

Applied Mathematical Sciences

Gadi Fibich

The Nonlinear Schrödinger Equation

Singular Solutions and Optical Collapse



Springer

Applied Mathematical Sciences

Volume 192

Editors-in-Chief

Stuart Antman, College Park, MD, USA
Leslie Greengard, New York, USA
Philip Holmes, Princeton, NJ, USA

Series editors

James Keener, Salt Lake City, UT, USA
Robert Kohn, New York, NY, USA
Bernard Matkowsky, Evanston, IL, USA
Paul Newton, Los Angeles, USA
R. Pego, Pittsburgh, PA, USA
Charles Peskin, New York, NY, USA
Lenya Ryzhik, Stanford, CA, USA
Amit Singer, Princeton, USA
Angela Stevens, Heidelberg, Germany
Andrew Stuart, Coventry, UK

More information about this series at <http://www.springer.com/series/34>

Gadi Fibich

The Nonlinear Schrödinger Equation

Singular Solutions and Optical Collapse



Springer

Gadi Fibich
School of Mathematical Sciences
Tel Aviv University
Tel Aviv
Israel

ISSN 0066-5452
ISBN 978-3-319-12747-7
DOI 10.1007/978-3-319-12748-4

ISSN 2196-968X (electronic)
ISBN 978-3-319-12748-4 (eBook)

Library of Congress Control Number: 2014954344

Mathematics Subject Classification: 35B44, 35Q55, 35Q60, 74J30, 78A60

Springer Cham Heidelberg New York Dordrecht London

© Springer International Publishing Switzerland 2015

This work is subject to copyright. All rights are reserved by the Publisher, whether the whole or part of the material is concerned, specifically the rights of translation, reprinting, reuse of illustrations, recitation, broadcasting, reproduction on microfilms or in any other physical way, and transmission or information storage and retrieval, electronic adaptation, computer software, or by similar or dissimilar methodology now known or hereafter developed. Exempted from this legal reservation are brief excerpts in connection with reviews or scholarly analysis or material supplied specifically for the purpose of being entered and executed on a computer system, for exclusive use by the purchaser of the work. Duplication of this publication or parts thereof is permitted only under the provisions of the Copyright Law of the Publisher's location, in its current version, and permission for use must always be obtained from Springer. Permissions for use may be obtained through RightsLink at the Copyright Clearance Center. Violations are liable to prosecution under the respective Copyright Law.

The use of general descriptive names, registered names, trademarks, service marks, etc. in this publication does not imply, even in the absence of a specific statement, that such names are exempt from the relevant protective laws and regulations and therefore free for general use.

While the advice and information in this book are believed to be true and accurate at the date of publication, neither the authors nor the editors nor the publisher can accept any legal responsibility for any errors or omissions that may be made. The publisher makes no warranty, express or implied, with respect to the material contained herein.

Printed on acid-free paper

Springer is part of Springer Science+Business Media (www.springer.com)

To Ravit, Maya, and Yael

Preface

Optical collapse is a fascinating research topic. The propagation of intense laser beams in a transparent medium is usually modeled by the two-dimensional nonlinear Schrödinger equation (NLS), and beam collapse corresponds to NLS solutions becoming singular. Since collapse occurs only when nonlinearity is stronger than diffraction, the analysis of singular NLS solutions requires a genuinely nonlinear approach.

This research field was started by experimental and theoretical physicists in the 1960s when high-power lasers became available. In the late 1970s, just as physicists started to lose interest, mathematicians joined in and began to develop the rigorous and asymptotic mathematical theory for NLS collapse. The availability of ultrashort lasers and new applications such as filamentation in air “brought back” the physicists, and nowadays this field is studied by both communities.

Because physicists and mathematicians tend to speak “different languages”, all too often the flow of information between them has been limited. One of the goals of this book is to lower the communication barrier between these communities, so that mathematicians would know the physical context of the mathematical theory and become familiar with the experimental research, while physicists know the mathematical theory and how it relates to the physics. To achieve this goal, the book adopts a “multi-lingual approach” and combines rigorous analysis, asymptotic analysis, informal arguments, numerical simulations, and physical experiments, repeatedly emphasizing the relations between these approaches and the intuition behind results.

The book covers material from the early 1960s and up to the present. Chapter 1 provides an informal derivation of the two-dimensional cubic NLS from Maxwell’s equations. Chapter 2 covers the relevant linear theory. Chapter 3 presents the pioneering early studies from the 1960s, and offers a historical perspective. NLS models in nonlinear optics and in Bose-Einstein condensates (BEC) are discussed in Chap. 4. The rigorous NLS theory begins in Chap. 5 with the topic of global existence. Properties of solitary waves are discussed in Chap. 6. Chapter 7

introduces the variance identity and its consequences. NLS symmetries are presented in Chap. 8, with special emphasis on the consequences of lens transformation. Stability of solitary waves is briefly discussed in Chap. 9. Chapters 10–12 present the explicit blowup solutions ψ_R^{explicit} , ψ_G^{explicit} , and ψ_Q^{explicit} . Properties shared by all blowup solutions of the critical NLS are presented in Chap. 13, and those that are unique to solutions that collapse with the $\psi_{R^{(0)}}$ profile are presented in Chap. 14. Chapter 15 concerns singular vortex solutions. Chapter 16 studies the effect of reflecting boundaries, by considering the NLS on bounded domains.

The blowup rate of peak-type solutions of the critical NLS is called the *loglog law*. The asymptotic analysis that leads to the loglog law, its “failure” in the regime of physical interest, and how to correct it with an adiabatic approach are presented in Chaps. 17 and 18. Other kinds of collapsing solutions of the critical NLS, namely ring-type and vortex solutions, are discussed in Chaps. 19 and 20. Collapsing peak-type and ring-type solutions of the supercritical NLS are covered in Chaps. 21–23. Going back to the nonlinear optics context, Chaps. 24 and 25 discuss the critical power for collapse and the breakup of high-power laser beams into multiple filaments. An asymptotic theory for strongly nonlinear solutions, the nonlinear geometrical optics (NGO) method, is presented in Chap. 26. Theoretical and experimental results on the location of singularity and on how to control it are given in Chap. 27. Numerical methods are discussed in Chaps. 28–30.

One of the advantages of this research field is that theoretical predictions that are based on the NLS can be observed in nonlinear optics experiments. This is because the NLS model is valid before and during the initial stages of the collapse. To model beam propagation beyond the NLS singularity, however, the mathematical model should include some of the terms that were neglected in the derivation of the NLS from Maxwell’s equations. A systematic asymptotic method for approximating perturbations of the critical NLS by simpler equations, called modulation theory, is derived in Chap. 31. The effects of various small terms neglected in the NLS model (high-order nonlinearities, linear and nonlinear damping, non-paraxiality, backscattering, and dispersion) on collapsing beams are discussed in Chaps. 32–37. Chapters 38 and 39 conclude with recent results on continuations of singular NLS solutions beyond the singularity.

This book could not have been written without the help of many friends and colleagues. George Papanicolaou introduced me to this field when he was my Ph.D. advisor at the Courant Institute, and he has been a continuing source of inspiration ever since. Russel Caflisch invited me to UCLA as a CAM postdoc, and suggested that I teach a graduate class on the NLS. This book grew out of lecture notes that I prepared for that class nearly 20 years ago. I deeply thank my former students Boaz Ilan, Yonatan Sivan, Nir Gavish, and Guy Baruch for their help and useful suggestions. Special thanks go to Steven Schochet for his enormous help and patience. Over the years, I benefited from collaborations and interactions with Reika Fukuizumi, Alexander Gaeta, Frank Merle, Hayato Nawa, Pierre Raphael, Semyon

Tsynkov, Xiao-Ping Wang, Michael Weinstein, and Arie Zigler. I am grateful to Andrei Iacob who voluntarily copy edited the entire manuscript, to Michal Shur-Ofry for legal advice, and to Shira Yechimovitz for technical help.

Tel Aviv, Israel, 2014

Gadi Fibich

How to Use This Book

The book assumes that the reader has taken an introductory PDE class. Other than that, all the necessary physical background and mathematical tools are introduced. For convenience, here are some suggested roadmaps:

Mathematical analysts: Start with the linear theory in Chap. 2, go over the classical rigorous analysis in Chaps. 5–16 (Chaps. 11, 12, 15 and 16 can be skipped on first reading), get familiarized with the asymptotic analysis of the critical NLS in Chaps. 17 and 18, the asymptotic analysis of the perturbed critical NLS in Chap. 31, and the NGO method for strongly-nonlinear solutions in Chap. 26, and conclude with Chaps. 38 and 39 on continuations beyond the singularity.

For challenging research problems, look for “Open Questions” throughout the book.

Applied mathematicians: Start with the physical background in Chaps. 1–4, go over the classical rigorous analysis in Chaps. 5–16 (Chaps. 11, 12, 15 and 16 can be skipped on first reading), go over the asymptotic analysis of the critical NLS in Chaps. 17 and 18, the asymptotic analysis of the perturbed critical NLS in Chap. 31, and the NGO method for strongly-nonlinear solutions in Chap. 26, and conclude with Chaps. 38 and 39 on continuations beyond the singularity.

Physicists and engineers: Start with the physical background in Chaps. 1–4, get familiarized with the classical rigorous results in Chaps. 5–8 and 14, go “back to the physics” in Chaps. 24–27, continue with perturbations of the NLS in Chaps. 31–37, and conclude with Chaps. 38 and 39 on continuations beyond the singularity.

Exercises

There are many exercises in this book, almost all of which are elementary. For example, the reader may be asked to modify a proof or a derivation that appears in the text. In my experience, these exercises enhance the understanding of the material.

Level of Rigor

Being interdisciplinary, this book contains various types of results: From rigorous theorems to asymptotic derivations, numerical simulations, and physical experiments. To aid readers identify the level of rigor of results, we adopt the following conventions:

Theorems are always rigorous results.

Propositions refer to non-rigorous results that are derived systematically using asymptotic and perturbation analysis.

Conclusions are non-rigorous results that are derived using informal arguments, such as dimensional arguments.

Observations are based on numerical or physical evidence.

Lemmas and **Corollaries** can be rigorous or informal, depending on the context. Similarly, the word **proof** refers both to rigorous proofs and informal ones. In the latter case, we state that the “proof” is informal.

Contents

Part I NLS in Nonlinear Optics I

1	Derivation of the NLS	3
1.1	Propagation in Vacuum	3
1.2	Linear Polarization	5
1.3	Paraxial Propagation	6
1.4	Polarization Field	9
1.4.1	Linear Polarization Field	10
1.4.2	Weakly-Nonlinear Polarization Field	11
1.4.3	Kerr Nonlinearity	12
1.4.4	Vectorial Kerr Nonlinearity	14
1.5	Weakly Nonlinear Helmholtz Equation	15
1.6	Nonlinear Schrödinger Equation	15
1.7	Relative Magnitude of the Kerr Effect	15
1.8	Physical Validity of the NLS Model	17
2	Linear Propagation	19
2.1	Geometrical Optics	19
2.1.1	Eikonal Equation	20
2.1.2	Transport Equation	23
2.2	Applications of Geometrical Optics	25
2.2.1	Homogeneous Medium	25
2.2.2	Snell's Law	25
2.2.3	Linear Waveguides	26
2.3	Collimated Beams (Helmholtz Model)	29
2.4	Fundamental Solution of Helmholtz Equation	29
2.5	Focused Beams (Helmholtz Model)	31
2.6	Singularity in the Helmholtz Model	31
2.7	Global Existence in the Linear Helmholtz Equation in the Half Space	32
2.8	Representations of Input Beams	34

2.8.1	Relation Between $S^{(E)}$ and $S^{(\psi)}$	34
2.8.2	Collimated Beams (Schrödinger Model)	34
2.8.3	From Spherical to Parabolic Waves	35
2.8.4	Focused Beams (Schrödinger Model)	35
2.8.5	Tilted Beams	36
2.8.6	Vortex Beams	37
2.8.7	Generic Input Beams	38
2.9	Geometrical Optics Analysis of Paraxial Propagation	39
2.10	Arrest of Linear Collapse by Diffraction (Gaussian Beams)	41
2.11	Diffraction Length (L_{diff})	45
2.12	The Dimensionless Linear Schrödinger Equation	47
2.12.1	Paraxial Approximation	47
2.12.2	Focused Beams	48
2.12.3	Tilted Beams	49
2.12.4	Linear Schrödinger Equation in d Dimensions	50
2.12.5	Generic Input Beams	50
2.13	Fourier Transform	51
2.14	L^p , H^1 , and H^2 Norms	51
2.15	Linear Schrödinger Equation—Analysis	52
2.15.1	Fundamental Solution	52
2.15.2	Existence and Smoothness	53
2.15.3	Gaussian Beams	55
2.15.4	Dispersive Equation	57
2.16	Non-directionality (Reversibility)	57
2.16.1	Symmetry with Respect to z_{\min}	58
2.16.2	Sign of Diffraction (and Nonlinearity)	59
2.17	Singularities in Linear and Nonlinear Optics	59
3	Early Self-focusing Research	61
3.1	Dimensionless NLH and NLS	61
3.1.1	Dimensionless NLH	61
3.1.2	Dimensionless NLS	62
3.1.3	No Wavelength in NLS Model	63
3.1.4	Vectorial Effects and Backscattering	63
3.2	Geometrical Optics Explanation of Self Focusing	64
3.2.1	Self Defocusing	65
3.2.2	Coupled Optical Beams	65
3.3	Self Trapping [46]	66
3.3.1	Hercher's Experiments	66
3.3.2	Self-trapping Analysis	67
3.3.3	Beyond the Diffraction Limit	69
3.4	Optical Collapse [140]	70
3.4.1	Self-focusing Distance (L_{SF})	71
3.4.2	Critical Power for Collapse	74

3.4.3	First Simulations of Blowup Solutions	75
3.4.4	In Retrospect	75
3.5	Aberrationless Approximation Method [4]	76
3.5.1	Effect of a Lens	81
3.5.2	Blowup Rate.	82
3.5.3	In Retrospect	82
3.6	Multiple Filamentation [27]	83
3.6.1	Early Experiments	83
3.6.2	Multiple Filamentation and Loss of Radial Symmetry.	84
3.6.3	Bespalov-Talanov Model	84
3.6.4	In Retrospect	87
3.7	Self Focusing Until 1975	88
4	NLS Models	89
4.1	NLS Models in Nonlinear Optics	89
4.1.1	Planar Waveguides	90
4.1.2	Ultrashort Pulses	91
4.2	NLS Models in BEC	92

Part II Rigorous Analysis

5	Existence of NLS Solutions	95
5.1	Biharmonic NLS (BNLS).	96
5.2	Power, Hamiltonian, and Linear Momentum.	96
5.3	Invariance	97
5.4	Gagliardo-Nirenberg Inequality	99
5.5	Existence in H^1	99
5.6	Local Existence and the Blowup Alternative.	100
5.7	Type of Singularity	103
5.7.1	Singularity Point \mathbf{x}_c	104
5.7.2	Singularity in L^2	105
5.8	Radial Solutions	107
5.9	Focusing and Defocusing NLS	107
5.10	Global Existence	108
5.10.1	Defocusing NLS	108
5.10.2	Focusing NLS.	109
5.11	Subcritical, Critical, and Supercritical NLS	111
5.11.1	Subcritical NLS	112
5.11.2	Critical NLS	112
5.11.3	Supercritical NLS	113
5.11.4	L^2 -Critical and H^1 -Subcritical	114

5.12	Optimal Constant $C_{\sigma,d}$ [272]	115
5.12.1	Critical Case	120
5.12.2	Existence of a Minimizer to $J[f]$	122
6	Solitary Waves	125
6.1	Solitary Waves $\psi_\omega^{\text{solitary}} = e^{i\omega z} R_\omega(\mathbf{x})$	126
6.2	Pohozaev Identities	127
6.3	The Ground State $R^{(0)}$	131
6.3.1	Critical Case	134
6.3.2	Variational Characterizations (Critical Case)	136
6.3.3	Variational Characterization (Subcritical Case)	136
6.4	Radial States $R^{(n)}(r)$	138
6.4.1	Uniqueness of Initial Value Problems	138
6.4.2	Asymptotic Behavior for $r \gg 1$	140
6.4.3	$d = 1$	141
6.4.4	$d \geq 2$	142
6.4.5	Asymptotic Behavior for $0 \leq r \ll 1$	145
7	Variance Identity	147
7.1	Variance	147
7.2	Variance Identity	148
7.2.1	Critical NLS	151
7.2.2	General Nonlinearity	151
7.2.3	Biharmonic NLS	152
7.3	Sufficient Conditions for Collapse	153
7.3.1	Sharper Conditions in the Supercritical Case	156
7.4	Limitations of the Variance Identity	157
7.5	Physical Interpretation of Theorem 7.2	158
7.6	The Sufficient Condition $H_G(0) < 0$	161
7.7	Whole-Beam and Partial-Beam Collapse	163
7.7.1	Critical NLS	164
7.7.2	Supercritical NLS	167
7.8	Wrong Conclusions	167
7.9	The Variance Identity and the Aberrationless Approximation	168
7.10	Sufficient Power ($P_{\text{sufficient}}$) and Threshold Power (P_{th}) for Collapse	168
7.10.1	Critical NLS	170
7.11	Calculation of $H(R)$	172
7.11.1	Critical NLS	173
7.12	Dual Borderline Properties of $R^{(0)}$	174

8 Symmetries and the Lens Transformation	175
8.1 NLS Symmetries.	175
8.1.1 Biharmonic NLS	176
8.2 Galilean Invariance	176
8.3 Lens Transformation (Critical NLS).	177
8.4 Consequences of the Lens Transformation	181
8.4.1 Effect of a Lens (Critical NLS)	181
8.4.2 Effect of a Lens (Subcritical and Supercritical NLS)	181
8.4.3 The Explicit Blowup Solution ψ_R^{explicit}	183
8.4.4 Arresting Collapse with a Defocusing Lens	184
8.4.5 Controlling the Collapse Distance with a Lens	185
8.4.6 Sharper Conditions for Blowup?	186
8.4.7 Scattering ($P < P_{\text{cr}}$)	187
8.4.8 NLS with a Quadratic Potential.	189
9 Stability of Solitary Waves	193
9.1 Orbital Stability	193
9.2 Linear Stability	195
9.3 Vakhitov-Kolokolov (VK) Condition	198
9.4 Orbital Stability of Ground States	199
9.4.1 Subcritical Case	199
9.4.2 General Case	199
9.4.3 Instability and Collapse	200
9.5 Critical NLS.	201
9.5.1 Strong Instability and Scattering	201
9.5.2 Dual Instabilities of the Ground State	202
9.5.3 Instability of Excited States	203
9.6 Instability Rate and Dynamics	203
9.7 Random Versus Deterministic Perturbations	204
10 The Explicit Critical Singular Peak-Type Solution ψ_R^{explicit}	205
10.1 Singular Peak-Type Solutions	205
10.2 Whole-Beam Collapse	206
10.3 $\psi_{R,\alpha}^{\text{explicit}}$ and $\psi_{R,\alpha,c}^{\text{explicit}}$	207
10.4 Blowup Rate $l(z)$	208
10.4.1 Blowup Rate of ψ_R^{explicit}	208
10.5 How to Define Stability of Singular Solutions?	209
10.6 Instability of ψ_R^{explicit}	211
10.6.1 Instability of $\psi_{R^{(0)}}^{\text{explicit}}$	211
10.6.2 Dual Instabilities of $\psi_{R^{(0)}}^{\text{explicit}}$	212
10.6.3 Instability of $\psi_{R^{(n)}}^{\text{explicit}}$ for $n \geq 1$	213
10.7 Non-generic Character of ψ_R^{explicit}	213

10.8	Bourgain-Wang Solutions (ψ_{BW})	214
10.8.1	Dual Instabilities of ψ_{BW}	215
10.8.2	Bourgain-Wang Solutions are “Generic”	216
10.9	Biharmonic BLS	216
11	The Explicit Critical Singular Ring-Type Solution ψ_G^{explicit}	219
11.1	Derivation of ψ_G^{explicit}	221
11.1.1	$\psi_{G,0}^{\text{explicit}} = G(r)e^{-i\frac{r^2}{4r}}$	224
11.2	Analysis of the G Equation	225
11.2.1	Asymptotic Behavior for $r \gg 1$	225
11.2.2	Asymptotic Behavior for $r \ll 1$	229
11.2.3	Ring Profile with an Algebraically-Decaying Tail	230
11.2.4	Families of Multi-ring Profiles	233
11.2.5	Single-Ring Profiles	235
11.3	Blowup Rate of Non- H^1 Solutions	239
11.4	Stability of ψ_G^{explicit}	241
11.4.1	Radial Stability	241
11.4.2	Azimuthal Instability	244
11.4.3	Non-integer d	245
11.5	Azimuthal Instability of Collapsing Rings	245
12	The Explicit Supercritical Singular Peak-Type Solution ψ_Q^{explicit}	249
12.1	Derivation of ψ_Q^{explicit}	249
12.2	Analysis of the Q Equation	252
12.3	Blowup Rate of ψ_Q^{explicit}	258
12.3.1	Weak Collapse	259
12.4	Zero-Hamiltonian Solutions	260
12.4.1	Computation of Zero-Hamiltonian Solutions	262
12.5	$Q(\rho) = e^{-i\frac{a\rho^2}{4}}P(\rho)$	263
12.6	Admissible Solutions	265
12.6.1	Admissible P Profile	266
12.6.2	$d = 1$	267
12.7	Multi-bump Solutions	269
12.8	Singular Solutions of the Subcritical NLS	270
12.8.1	The Q Equation in the Subcritical Case	271
13	Blowup Rate, Blowup Profile, and Power Concentration	273
13.1	Blowup Rate $l(z)$	273
13.1.1	Linear Blowup Rate	274
13.1.2	Loglog Law Blowup Rate	274
13.1.3	Square-Root Blowup Rate	274
13.1.4	Square-Root Bound	275

13.1.5	Blowup Rate of L^p Norms	277
13.1.6	Blowup Rate and the Lens Transformation	277
13.2	Convergence to a Self-similar Blowup Profile	280
13.2.1	Radial Solutions	283
13.2.2	Quasi Self-similar Collapse	284
13.2.3	$l(z) \sim c_l L(z)$ in the Critical NLS	285
13.2.4	$l_B(z) \sim c_{l_B} L(z)$ in the Critical BNLS	286
13.2.5	Nawa's Theorem	287
13.3	Power Concentration	288
13.3.1	Is $P_{\text{collapse}} = P_{\text{cr}}$?	292
13.3.2	Rate of Power Concentration	293
13.4	Collapse at k Points	296
13.4.1	Is $k \leq P/P_{\text{cr}}$?	298
13.5	Minimal-Power Blowup Solutions	299
13.5.1	Is $P_{\text{th}}[f] > P_{\text{cr}}$ for $f \not\equiv R^{(0)}$?	300
13.6	Supercritical NLS	301
13.6.1	Blowup Rate	301
13.6.2	Types of Singular Solutions	304
13.6.3	No Minimal-Power and Power-Concentration Properties	305
14	The Peak-Type Blowup Profile $\psi_{R^{(0)}}$	307
14.1	Numerical Observations—Convergence to $\psi_{R^{(0)}}$	309
14.1.1	Radial Initial Conditions	309
14.1.2	Convergence to a Radial Profile	312
14.2	Numerical Observations—Blowup Rate	314
14.2.1	How to Determine Numerically a Power-Law Blowup Rate?	315
14.2.2	How to Distinguish Between Loglog and Square-Root Blowup Rates?	316
14.2.3	Blowup Rate	318
14.3	Numerical Observations—Perturbed Excited Solitary Waves	319
14.4	Numerical Observations—Perturbed Excited Explicit Blowup Solutions	322
14.5	Experimental Observations	322
14.6	Collapse with the $\psi_{R^{(0)}}$ Profile at the Loglog Law Blowup Rate	324
14.6.1	Universal Blowup Profile and Power Quantification	326
14.6.2	Blowup Rate	328
14.6.3	Sufficient Condition for Loglog Collapse	329
14.6.4	Stability of Loglog Blowup	329

14.6.5	Instability of Linear Collapse?	329
14.6.6	Spectral Property	329
14.6.7	Value of $\alpha^*(d)$	329
14.6.8	Universality of $\psi_{R^{(0)}}$ and of Loglog Collapse?	331
14.7	Critical Biharmonic NLS ($\psi_{R_B^{(0)}}$)	331
15	Vortex Solutions	333
15.1	Preliminary Results	334
15.2	Solitary Vortex Profiles ($R_m^{(n)}$)	337
15.2.1	Pohozaev Identities	338
15.2.2	Infinite Number of Solutions	339
15.2.3	Asymptotic Behavior for $r \ll 1$	339
15.2.4	Ring Profile with an Exponential Tail	341
15.2.5	The Ground State ($R_m^{(0)}$)	341
15.2.6	Critical Case	345
15.3	Optimal Constant $C_{\sigma,2}(m)$	346
15.4	Critical Power for Vortex Collapse $P_{\text{cr}}(m)$	347
15.4.1	Nonradial Vortex Initial Conditions	350
15.5	Explicit Blowup Solutions (Critical NLS)	354
15.5.1	The Explicit Vortex Blowup Solution $\psi_{R_m^{(n)}}^{\text{explicit}}$	354
15.6	The Explicit Vortex Blowup Solution $\psi_{G_m}^{\text{explicit}}$	356
15.6.1	$\psi_0 = e^{im\theta} G_m(r) e^{-i\frac{r^2}{4F}}$	358
15.6.2	Analysis of the G_m Equation	358
15.6.3	Square-Root Blowup Rate (in L^4)	362
15.7	The Explicit Blowup Solution $\psi_{Q_m}^{\text{explicit}}$ (Supercritical NLS)	363
15.8	Stability of Solitary Vortex Solutions $\psi_{\text{vortex}}^{\text{solitary},(n)}$	364
15.8.1	Radial Stability	365
15.8.2	A Surprising Result	366
15.8.3	Azimuthal Instability	368
15.9	Stability of $\psi_{R_m^{(n)}}^{\text{explicit}}$ and $\psi_{G_m}^{\text{explicit}}$	371
15.9.1	Radial Stability	371
15.9.2	Azimuthal Instability	373
15.10	Radial Instability of $\psi_{Q_m}^{\text{explicit}}$	373
15.11	Asymptotic Blowup Profile (Critical NLS)	374
15.11.1	Quasi Self-similar Profile	374
15.11.2	Blowup Profile is Different from $\psi_{R^{(0)}}$	376
15.11.3	Upper Bound for $\alpha^*(d=2)$	377
15.11.4	Azimuthal Instability	377
15.11.5	Power Concentration	377
15.11.6	Rate of Power Concentration	378
15.11.7	Collapse at the Origin	378
15.12	Vortex Solutions in Three Dimensions	380
15.13	Necklace Solutions	381

16 NLS on a Bounded Domain	385
16.1 Physical Motivation.	386
16.2 Numerical Motivation	387
16.3 Invariance and Symmetries.	387
16.4 Solitary Waves	388
16.4.1 Pohozaev Identities	389
16.4.2 Critical Case.	391
16.4.3 Linear Solitary Waves	391
16.4.4 Large-Amplitude and Small-Amplitude Regimes	392
16.4.5 Radial Solitary Waves	395
16.4.6 Solitary Vortex Solutions	396
16.4.7 Necklace Solitary Waves	397
16.4.8 Critical Radial Solitary Waves	398
16.5 Stability of Solitary Waves.	402
16.5.1 Orbital Stability on a Bounded Domain	402
16.5.2 Critical NLS	402
16.5.3 Linear and Weakly-Nonlinear Modes	405
16.5.4 Supercritical NLS	406
16.5.5 Excited States	406
16.6 Optimal Constant $C_{\sigma,d}(\Omega)$	407
16.6.1 Critical Case.	409
16.7 Global Existence.	410
16.8 Blowup Solutions	411
16.8.1 Variance Identity.	411
16.8.2 Threshold Power for Collapse (Critical NLS)	413
16.8.3 Local Behavior Near the Singularity (Critical NLS).	414
16.9 Oscillations for $P < P_{\text{cr}}$	415
16.9.1 Informal Analysis	416
16.10 Experiments	417

Part III Asymptotic Analysis of the Critical NLS

17 Derivation of Reduced Equations.	421
17.1 “Failure” of Self-similar Analysis	422
17.1.1 Identifying All Self-similar Solutions	423
17.1.2 Relation to the Aberrationless Approximation	425
17.2 Dual Borderline Properties of $\psi_{R^{(0)}}$	426
17.3 Quasi Self-similar Collapse	427
17.4 Perturbation Analysis for $U = R^{(0)} + \epsilon h$	432
17.4.1 Perturbation Analysis for $V_0 \sim R^{(0)} + \beta g$	435

17.5	Calculation of $\frac{dP_{\text{coll}}}{d\zeta}$ (Proof of Proposition 17.2)	436
17.5.1	A Remark on the Derivation	442
17.6	Derivation of Reduced Equations from a Solvability Condition	443
17.6.1	“Correct” Equation for V_0	443
17.6.2	Solvability Condition	444
17.6.3	Alternative Proof of Proposition 17.2	446
17.7	Numerical Values of P_{cr} , M , A_R , and c_v	446
17.7.1	$d = 1$	447
17.7.2	$d = 2$	447
18	Loglog Law and Adiabatic Collapse	449
18.1	Preliminary Observations	450
18.2	Derivation of the Loglog Law (Proof of Proposition 18.1)	452
18.2.1	Solve Eq. (18.10b) for $\beta(\zeta)$	453
18.2.2	Use the Solution for $\beta(\zeta)$ and Eq. (18.10a) to Solve for $A(\zeta)$	454
18.2.3	Use the Solution for $A(\zeta)$ and Eq. (18.10c) to Express A as a Function of z	455
18.3	“Failure” of the Loglog Law	457
18.4	Adiabatic Approach	460
18.5	Strict Adiabatic Law	462
18.5.1	$Z_c - z_0 \approx Z_c^{\text{adiabatic}}$	463
18.5.2	Blowup Rate	465
18.6	Delicate Balance Between Two Giants	465
18.7	Nonadiabatic Effects	467
18.8	Comparison of the Adiabatic and Loglog Laws	468
18.8.1	Simulations	469
18.9	In Retrospect	470
19	Singular H^1 Ring-Type Solutions (ψ_G)	473
19.1	Preliminary Simulations	473
19.1.1	Quasi Self-similar Ring Profile	474
19.2	Blowup Profile and Blow Rate	476
19.2.1	Quasi Self-similar Blowup Profile	478
19.2.2	Blowup Rate of ψ_G	480
19.2.3	$d = 7/4$	481
19.3	Azimuthal Instability	481
19.4	Experiments with Super-Gaussian Beams	481
19.5	Ring Power Collapsing into the Singularity	482
19.6	Open Question	483
19.7	Critical Biharmonic NLS (ψ_{G_B})	485

20 Singular H^1 Vortex Solutions (ψ_{R_m} and ψ_{G_m})	487
20.1 Two Potential Blowup Profiles	487
20.2 Simulations	489
20.2.1 Quasi Self-similar Collapse	491
20.3 Open Question	492
20.4 Azimuthal Instability	492
Part IV Asymptotic Analysis of the Supercritical NLS	
21 Singular H^1 Peak-Type Solutions (ψ_Q)	495
21.1 Quasi Self-similar Collapse	496
21.2 Weak Collapse	498
21.3 Blowup of L^p Norms	499
21.4 Blowup Rate	499
21.5 Rigorous Results	500
21.6 Simulations	501
21.7 Supercritical Biharmonic NLS (ψ_{Q_B})	504
22 Singular Standing-Ring Solutions (ψ_F)	505
22.1 Standing-Ring and Shrinking-Ring Solutions	505
22.2 Preliminary Observations	507
22.2.1 Standing-Ring Solutions of the BNLS and Other Nonlinear PDEs	509
22.3 “Critical” Standing Rings ($\sigma = 2$)	509
22.3.1 Informal Analysis	510
22.3.2 Rigorous Results	511
22.3.3 Simulations	512
22.4 “Supercritical” Standing Rings ($\sigma > 2$)	516
22.4.1 Informal Analysis	516
22.4.2 Simulations	517
22.5 Singular Standing Vortex Solutions	518
22.6 Azimuthal Instability	519
22.7 Mixed Standing-Ring/Peak-Type Solutions	520
23 Singular Shrinking-Ring Solutions (ψ_S)	523
23.1 Review of Ring-Type Blowup Solutions	523
23.2 A New Type of Ring-Type Blowup Solutions	524
23.2.1 $\frac{d-1}{r} \psi_r$ Is Not Negligible	526
23.3 Finding the Blowup Profile and Blowup Rate	527
23.3.1 “Interpolation” of ψ_G and ψ_F	527
23.3.2 The Shrinkage Parameter α	529

23.3.3	Bounds for the Blowup Rate	531
23.3.4	Self-similar Profile	533
23.3.5	$\alpha = \alpha_{\text{ring}}$ and $p = \frac{1}{1+\alpha_{\text{ring}}}$	538
23.4	Strong Collapse	538
23.5	“Minimal-Power” Shrinking-Ring Solutions	539
23.6	Simulations	540
23.6.1	Self-similar Ring-Type Profile	540
23.6.2	$\alpha = \alpha_{\text{ring}}$ and $p = \frac{1}{1+\alpha_{\text{ring}}}$	540
23.6.3	Stability of ψ_S	542
23.7	Singular Shrinking-Vortex Solutions (ψ_{S_m})	544
23.7.1	Stability of Collapsing Supercritical Vortex Solutions	544
23.8	Non-existence of Expanding Rings	545
23.9	Classification of Ring-Type Blowup Solutions	546
23.9.1	Critical Exponent and Phase Transition	547
23.10	Biharmonic NLS	548
23.10.1	Shrinking-Ring Blowup Solutions (ψ_{S_B})	548
23.10.2	Classification of Ring-Type Blowup Solutions	549

Part V NLS in Nonlinear Optics II

24	Critical and Threshold Powers for Collapse (P_{cr} and P_{th})	553
24.1	Review: P_{cr} , P_{th} , and $P_{\text{sufficient}}$	554
24.1.1	A Historical Note	555
24.2	Dimensional Dependence	556
24.3	Threshold Power	557
24.3.1	Inaccuracy of the Zero-Hamiltonian Condition	557
24.3.2	Failure of the Aberrationless Approximation	558
24.4	Biharmonic NLS	560
24.5	Bounded Domains (Hollow-Core Fibers)	560
24.6	Elliptic Input Beams	561
24.6.1	Lower and Upper Bounds	562
24.6.2	Threshold Power	563
24.7	Vortex Beams	564
24.7.1	Effect of Symmetry Breaking	566
24.8	Circular, Radial, and Azimuthal Polarizations	566
24.9	Interpretation of the Ratio P/P_{cr}	567
24.10	Local Nature of the Critical Power	568
24.11	Critical and Threshold Powers for Self Trapping	569

25	Multiple Filamentation	571
25.1	Validity of Bespalov-Talanov Analysis	571
25.1.1	Threshold Power for a Bespalov-Talanov Multiple Filamentation ($P_{\text{th}}^{\text{MF}}$)	572
25.1.2	Experiments	576
25.2	Noise and Saturated Nonlinearities	576
25.3	Deterministic Multiple Filamentation	577
25.3.1	Vectorial Effects	578
25.3.2	Elliptic (Astigmatic) Input Beams	581
25.3.3	Tilted Lens Setup	585
25.3.4	Amplitude and Phase Masks	587
25.3.5	Chaotic Post-collapse Interactions	587
25.4	Predicting the Initial Filamentation Pattern	587
25.5	Summary—Four Types of Multiple Filamentation	588
26	Nonlinear Geometrical Optics (NGO) Method	589
26.1	Derivation of NGO Equations	590
26.2	NGO Method	592
26.2.1	Direction of NGO Rays	596
26.3	(In)dependence on Beam Power	596
26.3.1	L_{SPM} and L_{SF}	597
26.3.2	“Counter-Intuitive” Effect of Small Diffraction	598
26.4	Limitations of the NGO Method	599
26.5	One Spatial Dimension	600
26.5.1	Analysis	600
26.5.2	Simulations	602
26.6	“Failure” of the Linear Schrödinger Model	603
26.7	Two Spatial Dimensions	604
26.7.1	Radial Beams	604
26.7.2	Experiments	606
26.7.3	Square Input Beams	607
26.7.4	One-Dimensional Building Blocks	608
26.7.5	Rectangular Beams	609
26.8	Effect of a Lens	611
26.9	Robustness of NGO Method	611
27	Location of Singularity (Z_c)	613
27.1	Rigorous Results	613
27.1.1	Consequences of NLS Symmetries	613
27.1.2	Upper Bound for Z_c	614
27.2	Asymptotic Results	617
27.2.1	Adiabatic Approximation (Critical NLS)	617
27.2.2	Clean High-Power Initial Conditions	618
27.2.3	Noisy High-Power Initial Conditions	618

27.3	Gaussian Initial Conditions (Critical NLS)	620
27.4	Experiments	621
27.5	Coupled Optical Beams	622
27.6	Monotonicity and Non-monotonicity of $Z_c(P)$	624
27.6.1	Loss of Monotonicity	626
27.7	Effect of a Lens	628
27.7.1	Monotonicity (Critical Case)	628
27.7.2	Loss of Monotonicity (Supercritical Case)	630
27.8	Controlling the Collapse Distance	631
27.8.1	Deformable Mirror	631
27.8.2	Double Lens Setup	632

Part VI Numerical Methods

28	Computation of Solitary Waves	637
28.1	Shooting Method	637
28.2	Spectral Renormalization Method	638
28.3	Non-spectral Renormalization Method	643
28.4	Biharmonic Solitary Waves	644
28.5	Consistency Checks	646
29	Numerical Methods for the NLS	647
29.1	Spatial Discretization	647
29.1.1	Radial NLS	648
29.2	“Temporal” Discretization	649
29.2.1	Explicit Methods	649
29.2.2	Implicit Methods	649
29.2.3	Explicit or Implicit?	650
29.3	Boundary Conditions	650
29.4	Moving-Mesh Methods	651
29.4.1	Dynamic Rescaling	651
29.4.2	Remeshing Without Prior Knowledge	652
29.5	Consistency Checks	653
30	Effects of Spatial Discretization	655
30.1	Spatial Discretization	655
30.2	Modified Equations	656
30.2.1	Rigorous Analysis	658
30.3	Analysis of the Semi-discrete NLS	660
30.4	Informal Analysis	662
30.5	Simulations	664

Part VII The Perturbed Critical NLS

31 Modulation Theory	669
31.1 Derivation of Reduced Equations	670
31.1.1 Three Conditions for Validity of Modulation Theory	671
31.1.2 Three (or Five) Stages of Propagation	671
31.1.3 Main Result	673
31.1.4 The Physical Case $d = 2$	675
31.1.5 Multiple Perturbations	676
31.1.6 Perturbations that “Add a Dimension”	677
31.2 Derivation of Main Result (Proposition 31.1)	677
31.2.1 Derivation from a Solvability Condition	678
31.2.2 Derivation from Balance of Power	680
31.2.3 Variational Derivation	681
31.3 The β Principle	682
31.4 Conservative and Non-conservative Perturbations	684
31.4.1 Dual Interpretations for β	685
31.4.2 Non-conservative Perturbations	686
31.4.3 Conservative Perturbations	687
31.5 Generic Effect of Conservative Perturbations	689
31.5.1 Periodic Focusing-Defocusing Oscillations	691
31.5.2 Self Trapping (Filamentation)	693
31.5.3 Other Cases	694
31.5.4 Nonadiabatic Effects	695
31.5.5 Global Validity of Modulation Theory	699
32 Cubic-Quintic and Saturated Nonlinearities	701
32.1 Physical Motivation	701
32.2 Global Existence and Singular Solutions	702
32.2.1 Focusing Quintic Nonlinearity	703
32.2.2 Defocusing Quintic Nonlinearity	703
32.3 Dynamics	704
32.3.1 Small Defocusing Quintic Nonlinearity	705
32.3.2 Small Focusing Quintic Nonlinearity	706
32.4 Saturated Nonlinearities	707
32.4.1 Physical Motivation	707
32.4.2 Equivalence of Cubic-Quintic and Saturated Nonlinearities	707
32.5 Filamentation and Multiple Filamentation	709
33 Linear and Nonlinear Damping	711
33.1 Linear Damping	711
33.1.1 Physical Origin	711

33.1.2	Linear Damping Parameter (δ)	712
33.1.3	Conditions for Collapse	713
33.1.4	$u = e^{\delta z} \psi$	714
33.1.5	Blowup Profile and Rate	715
33.1.6	Monotonicity and Non-monotonicity of Z_c^δ	715
33.1.7	Threshold Damping Parameter (δ_{th})	715
33.2	Nonlinear Damping	716
33.2.1	Physical Motivation	716
33.2.2	Power Losses	716
33.2.3	Arrest of Collapse—Rigorous Results	717
33.3	Asymptotic Analysis	718
33.3.1	Derivation of Reduced Equations	718
33.3.2	Dynamics	719
34	Nonparaxiality and Backscattering	
	(Nonlinear Helmholtz Equation)	723
34.1	Breakdown of the Paraxial Approximation	723
34.2	Early Simulations	725
34.3	Asymptotic Analysis of Nonparaxial Effects	726
34.3.1	Global Validity of Reduced Equations	730
34.4	Backscattering and Vectorial Effects	730
34.5	Continuity of E and E_z Across Interfaces	733
34.6	The $(0 + 1)$ D NLH	734
34.6.1	Radiation Boundary Conditions	737
34.7	Boundary Conditions for the $(2 + 1)$ D NLH	737
34.8	Genuine Boundary Value Simulations	738
34.8.1	Arrest of Collapse in the NLH	740
34.8.2	Nonparaxial Solitons	741
34.9	Rigorous Analysis	742
35	Ultrashort Pulses	743
35.1	Derivation from Maxwell's Equations	743
35.1.1	Dispersion	744
35.1.2	Slowly-Varying Envelope Approximation	745
35.1.3	Moving-Frame Coordinate System	747
35.1.4	Boundary Conditions	749
35.1.5	The Slowly-Varying Envelope Parameter $\delta = \frac{1}{T_0 \omega_0}$	749
35.1.6	Instantaneous Kerr Response	750
35.2	Dispersion and Transparency	751
35.3	Models for Propagation of Ultrashort Pulses	752

36 Normal and Anomalous Dispersion	755
36.1 Initial Conditions	755
36.2 Linear Dispersive Propagation	756
36.2.1 Dispersion Length (L_{disp})	756
36.2.2 Dispersion Parameter (γ_2)	757
36.2.3 Temporal Broadening	757
36.2.4 Chirping	758
36.3 Temporal Solitons	758
36.4 Invariance	759
36.5 Solitary Waves	760
36.5.1 Optical Bullets	761
36.6 Initial Propagation Stage ($ \gamma_2 \ll 1$)	761
36.7 Small Anomalous Dispersion	763
36.7.1 Cigar-Shaped Bose-Einstein Condensates	764
36.8 Small Normal Dispersion	764
36.8.1 Failure of Linear Superposition Analysis	765
36.8.2 Early Simulations	765
36.8.3 Reduced Equations	765
36.8.4 Analysis of Pulse Splitting	769
36.8.5 Self-similar Analysis	770
36.8.6 Simulations	772
36.8.7 Why only One Splitting?	773
36.8.8 Post-splitting Simulations	774
36.8.9 Summary: Self-focusing with Small Normal Dispersion	777
36.8.10 Open Question	778
36.9 Asymmetric Pulse Splitting	778
36.9.1 Reduced Equations	779
36.9.2 Simulations	780
36.10 Experimental Observation of Pulse Splitting (Normal Regime)	780
37 NGO Method for Ultrashort Pulses with Anomalous Dispersion	783
37.1 NGO Method	783
37.2 One Temporal Dimension	784
37.3 Spherical Spatio-Temporal Input Pulses	785
37.4 Cylindrical Spatio-Temporal Input Pulses	786
37.4.1 Non-isotropic Case	788
37.5 Experimental Observation of Pulse Splitting (Anomalous Regime)	790
37.6 Spatio-Temporal Cubic Input Pulses	791

38 Continuations Beyond the Singularity	793
38.1 Rigorous Continuations	794
38.1.1 Merle's Explicit Continuation of $\psi_{R^{(0)},\alpha}^{\text{explicit}}$	794
38.1.2 Continuation of Bourgain-Wang Solutions	797
38.1.3 Tao's Continuation	799
38.1.4 Vanishing Nonlinear-Saturation Continuation	799
38.2 Sub-threshold Power Continuation.	799
38.2.1 Proof of Proposition 38.1	801
38.2.2 Comparison of Proposition 38.1 and Theorem 10.2	803
38.3 Reversible Continuations	804
38.4 Vanishing Nonlinear-Saturation Continuation	806
38.4.1 Merle's Rigorous Analysis	806
38.4.2 Malkin's Asymptotic Analysis	807
38.4.3 Importance of Power Radiation	808
38.5 Shrinking-Hole Continuation	809
38.5.1 Theory Review	809
38.5.2 Explicit Continuation of ψ_G^{explicit}	809
38.6 Vanishing Nonlinear-Damping Continuation.	812
38.6.1 Physical Motivation	812
38.6.2 Arrest of Collapse by Nonlinear Damping—Review	812
38.6.3 Explicit Continuation of $\psi_{R^{(0)},\alpha}^{\text{explicit}}$ with Critical Nonlinear Damping.	813
38.6.4 Proof of Proposition 38.3	815
38.6.5 Nonlinear Damping and the Hamiltonian	823
38.6.6 Continuations of $\psi_{R^{(0)},\alpha}^{\text{explicit}}$ with Subcritical and Supercritical Nonlinear Damping.	825
38.6.7 Continuation of Loglog Collapse	826
38.6.8 Continuation of the Supercritical NLS	827
38.7 Complex Ginzburg-Landau Continuation	828
38.8 Vanishing-Diffraction Continuation of the Linear Schrödinger Equation	829
38.9 Summary	831
39 Loss of Phase and Chaotic Interactions	833
39.1 Phase-Loss Property	833
39.1.1 Physical Perspective	833
39.1.2 Simulations	834
39.1.3 Experiments	834
39.2 Chaotic Interactions	836
39.2.1 Simulations	836
39.2.2 Experiments	839
39.3 Summary	840

Contents	xxxi
Appendix A: Elementary Inequalities	843
Appendix B: Strong and Weak Convergence	845
References	847
Index	859

Part I

NLS in Nonlinear Optics I

Chapter 1

Derivation of the NLS

In this chapter we present a quick, informal derivation of the nonlinear Schrödinger equation (NLS) as the leading-order model for propagation of intense laser beams in an isotropic bulk medium. During the derivation, we introduce some terminology from linear and nonlinear optics, such as *linear polarization*, the *paraxial approximation*, and a *Kerr nonlinearity*.

1.1 Propagation in Vacuum

A laser pulse is an electromagnetic wave. Therefore, its propagation in a medium with no external charges or currents is governed by Maxwell's equations, which in MKS units are given by [134]

$$\begin{aligned}\nabla \times \vec{\mathcal{E}}(x, y, z, t) &= -\frac{\partial \vec{\mathcal{B}}}{\partial t}, & \nabla \times \vec{\mathcal{H}}(x, y, z, t) &= \frac{\partial \vec{\mathcal{D}}}{\partial t}, \\ \nabla \cdot \vec{\mathcal{D}}(x, y, z, t) &= 0, & \nabla \cdot \vec{\mathcal{B}}(x, y, z, t) &= 0.\end{aligned}\tag{1.1a}$$

Here x , y , and z are the spatial coordinates, t is time, $\vec{\mathcal{E}} = (\mathcal{E}_1, \mathcal{E}_2, \mathcal{E}_3)$ is the electric field in the x , y , and z directions, respectively, $\vec{\mathcal{H}} = (\mathcal{H}_1, \mathcal{H}_2, \mathcal{H}_3)$ is the magnetic field, $\vec{\mathcal{D}} = (\mathcal{D}_1, \mathcal{D}_2, \mathcal{D}_3)$ is the electric induction field, and $\vec{\mathcal{B}} = (\mathcal{B}_1, \mathcal{B}_2, \mathcal{B}_3)$ is the magnetic induction field. In vacuum, $\vec{\mathcal{B}}$ and $\vec{\mathcal{D}}$ are related to $\vec{\mathcal{H}}$ and $\vec{\mathcal{E}}$ by the constitutive relations

$$\vec{\mathcal{B}} = \mu_0 \vec{\mathcal{H}}, \quad \vec{\mathcal{D}} = \epsilon_0 \vec{\mathcal{E}},\tag{1.1b}$$

where ϵ_0 and μ_0 are vacuum permittivity and permeability, respectively.

Let us recall the standard derivation of the wave equation from Maxwell's equations:

Lemma 1.1 *Let $\vec{\mathcal{E}}$ and $\vec{\mathcal{B}}$ be solutions of Maxwell's equations in vacuum, see (1.1). Then*

$$\Delta \vec{\mathcal{E}} = \frac{1}{c^2} \frac{\partial^2 \vec{\mathcal{E}}}{\partial t^2}, \quad (1.2)$$

where $c = (\mu_0 \epsilon_0)^{-\frac{1}{2}}$ is the speed of light in vacuum.

Proof By Eqs. (1.1a) and (1.1b),

$$\nabla \times \vec{\mathcal{B}} = \mu_0 \nabla \times \vec{\mathcal{H}} = \mu_0 \frac{\partial \vec{\mathcal{D}}}{\partial t}.$$

From the last equation and (1.1a) we get that

$$\nabla \times \nabla \times \vec{\mathcal{E}} = -\frac{\partial}{\partial t}(\nabla \times \vec{\mathcal{B}}) = -\mu_0 \frac{\partial^2 \vec{\mathcal{D}}}{\partial t^2}.$$

Using the vector identity $\nabla \times \nabla \times \vec{\mathcal{E}} = -\Delta \vec{\mathcal{E}} + \nabla(\nabla \cdot \vec{\mathcal{E}})$, we can rewrite the last equation as

$$\Delta \vec{\mathcal{E}} - \nabla(\nabla \cdot \vec{\mathcal{E}}) = \mu_0 \frac{\partial^2 \vec{\mathcal{D}}}{\partial t^2}. \quad (1.3)$$

Using (1.1b) and the relation $\mu_0 \epsilon_0 = c^{-2}$ gives

$$\Delta \vec{\mathcal{E}} - \nabla(\nabla \cdot \vec{\mathcal{E}}) = \frac{1}{c^2} \frac{\partial^2 \vec{\mathcal{E}}}{\partial t^2}. \quad (1.4)$$

Since $\nabla \cdot \vec{\mathcal{D}} = 0$ and $\vec{\mathcal{D}} = \epsilon_0 \vec{\mathcal{E}}$, we have that

$$\nabla \cdot \vec{\mathcal{E}} = 0. \quad (1.5)$$

Therefore, (1.4) reduces to (1.2). \square

Equation (1.2) shows that the equations for \mathcal{E}_1 , \mathcal{E}_2 , and \mathcal{E}_3 are decoupled. Each component of the electric field satisfies the *scalar wave equation*

$$\Delta \mathcal{E}_j(x, y, z, t) = \frac{1}{c^2} \frac{\partial^2 \mathcal{E}_j}{\partial t^2}, \quad j = 1, 2, 3. \quad (1.6)$$

We can look for solutions of (1.6) of the form

$$\mathcal{E}_j = E_c e^{i(k_0 z - \omega_0 t)} + \text{c.c.} = 2E_c \cos(k_0 z - \omega_0 t), \quad (1.7)$$

where E_c is a real constant, k_0 is the wavenumber, ω_0 is the frequency, and “c.c.” stands for complex conjugate.^{1,2} Substituting (1.7) in (1.6) gives the *dispersion relation*³ in vacuum

$$k_0^2 = \frac{\omega_0^2}{c^2}. \quad (1.8)$$

The solution (1.7) is called a *plane wave*, because for any given $z = z_0$, its value is constant in the (x, y, z_0) -plane. This plane wave travels in the positive z -direction when $k_0 > 0$, and in the negative z -direction when $k_0 < 0$. More generally, let $\mathbf{k}_0 = (k_x, k_y, k_z)$ satisfy

$$|\mathbf{k}_0|^2 = \frac{\omega_0^2}{c_0^2}, \quad |\mathbf{k}_0|^2 = k_x^2 + k_y^2 + k_z^2.$$

Then, (1.6) admits the solution

$$\mathcal{E}_j = E_c e^{i(k_x x + k_y y + k_z z - \omega_0 t)} + \text{c.c.}, \quad (1.9)$$

which is a plane wave that propagates in the direction of the vector \mathbf{k}_0 .

1.2 Linear Polarization

The electric field

$$\vec{\mathcal{E}} = (\mathcal{E}_1, 0, 0), \quad \mathcal{E}_1 = E_c e^{i(k_0 z - \omega_0 t)} + \text{c.c.}, \quad k_0^2 = \frac{\omega_0^2}{c_0^2}, \quad (1.10)$$

is a solution of the wave equation (1.2), and also of Maxwell's equations. This plane wave points in a fixed direction \hat{e}_x , which is perpendicular to its direction of propagation \hat{e}_z .

Definition 1.1 (Linear polarization) An electric field is called linearly-polarized, if it points in a fixed direction, which is perpendicular to its direction of propagation.

Thus, the plane wave (1.10) is linearly polarized in the x -direction.

¹ The electric field $\vec{\mathcal{E}}$ in Maxwell's equations is a physical entity. Therefore, it has to be real.

² In linear optics, it is often convenient to “drop the complex conjugate”, i.e., carry out the calculations with a complex electric field, with the implicit understanding that the physical electric field corresponds to its real or imaginary part (this can be done because the real and imaginary parts of solutions of a linear equation with real coefficients are also solutions of that equation). This, however, is not the case in nonlinear optics. Nevertheless, “dropping the complex conjugate” is often a legitimate approximation in nonlinear optics (Sect. 34.4).

³ I.e., the relation between the wavenumber k_0 and the frequency ω_0 .

Conclusion 1.1 *The assumption that a physical laser beam is linearly polarized is inconsistent with Maxwell's equations.*

Proof Without loss of generality, assume that $\vec{\mathcal{E}} = (\mathcal{E}_1, \mathcal{E}_2, \mathcal{E}_3)$ propagates in the z -direction and is linearly-polarized in the x -direction. Then

$$0 = \nabla \cdot \vec{\mathcal{D}} = \epsilon_0 \nabla \cdot \vec{\mathcal{E}} = \epsilon_0 (\mathcal{E}_1)_x.$$

Hence, the electric field is not localized in the x -direction. Physical laser beams that propagate in the z -direction, however, are localized in the transverse (x, y) -plane. \square

Nevertheless, the assumption that laser beams are linearly polarized is frequently used in linear and in nonlinear optics, and it usually leads to predictions which are in excellent agreement with experimental results. This apparent ‘contradiction’ was resolved in 1975 by Lax et al. [153].⁴ Briefly, they noted that physical beams which are referred to as being “linearly-polarized”, are in fact linearly-polarized only to leading-order, i.e., \mathcal{E}_2 and \mathcal{E}_3 are not identically zero, but are much smaller than \mathcal{E}_1 . Thus, the linearly-polarized beam $\tilde{\mathcal{E}}_{\text{lin-polarized}} = (\tilde{\mathcal{E}}_1(x, y, z, t), 0, 0)$, where $\tilde{\mathcal{E}}_1$ is a solution of the scalar wave equation (1.6), is the leading-order approximation of the solution of Maxwell's equations $\vec{\mathcal{E}} = (\mathcal{E}_1, \mathcal{E}_2, \mathcal{E}_3)$, in the sense that $\tilde{\mathcal{E}}_1$ is the leading-order approximation of \mathcal{E}_1 , and $\mathcal{E}_2, \mathcal{E}_3 \ll \mathcal{E}_1$.

1.3 Paraxial Propagation

Consider the time-harmonic solution of the scalar wave equation (1.6)

$$\mathcal{E}_j(x, y, z, t) = e^{-i\omega_0 t} E(x, y, z) + \text{c.c.} .$$

In optics, this solution corresponds to a *continuous wave (cw)* beam.⁵ Substitution in (1.6) shows that the equation for E is the *scalar linear Helmholtz equation*

$$\Delta E(x, y, z) + k_0^2 E = 0, \quad (1.11)$$

where k_0 is given by (1.8). For example, the plane waves (1.9) correspond to solutions of the Helmholtz equation (1.11) of the form⁶

$$E = E_c e^{i(k_x x + k_y y + k_z z)}, \quad k_x^2 + k_y^2 + k_z^2 = k_0^2. \quad (1.12)$$

⁴ See also [76] for a more systematic treatment.

⁵ A *continuous wave* refers to a laser that produces a continuous (in time) output beam, as opposed to lasers that produce pulsed output beams.

⁶ There is no complex-conjugate in expression (1.12). Indeed, traveling solutions of Helmholtz equation are complex. Mathematically, this is because they satisfy radiation boundary conditions (Sect. 34.6.1), and because the Helmholtz solution E is the Fourier transform of the (real) electric field \mathcal{E} .

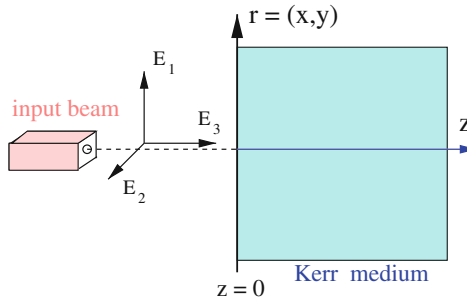


Fig. 1.1 The coordinate system

Let us consider a laser beam that propagates in vacuum in the positive z -direction (see Fig. 1.1), and denote by $E_0^{\text{inc}}(x, y)$ the incoming electric field at $z = 0$. Unlike a plane wave, the electric field of a laser beam decays to zero as the transverse distance from the beam axis goes to infinity. Nevertheless, the electric field of a laser beam can be written as a linear superposition of plane waves. Indeed, the Fourier expansion of $E_0^{\text{inc}}(x, y)$ reads

$$E_0^{\text{inc}}(x, y) = \frac{1}{2\pi} \int E_c(k_x, k_y) e^{i(k_x x + k_y y)} dk_x dk_y.$$

Therefore, the corresponding right-propagating solution of (1.11) is

$$E(x, y, z) = \frac{1}{2\pi} \int E_c(k_x, k_y) e^{i(k_x x + k_y y + \sqrt{k_0^2 - k_x^2 - k_y^2} z)} dk_x dk_y. \quad (1.13)$$

Indeed,

1. Expression (1.13) is a solution of Helmholtz equation, since each mode is a plane wave of the form (1.12).
2. It is equal to $E_0^{\text{inc}}(x, y)$ at $z = 0$.
3. It propagates to the right, since $k_z = \sqrt{k_0^2 - k_x^2 - k_y^2}$ is positive.⁷

Consider expression (1.13) for a laser beam that propagates in the positive z -direction. Without being too precise, it is clear that the direction of propagation of “most” of the plane-wave modes in (1.13) is nearly parallel to the z -axis. These *paraxial plane waves* satisfy

$$k_{\perp}^2 \ll k_z^2, \quad k_{\perp}^2 = k_x^2 + k_y^2.$$

Since $k_0^2 = k_{\perp}^2 + k_z^2$, this implies that $k_z \approx k_0$.

⁷ When $k_x^2 + k_y^2 > k_0^2$, we take the branch of the root with a positive imaginary value, so that this mode will decay (exponentially) in z .

This informal discussion suggests that we look for solutions of the Helmholtz equation (1.11) of the form

$$E = e^{ik_0 z} \psi(x, y, z), \quad (1.14)$$

where $\psi(x, y, z)$ is the *electric-field envelope* (or *amplitude*). The Helmholtz equation for ψ reads

$$\psi_{zz}(x, y, z) + 2ik_0\psi_z + \Delta_{\perp}\psi = 0, \quad \Delta_{\perp}\psi = \psi_{xx} + \psi_{yy}, \quad (1.15)$$

where $\Delta_{\perp}\psi$ is the transverse Laplacian, or the *diffraction* term. The plane waves $E = E_c e^{i(k_x x + k_y y + k_z z)}$, see (1.12), correspond to

$$\psi = E_c e^{i(k_x x + k_y y + (k_z - k_0)z)}. \quad (1.16)$$

Since for paraxial plane waves $k_z - k_0 \ll k_0$, the amplitude ψ of paraxial plane waves is slowly-varying in z , compared with the carrier oscillations $e^{ik_0 z}$.

Lemma 1.2 *In the case of paraxial plane waves,*

$$\psi_{zz} \ll k_0\psi_z \text{ and } \psi_{zz} \ll \Delta_{\perp}\psi. \quad (1.17)$$

Proof We first note that since $\frac{k_{\perp}}{k_0} \ll 1$ and $k_z^2 = k_0^2 - k_{\perp}^2$, then

$$k_z = k_0 \left(1 - \frac{k_{\perp}^2}{k_0^2} \right)^{\frac{1}{2}} \sim k_0 \left(1 - \frac{1}{2} \frac{k_{\perp}^2}{k_0^2} \right).$$

Therefore,

$$k_0 - k_z \sim \frac{1}{2} \frac{k_{\perp}^2}{k_0}.$$

By (1.16), the ratio of the magnitudes of ψ_{zz} and $k_0\psi_z$ satisfies⁸

$$\frac{[\psi_{zz}]}{[k_0\psi_z]} = \frac{(k_0 - k_z)^2 E_c}{k_0(k_0 - k_z) E_c} = \frac{k_0 - k_z}{k_0} \sim \frac{1}{2} \frac{k_{\perp}^2}{k_0^2} \ll 1.$$

Similarly,

$$\frac{[\psi_{zz}]}{[\Delta_{\perp}\psi]} = \frac{(k_0 - k_z)^2 E_c}{k_{\perp}^2 E_c} \sim \frac{1}{4} \frac{k_{\perp}^2}{k_0^2} \ll 1.$$

□

Since a paraxial laser beam (1.13) is “mainly” composed of paraxial plane waves, it is reasonable to assume that relations (1.17) also hold for paraxial laser beams.

⁸ Here and elsewhere in this book, $[\cdot]$ denotes “the characteristic magnitude of”.

This suggests that we can neglect ψ_{zz} in the scalar Helmholtz equation (1.15).⁹ Under this approximation, which is called the *paraxial approximation* or the *parabolic approximation*,¹⁰ the equation for ψ becomes the *linear Schrödinger equation*

$$2ik_0\psi_z(z, x, y) + \Delta_{\perp}\psi = 0. \quad (1.18)$$

Remark The Schrödinger equation (1.18) is an initial value problem in z . Indeed, it is solved for $z > 0$, subject to the initial condition

$$\psi(z = 0, x, y) = \psi_0(x, y) = E_0^{\text{inc}}(x, y),$$

see Fig. 1.1 and (1.14).

Remark The Schrödinger equation is usually associated with quantum mechanics. In optics, however, it arises within the context of classical physics. Indeed, the starting point of the derivation of (1.18) is Maxwell's equations, which are classical.

Remark From a mathematical point of view, the validity of the paraxial approximation is highly questionable, since by neglecting the highest-order derivative in z , we changed the character of the equation from a boundary value problem (Helmholtz) to an initial value one (Schrödinger). Nevertheless, in most cases in optics the paraxial approximation leads to results that are in excellent agreement with experiments. See Chap. 34 for discussion of the validity of the paraxial approximation in nonlinear propagation.

1.4 Polarization Field

When an electric field is applied to a dielectric medium, it induces an additional electric field, which is called the polarization field. The polarization field can be induced by the effect of the electric field on molecular orientation, on electrostriction, or on non-resonant electrons. For example, in polarization due to non-resonant electrons, the electric field which is applied to the dielectric medium exerts a force on the electrons. As a result, the orbits of the electrons around the nucleus are deformed. In particular, the centers of these orbits do not coincide anymore with the nucleus. Hence, the material becomes polarized, i.e., the atoms have nonzero electrical dipole moments. These microscopic dipole moments, in turn, induce a macroscopic electric field, the *polarization field*, which is denoted by $\vec{\mathcal{P}}$. The electrical induction field $\vec{\mathcal{D}}$ which appears in Maxwell's equations is the sum of the original electric field and the polarization field, i.e.,

$$\vec{\mathcal{D}} = \epsilon_0 \vec{\mathcal{E}} + \vec{\mathcal{P}}.$$

⁹ See Sect. 2.12 for another informal justification for neglecting ψ_{zz} .

¹⁰ See Sect. 2.8.3 for an explanation of the terminology *parabolic approximation*.

To simplify the presentation, in what follows, we make the following assumptions and approximations:

1. We assume that the electric field is linearly-polarized, i.e., that $\vec{\mathcal{E}} = (\mathcal{E}, 0, 0)$, $\vec{\mathcal{P}} = (\mathcal{P}, 0, 0)$, and $\vec{\mathcal{D}} = (\mathcal{D}, 0, 0)$.
2. We consider the cw electric field

$$\mathcal{E}(x, y, z, t) = e^{-i\omega_0 t} E(x, y, z) + \text{c.c.} \quad (1.19)$$

3. We assume that the dielectric medium is isotropic and homogeneous.

1.4.1 Linear Polarization Field

At “low” intensities of the electric field,¹¹ the shift of the centers of the electron orbits, hence the polarization field, is linearly proportional to the electric field, i.e., $\mathcal{P} = \mathcal{P}_{\text{lin}} = c\mathcal{E}$. The relation between \mathcal{P}_{lin} and \mathcal{E} is written as

$$\mathcal{P}_{\text{lin}} = \epsilon_0 \chi^{(1)}(\omega_0) \mathcal{E}, \quad (1.20)$$

where $\chi^{(1)}$ is the *first-order optical susceptibility*, whose value depends on the frequency ω_0 . Thus, the electric induction field is given by¹²

$$\mathcal{D} = \epsilon_0 \mathcal{E} + \mathcal{P}_{\text{lin}} = \epsilon_0 n_0^2(\omega_0) \mathcal{E}, \quad n_0^2(\omega_0) := 1 + \chi^{(1)}(\omega_0), \quad (1.21)$$

where n_0 is the (linear) *index of refraction* (or *refractive index*) of the medium. The value of n_0^2 is equal to one in vacuum, and is larger than one for dielectrics in their transparency spectrum. For example, $n_0 \approx 1.33$ for water in the visible spectrum.

The only difference between Maxwell’s equations in vacuum and in a linear dielectric^{13,14} is in the multiplicative term n_0^2 in the constitutive relation between \mathcal{D} and \mathcal{E} , cf. (1.1b) and (1.21). Therefore, a derivation identical to that of (1.11) shows that propagation of cw linearly-polarized laser beams in a linear dielectric is governed by the scalar Helmholtz equation

$$\Delta E(x, y, z) + k_0^2 E = 0, \quad k_0^2 = \frac{\omega_0^2}{c^2} n_0^2. \quad (1.22)$$

Exercise 1.1 Derive (1.22) from Maxwell’s equations.

¹¹ The definition of “low” will be made precise in relation (1.37).

¹² This relation holds for the cw field (1.19). When the electric field consists of more than one frequency (as, e.g., in the case of laser pulses), relation (1.21) holds for each frequency component, with a proportionality constant that depends on the frequency.

¹³ I.e., a material for which \mathcal{D} is given by (1.21) and $\vec{\mathcal{B}} = \mu_0 \vec{\mathcal{H}}$.

¹⁴ The term *linear* dielectric is somewhat misleading, because whether the dielectric is linear or nonlinear depends on the electric-field intensity (Sect. 1.4.2).

1.4.2 Weakly-Nonlinear Polarization Field

In this section we show that in an isotropic medium, the leading-order nonlinear response is cubic. The analysis here is very elementary. See, e.g., [32] for further discussion.

It is convenient to write the polarization field \mathcal{P} as

$$\mathcal{P} = \mathcal{P}_{\text{lin}} + \mathcal{P}_{\text{nl}},$$

where \mathcal{P}_{lin} is given by (1.20) and $\mathcal{P}_{\text{nl}} = \mathcal{P} - \mathcal{P}_{\text{lin}}$ is the nonlinear component of the polarization field. As noted, at low intensities, the dependence of \mathcal{P} on the electric field \mathcal{E} is linear. As \mathcal{E} increases, the shift of the centers of the electrons orbits, hence the polarization field \mathcal{P} , begins to have a nonlinear dependence on \mathcal{E} . Let us consider the regime where \mathcal{E} is sufficiently strong so that \mathcal{P}_{nl} is no longer negligible, but not too strong so that \mathcal{P}_{nl} is still much smaller than \mathcal{P}_{lin} , i.e.,

$$\mathcal{P}_{\text{nl}} \ll \mathcal{P}_{\text{lin}}.$$

In other words, we consider the regime where the material response is *weakly nonlinear*. Therefore, we can expand \mathcal{P}_{nl} in a Taylor series in \mathcal{E} , i.e.,

$$\mathcal{P}_{\text{nl}} = \chi^{(2)}(\omega_0)\mathcal{E}^2 + \chi^{(3)}(\omega_0)\mathcal{E}^3 + \dots, \quad (1.23)$$

where $\chi^{(i)}$ is the *i*th-order optical susceptibility. In the weakly-nonlinear regime, a “Taylor-series argument” implies that each additional term is substantially smaller than its predecessor. Therefore, the leading-order nonlinear material-response is quadratic in \mathcal{E} , i.e., $\mathcal{P}_{\text{nl}} \approx \chi^{(2)}\mathcal{E}^2$. This is indeed the case for *noncentrosymmetric crystals*, i.e., crystals that do not possess a center of inversion. Such $\chi^{(2)}$ materials will not be considered in this book. See e.g., [32] for more details.

In the case of isotropic materials, ¹⁵ all the even-order optical susceptibilities must vanish:

Lemma 1.3 *For isotropic materials, $\chi^{(2j)}(\omega_0) \equiv 0$ for $j = 1, 2, \dots$*

Proof Since there are no preferred directions in an isotropic material, $\vec{\mathcal{P}}_{\text{nl}}$ and $\vec{\mathcal{E}}$ should point in the same direction, and the relation between them should be independent of that direction. In particular, the relation between $\vec{\mathcal{P}}_{\text{nl}} = (\mathcal{P}_{\text{nl}}, 0, 0)$ and $\vec{\mathcal{E}} = (\mathcal{E}, 0, 0)$ should be the same as between $\vec{\mathcal{P}}_{\text{nl}} = (-\mathcal{P}_{\text{nl}}, 0, 0)$ and $\vec{\mathcal{E}} = (-\mathcal{E}, 0, 0)$, which point in the opposite direction. In other words, relation (1.23) between \mathcal{P}_{nl} and \mathcal{E} should remain the same if we simultaneously change \mathcal{P}_{nl} to $-\mathcal{P}_{\text{nl}}$ and \mathcal{E} to $-\mathcal{E}$. Under this simultaneous sign change, relation (1.23) reads

$$-\mathcal{P}_{\text{nl}} = \chi^{(2)}(-\mathcal{E})^2 + \chi^{(3)}(-\mathcal{E})^3 + \dots.$$

Since this relation should be identical to (1.23), the result follows. \square

¹⁵ Or, more generally, of centrosymmetric materials.

We thus see that for isotropic materials

$$\mathcal{P}_{\text{nl}} = \chi^{(3)} \mathcal{E}^3 + \chi^{(5)} \mathcal{E}^5 + \dots$$

In particular, in the weakly-nonlinear regime, the leading-order nonlinear contribution to the polarization field is cubic in \mathcal{E} , i.e.,

$$\mathcal{P}_{\text{nl}} \approx \chi^{(3)} \mathcal{E}^3. \quad (1.24)$$

In this book we will mostly consider power-law nonlinearities, such as (1.24). Higher-order corrections to (1.24) will be discussed in Sects. 32.1 and 32.4.1.

1.4.3 Kerr Nonlinearity

By (1.24), the nonlinear polarization field which is induced by the cw electric field $\mathcal{E} = (e^{-i\omega_0 t} E + \text{c.c.})$ is

$$\mathcal{P}_{\text{nl}} \approx \chi^{(3)} \mathcal{E}^3 = \chi^{(3)} \left(3|E|^2 E e^{-i\omega_0 t} + E^3 e^{-3i\omega_0 t} + \text{c.c.} \right).$$

The first component of \mathcal{P}_{nl} has the same frequency as the electric field. The second component, however, has frequency $3\omega_0$, a nonlinear phenomenon known as *third-harmonic generation*. In general, the third harmonic component has a small effect on the propagation, since it is phase-mismatched with the first-harmonic component. Therefore, almost all studies neglect this term and make the approximation

$$\mathcal{P}_{\text{nl}} \approx 3\chi^{(3)} |E|^2 E e^{-i\omega_0 t} + \text{c.c.} = 3\chi^{(3)} |E|^2 \mathcal{E}. \quad (1.25)$$

Exercise 1.2 Show that if $\mathcal{P}_{\text{nl}} = \chi^{(3)} \mathcal{E}^3 + \chi^{(5)} \mathcal{E}^5$, then

$$\mathcal{P}_{\text{nl}} \approx \left(3\chi^{(3)} |E|^2 + \binom{5}{3} \chi^{(5)} |E|^4 \right) \mathcal{E}.$$

Let us define the *Kerr coefficient* as¹⁶

$$n_2 := \frac{3\chi^{(3)}}{4\epsilon_0 n_0}.$$

Then, the nonlinear polarization field (1.25) reads

$$\mathcal{P}_{\text{nl}} = 4\epsilon_0 n_0 n_2 |E|^2 \mathcal{E}. \quad (1.26)$$

¹⁶ There are several definitions for n_2 in the literature, which differ from each other by a multiplicative constant (see e.g., [32]).

Therefore,

$$\mathcal{D} = \epsilon_0 \mathcal{E} + \mathcal{P}_{\text{lin}} + \mathcal{P}_{\text{nl}} = \epsilon_0 n^2 \mathcal{E}, \quad (1.27)$$

where n , the *index of refraction*, is given by

$$n^2 = n^2(\omega_0, |E|^2) = n_0^2 \left(1 + \frac{4n_2}{n_0} |E|^2\right). \quad (1.28)$$

Materials for which the index of refraction is given by (1.28) are called *Kerr materials*. As the above derivation shows, *any isotropic material is a Kerr material*. Thus, Kerr materials can be solids (e.g., glass, silica), liquids (e.g., water), or gases (e.g., air, noble gases). For all these materials, however, the value of n_2 turned out to be extremely small. For example, for water $n_0 \approx 1.33$ and $n_2 \approx 10^{-22} \frac{m^2}{V^2}$. Hence, the nonlinear contribution to the index of refraction which is induced by natural light sources (e.g., sunlight $\approx 10^3 \frac{V}{m}$) is $n_2 |E|^2 \approx 10^{-16}$. Even when the sunlight is focused by a lens, \mathcal{P}_{nl} is too small to have any noticeable effect. As a result, the propagation of electromagnetic waves produced by natural light sources is for all practical purposes linear. It is because of the smallness of the Kerr coefficient that optics was traditionally a linear science. This changed “overnight” in the 1960s with the invention of the laser, which could produce artificial electromagnetic radiation with intensities far above those possible from natural light sources. Even with powerful lasers, however, the contribution of the nonlinear polarization to the index of refraction is usually small, i.e.,

$$n_2 |E|^2 \ll n_0. \quad (1.29)$$

For example, a typical value for a powerful laser beam is $|E| = O\left(10^9 \frac{V}{m}\right)$. At such intensities the magnitude of the Kerr nonlinearity in water is

$$n_2 |E|^2 \approx 10^{-4} \ll n_0 \approx 1.33.$$

Therefore, even with high-power lasers, the assumption of a weak nonlinear response is usually justified.^{17, 18}

Remark When the nonlinearity is weak, see (1.29), relation (1.28) can also be written as

$$n = n_0 + 2n_2 |E|^2. \quad (1.30)$$

¹⁷ In fact, the intensities at which nonlinear polarization becomes comparable to linear polarization in transparent dielectrics are typically those at which the electrons are torn away from the atoms (i.e., the intensities at which the dielectric medium becomes ionized).

¹⁸ Nevertheless, a weak nonlinear response can have a large effect on the propagation (Sect. 1.7).

1.4.4 Vectorial Kerr Nonlinearity

Relation (1.28) is sometimes called the *scalar Kerr effect*, since it is derived under the approximation that the electric and polarization fields are linearly-polarized. When the vectorial nature of these fields is not neglected, $\vec{\mathcal{P}}_{\text{NL}}$ and $\vec{\mathcal{E}}$ are connected by the nonlinear tensorial relation [161, 162]

$$\begin{aligned} \vec{\mathcal{P}}_{\text{NL}}(\vec{\mathcal{E}}) &= \frac{4\epsilon_0 n_0 n_2}{1 + \gamma} \left[(\vec{\mathcal{E}} \cdot \vec{\mathcal{E}}^*) \vec{\mathcal{E}} + \gamma (\vec{\mathcal{E}} \cdot \vec{\mathcal{E}}) \vec{\mathcal{E}}^* \right] \\ &= \frac{4\epsilon_0 n_0 n_2}{1 + \gamma} \left[|\vec{\mathcal{E}}|^2 \begin{pmatrix} 1 & 0 & 0 \\ 0 & 1 & 0 \\ 0 & 0 & 1 \end{pmatrix} + \gamma \begin{pmatrix} |\mathcal{E}_1|^2 & \mathcal{E}_2 \mathcal{E}_1^* & \mathcal{E}_3 \mathcal{E}_1^* \\ \mathcal{E}_1 \mathcal{E}_2^* & |\mathcal{E}_2|^2 & \mathcal{E}_3 \mathcal{E}_2^* \\ \mathcal{E}_1 \mathcal{E}_3^* & \mathcal{E}_2 \mathcal{E}_3^* & |\mathcal{E}_3|^2 \end{pmatrix} \right] \begin{pmatrix} \mathcal{E}_1 \\ \mathcal{E}_2 \\ \mathcal{E}_3 \end{pmatrix}, \end{aligned} \quad (1.31)$$

where n_2 is the Kerr coefficient, and γ is a constant, whose value depends on the physical origin of the Kerr effect (Table 1.1). In that case, the propagation is governed by the *vectorial nonlinear Helmholtz equation*

$$\begin{cases} \Delta \vec{\mathcal{E}} - \vec{\nabla}(\nabla \cdot \vec{\mathcal{E}}) + k_0^2 \vec{\mathcal{E}} = -\frac{k_0^2}{\epsilon_0 n_0^2} \vec{\mathcal{P}}_{\text{NL}}, \\ \nabla \cdot \vec{\mathcal{E}} = -\frac{1}{\epsilon_0 n_0^2} \nabla \cdot \vec{\mathcal{P}}_{\text{NL}}. \end{cases} \quad (1.32)$$

Except for Sect. 25.3.1, in this book we only consider the scalar Kerr effect. See [45, 76, 77] for analysis of vectorial effects in self-focusing.

Exercise 1.3 Derive Eq. (1.32) from Maxwell's equations.

Remark When $\gamma = 0$ the Kerr effect is “semi-vectorial”, in the sense that $\vec{\mathcal{P}}_{\text{NL}} = 4\epsilon_0 n_0 \bar{n}_2 |\vec{\mathcal{E}}|^2 \vec{\mathcal{E}}$. In other words, the “semi-vectorial” Kerr effect is given by the scalar index of refraction

$$n^2 = n_0^2 \left(1 + \frac{4n_2}{n_0} |\vec{\mathcal{E}}|^2 \right). \quad (1.33)$$

When $\gamma \neq 0$, however, the Kerr effect is “genuinely vectorial”, in the sense that it cannot be written in the form (1.33).

Table 1.1 Values of γ for common Kerr mechanisms

Kerr mechanism	γ
Electrostriction	0
Non-resonant electrons	0.5
Molecular orientation	3

1.5 Weakly Nonlinear Helmholtz Equation

In Sect. 1.4.1 we saw that the propagation of a linearly-polarized cw laser beam in a linear dielectric is governed by the linear Helmholtz equation (1.22) with $k_0^2 = \omega_0^2 n_0^2 / c^2$. Then, in Sect. 1.4.3 we saw that in a Kerr medium the index of refraction is given by $n^2 = n_0^2 + 4n_2 n_0 |E|^2$, rather than by n_0^2 . Therefore, if we formally replace n_0^2 with n^2 in (1.22), we get that the propagation of a linearly-polarized cw laser beam in a Kerr medium is governed by the *scalar nonlinear Helmholtz equation* (NLH)

$$\Delta E(x, y, z) + k^2 E = 0, \quad k^2 = k_0^2 \left(1 + \frac{4n_2}{n_0} |E|^2 \right). \quad (1.34)$$

Since the refractive index is typically weakly nonlinear, see (1.29), then so is the NLH (1.34).

1.6 Nonlinear Schrödinger Equation

If we substitute $E = e^{ik_0 z} \psi$ in the NLH (1.34) and apply the paraxial approximation $\psi_{zz} \ll k_0 \psi_z$, we obtain that ψ satisfies the *nonlinear Schrödinger equation* (NLS)

$$2ik_0 \psi_z(x, y, z) + \underbrace{\Delta_\perp \psi}_{\text{diffraction}} + \underbrace{k_0^2 \frac{4n_2}{n_0} |\psi|^2 \psi}_{\text{Kerr nonlinearity}} = 0, \quad \Delta_\perp = \frac{\partial^2}{\partial x^2} + \frac{\partial^2}{\partial y^2}. \quad (1.35)$$

Conclusion 1.2 *The NLS (1.35) is the leading-order model for paraxial propagation of intense linearly-polarized cw laser beams in a homogeneous Kerr medium, in which ψ is the slowly-varying amplitude of the electric field, z is the direction of propagation, and x and y are the coordinates in the transverse plane.*

As in the linear case, see Sect. 1.3,

- The NLS (1.35) is an initial value problem in z , which is solved for $z > 0$, subject to the initial condition $\psi(z = 0, x, y) = \psi_0(x, y)$.
- The NLS is derived within the context of classical physics.

1.7 Relative Magnitude of the Kerr Effect

The NLS (1.35) shows that as the beam propagates, its evolution is determined by the combined effects of diffraction and the Kerr nonlinearity (second and third terms in (1.35), respectively). The ratio of the magnitudes of the Kerr effect and diffraction is

$$\frac{[\text{Kerr effect}]}{[\text{diffraction}]} = \frac{\left[k_0^2 \frac{4n_2}{n_0} |\psi|^2 \psi \right]}{[\Delta_{\perp} \psi]} = \frac{k_0^2 \frac{4n_2}{n_0} [E]^3}{\frac{[E]}{r_0^2}} = \frac{1}{f^2} \frac{4n_2 E_c^2}{n_0}, \quad (1.36)$$

where E_c is the characteristic magnitude of the electric-field amplitude, r_0 is the characteristic length-scale in the transverse direction (e.g., the radius of the incoming laser beam), and

$$f := \frac{1}{r_0 k_0}$$

is the *nonparaxiality parameter*, to be defined in Sect. 2.12.

Conclusion 1.3

- Diffraction dominates over the Kerr effect (i.e., the propagation is weakly nonlinear) when

$$\frac{4n_2 E_c^2}{n_0} \ll f^2. \quad (1.37)$$

- Diffraction and the Kerr effect are of comparable magnitudes (i.e., the propagation is nonlinear) when $\frac{4n_2 E_c^2}{n_0} = O(f^2)$.
- The Kerr effect dominates over diffraction (i.e., the propagation is strongly nonlinear) when $\frac{4n_2 E_c^2}{n_0} \gg f^2$.

To estimate the magnitude of f , we note that the visible spectrum is $0.4 \mu\text{m} \leq \lambda \leq 0.7 \mu\text{m}$, and the width of laser beams is typically much larger than $1 \mu\text{m}$.

Observation 1.1 In most physical setups, the width of a laser beam is much larger than its wavelength, i.e., $r_0 \gg \lambda$.

Therefore, since $f = 1/r_0 k_0 = \lambda/2\pi r_0$, we have

Observation 1.2 In most physical setups, $f \ll 1$.

Let us rewrite the refractive index as

$$n^2 = n_0^2 + \Delta_{\text{nl}},$$

where n_0^2 and $\Delta_{\text{nl}} = n^2 - n_0^2$ are the linear and nonlinear components of n^2 , respectively. By (1.28),

$$\frac{4n_2 |E|^2}{n_0} = \frac{\Delta_{\text{nl}}}{n_0^2}, \quad (1.38)$$

which is the ratio of the linear and nonlinear components of n^2 . Therefore, we can rewrite (1.36) as

$$\frac{[\text{Kerr effect}]}{[\text{diffraction}]} = \frac{1}{f^2} \frac{\Delta_{\text{nl}}}{n_0^2}. \quad (1.39)$$

From Eq. (1.39) and Observation 1.2 follows

Conclusion 1.4 *The Kerr effect is comparable in magnitude to diffraction when*

$$\frac{\Delta_{\text{nl}}}{n_0^2} = O(f^2) \ll 1,$$

i.e., when the nonlinear contribution to the index of refraction is $O(f^2)$ smaller than the linear index of refraction. In other words, an $O(f^2)$ nonlinearity in the NLH model corresponds to an $O(1)$ nonlinearity in the NLS model.

For example, let $\lambda = 0.5 \mu\text{m}$ and $r_0 = 100 \mu\text{m}$. Since $f = \frac{0.5}{200\pi} \approx 8 \cdot 10^{-4}$, nonlinear effects become important when $4n_2|E|^2 = O(10^{-6})$, i.e., when the nonlinear contribution to the index of refraction is 0.0001%.

How is it possible that a Kerr nonlinearity can have an $O(f^2)$ effect on the index of refraction, yet have an $O(1)$ effect on the propagation dynamics? To answer this question, it is useful to adopt a multiple-scales perspective. The balance of the leading-order terms in the weakly-nonlinear Helmholtz equation (1.34) is given by the linear Helmholtz equation (1.22). This leading-order equation determines the fast-scale dynamics, namely, the carrier oscillations $e^{ik_0 z}$. The weak nonlinearity only enters in the equation for the next-order terms, which determines the slow-scale evolution of the amplitude ψ . Thus, over propagation distances of a few wavelengths, the propagation is essentially linear. Over longer propagation distances of many wavelengths, however, the effect of the weak nonlinearity becomes important.

1.8 Physical Validity of the NLS Model

The NLS (1.35) models the propagation of intense laser beams in isotropic media. As we shall see, this equation admits solutions that become infinitely large (collapse, blowup, become singular) after a finite propagation distance. Since physical quantities do not become infinite, we have

Conclusion 1.5 *The physical validity of the NLS model breaks down at or before the NLS blowup point.*

This breakdown indicates that some of the approximations made in the derivation of the NLS break down at or before the NLS blowup point. Let us recall these approximations:

1. We assumed that the electric field is linearly polarized. Physical laser beams, however, can be linearly polarized only to leading order.
2. We used the scalar Kerr effect (1.26), and not the more accurate vectorial Kerr effect (1.31).
3. We applied the paraxial approximation and neglected the ψ_{zz} term.
4. We neglected third-harmonic generation.

There are various other physical mechanisms which are neglected in the NLS model but can affect the propagation. For example, the NLS (1.35) models the propagation of cw laser beams. In the case of ultrashort laser pulses, temporal effects (such as dispersion) can become important. In addition, at sufficiently high intensities the electric field ionizes the medium, resulting in plasma formation. This, in turn, leads to changes in the optical properties of the medium, which are unaccounted for in (1.35). The NLS model also neglects high-order nonlinear polarizations (such as $\chi^{(5)}\mathcal{E}^5$), and absorption (damping) by the medium.

As noted, the NLS model breaks down at or before the NLS blowup point. “Fortunately”, this model is valid until shortly before the NLS blowup point (typically, until the beam intensity increases by a factor of 10–100). Indeed, experiments with intense laser beams show that the NLS model correctly predicts:

1. The existence of a critical power, above which laser beams undergo optical collapse [267].
2. That collapsing beams undergo a quasi self-similar collapse with a universal radial profile, which is the Townes profile (Sect. 14.5).
3. The azimuthal instability of collapsing rings (Sect. 19.4).
4. The initial filamentation pattern of high-power beams (Sect. 26.7.2).
5. The collapse distance (Sect. 27.4).
6. The effect of a lens on the collapse distance (Sects. 27.8.1 and 27.8.2).
7. The dynamics of coupled optical beams (Sect. 27.5).
8. The pulse splitting in the normal regime (Sect. 36.10) and in the anomalous regime (Sect. 37.5).
9. The loss of phase of collapsing beams (Sect. 39.1.3).
10. That interactions between beams that already underwent collapse are chaotic (Sect. 39.2.2).

Observation 1.3 *The NLS (1.35) models the propagation of intense cw laser beams from the location where the beam enters the Kerr medium, and until shortly before the NLS singularity point.*

While the NLS model breaks down at the singularity point, the laser beam continues to propagate forward. Therefore, to model the propagation beyond the singularity, one needs to retain some of the small terms that were neglected in the NLS model.

Most of this book concerns the unperturbed NLS. Perturbations of the NLS are considered in Chaps. 31–37, and continuations of singular NLS solutions beyond the singularity are considered in Chaps. 38 and 39.

Chapter 2

Linear Propagation

In this chapter we consider the propagation of continuous-wave (cw) laser beams in a linear medium.¹

2.1 Geometrical Optics

Laser beams that propagate in a Kerr medium can become narrower with propagation, a phenomenon called *self focusing*. The simplest and most intuitive way to understand why a Kerr nonlinearity leads to self focusing is to use *geometrical optics* (Sect. 3.2).² Therefore, we begin by introducing the geometrical optics approximation.

Our starting point is the dimensional linear Helmholtz equation

$$\Delta E(\mathbf{x}) + k^2 \left(\frac{\mathbf{x}}{X} \right) E = 0, \quad k^2 \left(\frac{\mathbf{x}}{X} \right) = \frac{\omega_0^2}{c^2} n^2 \left(\frac{\mathbf{x}}{X} \right), \quad (2.1)$$

which models propagation in an inhomogeneous linear medium. Here, $\mathbf{x} = (x, y, z)$, n is the linear index of refraction,³ and X is the characteristic length-scale for changes in n (hence in k). We assume that the medium is weakly inhomogeneous, i.e., $k \approx k_0 = \omega_0 n_0 / c$.⁴ Let $\lambda = 2\pi/k_0$ be the wavelength. The geometrical optics approximation is valid when $X \gg \lambda$, i.e., when changes in n occur over distances much longer than the wavelength, so that locally (i.e., over a few wavelengths) the material can be viewed as homogeneous.

¹ Since all media are nonlinear (Sect. 1.4.2), the term *linear medium* refers to the situation where the electric field is sufficiently weak, see (1.37), so that nonlinear effects are negligible.

² Indeed, the early studies on self-focusing employed a geometrical optics approach (Sects. 3.2 and 3.3.2).

³ To simplify the notations, in this chapter (only) we denote the inhomogeneous linear index of refraction by $n(\cdot)$, and its value in the absence of inhomogeneities by n_0 .

⁴ This is the linear analog of a weakly-nonlinear homogeneous Kerr medium, i.e., when the contribution of the nonlinear Kerr effect to the index of refraction is small, see (1.29).

Let us change to the dimensionless variables

$$\tilde{\mathbf{x}} = \frac{\mathbf{x}}{X}, \quad \tilde{E} = \frac{E}{E_c},$$

where E_c is the characteristic magnitude of E . Then the dimensionless Helmholtz equation reads

$$\Delta_{\tilde{\mathbf{x}}} \tilde{E}(\tilde{\mathbf{x}}) + \tilde{k}^2(\tilde{\mathbf{x}}) \tilde{E} = 0,$$

where $\tilde{k} = Xk$ is the dimensionless wavenumber. Since $X \gg \lambda$,

$$\tilde{k} \approx \tilde{k}_0 := Xk_0 = \frac{2\pi X}{\lambda} \gg 1.$$

To simplify the notations, from now on we drop the tildes. Thus, the dimensionless Helmholtz equation reads

$$\Delta E(\mathbf{x}) + k^2(\mathbf{x}) E = 0, \quad (2.2)$$

and the dimensionless geometrical optics regime is $k^2 \gg 1$.

2.1.1 Eikonal Equation

When $k \approx k_0 \gg 1$, we can look for solutions of (2.2) of the form⁵

$$E = A(\mathbf{x}) e^{ik_0 S(\mathbf{x})},$$

where A and S are real. Here, A is the *slowly-varying envelope* and $k_0 S$ is the *phase*. Substitution in (2.2) gives

$$\Delta A + 2ik_0 \nabla A \cdot \nabla S + A(i k_0 \Delta S - k_0^2 \nabla S \cdot \nabla S) + k^2 A = 0, \quad (2.3)$$

where $\nabla = \left(\frac{\partial}{\partial x}, \frac{\partial}{\partial y}, \frac{\partial}{\partial z} \right)$. Balancing the leading $O(k_0^2)$ terms in (2.3) gives the *eikonal equation*

$$\nabla S \cdot \nabla S = \tilde{n}^2(\mathbf{x}), \quad (2.4)$$

where

$$\tilde{n}(\mathbf{x}) = \frac{k(\mathbf{x})}{k_0} = \frac{n(\mathbf{x})}{n_0} \approx 1.$$

The initial condition for the eikonal equation is $S(\mathbf{x}) = S_0(\mathbf{x})$ for $\mathbf{x} \in \Sigma_0$, where Σ_0 is a given surface in \mathbb{R}^3 . For example, the model problem studied in this

⁵ This ansatz can be viewed as a generalization of the plane-wave solution (1.12).

book is the propagation of a laser beam in the half-space $z > 0$, given an incoming beam $E_0^{\text{inc}}(x, y)$ at $z = 0$ (Fig. 1.1). In this case, Σ_0 is the (x, y) -plane $z \equiv 0$.

The eikonal equation is a nonlinear first-order PDE. As such, it can be solved using the *method of characteristics*.^{6,7} To do that, let us recall the method of characteristics for the first-order linear PDE

$$a(\mathbf{x})u_x(\mathbf{x}) + b(\mathbf{x})u_y + c(\mathbf{x})u_z = e(\mathbf{x}). \quad (2.5)$$

The characteristic curves $\mathbf{x}(\sigma) = (x(\sigma), y(\sigma), z(\sigma))$ of (2.5), where σ is the curve parameter, are parallel to (a, b, c) . Therefore,

$$\frac{d\mathbf{x}(\sigma)}{d\sigma} = \eta(\sigma) (a(\mathbf{x}(\sigma)), b(\mathbf{x}(\sigma)), c(\mathbf{x}(\sigma))), \quad (2.6a)$$

where $\eta(\sigma)$ is an arbitrary positive function. By the chain rule, the evolution of u along characteristics is

$$\frac{du(\mathbf{x}(\sigma))}{d\sigma} = \nabla u \cdot \frac{d\mathbf{x}}{d\sigma} = \eta(\sigma) e(\mathbf{x}(\sigma)). \quad (2.6b)$$

Therefore, to solve the PDE (2.5), one only needs to solve the ODEs (2.6).

Unlike (2.5), the eikonal equation (2.4) is nonlinear. Nevertheless, since the vector ∇S in (2.4) “corresponds” to the vector (a, b, c) in (2.5), this suggests that the characteristics of the eikonal equation are parallel to ∇S , i.e.,

$$\frac{d\mathbf{x}}{d\sigma} = \eta(\sigma) \nabla S.$$

Let σ be the arclength. Then

$$1 = \left| \frac{d\mathbf{x}}{d\sigma} \right|^2 = \eta^2 (\nabla S)^2 = \eta^2 \tilde{n}^2.$$

Hence, $\eta = 1/\tilde{n}$ and

$$\frac{d\mathbf{x}}{d\sigma} = \frac{1}{\tilde{n}} \nabla S. \quad (2.7)$$

To close the system (2.7), we note that

$$\begin{aligned} \frac{d}{d\sigma} \nabla S(\mathbf{x}(\sigma)) &= \nabla(\nabla S) \cdot \frac{d\mathbf{x}}{d\sigma} = \nabla(\nabla S) \cdot \frac{1}{\tilde{n}} \nabla S = \frac{1}{2\tilde{n}} \nabla(\nabla S)^2 \\ &= \frac{1}{2\tilde{n}} \nabla(\tilde{n}^2) = \nabla \tilde{n}. \end{aligned}$$

⁶ See e.g., [210].

⁷ In geometrical optics the characteristics are also called *rays*, because they correspond to the curves followed by light rays.

Therefore, the rays of the eikonal equation are determined by the system of six linear ODEs

$$\frac{d\mathbf{x}}{d\sigma} = \frac{1}{\tilde{n}} \mathbf{p}, \quad \frac{d\mathbf{p}}{d\sigma} = \nabla \tilde{n}, \quad (2.8)$$

where $\mathbf{p} = \nabla S$ and $\tilde{n} = n/n_0$.

Definition 2.1 (wavefront) *In optics, a surface of points that have the same phase is called a wavefront.*

Since ∇S is perpendicular to the wavefronts, we have

Lemma 2.1 *Under the geometrical optics approximation, the rays of the eikonal equation are perpendicular to the wavefronts of the Helmholtz solution.*

The evolution of S along a ray is given by

$$\frac{d}{d\sigma} S(\mathbf{x}(\sigma)) = \nabla S \cdot \frac{d\mathbf{x}}{d\sigma} = \frac{1}{\tilde{n}} (\nabla S)^2 = \tilde{n}. \quad (2.9)$$

Therefore,

$$dS = \tilde{n} d\sigma = \frac{n}{n_0} d\sigma = \frac{c/n_0}{c/n} d\sigma = \frac{c}{n_0} \frac{d\sigma}{v},$$

where $v(\mathbf{x}) = c/n(\mathbf{x})$ is the local speed of propagation. Since $d\sigma/v = dt$, then

$$dS = \frac{c}{n_0} dt. \quad (2.10)$$

Therefore, $S(\mathbf{x}(\sigma))$ measures the *travel time* along the ray.

Fermat's principle of least time states that out of all possible paths from one point to another, a light ray travels along the path with the shortest travel-time. It later turned out that a more accurate formulation is the *principle of stationary time*, which states that out of all possible paths from point \mathbf{x}_0 to point \mathbf{x}_1 , a light ray travels along the path whose travel-time is stationary with respect to neighboring paths that connect \mathbf{x}_0 and \mathbf{x}_1 . In other words, the ray that connects \mathbf{x}_0 and \mathbf{x}_1 is an extremal of the functional

$$T = \int_{\text{path } \mathbf{x}_0 \rightarrow \mathbf{x}_1} \frac{d\sigma}{v(\mathbf{x}(\sigma))}. \quad (2.11)$$

Exercise 2.1 *Show that the trajectories of the rays, as given by Eq. (2.8), are indeed the extremals of the functional (2.11).*

1. Write the functional using a parameter μ with fixed boundary values

$$T = \frac{1}{c} \int_{\mu=0}^1 \mathcal{F}(x(\mu), y(\mu), z(\mu), x_\mu, y_\mu, z_\mu) d\mu,$$

where $\mathcal{F} = n(x, y, z) \sqrt{(x_\mu)^2 + (y_\mu)^2 + (z_\mu)^2}$.

2. Write the Euler-Lagrange equations for an extremal

$$\mathcal{F}_x - \frac{d}{d\mu} \mathcal{F}_{x_\mu} = 0, \quad \mathcal{F}_y - \frac{d}{d\mu} \mathcal{F}_{y_\mu} = 0, \quad \mathcal{F}_z - \frac{d}{d\mu} \mathcal{F}_{z_\mu} = 0.$$

3. Change back from μ to σ .

Fermat's principle is not an exact physical law. Rather, it is an approximate physical law, which is valid under the geometrical optics approximation. This is not really surprising, since it is based on a ray description of light propagation.

Lemma 2.2 *Rays follow the same path in both directions.*

Proof This follows from the fact that the characteristic equations (2.8) remain unchanged under the *reversibility transformation* $\sigma \rightarrow -\sigma$ and $S \rightarrow -S$. Alternatively, it follows directly from Fermat's principle. \square

Remark Since S increases in the direction of propagation of the ray, see (2.10), S changes to $-S$ when we reverse the direction of propagation.

2.1.2 Transport Equation

The balance of the $O(k_0)$ terms in (2.3) gives the *transport equation*

$$2\nabla S \cdot \nabla A + A \Delta S = 0. \quad (2.12)$$

Since S has already been determined by the eikonal equation, (2.12) is a first-order linear PDE for A . By (2.6), the characteristics of this equation are parallel to ∇S . Therefore, they identify with the rays of S . The change in A along a ray is

$$\frac{d}{d\sigma} A(\mathbf{x}(\sigma)) = \nabla A \cdot \frac{d\mathbf{x}}{d\sigma} = \frac{1}{\tilde{n}} \nabla A \cdot \nabla S = -\frac{1}{2\tilde{n}} A \Delta S,$$

where $\mathbf{x}(\sigma)$ and $S = S(\mathbf{x}(\sigma))$ were already calculated from (2.8) and (2.9), respectively, and $\tilde{n} = \tilde{n}(\mathbf{x}(\sigma))$ is given. Therefore, $A(\mathbf{x}(\sigma))$ is calculated from the ODE

$$\frac{1}{A} \frac{dA}{d\sigma} = -\frac{1}{2\tilde{n}} \Delta S.$$

The transport equation can be written as

$$A^2 \Delta S + \nabla \left(A^2 \right) \cdot \nabla S = 0, \quad (2.13)$$

or, in divergence form, as

$$\nabla \cdot (A^2 \nabla S) = 0.$$

To understand the conservation law associated with this equation, consider a *bundle (tube) of rays* that start from a surface Σ_0 , and denote by Σ_1 the surface defined by the positions of the rays at $\sigma = \sigma_1$.⁸ These rays form a tube with ends Σ_0 and Σ_1 and sides Σ_{sides} . By the divergence theorem,

$$0 = \int_{\substack{\text{tube} \\ \text{volume}}} \nabla \cdot (A^2 \nabla S) \, d\mathbf{x} = \int_{\substack{\text{tube} \\ \text{surface}}} A^2 \nabla S \cdot \mathbf{n} \, d\mathbf{s},$$

where \mathbf{n} is the outward normal to the ray bundle,⁹ and $d\mathbf{s}$ is a surface element. Since the rays are parallel to ∇S ,

$$\nabla S \cdot \mathbf{n} = \begin{cases} 0, & \text{on } \Sigma_{\text{sides}}, \\ -|\nabla S|, & \text{on } \Sigma_0, \\ |\nabla S|, & \text{on } \Sigma_1. \end{cases}$$

Combining the above and using (2.4) and $\tilde{n}(\mathbf{x}) = n(\mathbf{x})/n_0$ gives

$$\int_{\Sigma_0} n A^2 \, d\mathbf{s} = \int_{\Sigma_1} n A^2 \, d\mathbf{s}. \quad (2.14)$$

In optics $\int_{\Sigma} n |A|^2 \, d\mathbf{s}$ is the *beam power* at Σ . Hence, the transport equation leads to

Lemma 2.3 *Under the geometrical optics approximation, the power of a ray bundle at any cross-section $\sigma \equiv \text{constant}$ is constant.*

Relation (2.14) shows that when an input beam is focused by a lens, all the beam power concentrates at the focal point:¹⁰

Corollary 2.1 *Consider a focused input beam that propagates in a homogeneous medium. Then under the geometrical optics approximation*

$$n|A|^2 \rightarrow P \cdot \delta(\mathbf{x} - \mathbf{x}_c), \quad \mathbf{x} \rightarrow \mathbf{x}_c,$$

where P is the input power, $\mathbf{x}_c \in \mathbb{R}^3$ is the focal point of the lens, and the limit is in the sense of distributions. In particular, $A(\mathbf{x})$ becomes infinite as $\mathbf{x} \rightarrow \mathbf{x}_c$.

Proof Let the input beam be prescribed at Σ_0 . Then its power is $P = \int_{\Sigma_0} n A^2$. Since all the rays reach the focal point with the same σ (see Exercise 2.5 below), the result follows from relation (2.14) with $\Sigma_1 = \mathbf{x}_c$. \square

⁸ I.e., $\Sigma_1 = \{\mathbf{x}(\sigma_1) \mid \mathbf{x}(0) \in \Sigma_0\}$.

⁹ Not to be confused with n , the index of refraction.

¹⁰ This property is called *whole-beam collapse* (Sect. 7.7).

Remark Let S and A be the solutions of the eikonal equation (2.4) and the transport equation (2.12), respectively. Then $E_{\text{go}} := Ae^{ik_0 S}$ is only an approximate solution of the Helmholtz equation (2.2), since we neglected the diffraction term ΔA in (2.3).

2.2 Applications of Geometrical Optics

2.2.1 Homogeneous Medium

When $n \equiv n_0$, Fermat's principle of "least time" is the same as the principle of "least distance", showing that rays move in straight lines. This also follows from Eq. (2.8), which in a homogeneous medium ($\tilde{n} \equiv 1$) read

$$\frac{d\mathbf{x}}{d\sigma} = \mathbf{p}, \quad \frac{d\mathbf{p}}{d\sigma} = 0.$$

2.2.2 Snell's Law

Consider a two-layer medium that consists of material 1 with linear refractive index $n(x, y, z) \equiv n_1$ at $y > 0$, and material 2 with $n(x, y, z) \equiv n_2$ at $y < 0$. Now, consider a ray which travels from point $\mathbf{A} = (x_1, y_1, z_1)$ inside material 1 to point $\mathbf{B} = (x_2, y_2, z_2)$ inside material 2, and crosses the interface $y = 0$ at point $\mathbf{C} = (x, 0, z)$, see Fig. 2.1. Within each material the ray travels in a straight line, i.e., $\overline{\mathbf{AC}}$ and $\overline{\mathbf{CB}}$ are straight lines. Since the propagation velocity in material i is c/n_i , the overall travel-time from \mathbf{A} to \mathbf{C} to \mathbf{B} is

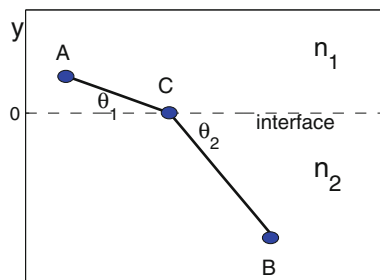


Fig. 2.1 Derivation of Snell's law

$$T = \frac{n_1}{c} \overline{AC} + \frac{n_2}{c} \overline{CB} = \sum_{i=1}^2 \frac{n_i}{c} \sqrt{(x - x_i)^2 + y_i^2 + (z - z_i)^2}.$$

Exercise 2.2 Use Fermat's principle of least time to show that

$$n_1 \cos \theta_1 = n_2 \cos \theta_2, \quad (\text{Snell's law}) \quad (2.15)$$

where θ_i is the angle that a ray inside material i makes with the interface (see Fig. 2.1).¹¹

Remark From Snell's law we see that

$$n_2 > n_1 \implies \cos \theta_2 < \cos \theta_1 \implies \theta_2 > \theta_1,$$

i.e., rays bend towards regions with a higher index of refraction.

Remark Snell's law explains why a teaspoon which is partially immersed in a cup of tea appears to be bent (and also why n is called the *index of refraction*).

Exercise 2.3 Show that if a ray is reflected back by a planar mirror, the angle of incidence is equal to the angle of reflection.

2.2.3 Linear Waveguides

Two Layers

Consider a *planar waveguide* made out of an inner core with index of refraction n_1 at $0 \leq |y| < y_1$, and an outer cladding with index of refraction n_2 at $y_1 < |y| < y_2$. Inside each dielectric the rays travel in straight lines. Let us denote by θ_1 the angle at which an inner-core ray impinges on the interface with the outer cladding at $y = \pm y_1$, and by θ_2 the angle at which the ray enters the outer cladding. By Snell's law,

$$n_1 \cos \theta_1 = n_2 \cos \theta_2.$$

Therefore, θ_2 can be found from the equation

$$\cos \theta_2 = \frac{n_1}{n_2} \cos \theta_1. \quad (2.16)$$

If $n_1 < n_2$, Eq. (2.16) can always be solved for θ_2 , since for any θ_1 the magnitude of the right-hand side of (2.16) is less than one. Physically, this means that rays can always cross the interface. If $n_1 > n_2$, however, then for all the inner-core rays for which

¹¹ Here the angle is defined with respect to the interface, hence the use of cosines instead of sines.

$$|\theta_1| < \Theta_{\text{cr}} := \cos^{-1} \left(\frac{n_2}{n_1} \right), \quad (2.17)$$

the right-hand side of (2.16) is larger than one, and so we cannot solve for θ_2 . Physically, this means that these rays cannot cross the interface. Instead, they are reflected backwards into the inner core. We thus see that when $n_1 > n_2$, the planar waveguide traps the paraxial rays $|\theta_1| \leq \Theta_{\text{cr}}$ inside the inner core, and that the *trapping efficiency* increases with the ratio n_1/n_2 .

K Layers

Let us consider now a planar waveguide made out of K dielectric materials, such that the index of refraction is n_k for $y_{k-1} < |y| < y_k$, where $k = 1, \dots, K$, and $y_0 = 0$. Since at each interface

$$n_k \cos \theta_k = n_{k+1} \cos \theta_{k+1}, \quad k = 1, \dots, K-1,$$

and since between interfaces rays travel in straight lines, it follows that for any given ray,

$$n_1 \cos \theta_1 = n_2 \cos \theta_2 = \dots = n_K \cos \theta_K. \quad (2.18)$$

Therefore, if n_k is monotonically decreasing in k , then so does θ_k , i.e., at each interface the ray bends back towards the center ($y = 0$). In addition, relation (2.18) shows that the overall trapping efficiency depends on n_1/n_K .

Continuous Variation

Consider now a planar waveguide made out of a dielectric material with a continuously-varying index of refraction $n = n(y)$. Intuitively, we can think of this waveguide as the limit as $K \rightarrow \infty$ of a planar waveguide with K homogeneous layers. Taking the limit of (2.18) as $K \rightarrow \infty$ shows that the trajectory of the ray satisfies

$$n(y) \cos \theta(y) \equiv n(0) \cos \theta(0). \quad (2.19)$$

We can also derive (2.19) from the eikonal equation. Indeed, when $n = n(y)$, Eqs.(2.8) for the trajectories of the rays read

$$\begin{aligned} \frac{dx}{d\sigma} &= \frac{p_1}{\tilde{n}}, & \frac{dy}{d\sigma} &= \frac{p_2}{\tilde{n}}, & \frac{dz}{d\sigma} &= \frac{p_3}{\tilde{n}}, \\ \frac{dp_1}{d\sigma} &= 0, & \frac{dp_2}{d\sigma} &= \frac{d\tilde{n}}{dy}, & \frac{dp_3}{d\sigma} &= 0. \end{aligned}$$

Therefore, p_1 and p_3 are constants. Let $\theta(\sigma)$ denote the angle at $\mathbf{x}(\sigma)$ between the ray and its projection on the (x, z) -plane $y \equiv y(\sigma)$. Then, since $|\frac{dx}{d\sigma}| = 1$,

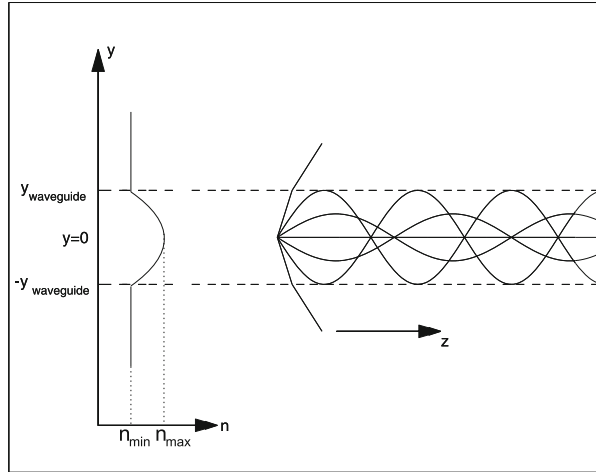


Fig. 2.2 Propagation of rays in a planar waveguide with a continuously-varying index of refraction $n = n(y)$

$$\cos \theta = \frac{\sqrt{\left(\frac{dx}{d\sigma}\right)^2 + \left(\frac{dz}{d\sigma}\right)^2}}{\left|\frac{d\mathbf{x}}{d\sigma}\right|} = \sqrt{\frac{p_1^2(0)}{\tilde{n}^2(y)} + \frac{p_3^2(0)}{\tilde{n}^2(y)}}.$$

Hence, $n(y) \cos \theta \equiv \text{constant}$, which is (2.19).

Let us assume that $n(y)$ is continuous and monotonically decreasing in $|y|$ for $0 \leq |y| \leq y_{\text{waveguide}}$, and $n(y) \equiv n_{\min}$ for $|y| \geq y_{\text{waveguide}}$, see Fig. 2.2. Then (2.19) shows that as $|y|$ increases, so does $\cos \theta$, hence also $|\theta|$. In other words, the rays continuously bend towards the center as they propagate.

Let us denote by θ_0 the angle at which a ray crosses the plane $y \equiv 0$. As before, Eq. (2.19) shows that there is a critical angle $\Theta_{\text{cr}} := \cos^{-1}\left(\frac{n_{\min}}{n_{\max}}\right)$, where $n_{\max} = n(0)$, such that all rays with $|\theta_0| \geq \Theta_{\text{cr}}$ escape to the outer region $|y| > y_{\text{waveguide}}$, where they continue to propagate as straight lines. The paraxial rays for which $|\theta_0| < \Theta_{\text{cr}}$, however, are trapped inside the waveguide. Furthermore, Eq. (2.19) shows that these rays oscillate periodically above and below $y = 0$ as they propagate (Fig. 2.2).

Cylindrical Waveguides (Optical Fibers)

An *optical fiber* is a cylindrical waveguide in which the linear refractive index is a function of $r = \sqrt{x^2 + y^2}$. For example, *step-index fibers* consist of a central glass core, surrounded by a cladding layer whose refractive index is slightly lower than that of the core. In *graded-index fibers*, the refractive index decreases gradually from the fiber center to the boundary [2].

Ray analysis of cylindrical waveguides is similar to that of planar waveguides. Thus, in step-index fibers, the paraxial rays are reflected back by the core-cladding interface. In graded-index fibers, the rays continuously bend toward the fiber center as they propagate. In both cases, the cylindrical waveguide traps the paraxial rays, and the trapping efficiency increases with $\frac{n(r=0)}{n(r=r_f)}$, where r_f is the fiber radius.

2.3 Collimated Beams (Helmholtz Model)

In a homogeneous medium, the eikonal equation reads¹²

$$\nabla S^{(E)} \cdot \nabla S^{(E)} = 1. \quad (2.20)$$

Let us consider this equation with the constant-phase initial condition

$$S^{(E)}(x, y, z = 0) \equiv \alpha, \quad -\infty < x, y < \infty, \quad \alpha \in \mathbb{R}. \quad (2.21)$$

Since both (2.20) and (2.21) are invariant under translations $(x, y) \rightarrow (x + x_0, y + y_0)$, $S^{(E)}$ only depends on z . Therefore, (2.20) reduces to $\frac{dS^{(E)}}{dz} = \pm 1$. In particular, the right-propagating solution is

$$S^{(E)}(x, y, z) = \alpha + z.$$

Since $\nabla S^{(E)} \equiv (0, 0, 1)$, the rays are everywhere parallel to the z -axis, and in particular at $z = 0$. Therefore, the initial condition (2.21) corresponds to a collimated input beam.

Conclusion 2.1 *In the Helmholtz model, a collimated input beam that propagates in the z -direction is represented by the constant-phase initial condition (2.21).*

Indeed, since the rays are perpendicular to the wavefronts, and since a collimated input beam is perpendicular to the (x, y) -plane $z \equiv 0$, this plane has to be a wavefront.

2.4 Fundamental Solution of Helmholtz Equation

We now begin to analyze the Helmholtz equation without applying the geometrical optics approximation (i.e., without neglecting diffraction).

In a homogeneous linear medium, the scalar Helmholtz equation reads

$$\Delta E(\mathbf{x}) + k_0^2 E = 0, \quad \mathbf{x} = (x, y, z). \quad (2.22)$$

¹² We use the notations $S^{(E)}$ and $S^{(\psi)}$ whenever we want to distinguish between the phases of the Helmholtz and Schrödinger solutions, respectively.

In Sect. 1.3 we saw that this equation has plane-wave solutions $E = E_c e^{i\mathbf{k} \cdot \mathbf{x}}$, where $|\mathbf{k}| = k_0$. Equation (2.22) also admits the spherical-wave solution

$$G(\mathbf{x}) = \frac{1}{4\pi\rho} e^{ik_0\rho}, \quad \rho = |\mathbf{x}| = \sqrt{x^2 + y^2 + z^2}. \quad (2.23)$$

Lemma 2.4 *Let G be given by (2.23). Then*

$$\Delta G + k_0^2 G = -\delta(\mathbf{x}),$$

i.e., $\Delta G + k_0^2 G = 0$ for $|\mathbf{x}| > 0$, and $\int_{\mathbb{R}^3} f(\mathbf{x}) (\Delta G + k_0^2 G) d\mathbf{x} = -f(0)$.

Proof Direct differentiation yields

$$G' = \frac{e^{ik_0\rho}}{4\pi} \left(\left(\frac{1}{\rho} \right)' + \frac{ik_0}{\rho} \right), \quad G'' = \frac{e^{ik_0\rho}}{4\pi} \left(\left(\frac{1}{\rho} \right)'' + 2 \left(\frac{1}{\rho} \right)' ik_0 - k_0^2 \right).$$

Therefore,

$$\Delta G + k_0^2 G = G'' + \frac{2}{\rho} G' + k_0^2 G = \frac{e^{ik_0\rho}}{4\pi} \Delta \left(\frac{1}{\rho} \right).$$

Since $\Delta \left(\frac{1}{\rho} \right) = -4\pi\delta(\rho)$, the result follows. \square

If we write $G = A e^{ik_0 S^{(E)}}$, then $A = \frac{1}{4\pi\rho}$ and $S^{(E)} = \rho$. Therefore, the wavefronts of G are the spheres $\rho \equiv \text{constant}$. Since the rays are perpendicular to the wavefronts, they are the lines emanating from $\rho = 0$. We thus see that G describes spherical propagation of radiation from a *point source* at $\rho = 0$.

Exercise 2.4 Verify that $G(\mathbf{x})$ satisfies relation (2.14), i.e., that the power in the intersection of a cone of rays that starts at $\rho = 0$ with a sphere of radius ρ , is independent of ρ .

The Helmholtz equation (2.22) also admits the spherical-wave solution

$$G_-(\mathbf{x}) = \frac{1}{4\pi\rho} e^{-ik_0\rho}, \quad \rho = \sqrt{x^2 + y^2 + z^2}. \quad (2.24)$$

In this case, $A = \frac{1}{4\pi\rho}$ and $S^{(E)} = -\rho$. Therefore, the wavefronts of G_- are the spheres $\rho \equiv \text{constant}$, and the rays are the lines pointing towards $\rho = 0$.¹³ Hence, expression (2.24) describes a *point sink* located at $\rho = 0$.

¹³ Recall that $S^{(E)}$ increases in the direction of propagation of the ray (Sect. 2.1.1).

2.5 Focused Beams (Helmholtz Model)

In many applications, the incoming laser beam is focused by a lens. To represent the effect of a lens on an input beam, we first note that the solution of Helmholtz equation (2.22) with a point sink located at $(0, 0, F)$ is

$$G_- = \frac{1}{4\pi\sqrt{x^2 + y^2 + (z - F)^2}} e^{ik_0 S^{(E)}}, \quad (2.25a)$$

where

$$S^{(E)} = -\sqrt{x^2 + y^2 + (z - F)^2}. \quad (2.25b)$$

Hence, the rays are the lines pointing towards $(0, 0, F)$. In particular, all the rays that start at the (x, y) -plane $z \equiv 0$ intersect at $(0, 0, F)$. Therefore, expression (2.25b) describes the phase of a beam which is focused at $z = 0$ by a lens with focal point at $(0, 0, F)$. In particular, the phase at $z = 0$ is

$$k_0 S^{(E)}(x, y, 0) = -k_0 \sqrt{x^2 + y^2 + F^2}. \quad (2.26)$$

Conclusion 2.2 *In the Helmholtz model, a lens located at $z = 0$ with a focal point at $(0, 0, F)$ is represented by the phase term (2.26).*

Indeed, the solution of the eikonal equation (2.20) with the initial condition (2.26) is given by (2.25b).

Exercise 2.5 *Derive expression (2.26) from the condition that all the rays that emanate from the (x, y) -plane $z \equiv 0$ should reach the focal point $(0, 0, F)$ with the same travel time (phase), so that they would interfere constructively.*

The representation of a lens in an inhomogeneous or nonlinear medium is also given by (2.26). Indeed, although we derived this expression for a linear homogeneous medium, the lens effect is independent of the subsequent propagation. Of course, if the medium is inhomogeneous or nonlinear, the lens will not focus all rays to the point $(0, 0, F)$.¹⁴

2.6 Singularity in the Helmholtz Model

We now show that under the geometrical optics approximation, solutions of the Helmholtz equation can become singular:

¹⁴ Even in a linear homogeneous medium, if we do not apply the geometrical optics approximation, the lens does not focus the solution to a point (Sect. 2.10).

Lemma 2.5 Consider the Helmholtz equation (2.22) for propagation in a homogeneous linear medium. Then under the geometrical optics approximation, a focused incoming beam has a δ -function singularity at the focal point.

Proof Under the geometrical optics approximation, the phase evolves according to the eikonal equation. In Sect. 2.5 we saw that the initial phase is given by (2.26), and the corresponding solution of the eikonal equation (2.20) is $S^{(E)} = -\sqrt{x^2 + y^2 + (z - F)^2}$. Therefore, all rays that start at the (x, y) -plane $z \equiv 0$ intersect at the focal point $(0, 0, F)$. Hence, by Corollary 2.1, all the beam power concentrates at the focal point. \square

It is not really surprising that the solution becomes singular at the focal point, since under the geometrical optics approximation, a lens focuses all the rays into a single point, and classical solutions break down whenever their characteristics intersect. For example, in hyperbolic equations, the crossing of characteristics corresponds to a shock wave (see, e.g., [157]). Note, however, that our analysis also reveals that the singularity is of a delta-function type, whereby all the solution power concentrates at the focal point. In particular, the solution becomes infinite at the singularity point. This is different from hyperbolic shock waves, where only the derivative becomes infinite when the characteristics intersect.

2.7 Global Existence in the Linear Helmholtz Equation in the Half Space

In the scalar linear Helmholtz equation (2.22), under the geometrical optics approximation, a focused input beam become singular at the focal point (Lemma 2.5). Since physical quantities do not become singular, we would like to know which approximation is “responsible” for this singularity.¹⁵

Equation (2.22) is already an approximate model, since it neglects the vectorial nature of the electric field (Sect. 1.2). We now show that when Eq. (2.22) is driven by right-propagating incoming beam at $z = 0$, its solution exists for all $z > 0$. Therefore, the singularity in Lemma 2.5 is not due to approximations made in the derivation of the scalar Helmholtz equation, but rather due to the geometrical optics approximation.

Consider the Helmholtz equation in the positive half space

$$\Delta E(x, y, z) + k_0^2 E = 0, \quad z > 0, \quad -\infty < x, y < \infty, \quad (2.27)$$

¹⁵ This book is mainly concerned with singular NLS solutions. Therefore, understanding the origin of singularities in the linear case will help us to determine whether NLS singularity is a linear or a nonlinear phenomenon.

with a right-propagating incoming beam, whose value at $z = 0$ is $E_0^{\text{inc}}(x, y)$.¹⁶ To solve this problem, we first write the incoming beam as

$$E_0^{\text{inc}}(x, y) = \frac{1}{2\pi} \int \widehat{E_0^{\text{inc}}}(k_x, k_y) e^{i(k_x x + k_y y)} dk_x dk_y.$$

The corresponding right-propagating solution of (2.27) is, see (1.13),

$$E(x, y, z) = \frac{1}{2\pi} \int \widehat{E_0^{\text{inc}}}(k_x, k_y) e^{i(k_x x + k_y y + \sqrt{k_0^2 - k_x^2 - k_y^2} z)} dk_x dk_y. \quad (2.28)$$

Lemma 2.6 *Assume that $E_0^{\text{inc}}(x, y)$ is sufficiently smooth and decays sufficiently fast to zero as $\sqrt{x^2 + y^2} \rightarrow \infty$. Then expression (2.28) is smooth and bounded for all $z > 0$.*

Proof Recall that the decay rate of Fourier coefficients as $\sqrt{k_x^2 + k_y^2} \rightarrow \infty$ increases with the smoothness of the function. Therefore, since $E_0^{\text{inc}}(x, y)$ is sufficiently smooth and decays sufficiently fast to zero as $\sqrt{x^2 + y^2} \rightarrow \infty$, $\widehat{E_0^{\text{inc}}}(k_x, k_y)$ is also sufficiently smooth and decays sufficiently fast as $\sqrt{k_x^2 + k_y^2} \rightarrow \infty$. Hence, so does $\hat{E}(k_x, k_y, z) = \widehat{E_0^{\text{inc}}}(k_x, k_y) e^{i(\sqrt{k_0^2 - k_x^2 - k_y^2} z)}$. Therefore, $E(x, y, z)$ exists and is bounded for all z . \square

Corollary 2.2 *Let the scalar linear Helmholtz equation (2.27) be driven at $z = 0$ by a focused incoming beam which is smooth and decays sufficiently fast to zero as $\sqrt{x^2 + y^2} \rightarrow \infty$. Then the solution does not become singular.*

Comparison of Lemma 2.5 with Corollary 2.2 leads to

Conclusion 2.3 *The singularity in Lemma 2.5 is due to the geometrical optics approximation.*

Remark The spherical wave G_- , see (2.25), is a solution of Helmholtz equation with the focused incoming beam

$$E_0^{\text{inc}}(x, y) = G_-(x, y, z = 0) = \frac{1}{4\pi \sqrt{x^2 + y^2 + F^2}} e^{-ik_0 \sqrt{x^2 + y^2 + F^2}}. \quad (2.29)$$

Since this solution becomes singular at $(0, 0, F)$, it appears to be a “counter-example” to Corollary 2.2. In Sect. 34.7 we shall see, however, that physical solutions of Helmholtz equation that are driven at $z = 0$ by a right-propagating incoming beam, should propagate to the right as $z \rightarrow +\infty$. The spherical wave G_- , however, propagates to the left as $z \rightarrow +\infty$. Thus, the resolution of this “contradiction” is that the

¹⁶ The discussion here is very informal. The formulation of boundary conditions for the Helmholtz equation in the positive half space will be discussed in Sect. 34.7.

solution of Helmholtz equation with the incoming beam (2.29) is non-unique. The unique physical solution that satisfies the *radiation-to-the-right boundary condition* as $z \rightarrow +\infty$ exists globally and is bounded, but solutions that do not satisfy this radiation boundary condition may become unbounded.

2.8 Representations of Input Beams

2.8.1 Relation Between $S^{(E)}$ and $S^{(\psi)}$

Let $E(x, y, z)$ be a solution of Helmholtz equation (2.22). As in Sect. 1.3, if we substitute $E = e^{ik_0 z} \psi(x, y, z)$ and apply the paraxial approximation, then ψ satisfies the Schrödinger equation

$$2ik_0 \psi_z(x, y, z) + \Delta_{\perp} \psi = 0, \quad \Delta_{\perp} = \frac{\partial^2}{\partial x^2} + \frac{\partial^2}{\partial y^2}. \quad (2.30)$$

In Sect. 2.1.1 we decomposed the Helmholtz solution as

$$E = A(x, y, z) e^{ik_0 S^{(E)}(x, y, z)},$$

where A and $S^{(E)}$ are real. Similarly, we can decompose the Schrödinger solution as

$$\psi = A(x, y, z) e^{ik_0 S^{(\psi)}(x, y, z)},$$

where A and $S^{(\psi)}$ are real. Since $E = e^{ik_0 z} \psi$, the amplitudes of E and ψ are the same, but their phases are not. Rather, they are related through

$$k_0 S^{(E)} = k_0 z + k_0 S^{(\psi)}. \quad (2.31)$$

The paraxial approximation implies that $k_0 S^{(\psi)}$ is slowly-varying in z , compared with $k_0 z$. Therefore,

$$\frac{\partial}{\partial z} S^{(\psi)} \ll 1. \quad (2.32)$$

In Sects. 2.8.2, 2.8.4, and 2.8.5 we will use relation (2.31) to find the representations of collimated, focused, and tilted input beams in the Schrödinger model, from their respective representations in the Helmholtz model.

2.8.2 Collimated Beams (Schrödinger Model)

In Conclusion 2.1 we saw that in the Helmholtz model, a collimated input beam is represented by the constant-phase initial condition $S^{(E)}(z = 0) \equiv \alpha$. Therefore, by relation (2.31) we have

Conclusion 2.4 *In the Schrödinger model, a collimated input beam that propagates in the z -direction is represented by the constant-phase initial condition*

$$S^{(\psi)}(x, y, z = 0) \equiv \alpha, \quad -\infty < x, y < \infty, \quad \alpha \in \mathbb{R}.$$

Corollary 2.3 *If the initial condition ψ_0 of the Schrödinger equation is real, then it corresponds to a collimated input beam that propagates in the z -direction.*

2.8.3 From Spherical to Parabolic Waves

Consider the spherical-wave solution G . Since the phase of G is $k_0 S^{(E)} = k_0 \rho$, see (2.23), the corresponding phase of ψ is

$$k_0 S^{(\psi)} = k_0(\rho - z).$$

Let us consider the narrow paraxial portion of the spherical-wave solution G that propagates in the direction of the positive z -axis. Then $x, y \ll z$, and so we can approximate

$$\rho = (x^2 + y^2 + z^2)^{\frac{1}{2}} = z \left(1 + \frac{x^2 + y^2}{z^2} \right)^{\frac{1}{2}} \approx z \left(1 + \frac{1}{2} \frac{x^2 + y^2}{z^2} \right).$$

Hence,

$$S^{(\psi)}(x, y, z) \approx \frac{r^2}{2z}, \quad r = \sqrt{x^2 + y^2}, \quad (2.33)$$

i.e., the wavefronts of ψ are parabolic.

Conclusion 2.5 *Under the paraxial approximation, a spherical wave turns into a parabolic one.*

For that reason, the *paraxial approximation* is also called the *parabolic approximation*.

2.8.4 Focused Beams (Schrödinger Model)

In order to represent a focusing lens ($F > 0$) in the Schrödinger model, let $G_- = e^{ik_0 z} \psi$, where G_- is given by (2.25). Since $S^{(E)}$ is given by (2.25b), then by (2.31), for $0 < z < F$,

$$S^{(\psi)} = -\sqrt{x^2 + y^2 + (z - F)^2} - z = (z - F) \sqrt{1 + \frac{r^2}{(z - F)^2}} - z. \quad (2.34)$$

Application of the paraxial approximation $r \ll z - F$ gives $\left(1 + \frac{r^2}{(z-F)^2}\right)^{\frac{1}{2}} \approx 1 + \frac{r^2}{2(z-F)^2}$. Therefore,

$$S^{(\psi)}(x, y, z) \approx \frac{r^2}{2(z-F)} - F.$$

Since a constant phase term has no effect, we can also write

$$S^{(\psi)}(x, y, z) \approx \frac{r^2}{2(z-F)}. \quad (2.35)$$

In particular, the phase at $z = 0$ is

$$k_0 S^{(\psi)}(x, y, 0) \approx -k_0 \frac{r^2}{2F}. \quad (2.36)$$

Therefore, we have

Conclusion 2.6 *In the Schrödinger model (2.30), a lens located at $z = 0$ whose focal point is at $(0, 0, F)$, is represented by adding a quadratic phase term to the initial condition as follows:*

$$\underbrace{\psi_0(x, y)}_{\text{no lens}} \rightarrow \underbrace{\psi_0(x, y) e^{-ik_0 \frac{r^2}{2F}}}_{\text{with lens}}. \quad (2.37)$$

As expected, the addition of a lens does not affect the input beam amplitude $|\psi_0|$.

Remark The dimensionless representation of a lens is given in Conclusion 2.12.

2.8.5 Tilted Beams

We can use a similar approach to find the representation of a tilted input beam, i.e., a collimated input beam whose direction of propagation is not parallel to the z -axis. Recall that the Helmholtz equation (2.22) admits the plane-wave solution $E = E_c e^{i(k_x x + k_y y + k_z z)}$, where $k_x^2 + k_y^2 + k_z^2 = k_0^2$. This solution can be written as $E = E_c e^{ik_0(n_x x + n_y y + n_z z)}$, where $\mathbf{n} = (n_x, n_y, n_z)$ is the unit vector in the direction of propagation ($n_x^2 + n_y^2 + n_z^2 = 1$). For this plane wave, $S^{(E)} = n_x x + n_y y + n_z z$. Hence, for the corresponding Schrödinger solution

$$S^{(\psi)}(x, y, z) = S^{(E)} - z = n_x x + n_y y + (n_z - 1)z.$$

In particular,

$$S^{(\psi)}(x, y, 0) = n_x x + n_y y.$$

In fact, in Sect. 2.12.3 we will see that the correct expression is¹⁷

$$S^{(\psi)}(x, y, 0) = \frac{n_x}{n_z} x + \frac{n_y}{n_z} y.$$

Since in paraxial propagation $n_z = 1 + O(f^2)$, see (2.66), these two expressions for $S^{(\psi)}(x, y, 0)$ are equivalent, up to the $O(f^2)$ accuracy of the paraxial Schrödinger model (Sect. 2.12.1).¹⁸

Conclusion 2.7 *In the Schrödinger model (2.30), a tilt of the input beam in the direction of the unit vector $\mathbf{n} = (n_x, n_y, n_z)$ is represented by adding a linear phase term to the initial condition, as follows:*

$$\underbrace{\psi_0(x, y)}_{\text{no tilt}} \rightarrow \underbrace{\psi_0(x, y) e^{ik_0(\frac{n_x}{n_z}x + \frac{n_y}{n_z}y)}}_{\text{with tilt}}.$$

Remark The tilt angle θ is given by $\tan \theta = \frac{|\mathbf{n}_\perp|}{|n_z|}$, where $\mathbf{n}_\perp = (n_x, n_y)$.

Remark The dimensionless expression for a tilted beam is given in Conclusion 2.13.

Exercise 2.6 *Analyze the effect of the phase in the initial condition*

$$\psi_0(x) = e^{-(\frac{x}{3})^2} e^{ik_0 \log(e^x + e^{-x})}.$$

2.8.6 Vortex Beams

The Helmholtz equation (2.22) admits solutions of the form

$$E(z, r, \theta) = e^{im\theta} A(z, r),$$

where (z, r, θ) are the cylindrical coordinates, m is an integer, and A is the solution of

$$A_{zz} + A_{rr} + \frac{1}{r} A_r + \left(k_0^2 - \frac{m^2}{r^2} \right) A = 0.$$

¹⁷ That this is the correct expression will follow from Galilean invariance of the Schrödinger equation.

¹⁸ The quadratic phase term (2.35) for the effect of a lens in the Schrödinger model is also not equal to $S^{(E)} - z$, see (2.34). It is, however, $O(f^2)$ equivalent to it, since under the paraxial approximation $\frac{r}{z-f} = O(f)$, see (2.64). We “prefer” approximation (2.35) over the “exact” expression (2.34), because (2.35) agrees with the lens transformation of the linear Schrödinger equation (Corollary 8.1).

These solutions are called *vortex solutions*, because they rotate around the z -axis as they propagate in the z -direction.¹⁹ Indeed, if $A(z, r)$ is real, then the equal-phase curves in the (r, θ) -plane are $m\theta \equiv \text{constant}$, i.e., lines emanating from $r = 0$. Since the rays are perpendicular to these lines, they point in the azimuthal direction.

By (2.31), the initial phase of the corresponding Schrödinger solution is $\arg \psi(x, y, 0) = m\theta$. Therefore we have

Conclusion 2.8 *In the Schrödinger model (2.30), a rotation of the incoming beam around the z -axis is represented by adding the phase-term $e^{im\theta}$ to the initial condition, as follows:*

$$\underbrace{\psi_0(x, y)}_{\text{no rotation}} \rightarrow \underbrace{\psi_0(x, y)e^{im\theta}}_{\text{with rotation}}.$$

2.8.7 Generic Input Beams

We can summarize the results of Sect. 2.8, as follows. In the dimensional Schrödinger model (2.30):

1. A collimated input beam that propagates in the z -direction is represented by a real initial condition ψ_0 .
2. A focused input beam that propagates in the z -direction is represented by

$$\psi_0 = A_0(x, y)e^{-ik_0 \frac{r^2}{2F}}, \quad (2.38)$$

where $A_0(x, y) = |\psi_0(x, y)|$ is the input beam amplitude and F is the focal length.

3. A tilted collimated input beam that propagates in the direction of the unit vector $\mathbf{n} = (n_x, n_y, n_z)$ is represented by

$$\psi_0 = A_0(x, y)e^{ik_0 \left(\frac{n_x}{n_z}x + \frac{n_y}{n_z}y \right)}.$$

4. A tilted focused input beam that propagates in the direction of the unit vector $\mathbf{n} = (n_x, n_y, n_z)$ is represented by

$$\psi_0 = A_0(x, y)e^{-ik_0 \frac{r^2}{2F}} e^{ik_0 \left(\frac{n_x}{n_z}x + \frac{n_y}{n_z}y \right)}. \quad (2.39)$$

5. A vortex input beam that propagates in the z -direction is represented by

$$\psi_0 = A_0(x, y)e^{im\theta}, \quad m = \pm 1, \pm 2, \dots$$

¹⁹ Vortex solutions are studied in Chaps. 15 and 20 and in Sects. 23.7 and 24.7.

2.9 Geometrical Optics Analysis of Paraxial Propagation

In Sect. 1.3 we saw that under the paraxial approximation, the Helmholtz equation (2.22) reduces to the Schrödinger equation (2.30). We now analyze the Schrödinger equation under the geometrical optics approximation.

Substituting $\psi = Ae^{ik_0 S^{(\psi)}}$ in (2.30), where A and $S^{(\psi)}$ are real, gives

$$\begin{aligned} -2k_0^2 AS_z^{(\psi)} - 2ik_0 A_z + \Delta_{\perp} A + 2ik_0 \nabla_{\perp} A \cdot \nabla_{\perp} S^{(\psi)} \\ + A \left(-k_0^2 (\nabla_{\perp} S^{(\psi)})^2 + ik_0 \Delta_{\perp} S^{(\psi)} \right) = 0, \end{aligned}$$

where $\nabla_{\perp} = \left(\frac{\partial}{\partial x}, \frac{\partial}{\partial y} \right)$ and $\Delta_{\perp} = \frac{\partial^2}{\partial x^2} + \frac{\partial^2}{\partial y^2}$. The equation for the real parts, after division by $k_0^2 A$, is

$$2S_z^{(\psi)} + (\nabla_{\perp} S^{(\psi)})^2 - \frac{1}{k_0^2} \frac{\Delta_{\perp} A}{A} = 0. \quad (2.40a)$$

Similarly, the equation for the imaginary parts, after multiplication by A , is

$$(A^2)_z + \nabla_{\perp} S^{(\psi)} \cdot \nabla_{\perp} (A^2) + A^2 \Delta_{\perp} S^{(\psi)} = 0. \quad (2.40b)$$

When $k_0 \gg 1$, we can apply the geometrical optics approximation and neglect the diffraction term $\Delta_{\perp} A$. In this case, (2.40a) becomes

$$2S_z^{(\psi)} + (\nabla_{\perp} S^{(\psi)})^2 = 0. \quad (2.41)$$

Equation (2.41) is the *paraxial eikonal equation* in a homogeneous medium, as is confirmed in the following exercise:

Exercise 2.7 Derive (2.41) from the eikonal equation for a homogeneous medium (2.4), by using relation (2.31) and the paraxial approximation (2.32).

Unlike Eq. (2.40a), Eq. (2.40b) remains unchanged under the geometrical optics approximation. Equation (2.40b) is the *paraxial transport equation* in a homogeneous medium, as is confirmed in the following exercise:

Exercise 2.8 Derive (2.40b) from the transport equation (2.13), by using relation (2.31) and the paraxial approximation (2.32).

In Sect. 2.1 we saw that the eikonal and transport equations have the same characteristics. Interestingly, the characteristics of the paraxial eikonal and transport equations are not the same. Rather, they are given by

$$\frac{dz}{d\sigma} = 2, \quad \frac{dx}{d\sigma} = S_x^{(\psi)}, \quad \frac{dy}{d\sigma} = S_y^{(\psi)},$$

and

$$\frac{dz}{d\sigma} = 1, \quad \frac{dx}{d\sigma} = S_x^{(\psi)}, \quad \frac{dy}{d\sigma} = S_y^{(\psi)}, \quad (2.42)$$

respectively.

Exercise 2.9 Derive (2.42) for the characteristics of the paraxial transport equation from Eq. (2.7) for the characteristics of the transport equation, by using relation (2.31) and the paraxial approximation (2.32).

Let ψ_0 be the generic focused input beam (2.38). Then the corresponding initial conditions for $S^{(\psi)}$ and A^2 are

$$S^{(\psi)}(x, y, 0) = -\frac{r^2}{2F} \quad (2.43a)$$

and

$$A^2(x, y, 0) = |\psi_0(x, y)|^2. \quad (2.43b)$$

It is easy to verify that the solution of the paraxial eikonal equation (2.41), subject to the initial condition (2.43a), is²⁰

$$S^{(\psi)} = \frac{r^2}{2(z - F)}. \quad (2.44)$$

Substituting (2.44) in the paraxial transport equation (2.40b) gives

$$\left(A^2\right)_z + \frac{1}{z - F}(x, y) \cdot \nabla_{\perp} \left(A^2\right) + \frac{2}{z - F} A^2 = 0. \quad (2.45)$$

The solution of this equation, subject to the initial condition (2.43b), can be calculated by the method of characteristics, yielding

$$A^2(x, y, z) = \frac{1}{L^2(z)} \left| \psi_0 \left(\frac{x}{L(z)}, \frac{y}{L(z)} \right) \right|^2, \quad L(z) = 1 - \frac{z}{F}.$$

Here $L(z)$ is the beam width, and $L^{-1}(z)$ is proportional to the on-axis amplitude $A(0, 0, z) = |\psi(0, 0, z)|$.

Let $\psi_{go} := Ae^{ik_0 S^{(\psi)}}$, where A and $S^{(\psi)}$ are the solutions of (2.40b) and (2.41), respectively.²¹ Then

²⁰ We already derived this expression by applying the geometrical optics approximation and then the paraxial approximation, see (2.35). In the derivation here the order of the approximations is reversed.

²¹ The subscript *go* emphasizes that ψ_{go} is not an exact solution of the Schrödinger equation, as it is obtained under the geometrical optics approximation.

$$\psi_{\text{go}}(x, y, z) = \frac{1}{L(z)} \left| \psi_0 \left(\frac{x}{L}, \frac{y}{L} \right) \right| e^{ik_0 \frac{r^2}{2(z-F)}}, \quad L(z) = 1 - \frac{z}{F}. \quad (2.46)$$

Expression (2.46) with $F > 0$ describes the propagation of a focused input beam under the paraxial and geometrical optics approximations. In particular, the beam width $L(z)$ decreases linearly with z , and vanishes at the focal point $z = F$. Moreover,

$$|\psi_{\text{go}}|^2 = \frac{1}{L^2(z)} \left| \psi_0 \left(\frac{x}{L}, \frac{y}{L} \right) \right|^2 \rightarrow P \cdot \delta(\mathbf{x}), \quad z \rightarrow F-, \quad (2.47)$$

where $P = \int |\psi_0|^2 dx dy$ is the input power, and the limit is in the sense of distributions.

Lemma 2.7 *In the linear Schrödinger model, under the geometrical optics approximation, a focusing lens leads to a δ -function singularity at the focal point.*

Remark Lemma 2.7 is the paraxial analog of Lemma 2.5.

Remark The singularity in Lemma 2.7 is not related to non-smoothness or insufficient decay at infinity of the initial condition, as it occurs e.g., for a focused Gaussian input beam.

Remark See Sect. 38.8 for a continuation of ψ_{go} beyond the singularity.

2.10 Arrest of Linear Collapse by Diffraction (Gaussian Beams)

In Lemma 2.7 we saw that in the linear Schrödinger model, under the geometrical optics approximation, a focused input beam becomes singular at the lens focal point. We now show that if one does not apply the geometrical optics approximation (i.e., when diffraction is not neglected in the Schrödinger model), the focused beam does not collapse to a point. Rather, it narrows down to a positive *diffraction-limited width*, and then spreads out with further propagation.

Our starting point is the linear Schrödinger equation (2.30). As in the diffractionless case (Sect. 2.9), let $\psi = Ae^{ik_0 S^{(\psi)}}$, where A and $S^{(\psi)}$ are real. Therefore, A and $S^{(\psi)}$ are solutions of

$$2S_z^{(\psi)} + \left(\nabla_{\perp} S^{(\psi)} \right)^2 - \frac{1}{k_0^2} \frac{\Delta_{\perp} A}{A} = 0, \quad (2.48a)$$

and

$$\left(A^2 \right)_z + \nabla_{\perp} S^{(\psi)} \cdot \nabla_{\perp} \left(A^2 \right) + A^2 \Delta_{\perp} S^{(\psi)} = 0, \quad (2.48b)$$

respectively, see (2.40). Unlike the analysis in Sect. 2.9, here we do not neglect the diffraction term $\Delta_{\perp} A$.

In general, Eqs. (2.48) cannot be solved explicitly. An explicit solution can be obtained, however, for the focused Gaussian input beam²²

$$\psi_0(x, y) = E_c e^{-\frac{r^2}{2r_0^2} - i \frac{k_0 r^2}{2F}}, \quad r = \sqrt{x^2 + y^2},$$

where F is the focal distance and r_0 is the input beam width. By (2.43), the initial conditions for (2.48) are

$$S^{(\psi)}(x, y, 0) = -\frac{r^2}{2F}, \quad A^2(x, y, 0) = E_c^2 e^{-\frac{r^2}{r_0^2}}. \quad (2.48c)$$

Let us look for a solution of (2.48) of the form

$$S^{(\psi)} = \frac{a(z)r^2}{2} + \zeta(z), \quad A^2 = \frac{E_c^2}{L^2(z)} e^{-\frac{r^2}{r_0^2 L^2(z)}}, \quad (2.49)$$

i.e., for a solution that maintains a self-similar Gaussian profile during its propagation.

Exercise 2.10 Verify that the self-similar Gaussian ansatz (2.49) is an exact solution of (2.48), provided that $a(z)$, $\zeta(z)$, and $L(z)$ satisfy

$$a^2 + a_z = \frac{1}{k_0^2 r_0^4} \frac{1}{L^4}, \quad \zeta_z = -\frac{1}{k_0^2 r_0^2} \frac{1}{L^2}, \quad a = \frac{L_z}{L}, \quad (2.50)$$

subject to the initial conditions

$$a(0) = -\frac{1}{F}, \quad \zeta(0) = 0, \quad L(0) = 1.$$

Thus, the assumption that the solution maintains a self-similar Gaussian profile is fully consistent with the linear Schrödinger equation (2.30).²³

Substitution (2.49) allows us to replace a PDE (the Schrödinger equation) with a system of ODEs.²⁴ In general, it is considerably simpler to analyze ODEs than a PDE. Moreover, the ODEs (2.50) can be explicitly solved, as follows. Since $a = L_z/L$, then

²² The assumption that the input beam has a Gaussian profile is common in optics.

²³ This is not the case in nonlinear propagation of Gaussian input beams (Sect. 3.5). Even in linear propagation, this *aberrationless propagation* property holds only for Gaussian profiles. Thus, for example, if the input beam has a *sech* profile, the beam does not maintain a *sech* profile during linear propagation. The reason why this aberrationless property only holds for linear Gaussian beams will become clear in Sect. 2.15.3.

²⁴ This is possible because the transverse profile of the solution is “known” to be a rescaled Gaussian.

$$a^2 + a_z = \frac{L_{zz}}{L}.$$

Therefore, the dynamics of $L(z)$ is governed by

$$L_{zz}(z) = \frac{1}{L_{\text{diff}}^2} \frac{1}{L^3}, \quad (2.51\text{a})$$

where $L_{\text{diff}} = k_0 r_0^2$ is the *diffraction length*.²⁵ The initial conditions for (2.51a) are

$$L(0) = 1, \quad L_z(0) = a(0)L(0) = -\frac{1}{F}. \quad (2.51\text{b})$$

Since a converging, collimated, or diverging beam corresponds to $F > 0$, $F = \infty$, or $F < 0$, respectively, from (2.51b) we have

Conclusion 2.9 *An input beam is collimated when $L_z(0) = 0$, converging (focused) when $L_z(0) < 0$, and diverging (defocused) when $L_z(0) > 0$.*

This conclusion is intuitive since, for example, a beam is focused if and only if its width L is decreasing.

The solution of (2.51) follows from

Lemma 2.8 *The solution of*

$$L_{zz}(z) = \frac{K}{L^3}, \quad L(0) = L_0 > 0, \quad L_z(0) = L'_0, \quad (2.52)$$

where K is a constant, is given by

$$L^2(z) = c_1 \left(z + \frac{L_0 L'_0}{c_1} \right)^2 + \frac{K}{c_1}, \quad c_1 = (L'_0)^2 + \frac{K}{L_0^2}. \quad (2.53)$$

This solution can also be written as

$$L^2(z) = c_1 z^2 + 2L_0 L'_0 z + L_0^2, \quad (2.54)$$

and as

$$L^2(z) = (L_0 + z L'_0)^2 + \frac{K}{L_0^2} z^2. \quad (2.55)$$

Proof Multiplying (2.52) by $2L_z$ and integrating gives

$$(L_z)^2 = \frac{-K}{L^2} + c_1, \quad c_1 = (L'_0)^2 + \frac{K}{L_0^2}.$$

²⁵ See Sect. 2.11.

If we multiply this equation by L^2 we can rewrite it as

$$\frac{1}{2}y_z = \pm\sqrt{c_1y - K}, \quad y := L^2,$$

where the \pm sign corresponds to the sign of L'_0 . Integrating this equation and using the initial conditions gives

$$\frac{1}{c_1}\sqrt{c_1y - K} = \pm z + \frac{L_0|L'_0|}{c_1} = \text{sign}(L'_0) \left(z + \frac{L_0L'_0}{c_1} \right),$$

which leads to (2.53). \square

In the case of Eq.(2.51),

$$K = \frac{1}{L_{\text{diff}}^2}, \quad L_0 = 1, \quad L'_0 = -\frac{1}{F}.$$

Therefore, by (2.55), the solution of (2.51) is

$$L^2(z) = \left(1 - \frac{z}{F} \right)^2 + \left(\frac{z}{L_{\text{diff}}} \right)^2. \quad (2.56)$$

The first and second terms on the right-hand side correspond to focusing (or defocusing) by the lens and to defocusing due to diffraction, respectively.

We can rewrite the solution of (2.51) as, see (2.53),

$$L^2(z) = \left(\frac{1}{F^2} + \frac{1}{L_{\text{diff}}^2} \right) (z - z_{\min})^2 + L_{\min}^2, \quad (2.57)$$

where

$$z_{\min} = \frac{F}{1 + F^2/L_{\text{diff}}^2}, \quad L_{\min} = \frac{F}{\sqrt{F^2 + L_{\text{diff}}^2}}.$$

Expression (2.57) shows that $L(z)$ does not shrink to zero at any $z > 0$.

Corollary 2.4 *Diffraction arrests collapse of focused Gaussian input beams in paraxial linear propagation.*

Equation (2.57) also shows that when $F > 0$, the beam focuses for $0 < z < z_{\min}$, and defocuses for $z > z_{\min}$. The minimal value of L is $L_{\min} > 0$. It is attained at $z = z_{\min} < F$, i.e., before the focal point (Fig. 2.3).

Let us consider the case where the focusing lens is much stronger than diffraction (*tight focusing*), i.e., $0 < F \ll L_{\text{diff}}$. In this case, $z_{\min} \approx F$ and $L_{\min} \approx F/L_{\text{diff}}$.

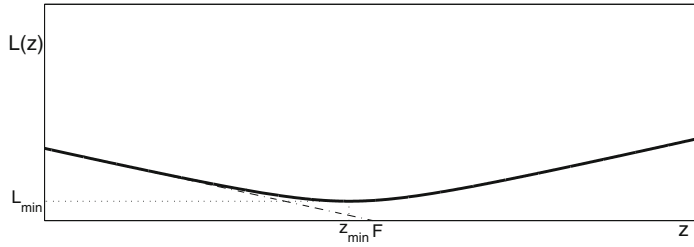


Fig. 2.3 The collapse of a focused input beam under the geometrical optics approximation in linear propagation (dashed line), is arrested by diffraction (solid line)

Since the dimensional beam width is $r_0 L(z)$, see (2.49), the minimal dimensional beam width (*diffraction-limited width*) is

$$r_{\min} = r_0 L_{\min} \approx \frac{F}{k_0 r_0} = \frac{\lambda}{2\pi} \frac{F}{r_0}.$$

Remark One of the earliest indications that propagation of intense laser beams in a bulk medium is nonlinear, was provided by the experiments of Hercher, in which high-power laser beams that propagated in glass created thin threads of damage, whose widths were well below the diffraction-limited widths expected in linear propagation. See Sect. 3.3.1 for further details.

2.11 Diffraction Length (L_{diff})

We now consider the physical meaning of the diffraction length (also called the *Rayleigh length*) $L_{\text{diff}} := k_0 r_0^2$, which appeared in the derivation of (2.51a). We first note that since $k_0 = 2\pi/\lambda$ has units of 1/length, L_{diff} has units of length. It is also easy to see that L_{diff} is the characteristic length scale of z in (2.51a).²⁶ In addition, the solution of (2.51) with a collimated Gaussian input beam ($F = \infty$, $L_z(0) = 0$) is, see (2.56),

$$L^2(z) = 1 + \left(\frac{z}{L_{\text{diff}}} \right)^2.$$

For comparison, in the absence of diffraction (i.e., under the geometrical optics approximation), the beam remains collimated, and so $L^2(z) \equiv 1$.

Conclusion 2.10 *The diffraction length $L_{\text{diff}} := k_0 r_0^2$ is the characteristic distance for diffraction effects, i.e., the characteristic propagation distance over which the beam width undergoes $O(1)$ changes because of diffraction.*

²⁶ Indeed, under the rescaling $\tilde{z} = z/L_{\text{diff}}$, (2.51a) reads $L_{\tilde{z}\tilde{z}} = L^{-3}$, and so $[L_{\tilde{z}\tilde{z}}] = O(1)$.

In other words, L_{diff} is the characteristic distance at which neighboring rays begin to interact with each other, so that the validity of the geometrical optics approximation breaks down.

We can also derive the expression for L_{diff} from a dimensional argument.²⁷ Consider the Schrödinger equation

$$2ik_0\psi_z + \psi_{xx} + \psi_{yy} = 0.$$

If we change to the dimensionless variables

$$\tilde{x} = \frac{x}{r_0}, \quad \tilde{y} = \frac{y}{r_0}, \quad \tilde{z} = \frac{z}{Z}, \quad \tilde{\psi} = \frac{\psi}{E_c},$$

where r_0 and Z are the characteristic length-scales in the transverse and axial directions, respectively, and E_c is the characteristic magnitude of ψ , we get

$$2ik_0 \frac{E_c}{Z} \tilde{\psi}_{\tilde{z}} + \frac{E_c}{r_0^2} \left[\tilde{\psi}_{\tilde{x}\tilde{x}} + \tilde{\psi}_{\tilde{y}\tilde{y}} \right] = 0. \quad (2.58)$$

The diffraction length is the distance Z at which diffraction has an $O(1)$ effect, i.e., $\tilde{\psi}_{\tilde{z}} = O(1)$. This occurs when the two terms in (2.58) are of comparable magnitudes, i.e.,

$$\frac{k_0 E_c}{Z} = \frac{E_c}{r_0^2}.$$

Therefore, $Z = k_0 r_0^2$.

Exercise 2.11 Calculate the diffraction length for an input beam with wavelength $\lambda = 0.5 \mu\text{m}$ and width $r_0 = 1 \text{ cm}$.

In Observation 1.2 we noted that the width of a laser beam is typically much larger than its wavelength (i.e., $r_0 \gg \lambda$). Therefore, there are *three distinct length-scales* in paraxial propagation:

$$\lambda \ll r_0 = [x], [y] \ll L_{\text{diff}} = [z].$$

The ratios between these three length-scales are characterized, however, by a *single* nondimensional parameter, since

$$\frac{\lambda}{r_0} = 2\pi f \quad \text{and} \quad \frac{r_0}{L_{\text{diff}}} = f,$$

²⁷ This approach has the advantage that it applies also to non-Gaussian beams.

where

$$f := \frac{1}{r_0 k_0} \ll 1, \quad (2.59)$$

is the *nonparaxiality parameter*.²⁸

Remark As noted, the characteristic length-scales in x and y are significantly smaller than in z . This anisotropy has nothing to do with the medium, which is assumed to be homogeneous and isotropic. Rather, this anisotropy is induced by the initial condition, which propagates in the z -direction. Thus, it is only because of the initial condition that the dynamics in z occurs on a different length-scale than in x and y .

2.12 The Dimensionless Linear Schrödinger Equation

2.12.1 Paraxial Approximation

In Sect. 1.3 we derived the linear Schrödinger equation by applying the paraxial approximation to the scalar Helmholtz equation. The justification given there for the paraxial approximation was that solutions that propagate in the z -direction are “mainly” composed of paraxial plane waves. We now utilize the understanding that the characteristic length-scale for changes in z is given by the diffraction length (Sect. 2.11), to provide a different informal justification for the paraxial approximation.

Our starting point is the dimensional scalar Helmholtz equation

$$\Delta E(x, y, z) + k_0^2 E = 0.$$

Substituting $E = \psi(x, y, z)e^{ik_0 z}$ gives

$$\psi_{zz}(z, x, y) + 2ik_0 \psi_z + \psi_{xx} + \psi_{yy} = 0, \quad (2.60)$$

which is the Helmholtz equation in terms of ψ . In Sect. 2.11 we saw that the scaling of the independent variables is

$$\tilde{x} = \frac{x}{r_0}, \quad \tilde{y} = \frac{y}{r_0}, \quad \tilde{z} = \frac{z}{2L_{\text{diff}}}, \quad (2.61)$$

where r_0 is the input beam width, and $L_{\text{diff}} = r_0^2 k_0$ is the diffraction length. Substituting (2.61) in (2.60) and multiplying by r_0^2 gives the dimensionless Helmholtz equation

²⁸ See Sects. 1.7 and 2.12.

$$\frac{f^2}{4} \psi_{\tilde{z}\tilde{z}}(\tilde{z}, \tilde{x}, \tilde{y}) + i \psi_{\tilde{z}} + \psi_{\tilde{x}\tilde{x}} + \psi_{\tilde{y}\tilde{y}} = 0, \quad (2.62)$$

where f is given by (2.59).

Typically f^2 is very small (Observation 1.2). Therefore,²⁹

$$f^2 \tilde{\psi}_{\tilde{z}\tilde{z}} \ll \tilde{\psi}_{\tilde{z}}.$$

This suggests that we can apply the *paraxial approximation* and neglect $\tilde{\psi}_{\tilde{z}\tilde{z}}$, i.e., approximate (2.62) by the dimensionless Schrödinger equation

$$i \psi_{\tilde{z}}(\tilde{z}, \tilde{x}, \tilde{y}) + \psi_{\tilde{x}\tilde{x}} + \psi_{\tilde{y}\tilde{y}} = 0. \quad (2.63)$$

Conclusion 2.11 *The paraxial approximation amounts to neglecting $O(f^2)$ terms in the Helmholtz equation.*

Since the relative magnitude of nonparaxial effects is $O(f^2)$, f is called the *nonparaxiality parameter*.

Remark The parameter f also represents the ratio of the length-scale of the transverse and longitudinal coordinates, i.e.,

$$\frac{[x]}{[z]} = \frac{[y]}{[z]} = O(f), \quad (2.64)$$

see Sect. 2.11.

2.12.2 Focused Beams

In Conclusion 2.6 we saw that a lens located at $z = 0$ with a focal point at $(0, 0, F)$ is represented by the quadratic phase term $e^{-i \frac{k_0(x^2+y^2)}{2F}}$. To derive the corresponding expression for the dimensionless Schrödinger equation (2.63), we change to the dimensionless variables (2.61) and $\tilde{F} = \frac{F}{2L_{\text{diff}}}$. This gives

Conclusion 2.12 *In the dimensionless Schrödinger equation (2.63), the effect of a lens located at $\tilde{z} = 0$, whose focal point is at $(0, 0, \tilde{F})$, is represented by adding a quadratic phase term to the initial condition as follows:*

$$\underbrace{\tilde{\psi}_0(\tilde{x}, \tilde{y})}_{\text{no lens}} \rightarrow \underbrace{\tilde{\psi}_0(\tilde{x}, \tilde{y}) e^{-i \frac{\tilde{x}^2 + \tilde{y}^2}{4\tilde{F}}}}_{\text{with lens}}. \quad (2.65)$$

²⁹ This is the dimensionless analog of $\psi_{zz} \ll k_0 \psi_z$.

Remark Since the dimensional and dimensionless Schrödinger equations are $2ik_0\psi_z + \Delta_{\perp}\psi = 0$ and $i\psi_z + \Delta_{\perp}\psi = 0$, respectively, one can obtain the dimensionless expression of the phase by “substituting $k_0 = 1/2$ ” in the dimensional expression.

Exercise 2.12 Verify that $\tilde{F} = O(1) \iff \frac{r_0}{F} = O(f)$. Conclude that if the rescaled focal distance is $O(1)$, the (dimensional) input beam is paraxial.

2.12.3 Tilted Beams

In Conclusion 2.7 we saw that in the dimensional Schrödinger model, a tilt in the direction of the unit vector $\mathbf{n} = (n_x, n_y, n_z)$ is represented by the linear phase term $e^{i\frac{k_0}{n_z}(n_x x + n_y y)}$. To derive the corresponding dimensionless expression, we change to the dimensionless variables (2.61). This yields

$$e^{i\frac{k_0}{n_z}(n_x x + n_y y)} = e^{i\frac{k_0}{n_z}r_0(n_x \tilde{x} + n_y \tilde{y})} = e^{i\frac{c_x \tilde{x} + c_y \tilde{y}}{2}}, \quad (c_x, c_y) = \frac{2r_0 k_0}{n_z} (n_x, n_y).$$

Since the scaling of x and y is different from that of z , the direction of the tilted beam in the dimensionless coordinates is

$$\left(\frac{n_x}{r_0}, \frac{n_y}{r_0}, \frac{n_z}{2L_{\text{diff}}} \right) = \frac{n_z}{2L_{\text{diff}}} (c_x, c_y, 1),$$

i.e., it points in the direction of $(c_x, c_y, 1)$.

Conclusion 2.13 In the dimensionless Schrödinger model (2.63), a tilt of the incoming beam in the direction of the vector $(c_x, c_y, 1)$ is represented by adding a linear phase term to the initial condition as follows:

$$\underbrace{\tilde{\psi}_0(\tilde{x}, \tilde{y})}_{\text{no tilt}} \rightarrow \underbrace{\tilde{\psi}_0(\tilde{x}, \tilde{y})e^{i\frac{c_x \tilde{x} + c_y \tilde{y}}{2}}}_{\text{with tilt}}.$$

Remark The dimensionless tilt angle $\tilde{\theta}$ is given by $\tan \tilde{\theta} = \frac{|\mathbf{c}|}{1} = |\mathbf{c}|$, where $\mathbf{c} = (c_x, c_y)$.

Exercise 2.13 Verify that $\mathbf{c} = O(1) \iff \frac{|\mathbf{n}_{\perp}|}{|n_z|} = O(f)$, where $\mathbf{n}_{\perp} = (n_x, n_y)$. Therefore, if the rescaled tilt angle $\tilde{\theta} = \arctan |\mathbf{c}|$ is $O(1)$, the dimensional tilt angle $\theta = \arctan \frac{|\mathbf{n}_{\perp}|}{|n_z|}$ is $O(f)$, and so the (dimensional) tilted beam is paraxial.

Exercise 2.14 Verify that if the dimensional tilted beam is paraxial, then

$$n_z = 1 + O(f^2). \quad (2.66)$$

Remark In Sect. 8.2 we will re-derive Conclusion 2.13 by using the (exact) Galilean invariance of the Schrödinger equation. This will show that the result of Conclusion 2.13 is exact, which is why in Sect. 2.8.5 we divided the phase by n_z .

2.12.4 Linear Schrödinger Equation in d Dimensions

In what follows, we drop the tilde signs and consider the dimensionless linear Schrödinger equation in d transverse dimensions

$$i\psi_z(z, \mathbf{x}) + \Delta_{\perp}\psi = 0, \quad \psi(0, \mathbf{x}) = \psi_0(\mathbf{x}), \quad (2.67)$$

where

$$\mathbf{x} = (x_1, \dots, x_d) \in \mathbb{R}^d, \quad \Delta_{\perp} = \frac{\partial^2}{\partial x_1^2} + \dots + \frac{\partial^2}{\partial x_d^2}.$$

The physical case of propagation of laser beams in a bulk medium is $d = 2$. Other dimensions, however, are also of physical interest. For example, $d = 1$ corresponds to propagation of laser beams in a planar waveguide, and $d = 3$ to propagation of laser pulses in a bulk medium in the anomalous dispersion regime (Sect. 4.1). The cases $d = 1, 2, 3$ are also of physical interest in quantum mechanics, where linear Schrödinger equation describes the temporal evolution of the quantum state of physical systems. In addition, in the nonlinear case, the cases $d = 1, 2, 3$ are of physical interest in the context of Bose-Einstein condensates (Sect. 4.2).

2.12.5 Generic Input Beams

We now extend the results of Sects. 2.12.2 and 2.12.3 to the d -dimensional linear Schrödinger equation (2.67).

- A real initial condition corresponds to a collimated input beam that propagates in the z -direction.
- A focused input beam that propagates in the z -direction is represented by

$$\psi_0(\mathbf{x}) = A_0(\mathbf{x})e^{-i\frac{|\mathbf{x}|^2}{4F}}, \quad (2.68)$$

where $A_0(\mathbf{x}) = |\psi_0(\mathbf{x})|$ is the beam amplitude, and F is the focal length.

- A tilted focused input beam that propagates in the (\mathbf{x}, z) -space in the direction of the vector $(\mathbf{c}, 1) \in \mathbb{R}^{d+1}$, where $\mathbf{c} = (c_1, \dots, c_d)$, is represented by

$$\psi_0(\mathbf{x}) = A_0(\mathbf{x})e^{-i\frac{|\mathbf{x}|^2}{4F}}e^{i\frac{\mathbf{c}\cdot\mathbf{x}}{2}}. \quad (2.69)$$

2.13 Fourier Transform

Before we begin to analyze the linear Schrödinger equation, let us recall some facts about the Fourier transform. Let $f(\mathbf{x})$ be a function defined for $\mathbf{x} \in \mathbb{R}^d$. The d -dimensional *Fourier transform* of f is

$$\hat{f}(\mathbf{k}) = \mathcal{F}(f(\mathbf{x})) := \frac{1}{(2\pi)^{\frac{d}{2}}} \int_{\mathbb{R}^d} f(\mathbf{x}) e^{-i\mathbf{k}\cdot\mathbf{x}} d\mathbf{x}, \quad (2.70)$$

where $\mathbf{k} = (k_1, \dots, k_d)$. The *inverse Fourier transform* is

$$f(\mathbf{x}) = \mathcal{F}^{-1}(\hat{f}(\mathbf{k})) := \frac{1}{(2\pi)^{\frac{d}{2}}} \int_{\mathbb{R}^d} \hat{f}(\mathbf{k}) e^{i\mathbf{k}\cdot\mathbf{x}} d\mathbf{k}.$$

The inverse Fourier transform of a product is a convolution, i.e.,

$$\mathcal{F}^{-1}(\hat{f}(\mathbf{k})\hat{g}(\mathbf{k})) = f * g(\mathbf{x}), \quad (2.71)$$

where

$$(f * g)(\mathbf{x}) := \frac{1}{(2\pi)^{\frac{d}{2}}} \int_{\mathbb{R}^d} f(\mathbf{x} - \mathbf{y}) g(\mathbf{y}) d\mathbf{y}.$$

The Fourier transform of a Gaussian is a Gaussian, i.e.,

$$\mathcal{F}\left(e^{-p|\mathbf{x}|^2/2}\right) = p^{-\frac{d}{2}} e^{-|\mathbf{k}|^2/2p}, \quad \operatorname{Re}(p) \geq 0. \quad (2.72)$$

Finally, *Parseval's relation* is

$$\int_{\mathbb{R}^d} |f(\mathbf{x})|^2 d\mathbf{x} = \int_{\mathbb{R}^d} |\hat{f}(\mathbf{k})|^2 d\mathbf{k}. \quad (2.73)$$

2.14 L^p , H^1 , and H^2 Norms

For the analysis of the linear Schrödinger equation, we will need the following definitions.

Definition 2.2 (L^p norm) *The L^p norm of a function $f(\mathbf{x})$ is*

$$\|f\|_p := \begin{cases} \left(\int_{\mathbb{R}^d} |f(\mathbf{x})|^p d\mathbf{x} \right)^{\frac{1}{p}}, & \text{if } 1 \leq p < \infty, \\ \sup_{\mathbf{x} \in \mathbb{R}^d} |f(\mathbf{x})|, & \text{if } p = \infty. \end{cases}$$

Definition 2.3 (H^1 norm) *The H^1 norm of $f(\mathbf{x})$ is*

$$\|f\|_{H^1} := \left(\|f\|_2^2 + \|\nabla_{\perp} f\|_2^2 \right)^{\frac{1}{2}} = \left(\int_{\mathbb{R}^d} |f(\mathbf{x})|^2 d\mathbf{x} + \int_{\mathbb{R}^d} |\nabla_{\perp} f(\mathbf{x})|^2 d\mathbf{x} \right)^{\frac{1}{2}},$$

where $\nabla_{\perp} = \left(\frac{\partial}{\partial x_1}, \dots, \frac{\partial}{\partial x_d} \right)$ and $|\nabla_{\perp} f|^2 = |\frac{\partial f}{\partial x_1}|^2 + \dots + |\frac{\partial f}{\partial x_d}|^2$.

Definition 2.4 (H^2 norm) The H^2 norm of $f(\mathbf{x})$ is

$$\|f\|_{H^2} := \left(\|f\|_2^2 + \|\nabla f\|_2^2 + \|\Delta f\|_2^2 \right)^{\frac{1}{2}}.$$

If $\|f\|_p < \infty$, we say that f is in L^p , and similarly for H^1 and H^2 .

2.15 Linear Schrödinger Equation—Analysis

In this section we analyze the linear Schrödinger equation (2.67).

2.15.1 Fundamental Solution

Lemma 2.9 The solution of the linear Schrödinger equation (2.67) is

$$\psi(z, \mathbf{x}) = \frac{1}{(4\pi iz)^{\frac{d}{2}}} \int e^{i\frac{|\mathbf{x}-\mathbf{y}|^2}{4z}} \psi_0(\mathbf{y}) d\mathbf{y}. \quad (2.74)$$

Proof Let $\hat{\psi}(z, \mathbf{k}) = \mathcal{F}(\psi(z, \mathbf{x}))$. Taking the Fourier transform of Eq. (2.67) gives

$$i(\hat{\psi})_z - |\mathbf{k}|^2 \hat{\psi} = 0, \quad \hat{\psi}(0, \mathbf{k}) = \hat{\psi}_0(\mathbf{k}).$$

The solution of this ODE is

$$\hat{\psi}(z, \mathbf{k}) = e^{-i|\mathbf{k}|^2 z} \hat{\psi}_0(\mathbf{k}). \quad (2.75)$$

Therefore, by (2.71),

$$\psi = \mathcal{F}^{-1} \left(e^{-i|\mathbf{k}|^2 z} \right) * \psi_0.$$

Substituting $p = 1/2iz$ in (2.72) gives

$$\mathcal{F}^{-1} \left(e^{-i|\mathbf{k}|^2 z} \right) = \frac{1}{(2iz)^{\frac{d}{2}}} e^{i\frac{|\mathbf{x}|^2}{4z}}. \quad (2.76)$$

Hence, the result follows. \square

Remark A different explicit expression for the solution of (2.67) is given in Lemma 2.14.

If $\psi_0 = \delta(\mathbf{x})$, then $\psi = G$, where

$$G(z, \mathbf{x}) = \frac{1}{(4\pi iz)^{\frac{d}{2}}} e^{i\frac{|\mathbf{x}|^2}{4z}}. \quad (2.77)$$

Therefore, $G(z, \mathbf{x})$ is the fundamental solution of the linear Schrödinger equation (2.67):

Lemma 2.10 *Let G be given by (2.77). Then*

$$iG_z(z, \mathbf{x}) + \Delta_{\perp}G = 0, \quad z > 0, \quad \mathbf{x} \in \mathbb{R}^d,$$

and $\lim_{z \rightarrow 0+} G(z, \mathbf{x}) = \delta(\mathbf{x})$.

The result of Lemma 2.9 can also be rewritten as

Corollary 2.5 *The solution of the linear Schrödinger equation (2.67) is*

$$\psi(z, \mathbf{x}) = (2\pi)^{\frac{d}{2}} G * \psi_0. \quad (2.78)$$

Exercise 2.15 *Prove Lemmas 2.9 and 2.10 directly, by using the definition of G and the relation $\int_{-\infty}^{\infty} e^{is^2} ds = e^{i\pi/4} \sqrt{\pi}$.*

Remark A “careless derivation” of the fundamental solution of the Schrödinger equation is as follows. If we formally make the change of variables $z = -it$, then (2.67) becomes the heat equation $\psi_t(t, \mathbf{x}) = \Delta_{\perp}\psi$. It is well known that the fundamental solution of the heat equation is $G(t, \mathbf{x}) = (4\pi t)^{-\frac{d}{2}} e^{-\frac{|\mathbf{x}|^2}{4t}}$. If we change back from t to z , we “get” that the fundamental solution of the Schrödinger equation is given by (2.77). There is, however, a fundamental difference between these two kernels: The heat kernel is exponentially decaying, hence it is highly regularizing. In contrast, the Schrödinger kernel is oscillatory. Hence, it is only mildly regularizing.

2.15.2 Existence and Smoothness

In Sect. 2.10 we saw that in linear paraxial propagation³⁰ of focused Gaussian input beams, collapse occurs under the geometrical optics approximation, but not if diffraction is not neglected. More generally, one can prove that diffraction prevents singularities in linear optics, by showing that all solutions of the linear Schrödinger equation exist and are bounded for $0 \leq z < \infty$.

³⁰ I.e., in the linear Schrödinger model.

In general, existence and smoothness of solutions of the linear Schrödinger equation (2.67) depend on properties of their initial condition. When ψ_0 corresponds to an input laser beam, we can assume that it is bounded and that it decays sufficiently fast as $|\mathbf{x}| \rightarrow \infty$. In what follows, we present some rigorous results that show that under these conditions, the solution of (2.67) exists for all $z \geq 0$. This implies, in particular, that a focusing lens does not lead to a singularity if one applies the paraxial approximation (i.e., uses the Schrödinger model instead of the Helmholtz model), but does not apply the geometrical optics approximation (i.e., does not neglect diffraction). Therefore, we have

Conclusion 2.14 *Diffraction arrests collapse in linear paraxial propagation.*

Let us begin with the case where $\psi_0 \in L^1$, i.e., $\int_{\mathbb{R}^d} |\psi_0| d\mathbf{x} < \infty$.³¹ By (2.74),

$$\sup_{\mathbf{x} \in \mathbb{R}^d} |\psi(\mathbf{x}, z)| \leq (4\pi z)^{-\frac{d}{2}} \int_{\mathbb{R}^d} |\psi_0| d\mathbf{x}, \quad z > 0.$$

Therefore, the solution of (2.67) is bounded for all $\mathbf{x} \in \mathbb{R}^d$ and $z > 0$. In particular, diffraction prevents the amplitude $|\psi|$ from becoming infinite. Moreover, if $\psi_0 \in L^1$ and has a compact support, then ψ is analytic, since differentiation under the integral sign in (2.74) is justified.

“Unfortunately”, the L^1 norm does not have a physical meaning in optics. Rather, the physical condition that the input beam has a finite power is $\psi_0 \in L^2$, i.e., $\int_{\mathbb{R}^d} |\psi_0|^2 d\mathbf{x} < \infty$. In that case, the following holds:

Lemma 2.11 (conservation of L^2 norm) *Let ψ be a solution of linear Schrödinger equation (2.67), such that $\psi_0 \in L^2(\mathbb{R}^d)$. Then*

$$\|\psi\|_2^2 \equiv \|\psi_0\|_2^2, \quad z > 0,$$

where $\|\psi\|_2^2 := \int_{\mathbb{R}^d} |\psi|^2 d\mathbf{x}$.

Proof By (2.75), $|\hat{\psi}(z, \mathbf{k})| = |\hat{\psi}_0(\mathbf{k})|$. Therefore,

$$\int_{\mathbb{R}^d} |\psi(z, \mathbf{x})|^2 d\mathbf{x} = \int_{\mathbb{R}^d} |\hat{\psi}(z, \mathbf{k})|^2 d\mathbf{k} = \int_{\mathbb{R}^d} |\hat{\psi}_0|^2 d\mathbf{k} = \int_{\mathbb{R}^d} |\psi_0(\mathbf{x})|^2 d\mathbf{x},$$

where in the first and last equalities we used Parseval’s relation (2.73). \square

Remark See Lemma 5.1 for a different proof of this result.

Remark Lemma 2.11 implies that *the power of a laser beam is conserved* in linear paraxial propagation.

³¹ See Sect. 2.14 for definitions of L^p and H^1 norms and spaces.

The NLS theory presented in this book is mostly in H^1 , i.e., for solutions $\psi(z, \mathbf{x})$ such that $\psi(z) \in H^1(\mathbb{R}^d)$, see Sect. 5.5. In particular, an NLS solution becomes singular if and only if its H^1 norm becomes infinite (Corollary 5.3). We now show that in the linear case, the H^1 norm of ψ is conserved:

Corollary 2.6 (conservation of H^1 norm) *Let ψ be a solution of linear Schrödinger equation (2.67), such that $\psi_0 \in H^1$. Then*

$$\|\psi\|_{H^1} \equiv \|\psi_0\|_{H^1}, \quad z > 0,$$

where $\|\psi\|_{H^1}^2 := \int_{\mathbb{R}^d} (|\psi|^2 + |\nabla_{\perp} \psi|^2) d\mathbf{x}$ and $|\nabla_{\perp} \psi|^2 = \sum_{k=1}^d |\frac{\partial \psi}{\partial x_k}|^2$.

Exercise 2.16 *Prove Corollary 2.6.*

Thus, when $\psi_0 \in H^1$, the H^1 norm of the solution ψ of the linear Schrödinger equation does not become infinite. If, in addition, ψ_0 decays sufficiently fast as $|\mathbf{x}| \rightarrow \infty$, then ψ is smooth, since differentiation under the integral sign in (2.74) is justified.

For comprehensive surveys of rigorous results on existence and smoothness of solutions of the linear Schrödinger equation, see e.g., [249, Sect. 3.1] and [39, Chap. 2].

2.15.3 Gaussian Beams

From expression (2.78) follows

Lemma 2.12 *Any solution of the linear Schrödinger equation (2.67) with a Gaussian initial condition maintains a Gaussian profile for all $z > 0$.*

Proof Since the Fourier transform of a Gaussian is a Gaussian, see (2.72), and the product of two Gaussians is a Gaussian, it follows that $\hat{\psi} = e^{-i|\mathbf{k}|^2 z} \hat{\psi}_0$ is a Gaussian. Hence, by (2.72), so is ψ . \square

Lemma 2.12 explains why the Gaussian ansatz (2.49) leads to an exact solution of the linear Schrödinger equation, and also why this aberrationless property is unique to Gaussian profiles in linear propagation. In Sect. 3.5 we shall see that the Gaussian ansatz was also used in nonlinear propagation. In that case, however, it is an *approximation*.

Expression (2.78) enables us to explicitly solve the linear Schrödinger equation with a Gaussian initial condition:

Lemma 2.13 *The solution of the linear Schrödinger equation (2.67) with $\psi_0(\mathbf{x}) = e^{-|\mathbf{x}|^2}$ is*

$$\psi(z, \mathbf{x}) = \frac{1}{(1 + 4iz)^{\frac{d}{2}}} e^{-\frac{|\mathbf{x}|^2}{1+4iz}}. \quad (2.79)$$

Proof Let us first recall that if $G_\sigma(\mathbf{x}) = \left(\frac{1}{2\pi\sigma}\right)^{\frac{d}{2}} e^{-\frac{|\mathbf{x}|^2}{2\sigma}}$, then

$$G_{\sigma_1} * G_{\sigma_2} = \left(\frac{1}{2\pi}\right)^{\frac{d}{2}} G_{\sigma_1+\sigma_2}. \quad (2.80)$$

Indeed, (2.72) implies that $\widehat{G_\sigma} = \left(\frac{1}{2\pi}\right)^{\frac{d}{2}} e^{-\frac{\sigma|\mathbf{k}|^2}{2}}$. Therefore,

$$\widehat{G_{\sigma_1}} \widehat{G_{\sigma_2}} = \left(\frac{1}{2\pi}\right)^d \widehat{G_{\sigma_1+\sigma_2}}.$$

Transforming back and using (2.71) gives (2.80).

Returning to the solution of the linear Schrödinger equation, let us note that $\psi_0 = e^{-|\mathbf{x}|^2} = \pi^{\frac{d}{2}} G_{\sigma=\frac{1}{2}}$, and the Schrödinger kernel (2.77) is equal to $G_{\sigma=2iz}$. By relations (2.78) and (2.80),

$$\psi = (2\pi)^{\frac{d}{2}} G * \psi_0 = (2\pi)^{\frac{d}{2}} G_{2iz} * \pi^{\frac{d}{2}} G_{\frac{1}{2}} = \pi^{\frac{d}{2}} G_{2iz + \frac{1}{2}}.$$

Therefore, we proved (2.79). \square

Remark Expression (2.79) is useful, among other things, for testing the linear part of numerical solvers of the NLS (Sect. 29.5).

We can rewrite (2.79) as

$$\psi(z, \mathbf{x}) = \frac{1}{(1+4iz)^{\frac{d}{2}}} e^{-\frac{1-4iz}{1+16z^2} |\mathbf{x}|^2}.$$

Since

$$|\psi| = \frac{1}{L^{\frac{d}{2}}(z)} e^{-\frac{|\mathbf{x}|^2}{L^2(z)}}, \quad L(z) = \sqrt{1+16z^2},$$

it follows that ψ has a self-similar Gaussian profile, whose width and amplitude are proportional to $L(z)$ and $L^{-\frac{d}{2}}(z)$, respectively. In addition, since

$$\arg \psi(z, \mathbf{x}) = \arg \psi(z, 0) + \frac{4z|\mathbf{x}|^2}{1+16z^2},$$

where

$$\arg \psi(z, 0) = \arg \frac{1}{(1+4iz)^{\frac{d}{2}}} = -\frac{d}{2} \arctan(4z),$$

the real and imaginary parts of ψ develop spatial oscillations, which become ever faster as $|\mathbf{x}| \rightarrow \infty$.

2.15.4 Dispersive Equation

To understand why the Gaussian beam (2.79) develops spatial oscillations, let us first note that $\psi = e^{-i\omega z + i\mathbf{k} \cdot \mathbf{x}}$ is a linear mode of the Schrödinger equation (2.67), provided that ω and \mathbf{k} satisfy the dispersion relation $\omega = |\mathbf{k}|^2$. Therefore, we can explicitly write the solution of the linear Schrödinger equation as follows:

Lemma 2.14 *The solution of the linear Schrödinger equation (2.67) is*

$$\psi(z, \mathbf{x}) = \frac{1}{(2\pi)^{\frac{d}{2}}} \int \hat{\psi}_0(\mathbf{k}) e^{-i\omega(\mathbf{k})z + i\mathbf{k} \cdot \mathbf{x}} d\mathbf{k}, \quad \omega(\mathbf{k}) = |\mathbf{k}|^2. \quad (2.81)$$

The linear modes can be written as

$$e^{-i\omega(\mathbf{k})z + i\mathbf{k} \cdot \mathbf{x}} = e^{-i|\mathbf{k}|(v_{\text{phase}}z - \frac{\mathbf{k}}{|\mathbf{k}|} \cdot \mathbf{x})}, \quad v_{\text{phase}} := \frac{\omega(\mathbf{k})}{|\mathbf{k}|} = |\mathbf{k}|.$$

Since each wavenumber travels at a different phase velocity, “any” solution of the linear Schrödinger equation (and not only Gaussian beams) “disintegrates” and develops spatial oscillations as it propagates.

Exercise 2.17 *Explain why the spatial oscillations become faster as $|\mathbf{x}| \rightarrow \infty$.*

The term *dispersive* is misleading in the context of the Schrödinger equation in optics. Indeed, physical dispersion refers to the situation where different temporal frequencies propagate at different phase velocities $v_{\text{phase}} = c/n_0(\omega)$, see Sect. 35.1.1. Since the Schrödinger equation models the propagation of a single temporal frequency, there is no “physical dispersion” in this model. The “dispersion” in the Schrödinger model should thus be viewed as “mathematical dispersion”, i.e., it has the mathematical properties of physical dispersion. This is analogous (and related) to viewing the variable z in the Schrödinger equation in optics as a “time-like” variable, although z has nothing to do with physical time.³²

2.16 Non-directionality (Reversibility)

In most of this book we will consider the nonlinear Schrödinger equation

$$i\psi_z(z, \mathbf{x}) + \Delta\psi + |\psi|^{2\sigma}\psi = 0, \quad z > 0, \quad \psi(0, \mathbf{x}) = \psi_0(\mathbf{x}). \quad (2.82)$$

³² The dispersive character of the Schrödinger equation in optics is not due to the paraxial approximation, since the linear Helmholtz equation is also “mathematically dispersive”. Indeed, the dispersion relation for the linear modes $E = e^{-i\omega z + i\mathbf{k} \cdot \mathbf{x}}$ of the Helmholtz equation (2.22) is $\omega = \sqrt{k_0^2 - |\mathbf{k}|^2}$, and so $\omega/|\mathbf{k}| \neq \text{constant}$. This dispersion is also mathematical and not optical, since the Helmholtz equation models the propagation of a single temporal frequency.

Both the linear and the nonlinear Schrödinger equation are considered as initial value problems, solved for increasing values of z . Any result for these equations can be applied, however, to the Schrödinger equation with decreasing values of z . This follows from the fact that the Schrödinger equation is invariant under the *reversibility transformation*³³

$$z \rightarrow -z \quad \text{and} \quad \psi \rightarrow \psi^*.$$

Lemma 2.15 *Let $\psi(z, \mathbf{x})$ is a solution of the linear or nonlinear Schrödinger equation with initial condition $\psi_0(\mathbf{x})$. Then $\psi^*(-z, \mathbf{x})$ is a solution of the Schrödinger equation with initial condition $\psi_0^*(\mathbf{x})$.*

In particular, since ψ becomes singular if and only if ψ^* does so, as far as collapse is concerned, it “does not matter” whether the equation is for ψ or for ψ^* .

The reversibility in z of the Schrödinger equation sets it apart from the heat equation $i u_t(t, \mathbf{x}) = \Delta u$, which is well-posed for increasing values of t , but ill-posed for decreasing values of t . In the case of the heat equation, this directionality reflects the difference between moving forward and backward in time. In contrast, in the Schrödinger model, there is no physical difference between increasing z (moving to the right) and decreasing z (moving to the left).

2.16.1 Symmetry with Respect to z_{\min}

The width of a focused Gaussian beam is, see (2.57),

$$L^2(z) = \left(\frac{1}{F^2} + \frac{1}{L_{\text{diff}}^2} \right) (z - z_{\min})^2 + L_{\min}^2,$$

where z_{\min} is the location of the minimal width L_{\min} . Therefore,

$$L(z_{\min} - z) = L(z_{\min} + z),$$

i.e., $L(z)$ is symmetric with respect to z_{\min} . Indeed, because of the non-directionality in z , for any beam collimated at z_{\min} ,³⁴ the propagation dynamics to the right of z_{\min} is the same as that to the left of z_{\min} :

Lemma 2.16 *Let ψ be a solution of the linear or nonlinear Schrödinger equation which is is collimated at z_{\min} , i.e.,*

$$\psi(z_{\min}, \mathbf{x}) = e^{i\alpha} f(\mathbf{x}), \quad \text{where } \alpha \text{ and } f(\mathbf{x}) \text{ are real.} \quad (2.83)$$

³³ This reversibility property also holds for the rays of the eikonal equation (Lemma 2.2).

³⁴ To see that the Gaussian beam is collimated at z_{\min} , note that by (2.49), it can be written as $\psi = A(z, \mathbf{x}) e^{i \frac{L_z(z)}{L} \frac{|\mathbf{x}|^2}{2} + \zeta(z)}$, where A is real. Since $L(z)$ attains its minimum at z_{\min} , then $L_z(z_{\min}) = 0$, and so (2.83) holds. Intuitively, the Gaussian beam is collimated at z_{\min} , since it is focusing for $z < z_{\min}$ and defocusing for $z > z_{\min}$.

Then

$$\psi(z_{\min} + z, \mathbf{x}) = e^{2i\alpha} \psi^*(z_{\min} - z, \mathbf{x}).$$

In particular,

$$|\psi(z_{\min} + z, \mathbf{x})| = |\psi(z_{\min} - z, \mathbf{x})|.$$

Proof Let $\psi_{-\alpha} := e^{-i\alpha}\psi$. Then $\psi_{-\alpha}$ is a solution of the Schrödinger equation that satisfies $\psi_{-\alpha}(z_{\min}, \mathbf{x}) = f(\mathbf{x})$, where $f(\mathbf{x})$ is real. Therefore, by Lemma 2.15, $\psi_{-\alpha}(z_{\min} + z, \mathbf{x}) = \psi_{-\alpha}^*(z_{\min} - z, \mathbf{x})$. Hence, the result follows. \square

Remark In Lemma 38.4 we will use this result to characterize the continuations of singular NLS solutions which are symmetric with respect to the singularity point Z_c .

2.16.2 Sign of Diffraction (and Nonlinearity)

Let $\psi(z, \mathbf{x})$ be a solution of the linear Schrödinger equation

$$i\psi_z(z, \mathbf{x}) + \Delta\psi = 0, \quad z > 0, \quad \psi(0, \mathbf{x}) = \psi_0(\mathbf{x}),$$

where ψ_0 is real. Then, $\psi^*(z, \mathbf{x})$ is a solution of the Schrödinger equation with the opposite sign of diffraction but the same initial condition

$$i\psi_z^*(z, \mathbf{x}) - \Delta\psi^* = 0, \quad z > 0, \quad \psi^*(0, \mathbf{x}) = \psi_0(\mathbf{x}).$$

Since $|\psi| = |\psi^*|$, we conclude that, by itself, the sign of the diffraction term does not affect the dynamics of $|\psi|$.

The above conclusion also holds in the nonlinear case. Indeed, let ψ be a solution of the NLS (2.82), and let ψ_0 be a real function. Then ψ^* is a solution of

$$i\psi_z^*(z, \mathbf{x}) - \Delta\psi^* - |\psi^*|^{2\sigma} \psi^* = 0, \quad z > 0, \quad \psi^*(0, \mathbf{x}) = \psi_0(\mathbf{x}),$$

i.e., of the NLS with the opposite signs of diffraction and nonlinearity but the same initial condition. Since $|\psi| = |\psi^*|$, the sign of nonlinearity by itself does not determine whether the nonlinearity is focusing or defocusing.³⁵

2.17 Singularities in Linear and Nonlinear Optics

In this chapter we saw that under the geometrical optics approximation, solutions of the Helmholtz and Schrödinger equations with initial conditions that correspond to a focused input beam, collapse at the focal point as a δ -function. If one does not

³⁵ Whether the nonlinearity is focusing or defocusing depends on the *relative signs* of nonlinearity and diffraction (Sect. 5.9).

make the geometrical optics approximation, however, these solutions do not shrink to a point.

Conclusion 2.15 *In linear propagation, focused initial conditions become singular if and only if we apply the geometrical optics approximation. In other words, diffraction arrests collapse in linear optics.*

In Sect. 3.4 we shall see that Conclusion 2.15 does not extend to the nonlinear case, i.e., diffraction does not always arrest collapse of NLS solutions.

Since solutions of the linear Schrödinger equation exist globally, we have

Conclusion 2.16 *In linear propagation, the paraxial approximation does not lead to a singularity.*

In Sect. 34.8 we shall see that there exist solutions of the scalar nonlinear Helmholtz equation that exist globally, for which the corresponding NLS solutions become singular. Therefore, Conclusion 2.16 does not extend to nonlinear propagation.

Chapter 3

Early Self-focusing Research

In this chapter we present several key studies from the beginning of self focusing research, which were carried out in the 1960s. Some results of these studies turned out later to be inaccurate, or even incorrect. Nevertheless, there is value in presenting the historical evolution of a research topic, and not just the “final outcome”.

The chapter is organized as follows. In Sect. 3.1 we derive the dimensionless NLH and NLS models. In Sect. 3.2 we use geometrical optics to explain why a Kerr nonlinearity is self focusing. In Sect. 3.3 we present the 1964 paper of Chiao et al. [46] on *self trapping* in a Kerr medium. In Sect. 3.4 we present the 1965 paper of Kelley [140], who predicted that above a certain *critical power*, the Kerr nonlinearity dominates over diffraction, resulting in a *catastrophic collapse*. In Sect. 3.5 we present the 1966 paper of Akhmanov et al. [4], who analyzed the *dynamics* of self focusing using the *aberrationless approximation method*. Section 3.6 presents the 1966 model of Bespalov and Talanov for *multiple filamentation*. Section 3.7 concludes with the “state of the art” in 1975. For more information on the history of self focusing, see the book *Self focusing—past and present* [33].

3.1 Dimensionless NLH and NLS

In this section we derive the dimensionless NLH and NLS models.

3.1.1 Dimensionless NLH

In Sect. 1.6 we saw that the propagation of intense, linearly-polarized cw laser beams in a bulk Kerr medium is governed by the dimensional nonlinear Helmholtz equation (NLH)

$$\Delta_{x,y,z} E(x, y, z) + k^2 E = 0, \quad k^2 = k_0^2 \left(1 + \frac{4n_2}{n_0} |E|^2 \right).$$

Substituting $E = e^{ik_0 z} \psi$ gives

$$\psi_{zz} + 2ik_0\psi_z + \Delta_\perp\psi + k_0^2 \frac{4n_2}{n_0} |\psi|^2 \psi = 0, \quad \Delta_\perp = \frac{\partial^2}{\partial x^2} + \frac{\partial^2}{\partial y^2}. \quad (3.1)$$

By Sects. 2.11 and 2.12.1, the scaling of the independent variables is

$$\tilde{x} = \frac{x}{r_0}, \quad \tilde{y} = \frac{y}{r_0}, \quad \tilde{z} = \frac{z}{2L_{\text{diff}}}, \quad (3.2a)$$

where r_0 is the input-beam width and $L_{\text{diff}} = k_0 r_0^2$ is the diffraction length. Let us also rescale the independent variable ψ as

$$\tilde{\psi} = \frac{\psi}{E_c}, \quad E_c := \max_{x,y} |\psi_0(x,y)|. \quad (3.2b)$$

Applying rescaling (3.2) to (3.1) gives the dimensionless NLH

$$\frac{f^2}{4} \psi_{\tilde{z}\tilde{z}}(\tilde{z}, \tilde{x}, \tilde{y}) + i\tilde{\psi}_{\tilde{z}} + \Delta_\perp \tilde{\psi} + \nu |\tilde{\psi}|^2 \tilde{\psi} = 0, \quad \Delta_\perp = \frac{\partial^2}{\partial \tilde{x}^2} + \frac{\partial^2}{\partial \tilde{y}^2}, \quad (3.3a)$$

where

$$\nu = r_0^2 k_0^2 \frac{4n_2 E_c^2}{n_0}. \quad (3.3b)$$

Therefore, the propagation dynamics in the NLH depends on two dimensionless parameters: The nonparaxiality parameter f , and the nonlinearity parameter ν .

3.1.2 Dimensionless NLS

As in the linear case (Sect. 2.12.1), f^2 is typically very small, and so

$$f^2 \tilde{\psi}_{\tilde{z}\tilde{z}} \ll \tilde{\psi}_{\tilde{z}}.$$

This suggests that one can apply the paraxial approximation and approximate the dimensionless NLH (3.3a) with the dimensionless NLS

$$i\tilde{\psi}_{\tilde{z}}(\tilde{z}, \tilde{x}, \tilde{y}) + \Delta_\perp \tilde{\psi} + \nu |\tilde{\psi}|^2 \tilde{\psi} = 0. \quad (3.4)$$

Note that NLS dynamics depends on ν , but not on f .

In Eqs. (3.3a) and (3.4), the coefficients of diffraction and the Kerr nonlinearity are 1 and ν , respectively. Hence, ν expresses the ratio between the magnitudes of the Kerr effect and diffraction. Thus, when $\nu \ll 1$ diffraction dominates over nonlinearity and the propagation is weakly nonlinear, when $\nu = O(1)$ diffraction and nonlinearity are of comparable magnitudes and the propagation is nonlinear, and when $\nu \gg 1$

nonlinearity dominates over diffraction and the propagation is strongly nonlinear. Therefore, ν is the “*nonlinearity parameter*”.

The parameter ν can be written as

$$\nu = \frac{1}{f^2} \frac{\Delta_{\text{nl}}}{n_0^2},$$

where Δ_{nl}/n_0^2 is the ratio of the nonlinear and linear components of n^2 , see (1.28). Therefore, as already noted in Conclusion 1.4, the magnitude of the Kerr effect is comparable to that of diffraction [i.e., $\nu = O(1)$] when the nonlinear component of the index of refraction is $O(f^2)$ smaller than the linear index of refraction, i.e., when the index of refraction is weakly nonlinear.

3.1.3 No Wavelength in NLS Model

The NLS is the limit of the NLH as $f \rightarrow 0$. Since $f = \lambda/2\pi r_0$, “there is no wavelength” in the NLS model. Indeed, unlike the NLH solution $E = e^{ik_0 z} \psi$ that undergoes fast oscillations at the carrier wavelength, the NLS solution ψ is “just” the slowly-varying envelope.

In the NLH model, we can define a *wide beam* as one whose radius is much larger than its wavelength. This notion of a wide beam does not exist in the NLS model, because there is no wavelength in the NLS model. Thus, NLH solutions can “feel” when the beam width becomes comparable to the wavelength, but NLS solutions cannot. In other words, in the NLH model, the dynamics of an input beam with $r_0 = 10^3 \lambda_0$ is very different from that with $r_0 = 10^{-3} \lambda_0$. In the NLS model, however, their dynamics are identical, up to dilations.¹

3.1.4 Vectorial Effects and Backscattering

In Chap. 1 we derived the scalar Helmholtz equation from the vectorial Helmholtz equation by assuming that the laser beam is linearly polarized. Since this assumption is inconsistent with Maxwell’s equations, the scalar Helmholtz equation is only an approximate model. Indeed, neglecting the effects of E_2 and E_3 on E_1 amounts to neglecting $O(f^2)$ terms, see Sect. 25.3.1 and [45, 76, 77].

The derivation of the NLS from the scalar NLH via the paraxial approximation also amounts to neglecting $O(f^2)$ terms, see Sect. 3.1.2. In fact, this derivation also involves neglecting the backscattered wave that propagates in the negative z -direction. Briefly, the scalar NLH solution can be written as

$$E \sim e^{ik_0 z} \psi(z, x, y) + e^{-ik_0 z} B(z, x, y),$$

¹ This follows from the NLS dilation symmetry (Sect. 8.1).

where ψ and B are the slowly-varying envelopes of the forward and backward moving waves, respectively. Therefore, when passing to the NLS via the substitution $E = e^{ik_0 z} \psi(z, x, y)$, we implicitly assume that the backscattered wave can be neglected. This approximation also amounts to neglecting $O(f^2)$ terms. See Sect. 34.4 for more details.

Conclusion 3.1 *The NLS is the leading-order equation for propagation of paraxial, linearly-polarized cw beams, in which the $O(f^2)$ terms due to nonparaxiality, backscattering, and vectorial effects are neglected.*

3.2 Geometrical Optics Explanation of Self Focusing

The first analytical approach for studying self-focusing was geometrical optics. Indeed, the possibility that strong electromagnetic waves that propagate in a Kerr medium undergo self-focusing was first suggested in 1962 by Askar'yan [8], who predicted that “*the strong ... effects of the ray on the medium can be used to set up waveguide propagation conditions and to eliminate divergence of the beam (self focusing)*”.² This prediction was based on a geometrical optics description of trapping of light by linear waveguides (Sect. 2.2.3). Subsequently, Chiao, Garmire, and Townes used a geometrical optics argument to estimate the critical power for self trapping (Sect. 3.3.2).

We now use geometrical optics to give a simple and intuitive explanation to why a positive Kerr nonlinearity ($n_2 > 0$) leads to self-focusing. Consider a right-propagating collimated Gaussian input beam

$$E_0^{\text{inc}}(x, y) = E_c e^{-\frac{r^2}{r_0^2}}, \quad r = \sqrt{x^2 + y^2}$$

that enters a Kerr medium located in the half-space $z > 0$, see Fig. 1.1. Under the geometrical optics approximation, the beam remains collimated (i.e., the rays remain parallel) and so

$$|E(x, y, z)| \approx E_c e^{-\frac{r^2}{r_0^2}}, \quad z > 0.$$

The electric field induces a nonlinear change in the index of refraction, see (1.28), so that

$$n^2 = n_0^2 + 4n_2 n_0 |E|^2 \approx n_0^2 + 4n_2 n_0 E_c^2 e^{-\frac{2r^2}{r_0^2}}.$$

Thus, $n^2 = n^2(r)$ attains the maximal value of $n_0^2 + 4n_2 n_0 E_c^2$ at $r = 0$, and it decreases monotonically with r . This distribution of n^2 is similar to that of graded-index fibers (Sect. 2.2.3). Therefore, the rays bend towards the beam center. In other

² Askar'yan was the first to use the term *self focusing*.

words, the change in the index of refraction has a focusing effect. Since this focusing effect is caused by the beam (through the changes it induces in the index of refraction) and not by external effects (such as the variations of the linear index of refraction in linear waveguides or a lens), this phenomenon is called *self focusing*.

If the self-focusing effect is stronger than diffraction, the beam intensity increases at and near its center. Hence, so does the index of refraction, see (1.28). Consequently, the Kerr effect becomes stronger with distance. As a result, the self-focusing process accelerates as the beam propagates. This is different from linear waveguides, whose *trapping efficiency* does not change with propagation.

3.2.1 Self Defocusing

A similar geometrical optics analysis shows that a negative Kerr nonlinearity ($n_2 < 0$) leads to *self defocusing*. Indeed, since rays are attracted towards regions with higher index of refraction, they bend away from the beam center.

The Kerr coefficient of most natural materials (e.g., air, water, and silica) is positive. Nevertheless, self defocusing is “physical”. Indeed, in Conclusion 5.1 we will see that whether nonlinearity is self focusing or self defocusing is not determined by its sign, but rather by the relative signs of nonlinearity and diffraction. Therefore, when the sign of diffraction is negative, a positive Kerr nonlinearity is self defocusing. Of course, the sign of diffraction in homogeneous media is always positive. In propagation of laser pulses, however, “diffraction” in time is given by temporal dispersion, whose sign is negative (*normal dispersion*) at most wavelengths, see Sect. 36.2.2.³ Hence, in the normal dispersion regime, a positive Kerr nonlinearity ($n_2 > 0$) leads to temporal self defocusing.

The NLS also models the temporal evolution of *Bose-Einstein condensates* (BEC), where it is usually referred to as the Gross-Pitaevskii equation (Sect. 4.2). In this case, the focusing and defocusing cases correspond to attractive and repulsive interactions, respectively. Both cases are physical.

3.2.2 Coupled Optical Beams

We now show that whether two beams attract or repel each other depends on their relative phases:

Conclusion 3.2 *In a Kerr medium, two beams attract each other when they are in phase ($\phi_0 = 0$), and repel each other when they are out of phase ($\phi_0 = \pi$), where ϕ_0 is the phase difference between the beams.*

³ In addition, diffraction can be negative in waveguide arrays [59].

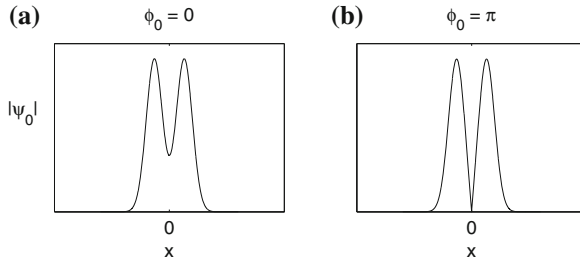


Fig. 3.1 Amplitude of two identical coupled beams when they are **a** in phase, and **b** out of phase

Proof We give an informal proof. Let

$$\psi_0(x, y) = f_1 \left(x - \frac{\Delta_0}{2}, y \right) + e^{i\phi_0} f_2 \left(x + \frac{\Delta_0}{2}, y \right),$$

where $f_i(x, y)$ is a positive radial function localized around the origin (e.g., $f_i = c_i e^{-x^2-y^2}$). This initial condition corresponds to two parallel collimated input beams with spatial separation Δ_0 and phase difference ϕ_0 .

When two beams are in phase, the magnitude of the Kerr nonlinearity in the overlapping area is higher than in the outer sides of the beams (Fig. 3.1a). Since beams are attracted toward regions with a higher index of refraction, each beam “feels” a stronger attraction toward the other beam than toward the outward direction. Hence, the two beams attract each other.

When two beams are out of phase, the magnitude of the Kerr nonlinearity in the overlapping area is lower than in the outer sides of the beams (Fig. 3.1b). Hence, each beam “feels” a stronger attraction toward the outward direction than toward the other beam. Therefore, the two beams repel each other. \square

Remark The dynamics of coupled optical beams will be further discussed in Sects. 27.5 and 39.2.

3.3 Self Trapping [46]

3.3.1 Hercher’s Experiments

In experiments carried out by Hercher in 1964, high-power lasers produced damage in transparent glass samples. The damage had the shape of a long and thin filament, near and beyond the focal point [125].⁴ Chiao et al. [46] noted that it was difficult to explain these experimental results using linear optics, because:

⁴ The full text of Hercher’s manuscript is available at [33].

1. The filaments could be as long as two centimeters, which was considerably longer than the diffraction length (Sect. 2.11).
2. The diameters of the filaments were only a few wavelengths, which in some cases was two orders of magnitude smaller than what would be expected in linear optics (Sect. 2.10).

3.3.2 Self-trapping Analysis

The long filaments observed by Hercher were interpreted by Chiao et al. as nonlinear *self-trapping* of laser beams, i.e., a situation where “an electro-magnetic beam can produce its own dielectric waveguide and propagate without spreading” [46]. In other words, the Kerr nonlinearity induced spatial variations in the index of refraction, similar to those in linear waveguides (Sect. 3.2), which prevented the beam from spreading. Unlike linear waveguides, the glass samples in Hercher’s experiments were homogeneous. Therefore, the variations in the index of refraction could only be induced by the propagating laser beam.

To analyze self trapping of cw laser beams in a Kerr medium, Chiao et al. considered an idealized situation in which the self-trapped filament is uniform and circular with radius r_0 , i.e.,

$$E(z, r) = \begin{cases} E_c, & \text{if } 0 \leq r \leq r_0, \quad z > 0, \\ 0, & \text{if } r_0 < r < \infty, \quad z > 0. \end{cases} \quad (3.5)$$

Therefore, the index of refraction is, see (1.30),⁵

$$n = n_0 + 2n_2|E|^2 = \begin{cases} n_0 + 2n_2E_c^2, & \text{if } 0 \leq r \leq r_0, \quad z > 0, \\ n_0, & \text{if } r_0 < r < \infty, \quad z > 0. \end{cases} \quad (3.6)$$

Chiao et al. argued that a necessary condition for self trapping is that the Kerr nonlinearity will be able to prevent beam spreading due to diffraction. To estimate the magnitude of diffraction, they suggested that at each z , one can view the beam as though it had just passed through a circular aperture with radius r_0 . In that case, the diffraction angle θ_{diff} is given by⁶

$$\theta_{\text{diff}} \approx \frac{1.22\lambda}{2r_0n_0}. \quad (3.7)$$

The magnitude of the Kerr nonlinearity was estimated as follows. By (3.6), the index of refraction inside the beam is higher than outside. Therefore, by Snell’s law,

⁵ Our definition of n_2 is different by a factor of two from the one used by Chiao et al.

⁶ This formula follows from the theory of Fraunhofer diffraction through a circular aperture (see, e.g., [228]).

there is a critical angle θ_{nl} , defined by

$$\cos \theta_{\text{nl}} = \frac{n_0}{n_0 + 2n_2 E_c^2}, \quad (3.8)$$

see (2.17), such that all rays that reach the interface $r = r_0$ at angles smaller than θ_{nl} are reflected backwards. Since the Kerr nonlinearity is weak (i.e., $n_2 E_c^2 \ll n_0$, see Sect. 1.4.3), it follows from (3.8) that $\cos \theta_{\text{nl}} \approx 1$. Hence $\theta_{\text{nl}} \ll 1$, and so (3.8) can be approximated by

$$\left(n_0 + 2n_2 E_c^2 \right) \left(1 - \frac{\theta_{\text{nl}}^2}{2} \right) \approx n_0.$$

Consequently, the critical angle satisfies $\theta_{\text{nl}} \approx 4n_2 E_c^2 / n_0$.

The Kerr nonlinearity can overcome diffraction (i.e., reflect back the diffracting rays) when

$$\theta_{\text{nl}} \geq \theta_{\text{diff}},$$

or equivalently, when

$$\sqrt{\frac{4n_2 E_c^2}{n_0}} \geq \frac{1.22\lambda}{2r_0 n_0}.$$

This inequality can be rewritten as

$$r_0^2 E_c^2 \geq \frac{(1.22\lambda)^2}{16n_0 n_2}. \quad (3.9)$$

To write (3.9) in a more meaningful form, we recall that the input beam power (in MKS units) is

$$P = 2\epsilon_0 n_0 c \int |E_0^{\text{inc}}(x, y)|^2 dx dy.$$

For the uniform circular beam (3.5) we have that $\int |E_0^{\text{inc}}|^2 dx dy = \pi E_c^2$ and so $P = 2\epsilon_0 n_0 c \pi r_0^2 E_c^2$. Hence, condition (3.9) for self trapping reads

$$P \geq P_{\text{cr}}^{\text{Chiao}}, \quad P_{\text{cr}}^{\text{Chiao}} := \frac{\epsilon_0 c \pi (1.22\lambda)^2}{8n_2}. \quad (3.10)$$

Therefore, $P_{\text{cr}}^{\text{Chiao}}$ is the *critical power for self trapping*, according to Chiao et al.

In Retrospect

The analysis of Chiao et al. assumes that the beam can maintain a discontinuous profile during its propagation, and that the strength of the Kerr nonlinearity can be estimated using Snell's law. Both assumptions are based on the geometrical optics

approximation. A less obvious assumption is that self trapping is possible in a Kerr medium. Indeed, it later turned out that this assumption is wrong: NLS solitary waves are unstable, and when perturbed, they either scatter (diffract) or collapse to a point (Sect. 7.11.1).⁷ Thus, the conclusion that beams are self-trapped in a Kerr medium when $P \geq P_{\text{cr}}^{\text{Chiao}}$ is wrong.

The analysis of Chiao et al. correctly showed that whether the Kerr effect is stronger than diffraction is determined by the beam power. In retrospect, there is no reason why beams should “only” be self-trapped when $P > P_{\text{cr}}^{\text{Chiao}}$, since this condition implies that nonlinearity is stronger than diffraction, whereas in self-trapping nonlinearity merely balances diffraction. This interpretation, however, requires to allow for a focusing effect which is not balanced by diffraction, which did not seem possible in 1964. It is interesting to note that if relation (3.10) is re-interpreted as the condition for catastrophic collapse, the value of $P_{\text{cr}}^{\text{Chiao}}$ is surprisingly close to the actual value of the critical power for collapse. See Sects. 24.1.1 and 24.11 for further discussion.

3.3.3 Beyond the Diffraction Limit

To explain Hercher’s observation that the filaments widths were considerably smaller than the linear diffraction limit, Chiao et al. considered radial solitary-wave solutions of the dimensionless NLS

$$i\psi_z(z, r) + \Delta_{\perp}\psi + |\psi|^2\psi = 0, \quad r = \sqrt{x^2 + y^2}.$$

These solutions propagate without changing their transverse shape, as filaments appear to be doing.⁸ Specifically, they considered the NLS solutions

$$\psi_{\omega}^{\text{solitary}}(r, z) = e^{i\omega z} R_{\omega}(r), \quad (3.11)$$

where ω is a real number and R_{ω} is the real solution of

$$-\omega R_{\omega} + \Delta_{\perp} R_{\omega}(r) + R_{\omega}^3 = 0.$$

Since R_{ω} is radial, $R'_{\omega}(0) = 0$ and $\Delta_{\perp} = \frac{d^2}{dr^2} + \frac{1}{r} \frac{d}{dr}$. In addition, since R_{ω} has a finite power, it decays to zero at infinity, i.e., $\lim_{r \rightarrow \infty} R_{\omega}(r) = 0$.

Let

$$R_{\omega}(r) = \omega^{\frac{1}{2}} R\left(\omega^{\frac{1}{2}} r\right). \quad (3.12)$$

⁷ Self trapping is possible if one adds a small collapse-arresting dispersive mechanism (Sect. 31.5), such as a saturating nonlinearity (Sect. 32.4.2) or nonparaxiality (Sect. 34.3).

⁸ It was later shown experimentally that the width of laser filaments undergoes focusing–defocusing oscillations (Sect. 31.5.2).

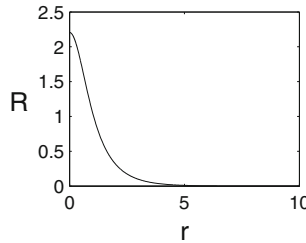


Fig. 3.2 The Townes profile

Then $R(r) := R_{\omega=1}(r)$ is the solution of

$$R''(r) + \frac{1}{r} R' - R + R^3 = 0, \quad 0 < r < \infty, \quad (3.13a)$$

subject to

$$R'(0) = 0, \quad \lim_{r \rightarrow \infty} R(r) = 0. \quad (3.13b)$$

Equation (3.13) is a nonlinear boundary value problem. Since it cannot be solved analytically, Chiao et al. solved it numerically,⁹ and found that it has a positive solution which is monotonically decreasing in r , see Fig. 3.2.¹⁰ This positive solution became known as the *Townes profile*.

Since the radius of $\psi_\omega^{\text{solitary}}$ scales as $\omega^{-\frac{1}{2}}$, see (3.12), and since ω can be arbitrarily large, Chiao et al. concluded that the Kerr nonlinearity can balance diffraction and support filaments whose width is much smaller than the linear diffraction limit, in accordance with Hercher's experiments.

In Retrospect

The analysis of Chiao et al. showed that a Kerr nonlinearity can support solitary waves $\psi_\omega^{\text{solitary}} = e^{i\omega z} R_\omega(r)$ with arbitrarily small radius. As already noted, however, later studies showed that these solitary waves are unstable. Therefore, in retrospect, the explanation of Chiao et al. to Hercher's observation that the width of filaments can be considerably smaller than the diffraction limit, is problematic.

3.4 Optical Collapse [140]

In Chap. 2 we saw that in linear propagation, under the geometrical optics approximation, any focused input beam collapses to a point (blows up/becomes singular) at a finite propagation distance. Once diffraction is added, however, the beam width

⁹ Numerical methods for solving (3.13) are described in Chap. 28.

¹⁰ The boundary value problem (3.13) has an infinite number of solutions. The solution computed by Chiao et al. is the one with the minimal power (the *ground state*), which will be denoted later in this book by $R^{(0)}$. See Sect. 6.4 for more details.

remains positive, and the solution exists for all z . Therefore, we concluded that *in linear optics, singularities can occur under the geometrical optics approximation, but not if diffraction is not neglected.*

In Sect. 3.2 we saw that under the geometrical optics approximation, collimated input beams that propagate in a Kerr medium undergo self-focusing. In Conclusion 3.3 we will see that such beams collapse to a point at a finite propagation distance. It was widely believed, however, that once diffraction is added, it would arrest collapse, much as it does in linear propagation. Probably because of this belief, the early self-focusing studies considered the possibility that nonlinearity can balance diffraction (i.e., self trapping), but did not go so far as to suggest that nonlinearity can dominate over diffraction. It was P.L. Kelley, in his celebrated 1965 Physical Review Letter titled *Self-focusing of optical beams*, who suggested the possibility that “the self-focusing effect . . . is not compensated for by diffraction”, and that, as a result, the intensity would become “anomalously large” after a finite propagation distance [140]. The key contribution of Kelley’s paper is thus the recognition that diffraction cannot always prevent self-focusing beams from collapsing to a point.¹¹

To show that, Kelley used the following dimensional argument. He estimated the self-focusing distance L_{SF} , i.e., the distance over which nonlinearity leads to a significant self-focusing. Then, he argued that when L_{SF} is smaller than the diffraction length L_{diff} , self focusing dominates over diffraction, and so the beam undergoes a “catastrophic collapse”.¹²

3.4.1 Self-focusing Distance (L_{SF})

In what follows, we sketch Kelley’s estimation of L_{SF} . Our starting point is the dimensional NLS

$$2ik_0\psi_z(z, x, y) + \Delta_{\perp}\psi + k_0^2 \frac{4n_2}{n_0} |\psi|^2 \psi = 0, \quad \psi(0, x, y) = \psi_0(x, y) \quad (3.14)$$

with input beams that are sufficiently intense so that initially nonlinearity dominates over diffraction, i.e.,

$$\Delta_{\perp}\psi_0 \ll k_0^2 \frac{4n_2}{n_0} |\psi_0|^2 \psi_0. \quad (3.15)$$

¹¹ Since physical quantities do not become infinite, there must be some other physical mechanisms, which are neglected in the NLS model, that arrest the collapse.

¹² Kelley’s dimensional argument is similar to that of Chiao et al. (Sect. 3.3.2). In retrospect, the condition $\theta_{\text{nl}} \geq \theta_{\text{diff}}$ could have also been interpreted as implying the dominance of nonlinear self-focusing over diffraction. Therefore, the analysis of Chiao et al. could (and should) be reinterpreted as implying that the beam collapses if $P \geq P_{\text{cr}}^{\text{Chiao}}$. The relation between the critical power for self trapping and for collapse is further explored in Sect. 24.11.

By continuity, during the initial stage of the propagation

$$\Delta_{\perp} \psi \ll k_0^2 \frac{4n_2}{n_0} |\psi|^2 \psi. \quad (3.16)$$

Therefore, the NLS (3.14) reduces to

$$2ik_0\psi_z + k_0^2 \frac{4n_2}{n_0} |\psi|^2 \psi = 0, \quad \psi(0, x, y) = \psi_0(x, y). \quad (3.17)$$

This ODE can be solved explicitly:

Lemma 3.1 *The solution of (3.17) is*

$$\psi_{\text{SPM}}(z, x, y) := \psi_0(x, y) e^{ik_0 S^{(\psi)}(z, x, y)}, \quad S^{(\psi)} = \frac{2n_2}{n_0} |\psi_0(x, y)|^2 z. \quad (3.18)$$

Proof This can be verified by direct substitution. \square

The explicit solution (3.18) shows that the Kerr nonlinearity induces phase modulations, a nonlinear phenomenon called *selfphase modulations* (SPM). Consequently, since the rays are perpendicular to the wavefronts of the Helmholtz solution, they bend as they propagate. To visualize that, we recall that the phases of the Helmholtz and NLS solutions are related through $k_0 S^{(E)} = k_0 (z + S^{(\psi)})$, see (2.31).¹³ Therefore, the Helmholtz solution that corresponds to the (approximate) NLS solution (3.18) satisfies

$$S^{(E)}(x, y, z) = S^{(\psi)}(x, y, 0) + z \left(1 + \frac{2n_2}{n_0} |\psi_0(x, y)|^2 \right). \quad (3.19)$$

Hence, as z increases, the level sets of $S^{(E)}$ become more and more depressed at the beam center where the beam is most intense. Since rays are parallel to $\nabla S^{(E)}$, this implies that as z increases the rays bend more and more towards the beam center (Fig. 3.3). In other words, the beam becomes narrower with propagation.

As a result of this nonlinear self-focusing, the intensity near the beam axis increases. These transverse intensity changes, however, are not captured by the diffractionless NLS (3.17). Therefore, to model the transverse intensity changes, we should include the diffraction term. This may seem counterintuitive, as diffraction is expected to defocus the beam. This “expectation”, however, is based on a linear approach, in which the overall dynamics is a superposition of the separate effect of each term. Such a linear approach is inappropriate for the NLS, and in particular in the strongly-nonlinear regime (3.16).¹⁴

¹³ This analysis can also be carried using the NLS model (Sect. 26.1).

¹⁴ Another example that NLS dynamics is not a superposition of the separate effects of nonlinearity and diffraction, is that the effect of nonlinearity (i.e., whether it is focusing or defocusing) depends on the sign of the diffraction term (Conclusion 5.1). For more examples, see Sects. 26.3.2, 30.4, and 36.8.1.

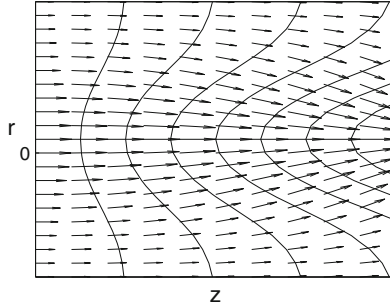


Fig. 3.3 Bending of rays (arrows) towards the beam center. The solid lines are the wavefronts $S^{(E)} \equiv \text{constant}$, where $S^{(E)} = z \left(1 + \frac{2n_2}{n_0} e^{-\frac{r^2}{r_0^2}} \right)$

The characteristic distance for intensity changes was estimated by Kelley from the condition that $2ik_0\psi_z$ and $\Delta_{\perp}\psi$ have the same magnitude,^{15, 16} i.e.,

$$[2ik_0\psi_z] = [\Delta_{\perp}\psi],$$

where $\psi \approx \psi_{\text{SPM}}$, see (3.18). Now,

$$\Delta_{\perp}\psi \approx \Delta_{\perp}\psi_{\text{SPM}} = \Delta_{\perp} \left(\psi_0 e^{ik_0 S^{(\psi)}} \right), \quad S^{(\psi)} = \frac{2n_2}{n_0} |\psi_0(x, y)|^2 z.$$

Since $\Delta_{\perp}\psi_0$ is “small”, see (3.15), the self-focusing dynamics is driven by the induced self-phase modulations. Therefore, $\Delta_{\perp}\psi_{\text{SPM}} \approx \psi_0 \Delta_{\perp} e^{ik_0 S^{(\psi)}}$.

In order to proceed, consider the collimated Gaussian input beam $\psi_0 = E_c e^{-\frac{r^2}{2r_0^2}}$. For this beam $\psi_{\text{SPM}} = E_c e^{-\frac{r^2}{2r_0^2} + ik_0 S^{(\psi)}}$, where $S^{(\psi)} = \frac{2n_2}{n_0} E_c^2 e^{-\frac{r^2}{r_0^2}}$. Since the highest intensity is at $r = 0$, nonlinear effects are most pronounced near $r = 0$. Therefore, we can estimate the magnitudes of ψ_z and $\Delta_{\perp}\psi = \psi_{rr} + \frac{1}{r}\psi_r$ from their values at $r = 0$:

$$[2ik_0\psi_z] = \frac{2k_0 E_c}{Z}, \quad [\Delta_{\perp}\psi] \approx [\psi_0] \left[\Delta_{\perp} e^{ik_0 S^{(\psi)}} \right] = E_c k_0 Z \frac{2n_2}{n_0} \frac{4E_c^2}{r_0^2},$$

where Z is the (yet unknown) characteristic length of z . These two terms are of comparable magnitudes if

$$Z = \frac{r_0}{2E_c} \sqrt{\frac{n_0}{n_2}}.$$

¹⁵ When this condition holds, $\Delta_{\perp}\psi$ leads to $O(1)$ changes in the solution. Therefore, it is no longer justified to neglect diffraction (i.e., approximation (3.18) is no longer valid).

¹⁶ In Sect. 2.11 we used a similar argument to estimate the diffraction length.

Corollary 3.1 *The characteristic distance for intensity and width changes due to self-focusing is*

$$L_{\text{SF}} = \frac{r_0}{2E_c} \sqrt{\frac{n_0}{n_2}}. \quad (3.20)$$

Since the beam power P scales as $r_0^2 E_c^2$, the self-focusing distance scales as

$$L_{\text{SF}} \sim \frac{r_0^2}{\sqrt{P}}. \quad (3.21)$$

3.4.2 Critical Power for Collapse

Beam propagation in a Kerr medium is characterized by the competition between the focusing nonlinearity and diffraction. Since nonlinearity dominates when $L_{\text{diff}} \gg L_{\text{SF}}$ and diffraction dominates when $L_{\text{diff}} \ll L_{\text{SF}}$, the condition for dominance of nonlinearity over diffraction can be estimated from the inequality

$$L_{\text{diff}} \geq L_{\text{SF}}. \quad (3.22)$$

The value of the diffraction length used by Kelley was $L_{\text{diff}} = \frac{r_0}{\theta_{\text{diff}}} = \frac{2r_0^2 n_0}{1.22\lambda}$, where θ_{diff} is given by (3.7).^{17,18} Substitution in (3.22) gives

$$r_0^2 E_c^2 \geq \frac{(1.22\lambda)^2}{16n_0 n_2},$$

which is the same as condition (3.9) of Chiao et al. Hence, as in Sect. 3.3.2, this inequality can be rewritten as

$$P \geq P_{\text{cr}}^{\text{Chiao}}, \quad (3.23)$$

where $P_{\text{cr}}^{\text{Chiao}}$ is given by (3.10).¹⁹ Unlike Chiao et al., however, Kelley correctly interpreted (3.23) as implying that diffraction is unable to arrest beam collapse driven by the Kerr nonlinearity, rather than that nonlinearity is able to prevent beam spreading due to diffraction (i.e., self trapping).

¹⁷ This expression for L_{diff} differs by a factor of $\frac{n_0}{1.22\pi}$ from our definition $L_{\text{diff}} = k_0 r_0^2$.

¹⁸ The motivation for this expression is as follows. At the propagation distance z , the beam radius increases by $z \tan \theta_{\text{diff}} \approx z\theta_{\text{diff}}$. Therefore, the beam radius undergoes $O(1)$ changes at $z = \frac{r_0}{\theta_{\text{diff}}}$.

¹⁹ The value of the critical power obtained by Kelley was one-fourth of that obtained by Chiao et al., since he defined L_{SF} to be one-half of expression (3.20). Such differences are to be expected in dimensional arguments, where multiplicative constants in definitions of characteristic distances are arbitrary.

Kelley's analysis suggested that catastrophic self-focusing occurs when the beam power exceeds the critical value $P_{\text{cr}}^{\text{Chiao}}$. This value is proportional to the square of the wavelength, and is inversely proportional to the Kerr coefficient n_2 . *The critical power, however, does not depend on the input-beam width r_0 .* At first, this may seem counterintuitive, since a narrower input beam may seem more likely to collapse. Note, however, that if we change the input-beam width by a factor of L_0 while keeping the input power $\int |\psi_0|^2 dx dy$ fixed, the initial condition changes from $\psi_0(x, y)$ to $\frac{1}{L_0} \psi_0(\frac{x}{L_0}, \frac{y}{L_0})$. Since both nonlinearity and diffraction scale as L_0^{-3} , changing the input-beam width while keeping its power fixed does not affect the balance between nonlinearity and diffraction. This explains why the critical power is independent of r_0 , as indeed was confirmed experimentally in 1966 by Wang [267].

Remark See Chap. 24 for further discussion of the critical power.

3.4.3 First Simulations of Blowup Solutions

Kelley's conclusion that collapse of high-power beams is not arrested by diffraction, was based on an informal dimensional argument. Kelley supported this conclusion with numerical simulations. For example, in Fig. 3.4 Kelley solved the NLS with a Gaussian initial condition and observed that the on-axis amplitude is fairly constant during the early stages of the propagation. Then, “all of a sudden”, it undergoes an abrupt increase “towards infinity”²⁰

In Kelley's simulation, the on-axis intensity only increased by a factor of 10. Even this level of focusing was a numerical challenge at the time, because of the steep gradients in z and r that develop near the singularity. For a more “modern” simulation of a singular NLS solution, see, e.g., Fig. 14.8.

3.4.4 In Retrospect

Kelley's 1965 article was the starting point of the research on singular NLS solutions, which is the main topic of this book. This three-page letter touched upon many of the issues that later played an important role in NLS research, such as conditions for a singularity, simulations of blowup solutions, location of the blowup point, and the blowup rate. Kelley was also careful to note that the validity of the paraxial approximation breaks down near the NLS blowup point, and therefore that predictions based on the NLS model are not valid within a few wavelengths from the blowup point.

²⁰ The acceleration of the self-focusing process was discussed in Sect. 3.2.

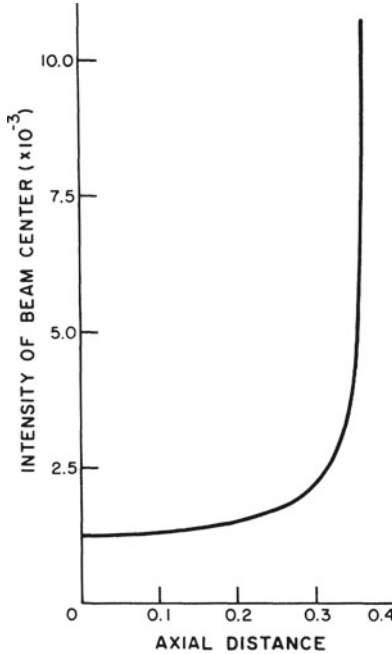


Fig. 3.4 Kelley's simulation of a collapsing NLS solution. From [140]

3.5 Aberrationless Approximation Method [4]

In the papers of Chiao et al. and Kelley, the analysis was based on a comparison between the magnitudes of the Kerr nonlinearity (θ_{nl} , $\frac{1}{L_{SF}}$) and diffraction (θ_{diff} , $\frac{1}{L_{diff}}$). This dimensional argument showed that nonlinearity is stronger than diffraction when the input power exceeds a certain critical value, but did not reveal the self-focusing *dynamics*.

The first analysis of the self-focusing dynamics was performed in 1966 by Akhmanov et al. [4] using the *aberrationless approximation method*, as follows. Consider the radial NLS

$$2ik_0\psi_z(z, r) + \Delta_\perp\psi + k_0^2 \frac{4n_2}{n_0} |\psi|^2 \psi = 0, \quad (3.24a)$$

with the focused Gaussian input beam

$$\psi_0(r) = E_c e^{\frac{-r^2}{2r_0^2}} e^{-i \frac{k_0 r^2}{2F}}, \quad (3.24b)$$

where r_0 is the input beam width and F is the focal length of the lens. As in the linear case (Sect. 2.10), let $\psi = A(z, r)e^{ik_0 S(z, r)}$, where S and A are real.²¹ Substitution in (3.24a) gives

$$-2k_0^2 AS_z + 2ik_0 A_z + \Delta_{\perp} A + 2ik_0 A_r S_r + A \left[-k_0^2 S_r^2 + ik_0 \Delta_{\perp} S \right] + k_0^2 \frac{4n_2}{n_0} A^3 = 0.$$

The equations for the real and imaginary parts are

$$2S_z + (S_r)^2 = \frac{1}{k_0^2} \frac{\Delta_{\perp} A}{A} + \frac{4n_2}{n_0} A^2, \quad (A^2)_z + S_r (A^2)_r + A^2 \Delta_{\perp} S = 0, \quad (3.25)$$

respectively, with the initial conditions

$$S(z=0, r) = -\frac{r^2}{2F}, \quad A^2(z=0, r) = E_c^2 e^{-\frac{r^2}{r_0^2}}. \quad (3.26)$$

Motivated by the success of the Gaussian ansatz in linear propagation (Sect. 2.10), we look for a solution of (3.25) of the form

$$S = \frac{a(z)r^2}{2} + \zeta(z), \quad A^2 = \frac{E_c^2}{L^2(z)} e^{-\frac{r^2}{r_0^2 L^2}}. \quad (3.27)$$

Unlike the linear case, however, the Gaussian ansatz (3.27) does not correspond to an exact solution of the NLS. Therefore, in order to proceed, we restrict our attention to the near-axis region where the main nonlinear dynamics takes place, i.e., to $0 \leq r \ll r_0 L(z)$. In this region, we can expand A^2 in a Taylor series in r , i.e.,

$$A^2 = \frac{E_c^2}{L^2(z)} \left(1 - \frac{r^2}{r_0^2 L^2} + O\left(\frac{r^4}{r_0^4 L^4}\right) \right).$$

Exercise 3.1 Show that if we substitute the ansatz (3.27) in (3.25) and neglect $O\left(\frac{r^4}{r_0^4 L^4}\right)$ terms, the equations for $L(z)$, $a(z)$, and $\zeta(z)$ are

$$a_z + a^2 = \left[\frac{1}{k_0^2 r_0^4} - \frac{4n_2 E_c^2}{n_0 r_0^2} \right] \frac{1}{L^4}, \quad \zeta_z = \left[-\frac{1}{k_0^2 r_0^2} + \frac{2n_2 E_c^2}{n_0} \right] \frac{1}{L^2}, \quad \frac{L_z}{L} = a, \quad (3.28)$$

subject to

$$a(0) = -\frac{1}{F}, \quad \zeta(0) = 0, \quad L(0) = 1.$$

²¹ Here $S = S^{(\psi)}$, the phase of the NLS solution.

Therefore, the aberrationless approximation method replaces a nonlinear PDE (the NLS) with a system of ODEs, see (3.28). Moreover, as in Sect. 2.10, Eq. (3.28) can be solved explicitly, as follows. Since $a^2 + a_z = L_{zz}/L$, the equation for $L(z)$ reads

$$L_{zz}(z) = \left[\frac{1}{L_{\text{diff}}^2} - \frac{1}{L_{\text{SF}}^2} \right] \frac{1}{L^3}, \quad (3.29a)$$

where $L_{\text{diff}} = k_0 r_0^2$ is the *diffraction length* and $L_{\text{SF}} = \frac{r_0}{2E_c} \sqrt{\frac{n_0}{n_2}}$ is the *self-focusing distance*.²² The initial conditions for (3.29a) are

$$L(0) = 1, \quad L_z(0) = -\frac{1}{F}. \quad (3.29b)$$

Therefore, the beam dynamics is determined by the competing effects of diffraction and nonlinearity (first and second terms on the right-hand side of (3.29b), respectively), and by the lens at $z = 0$, see (3.29b).

By Lemma 2.8, the solution of (3.29) is

$$L^2(z) = \left(1 - \frac{z}{F}\right)^2 + \frac{z^2}{L_{\text{diff}}^2} - \frac{z^2}{L_{\text{SF}}^2}. \quad (3.30)$$

Therefore, we obtained a complete description of the self-focusing dynamics in the presence of a focusing (or defocusing) lens, diffraction, and nonlinearity (the three terms on the right-hand side of (3.30), respectively).

To determine whether the beam collapses, i.e., whether there exists $Z_c^{(F)} > 0$ such that $L(Z_c^{(F)}) = 0$,²³ we rewrite (3.30) as

$$L^2(z) = \left(\frac{1}{F^2} + \frac{1}{L_{\text{diff}}^2} - \frac{1}{L_{\text{SF}}^2} \right) z^2 - \frac{2}{F} z + 1.$$

Substituting $L = 0$ and solving for $Z_c^{(F)}$ gives

$$Z_c^{(F)} = \frac{\frac{1}{F} \pm \sqrt{\frac{1}{L_{\text{SF}}^2} - \frac{1}{L_{\text{diff}}^2}}}{\frac{1}{F^2} - \left(\frac{1}{L_{\text{SF}}^2} - \frac{1}{L_{\text{diff}}^2} \right)} = \frac{1}{\frac{1}{F} \mp \sqrt{\frac{1}{L_{\text{SF}}^2} - \frac{1}{L_{\text{diff}}^2}}}.$$

²² See Sects. 2.11 and 3.4.1, respectively.

²³ If there are two positive roots, only the smaller one corresponds to optical collapse, because the validity of the NLS model breaks down at the (first) collapse point.

Therefore, $Z_c^{(F)}$ satisfies the lens relation

$$\frac{1}{Z_c^{(F)}} = \frac{1}{F} \pm \frac{1}{Z_c}, \quad Z_c := \left(\frac{1}{L_{SF}^2} - \frac{1}{L_{\text{diff}}^2} \right)^{-\frac{1}{2}}. \quad (3.31)$$

In particular, in the case of a collimated beam ($F = \infty$),

$$\frac{1}{Z_c^{(F)}} = \pm \frac{1}{Z_c}.$$

Therefore, if Z_c as defined in (3.31) is real, it corresponds to the collapse distance of the collimated beam.

Since $Z_c^{(F)}$ should be real, we immediately see that a necessary condition for collapse is $L_{SF}^2 > 0$. This, in turn, is the case if and only if $n_2 > 0$, i.e., if the Kerr nonlinearity is focusing. Therefore, from now on we only consider the focusing case $n_2 > 0$.

Let us begin with the geometrical optics limit $k_0 \rightarrow \infty$, i.e., when diffraction is neglected ($L_{\text{diff}} = \infty$). In that case $Z_c = L_{SF}$, and the following possibilities exist:

1. **Collimated beam ($F = \infty$)**: The beam collapses at $Z_c^{(F)} = L_{SF}$. By (3.21), the collapse distance decreases as the beam power increases.
2. **Converging beam ($0 < F < \infty$)**: The beam collapses at $Z_c^{(F)} = (\frac{1}{L_{SF}} + \frac{1}{F})^{-1}$. As expected, the collapse distance is shorter than for the collimated beam (i.e., $Z_c^{(F)} < Z_c$), and it decreases monotonically as the lens power $1/F$ increases.

If $0 < F < L_{SF}$, then the second root $(\frac{1}{F} - \frac{1}{L_{SF}})^{-1}$ is also positive. This second root is not a collapse point, however, since it is larger than the first (positive) root $(\frac{1}{F} + \frac{1}{L_{SF}})^{-1}$.

3. **Weakly-diverging beam ($F < -L_{SF} < 0$)**: The beam collapses at $Z_c^{(F)} = (\frac{1}{L_{SF}} + \frac{1}{F})^{-1}$. As expected, the collapse distance is longer than for the collimated beam (i.e., $Z_c^{(F)} > Z_c$), and it increases monotonically as $1/|F|$ increases.
4. **Strongly-diverging beam ($-L_{SF} < F < 0$)**: The beam does not collapse.

Conclusion 3.3 *Under the geometrical optics, paraxial, and aberrationless approximations:*

1. Any collimated, focused, or weakly-defocused input beam that propagates in a focusing Kerr medium will collapse to a point at a finite propagation distance.

2. A defocusing lens arrests collapse if and only if it is stronger than the Kerr effect, i.e., if $-L_{\text{SF}} < F < 0$.

When diffraction is included, the requirement that $Z_c^{(F)}$ be real implies that $n_2 > 0$ and $L_{\text{SF}} \leq L_{\text{diff}}$, i.e., that the Kerr effect is focusing and is stronger than diffraction. As in Sect. 3.4.2, this condition reads

$$E_c^2 r_0^2 \geq \frac{n_0}{4n_2 k_0^2} = \frac{\lambda^2 n_0}{16\pi^2 n_2},$$

or

$$P \geq P_{\text{cr}}^{\text{Akhmanov}}, \quad P_{\text{cr}}^{\text{Akhmanov}} = \frac{\epsilon_0 c n_0^2}{8\pi n_2}. \quad (3.32)$$

Therefore, $P_{\text{cr}}^{\text{Akhmanov}} = \frac{n_0^2}{1.222\pi^2} P_{\text{cr}}^{\text{Chiao}}$, where $P_{\text{cr}}^{\text{Chiao}}$ is the critical power obtained by Chiao et al., see (3.10).²⁴ Thus, under the aberrationless approximation, if $P < P_{\text{cr}}^{\text{Akhmanov}}$ there is no collapse. If $P > P_{\text{cr}}^{\text{Akhmanov}}$, however, the following possibilities exist:

1. **Collimated beam ($F = \infty$)**: The beam collapses at $Z_c^{(F)} = Z_c$, where

$$Z_c := \left(\frac{1}{L_{\text{SF}}^2} - \frac{1}{L_{\text{diff}}^2} \right)^{-\frac{1}{2}}.$$

As expected, $Z_c > L_{\text{SF}}$, i.e., the collapse distance is longer than in the diffractionless case.

2. **Converging beam ($0 < F < \infty$)**: The beam collapses at $Z_c^{(F)} = \left(\frac{1}{Z_c} + \frac{1}{F} \right)^{-1}$. As expected, the collapse distance decreases monotonically as the lens power $1/F$ increases.
3. **Weakly-diverging beam ($F < -Z_c$)**: The beam collapses at $Z_c^{(F)} = \left(\frac{1}{Z_c} + \frac{1}{F} \right)^{-1}$. As expected, the collapse distance increases monotonically as $1/|F|$ increases.
4. **Strongly-diverging beam ($-Z_c < F < 0$)**: The beam does not collapse.

²⁴ The actual value of the critical power is within a few percent from $P_{\text{cr}}^{\text{Chiao}}$, see Sect. 24.1.1. Hence, the critical power $P_{\text{cr}}^{\text{Akhmanov}}$, which was derived under the aberrationless approximation method, is off by a factor of ≈ 10 . Indeed, predictions of the critical power which are based on the aberrationless approximation can be very inaccurate (Observation 24.4).

Conclusion 3.4 *Under the paraxial and aberrationless approximations:*

1. *A necessary condition for collapse is $L_{\text{SF}} \leq L_{\text{diff}}$, i.e., the focusing nonlinearity is stronger than diffraction. This condition holds when $P \geq P_{\text{cr}}^{\text{Akhmanov}}$.*
2. *A sufficient condition for collapse is $\frac{1}{F^2} < \frac{1}{Z_c^2}$, or equivalently*

$$\frac{1}{L_{\text{SF}}^2} > \frac{1}{L_{\text{diff}}^2} + \frac{1}{F^2}, \quad (3.33)$$

i.e., the focusing nonlinearity is stronger than the combined effects of diffraction and the lens.

Remark In Theorem 7.2 we will rigorously prove that solutions of the NLS (3.24a) always collapse when their initial Hamiltonian is negative, i.e.,

$$H(0) := \int |\nabla_{\perp} \psi_0|^2 dx dy - k_0^2 \frac{2n_2}{n_0} \int |\psi_0|^4 dx dy < 0.$$

It can be verified that for the initial condition (3.24b),

$$H(0) = \frac{E_c^2 k_0^2 r_0^4}{2} \left(\frac{1}{L_{\text{diff}}^2} + \frac{1}{F^2} - \frac{1}{8L_{\text{SF}}^2} \right).$$

Therefore,

- The sufficient condition (3.33) is essentially the negative Hamiltonian condition, up to the $\frac{1}{8}$ multiplicative constant which is “missed” by the aberrationless approximation.
- The physical interpretation of the condition $H(0) < 0$ is that the focusing nonlinearity is stronger than the combined effects of diffraction and the lens.²⁵

3.5.1 Effect of a Lens

The predictions of the aberrationless approximation method on the effect of a lens can be summarized as follows:

1. If the beam power is below critical, the beam will not collapse, even if focused by a powerful lens.

²⁵ We will re-derive this interpretation in Sect. 7.5.

2. The relation between the collapse distance with and without a lens is

$$\frac{1}{Z_c^{(F)}} = \frac{1}{F} + \frac{1}{Z_c}. \quad (3.34)$$

3. If a collimated beam collapses at Z_c , adding a defocusing lens arrests collapse if and only if the lens is stronger than the balance between the Kerr nonlinearity and diffraction, i.e., if $-Z_c < F < 0$. Otherwise, adding a defocusing lens only delays the collapse, and adding a focusing lens accelerates it.

In what follows, we will prove these predictions rigorously (i.e., without using the aberrationless approximation), see Theorem 5.11, Sect. 8.4.5, and Lemma 8.5, respectively. In particular, we will see that the lens relation (3.34) is an exact result.

3.5.2 Blowup Rate

As noted, one advantage of the aberrationless approximation method is that it provides information of the collapse dynamics. For example, we have

Conclusion 3.5 *Under the aberrationless approximation, the blowup rate of $L(z)$ is a square root.*

Proof Equation (3.30) can be rewritten as $L^2(z) = \left(1 - \frac{z}{Z_c^{(F)}}\right)\left(1 - \frac{z}{Z_c^{(2)}}\right)$, where $Z_c^{(2)}$ is the second root of the quadratic equation $L^2(z) = 0$. Therefore, $L(z) \sim c(Z_c^{(F)} - z)^{\frac{1}{2}}$ as $z \rightarrow Z_c^{(F)}$. \square

3.5.3 In Retrospect

The aberrationless approximation method was very successful in advancing the understanding of self-focusing dynamics. Thus, it provided an analytic approximation for the beam width $L(z)$ and for the collapse distance, it predicted the effect of a lens on the possibility of collapse and on the collapse distance, and it provided a reasonable prediction for the blowup rate.²⁶

Following Akhmanov et al., the aberrationless approximation method became popular in self-focusing analysis, and for a good reason, as it provides a simple method for deriving reduced equations that do not depend on the transverse

²⁶ The actual blowup rate is slightly faster than a square root, due to a double logarithmic correction (Chap. 18).

coordinates. It gradually became clear, however, that predictions based on the original aberrationless approximation method of Akhmanov et al. can be quantitatively inaccurate or even qualitatively incorrect [6, 55, 165]. Consequently, various modifications were suggested, such as using a variational approach [55], and replacing the Gaussian ansatz with super-Gaussian or sech profile [55, 138]. These methods were sometimes called the *variational method* and the *collective coordinate method*. Nevertheless, all these methods are essentially the same, as they are based on the aberrationless approximation, i.e., the assumption that the beam maintains a self-similar profile during its propagation. As a result, all these methods can lead to predictions that are quantitatively or qualitatively incorrect.

In Sect. 7.9 we will discuss why the assumption of aberrationless self focusing is problematic, and in Sect. 24.3.2 we will explain why the aberrationless approximation leads to significant over-estimates of the critical power. In Chap. 31 we will present an alternative method for deriving reduced equations, called *modulation theory*, which does not suffer from the weaknesses of aberrationless approximation methods. For further discussion of the failure of the aberrationless approximation in self focusing, see [75].

3.6 Multiple Filamentation [27]

Experiments carried out during the early 1960s showed that when the input power is much larger than the critical power for collapse, the beam can break up into several long and narrow filaments. This phenomenon has been called *multiple filamentation*, *small-scale self focusing*, and *beam breakup*. In this section we present the theoretical model proposed by Bespalov and Talanov for multiple filamentation.

3.6.1 Early Experiments

In 1965, Pilipetskii and Rustamov [209] carried out self-focusing experiments and observed that in some cases, a single input beam produced two or three filaments. Bespalov and Talanov [27] noted that when several filaments were formed, the collapse distance of the filaments was at least one order of magnitude shorter than for an equal-power beam that collapsed as a single filament. In 1966, Chiao et al. [47] observed that when a self-focusing beam disintegrated into *small-scale filaments*, all filaments had nearly the same intensity and diameter ($\approx 5 \mu\text{m}$). Furthermore, the intensities and diameters of the filaments were independent of the initial conditions.

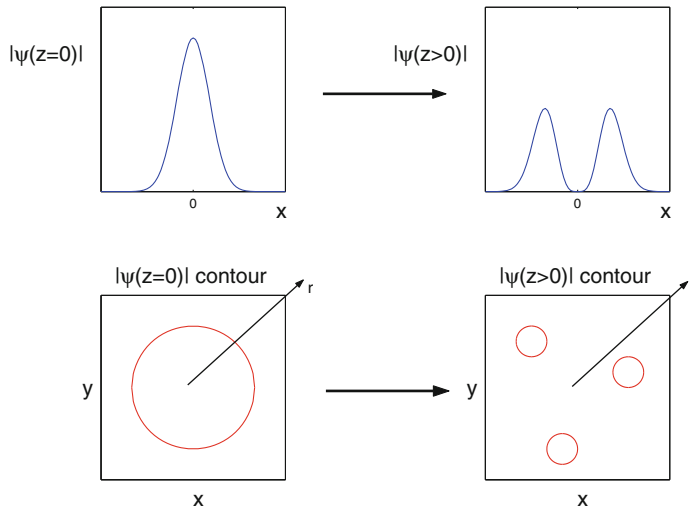


Fig. 3.5 Symmetry with respect to the origin can be maintained in multiple filamentation in one dimension (*top*), but not in two dimensions (*bottom*). From [131]

3.6.2 Multiple Filamentation and Loss of Radial Symmetry

In linear and nonlinear optics, it is customary to assume that the input beam is radial (e.g., $\psi_0(x, y) = c e^{-r^2}$). Since both diffraction and the Kerr nonlinearity preserve radial symmetry, radial input beams maintain radial symmetry during their propagation (Lemma 5.5).

In one transverse dimension, “multiple filamentation” (i.e., beam splitting) can occur *without* loss of symmetry with respect to $x = 0$, see Fig. 3.5. In two transverse dimensions, however, multiple filamentation *cannot* occur without a complete breakup of radial symmetry. Therefore, in order to explain the phenomenon of multiple filamentation in a bulk medium, one has to add a symmetry-breaking mechanism to the NLS model.

3.6.3 Bespalov-Talanov Model

In 1966, Bespalov and Talanov proposed the first theoretical model of multiple filamentation. In this model, breakup of radial symmetry is initiated by random noise in the input-beam profile.²⁷ Specifically, Bespalov and Talanov proved that plane-wave solutions of the NLS are linearly unstable.

²⁷ The assumption that the input profile of an intense laser beam is noisy is physical. See, e.g., Figs. 26.14a, c and 25.7.

Proposition 3.1 ([27]) Let $\psi^{\text{pw}}(z) = \alpha e^{i\alpha^2 z}$, where α is a real constant, be a plane-wave solution of the NLS

$$i\psi_z(z, x, y) + \Delta_{\perp}\psi + |\psi|^2\psi = 0. \quad (3.35)$$

Then, ψ^{pw} is linearly unstable.

Proof Clearly, ψ^{pw} is a plane-wave solution of (3.35). To analyze the effect of input-beam noise, let us perturb the initial condition as

$$\psi_0 = \psi^{\text{pw}}(z = 0) + g_0(x, y) = \alpha + g_0(x, y), \quad g_0(x, y) \ll \alpha,$$

and look for a solution of the form

$$\psi(z, x, y) = (\alpha + g(z, x, y))e^{i\alpha^2 z}, \quad |g| \ll \alpha,$$

where $g(0, x, y) = g_0(x, y)$. Substitution in (3.35) gives

$$ig_z(z, x, y) - \alpha^2(\alpha + g) + \Delta_{\perp}g + (\alpha + g)^2(\alpha + g^*) = 0.$$

The leading order, linearized equation for g reads

$$ig_z + \Delta_{\perp}g + \alpha^2(g + g^*) = 0.$$

Let $g = u + iv$, where u and v are real. Then the equations for u and v are

$$v_z - \Delta_{\perp}u - 2\alpha^2u = 0, \quad u_z + \Delta_{\perp}v = 0.$$

If we differentiate the left equation with respect to z and substitute u_z from the right equation, we get the decoupled equation for v

$$v_{zz}(z, x, y) + \Delta_{\perp}^2v + 2\alpha^2\Delta_{\perp}v = 0, \quad \Delta_{\perp}^2 := \left(\frac{\partial^2}{\partial x^2} + \frac{\partial^2}{\partial y^2}\right)^2. \quad (3.36)$$

Let

$$v(0) = \text{Im}(g_0) = \int \left[a(k_x, k_y) \cos(k_x x + k_y y) + b(k_x, k_y) \sin(k_x x + k_y y) \right] dk_x dk_y.$$

Then²⁸

$$v = \int \left[a(k_x, k_y) \cos(k_x x + k_y y + k_z z) + b(k_x, k_y) \sin(k_x x + k_y y + k_z z) \right] dk_x dk_y.$$

²⁸ We expand in cosines and sines, because v is real.

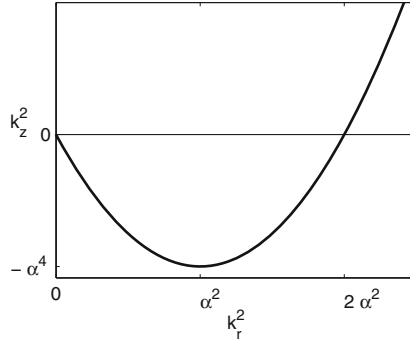


Fig. 3.6 The parabola $k_z^2 = k_r^2(k_r^2 - 2\alpha^2)$

Substitution in (3.36) gives the dispersion relation

$$k_z^2 = k_r^2 \left(k_r^2 - 2\alpha^2 \right), \quad k_r = \sqrt{k_x^2 + k_y^2}.$$

Therefore, for the small wavenumbers $0 < k_r < \sqrt{2}\alpha$ we have that $k_z^2 < 0$. Consequently, for $z \gg 1/k_z$, using $\cos a = \frac{e^{ia} + e^{-ia}}{2}$ and $\sin a = \frac{e^{ia} - e^{-ia}}{2i}$,

$$\begin{aligned} & \left[a(k_x, k_y) \cos(k_x x + k_y y + k_z z) + b(k_x, k_y) \sin(k_x x + k_y y + k_z z) \right] \\ & \sim \left[c(k_x, k_y) \cos(k_x x + k_y y) + d(k_x, k_y) \sin(k_x x + k_y y) \right] e^{|k_z|z}, \end{aligned} \quad (3.37)$$

i.e., the amplitude of these modes grows exponentially in z . \square

Remark This type of instability is called *modulational instability* (MI).

The Bespalov-Talanov analysis shows that plane waves are destabilized by the small wavenumbers, rather than by the large ones. In particular, the fastest-growing wavenumbers are those for which k_z^2 attains its minimum. Since k_z^2 is a parabola in k_r^2 that vanishes at $k_r^2 = 0, 2\alpha^2$, the minimum of k_z^2 is attained at $k_r^2 = \alpha^2$ and is equal to $-\alpha^4$, see Fig. 3.6. Therefore, regardless of the specific noise details, *modulational instability always leads to the emergence of modulations at the wavenumber $k_r = \alpha$.*

Let ψ be the solution of the NLS (3.35) with $\psi_0 = \alpha e^{-r^2}$. Since $\psi^{\text{PW}}(z = 0) \equiv \alpha$ is the zeroth-order Taylor approximation of ψ_0 near $r = 0$, one could argue that ψ^{PW} is the leading-order approximation of ψ , at least initially. Therefore, the Bespalov-Talanov analysis (for ψ^{PW}) suggests that the characteristic distance for the growth of the unstable modes of ψ is $L_{\text{MI}} = \frac{1}{k_z}$, see (3.37). Since $|k_z| = \alpha^2$ for the fastest-growing unstable mode, and since the beam power P scales as α^2 , we have that

$$L_{\text{MI}} \sim \frac{1}{\alpha^2} \sim \frac{1}{P}. \quad (3.38)$$

The Bespalov-Talanov linear-stability analysis does not tell us what happens once the solution develops small modulations. Intuitively, each local-intensity spike attracts power from its surroundings.²⁹ Consequently, the instability become even more pronounced,³⁰ so that ultimately, some local spikes attract enough power to undergo collapse. Since the collapse distance scales as the square of the width, see (3.21) and Lemma 27.1, the remaining distance to the collapse point of a spike is much smaller than L_{MI} . Therefore,

$$L_{\text{MF}} \approx L_{\text{MI}},$$

where L_{MF} is the characteristic distance for multiple filamentation.

Conclusion 3.6 *The characteristic distances for modulational instability (L_{MI}) and for multiple filamentation (L_{MF}) scale as $1/P$.*

As noted, the self focusing distance of a single filament scales as $1/\sqrt{P}$, see (3.21). Therefore, the Bespalov-Talanov analysis explains the experimental observation in Sect. 3.6.1 that the collapse distance in multiple filamentation is considerably shorter than in a single-filament collapse.

3.6.4 In Retrospect

The Bespalov-Talanov model for multiple filamentation is based on a linear stability analysis of plane-wave solutions. The validity of this analysis for laser beams is not obvious, because unlike plane waves, physical laser beams have a finite power, and they evolve in the transverse coordinates. Nevertheless, it was widely believed that the Bespalov-Talanov analysis is valid when the input power is sufficiently high, namely, when $P \gg P_{\text{cr}}$. In fact, for over thirty years, the Bespalov-Talanov model was the only theoretical explanation for multiple filamentation.

It later turned out that the picture is more complex. For example, numerical simulations of the NLS (3.35) showed that an input Gaussian beam with $P = 15P_{\text{cr}}$ and 10% random noise does not break up into multiple filaments, but collapses as a single filament. The same noisy input beam with $P = 150P_{\text{cr}}$, however, does break up into multiple filaments. The situation was clarified when it was discovered that the Bespalov-Talanov model is only valid at input powers above a certain power threshold which is on the order of $100P_{\text{cr}}$. While noise can lead to multiple filamentation at lower powers, such multiple filamentation has different characteristics, and is not of a Bespalov-Talanov type. In fact, there are four different types of multiple filamentation processes. In addition, multiple filamentation can also be induced by deterministic effects. See Chap. 25 for more details.

²⁹ Recall that rays bends towards regions with higher refractive index.

³⁰ The evolution of an intensity spike can be seen in Fig. 22.9.

As noted, the Bespalov-Talanov model only describes the onset of multiple filamentation. In particular, it does not provide an explanation to the experimental observation that all filaments have the same power and diameter. The explanation of this observation came many years later, when it was discovered that all solutions of the two-dimensional cubic NLS collapse with a universal blowup profile, which is a self-similar Townes profile (Chap. 14).

3.7 Self Focusing Until 1975

The year 1975 saw the publication of two comprehensive review articles on self focusing: *Self focusing: Experimental* by Shen [233], and *Self focusing: Theory* by Marburger [165]. These articles summarized the extensive theoretical and experimental research on self-focusing since the early 1960s (each paper has more than a hundred references). The two papers differ in style; Shen's paper describes the historical development of the subject, while Marburger's does not. Both papers, however, convey an overall feeling that self focusing has become a mature field in which “most of [the] controversies have now been resolved” [233]. This feeling is also reflected in the gradual decline in the number of papers on self focusing in leading general-audience physics journals, such as Physical Review Letters.

About that time, mathematicians started to become interested in self-focusing theory. This interest had to do with the realization that the NLS has solutions which become singular in finite “time”. The possibility of finite-time singularities led to “natural mathematical questions”, such as conditions for local and global existence, and properties of singular solutions. The mathematical research on singular NLS solutions, which is still on going, resulted in a theory of optical collapse very different from the one in 1975.

A lot of attention was also given to the one-dimensional cubic NLS, mainly in the context of propagation of *solitons*. In 1972, Zakharov and Shabat [282] showed that the inverse scattering approach, which was developed by Lax in 1968 for the KdV equation, can be applied to the one-dimensional cubic NLS. This discovery led to extensive research of the one-dimensional NLS, which found important applications in optical fiber communications [2].

The two-dimensional cubic NLS is fundamentally different from the one-dimensional cubic NLS, since the latter is integrable whereas the former is not. Therefore, analytical tools based on integrability (such as inverse scattering theory) are applicable to the one-dimensional cubic NLS, but not to the two-dimensional cubic NLS. The fundamental difference between the one-dimensional and two-dimensional NLS with regard to singular solutions will become clear when we begin to present the rigorous theory for the NLS in Chap. 5.

Chapter 4

NLS Models

In Chap. 1 we saw that propagation of linearly-polarized paraxial cw laser beams in a bulk Kerr medium is modeled by the two-dimensional cubic NLS

$$i\psi_z(z, x, y) + \Delta_{\perp}\psi + |\psi|^2\psi = 0, \quad \psi(0, x, y) = \psi_0(x, y), \quad (4.1)$$

where z is the direction of propagation, x and y are the transverse coordinates, and $\Delta_{\perp} = \frac{\partial^2}{\partial x^2} + \frac{\partial^2}{\partial y^2}$. In this chapter we briefly show that the one-dimensional and three-dimensional cubic NLS also arise in physical models.

4.1 NLS Models in Nonlinear Optics

In some physical setups we can ignore the dynamics in one of the transverse coordinates. For example, if the input beam only depends on x , i.e., $\psi_0(x, y) = \psi_0(x)$, then there is no dynamics in y , and so the propagation is governed by the one-dimensional cubic NLS

$$i\psi_z(z, x) + \psi_{xx} + |\psi|^2\psi = 0. \quad (4.2)$$

Of course, a physical laser beam that propagates in a bulk medium cannot be truly uniform in y . Experimentally, one way to suppress the dynamics in y is to use a highly-elliptic input beam, e.g.,

$$\psi_0(x, y) = ce^{-x^2-\epsilon y^2}, \quad 0 < \epsilon \ll 1.$$

Because $\frac{\partial^2\psi_0}{\partial y^2} \ll \frac{\partial^2\psi_0}{\partial x^2}$, one can neglect the dynamics in the y -direction, at least initially. For Eq. (4.2) to remain a valid physical model, however, its solution $\psi(z, x)$

should be stable under small perturbations in the y -direction.^{1,2} In other words, one has to check whether the assumption that

$$\psi_{yy} \ll \psi_{xx}, \quad (4.3)$$

remains valid as the solution of (4.1) evolves.

4.1.1 Planar Waveguides

The one-dimensional cubic NLS (4.2) also models beam propagation in a Kerr medium with a *planar waveguide* geometry, i.e., when the Kerr medium is narrow in the y -direction and wide (or infinite) in the x -direction. To see that, let E be the solution of the nonlinear Helmholtz equation (NLH)

$$E_{xx}(x, y, z) + E_{yy} + E_{zz} + k^2 E = 0, \quad k^2 = k_0^2 \left(1 + \frac{4n_2}{n_0} |E|^2 \right). \quad (4.4)$$

This equation should be supplemented with boundary conditions in the y -direction. For example, if the planar waveguide is located between $y = 0$ and $y = Y$, and if the electric field vanishes outside the waveguide, then from the continuity of the electric field it follows that

$$E(y = 0) = E(y = Y) = 0.$$

Because of these boundary conditions, changes in y occur on a much shorter length-scale than in x and z , i.e.,

$$E_{xx} + E_{zz} \ll E_{yy}. \quad (4.5)$$

Consequently, to leading order, (4.4) reduces to

$$E_{yy} + k^2 E = 0, \quad E(y = 0) = E(y = Y) = 0.$$

In order to proceed, consider the eigenvalue problem

$$F''(y) + \lambda^2 F = 0, \quad F(0) = F(Y) = 0.$$

This problem admits the solutions

$$F_n(y) = \sin(\lambda_n y), \quad \lambda_n = \frac{n\pi}{Y}.$$

¹ i.e., the solution $\tilde{\psi}(z, x, y)$ of (4.1) with $\tilde{\psi}_0(x, y) = \psi_0(x)(1 + \epsilon g(x, y))$ should remain close to $\psi(z, x)$ for any $g(x, y)$ and $\epsilon \ll 1$.

² For example, one-dimensional solitons are stable as solutions of (4.2), but unstable under transverse perturbations in the y -direction as solutions of (4.1), see [249, Sect. 1.3.3].

Let us assume that there exists an eigenvalue $\lambda_n^2 \approx k_0^2$. Then we can look for a solution of (4.4), whose profile in the narrow transverse direction is $F_n(y)$:

Exercise 4.1 Show that if $\lambda_n^2 \approx k^2$, the solution $E(x, y, z) = F_n(y)A(x, z)$ of (4.4) satisfies relation (4.5).

The function A satisfies the two-dimensional NLH

$$A_{xx}(x, z) + A_{zz} + k_n^2 A = 0, \quad k_n^2 = k^2 - \lambda_n^2.$$

Substituting $E = e^{ik_n z} \psi(z, x)$ and applying the paraxial approximation $\psi_{zz} \ll k_n \psi_z$ leads to the one-dimensional cubic NLS (4.2).

Remark There is an important difference between the above two examples where propagation in two transverse dimensions can be modeled by the one-dimensional NLS (4.2). In the case of highly-elliptic input beams, there is no dynamics in y because the dynamics in y is negligible compared with that in x , see (4.3). In contrast, in the planar-waveguide case, there is no dynamics in y because the “dynamics” in y dominates that in x , see (4.5).

4.1.2 Ultrashort Pulses

In Sect. 35.3 we will see that the canonical model for propagation of ultrashort laser pulses in a bulk Kerr medium is

$$i\psi_z(z, x, y, t) + \Delta_\perp \psi - \gamma_2 \psi_{tt} + |\psi|^2 \psi = 0, \quad \Delta_\perp = \frac{\partial^2}{\partial x^2} + \frac{\partial^2}{\partial y^2},$$

where ψ_{tt} accounts for temporal dispersion. The sign of γ_2 depends on the medium and on the wavelength (Sect. 36.2.2). When $\gamma_2 < 0$, dispersion is called anomalous. In that case, if we change to the rescaled time $\tilde{t} := t / \sqrt{|\gamma_2|}$, the NLS with anomalous dispersion reads

$$i\psi_z(z, x, y, \tilde{t}) + \Delta_\perp \psi + |\psi|^2 \psi = 0, \quad \Delta_\perp = \frac{\partial^2}{\partial x^2} + \frac{\partial^2}{\partial y^2} + \frac{\partial^2}{\partial \tilde{t}^2}.$$

Therefore, the propagation of laser pulses in a bulk Kerr medium in the anomalous regime is governed by the three-dimensional cubic NLS.

Similarly, the propagation of laser pulses in a Kerr-type *planar waveguide* in the anomalous regime is governed by the two-dimensional cubic NLS

$$i\psi_z(z, x, \tilde{t}) + \Delta_\perp \psi + |\psi|^2 \psi = 0, \quad \Delta_\perp = \frac{\partial^2}{\partial x^2} + \frac{\partial^2}{\partial \tilde{t}^2}.$$

Finally, the propagation of laser pulses in an *optical fiber* in the anomalous regime is governed by the one-dimensional cubic NLS

$$i\psi_z(z, \tilde{t}) + \psi_{\tilde{t}\tilde{t}} + |\psi|^2\psi = 0.$$

As with planar waveguides (Sect. 4.1.1), there is no dynamics in the transverse (x, y) coordinates, because the transverse profile is determined by the linear modes of the fiber (see, e.g., [2, Sect. 2.3.1]).

4.2 NLS Models in BEC

In recent years, there has been a considerable experimental and theoretical interest in the dynamics of Bose-Einstein condensates (BEC). A Bose-Einstein condensate is a state of matter of bosons that are cooled to temperatures near the absolute zero. Under such conditions, a large fraction of the atoms collapse into the lowest quantum state.

The state of the condensate is described by the wavefunction $\psi(t, x, y, z)$, so that $|\psi|^2$ is the particle density and $N = \int |\psi|^2 dx dy dz$ is the total number of atoms. Provided that essentially all atoms are in the condensate (that is, have condensed to the ground state), and treating the bosons using mean-field theory, the dynamics of the condensate is governed by the Gross-Pitaevski equation (GP)

$$i\bar{h}\psi_t(t, x, y, z) + \frac{\bar{h}^2}{2m}\Delta\psi - U_0|\psi|^2\psi - V\psi = 0, \quad \Delta = \frac{\partial^2}{\partial x^2} + \frac{\partial^2}{\partial y^2} + \frac{\partial^2}{\partial z^2},$$

where t is time, x, y , and z are the spatial coordinates, \bar{h} is Planck's constant, m is the mass of the bosons, V is the external potential, and U_0 is the scattering length. Therefore, the dynamics of BEC is governed by the three-dimensional NLS with a linear potential. The scattering length is positive in some setups and negative in others, corresponding to repulsive and attractive interactions, respectively. See e.g., [9] for a recent review.

In some cases, the external potential confines the condensate to a one-dimensional or a two-dimensional trap. In such cases, one usually models the dynamics with the one-dimensional or two-dimensional GP/NLS.³

Although this book focuses on optical collapse, we note that collapse of BEC condensates with attractive interactions was observed experimentally [109, 277].

³ See, e.g., [10] for analysis of dimension reduction in the GP/NLS equation.

Part II

Rigorous Analysis

Chapter 5

Existence of NLS Solutions

In this chapter we begin to present the rigorous theory of singular solutions of the NLS. We consider the NLS in d transverse dimensions¹ and a nonlinearity of order $2\sigma + 1$, i.e.,²

$$i\psi_z(z, \mathbf{x}) + \Delta\psi + \nu|\psi|^{2\sigma}\psi = 0, \quad z > 0, \quad \mathbf{x} \in \mathbb{R}^d, \quad (5.1a)$$

where $\mathbf{x} = (x_1, \dots, x_d)$, $\Delta = \frac{\partial^2}{\partial x_1^2} + \dots + \frac{\partial^2}{\partial x_d^2}$, and ν is a real constant. The NLS is solved for $z > 0$, subject to the initial condition

$$\psi(z = 0, \mathbf{x}) = \psi_0(\mathbf{x}), \quad \mathbf{x} \in \mathbb{R}^d. \quad (5.1b)$$

Hence, (5.1) is an initial value problem, in which the variable z plays the role of ‘time’.

Throughout this book, the parameter σ will be in the H^1 -subcritical regime³

$$\begin{cases} 0 < \sigma < \infty, & \text{if } d \leq 2, \\ 0 < \sigma < \frac{2}{d-2}, & \text{if } d > 2. \end{cases} \quad (5.2)$$

In Chap. 4 we saw that the cubic NLS ($\sigma = 1$) in one, two, and three dimensions arises in nonlinear optics and in Bose-Einstein condensates. Our main interest in this book is in the case $d = 2$ and $\sigma = 1$, which corresponds to laser propagation in a bulk Kerr medium. Only by considering the more general NLS (5.1), however, we will be able to realize that this case lies between the *subcritical* NLS ($\sigma d < 2$), where all solutions exist globally, and the *supercritical* NLS ($\sigma d > 2$), where singular solutions exist. This borderline property of the *critical* NLS ($\sigma d = 2$) has many important consequences. For example, it is related to the dual borderline properties

¹ Equation (5.1) is sometimes called the NLS in $d + 1$ dimensions, where the “1” refers to the z -coordinate.

² To simplify the notations, from now on we denote the transverse Laplacian by Δ instead of by Δ_\perp .

³ See Sect. 5.11.4 for the terminology H^1 -subcritical.

of the ground state (Sect. 7.12), and to the sensitivity of collapsing solutions of the critical NLS to small perturbations (Sect. 18.6).

5.1 Biharmonic NLS (BNLS)

The biharmonic NLS equation (BNLS) is defined as

$$i\psi_z(z, \mathbf{x}) + \nu\Delta^2\psi + |\psi|^{2\sigma}\psi = 0, \quad (5.3)$$

where Δ^2 is the biharmonic operator. For example, the one-dimensional BNLS reads

$$i\psi_z(z, x) + \nu\psi_{xxxx} + |\psi|^{2\sigma}\psi = 0,$$

and the two-dimensional BNLS reads

$$i\psi_z(z, x, y) + \nu(\psi_{xxxx} + 2\psi_{xxyy} + \psi_{yyyy}) + |\psi|^{2\sigma}\psi = 0.$$

Unlike the NLS, the interest in the BNLS is predominantly mathematical. In this book we repeatedly use the BNLS as a pedagogical tool, asking the reader to extend NLS results to the BNLS.

5.2 Power, Hamiltonian, and Linear Momentum

In many applications $\|\psi\|_2^2$ is called the *mass*.⁴ In this book $\|\psi\|_2^2$ is referred to as the *power*, because in optics it corresponds to the beam power (e.g., in watts), see Sect. 24.2.

Definition 5.1 (power) *The power of ψ is*

$$P(z) := \|\psi\|_2^2 = \int |\psi|^2 d\mathbf{x}.$$

In most applications, the Hamiltonian corresponds to *energy*. This is not the case in optics, however, where the Hamiltonian does not have a clear physical analog. Therefore, we simply call it the Hamiltonian.

Definition 5.2 (Hamiltonian) *Let ψ be a solution of the NLS (5.1). Then the Hamiltonian of ψ is*

$$H(z) := \|\nabla\psi\|_2^2 - \frac{\nu}{\sigma+1}\|\psi\|_{2\sigma+2}^{2\sigma+2} = \int |\nabla\psi|^2 d\mathbf{x} - \frac{\nu}{\sigma+1} \int |\psi|^{2\sigma+2} d\mathbf{x}.$$

The definition of *linear momentum* is as follows.

⁴ See Definition 2.2 of L^p norms.

Definition 5.3 (linear momentum) Let ψ be a solution of the NLS (5.1). Then the linear momentum of ψ is

$$\mathbf{M}(z) := i \int (\psi \nabla \psi^* - \psi^* \nabla \psi) d\mathbf{x}.$$

Finally, we define the *center of mass*.

Definition 5.4 (center of mass) The center of mass of ψ is

$$\bar{\mathbf{x}}(z) := \frac{\int \mathbf{x} |\psi|^2 d\mathbf{x}}{\int |\psi|^2 d\mathbf{x}} = \frac{\int \mathbf{x} |\psi|^2 d\mathbf{x}}{P}.$$

5.3 Invariance

We first prove the conservation of power and Hamiltonian, both of which play a key role in NLS theory.

Lemma 5.1 (Conservation of power) Let ψ be a solution of the NLS (5.1) which is in H^1 , and let $P(z)$ be its power. Then

$$P(z) \equiv P(0). \quad (5.4)$$

Proof If we multiply (5.1) by ψ^* , we get

$$i\psi^*\psi_z + \psi^*\Delta\psi + \nu|\psi|^{2\sigma+2} = 0.$$

Taking the complex-conjugate of this equation, one obtains

$$-i\psi\psi_z^* + \psi\Delta\psi^* + \nu|\psi|^{2\sigma+2} = 0.$$

Subtracting the second equation from the first gives

$$i(\psi^*\psi_z + \psi\psi_z^*) + \psi^*\Delta\psi - \psi\Delta\psi^* = 0.$$

Taking the integral over \mathbb{R}^d , using the relation

$$\psi^*\psi_z + \psi\psi_z^* = (\psi\psi^*)_z = (|\psi|^2)_z,$$

and integrating by parts gives⁵

$$i \frac{d}{dz} \int |\psi|^2 d\mathbf{x} - \int \nabla\psi^* \nabla\psi d\mathbf{x} + \int \nabla\psi \nabla\psi^* d\mathbf{x} = 0,$$

from which conservation of power follows. \square

⁵ The justification that there is no contribution from boundary integrals in the integration by parts requires further analysis (see e.g. [39]).

Remark If in the proof of Lemma 5.1 we take the integral over a domain $\Omega \subset \mathbb{R}^d$ and integrate by parts, we get that

$$\frac{d}{dz} \int_{\Omega} |\psi|^2 d\mathbf{x} = \int_{\partial\Omega} i (\psi^* \nabla \psi - \psi \nabla \psi^*) \cdot \mathbf{n} ds, \quad (5.5)$$

where \mathbf{n} is the outward unit normal to $\partial\Omega$. Therefore, $i(\psi^* \nabla \psi - \psi \nabla \psi^*)$ is the *power flux density*.

Lemma 5.2 (Conservation of Hamiltonian) *Let ψ be a solution of the NLS (5.1) which is in H^1 , and let $H(z)$ be its Hamiltonian. Then*

$$H(z) \equiv H(0). \quad (5.6)$$

Proof Multiplying (5.1) by ψ_z^* gives

$$i|\psi_z|^2 + \psi_z^* \Delta \psi + \nu |\psi|^{2\sigma} \psi \psi_z^* = 0.$$

Adding the complex-conjugate equation, one obtains

$$\psi_z^* \Delta \psi + \psi_z \Delta \psi^* + \frac{\nu}{\sigma+1} (|\psi|^{2\sigma+2})_z = 0.$$

Taking the integral over \mathbb{R}^d and integrating by parts gives⁶

$$\begin{aligned} 0 &= - \int (\nabla \psi_z^* \nabla \psi + \nabla \psi_z \nabla \psi^*) d\mathbf{x} + \frac{\nu}{\sigma+1} \int (|\psi|^{2\sigma+2})_z d\mathbf{x} \\ &= - \frac{d}{dz} \int |\nabla \psi|^2 d\mathbf{x} + \frac{\nu}{\sigma+1} \frac{d}{dz} \int |\psi|^{2\sigma+2} d\mathbf{x} = - \frac{d}{dz} H, \end{aligned}$$

as claimed. \square

We now present all the other conservation laws of the NLS (5.1). These conservation laws can be proved in a similar fashion, or by using Noether's Theorem (see, e.g., [220, 247, 249]).

NLS solutions conserve the linear momentum, i.e.,

$$\mathbf{M}(z) \equiv \mathbf{M}(0). \quad (5.7)$$

Similarly, NLS solutions conserve the angular momentum, i.e.,

$$i \int \mathbf{x} \times (\psi^* \nabla \psi - \psi \nabla \psi^*) d\mathbf{x} \equiv \text{constant}.$$

⁶ The justification that there is no contribution from boundary integrals in the integration by parts requires further analysis (see e.g. [39]).

The conservation law for the center of mass reads

$$\frac{d\bar{\mathbf{x}}(z)}{dz} = \frac{\mathbf{M}}{P}. \quad (5.8)$$

Therefore, the center of mass moves at a constant velocity, which is equal to linear momentum divided by “mass” (power).

A conservation law which is valid only in the critical case $\sigma d = 2$ is

$$\frac{d}{dz} \int i\mathbf{x} \cdot (\psi \nabla \psi^* - \psi^* \nabla \psi) d\mathbf{x} \equiv 4H. \quad (5.9)$$

This relation is better known as the *variance identity*, see Corollary 7.1.

Exercise 5.1 Show that conservation of power and Hamiltonian for the BNLS (5.3) reads $P(z) \equiv P(0)$ and $H_B(z) \equiv H_B(0)$, where

$$P = \|\psi\|_2^2, \quad H_B = -v \|\Delta \psi\|_2^2 - \frac{1}{\sigma+1} \|\psi\|_{2\sigma+2}^{2\sigma+2}. \quad (5.10)$$

5.4 Gagliardo-Nirenberg Inequality

An key tool in NLS theory is the following *Gagliardo-Nirenberg inequality*:

Lemma 5.3 ([104, 105, 202]) Let $f(\mathbf{x})$ be in $H^1(\mathbb{R}^d)$, and let σ be in the H^1 -subcritical regime (5.2). Then

$$\|f\|_{2\sigma+2}^{2\sigma+2} \leq C_{\sigma,d} \|\nabla f\|_2^{\sigma d} \|f\|_2^{2+\sigma(2-d)}, \quad (5.11)$$

where $C_{\sigma,d}$ is a positive constant that depends only on σ and d .

Corollary 5.1 Let σ be in the H^1 -subcritical regime (5.2).

1. If $f \in H^1$, then $f \in L^{2\sigma+2}$ and $H(f) < \infty$, where H is the Hamiltonian.
2. If $f_n \rightarrow f$ in H^1 , then $f_n \rightarrow f$ in $L^{2\sigma+2}$.⁷
3. If $f_n \rightarrow f$ in H^1 , then $H(f_n) \rightarrow H(f)$.

Exercise 5.2 Prove Corollary 5.1.

5.5 Existence in H^1

Most of NLS theory is carried out in H^1 ,⁸ i.e., for solutions $\psi(z, \mathbf{x})$ such that for each z , $\psi(z) \in H^1(\mathbb{R}^d)$. The advantage of working in H^1 is as follows. In NLS

⁷ i.e., $\lim_{n \rightarrow \infty} \|f_n - f\|_{H^1} = 0 \implies \lim_{n \rightarrow \infty} \|f_n - f\|_{L^{2\sigma+2}} = 0$.

⁸ See Definition 2.3 of the H^1 norm.

theory we heavily rely on power and Hamiltonian conservation. To do that, however, the power and the Hamiltonian should be finite. When ψ is in H^1 , this is indeed the case:

Lemma 5.4 *Let $\psi(z) \in H^1$, and let σ be in the H^1 -subcritical regime (5.2). Then the power, Hamiltonian, and linear momentum of ψ are finite.*

Proof Clearly, $P(\psi)$ is finite. By Corollary 5.1, $H(\psi)$ is finite. Finally, since

$$|\mathbf{M}| \leq 2 \int |\psi| |\nabla \psi| d\mathbf{x} \leq \int |\psi|^2 d\mathbf{x} + \int |\nabla \psi|^2 d\mathbf{x},$$

$\mathbf{M}(\psi)$ is also finite. \square

Therefore, throughout this book, we adopt the following definition for existence of solutions:

Definition 5.5 (existence) *We say that a solution ψ of the NLS (5.1) exists in H^1 for $0 \leq z \leq Z$ if $\psi(z, \mathbf{x}) \in C([0, Z], H^1(\mathbb{R}^d))$, i.e., if $\psi(z)$ is a continuous function from $[0, Z]$ to $H^1(\mathbb{R}^d)$.⁹*

Exercise 5.3 *Most of BNLS theory is carried out in H^2 , i.e., for solutions $\psi(z, \mathbf{x})$ such that for each z , $\psi(z) \in H^2(\mathbb{R}^d)$.¹⁰ Show that if $\|\psi\|_{H^2} < \infty$, then $P(\psi)$ and $H_B(\psi)$ are finite, where P and H_B are given by (5.10). In this case, the relevant Gagliardo-Nirenberg inequality reads [104, 105, 202]*

$$\|f\|_{2\sigma+2}^{2\sigma+2} \leq B_{\sigma,d} \|\Delta f\|_2^{\frac{\sigma d}{2}} \|f\|_2^{2+2\sigma-\frac{\sigma d}{2}}, \quad (5.12)$$

where σ is in the H^2 -subcritical regime¹¹

$$\begin{cases} 0 < \sigma < \infty, & \text{if } d \leq 4, \\ 0 < \sigma < \frac{4}{d-4}, & \text{if } d > 4, \end{cases} \quad (5.13)$$

and $B_{\sigma,d}$ is a constant which depends only on σ and d .

5.6 Local Existence and the Blowup Alternative

Local existence and uniqueness for the NLS were first proved in 1979 by Ginibre and Velo. A more comprehensive result was proved in 1987 by Kato:¹²

⁹ By continuous we mean that $\lim_{n \rightarrow \infty} z_n = z \implies \lim_{n \rightarrow \infty} \|\psi(z_n) - \psi(z)\|_{H^1(\mathbb{R}^d)} = 0$.

¹⁰ See Definition 2.4.

¹¹ See Sect. 5.11.4.

¹² Kato's proof is based on the standard iteration method for the equivalent integral equation, using space-time estimates of the linear Schrödinger operator $e^{iz\Delta}$.

Theorem 5.1 (local existence and uniqueness [112, 139]) *Let $\|\psi_0\|_{H^1} < \infty$, and let σ be in the H^1 -subcritical regime (5.2). Then there exists a positive number Z , which depends only on $\|\psi_0\|_{H^1}$, such that there exists a unique solution of the NLS (5.1) for $0 \leq z \leq Z$. In addition, $Z(\|\psi_0\|_{H^1})$ is monotonically decreasing in $\|\psi_0\|_{H^1}$.*

In what follows, we will prove global existence by using power and Hamiltonian conservation to find conditions under which the H^1 norm of ψ remains bounded. Deriving a global bound for the H^1 norm, however, does not immediately imply global existence. This is because in the proof of power and Hamiltonian conservation we implicitly assumed the existence of the solution. Moreover, until proved otherwise (in Corollary 5.3), we have to allow for the possibility that an NLS solution can cease to be in H^1 while its H^1 norm remains bounded. Therefore, we first establish that an *a priori bound*¹³ for the H^1 norm implies global existence.¹⁴

Corollary 5.2 *Let ψ be a solution of the NLS (5.1). If ψ satisfies the a priori bound $\|\psi\|_{H^1} \leq M$ for some $0 < M < \infty$, then ψ exists in H^1 and is unique for $0 \leq z < \infty$.*

Proof Since $\|\psi_0\|_{H^1} \leq M$, by Theorem 5.1, there exists $Z_M = Z(M)$, such that the NLS solution $\psi(z)$ exists and is unique in $[0, Z_M]$. In particular, $\psi\left(\frac{Z_M}{2}\right)$ exists and $\|\psi\left(\frac{Z_M}{2}\right)\|_{H^1} \leq M$.

Let $\tilde{\psi}$ be the solution of (5.1) for $z \geq \frac{Z_M}{2}$, subject to the initial condition $\tilde{\psi}\left(\frac{Z_M}{2}\right) = \psi\left(\frac{Z_M}{2}\right)$. Since $\|\tilde{\psi}\left(\frac{Z_M}{2}\right)\|_{H^1} \leq M$, we know from Theorem 5.1 that $\tilde{\psi}$ exists in $\left[\frac{Z_M}{2}, \frac{3Z_M}{2}\right]$. By uniqueness, ψ and $\tilde{\psi}$ are identical in their interval of overlap $\left[\frac{Z_M}{2}, Z_M\right]$. Therefore, ψ exists and is unique in $\left[0, \frac{3Z_M}{2}\right]$. Repetition of this argument shows that ψ exists globally. \square

We now show that NLS solutions have a *blowup alternative* in H^1 : Either they exist globally, or their H^1 norm blows up when they cease to be in H^1 . This is not true in L^2 , where NLS solutions can cease to exist while their L^2 norm remains bounded (Sect. 5.7.2).

¹³ An *a priori estimate* is one derived from the equation before the solution is known to exist. An example in NLS theory where an *a priori estimate* bifurcates from the actual NLS solution is given in Sect. 7.3.

¹⁴ To clarify that the result of Corollary 5.2 is not obvious, consider the case where we replace H^1 with L^2 . In that case, Corollary 5.2 reads: “If ψ satisfies the a priori bound $\|\psi\|_2 \leq M < \infty$, then ψ exists in L^2 for all $z \geq 0$ ”. This, however, is not true. Indeed, if $\|\psi_0\|_2 < \infty$, then power conservation implies that $\|\psi\|_2 \equiv \|\psi_0\|_2$ for all $z > 0$. This does not imply, however, that ψ exists in L^2 for all $z \geq 0$. Indeed, in Theorem 5.3 we saw that if $\psi_0 \in H^1$, $\sigma d = 2$, and the solution blows up in H^1 at Z_c , then its limit as $z \rightarrow Z_c$ cannot be in L^2 . Another “counterexample” is Theorem 7.2, which shows that if $\psi_0 \in H^1$, $H(\psi_0) < 0$, $\sigma d \geq 2$, and $v > 0$, then ψ cannot exist globally in any space (H^1 , L^2 , etc.). Thus, the “success” of Corollary 5.2 reflects the fact that H^1 is the “natural” space for studying existence and singularity in the NLS.

Corollary 5.3 (blowup alternative) *Let $\psi_0 \in H^1$, and let $[0, Z_c)$ be the maximal existence interval for the NLS (5.1). Then either $Z_c = \infty$, or $0 < Z_c < \infty$ and $\lim_{z \rightarrow Z_c} \|\psi\|_{H^1} = \infty$.*

Proof Let

$$Z_c := \sup \left\{ Z \mid \exists M = M(Z), \quad 0 < M < \infty, \quad \sup_{0 \leq z \leq Z} \|\psi(z)\|_{H^1} < M \right\}.$$

Since $\|\psi_0\|_{H^1} < \infty$, then by Theorem 5.1, there exists $Z = Z(\|\psi_0\|_{H^1}) > 0$, such that ψ exists in $[0, Z]$. Therefore, $Z_c \geq Z(\|\psi_0\|_{H^1}) > 0$. In addition, from the proof of Corollary 5.2 it follows that for any $0 < Z < Z_c$, the NLS has a unique solution in $[0, Z]$. If $Z_c = \infty$, we are done.¹⁵ If $Z_c < \infty$, then $\lim_{z \rightarrow Z_c} \|\psi\|_{H^1} = \infty$, since if $\liminf_{z \rightarrow Z_c} \|\psi\|_{H^1} < \infty$, Theorem 5.1 implies that the solution can be extended beyond Z_c . Hence, the maximal existence interval is $[0, Z_c]$. \square

Remark In general, a function $\phi(z, \mathbf{x})$ can cease to belong to H^1 when its H^1 norm is bounded. This is the case, for example, if $\nabla \phi$ approaches a delta function in L^2 (Exercise 5.4). Thus, the blowup alternative (Corollary 5.3) shows that H^1 is the “natural” space for studying existence and singularity in the NLS.

Exercise 5.4 *Let $f(\mathbf{x}) \in H^1$ and $\phi(z, \mathbf{x}) = \frac{1}{L^{\frac{d}{2}-1}(z)} f\left(\frac{\mathbf{x}}{L(z)}\right)$. Show that as $L(z) \rightarrow 0$,*

$$|\nabla \phi|^2 \rightarrow \|\nabla f\|_2^2 \delta(\mathbf{x}), \quad \|\phi\|_2^2 \rightarrow 0, \quad \|\phi\|_{H^1}^2 \rightarrow \|\nabla f\|_2^2.$$

Hence, ϕ ceases to belong to H^1 even though its H^1 norm is bounded.

The issue of local existence and uniqueness is closely related to that of continuous dependence on initial conditions.

Theorem 5.2 (continuous dependence on initial conditions [112, 139]) *Let $\psi_0 \in H^1$, let $[0, Z_c)$ be the maximal existence interval for the solution ψ of the NLS (5.1), and let $0 < Z < Z_c$. Then the mapping $\psi_0 \mapsto \psi$ is continuous from H^1 into $C([0, Z], H^1)$. By this we mean that if $\psi_{0,n} \rightarrow \psi_0$ in H^1 as $n \rightarrow \infty$, then for n sufficiently large the solution ψ_n of (5.1) with $\psi_n(z = 0) = \psi_{0,n}$ exists in $[0, Z]$, and $\psi_n \rightarrow \psi$ in $C([0, Z], H^1)$, i.e.,*

$$\lim_{n \rightarrow \infty} \sup_{0 \leq z \leq Z} \|\psi_n - \psi\|_{H^1} = 0.$$

Corollary 5.4 *Under the conditions of Theorem 5.2, for any $\epsilon > 0$ and $0 < Z < Z_c$, there exists $\delta = \delta(\epsilon; Z)$ such that if $\|\psi_0 - \phi_0\|_{H^1} \leq \delta$, and if the solution $\phi(z, \mathbf{x})$ of (5.1) with the initial condition ϕ_0 exists in $[0, Z]$, then $\sup_{0 \leq z \leq Z} \|\psi(z) - \phi(z)\|_{H^1} \leq \epsilon$.*

¹⁵ In that case $\lim_{z \rightarrow \infty} \|\psi(z)\|_{H^1}$ can be either finite or infinite.

Proof Suppose no such $\delta(\epsilon; Z)$ exists. Then for some ϵ_0 there is no such $\delta(\epsilon)$. That means that, taking a sequence $\delta_n \rightarrow 0$, there exist NLS solutions $\{\psi_n\}$ such that $\|\psi_n(0, \mathbf{x}) - \psi_0\|_{H^1} \leq \delta_n$ but $\sup_{0 \leq z \leq Z} \|\psi_n - \psi\|_{H^1} > \epsilon_0$. This, however, contradicts with Theorem 5.2. \square

5.7 Type of Singularity

Since we defined existence as belonging to H^1 , we say that an NLS solution becomes singular if it ceases to be in H^1 . By Corollary 5.3, this occurs only if its H^1 norm becomes infinite. Therefore, we adopt the following definition:

Definition 5.6 (singularity) A solution of the NLS (5.1) becomes singular at Z_c , where $0 < Z_c < \infty$, if $\psi(z) \in H^1$ for $0 \leq z < Z_c$, and if $\lim_{z \rightarrow Z_c} \|\psi(z)\|_{H^1} = \infty$.

In light of power conservation (Lemma 5.1), we immediately have

Corollary 5.5 ψ becomes singular at Z_c if and only if $\lim_{z \rightarrow Z_c} \|\nabla \psi\|_2 = \infty$.

By Hamiltonian conservation (Lemma 5.2), $\|\nabla \psi\|_2$ goes to infinity if and only if $v > 0$ and $\|\psi\|_{2\sigma+2}$ goes to infinity.

Corollary 5.6 ψ becomes singular at Z_c if and only if $\lim_{z \rightarrow Z_c} \|\psi\|_{2\sigma+2} = \infty$.

The L^∞ norm (i.e., the maximal amplitude) also becomes infinite at the singularity:

Corollary 5.7 If ψ becomes singular at Z_c , then $\lim_{z \rightarrow Z_c} \|\psi\|_\infty = \infty$.

Proof By negation. Assume that $\limsup_{z \rightarrow Z_c} \|\psi\|_\infty = M < \infty$. Then

$$\lim_{z \rightarrow Z_c} \|\psi\|_{2\sigma+2}^{2\sigma+2} \leq M^{2\sigma} \lim_{z \rightarrow Z_c} \|\psi\|_2^2 = M^{2\sigma} \|\psi_0\|_2^2 < \infty,$$

which contradicts with Corollary 5.6. \square

In fact, since the L^2 norm is conserved and the $L^{2\sigma+2}$ norm becomes infinite, the solution blows up in L^p for $p \geq 2\sigma + 2$:

Corollary 5.8 ψ becomes singular at Z_c if and only if $\lim_{z \rightarrow Z_c} \|\psi\|_p = \infty$ for all p such that $2\sigma + 2 \leq p \leq \infty$.

Proof If $\lim_{z \rightarrow Z_c} \|\psi\|_p = \infty$ for $2\sigma + 2 \leq p \leq \infty$, then by Corollary 5.6, ψ becomes singular. To prove the converse, recall the *interpolation inequality for L^p norms* (Appendix A)

$$\|f\|_q \leq \|f\|_r^\alpha \|f\|_p^{1-\alpha}, \quad 1 \leq r \leq q \leq p \leq \infty, \quad (5.14)$$

where $0 \leq \alpha \leq 1$ is given by

$$\frac{1}{q} = \frac{\alpha}{r} + \frac{1-\alpha}{p}.$$

Substituting $f = \psi$, $r = 2$, and $q = 2\sigma + 2$, shows that for $2\sigma + 2 < p \leq \infty$,

$$\|\psi\|_{2\sigma+2} \leq \|\psi\|_2^\alpha \|\psi\|_p^{1-\alpha}, \quad \alpha = \frac{p - (2\sigma + 2)}{(\sigma + 1)(p - 2)}. \quad (5.15)$$

Hence, $0 < \alpha \leq (\sigma + 1)^{-1}$. Since $\lim_{z \rightarrow Z_c} \|\psi\|_{2\sigma+2} = \infty$, $\|\psi\|_2 \equiv \|\psi_0\|_2$ and $1 - \alpha > 0$, the result follows. \square

Remark The proof of Corollary 5.8 also provides information on the blowup rate of L^p norms (Corollary 13.2).

Remark Corollary 5.8 shows that singular NLS solutions blow up simultaneously in L^p for all p such that $2\sigma + 2 \leq p \leq \infty$. In some cases, one can prove a stronger result that ψ blows up in L^p for $\sigma d < p \leq \infty$.^{16,17,18}

Exercise 5.5 We say that a solution of the BNLS (5.3) becomes singular at Z_c , if $\psi(z) \in H^2$ for $0 \leq z < Z_c$ and if $\lim_{z \rightarrow Z_c} \|\psi(z)\|_{H^2} = \infty$.

1. Show that if $\psi \in H^2$, then

$$\|\nabla \psi\|_2^2 \leq \|\Delta \psi\|_2 \|\psi\|_2. \quad (5.16)$$

2. Show that ψ becomes singular at Z_c if and only if $\lim_{z \rightarrow Z_c} \|\Delta \psi\|_2 = \infty$.
3. Show that ψ becomes singular at Z_c if and only if $\lim_{z \rightarrow Z_c} \|\psi\|_p = \infty$ for all p such that $2\sigma + 2 \leq p \leq \infty$.

5.7.1 Singularity Point \mathbf{x}_c

NLS singularity is typically a local phenomenon, i.e., the solution collapses at a point $\mathbf{x}_c \in \mathbb{R}^d$.

Definition 5.7 (singularity point \mathbf{x}_c) Let ψ be a solution of the NLS (5.1) that becomes singular in H^1 at $z = Z_c$. We say that ψ becomes singular at $\mathbf{x} = \mathbf{x}_c \in \mathbb{R}^d$, iff for any $\epsilon > 0$,

$$\lim_{z \rightarrow Z_c} \|\psi\|_{H^1(|\mathbf{x}-\mathbf{x}_c|<\epsilon)} = \infty \quad \text{and/or} \quad \lim_{z \rightarrow Z_c} \|\psi\|_{L^{2\sigma+2}(|\mathbf{x}-\mathbf{x}_c|<\epsilon)} = \infty.$$

¹⁶ This result is stronger because $\sigma d < 2\sigma + 2$ in the H^1 -subcritical regime (5.2).

¹⁷ See e.g., Corollary 13.6 and Theorem 14.2.

¹⁸ Intuitively, near the singularity, peak-type solutions approach a quasi self-similar asymptotic profile, so that $|\psi| \sim L^{-\frac{1}{\sigma}}(z) F\left(\frac{|\mathbf{x}|}{L(z)}\right)$ and $\lim_{z \rightarrow Z_c} L(z) = 0$, see Chaps. 14 and 21. Therefore, $\|\psi\|_p^p \sim L^{d-\frac{p}{\sigma}}(z) \|F\|_p^p$ becomes infinite for $p > \sigma d$.

Since $\lim_{z \rightarrow Z_c} \|\psi\|_\infty = \infty$ (Corollary 5.7), this may seem to suggest that $\lim_{z \rightarrow Z_c} |\psi(z, \mathbf{x}_c)| = \infty$. This is indeed the case with peak-type and shrinking-ring solutions,¹⁹ but not with singular vortex solutions which *vanish* at the singularity point (i.e., they satisfy $\psi(z, \mathbf{x}_c) \equiv 0$, see Chap. 15). Thus, the blowup of the global L^∞ norm “only” implies the blowup of the local L^∞ norm in any finite-size ball around the singularity point, i.e., $\lim_{z \rightarrow Z_c} \|\psi\|_{\infty(|\mathbf{x} - \mathbf{x}_c| < \epsilon)} = \infty$ for any $\epsilon > 0$, see Corollary 13.5.

NLS solutions can also simultaneously collapse at k points (Sect. 13.4). For many years, it was believed that NLS solutions can only collapse at a finite number of points. In the early 2000s however, it was discovered, that the NLS with $\sigma \geq 2$ and $d > 1$ admits *standing-ring* solutions that collapse on a d -dimensional sphere. See Chap. 22 for more details.

5.7.2 Singularity in L^2

Unlike the H^1 norm, the L^2 norm of NLS solutions is conserved. This may seem to suggest that NLS solutions remain in L^2 as $z \rightarrow Z_c$. When $v > 0$ and $\sigma d = 2$, however, Merle and Tsutsumi proved that if ψ becomes singular in H^1 , then it also becomes singular in L^2 :

Theorem 5.3 ([188]) *Let ψ be a solution of the NLS (5.1) with $v > 0$ and $\sigma d = 2$ that becomes singular at Z_c . Then ψ does not have a strong limit in L^2 as $z \rightarrow Z_c$. Moreover, there is no sequence $z_n \rightarrow Z_c$, such that $\psi(z_n, \mathbf{x})$ converges in L^2 as $n \rightarrow \infty$.*

Proof Assume, by negation, that there exists a sequence $z_n \rightarrow Z_c$ such that $\psi(z_n)$ has a strong limit in L^2 as $n \rightarrow \infty$. We now show that this implies that $\|\nabla \psi(z_n)\|_2$ is bounded as $n \rightarrow \infty$, which is a contradiction.

To see that, note that by Hamiltonian conservation,

$$\|\nabla \psi(z_n)\|_2^2 = H(0) + \frac{v}{\sigma + 1} \|\psi(z_n)\|_{2\sigma+2}^{2\sigma+2}.$$

Since for any $p \geq 0$,

$$|f + g|^p \leq (|f| + |g|)^p \leq (2 \max\{|f|, |g|\})^p \leq 2^p (|f|^p + |g|^p),$$

it follows that

$$\|f + g\|_p^p \leq 2^p (\|f\|_p^p + \|g\|_p^p). \quad (5.17)$$

¹⁹ See Chaps. 14, 21, and 23.

Hence,

$$\|\psi(z_n)\|_{2\sigma+2}^{2\sigma+2} \leq 2^{2\sigma+2} \left(\|(\psi(z_n) - \psi(z_k))\|_{2\sigma+2}^{2\sigma+2} + \|\psi(z_k)\|_{2\sigma+2}^{2\sigma+2} \right).$$

By the Gagliardo-Nirenberg inequality (5.11) with $\sigma d = 2$ and (5.17),

$$\begin{aligned} \|\psi(z_n) - \psi(z_k)\|_{2\sigma+2}^{2\sigma+2} &\leq C_{\sigma,d} \|\psi(z_n) - \psi(z_k)\|_2^{2\sigma} \|\nabla \psi(z_n) - \nabla \psi(z_k)\|_2^2 \\ &\leq C_{\sigma,d} \|\psi(z_n) - \psi(z_k)\|_2^{2\sigma} 2^2 \left(\|\nabla \psi(z_n)\|_2^2 + \|\nabla \psi(z_k)\|_2^2 \right). \end{aligned}$$

Since we assumed that $\psi(z_n)$ converges strongly in L^2 , there exists a positive integer k , such that for all $n > k$,

$$\frac{\nu C_{\sigma,d}}{\sigma+1} 2^{2\sigma+4} \|\psi(z_n) - \psi(z_k)\|_2^{2\sigma} < \frac{1}{2}.$$

Combining the above, we have

$$\begin{aligned} \|\nabla \psi(z_n)\|_2^2 &\leq H(0) + \frac{2^{2\sigma+2}\nu}{\sigma+1} \\ &\times \left(C_{\sigma,d} \|\psi(z_n) - \psi(z_k)\|_2^{2\sigma} 2^2 \left(\|\nabla \psi(z_n)\|_2^2 + \|\nabla \psi(z_k)\|_2^2 \right) + \|\psi(z_k)\|_{2\sigma+2}^{2\sigma+2} \right) \\ &\leq \frac{1}{2} \left(\|\nabla \psi(z_n)\|_2^2 + \|\nabla \psi(z_k)\|_2^2 \right) + \frac{2^{2\sigma+2}\nu}{\sigma+1} \|\psi(z_k)\|_{2\sigma+2}^{2\sigma+2} \\ &= \frac{1}{2} \|\nabla \psi(z_n)\|_2^2 + c_k. \end{aligned}$$

Thus, $\|\nabla \psi(z_n)\|_2^2$ is bounded as $n \rightarrow \infty$, which is a contradiction. \square

Theorem 5.3 shows that when $\nu > 0$ and $\sigma d = 2$, the location of the singularity in L^2 and in H^1 is the same. The “reasons” why the solution leaves these two spaces are different. Thus, the solution leaves H^1 because its H^1 norm becomes infinite (Corollary 5.3). In contrast, the solution leaves L^2 not because its L^2 norm becomes infinite,²⁰ but rather because it approaches a delta function (Sect. 13.3), which is not an L^2 function.

Exercise 5.6 Let ψ be a solution of the BNLS (5.3) with $\nu < 0$ and $\sigma d = 4$ that becomes singular in H^2 at Z_c . Show that ψ does not have a strong limit in L^2 as $z \rightarrow Z_c$.

²⁰ By power conservation, the L^2 norm of the solution remains finite at the singularity.

5.8 Radial Solutions

The assumption that the initial condition (input beam) is radially symmetric is common in optics. In this case, the solution (beam) preserves this symmetry:

Lemma 5.5 *Let ψ be a solution of the NLS (5.1). If $\psi_0 \in H^1$ and $\psi_0 = \psi_0(|\mathbf{x}|)$, then $\psi = \psi(z, |\mathbf{x}|)$ for all $0 < z < Z_c$.*

Proof Consider any rotation of the d -dimensional transverse plane around the origin, and let $\tilde{\psi}$ be the solution of the NLS in the rotated coordinate system. Both the Laplacian and the nonlinearity, hence the NLS, are invariant under rotations. In addition, if $\psi_0 = \psi_0(|\mathbf{x}|)$, then $\tilde{\psi}_0 = \psi_0$. Therefore, from uniqueness of NLS solutions (Theorem 5.1) it follows that $\psi \equiv \tilde{\psi}$. Since $\psi \equiv \tilde{\psi}$ for any rotation, ψ is radial. \square

Remark Input laser beams are never truly radial. Therefore, when making use of Lemma 5.5, an important issue is that of *azimuthal stability*, i.e., to what extent laser beams are affected by small departures from radial symmetry of the input beam.²¹

A similar argument shows that if $\psi_0 = \psi_0(|x_1|, x_2, \dots, x_d)$, then $\psi(z, \mathbf{x})$ is invariant under the transformation $x_1 \rightarrow -x_1$.

Corollary 5.9 *Let ψ be a solution of the NLS (5.1). If $\psi_0 \in H^1$ and is elliptically shaped, i.e., if $\psi_0 = \psi_0\left(\sum_{k=1}^d \frac{x_k^2}{a_k^2}\right)$, then $\psi(z, \mathbf{x})$ is invariant under the transformations $x_k \rightarrow -x_k$ for $k = 1, \dots, d$.*

In Lemma 25.1 we will use this result to characterize the multiple filamentation patterns of elliptic input beams.

5.9 Focusing and Defocusing NLS

In Sect. 3.2 we used geometrical optics to show that laser beams that propagate in a Kerr medium undergo self-focusing if the Kerr coefficient n_2 is positive, and self-defocusing if n_2 is negative. Since the sign of v is the same as that of n_2 , see (3.3b), we make the following definitions.

Definition 5.8 (focusing and defocusing NLS) *The NLS (5.1) is called focusing if $v > 0$, and defocusing if $v < 0$.*

An informal way to determine whether the nonlinearity is focusing or defocusing is to use the following two “rules”, which are valid when the nonlinearity is weaker than or comparable to diffraction:²²

²¹ This issue will be discussed in Sects. 11.4.2, 11.5, 14.1.2, 14.5, 14.6.1, 19.3, 20.4, 22.6, and 25.3.2.

²² These “rules” do not necessarily apply when nonlinearity dominates over diffraction (Sects. 3.4.1 and 26.3.2).

1. Diffraction is always defocusing.
2. Nonlinearity is defocusing when it “works with diffraction” (i.e., when they have the “same sign”), and focusing when it “works against diffraction” (i.e., when they have “opposite signs”).

Since the Laplacian is a negative operator, it has “the same sign” as nonlinearity when $\nu < 0$, but the “opposite sign” when $\nu > 0$. This conclusion can also be reached by inspecting the relative signs of diffraction and nonlinearity in the Hamiltonian

$$H = \underbrace{\|\nabla\psi\|_2^2}_{\text{diffraction}} - \underbrace{\frac{\nu}{\sigma+1} \|\psi\|_{2\sigma+2}^{2\sigma+2}}_{\text{nonlinearity}}.$$

Indeed, the two terms are of the same sign when $\nu < 0$, but have opposite signs when $\nu > 0$.

The second “rule” implies

Conclusion 5.1 *Whether nonlinearity is self focusing or self defocusing depends on the relative signs of nonlinearity and diffraction, and not just on the sign of nonlinearity.*

This conclusion is consistent with the discussion in Sect. 2.16.2.

Exercise 5.7 *Determine the focusing and defocusing cases for the biharmonic NLS (5.3):*

1. *From the “signs” of $\nu\Delta^2$ and nonlinearity.*
2. *From the Hamiltonian (5.10).*

Note that $\Delta^2\psi$ is always defocusing.

5.10 Global Existence

5.10.1 Defocusing NLS

As noted, when $\nu < 0$ nonlinearity works together with diffraction to defocus the beam. Therefore, one does not expect the solution to collapse. Indeed, the defocusing NLS does not admit singular solutions:

Theorem 5.4 *Let ψ be a solution of the NLS (5.1) such that $\|\psi_0\|_{H^1} < \infty$, and let $\nu < 0$. Then ψ exists and is unique for all $0 \leq z < \infty$.*

Proof By Corollary 5.1, $H(\psi_0) < \infty$. In addition, when $\nu < 0$, Hamiltonian conservation implies that $\|\nabla\psi\|_2^2 \leq H(0)$. Since $\|\psi\|_2^2$ is conserved, global existence follows from Corollary 5.2. \square

Remark We already “derived” this result using the aberrationless approximation (Sect. 3.5).

Since $n_2 > 0$ for almost all Kerr materials, the two-dimensional defocusing NLS does not serve as a physical model for beam propagation in a bulk Kerr medium.²³ In addition, Theorem 5.4 indicates that solutions of the defocusing NLS do not become singular. Since the emphasis in this book is on optical collapse of laser beams, from now on we only consider the focusing NLS.

5.10.2 Focusing NLS

Without loss of generality, we can limit the discussion of the focusing NLS to the case $\nu = 1$, i.e.,

$$i\psi_z(z, \mathbf{x}) + \Delta\psi + |\psi|^{2\sigma}\psi = 0, \quad \psi(0, \mathbf{x}) = \psi_0(\mathbf{x}). \quad (5.18)$$

Indeed, let ψ be a solution of the NLS (5.1) such that $\|\psi_0\|_{H^1} < \infty$, and let $\nu > 0$. Then $\tilde{\psi} = \nu^{\frac{1}{2\sigma}}\psi$ is a solution of (5.18) with $\|\tilde{\psi}_0\|_{H^1} < \infty$. Therefore, from now on, we mainly consider the NLS (5.18).

The following result was proved in 1983 by Weinstein:

Theorem 5.5 ([272]) *Let $\|\psi_0\|_{H^1} < \infty$. Then any of the following two conditions is sufficient for global existence in the focusing NLS (5.18):*

1. $0 < \sigma d < 2$.
2. $\sigma d = 2$ and $\|\psi_0\|_2^2 < P_{\text{cr}}$, where P_{cr} is a constant that depends only on the dimension d .

Proof By Corollary 5.2, we can prove global existence by deriving an a priori bound on $\|\nabla\psi\|_2$. Unlike the defocusing NLS (see Theorem 5.4), however, Hamiltonian conservation does not necessarily imply that $\|\nabla\psi\|_2$ remains bounded, because the two terms in the Hamiltonian have opposite signs.

To bound $\|\nabla\psi\|_2$, we rewrite Hamiltonian conservation as, see (5.6),

$$\|\nabla\psi\|_2^2 = H(0) + \frac{1}{\sigma+1}\|\psi\|_{2\sigma+2}^{2\sigma+2}. \quad (5.19)$$

²³ Defocusing NLS equations do arise, however, in physical models (Sect. 3.2.1).

Combining (5.19) with the Gagliardo-Nirenberg inequality (5.11) and power conservation, see (5.4), one obtains

$$\|\nabla\psi\|_2^2 \leq H(0) + \kappa \|\nabla\psi\|_2^{\sigma d}, \quad \kappa := \frac{C_{\sigma,d}}{\sigma+1} \|\psi_0\|_2^{2+\sigma(2-d)}. \quad (5.20)$$

Since $\kappa \geq 0$, inequality (5.20) shows that $\|\nabla\psi\|_2$ is bounded when $\sigma d < 2$.

When $\sigma d = 2$, inequality (5.20) reads

$$\|\nabla\psi\|_2^2 \leq H(0) + \kappa \|\nabla\psi\|_2^2. \quad (5.21)$$

A sufficient condition for global existence is thus $\kappa < 1$. This condition can be rewritten as $\|\psi_0\|_2^2 < P_{\text{cr}}$, where

$$P_{\text{cr}} := \left(\frac{\sigma+1}{C_{\sigma,d}} \right)^{\frac{1}{\sigma}}, \quad \sigma = \frac{2}{d}. \quad (5.22)$$

Hence, P_{cr} depends only on the dimension d . \square

Remark The constant P_{cr} is the minimal power required for collapse in the focusing NLS with $\sigma d = 2$, and is called the *critical power for collapse*, or simply the *critical power*.

For completeness, we present the equivalent results for the NLS (5.1):

Theorem 5.6 *Let $\|\psi_0\|_{H^1} < \infty$. Then any of the following three conditions is sufficient for global existence in the NLS (5.1):*

1. $v < 0$.
2. $v > 0$ and $0 < \sigma d < 2$.
3. $v > 0$, $\sigma d = 2$, and $\|\psi_0\|_2^2 < v^{-\frac{1}{\sigma}} P_{\text{cr}}$, where P_{cr} is given by (5.22).

Remark The scaling of the critical power by $v^{-\frac{1}{\sigma}} = v^{-\frac{d}{2}}$ can be explained as follows. The critical power represents the minimal power needed for the nonlinearity $v|\psi|^{2\sigma}$ to overcome diffraction. Therefore, as v increases, less power is required for $v|\psi|^{2\sigma}$ to overcome diffraction.

The generalization of Theorem 5.6 to the BNLS is due to Fibich, Ilan, and Papanicolaou:

Theorem 5.7 ([82]) *Let $\|\psi_0\|_{H^2} < \infty$. Then any of the following three conditions is sufficient for global existence in the biharmonic NLS (5.3):*

1. $v > 0$.
2. $v < 0$ and $0 < \sigma d < 4$.

3. $\nu < 0$, $\sigma d = 4$, and $\|\psi_0\|_2^2 < |\nu|^{\frac{1}{\sigma}} P_{\text{cr}}^B$, where

$$P_{\text{cr}}^B = \left(\frac{\sigma + 1}{B_{\sigma,d}} \right)^{\frac{1}{\sigma}}, \quad \sigma = \frac{4}{d}. \quad (5.23)$$

Remark Unlike the NLS, the critical power in the BNLS (5.3) scales as $|\nu|^{+\frac{1}{\sigma}}$, since ν multiplies the diffraction term and not the nonlinearity.

Exercise 5.8 Prove Theorem 5.7. Note that:

- The conserved power and Hamiltonian are given by (5.10).
- The focusing and defocusing cases were determined in Exercise 5.7.
- As in the case of the NLS, from the BNLS local existence theory [19] it follows that an a priori bound of the H^2 norm implies global existence.
- It is sufficient to derive an a priori bound for $\|\Delta\psi\|_2^2$, since $\|\psi\|_2^2$ is conserved, and $\|\nabla\psi\|_2^2$ can be bounded by $\|\Delta\psi\|_2^2$ and $\|\psi\|_2^2$ (Exercise 5.5).
- The relevant Gagliardo-Nirenberg inequality is (5.12).

Theorem 5.7 can be extended to the NLS with mixed-order dispersion:

Theorem 5.8 ([82]) The result of Theorem 5.7 is also valid for the NLS

$$i\psi_z(z, \mathbf{x}) + \Delta\psi + |\psi|^{2\sigma}\psi + \nu\Delta^2\psi = 0, \quad \psi(0, \mathbf{x}) = \psi_0 \in H^2. \quad (5.24)$$

Exercise 5.9 Prove Theorem 5.8. Note that the conserved power and Hamiltonian are $\|\psi\|_2^2$ and $H_{\text{mix}} := \|\nabla\psi\|_2^2 - \frac{1}{\sigma+1}\|\psi\|_{2\sigma+2}^{2\sigma+2} - \nu\|\Delta\psi\|_2^2$, respectively, and that from the estimates of the linear operator associated with (5.24), see [19], it follows that a priori bound of $\|\psi\|_{H^2}$ implies global existence.

Finally, we note that in [83], Fibich, Ilan and Schochet extended Theorem 5.7 to the NLS with *non-isotropic mixed-order dispersion*

$$i\psi_z(z, \mathbf{x}) + \Delta\psi + |\psi|^{2\sigma}\psi - \sum_{i=1}^k \psi_{x_i x_i x_i x_i} = 0, \quad 1 \leq k \leq d.$$

5.11 Subcritical, Critical, and Supercritical NLS

Theorem 5.5 showed that when $\sigma d < 2$, all solutions exist globally. In Theorem 7.2 we will see that when $\sigma d \geq 2$, the focusing NLS admits blowup solutions. Therefore, we say that *the critical exponent for blowup of NLS solutions is $\sigma = 2/d$* . This motivates the following definitions:

Definition 5.9 (subcritical, critical, and supercritical NLS) *The NLS is called subcritical if $0 < \sigma d < 2$, critical if $\sigma d = 2$, and supercritical if $\sigma d > 2$.*

Remark Definitions 5.9 are also known as the L^2 -subcritical, L^2 -critical, and L^2 -supercritical NLS, see Sect. 5.11.4.

By Theorem 5.7, when $\sigma d < 4$ all solutions of the BNLS (5.3) exist globally. In addition, there is extensive numerical evidence that the focusing BNLS admits blowup solutions when $\sigma d \geq 4$.²⁴ Therefore, the *critical exponent* for blowup of BNLS solutions is $\sigma = 4/d$, and the BNLS is called subcritical, critical, and supercritical, if $0 < \sigma d < 4$, $\sigma d = 4$, and $\sigma d > 4$, respectively.²⁵

5.11.1 Subcritical NLS

In Theorem 5.5 we proved that all solutions of the subcritical focusing NLS exist globally. For example, the one-dimensional cubic focusing NLS

$$i\psi_z(z, x) + \psi_{xx} + |\psi|^2\psi = 0$$

is subcritical, since $\sigma = d = 1$. This equation admits stable solitary waves called *solitons*, but does not admit singular solutions.

Remark More precisely, Theorem 5.5 shows that the subcritical NLS does not admit H^1 blowup solutions. The subcritical NLS does admit blowup solutions which are not in H^1 (Sect. 12.8).

5.11.2 Critical NLS

The critical focusing NLS reads

$$i\psi_z(z, \mathbf{x}) + \Delta\psi + |\psi|^{\frac{4}{d}}\psi = 0. \quad (5.25)$$

This book is mostly concerned with this equation, because the model for beam propagation in a bulk medium is the NLS with $v > 0$, $d = 2$, and $\sigma = 1$.

In Theorem 5.5 we saw that $\|\psi_0\|_2^2 < P_{\text{cr}}$ is a sufficient condition for global existence in (5.25). In Theorem 7.2 we will see that $H(\psi_0) < 0$ is a sufficient condition for collapse in (5.25). Therefore, in the critical case the two conditions $\|\psi_0\|_2^2 < P_{\text{cr}}$ and $H(\psi_0) < 0$ cannot be simultaneously satisfied. Indeed, we have

²⁴ See Sects. 14.7, 19.7, 21.7, 22.2.1, and 23.10.

²⁵ See also Exercise 5.13.

Corollary 5.10 Let $\sigma d = 2$ and $\psi_0 \in H^1$. Then

$$0 < \|\psi_0\|_2^2 < P_{\text{cr}} \implies H(\psi_0) > 0, \quad (5.26)$$

or, equivalently,

$$H(\psi_0) \leq 0 \implies \|\psi_0\|_2^2 \geq P_{\text{cr}}.$$

Proof Consider inequality (5.21). If $0 < \|\psi_0\|_2^2 < P_{\text{cr}}$, then $\kappa < 1$, and so $H(\psi_0) \geq (1 - \kappa)\|\nabla\psi_0\|_2 > 0$. \square

Exercise 5.10 Let $f \in H^1$ such that $\|\nabla f\|_2 \leq M$ and $\|f\|_{\frac{4}{d}+2} \geq m$. Show that $\|f\|_2^2 \geq \left(\frac{d}{d+2}\right)^{\frac{d}{2}} \frac{m^{d+2}}{M^d} P_{\text{cr}}$.

By Theorems 5.5 and 7.2, relation (5.26) has the following interpretation:

sufficient condition for global existence in the critical NLS is true \implies sufficient condition for blowup in the critical NLS is false

Corollary 5.11 Let $\sigma d = 2$ and $\psi_0 \in H^1$. If $\|\psi_0\|_2^2 = P_{\text{cr}}$, then $H(\psi_0) \geq 0$.

Exercise 5.11 Prove Corollary 5.11.

Remark See Corollary 6.7 for additional results on the case $\|\psi_0\|_2^2 = P_{\text{cr}}$.

Exercise 5.12 Consider the focusing critical BNLS ($v = -1$, $\sigma d = 4$) with $\psi_0 \in H^2$. Show that

$$0 < \|\psi_0\|_2^2 < P_{\text{cr}}^B \implies H_B(\psi_0) > 0, \quad (5.27)$$

where P_{cr}^B is given by (5.23) and $H_B = \|\Delta\psi\|_2^2 - \frac{1}{\frac{4}{d}+1} \|\psi\|_{\frac{8}{d}+2}^{\frac{8}{d}+2}$.

5.11.3 Supercritical NLS

In Theorem 5.5 we saw that there exists a positive number P_{cr} , such that $\|\psi_0\|_2^2 \geq P_{\text{cr}}$ is a necessary condition for collapse in the critical NLS (5.25). This is not the case, however, in the supercritical NLS:

Lemma 5.6 The supercritical NLS admits singular solutions with arbitrarily small power.

Proof Let ψ be a singular solution of the supercritical NLS (existence of singular supercritical solutions follows e.g., from Lemma 7.9). Then $\psi^{(\lambda)}(z, \mathbf{x}) := \lambda^{\frac{1}{\sigma}} \psi(\lambda^2 z, \lambda \mathbf{x})$ is also a singular solution of the supercritical NLS (Sect. 8.1 and Lemma 27.1). Since $\|\psi_0^{(\lambda)}\|_2^2 = \lambda^{\frac{2}{\sigma}-d} \|\psi_0\|_2^2$, then $\lim_{\lambda \rightarrow \infty} \|\psi_0^{(\lambda)}\|_2^2 = 0$. Hence, the result follows. \square

Thus, there is no critical power for collapse in the supercritical case. There is, however, a *critical H^1 norm for collapse*:²⁶

Theorem 5.9 ([39]) *Consider the critical and supercritical NLS (5.1), where*

$$\begin{cases} \frac{2}{d} \leq \sigma < \infty, & \text{if } d \leq 2, \\ \frac{2}{d} \leq \sigma < \frac{2}{d-2}, & \text{if } d > 2. \end{cases}$$

Then there exists ϵ_0 such that if $\|\psi_0\|_{H^1} \leq \epsilon_0$, the solution ψ exists globally.

5.11.4 L^2 -Critical and H^1 -Subcritical

If $\psi(z, \mathbf{x})$ is a solution of the NLS (5.1), then so is $\psi^{(\lambda)}(z, \mathbf{x}) := \lambda^{\frac{1}{\sigma}} \psi(\lambda^2 z, \lambda \mathbf{x})$. Therefore, we define the NLS dilation of $f(\mathbf{x})$ as $f^{(\lambda)}(\mathbf{x}) := \lambda^{\frac{1}{\sigma}} f(\lambda \mathbf{x})$. We say that the NLS is *L^2 -critical*, if the L^2 norm of $f^{(\lambda)}$ is independent of λ . Since

$$\|f^{(\lambda)}\|_2^2 = \lambda^{\frac{2}{\sigma}-d} \|f\|_2^2,$$

the NLS is *L^2 -critical* when $\sigma d = 2$. In addition, we say that the NLS is *L^2 -subcritical* or *L^2 -supercritical*, if for any $0 \not\equiv f \in L^2$, $\lim_{\lambda \rightarrow 0} \|f^{(\lambda)}\|_{L^2}$ is equal to zero or to infinity, respectively. These cases correspond to $\sigma d < 2$ and $\sigma d > 2$, respectively.

Similarly, we say that the NLS is *H^1 -critical*, if $\|f^{(\lambda)}\|_{\dot{H}^1}$ is independent of λ , where $\|f\|_{\dot{H}^1} := \|\nabla f\|_2$. Since

$$\|f^{(\lambda)}\|_{\dot{H}^1}^2 = \|\nabla f^{(\lambda)}\|_2^2 = \lambda^{\frac{2}{\sigma}+2-d} \|\nabla f\|_2^2,$$

the NLS is *H^1 -critical* if $d = 2 + \frac{2}{\sigma}$.²⁷ In addition, the NLS is called *H^1 -subcritical* or *H^1 -supercritical*, if for any $0 \not\equiv f \in H^1$, $\lim_{\lambda \rightarrow 0} \|f^{(\lambda)}\|_{\dot{H}^1}$ is equal to zero or to infinity, respectively. Therefore, the NLS with $\sigma > 0$ is *H^1 -subcritical* if

$$\begin{cases} 0 < \sigma < \infty, & \text{if } d \leq 2, \\ 0 < \sigma < \frac{2}{d-2}, & \text{if } d > 2. \end{cases}$$

²⁶ Theorem 5.9 is a special case of Theorem 6.2.1 in [39], due to Cazenave. See also Remark 6.2.2 therein.

²⁷ This is the case, e.g., with the three-dimensional cubic NLS.

In this book we always assume that the NLS is H^1 -subcritical. This ensures that H^1 solutions have a finite Hamiltonian (Lemma 5.4). Note that the L^2 -subcritical and L^2 -critical NLS are always H^1 -subcritical.

Exercise 5.13 Let $\psi(z, \mathbf{x})$ be a solution of the biharmonic NLS (5.3) with $\sigma > 0$. Then $\psi^{(\lambda)}(z, \mathbf{x}) := \lambda^{\frac{2}{\sigma}} \psi(\lambda^4 z, \lambda \mathbf{x})$ is also a solution of the BNLS. Therefore, we define the BNLS dilation of $f(\mathbf{x})$ as $f^{(\lambda)}(\mathbf{x}) := \lambda^{\frac{2}{\sigma}} f(\lambda \mathbf{x})$.

1. Show that the BNLS is L^2 -subcritical, L^2 -critical, and L^2 -supercritical, if $\sigma d < 4$, $\sigma d = 4$, and $\sigma d > 4$, respectively.
2. Show that the BNLS is H^2 -subcritical if σ is given by (5.13). Here, $\|f\|_{\dot{H}^2} := \|\Delta f\|_2$.

5.12 Optimal Constant $C_{\sigma,d}$ [272]

The result of Theorem 5.5 for the critical case can be restated as

Corollary 5.12 ([272]) A necessary condition for a singularity in the critical NLS (5.25) is that $\|\psi_0\|_2^2 \geq P_{\text{cr}}$, where P_{cr} is given by (5.22).

Since $\|\psi\|_2^2$ is the power, we have

Corollary 5.13 P_{cr} is a lower bound for the power required for collapse.

By Theorem 5.5, the value of P_{cr} depends on the optimal constant $C_{\sigma,d}$ in the Gagliardo-Nirenberg inequality (5.11). Thus, the practical problem of calculating the critical power for collapse of laser beams reduces to a theoretical calculation of an optimal constant in a Sobolev inequality.

The original proofs of Gagliardo and Nirenberg [104, 105, 202] “only” showed that there exists a positive constant C for which inequality (5.11) holds. Therefore, for this value of C ,

$$0 < \frac{1}{C} \leq J[f], \quad 0 \not\equiv f \in H^1, \quad (5.28a)$$

where

$$J[f] = \frac{\|\nabla f\|_2^{\sigma d} \|f\|_2^{2+\sigma(2-d)}}{\|f\|_{2\sigma+2}^{2\sigma+2}}. \quad (5.28b)$$

Clearly, if we replace C with a larger constant, inequalities (5.11) and (5.28) still hold. If we replace C with a smaller constant, however, these inequalities might not hold for all f .

Definition 5.10 (optimal constant) The optimal constant $C_{\sigma,d}$ is the smallest positive number for which the Gagliardo-Nirenberg inequality (5.11) holds for all $f \in H^1$.

Therefore,

$$\frac{1}{C_{\sigma,d}} = \inf_{0 \not\equiv f \in H^1} J[f]. \quad (5.29)$$

If there exists a minimizer \tilde{f} to $J[f]$, then $C_{\sigma,d} = 1/J[\tilde{f}]$, and so the Gagliardo-Nirenberg inequality (5.11) becomes an equality for \tilde{f} . The existence of such a minimizer was first proved by Weinstein for $d \geq 2$. A different proof, which holds for $d \geq 1$, was given by Nawa.

Theorem 5.10 ([196, 272]) *Let σ be in the H^1 -subcritical regime (5.2), and let $J[f]$ be given by (5.28b). Then $\inf_{0 \not\equiv f \in H^1} J[f]$ is attained.*

Proof See Sect. 5.12.2. □

Remark The existence of a minimizer to $J[f]$ is not obvious. Indeed, on a bounded domain the infimum of $J[f]$ is not attained (Corollary 16.6).

We now present the calculation of the optimal constant $C_{\sigma,d}$, due to Weinstein [272]. Note that for the purpose of calculating the critical power, we only need to calculate the optimal constant in the critical case. For completeness, however, we calculate it for any σ and d .

By Theorem 5.10, there exists a function $0 \not\equiv \tilde{f} \in H^1$ such that

$$J[\tilde{f}] = \min_{0 \not\equiv f \in H^1} J[f].$$

We first show that the minimizer is real, up to multiplication by $e^{i\alpha}$:

Lemma 5.7 *Let \tilde{f} be a minimizer of $J[f]$ over all functions $0 \not\equiv f \in H^1$ which are complex. Then $\tilde{f} = e^{i\alpha} A(\mathbf{x})$, where α is a real constant and A is a real function.*

Proof Let $\tilde{f} = Ae^{iS}$, where A and S are real functions. Then

$$J[\tilde{f}] = \frac{\left(\|\nabla A\|_2^2 + \|A\nabla S\|_2^2 \right)^{\frac{\sigma d}{2}} \|A\|_2^{2+\sigma(2-d)}}{\|A\|_{2\sigma+2}^{2\sigma+2}} = \left(1 + \frac{\|A\nabla S\|_2^2}{\|\nabla A\|_2^2} \right)^{\frac{\sigma d}{2}} J[A].$$

Therefore, if $\nabla S \not\equiv 0$, then $J[\tilde{f}] > J[A]$, which is a contradiction. □

Thus, without loss of generality, we can assume from now on that the minimizer \tilde{f} is real. Since \tilde{f} is a minimizer, $J[\tilde{f} + \epsilon g] \geq J[\tilde{f}]$ for all $g \in H^1$ and for all ϵ . Therefore,

$$\frac{d}{d\epsilon} \Big|_{\epsilon=0} J[\tilde{f} + \epsilon g] = 0, \quad \forall g \in H^1. \quad (5.30)$$

To calculate this derivative, we first note that

$$\begin{aligned} \frac{d}{d\epsilon} \Big|_{\epsilon=0} \|\nabla(\tilde{f} + \epsilon g)\|_2^{\sigma d} &= \frac{d}{d\epsilon} \Big|_{\epsilon=0} \left(\int (\nabla \tilde{f} + \epsilon \nabla g)^2 d\mathbf{x} \right)^{\frac{\sigma d}{2}} \\ &= \frac{\sigma d}{2} \left(\int (\nabla \tilde{f})^2 d\mathbf{x} \right)^{\frac{\sigma d}{2}-1} \int 2\nabla \tilde{f} \nabla g d\mathbf{x} = \sigma d \|\nabla \tilde{f}\|_2^{\sigma d-2} \int \nabla \tilde{f} \nabla g d\mathbf{x}. \end{aligned}$$

Similarly,

$$\frac{d}{d\epsilon} \Big|_{\epsilon=0} \|\tilde{f} + \epsilon g\|_2^{2+\sigma(2-d)} = (2 + \sigma(2-d)) \|\tilde{f}\|_2^{\sigma(2-d)} \int \tilde{f} g d\mathbf{x},$$

and

$$\frac{d}{d\epsilon} \Big|_{\epsilon=0} \|\tilde{f} + \epsilon g\|_{2\sigma+2}^{2\sigma+2} = (2\sigma+2) \int |\tilde{f}|^{2\sigma} \tilde{f} g d\mathbf{x}.$$

Substituting the above in (5.30), dividing by $J[\tilde{f}]$, and dropping the tilde signs, one obtains

$$\begin{aligned} \frac{\sigma d}{\|\nabla f\|_2^2} \int \nabla f \nabla g d\mathbf{x} + \frac{2 + \sigma(2-d)}{\|f\|_2^2} \int f g d\mathbf{x} \\ - \frac{2\sigma+2}{\|f\|_{2\sigma+2}^{2\sigma+2}} \int |f|^{2\sigma} f g d\mathbf{x} = 0. \end{aligned} \quad (5.31)$$

Let $f^{\lambda,\mu}(\mathbf{x}) = \mu f(\lambda \mathbf{x})$. It is easy to see that

$$J[f^{\lambda,\mu}] = J[f]. \quad (5.32)$$

Therefore, we can choose λ_0 and μ_0 so that²⁸

$$\|f^{\lambda_0,\mu_0}\|_2^2 = 2 + \sigma(2-d), \quad \|\nabla f^{\lambda_0,\mu_0}\|_2^2 = \sigma d. \quad (5.33)$$

Indeed, since

$$\|f^{\lambda,\mu}\|_2^2 = \mu^2 \lambda^{-d} \|f\|_2^2, \quad \|\nabla f^{\lambda,\mu}\|_2^2 = \mu^2 \lambda^{2-d} \|\nabla f\|_2^2,$$

we have that

$$\lambda_0 = \left(\frac{\sigma d}{2 + \sigma(2-d)} \right)^{\frac{1}{2}} \frac{\|f\|_2}{\|\nabla f\|_2}, \quad \mu_0 = \frac{[2 + \sigma(2-d)]^{\frac{1}{2}} \lambda_0^{\frac{d}{2}}}{\|f\|_2}.$$

²⁸ Note that $2 + \sigma(2-d) > 0$ for σ in the H^1 -subcritical regime (5.2).

Therefore, substituting $f = f^{\lambda_0, \mu_0}$ in (5.31) gives

$$\int \left[\nabla f^{\lambda_0, \mu_0} \nabla g + f^{\lambda_0, \mu_0} g - \frac{2\sigma + 2}{\|f^{\lambda_0, \mu_0}\|_{2\sigma+2}^{2\sigma+2}} |f^{\lambda_0, \mu_0}|^{2\sigma} f^{\lambda_0, \mu_0} g \right] d\mathbf{x} = 0.$$

To simplify the notation, from now on we denote f^{λ_0, μ_0} by f . Using integration by parts, the last equation can be rewritten as

$$\int g \left[\Delta f - f + \alpha_f |f|^{2\sigma} f \right] d\mathbf{x} = 0, \quad \alpha_f = \frac{2(\sigma + 1)}{\|f\|_{2\sigma+2}^{2\sigma+2}}. \quad (5.34)$$

Since Eq. (5.34) is valid for all $g \in H^1$, we have that²⁹

$$\Delta f(\mathbf{x}) - f + \alpha_f |f|^{2\sigma} f \equiv 0.$$

To eliminate the unknown constant α_f , we substitute

$$f(\mathbf{x}) = \alpha_f^{-\frac{1}{2\sigma}} R(\mathbf{x}). \quad (5.35)$$

Then $R(\mathbf{x})$ is the solution of

$$\Delta R(\mathbf{x}) - R + |R|^{2\sigma} R = 0. \quad (5.36)$$

By (5.32) and (5.35), $R(\mathbf{x})$ is also a minimizer. Hence,

$$\min_{0 \neq f \in H^1} J[f] = J[R] = \frac{\|\nabla R\|_2^{\sigma d} \|R\|_2^{2+\sigma(2-d)}}{\|R\|_{2\sigma+2}^{2\sigma+2}}.$$

At this stage, we would like to eliminate $\|\nabla R\|_2$ and $\|R\|_{2\sigma+2}$ from the expression for $J[R]$. One way to do that is to use the Pohozaev identities (6.7), see Exercise 6.5. Alternatively, we can proceed as follows. By (5.28b), (5.34), and (5.35),

$$\|R\|_2^{2\sigma} = \alpha_f \|f\|_2^{2\sigma} = \frac{2(\sigma + 1)}{\|f\|_{2\sigma+2}^{2\sigma+2}} \|f\|_2^{2\sigma} = \frac{2(\sigma + 1) J[f]}{\|\nabla f\|_2^{\sigma d} \|f\|_2^{2-\sigma d}}.$$

From this relation, (5.32), and (5.33), it follows that

$$\begin{aligned} J[R] = J[f] &= \frac{\|\nabla f\|_2^{\sigma d} \|f\|_2^{2-\sigma d}}{2(\sigma + 1)} \|R\|_2^{2\sigma} \\ &= \frac{(\sigma d)^{\frac{\sigma d}{2}}}{2(\sigma + 1)} [2 + \sigma(2 - d)]^{1 - \frac{\sigma d}{2}} \|R\|_2^{2\sigma}. \end{aligned} \quad (5.37)$$

²⁹ This conclusion is known as *the Fundamental Lemma of the Calculus of Variations* (see, e.g., [107]). Intuitively, we can prove this result by substituting $g = \delta(\mathbf{x})$, or, more accurately, by choosing a sequence $g_n \in H^1$ such that $g_n \rightarrow \delta(\mathbf{x})$.

In Sect. 6.4 we shall see that when $d = 1$, Eq.(5.36) has a unique solution in H^1 . When $d \geq 2$, however, Eq.(5.36) has a countable number of radial solutions $\{R^{(n)}(r)\}_{n=0}^\infty$ in H^1 .³⁰ Each $R^{(n)}$ is an extremal of $J[f]$, i.e., it satisfies Eq.(5.30). In addition,

$$J[R^{(n)}] = \frac{(\sigma d)^{\frac{\sigma d}{2}}}{2(\sigma + 1)} [2 + \sigma(2 - d)]^{1 - \frac{\sigma d}{2}} \|R^{(n)}\|_2^{2\sigma}. \quad (5.38)$$

Therefore, the minimum of J is attained by the extremal $R^{(n)}$ that has the minimal power.

Definition 5.11 (ground state) *A ground state of an equation is its lowest-power (L^2 norm) nontrivial solution.*

Definition 5.12 (excited state) *An excited state of an equation is a solution of that equation with power greater than the ground state.*

Let R^{gs} and R^{es} denote a ground state and an excited state of Eq.(5.36), respectively. Therefore,

$$\|R^{\text{gs}}\|_2^2 < \|R^{\text{es}}\|_2^2.$$

Hence, by (5.38),

$$J[R^{\text{gs}}] < J[R^{\text{es}}].$$

Consequently, the minimum of J is attained by R^{gs} , i.e.,

$$\min_{0 \neq f \in H^1} J[f] = J[R^{\text{gs}}].$$

By (5.32), the minimum of J is attained by $\mu R^{\text{gs}}(\lambda \mathbf{x})$. More generally, it is attained by $\mu e^{i\alpha} R^{\text{gs}}(\lambda(\mathbf{x} - \mathbf{x}_0))$. Therefore, we have

Lemma 5.8 $\min_{0 \neq f \in H^1} J[f]$ is attained by the $d + 3$ parameter family

$$R_{\lambda, \mu, \alpha, \mathbf{x}_0}^{\text{gs}}(\mathbf{x}) = \mu e^{i\alpha} R^{\text{gs}}(\lambda(\mathbf{x} - \mathbf{x}_0)), \quad (5.39)$$

where $\lambda, \mu, \alpha > 0$, $\mathbf{x}_0 \in \mathbb{R}^d$, and R^{gs} is a ground state of (5.36). In addition,

$$\min_{0 \neq f \in H^1} J[f] = \frac{(\sigma d)^{\frac{\sigma d}{2}}}{2(\sigma + 1)} [2 + \sigma(2 - d)]^{1 - \frac{\sigma d}{2}} \|R^{\text{gs}}\|_2^{2\sigma}.$$

In Theorem 6.3 we will show that

Lemma 5.9 Up to scaling, Eq.(5.36) has a unique ground state.

³⁰ When $d = 2$, Eq.(5.36) also admits a doubly-countable number of non-radial vortex solutions $R = e^{im\theta} R_m^{(n)}(r)$, see Sect. 15.2.2.

Therefore, from now on we denote this unique ground state by $R^{(0)}$.

From Eq. (5.29), Lemma 5.8, and Lemma 5.9 we get

Lemma 5.10 *The optimal constant in the Gagliardo-Nirenberg inequality (5.11) is*

$$C_{\sigma,d} = \frac{2(\sigma+1)}{(\sigma d)^{\frac{\sigma d}{2}}} [2 + \sigma(2-d)]^{-(1-\frac{\sigma d}{2})} \frac{1}{\|R^{(0)}\|_2^{2\sigma}}, \quad (5.40)$$

where $R^{(0)}$ is the ground state of (5.36).

Remark In the process of calculating the optimal constant in the Gagliardo-Nirenberg inequality, we obtained Eq.(5.36) for $R(\mathbf{x})$ from the first-order condition for minimizers of $J[f]$. Remarkably, the same equation governs the profile of NLS solitary wave $\psi^{\text{solitary}} = e^{iz} R(\mathbf{x})$. These “dual origins” of the R profile will be exploited in Chap. 6 where we analyze Eq. (5.36).

Exercise 5.14 ([82]) *The optimal constant in the Gagliardo-Nirenberg inequality (5.12) satisfies*

$$B_{\sigma,d} = \frac{1}{\inf_{0 \neq f \in H^2} J_B[f]}, \quad J_B[f] = \frac{\|\Delta f\|_2^{\frac{\sigma d}{2}} \|f\|_2^{2+2\sigma-\frac{\sigma d}{2}}}{\|f\|_{2\sigma+2}^{2\sigma+2}}. \quad (5.41)$$

Show that if the infimum of J_B is attained by a real function, then it is attained by $R_B^{(0)}$, the ground state of

$$-\Delta^2 R_B - R_B + |R_B|^{2\sigma} R_B = 0. \quad (5.42)$$

In this case

$$\min_{0 \neq f \in H^2} J_B[f] = \frac{1}{\sigma+1} \left(\frac{\sigma d}{4} \right)^{\frac{\sigma d}{4}} \left(1 + \frac{\sigma(4-d)}{4} \right)^{1-\frac{\sigma d}{4}} \|R_B^{(0)}\|_2^{2\sigma}.$$

Therefore, the optimal constant in the Gagliardo-Nirenberg inequality (5.12) is

$$B_{\sigma,d} = \left(\frac{\sigma d}{4} \right)^{-\frac{\sigma d}{4}} \left(1 + \frac{\sigma(4-d)}{4} \right)^{\frac{\sigma d}{4}-1} \frac{\sigma+1}{\|R_B^{(0)}\|_2^{2\sigma}}.$$

Remark The existence of a minimizer to J_B in the critical case $\sigma d = 4$ was proved in 2010 by Zhu et al. [286], and independently by Baruch et al. [14].

5.12.1 Critical Case

The expressions in Lemmas 5.8 and 5.10 become considerably simpler in the critical case. For example, the critical-case version of Lemma 5.8 is

Lemma 5.11 Let $\sigma d = 2$. Then $\min_{0 \neq f \in H^1} J[f]$ is attained by $R^{(0)}$, the ground state of

$$\Delta R - R + |R|^{\frac{4}{d}} R = 0. \quad (5.43)$$

In addition,

$$\min_{0 \neq f \in H^1} J[f] = \frac{1}{\sigma + 1} \|R^{(0)}\|_2^{2\sigma}.$$

Similarly, the critical-case version of Lemma 5.10 is

Lemma 5.12 Let $\sigma d = 2$. Then the optimal constant in the Gagliardo-Nirenberg inequality (5.11) is

$$C_{\sigma,d} = \frac{\sigma + 1}{\|R^{(0)}\|_2^{2\sigma}} = \frac{\frac{2}{d} + 1}{\|R^{(0)}\|_2^{\frac{4}{d}}}, \quad (5.44)$$

where $R^{(0)}$ is the ground state of (5.43).

In Theorem 5.5 we saw that a sufficient condition for global existence in the critical NLS is $\|\psi_0\|_2^2 < P_{\text{cr}} = \left(\frac{\sigma+1}{C_{\sigma,d}}\right)^{\frac{1}{\sigma}}$. Combining this result with expression (5.44) for $C_{\sigma,d}$ gives

Theorem 5.11 ([272]) A sufficient condition for global existence in the critical NLS is

$$\|\psi_0\|_2^2 < \|R^{(0)}\|_2^2,$$

where $R^{(0)}$ is the ground state of (5.43).

In other words, a necessary condition for collapse in the critical NLS is that the solution power be at least that of the ground state $R^{(0)}$.³¹

Corollary 5.14 The critical power for collapse in the critical NLS is given by $P_{\text{cr}} = \|R^{(0)}\|_2^2$, where $R^{(0)}$ is the ground state of (5.43).

Remark Theorem 5.11 provides a rigorous and exact calculation of the critical power for collapse, first estimated 18 years earlier by Kelley (Sect. 3.4.2).

Remark Theorem 5.11 is sharp, in the sense that all solutions with $\|\psi_0\|_2^2 < P_{\text{cr}}$ exist globally, and there exist blowup solutions with $\|\psi_0\|_2^2 = P_{\text{cr}}$, see Exercise 7.8 and Sect. 13.5.

Exercise 5.15 ([82]) Show that when $\sigma = 4/d$, the optimal constant in the BNLS Gagliardo-Nirenberg inequality (5.12) is

³¹ This result can be motivated as follows. Consider the solitary waves $\psi^{\text{solitary}} = e^{iz} R(\mathbf{x})$ of the critical NLS. Then R is a solution of (5.43). Since these solutions propagate without changing their profile, diffraction and nonlinearity are exactly balanced. Hence, the ground state $R^{(0)}$ is the borderline case between diffraction-dominated and nonlinearity-dominated propagation.

$$B_{\sigma,d} = \frac{\sigma + 1}{\|R_B^{(0)}\|_2^{2\sigma}},$$

where $R_B^{(0)}$ is the ground state of

$$-\Delta^2 R_B - R_B + |R_B|^{\frac{8}{d}} R_B = 0. \quad (5.45)$$

Exercise 5.16 ([82]) Show that a sufficient condition for global existence in the focusing critical BNLS

$$i\psi_z(z, \mathbf{x}) - \Delta^2 \psi + |\psi|^{\frac{4}{d}} \psi = 0$$

is $\|\psi_0\|_2^2 < \|R_B^{(0)}\|_2^2$, where $R_B^{(0)}$ is the ground state of (5.45). Therefore, $P_{\text{cr}}^B := \|R_B^{(0)}\|_2^2$ is the critical power for collapse in the critical BNLS.

5.12.2 Existence of a Minimizer to $J[f]$

We now turn to the proof of Theorem 5.10 of the existence of a minimizer for the functional $J[f]$. We present the original proof by Weinstein, which holds for $d \geq 2$. A different proof, which holds for $d \geq 1$ and does not make use of symmetrization, was given by Nawa [196, Proposition 2.5].

Proof of Theorem 5.10 By the definition of infimum, there exists a sequence $u_n \in H^1$ such that $\lim_{n \rightarrow \infty} J[u_n] = \inf_{0 \neq f \in H^1} J[f]$. From (5.28) it follows that $\inf_{0 \neq f \in H^1} J[f] > 0$. By Lemma 5.7 we can assume that u_n is real. Recall that if $f \in H^1$ is real, then $|\nabla|f|| = |\nabla f|$ almost everywhere (see, e.g., [158, Theorem 6.17]). Hence,

$$\|\nabla|f|\|_2 = \|\nabla f\|_2, \quad f \in H^1 \text{ and } f \text{ is real.} \quad (5.46)$$

Therefore,

$$J[f] = J[|f|], \quad f \in H^1 \text{ and } f \text{ is real.} \quad (5.47)$$

As a result, we can take $u_n \geq 0$. By *Steiner symmetrization*, we can also take u_n to be radial.³² In addition, as in Sect. 5.12, we can rescale u_n without changing the

³² The main result of Steiner symmetrization is as follows (see, e.g., [213, 271]):

Theorem 5.12 Let $u(\mathbf{x})$ be a function in \mathbb{R}^d such that $u \geq 0$ and $u \in C^1 \cap H^1$. Then there exists a function \tilde{u} in \mathbb{R}^d , “the Steiner symmetrization of u ”, such that $\tilde{u} \geq 0$, $\tilde{u} \in H^1$, and in addition:

1. \tilde{u} is radial, i.e., $\tilde{u} = \tilde{u}(|\mathbf{x}|)$.
2. For all $p > 0$, $\|\tilde{u}\|_p = \|u\|_p$.
3. $\|\nabla \tilde{u}\|_2 \leq \|\nabla u\|_2$.

Therefore, $\tilde{u}_n \in H^1$ and $J[\tilde{u}_n] \leq J[u_n]$.

value of $J[u_n]$, so that $\|u_n\|_2 = \|\nabla u_n\|_2 = 1$. Therefore, we obtain a sequence $\{u_n\}$ with the following properties:

$$u_n = u_n(r) \geq 0, \quad u_n \in H^1,$$

$$\|u_n\|_2 = \|\nabla u_n\|_2 = 1, \quad J[u_n] = \frac{1}{\|u_n\|_{2\sigma+2}^{2\sigma+2}} \rightarrow \inf_{0 \neq f \in H^1} J[f].$$

Since u_n is bounded in H^1 , it has a subsequence, also denoted by u_n , such that $u_n \rightharpoonup u$ weakly in H^1 , see Lemma B.5. Therefore, u_n and ∇u_n converge weakly in L^2 to u and ∇u , respectively. Hence, by Lemma B.3,

$$\|u\|_2 \leq \liminf_{n \rightarrow \infty} \|u_n\|_2 = 1, \quad \|\nabla u\|_2 \leq \liminf_{n \rightarrow \infty} \|\nabla u_n\|_2 = 1.$$

By Lemma 5.14, which will be proved next, $u_n \rightarrow u$ strongly in $L^{2\sigma+2}$. Therefore,

$$\inf J[f] \leq J[u] \leq \frac{1}{\|u\|_{2\sigma+2}^{2\sigma+2}} = \lim_{n \rightarrow \infty} \frac{1}{\|u_n\|_{2\sigma+2}^{2\sigma+2}} = \lim_{n \rightarrow \infty} J[u_n] = \inf_{0 \neq f \in H^1} J[f].$$

Hence, $J[u] = \inf_{0 \neq f \in H^1} J[f]$. Thus, the infimum of $J[f]$ is attained at $u \in H^1$. \square

To prove Lemma 5.14, we begin with an estimate of the decay of radial functions in H^1 :

Lemma 5.13 (Strauss radial lemma [246]) *Let $d \geq 2$ and $f = f(|\mathbf{x}|) \in H^1$. Then*

$$|f(\mathbf{x})| \leq \frac{C(d) \|f\|_{H^1}}{|\mathbf{x}|^{\frac{d-1}{2}}}, \quad |\mathbf{x}| \geq 1.$$

Proof Let $r = |\mathbf{x}|$. Then

$$-r^{d-1} f^2 = \int_r^\infty (r^{d-1} f^2)_r dr = \int_r^\infty [(d-1)r^{d-2} f^2 + 2ff_r r^{d-1}] dr.$$

Taking the absolute value and using $2ab \leq a^2 + b^2$ with $a = f$ and $b = f_r$, we have that for $r > 1$,

$$r^{d-1} f^2 \leq (d-1) \int_r^\infty r^{d-1} f^2 dr + \int_r^\infty r^{d-1} f^2 dr + \int_r^\infty r^{d-1} f_r^2 dr \leq \frac{d}{s_d} \|f\|_{H^1}^2,$$

where s_d is the surface area of the unit sphere in \mathbb{R}^d . \square

We now use Lemma 5.13 to prove

Lemma 5.14 (Compactness lemma) *Let $d \geq 2$, and let σ be in the H^1 -subcritical regime (5.2). Then the embedding $H_{\text{radial}}^1(\mathbb{R}^d) \rightarrow L^{2\sigma+2}(\mathbb{R}^d)$ is compact, i.e., every*

bounded sequence $\{u_n\} \in H_{\text{radial}}^1(\mathbb{R}^d)$ has a subsequence that converges strongly in $L^{2\sigma+2}(\mathbb{R}^d)$.

Proof Since $\|u_n\|_{H^1} \leq M$, the sequence $\{u_n\}$ contains a subsequence that converges weakly to u in H^1 . Since the limit of radial functions is a radial function, $u \in H_{\text{radial}}^1$. In addition, since for any bounded domain Ω the embedding $H^1(\Omega) \rightarrow L^2(\Omega)$ is compact, there is a subsequence, also denoted by u_n , that converges strongly to u in $L^2(\Omega)$, i.e., $\lim_{n \rightarrow \infty} \int_{\Omega} |u_n - u|^2 d\mathbf{x} = 0$. Therefore, from the Gagliardo-Nirenberg inequality on Ω

$$\|f\|_{L^{2\sigma+2}(\Omega)}^{2\sigma+2} \leq C_{\sigma,d,\Omega} \|\nabla f\|_{L^2(\Omega)}^{\sigma d} \|f\|_{L^2(\Omega)}^{2+\sigma(2-d)},$$

it follows that $u_n \rightarrow u$ strongly in $L^{2\sigma+2}(\Omega)$, i.e.,

$$\lim_{n \rightarrow \infty} \|u_n - u\|_{L^{2\sigma+2}(\Omega)} = 0.$$

To extend this result to \mathbb{R}^d , we first use Strauss' radial lemma to show that for any $\rho_\epsilon > 1$ and any n ,

$$\int_{|\mathbf{x}| > \rho_\epsilon} |u_n|^{2\sigma+2} d\mathbf{x} = \int_{|\mathbf{x}| > \rho_\epsilon} |u_n|^{2\sigma} |u_n|^2 \leq \frac{C \|u_n\|_{H^1}^{2\sigma}}{\rho_\epsilon^{(d-1)\sigma}} \int_{|\mathbf{x}| > \rho_\epsilon} |u_n|^2 \leq \frac{\tilde{C}}{\rho_\epsilon^{(d-1)\sigma}}.$$

Therefore, for any ϵ , there exists ρ_ϵ , such that for any n ,

$$\int_{|\mathbf{x}| > \rho_\epsilon} |u_n|^{2\sigma+2} d\mathbf{x} \leq \epsilon.$$

The proof is completed by using the above estimates in

$$\begin{aligned} \|u_n - u\|_{L^{2\sigma+2}(\mathbb{R}^d)}^{2\sigma+2} &= \|u_n - u\|_{L^{2\sigma+2}(|\mathbf{x}| \leq \rho_\epsilon)}^{2\sigma+2} + \|u_n - u\|_{L^{2\sigma+2}(|\mathbf{x}| \geq \rho_\epsilon)}^{2\sigma+2} \\ &\leq \|u_n - u\|_{L^{2\sigma+2}(|\mathbf{x}| \leq \rho_\epsilon)}^{2\sigma+2} + (\|u_n\|_{L^{2\sigma+2}(|\mathbf{x}| \geq \rho_\epsilon)} + \|u\|_{L^{2\sigma+2}(|\mathbf{x}| \geq \rho_\epsilon)})^{2\sigma+2}. \end{aligned}$$

□

In the analysis of the BNLS, we will make use of a compactness lemma for functions in H_{radial}^2 :

Lemma 5.15 ([14]) *Let $d \geq 2$ and let σ be in the H^2 -subcritical regime (5.13). Then the embedding $H_{\text{radial}}^2(\mathbb{R}^d) \rightarrow L^{2\sigma+2}(\mathbb{R}^d)$ is compact, i.e., every bounded sequence $\{u_n\} \in H_{\text{radial}}^2(\mathbb{R}^d)$ has a subsequence that converges strongly in $L^{2\sigma+2}(\mathbb{R}^d)$.*

Exercise 5.17 Prove Lemma 5.15.

Chapter 6

Solitary Waves

In this chapter, we analyze the semilinear elliptic equation

$$\Delta R(\mathbf{x}) - R + |R|^{2\sigma} R = 0, \quad (6.1)$$

where $\mathbf{x} = (x_1, \dots, x_d) \in \mathbb{R}^d$, $\Delta = \frac{\partial^2}{\partial x_1^2} + \dots + \frac{\partial^2}{\partial x_d^2}$, $R(\mathbf{x}) \in H^1(\mathbb{R}^d)$, and σ is in the H^1 -subcritical regime

$$\begin{cases} 0 < \sigma < \infty, & \text{if } d \leq 2, \\ 0 < \sigma < \frac{2}{d-2}, & \text{if } d > 2. \end{cases} \quad (6.2)$$

This equation arises in NLS theory in various contexts:

1. It governs the profile of the solitary waves $\psi^{\text{solitary}} = e^{iz}R(\mathbf{x})$ of the focusing NLS, see Sect. 6.1.
2. It is satisfied by the minimizers/extremals of the functional

$$J[f] = \frac{\|\nabla f\|_2^{\sigma d} \|f\|_2^{2+\sigma(2-d)}}{\|f\|_{2\sigma+2}^{2\sigma+2}}, \quad (6.3)$$

see Lemma 5.8, which arises in the calculation of the optimal constant $C_{\sigma,d}$.

The analysis in this chapter utilizes both the PDE and variational characterizations of $R(\mathbf{x})$

Remark In the critical case, $R(\mathbf{x})$ is also the self-similar profile of the explicit blowup solutions ψ_R^{explicit} , see Chap. 10, and of the asymptotic blowup profile $\psi_{R^{(0)}}$, see Chap. 14.

Remark Stability of solitary waves will be discussed in Chap. 9. Numerical methods for Eq. (6.1) are presented in Chap. 28.

6.1 Solitary Waves $\psi_\omega^{\text{solitary}} = e^{i\omega z} R_\omega(\mathbf{x})$

A solitary wave is a solution that travels at a constant velocity without changing its shape. Specifically, let $\psi_\omega^{\text{solitary}} = e^{i\omega z} R_\omega(\mathbf{x})$ be a solitary wave of the focusing NLS

$$i\psi_z(z, \mathbf{x}) + \Delta\psi + |\psi|^{2\sigma}\psi = 0,$$

where R_ω is a real function.¹ Then the equation for R_ω reads

$$\Delta R_\omega(\mathbf{x}) - \omega R_\omega + |R_\omega|^{2\sigma} R_\omega = 0. \quad (6.4)$$

Lemma 6.1 *A necessary condition for existence of H^1 solutions to Eq. (6.4) is $\omega > 0$.*

Proof We only give informal arguments, which would later clarify why this condition is not necessary on bounded domains (Sect. 16.4). Since $R_\omega \in H^1$, then $\lim_{|\mathbf{x}| \rightarrow \infty} R_\omega = 0$. Therefore, as $|\mathbf{x}| \rightarrow \infty$ the nonlinearity becomes negligible. Hence, to leading order, Eq. (6.4) reduces to

$$\Delta R_\omega(\mathbf{x}) - \omega R_\omega = 0. \quad (6.5)$$

When $\omega < 0$, solutions of (6.5) are oscillatory. Therefore, they do not have sufficient decay to be in H^1 . For example, the one-dimensional solutions $R_\omega = \sin(\sqrt{-\omega}x_i)$ do not decay as $|\mathbf{x}| \rightarrow \infty$. Radial solutions of (6.5) do decay, but only as $r^{-\frac{d-1}{2}}$, see Exercise 6.9. Therefore, they are not in L^2 . \square

Lemma 6.2 *Let R_ω be a solution of (6.4). Then*

$$\frac{d}{d\omega} H(R_\omega) = -\omega \frac{d}{d\omega} \|R_\omega\|_2^2.$$

Proof

$$\begin{aligned} \frac{d}{d\omega} H(R_\omega) &= \int (\nabla R_\omega) \left(\frac{\partial}{\partial \omega} \nabla R_\omega^* \right) - \int |R_\omega|^{2\sigma} R_\omega \frac{\partial}{\partial \omega} R_\omega^* + \text{c.c.} \\ &= - \int \left(\Delta R_\omega + |R_\omega|^{2\sigma} R_\omega \right) \frac{\partial}{\partial \omega} R_\omega^* + \text{c.c.} \\ &= - \int \omega R_\omega \frac{\partial}{\partial \omega} R_\omega^* + \text{c.c.} = -\omega \frac{d}{d\omega} \|R_\omega\|_2^2. \end{aligned}$$

See also Exercise 6.6 for a different proof. \square

¹ When R_ω is radial, it has to be real (up to multiplication by $e^{i\alpha}$), see Lemma 6.12. However, Eq. (6.1) can also admit genuinely-complex solutions (Sect. 15.2).

Exercise 6.1 Let $\psi_{B,\omega}^{\text{solitary}} = e^{i\omega z} R_{B,\omega}(\mathbf{x})$ be a solitary wave of the focusing biharmonic NLS $i\psi_z(z, \mathbf{x}) - \Delta^2 \psi + |\psi|^{2\sigma} \psi = 0$, where $R_B \in H^2$, and let $H_B(R_{B,\omega}) := \|\Delta R_{B,\omega}\|_2^2 - \frac{1}{\sigma+1} \|R_{B,\omega}\|_{2\sigma+2}^{2\sigma+2}$ be its Hamiltonian. Show that

$$\frac{d}{d\omega} H_B(R_{B,\omega}) = -\omega \frac{d}{d\omega} \|R_{B,\omega}\|_2^2.$$

It is easy to verify that when $\omega > 0$,

$$R_\omega(\mathbf{x}) = \omega^{\frac{1}{2\sigma}} R\left(\omega^{\frac{1}{2}} \mathbf{x}\right), \quad (6.6)$$

where $R := R_{\omega=1}$ is a solution of (6.1). Therefore, without loss of generality, from now on we set $\omega = 1$.

Exercise 6.2 Show that

$$\|R_\omega\|_2^2 = \omega^{\frac{2-\sigma d}{2\sigma}} \|R\|_2^2, \quad H(R_\omega) = \omega^{1+\frac{2-\sigma d}{2\sigma}} H(R).$$

Corollary 6.1 Let $R_\omega(\mathbf{x})$ be given by (6.6). Then

$$\begin{cases} \frac{d}{d\omega} \|R_\omega\|_2^2 > 0, & \text{if } \sigma d < 2, \\ \frac{d}{d\omega} \|R_\omega\|_2^2 = 0, & \text{if } \sigma d = 2, \\ \frac{d}{d\omega} \|R_\omega\|_2^2 < 0, & \text{if } \sigma d > 2. \end{cases}$$

This result will play a key role in the stability analysis of solitary waves (Sect. 9.4).

6.2 Pohozaev Identities

The following relations are known as the *Pohozaev identities* [212] for the NLS:

Lemma 6.3 (Pohozaev identities) Let $R(\mathbf{x})$ be a solution of (6.1). Then

$$\|R\|_2^2 = \frac{2-\sigma(d-2)}{2(\sigma+1)} \|R\|_{2\sigma+2}^{2\sigma+2}, \quad (6.7a)$$

$$\|\nabla R\|_2^2 = \frac{\sigma d}{2(\sigma+1)} \|R\|_{2\sigma+2}^{2\sigma+2}. \quad (6.7b)$$

Proof If we multiply (6.1) by R and integrate, we get

$$\|\nabla R\|_2^2 + \|R\|_2^2 = \|R\|_{2\sigma+2}^{2\sigma+2}. \quad (6.8)$$

Similarly, if we multiply (6.1) by $\mathbf{x} \cdot \nabla R$ and integrate, we get

$$\begin{aligned} 0 &= \int (\mathbf{x} \cdot \nabla R) \left(\Delta R - R + |R|^{2\sigma} R \right) \\ &= \int -\nabla(\mathbf{x} \cdot \nabla R) \cdot \nabla R + \int \mathbf{x} \cdot \left(-\nabla \frac{R^2}{2} + \nabla \frac{|R|^{2\sigma+2}}{2\sigma+2} \right). \end{aligned} \quad (6.9)$$

To evaluate the first integral on the right-hand side, we first note that

$$\frac{\partial}{\partial x_j} (\mathbf{x} \cdot \nabla R) = \frac{\partial R}{\partial x_j} + \mathbf{x} \cdot \nabla \frac{\partial R}{\partial x_j}.$$

Hence,

$$\nabla(\mathbf{x} \cdot \nabla R) = \nabla R + (\mathbf{x} \cdot \nabla) \nabla R. \quad (6.10)$$

Therefore,

$$\begin{aligned} - \int \nabla(\mathbf{x} \cdot \nabla R) \cdot \nabla R &= - \int (\nabla R + (\mathbf{x} \cdot \nabla) \nabla R) \cdot \nabla R \\ &= - \int (\nabla R)^2 - \int \mathbf{x} \cdot \nabla \frac{(\nabla R)^2}{2} = \left(-1 + \frac{d}{2} \right) \int (\nabla R)^2. \end{aligned}$$

The second integral on the right-hand side of (6.9) is equal to

$$\int \mathbf{x} \cdot \left(-\nabla \frac{R^2}{2} + \nabla \frac{|R|^{2\sigma+2}}{2\sigma+2} \right) = \frac{d}{2} \int R^2 - \frac{d}{2\sigma+2} \int |R|^{2\sigma+2}. \quad (6.11)$$

Hence, (6.9) implies that

$$\frac{d-2}{2} \|\nabla R\|_2^2 + \frac{d}{2} \|R\|_2^2 = \frac{d}{2(\sigma+1)} \|R\|_{2\sigma+2}^{2\sigma+2}. \quad (6.12)$$

Therefore,

$$\frac{d-2}{2} \times (6.8) - (6.12) \implies (6.7a)$$

$$\frac{d}{2} \times (6.8) - (6.12) \implies (6.7b).$$

□

Exercise 6.3 Use Lemma 6.3 and relation (6.6) to show that the Pohozaev identities for R_ω are

$$\omega \|R_\omega\|_2^2 = \frac{2-\sigma(d-2)}{2(\sigma+1)} \|R_\omega\|_{2\sigma+2}^{2\sigma+2}, \quad \|\nabla R_\omega\|_2^2 = \frac{d\sigma}{2(\sigma+1)} \|R_\omega\|_{2\sigma+2}^{2\sigma+2}.$$

From Lemma 6.3 one immediately has

Corollary 6.2 *Let $R(\mathbf{x})$ be a solution of (6.1). Then*

$$\|R\|_2^2 = \frac{2 - \sigma(d - 2)}{\sigma d} \|\nabla R\|_2^2. \quad (6.13)$$

In particular, in the critical case $\sigma d = 2$,

$$\|R\|_2^2 = \frac{2}{d} \|\nabla R\|_2^2. \quad (6.14)$$

Similarly, from relations (6.7) follows

Corollary 6.3 *Let $R(\mathbf{x})$ be a solution of (6.1). Then*

$$H(R) = \frac{d\sigma - 2}{2\sigma + 2} \|R\|_{2\sigma+2}^{2\sigma+2} = \frac{d\sigma - 2}{2 - \sigma(d - 2)} \|R\|_2^2. \quad (6.15)$$

Remark A different proof of relation (6.15) is given in Corollary 7.14.

Corollary 6.4 *Let $R(\mathbf{x})$ be a nontrivial solution of (6.1). Then*

$$\begin{cases} H(R) < 0, & \text{if } \sigma d < 2, \\ H(R) = 0, & \text{if } \sigma d = 2, \\ H(R) > 0, & \text{if } \sigma d > 2. \end{cases}$$

Proof This follows directly from (6.15). \square

Remark See Sect. 7.11 for “why” $H(R)$ cannot be negative in the critical and supercritical cases.

Corollary 6.5 *Let $R_\omega(\mathbf{x})$ be a nontrivial solution of (6.4). Then*

$$\begin{cases} H(R_\omega) < 0, & \text{if } \sigma d < 2, \\ H(R_\omega) = 0, & \text{if } \sigma d = 2, \\ H(R_\omega) > 0, & \text{if } \sigma d > 2. \end{cases}$$

Proof This follows directly from Corollary 6.4 and Exercise 6.2. \square

Lemma 6.4 *A necessary condition for existence of nontrivial H^1 solutions to Eq. (6.1) is that σ be in the H^1 -subcritical regime (6.2).*

Proof By (6.1), for R to decay as $|\mathbf{x}| \rightarrow \infty$, one should have that $|R|^{2\sigma} R \rightarrow 0$ as $R \rightarrow 0$. Hence, $2\sigma + 1 > 0$. Consequently, $2(\sigma + 1) > 0$. The necessary condition follows from the requirement that the right-hand sides of Eq. (6.7) be strictly positive. \square

A similar argument shows that the *defocusing NLS*

$$i\psi_z(z, \mathbf{x}) + \Delta\psi - |\psi|^{2\sigma}\psi = 0$$

does not admit localized solitary-wave solutions:

Exercise 6.4 Show that there are no nontrivial H^1 solutions to the equation

$$\Delta R(\mathbf{x}) - R - |R|^{2\sigma}R = 0.$$

Intuitively, there are no localized solitary waves in the defocusing case, because in a solitary wave diffraction effects are balanced by the nonlinearity, whereas a defocusing nonlinearity works together with diffraction.²

The Pohozaev identities provide an alternative proof to relation (5.37):

Exercise 6.5 Use the Pohozaev identities (6.7) to prove that $J[R] = \frac{(\sigma d)^{\frac{\sigma d}{2}}}{2(\sigma+1)} [2 + \sigma(2-d)]^{1-\frac{\sigma d}{2}} \|R\|_2^{2\sigma}$, where R is a solution of (6.1) and $J[R] = \frac{\|\nabla R\|_2^{\sigma d} \|R\|_2^{2+\sigma(2-d)}}{\|R\|_{2\sigma+2}^{2\sigma+2}}$.

The Pohozaev identities also provide an alternative proof to Lemma 6.2:

Exercise 6.6 Prove Lemma 6.2 using Eqs. (6.6) and (6.7).

In the following exercise we derive the Pohozaev identities for the BNLS:

Exercise 6.7 Let $\psi_{B,\omega}^{\text{solitary}} = e^{iz}R_B(\mathbf{x})$ be a solitary wave of the BNLS

$$i\psi_z(z, \mathbf{x}) + v\Delta^2\psi + |\psi|^{2\sigma}\psi = 0, \quad v = \pm 1,$$

where R_B is a real function in H^2 . Then R_B satisfies

$$v\Delta^2R_B(\mathbf{x}) - R_B + |R_B|^{2\sigma}R_B = 0. \quad (6.16)$$

1. Show that the Pohozaev identities for R_B are

$$\|R_B\|_2^2 = \frac{4 - (d - 4)\sigma}{4(\sigma + 1)} \|R_B\|_{2\sigma+2}^{2\sigma+2},$$

$$\sigma \|R_B\|_2^2 = -v \frac{4 - (d - 4)\sigma}{d} \|\Delta R_B\|_2^2.$$

² The defocusing NLS admits non-localized solitary wave solutions, known as *dark solitons*, whose intensity profile exhibit a dip in a uniform background, see e.g., [141, Chap. 4]. In this case, the defocusing nonlinearity and diffraction are balanced by the uniform background.

2. Show that two necessary conditions for existence of nontrivial solutions to Eq. (6.16) in H^2 are:
- $v < 0$.
 - σ is in the H^2 subcritical regime (5.13).
3. Show that in the focusing case $v = -1$,

$$\begin{cases} H_B(R_B) < 0, & \text{if } \sigma d < 4, \\ H_B(R_B) = 0, & \text{if } \sigma d = 4, \\ H_B(R_B) > 0, & \text{if } \sigma d > 4, \end{cases}$$

where $H_B(R_{B,\omega}) := \|\Delta R_{B,\omega}\|_2^2 - \frac{1}{\sigma+1} \|R_{B,\omega}\|_{2\sigma+2}^{2\sigma+2}$.

6.3 The Ground State $R^{(0)}$

Let us first recall some properties of the minimizers of $J[f]$ which were already proved in Chap. 5. In Theorem 5.10 we proved that the minimum of $J[f]$ in H^1 is attained. In Lemma 5.7 we showed that, up to multiplication by $e^{i\alpha}$, the minimizers of $J[f]$ are real. In Lemma 5.8 we saw that if R^{gs} is a ground state of (6.1), then the minimum of $J[f]$ is attained by R^{gs} .

We now prove that the ground state is:

1. Strictly positive (up to multiplication by $e^{i\alpha}$).
2. Analytic.
3. Radially-symmetric about some point $\mathbf{x}_0 \in \mathbb{R}^d$.
4. Monotonically decreasing in $r = |\mathbf{x} - \mathbf{x}_0|$.
5. Unique (up to NLS symmetries).

We first establish the following result:

Lemma 6.5 All non-trivial, non-negative solutions of (6.1) are strictly positive.

Proof We present the proof of Tao [253]. Taking the Fourier transform of Eq. (6.1) gives

$$(1 + |\mathbf{k}|^2) \hat{R}(\mathbf{k}) = \widehat{|R|^{2\sigma} R}.$$

Therefore,

$$\hat{R} = \frac{1}{1 + |\mathbf{k}|^2} \widehat{|R|^{2\sigma} R}.$$

Transforming back gives, see (2.71),

$$R = h * |R|^{2\sigma} R, \quad h(\mathbf{x}) = \mathcal{F}^{-1} \left(\frac{1}{1 + |\mathbf{k}|^2} \right).$$

We claim that $h > 0$. Therefore, if $|R|^{2\sigma} R \geq 0$, then

$$R(\mathbf{x}) = (2\pi)^{-\frac{d}{2}} \int h(\mathbf{x} - \mathbf{y}) |R|^{2\sigma} R(\mathbf{y}) d\mathbf{y} > 0.$$

To finish the proof, we need to verify that

$$h(\mathbf{x}) = \frac{1}{(2\pi)^{\frac{d}{2}}} \int_{\mathbb{R}^d} \frac{1}{1 + |\mathbf{k}|^2} e^{i\mathbf{k}\cdot\mathbf{x}} d\mathbf{k} > 0.$$

Tao [253] lists several ways to show that. Here we give yet another proof. When $d = 1$,

$$h(x) = \frac{1}{(2\pi)^{\frac{1}{2}}} \int_{-\infty}^{\infty} \frac{e^{ikx}}{1 + k^2} dk = \frac{2}{(2\pi)^{\frac{1}{2}}} \int_0^{\infty} \frac{\cos(kx)}{1 + k^2} dk.$$

The integral can be calculated explicitly using contour integration in the complex plane, yielding

$$\int_0^{\infty} \frac{\cos(kx)}{1 + k^2} dk = \frac{\pi}{2} e^{-|x|}. \quad (6.17)$$

Therefore, $h(x) > 0$.

When $d \geq 2$, we can assume, without loss of generality, that $\mathbf{x} = (|\mathbf{x}|, 0, \dots, 0)$, since we can always rotate the \mathbf{k} -space coordinate system so that $\mathbf{k} = (1, 0, \dots, 0)$ points in the direction of \mathbf{x} . Therefore, $\mathbf{k} \cdot \mathbf{x} = k_1 |\mathbf{x}|$, and

$$h(\mathbf{x}) = \frac{1}{(2\pi)^{\frac{d}{2}}} \int h_1(|\mathbf{x}|, s^2) dk_2 \cdots dk_d,$$

where

$$s^2 = \sum_{j=2}^d k_j^2, \quad h_1 = 2 \int_0^{\infty} \frac{\cos(k_1 |\mathbf{x}|)}{a^2 + k_1^2} dk_1, \quad a = \sqrt{1 + s^2}.$$

Since $h_1 = 2 \frac{\pi}{2a} e^{-a|\mathbf{x}|} > 0$, see (6.17), the result follows. \square

Lemma 6.6 All non-negative solutions of (6.1) are analytic.

Proof Equation (6.1) can be rewritten as

$$\Delta u(\mathbf{x}) + F(u(\mathbf{x})) = 0, \quad F(s) = |s|^{2\sigma} s - s. \quad (6.18)$$

Let $u \geq 0$ be a solution of (6.18). Since $u > 0$ for all \mathbf{x} (Lemma 6.5), the function $F(u)$ is analytic. Since (6.18) is a semilinear elliptic equation and F is analytic, the solution u of (6.18) is analytic (see, e.g., [51, p. 502] or [253, p. 353]). \square

Until now we assumed that $R \geq 0$. We now remove this assumption.

Lemma 6.7 *All minimizers of $J[f]$ are positive and analytic.*

Proof Let $f \in H^1$ be a minimizer of $J[f]$. Since $J[f] = J[|f|]$, see (5.47), $|f|$ is also a minimizer of $J[f]$. Therefore, by Lemma 5.8,

$$|f(\mathbf{x})| = \mu R^{\text{gs}}(\lambda(\mathbf{x} - \mathbf{x}_0)), \quad (6.19)$$

where R^{gs} is a ground state of (6.1). Since $|f| \geq 0$, it follows that R^{gs} is non-negative.³ Therefore, by Lemmas 6.5 and 6.6, R^{gs} is positive and analytic. Hence, by (6.19), $|f|$ is positive and analytic. Consequently, so is f . \square

Lemma 6.8 *Let R^{gs} be a ground state of (6.1). Then R^{gs} is positive and analytic.*

Proof By Lemma 5.8, R^{gs} is a minimizer of $J[f]$. Therefore, the result follows from Lemma 6.7. \square

From the proof of Theorem 5.10 we know that there exists a minimizer of J which is radial (Sect. 5.12.2). By Lemma 5.8, this minimizer is, up to scaling, a ground state of (6.1). In order to show that any ground state of (6.1) is radial, we recall the classical result of Gidas, Ni, and Nirenberg:

Theorem 6.1 ([110]) *Let $u(\mathbf{x}) > 0$ be a positive C^2 solution of $\Delta u + F(u) = 0$, such that $u(\mathbf{x}) \rightarrow 0$ as $|\mathbf{x}| \rightarrow \infty$, $F(0) = 0$, $F'(0) < 0$ and $F \in C^{1+\mu}$ for some $\mu > 0$. Then u is radially-symmetric about some point $\mathbf{x}_0 \in \mathbb{R}^d$, and monotonically decreasing in $r = |\mathbf{x} - \mathbf{x}_0|$.*

Since R^{gs} is smooth and positive, and since $F(u) = -u + |u|^{2\sigma}u$ satisfies the requirements of Theorem 6.1, we have

Corollary 6.6 *Any ground state of (6.1), hence any minimizer of $J[f]$, is radial about some point $\mathbf{x}_0 \in \mathbb{R}^d$, and monotonically decreasing in $r = |\mathbf{x} - \mathbf{x}_0|$.*

Since Eq. (6.1) is translation invariant, we can set $\mathbf{x}_0 = 0$. In this case, the ground state R^{gs} is radial about the origin, and so Eq. (6.1) can be written as the ODE

$$R''(r) + \frac{d-1}{r}R' - R + |R|^{2\sigma}R = 0, \quad 0 < r < \infty, \quad (6.20a)$$

subject to

$$R'(0) = 0, \quad \lim_{r \rightarrow \infty} R(r) = 0. \quad (6.20b)$$

Uniqueness of positive solutions to the boundary value problem (6.20) was proved in 1989 by Kwong:

³ By non-negative we mean that R^{gs} does not change its sign.

Theorem 6.2 ([149]) *For any σ in the H^1 -subcritical regime (6.2), there exists a unique positive solution to (6.20).*

In summary, Theorem 5.10 showed that there exist a minimizer of $J[f]$. Lemmas 6.5 and 6.6 showed that the minimizers of $J[f]$ are positive and analytic. Hence, Theorem 6.1 showed that they are radial about some point $\mathbf{x}_0 \in \mathbb{R}^d$, and monotonically decreasing in $r = |\mathbf{x} - \mathbf{x}_0|$. Finally, Theorem 6.2 showed that there is a unique positive, radial ground state. Therefore, we proved

Theorem 6.3 (Unique ground state and minimizer) *Let σ be in the H^1 -subcritical regime (6.2). Then there exists a unique positive solution of (6.20). This positive radial solution, which we denote by $R^{(0)}(r)$, is analytic and monotonically decreasing in r . It is the unique ground state of (6.20) which is positive. It is also the unique minimizer of $J[f]$, see (6.3), which is positive and radial.*

More generally, the ground states of (6.20) are given by one-parameter family $e^{i\alpha} R^{(0)}(r)$, the ground states of (6.1) are given by the $(d+1)$ -parameter family $e^{i\alpha} R^{(0)}(|\mathbf{x} - \mathbf{x}_0|)$, and the minimizers of $J[f]$ are given by the $(d+3)$ -parameter family $\mu e^{i\alpha} R^{(0)}(\lambda|\mathbf{x} - \mathbf{x}_0|)$, where $\alpha, \mu \in \mathbb{R}$, $\lambda > 0$, and $\mathbf{x}_0 \in \mathbb{R}^d$.⁴

6.3.1 Critical Case

In the critical case, $R^{(0)}$ is the positive solution of

$$\Delta R - R + |R|^{\frac{4}{d}} R = 0. \quad (6.21)$$

By Corollary 5.11, if $\|\psi_0\|_2^2 = P_{\text{cr}}$, then $H(\psi_0) \geq 0$. We now identify the initial conditions for which $H(\psi_0) = 0$:

Corollary 6.7 *Let $\sigma d = 2$. Then $\|\psi_0\|_2^2 = P_{\text{cr}}$ and $H(\psi_0) = 0$ if and only if $\psi_0 = e^{i\alpha} \lambda^{\frac{d}{2}} R^{(0)}(\lambda|\mathbf{x} - \mathbf{x}_0|)$ for some $\alpha \in \mathbb{R}$, $\lambda > 0$, and $\mathbf{x}_0 \in \mathbb{R}^d$.*

Proof If $\psi_0 = e^{i\alpha} \lambda^{\frac{d}{2}} R^{(0)}(\lambda|\mathbf{x} - \mathbf{x}_0|)$, the proof follows from Corollaries 5.14 and 6.5. To prove the opposite direction, note that in the critical case, the Gagliardo-Nirenberg inequality reads, see (5.11) and (5.22),

$$\|f\|_{\frac{4}{d}+2}^{\frac{4}{d}+2} \leq \left(\frac{2}{d} + 1 \right) \left(\frac{\|f\|_2^2}{P_{\text{cr}}} \right)^{\frac{2}{d}} \|\nabla f\|_2^2. \quad (6.22)$$

⁴ The number of degrees of freedom of the minimizers of $J[f]$ is larger by two than that of the ground states, because $f = \mu e^{i\alpha} R^{(0)}(\lambda|\mathbf{x} - \mathbf{x}_0|)$ is a minimizer of $J[f]$ for any $\mu, \lambda > 0$, but is a solution of (6.1) only for $\mu = \lambda = 1$.

Therefore, if $f \in H^1$ and $\sigma d = 2$,

$$H(f) := \|\nabla f\|_2^2 - \frac{1}{\frac{2}{d} + 1} \|f\|_{\frac{4}{d}+2}^{\frac{4}{d}+2} \geq \left[1 - \left(\frac{\|f\|_2^2}{P_{\text{cr}}} \right)^{\frac{2}{d}} \right] \|\nabla f\|_2^2. \quad (6.23)$$

If $\|\psi_0\|_2^2 = P_{\text{cr}}$ and $H(\psi_0) = 0$, the inequality in (6.23) is an equality for ψ_0 . This, in turn, is the case if and only if the Gagliardo-Nirenberg inequality (6.22) is an equality for ψ_0 , i.e., if and only if ψ_0 is a minimizer of $J[f]$ (Sect. 5.12). By Theorem 6.3, the minimizers of $J[f]$ are given by $\mu e^{i\alpha} R^{(0)}(\lambda|\mathbf{x} - \mathbf{x}_0|)$. Since $\|\psi_0\|_2^2 = P_{\text{cr}}$, it follows that $\mu = \lambda^{\frac{d}{2}}$. \square

We thus obtain

Corollary 6.8 (Dual borderline properties of $R^{(0)}$) *In the critical case, the ground state $R^{(0)}$ is the unique profile (up to scaling) that has the critical power for collapse and a zero Hamiltonian (i.e., that satisfies $\|f\|_2^2 = P_{\text{cr}}$ and $H(f) = 0$).*

Remark The terminology *dual borderline properties* will become clear in Sect. 7.12.

The result of Corollary 6.8 is surprising, for the following reason. Let $f(\mathbf{x})$ be a nontrivial function in H^1 , and let $f^{\mu,\lambda}(\mathbf{x}) := \mu f(\lambda \mathbf{x})$. Since there are two degrees of freedom, it seems that we should be able to choose μ and λ so that $H(f^{\mu,\lambda}) = 0$ and $\|f^{\mu,\lambda}\|_2^2 = P_{\text{cr}}$. To do that, we note that

$$\|f^{\mu,\lambda}\|_2^2 = \mu^2 \lambda^{-d} \|f\|_2^2$$

and

$$\begin{aligned} H(f^{\mu,\lambda}) &= \mu^2 \lambda^{2-d} \|\nabla f\|_2^2 - \mu^{2\sigma+2} \lambda^{-d} \|f\|_{2\sigma+2}^{2\sigma+2} \\ &= \mu^2 \lambda^{2-d} \left(\|\nabla f\|_2^2 - \mu^{2\sigma} \lambda^{-2} \|f\|_{2\sigma+2}^{2\sigma+2} \right). \end{aligned}$$

Therefore, μ and λ must satisfy

$$\mu^2 \lambda^{-d} = \frac{P_{\text{cr}}}{\|f\|_2^2}, \quad \mu^{2\sigma} \lambda^{-2} = \frac{\|\nabla f\|_2^2}{\|f\|_{2\sigma+2}^{2\sigma+2}}. \quad (6.24)$$

In the critical case, however, $(\mu^2 \lambda^{-d})^\sigma = \mu^{2\sigma} \lambda^{-2}$. Because of this degeneracy, Eq. (6.24) can be solved for λ and μ only if $\left(\frac{P_{\text{cr}}}{\|f\|_2^2} \right)^\sigma = \frac{\|\nabla f\|_2^2}{\|f\|_{2\sigma+2}^{2\sigma+2}}$.

Exercise 6.8 Prove that in the critical case, if $H(\psi_0) = 0$ then

$$\begin{aligned} \|\psi_0\|_2^2 = P_{\text{cr}} &\iff \psi_0 \equiv e^{i\alpha} \lambda^{\frac{d}{2}} R^{(0)}(\lambda(\mathbf{x} - \mathbf{x}_0)), \\ \|\psi_0\|_2^2 > P_{\text{cr}} &\iff \psi_0 \not\equiv e^{i\alpha} \lambda^{\frac{d}{2}} R^{(0)}(\lambda(\mathbf{x} - \mathbf{x}_0)). \end{aligned}$$

6.3.2 Variational Characterizations (Critical Case)

The critical ground state $R^{(0)}$ is the minimizer of $J[f]$, as well as of several other variational problems. For example, we have

Lemma 6.9 ([196]) *Let $\sigma d = 2$. Then*

$$P_{\text{cr}} = \inf_{0 \neq f \in H^1} \left\{ \|f\|_2^2 \mid H(f) \leq 0 \right\}. \quad (6.25)$$

In addition, the minimum is attained by the ground state $R^{(0)}$ of (6.21).

Proof By Corollary 5.10, if $H(f) \leq 0$, then $\|f\|_2^2 \geq P_{\text{cr}}$. By Corollary 6.8, $H(R^{(0)}) = 0$ and $\|R^{(0)}\|_2^2 = P_{\text{cr}}$. Hence, the result follows. \square

Remark In the above proof we relied on the existence of a minimizer to $J[f]$. In [196, Proposition 2.5], Nawa proved directly the existence of a minimizer to variational problem (6.25), and then used this result to prove the existence of a minimizer to $J[f]$.

Another variational characterization of the critical ground state is

Lemma 6.10 *Let $\sigma d = 2$. Then*

$$\inf_{f \in H^1} \left\{ H(f) \mid \|f\|_2^2 = P_{\text{cr}} \right\} = 0.$$

In addition, the infimum is attained by the ground state $R^{(0)}$ of (6.21).

Proof This follows from Corollaries 5.11 and 6.4. \square

6.3.3 Variational Characterization (Subcritical Case)

Consider the following problem: For a given $0 < P < \infty$, find the minimizer, if it exists, of

$$\inf_{f(\mathbf{x}) \in H^1} \left\{ H(f) \mid \|f\|_2^2 = P \right\}. \quad (6.26)$$

We first note that by the Gagliardo-Nirenberg inequality (5.11),

$$\begin{aligned} H(f) &= \|\nabla f\|_2^2 - \frac{1}{1+\sigma} \|f\|_{2\sigma+2}^{2\sigma+2} \geq \|\nabla f\|_2^2 - \frac{C_{\sigma,d}}{1+\sigma} P^{1+\sigma-\frac{\sigma d}{2}} \|\nabla f\|_2^{\sigma d} \\ &= \|\nabla f\|_2^2 - \alpha \|\nabla f\|_2^{\sigma d}, \end{aligned}$$

where $\alpha = \frac{C_{\sigma,d}}{1+\sigma} P^{1+\sigma-\frac{\sigma d}{2}} > 0$. The function $h(x) = x^2 - \alpha x^{\sigma d}$ with $\alpha > 0$ and $0 < \sigma d < 2$ is bounded from below in the domain $0 < x < \infty$. Hence, we conclude that in the subcritical case, the infimum (6.26) is finite.

Existence of a minimizer to (6.26) in the subcritical case was proved by Cazenave and Lions using the concentration-compactness method [40]. As in Sect. 5.12.2, one can show that this minimizer, denoted by $f_P^{(0)}$, is positive, radial, and monotonically decreasing. Since (6.26) is a constrained minimization problem, $f_P^{(0)}$ satisfies the Euler-Lagrange equation for the constrained functional

$$F(f, \nabla f) := \|\nabla f\|_2^2 - \frac{1}{1+\sigma} \|f\|_{2\sigma+2}^{2\sigma+2} - \omega_P \left(\|f\|_2^2 - P \right),$$

where ω_P is a Lagrange multiplier. Therefore, $f_P^{(0)}$ is the solution of

$$\Delta f + |f|^{2\sigma} f - \omega_P f = 0.$$

Since $f_P^{(0)}$ is positive, it follows that $f_P^{(0)} = \omega_P^{\frac{1}{2\sigma}} R^{(0)} \left(\omega_P^{\frac{1}{2}} r \right)$, where $R^{(0)}$ is the unique positive solution of (6.20). Finally, by Exercise 6.2, $P = \|f_P^{(0)}\|_2^2 = \omega_P^{\frac{2-\sigma d}{2\sigma}} \|R^{(0)}\|_2^2$. Therefore,

$$\omega_P = \left(\frac{P}{\|R^{(0)}\|_2^2} \right)^{\frac{2\sigma}{2-\sigma d}}. \quad (6.27)$$

Theorem 6.4 ([40]) *Let $0 < \sigma d < 2$. Then for any $0 < P < \infty$, the function $R_{\omega_P}^{(0)}(r) = \omega_P^{\frac{1}{2\sigma}} R^{(0)} \left(\omega_P^{\frac{1}{2}} r \right)$, where ω_P is given by (6.27), is a minimizer of*

$$\inf_{f(\mathbf{x}) \in H^1} \left\{ H(f) \mid \|f\|_2^2 = P \right\}. \quad (6.28)$$

Furthermore, $R_{\omega_P}^{(0)}(r)$ is the unique minimizer up to phase shifts and translations, i.e., the minimizers are given by $e^{i\theta} R_{\omega_P}^{(0)}(|\mathbf{x} - \mathbf{x}_c|)$, where $\theta \in \mathbb{R}$ and $\mathbf{x}_c \in \mathbb{R}^d$.

Remark The variational characterization (6.28) implies that the subcritical ground-state solitary waves are orbitally stable (Sect. 9.4.1).

Let $f \in H^1$, $P = \|f\|_2^2$, and $f^\lambda(\mathbf{x}) := \lambda^{\frac{d}{2}} f(\lambda \mathbf{x})$. Then

$$\|f^\lambda\|_2^2 = P, \quad H(f^\lambda) = \lambda^2 \|\nabla f\|_2^2 - \frac{\lambda^{\sigma d}}{\sigma + 1} \|f\|_{2\sigma+2}^{2\sigma+2}.$$

Therefore, if $\sigma d > 2$, then $\lim_{\lambda \rightarrow \infty} H(f^\lambda) = -\infty$, and so the infimum (6.28) is equal to $-\infty$.⁵ In particular, since there is no minimizer, the variational characterization (6.28) of the ground state does not hold in the supercritical case.

⁵ Indeed, when $\sigma d > 2$, the function $h(x) = x^2 - \alpha x^{\sigma d}$ is unbounded from below in $0 < x < \infty$.

The variational characterization (6.28) does not hold in the critical case either.⁶ Indeed, if there is a minimizer to (6.28) with $P \neq P_{\text{cr}}$, then it is given by some $R_\omega^{(0)}$. In the critical case, however, $\|R_\omega^{(0)}\|_2^2 = P_{\text{cr}}$ for any ω . We note, however, that the variational characterization (6.28) does hold in the critical case on a bounded domain for $0 < P < P_{\text{cr}}$ (Theorem 16.1).

6.4 Radial States $R^{(n)}(r)$

In Theorem 6.3 we saw that the ground state of (6.1) is radial. In this section we analyze the radial solutions of (6.1).

6.4.1 Uniqueness of Initial Value Problems

We begin with an auxiliary result.

Lemma 6.11 *Let $d \geq 1$, let F be a continuous function, and let u be a continuous solution of the initial value problem*

$$u''(r) + \frac{d-1}{r}u' + F(r, |u|)u = 0, \quad 0 < r < \infty, \quad (6.29a)$$

subject to

$$u(0) = u'(0) = 0. \quad (6.29b)$$

Then $u(r) \equiv 0$ for $0 \leq r < \infty$.

Proof When $d = 1$, the result follows directly from the standard uniqueness theorem for ODEs. This is not the case when $d > 1$, however, because of the singularity at $r = 0$. To prove the result for $d > 1$, let $g(r) := F(r, |u(r)|)$. Multiplying (6.29a) by r^{d-1} , one obtains

$$\left(r^{d-1}u' \right)' = -r^{d-1}g(r)u. \quad (6.30)$$

Since $u'(0) = 0$ and $d \geq 1$, $\lim_{r \rightarrow 0} r^{d-1}u'(r) = 0$. Therefore, integrating Eq. (6.30) from zero to r and dividing by r^{d-1} yields

$$u'(r) = -\frac{1}{r^{d-1}} \int_0^r s^{d-1}g(s)u(s) ds. \quad (6.31)$$

Since $u(0) = 0$, integrating Eq. (6.31) from zero to r yields

$$u(r) = - \int_0^r \left(\frac{1}{\rho^{d-1}} \int_0^\rho s^{d-1}g(s)u(s) ds \right) d\rho. \quad (6.32)$$

⁶ Unless $P = P_{\text{cr}}$, in which case it “reduces” to that of Lemma 6.10.

Since g and u are continuous, they are bounded on every finite interval $[0, r_0]$. Taking the maximum of (6.32) over $[0, r_0]$ yields

$$\begin{aligned} \max_{0 \leq r \leq r_0} |u(r)| &\leq \left[\max_{0 \leq r \leq r_0} |g(r)| \right] \left[\max_{0 \leq r \leq r_0} |u(r)| \right] \int_0^{r_0} \frac{1}{\rho^{d-1}} \left(\int_0^\rho s^{d-1} ds \right) d\rho \\ &= \frac{r_0^2}{2d} \left[\max_{0 \leq r \leq r_0} |g(r)| \right] \max_{0 \leq r \leq r_0} |u(r)|. \end{aligned}$$

Choosing r_0 small enough so that $\theta := \frac{r_0^2 [\max_{0 \leq r \leq r_0} |g(r)|]}{2d} < 1$, we obtain the estimate $(1-\theta) \max_{0 \leq r \leq r_0} |u(r)| \leq 0$, which implies that $u \equiv 0$ in $[0, r_0]$. Since ODE (6.29a) is regular except at $r = 0$, the standard uniqueness theorem for ODEs then implies that $u \equiv 0$ for all r . \square

A similar approach was used by Franchi, Lanconelli, and Serrin to prove

Corollary 6.9 ([101, Proposition A2]) *The solution of the initial value problem*

$$R''(r) + \frac{d-1}{r} R' - R + |R|^{2\sigma} R = 0, \quad R(0) = R_0, \quad R'(0) = 0,$$

is unique.

We now show that all radial states are real (up to multiplication by $e^{i\alpha}$):

Lemma 6.12 *Let $R(r)$ be a solution of (6.20). Then $R = e^{i\alpha} \tilde{R}(r)$, where α is a real number and $\tilde{R}(r)$ is real.*

Proof Substituting $R = S + iT$ in (6.20), where S and T are real, gives

$$\Delta_r(S + iT) - (S + iT) + (S^2 + T^2)^\sigma (S + iT) = 0, \quad \Delta_r = \frac{d^2}{dr^2} + \frac{d-1}{r} \frac{d}{dr}.$$

Therefore, T satisfies the ODE

$$\Delta_r T(r) - T + (S^2 + T^2)^\sigma T = 0. \quad (6.33)$$

Assume first that $R(0)$ is real. Therefore, $T(0) = 0$. Since R is radial, $R'(0) = 0$. In particular, $T'(0) = 0$. Hence, T is the solution of the homogeneous equation (6.33), subject to $T(0) = T'(0) = 0$. Therefore, by Lemma 6.11, $T \equiv 0$, i.e., R is real for all $r > 0$.

If $R(0)$ is not real, let $\alpha = \arg R(0)$ and $\tilde{R} = e^{-i\alpha} R$. Then \tilde{R} is a solution of (6.4) such that $\tilde{R}(0)$ is real. By the previous argument, $\tilde{R}(r)$ is real. \square

Remark Equation (6.1) also admits non-radial solutions, which are indeed complex (Sect. 15.2).

6.4.2 Asymptotic Behavior for $r \gg 1$

If $f(r) \in H_{\text{radial}}^1$ then $\lim_{r \rightarrow \infty} f(r) = 0$, see Lemma 5.13. In addition, either $\lim_{r \rightarrow \infty} f'(r) = 0$, or $f'(r)$ does not have a limit as $r \rightarrow \infty$. The last possibility can be ruled out for H^1 solutions of (6.20):

Lemma 6.13 *Let $R(r)$ be a solution of (6.20) in H^1 . Then*

$$\lim_{r \rightarrow \infty} R'(r) = 0. \quad (6.34)$$

Proof If we multiply (6.20) by $2R'$ and integrate from 0 to r , we get

$$N(r) - N(0) = -2(d-1) \int_0^r \frac{1}{s} (R'(s))^2 ds,$$

where

$$N(r) := (R')^2 - R^2 + \frac{1}{1+\sigma} |R|^{2\sigma+2}.$$

If $d = 1$, then $N(r) \equiv N(0)$. Therefore, $\lim_{r \rightarrow \infty} R = 0$ implies that

$$N(0) = \lim_{r \rightarrow \infty} N(r) = \lim_{r \rightarrow \infty} (R'(r))^2.$$

Hence, $\lim_{r \rightarrow \infty} R'$ exists, and is therefore equal to zero.

If $d > 1$, then $N(r)$ is monotonically decreasing in r . This implies that $N(r)$ has a limit as $r \rightarrow \infty$, i.e.,

$$\lim_{r \rightarrow \infty} N(r) = N_\infty, \quad -\infty \leq N_\infty < \infty.$$

In addition, since $\lim_{r \rightarrow \infty} R(r) = 0$, then

$$N_\infty = \lim_{r \rightarrow \infty} N(r) = \lim_{r \rightarrow \infty} (R'(r))^2 \geq 0.$$

Therefore, N_∞ is finite. Hence, $\lim_{r \rightarrow \infty} R'$ exists, and is therefore equal to zero. and so $\lim_{r \rightarrow \infty} R'(r) = 0$. \square

We now calculate the asymptotic behavior of $R(r)$ for large r :

Lemma 6.14 *Let $R(r)$ be a nontrivial solution of (6.20) in H^1 . Then*

$$R(r) \sim A_R r^{-\frac{d-1}{2}} e^{-r}, \quad r \gg 1, \quad (6.35)$$

where A_R is a constant.

Proof Since $\lim_{r \rightarrow \infty} R = 0$, the nonlinearity becomes negligible as $r \rightarrow \infty$. Hence, to leading order, Eq. (6.20) reduces to

$$R''(r) + \frac{d-1}{r} R' - R = 0.$$

To eliminate the first derivative, we substitute $R = r^{-\frac{d-1}{2}} U(r)$. The equation for U is

$$U''(r) - (1 + O(r^{-2})) U = 0.$$

This equation has two independent solutions $U = e^{\pm r} (1 + O(\frac{1}{r}))$.⁷ Therefore, the solution which decays at infinity satisfies $U \sim Ae^{-r}$. \square

Remark In Theorem 6.5 we will see that in dimension $d \geq 2$, Eq. (6.20) has an countable number of solutions $\{R^{(n)}\}_{n=0}^\infty$. In that case, expansion (6.35) is valid for any $R^{(n)}$, but the value of A_R depends on n .

Exercise 6.9 Let $f(r)$ be a radial solution of $\Delta f + \omega f = 0$. Show that if $\omega > 0$, then $f \sim cr^{-\frac{d-1}{2}} e^{\pm i\sqrt{-\omega}r}$ as $r \rightarrow \infty$.

Exercise 6.10 Let $f(r)$ be a radial solution of $\Delta f = f$, such that $\lim_{r \rightarrow \infty} f = \infty$. Show that $f \sim c_f r^{-\frac{d-1}{2}} e^r$ as $r \rightarrow \infty$.

Exercise 6.11 Let $R_B(r)$ be a radial solution of (6.16) in H^2 . Show that

$$R_B(r) \sim B_R r^{-\frac{d-1}{2}} e^{-\frac{r}{\sqrt{2}}} \cos\left(\frac{r}{\sqrt{2}}\right), \quad r \gg 1. \quad (6.36)$$

6.4.3 $d = 1$

In Theorem 6.2 we saw that Eq. (6.20) has a unique positive solution. We now show that when $d = 1$, this is the *only* real solution of (6.20), up to multiplication by -1 . Therefore, in one dimension there is a unique ground state, and no excited states.

Lemma 6.15 When $d = 1$, the unique real solutions of (6.20) in H^1 are

$$R_{1D}(x) = \pm \frac{(1+\sigma)^{\frac{1}{2\sigma}}}{\cosh^{\frac{1}{\sigma}}(\sigma x)} = \pm(1+\sigma)^{\frac{1}{2\sigma}} \operatorname{sech}^{\frac{1}{\sigma}}(\sigma x). \quad (6.37)$$

⁷ See e.g., [193, Eq.(6.12)].

Proof When $d = 1$, Eq. (6.20) reads

$$R''(x) - R + |R|^{2\sigma}R = 0.$$

If we multiply this equation by $2R'$ and integrate, we get

$$(R')^2 - R^2 + \frac{1}{\sigma+1}|R|^{2\sigma+2} \equiv C.$$

Since $\lim_{x \rightarrow \infty} R = \lim_{x \rightarrow \infty} R' = 0$, see (6.34), this implies that $C = 0$ and

$$R^2 - (R')^2 = \frac{1}{\sigma+1}|R|^{2\sigma+2}.$$

Let $R(x) = \pm(1 + \sigma)^{\frac{1}{2\sigma}}u^{-\frac{1}{\sigma}}(\sigma x)$. Then $u(x)$ is the positive solution of

$$u^2 - (u')^2 = 1, \quad u'(0) = 0, \quad \lim_{x \rightarrow \infty} u = 0.$$

Therefore, $u = \cosh(x)$. □

For example, in the subcritical one-dimensional cubic case ($d = \sigma = 1$),

$$R_{1D}(x) = \frac{\sqrt{2}}{\cosh(x)} = \sqrt{2} \operatorname{sech}(x). \quad (6.38)$$

This is the well-known profile of NLS solitons. In the critical one-dimensional quintic case ($d = 1, \sigma = 2$), the ground state is

$$R_{1D}(x) = \frac{3^{\frac{1}{4}}}{\cosh^{\frac{1}{2}}(2x)} = 3^{\frac{1}{4}} \operatorname{sech}^{\frac{1}{2}}(2x). \quad (6.39)$$

6.4.4 $d \geq 2$

In Lemma 6.15 we saw that when $d = 1$, Eq. (6.20) has a unique solution, which can be written explicitly. In contrast, when $d \geq 2$, Eq. (6.20) has a *countable* number of solutions, for which an explicit expression is not available:

Theorem 6.5 *Let $d \geq 2$. Then Eq. (6.20) has a countable number of solutions $\{R^{(n)}(r)\}_{n=0}^\infty$ in C^2 , such that*

$$\lim_{n \rightarrow \infty} \|\nabla R^{(n)}\|_2^2 = \infty \quad \text{and} \quad \lim_{n \rightarrow \infty} I(R^{(n)}) = \infty,$$

where $I(R) := H(R) + \|R\|_2^2$.

By Theorem 6.5 and the Pohozaev identities (6.7)

$$\lim_{n \rightarrow \infty} \|R^{(n)}\|_2^2 = \infty \quad \text{and} \quad \lim_{n \rightarrow \infty} \|R^{(n)}\|_{2\sigma+2}^{2\sigma+2} = \infty. \quad (6.40)$$

Therefore, the solutions of (6.20) can be arranged in order of increasing power, i.e.,⁸

$$\|R^{(0)}\|_2^2 < \|R^{(1)}\|_2^2 \leq \|R^{(2)}\|_2^2 \leq \dots$$

Theorem 6.5 was proved by Berestycki et al. [21] for $d = 2$, and by Berestycki and Lions [22] for $d \geq 3$. Grillakis [117] proved that in dimension $d \geq 2$, for any $n = 0, 1, 2, \dots$, there exists a solution of (6.20) with n roots in the interval $0 < r < \infty$. These results and numerical simulations suggest

Conjecture 6.1 *For any $n = 0, 1, 2, \dots$, Eq. (6.20) has a unique solution with n roots. In addition, the power of these solutions is strictly monotonically increasing in n , i.e., $\|R^{(0)}\|_2^2 < \|R^{(1)}\|_2^2 < \|R^{(2)}\|_2^2 < \dots$*

So far, however, it has only been proved that there is a unique solution of (6.20) with $n = 0$ roots (Theorem 6.2), that $\|R^{(n)}\|_2^2 > \|R^{(0)}\|_2^2$ for $n \geq 1$ (Theorem 6.3), and that $\lim_{n \rightarrow \infty} \|R^{(n)}\|_2^2 = \infty$ (Theorem 6.5).

Figure 6.1 shows the first four states of Eq. (6.20) in the critical case $\sigma = 1$ and $d = 2$.⁹ The radial powers $\int_0^\infty (R^{(n)})^2 r dr$ of these states are 1.8623, 12.28, 31.17, and 58.47, for $n = 0, 1, 2$, and 3, respectively. These numerical results are in agreement with Conjecture 6.1: There is a unique solution with n zeros, and the power of $R^{(n)}$ increases with n .

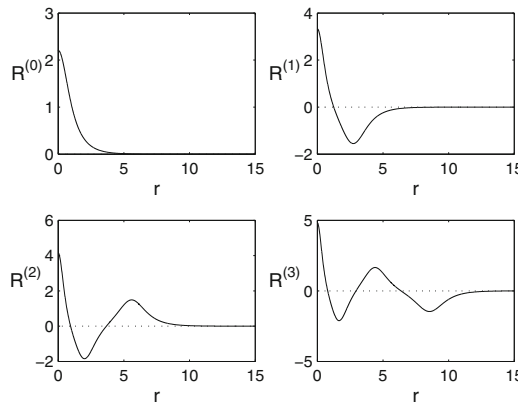


Fig. 6.1 The first four states of Eq. (6.20) with $\sigma = 1$ and $d = 2$

⁸ The strict inequality between $\|R^{(0)}\|_2^2$ and $\|R^{(1)}\|_2^2$ follows from Theorem 6.3.

⁹ These solutions were computed using the *shooting method* (Sect. 28.1).

In Theorem 6.3 we proved that the ground state of (6.20) attains its global maximum at $r = 0$. Figure 6.1 shows that the first three excited states also attain their maximum at $r = 0$. This property was proved by Fibich, Gavish, and Wang:

Lemma 6.16 ([74]) *Let $R^{(n)}$ be a nontrivial solution of (6.20) in H^1 , and let $d > 1$. Then for any two extremum points $0 \leq r_k < r_m$ such that $\frac{dR^{(n)}}{dr}(r_k) = \frac{dR^{(n)}}{dr}(r_m) = 0$, we have that $|R^{(n)}(r_k)| > |R^{(n)}(r_m)|$. In particular, the global maximum of $|R^{(n)}|$ is attained at $r = 0$.*

Proof In Lemma 6.13 we showed that $\lim_{r \rightarrow \infty} R(r) = \lim_{r \rightarrow \infty} R'(r) = 0$, and

$$N(r) - N(0) = -2(d-1) \int_0^r \frac{1}{s} (R'(s))^2 ds, \quad N = (R')^2 - R^2 + \frac{1}{1+\sigma} |R|^{2\sigma+2}.$$

Therefore, $\lim_{r \rightarrow \infty} N(r) = 0$. Since $N(r)$ is monotonically decreasing in r , this implies that $N(r) > 0$ for any $0 \leq r < \infty$.

Let us rewrite N as

$$N = (R')^2 + R^2 \left(\left(\frac{R}{R_c} \right)^{2\sigma} - 1 \right), \quad R_c = (1+\sigma)^{\frac{1}{2\sigma}}. \quad (6.41)$$

Since $N > 0$, it follows that

$$\text{if } R'(r_k) = 0 \text{ then } |R(r_k)| > R_c. \quad (6.42)$$

Assume that there exists $0 \leq r_k < r_m$ such that $R'(r_k) = R'(r_m) = 0$. By (6.42), both $|R(r_k)|$ and $|R(r_m)|$ are above R_c . In addition, since $N(r)$ is monotonically decreasing in r , then $N(r_k) > N(r_m)$.

By (6.41), for $|R| > R_c$, $N(R, R' = 0)$ is monotonically increasing in $|R|$. Therefore, the inequality

$$N(R(r_k), R' = 0) = N(r = r_k) > N(r = r_m) = N(R(r_m), R' = 0)$$

implies that $|R(r_k)| > |R(r_m)|$. □

From (6.42) follows a lower bound for the extremal values of $R^{(n)}$:

Corollary 6.10 *Let $R^{(n)}$ be a nontrivial solution of (6.20) in H^1 , and let $d > 1$. If $\frac{dR^{(n)}}{dr}(r_k) = 0$, then $|R^{(n)}(r_k)|^{2\sigma} > 1 + \sigma$. In particular, $|R^{(n)}(0)|^{2\sigma} > 1 + \sigma$.*

Figure 6.1 also shows that the ground state of (6.20) is monotonically decreasing in r , but the first three excited states are non-monotone. Indeed, we have

Corollary 6.11 *The only nontrivial solution of (6.20) which is monotone in r is the ground state.*

Proof By Theorem 6.3, the ground state of (6.20) is monotonically decreasing in r . In addition, by Theorem 6.2, any other solution $R^{(n)}$ of (6.20) has a root at some $0 < r_0 < \infty$. Since $\lim_{r \rightarrow \infty} R^{(n)}(r) = 0$, this implies that $R^{(n)}$ is non-monotone. \square

Although the excited states are non-monotone, they cannot have a ring profile:

Corollary 6.12 *Equation (6.20) does not admit ring-type solutions.*

Proof By Lemma 6.16, the global maximum of $|R^{(n)}|$ is attained at $r = 0$. \square

6.4.5 Asymptotic Behavior for $0 \leq r \ll 1$

If we let $r \rightarrow 0$ in Eq. (6.20) and apply l'Hospital's rule, we get that

$$d \cdot R''(0) = \lim_{r \rightarrow 0} \Delta R = R(0) \left(1 - |R(0)|^{2\sigma} \right).$$

Therefore,

$$R''(0) = \frac{R(0)}{d} \left(1 - |R(0)|^{2\sigma} \right). \quad (6.43)$$

Since $|R(0)|^{2\sigma} > 1 + \sigma > 1$, it follows that if $R(0) > 0$, then $R''(0) < 0$. This is consistent with the result in Lemma 6.16 that the global maximum of $|R|$ is attained at $r = 0$.

By (6.43), the Taylor expansion of R near the origin is

$$R(r) = R(0) + \frac{R(0)}{2d} \left(1 - |R(0)|^{2\sigma} \right) r^2 + O(r^4), \quad 0 \leq r \ll 1.$$

Exercise 6.12 *Show that*

$$R'''(0) = \frac{3}{d+2} R''(0) \left(1 - (2\sigma + 1)|R(0)|^{2\sigma} \right). \quad (6.44)$$

Remark The relations in this subsection are valid for any solution of (6.20), i.e., for the ground state and for excited states.

Chapter 7

Variance Identity

In this chapter we derive the variance identity for the focusing NLS

$$i\psi_z(z, \mathbf{x}) + \Delta\psi + |\psi|^{2\sigma}\psi = 0, \quad \psi(0, \mathbf{x}) = \psi_0(\mathbf{x}) \in \Sigma, \quad (7.1)$$

where

$$\Sigma = H^1 \cap \left\{ f(\mathbf{x}) \mid \mathbf{x}f \in L^2 \right\}.$$

This identity provided the first rigorous proof that NLS solutions can become singular, that NLS singularity is not related to insufficient smoothness of the initial conditions, and that singularity occurs for large classes of initial conditions (e.g., for all initial conditions with a negative Hamiltonian). The variance identity also led to numerous other results, some of which are presented in this chapter. Unfortunately, over the years, the variance identity has been frequently misinterpreted. These misinterpretations are also pointed out.

7.1 Variance

We begin with the definition of the variance.

Definition 7.1 (variance) *The variance of $f(\mathbf{x})$ is $V[f] := \int |\mathbf{x}|^2 |f(\mathbf{x})|^2 d\mathbf{x}$.*

Therefore, the variance of $\psi(z, \mathbf{x})$ is

$$V(z) = V[\psi(z, \mathbf{x})] = \int |\mathbf{x}|^2 |\psi(z, \mathbf{x})|^2 d\mathbf{x}, \quad (7.2)$$

and the requirement that $\psi_0 \in \Sigma$ ensures that $V(\psi_0) < \infty$.

To understand the meaning of the variance, assume that a propagating laser beam maintains a self-similar profile (*aberrationless propagation*). Then

$$|\psi| = \frac{1}{L^{\frac{d}{2}}(z)} F \left(\frac{\mathbf{x}}{L(z)} \right), \quad (7.3)$$

where the scaling by $L^{-\frac{d}{2}}(z)$ follows from power conservation. By (7.3),

$$L^2(z) = \frac{V(z)}{V[F]}, \quad V[F] = \int |\mathbf{x}|^2 |F(\mathbf{x})|^2 d\mathbf{x}. \quad (7.4)$$

Therefore, in an aberrationless propagation, the variance is proportional to the square of the solution width. In particular, $V \rightarrow 0$ if and only if $L \rightarrow 0$.

In linear optics, if the input beam is a Gaussian, the propagating beam maintains a self-similar profile (Sect. 2.15.3). In that case, relations (7.3) and (7.4) are exact. When the input beam is not a Gaussian, the beam does not maintain a self-similar profile. Nevertheless, in linear optics the variance typically provides a reasonable estimate for the beam width, i.e., (7.4) is a reasonable approximation.

As we shall see in this chapter, the situation is very different in nonlinear propagation of collapsing beams. This is because generically, only the beam core undergoes collapse while the rest of the beam propagates forward (*partial-beam collapse*). As a result, the variance is positive (and not zero) at the singularity. In this case, using the variance (which is a global quantity) as a measure for the width of the collapsing core (which is a local quantity) can lead to results which are quantitatively and even qualitatively wrong. Therefore, in the case of collapsing solutions, one has to be careful about interpretations and consequences of the variance identity.

7.2 Variance Identity

The *variance identity*, which is also known as the *virial theorem*, was derived in 1971 by Vlasov, Petrishchev, and Talanov:

Theorem 7.1 (Variance identity [262]) *Let ψ be a solution of the NLS (7.1) in $[0, Z_c]$, where $0 < Z_c \leq \infty$, and let $V(z)$ be given by (7.2). Then*

$$V'(z) = 4 \operatorname{Im} \int \psi^* \mathbf{x} \cdot \nabla \psi d\mathbf{x}, \quad 0 \leq z < Z_c, \quad (7.5)$$

and

$$V''(z) = 8 \left[H - \frac{d\sigma - 2}{2\sigma + 2} \|\psi\|_{2\sigma+2}^{2\sigma+2} \right], \quad 0 \leq z < Z_c, \quad (7.6)$$

where $H = \|\nabla \psi\|_2^2 - \frac{1}{\sigma+1} \|\psi\|_{2\sigma+2}^{2\sigma+2}$ is the Hamiltonian.

Proof If we differentiate $V = \int |\mathbf{x}|^2 \psi^* \psi d\mathbf{x}$ with respect to z , we get that

$$V'(z) = \int |\mathbf{x}|^2 \psi^* \psi_z d\mathbf{x} + \text{c.c.},$$

where “c.c.” stands for complex conjugate. Since ψ is a solution of (7.1),

$$\psi_z = i \Delta \psi + i |\psi|^{2\sigma} \psi. \quad (7.7)$$

Therefore,

$$\begin{aligned}
 V'(z) &= \int |\mathbf{x}|^2 \psi^* (i\Delta\psi + i|\psi|^{2\sigma}\psi) d\mathbf{x} + \text{c.c.} = \int i|\mathbf{x}|^2 \psi^* \Delta\psi d\mathbf{x} + \text{c.c.} \\
 &= - \int i \nabla(|\mathbf{x}|^2 \psi^*) \cdot \nabla\psi d\mathbf{x} + \text{c.c.} \\
 &= - \int i(2\mathbf{x}\psi^* + |\mathbf{x}|^2 \nabla\psi^*) \cdot \nabla\psi d\mathbf{x} + \text{c.c.} \\
 &= -2 \int i\psi^* \mathbf{x} \cdot \nabla\psi d\mathbf{x} + \text{c.c.},
 \end{aligned}$$

which proves (7.5). Differentiating again with respect to z , one obtains

$$\begin{aligned}
 V''(z) &= -2 \int i\mathbf{x} [\psi_z^* \cdot \nabla\psi + \psi^* \cdot \nabla\psi_z] d\mathbf{x} + \text{c.c.} \\
 &= -2 \int i [\mathbf{x}\psi_z^* \cdot \nabla\psi - \mathbf{x} \cdot \nabla\psi^* \psi_z - d\psi^* \psi_z] d\mathbf{x} + \text{c.c.} \\
 &= 2 \int i [2\mathbf{x} \cdot \nabla\psi^* + d\psi^*] \psi_z d\mathbf{x} + \text{c.c.} .
 \end{aligned}$$

Using (7.7), we get that

$$V''(z) = -2 \int [2\mathbf{x} \cdot \nabla\psi^* + d\psi^*] [\Delta\psi + |\psi|^{2\sigma}\psi] d\mathbf{x} + \text{c.c.} .$$

We calculate the right-hand side terms as follows. Since

$$\nabla(\mathbf{x} \cdot \nabla\psi^*) = \nabla\psi^* + (\mathbf{x} \cdot \nabla)\nabla\psi^*,$$

see (6.10), then

$$\begin{aligned}
 \int \mathbf{x} \cdot \nabla\psi^* \Delta\psi d\mathbf{x} + \text{c.c.} &= - \int \nabla(\mathbf{x} \cdot \nabla\psi^*) \cdot \nabla\psi d\mathbf{x} + \text{c.c.} \\
 &= - \int (\nabla\psi^* + (\mathbf{x} \cdot \nabla)\nabla\psi^*) \cdot \nabla\psi d\mathbf{x} + \text{c.c.} \\
 &= -2\|\nabla\psi\|_2^2 - \int \mathbf{x} \cdot \nabla|\nabla\psi|^2 d\mathbf{x} = (d-2)\|\nabla\psi\|_2^2.
 \end{aligned} \tag{7.8}$$

In addition,

$$\int \mathbf{x} \cdot \nabla\psi^* |\psi|^{2\sigma}\psi d\mathbf{x} + \text{c.c.} = \frac{1}{\sigma+1} \int \mathbf{x} \cdot \nabla |\psi|^{2\sigma+2} d\mathbf{x} = -\frac{d}{\sigma+1} \|\psi\|_{2\sigma+2}^{2\sigma+2}.$$

Finally,

$$\int \psi^* [\Delta\psi + |\psi|^{2\sigma}\psi] d\mathbf{x} + \text{c.c.} = -2\|\nabla\psi\|_2^2 + 2\|\psi\|_{2\sigma+2}^{2\sigma+2}.$$

Collecting terms, we get

$$V''(z) = 8\|\nabla\psi\|_2^2 - \frac{4d\sigma}{\sigma+1}\|\psi\|_{2\sigma+2}^{2\sigma+2}, \quad (7.9)$$

which yields (7.6). \square

More generally, we can define the variance around \mathbf{x}_0 as

$$V(z; \mathbf{x}_0) := \int |\mathbf{x} - \mathbf{x}_0|^2 |\psi(z, \mathbf{x})|^2 d\mathbf{x}. \quad (7.10)$$

Lemma 7.1 *Let ψ be a solution of the NLS (7.1) in $[0, Z_c]$, where $0 < Z_c \leq \infty$, and let $V(z; \mathbf{x}_0)$ be given by (7.10). Then*

$$\frac{d}{dz} V(z; \mathbf{x}_0) = 4 \operatorname{Im} \int \psi^* \nabla \psi \cdot (\mathbf{x} - \mathbf{x}_0) d\mathbf{x}, \quad (7.11)$$

and

$$\frac{d^2}{dz^2} V(z; \mathbf{x}_0) = 8 \left[H - \frac{d\sigma - 2}{2\sigma + 2} \|\psi\|_{2\sigma+2}^{2\sigma+2} \right]. \quad (7.12)$$

Proof NLS solutions are invariant under spatial translation $\mathbf{x} \rightarrow \mathbf{x} - \mathbf{x}_0$, see Sect. 8.1. Hence, the results follow directly from Theorem 7.1.

We can also prove Lemma 7.1 as follows.¹ Since

$$|\mathbf{x} - \mathbf{x}_0|^2 = |\mathbf{x}|^2 + 2\mathbf{x}_0 \cdot \mathbf{x} + |\mathbf{x}_0|^2,$$

we have that

$$\begin{aligned} V(z; \mathbf{x}_0) &= V(z; 0) + 2\mathbf{x}_0 \cdot \int \mathbf{x} |\psi|^2 d\mathbf{x} + |\mathbf{x}_0|^2 \int |\psi|^2 d\mathbf{x} \\ &= V(z) + 2\mathbf{x}_0 \cdot \int \mathbf{x} |\psi|^2 d\mathbf{x} + |\mathbf{x}_0|^2 \int |\psi_0|^2 d\mathbf{x}. \end{aligned}$$

By (5.8),

$$\frac{d}{dz} \int \mathbf{x} |\psi|^2 d\mathbf{x} = M,$$

¹ This second proof will become useful when we discuss the variance identity on a bounded domain (Sect. 16.8.1).

where $M = -2 \operatorname{Im} \int \psi \nabla \psi^* d\mathbf{x}$ is the conserved linear momentum. Therefore,

$$\frac{d}{dz} V(z; \mathbf{x}_0) = \frac{d}{dz} V(z) + 2\mathbf{x}_0 \cdot M = 4 \operatorname{Im} \int \psi^* \nabla \psi \cdot (\mathbf{x} - \mathbf{x}_0) d\mathbf{x},$$

and

$$\frac{d^2}{dz^2} V(z; \mathbf{x}_0) = \frac{d^2}{dz^2} V(z) = 8 \left[H - \frac{d\sigma - 2}{2\sigma + 2} \|\psi\|_{2\sigma+2}^{2\sigma+2} \right].$$

□

7.2.1 Critical NLS

The variance identity has a simpler form in the critical case:

Corollary 7.1 *Let ψ be a solution of the critical NLS*

$$i\psi_z(z, \mathbf{x}) + \Delta\psi + |\psi|^{\frac{4}{d}}\psi = 0, \quad \psi(0, \mathbf{x}) = \psi_0(\mathbf{x}) \in \Sigma \quad (7.13)$$

in $[0, Z_c]$, where $0 < Z_c \leq \infty$. Then $V'(z) = 4 \operatorname{Im} \int \psi^* \mathbf{x} \cdot \nabla \psi d\mathbf{x}$, and

$$V''(z) = 8H, \quad 0 \leq z < Z_c. \quad (7.14)$$

The critical variance identity (7.14) is one of the conservation laws of the critical NLS, see (5.9).

7.2.2 General Nonlinearity

The variance identity can be generalized to NLS equations of the form

$$i\psi_z(z, \mathbf{x}) + \Delta\psi + f(|\psi|^2)\psi = 0, \quad (7.15)$$

where $f(s)$ is a smooth real function, as follows. Let ψ be a solution of (7.15), and let $V(z)$ be given by (7.2). Then

$$V''(z) = 8H - 4 \int \left[d|\psi|^2 f'(|\psi|^2) - (d+2)F(|\psi|^2) \right] d\mathbf{x}, \quad (7.16)$$

where $F(s) = \int_0^s f(s') ds'$, and $H = \int [|\nabla \psi|^2 - F(|\psi|^2)] d\mathbf{x}$ is the conserved Hamiltonian of (7.15).

Exercise 7.1 Derive (7.16).

7.2.3 Biharmonic NLS

In [14], Baruch et al. derived the variance identity for the biharmonic NLS, as follows. By Noether's Theorem, the conservation law of the critical BNLS

$$i\psi_z(z, \mathbf{x}) - \Delta^2\psi + |\psi|^{\frac{8}{d}}\psi = 0,$$

which is *equivalent*² to relation (5.9), is

$$\frac{d}{dz} \operatorname{Im} \int \psi^* \mathbf{x} \cdot \nabla \psi d\mathbf{x} = 4H_B,$$

where H_B is the conserved BNLS Hamiltonian, see (5.10). More generally, solutions of the focusing BNLS

$$i\psi_z(z, \mathbf{x}) - \Delta^2\psi + |\psi|^{2\sigma}\psi = 0$$

satisfy

$$\frac{d}{dz} \operatorname{Im} \int \psi^* \mathbf{x} \cdot \nabla \psi d\mathbf{x} = 4H_B - \frac{\sigma d - 4}{\sigma + 1} \|\psi\|_{2\sigma+2}^{2\sigma+2}. \quad (7.17)$$

Exercise 7.2 Prove (7.17) by direct differentiation.

Therefore, if we define

$$V_B(z) := V_B(0) + \int_0^z \left(\operatorname{Im} \int \psi^*(\tilde{z}, \mathbf{x}) \nabla \psi \cdot \mathbf{x} d\mathbf{x} \right) d\tilde{z}, \quad (7.18)$$

where $V_B(0)$ is a positive constant, then V_B satisfies the *BNLS variance identity* [14]

$$V''_B(z) = 4H_B - \frac{\sigma d - 4}{\sigma + 1} \|\psi\|_{2\sigma+2}^{2\sigma+2}.$$

Unfortunately, it is not clear whether $V_B(z)$, as defined by (7.18), has to remain positive. Therefore, one cannot use the BNLS variance identity to prove blowup. Indeed, at present the following problem is open:

Open Question 7.1 Does the BNLS admit singular solutions?

We stress that what is lacking is a rigorous proof, as there is plenty of asymptotic and numerical evidence that BNLS solutions can become singular [11, 12, 13, 14, 82].

² By *equivalent* we mean that both conservation laws follow from the invariance of the action integral under dilations (see [220, 247, 249] for derivation of NLS conservation laws via Noether Theorem).

7.3 Sufficient Conditions for Collapse

The variance identity (7.6) leads to

Lemma 7.2 *Let ψ be a solution of the NLS (7.1) in $[0, Z_c)$, where $0 < Z_c \leq \infty$, let $\sigma d \geq 2$, and let $V(z)$ be given by (7.2). Then*

$$V(z) \leq P_2(z), \quad 0 \leq z < Z_c, \quad (7.19a)$$

where

$$P_2(z) = V(0) + zV'(0) + 4z^2 H(0) \quad (7.19b)$$

and

$$V'(0) = 4 \operatorname{Im} \int \psi_0^* \mathbf{x} \cdot \nabla \psi_0 d\mathbf{x}. \quad (7.19c)$$

Specifically,

1. If $\sigma d = 2$, then $V(z) \equiv P_2(z)$ for $0 \leq z < Z_c$.
2. If $\sigma d > 2$ and $\psi \not\equiv 0$, then $V(z) < P_2(z)$ for $0 < z < Z_c$.

Proof By the variance identity (7.6) and Hamiltonian conservation (5.6),

$$V''(z) \leq 8H(0). \quad (7.20)$$

Integrating this inequality from 0 to z gives

$$V'(z) \leq V'(0) + 8H(0)z, \quad 0 \leq z < Z_c.$$

Integrating one more time and using (7.5) proves (7.19). Equation (7.19c) follows from (7.5). Finally, we note that (7.20), hence (7.19a), is a strict inequality if $\sigma d > 2$ and $\psi \not\equiv 0$, and an equality if $\sigma d = 2$. \square

The most important consequence of the variance identity is

Theorem 7.2 (Sufficient conditions for collapse [262]) *Let ψ be a solution of the NLS (7.1), let $\sigma d \geq 2$, and assume that one of the following three conditions holds:*

1. $H(0) < 0$.
2. $H(0) = 0$ and $\operatorname{Im} \int \psi_0^* \mathbf{x} \cdot \nabla \psi_0 d\mathbf{x} < 0$.
3. $H(0) > 0$ and $\operatorname{Im} \int \psi_0^* \mathbf{x} \cdot \nabla \psi_0 d\mathbf{x} \leq -\sqrt{H(0)V(0)}$.

Then ψ becomes singular at a finite distance Z_c .

Proof By negation. Assume that ψ exists for all z . In that case, (7.19) holds for $0 \leq z < \infty$. Recall that when $C > 0$, the parabola $P_2(z) = Az^2 + Bz + C$ has a positive root if either of the following three conditions hold:

1. $A < 0$.
2. $A = 0$ and $B < 0$.
3. $A > 0$, $B < 0$ and $B^2 - 4AC \geq 0$, or equivalently, $A > 0$ and $B \leq -2\sqrt{AC}$.

The coefficients of the parabola P_2 are, see (7.19b),

$$A = 4H(0), \quad B = 4 \operatorname{Im} \int \psi_0^* \mathbf{x} \cdot \nabla \psi_0 d\mathbf{x}, \quad C = V(0).$$

Therefore, conditions 1–3 of the theorem correspond to conditions 1–3 for $P_2(z)$ to have a positive root. In that case, by (7.19a), $V(Z_*) \leq 0$. This however, is not possible. Indeed, by (7.2), $V(z) \geq 0$ and $V(z) = 0$ if and only if $\psi \equiv 0$. In the latter case, however, ψ cannot satisfy any of the three conditions of the theorem. \square

Remark The conditions of Theorem 7.2 are not sharp, i.e., NLS solutions can become singular even when none of these three conditions is satisfied (Sect. 7.4).

Remark A physical interpretation of Theorem 7.2 is presented in Sect. 7.5.

Remark An extension of Theorem 7.2 is presented in Sect. 7.6.

Corollary 7.2 *The only condition in Theorem 7.2 which is relevant for real initial conditions is $H(\psi_0) < 0$.*

Proof If ψ_0 is real, then $\operatorname{Im} \int \psi_0^* \mathbf{x} \cdot \nabla \psi_0 d\mathbf{x} = 0$. Therefore, Conditions 2 and 3 of Theorem 7.2 cannot be satisfied. \square

Exercise 7.3 “Prove” that solutions of the defocusing NLS can also become singular, as follows:

1. Verify that the variance identity for the NLS

$$i\psi_z + \Delta\psi + \nu|\psi|^{2\sigma}\psi = 0$$

is

$$V''(z) = 8 \left[H - \nu \frac{d\sigma - 2}{2\sigma + 2} \|\psi\|_{2\sigma+2}^{2\sigma+2} \right], \quad H := \|\nabla\psi\|_2^2 - \frac{\nu}{\sigma + 1} \|\psi\|_{2\sigma+2}^{2\sigma+2}.$$

2. “Conclude” that when $\nu < 0$, $\sigma d < 2$, and $H(0) < 0$, the solution becomes singular at a finite z .

What is the logical failure of this argument?

To relate the vanishing of the variance to blowup of the H^1 norm (which is our definition of a singularity), we first recall the following classical result:

Lemma 7.3 (Uncertainty principle) *Let $\phi(\mathbf{x}) \in \Sigma(\mathbb{R}^d)$ be a complex function. Then*

$$\|\phi\|_2^4 \leq \left(\frac{2}{d}\right)^2 \|\nabla\phi\|_2^2 V(\phi).$$

Proof We first note that

$$0 = \int \nabla \cdot (\mathbf{x} |\phi|^2) d\mathbf{x} = d \int |\phi|^2 d\mathbf{x} + 2 \operatorname{Re} \int \phi^* \mathbf{x} \cdot \nabla \phi d\mathbf{x}.$$

Therefore, using the Cauchy-Schwartz inequality, we have

$$d \int |\phi|^2 d\mathbf{x} \leq 2 \int |\phi^* \mathbf{x} \cdot \nabla \phi| d\mathbf{x} \leq 2 \left(\int |\mathbf{x}|^2 |\phi|^2 d\mathbf{x} \right)^{\frac{1}{2}} \left(\int |\nabla \phi|^2 d\mathbf{x} \right)^{\frac{1}{2}}.$$

□

Remark Let $\hat{\phi}(\mathbf{k})$ be the Fourier transform of $\phi(\mathbf{x})$, see (2.70). By Parseval relation and the relation $\widehat{\nabla \phi} = i\mathbf{k}\hat{\phi}$,

$$\int |\nabla \phi|^2 d\mathbf{x} = \int |\widehat{\nabla \phi}|^2 d\mathbf{k} = \int |\mathbf{k}|^2 |\hat{\phi}|^2 d\mathbf{k}.$$

Therefore, we can rewrite the uncertainty principle (Lemma 7.3) in the more familiar form

$$\left(\frac{d}{2}\right)^2 \left(\int |\phi|^2 d\mathbf{x} \right)^2 \leq \int |\mathbf{x}|^2 |\phi|^2 d\mathbf{x} \int |\mathbf{k}|^2 |\hat{\phi}|^2 d\mathbf{k}. \quad (7.21)$$

We now use Lemma 7.3 to relate the vanishing of the variance to blowup of the H^1 norm:

Corollary 7.3 *Let ψ be a solution of the NLS (7.1) which exists for $0 \leq z < Z_{**}$. If $\lim_{z \rightarrow Z_{**}} V(z) = 0$, then $\lim_{z \rightarrow Z_{**}} \|\psi\|_{H^1} = \infty$.*

Proof By Lemma 7.3 and power conservation,

$$\|\psi_0\|_2^4 = \|\psi\|_2^4 \leq \left(\frac{2}{d}\right)^2 \|\nabla\psi\|_2^2 V(z). \quad (7.22)$$

Hence, $\lim_{z \rightarrow Z_{**}} V = 0$ implies that $\lim_{z \rightarrow Z_{**}} \|\nabla\psi\|_2 = \infty$. □

Remark When $Z_{**} < \infty$, then $Z_c = Z_{**}$, and so Corollary 7.3 also follows from the blowup alternative (Corollary 5.3).

Inequality (7.22) does not imply that the converse of Corollary 7.3 also holds, namely, that $\lim_{z \rightarrow Z_c} \|\nabla\psi\|_2 = \infty \implies \lim_{z \rightarrow Z_c} V(z) = 0$. Indeed, there are two possibilities for a solution that becomes singular at Z_c :

1. $\lim_{z \rightarrow Z_c} V(z) = 0.$
2. $\lim_{z \rightarrow Z_c} V(z) > 0.$

Therefore, the correct interpretation of the variance identity, with regard to the location of the singularity, is as follows:

Corollary 7.4 *Assume that one of the three conditions of Theorem 7.2 holds, so that there exists $0 < Z_* < \infty$ such that $P_2(Z_*) = 0$, where $P_2(z)$ is given by (7.19b). Then there exists Z_c , such that $0 < Z_c \leq Z_*$ and $\lim_{z \rightarrow Z_c} \|\nabla \psi\|_2 = \infty$.*

In other words, the variance identity does not predict the location of the singularity Z_c , but only provides an *upper bound* for Z_c .

Remark In this chapter we use the following notations:

1. The point where $P_2(z)$ vanishes is denoted by Z_* .
2. The point where $V(z)$ vanishes is denoted by Z_{**} .
3. The point where ψ becomes singular is denoted by Z_c .

The relations between these points are as follows. By Corollary 7.4,

$$0 < Z_c \leq Z_*.$$

The variance $V = \int |\mathbf{x}|^2 |\psi|^2 d\mathbf{x}$ is not defined for $z > Z_c$. Therefore, if $\lim_{z \rightarrow Z_c} V(z) > 0$, there is no point Z_{**} such that $\lim_{z \rightarrow Z_{**}} V(z) = 0$. Hence, if there is such a point, then $Z_{**} = Z_c$.

Remark The variance identity is a good example of an *a priori estimate* that bifurcates from the actual solution. For example, in the critical case the variance identity reads $V''(z) = 8H(0)$. The solution of this ODE exists for all $z \geq 0$. If one adds the constraint that $V \geq 0$, the variance identity suggests that the NLS solution blows up at the point Z_* where P_2 vanishes. The variance identity is derived, however, under the implicit assumption that the NLS solution exists. Therefore, if the NLS solution blows up at some $Z_c < Z_*$, the variance according to the variance-identity ODE bifurcates from the variance of the NLS solution for $z \geq Z_c$.

7.3.1 Sharper Conditions in the Supercritical Case

The three conditions for collapse in Theorem 7.2 were derived by replacing the variance identity (7.6) with the inequality $V''(z) \leq 8H$. In the supercritical case, Turitsyn and Kuznetsov et al. obtained a sharper result, by using the Gagliardo-Nirenberg inequality to bound (rather than neglect) the term $\frac{d\sigma-2}{2\sigma+2} \|\psi\|_{2\sigma+2}^{2\sigma+2}$ in (7.6):

Theorem 7.3 ([148, 257]) Let ψ be a solution of the NLS (7.1), let $\sigma d > 2$, let $R_\omega^{(0)}$ be the ground state of

$$\Delta R_\omega(\mathbf{x}) - \omega R_\omega + |R_\omega|^{2\sigma} R_\omega = 0,$$

and let ω be such that $\|R_\omega^{(0)}\|_2^2 = \|\psi_0\|_2^2$. If $\|\nabla \psi_0\|_2^2 > \|\nabla R_\omega^{(0)}\|_2^2$ and $H(\psi_0) < H(R_\omega^{(0)})$, then ψ becomes singular at a finite distance Z_c .

Remark In the supercritical case, there is a unique ω for which $\|R_\omega^{(0)}\|_2^2 = \|\psi_0\|_2^2$, see Sect. 6.1.

Remark Since $H(R^{(0)}) = 0$ in the critical case (Corollary 6.4), there is an analogy between the sufficient condition for collapse in the critical case $H(\psi_0) < H(R^{(0)})$, and the condition $H(\psi_0) < H(R_\omega^{(0)})$ in the supercritical case. Note, however, that the condition $H(\psi_0) < H(R_\omega^{(0)})$, by itself, is not sufficient for collapse in the supercritical case.

Remark For additional conditions for collapse in the three-dimensional cubic NLS, see Holmer et al. [128] and Akahori and Nawa [3].

7.4 Limitations of the Variance Identity

In general, the variance is not a good measure for the width of a collapsing solution. This is because NLS blowup is generically a local phenomenon, whereas the variance is a global quantity. To illustrate this point, consider the critical or supercritical NLS with the initial condition

$$\psi_0 = c_1 e^{-|\mathbf{x}-\mathbf{x}_1|^2} + c_2 e^{-|\mathbf{x}-\mathbf{x}_2|^2},$$

which models two parallel collimated input beams. Let \mathbf{x}_1 and \mathbf{x}_2 be sufficiently far from each other, so that interactions between the two beams are negligible. Let c_1 and c_2 be sufficiently large, so that each of the two beams, by itself, would collapse at a finite distance (Lemma 7.9). Assume that $|c_1| > |c_2|$. Then the beam initially centered at \mathbf{x}_1 will collapse before that centered at \mathbf{x}_2 (Sect. 27.6). The variance around the collapse point $\mathbf{x}_c \approx \mathbf{x}_1$ will be positive as $z \rightarrow Z_c$, because the power of the second beam remains away from \mathbf{x}_c .

One could ask whether in the case of a single-beam initial condition, such as $\psi_0 = c_1 e^{-|\mathbf{x}|^2}$, the variance does vanish at the singularity. It turns out, however, that this is not the case. For example, in Corollary 7.10 we will prove that $\lim_{z \rightarrow Z_c} V(z) > 0$ for all singular solutions of the critical NLS whose power is slightly above P_{cr} . Moreover, numerical simulations show that $\lim_{z \rightarrow Z_c} V(z) > 0$ also for high-power singular solutions not covered by Corollary 7.10. Intuitively, this is because only

the inner core of these solutions collapses into \mathbf{x}_c , leaving a positive amount of power outside. In fact, the only known H^1 solutions of the critical NLS for which the variance vanishes at the singularity are the explicit blowup solutions ψ_R^{explicit} (Chap. 10). These solutions, however, are unstable. Therefore, we make

Observation 7.1 *Generically, the variance of singular solutions of the critical NLS does not vanish at the singularity, i.e., $\lim_{z \rightarrow Z_c} V(z; \mathbf{x}_c) > 0$.*

Since the variance is not a good measure of the width of a collapsing beam, this implies

Observation 7.2 *Generically, the sufficient conditions for collapse in the critical NLS that are based on the variance identity are not sharp.*

Indeed, according to the variance identity, when the initial condition is real, the variance vanishes (and hence the solution becomes singular) only if the Hamiltonian is negative. However, real initial conditions with a positive Hamiltonian can also become singular. For example, numerical simulations show that solutions of the two-dimensional critical NLS with $\psi_0 = ce^{-r^2}$ become singular for $c > c_{\text{th}} \approx 2.75$ [70]. The Hamiltonian of ψ_0 , however, becomes negative for $c > c_H = \sqrt{8} \approx 2.83$. Therefore, Gaussian initial conditions with $c_{\text{th}} < c < c_H$ have a positive Hamiltonian, yet they become singular. Similarly, the Hamiltonian of $\psi_0 = ce^{-r^4}$ becomes negative for $c > c_H \approx 3.0$, but these super-Gaussian initial conditions become singular for $c \geq c_{\text{th}} \approx 2.54$.

From Observation 7.1 follows

Observation 7.3 *Generically, the blowup point Z_c of a singular solution of the critical NLS lies to the left of the point Z_* where $P_2(z)$ vanishes, i.e., $Z_c < Z_*$.*

In fact, the upper bound Z_* typically provides a significant overestimate for Z_c . Moreover, it can even lead to erroneous qualitative predictions. See Sect. 27.1.2 for more details.

In the case of the *supercritical NLS*, the theory is considerably less developed. Since $V(z) < P_2(z)$, see Lemma 7.2, the conditions of Theorem 7.2 are not sharp. Moreover, asymptotic analysis shows that peak-type supercritical solutions collapse with a positive variance (Sect. 21.2). Therefore, Observations 7.2 and 7.3 are also valid for these supercritical solutions.

7.5 Physical Interpretation of Theorem 7.2

To motivate the conditions of Theorem 7.2, we consider the focused input beam

$$\tilde{\psi}_0(\mathbf{x}) = \psi_0(\mathbf{x}) e^{-i \frac{|\mathbf{x}|^2}{4F}}, \quad (7.23)$$

where ψ_0 is real and F is the focal distance of the lens.³ Let us begin with the case of a collimated input beam ($\tilde{\psi}_0 = \psi_0$, $F = \infty$). By Corollary 7.2, the only condition in

³ See Conclusion 2.12.

Theorem 7.2 which is relevant for ψ_0 real is $H(\psi_0) < 0$. To motivate this condition, we note that the first and second term in

$$H(\psi_0) = \underbrace{\|\nabla\psi_0\|_2^2}_{\text{diffraction}} - \underbrace{\frac{1}{\sigma+1}\|\psi_0\|_{2\sigma+2}^{2\sigma+2}}_{\text{nonlinearity}} \quad (7.24)$$

correspond to diffraction and nonlinearity, respectively. Therefore, the condition $H(\psi_0) < 0$ has the interpretation that “*nonlinearity > diffraction*”, i.e., that the focusing nonlinearity is stronger than diffraction.⁴

We now consider the case where the input beam is not collimated ($0 < |F| < \infty$). Since $\nabla\tilde{\psi}_0 = (\nabla\psi_0 - i\frac{\mathbf{x}}{2F}\psi_0)e^{-i\frac{|\mathbf{x}|^2}{4F}}$ and ψ_0 is real,

$$H(\tilde{\psi}_0) = H(\psi_0) + \frac{V(\psi_0)}{4F^2}. \quad (7.25)$$

In addition, by (7.19c),

$$\tilde{V}_z(0) = 4 \operatorname{Im} \int \tilde{\psi}_0^* \mathbf{x} \cdot \nabla \tilde{\psi}_0 d\mathbf{x} = -\frac{2V(\psi_0)}{F},$$

where we adopt the notation $\tilde{V} := V(\tilde{\psi})$. Therefore, by (7.19),

$$\tilde{V}(z) \leq \tilde{P}_2(z), \quad (7.26a)$$

where

$$\tilde{P}_2(z) := \tilde{V}(0) + z\tilde{V}_z(0) + 4z^2 H(\tilde{\psi}_0) = V(0) \left(1 - \frac{z}{F}\right)^2 + 4z^2 H(\psi_0). \quad (7.26b)$$

When the lens is focusing ($F > 0$) and the Hamiltonian of the original collimated input beam is negative ($H(\psi_0) < 0$), it follows from (7.26) that $\tilde{P}_2(z = F) < 0$. Therefore, both the focused and the collimated beam collapse at a finite distance:

Corollary 7.5 *Let $\tilde{\psi}$ be a solution of the NLS (7.1) with the initial condition (7.23). If $\sigma d \geq 2$, ψ_0 is real, $H(\psi_0) < 0$, and $0 < F \leq \infty$, then $\tilde{\psi}$ becomes singular at a finite distance.*

This result is intuitive: If a collimated beam undergoes collapse, the addition of a focusing lens is not expected to arrest collapse.

When $H(\psi_0) < 0$ and $0 < F \ll 1$ (i.e., tight focusing), then $H(\tilde{\psi}_0) > 0$. This may seem to suggest that the beam does not collapse. Equation (7.26) shows, however, that the focused beam does collapse. Indeed, in that case collapse follows from Condition 3 of Theorem 7.2:

⁴ The condition $H(\psi_0) < 0$ is not sharp, i.e., collapse can also occur for real initial conditions with a positive Hamiltonian (Sect. 7.4). Hence, nonlinearity can be stronger than diffraction even when $H(\psi_0) > 0$.

Exercise 7.4 Let $\tilde{\psi}$ be a solution of the NLS (7.1) with the initial condition (7.23), let $\sigma d \geq 2$, let $H(\psi_0) < 0$, and let $F > 0$. Show that if F is sufficiently small so that $H(\tilde{\psi}_0) > 0$, collapse of $\tilde{\psi}$ follows from Condition 3 of Theorem 7.2.

Finally, consider the case of a defocusing lens ($F < 0$) and $H(\psi_0) < 0$. Then the original collimated beam undergoes collapse. Whether the defocused beam collapses, however, depends on the lens strength. If $-F$ is sufficiently large (i.e., weak defocusing), then $H(\tilde{\psi}_0)$ remains negative and so the beam will collapse. If $-F$ is sufficiently small (i.e., strong defocusing), however, then $H(\tilde{\psi}_0)$ becomes positive. As noted, the condition $H(\tilde{\psi}_0) > 0$ does not imply that the beam does not collapse. Intuitively, however, one can expect collapse to be arrested by a sufficiently strong defocusing lens.⁵ Therefore, in the case of a defocusing lens, the condition $H(\tilde{\psi}_0) < 0$ implies that the focusing nonlinearity is stronger than the combined effects of diffraction and the defocusing lens.^{6,7} This interpretation also follows from the Hamiltonian of $\tilde{\psi}_0$, see (7.24) and (7.25), which reads

$$H(\tilde{\psi}_0) = \underbrace{\|\nabla\psi_0\|_2^2}_{\text{diffraction}} + \underbrace{\frac{1}{4F^2}V(\psi_0)}_{\text{lens}} - \underbrace{\frac{1}{\sigma+1}\|\psi_0\|_{2\sigma+2}^{2\sigma+2}}_{\text{nonlinearity}}.$$

In summary, according to Theorem 7.2, collapse occurs when

1. The input beam is collimated, and the focusing nonlinearity is stronger than diffraction (Condition 1 of Theorem 7.2).
2. The input beam is focused, and the focusing nonlinearity is stronger than diffraction for the corresponding collimated beam (Condition 3 of Theorem 7.2).
3. The input beam is defocused, and the focusing nonlinearity is stronger than the combined effects of diffraction and the defocusing lens (Condition 1 of Theorem 7.2).

Remark In the critical NLS, the effect of a lens on the possibility and location of collapse is completely understood, as it follows from the *lens transformation* (Sect. 8.4). In particular, the location of the singularity is monotone in F (Corollary 27.1). In contrast, the effect of a lens in the supercritical NLS is more complex. Thus, for example, the location of the singularity is not necessarily monotone in F (Sect. 27.6).

⁵ In the critical case, it can be rigorously shown that if $0 < -F \leq Z_c$, where Z_c is the blowup point of ψ , then $\tilde{\psi}$ does not blowup (Sect. 8.4.6). In the supercritical case, it can be informally shown that collapse is arrested when $-F$ is sufficiently small (Sect. 8.4.2).

⁶ The converse statement is not true, i.e., the condition $H(\tilde{\psi}_0) > 0$ does not necessarily imply that nonlinearity is weaker than the combined effects of diffraction and the lens.

⁷ We already reached this conclusion when we analyzed the NLS with the aberrationless approximation method (Sect. 3.5).

7.6 The Sufficient Condition $H_G(0) < 0$

In Sect. 7.5 we saw that Condition 3 of Theorem 7.2 can be viewed as an extension of the condition $H(0) < 0$ to focused beams. We now derive a *sharper sufficient condition for collapse*, by extending the negative Hamiltonian condition to tilted beams.⁸

Let ψ be the solution of the NLS with initial condition ψ_0 , and let ψ^c be the solution of the same NLS with the initial condition

$$\psi_0^c(\mathbf{x}) = \psi_0(\mathbf{x}) e^{i \frac{c \cdot \mathbf{x}}{2}}.$$

In Sect. 8.1 we shall see that by Galilean invariance,

$$\psi^c(z, \mathbf{x}) = \psi(z, \mathbf{x} - \mathbf{c}z) e^{i \frac{c \cdot \mathbf{x}}{2} - i \frac{|\mathbf{c}|^2 z}{4}}. \quad (7.27)$$

Since

$$\|\psi^c(z)\|_{2\sigma+2} = \|\psi(z)\|_{2\sigma+2}, \quad (7.28)$$

ψ and ψ^c blowup at the same z , if at all. Therefore, if there exists $\mathbf{c} \in \mathbb{R}^d$ for which $H(\psi_0^c) < 0$, then ψ^c , hence also ψ , become singular. This suggests that in order to get a sharper sufficient condition for collapse, we look for the value of \mathbf{c} that minimizes the Hamiltonian of ψ_0^c :

Lemma 7.4 *The minimal value of $H(\psi_0^c)$ is attained at*

$$\mathbf{c} = -2 \frac{\operatorname{Im} \int \psi_0^* \nabla \psi_0 d\mathbf{x}}{\int |\psi_0|^2 d\mathbf{x}}. \quad (7.29)$$

Proof Since $\nabla \psi_0^c = (\nabla \psi_0 + \frac{i\mathbf{c}}{2} \psi_0) e^{i \frac{c \cdot \mathbf{x}}{2}}$, then

$$H(\psi_0^c) = H(\psi_0) + \frac{|\mathbf{c}|^2}{4} \|\psi_0\|_2^2 + \mathbf{c} \cdot \operatorname{Im} \int \psi_0^* \nabla \psi_0 d\mathbf{x}. \quad (7.30)$$

Hence, $H(\psi_0^c)$ is a parabola in each coordinate c_j . Therefore, the result follows. \square

The minimal Hamiltonian is attained when the initial condition has a zero linear momentum:

Lemma 7.5 *Let $\psi_0^c(\mathbf{x}) = \psi_0(\mathbf{x}) e^{i \frac{c \cdot \mathbf{x}}{2}}$, where \mathbf{c} is given by (7.29). Then*

1. ψ_0^c has a zero linear momentum.
2. $H(\psi_0^c) = H_G(\psi_0)$, where

$$H_G(\psi) := H(\psi) - \frac{(\operatorname{Im} \int \psi^* \nabla \psi d\mathbf{x})^2}{\|\psi\|_2^2}. \quad (7.31)$$

⁸ See Sects. 2.12.3 and 8.2 for the mathematical representation of tilted beams.

Proof 1. The linear momentum of ψ_0^c is equal to (Definition 5.3)

$$\operatorname{Im} \int (\psi_0^c)^* \nabla \psi_0^c d\mathbf{x} = \frac{\mathbf{c}}{2} \int |\psi_0|^2 d\mathbf{x} + \operatorname{Im} \int \psi_0^* \nabla \psi_0 d\mathbf{x}.$$

Therefore, when \mathbf{c} is given by (7.29), $\operatorname{Im} \int (\psi_0^c)^* \nabla \psi_0^c d\mathbf{x} = 0$.

2. Substitution of (7.29) in (7.30) gives

$$H(\psi_0^c) = H(\psi_0) + \frac{(\operatorname{Im} \int \psi_0^* \nabla \psi_0 d\mathbf{x})^2}{\|\psi_0\|_2^2} - 2 \frac{(\operatorname{Im} \int \psi_0^* \nabla \psi_0 d\mathbf{x})^2}{\|\psi_0\|_2^2} = H_G(\psi_0).$$

□

The “generalized Hamiltonian” $H_G(\psi)$ is a conserved quantity, since it is a combination of the conserved Hamiltonian, linear momentum, and power (Sect. 5.3). In addition, $H_G(\psi) = H(\psi)$ when ψ has a zero linear momentum i.e., when $\operatorname{Im} \int \psi_0^* \nabla \psi_0 d\mathbf{x} = 0$.⁹ When ψ has a non-zero linear momentum, then $H_G(\psi) = H(\psi^c)$, where ψ^c is the same as ψ , except that it is tilted at such an angle so that it has a zero linear momentum.

The condition $H_G(\psi_0) < 0$ is sufficient for collapse:

Theorem 7.4 *Let ψ be a solution of the NLS (7.1) and let $\sigma d \geq 2$. If*

$$H_G(\psi_0) < 0, \quad (7.32)$$

then ψ becomes singular at a finite distance.

Proof By Lemma 7.5 and (7.32), $H(\psi_0^c) = H_G(\psi_0) < 0$. Therefore, ψ^c collapses at a finite distance Z_c . Hence, by (7.28), ψ also collapses at Z_c . □

Remark Since

$$H_G(\psi_0) \leq H(\psi_0),$$

the condition $H_G(\psi_0) < 0$ is sharper than the condition $H(\psi_0) < 0$.

Remark If ψ becomes singular, then ψ^c becomes singular for any \mathbf{c} . Since

$$H(\psi_0^c) \sim \frac{|\mathbf{c}|^2}{4} \|\psi_0\|_2^2, \quad |\mathbf{c}| \rightarrow \infty,$$

see (7.30), this shows (again) that NLS solutions can collapse with an arbitrarily large positive Hamiltonian.

⁹ This is the case, e.g., when ψ_0 is real or radially-symmetric.

7.7 Whole-Beam and Partial-Beam Collapse

In Sect. 7.4 we asked whether the variance always or sometimes vanishes at the singularity. Intuitively, the variance vanishes at the singularity if and only if all the beam power collapses into the singularity point \mathbf{x}_c . Therefore, in what follows, we consider the amount of power that collapses into the singularity.¹⁰ We begin with a few definitions.

Definition 7.2 (amount of power that collapses into the singularity) *Let ψ be an NLS solution that collapses at $\mathbf{x} = \mathbf{x}_c$ as $z \rightarrow Z_c$, and let*

$$P_\epsilon := \liminf_{z \rightarrow Z_c} \int_{|\mathbf{x} - \mathbf{x}_c| < \epsilon} |\psi|^2 d\mathbf{x}$$

be the limiting power in a ball of radius ϵ centered at \mathbf{x}_c . Then the amount of power that collapses into the singularity is

$$P_{\text{collapse}} := \lim_{\epsilon \rightarrow 0^+} P_\epsilon.$$

Definition 7.3 (whole-beam collapse) *A beam undergoes a whole-beam collapse, if it collapses into the singularity point \mathbf{x}_c as a delta function that contains all the beam power, i.e., if*

$$\lim_{z \rightarrow Z_c} |\psi|^2 = \|\psi_0\|_2^2 \delta(\mathbf{x} - \mathbf{x}_c), \quad (7.33)$$

where the limit is in the sense of distributions.

Remark In Corollary 2.1 we saw that in linear propagation, under the geometrical optics approximation, focused input beams undergo a whole-beam collapse.

Definition 7.4 (partial-beam collapse) *A beam undergoes a partial-beam collapse, if it collapses into the singularity point \mathbf{x}_c as a delta function that contains a positive fraction of the beam power, i.e., if*

$$\lim_{z \rightarrow Z_c} |\psi|^2 = P_{\text{partial}} \delta(\mathbf{x} - \mathbf{x}_c) + |\phi(\mathbf{x})|^2,$$

where $0 < P_{\text{partial}} < \|\psi_0\|_2^2$, $0 \not\equiv \phi \in L^2$ is the limit of the non-collapsing “tail”, and the limit is in the sense of distributions.

Thus, $P_{\text{collapse}} = \|\psi_0\|_2^2$ in whole-beam collapse, and $P_{\text{collapse}} = P_{\text{partial}}$ in partial-beam collapse.

Definition 7.5 (strong collapse) *A beam undergoes a strong collapse, if the amount of power that collapses into the singularity is positive ($P_{\text{collapse}} > 0$).*

¹⁰ Knowing the amount of power that collapses into the singularity is important in applications where one wants to maximize (or control) the amount of power at the “target”.

Definition 7.6 (weak collapse) A beam undergoes a weak collapse, if the amount of power that collapses into the singularity is zero ($P_{\text{collapse}} = 0$).

Therefore, both whole-beam collapse and partial-beam collapse are examples of a strong collapse.

Whole-beam collapse is closely related to the vanishing of the variance at the blowup point. Indeed, Nawa and Tsutsumi showed that if the variance vanishes at the singularity, then the solution undergoes a whole-beam collapse:

Lemma 7.6 ([200]) Let ψ be a solution of the NLS (7.1) that becomes singular at \mathbf{x}_c as $z \rightarrow Z_c$. If the variance vanishes at the singularity, i.e., if

$$\lim_{z \rightarrow Z_c} V(z; \mathbf{x}_c) = \lim_{z \rightarrow Z_c} \int |\mathbf{x} - \mathbf{x}_c|^2 |\psi(z, \mathbf{x})|^2 d\mathbf{x} = 0, \quad (7.34)$$

then the solution undergoes a whole-beam collapse, i.e., relation (7.33) holds.

Proof Let $\epsilon > 0$. Then

$$\int_{|\mathbf{x} - \mathbf{x}_c| > \epsilon} |\psi|^2 d\mathbf{x} \leq \frac{1}{\epsilon^2} \int_{|\mathbf{x} - \mathbf{x}_c| > \epsilon} |\mathbf{x} - \mathbf{x}_c|^2 |\psi|^2 d\mathbf{x} \leq \frac{1}{\epsilon^2} \int_{\mathbb{R}^d} |\mathbf{x} - \mathbf{x}_c|^2 |\psi|^2 d\mathbf{x}.$$

Therefore, if relation (7.34) holds, then $\lim_{z \rightarrow Z_c} \int_{|\mathbf{x} - \mathbf{x}_c| > \epsilon} |\psi|^2 d\mathbf{x} = 0$. Hence, by power conservation, $\lim_{z \rightarrow Z_c} \int_{|\mathbf{x} - \mathbf{x}_c| < \epsilon} |\psi|^2 d\mathbf{x} = \|\psi_0\|_2^2$. \square

Corollary 7.6 If an NLS solution undergoes a weak collapse or a partial-beam collapse, then its variance does not vanish at the singularity.

7.7.1 Critical NLS

In [201], Nawa and Tsutsumi showed for the critical NLS that when either $d = 1$, or $d \geq 2$ and ψ_0 is radial, the converse of Lemma 7.6 also holds, namely, whole-beam collapse, see (7.33), implies that the variance vanishes at the singularity, see (7.34). Therefore, we have

Theorem 7.5 ([201]) Let ψ be a singular solution of the critical NLS (7.13). Suppose that either $d = 1$, or $d \geq 2$ and ψ_0 is radial. Then ψ undergoes a whole-beam collapse if and only if the variance vanishes at the singularity.

In Sect. 13.3 we will prove

Corollary 7.7 All singular solutions of the critical NLS undergo a strong collapse with $P_{\text{collapse}} \geq P_{\text{cr}}$.

Therefore, singular solutions of the critical NLS undergo either a whole-beam collapse or a partial-beam collapse.

The following result, due to Nawa and Tsutsumi, characterizes the initial conditions that lead to a whole-beam collapse in the critical NLS:

Theorem 7.6 ([200]) *Let ψ be a solution of the critical NLS (7.13) which becomes singular at \mathbf{x}_c as $z \rightarrow Z_c$. Then the variance $V(z; \mathbf{x}_c)$ vanishes at the singularity (hence, ψ undergoes a whole-beam collapse) if and only if*

$$\psi_0(\mathbf{x}) = e^{-i\frac{|\mathbf{x}-\mathbf{x}_c|^2}{4Z_c}} S(\mathbf{x}), \quad (7.35)$$

where $0 \not\equiv S \in \Sigma$, $H(S) = 0$ and the solution $\tilde{\psi}$ of the critical NLS (7.13) with the initial condition $\tilde{\psi}_0 = S$ exists globally.

Proof Without loss of generality, we can set $\mathbf{x}_c = 0$. By Lemma 7.2,

$$V(z) = P_2(z) = V(\psi_0) + 4z \operatorname{Im} \int \psi_0^* \mathbf{x} \cdot \nabla \psi_0 d\mathbf{x} + 4H(\psi_0)z^2.$$

Therefore,

$$\lim_{z \rightarrow Z_c} V(z) = V(\psi_0) + 4Z_c \operatorname{Im} \int \psi_0^* \mathbf{x} \cdot \nabla \psi_0 d\mathbf{x} + 4H(\psi_0)Z_c^2.$$

If $S(\mathbf{x}) = e^{i\frac{|\mathbf{x}|^2}{4Z_c}} \psi_0$, then

$$\begin{aligned} H(S) &= \int \left| \nabla \psi_0 + i \frac{\mathbf{x}}{2Z_c} \psi_0 \right|^2 d\mathbf{x} - \frac{1}{\sigma+1} \int |\psi_0|^{2\sigma+2} d\mathbf{x} \\ &= H(\psi_0) + \frac{1}{Z_c} \cdot \operatorname{Im} \int \psi_0^* \mathbf{x} \cdot \nabla \psi_0 d\mathbf{x} + \frac{V(\psi_0)}{4Z_c^2}. \end{aligned}$$

Comparison of the last two relations shows that $\lim_{z \rightarrow Z_c} V(z) = 4Z_c^2 H(S)$. In particular,

$$\lim_{z \rightarrow Z_c} V(z) = 0 \iff H(S) = 0. \quad (7.36)$$

To prove the first direction, assume that $V(Z_c) = 0$. By (7.36), $H(S) = 0$. In addition, in Lemma 8.4 we will prove that if ψ is a solution of the critical NLS with an initial condition ψ_0 that becomes singular at Z_c , then the solution $\tilde{\psi}$ of the critical NLS with the initial condition $\tilde{\psi}_0 = \psi_0 \cdot e^{-i\frac{|\mathbf{x}|^2}{4F}}$ exists globally for $0 < -F \leq Z_c$. Therefore, the solution $\tilde{\psi}$ of the NLS (7.13) with $\tilde{\psi}_0 = S = e^{i\frac{|\mathbf{x}|^2}{4Z_c}} \psi_0$ exists globally.

The opposite direction follows from the facts that if ψ becomes singular at Z_c and if $H(S) = 0$, then by (7.36), the variance vanishes at Z_c . \square

Unfortunately, Theorem 7.6 tells us whether a given initial condition will undergo a whole-beam collapse only if we know the value of Z_c for that solution. In that case, however, we can determine whether the solution undergoes a whole-beam collapse directly from the variance identity, namely, by checking whether the collapse point Z_c is equal to the positive root Z_* of $P_2(z)$.

The function $S(\mathbf{x})$ in Theorem 7.6 can be any nontrivial solution of

$$\Delta R(\mathbf{x}) - R + |R|^{\frac{4}{d}} R = 0, \quad R \in H^1. \quad (7.37)$$

In that case, ψ is the explicit blowup solution ψ_R^{explicit} , which indeed undergoes a whole-beam collapse (Sect. 10.2). It is believed that these are the only H^1 solutions that undergo a whole-beam collapse. Theorem 7.6 does not show, however, that this is the case.

We can identify initial conditions for which a whole-beam collapse cannot occur:

Lemma 7.7 *Let ψ be a singular solution of the critical NLS (7.13) with $\psi_0 = f(\mathbf{x})e^{-i\frac{|\mathbf{x}|^2}{4F}}$, where $f(\mathbf{x})$ is a real function and $H(f) > 0$. Suppose that either $d = 1$, or $d \geq 2$ and ψ_0 is radial. Then ψ does not undergo a whole-beam collapse.*

Proof By Lemma 7.2, $V(z) \equiv P_2(z)$. In addition, by (7.26),

$$P_2(z) = V(0) \left(1 - \frac{z}{F}\right)^2 + 4z^2 H(f).$$

Hence, $V(z)$ cannot vanish at any $z > 0$. Consequently, by Theorem 7.5, ψ does not undergo a whole-beam collapse. \square

Lemma 7.7 should not be interpreted as implying that whole-beam collapse does occur when $H(f) < 0$. Indeed, it can be shown that, regardless of the sign of $H(\psi_0)$, for all singular solutions whose power is slightly above P_{cr} , the amount of power that collapses into the singularity is exactly P_{cr} :

Corollary 7.8 *Let ψ be a singular solution of the critical NLS with $\psi_0 \in H^1$, and let $1 \leq d \leq 5$. Then there exists a universal constant $\alpha^* > 0$, such that if $P_{\text{cr}} < \|\psi_0\|_2^2 \leq P_{\text{cr}} + \alpha^*$, the amount of power that collapses into the singularity is exactly P_{cr} , i.e., $P_{\text{collapse}} = P_{\text{cr}}$.*

Proof See Corollary 14.1. \square

Corollary 7.9 *Under the conditions of Corollary 7.8, ψ undergoes a partial-beam collapse, and not a whole-beam collapse.*

Proof Since $P_{\text{collapse}} = P_{\text{cr}}$ and $0 < P_{\text{cr}} < \|\psi_0\|_2^2$, the result follows. \square

Since Corollary 7.9 holds for initial conditions with both positive and negative Hamiltonians, this shows that the condition $H(\psi_0) < 0$ does not imply whole-beam collapse.

Remark In Sect. 14.5 we present *experimental evidence* that collapsing laser beams undergo a partial-beam collapse.

Corollary 7.10 *Under the conditions of Corollary 7.8, $\lim_{z \rightarrow z_c} V(z; \mathbf{x}_c) > 0$.*

Proof This follows from Corollaries 7.6 and 7.9. \square

7.7.2 Supercritical NLS

For many years it was believed, based on asymptotic analysis and simulations (Sect. 21.2), that all singular solutions of the supercritical NLS undergo a weak collapse. Thus, it was argued that singular NLS solutions undergo a strong collapse in the critical case but a weak collapse in the supercritical case, because in both cases the scaling of the asymptotic blowup profile is¹¹

$$|\psi(z, r)| \sim \frac{1}{L^{\frac{1}{\sigma}}(z)} F\left(\frac{r}{L(z)}\right). \quad (7.38)$$

Exercise 7.5 Show that if $|\psi|$ is given by (7.38) and $\lim_{z \rightarrow Z_c} L(z) = 0$, ψ undergoes a strong collapse if $\sigma d = 2$, and a weak collapse if $\sigma d > 2$.

Thus, in the critical case the amplitude increases at the rate that exactly “balances” the narrowing of the solution, so that the power of $L^{-\frac{1}{\sigma}} F\left(\frac{r}{L}\right)$ remains unchanged as $L \rightarrow 0$. In the supercritical case, however, the rate at which the amplitude increases is slower. Hence, the power of $L^{-\frac{1}{\sigma}} F\left(\frac{r}{L}\right)$ goes to zero as $L \rightarrow 0$.

The scaling (7.38) applies to blowup solutions which are peak-type. In 2007, Fibich et al. showed that the supercritical subquintic NLS ($\frac{2}{d} < \sigma < 2$) admits blowup solutions that are ring-type [74]. In particular, these solutions undergo a strong collapse (Sect. 23.4). Therefore, while critical collapse is always strong, there is no such characterization of supercritical collapse.

7.8 Wrong Conclusions

In the remainder of this chapter we will present additional consequences of the variance identity. Before doing that, we caution against some incorrect conclusions which have been sometimes deduced from the variance identity:

Wrong conclusion 1. The variance vanishes at the blowup point.

Wrong conclusion 2. The blowup point Z_c is given by (or is well approximated by) the point Z_{**} , where the variance should vanish according to the variance identity.

Wrong conclusion 3. As $z \rightarrow Z_c$, all the beam power collapses into the singularity point x_c (*whole-beam collapse*).

Wrong conclusion 4. There is a qualitative difference between collapse when $H(0) < 0$ and when $H(0) > 0$, in the sense that the former is a *whole-beam collapse* and the latter is a *partial-beam collapse*.

Wrong conclusion 5. The condition $H(0) = 0$ provides a good estimate for the critical power P_{cr} .

¹¹ See Sects. 13.2 and 14.6 for the critical case, and Sect. 21.1 for the supercritical case.

The above misinterpretations of the variance identity are based on the assumption that $V(z) \sim c L^2(z)$, so that the variance vanishes at the singularity. As pointed out in Sect. 7.4, this assumption is incorrect: Generically NLS solutions undergo a *partial-beam collapse*. Consequently $V(z) \not\sim c L^2(z)$. In particular, the variance is positive at the blowup point.

7.9 The Variance Identity and the Aberrationless Approximation

The results in Sect. 7.5 on the effect of a lens are reminiscent of those obtained in Sect. 3.5, where we analyzed the NLS with the aberrationless approximation method. Indeed, these results were deduced from Eq. (7.26) and from Eq. (3.30), respectively, which agree with each other if we identify $P_2(z)$ with $V(z)$ and $V(z)/V[F]$ with $L^2(z)$.

The similarity between consequences of the aberrationless approximation and consequences of the variance identity coupled with the approximation $V \sim cL^2$, is not a coincidence. Indeed, we already saw that the aberrationless approximation (7.3) implies that $V \sim cL^2$, see (7.4).

Conclusion 7.1 *The aberrationless approximation and the approximation $V \sim cL^2$ are essentially the same approximation.*

Therefore, application of the aberrationless approximation to collapsing NLS solutions can lead to all the wrong conclusions outlined in Sect. 7.8. We stress that by the *aberrationless approximation* we do not refer only to the original aberrationless approximation method of Akhmanov et al. (Sect. 3.5), but to any method that assumes that the solution profile is a modulated test function (e.g., *variational method*). Obviously, not all predictions of the aberrationless approximation are incorrect or inaccurate. A priori, however, it is not possible to know which prediction would turn out to be “correct”.

Conclusion 7.2 *One should always test predictions that are based on the aberrationless approximation with direct numerical simulations of the NLS.*

See [75] and Sect. 24.3.1 for further ‘failures’ of the aberrationless approximation.

7.10 Sufficient Power ($P_{\text{sufficient}}$) and Threshold Power (P_{th}) for Collapse

Consider the critical or supercritical NLS with the one-parameter family of initial conditions

$$\psi_0 = c f(\mathbf{x}), \quad c > 0, \quad f(\mathbf{x}) \in \Sigma.$$

Lemma 7.8 Let ψ be a solution of the NLS (7.1) with $\sigma d \geq 2$ and $\psi_0 = c f(\mathbf{x})$. For any $f \in H^1$, there exists $c_m = c_m[f]$, such that ψ exists globally for $0 < c < c_m$.

Proof This follows from Theorem 5.9. In the critical case, it also follows from Theorem 5.5. \square

We now show that for any $f \in \Sigma$, there exists $c_{\text{th}} = c_{\text{th}}[f]$, such that ψ becomes singular for $c > c_{\text{th}}$.

Lemma 7.9 Let ψ be a solution of the NLS (7.1) with $\sigma d \geq 2$ and $\psi_0 = c f(\mathbf{x}) \in \Sigma$, and let $c_{\text{collapse}} := \left((\sigma + 1) \frac{\|\nabla f\|_2^2}{\|f\|_{2\sigma+2}^{2\sigma+2}} \right)^{\frac{1}{2\sigma}}$. If $c > c_{\text{collapse}}$, then ψ becomes singular at a finite distance.

Proof The sufficient condition for collapse $H(\psi_0) < 0$, see Theorem 7.2, is satisfied if $c^2 \|\nabla f\|_2^2 < \frac{c^{2\sigma+2}}{\sigma+1} \|f\|_{2\sigma+2}^{2\sigma+2}$, i.e., if $c > c_{\text{collapse}}$. \square

Since Lemma 7.9 holds even if f is analytic, we have

Corollary 7.11 Singularity formation in the critical and supercritical NLS is not related to insufficient smoothness of the initial condition.

Since $\|\psi_0\|_2^2 = c^2 \|f\|_2^2$, we can rewrite Lemma 7.9 in terms of the input power:

Lemma 7.10 ([70, 75]) Let ψ be a solution of the NLS (7.1) with $\sigma d \geq 2$ and $\psi_0 = c f(\mathbf{x}) \in \Sigma$, and let

$$P_{\text{sufficient}}[f] := \left((\sigma + 1) \frac{\|f\|_2^{2\sigma} \|\nabla f\|_2^2}{\|f\|_{2\sigma+2}^{2\sigma+2}} \right)^{\frac{1}{\sigma}}. \quad (7.39a)$$

If

$$\|\psi_0\|_2^2 > P_{\text{sufficient}}[f], \quad (7.39b)$$

then ψ becomes singular at a finite distance.

Definition 7.7 (threshold power for collapse) Let ψ be a solution of the NLS with $\psi_0 = c f(\mathbf{x})$. We say that $P_{\text{th}}[f]$ is the threshold power for collapse, if it is the minimal power for which the following statement holds:

$$\|\psi_0\|_2^2 > P_{\text{th}}[f] \implies \psi \text{ becomes singular at a finite distance.}$$

Corollary 7.12 Let $f(\mathbf{x}) \in \Sigma$. Then $0 < P_{\text{th}}[f] \leq P_{\text{sufficient}}[f] < \infty$.

Proof This follows from Lemmas 7.8 and 7.10. \square

Since Lemma 7.10 is a restatement of the sufficient condition for collapse $H(0) < 0$, the condition $\|\psi_0\|_2^2 > P_{\text{sufficient}}[f]$ is not sharp. In other words, generically,

$$P_{\text{th}}[f] < P_{\text{sufficient}}[f].$$

In Corollary 7.5 we generalized the condition $H(0) < 0$ to the case of focused input beams. Using this result, Lemma 7.10 can be generalized as follows:

Lemma 7.11 *Let ψ be a solution of the NLS (7.1) with $\sigma d \geq 2$ and $\psi_0 = c f(\mathbf{x}) e^{-i\frac{|\mathbf{x}|^2}{4F}} \in \Sigma$, where $f(\mathbf{x})$ is a real function and $F > 0$. If $\|\psi_0\|_2^2 > P_{\text{sufficient}}[f]$, then ψ becomes singular at a finite distance.*

Note that unlike the necessary condition for collapse $P \geq P_{\text{cr}}$, which is only valid in the critical case, the sufficient condition for collapse $P > P_{\text{sufficient}}[f]$ is valid for both the critical and the supercritical NLS.

7.10.1 Critical NLS

When $\sigma d = 2$, the expression for $P_{\text{sufficient}}[f]$ reads

$$P_{\text{sufficient}}[f] = ((\sigma + 1)J[f])^{\frac{1}{\sigma}}, \quad (7.40)$$

see (7.39a), where $J[f]$ is the functional used in the calculation of the optimal constant $C_{\sigma,d}$, see (5.28b). Since

$$\inf_{0 \not\equiv f \in H_1} J[f] = \frac{1}{C_{\sigma,d}}, \quad \left(\frac{\sigma + 1}{C_{\sigma,d}}\right)^{\frac{1}{\sigma}} = P_{\text{cr}},$$

see (5.22) and (5.29), we conclude that for all $0 \not\equiv f \in H^1$,

$$P_{\text{sufficient}}[f] \geq \left((\sigma + 1) \inf_{0 \not\equiv f \in H_1} J[f]\right)^{\frac{1}{\sigma}} = \left(\frac{\sigma + 1}{C_{\sigma,d}}\right)^{\frac{1}{\sigma}} = P_{\text{cr}}. \quad (7.41)$$

Since the minimum of $J[f]$ is attained if and only if $f = \mu e^{i\alpha} R^{(0)}(\lambda(\mathbf{x} - \mathbf{x}_0))$, see Theorem 6.3, it follows that for any $0 \not\equiv f \in H^1$,

$$P_{\text{sufficient}}[f] = P_{\text{cr}} \iff f = \mu e^{i\alpha} R^{(0)}(\lambda(\mathbf{x} - \mathbf{x}_0)), \quad (7.42a)$$

$$P_{\text{sufficient}}[f] > P_{\text{cr}} \iff f \neq \mu e^{i\alpha} R^{(0)}(\lambda(\mathbf{x} - \mathbf{x}_0)). \quad (7.42b)$$

Remark This result was already proved in Exercise 6.8.

Since

$$P_{\text{th}}[f] \geq P_{\text{cr}},$$

see Theorem 5.11, $P_{\text{cr}} = \|R^{(0)}\|_2^2$ is a *lower bound* for the threshold power $P_{\text{th}}[f]$. Similarly, since

$$P_{\text{sufficient}}[f] \geq P_{\text{th}}[f],$$

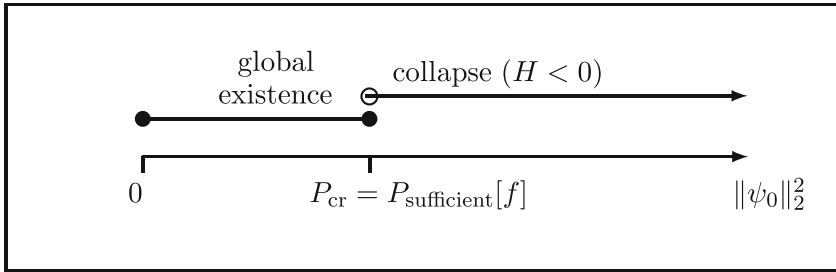


Fig. 7.1 Domains of global existence and collapse in the critical NLS, as a function of input power, for $\psi_0 = c R^{(0)}(\lambda(\mathbf{x} - \mathbf{x}_0))$

see Lemma 7.10, $P_{\text{sufficient}}[f]$ is an *upper bound* for the threshold power $P_{\text{th}}[f]$. Combining the last two inequalities gives

$$P_{\text{sufficient}}[f] \geq P_{\text{cr}},$$

which was already derived in (7.41).

Exercise 7.6 Show that if $f_n \rightarrow R^{(0)}$ in H^1 , then $P_{\text{sufficient}}[f_n] \rightarrow P_{\text{cr}}$ and $P_{\text{th}}[f_n] \rightarrow P_{\text{cr}}$.

We now consider the domains of global existence and collapse in the critical NLS for two families of real initial conditions.¹²

1. $\psi_0 = c R^{(0)}(\lambda(\mathbf{x} - \mathbf{x}_0))$, where $R^{(0)}$ is the ground state of (7.37).

In this case $P_{\text{cr}} = P_{\text{sufficient}}$, see (7.42a). Therefore,

Corollary 7.13 Let ψ be a solution of the critical NLS (7.13) with $\psi_0 = c R^{(0)}(\lambda(\mathbf{x} - \mathbf{x}_0))$. Then ψ exists globally when $\|\psi_0\|_2^2 \leq P_{\text{cr}}$, and blows up when $\|\psi_0\|_2^2 > P_{\text{cr}}$. Hence, $P_{\text{th}}[R^{(0)}] = P_{\text{cr}}$.

Proof Since $P_{\text{sufficient}}[R^{(0)}] = P_{\text{cr}} = \|R^{(0)}\|_2^2$, ψ exists globally for $\|\psi_0\|_2^2 < P_{\text{cr}}$ and becomes singular for $\|\psi_0\|_2^2 > P_{\text{cr}}$. When $\|\psi_0\|_2^2 = P_{\text{cr}}$, then $c = \lambda^{\frac{d}{2}}$. In this case, $\psi = \lambda^{\frac{d}{2}} e^{i\lambda^2 z} R^{(0)}(\lambda(\mathbf{x} - \mathbf{x}_0))$. In particular, it exists globally. \square

This case is illustrated in Fig. 7.1.

2. $\psi_0 = c f(\mathbf{x})$, where $f(\mathbf{x}) \neq R^{(0)}(\lambda(\mathbf{x} - \mathbf{x}_0))$, and c and $f(\mathbf{x})$ are real. In this case $P_{\text{sufficient}}[f] > P_{\text{cr}}$, see (7.42b). In addition, in Corollary 13.8 we shall see that when $f \neq R^{(0)}(\lambda(\mathbf{x} - \mathbf{x}_0))$, the NLS solution ψ can become singular only if its power is strictly above P_{cr} .

¹² These results can be generalized to focused initial conditions by using Lemma 7.11.

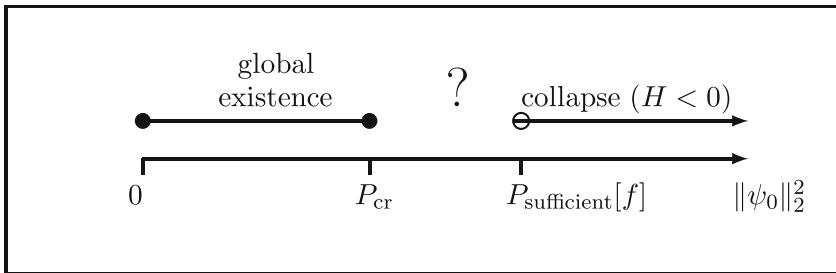


Fig. 7.2 Same as Fig. 7.1, for real initial condition $\psi_0 \neq c R^{(0)}(\lambda(\mathbf{x} - \mathbf{x}_0))$

Conclusion 7.3 (gap in the theory) *When f is real and is different from $R^{(0)}(\lambda(\mathbf{x} - \mathbf{x}_0))$, there is a gap in the theory, in the sense that there is no analytic way to determine whether blowup occurs when $P_{\text{cr}} < \|\psi_0\|_2^2 \leq P_{\text{sufficient}}[f]$, i.e., when $\|\psi_0\|_2^2 > P_{\text{cr}}$ and $H(\psi_0) \geq 0$.*

This case is illustrated in Fig. 7.2.

Numerical simulations suggest that $P_{\text{th}}[f]$ is strictly above P_{cr} and strictly below $P_{\text{sufficient}}[f]$, i.e.,

$$P_{\text{cr}} < P_{\text{th}}[f] < P_{\text{sufficient}}[f]. \quad (7.43)$$

The left inequality is further discussed in Sect. 13.5.1. The right inequality implies that the transition from global existence to collapse for real initial conditions occurs at $H > 0$ and not at $H = 0$ (Sect. 7.4). In fact, numerical simulations suggest that $P_{\text{th}}[f]$ is closer to P_{cr} than to $P_{\text{sufficient}}[f]$, i.e.,

$$P_{\text{th}}[f] - P_{\text{cr}} < P_{\text{sufficient}}[f] - P_{\text{th}}[f]. \quad (7.44)$$

At present, however, relations (7.43) and (7.44) are only based on numerical evidence. See Chap. 24 for further details.

7.11 Calculation of $H(R)$

Let R be a solution of

$$\Delta R(\mathbf{x}) - R + |R|^{2\sigma} R = 0, \quad R \in H^1. \quad (7.45)$$

In Corollary 6.3 we used the Pohozaev identities to calculate the Hamiltonian of R . We now provide an alternative, variance-identity based calculation.

Corollary 7.14 *Let R be a solution of (7.45). Then*

$$H(R) = \frac{d\sigma - 2}{2\sigma + 2} \|R\|_{2\sigma+2}^{2\sigma+2}. \quad (7.46)$$

Proof The solitary wave $\psi^{\text{solitary}} = e^{iz} R(\mathbf{x})$ is a solution of the NLS (7.1). For this NLS solution we have that $V(z) \equiv V(0)$, hence $V''(z) \equiv 0$. Substitution in the variance identity (7.6) yields (7.46). \square

Remark The variance identity shows “why” $H(R)$ cannot be negative in the critical and supercritical cases. Indeed, if $H(R) < 0$, then $\psi^{\text{solitary}} = e^{iz} R(\mathbf{x})$ would become singular, as its Hamiltonian is negative. This, however, is not the case, since ψ^{solitary} exists globally.

Exercise 7.7 Use the BNLS variance identity (Sect. 7.2.3) to generalize the result of Corollary 7.14 to solitary waves of the biharmonic NLS.

7.11.1 Critical NLS

By Corollary 7.14, $H(R) = 0$ in the critical case. More generally, we have

Lemma 7.12 Let R be a nontrivial solution of (7.37). Then

$$\begin{cases} H(cR) > 0, & \text{if } 0 < c < 1, \\ H(cR) = 0, & \text{if } c = 1, \\ H(cR) < 0, & \text{if } c > 1. \end{cases}$$

Proof Since $H(R) = 0$, then

$$\begin{aligned} H(cR) &= c^2 \|\nabla R\|_2^2 - \frac{c^{2\sigma+2}}{\sigma+1} \|R\|_{2\sigma+2}^{2\sigma+2} \\ &= c^2 \left[H(R) - \left(c^{2\sigma} - 1 \right) \frac{1}{\sigma+1} \|R\|_{2\sigma+2}^{2\sigma+2} \right] \\ &= -c^2 \left(c^{2\sigma} - 1 \right) \frac{1}{\sigma+1} \|R\|_{2\sigma+2}^{2\sigma+2}. \end{aligned}$$

\square

Lemma 7.13 Let $\psi^{(\epsilon)}$ be the solution of the critical NLS (7.13) with $\psi_0^{(\epsilon)} = (1+\epsilon)R(\mathbf{x})$, where $\epsilon > 0$ and R is a nontrivial solution of (7.37). Then ψ becomes singular at a finite z .

Proof By Lemma 7.12, $H(\psi_0^{(\epsilon)}) < 0$. Therefore, by Theorem 7.2, $\psi^{(\epsilon)}$ becomes singular. \square

Remark Lemma 7.13 was already proved in Corollary 7.13 for $n = 0$.

By Lemma 7.13, the critical NLS admits blowup solutions with power slightly above P_{cr} :

Corollary 7.15 For any $\epsilon > 0$, there exists a singular solution ψ of the critical NLS (7.13), such that $\|\psi_0\|_2^2 \leq P_{\text{cr}}(1 + \epsilon)$.

Proof Let $\psi_0 = \sqrt{1 + \epsilon} R^{(0)}$, where $R^{(0)}$ is the ground state of (7.37). Then $\|\psi_0\|_2^2 = (1 + \epsilon) \|R^{(0)}\|_2^2 = P_{\text{cr}}(1 + \epsilon)$, and by Lemma 7.13, the corresponding NLS solution becomes singular. \square

Corollary 7.16 The sufficient condition $\|\psi_0\|_2^2 < P_{\text{cr}}$ for global existence in the critical NLS is sharp, in the sense that all solutions with $\|\psi_0\|_2^2 < P_{\text{cr}}$ exist globally, and for any $\epsilon > 0$ there exist singular solutions with $\|\psi_0\|_2^2 < P_{\text{cr}}(1 + \epsilon)$.

In fact, there exist blowup solutions with $\|\psi_0\|_2^2 = P_{\text{cr}}$:

Exercise 7.8 Let $\psi^{(F)}$ be the solution of the critical NLS with

$$\psi_0^{(F)} = R(\mathbf{x})e^{-i\frac{r^2}{4F}}, \quad (7.47)$$

where R is a nontrivial solution of (7.37) and $F > 0$. Use the variance identity (Theorem 7.2) to show that $\psi^{(F)}$ becomes singular at a finite z .¹³

When $R = R^{(0)}$ in (7.47), the power of $\psi^{(F)}$ is exactly P_{cr} . Since there are no blowup solutions with power smaller than P_{cr} , this solution is called a *minimal-power blowup solution*. In Sect. 13.5 we shall see that, up to NLS symmetries, the initial conditions of all minimal-power blowup solutions are given by (7.47).

7.12 Dual Borderline Properties of $R^{(0)}$

As noted, in the critical NLS the two conditions $\|\psi_0\|_2^2 \geq P_{\text{cr}}$ and $H(\psi_0) < 0$ are necessary and sufficient for collapse, respectively. In Corollary 6.8 we saw that the critical ground state $R^{(0)}$ is the unique (up to NLS symmetries) profile that simultaneously satisfies $\|f\|_2^2 = P_{\text{cr}}$ and $H(f) = 0$. Hence, $R^{(0)}$ is the unique profile which is a “borderline case” for these two conditions. It is because of this *dual borderline properties* that the critical solitary wave $\psi^{\text{solitary},(0)} = e^{iz} R^{(0)}(r)$ and explicit blowup solution $\psi_{R^{(0)}}^{\text{explicit}}$ have the *dual instabilities property* (Sects. 9.5.2 and 10.6.2), and the asymptotic blowup profile $\psi_{R^{(0)}}$ has the *dual borderline properties* (Sect. 17.2).

¹³ See Sect. 8.4.3 for an alternative proof, which is based on the *lens transformation*.

Chapter 8

Symmetries and the Lens Transformation

In this chapter we present the symmetries of the NLS

$$i\psi_z(z, \mathbf{x}) + \Delta\psi + \nu|\psi|^{2\sigma}\psi = 0, \quad \psi(0, \mathbf{x}) = \psi_0(\mathbf{x}) \in H^1, \quad (8.1)$$

where $\nu \in \mathbb{R}$. We mainly focus on consequences of the lens transformation, which is a symmetry of the critical NLS

$$i\psi_z(z, \mathbf{x}) + \Delta\psi + \nu|\psi|^{\frac{4}{d}}\psi = 0, \quad \psi(0, \mathbf{x}) = \psi_0(\mathbf{x}) \in H^1. \quad (8.2)$$

8.1 NLS Symmetries

Let $\psi(z, \mathbf{x})$ be a solution of the NLS (8.1). Then ψ remains a solution of (8.1) under the following transformations:

1. Spatial translations: $\psi(z, \mathbf{x}) \rightarrow \psi(z, \mathbf{x} + \mathbf{x}_0)$, where $\mathbf{x}_0 \in \mathbb{R}^d$.
2. Axial ('time') translations: $\psi(z, \mathbf{x}) \rightarrow \psi(z + z_0, \mathbf{x})$, where $z_0 \in \mathbb{R}$.
3. Rotations: $\psi(z, \mathbf{x}) \rightarrow \psi(z, \mathbf{x} + \mathbf{x} \times \mathbf{n})$, where $\mathbf{n} \in \mathbb{R}^d$.
4. Phase shifts: $\psi(z, \mathbf{x}) \rightarrow e^{i\theta}\psi(z, \mathbf{x})$, where $\theta \in \mathbb{R}$.
5. Dilations: $\psi(z, \mathbf{x}) \rightarrow \psi^\lambda(z, \mathbf{x}) := \lambda^{\frac{1}{\sigma}}\psi(\lambda^2z, \lambda\mathbf{x})$, where $\lambda \in \mathbb{R}^+$.
6. Galilean transformation:

$$\psi(z, \mathbf{x}) \rightarrow \psi_{\text{GL}}(z, \mathbf{x}) := \psi(z, \mathbf{x} - z\mathbf{c})e^{i\frac{\mathbf{c}\mathbf{x}}{2} - i\frac{|\mathbf{c}|^2 z}{4}}, \quad \mathbf{c} \in \mathbb{R}^d.$$

Exercise 8.1 Show that power and Hamiltonian change under dilation as

$$\|\psi^\lambda\|^2 = \lambda^{\frac{2-\sigma d}{\sigma}} \|\psi\|^2, \quad H(\psi^\lambda) = \lambda^{\frac{2-\sigma d+2\sigma}{\sigma}} H(\psi).$$

8.1.1 Biharmonic NLS

The BNLS (5.3) remains invariant under transformations 1–4. The dilation symmetry for the BNLS reads $\psi(z, \mathbf{x}) \rightarrow \psi^\lambda(z, \mathbf{x}) := \lambda^{\frac{1}{\sigma}} \psi\left(\lambda^2 z, \lambda^{\frac{1}{2}} \mathbf{x}\right)$. It is not known whether there is a Galilean invariance for the BNLS.

8.2 Galilean Invariance

The Galilean transformation shows that if the initial condition changes from $\psi_0(\mathbf{x})$ to $\psi_{\text{GL},0} := \psi_0(\mathbf{x})e^{i\frac{\mathbf{c}\mathbf{x}}{2}}$, the NLS solution changes from ψ to ψ_{GL} . In particular, since

$$|\psi(z, \mathbf{x} \equiv \mathbf{x}_0)| = |\psi_{\text{GL}}(z, \mathbf{x}_0 + z\mathbf{c})|, \quad (8.3)$$

the line $\mathbf{x} \equiv \mathbf{x}_0$ in the (z, \mathbf{x}) plane is mapped to the line $\mathbf{x} = \mathbf{x}_0 + z\mathbf{c}$.

Conclusion 8.1 In the NLS model (8.1), a tilt of an incoming beam in the direction $\mathbf{n} = (1, \mathbf{c}) \in \mathbb{R} \times \mathbb{R}^d$, where the first coordinate of \mathbf{n} points in the z -direction and $\mathbf{c} = (c_1, \dots, c_d)$ points in the transverse d -dimensional plane, is represented mathematically by adding a linear phase term to the initial condition as follows:

$$\underbrace{\psi_0(\mathbf{x})}_{\text{no tilt}} \rightarrow \underbrace{\psi_0(\mathbf{x})e^{i\frac{\mathbf{c}\mathbf{x}}{2}}}_{\text{with tilt}}.$$

Remark We already derived this result from a geometrical optics analysis of the Helmholtz equation (Conclusion 2.13).

Remark The tilt angle θ is given by $\tan \theta = \frac{|\mathbf{c}|}{1} = |\mathbf{c}|$.

Remark In Conclusion 8.1, \mathbf{n} is not a unit vector, as its z -coordinate is equal to 1.

Remark We already used the Galilean transformation to show that the condition $H_G(0) < 0$ is sufficient for collapse (Theorem 7.4).

Lemma 8.1 In the NLS model (8.1), tilting the incoming beam does not change its propagation dynamics.

Proof This follows from Galilean invariance. \square

This result is intuitive, because in an isotropic homogeneous medium the dynamics is independent of the direction of propagation.¹

8.3 Lens Transformation (Critical NLS)

We begin with an auxiliary result.

Lemma 8.2 *Let $L(z)$ be a positive function, let $p > 0$, and let*

$$\tilde{\psi}(z, \mathbf{x}) := \frac{1}{L^p(z)} \psi(\zeta, \xi) e^{i \frac{L_z}{L} \frac{|\mathbf{x}|^2}{4}}, \quad \zeta = \int_0^z \frac{1}{L^2}, \quad \xi = \frac{\mathbf{x}}{L(z)} \in \mathbb{R}^d.$$

Then $\tilde{\psi}(z, \mathbf{x})$ is a solution of the NLS (8.1) if and only if $\psi(\zeta, \xi)$ is a solution of

$$i\psi_\zeta(\zeta, \xi) + \Delta_\xi \psi + L^{2-2\sigma p}(z)|\psi|^{2\sigma}\psi + i \left(\frac{d}{2} - p \right) LL_z \psi - \frac{1}{4} L^3 L_{zz} |\xi|^2 \psi = 0, \quad (8.4)$$

where $z = z(\zeta) = \int_0^\zeta L^2$.

Proof Since

$$\begin{aligned} \frac{\partial}{\partial z} L^{-p} &= -p L^{-p} \frac{L_z}{L}, & \frac{\partial}{\partial z} \psi(\zeta, \xi) &= \psi_\zeta \frac{1}{L^2} - \frac{L_z}{L^2} \mathbf{x} \cdot \nabla \psi, \\ \frac{\partial}{\partial z} e^{i \frac{L_z}{L} \frac{|\mathbf{x}|^2}{4}} &= i \left(\frac{L_{zz}}{L} - \frac{L_z^2}{L^2} \right) \frac{|\mathbf{x}|^2}{4} e^{i \frac{L_z}{L} \frac{|\mathbf{x}|^2}{4}}, \end{aligned}$$

we have that

$$i \frac{\partial}{\partial z} \tilde{\psi} = \frac{1}{L^p} \left[-ip \frac{L_z}{L} \psi + i \frac{\psi_\zeta}{L^2} - i \frac{L_z}{L^2} \mathbf{x} \cdot \nabla \psi + \frac{|\mathbf{x}|^2}{4} \frac{L_z^2}{L^2} \psi - \frac{|\mathbf{x}|^2}{4} \frac{L_{zz}}{L} \psi \right] e^{i \frac{L_z}{L} \frac{|\mathbf{x}|^2}{4}}. \quad (8.5a)$$

In addition,

$$\Delta_{\mathbf{x}} \psi(\zeta, \xi) = \frac{1}{L^2} \Delta_\xi \psi, \quad \frac{\partial}{\partial x_i} e^{i \frac{L_z}{L} \frac{|\mathbf{x}|^2}{4}} = i \frac{L_z}{L} \frac{x_i}{2} e^{i \frac{L_z}{L} \frac{|\mathbf{x}|^2}{4}}.$$

¹ While the tilted beam undergoes the same dynamics as the un-tilted one, it does so over a longer propagation distance. This is not an inconsistency, however, because the NLS is derived for paraxial beams for which $[r]/[z] = O(f)$, see Sect. 2.11. Consequently, the difference between the propagation distance of the tilted and un-tilted beams is $O(f^2)$, which is the order of accuracy of the NLS model (Conclusion 3.1).

Therefore,

$$\frac{\partial^2}{\partial x_i x_i} e^{i \frac{L_z}{L} \frac{|\mathbf{x}|^2}{4}} = \left(i \frac{L_z}{2L} - \frac{L_z^2}{L^2} \frac{x_i^2}{4} \right) e^{i \frac{L_z}{L} \frac{|\mathbf{x}|^2}{4}},$$

$$2(\nabla_{\mathbf{x}} \psi) \cdot \nabla_{\mathbf{x}} e^{i \frac{L_z}{L} \frac{|\mathbf{x}|^2}{4}} = i \left(\nabla \psi \cdot \frac{\mathbf{x} L_z}{L^2} \right) e^{i \frac{L_z}{L} \frac{|\mathbf{x}|^2}{4}},$$

and

$$\Delta_{\mathbf{x}} e^{i \frac{L_z}{L} \frac{|\mathbf{x}|^2}{4}} = \sum_{i=1}^d \frac{\partial^2}{\partial x_i x_i} e^{i \frac{L_z}{L} \frac{|\mathbf{x}|^2}{4}} = \left(i \frac{d L_z}{2L} - \frac{L_z^2}{L^2} \frac{|\mathbf{x}|^2}{4} \right) e^{i \frac{L_z}{L} \frac{|\mathbf{x}|^2}{4}}.$$

Hence,

$$\Delta_{\mathbf{x}} \tilde{\psi} = \frac{1}{L^p} \left[\frac{\Delta_{\xi} \psi}{L^2} + i \nabla \psi \frac{L_z}{L^2} \mathbf{x} + i \frac{d}{2} \frac{L_z}{L} \psi - \frac{|\mathbf{x}|^2}{4} \frac{(L_z)^2}{L^2} \psi \right] e^{i \frac{L_z}{L} \frac{|\mathbf{x}|^2}{4}}. \quad (8.5b)$$

Finally,

$$|\tilde{\psi}|^{2\sigma} \tilde{\psi} = \frac{1}{L^p} \left[\frac{1}{L^{2\sigma p}} |\psi|^{2\sigma} \psi \right] e^{i \frac{L_z}{L} \frac{|\mathbf{x}|^2}{4}}. \quad (8.5c)$$

Collecting (8.5) shows that $\tilde{\psi}$ satisfies (8.1) if and only if ψ satisfies (8.4). \square

By Lemma 8.2, if

$$p = \frac{d}{2}, \quad \sigma = \frac{1}{p} = \frac{2}{d}, \quad L_{zz} = 0,$$

then ψ is also a solution of the NLS. Therefore, in the critical case $\sigma d = 2$ the NLS has an additional symmetry, which was discovered in 1970 by Talanov:

Lemma 8.3 (Lens transformation [252]) *Let*

$$\tilde{\psi}(z, \mathbf{x}) := \frac{1}{L^{\frac{d}{2}}(z)} \psi(\zeta, \xi) e^{i \frac{L_z}{L} \frac{|\mathbf{x}|^2}{4}}, \quad (8.6a)$$

where

$$\xi = \frac{\mathbf{x}}{L(z)}, \quad \zeta = \int_0^z \frac{ds}{L^2(s)}, \quad (8.6b)$$

and $L(z)$ depends linearly on z , i.e.,

$$L = \alpha(Z_c - z), \quad (8.6c)$$

where α and Z_c are constants. Then $\psi(z, \mathbf{x})$ is a solution of the critical NLS (8.2) if and only if $\tilde{\psi}(z, \mathbf{x})$ is a solution of (8.2).

Remark In the lens transformation, the function $L(z)$ is used:

1. To rescale the amplitude by $L^{-\frac{d}{2}}(z)$.
2. To rescale the transverse coordinates by $L^{-1}(z)$.
3. To locally rescale the axial coordinate by $L^{-2}(z)$, i.e., $d\xi = L^{-2}(z) dz$.
4. To “add a continuum of focusing lenses” with a variable focal distance $F(z) = \frac{L(z)}{L_z(z)} = Z_c - z$, so that the focal point of all the “lenses” is located at $z = Z_c$.

Remark Under the substitution $L(z) \equiv 1/\lambda$, where λ is a constant, the lens transformation reduces to the dilation transformation.

Remark The lens transformation is also called the *pseudo-conformal transformation*.

To motivate the name *lens transformation*, let

$$L(z) = 1 - \frac{z}{F}, \quad (8.7)$$

where F is a constant. Therefore, if $\psi(z, \mathbf{x})$ is the solution of the critical NLS (8.2) with the initial condition $\psi_0(\mathbf{x})$, then $\tilde{\psi}(z, \mathbf{x})$ is the solution of (8.2) with the initial condition

$$\tilde{\psi}_0(\mathbf{x}) = \psi_0(\mathbf{x}) e^{-i \frac{|\mathbf{x}|^2}{4F}}. \quad (8.8)$$

By Conclusion 2.12, the quadratic phase term in (8.8) corresponds to a lens with focal length F at $z = 0$. Therefore, we can use the lens transformation to find the effect of a lens in the critical NLS. Indeed, by (8.6b),

$$\xi = \int_0^z \frac{ds}{\left(1 - \frac{s}{F}\right)^2} = \frac{z}{1 - \frac{z}{F}}.$$

Therefore, z and ξ are related by the lens relation

$$\frac{1}{z} = \frac{1}{F} + \frac{1}{\xi}. \quad (8.9a)$$

In particular, under the lens transformation, the values of $\psi(\xi, \mathbf{x})$ at $\xi = \infty$ correspond to the values of $\tilde{\psi}(z, \mathbf{x})$ at $z = F$. In addition, the values of $\psi(\xi, \mathbf{x})$ at ξ correspond to the values of $\tilde{\psi}(z, \mathbf{x})$ at

$$\mathbf{x} = L\xi = \left(1 - \frac{z}{F}\right)\xi \mathbf{x}. \quad (8.9b)$$

Hence, under the lens transformation with $L(z) = 1 - z/F$, the value of ψ at (ξ, \mathbf{x}) is mapped to the value of $\tilde{\psi}$ at $(z(\xi), \mathbf{x}(\xi, \mathbf{x}))$, where $z(\xi)$ and $\mathbf{x}(\xi, \mathbf{x})$ are given by (8.9).

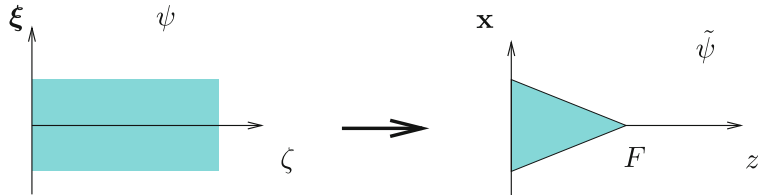


Fig. 8.1 The lens transformation (8.6) with $L(z) = 1 - \frac{z}{F}$ and $F > 0$ maps the values of ψ in the shaded semi-infinite strip into the values of $\tilde{\psi}$ in the shaded triangle

For example, as illustrated in Fig. 8.1, the lens transformation with $L(z) = 1 - z/F$ maps the values of ψ in the shaded semi-infinite strip into the values of $\tilde{\psi}$ in the shaded triangle.

Conclusion 8.2 *The effect of a lens at $z = 0$ in the critical NLS is to map the solution exactly as in geometrical optics.*

This result is surprising, because the lens relations (8.9) are usually associated with the geometrical optics approximation, where diffraction and nonlinear effects are not included.

Exercise 8.2 *Let ψ be a solution of the critical NLS (8.2).*

1. *Show that if $\tilde{\psi}$ is the lens transformation of ψ with $L = 1 - \frac{z}{F_1}$, and $\tilde{\tilde{\psi}}$ is the lens transformation of $\tilde{\psi}$ with $L = 1 - \frac{z}{F_2}$, then $\tilde{\tilde{\psi}}$ is the lens transformation of ψ with*

$$L = 1 - \frac{z}{F_{1,2}}, \quad \frac{1}{F_{1,2}} = \frac{1}{F_1} + \frac{1}{F_2}.$$

2. *Deduce that if $\tilde{\psi}$ is the lens transformation of ψ with $L = 1 - z/F$, and $\tilde{\tilde{\psi}}$ is the lens transformation of $\tilde{\psi}$ with $L = 1 + z/F$, then $\tilde{\tilde{\psi}} \equiv \psi$.*

Corollary 8.1 *The lens transformation is valid in the linear Schrödinger equation $i\psi_z(z, \mathbf{x}) + \Delta\psi = 0$ in any dimension.*

Exercise 8.3 *Prove Corollary 8.1.*

Thus, the linear Schrödinger equation has seven symmetries: The six mentioned in Sect. 8.1 and the lens transformation. In the nonlinear case the first six remain symmetries. The lens transformation, however, remains a symmetry only if $\sigma d = 2$.

Remark It is not known whether there is a “lens transformation” for the critical biharmonic NLS. Therefore, it is not clear whether the consequences of the lens transformation, which are described in Sect. 8.4, extend to the BNLS. In particular, it is not known whether the critical BNLS admits explicit blowup solutions (see Open Question 7.1).

8.4 Consequences of the Lens Transformation

8.4.1 Effect of a Lens (Critical NLS)

In Sect. 8.3 we saw that if we apply the lens transformation with $L = 1 - z/F$ to the solution of the critical NLS (8.2) with initial condition ψ_0 , we obtain the solution of (8.2) with the initial condition

$$\tilde{\psi}_0(\mathbf{x}) = \psi_0(\mathbf{x})e^{-i\frac{|\mathbf{x}|^2}{4F}}. \quad (8.10)$$

As noted, the quadratic phase term corresponds to the addition of a lens with focal distance F at $z = 0$. Therefore, if we know (analytically or numerically) the NLS solution for some initial condition ψ_0 , we can use the lens transformation to obtain the NLS solution for the same initial condition, but with the addition of a lens. Consequently, there is no need to carry out repeated numerical simulations of the critical NLS for the same input profile, but with different lenses. In particular, one can use the lens transformation to write explicitly the effect of a lens on the collapse point (Sect. 8.4.5).

8.4.2 Effect of a Lens (Subcritical and Supercritical NLS)

Although the lens transformation is an NLS symmetry only in the critical case, it can still be used to gain some insight on the effect of a lens in the subcritical and supercritical cases. To do this, let $\tilde{\psi}$ be the solution of the NLS with the focused input beam ψ_0 , i.e.,

$$i\tilde{\psi}_z(z, \mathbf{x}) + \Delta\tilde{\psi} + |\tilde{\psi}|^{2\sigma}\tilde{\psi} = 0, \quad \tilde{\psi}_0(\mathbf{x}) = \psi_0(\mathbf{x})e^{-i\frac{|\mathbf{x}|^2}{4F}}, \quad (8.11)$$

and let ψ be defined by the lens transformation (8.6) with $L(z) = 1 - z/F$, i.e., ψ is the “inverse lens transformation” of $\tilde{\psi}$. Then ψ is the solution of, see (8.4),

$$i\psi_\xi(\xi, \mathbf{x}) + \Delta_\xi\psi + L^{2-\sigma d}(z(\xi))|\psi|^{2\sigma}\psi = 0, \quad \psi(0, \mathbf{x}) = \psi_0(\mathbf{x}). \quad (8.12a)$$

Since $z(\xi) = 1/(\frac{1}{\xi} + \frac{1}{F})$, see (8.9a), and $L(z) = 1 - z/F$, we have that

$$L(z(\xi)) = 1 - \frac{\xi}{\xi + F}. \quad (8.12b)$$

Exercise 8.4 Derive (8.12).

Therefore, we can understand the effect of the lens in (8.11) by analyzing (8.12). Indeed, from (8.12) follows

Conclusion 8.3 A lens with focal distance F changes the relative magnitude of nonlinearity, compared with that of diffraction, by

$$L^{2-\sigma d} = \left(1 - \frac{\zeta}{\zeta + F}\right)^{2-\sigma d}.$$

To motivate this conclusion, note that if the beam propagation is aberrationless so that $\psi \sim L^{-\frac{d}{2}} G\left(\frac{x}{L}\right)$, then

$$\frac{[|\psi|^{2\sigma} \psi]}{[\Delta \psi]} \sim \frac{L^{-\sigma d - \frac{d}{2}}}{L^{-2 - \frac{d}{2}}} = L^{2-\sigma d}.$$

Therefore, both nonlinearity and diffraction increase when the beam is focusing, and decrease when the beam is defocusing. Only in the critical case, however, they increase (or decrease) at exactly the same rate.

Conclusion 8.3 shows that when the lens is focusing ($F > 0$), as z increases, the relative magnitude of nonlinearity decreases in the subcritical case and increases in the supercritical case. Therefore, a focusing lens “helps” diffraction in the subcritical case and nonlinearity in the supercritical case. Conversely, in the case of a defocusing lens ($F < 0$), as z increases, the relative magnitude of nonlinearity increases in the subcritical case and decreases in the supercritical case. Therefore, a defocusing lens “helps” nonlinearity in the subcritical case and diffraction in the supercritical case. These results are summarized in Table 8.1.

In Chap. 9 we will analyze the stability of ground-state solitary wave $\psi^{\text{solitary},(0)} = e^{iz} R^{(0)}(r)$ of the NLS (8.1). In particular, in Theorem 9.3 we will see that $\psi^{\text{solitary},(0)}$ is orbitally stable in the subcritical case but unstable in the critical and supercritical cases. To motivate these results, let us perturb the solitary wave by adding a lens at $z = 0$, i.e.,

$$\psi_0^{(F)} = \psi^{\text{solitary},(0)}(z = 0, r) e^{-i \frac{|x|^2}{4F}} = R^{(0)}(r) e^{-i \frac{|x|^2}{4F}}. \quad (8.13)$$

A solitary wave represents a perfect balance between diffraction and nonlinearity. Therefore, in the subcritical case, if the lens is focusing ($F > 0$), nonlinearity

Table 8.1 Qualitative effect of a focusing ($F > 0$) and defocusing ($F < 0$) lens on the relative magnitudes of nonlinearity and diffraction

	$F > 0$	$F < 0$
Subcritical NLS	$\frac{[\psi ^{2\sigma} \psi]}{[\Delta \psi]}$ decreases	$\frac{[\psi ^{2\sigma} \psi]}{[\Delta \psi]}$ increases
Critical NLS	$\frac{[\psi ^{2\sigma} \psi]}{[\Delta \psi]}$ does not change	$\frac{[\psi ^{2\sigma} \psi]}{[\Delta \psi]}$ does not change
Supercritical NLS	$\frac{[\psi ^{2\sigma} \psi]}{[\Delta \psi]}$ increases	$\frac{[\psi ^{2\sigma} \psi]}{[\Delta \psi]}$ decreases

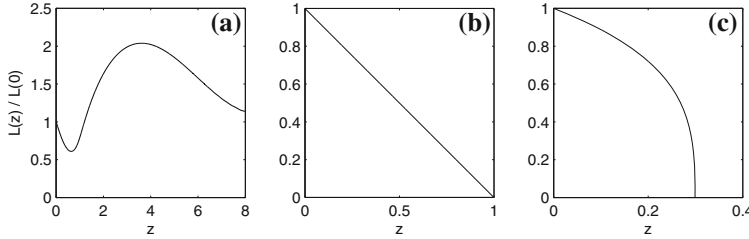


Fig. 8.2 The normalized width $L(z) = \left| \frac{\psi(z, x=0)}{R^{(0)}(0)} \right|^{-\frac{2}{d}}$ of the solution of the NLS (8.1) with the initial condition (8.13). Here, $d = 1$ and $F = 1$. **a** $\sigma = 1$ (subcritical). **b** $\sigma = 2$ (critical). **c** $\sigma = 3$ (supercritical)

becomes weaker than diffraction, whereas if the lens is defocusing ($F < 0$) nonlinearity becomes stronger than diffraction. Thus, in both cases, the solution tends to return to its original width. Therefore, the solitary wave is stable. In contrast, in the supercritical case, if the lens is focusing, nonlinearity becomes stronger, and so beam focusing is further accelerated, whereas if the lens is defocusing, nonlinearity becomes weaker, and so beam defocusing is further accelerated. Therefore, the solitary wave is unstable. In the borderline critical case, nonlinearity and diffraction remain balanced, hence the beam focuses or defocuses at the constant rate induced by the lens. Therefore, the solitary wave is also unstable. These results are illustrated in Fig. 8.2 for the case of a focusing lens.

Similar informal arguments lead to

Conclusion 8.4 *In the supercritical case, the addition of a sufficiently strong defocusing lens arrests collapse.*

Remark A rigorous proof of this result exists only in the critical case (Lemma 8.4).

The above discussion shows that the effect of a lens in the subcritical and supercritical NLS is more complex than in the critical case. Indeed, in the critical case the lens transformation implies that the collapse distance is monotone in F (Corollary 27.1). In the supercritical case, however, the collapse distance can be non-monotone in F (Sect. 27.7.2).

8.4.3 The Explicit Blowup Solution ψ_R^{explicit}

In Sect. 6.4 we saw that the critical NLS (8.2) admits the solitary wave solution $\psi^{\text{solitary}} = e^{iz} R(\mathbf{x})$, where R is a nontrivial solution of

$$\Delta R - R + |R|^{\frac{4}{d}} R = 0, \quad R \in H^1.$$

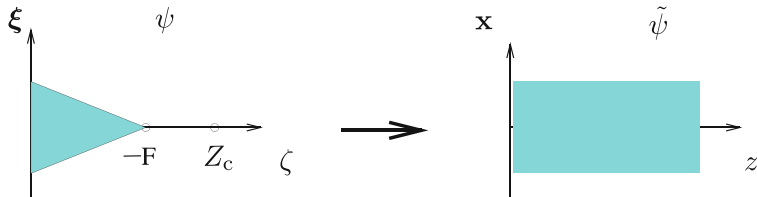


Fig. 8.3 Sketch of Lemma 8.4. Let ψ blow up at Z_c . If one adds at $z = 0$ a defocusing lens with focal point $0 < -F < Z_c$, the defocused solution $\tilde{\psi}$ does not blowup, because the blowup point is mapped ‘beyond infinity’

Let us apply the lens transformation with $L(z) = Z_c - z$ to ψ^{solitary} . Since

$$\zeta = \int_0^z \frac{ds}{L^2(s)} = \frac{1}{Z_c - z} - \frac{1}{Z_c} = \frac{z/Z_c}{Z_c - z},$$

the lens-transformed solitary wave is given by

$$\psi_R^{\text{explicit}}(z, \mathbf{x}) = \frac{1}{(Z_c - z)^{\frac{d}{2}}} R\left(\frac{\mathbf{x}}{Z_c - z}\right) e^{i \frac{z/Z_c}{Z_c - z} - i \frac{|\mathbf{x}|^2}{4(Z_c - z)}}. \quad (8.14)$$

This solution blows up as $z \rightarrow Z_c$. Chapter 10 is devoted to this explicit blowup solution.

8.4.4 Arresting Collapse with a Defocusing Lens

The lens transformation shows that for any initial condition that collapses at a finite distance Z_c , the addition at $z = 0$ of a sufficiently powerful defocusing lens arrests collapse. Intuitively, this is because if one adds a defocusing lens with focal point $0 < -F < Z_c$, the defocused solution does not blowup, since the blowup point is mapped ‘beyond infinity’ (Fig. 8.3):

Lemma 8.4 ([93]) *Let ψ be a solution of the critical NLS (8.2) with the initial condition $\psi_0(\mathbf{x})$ that becomes singular at Z_c , where $0 < Z_c < \infty$. Let $\tilde{\psi}(z, \mathbf{x})$ be the solution of (8.2) with the initial condition*

$$\tilde{\psi}_0 = \psi_0(\mathbf{x}) e^{-i \frac{|\mathbf{x}|^2}{4F}}. \quad (8.15)$$

If

$$0 < -F \leq Z_c, \quad (8.16)$$

then $\tilde{\psi}$ exists globally.

Proof By the lens transformation (8.6),

$$|\tilde{\psi}(z, \mathbf{x})| = \frac{1}{L^{\frac{d}{2}}(z)} |\psi(\zeta(z), \xi)|, \quad L = 1 - \frac{z}{F}.$$

Therefore,

$$\|\tilde{\psi}(z)\|_{\frac{4}{d}+2}^{\frac{4}{d}+2} = \frac{1}{L^2(z)} \|\psi(\zeta(z))\|_{\frac{4}{d}+2}^{\frac{4}{d}+2}.$$

To prove that $\tilde{\psi}$ exists globally, we need to show that the right-hand side is finite for $0 \leq z < \infty$. Since the lens is defocusing, $L(z) > 0$ for $0 \leq z < \infty$. Therefore, the right-hand side is finite for $0 \leq \zeta(z) < Z_c$, and becomes infinite as $\zeta(z) \rightarrow Z_c$. By (8.9a),

$$\frac{1}{\zeta(z)} = \frac{1}{z} - \frac{1}{F}. \quad (8.17)$$

Therefore, for $0 \leq z < \infty$,

$$\frac{1}{\zeta(z)} > -\frac{1}{F} > 0$$

and

$$0 \leq \zeta(z) < -F. \quad (8.18)$$

From (8.16) and (8.18) it follows that $\zeta(z) < Z_c$ for any $0 \leq z < \infty$. Therefore, $\tilde{\psi}$ cannot become singular at a finite distance. \square

Thus, any input beam, however powerful it may be, will not collapse if defocused by a sufficiently strong defocusing lens. Here, “sufficiently strong” means that the defocusing lens maps the blowup point Z_c ‘beyond infinity’.²

8.4.5 Controlling the Collapse Distance with a Lens

We now consider the effect of a lens on the possibility of collapse and on the collapse distance.

Lemma 8.5 *Let ψ be a solution of the critical NLS (8.2) with an initial condition ψ_0 that collapses at Z_c , where $0 < Z_c < \infty$. Let $\psi^{(F)}(z, \mathbf{x})$ be the solution of (8.2) with the initial condition*

$$\psi_0^{(F)}(\mathbf{x}) = \psi_0(\mathbf{x}) e^{-i \frac{|\mathbf{x}|^2}{4F}}.$$

² We already “derived” this result using the aberrationless approximation method (Sect. 3.5). Unlike the aberrationless approximation, however, the lens transformation is an exact relation. Hence, it allows us to find the exact values of F that arrest collapse.

Then $\psi^{(F)}$ collapses at some $Z_c^{(F)}$, where $0 < Z_c^{(F)} < \infty$, if and only if

$$F > 0 \text{ or } F < -Z_c < 0,$$

i.e., if the lens is focusing or is weakly defocusing, respectively. In that case,

$$\frac{1}{Z_c^{(F)}} = \frac{1}{Z_c} + \frac{1}{F}. \quad (8.19)$$

Proof From the proof of Lemma 8.4 it follows that if $\psi^{(F)}$ collapses at z , then ψ collapses at $\zeta(z)$, where z and $\zeta(z)$ are related by (8.17). Therefore,

$$\frac{1}{Z_c} = \frac{1}{Z_c^{(F)}} - \frac{1}{F}.$$

Hence, $0 < Z_c^{(F)} < \infty$ if and only if $F > 0$ or $F < -Z_c < 0$. \square

See Sects. 27.7–27.8.2 for additional results on controlling the collapse distance with one or two lenses.

8.4.6 Sharper Conditions for Blowup?

As noted in Observation 7.2, the sufficient conditions for collapse in Theorem 7.2 which follow from the variance identity are not sharp, i.e., there exist singular solutions that do not satisfy these conditions. The necessary condition for collapse $P \geq P_{\text{cr}}$ (Theorem 5.11) is also not sharp, i.e., the threshold power for collapse P_{th} is generically above P_{cr} (Corollary 13.8 and Chap. 24). Thus, the problem of finding sharp conditions for global existence or for collapse in the critical NLS is still open. The following result rules out many potential candidates:

Lemma 8.6 ([93]) *Let ψ be a solution of the critical NLS (8.2). Any condition which only involves $|\psi_0|$, the amplitude of the initial condition, cannot be a sufficient condition for collapse.*

Proof Assume, by negation, that there exists such a condition. Let ψ be a solution of (8.2) with an initial condition ψ_0 that satisfies this condition. Let $\tilde{\psi}$ be the solution of (8.2) with the initial condition (8.15), such that condition (8.16) holds. Since $|\tilde{\psi}_0| = |\psi_0|$, then $\tilde{\psi}$ also satisfies this condition. Hence, it should become singular at a finite distance. This is not possible, however, since by Lemma 8.4, $\tilde{\psi}$ exists globally. \square

Therefore, any condition that only involves the L_p norms of the initial condition (e.g., $\|\psi_0\|_{2\sigma+2} \geq 10^6$) cannot be sufficient for collapse.

Corollary 8.2 *There is no universal threshold power P_{th} , such that $P(\psi_0) > P_{\text{th}}$ is a sufficient condition for collapse in the critical NLS (8.2).*

This result also follows from the fact that the critical NLS admits the globally-existing solitary waves $\psi^{\text{solitary},(n)} = e^{iz} R^{(n)}(r)$, whose power can be arbitrarily large, see (6.40).

8.4.7 Scattering ($P < P_{\text{cr}}$)

In Theorem 5.11 we proved that solutions of the critical NLS with power below P_{cr} do not collapse. So far, however, we did not discuss the *dynamics* of these solutions. These solutions cannot be solitary waves, because the minimal power of the solitary waves is $P_{\text{cr}} = \|R^{(0)}\|_2^2$, see Theorem 6.3. Nevertheless, one could ask whether these solutions can somehow maintain a balance between nonlinearity and diffraction, e.g., be of the form $\psi \sim f(z)g(\mathbf{x})$, where $f(z)$ is periodic in z . To see that this is not possible, we first note that if $P < P_{\text{cr}}$, then $H(\psi) > 0$, see (5.26). Hence, by the variance identity (7.14),

$$\lim_{z \rightarrow \infty} V(z) = \infty. \quad (8.20)$$

This however, still leaves the possibility that part of the solution remains localized.

We now use the lens transformation to show that any solution ψ with power below P_{cr} scatters (diffracts) as $z \rightarrow \infty$. The idea of the proof is as follows. Let $\tilde{\psi}$ be the lens transformation of ψ with a focusing lens (i.e., with $L(z) = 1 - z/F$ where $F > 0$). Therefore,

$$|\tilde{\psi}(z, \mathbf{x})| = \frac{1}{L^{\frac{d}{2}}(z)} |\psi(\xi(z), \xi)|.$$

Because the power of $\tilde{\psi}$ is also below P_{cr} , it does not blowup as $z \rightarrow F$. Therefore, $\psi(\xi(z), \cdot)$ should decay to zero faster than $L^{\frac{d}{2}}(z)$ as $z \rightarrow F$, or equivalently, $\psi(\xi, \cdot)$ should decay to zero faster than $L^{\frac{d}{2}}(z(\xi))$ as $\xi \rightarrow \infty$.

Lemma 8.7 *Let $\psi(z, \mathbf{x})$ be a solution of the critical NLS (8.2), and let $\|\psi_0\|_2^2 < P_{\text{cr}}$. Then there exists a constant $M > 0$, such that*

$$\|\psi\|_{2\sigma+2}^{2\sigma+2} \leq M(1+z)^{-2}, \quad 0 \leq z < \infty.$$

Proof Let $\tilde{\psi}$ be the lens transformation (8.6) of ψ with $L(z) = 1 - z$. Then

$$|\tilde{\psi}(z, \mathbf{x})| = \frac{1}{L^{\frac{d}{2}}(z)} |\psi(\xi, \xi)|, \quad 0 \leq z < 1,$$

where

$$\xi = \frac{\mathbf{x}}{L}, \quad \zeta = \int_0^z \frac{ds}{L^2(s)} = \frac{z}{1-z}.$$

Since $\|\tilde{\psi}_0\|_2^2 = \|\psi_0\|_2^2 < P_{\text{cr}}$, $\tilde{\psi}$ is a global H^1 solution of the NLS. Therefore, $\tilde{\psi}$ is bounded in $L^{2\sigma+2}$ for $z \in [0, 1]$, i.e., there exists $M > 0$, such that

$$\int |\tilde{\psi}(z, \mathbf{x})|^{2\sigma+2} d\mathbf{x} < M, \quad 0 \leq z < 1. \quad (8.21)$$

Since

$$\int |\tilde{\psi}(z, \mathbf{x})|^{2\sigma+2} d\mathbf{x} = \frac{1}{(1-z)^2} \int |\psi(\zeta(z), \xi)|^{2\sigma+2} d\xi$$

and $1 + \zeta = \frac{1}{1-z}$, relation (8.21) can be rewritten as

$$(1 + \zeta)^2 \int |\psi(\zeta, \xi)|^{2\sigma+2} d\xi < M, \quad 0 \leq \zeta < \infty.$$

□

Corollary 8.3 *Under the conditions of Lemma 8.7, $\lim_{z \rightarrow \infty} \|\nabla \psi\|_2^2 = H(\psi_0)$.*

Proof This follows from Lemma 8.7 and Hamiltonian conservation. □

Lemma 8.7 is a special case of the following result, due to Weinstein:

Lemma 8.8 ([276]) *Under the conditions of Lemma 8.7,*

$$\|\psi\|_p^p \leq c_{p,d,\psi_0} (1+z)^{-d(\frac{p}{2}-1)}, \quad 0 \leq z < \infty$$

for all p such that

$$\begin{cases} 2 < p < \infty, & \text{if } d \leq 2, \\ 2 < p < \frac{2d}{d-2}, & \text{if } d > 2, \end{cases} \quad (8.22)$$

where c_{p,d,ψ_0} is a constant that depends on p , d , and ψ_0 . In particular, ψ scatters as $z \rightarrow \infty$, in the sense that $\lim_{z \rightarrow \infty} \|\psi\|_p = 0$, for all p in the range (8.22).

Proof As in the proof of Lemma 8.7, let $\tilde{\psi}$ be the lens transformation (8.6) of ψ with $L(z) = 1 - z$. Since $\tilde{\psi}$ is an NLS solution, from Hamiltonian conservation it follows that

$$H(\tilde{\psi}(z)) \equiv H(\tilde{\psi}_0).$$

We claim that

$$H(|\tilde{\psi}(z)|) \leq H(\tilde{\psi}(z)).$$

Indeed, let $\tilde{\psi} = Ae^{iS}$, where A and S are real. Then

$$\|\nabla \tilde{\psi}\|_2^2 = \|\nabla A\|_2^2 + \|A \nabla S\|_2^2 \geq \|\nabla A\|_2^2 = \|\nabla |A|\|_2^2 = \|\nabla |\tilde{\psi}| \|_2^2,$$

where in last but one equality we used (5.46). As in the proof of Lemma 8.7,

$$H(|\tilde{\psi}(z)|) = \frac{1}{(1-z)^2} H(|\psi(\xi(z))|) = (1+\xi)^2 H(|\psi(\xi)|).$$

Combining the above, we get that

$$H(|\psi(\xi)|) \leq C_{\psi_0} (1+\xi)^{-2}, \quad C_{\psi_0} = H(\tilde{\psi}_0).$$

Recall that for any $f \in H^1$, $\left(1 - \left(\frac{\|f\|_2^2}{P_{\text{cr}}}\right)^{\frac{2}{d}}\right) \|\nabla f\|_2^2 \leq H(f)$, see (6.23).

Since $\|\psi\|_2^2 < P_{\text{cr}}$, from the last two inequalities we have that

$$\|\nabla|\psi(\xi)|\|_2^2 \leq \frac{H(|\psi(\xi)|)}{1 - \left(\frac{\|\psi\|_2^2}{P_{\text{cr}}}\right)^{\frac{2}{d}}} \leq \frac{C_{\psi_0}}{1 - \left(\frac{\|\psi_0\|_2^2}{P_{\text{cr}}}\right)^{\frac{2}{d}}} (1+\xi)^{-2}. \quad (8.23)$$

The result follows from power conservation and the Gagliardo-Nirenberg inequality (see Lemma 5.3)

$$\|f\|_p^p \leq C_{\sigma=\frac{p}{2}-1,d} \|\nabla f\|_2^{d(\frac{p}{2}-1)} \|f\|_2^{p-\frac{d(p-2)}{2}},$$

applied to $f = |\psi|$. \square

Remark In contrast with Lemma 8.8, the L^p norms of singular solutions become infinite at the blowup point (Corollary 13.6).

As a solution with $P < P_{\text{cr}}$ scatters, its amplitude variations decay to zero, but its phase variations do not:

Corollary 8.4 *Let $\psi = Ae^{iS}$, where A and S are real. Then under the conditions of Lemma 8.7,*

$$\lim_{z \rightarrow \infty} \|\nabla A\|_2^2 = 0, \quad \lim_{z \rightarrow \infty} \|A \nabla S\|_2^2 > 0.$$

Proof The left limit follows from (8.23). Since $\|\nabla \psi\|_2^2 = \|\nabla A\|_2^2 + \|A \nabla S\|_2^2$, the right limit follows from Corollary 8.3, the left limit, and the result that if $P < P_{\text{cr}}$ then $H(\psi_0) > 0$, see (5.10). \square

8.4.8 NLS with a Quadratic Potential

The NLS with a linear quadratic potential arises in various physical models. For example, in Bose-Einstein condensates, the quadratic potential represents the magnetic trap that confines the condensate (Sect. 4.2). A useful tool in the analysis of the

critical NLS with a quadratic potential is the generalized lens transformation, which is the lens transformation (8.6), but with a function $L(z)$ which is not necessarily linear in z .

Definition 8.1 (Generalized lens transformation) *The generalized lens transformation of $\psi(z, \mathbf{x})$ is*

$$\tilde{\psi}(z, \mathbf{x}) = \frac{1}{L^{\frac{d}{2}}(z)} \psi(\xi, \mathbf{x}) e^{i \frac{L_z}{L} \frac{|\mathbf{x}|^2}{4}}, \quad \xi = \frac{\mathbf{x}}{L(z)}, \quad \xi = \int_0^z \frac{ds}{L^2(s)}. \quad (8.24)$$

Let $\psi(z, \mathbf{x})$ be a solution of the NLS with a z -dependent quadratic potential

$$i\psi_z(z, \mathbf{x}) + \Delta\psi + |\psi|^{\frac{4}{d}}\psi + \gamma(z)|\mathbf{x}|^2\psi = 0, \quad (8.25)$$

and let $\tilde{\psi}(z, \mathbf{x})$ be the generalized lens transformation (8.24) of ψ . Then $\tilde{\psi}$ is the solution of the NLS with a (different) z -dependent quadratic potential

$$i\tilde{\psi}_z(z, \mathbf{x}) + \Delta\tilde{\psi} + |\tilde{\psi}|^{\frac{4}{d}}\tilde{\psi} + \tilde{\gamma}(z)|\mathbf{x}|^2\tilde{\psi} = 0, \quad (8.26a)$$

where

$$\tilde{\gamma}(z) = \frac{\gamma(\xi(z)) - \frac{1}{4}L^3 L_{zz}}{L^4(z)}, \quad \xi(z) = \int_0^z \frac{ds}{L^2(s)}. \quad (8.26b)$$

Exercise 8.5 Derive (8.26).

Therefore,

Lemma 8.9 *The family of solutions of the critical NLS with a z -dependent quadratic potential, Eq. (8.25), is closed under the generalized lens transformation (8.24).*

Now, let $\tilde{\psi}(z, \mathbf{x})$ be a solution of (8.26) with some given function $\tilde{\gamma}(z)$. Let $L(z)$ be chosen so that it satisfies the ODE

$$L_{zz}(z) = 4\tilde{\gamma}(z)L, \quad (8.27)$$

and let ψ be defined by Eq. (8.24). By (8.26b),

$$\gamma(\xi(z)) = \frac{-L^3(z)L_{zz}}{4} + L^4\tilde{\gamma}(z) = \frac{L^3}{4}(4\tilde{\gamma}L - L_{zz}) \equiv 0.$$

Since $\gamma \equiv 0$, ψ is a solution of the critical NLS (8.2).

Conclusion 8.5 *The critical NLS with a z -dependent quadratic potential can always be reduced to the critical NLS without a quadratic potential via the generalized lens transformation with an appropriately chosen $L(z)$.*

Exercise 8.6 Use (8.14) to construct explicit blowup solutions of

$$i\psi_z(z, \mathbf{x}) + \Delta\psi + |\psi|^{\frac{4}{d}}\psi + c|\mathbf{x}|^2\psi = 0, \quad (8.28)$$

where c is a constant.

Hint:

$$\tilde{\psi}^{\text{explicit}}(z, \mathbf{x}) = \frac{1}{[L(z)(Z_c - \zeta(z))]^{\frac{d}{2}}} R \left(\frac{\mathbf{x}/L(z)}{Z_c - \zeta(z)} \right) e^{i \frac{L_z}{L} \frac{|\mathbf{x}|^2}{4}} e^{i \frac{1-|\mathbf{x}|^2/4}{Z_c - \zeta(z)}},$$

where

$$\zeta(z) = \int_0^z \frac{ds}{L^2(s)}, \quad L(z) = L_0 \operatorname{Re} \left\{ e^{\pm 2\sqrt{c}z} \right\}.$$

Show that with a proper choice of L_0 it is possible to construct blowup solutions of (8.28) for both positive and negative values of c .

Chapter 9

Stability of Solitary Waves

In Chap. 6 we saw that the NLS

$$i\psi_z(z, \mathbf{x}) + \Delta\psi + |\psi|^{2\sigma}\psi = 0, \quad \psi(0, \mathbf{x}) = \psi_0(\mathbf{x}) \in H^1 \quad (9.1)$$

admits the solitary-wave solutions $\psi_\omega^{\text{solitary}} = e^{i\omega z} R_\omega(\mathbf{x})$, where R_ω is a nontrivial solution of

$$\Delta R_\omega(\mathbf{x}) - \omega R_\omega + |R_\omega|^{2\sigma} R_\omega = 0, \quad R_\omega \in H^1. \quad (9.2)$$

In addition, $R_\omega(\mathbf{x}) = \omega^{\frac{1}{2\sigma}} R(\omega^{\frac{1}{2}} \mathbf{x})$, where $R := R_{\omega=1}$ is a solution of

$$\Delta R(\mathbf{x}) - R + |R|^{2\sigma} R = 0, \quad R \in H^1. \quad (9.3)$$

Equation (9.3) has a unique ground-state solution, denoted by $R^{(0)}$, which is radial, positive, and monotonically decreasing. When $d \geq 2$, Eq. (9.3) also admits a countable number of non-monotone radial solutions $\{R^{(n)}(r)\}_{n=1}^\infty$, which change their sign n times in $0 < r < \infty$. In addition, when $d = 2$, Eq. (9.3) admits a doubly-countable number of non-radial vortex solutions $R = R_m^{(n)}(r)e^{im\theta}$, see Sect. 15.2.

Solitary waves are important for applications, because they propagate localized packets of power over long distances. For that to happen, however, the solitary wave has to be stable. The issue of stability arises also in the analysis of the convergence of the profile of collapsing NLS solutions to a self-similar profile.

In this chapter we consider the stability of solitary waves. Our discussion is very brief. For more details, see e.g., [249, Chap. 4].

9.1 Orbital Stability

We first need to define what we mean by stability. Typically, the notion of stability is that “small perturbations lead to small changes”. Therefore, intuitively, $\psi_\omega^{\text{solitary}}$ is stable, if for any initial condition which is sufficiently close to $\psi_\omega^{\text{solitary}}(z = 0)$, the

corresponding NLS solution remains close to $\psi_\omega^{\text{solitary}}$ for $0 \leq z < \infty$.¹ Under this definition, however, all solitary waves are unstable:

Lemma 9.1 *If stability means that the perturbed solution remains close to the unperturbed solitary wave for $0 \leq z < \infty$, then all solitary waves of the NLS (9.1) are unstable.*

Proof Let $\psi_\omega^{\text{solitary}} = e^{i\omega z} R_\omega(\mathbf{x})$ and $\psi_{\tilde{\omega}}^{\text{solitary}} = e^{i\tilde{\omega} z} R_{\tilde{\omega}}(\mathbf{x})$ be two solitary waves of (9.1). Since $R_\omega(\mathbf{x}) = \omega^{\frac{1}{2\sigma}} R(\omega^{\frac{1}{2}} \mathbf{x})$, then for any $0 < \epsilon \ll 1$, if $\tilde{\omega}$ is sufficiently close to ω , then

$$\|\psi_{\tilde{\omega}}^{\text{solitary}}(z=0) - \psi_\omega^{\text{solitary}}(z=0)\|_{H^1} = \|R_{\tilde{\omega}} - R_\omega\|_{H^1} < \epsilon.$$

However,

$$\begin{aligned} \|\psi_{\tilde{\omega}}^{\text{solitary}} - \psi_\omega^{\text{solitary}}\|_{H^1} &= \|e^{i\tilde{\omega} z} R_{\tilde{\omega}} - e^{i\omega z} R_\omega\|_{H^1} \\ &= \|e^{i\tilde{\omega} z} (R_{\tilde{\omega}} - R_\omega) + (e^{i\tilde{\omega} z} - e^{i\omega z}) R_\omega\|_{H^1} \\ &\geq \|(e^{i\tilde{\omega} z} - e^{i\omega z}) R_\omega\|_{H^1} - \|e^{i\tilde{\omega} z} (R_{\tilde{\omega}} - R_\omega)\|_{H^1} \\ &\geq |e^{i(\tilde{\omega}-\omega)z} - 1| \|R_\omega\|_{H^1} - \epsilon. \end{aligned}$$

Hence, $\psi_{\tilde{\omega}}^{\text{solitary}}$ does not remain close to $\psi_\omega^{\text{solitary}}$ for all z .

Similarly, let $\psi_{\omega,\text{GL}}^{\text{solitary}}$ be the solution of (9.1) with the initial condition $\psi_{\omega,\text{GL}}^{\text{solitary}}(z=0) = e^{i\frac{\mathbf{c}\cdot\mathbf{x}}{2}} R_\omega(\mathbf{x})$, where $\mathbf{c} \in \mathbb{R}^d$. For any $0 < \epsilon \ll 1$, if $|\mathbf{c}|$ is sufficiently small,

$$\|\psi_{\omega,\text{GL}}^{\text{solitary}}(z=0) - \psi_\omega^{\text{solitary}}(z=0)\|_{H^1} < \epsilon.$$

By Galilean invariance (Sect. 8.2),

$$\psi_{\omega,\text{GL}}^{\text{solitary}}(z, \mathbf{x}) = \psi_\omega^{\text{solitary}}(z, \mathbf{x} - z\mathbf{c}) e^{i\frac{\mathbf{c}\cdot\mathbf{x}}{2} - i\frac{|\mathbf{c}|^2 z}{4}} = R_\omega(\mathbf{x} - z\mathbf{c}) e^{i\omega z + i\frac{\mathbf{c}\cdot\mathbf{x}}{2} - i\frac{|\mathbf{c}|^2 z}{4}}.$$

Since $\psi_\omega^{\text{solitary}}$ and $\psi_{\omega,\text{GL}}^{\text{solitary}}$ are localized around $\mathbf{x} = 0$ and $\mathbf{x} = z\mathbf{c}$, respectively, the overlap between them becomes negligible as $z \rightarrow \infty$. Therefore,

$$\|\psi_{\omega,\text{GL}}^{\text{solitary}} - \psi_\omega^{\text{solitary}}\|_{H^1} \sim \|\psi_{\omega,\text{GL}}^{\text{solitary}}\|_{H^1} + \|\psi_\omega^{\text{solitary}}\|_{H^1}, \quad z \rightarrow \infty.$$

Hence, $\psi_{\omega,\text{GL}}^{\text{solitary}}$ does not remain close to $\psi_\omega^{\text{solitary}}$ for all $z \geq 0$. \square

One could argue, however, that if stability refers to the possibility to propagate localized packets of power over long distances, then the solitary wave “does not really

¹ It is not enough to require that the perturbed solitary wave remains close to $\psi_\omega^{\text{solitary}}$ for $0 \leq z \leq Z$, where $0 < Z < \infty$, since by Corollary 5.4, all the perturbed solitary waves that exist in $[0, Z]$ satisfy this requirement.

becomes unstable” under a phase shift or a tilt. Therefore, we modify the definition of stability, so that it allows for phase shifts and tilts.

Definition 9.1 (orbital stability) Let $\psi_\omega^{\text{solitary}} = e^{i\omega z} R_\omega(\mathbf{x})$ be a solitary wave of the NLS (9.1). We say that $\psi_\omega^{\text{solitary}}$ is orbitally stable, if for any $\epsilon > 0$, there exists $\delta > 0$, such that if $\|\psi_0 - \psi_\omega^{\text{solitary}}(z=0)\|_{H^1} < \delta$, and if ψ is the solution of (9.1) with the initial condition ψ_0 , then

$$\inf_{\zeta(z) \in \mathbb{R}, \mathbf{x}_0(z) \in \mathbb{R}^d} \|\psi(z, \mathbf{x}) - e^{i\zeta(z)} R_\omega(\mathbf{x} - \mathbf{x}_0(z))\|_{H^1} < \epsilon, \quad 0 \leq z < \infty.$$

Thus, orbital stability refers to stability within the orbit of the solitary wave, which is defined by the transformations that keep the NLS invariant.²

9.2 Linear Stability

Before we consider orbital stability, we begin with the simpler problem of linear stability. To simplify the presentation, we consider the case where R_ω is real.³ Following Vakhitov and Kolokolov [258], we perturb the initial condition as

$$\psi_0(\mathbf{x}) = R_\omega(\mathbf{x}) + \epsilon h_0(\mathbf{x}), \quad \epsilon \ll 1.$$

Initially the perturbed solution remains close to the solitary wave. Therefore, it can be written as

$$\psi(z, \mathbf{x}) = [R_\omega(\mathbf{x}) + \epsilon h(z, \mathbf{x}; \omega) + O(\epsilon^2)]e^{i\omega z}, \quad (9.4)$$

where $h(0, \mathbf{x}) = h_0(\mathbf{x})$. Let us substitute (9.4) in the NLS (9.1) and expand in powers of ϵ . Since $\psi_\omega^{\text{solitary}} = e^{i\omega z} R_\omega$ is an exact solution of (9.1), the equation for the $O(1)$ terms is automatically satisfied. To balance the $O(\epsilon)$ terms, we first note that

$$|R_\omega + \epsilon h|^2 = (R_\omega + \epsilon h)(R_\omega + \epsilon h)^* = |R_\omega|^2 + \epsilon R_\omega(h^* + h) + O(\epsilon^2).$$

Therefore,

$$|\psi|^{2\sigma} = (|R_\omega + \epsilon h|^2 + O(\epsilon^2))^\sigma = |R_\omega|^{2\sigma} + \epsilon R_\omega(h^* + h)\sigma|R_\omega|^{2(\sigma-1)} + O(\epsilon^2),$$

² When the NLS is not invariant under translations in \mathbf{x} , orbital stability refers to stability up to phase shifts. This is the case, e.g., with the NLS on a bounded domain (Sect. 16.5.2), or the NLS with a potential that depends on \mathbf{x} .

³ When R_ω is radial, it has to be real (Lemma 6.12). Note, however, that R_ω can be complex (Sect. 15.2).

and

$$\begin{aligned} |\psi|^{2\sigma}\psi &= \left(|R_\omega|^{2\sigma} + \epsilon R_\omega(h^* + h)\sigma|R_\omega|^{2(\sigma-1)}\right)(R_\omega + \epsilon h) + O(\epsilon^2) \\ &= |R_\omega|^{2\sigma}R_\omega + \epsilon|R_\omega|^{2\sigma}\left((1+\sigma)h + \sigma h^*\right) + O(\epsilon^2). \end{aligned}$$

Hence, the balance of the $O(\epsilon)$ terms gives the linearized equation for h

$$ih_z(z, \mathbf{x}; \omega) + L_{0,\omega}h + \sigma|R_\omega|^{2\sigma}h^* = 0, \quad L_{0,\omega} := \Delta - \omega + (1+\sigma)|R_\omega|^{2\sigma}. \quad (9.5)$$

We now show that solutions of (9.5) can be constructed from solutions of the eigenvalue problem

$$\begin{pmatrix} 0 & L_{+, \omega} \\ -L_{-, \omega} & 0 \end{pmatrix} \begin{pmatrix} v \\ u \end{pmatrix} = \Omega \begin{pmatrix} v \\ u \end{pmatrix}, \quad (9.6)$$

where $\Omega \in \mathbb{C}$ is the eigenvalue, $\begin{pmatrix} v \\ u \end{pmatrix} = \begin{pmatrix} v(\mathbf{x}) \\ u(\mathbf{x}) \end{pmatrix}$ is the eigenfunction, and

$$L_{+, \omega} := \Delta - \omega + (1+2\sigma)|R_\omega|^{2\sigma}, \quad L_{-, \omega} := \Delta - \omega + |R_\omega|^{2\sigma}.$$

Lemma 9.2 *Let $\left\{\Omega, \begin{pmatrix} v \\ u \end{pmatrix}\right\}$ be an eigenpair of (9.6).*

1. *If Ω is real, then*

$$h(z, \mathbf{x}) = [u(\mathbf{x}) + iv(\mathbf{x})]e^{\Omega z} \quad (9.7a)$$

is a solution of (9.5), where u and v are real.

2. *If $\text{Im}(\Omega) \neq 0$, then*

$$h(z, \mathbf{x}) = \frac{u(\mathbf{x}) + iv(\mathbf{x})}{2}e^{\Omega z} + \frac{u^*(\mathbf{x}) + iv^*(\mathbf{x})}{2}e^{\Omega^*z} \quad (9.7b)$$

is a solution of (9.5), where u and v are complex.

Proof

1. We substitute (9.7a) into Eq. (9.5). Because Ω is real, the equations for the real and imaginary parts are

$$L_{+, \omega}u = \Omega v, \quad (9.8a)$$

$$L_{-, \omega}v = -\Omega u, \quad (9.8b)$$

which is exactly (9.6).

2. When Ω has an imaginary component, we look for a solution of the form $h = f(\mathbf{x})e^{\Omega z} + g^*(\mathbf{x})e^{\Omega^* z}$. Substitution in (9.5) gives

$$e^{\Omega z} \left[i\Omega f + L_{0,\omega} f + \sigma |R_\omega|^{2\sigma} g \right] + e^{\Omega^* z} \left[i\Omega^* g^* + L_{0,\omega} g^* + \sigma |R_\omega|^{2\sigma} f^* \right] = 0.$$

Since $\Omega \neq \Omega^*$ and f, g , and R_ω are independent of z , we get that

$$i\Omega f + L_{0,\omega} f + \sigma |R_\omega|^{2\sigma} g = 0, \quad i\Omega^* g^* + L_{0,\omega} g^* + \sigma |R_\omega|^{2\sigma} f^* = 0.$$

Taking the conjugate of the second equation and rearranging gives

$$L_{0,\omega} f + \sigma |R_\omega|^{2\sigma} g = -i\Omega f, \quad L_{0,\omega} g + \sigma |R_\omega|^{2\sigma} f = i\Omega g.$$

Summing and subtracting these equations gives

$$\begin{aligned} L_{0,\omega}(f+g) + \sigma |R_\omega|^{2\sigma}(f+g) &= -i\Omega(f-g), \\ L_{0,\omega}(f-g) - \sigma |R_\omega|^{2\sigma}(f-g) &= -i\Omega(f+g). \end{aligned}$$

Let $f+g = u$ and $f-g = iv$. Then u and v satisfy (9.8), and h is given by (9.7b). \square

Remark We can rewrite (9.7b) as

$$h = e^{\Omega_{\text{re}} z} \left[\cos(\Omega_{\text{im}} z) (u_{\text{re}}(\mathbf{x}) + i v_{\text{re}}(\mathbf{x})) - \sin(\Omega_{\text{im}} z) (u_{\text{im}}(\mathbf{x}) + i v_{\text{im}}(\mathbf{x})) \right], \quad (9.9)$$

where $\Omega_{\text{re}} = \text{Re}(\Omega)$, $\Omega_{\text{im}} = \text{Im}(\Omega)$, $u_{\text{re}} = \text{Re}(u)$, $u_{\text{im}} = \text{Im}(u)$, $v_{\text{re}} = \text{Re}(v)$, and $v_{\text{im}} = \text{Im}(v)$.⁴

Remark If $\left\{ \Omega, \begin{pmatrix} v \\ u \end{pmatrix} \right\}$ is an eigenpair of (9.6), then so is $\left\{ -\Omega, \begin{pmatrix} -v \\ u \end{pmatrix} \right\}$, as well as $\left\{ \Omega^*, \begin{pmatrix} v^* \\ u^* \end{pmatrix} \right\}$. Therefore, non-zero real and imaginary eigenvalues of (9.6) always come in pairs, and complex eigenvalues always come in quadruples.

Lemma 9.3 Let $\psi_\omega^{\text{solitary}} = e^{i\omega z} R_\omega$ be a solitary wave of the NLS (9.1), and let

$$\Omega_{\text{re}}^{\max} := \max\{ \text{Re}(\Omega) \mid \Omega \text{ is an eigenvalue of (9.6)} \}.$$

If $\Omega_{\text{re}}^{\max} > 0$, then $\psi_\omega^{\text{solitary}}$ is linearly unstable.

Proof Let $\left\{ \Omega, \begin{pmatrix} v \\ u \end{pmatrix} \right\}$ be the eigenpair that corresponds to $\Omega_{\text{re}}^{\max}$, and let $h(z=0) = \text{Re}(u) + i\text{Re}(v)$. Then h is given by (9.9). Since $\text{Re}(\Omega) = \Omega_{\text{re}}^{\max} > 0$, h increases exponentially in z . \square

⁴ When $\Omega_{\text{im}} = 0$, this expression reduces to (9.7a).

Exercise 9.1 Show that if $\Omega_{\text{re}}^{\max} \leq 0$, all the eigenvalues of (9.6) are purely imaginary.

If we apply $L_{-, \omega}$ to Eq.(9.8a) and use Eq.(9.8b), we obtain the equivalent fourth-order eigenvalue problem

$$L_{-, \omega} L_{+, \omega} u = \lambda u, \quad \lambda = -\Omega^2. \quad (9.10)$$

Lemma 9.4 Let $\psi_\omega^{\text{solitary}} = R_\omega e^{i\omega z}$ be a solitary wave of the NLS (9.1). If there exists an eigenvalue λ of (9.10) such that $\text{Re}(\sqrt{-\lambda}) \neq 0$, then $\psi_\omega^{\text{solitary}}$ is linearly unstable.

Exercise 9.2 Prove Lemma 9.4.

9.3 Vakhitov-Kolokolov (VK) Condition

The result of Lemma 9.3 holds for any solitary wave. In 1973, Vakhitov and Kolokolov showed that when the solitary wave is positive (i.e., when R_ω is the ground state $R_\omega^{(0)}$), the instability condition $\Omega_{\text{re}}^{\max} > 0$, see Lemma 9.3, can be replaced with a different condition, which became known as the Vakhitov-Kolokolov (VK) condition:

Lemma 9.5 ([258]) Let $R_\omega^{(0)}$ be the positive solution of (9.2), and denote its power by $P(\omega) := \|R_\omega^{(0)}\|_2^2$. If

$$P'(\omega) < 0, \quad (\textbf{VK condition})$$

the solitary wave $\psi_\omega^{\text{solitary}, (0)} = e^{i\omega z} R_\omega^{(0)}$ is linearly unstable.

For the NLS (9.1) with a power-law nonlinearity, $P(\omega) = \omega^{\frac{2-\sigma d}{2\sigma}} \|R^{(0)}\|_2^2$, see Exercise 6.2. Therefore,

$$P'(\omega) = \frac{2-\sigma d}{2\sigma} \omega^{\frac{2-\sigma d}{2\sigma}-1} \|R^{(0)}\|_2^2, \quad (9.11)$$

and so

$$\begin{cases} P'(\omega) > 0, & \text{if } \sigma d < 2, \\ P'(\omega) = 0, & \text{if } \sigma d = 2, \\ P'(\omega) < 0, & \text{if } \sigma d > 2. \end{cases} \quad (9.12)$$

Hence, checking the VK condition for a power-law nonlinearity is trivial.

The conditions $\Omega_{\text{re}}^{\max} > 0$ and $P'(\omega) < 0$ can be extended to other NLS equations. In such cases, checking the VK condition requires calculating $R_\omega^{(0)}$ analytically or numerically. Checking the condition $\Omega_{\text{re}}^{\max} > 0$ is considerably more demanding, as

one needs to calculate $R_\omega^{(0)}$, and then use it to solve the eigenvalue problem (9.6). For that reason, most studies on stability used the VK condition. We note, however, that the condition $\Omega_{\text{re}}^{\max} > 0$ is more general, since it is not restricted to positive solitary waves, and since there are cases where $\Omega_{\text{re}}^{\max} > 0$ even though $P'(\omega) > 0$. Another advantage of the condition $\Omega_{\text{re}}^{\max} > 0$ is that it provides the instability rate and dynamics. See Sect. 9.6 for further discussion.

9.4 Orbital Stability of Ground States

9.4.1 Subcritical Case

Consider the ground-state solitary wave $\psi_\omega^{\text{solitary},(0)} = e^{i\omega z} R_\omega^{(0)}$ of the subcritical NLS. If we slightly perturb its initial condition $\psi_\omega^{\text{solitary},(0)}(z=0) = R_\omega^{(0)}$, the power of the perturbed solution will be equal to that of $R_{\tilde{\omega}}^{(0)}$ for some $\tilde{\omega} \approx \omega$, and its Hamiltonian will be close to that of $R_{\tilde{\omega}}^{(0)}$. In Theorem 6.4 we saw that in the subcritical case, the minimizers of

$$\inf_{f(\mathbf{x}) \in H^1} \left\{ H(f) \mid \|f\|_2^2 = \|R_{\tilde{\omega}}^{(0)}\|_2^2 \right\}, \quad (9.13)$$

are given by the $(d+1)$ -parameter orbit $\left\{ e^{i\theta} R_{\tilde{\omega}}^{(0)}(|\mathbf{x} - \mathbf{x}_c|) \right\}$. Since the Hamiltonian of the perturbed solution is close to $H(R_{\tilde{\omega}}^{(0)})$, which is the minimal value of (9.13), this implies that the perturbed solution has to remain close to the minimizing orbit $\left\{ e^{i\theta} R_{\tilde{\omega}}^{(0)}(|\mathbf{x} - \mathbf{x}_c|) \right\}$. Indeed, in 1982 Cazenave and Lions used the variational characterization (9.13) to prove orbital stability for the subcritical ground-state solitary waves:

Theorem 9.1 ([40]) *Let $\sigma d < 2$. Then the ground-state solitary waves $\psi_\omega^{\text{solitary},(0)} = e^{i\omega z} R_\omega^{(0)}$ of the NLS (9.1) are orbitally stable.*

The subcritical case of most interest is the one-dimensional cubic NLS. In this case, the solitary waves are called *solitons*, in order to emphasize that in addition to being stable, they have the property that when two solitons collide, they emerge from the collision unchanged, except for a phase shift (i.e. they collide *elastically*).

9.4.2 General Case

During the 1980s, Weinstein, Grillakis, Shatah, and Strauss rigorously showed that the VK condition for linear stability also determines orbital stability:

Theorem 9.2 ([116, 118, 232, 274]) Consider the ground-state solitary waves $\psi_\omega^{\text{solitary},(0)} = e^{i\omega z} R_\omega^{(0)}$ of the NLS (9.1). Then $\psi_\omega^{\text{solitary},(0)}$ is orbitally stable if $P'(\omega) > 0$ and orbitally unstable if $P'(\omega) < 0$.

In the case of a power-law nonlinearity, $P'(\omega) > 0$ if and only if $\sigma d < 2$, see (9.12). Therefore, Theorem 9.2 provides an alternative proof for the orbital stability of the subcritical solitary waves. Theorem 9.2 also shows that the supercritical ground-state solitary waves are orbitally unstable. As for the critical ground-state solitary waves, since they are strongly unstable (see Theorem 9.4 below), they are also orbitally unstable.

Theorem 9.3 The ground-state solitary waves $\psi_\omega^{\text{solitary},(0)} = e^{i\omega z} R_\omega^{(0)}$ of the NLS (9.1) are orbitally stable if $\sigma d < 2$, and orbitally unstable if $\sigma d \geq 2$.

Hence, the *critical exponent* for stability of NLS solitary waves is $\sigma = 2/d$.

Remark See Sect. 8.4.2 for an informal explanation of why solitary waves are stable in the subcritical case and unstable in the supercritical case.

9.4.3 Instability and Collapse

In Sect. 5.11 we saw that the *critical exponent* for blowup of NLS solutions is also $\sigma = 2/d$.⁵

Corollary 9.1 The NLS (9.1) admits singular solutions if and only if its ground-state solitary waves are orbitally unstable.

Stubbe showed that this relation between collapse and stability extends to a large class of NLS equations [248]. There are, however, NLS equations for which this relation does not hold: Either the solitary wave is unstable even though all solutions exist globally, or conversely, the solitary wave is stable yet there exist singular solutions. For example, the critical NLS on a bounded domain admits singular solutions (Sect. 16.8.1), yet its ground-state solitary waves are orbitally stable (Sect. 16.5.2). See [52, 96, 239, 242] for additional examples of “decoupling” between instability and collapse. In all of these examples, this “decoupling” appears to be related to the absence of translation invariance in \mathbf{x} .

⁵ I.e., all solutions of the subcritical NLS exist globally, whereas the critical and supercritical NLS admit singular solutions.

9.5 Critical NLS

9.5.1 Strong Instability and Scattering

We begin with the following definition of instability.

Definition 9.2 (strong instability of solitary waves) A solitary wave ψ^{solitary} is strongly unstable if for every $\epsilon > 0$ there is an initial condition $\psi_0^{(\epsilon)}(\mathbf{x})$ such that $\|\psi_0^{(\epsilon)} - \psi^{\text{solitary}}(z = 0)\|_{H^1} \leq \epsilon$, and the corresponding NLS solution $\psi^{(\epsilon)}(z, \mathbf{x})$ becomes singular at a finite distance z .

In the critical NLS, all solitary waves (ground state, excited states, and vortex states) are strongly unstable:

Theorem 9.4 Let $\psi^{\text{solitary}} = e^{iz} R(\mathbf{x})$ be a solitary wave of the critical NLS. Then ψ^{solitary} is strongly unstable.

Proof Let $\psi_0^{(\epsilon)} = (1 + \epsilon)R(\mathbf{x})$ and $0 < \epsilon \ll 1$. Then $\|\psi_0^{(\epsilon)} - R\|_{H^1} = \epsilon \|R\|_{H^1}$. In addition, by Lemma 7.13, $\psi^{(\epsilon)}$ blows up at a finite z . \square

Exercise 9.3 Use Exercise 7.8 to give a different proof for Theorem 9.4.

In the case of the ground-state solitary wave, if we perturb it in the opposite direction, i.e., $\psi_0^{(\epsilon)} = (1 - \epsilon)R^{(0)}$, the perturbed solution exists globally:

Lemma 9.6 Let $\psi^{(\epsilon)}$ be the solution of the critical NLS with the initial condition $\psi_0^{(\epsilon)} = (1 - \epsilon)R^{(0)}$, where $0 < \epsilon < 1$, and $R^{(0)}$ is the ground state. Then $\psi^{(\epsilon)}$ exists for all $0 \leq z < \infty$.

Proof Since $\|\psi_0^{(\epsilon)}\|_2^2 = (1 - \epsilon)^2 \|R^{(0)}\|_2^2 < \|R^{(0)}\|_2^2 = P_{\text{cr}}$, it follows from Theorem 5.11 that the solution exists for all $z \geq 0$. \square

Lemma 9.6 does not imply that $\psi^{\text{solitary},(0)} = e^{iz} R^{(0)}(r)$ becomes unstable under multiplication by $1 - \epsilon$, since both the unperturbed and perturbed solutions exist globally. Rather, the instability under multiplication by $1 - \epsilon$ follows from Lemma 9.7, which shows that, unlike $\psi^{\text{solitary},(0)}$, $\psi^{(\epsilon)}$ scatters (diffracts) as $z \rightarrow \infty$:

Lemma 9.7 Under the conditions of Lemma 9.6,

$$\|\psi^{(\epsilon)}\|_p^p \leq c_{p,d,\psi_0}(1+z)^{-d(\frac{p}{2}-1)}, \quad 0 \leq z < \infty,$$

for all p such that

$$\begin{cases} 2 < p < \infty, & \text{if } d \leq 2, \\ 2 < p < \frac{2d}{d-2}, & \text{if } d > 2, \end{cases} \quad (9.14)$$

where c_{p,d,ψ_0} is a constant that depends on p , d , and ψ_0 . In particular, $\psi^{(\epsilon)}$ scatters as $z \rightarrow \infty$, in the sense that $\lim_{z \rightarrow \infty} \|\psi^{(\epsilon)}\|_p = 0$.

Proof This is a special case of Lemma 8.8. \square

9.5.2 Dual Instabilities of the Ground State

Because of the dual borderline properties of $R^{(0)}$, see Sect. 7.12, the ground-state solitary wave $\psi^{\text{solitary},(0)} = e^{iz} R^{(0)}(r)$ of the critical NLS can become unstable in two opposite ways:

1. Perturbations of the initial condition $\psi^{\text{solitary},(0)}(z=0) = R^{(0)}$ that lower its power lead to scattering (Lemma 9.7).
2. Perturbations of the initial condition that lower its Hamiltonian lead to collapse (Theorem 9.4).

Remark More generally, the critical NLS admits the solitary waves $\psi_\omega^{\text{solitary},(0)} = e^{i\omega z} R_\omega^{(0)}(r)$. Since $\|R_\omega^{(0)}\|_2^2 = P_{\text{cr}}$ and $H(R_\omega^{(0)}) = 0$, these solitary waves are also “borderline cases” for the above two conditions.

Remark The dual instabilities of $\psi^{\text{solitary},(0)}$ imply similar dual instabilities for the explicit blowup solution $\psi_{R^{(0)}}^{\text{explicit}}$, see Sect. 10.6.2.

In Sect. 9.5.1 we saw that if $\psi^{\text{solitary},(0)}$ is embedded into the one-parameter family of NLS solutions with the initial conditions $\psi_0^{(\epsilon)} = (1+\epsilon)R^{(0)}$, these NLS solutions scatter when $\psi^{\text{solitary},(0)}$ is perturbed in one direction ($-1 \ll \epsilon < 0$), but collapse when it is perturbed in the opposite direction ($0 < \epsilon \ll 1$). In fact, these dual instabilities occur for “any” embedding of $\psi^{\text{solitary},(0)}$:

Lemma 9.8 *Let $\psi^{(\epsilon)}$ be the solution of the critical NLS with the initial condition $\psi_0^{(\epsilon)}(\mathbf{x}) = R^{(0)}(r) + \epsilon h(\mathbf{x})$, where $h \in H^1$ and $\int R^{(0)} h \, d\mathbf{x} > 0$. Then $\psi^{(\epsilon=0)} = \psi^{\text{solitary},(0)}$, $\psi^{(\epsilon)}$ scatters for $-1 \ll \epsilon < 0$, and collapses for $0 < \epsilon \ll 1$.*

Proof If $-1 \ll \epsilon < 0$ then $\|\psi_0^{(\epsilon)}\|_2^2 < P_{\text{cr}}$ (Exercise 17.3). Therefore, $\psi^{(\epsilon)}$ scatters (Lemma 8.8). If $0 < \epsilon \ll 1$ then $H(\psi_0^{(\epsilon)}) < 0$ (Exercise 17.3). Therefore, $\psi^{(\epsilon)}$ collapses (Theorem 7.2). \square

Since $\psi^{\text{solitary},(0)} = e^{iz} R^{(0)}(r)$ is unstable, it may seem that the profile $R^{(0)}$ has no physical relevance. In fact, the profile $R^{(0)}$ plays a key role in NLS theory! Indeed, we already saw that it has exactly the critical power for collapse. In addition, in Chap. 14 we will see that peak-type singular solutions of the critical NLS approach the universal asymptotic blowup profile $\psi_{R^{(0)}}$, whose profile is a rescaled $R^{(0)}$ profile. Because of the dual borderline properties of $R^{(0)}$, however, the asymptotic profile $\psi_{R^{(0)}}$ is highly sensitive to small perturbations. See Sect. 17.2 for more details.

9.5.3 Instability of Excited States

In Sect. 6.4.4 we saw that in dimension $d \geq 2$, the critical NLS admits a countable number of radial solitary waves $\psi^{\text{solitary},(n)} = e^{iz} R^{(n)}(r)$, where $n = 0$ is the ground state and $n \geq 1$ are the excited states.

Corollary 9.2 *The excited-state solitary waves of the critical NLS are strongly unstable. In particular, they are orbitally unstable.*

Proof By Lemma 7.13, for any $0 < \epsilon \ll 1$, the solution of the critical NLS with the initial condition $\psi_0^{(\epsilon)} = (1 + \epsilon)R^{(n)}$ blows up at a finite distance. \square

When $\psi_0^{(\epsilon)} = (1 - \epsilon)R^{(n)}$, $0 < \epsilon \ll 1$, and $n \geq 1$, then $H(\psi_0) > 0$, see Lemma 7.12, and $\|R^{(n)}\|_2^2 > \|R^{(0)}\|_2^2 = P_{\text{cr}}$, see Theorem 6.3. Hence, these initial conditions are in the *gap* for which there are no analytic results on whether the solution exists globally or becomes singular (Conclusion 7.3). What we do know, however, is that if these solutions become singular, they do not undergo a *whole-beam collapse* (Lemma 7.7). Numerical simulations suggest that these solutions become singular (Fig. 14.11). See Sect. 14.3 for a numerical investigation of the instability dynamics of perturbed excited-state solitary waves.

9.6 Instability Rate and Dynamics

So far, we “only” asked whether the solitary wave is stable. In [96], Fibich et al. moved beyond this yes/no approach and developed qualitative and quantitative approaches to stability. Specifically, we considered the instability rate and the instability dynamics. See [241] for a review of these approaches.

Briefly, by (9.7), the instability rate is given by $\Omega_{\text{re}}^{\max}$. Therefore, when $0 < \Omega_{\text{re}}^{\max} \ll 1$, the instability might not become noticeable over the propagation distance of the experiment. Such a solitary wave is therefore “mathematically unstable”, but “physically stable”.

As noted, when checking for stability, it is considerably easier to compute $P'(\omega)$, than it is to compute $\Omega_{\text{re}}^{\max}$. Since the solitary wave is stable when $P'(\omega) > 0$ and unstable when $P'(\omega) < 0$, it is tempting to conclude that the instability rate is small when $0 < -P'(\omega) \ll 1$. The following result, however, due to Ilan, Sivan, and Fibich, shows that the magnitude of $P'(\omega)$ is unrelated to the instability rate $\Omega_{\text{re}}^{\max}$:

Lemma 9.9 ([132]) *Consider the unstable solitary waves of the NLS (9.1) in the supercritical case $\sigma d > 2$. Then*

1. $|P'(\omega)|$ decreases with ω .
2. Ω_{max} increases (linearly) with ω .

Proof

1. This follows from Eq. (9.11).
2. Under the NLS dilation transformation (see Sect. 8.1), $\psi(z, \mathbf{x}) \rightarrow \omega^{\frac{1}{2\sigma}} \psi(\omega z, \sqrt{\omega} \mathbf{x})$. Therefore, by (9.4), so does $h(z, \mathbf{x})$, i.e., $h(z, \mathbf{x}) \rightarrow \omega^{\frac{1}{2\sigma}} h(\omega z, \sqrt{\omega} \mathbf{x})$. Hence, $\Omega z \rightarrow \Omega \omega z$, see (9.7). \square

Thus, $|P'(\omega)|$ is inversely proportional to $\Omega_{\text{re}}^{\max}$. In particular, the instability rate is large when $|P'(\omega)|$ is small, and vice versa. See [132] for further discussion of why $|P'(\omega)|$ is unrelated to the instability rate.

As noted, one advantage of determining stability by solving the eigenvalue problem (9.6) is that it provides the instability rate. Another advantage of this “spectral approach” is that the eigenfunctions of the unstable eigenvalues indicate the type of the instability dynamics. In the case of the NLS (9.1) with a power-law non-linearity, perturbed unstable solitary waves either collapse or scatter (diffract). More generally, violation of the VK condition results in a *width instability*, whereby small perturbations lead to large changes of the solution width and amplitude. Other types of instability dynamics are also possible. For example, in the case of positive solitary waves of inhomogeneous NLS equations, violation of the so-called *spectral condition* leads to a *drift instability* [240]. In this case, the associated positive eigenvalue provides the drift rate. Note that if the solitary wave is “width stable” but “drift unstable”, the VK condition fails to detect the instability. See [52, 96, 132, 239, 241, 242] for further details.

9.7 Random Versus Deterministic Perturbations

In most numerical studies of stability, the solitary wave is perturbed by adding noise to the initial condition, and/or by the round-off error that accumulates during the simulation. When the computed solution appears to be unstable, however, deterministic perturbations provide better confidence that the observed instability is not a numerical artifact. This is because it is much easier to test for grid convergence with deterministic initial conditions. Another advantage of deterministic perturbations is that they can reveal the relation between the type of the perturbation and the resulting instability dynamics. When, however, the computed solution appears to be stable, it is much easier to “trust” computations with random perturbations. In fact, in that case random perturbations have the advantage that they excite all possible modes, unlike deterministic perturbations which might only excite the stable modes, and therefore lead to the misperception that an unstable solution is stable. See [96, 241] for more details.

Chapter 10

The Explicit Critical Singular Peak-Type Solution ψ_R^{explicit}

In Chap. 6 we saw that the critical NLS

$$i\psi_z(z, \mathbf{x}) + \Delta\psi + |\psi|^{\frac{4}{d}}\psi = 0, \quad \psi(0, \mathbf{x}) = \psi_0(\mathbf{x}) \in H^1 \quad (10.1)$$

admits the solitary-wave solutions $\psi^{\text{solitary}}(z, \mathbf{x}) = e^{iz}R(\mathbf{x})$, where $R(\mathbf{x})$ is a solution of

$$\Delta R(\mathbf{x}) - R + |R|^{2\sigma}R = 0, \quad R \in H^1. \quad (10.2)$$

In Sect. 8.4.3 we applied the lens transformation with $L(z) = Z_c - z$ to $\psi^{\text{solitary}}(z, \mathbf{x})$. This showed that

$$\psi_R^{\text{explicit}}(z, \mathbf{x}) = \frac{1}{(Z_c - z)^{\frac{d}{2}}} R(\xi) e^{i\xi(z) - i\frac{|\mathbf{x}|^2}{4(Z_c - z)}}, \quad (10.3a)$$

where

$$\xi = \frac{\mathbf{x}}{L(z)} = \frac{\mathbf{x}}{Z_c - z}, \quad \xi = \int_0^z \frac{ds}{L^2(s)} = \frac{z/Z_c}{Z_c - z}, \quad (10.3b)$$

is the solution of (10.1) with

$$\psi_0(\mathbf{x}) = \frac{1}{Z_c^{d/2}} R\left(\frac{\mathbf{x}}{Z_c}\right) e^{-i\frac{|\mathbf{x}|^2}{4Z_c}}.$$

This chapter is devoted to analysis of these explicit solutions.

10.1 Singular Peak-Type Solutions

We first confirm that ψ_R^{explicit} is a blowup solution.

Lemma 10.1 ψ_R^{explicit} is an H^1 solution of the critical NLS (10.1) that becomes singular at Z_c .

Proof Since $R \in H^1$, $\psi_R^{\text{explicit}} \in H^1$ for $0 \leq z < Z_c$. In addition, since

$$\|\psi_R^{\text{explicit}}\|_{\frac{4}{d}+2}^{\frac{4}{d}+2} = \|R\|_{\frac{4}{d}+2}^{\frac{4}{d}+2} \frac{1}{(Z_c - z)^2}, \quad (10.4)$$

then $\lim_{z \rightarrow Z_c^-} \|\psi_R^{\text{explicit}}\|_{\frac{4}{d}+2}^{\frac{4}{d}+2} = \infty$. Hence, ψ_R^{explicit} becomes singular at Z_c (Corollary 5.6). \square

Radial solutions are called *peak-type* if their maximum is attained at the origin.

Lemma 10.2 *Let $R^{(n)}(r)$ be a radial solution of (10.2). Then $\psi_{R^{(n)}}^{\text{explicit}}$ is a peak-type solution.*

Proof By Lemma 6.16, the maximum of $R^{(n)}$ is attained at the origin. \square

In Sect. 15.5.1 we will see that ψ_R^{explicit} can also be *ring-type*.

Lemma 10.3 *ψ_R^{explicit} becomes singular at $\mathbf{x}_c = \mathbf{0}$ as $z \rightarrow Z_c$.*

Proof It is easy to verify that for all $\epsilon > 0$, $\lim_{z \rightarrow Z_c^-} \int_{|\mathbf{x}| < \epsilon} |\psi_R^{\text{explicit}}|^{2\sigma+2} d\mathbf{x} = \infty$. Therefore, by Definition 5.7, the solution becomes singular at $\mathbf{x}_c = \mathbf{0}$. \square

10.2 Whole-Beam Collapse

The power and variance of ψ_R^{explicit} are

$$\|\psi_R^{\text{explicit}}\|_2^2 = \|R\|_2^2, \quad V(\psi_R^{\text{explicit}}) = (Z_c - z)^2 V(R).$$

The variance vanishes at the singularity, i.e.,

$$\lim_{z \rightarrow Z_c} V(\psi_R^{\text{explicit}}) = 0.$$

Hence, by Lemma 7.6, these solutions undergo a whole-beam collapse. Indeed, as $z \rightarrow Z_c$,

$$|\psi_R^{\text{explicit}}|^2 = \frac{1}{L^d(z)} R^2 \left(\frac{\mathbf{x}}{L(z)} \right) \rightarrow \|R\|_2^2 \delta(\mathbf{x}) = \|\psi_R^{\text{explicit}}\|_2^2 \delta(\mathbf{x}).$$

By (10.3b),

$$\lim_{z \rightarrow Z_c} \zeta(z) = \infty, \quad \zeta(z) = \arg \psi(z, r = 0), \quad (10.5)$$

i.e., the on-axis phase of $\psi_{R^{(n)}}^{\text{explicit}}$ also blows up at the singularity. This observation will become important when we consider continuations of $\psi_{R^{(0)}}^{\text{explicit}}$ beyond the singularity (Sects. 38.1.1, 38.6.3, and 38.6.6).

10.3 $\psi_{R,\alpha}^{\text{explicit}}$ and $\psi_{R,\alpha,c}^{\text{explicit}}$

We can use NLS symmetries (Sect. 8.1) to obtain more general expressions for explicit solutions that blowup at Z_c . Thus, applying the lens transformation with $L_\alpha(z) = \alpha(Z_c - z)$ to $\psi^{\text{solitary}} = e^{iz} R(\mathbf{x})$ shows that

$$\psi_{R,\alpha}^{\text{explicit}}(z, \mathbf{x}) = \frac{1}{L_\alpha^{\frac{d}{2}}(z)} R\left(\frac{\mathbf{x}}{L_\alpha(z)}\right) e^{i\zeta_\alpha + i\frac{(L_\alpha)_z}{L_\alpha} \frac{|\mathbf{x}|^2}{4}}, \quad (10.6a)$$

where

$$\zeta_\alpha(z) = \int_0^z \frac{ds}{L_\alpha^2(s)} = \frac{1}{\alpha^2} \left(\frac{1}{Z_c - z} - \frac{1}{Z_c} \right), \quad (10.6b)$$

is the solution of the critical NLS (10.1) with

$$\psi_0(\mathbf{x}) = \frac{1}{(\alpha Z_c)^{\frac{d}{2}}} R\left(\frac{\mathbf{x}}{\alpha Z_c}\right) e^{-i\frac{|\mathbf{x}|^2}{4Z_c}}.$$

More generally, by Galilean invariance,

$$\psi_{R,\alpha,c}^{\text{explicit}}(z, \mathbf{x}) = \psi_{R,\alpha}^{\text{explicit}}(z, |\mathbf{x} - z\mathbf{c}|) e^{i\frac{\mathbf{c}\cdot\mathbf{x}}{2} - i\frac{|\mathbf{c}|^2 z}{4}} \quad (10.7)$$

is the solution of (10.1) with

$$\psi_0(\mathbf{x}) = \frac{1}{(\alpha Z_c)^{\frac{d}{2}}} R\left(\frac{|\mathbf{x}|}{\alpha Z_c}\right) e^{i\frac{\mathbf{c}\cdot\mathbf{x}}{2} - i\frac{|\mathbf{x}|^2}{4Z_c}}.$$

Even more generally, from the invariance under phase changes and spatial translations we have that

$$\psi(z, \mathbf{x}) = e^{i\theta} \psi_{R,\alpha,c}^{\text{explicit}}(z, \mathbf{x} - \mathbf{x}_0)$$

is the solution of (10.1) with

$$\psi_0(\mathbf{x}) = \frac{1}{(\alpha Z_c)^{\frac{d}{2}}} R\left(\frac{|\mathbf{x} - \mathbf{x}_0|}{\alpha Z_c}\right) e^{i\theta + i\frac{\mathbf{c}\cdot(\mathbf{x}-\mathbf{x}_0)}{2} - i\frac{|(\mathbf{x}-\mathbf{x}_0)|^2}{4Z_c}}.$$

10.4 Blowup Rate $l(z)$

A key property of blowup solutions is their blowup rate.

Definition 10.1 (blowup rate) *Let ψ be an NLS solution that blows up at Z_c . The blowup rate of ψ is the rate at which*

$$l(z) := \frac{1}{\|\nabla\psi\|_2} \quad (10.8)$$

goes to zero as $z \rightarrow Z_c$.

By Hamiltonian conservation (Lemma 5.2), if ψ becomes singular at Z_c , then

$$\lim_{z \rightarrow Z_c} \frac{\|\nabla\psi\|_2^2}{\frac{1}{\sigma+1} \|\psi\|_{2\sigma+2}^{2\sigma+2}} = 1. \quad (10.9)$$

Therefore, the blowup rate can also be defined as the rate at which

$$l(z) := \left(\frac{\sigma+1}{\|\psi\|_{2\sigma+2}^{2\sigma+2}} \right)^{\frac{1}{2}} \quad (10.10)$$

goes to zero as $z \rightarrow Z_c$. In particular, in the critical case,

$$l(z) := \left(\frac{\frac{2}{d} + 1}{\|\psi\|_{\frac{4}{d}+2}^{\frac{4}{d}+2}} \right)^{\frac{1}{2}}, \quad \sigma d = 2. \quad (10.11)$$

One advantage of this alternative definition is that it extends to singular solutions which are in $L^{2\sigma+2}$ but not in H^1 (Sects. 11.3 and 12.3). Another advantage, both in the analysis and in simulations, is that $\|\psi\|_{\frac{4}{d}+2}^{\frac{4}{d}+2}$ only depends on the amplitude of ψ , whereas $\|\nabla\psi\|_2$ also depends on its phase.

10.4.1 Blowup Rate of ψ_R^{explicit}

We say that ψ has a *linear blowup rate* if $l(z) \sim c(Z_c - z)$ as $z \rightarrow Z_c$, where c is a positive constant.

Lemma 10.4 ψ_R^{explicit} has a linear blowup rate.

Proof By (10.4) and (10.11),

$$l(z) = \frac{\left(\frac{2}{d} + 1\right)^{\frac{1}{2}}}{\left\|\psi_R^{\text{explicit}}\right\|^{\frac{2}{d}+1}_{\frac{4}{d}+2}} = \frac{\left(\frac{2}{d} + 1\right)^{\frac{1}{2}}}{\|R\|^{\frac{2}{d}+1}_{\frac{4}{d}+2}} (Z_c - z). \quad (10.12)$$

□

Exercise 10.1 Calculate $l(z)$ for ψ_R^{explicit} using (10.8). Verify that it is not identical the one obtained from (10.11), but that the two definitions agree asymptotically as $z \rightarrow Z_c$.

10.5 How to Define Stability of Singular Solutions?

To analyze the stability of ψ_R^{explicit} , we need to define what we mean by stability of a singular solution. We first show that the standard notion of stability is not useful.

Conclusion 10.1 *If stability means that small perturbations of the initial condition lead to small changes in the solution, then all NLS singular solutions are unstable.*

Proof Let ψ collapse at Z_c , and let its initial condition be slightly perturbed, so that the corresponding perturbed solution $\tilde{\psi}$ collapses at $\tilde{Z}_c \neq Z_c$. By the triangle inequality, as $z \rightarrow Z_c^{\min} := \min\{Z_c, \tilde{Z}_c\}$,

$$\lim_{z \rightarrow Z_c^{\min}} \|\tilde{\psi} - \psi\|_{H^1} \geq \lim_{z \rightarrow Z_c^{\min}} |\|\tilde{\psi}\|_{H^1} - \|\psi\|_{H^1}| = \infty,$$

i.e., the distance between ψ and $\tilde{\psi}$ becomes infinite. □

It is easier to understand what we mean by an instability of a singular solution. One useful definition is

Definition 10.2 (Strong instability of a singular solution) *Let ψ be a singular NLS solution with the initial condition ψ_0 . We say that ψ is strongly unstable, if for every $\delta > 0$, there is an initial condition $\tilde{\psi}_0$, such that $\|\tilde{\psi}_0 - \psi_0\|_{H^1} < \delta$ and the corresponding NLS solution $\tilde{\psi}$ exists globally for $0 \leq z < \infty$.*

Definition 10.2 is the analog of Definition 9.2 of strong instability of solitary waves, in the sense that in both definitions, infinitesimal perturbations can completely change the dynamics from collapse to global existence or vice versa.

The notion of strong instability is sometimes too restrictive. This is the case when all initial conditions in an H^1 -neighborhood of ψ_0 lead to collapse, but some of these perturbed singular solutions are qualitatively different from the unperturbed solution. In that case, the singular NLS solution is not strongly unstable, yet it is “qualitatively” unstable.

Singular NLS solutions are typically characterized by their *blowup rate* and *blowup profile*. Therefore, we say that a collapsing solution is unstable, if either of these properties can undergo a *discontinuous* change under a continuous perturbation of ψ_0 . At present, for all known unstable singular NLS solutions, the blowup rate is discontinuous under some perturbations of ψ_0 . As for the blowup profile, in some cases (e.g., Observation 14.1) it is discontinuous under perturbations of ψ_0 . Lemma 10.6, however, provides an example of a perturbation of ψ_0 under which the blowup rate is discontinuous but the blowup profile is continuous. Therefore, it seems that the “correct” property for determining stability of singular solutions is the blowup rate.

Definition 10.3 (Instability of singular solutions) *Let ψ be a singular NLS solution with initial condition ψ_0 . We say that ψ is unstable, if there exists a one-parameter family of initial conditions $\psi_0^{(\epsilon)}$, which is smooth in ϵ , such that (i) the corresponding NLS solutions $\psi^{(\epsilon)}$ are singular for $0 < \epsilon \ll 1$, (ii) $\lim_{\epsilon \rightarrow 0+} \psi_0^{(\epsilon)} = \psi_0$, and (iii) the blowup rate of $\psi^{(\epsilon)}$ is discontinuous at $\epsilon = 0$.*

Since NLS solutions depend continuously on the initial conditions (Theorem 5.2), if $\psi_0^{(\epsilon)}(\mathbf{x})$ is smooth in ϵ , then so is $\psi^{(\epsilon)}(z, \mathbf{x})$. How is it possible, then, for the blowup rate $l := 1/\|\psi^{(\epsilon)}\|_2$ to be discontinuous in ϵ ? To answer this question, consider a toy model in which $L(z)$ is the solution of the ODE¹

$$L''(z) \equiv -\frac{\beta}{L^3}, \quad L(0) = 1, \quad L'(0) = -1, \quad (10.13)$$

where β is a constant. By Lemma 2.8, the solution of (10.13) is

$$L^2(z) = (1-z)^2 - \beta z^2 = (1-\beta)(Z_c^{(1)} - z)(Z_c^{(2)} - z),$$

where

$$Z_c^{(1),(2)} = \frac{1 \pm \sqrt{\beta}}{1 - \beta} = \frac{1}{1 \mp \sqrt{\beta}}.$$

Let

$$Z_c := \min\{Z_c^{(i)} \mid Z_c^{(i)} > 0\}.$$

If $\beta = 0$, then $Z_c = Z_c^{(1)} = Z_c^{(2)} = 1$ and so $L(z) = Z_c - z$. Hence, the blowup rate of $L(z)$ is linear.² For any $0 < \beta \ll 1$, however, $Z_c = 1/(1 + \sqrt{\beta})$, and so the blowup rate of $L(z)$ is a square root. We thus see that although $L(z; \beta)$ is continuous in β , its blowup rate has a discontinuity at $\beta = 0$.³

¹ This ODE describes self-similar collapse in the critical NLS (Sect. 11.1).

² Here by “blowup rate” we mean the rate at which $L(z)$ goes to zero.

³ See Sect. 23.9.1 for another example where the blowup rate has a discontinuity.

If a singular NLS is not unstable according to the above definitions, we call it a stable singular solution:

Definition 10.4 (*Stability of a singular solution*) We say that a singular NLS solution is stable, if it is not strongly unstable according to Definition 10.2, and not unstable according to Definition 10.3.

10.6 Instability of ψ_R^{explicit}

We are now ready to consider the stability (or rather the instability) of ψ_R^{explicit} .

10.6.1 Instability of $\psi_{R^{(0)}}^{\text{explicit}}$

We begin with $\psi_{R^{(0)}}^{\text{explicit}}$, where $R^{(0)}$ is the ground state of (10.2).

Lemma 10.5 $\psi_{R^{(0)}}^{\text{explicit}}$ is strongly unstable (in the sense of Definition 10.2).

Proof Let us perturb the initial condition of $\psi_{R^{(0)}}^{\text{explicit}}$ as

$$\psi_0^{(\epsilon)} = (1 - \epsilon)\psi_{R^{(0)}}^{\text{explicit}}(z = 0) = (1 - \epsilon)R^{(0)}(r)e^{-i\frac{r^2}{4Z_c}}, \quad 0 < \epsilon \ll 1. \quad (10.14)$$

The power of the perturbed solution is $\|\psi_0^{(\epsilon)}\|_2^2 = (1 - \epsilon)^2 \|R^{(0)}\|_2^2 < P_{\text{cr}}$. Therefore, the corresponding NLS solution does not become singular. \square

Figure 10.1 shows the dynamics of $\psi^{(\epsilon)}$, the perturbed solution with the initial condition (10.14). It initially collapses, because of the focusing quadratic phase term. Since its power is slightly below P_{cr} , however, collapse is arrested slightly before the focal point Z_c .

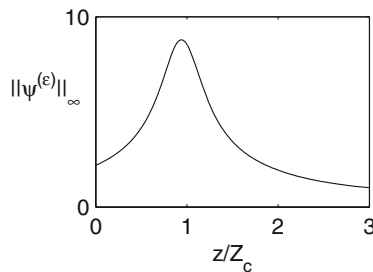


Fig. 10.1 The maximal amplitude of the solution of the critical NLS (10.1) with the initial condition (10.14). Here, $d = 2$, $Z_c = 1$, and $\epsilon = 0.01$

If we perturb the initial condition in the opposite direction, the corresponding NLS solution does blowup, but with a different blowup rate:

Lemma 10.6 *Let $\psi^{(\epsilon)}$ be the solution of the critical NLS (10.1) with*

$$\psi_0^{(\epsilon)}(r) = (1 + \epsilon)\psi_{R^{(0)}}^{\text{explicit}}(z = 0) = (1 + \epsilon)R^{(0)}(r)e^{-i\frac{r^2}{4Z_c}}, \quad (10.15)$$

where $0 < \epsilon \ll 1$ and $Z_c > 0$. Then $\psi^{(\epsilon)}$ becomes singular at a finite distance $Z_c^{(\epsilon)}$. Moreover,

$$\frac{1}{\|\nabla\psi^{(\epsilon)}\|_2} \sim \frac{\sqrt{2\pi}}{\|\nabla R^{(0)}\|_2} \left(\frac{Z_c^{(\epsilon)} - z}{\log |\log(Z_c^{(\epsilon)} - z)|} \right)^{\frac{1}{2}}, \quad z \rightarrow Z_c^{(\epsilon)}.$$

Proof Since $H((1 + \epsilon)R^{(0)}(r)) < 0$, see Lemma 7.13, the NLS solution with $\psi_0 = (1 + \epsilon)R^{(0)}$ collapses at the loglog law blowup rate (Theorem 14.1, part 3), i.e.,

$$\|\nabla\psi\|_2 \sim \frac{\|\nabla R^{(0)}\|_2}{\sqrt{2\pi}} \left(\frac{Z_c - z}{\log |\log(Z_c - z)|} \right)^{-\frac{1}{2}}, \quad z \rightarrow Z_c.$$

The addition of a focusing lens does not prevent the solution from collapsing (Corollary 7.5), nor does it affect the blowup rate (Lemma 13.1). Therefore, $\psi^{(\epsilon)}$ also collapses at the loglog law blowup rate. \square

The instability of $\psi_{R^{(0)}}^{\text{explicit}}$ in Lemma 10.6 is in the sense of Definition 10.3, since the blowup rate has a discontinuity at $\epsilon = 0$. Note that there is no discontinuity in the blowup profile, as $\psi^{(\epsilon)}$ also collapses with the $R^{(0)}$ profile (Theorem 14.1, part 1). Since $\psi_{R^{(0)}}^{\text{explicit}}$ is both strongly unstable (Lemma 10.5) and unstable (Lemma 10.6), and since there is always some physical or numerical noise present, this solution cannot be observed physically or numerically.

There is a close connection between the change of the blowup rate from linear to a square root in ODE (10.13), and from linear to a square root with a loglog correction in the critical NLS with the initial condition (10.15). Indeed, under the adiabatic approximation, the evolution of the blowup rate is governed by ODE (10.13) with $\beta \approx \frac{2P_{\text{cr}}}{M}\epsilon$. The loglog correction comes from the exponentially-small non-adiabatic radiation. See Chaps. 17 and 18 for more details.

10.6.2 Dual Instabilities of $\psi_{R^{(0)}}^{\text{explicit}}$

In Sect. 9.5.2 we saw that the ground-state solitary wave $\psi^{\text{solitary},(0)} = e^{iz}R^{(0)}(r)$ of the critical NLS has the following dual instabilities: Small perturbations of the initial

condition in “one direction” lower its power and lead to scattering, whereas small perturbations in the “opposite direction” lower its Hamiltonian and lead to collapse. The ground-state explicit blowup solution $\psi_{R^{(0)}}^{\text{explicit}}$ has similar dual instabilities. When unperturbed, it self-focuses at a constant velocity ($L_{zz} = 0$). Intuitively, this is because nonlinearity and diffraction are exactly balanced, and so there is no acceleration or deceleration of the initial focusing rate (which is induced by the focusing lens). This state of an exact balance between nonlinearity and diffraction, however, is unstable. Thus, small perturbations of the initial condition can lead to an acceleration of the collapse process ($L_{zz} < 0$) and thus change the blowup rate (Lemma 10.6), as well as to a deceleration of the collapse process ($L_{zz} > 0$) which arrests the collapse (Lemma 10.5).

10.6.3 Instability of $\psi_{R^{(n)}}^{\text{explicit}}$ for $n \geq 1$

We now consider the stability of the excited-state explicit blowup solutions ($\psi_{R^{(n)}}^{\text{explicit}}$ with $n \geq 1$). For these solutions one cannot prove instability as in Lemma 10.5, because the power of $\psi_0^{(\epsilon)} = (1 - \epsilon)\psi_{R^{(n)}}^{\text{explicit}}(0, r)$ for $0 < \epsilon \ll 1$ and $n \geq 1$ is strictly above P_{cr} . Similarly, one cannot prove instability as in Lemma 10.6. Indeed, while the initial conditions $\psi_0^{(\epsilon)} = (1 + \epsilon)\psi_{R^{(n)}}^{\text{explicit}}(0, r)$ with $0 < \epsilon \ll 1$ and $n \geq 1$ do lead to collapse (Exercise 10.2), one cannot use Theorem 14.1 to conclude that the perturbed solutions collapse at the loglog-law rate.⁴

Exercise 10.2 Let $\psi^{(\epsilon)}$ be a solution of the critical NLS (10.1) with the initial condition $\psi_0^{(\epsilon)} = (1 + \epsilon)\psi_{R^{(n)}}^{\text{explicit}}(0, r)$, where $0 < \epsilon \ll 1$ and $n \geq 1$. Show that $\psi^{(\epsilon)}$ becomes singular at a finite Z_c .

At present, we can only rely on numerical simulations to determine the stability of excited-state explicit blowup solutions. These simulations suggest that these solutions are unstable, but not strongly unstable. See Sect. 14.4 for more details.

10.7 Non-generic Character of ψ_R^{explicit}

A priori, the availability of explicit blowup solutions should have significantly advanced the understanding of collapse in the critical NLS, since one could have deduced its properties directly from the explicit solutions, rather than from the NLS equation. “Unfortunately”, not only are these explicit blowup solutions unstable, but

⁴ Theorem 14.1 does not apply for $\|\psi_0\|_2^2 \geq \|R^{(n=1)}\|_2^2$, see Lemma 14.20.

they also differ from the generic blowup solutions of the critical NLS in several important aspects:⁵

1. While all singular solutions of the critical NLS undergo a strong collapse (Sect. 13.3), NLS blowup is generically a partial-beam collapse (Sect. 7.7). In contrast, ψ_R^{explicit} undergoes a whole-beam collapse.
2. The blowup rate in the critical NLS is a square root with a loglog correction for solutions that collapse with the $\psi_{R^{(0)}}$ profile, and a square root for solutions that collapse with the ψ_G or ψ_{G_m} profiles. In contrast, the blowup rate of ψ_R^{explicit} is linear.
3. The excited-state explicit blowup solutions ($\psi_{R^{(n)}}$ with $n \geq 1$) collapse with the self-similar $R^{(n)}$ profile. This is different from the generic blowup solutions, which collapse with the $R^{(0)}$ profile, the G profile, or the G_m profile.

The ground-state explicit blowup solution $\psi_{R^{(0)}}$ does collapse with the self-similar $R^{(0)}$ profile. Even this solution is different, however, from stable solutions that collapse with the $\psi_{R^{(0)}}$ profile, because the rescaled profile of these stable solutions is not equal to $R^{(0)}$, but only approaches $R^{(0)}$ as $z \rightarrow Z_c$. It is precisely this small difference between the rescaled profile and $R^{(0)}$ that changes the blowup rate from linear to a square root with a loglog correction (Chap. 18).

Therefore, when searching for the generic properties of critical collapse, the availability of ψ_R^{explicit} is “misleading”, rather than “helpful”. Moreover, part of the difficulty in proving the “generic properties” of critical collapse (Theorem 14.1) is that such a proof should be able to distinguish between the generic blowup solutions and the “misleading” explicit blowup solutions.

10.8 Bourgain-Wang Solutions (ψ_{BW})

In 1997, Bourgain and Wang discovered a new type of blowup solutions of the critical NLS. The collapsing core of these solutions approaches $\psi_{R^{(0)}}$ and blows up at a linear rate. Unlike $\psi_{R^{(0)}}$, however, these solutions have a nontrivial tail, denoted by u , that does not collapse into the singularity. Therefore, unlike $\psi_{R^{(0)}}$ (Sect. 10.2), they undergo a partial-beam collapse.

⁵ Here, by “generic” we refer to solutions of the critical NLS that undergo a stable collapse with (i) the asymptotic $\psi_{R^{(0)}}$ profile at the loglog law rate (Sect. 14.6 and Chaps. 17 and 18), (ii) the asymptotic ψ_G profile at a square-root blowup rate (Chap. 19), and (iii) the asymptotic ψ_{G_m} vortex profile at a square-root blowup rate (Chap. 20).

Theorem 10.1 ([31]) Let $d = 1, 2$, let A_0 be a given integer, and let $A \geq A_0$ be a large enough integer. Let $\phi \in X_A = \{f \in H^A \text{ with } (1 + |x|^A)f \in L^2\}$, and let $u \in C([Z^*, Z_c], X^A)$ be the solution of the critical NLS (10.1), subject to $u(z = Z_c) = \phi$, where $(Z^*, Z_c]$ is the maximal existence interval of u . Assume that ϕ vanishes to high order at the origin, i.e.,

$$D^\alpha \phi(0) = 0, \quad |\alpha| \leq A - 1. \quad (10.16)$$

Then for all $\theta \in \mathbb{R}$, there exists $z_0 < Z_c$ and a unique solution $\psi_{\text{BW}}^\theta \in C([z_0, Z_c], X_{A_0})$ of (10.1), such that

$$\|\psi_{\text{BW}}^\theta(z) - e^{i\theta} \psi_{R^{(0)}}^{\text{explicit}}(z) - u(z)\|_{X_{A_0}} \leq |Z_c - z|^{A_0}, \quad z_0 < z < Z_c. \quad (10.17)$$

Theorem 10.1 is surprising, since the collapsing core is unstable, yet it “withstands” the interactions with the nontrivial tail u . Intuitively, this is possible because $u \rightarrow \phi$ as $z \rightarrow Z_c$, and ϕ vanishes to a high order at the singularity point $\mathbf{x}_c = 0$. Therefore, there is a decoupling between the collapsing core and the tail as $z \rightarrow Z_c$.

10.8.1 Dual Instabilities of ψ_{BW}

Bourgain-Wang solutions $\psi_{\text{BW}}(z, \mathbf{x})$ can be expected to be unstable, since their singular core is $\psi_{R^{(0)}}^{\text{explicit}}$, which is unstable. Indeed, in 2011 Merle, Raphaël, and Szeftel showed that ψ_{BW} inherits the dual instabilities of $\psi_{R^{(0)}}^{\text{explicit}}$,⁶ in the sense that it can be embedded into a one-parameter family of NLS solutions $\psi^{(\epsilon)}$, such that $\psi^{(\epsilon=0)} = \psi_{\text{BW}}$, $\psi^{(\epsilon)}$ scatters when perturbed in one direction ($\epsilon > 0$), but collapses when perturbed in the opposite direction ($\epsilon < 0$):

Theorem 10.2 ([185]) Let $d = 2$, let $\alpha^* > 0$ be a small enough universal constant, and let A be a large enough integer. Let $\phi \in X_A$ be radial function that satisfies the smallness assumption $\|\phi\|_{H^A} < \alpha^* \ll 1$ and the degeneracy at blowup point property (10.16). Let $\Sigma = \{u(\mathbf{x}) \mid \mathbf{x}u \in L^2\} \cap H^1$, and let $\psi_{\text{BW}}^{\theta=0} \in C((-\infty, Z_c), \Sigma)$ be the corresponding Bourgain-Wang solution given by Theorem 10.1 with $\theta = 0$. Then there exists a continuous map $\Gamma(\epsilon) : [-1, 1] \rightarrow \Sigma$, such that the following holds. Given $\epsilon \in [-1, 1]$, let $\psi^{(\epsilon)}(z, \mathbf{x})$ be the solution of the critical NLS (10.1), subject to the initial condition $\psi_0^{(\epsilon)} = \Gamma(\epsilon)$. Then

- $\Gamma(\epsilon = 0) = \psi_{\text{BW}}^{\theta=0}(z = 0)$. Hence, for all $z < Z_c$, $\psi^{(\epsilon=0)}(z)$ is equal to the Bourgain-Wang solution $\psi_{\text{BW}}(z)$ on $(-\infty, Z_c)$ with blowup profile $\psi_{R^{(0)}}^{\text{explicit}}$ and a regular part ϕ .

⁶ See Sect. 10.6.2.

- $\forall \epsilon \in (0, 1]$, $\psi^{(\epsilon)} \in C(\mathbb{R}, \Sigma)$ is global in z , and it scatters forward and backwards in the sense that $\int_{z=-\infty}^{\infty} dz \int_{\mathbb{R}^2} |\psi^{(\epsilon)}|^4 d\mathbf{x} < \infty$.
- $\forall \epsilon \in [-1, 0)$, $\psi^{(\epsilon)} \in C((-\infty, Z_c^{(\epsilon)}), \Sigma)$ scatters to the left (in the sense that $\int_{z=-\infty}^0 dz \int_{\mathbb{R}^2} |\psi^{(\epsilon)}|^4 d\mathbf{x} < \infty$), and undergoes a loglog law collapse to the right at a finite distance $Z_c^{(\epsilon)} < Z_c$, where $\lim_{\epsilon \rightarrow 0} Z_c^{(\epsilon)} = Z_c$.

See Sect. 38.2.2 for an informal asymptotic proof of Theorem 10.2. See also Sect. 38.1.2 on the continuation of Bourgain-Wang solutions beyond the singularity by taking the limit $\epsilon \rightarrow 0+$.

10.8.2 Bourgain-Wang Solutions are “Generic”

Because of the dual instabilities of Bourgain-Wang solutions, these solutions were believed to be “non-generic”. In 2011, however, Fibich and Klein [85] showed that these solutions are “very generic”, in the following sense. Consider the solution $\psi(z, \mathbf{x}; K)$ of the critical NLS (10.1) with

$$\psi_0(\mathbf{x}; K) = K f(\mathbf{x}), \quad f(\mathbf{x}) \in H^1, \quad K > 0.$$

Let

$$K_{\text{th}} := \inf\{K \mid \psi(z, \mathbf{x}; K) \text{ collapses at some } 0 < Z_c(K) < \infty\}.$$

Assume that the infimum is attained, i.e., that $\psi(z, \mathbf{x}; K_{\text{th}})$ is a blowup solution. Then, generically, $\psi(z, \mathbf{x}; K_{\text{th}})$ is a Bourgain-Wang solution. See Sect. 38.2 for more details.

10.9 Biharmonic BLS

We briefly discuss the corresponding results for the focusing BNLS

$$i\psi_z(z, \mathbf{x}) - \Delta^2 \psi + |\psi|^{2\sigma} \psi = 0.$$

The blowup rate of ψ is defined as the rate at which $l_B(z) := 1/\|\Delta \psi\|_2^{\frac{1}{2}}$ goes to zero as $z \rightarrow Z_c$. By Hamiltonian conservation (Exercise 5.1), BNLS blowup rate can also be defined as $l_B(z) := (\sigma + 1/\|\psi\|_{2\sigma+2}^{2\sigma+2})^{\frac{1}{4}}$. In particular, in the critical case,

$$l_B(z) := \left(\frac{\frac{4}{d} + 1}{\|\psi\|_{\frac{8}{d}+2}^{\frac{8}{d}+2}} \right)^{\frac{1}{4}}, \quad \sigma d = 4. \quad (10.18)$$

It is not known whether there is a lens transformation symmetry for the critical BNLS. Therefore, it is not clear whether the critical BNLS admits blowup solutions analogous to ψ_R^{explicit} . It is also not known whether it admits Bourgain-Wang type solutions.

Chapter 11

The Explicit Critical Singular Ring-Type Solution ψ_G^{explicit}

In this chapter we consider the critical NLS

$$i\psi_z(z, \mathbf{x}) + \Delta\psi + |\psi|^{\frac{4}{d}}\psi = 0, \quad d > 1. \quad (11.1)$$

We mainly focus on the radial case

$$i\psi_z(z, r) + \psi_{rr} + \frac{d-1}{r}\psi_r + |\psi|^{\frac{4}{d}}\psi = 0, \quad d > 1. \quad (11.2)$$

In Chap. 10 we saw that Eq. (11.2) admits the explicit solution ψ_R^{explicit} . This solution undergoes a self-similar collapse, i.e.,

$$|\psi_R^{\text{explicit}}(z, r)| = \frac{1}{L^{\frac{d}{2}}(z)}R(\rho), \quad \rho = \frac{r}{L(z)}.$$

The self-similar profile of ψ_R^{explicit} is a solution of the R equation

$$R''(\rho) + \frac{d-1}{\rho}R' - R + |R|^{\frac{4}{d}}R = 0, \quad 0 < \rho < \infty, \quad (11.3a)$$

subject to the boundary conditions

$$R'(0) = 0, \quad R(\infty) = 0. \quad (11.3b)$$

In this chapter we present a different explicit singular solution, denoted by ψ_G^{explicit} ¹. This solution also undergoes a self-similar collapse, i.e.,

$$|\psi_G^{\text{explicit}}(z, r)| = \frac{1}{L^{\frac{d}{2}}(z)}G(\rho), \quad \rho = \frac{r}{L(z)}.$$

¹ The critical NLS also admits the explicit blowup vortex solutions $\psi_{R_m^{(n)}}^{\text{explicit}}$ and $\psi_{G_m}^{\text{explicit}}$ (Sects. 15.5 and 15.6, respectively).

The self-similar profile of ψ_G^{explicit} is a solution of the G equation

$$G''(\rho) + \frac{d-1}{\rho} G' - G + |G|^{\frac{4}{d}} G + \gamma \rho^2 G = 0, \quad \gamma > 0, \quad d > 1 \quad (11.4a)$$

for $0 < \rho < \infty$, subject to the initial conditions

$$G(0) \in \mathbb{C}, \quad G'(0) = 0. \quad (11.4b)$$

When $\gamma = 0$, the G equation (11.4a) reduces to the R equation (11.3a). As we shall see, however, solutions of the G equation and of the R equation have very different characteristics.

The chapter is organized as follows. We begin in Sect. 11.1 with a derivation of ψ_G^{explicit} . In Sect. 11.2 we show that when $0 < G(0) \ll 1$, $G(\rho)$ has a ring profile, namely, it has a local minimum at $\rho = 0$, it attains its global maximum at $0 < \rho_{\max} < \infty$, and it decays to zero as $\rho \rightarrow \infty$. Therefore, unlike ψ_R^{explicit} which is peak-type, ψ_G^{explicit} is a ring-type singular solution.

Another difference between ψ_R^{explicit} and ψ_G^{explicit} is that R decays exponentially as $\rho \rightarrow \infty$, whereas G only decays algebraically. In fact, the algebraic decay of G is such that G and ∇G have an infinite power. Therefore, ψ_G^{explicit} is not in H^1 or even in L^2 . In particular, we cannot say that ψ_G^{explicit} becomes singular in H^1 . To overcome this “limitation”, in Sect. 11.3 we introduce a new definition of singularity in $L^{2\sigma+2}$, which generalizes the “old” definition for H^1 solutions. Under this new definition, ψ_G^{explicit} is a singular solution of the NLS that collapses with a square-root blowup rate. This is different from ψ_R^{explicit} , whose blowup rate is linear.

In Sect. 11.4 we study numerically the stability of ψ_G^{explicit} . These simulations show that ψ_G^{explicit} is unstable under radial perturbations if G has a multi-ring profile, but is stable under radial perturbations if G has a single-ring profile.² The single-ring ψ_G^{explicit} solutions, however, are unstable under azimuthal perturbations. Indeed, in Sect. 11.5 we use a perturbation method to show that all singular self-similar ring solutions of the two-dimensional critical NLS are azimuthally unstable.

Although G is not in H^1 , the G profile is relevant to the study of singular H^1 solutions. Indeed,

1. In the case of singular H^1 solutions that undergo a quasi self-similar collapse with the peak-type $\psi_{R^{(0)}}$ profile, the profile of the collapsing core is a solution of the G equation (Sect. 17.3).³

² This is different from $\psi_{R^{(n)}}^{\text{explicit}}$, which is unstable under radial perturbations for any n , and not just for the excited states.

³ In Sect. 17.3 the profile of the collapsing core is denoted by V_0 , in order to emphasize that it is peak-type and not ring-type.

2. The critical NLS “appears to” admit H^1 solutions that collapse with the quasi self-similar ring profile ψ_G , whose self-similar profile is a single-ring G profile (Chap. 19).

Remark In one dimension, there is no notion of a ring solution. Indeed, a one-dimensional “ring” solution (i.e., a solution that attains its maximum at $0 < x_{\max} < \infty$) is, up to translation, a peak-type solution that attain its maximum at $x_{\max} = 0$. Therefore, when studying ring solutions, we only consider the case $d > 1$.

11.1 Derivation of ψ_G^{explicit}

The explicit solution ψ_R^{explicit} of the critical NLS (11.2) can be written as

$$\psi(z, r) = \frac{1}{L^{\frac{d}{2}}(z)} G(\rho) e^{i\zeta(z) + i\frac{L_z}{L} \frac{r^2}{4}}, \quad \rho = \frac{r}{L(z)}, \quad \zeta = \int_0^z \frac{ds}{L^2(s)}, \quad (11.5)$$

where $L(z)$ is linear in z , and $G(\rho)$ is a solution of the R equation (11.3). We now look for explicit solutions of (11.2) of the self-similar form (11.5), for which $L(z)$ is not linear in z .⁴ It can be verified by direct substitution (Lemma 8.2) that the equation for G is

$$G''(\rho) + \frac{d-1}{\rho} G' - G + |G|^{\frac{4}{d}} G + \frac{1}{4} \beta(z) \rho^2 G = 0, \quad \beta = -L^3 L_{zz}. \quad (11.6)$$

Since $G = G(\rho)$ is independent of z , this implies that $\beta(z) \equiv \text{constant}$. Therefore, the equation for $L(z)$ reads

$$-L^3 L_{zz}(z) \equiv \beta. \quad (11.7a)$$

By Lemma 2.8, the solution of this equation, subject to

$$L(0) = L_0 > 0, \quad L_z(0) = L'_0, \quad (11.7b)$$

is

$$L^2(z) = (L_0 + z L'_0)^2 - \frac{\beta}{L_0^2} z^2. \quad (11.8)$$

Therefore, we have

Lemma 11.1 *Let*

$$\psi_G^{\text{explicit}}(z, r) = \frac{1}{L^{\frac{d}{2}}(z)} G(\rho) e^{i\zeta(z) + i\frac{L_z}{L} \frac{r^2}{4}}, \quad \rho = \frac{r}{L(z)}, \quad \zeta(z) = \int_0^z \frac{ds}{L^2(s)},$$

⁴ In Lemma we show that all self-similar radial solutions of the critical NLS are of the form (11.5).

where

$$L(z) = \left((L_0 + zL'_0)^2 - \frac{\beta}{L_0^2} z^2 \right)^{\frac{1}{2}}, \quad (11.9)$$

$L_0 > 0$, L'_0 and β are constants, and $G(\rho)$ is a solution of (11.4) with $\gamma = \beta/4$. Then ψ_G^{explicit} is an explicit solution of the critical NLS (11.2).

Our interest is in singular solutions, i.e., when $L(Z_c) = 0$ for some $0 < Z_c < \infty$. By (11.8), if $\beta < 0$, then $L(z)$ cannot go to zero. If $\beta = 0$, then $L(z)$ is linear in z , Eq. (11.6) for G reduces to Eq. (11.3a) for R , and so we recover the explicit solution ψ_R^{explicit} . If $\beta > 0$, then $L(z)$ can also go to zero. In that case, $L(z)$ has a square-root blowup rate:

Lemma 11.2 *Let $L(z)$ be given by (11.9), $\beta > 0$, $L_0 > 0$, and $L_0 L'_0 < \sqrt{\beta}$. Then*

$$L(z) \sim \alpha(Z_c - z)^{\frac{1}{2}}, \quad z \rightarrow Z_c,$$

where $\alpha = (4\beta)^{\frac{1}{4}}$ and $Z_c = \frac{L_0^2}{\sqrt{\beta} - L_0 L'_0} > 0$.

Proof Equation (11.8) can be rewritten as

$$L^2(z) = L_0^2 \left(1 - \frac{z}{Z_c^{(1)}} \right) \left(1 - \frac{z}{Z_c^{(2)}} \right), \quad (11.10)$$

where

$$Z_c^{(1)} = \frac{L_0^2}{\sqrt{\beta} - L_0 L'_0}, \quad Z_c^{(2)} = \frac{L_0^2}{-\sqrt{\beta} - L_0 L'_0}, \quad (11.11)$$

are the two roots of the quadratic equation $L^2(z) = 0$. Since $L_0 L'_0 < \sqrt{\beta}$, then $Z_c^{(1)} > 0$. When $L'_0 > 0$, then $Z_c^{(2)} < 0$. When $L'_0 < 0$ and $Z_c^{(2)} > 0$, then $0 < Z_c^{(1)} < Z_c^{(2)}$. Therefore, $Z_c^{(1)}$ is always the smaller positive root of $L(z)$. Hence, $Z_c := Z_c^{(1)}$, and

$$L^2(z) \sim L_0^2 \left(1 - \frac{z}{Z_c^{(1)}} \right) \left(1 - \frac{Z_c^{(1)}}{Z_c^{(2)}} \right), \quad z \rightarrow Z_c^{(1)}.$$

Therefore, $L^2(z) \sim \alpha^2(Z_c - z)$ as $z \rightarrow Z_c$, where $\alpha^2 = \frac{L_0^2}{Z_c^{(1)}} \left(1 - \frac{Z_c^{(1)}}{Z_c^{(2)}} \right) = 2\sqrt{\beta}$, and the last equality follows from (11.11).

We can also prove this lemma as follows. If we multiply (11.7a) by $2L_z$, integrate, and multiply by L^2 , we obtain

$$(LL_z)^2 = \beta + C_0 L^2, \quad C_0 = \frac{(L_0 L'_0)^2 - \beta}{L_0^2}. \quad (11.12)$$

Since $\lim_{z \rightarrow Z_c} L(z) = 0$, we have that $\lim_{z \rightarrow Z_c} (LL_z)^2 = \beta$. Therefore, $\lim_{z \rightarrow Z_c} LL_z = \pm\beta^{\frac{1}{2}}$. In addition, since near the singularity $L > 0$ and $L_z < 0$,

$$\lim_{z \rightarrow Z_c} LL_z = -\beta^{\frac{1}{2}}. \quad (11.13)$$

Hence, by l'Hospital's rule,

$$\lim_{z \rightarrow Z_c} \frac{L^2}{Z_c - z} = -2 \lim_{z \rightarrow Z_c} LL_z = 2\beta^{\frac{1}{2}}.$$

Therefore, the result follows. \square

The proof of Lemma 11.2 shows that in general, the square-root dependence of solutions of (11.7) holds only asymptotically as $z \rightarrow Z_c$. When $L_0 L'_0 = -\sqrt{\beta}$, however, then $C_0 = 0$ and so

$$\frac{1}{2}(L^2)_z = LL_z = -\sqrt{\beta},$$

see (11.12). The solution of this ODE is a “pure square-root”, i.e.,

$$L(z) = \alpha(Z_c - z)^{\frac{1}{2}}, \quad \alpha = (4\beta)^{\frac{1}{4}}.$$

Since

$$\frac{L_z}{L} \frac{r^2}{4} = LL_z \frac{\rho^2}{4} = -\frac{\alpha^2}{8} \rho^2,$$

in this special case Lemma 11.1 reduces to

Lemma 11.3 *Let*

$$\psi_G^{\text{explicit}}(z, r) = \frac{1}{L^{\frac{d}{2}}(z)} G(\rho) e^{i\zeta(z) + i \frac{L_z}{L} \frac{r^2}{4}} = \frac{1}{L^{\frac{d}{2}}(z)} G(\rho) e^{i\zeta(z) - i \frac{\alpha^2}{8} \rho^2}, \quad (11.14a)$$

where

$$L(z) = \alpha(Z_c - z)^{\frac{1}{2}}, \quad \rho = \frac{r}{L(z)}, \quad (11.14b)$$

$$\zeta(z) = \int_0^z \frac{ds}{L^2(s)} = -\frac{1}{\alpha^2} \ln \left(1 - \frac{z}{Z_c} \right), \quad (11.14c)$$

and $G(\rho)$ is a solution of (11.4) with

$$\gamma = \frac{\alpha^4}{16}. \quad (11.15)$$

Then ψ_G^{explicit} is an explicit solution of the critical NLS (11.2).

Since $\|\psi_G^{\text{explicit}}(z, r)\|_\infty = L^{-\frac{d}{2}}(z)\|G\|_\infty$ and $\|G\|_\infty < \infty$, see Lemma 11.5, we have that

$$\|\psi_G^{\text{explicit}}(z, r)\|_\infty < \infty, \quad 0 \leq z < Z_c$$

and

$$\lim_{z \rightarrow Z_c} \|\psi_G^{\text{explicit}}(z, r)\|_\infty = \infty.$$

Therefore, ψ_G^{explicit} becomes singular in L^∞ as $z \rightarrow Z_c$. As we shall see, however, ψ_G^{explicit} is not in H^1 . Therefore, we cannot say that ψ_G^{explicit} becomes singular in H^1 , see Definition 5.6. In Sect. 11.3, however, we will see that ψ_G^{explicit} becomes singular in $L^{2\sigma+2}$ with a square-root blowup rate.

11.1.1 $\psi_{G,0}^{\text{explicit}} = G(r)e^{-i\frac{r^2}{4F}}$

Expression (11.14) depends on two parameters: α and Z_c . If we set $L(0) = 1$, then $Z_c = \alpha^{-2}$ and so

$$\begin{aligned} \psi_G^{\text{explicit}}(z, r) &= \frac{1}{L^{\frac{d}{2}}(z)} G\left(\frac{r}{L(z)}\right) e^{i\xi(z)} e^{-i\frac{\alpha^2 r^2}{8(1-\alpha^2 z)}} \\ &= \frac{1}{L^{\frac{d}{2}}(z)} G\left(\frac{r}{L(z)}\right) e^{i\xi(z)} e^{-i\frac{r^2}{8(Z_c-z)}}, \end{aligned} \quad (11.16a)$$

where

$$L(z) = \sqrt{1 - \alpha^2 z} = \sqrt{1 - \frac{z}{Z_c}} \quad (11.16b)$$

and

$$\xi(z) = -\frac{\ln(1 - \alpha^2 z)}{\alpha^2} = -Z_c \ln\left(1 - \frac{z}{Z_c}\right). \quad (11.16c)$$

Substituting $z = 0$ in (11.16) shows that $\psi_G^{\text{explicit}}(z = 0) = \psi_{G,0}^{\text{explicit}}$, where

$$\psi_{G,0}^{\text{explicit}} = G(r)e^{-i\frac{\alpha^2 r^2}{8}} = G(r)e^{-i\frac{r^2}{8Z_c}}, \quad (11.17)$$

i.e., a G profile which is focused by a lens with a focal length $F = 2/\alpha^2 = 2Z_c$ (Conclusion 2.12).

Corollary 11.1 *The solution of the critical NLS (11.2) with the initial condition $\psi_{G,0}^{\text{explicit}} = G(r)e^{-i\frac{r^2}{4F}}$ is given by (11.16) with $Z_c = F/2$.*

Thus, a G profile which is focused by a lens with focal distance F , blows up (in L^∞ and in $L^{2\sigma+2}$) at $Z_c = F/2$. This is different from a focused R profile (i.e., $\psi_0(r) = R(r)e^{-\frac{ir^2}{4F}}$), which blows up at $Z_c = F$ (Chap. 10). Note that for both initial conditions $L(0) = 1$ and $L'(0) = -1/F$. The difference between the two cases is that R is a profile of a solitary wave. Therefore, it follows from the lens transformation that $L = 1 - z/F$. In contrast, G is not a solitary-wave profile. Consequently, L is not linear in z (but rather $L = \sqrt{1 - 2z/F}$), which is why it does not “have to” vanish at $z = F$.

11.2 Analysis of the G Equation

We begin with a simple observation.

Lemma 11.4 *Let $G(r)$ be a solution of (11.4). Then $G = e^{i\alpha}\tilde{G}(r)$, where α is a real number and $\tilde{G}(r)$ is real function.*

Proof The proof is the same as in Lemma 6.12. \square

Therefore, without loss of generality, from now on we assume that G is real and $G(0) > 0$.

11.2.1 Asymptotic Behavior for $r \gg 1$

As noted, when $\gamma = 0$, the equation for G reduces to that for R . Equation (11.3) for R , however, is a boundary value problem. To compare it with Eq. (11.4) for G , it is instructive to consider the R equation as an initial value problem, i.e.,

$$R''(r) + \frac{d-1}{r}R' - R + |R|^{\frac{4}{d}}R = 0, \quad R(0) = R_0 \neq 0, \quad R'(0) = 0. \quad (11.18)$$

In Theorem 6.5 we saw that when $d \geq 2$, the boundary value problem (11.3) has countably many H^1 solutions, denoted by $\{R^{(n)}(r)\}_{n=0}^\infty$, which decay exponentially as $r \rightarrow \infty$. Therefore, the solution $R(r)$ of (11.18) decays to zero as $r \rightarrow \infty$ if and only if $R_0 = R^{(n)}(0)$ for some n . In addition, all decaying solutions of (11.18) are in H^1 .

In 1993, Johnson and Pan [136] showed that the behavior of $G(r)$ as $r \rightarrow \infty$ is very different, in two key aspects:

1. Solutions of (11.4) decay to zero as $r \rightarrow \infty$ for *any* $G(0) \in \mathbb{C}$.
2. The decaying solutions of (11.4) are not in H^1 , or even in L^2 .

Following Johnson and Pan, we first show that all solutions of (11.4) decay to zero as $r \rightarrow \infty$:

Lemma 11.5 ([136]) *Let $G(r)$ be a solution of (11.4). Then for any $G(0) \in \mathbb{C}$, this initial value problem has a unique solution for $0 \leq r < \infty$. In addition,*

$$G = O\left(r^{-\frac{d-1}{2}}\right), \quad r \rightarrow \infty.$$

In particular, $\lim_{r \rightarrow \infty} G(r) = 0$.

Proof Local existence and uniqueness follow from the standard theorems (except near $r = 0$, where it can be shown as in Sect. 6.4). Global existence follows from the a priori bounds which we now derive.

To eliminate the first derivative, let $G(r) = r^{-\frac{d-1}{2}}v(r)$. The equation for v reads

$$v''(r) + \left[\gamma r^2 - 1 - \frac{A}{r^2} + r^{-(2-\frac{2}{d})}|v|^{\frac{4}{d}}\right]v = 0, \quad A = \frac{(d-1)(d-3)}{4}. \quad (11.19)$$

Let

$$t = r^2, \quad x(t) = v(r), \quad y(t) = \frac{dx}{dt}.$$

By the chain rule,

$$v'(r) = 2ry(t), \quad v''(r) = y'(t)4r^2 + 2y = 4ty'(t) + 2y.$$

Therefore, (11.19) becomes

$$x'(t) = y, \quad y'(t) = -\frac{y}{2t} + \left(-\frac{\gamma}{4} + \frac{1}{4t} + \frac{A}{4t^2} - \frac{1}{4t^q}|x|^{\frac{4}{d}}\right)x, \quad (11.20)$$

where $q = 2 - \frac{1}{d} > 1$. Let us define

$$J(t) = \frac{y^2(t)}{2} + \frac{\gamma x^2(t)}{8} - \frac{1}{8} \left(\frac{1}{t} + \frac{A}{t^2}\right)x^2(t) + \frac{|x(t)|^{\frac{4}{d}+2}}{4\left(\frac{4}{d}+2\right)t^q}. \quad (11.21)$$

By (11.20) and (11.21),

$$J'(t) = -\frac{y^2}{2t} + \frac{1}{8t^2} \left(1 + \frac{2A}{t}\right)x^2 - q \frac{|x|^{\frac{4}{d}+2}}{4\left(\frac{4}{d}+2\right)t^{q+1}} < \frac{1}{8t^2} \left(1 + \frac{2A}{t}\right)x^2.$$

In addition, by (11.21),

$$\frac{1}{8} \left(\gamma - \frac{1}{t} - \frac{A}{t^2}\right)x^2 \leq J(t).$$

From the last two inequalities, there exists t_0 sufficiently large, such that

$$J'(t) < \frac{1}{8t^2} 1.1x^2, \quad 0 < \frac{1}{8} \frac{\gamma}{2} x^2 \leq J(t), \quad t \geq t_0. \quad (11.22)$$

Therefore, there exists a constant $C_1 > 0$ such that

$$J'(t) \leq \frac{C_1 J(t)}{t^2}, \quad t \geq t_0.$$

Dividing by $J(t)$ and integrating between t_0 and t gives

$$\ln J(t) \Big|_{t_0}^t \leq -\frac{C_1}{t} \Big|_{t_0}^t.$$

Hence, for $t \geq t_0$,

$$\ln J(t) \leq C_2 - \frac{C_1}{t} < C_2, \quad C_2 = \ln J(t_0) + \frac{C_1}{t_0},$$

and so $J(t) \leq e^{C_2}$. Therefore, by (11.22), $x(t)$ is bounded for t sufficiently large. Hence, $v(r) = x(t=r^2)$ is bounded for r sufficiently large. Since $G = vr^{-\frac{d-1}{2}}$, the result follows. \square

We can use WKB analysis to find the asymptotic behavior of G :

Lemma 11.6 ([136]) *Let $G(r)$ be a solution of (11.4). Then for $r \gg \gamma^{-\frac{1}{2}}$,*

$$G(r) \sim \frac{c_G}{r^{\frac{d}{2}}} \cos(h(r)), \quad G'(r) \sim -\frac{c_G \sqrt{\gamma}}{r^{\frac{d}{2}-1}} \sin(h(r)), \quad (11.23a)$$

where

$$h(r) \sim \frac{\sqrt{\gamma}}{2} r^2 - \frac{1}{2\sqrt{\gamma}} \ln r + d_G, \quad (11.23b)$$

and c_G and d_G are constants that depend on the value of $G(0)$.

Proof By Lemma 11.5, $G(r) = r^{-\frac{d-1}{2}} v(r)$, where v is a solution of (11.19), and v is bounded as $r \rightarrow \infty$. Therefore, (11.19) can be written as

$$v''(r) + \left[\gamma r^2 - 1 + O\left(r^{-\left(2-\frac{2}{d}\right)}\right) \right] v = 0. \quad (11.24)$$

Let us look for a solution of (11.24) of the form

$$v \sim c_G e^{h_0(r)+h_1(r)+h_2(r)+\dots} \quad r \rightarrow \infty,$$

where $\{h_0(r), h_1(r), h_2(r), \dots\}$ is an asymptotic sequence as $r \rightarrow \infty$, i.e., for all n , $h_{n+1} = o(h_n)$, $h'_{n+1} = o(h'_n)$ and $h''_{n+1} = o(h''_n)$ as $r \rightarrow \infty$. Substitution in (11.24) gives

$$(h''_0 + h''_1 + \dots) + (h'_0 + h'_1 + \dots)^2 + \gamma r^2 - 1 = O\left(r^{-\left(2-\frac{2}{d}\right)}\right),$$

where $' = \frac{d}{dr}$. Since $r \gg \gamma^{-\frac{1}{2}}$, the equation for the leading-order terms is

$$h''_0 + (h'_0)^2 + \gamma r^2 = 0.$$

The substitution $h_0 = cr^n$ shows that the order of the terms in this equation is r^{n-2} , r^{2n-2} , and r^2 , respectively. Since the only consistent way to balance the leading-order terms is if $n = 2$, the equation for the leading-order terms is

$$(h'_0)^2 + \gamma r^2 = 0.$$

Therefore,

$$h'_0 = \pm i\sqrt{\gamma}r, \quad h_0 = \pm i\sqrt{\gamma} \frac{r^2}{2}.$$

Balancing the next-order terms gives

$$h''_0 + 2h'_0h'_1 - 1 = 0.$$

Therefore,

$$h'_1 = -\frac{1}{2} \left(1 \pm \frac{i}{\sqrt{\gamma}}\right) \frac{1}{r}, \quad h_1 = -\frac{1}{2} \left(1 \pm \frac{i}{\sqrt{\gamma}}\right) \ln r + d_G.$$

Balancing the next-order terms gives $h_2 = o(1)$, see Exercise 11.1. Therefore,

$$v \sim c_G r^{-\frac{1}{2}} e^{\pm i\left(\sqrt{\gamma} \frac{r^2}{2} - \frac{1}{2\sqrt{\gamma}} \ln r + d_G\right)}.$$

Since v is real, $v \sim c_G r^{-\frac{1}{2}} \cos(h(r))$, where h is given by (11.23b). Therefore,

$$G = r^{-\frac{d-1}{2}} v \sim c_G r^{-\frac{d}{2}} \cos(h(r))$$

and

$$G' = r^{-\frac{d-1}{2}} v' - \frac{d-1}{2} r^{-\frac{d+1}{2}} v \sim -c_G r^{-\frac{d}{2}} h'(r) \sin(h(r)), \quad h' \sim \sqrt{\gamma}r. \quad \square$$

Exercise 11.1 Show that $h_2 = o(1)$.

Lemma 11.6 shows that G has an algebraically-decaying tail, which oscillates faster and faster as $r \rightarrow \infty$. In fact, because of the slow algebraic decay, G has an infinite power:

Corollary 11.2 ([136]) Let $G(r)$ be a nontrivial solution of (11.4). Then G and ∇G are not in L^2 . In particular, G is not in H^1 . However, G is in L^p for any $p > 2$. In particular, G is in $L^{2\sigma+2}$.

Proof This follows directly from Lemma 11.6. \square

Exercise 11.2 In Sect. 15.6 we will present the explicit two-dimensional vortex singular solution $\psi_{G_m}^{\text{explicit}}$, whose self-similar profile is the solution of

$$G_m''(r) + \frac{1}{r}G_m' - G_m - \frac{m^2}{r^2}G_m + |G_m|^2G_m + \gamma r^2G_m = 0, \quad \gamma > 0$$

for $0 < r < \infty$, subject to $g_m(0) := \lim_{r \rightarrow 0} \frac{G_m(r)}{r^m} \neq 0$.

1. Show that $\lim_{r \rightarrow \infty} G_m(r) = 0$.
2. Show that as $r \rightarrow \infty$,

$$G_m(r) \sim \frac{c_m}{r} \cos(h(r)), \quad G_m'(r) \sim -c_m \sqrt{\gamma} \sin(h(r)),$$

where $h(r) \sim \frac{\sqrt{\gamma}}{2}r^2 - \frac{1}{2\sqrt{\gamma}} \ln r + d_m$, and c_m and d_m are constants that depend on the value of $g_m(0)$.

3. Show that G_m and ∇G_m are not in L^2 . In particular, G_m is not in H^1 . However, G_m is in L^p for any $p > 2$. In particular, G_m is in $L^{2\sigma+2} = L^4$.

11.2.2 Asymptotic Behavior for $r \ll 1$

By Lemma 6.16, any solution of the R equation (11.18) which decays to zero at infinity, attains its global maximum at $r = 0$. In contrast, solutions of the G equation (which always decay to zero at infinity, see Lemma 11.5) can have a local minimum at $r = 0$:

Lemma 11.7 Let $G(r)$ be a solution of (11.4). Then G has a local minimum at $r = 0$ if $0 < G(0) < 1$, and a local maximum if $G(0) > 1$.

Proof If we let $r \rightarrow 0$ in (11.4) and apply l'Hospital's rule, we get that

$$d \cdot G''(0) = G(0) \left(1 - |G(0)|^{\frac{4}{d}} \right). \quad (11.25)$$

Therefore, $G''(0) > 0$ if $0 < G(0) < 1$ and $G''(0) < 0$ if $G(0) > 1$. \square

Remark It is interesting to contrast the behavior of $G(r)$ near $r = 0$ with that of $R^{(n)}(r)$. Indeed, while $R^{(n)}$ also satisfies relation (11.25), see Sect. 6.4.5, the fact that

$R^{(n)} \in H^1$ implies that $R^{(n)}(0) > 1$ (Corollary 6.10). Therefore, $(R^{(n)})''(0) < 0$, i.e., $R^{(n)}$ has a local maximum at $r = 0$. In fact, $R^{(n)}$ has a global maximum at $r = 0$ (Lemma 6.16). Therefore, the R equation does not admit ring-type solutions.

Remark In Sect. 17.3 we shall consider solutions of the G equation (11.4),⁵ which bifurcate from the ground state $R^{(0)}$. For these solutions

$$G(0) \approx R^{(0)}(0) > 1.$$

Hence, G is decreasing near the origin, and is thus peak-type. In this chapter, however, we focus on solutions of (11.4) with $0 < G(0) \ll 1$. These solutions are increasing near the origin, and are therefore ring-type.

When $0 < G(0) \ll 1$, then for $0 \leq r \ll \min\{1, \gamma^{-\frac{1}{2}}\}$, Eq.(11.4) can be approximated by

$$\Delta G(r) = G, \quad G'(0) = 0. \quad (11.26)$$

Therefore, G is exponentially increasing or decreasing. Since, in addition, $G''(0) > 0$, this implies that $G(r)$ is exponentially increasing near the origin.

The solution of (11.26) that satisfies $G''(0) > 0$ is $G(r) = G(0)f(r)$, where f is the monotonically-increasing solution of

$$\Delta f(r) = f, \quad f(0) = 1, \quad f'(0) = 0. \quad (11.27)$$

For example, when $d = 2$, the solution of (11.26) is $G(r) = G(0)I_0(r)$, where $I_0(r)$ is the solution of the modified Bessel equation of order zero of the first kind, i.e., the solution of

$$r^2y''(r) + ry' - r^2y = 0, \quad y(0) = 1, \quad y'(0) = 0. \quad (11.28)$$

11.2.3 Ring Profile with an Algebraically-Decaying Tail

So far, we proved that if $0 < G(0) \ll 1$, the solution of the G equation increases exponentially near the origin, is bounded for all r , and has an oscillatory decay to zero as $r \rightarrow \infty$. The change from exponential increase to oscillations is due to the sign change of the coefficient $\gamma r^2 - 1$ of $G(r)$ in Eq.(11.4a) at the transition point $r_{\text{transition}} = \gamma^{-\frac{1}{2}}$.

In the physical case $d = 2$, Eq.(11.4) reads

$$G''(\rho) + \frac{1}{\rho}G' - G + |G|^2G + \gamma r^2G = 0, \quad \gamma > 0, \quad 0 < \rho < \infty, \quad (11.29a)$$

$$G(0) \in \mathbb{C}, \quad G'(0) = 0. \quad (11.29b)$$

⁵ Denoted therein by V_0 .

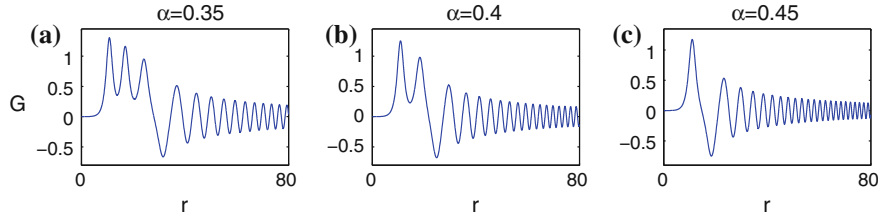


Fig. 11.1 Solutions of (11.29) with $G(0) = 5 \times 10^{-4}$ for several values of α . **a** $\alpha = 0.35$ **b** $\alpha = 0.4$ **c** $\alpha = 0.45$. From [73]

Figure 11.1 shows solutions of (11.29) with $0 < G(0) \ll 1$ and $\gamma = \alpha^4/16$ for various values of α . In general, these solutions can be separated into

1. **a ring region** for $0 \leq r \leq O\left(\gamma^{-\frac{1}{2}}\right)$, in which G is positive with one or several peaks (rings), and
2. **a tail region** for $r \gg \gamma^{-\frac{1}{2}}$, in which G is oscillatory and has an algebraic decay (Lemma 11.6).

The profile of $G(r)$ near the peak of its ring(s) is, up to scaling, that of a one-dimensional solitary wave:

Lemma 11.8 ([73]) *Let $G(r)$ be a solution of (11.4), and let r_{\max} be a local maximum point of G , such that⁶*

$$1 \ll r_{\max} \leq \gamma^{-\frac{1}{2}}. \quad (11.30)$$

Then for $r - r_{\max} = O(1)$,

$$G(r) \sim \left(1 + \frac{2}{d}\right)^{\frac{d}{4}} \lambda^{\frac{d}{2}} \operatorname{sech}^{\frac{d}{2}}(\lambda(r - r_{\max})), \quad (11.31a)$$

where

$$\lambda = \sqrt{1 - \gamma r_{\max}^2}. \quad (11.31b)$$

Proof Since $G'(r_{\max}) = 0$ and $r \gg 1$, the $\frac{d-1}{r}G'(r)$ term can be neglected for $r - r_{\max} = O(1)$. In addition, since $r \gg 1$ and $r - r_{\max} = O(1)$, then $r^2 = r_{\max}^2(1 + o(1))$. Hence, to leading order, Eq. (11.4) reduces to

$$G''(r) - \lambda^2 G + |G|^{\frac{4}{d}} G = 0, \quad G'(r_{\max}) = 0, \quad (11.32)$$

where λ^2 is given by (11.31b). Therefore, $G(r) \sim \lambda^{\frac{d}{2}} R(\lambda(r - r_{\max}))$, where R is the solution of

⁶ In Corollary 11.4 we will see that if $0 < G_0 \ll 1$ then $r_{\max} \gg 1$. The condition $r_{\max} \leq \gamma^{-\frac{1}{2}}$ ensures that r_{\max} is in the ring region and not in the tail region.

$$R''(x) - R + |R|^{\frac{4}{d}} R = 0, \quad R'(0) = 0$$

that attains its maximum at $x = 0$. By Lemma 6.15 with $\sigma = 2/d$, $R(x) = (1 + \frac{2}{d})^{\frac{d}{4}} \operatorname{sech}^{\frac{d}{2}}(x)$. Therefore, the result follows. \square

Thus, up to (radial) translations and dilations, all solutions of the G equation have the same profile near the ring peak.

When $d = 2$, expression (11.31) reads

$$G(r) \sim 2^{\frac{1}{2}} \lambda \operatorname{sech}(\lambda(r - r_{\max})), \quad \lambda^2 = 1 - \gamma r_{\max}^2. \quad (11.33)$$

Figure 11.2 shows that when G has a single-ring profile,⁷ approximation (11.33) is in excellent agreement with G in the ring region. In the case of multi-ring solutions, Lemma 11.8 can be applied to each of the peaks.

Figure 11.1 shows that when G has a multi-ring profile, the height of the peaks in the ring region decreases with r . Indeed, this result follows from Lemma 11.8:

Corollary 11.3 *Let $G(r)$ be a solution of (11.4), and let $r_{\max}^{(i)}$ and $r_{\max}^{(j)}$ be two local maximum points of G , such that $1 \ll r_{\max}^{(i)} < r_{\max}^{(j)} \leq \gamma^{-\frac{1}{2}}$. Then $G(r_{\max}^{(i)}) > G(r_{\max}^{(j)})$.*

Proof By (11.31),

$$G(r_{\max}) \sim \left(1 + \frac{2}{d}\right)^{\frac{d}{4}} \left(1 - \gamma r_{\max}^2\right)^{\frac{d}{4}}. \quad (11.34)$$

Therefore, the result follows. \square

In Lemma 6.16 we derived a similar result for the excited states of the R equation. Note, however, that all the peaks of a multi-ring G solution in the ring region are of the same sign, whereas the peaks of $R^{(n)}$ are of alternating signs (see, e.g., Fig. 6.1).

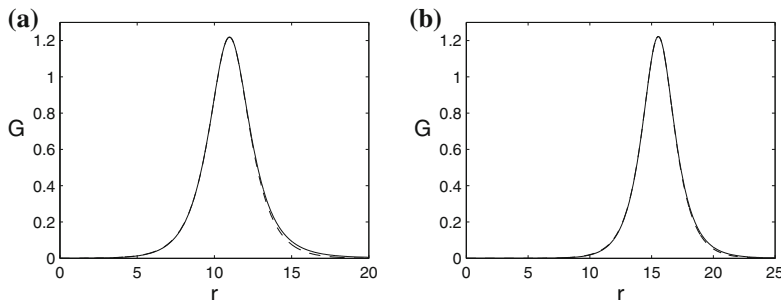


Fig. 11.2 Single-ring G profiles (solid) with **a** $G_0 = 5 \times 10^{-4}$ and $\alpha = \alpha^{(1)} = 0.424$, and **b** $G_0 = 7.6 \times 10^{-6}$ and $\alpha = \alpha^{(1)} = 0.357$. The dashed line is approximation (11.33)

⁷ i.e., when $\alpha = \alpha^{(1)}(G_0)$, see Sect. 11.2.5.

11.2.4 Families of Multi-ring Profiles

The G equation does not admit nontrivial solutions that do not have an infinite-power oscillatory tail. Indeed, by Lemma 11.6, if $c_G = 0$ then $G \equiv 0$. Therefore, Fibich et al. [73] suggested to look for ring solutions with *minimal tails*. Since the tail amplitude is determined by c_G , then for a given $G(0)$, we varied the value of α , and defined the single-ring profile of (11.4) as the single-ring solution with the smallest value of c_G . More generally, the n -ring profile is defined as the n -ring solution with the minimal c_G .

Figure 11.3 shows a graph of c_G as a function of α . In general, c_G is $O(10)$, but it sharply falls by two orders of magnitude at certain locations. Let us denote the values of α at the minimum points by, going from right to left, $\alpha^{(1)}, \alpha^{(2)}, \alpha^{(3)}$, etc. Plotting the corresponding G profiles shows that $\alpha = \alpha^{(n)}$ corresponds to an n -ring profile (Fig. 11.4). The sharp variations of c_G near the minima points in Fig. 11.3 indicate that small perturbations in the value of α from $\alpha^{(n)}$ result in solutions which are very different from ring profiles (Fig. 11.5). More generally, values of α in the range $\alpha^{(n)} < \alpha < \alpha^{(n-1)}$ give rise to n -ring solutions with “large” oscillating tails (as e.g., in Fig. 11.1).

Let us denote by $\alpha^{(n)}(G_0)$ the value of α for which the solution of (11.29) with $G(0) := G_0$ is an n -ring profile, i.e., $\alpha^{(n)}(G_0)$ is the n th (from the right) local minimum point of $c_G(\alpha)$. By repeating the above procedure for other values of G_0 ,⁸ we obtain curves $\alpha = \alpha^{(n)}(G_0)$ that describe families of n -ring profiles (Fig. 11.6). As pointed out earlier, values of α in the range $\alpha^{(n)}(G_0) < \alpha < \alpha^{(n-1)}(G_0)$ correspond to n -ring solutions with non-small oscillating tails.

Remark Instead of fixing G_0 and varying α , we could also fix α and vary G_0 . In this case, the family of n -ring profiles is parameterized by $(\alpha, G_0^{(n)}(\alpha))$, where $G_0^{(n)}(\alpha)$ is the value of G_0 that gives rise to the n -ring solution with a minimal tail.

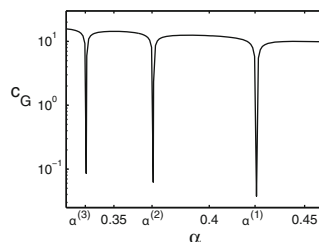


Fig. 11.3 c_G as a function of α , for solutions of (11.29) with $G(0) = 5 \times 10^{-4}$. From [73]

⁸ i.e., calculating c_G as a function of α , and finding the minimum points $\alpha^{(n)}$.

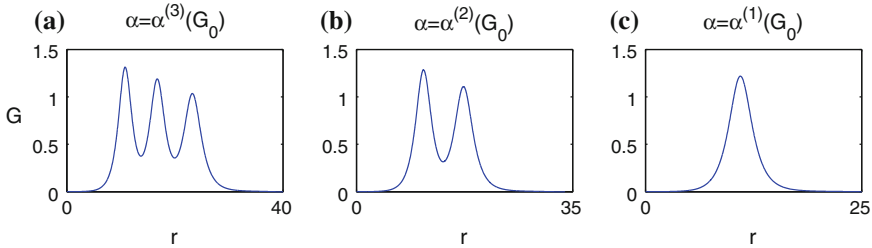


Fig. 11.4 Solutions of (11.29) with $G(0) = 5 \times 10^{-4}$ and **a** $\alpha = \alpha^{(3)}(G(0)) \cong 0.335$, **b** $\alpha = \alpha^{(2)}(G(0)) \cong 0.37$, **c** $\alpha = \alpha^{(1)}(G(0)) \cong 0.424$. From [73]

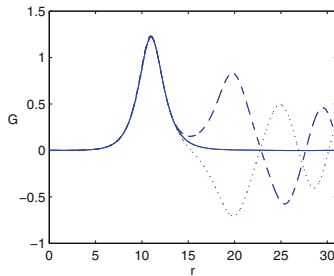


Fig. 11.5 Solutions of (11.29) with $G(0) = 5 \times 10^{-4}$ and $\alpha = \alpha^{(1)} \cong 0.424$ (solid), $\alpha = \alpha^{(1)} + 0.01$ (dotted), and $\alpha = \alpha^{(1)} - 0.01$ (dashed). From [73]

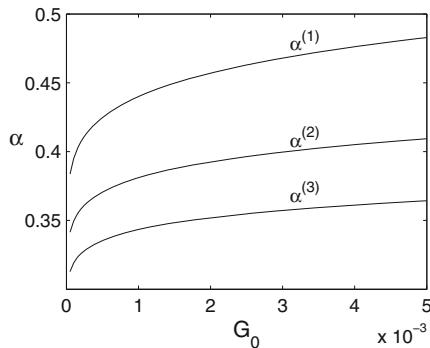


Fig. 11.6 The curves $\alpha^{(n)}(G_0)$ that correspond to n -ring solutions of (11.29). From [73]

Remark Figure 11.4 might lead to the misperception that n -ring solutions do not have an oscillatory tail. This, however, is incorrect, as the value of c_G cannot vanish at the minimum points. Indeed, we already noted that if $c_G = 0$ then $G \equiv 0$. The reason we do not see the tails in Fig. 11.4 is that they are of magnitude $\frac{c_G}{r} \approx \frac{0.1}{25} = O(0.001)$. Indeed, the oscillatory tails are clearly observed once we re-plot Fig. 11.4 on a semi-logarithmic scale (Fig. 11.7).

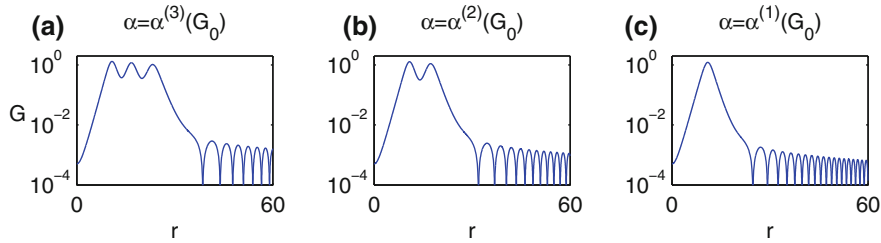


Fig. 11.7 Same as Fig. 11.4, but on a semi-logarithmic scale

11.2.5 Single-Ring Profiles

The one-parameter family of single-ring solutions of (11.4) can be parameterized by G_0 , so that $G(0) = G_0$ and $\alpha = \alpha^{(1)}(G_0)$.⁹ We now discuss how these solutions vary with G_0 .

Ring Peak (r_{\max})

We first ask how the location of the ring peak $r_{\max} := \arg \max_r |G(r)|$ varies with G_0 . In Sect. 11.2.2 we saw that when $0 < G_0 \ll 1$,

$$G(r) \approx G_0 f(r), \quad 0 \leq r \ll 1,$$

where f is the monotonically-increasing solution of (11.27). Therefore, intuitively, as G_0 becomes smaller, it takes a longer distance for G to reach the ring peak, hence r_{\max} increases.

The functional relation between r_{\max} and G_0 is as follows:

Conclusion 11.1

$$G_0 \sim \frac{c}{f(r_{\max})}, \quad c = O(1). \quad (11.35)$$

Proof We give a very informal derivation, which is based on two assumptions:

1. In the ring region, the nonlinearity $|G|^{\frac{4}{d}} G$ becomes comparable to the linear term G in the G equation, because otherwise it will not be able to arrest the exponential increase of the linear solution. Therefore, $G = O(|G|^{\frac{4}{d}} G)$.
2. In the ring region, we can still use the approximation $G(r) \approx G_0 f(r)$. Of course, this approximation does not hold at r_{\max} . It does hold, however, as the linear solution “just enters” the ring region.

⁹ See e.g., the top curve in Fig. 11.6.

From the first assumption we get that $|G|^{\frac{4}{d}} = O(1)$. Therefore, $G = O(1)$,¹⁰ and so the second assumption yields $G_0 f(r_{\max}) = O(1)$. \square

Although the derivation of (11.35) is quite informal, this relation appears to be in good agreement with numerical simulations. For example, when $d = 2$, then $f = I_0(r)$, the solution of (11.28). In this case, the approximation

$$G_0 \approx \frac{3.6}{I_0(r_{\max})} \quad (11.36)$$

turns out to be quite accurate (Fig. 11.8a). In addition, since $I_0(r) \sim e^r / \sqrt{2\pi r}$ for $r \gg 1$, we can replace (11.36) with

$$G_0 \approx 3.6 \frac{\sqrt{2\pi r_{\max}}}{e^{r_{\max}}}. \quad (11.37)$$

This approximation is also quite accurate (Fig. 11.8a).

By relation (11.35), $r_{\max} \sim f^{-1}\left(\frac{c}{G_0}\right)$. We can simplify this relation as follows:

Corollary 11.4 *If $0 < G_0 \ll 1$, then $r_{\max} \sim \log \frac{1}{G_0} \gg 1$.*

Proof If $0 < G_0 \ll 1$, then $f(r_{\max}) \gg 1$, see (11.35). Since $f(0) = 1$, this implies that $r_{\max} \gg 1$. By Exercise 6.10, $f(r) \sim cr^{-\frac{d-1}{2}}e^r$ for $r \gg 1$. Therefore, taking the log of relation (11.35) gives

$$\log \frac{1}{G_0} \sim \log(f(r_{\max})) \sim r_{\max}. \quad \square$$

It is interesting to note that while both r_{\max} and $\gamma = \frac{\alpha^4}{16}$ vary with G_0 , the value of $\gamma r_{\max}^2 = \frac{\alpha^4 r_{\max}^2}{16}$ is essentially independent of G_0 (Fig. 11.8b). Thus, as G_0 varies by a factor of 50 between 10^{-5} and 5×10^{-4} , γr_{\max}^2 varies between 0.245 and 0.248. Therefore, when $d = 2$, a reasonable approximation is

$$r_{\max} \approx 0.5\gamma^{-\frac{1}{2}}. \quad (11.38)$$

Ring Power (P_{ring})

We now consider the ring power as a function of G_0 . Of course, the power of G is infinite, because of the slow algebraic decay of its tail (Corollary 11.2). We can, however, define the ring power as the power of G in the ring region, i.e., between

¹⁰ The conclusion that $G = O(1)$ in the ring region also follows from (11.31).

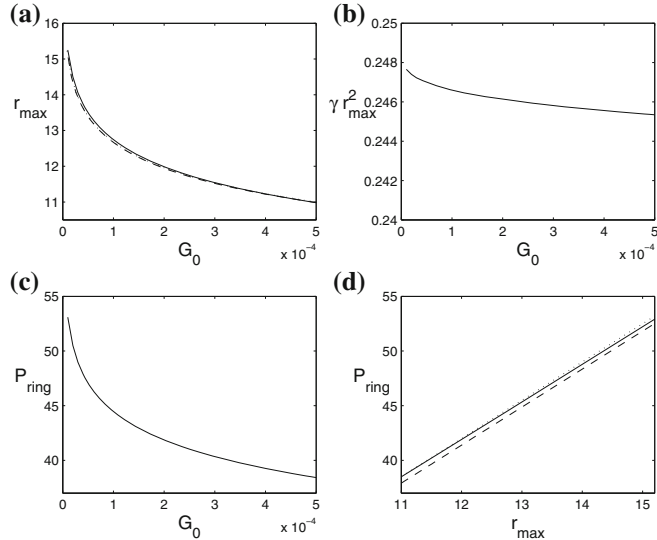


Fig. 11.8 Single-ring solutions of (11.29) with $G(0) = G_0$ and $\alpha = \alpha^{(1)}(G_0)$. **a** r_{\max} as a function of G_0 (*solid*). The *dashed* and *dotted* lines are approximations (11.36) and (11.37), respectively. **b** γr_{\max}^2 as a function of G_0 . **c** P_{ring} as a function of G_0 . **d** P_{ring} as a function of r_{\max} (*solid*). The *dashed* and *dotted* lines are approximation (11.39) and $P_{\text{ring}} \approx 3.5r_{\max}$, respectively

$r = 0$ and the transition point $r_{\text{transition}}$ where the coefficient of G in (11.29) changes its sign, i.e.,

$$P_{\text{ring}} := \int_0^{r_{\text{transition}}} |G|^2 r^{d-1} dr, \quad r_{\text{transition}} = \gamma^{-\frac{1}{2}} = \frac{4}{\alpha^2}.$$

For example, when $d = 2$, then $r_{\text{transition}} \approx 2r_{\max}$, see (11.38).

Clearly, P_{ring} is finite. To approximate it, we note that the ring power is mostly concentrated near the ring peak, where G is well approximated by (11.31). Hence,

$$\begin{aligned} P_{\text{ring}} &\approx \int_{r=0}^{\frac{4}{\alpha^2}} \left(1 + \frac{2}{d}\right)^{\frac{d}{2}} \lambda^d \operatorname{sech}^d(\lambda(r - r_{\max})) r^{d-1} dr \\ &\approx \left(1 + \frac{2}{d}\right)^{\frac{d}{2}} \int_{\tilde{r}=0}^{\frac{4\lambda}{\alpha^2}} \operatorname{sech}^d(\tilde{r} - \lambda r_{\max}) \tilde{r}^{d-1} d\tilde{r} \\ &\approx \left(1 + \frac{2}{d}\right)^{\frac{d}{2}} (\lambda r_{\max})^{d-1} \int_{-\infty}^{\infty} \operatorname{sech}^d(\tilde{r}) d\tilde{r}, \end{aligned}$$

where $\lambda = (1 - \gamma r_{\max}^2)^{\frac{1}{2}}$. For example, when $d = 2$, then $\int_{-\infty}^{\infty} \operatorname{sech}^2(r) dr = 2$.

Therefore,

$$P_{\text{ring}} \approx 4 \left(1 - \gamma r_{\max}^2\right)^{\frac{1}{2}} r_{\max}, \quad d = 2. \quad (11.39)$$

This approximation is in good agreement with numerical simulations (Fig. 11.8d). In addition, since $\gamma r_{\max}^2 \approx 0.246$, see Fig. 11.8b, approximation (11.39) is equivalent to $P_{\text{ring}} \approx 3.47r_{\max}$. Numerical simulations (Fig. 11.8d) show that $P_{\text{ring}} \approx 3.5r_{\max}$, and that approximation (11.39) has a 1%–2% error.

The above results show that, as expected, P_{ring} increases with r_{\max} . Since r_{\max} decreases with G_0 (Fig. 11.8a), this implies that the ring power decreases with G_0 , as is confirmed in Fig. 11.8c.

Rescaled Single-Ring Profiles $G_{\text{rescaled}}(r)$

Let ψ_G^{explicit} be given by (11.14). If we apply to it the dilation symmetry $\psi(z, r) \rightarrow \omega^{\frac{d}{4}} \psi(\omega z, \sqrt{\omega}r)$, see Sect. 8.1, we get the explicit blowup solution

$$\psi_{G_\omega}^{\text{explicit}}(z, r) = \frac{1}{L_{\omega}^{\frac{d}{2}}(z)} G_\omega(\rho) e^{i\zeta_\omega(z) - i\alpha^2 \omega \frac{\rho^2}{8}}, \quad (11.40)$$

where

$$L_\omega(z) = \alpha(Z_c - \omega z)^{\frac{1}{2}}, \quad \rho = \frac{\sqrt{\omega}r}{L_\omega(z)}, \quad \zeta_\omega(z) = \int_0^{\omega z} \frac{ds}{L_\omega^2(s)},$$

and $G_\omega(\rho) = \omega^{\frac{d}{4}} G(\sqrt{\omega}\rho)$. The function $G_\omega(r)$ is the solution of

$$G_\omega''(r) + \frac{d-1}{r} G_\omega' - \omega G_\omega + |G_\omega|^{\frac{4}{d}} G_\omega + \omega \frac{\alpha^4}{16} G_\omega = 0, \quad 0 < r < \infty,$$

subject to

$$G_\omega(0) = \omega^{\frac{d}{4}} G(0), \quad G_\omega'(0) = 0.$$

Remark In Sects. 11.4.1 and 19.2.1 we will search for the single-ring profile that provides the best fit to the self-similar profile of a collapsing ring-type NLS solution. A priori, this fitting involves a two-parameter search, since single-ring G_ω profiles depend on G_0 (or on α), and on ω . The fitting procedure can be simplified, however, by “factoring out” the dilation parameter ω , as follows. We define the rescaled ring profile

$$G_{\text{rescaled}}(r) := L^{\frac{d}{2}} G\left(\frac{r}{L}\right). \quad (11.41a)$$

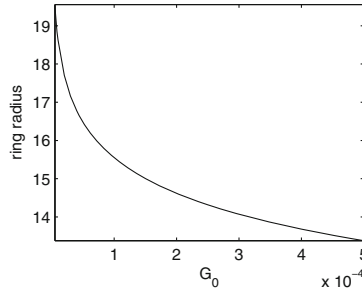


Fig. 11.9 r_{\max} as a function of G_0 for the rescaled single-ring profiles G_{rescaled} . From [73]

There are various ways for choosing L . For example, the choice

$$L = \left(\max_r |G| \right)^{-\frac{2}{d}} \quad (11.41b)$$

implies that $\|G_{\text{rescaled}}\|_\infty = 1$, i.e., that all rescaled rings have a maximal amplitude of 1. Since $G_{\omega, \text{rescaled}}$ is independent of ω , it only depends on G_0 . Figure 11.9 shows the ring radius r_{\max} of the rescaled G profiles, as a function of G_0 . As expected, r_{\max} is monotonically decreasing in G_0 . Therefore, the rescaled G profiles can be parameterized by their value of r_{\max} , which is convenient for the fitting procedure.

11.3 Blowup Rate of Non- H^1 Solutions

Intuitively, we would like to say that ψ_G^{explicit} blows up as $z \rightarrow Z_c$. Because G is not in H^1 , however, ψ_G^{explicit} is not in H^1 . Therefore, we cannot say that ψ_G^{explicit} blows up in H^1 as $z \rightarrow Z_c$, see Definition 5.6. Recall, however, that a finite H^1 norm implies a finite $L^{2\sigma+2}$ norm (Lemma 5.3), and blowup of the H^1 norm implies blowup of the $L^{2\sigma+2}$ norm (Corollary 5.6). Therefore, we can also define blowup as follows:

Definition 11.1 (blowup in $L^{2\sigma+2}$) *We say that ψ blows up in $L^{2\sigma+2}$ at Z_c , if $\|\psi\|_{2\sigma+2} < \infty$ for $0 \leq z < Z_c$ and $\lim_{z \rightarrow Z_c} \|\psi\|_{2\sigma+2} = \infty$.*

In the case of H^1 solutions, Definition 11.1 is equivalent to Definition 5.6. Definition 11.1, however, applies also to NLS solutions which are in $L^{2\sigma+2}$ but not in H^1 , such as ψ_G^{explicit} .

If ψ is in $L^{2\sigma+2}$ but not in H^1 , one cannot define the blowup rate as the rate at which $1/\|\nabla\psi\|$ goes to zero. One can, however, use the alternative definition of the blowup rate $l(z) = ((\sigma + 1)/\|\psi\|_{2\sigma+2}^{2\sigma+2})^{\frac{1}{2}}$, see Sect. 13.1. Since

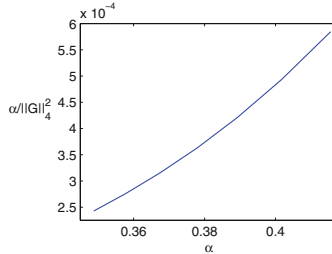


Fig. 11.10 The value of $\alpha/\|G\|_4^2$ as a function of α , for single-ring solutions of (11.29) with $\gamma = \alpha^4/16$ and $d = 2$

$$\frac{1}{\|\psi_G^{\text{explicit}}\|_{2\sigma+2}^{\sigma+1}} = \frac{L(z)}{\|G\|_{2\sigma+2}^{\sigma+1}}, \quad \|G\|_{2\sigma+2}^{2\sigma+2} < \infty$$

and $L(z)$ has a square-root blowup rate, we have

Lemma 11.9 ψ_G^{explicit} is an explicit solution of the critical NLS (11.2) that blows up in $L^{2\sigma+2}$ as $z \rightarrow Z_c$ at a square-root blowup rate, i.e.,

$$l(z) \sim \kappa \sqrt{Z_c - z}, \quad z \rightarrow Z_c.$$

Remark The value of κ is not universal, i.e., it depends on the initial condition. For example, when ψ_G^{explicit} is given by (11.14),

$$l(z) = \left(\frac{\sigma + 1}{\|\psi_G^{\text{explicit}}\|_{2\sigma+2}^{\sigma+1}} \right)^{\frac{1}{2}} = \frac{\sqrt{\sigma + 1} L(z)}{\|G\|_{2\sigma+2}^{\sigma+1}} = \frac{\sqrt{\sigma + 1} \alpha}{\|G\|_{2\sigma+2}^{\sigma+1}} \sqrt{Z_c - z}.$$

Figure 11.10 shows that $\frac{\alpha}{\|G\|_{2\sigma+2}^{\sigma+1}}$ depends on $G(0)$. Therefore, κ is not universal.

Remark If $G \not\equiv 0$, then $G(0) \neq 0$, and so

$$|\psi_G^{\text{explicit}}(z, r=0)| = \frac{G(0)}{L^{\frac{d}{2}}(z)} \rightarrow \infty, \quad z \rightarrow Z_c. \quad (11.42)$$

Therefore, although $\max_{0 \leq r < \infty} \psi_G^{\text{explicit}}(z, r) \gg \psi_G^{\text{explicit}}(z, 0)$, the value of ψ_G^{explicit} at the origin also goes to infinity. This is different from singular vortex solutions, which also have a ring shape, but for which ψ vanishes at the origin (Chap. 15).

11.4 Stability of ψ_G^{explicit}

In this section we investigate numerically the stability of ψ_G^{explicit} . We show that when G is a multi-ring solution, ψ_G^{explicit} is unstable under radial perturbations. When G is a single-ring solution, ψ_G^{explicit} is stable under radial perturbations, but unstable under azimuthal perturbations.

11.4.1 Radial Stability

We first consider the stability of ψ_G^{explicit} under radial perturbations, i.e., its stability as a solution of the radial critical NLS (11.2). Figure 11.11 shows the numerical solution of the two-dimensional radial critical NLS

$$i\psi_z(z, r) + \psi_{rr} + \frac{1}{r}\psi_r + |\psi|^2\psi = 0, \quad 0 < r < \infty, \quad (11.43a)$$

$$\psi_r(z, 0) = 0, \quad \psi(0, r) = \psi_0(r), \quad (11.43b)$$

where $\psi_0 = \psi_{G,0}^{\text{explicit}}$, see (11.17), and G is a single-ring solution of (11.29). The analytic solution is given by ψ_G^{explicit} , see (11.16). As expected, the numerical solution collapses with a ring profile (Fig. 11.11a). To confirm that the numerical solution remains self-similar, we rescale it as

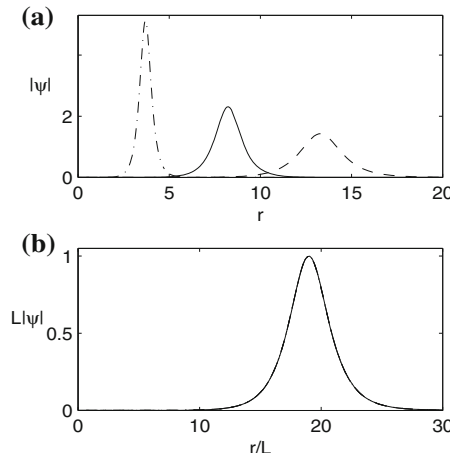


Fig. 11.11 **a** Solution of (11.43) with $\psi_0 = \psi_{G,0}^{\text{explicit}}$, at $z = 2.1$ (dashes), $z = 5.6$ (solid) and $z = 7.4$ (dash-dots). **b** The three lines from (a), rescaled according to (11.44) with $L^{-1} = 1.2, 1.9$, and 4.2 , respectively. Also plotted is the rescaled solution at focusing levels of $L^{-1}(z) = 2.2 \times 10^8$ (dots) and $L^{-1}(z) = 3.5 \times 10^{15}$ (dash-dots). All five lines are indistinguishable. From [73]

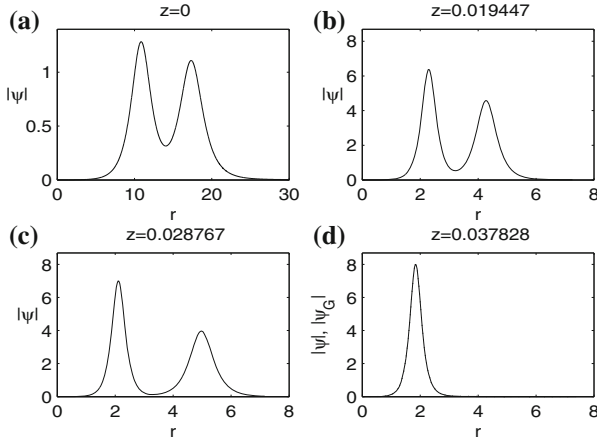


Fig. 11.12 Dynamics of a double-ring solution (*solid*). **a** $z = 0$; **b** $z = 0.019447$; **c** $z = 0.028767$; **d** $z = 0.037828$. *Dotted line* in **(d)** is the best-fitting single-ring profile $|\psi_G| = L^{-1}G\left(\frac{r}{L}\right)$; the two lines are indistinguishable. From [73]

$$\psi_{\text{rescaled}}(z, r) = L^{\frac{d}{2}}(z)\psi\left(\frac{r}{L(z)}\right), \quad L(z) = \left(\max_r |\psi|\right)^{-\frac{2}{d}}. \quad (11.44)$$

The rescaled solution remains unchanged while focusing by 10^{15} , see Fig. 11.11b, showing that the numerical solution indeed maintains the self-similar ring collapse of ψ_G^{explicit} .

In Fig. 11.12 we solve (11.43) with $\psi_0 = \psi_{G,0}^{\text{explicit}}$, where G is a double-ring solution of (11.29). The numerical solution initially remains close to the analytical solution ψ_G^{explicit} . After focusing by a factor of 5, the outer ring begins to diffract, and eventually ψ collapses with a single-ring profile (Fig. 11.12d). Similar results were observed when G had a triple-ring profile [73]. The simulations with the multi-ring profiles were conducted with the same numerical method and numerical parameters (e.g., grid resolution) as in Fig. 11.11. The fact that the single-ring solution maintained its self-similar profile in the presence of numerical noise while focusing by 10^{15} , whereas the multi-ring solutions disintegrated after focusing by 5, suggests

Observation 11.1 ([73]) *Single-ring solutions are radially stable, but multi-ring solutions are radially unstable.*

To further show the radial stability of single-ring solutions, we randomly perturbed the single-ring initial condition from Fig. 11.11 as

$$\psi_0^{\text{noise}} = (1 + \varepsilon_1(r))\psi_{G,0}^{\text{explicit}} + \varepsilon_2(r), \quad (11.45)$$

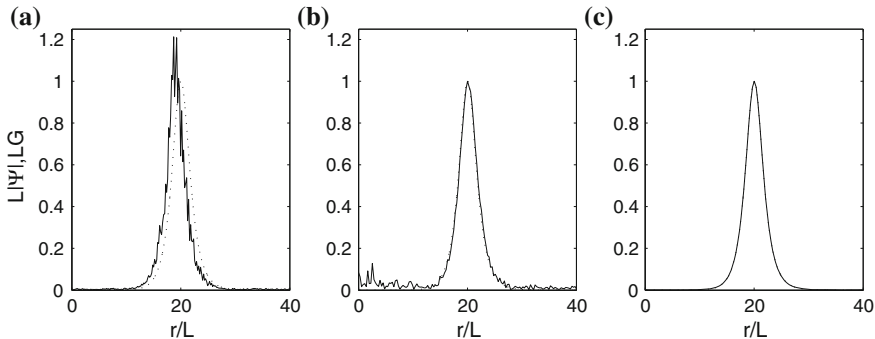


Fig. 11.13 Solution of the NLS (11.43) with the noisy initial condition (11.45); *solid line*. The *dotted line* is the G profile with $G_0 = 3.5 \times 10^{-6}$. Results are rescaled according to Eq. (11.44). **a** $z = 0$ ($L^{-1} = 1$); **b** $z \approx 5.9$ ($L^{-1} = 1.8$); **c** $z \approx 7.6$ ($L^{-1} = 150$). From [73]

where ε_1 and ε_2 are uniformly distributed in $[-0.25, 0.25]$ and $[-0.05, 0.05]$, respectively (Fig. 11.13a). After focusing by less than 2, the noise in the ring region (i.e., the area of high nonlinearity) disappears (Fig. 11.13b). Subsequently, the noise at the inner and outer regions slowly decreases, so that after focusing by 150, the solution approaches a clean ring profile. This simulation further suggests that the single-ring ψ_G^{explicit} is an attractor in the radial case.¹¹

Comparison with $\psi_{R^{(n)}}^{\text{explicit}}$

In Sect. 10.6 we saw that the explicit singular solutions $\psi_{R^{(n)}}^{\text{explicit}}$ are unstable under radial perturbations for any n . This is different from the explicit singular solutions ψ_G^{explicit} , which are radially unstable when G is a multi-ring, but stable when G is a single-ring. This difference may be related to the fact that $\{\psi_{R^{(n)}}^{\text{explicit}}\}_{n=0}^\infty$ have quantized powers $\{\|R^{(n)}\|_2^2\}_{n=0}^\infty$, whereas ψ_G^{explicit} is a one-parameter family of solutions, whose ring power P_{ring} varies continuously with G_0 (Sect. 11.2.5). Therefore, unlike $\psi_{R^{(n)}}^{\text{explicit}}$, when ψ_G^{explicit} is perturbed, it can collapse with a slightly different self-similar ring profile (as, e.g., in Fig. 11.13).¹²

¹¹ In the absence of noise, the radius of the (rescaled) G profile is $\rho_{\max} \approx 19$ (Fig. 11.11b). Once noise is added, however, the solution approaches a different G profile with $\rho_{\max} \approx 20$ (Fig. 11.13c). This is because the noise used in this simulation increases the input power. Therefore, the solution collapses with a self-similar ring profile that has more power, hence a larger radius (Sect. 11.2.5).

¹² The fact that the perturbed solution in Fig. 11.13 collapses with a different single-ring profile (Footnote 11), does not imply that ψ_G^{explicit} is unstable, because perturbations of a stable singular solution are allowed to lead to a continuous change of the blowup profile (Sect. 10.5).

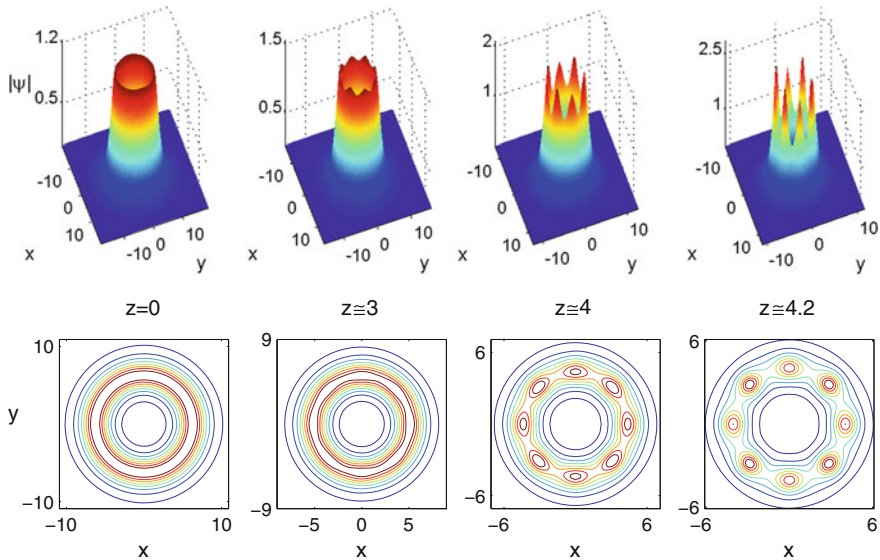


Fig. 11.14 Solution of the NLS (11.46) with the slightly-elliptic single-ring initial condition (11.47). **Top** surface plot. **Bottom** level sets of $|\psi|$. From [73]

11.4.2 Azimuthal Instability

In Sect. 11.4.1 we saw that the single-ring ψ_G^{explicit} is stable as a solution of the radial critical NLS (11.2). We now ask whether ψ_G^{explicit} is also stable as a solution of the critical NLS (11.1), i.e., under non-radial perturbations.

In Fig. 11.14 we solve the two-dimensional critical NLS

$$i\psi_z(z, x, y) + \Delta\psi + |\psi|^2\psi = 0, \quad \psi(0, x, y) = \psi_0(x, y), \quad (11.46)$$

with the slightly-elliptic single-ring initial condition¹³

$$\psi_0(x, y) = \psi_{G,0}^{\text{explicit}} \left(r = \sqrt{x^2 + 1.01y^2} \right). \quad (11.47)$$

As the ring becomes higher and narrower, it breaks into eight filaments located along a circle $r = r_{\text{fil}}$. Therefore, we conclude that ψ_G^{explicit} is unstable under azimuthal perturbations.

Remark In Sect. 11.5 we will show *asymptotically* that all collapsing rings are azimuthally unstable.

¹³ See Sect. 9.7 for the advantage of using a *deterministic* azimuthal perturbation.

Remark Although ψ_0 is only 1% elliptic, the azimuthal instability develops after the solution focuses by ≈ 1.5 , i.e., much faster than the self-focusing process. See Sect. 11.5 for further discussion.

Remark The eight filaments consist of a pair of identical filaments located at $(\pm r_{\text{fil}}, 0)$, another pair of identical filaments located at $(0, \pm r_{\text{fil}})$, and a quadruple of identical filaments located at $(\pm x_{\text{fil}}, \pm y_{\text{fil}})$ such that $x_{\text{fil}}^2 + y_{\text{fil}}^2 = r_{\text{fil}}^2$. This filamentation pattern is typical for elliptic input beams (Sect. 25.3.2).

11.4.3 Non-integer d

The explicit solution ψ_G^{explicit} can also be defined for non-integer values of d . For example, (radial) stability of the single-ring ψ_G^{explicit} was observed numerically for the critical radial NLS (11.2) with $d = 7/4$ in [74]. Since there is no notion of azimuthal stability when d is not an integer, these single-ring ψ_G^{explicit} solutions are stable “without any disclaimer”.

11.5 Azimuthal Instability of Collapsing Rings

In [244, 245], Soto-Crespo et al. developed a perturbation method, the *Approximate Modulational Instability (AMI) method*, for analyzing the azimuthal instability of stationary ring solutions (Sect. 15.8.3). Subsequently, Fibich and Gavish extended the AMI method to collapsing solutions, and showed that any collapsing self-similar ring solution is azimuthally unstable:

Lemma 11.10 ([72]) *Let $\psi_G(z, r)$ be a collapsing self-similar ring-type solution of the two-dimensional critical NLS (11.46), such that*

$$|\psi_G| \sim \frac{1}{L(z)} G(\rho), \quad \rho = \frac{r}{L(z)}, \quad (11.48)$$

and $G(\rho)$ is a ring profile. Then ψ_G is azimuthally unstable.

Proof We give an informal proof. Consider the perturbed initial condition

$$\psi_0(r, \theta) = \left(1 + \mu \cos(k\theta)\right) \psi_G(z = 0, r), \quad |\mu| \ll 1,$$

where $k = 1, 2, \dots$ is the frequency of the perturbation. Let us look for a solution of the form

$$\psi(z, r, \theta) = \left(1 + \mu \cos(k\theta) e^{\delta_k \zeta(z)} + O(\mu^2)\right) \psi_G(z, r), \quad \zeta = \int_0^z \frac{ds}{L^2}, \quad (11.49)$$

where δ_k is the growth rate of the k th mode. If $\delta_k > 0$ the k th mode will grow, if $\delta_k < 0$ it will decay, and if δ_k is imaginary it will neither grow nor decrease. Since we want to know to prove that there are unstable modes, in what follows we will show that there exist solutions of the form (11.49) for which δ_k is real and positive.

Substituting (11.49) in (11.46), denoting $C = \cos(k\theta)e^{\delta_k\zeta(z)}$ and $\mu = \mu_r + i\mu_i$, and using the relations

$$\begin{aligned} i\psi_z &= i(1 + \mu C)(\psi_G)_z + i\mu C\psi_G \frac{\delta_k}{L^2} + O(\mu^2), \\ \Delta\psi &= \Delta_r\psi + \frac{1}{r^2}\psi_{\theta\theta} = (1 + \mu C)\Delta_r\psi_G - \frac{k^2}{r^2}\mu C\psi_G + O(\mu^2) \\ &= (1 + \mu C)\Delta\psi_G - \frac{k^2}{L^2\rho^2}\mu C\psi_G + O(\mu^2), \\ |\psi|^2\psi &= |\psi_G(1 + \mu C)|^2\psi_G(1 + \mu C) + O(\mu^2) \\ &= |\psi_G|^2\psi_G(1 + \mu C)^2(1 + \mu^*C) + O(\mu^2) \\ &= |\psi_G|^2\psi_G(1 + 2\mu C)(1 + \mu^*C) + O(\mu^2) \\ &= |\psi_G|^2\psi_G(1 + 2\mu C + \mu^*C) + O(\mu^2) \\ &= |\psi_G|^2\psi_G(1 + \mu C + 2\mu_r C) + O(\mu^2), \end{aligned}$$

we obtain

$$\begin{aligned} &\underbrace{i\frac{d}{dz}\psi_G(z, r, \theta) + \Delta\psi_G + |\psi_G|^2\psi_G}_{=0} \\ &+ \mu \cos(k\theta)e^{\delta_k\zeta} \left[\underbrace{i\frac{d}{dz}\psi_G + \Delta\psi_G + |\psi_G|^2\psi_G}_{=0} + i\frac{\delta_k}{L^2(z)}\psi_G - \frac{k^2}{L^2(z)\rho^2}\psi_G \right] \\ &+ 2\mu_r \cos(k\theta)e^{\delta_k\zeta} |\psi_G|^2\psi_G = O(\mu^2). \end{aligned}$$

Balancing the $\mathcal{O}(\mu)$ terms and using (11.48) gives

$$(\mu_r + i\mu_i) \left(i\delta_k - \frac{k^2}{\rho^2} \right) + 2\mu_r |G|^2 = 0.$$

The equation for the real and imaginary parts reads¹⁴

¹⁴ Here we use the assumption that δ_k is real.

$$B \begin{pmatrix} \mu_r \\ \mu_i \end{pmatrix} = 0, \quad B = \begin{pmatrix} 2G^2(\rho) - \left(\frac{k}{\rho}\right)^2 & -\delta_k \\ \delta_k & -\left(\frac{k}{\rho}\right)^2 \end{pmatrix}.$$

A non-trivial solution exists only if $|B| = 0$, from which it follows that

$$\delta_k = \pm \frac{k}{\rho} \sqrt{2G^2(\rho) - \left(\frac{k}{\rho}\right)^2}.$$

The above result is inconsistent with the initial ansatz (11.49), in which δ_k does not depend on ρ . Nevertheless, one can argue that since the ring is localized around its peak at $\rho_{\max} := \arg \max G(\rho)$, one can replace ρ with its “average value” in the ring region, i.e.,

$$\delta_k = \pm \frac{k}{\rho_{\text{avg}}} \sqrt{2G^2(\rho_{\text{avg}}) - \left(\frac{k}{\rho_{\text{avg}}}\right)^2}, \quad \rho_{\text{avg}} \approx \rho_{\max}. \quad (11.50)$$

We thus see that for

$$0 < k \leq \sqrt{2\rho_{\text{avg}} G(\rho_{\text{avg}})}, \quad (11.51)$$

there exist a solution of the form (11.49), for which the growth rate δ_k is positive. Since generically $G(\rho_{\text{avg}}) \approx G(\rho_{\max}) = O(1)$ and $\rho_{\text{avg}} \approx \rho_{\max} \gg 1$, see (11.34) and Corollary 11.4, the $k = 1$ mode is always in the instability regime (11.51). Therefore, the collapsing ring is azimuthally unstable. \square

Interestingly, the unstable modes are the low frequencies and not the high ones, see (11.51).¹⁵ This observation explains why the addition of 1% ellipticity, which mainly excites the low frequencies, could lead to the “dramatic” azimuthal instability observed in Fig. 11.14.

Equation (11.50) shows that δ_k^2 is a parabola in $\left(\frac{k}{\rho_{\text{avg}}}\right)^2$ that vanishes at $\left(\frac{k}{\rho_{\text{avg}}}\right)^2 = 0$ and $\left(\frac{k}{\rho_{\text{avg}}}\right)^2 = 2G^2$. Hence, the maximum of δ_k^2 is attained at $\left(\frac{k}{\rho_{\text{avg}}}\right)^2 = G^2$. Since k has to be an integer, the fastest-growing mode is given by the integer which is the closest to $\rho_{\text{avg}} G(\rho_{\text{avg}})$. This value thus provides a quantitative prediction for the number of spikes (filaments) of the collapsing ring, as was indeed confirmed in NLS simulations of collapsing rings [72].

Remark We can also explain the azimuthal instability of collapsing rings with the following informal argument. Let us break radial symmetry by adding a small initial hump, somewhere along the ring. Since the intensity is higher at the hump, power will be attracted towards the hump. As a result, the hump will focus faster than the rest of the ring, resulting in the formation of a spike. This type of instability dynamics can be seen in Fig. 22.9.

¹⁵ This is typical for a modulational instability (Sect. 3.6.3).

Chapter 12

The Explicit Supercritical Singular Peak-Type Solution ψ_Q^{explicit}

In this chapter we present the explicit singular peak-type solution ψ_Q^{explicit} of the supercritical NLS. Although ψ_Q^{explicit} is not in H^1 , the results of this chapter are relevant to peak-type H^1 solutions of the supercritical NLS that undergo a quasi self-similar collapse with the ψ_Q profile (Chap. 21), and also to H^1 solutions of the supercritical NLS with $\sigma > 2$ and $d > 1$ that undergo a standing-ring collapse (Sect. 22.4). As always, we assume that the NLS is H^1 -subcritical, see (5.2). Therefore, we consider the NLS

$$i\psi_z(z, \mathbf{x}) + \Delta\psi + |\psi|^{2\sigma}\psi = 0, \quad (12.1a)$$

where σ is in the L^2 -supercritical and H^1 -subcritical regime

$$\begin{cases} \frac{2}{d} < \sigma < \infty, & \text{if } d \leq 2, \\ \frac{2}{d} < \sigma < \frac{2}{d-2}, & \text{if } d > 2. \end{cases} \quad (12.1b)$$

12.1 Derivation of ψ_Q^{explicit}

We look for self-similar radial solutions of (12.1), such that

$$\psi(z, r) = \frac{1}{L^{\frac{1}{\sigma}}(z)} Q(\rho) e^{i\zeta(z)}, \quad \rho = \frac{r}{L(z)}.$$

It can be verified by direct substitution that the equation for Q is

$$\Delta_\rho Q(\rho) - L^2 \frac{d\zeta}{dz} Q - iLL_z \left(\frac{1}{\sigma} Q + \rho Q' \right) + |Q|^{2\sigma} Q = 0, \quad 0 < \rho < \infty, \quad (12.2)$$

where $\Delta_\rho := \frac{\partial^2}{\partial \rho^2} + \frac{d-1}{\rho} \frac{\partial}{\partial \rho}$. Since Q is only a function of ρ , this implies that there exist real constants λ and a such that

$$L^2 \frac{d\zeta}{dz} \equiv \lambda, \quad -\frac{1}{2} \left(L^2 \right)_z = -LL_z \equiv a. \quad (12.3)$$

Therefore,

1. $\frac{d\zeta}{dz} = \lambda L^{-2}$, and so $\zeta = \lambda \int_0^z L^{-2} dz$.
2. There exists a real number Z_c such that $L^2 = 2a(Z_c - z)$.
3. Equation (12.2) for Q can be rewritten as

$$\Delta_\rho Q(\rho) - \lambda Q + ia \left(\frac{1}{\sigma} Q + \rho Q' \right) + |Q|^{2\sigma} Q = 0, \quad 0 < \rho < \infty. \quad (12.4a)$$

Since Q is radial, it satisfies the initial conditions

$$Q(0) = Q_0 \in \mathbb{C}, \quad Q'(0) = 0. \quad (12.4b)$$

Hence, we have the following result, which is due to Zakharov:

Lemma 12.1 ([281]) *Let Q be a solution of (12.4), and let*

$$\psi_Q^{\text{explicit}}(z, r) = \frac{1}{L^{\frac{1}{\sigma}}(z)} Q(\rho) e^{i\zeta(z)}, \quad (12.5a)$$

where

$$L(z) = \kappa \sqrt{Z_c - z}, \quad \kappa = \sqrt{2a}, \quad (12.5b)$$

and

$$\rho = \frac{r}{L(z)}, \quad \zeta = \lambda \int_0^z \frac{ds}{L^2(s)} = \frac{\lambda}{2a} \log \frac{Z_c}{Z_c - z}. \quad (12.5c)$$

Then, ψ_Q^{explicit} is an explicit solution of the NLS (12.1).

From Eq. (12.5b) we have that $L(0) = \sqrt{2aZ_c}$. Therefore,

$$Z_c = \frac{L^2(0)}{2a}.$$

In particular, setting $L(0) = 1$ leads to

Corollary 12.1 *Let Q be a solution of (12.4). Then the solution of the NLS (12.1) with $\psi_0 = Q$ is given by (12.5) with*

$$L(z) = \sqrt{1 - 2az} = \sqrt{1 - \frac{z}{Z_c}}, \quad Z_c = \frac{1}{2a}.$$

Remark Equation (12.4) depends on two parameters: λ and a . Note, however, that

$$Q(\rho; \lambda, a) := \lambda^{\frac{1}{2\sigma}} \tilde{Q}\left(\lambda^{\frac{1}{2}}\rho; \tilde{a} = \lambda a\right),$$

where $\tilde{Q}(\rho; a)$ is the solution of (12.4) with $\lambda = 1$, i.e., of

$$\Delta_\rho Q(\rho) - Q + ia \left(\frac{1}{\sigma} Q + \rho Q' \right) + |Q|^{2\sigma} Q = 0, \quad 0 < \rho < \infty, \quad (12.6a)$$

subject to

$$Q(0) = Q_0 \in \mathbb{C}, \quad Q'(0) = 0, \quad (12.6b)$$

Therefore, without loss of generality, from now on we can set $\lambda = 1$.

Exercise 12.1 ([11]) In this exercise we derive an explicit solution of the supercritical biharmonic NLS

$$i\psi_z(z, \mathbf{x}) - \Delta^2\psi + |\psi|^{2\sigma}\psi = 0, \quad \sigma d > 4. \quad (12.7)$$

Let

$$\psi_{Q_B}^{\text{explicit}}(z, r) = \frac{1}{L^{\frac{2}{\sigma}}(z)} Q_B(\rho) e^{i\zeta(z)}, \quad \rho = \frac{r}{L(z)},$$

be a solution of (12.7).

1. Derive the equation for Q_B .
2. Derive and solve the equations for $L(z)$ and $\zeta(z)$.
3. Conclude that if

$$L(z) = \kappa(Z_c - z)^{\frac{1}{4}}, \quad \zeta = \lambda \int_0^z \frac{ds}{L^4(s)} = \frac{\lambda}{\kappa^4} \log \frac{Z_c}{Z_c - z},$$

and if Q_B is a solution of the biharmonic Q equation¹

$$-\Delta^2 Q_B(\rho) - \lambda Q_B + i \frac{\kappa^4}{4} \left(\frac{2}{\sigma} Q_B + \rho Q'_B \right) + |Q_B|^{2\sigma} Q_B = 0, \quad (12.8)$$

then $\psi_{Q_B}^{\text{explicit}}$ is an explicit solution of (12.7).

¹ Unlike Eq. (12.6), see Theorem 12.1, there is currently no proof that solutions of (12.8) exist.

12.2 Analysis of the Q Equation

For ψ_Q^{explicit} to be a singular solution, $L^2(z)$ should go to zero. By (12.3), this implies that $a > 0$. In addition, for ψ_Q^{explicit} to be a singular solution, the Q equation (12.6) with $a > 0$ should admit nontrivial solutions.

Existence and uniqueness of solutions of the Q equation were proved by Wang for $d = 3$ and $\sigma = 1$, by Johnson and Pan for $d \geq 3$ and $\frac{2}{d} < \sigma < \frac{2}{d-2}$, and by Budd, Chen, and Russell for $2 < d < 4$ and $\sigma = 1$:

Theorem 12.1 ([35, 136, 269]) *Consider Eq. (12.6) with σ in the L^2 -supercritical and H^1 -subcritical range (12.1b) and $a > 0$. Then for any $Q_0 \in \mathbb{C}$, this initial value problem has a unique solution for $0 \leq \rho < \infty$. In addition, $Q = O\left(\rho^{-\frac{1}{\sigma}}\right)$ as $\rho \rightarrow \infty$. In particular, Q decays to zero as $\rho \rightarrow \infty$.*

Proof Local existence and uniqueness follow from standard arguments, except for $d > 1$ near $\rho = 0$, where it can be shown as in Sect. 6.4. Global existence follows from the a priori bounds which we now derive.

Following Johnson and Pan [136], let

$$Q(\rho) = u(\rho)e^{-i\frac{ap^2}{4}}, \quad u(\rho) = u_1(\rho) + iu_2(\rho),$$

where u_1 and u_2 are real functions, let

$$\begin{aligned} v_j(\rho) &= \rho^{\frac{d-1}{2}} u_j(\rho), \quad j = 1, 2, \\ t &= \rho^2, \quad x_j(t) = v_j(\rho), \quad f_j(t) = t^{\frac{1}{4}} x_j(t), \quad g_j(t) = \frac{df_j}{dt}, \end{aligned}$$

and

$$H(t) = \frac{1}{2} \left(g_1^2 + g_2^2 \right) + \frac{1}{8} \left(\lambda - \frac{1}{t} - \frac{e}{t^2} \right) \left(f_1^2 + f_2^2 \right) + \frac{t^{-\beta} (f_1^2 + f_2^2)^{\sigma+1}}{4(2\sigma+2)}, \quad (12.9)$$

where

$$\lambda = \frac{a^2}{4} > 0, \quad \beta = 1 + \frac{\sigma d}{2} > 0, \quad e = \frac{1}{4}d(d-4).$$

It can be verified by direct differentiation that

$$H'(t) = \frac{B}{4t} (f_1 g_2 - f_2 g_1) + \frac{1}{8t^2} \left(1 + \frac{2e}{t} \right) (f_1^2 + f_2^2) - \frac{\beta t^{-\beta-1}}{4(2\sigma+2)} (f_1^2 + f_2^2)^{\sigma+1},$$

where $B = a \left(\frac{d}{2} - \frac{1}{\sigma} \right) > 0$. In addition, by the weighted Cauchy-Schwartz inequality (Appendix A),

$$|f_1 g_2| \leq \frac{1}{2} \left[\frac{\sqrt{\lambda}}{2} f_1^2 + \frac{2}{\sqrt{\lambda}} g_2^2 \right], \quad |f_2 g_1| \leq \frac{1}{2} \left[\frac{\sqrt{\lambda}}{2} f_2^2 + \frac{2}{\sqrt{\lambda}} g_1^2 \right].$$

Therefore, since $\beta > 0$ and $B > 0$,

$$\begin{aligned} H'(t) &\leq \frac{B}{4t}(|f_1g_2| + |f_2g_1|) + \frac{1}{8t^2} \left(1 + \frac{2e}{t}\right) (f_1^2 + f_2^2) \\ &\leq \frac{B}{8t} \left(\frac{\sqrt{\lambda}}{2} (f_1^2 + f_2^2) + \frac{2}{\sqrt{\lambda}} (g_1^2 + g_2^2)\right) + \frac{1}{8t^2} \left(1 + \frac{2e}{t}\right) (f_1^2 + f_2^2) \\ &= \frac{B}{2\sqrt{\lambda}t} \left(\frac{\lambda}{8} (f_1^2 + f_2^2) + \frac{1}{2} (g_1^2 + g_2^2)\right) + \frac{1}{8t^2} \left(1 + \frac{2e}{t}\right) (f_1^2 + f_2^2) \\ &\leq \frac{B}{2\sqrt{\lambda}t} \left(1 + O\left(\frac{1}{t}\right)\right) H(t). \end{aligned}$$

By (12.9), there exists $t_0 \gg 1$, such that $H(t) > 0$ for $t \geq t_0$. Therefore,

$$\frac{H'}{H} \leq \frac{B}{2\sqrt{\lambda}t} + O\left(\frac{1}{t^2}\right).$$

Integrating this inequality between t_0 and t gives

$$\ln(H(t)) - \ln(H(t_0)) \leq \frac{B}{2\sqrt{\lambda}} (\ln t - \ln t_0) + C \left(\frac{1}{t_0} - \frac{1}{t}\right).$$

Therefore,

$$\ln(H(t)) \leq \frac{B}{2\sqrt{\lambda}} \ln t + \ln(H(t_0)) + \frac{C}{t_0},$$

and so

$$H(t) \leq c(t_0)t^{2\alpha}, \quad t_0 \leq t < \infty,$$

where

$$2\alpha = \frac{B}{2\sqrt{\lambda}} = \frac{d}{2} - \frac{1}{\sigma} > 0.$$

Hence,

$$|f_j(t)| \leq \tilde{c}(t_0) t^\alpha, \quad t_0 \leq t < \infty.$$

Therefore, there exists $c > 0$ such that

$$|f_j(t)| \leq c (1 + t^\alpha), \quad 0 \leq t < \infty,$$

$$|x_j(t)| \leq ct^{-\frac{1}{4}} (1 + t^\alpha), \quad 0 \leq t < \infty,$$

$$|v_j(\rho)| \leq c\rho^{-\frac{1}{2}} (1 + \rho^{2\alpha}), \quad 0 \leq \rho < \infty,$$

and

$$|u_j(\rho)| \leq c\rho^{-\frac{d}{2}} \left(1 + \rho^{2\alpha}\right) = c\rho^{-\frac{d}{2}} \left(1 + \rho^{\frac{d}{2} - \frac{1}{\sigma}}\right), \quad 0 \leq \rho < \infty.$$

Hence, $|u| = O(\rho^{-\frac{1}{\sigma}})$ as $\rho \rightarrow \infty$. \square

Remark If $Q(\rho)$ is a solution of (12.6), then so is $e^{i\alpha}Q(\rho)$ for any $\alpha \in \mathbb{R}$. Therefore, without loss of generality, we can assume that Q_0 is real.

The far-field asymptotics of Q was calculated by LeMesurier et al.:

Lemma 12.2 ([155]) *Let Q be a solution of (12.6), where σ is in the range (12.1b). Then*

$$Q(\rho) \sim c_1 Q_1(\rho) + c_2 Q_2(\rho), \quad \rho \rightarrow \infty,$$

where c_1 and c_2 are complex numbers, and

$$Q_1 = \rho^{-\frac{i}{a} - \frac{1}{\sigma}} \left(1 + O\left(\frac{1}{\rho^2}\right)\right), \quad Q_2 = e^{-i\frac{a\rho^2}{2}} \rho^{\frac{i}{a} - d + \frac{1}{\sigma}} \left(1 + O\left(\frac{1}{\rho^2}\right)\right).$$

Proof Equation (12.6) can be rewritten as

$$Q''(\rho) + \left(\frac{d-1}{\rho} + ia\rho\right) Q' - Q + ia\frac{1}{\sigma}Q + |Q|^{2\sigma}Q = 0.$$

To eliminate the first derivative, let

$$Q(\rho) = e^{-\frac{1}{2} \int \left(\frac{d-1}{\rho} + ia\rho\right)} Z(\rho) = e^{-i\frac{a\rho^2}{4}} \rho^{-\frac{d-1}{2}} Z(\rho).$$

The equation for Z reads

$$Z''(\rho) + \left(\frac{a^2}{4}\rho^2 - 1 - ia\frac{d\sigma - 2}{2\sigma} - \frac{(d-1)(d-3)}{4\rho^2}\right) Z + |Q|^{2\sigma}Z = 0.$$

By Theorem 12.1, $|Q| = O\left(\rho^{-\frac{1}{\sigma}}\right)$. Therefore,

$$Z''(\rho) + \left(\frac{a^2}{4}\rho^2 - 1 - ia\frac{d\sigma - 2}{2\sigma} + O\left(\frac{1}{\rho^2}\right)\right) Z = 0, \quad \rho \rightarrow \infty. \quad (12.10)$$

Let us look for an asymptotic solution of the form

$$Z = e^{w(\rho)}, \quad w(\rho) \sim w_0(\rho) + w_1(\rho) + \dots$$

The equation for $\{w_i(\rho)\}$ is

$$(w_0'' + w_1'' + \dots) + (w_0' + w_1' + \dots)^2 + \frac{a^2}{4}\rho^2 - 1 - ia\frac{d\sigma - 2}{2\sigma} = O\left(\frac{1}{\rho^2}\right).$$

A priori, the equation for the leading-order terms is

$$w_0'' + (w_0')^2 + \frac{a^2}{4}\rho^2 = 0.$$

The substitution $w_0 = c\rho^n$ shows that the orders of the terms in this equation are ρ^{n-2} , ρ^{2n-2} , and ρ^2 , respectively. The only consistent way to balance these terms is to set $n = 2$. Hence, the equation for the leading-order terms is

$$(w_0')^2 + \frac{a^2}{4}\rho^2 = 0.$$

Consequently,

$$w_0' = \pm \frac{ia}{2}\rho, \quad w_0 = \pm \frac{ia}{4}\rho^2.$$

The balance of the next-order terms is

$$w_0'' + 2w_0'w_1' - 1 - ia\frac{d\sigma - 2}{2\sigma} = 0.$$

Substituting $w_0' = \pm \frac{ia\rho}{2}$ and rearranging gives

$$w_1' = \mp \frac{i}{a\rho} \pm \frac{d\sigma - 2}{2\sigma} \frac{1}{\rho} - \frac{1}{2\rho}, \quad w_1 = \left(\mp \frac{i}{a} \pm \frac{d\sigma - 2}{2\sigma} - \frac{1}{2} \right) \log \rho.$$

The balance of the next-order terms is

$$w_1'' + (w_1')^2 + 2w_0'w_2' = O\left(\frac{1}{\rho^2}\right). \quad (12.11)$$

Substituting the expressions for w_0 and w_1 gives

$$w_2' = O\left(\frac{1}{\rho^3}\right), \quad w_2 = O\left(\frac{1}{\rho^2}\right).$$

Therefore, we obtained the two solutions

$$\begin{aligned} w^{(1)}(\rho) &= ia\frac{\rho^2}{4} + \left(-\frac{i}{a} - \frac{1-d}{2} - \frac{1}{\sigma} \right) \log \rho + O\left(\frac{1}{\rho^2}\right), \\ w^{(2)}(\rho) &= -ia\frac{\rho^2}{4} + \left(\frac{i}{a} + \frac{-1-d}{2} + \frac{1}{\sigma} \right) \log \rho + O\left(\frac{1}{\rho^2}\right). \end{aligned}$$

Substituting $Q_i(\rho) = e^{-i\frac{a\rho^2}{4}} \rho^{-\frac{d-1}{2}} e^{w^{(i)}(\rho)}$ leads to the result.

Finally, we note that this proof is rigorous, since solutions of linear ODEs always have their asymptotics obtained by WKB calculations, and ODE (12.10) for Z is “linear”. \square

Exercise 12.2 ([11]) Let Q_B be a solution of the biharmonic Q equation (12.8) that decays to zero as $\rho \rightarrow \infty$. Show that

$$Q_B(\rho) \sim c_1 Q_{B1}(\rho) + c_2 Q_{B2}(\rho) + c_3 Q_{B3}(\rho) + c_4 Q_{B4}(\rho), \quad \rho \rightarrow \infty,$$

where c_1, c_2, c_3 , and c_4 are complex numbers,

$$\begin{aligned} Q_{B1}(\rho) &\sim \rho^{-\frac{2}{\sigma} - \frac{i}{b^3}}, \\ Q_{B2}(\rho) &\sim \frac{1}{\rho^{\frac{2}{3\sigma}(\sigma d-1)}} \exp\left(-\frac{3i}{4} b \rho^{\frac{4}{3}} - \frac{i}{3b^3} \log \rho\right), \\ Q_{B3}(\rho) &\sim \frac{\exp\left(\frac{3\sqrt{3}}{8} b \rho^{\frac{4}{3}}\right)}{\rho^{\frac{2}{3\sigma}(\sigma d-1)}} \exp\left(\frac{3i}{8} b \rho^{\frac{4}{3}} - \frac{i}{3b^3} \log \rho\right), \\ Q_{B4}(\rho) &\sim \frac{\exp\left(-\frac{3\sqrt{3}}{8} b \rho^{\frac{4}{3}}\right)}{\rho^{\frac{2}{3\sigma}(\sigma d-1)}} \exp\left(\frac{3i}{8} b \rho^{\frac{4}{3}} - \frac{i}{3b^3} \log \rho\right), \end{aligned}$$

and $b = (\kappa^4/4)^{\frac{1}{3}}$.

Corollary 12.2 If σ is in the range (12.1b), then

$$Q_1 \notin L^2, \quad \nabla Q_1 \in L^2, \quad Q_1 \in L^{2\sigma+2},$$

and

$$Q_2 \in L^2, \quad \nabla Q_2 \notin L^2, \quad Q_2 \in L^{2\sigma+2}.$$

Proof By Lemma 12.2,

$$|Q_1| \sim \rho^{-\frac{1}{\sigma}}, \quad |\nabla Q_1| \sim \rho^{-\frac{1}{\sigma}-1}, \quad |Q_2| \sim \rho^{-d+\frac{1}{\sigma}}, \quad |\nabla Q_2| \sim \rho^{-d+\frac{1}{\sigma}+1}.$$

Therefore, the result follows. \square

Hence, while all nontrivial solutions of the Q equation (12.6) are decaying, none of these solutions is in H^1 .

Exercise 12.3 Show that if $c_1, c_2 \neq 0$, then as $\rho \rightarrow \infty$,

$$Q \sim c_1 Q_1 \quad \text{but} \quad \nabla Q \sim c_2 \nabla Q_2.$$

By Corollary 12.2,

$$H(Q_1) < \infty, \quad H(Q_2) = \infty.$$

In fact, the following lemma shows that $H(Q_1) = 0$:

Lemma 12.3 ([156]) *Let Q be a solution of (12.6), such that $a \neq 0$ and σ is in the range (12.1b). If $\nabla Q \in L^2$ and $Q \in L^{2\sigma+2}$, then $H(Q) = 0$.*

Proof If we multiply (12.6) by ΔQ^* , integrate over \mathbb{R}^d , and take the imaginary part, we get that $I_1 + I_2 = 0$, where

$$I_1 = a \operatorname{Re} \int \left(\frac{Q}{\sigma} + \rho Q' \right) \Delta Q^* \rho^{d-1} d\rho, \quad I_2 = \operatorname{Im} \int |Q|^{2\sigma} Q \Delta Q^* \rho^{d-1} d\rho.$$

Integration by parts gives

$$I_1 = a \left(\frac{d}{2} - 1 - \frac{1}{\sigma} \right) \int |Q'|^2 \rho^{d-1} d\rho.$$

In addition, by (12.6),

$$\Delta Q^* = -Q^* - ia \left(\frac{Q^*}{\sigma} + \rho Q'^* \right) - |Q|^{2\sigma} Q^*.$$

Substituting this in I_2 gives

$$I_2 = -a \operatorname{Re} \int |Q|^{2\sigma} Q \left(\frac{Q^*}{\sigma} + \rho Q'^* \right) \rho^{d-1} d\rho = -a \left(\frac{1}{\sigma} - \frac{d}{2\sigma+2} \right) \int |Q|^{2\sigma+2}.$$

Therefore,

$$0 = I_1 + I_2 = a \left(\frac{d}{2} - 1 - \frac{1}{\sigma} \right) H(Q).$$

Since σ is in the range (12.1b), then $d - 2 \neq \frac{2}{\sigma}$. Therefore, the result follows.

Alternatively, we can prove this lemma by noting that

$$H(\psi_Q^{\text{explicit}}) = L^{d-\frac{2}{\sigma}-2}(z) H(Q).$$

In addition, by (12.1b), $d - \frac{2}{\sigma} - 2 < 0$. Therefore, Hamiltonian conservation of ψ_Q^{explicit} implies that if $H(Q)$ is finite, then $H(Q) = 0$. \square

From Corollary 12.2 and Lemma 12.3 one immediately has

Corollary 12.3 *Let Q be a solution of (12.6), such that $a \neq 0$ and σ is in the range (12.1b). Then $H(Q) = 0$ if and only if $c_2 = 0$.*

Exercise 12.4 ([11]) Let Q_B be a solution of (12.8), such that $\kappa \neq 0$ and σ is in the L^2 -supercritical and H^2 subcritical range

$$\begin{cases} \frac{4}{d} < \sigma < \infty, & \text{if } d \leq 4, \\ \frac{4}{d} < \sigma < \frac{4}{d-4}, & \text{if } d > 4. \end{cases}$$

Show (in two different ways) that if $\Delta Q_B \in L^2$ and $Q_B \in L^{2\sigma+2}$, then $H_B(Q_B) = 0$, where $H_B(Q_B) = \|\Delta Q_B\|_2^2 - \frac{1}{\sigma+1} \|Q_B\|_{2\sigma+2}^{2\sigma+2}$ is the BNLS Hamiltonian.

12.3 Blowup Rate of ψ_Q^{explicit}

When $Q(0) \neq 0$,

$$\lim_{z \rightarrow Z_c} \|\psi_Q^{\text{explicit}}(z)\|_\infty \geq \lim_{z \rightarrow Z_c} |\psi_Q^{\text{explicit}}(z, 0)| = \lim_{z \rightarrow Z_c} \frac{|Q(0)|}{L^{\frac{1}{\sigma}}(z)} = \infty.$$

Therefore, ψ_Q^{explicit} is an NLS solution that becomes singular in L^∞ as $z \rightarrow Z_c$. Since Q is not in H^1 (Sect. 12.2), ψ_Q^{explicit} is also not in H^1 . Therefore, we cannot say that ψ_Q^{explicit} becomes singular in H^1 as $z \rightarrow Z_c$. However, since Q is in $L^{2\sigma+2}$, and since

$$\|\psi_Q^{\text{explicit}}\|_{2\sigma+2}^{2\sigma+2} = \frac{1}{L^{2+\frac{2}{\sigma}-d}} \|Q\|_{2\sigma+2}^{2\sigma+2},$$

ψ_Q^{explicit} is in $L^{2\sigma+2}$ for $0 \leq z < Z_c$, and it becomes singular in $L^{2\sigma+2}$ as $z \rightarrow Z_c$.²

The blowup rate of ψ_Q^{explicit} is, see (13.2),

$$l(z) := \frac{(\sigma+1)^{\frac{1}{2}}}{\|\psi_Q^{\text{explicit}}\|_{2\sigma+2}^{\sigma+1}} = \frac{(\sigma+1)^{\frac{1}{2}}}{\|Q\|_{2\sigma+2}^{\sigma+1}} L^{1+\frac{1}{\sigma}-\frac{d}{2}}(z) = c_l (Z_c - z)^p,$$

where

$$p = \frac{1}{2} + \frac{2 - \sigma d}{4\sigma}, \quad c_l = \frac{(\sigma+1)^{\frac{1}{2}}}{\|Q\|_{2\sigma+2}^{\sigma+1}} (2a)^p.$$

² See Definition 11.1.

Therefore, we have

Lemma 12.4 ψ_Q^{explicit} is an explicit solution of the supercritical NLS that becomes singular in $L^{2\sigma+2}$ at Z_c with the blowup rate $p = \frac{1}{2} + \frac{1}{2\sigma} - \frac{d}{4}$.

12.3.1 Weak Collapse

In Sect. 10.2 we saw that the blowup solution ψ_R^{explicit} of the critical NLS undergoes a whole-beam collapse. In particular, it undergoes a strong collapse. In contrast,

Lemma 12.5 ψ_Q^{explicit} undergoes a weak collapse.

Proof By (12.5a),

$$\begin{aligned} \int_0^{r_c} \left| \psi_Q^{\text{explicit}}(z, r) \right|^2 r^{d-1} dr &= L^{-\frac{2}{\sigma}}(z) \int_0^{r_c} \left| Q\left(\frac{r}{L}\right) \right|^2 r^{d-1} dr \\ &= L^{d-\frac{2}{\sigma}}(z) \int_0^{\frac{r_c}{L(z)}} |Q(\rho)|^2 \rho^{d-1} d\rho. \end{aligned}$$

As $L \rightarrow 0$ in the last expression, $L^{d-\frac{2}{\sigma}}$ goes to zero, but the integral diverges, since $Q \sim c_1 Q_1$ has an infinite power.³ To compute this expression, let us choose $\rho_1 \gg 1$, so that the asymptotic expansions

$$|Q_1| = \rho^{-\frac{1}{\sigma}} \left(1 + O\left(\frac{1}{\rho^2}\right) \right), \quad |Q_2| = \rho^{-d+\frac{1}{\sigma}} \left(1 + O\left(\frac{1}{\rho^2}\right) \right)$$

hold for $\rho \geq \rho_1$. Therefore,

$$|Q| = |c_1 Q_1 + c_2 Q_2| = |c_1| \rho^{-\frac{1}{\sigma}} \left(1 + O\left(\frac{1}{\rho^\alpha}\right) \right), \quad \rho \geq \rho_1,$$

where $\alpha = \min\{d - \frac{2}{\sigma}, 2\} > 0$. Now,

$$\begin{aligned} \int_0^{r_c} \left| \psi_Q^{\text{explicit}}(z, r) \right|^2 r^{d-1} dr &= L^{d-\frac{2}{\sigma}}(z) \int_0^{\frac{r_c}{L(z)}} |Q(\rho)|^2 \rho^{d-1} d\rho \\ &= L^{d-\frac{2}{\sigma}}(z) \int_0^{\rho_1} |Q(\rho)|^2 \rho^{d-1} d\rho + L^{d-\frac{2}{\sigma}}(z) \int_{\rho_1}^{\frac{r_c}{L(z)}} |Q(\rho)|^2 \rho^{d-1} d\rho. \end{aligned}$$

³ If $c_1 = 0$, then $Q \sim c_2 Q_2$. Therefore, the integral is finite, and the proof is immediate.

Since $\int_0^{\rho_1} |Q(\rho)|^2 \rho^{d-1} d\rho < \infty$, the first term goes to zero. The second integral can be approximated by

$$\begin{aligned} \int_{\rho_1}^{\frac{r_c}{L(z)}} |Q(\rho)|^2 \rho^{d-1} d\rho &= |c_1|^2 \int_{\rho_1}^{\frac{r_c}{L(z)}} \rho^{-\frac{2}{\sigma}} \left(1 + O\left(\frac{1}{\rho^\alpha}\right)\right) \rho^{d-1} d\rho \\ &= |c_1|^2 \frac{[r_c/(L(z))]^{d-\frac{2}{\sigma}}}{d - \frac{2}{\sigma}} \left(1 + O\left(\frac{L^\alpha(z)}{r_c^\alpha}\right)\right). \end{aligned}$$

Therefore, the limiting power in a ball of radius r_c centered at the origin is

$$P_{r_c}^{\text{radial}} := \lim_{z \rightarrow Z_c} \int_0^{r_c} \left| \psi_Q^{\text{explicit}}(z, r) \right|^2 r^{d-1} dr = |c_1|^2 \frac{r_c^{d-\frac{2}{\sigma}}}{d - \frac{2}{\sigma}}. \quad (12.12)$$

Hence, $P_{\text{collapse}}^{\text{radial}} = \lim_{r_c \rightarrow 0} P_{r_c}^{\text{radial}} = 0$. \square

Exercise 12.5 Show that if $c_1 \neq 0$, then for any $0 < r_c < \infty$,

$$\lim_{z \rightarrow Z_c} \int_0^{r_c} \left| \psi_Q^{\text{explicit}}(z, r) \right|^p r^{d-1} dr = \begin{cases} |c_1|^p \frac{r_c^{d-\frac{p}{\sigma}}}{d - \frac{p}{\sigma}} & \text{if } 2 \leq p < \sigma d, \\ \infty & \text{if } p \geq \sigma d. \end{cases}$$

12.4 Zero-Hamiltonian Solutions

From now on, we only consider the zero-Hamiltonian (and infinite-power) solution Q_1 .⁴ We first show that the global zero-Hamiltonian condition can be replaced with a local boundary condition:

Lemma 12.6 Let Q be a solution of (12.6), where σ is in the range (12.1b). Then $H(Q) = 0$ if and only if

$$\lim_{\rho \rightarrow \infty} \rho^\gamma Q'(\rho) = 0, \quad \gamma_0 < \gamma < \gamma_1, \quad (12.13)$$

where $\gamma_0 = d - 1 - \frac{1}{\sigma}$ and $\gamma_1 = 1 + \frac{1}{\sigma}$.

Proof We first note that if σ is in the range (12.1b), then indeed $\gamma_0 < \gamma_1$. By Lemma 12.2,

$$Q' \sim c_1 Q'_1 + c_2 Q'_2 \sim -c_1 \left(\frac{i}{a} + \frac{1}{\sigma} \right) \frac{Q_1}{\rho} - c_2 i a \rho Q_2, \quad \rho \rightarrow \infty.$$

⁴ The reason why the condition of a finite Hamiltonian is “more important” than that of a finite power will become clear in Sect. 21.1.

Therefore,

$$\rho^\gamma Q' \sim -c_1 \left(\frac{i}{a} + \frac{1}{\sigma} \right) \rho^{-\frac{i}{a}} \rho^{\gamma - \frac{1}{\sigma} - 1} - c_2 i a e^{-i \frac{a\rho^2}{2}} \rho^{\frac{i}{a}} \rho^{\gamma - d + \frac{1}{\sigma} + 1}. \quad (12.14)$$

If $\gamma_0 < \gamma < \gamma_1$, then

$$\lim_{\rho \rightarrow \infty} \rho^{\gamma - \frac{1}{\sigma} - 1} = 0, \quad \lim_{\rho \rightarrow \infty} \rho^{\gamma - d + \frac{1}{\sigma} + 1} = \infty.$$

Hence, condition (12.13) holds if and only if $c_2 = 0$, which, by Corollary 12.3, holds if and only if $H(Q) = 0$. \square

In light of Lemma 12.6, the zero-Hamiltonian Q profiles are solutions of

$$\Delta_\rho Q(\rho) - Q + |Q|^{2\sigma} Q = -ia \left(\frac{1}{\sigma} + \rho \frac{d}{d\rho} \right) Q, \quad 0 < \rho < \infty, \quad (12.15a)$$

subject to

$$Q'(0) = 0, \quad \lim_{\rho \rightarrow \infty} \rho^\gamma Q'(\rho) = 0. \quad (12.15b)$$

This ODE is a *nonlinear eigenvalue problem*, with eigenvalue a and eigenfunction Q . We can obtain a more accurate boundary condition (i.e., increase the upper bound for γ), by utilizing the relation

$$Q'_1 \sim \left(\frac{i}{a} + \frac{1}{\sigma} \right) \frac{Q_1}{\rho}.$$

Lemma 12.7 ([35]) *Under the conditions of Lemma 12.6, $H(Q) = 0$ if and only if*

$$\lim_{\rho \rightarrow \infty} \rho^\gamma \left(Q' + \left(\frac{i}{a} + \frac{1}{\sigma} \right) \frac{Q}{\rho} \right) = 0, \quad \gamma_0 < \gamma < \gamma_1 + 2. \quad (12.16)$$

Proof By Lemma 12.2, as $\rho \rightarrow \infty$,

$$\begin{aligned} Q' &\sim c_1 Q'_1 + c_2 Q'_2 \\ &\sim -c_1 \left(\frac{i}{a} + \frac{1}{\sigma} \right) \frac{Q_1}{\rho} \left(1 + O\left(\frac{1}{\rho^2}\right) \right) + c_1 Q_1 O\left(\frac{1}{\rho^3}\right) - c_2 i a \rho Q_2. \end{aligned}$$

Therefore,

$$Q' + \left(\frac{i}{a} + \frac{1}{\sigma} \right) \frac{Q}{\rho} \sim c_1 Q_1 O\left(\frac{1}{\rho^3}\right) - c_2 i a \rho Q_2.$$

Hence,

$$\rho^\gamma \left(Q' + \left(\frac{i}{a} + \frac{1}{\sigma} \right) \frac{Q}{\rho} \right) \sim c_1 \cdot O\left(\rho^{\gamma - \frac{1}{\sigma} - 3}\right) + c_2 \cdot O(\rho^{\gamma - d + \frac{1}{\sigma} + 1}). \quad (12.17)$$

Consequently, condition (12.16) holds if and only if $c_2 = 0$. \square

12.4.1 Computation of Zero-Hamiltonian Solutions

In [35], Budd et al. computed numerically the zero-Hamiltonian Q profiles. They used a boundary value formulation, in which the global zero-Hamiltonian condition is replaced with a local boundary condition, such as (12.13) or (12.16). In practice, the computational domain has to be truncated. Therefore, one solves

$$\Delta_\rho Q(\rho) - Q + ia \left(\frac{1}{\sigma} Q + \rho Q' \right) + |Q|^{2\sigma} Q = 0, \quad 0 < \rho < \rho_\infty$$

for some $1 \ll \rho_\infty < \infty$, subject to $Q'(0) = 0$, and to either

$$\rho^\gamma Q' \Big|_{\rho_\infty} = 0, \quad (12.18)$$

see (12.13), or to

$$\rho^\gamma \left(Q' + \left(\frac{i}{a} + \frac{1}{\sigma} \right) \frac{Q}{\rho} \right) \Big|_{\rho_\infty} = 0, \quad (12.19)$$

see (12.16). These boundary value problems can be solved using various approaches, such as *shooting* for the two unknowns $Q(0)$ and a (see a sample Matlab code in Fig. 12.1) or *collocation* methods [35].

As noted, the exact boundary condition (12.13) ensures that $c_2 = 0$. If we replace it with the approximate boundary condition (12.18) at $1 \ll \rho_\infty < \infty$, then by (12.14),

$$\frac{c_2}{c_1} \sim \frac{\rho_\infty^{\gamma - \frac{1}{\sigma} - 1}}{\rho_\infty^{\gamma - d + \frac{1}{\sigma} + 1}} = \rho_\infty^{d - \frac{2}{\sigma} - 2} = o(1).$$

Therefore, c_2 is small, but not zero. To further reduce c_2 , we can use the more accurate boundary condition (12.19). In this case, by (12.17),

$$\frac{c_2}{c_1} \sim \rho_\infty^{d - \frac{2}{\sigma} - 4}.$$

$$12.5 \quad Q(\rho) = e^{-i\frac{a\rho^2}{4}} P(\rho)$$

```

function Shooting4Qprofile(~)
global sigma x_inf x Q
x_inf=40;
param_initial=[1.2941,0.9669]; %initial guess for param=[Q0 aQ]
sigma=3;
param = fminsearch(@calcQ,param_initial,optimset('TolX',1e-4));
Q0=param(1)
aQ=param(2)
plot(x,abs(Q(:,1)));shg

function F = calcQ(input)
global x_inf sigma x Q;
Q0=input(1);aQ=input(2);
options=odeset('RelTol',1e-4);
initial_cond=[Q0 0];
[x,Q] = ode45(@ODE4Q,[0,x_inf],initial_cond,options,aQ,sigma);
F=abs(x_inf*(Q(end,2)+(1i/aQ+1/sigma)*Q(end,1)/x_inf));
return

function dQdx = ODE4Q(x,Q_dQ,aQ,sigma)
Q = Q_dQ(1);
dQ = Q_dQ(2);
ddQ = Q - 1i*aQ*(Q/sigma+x*dQ)-abs(Q)^(2*sigma)*Q;
dQdx= [dQ ; ddQ];
return

```

Fig. 12.1 A Matlab code for calculating the admissible solution of the one-dimensional Q equation (12.27)

$$12.5 \quad Q(\rho) = e^{-i\frac{a\rho^2}{4}} P(\rho)$$

In the critical case, the explicit blowup solutions can be written as

$$\psi_R^{\text{explicit}} = \frac{1}{L^{\frac{d}{2}}(z)} R\left(\frac{r}{L}\right) e^{i\xi(z)+i\frac{L_z r^2}{L^4}}, \quad \psi_G^{\text{explicit}} = \frac{1}{L^{\frac{d}{2}}(z)} G\left(\frac{r}{L}\right) e^{i\xi(z)+i\frac{L_z r^2}{L^4}},$$

see (10.3) and Lemma 11.1, respectively. Since both R and G are real, the radial phase of these solutions is $e^{i\frac{L_z r^2}{L^4}}$.⁵ In the expression $\psi_Q^{\text{explicit}} = \frac{1}{L^{\frac{1}{\sigma}}(z)} Q\left(\frac{r}{L}\right) e^{i\xi(z)}$ that appears in Lemma 12.1, the function Q represents both the profile and the radial phase. Comparison with ψ_Q^{explicit} and ψ_G^{explicit} suggests that we rewrite it as

⁵ This phase represents focusing with $F(z) = -L/L_z$, see Sect. 2.12.2.

$$\psi_Q^{\text{explicit}} = \frac{1}{L^{\frac{1}{\sigma}}(z)} P\left(\frac{r}{L}\right) e^{i\zeta(z)+i\frac{L_z}{L}r^2},$$

where L , ρ , and ζ are defined in (12.5). Since $\frac{L_z}{L}r^2 = LL_z\rho^2 = -a\rho^2$, then

$$\psi_Q^{\text{explicit}}(z, r) = \frac{1}{L^{\frac{1}{\sigma}}(z)} P(\rho) e^{i\zeta(z)-ia\frac{\rho^2}{4}}.$$

Therefore,

$$Q(\rho) = e^{-i\frac{a\rho^2}{4}} P(\rho). \quad (12.20)$$

Substitution in (12.6) shows that the equation for P is

$$P''(\rho) + \frac{d-1}{\rho} P' - P - ia\frac{\sigma d-2}{2\sigma} P + \frac{1}{4}a^2\rho^2 P + |P|^{2\sigma} P = 0 \quad (12.21a)$$

for $0 < \rho < \infty$, subject to

$$P(0) = Q_0, \quad P'(0) = 0. \quad (12.21b)$$

In the critical case, Eq. (12.21) for P reduces to Eq. (11.4) for G . In that case, if $G(0)$ is real, then G is real for all ρ , see Lemma 11.4. In the supercritical case, however, even if $P(0)$ is real, $P(\rho)$ is complex.

Conclusion 12.1 *In the supercritical case, the radial phase of ψ_Q^{explicit} is not given by $e^{i\frac{L_z}{L}r^2}$.*

From (12.20) and (12.21) immediately follows

Lemma 12.8 *If $a \rightarrow 0$ and $\sigma d \rightarrow 2$, then for any $0 \leq \rho < \infty$,*

$$Q(\rho; \sigma, d) \rightarrow P(\rho; \sigma, d) \rightarrow R(\rho),$$

where R is a solution of

$$R''(\rho) + \frac{d-1}{\rho} R' - R + |R|^{\frac{4}{d}} R = 0, \quad R'(0) = 0. \quad (12.22)$$

In particular, $Q(0; \sigma, d) = P(0; \sigma, d) \rightarrow R(0)$.

By Theorem 12.1 and (12.20), for any $P(0) \in \mathbb{C}$, there is a unique solution P to (12.21), which decays to zero as $\rho \rightarrow \infty$. By Lemma 12.2,

$$P(\rho) \sim c_1 P_1(\rho) + c_2 P_2(\rho), \quad \rho \rightarrow \infty,$$

$$12.5 \quad Q(\rho) = e^{-i\frac{a\rho^2}{4}} P(\rho)$$

265

where

$$P_1(\rho) \sim e^{+i\frac{a\rho^2}{4}} \rho^{-\frac{i}{a} - \frac{1}{\sigma}}, \quad P_2(\rho) \sim e^{-i\frac{a\rho^2}{4}} \rho^{\frac{i}{a} - d + \frac{1}{\sigma}}.$$

Zero-Hamiltonian Q profiles correspond to P profiles for which $H\left(e^{-i\frac{a\rho^2}{4}} P\right) = 0$. These solutions are of the form

$$P(\rho) \sim c_1 P_1(\rho), \quad \rho \rightarrow \infty.$$

Lemma 12.9 *Let P be a solution of (12.21) and let $\gamma > \gamma_0$, where $\gamma_0 = d - 1 - \frac{1}{\sigma}$. Then $H\left(e^{-i\frac{a\rho^2}{4}} P\right) = 0$ if and only if*

$$\lim_{\rho \rightarrow \infty} \rho^\gamma \left(P' + \left(-\frac{ia}{2} \rho + \left(\frac{i}{a} + \frac{1}{\sigma} \right) \frac{1}{\rho} \right) P \right) = 0. \quad (12.23)$$

Proof The proof is similar to that of Lemma 12.7. \square

The supercritical profile P is “less useful” than the critical profile R , since

1. $R(\rho)$ is real, whereas P is complex.
2. $H(R) = 0$, but $H(P) \neq 0$. Rather, $H(Q) = H\left(e^{-i\frac{a\rho^2}{4}} P\right) = 0$.

Hence, in the supercritical case it is “more natural” to work with the Q profile than with the P profile. The P profile is mainly used in the context of the supercritical limit of the critical NLS,⁶ since $P = R + o(1)$ when $0 < \sigma d - 2 \ll 1$.

12.6 Admissible Solutions

We now consider zero-Hamiltonian solutions which are also monotonically decreasing.

Definition 12.1 (admissible solution) *A solution of the Q equation (12.6) is called admissible, if $H(Q) = 0$ and if $|Q|$ is monotonically decreasing in ρ .*

Admissible solutions were first studied in 1988 by LeMesurier et al. [156]. Numerical simulations and asymptotic analysis suggested that for any σ and d , there exists a unique eigenpair $\{Q(\rho; \sigma, d), a_Q(\sigma, d)\}$ of the nonlinear eigenvalue problem (12.15), such that the eigenfunction $Q(\rho; \sigma, d)$ is an admissible solution, and $a = a_Q(\sigma, d)$ is the eigenvalue.⁷ Moreover,

⁶ See, e.g., Sect. 17.6.2.

⁷ For example, the unique value of a that corresponds to an admissible solution of the cubic three-dimensional NLS is

$$a_Q(\sigma = 1, d = 3) \approx 0.917.$$

$$a_Q(\sigma, d) \rightarrow 0+, \quad \sigma d \rightarrow 2+.$$

Therefore, by Lemma 12.8, Q approaches a solution of the R equation, see (12.22). Since the admissible solution is monotonically decreasing, and since $R^{(0)}$ is the only monotonically-decreasing solution of the R equation (Corollary 6.11), this implies that

$$Q(\rho; \sigma, d) \rightarrow R^{(0)}(\rho), \quad \sigma d \rightarrow 2+. \quad (12.24)$$

This pointwise convergence is not uniform, since Q has a polynomial decay as $\rho \rightarrow \infty$ (Lemma 12.2), whereas $R^{(0)}$ has an exponential decay (Lemma 6.14). Finally, WKB analysis shows that as $\sigma d \rightarrow 2+$, $a = a_Q(\sigma, d)$ satisfies the asymptotic relation

$$\sigma d - 2 \sim \frac{2\sigma A_R^2}{P_{\text{cr}}^{\text{radial}}} \frac{1}{a} e^{-\frac{\pi}{a}}, \quad (12.25)$$

where $A_R = \lim_{r \rightarrow \infty} r^{\frac{d-1}{2}} e^r R^{(0)}(r)$ and $P_{\text{cr}}^{\text{radial}} = \int_0^\infty |R^{(0)}|^2 r^{d-1} dr$. These results were later proved rigorously for $0 < \sigma d - 2 \ll 1$ by Koppel and Landman [144]. See [249, Chap. 8] for more details.

In Lemma 12.1, the explicit solutions ψ_Q^{explicit} are defined for *any* solution Q of (12.6). In particular, when Q is the unique admissible solution, the blowup rate of $L(z)$ is given by

$$L(z) = \kappa_Q(\sigma, d) \sqrt{Z_c - z}, \quad \kappa_Q(\sigma, d) = \sqrt{2a_Q(\sigma, d)}, \quad Z_c = \frac{L^2(0)}{2a_Q}.$$

12.6.1 Admissible P Profile

A solution of the P equation (12.21) is called *admissible*, if $H\left(e^{-i\frac{a\rho^2}{4}} P\right) = 0$, and if $|P|$ is monotonically decreasing in ρ . For each σ and d , Eq. (12.21) admits a unique admissible solution P . This solution is obtained for

$$a = a_Q(\sigma, d), \quad P(0) = Q_0(\sigma, d).$$

Therefore, when $0 < \sigma d - 2 \ll 1$, Eq. (12.21) can be approximated by

$$P''(\rho) + \frac{d-1}{\rho} P' - P - i \frac{A_R^2}{P_{\text{cr}}^{\text{radial}}} e^{-\frac{\pi}{a}} P + \frac{1}{4} a^2 \rho^2 P + |P|^{2\sigma} P = 0,$$

see (12.25). For future reference, we rewrite this equation as

$$P''(\rho) + \frac{d-1}{\rho} P' - P - i \frac{M^{\text{radial}}}{2P_{\text{cr}}^{\text{radial}}} v \left(a^2\right) P + \frac{1}{4} a^2 \rho^2 P + |P|^{2\sigma} P = 0, \quad (12.26)$$

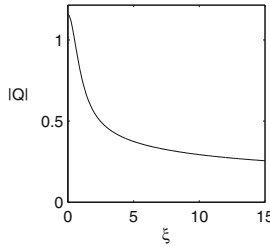


Fig. 12.2 The admissible solution of the one-dimensional Q equation (12.27) with $\sigma = 3$, as a function of ξ

where

$$\nu(a^2) = c_\nu e^{-\frac{\pi}{a}}, \quad c_\nu = \frac{2A_R^2}{M^{\text{radial}}}, \quad M^{\text{radial}} = \frac{1}{4} \int_0^\infty r^2 |R^{(0)}|^2 r^{d-1} dr.$$

In particular, as $\sigma d \rightarrow 2+$, both a and $\nu(a^2)$ go to zero, and so the equation for P reduces to Eq. (12.22) for R , and the admissible P profile approaches the monotonically-decreasing ground state $R^{(0)}$.

12.6.2 $d = 1$

In [12], Baruch et al. computed numerically⁸ the admissible solutions of the one-dimensional supercritical NLS, i.e., the solutions of

$$Q''(\xi) - Q + ia \left(\frac{1}{\sigma} Q + \xi Q' \right) + |Q|^{2\sigma} Q = 0, \quad \xi = \frac{x}{L(z)}, \quad (12.27a)$$

subject to⁹

$$Q'(0) = 0, \quad \lim_{\xi \rightarrow \infty} \xi \left(Q' + \left(\frac{i}{a} + \frac{1}{\sigma} \right) \frac{Q}{\xi} \right) = 0, \quad (12.27b)$$

which are monotonically decreasing. For example, Fig. 12.2 shows the admissible solution for $\sigma = 3$. In this case,

$$a_Q(3, 1) \approx 1.384, \quad \kappa_Q(3, 1) \approx 1.664, \quad Q_0(3, 1) \approx 1.155. \quad (12.28)$$

Note the slow algebraic decay to zero as $\xi \rightarrow \infty$.

⁸ Using the Matlab code in Fig. 12.1.

⁹ When $d = 1$ we can set $\gamma = 1$, since $\gamma_0 = -\frac{1}{\sigma}$ and $\gamma_1 + 2 = 3 + \frac{1}{\sigma}$ (Lemma 12.7).

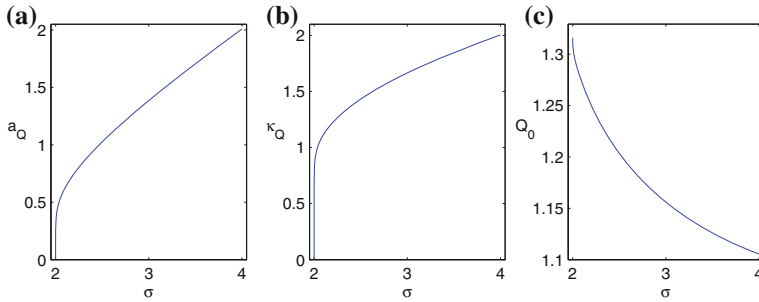


Fig. 12.3 The parameters of the admissible solutions of the one-dimensional Q equation (12.27), as a function of σ . **a** $a_Q(\sigma, d = 1)$. **b** $\kappa_Q(\sigma, d = 1)$. **c** $Q_0(\sigma, d = 1)$. Subplots (b) and (c) are from [12]

The values of a_Q , κ_Q , and $Q_0 = Q(0)$ for the admissible solutions of the one-dimensional Q equation (12.27), as functions of σ , are shown in Fig. 12.3. As expected,

$$\lim_{\sigma \rightarrow 2+} a_Q(\sigma, d = 1) = \lim_{\sigma \rightarrow 2+} \kappa_Q(\sigma, d = 1) = 0+,$$

see Fig. 12.3a, b. In addition, by (12.24) and Lemma 6.15,

$$Q(\rho; \sigma, d = 1) \rightarrow R^{(0)}(\rho; \sigma = 2, d = 1) = \frac{3^{\frac{1}{4}}}{\cosh^{\frac{1}{2}}(2\rho)}, \quad \sigma \rightarrow 2+.$$

In particular,

$$\lim_{\sigma \rightarrow 2+} Q_0(\sigma, d = 1) = R^{(0)}(0; \sigma = 2, d = 1) = 3^{\frac{1}{4}} \approx 1.32,$$

see Fig. 12.3c.

When $d = 1$, the asymptotic relation (12.25) reads

$$\sigma - 2 \sim \frac{2\sigma A_R^2}{\int_0^\infty |R^{(0)}(x)|^2 dx} \frac{1}{a} e^{-\frac{\pi}{a}}, \quad (12.29)$$

where $A_R^2 = 2\sqrt{3}$ and $\int_0^\infty |R^{(0)}(x)|^2 dx \approx 1.36$, see Sect. 17.7. In Fig. 12.4 we plot the ratio of the two sides of relation (12.29). This ratio approaches one as $\sigma \rightarrow 2+$, providing a numerical confirmation to relation (12.29). In fact, this relation is reasonably accurate for $2 < \sigma \leq 4$.

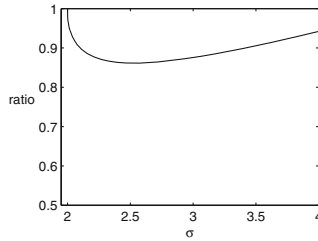


Fig. 12.4 The ratio $\frac{\sigma-2}{\frac{2\sigma A_R^2}{\int_0^\infty |R^{(0)}|^2} \frac{1}{d} e^{-\frac{\pi}{d}}}$ as a function of σ

12.7 Multi-bump Solutions

We now ask whether the Q equation (12.6) admits zero-Hamiltonian solutions which are non-admissible (i.e., non-monotone). To answer this question, we begin with the following informal argument. In Sect. 12.4 we saw that the zero-Hamiltonian solutions are eigenfunctions of the nonlinear eigenvalue problem (12.15). By analogy with linear eigenvalue problems, one can expect that (12.15) admits a countable number of eigenvalues, each with its corresponding (zero-Hamiltonian) eigenfunction. Since there is a unique admissible solution, all other zero-Hamiltonian solutions are non-monotone.

In [35], Budd et al. carried out a systematic numerical study of zero-Hamiltonian solutions for $\sigma = 1$ and $2 < d < 4$. This study showed that for each σ and d , (12.6) admits a doubly-countable set of zero-Hamiltonian solutions $\{Q_{K,J}(\rho)\}_{K,J=0}^\infty$, each with its corresponding eigenvalue $a_{K,J}$. The profile of $Q_{K,J}(\rho)$ has $K + J$ local maxima. As $\sigma d \rightarrow 2+$, $a_{K,J} \rightarrow 0+$, and $Q_{K,J}$ converges (non-uniformly) to $R^{(K-1)}(\rho)$,¹⁰ the $(K-1)$ th state of the R equation (12.22), which has K local maxima.¹¹ In particular, as $\sigma d \rightarrow 2+$, the monotonically-decreasing admissible solution $Q_{K=1,J=0}(\rho)$ approaches $R^{(0)}(\rho)$, the monotonically-decreasing ground state of (12.22). Since all other zero-Hamiltonian solutions are non-monotone, they are called *multibump solutions*.

Numerical simulations show that when Q is the admissible solution, the explicit blowup solution ψ_Q^{explicit} is stable. When Q has a multibump profile, however, ψ_Q^{explicit} is unstable [35].¹² A detailed asymptotic study of multibump solutions was carried out by Budd in [34].

¹⁰ See Lemma 12.8.

¹¹ Thus, for any J , $Q_{K=0,J}$ converges to the trivial solution $R^{(-1)}(\rho) \equiv 0$, $Q_{K=1,J}$ converges to the ground state $R^{(0)}(\rho)$, etc.

¹² This is different from the critical case, where all the explicit peak-type blowup solutions $\psi_{R^{(n)}}^{\text{explicit}}$ are unstable (Sect. 10.6). It is, however, analogous to the explicit ring-type blowup solutions ψ_G^{explicit} .

12.8 Singular Solutions of the Subcritical NLS

In Theorem 5.5 we proved that all H^1 solutions of the subcritical NLS exist globally. In [67] Fibich noted, however, that the explicit solutions ψ_Q^{explicit} exist also in the subcritical case. Therefore, if we do not restrict ourselves to H^1 solutions, the subcritical NLS also admits singular solutions. Here, by singular we mean that there exists some $2 < p < \infty$, such that ψ becomes singular in L^p , i.e., $\|\psi(z)\|_p < \infty$ for $0 \leq z < Z_c < \infty$, and $\lim_{z \rightarrow Z_c} \|\psi(z)\|_p = \infty$.¹³

Theorem 12.2 ([67]) *Let $1 < \sigma d < 2$, let*

$$p^* < p \leq \infty, \quad p^* := \frac{\sigma d}{\sigma d - 1}, \quad (12.30)$$

let $a > 0$ be a positive constant, let $Q(\rho)$ be a solution of (12.6) with $Q(0) \neq 0$, and let ψ_Q^{explicit} be given by (12.5). Then ψ_Q^{explicit} is an explicit solution of the subcritical NLS that becomes singular in L^p as $z \rightarrow Z_c$.

Proof In Lemma 12.10 we will prove that for any $Q(0) \neq 0$, there exists a solution Q of (12.6), and that $0 < \|Q\|_p < \infty$. Since $\|\psi_Q^{\text{explicit}}(z)\|_p = L^{-\frac{1}{\sigma}}(z)\|Q\|_p$ and $\lim_{z \rightarrow Z_c} L(z) = 0$, the result follows. \square

Remark Although Q , hence also ψ_Q^{explicit} , is not in H^1 , it is smooth, and it decays to zero as $r \rightarrow \infty$ (Lemma 12.10).

Corollary 12.4 ([67]) *Let p be in the range (12.30). Then the NLS (12.1a) in the subcritical regime $1 < \sigma d < 2$ admits classical solutions that become singular in L^p .*

Since

$$\lim_{\sigma d \rightarrow 2^-} p^* = 2+,$$

for any $2 < p < \infty$ there exists a singular solution of a subcritical NLS that becomes singular in L^p . In particular, if σd is sufficiently close to 2 from below, then ψ_Q^{explicit} becomes singular in $L^{2\sigma+2}$.

Remark The linear Schrödinger equation $i\psi_z + \Delta\psi = 0$ admits the fundamental solution $G(z, \mathbf{x}) = (4\pi iz)^{-\frac{d}{2}} e^{i\frac{|\mathbf{x}|^2}{4z}}$, see Sect. 2.15.1, which becomes singular in L^∞ as $z \rightarrow 0-$. Unlike ψ_Q^{explicit} , however, G does not become singular in L^p for any $p < \infty$.

(Footnote 12 continued)

of the critical NLS, for which the single-ring solution is stable but the multi-rings solutions are unstable (Sect. 11.4.1). In that case, the single-ring solution is the “least non-monotone”.

¹³ Recall that for H^1 NLS solutions, blowup of the H^1 norm implies blowup of the L^p norms for $2\sigma + 2 \leq p \leq \infty$ (Corollary 5.8).

Remark The question whether there exist singular solutions of the subcritical NLS which are different from ψ_Q^{explicit} is open. This question cannot be answered numerically, because even if the numerical solution reaches extremely high focusing levels, we can never know whether its collapse will be arrested at some higher focusing level.

12.8.1 The Q Equation in the Subcritical Case

We now establish existence and uniqueness for solutions of the Q equation in the subcritical regime:

Lemma 12.10 ([67]) *Let $a > 0$. Then for any $Q(0) \in \mathbb{C}$, the solution of (12.6) in the subcritical regime $1 < \sigma d < 2$ exists, is unique, and decays to zero as $\rho \rightarrow \infty$. In particular,*

$$|Q| = O\left(\rho^{-d+\frac{1}{\sigma}}\right), \quad \rho \rightarrow \infty.$$

Therefore, Q is in L^p for any $p^* < p \leq \infty$.

Proof The proof is nearly identical to that of Theorem 12.1. \square

The far-field asymptotics of Q can be calculated using the WKB method:

Lemma 12.11 *Let $Q(\rho)$ be a solution of (12.6) in the subcritical regime $1 < \sigma d < 2$. Then*

$$Q(\rho) \sim c_1 Q_1(\rho) + c_2 Q_2(\rho), \quad \rho \rightarrow \infty, \tag{12.31}$$

where c_1 and c_2 are complex numbers, and

$$Q_1 \sim \rho^{-\frac{i}{a}-\frac{1}{\sigma}}, \quad Q_2 \sim e^{-i\frac{ap^2}{2}} \rho^{\frac{i}{a}-d+\frac{1}{\sigma}}.$$

Proof The proof is nearly identical to that of Lemma 12.2. \square

Exercise 12.6 Prove Lemmas 12.10 and 12.11.

Corollary 12.5 If $1 < \sigma d < 2$, then

$$Q_1, \nabla Q_1 \in L^2, \quad Q_2, \nabla Q_2 \notin L^2.$$

In addition, $Q_1 \in L^p$ for any $2 \leq p \leq \infty$, and

$$Q_2 \in L^p, \quad p^* < p \leq \infty.$$

Proof This follows from Lemma 12.11. \square

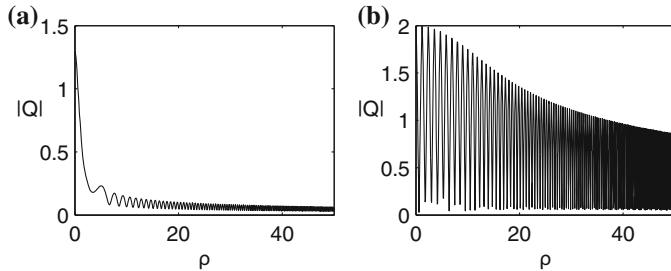


Fig. 12.5 Solution of (12.6) with $d = 1$, $\sigma = 1.9$, $a = 0.5145$, and **a** $Q(0) = 1.2953$, and **b** $Q(0) = 3$. From [67]

In the supercritical case, a key role is played by the zero-Hamiltonian solutions of the Q equation, for which $c_2 = 0$ (Corollary 12.3). In the subcritical case, however, there are no such solutions:

Lemma 12.12 *There are no solutions of the Q equation (12.6) in the subcritical regime $1 < \sigma d < 2$, for which $c_1 \neq 0$ and $c_2 = 0$.*

Proof By Corollary 12.5, $Q_1 \in H^1$. Therefore, if there exists a solution $Q \sim c_1 Q_1$, then $Q \in H^1$. Hence, ψ_Q^{explicit} is an H^1 solution of the subcritical NLS that becomes singular, which is in contradiction with Theorem 5.5. \square

Figure 12.5 shows two numerical solutions of (12.6) in the subcritical regime. As expected, see Lemma 12.11,

$$|Q| \sim |c_1 \rho^{-\frac{i}{a} - \frac{1}{\sigma}} + c_2 e^{-i \frac{a\rho^2}{2}} \rho^{\frac{i}{a} - d + \frac{1}{\sigma}}|$$

decreases to zero as $\rho \rightarrow \infty$, while undergoing faster and faster oscillations. The picture in Fig. 12.5a is “cleaner”, because the values of a and $Q(0)$ were chosen so as to minimize the value of c_2 .¹⁴

¹⁴ The value of c_2 cannot be equal to zero, see Lemma 12.12.

Chapter 13

Blowup Rate, Blowup Profile, and Power Concentration

In this chapter we rigorously study properties shared by *all* singular solutions of the critical NLS

$$i\psi_z(z, \mathbf{x}) + \Delta\psi + |\psi|^{\frac{4}{d}}\psi = 0, \quad \psi(0, \mathbf{x}) = \psi_0(\mathbf{x}) \in H^1. \quad (13.1)$$

Stronger results can be obtained when we restrict ourselves to solutions with power slightly above P_{cr} (Sect. 14.6) or to vortex solutions (Sect. 15.11). The chapter is organized as follows. In Sect. 13.1 we prove that the *blowup rate* is at least a square root. In Sect. 13.2 we prove that all singular solutions of the critical NLS collapse with a *quasi self-similar* profile. This, in turn, implies that all singular solutions of the critical NLS have the *power concentration property* that the amount of power that collapses into the singularity is at least P_{cr} (Sect. 13.3). In Sect. 13.4 we consider solutions that simultaneously *collapse at k points*. In Sect. 13.5 we show that, up to NLS symmetries, the only *minimal-power blowup solution* is $\psi_{R^{(0)}}^{\text{explicit}}$. Section 13.6 concludes with the equivalent results for the supercritical NLS.

13.1 Blowup Rate $l(z)$

In Sect. 10.4 we defined the blowup rate as $l(z) := 1/\|\nabla\psi\|_2$, and saw that it can also be defined as

$$l(z) := \left(\frac{\sigma + 1}{\|\psi\|_{2\sigma+2}^{2\sigma+2}} \right)^{\frac{1}{2}}. \quad (13.2)$$

In particular, in the critical case,

$$l(z) := \left(\frac{\frac{2}{d} + 1}{\|\psi\|_{\frac{4}{d}+2}^{\frac{4}{d}+2}} \right)^{\frac{1}{2}}, \quad \sigma d = 2. \quad (13.3)$$

13.1.1 Linear Blowup Rate

Singular solutions of the critical NLS that are known to have a linear blowup rate are the explicit blowup solution ψ_R^{explicit} (Sect. 10.1), the Bourgain-Wang solutions $\psi_{\text{BW}} \sim \psi_{R^{(0)}}^{\text{explicit}} + u$, where $0 \not\equiv u \in L^2$ (Sect. 10.8), and Merle's solutions that blow up simultaneously at k points, such that near each blowup point the solution approaches $\psi_{R^{(n)}}^{\text{explicit}}$ (Sect. 13.4).

The blowup solutions of Bourgain and Wang and of Merle are unstable, as they are “based” on $\psi_{R^{(0)}}^{\text{explicit}}$ and $\psi_{R^{(n)}}^{\text{explicit}}$, respectively, which are unstable. Thus, all known singular solutions of the critical NLS that collapse at a linear blowup rate are unstable. Whether this is always the case, however, is an open problem.

Remark The blowup solution ψ_R^{explicit} has a linear blowup rate, and it undergoes a whole-beam collapse. In contrast, stable blowup solutions that collapse with the $\psi_{R^{(0)}}$ profile have a slightly-faster-than-a-square-root blowup rate, and they undergo a partial-beam collapse (Sect. 14.6). Therefore, it is reasonable to conjecture that a solution has a linear blowup rate if and only if it undergoes a whole-beam collapse. The above example of Merle shows, however, that this is not the case, since a solution that collapses at k points cannot undergo a whole-beam collapse. One could argue, though, that this is not a “good” counter-example, because Merle's solution effectively undergoes a whole-beam collapse, in the sense that all the power collapses into the k singularity points. The Bourgain-Wang solutions show, however, that singular solutions can have a linear blowup rate, yet undergo a “genuine” partial-beam collapse.

13.1.2 Loglog Law Blowup Rate

In Sect. 14.6 we shall see that the critical NLS admits singular H^1 solutions that collapse with the peak-type $\psi_{R^{(0)}}$ profile. The blowup rate of these solutions is a square root with a loglog correction (the *loglog law*), i.e.,

$$l(z) \sim \frac{\sqrt{2\pi}}{\|\nabla R^{(0)}\|_2} \left(\frac{Z_c - z}{\log |\log(Z_c - z)|} \right)^{\frac{1}{2}}, \quad z \rightarrow Z_c. \quad (13.4)$$

13.1.3 Square-Root Blowup Rate

The critical NLS “appears to” admit singular H^1 solutions that collapse with the ring-type ψ_G profile (Chap. 19) or with the vortex profile ψ_{G_m} (Chap. 20).¹ The blowup

¹ See Sects. 19.6 and 20.3 for an explanation of the disclaimer “appears to”.

rate of these solutions is a *square root*, i.e.,

$$l(z) \sim \kappa \cdot (Z_c - z)^{\frac{1}{2}}, \quad z \rightarrow Z_c. \quad (13.5)$$

13.1.4 Square-Root Bound

The only rigorous bound for the blowup rate of *all* H^1 singular solutions of the critical NLS is the following theorem, due to Cazenave and Weissler:²

Theorem 13.1 ([41]) *Let $\psi(z, \mathbf{x})$ be a solution of the critical NLS (13.1) that becomes singular at Z_c . Then there exists a positive constant $K = K(\|\psi_0\|_2)$ such that*

$$\|\nabla \psi\|_2 \geq \frac{K}{\sqrt{Z_c - z}}, \quad 0 \leq z < Z_c. \quad (13.6)$$

Proof We present here a simpler proof, due to Merle [176]. Consider a given z such that $0 \leq z < Z_c$, let $\lambda(z) := \|\nabla \psi(z, \mathbf{x})\|_2$, and let

$$\phi(s, \mathbf{x}) := \frac{1}{\lambda^{\frac{d}{2}}(z)} \psi \left(z + \frac{s}{\lambda^2(z)}, \frac{\mathbf{x}}{\lambda(z)} \right).$$

Then ϕ is defined for $z + \frac{s}{\lambda^2(z)} < Z_c$, i.e., for $s < S_c(z) := \lambda^2(z)(Z_c - z)$. It is easy to verify that

$$i\phi_s(s, \mathbf{x}) + \Delta\phi + |\phi|^{\frac{4}{d}}\phi = 0, \quad 0 \leq s < S_c \quad (13.7)$$

and

$$\lim_{s \rightarrow S_c} \|\nabla \phi(s, \mathbf{x})\|_2 = \frac{1}{\lambda(z)} \lim_{\tilde{z} \rightarrow Z_c} \|\nabla \psi \left(\tilde{z} = z + \frac{s}{\lambda^2(z)}, \frac{\mathbf{x}}{\lambda(z)} \right)\|_2 = \infty.$$

In addition, we have that

$$\|\phi(s = 0, \mathbf{x})\|_2 = \|\psi(z, \mathbf{x})\|_2 = \|\psi_0(\mathbf{x})\|_2$$

and

$$\|\nabla \phi(s = 0, \mathbf{x})\|_2 = \frac{1}{\lambda(z)} \|\nabla \psi(z, \mathbf{x})\|_2 = 1.$$

Thus, for any fixed z such that $0 \leq z < Z_c$,

$$\|\phi(s = 0, \mathbf{x})\|_{H^1}^2 = \|\psi_0(\mathbf{x})\|_2^2 + 1.$$

² Additional rigorous results on the blowup rate are given in Sect. 14.6. These results, however, are not valid for all singular solutions.

By NLS local existence theory (Theorem 5.1), ϕ exists in the interval $0 \leq s \leq S_M$, where S_M depends only on the H^1 norm of the initial condition, i.e., $S_M(z) = S_M(\|\phi(0, \mathbf{x})\|_{H^1})$. Since $\|\phi(0, \mathbf{x})\|_{H^1} = \|\psi_0\|_2^2 + 1$, we see that S_M is independent of z .

Now, since ϕ blows up at S_c ,

$$S_M < S_c(z), \quad 0 \leq z < Z_c. \quad (13.8)$$

Let $K = \sqrt{S_M}$. Then (13.8) can be rewritten as $K^2 < \lambda^2(z)(Z_c - z)$. Hence, (13.6) follows. \square

Theorem 13.1 yields an upper bound for the blowup rate:

Corollary 13.1 *The blowup rate of singular solutions of the critical NLS is at least a square root, i.e.,*

$$l(z) \leq M(Z_c - z)^{\frac{1}{2}}, \quad 0 \leq z < Z_c, \quad (13.9)$$

where M is a positive constant that depends only on $\|\psi_0\|_2^2$.

The upper bound (13.9) is crude for singular solutions that have a linear blowup rate (Sect. 13.1.1). These solutions, however, are unstable. This bound is “almost sharp” for solutions that undergo a stable collapse with the $\psi_{R^{(0)}}$ profile at the loglog law blowup rate (13.4). Moreover, this upper bound is sharp for the ring and vortex solutions that collapse at the square-root blowup rate (13.5) with the ψ_G and ψ_{G_m} profiles, respectively.

Remark In Sect. 3.5.2 we saw that under the aberrationless approximation, the blowup rate is a square root.

Remark A lower bound for the blowup rate is not known.

The BNLS analog of Corollary 13.1 is

Theorem 13.2 ([14]) *Let ψ be a solution of the critical biharmonic NLS*

$$i\psi_z(z, \mathbf{x}) - \Delta^2\psi + |\psi|^{\frac{8}{d}}\psi = 0, \quad \psi(0, \mathbf{x}) = \psi_0(\mathbf{x}) \in H^2, \quad (13.10)$$

that becomes singular at Z_c , and let $l_B(z) := \|\Delta\psi\|_2^{-\frac{1}{2}}$ be its blowup rate. Then

$$l_B(z) \leq M_B(Z_c - z)^{\frac{1}{4}}, \quad 0 \leq z < Z_c, \quad (13.11)$$

where M_B is a positive constant that depends only on $\|\psi_0\|_2^2$.

Exercise 13.1 Prove Theorem 13.2. Note that by BNLS local existence theory, see [19], if $\psi_0 \in H^2$ then the BNLS solution exists in an interval $[0, Z_M]$, where $Z_M = Z_M(\|\psi_0\|_{H^2})$.

13.1.5 Blowup Rate of L^p Norms

Theorem 13.1 provides information on the blowup rate of the L^p norms:

Corollary 13.2 *Let ψ be a solution of the critical NLS (13.1) that becomes singular at Z_c . Then for any p such that $2\sigma + 2 \leq p \leq \infty$, there exists a constant K_p , such that*

$$\|\psi\|_p \geq K_p(Z_c - z)^{-\frac{p-2}{2\sigma p}} = K_p(Z_c - z)^{-\frac{(p-2)d}{4p}}, \quad 0 \leq z < Z_c.$$

In particular,

$$\|\psi\|_\infty \geq K_\infty(Z_c - z)^{-\frac{1}{2\sigma}} = K_\infty(Z_c - z)^{-\frac{d}{4}}, \quad 0 \leq z < Z_c.$$

Proof By (10.9) and Theorem 13.1,

$$\tilde{K}(Z_c - z)^{-\frac{1}{2\sigma+2}} \leq \|\psi\|_{2\sigma+2}, \quad 0 \leq z < Z_c.$$

In addition, by the interpolation inequality (5.15) for L^p norms and power conservation, for $p \geq 2\sigma + 2$,

$$\|\psi\|_{2\sigma+2} \leq \|\psi_0\|_2^\alpha \|\psi\|_p^{1-\alpha}, \quad 1-\alpha = \frac{\sigma p}{(\sigma+1)(p-2)}.$$

Therefore, the result follows. \square

Remark In Corollary 5.8 we proved that $\|\psi\|_p$ blows up at Z_c for $2\sigma + 2 \leq p \leq \infty$. Corollary 13.2 improves this result in the critical case, by providing a lower bound for the blowup rate of $\|\psi\|_p$.

Remark In Corollary 13.6 we will extend this result to $2 < p \leq \infty$.

Exercise 13.2 Generalize Corollary 13.2 to the critical BNLS (13.10).

13.1.6 Blowup Rate and the Lens Transformation

Let $\psi(z, \mathbf{x})$ be a solution of the critical NLS with initial condition $\psi_0(\mathbf{x})$ that collapses at Z_c , and let $\tilde{\psi}(z, \mathbf{x})$ be the solution of the critical NLS with the initial condition

$$\tilde{\psi}_0(\mathbf{x}) = \psi_0(\mathbf{x}) e^{-i \frac{|\mathbf{x}|^2}{4F}}, \quad (13.12)$$

i.e., the initial condition $\psi_0(\mathbf{x})$, focused by a lens with a focal distance F . In Sect. 8.4.5 we used the lens transformation to show that if

$$F > 0 \quad \text{or} \quad F < -Z_c < 0,$$

i.e., if the lens is focusing or weakly defocusing, respectively, then the focused solution $\tilde{\psi}$ collapses at \tilde{Z}_c , where $0 < \tilde{Z}_c < \infty$ and

$$\frac{1}{\tilde{Z}_c} = \frac{1}{Z_c} + \frac{1}{F}. \quad (13.13)$$

We now ask whether the addition of a lens affects the blowup rate. To see that, let

$l(z) := \left(\frac{\frac{2}{d}+1}{\|\psi(z, \mathbf{x})\|^{\frac{4}{d}+2}} \right)^{\frac{1}{2}}$ and $\tilde{l}(z) := \left(\frac{\frac{2}{d}+1}{\|\tilde{\psi}(z, \mathbf{x})\|^{\frac{4}{d}+2}} \right)^{\frac{1}{2}}$ denote the blowup rates of ψ and $\tilde{\psi}$, respectively, see (13.2). Let us further define

$$f(z) = l(Z_c - z), \quad \tilde{f}(z) = \tilde{l}(\tilde{Z}_c - z), \quad (13.14)$$

so that both functions would vanish at the same point ($z = 0$). For example, if

$$l(z) = \kappa \cdot (Z_c - z)^p, \quad \tilde{l}(z) = \tilde{\kappa} \cdot (\tilde{Z}_c - z)^{\tilde{p}},$$

then

$$f(z) = l(Z_c - z) = \kappa \cdot z^p, \quad \tilde{f}(z) = \tilde{\kappa} \cdot z^{\tilde{p}}.$$

We say that $\tilde{\psi}$ has the same blowup rate as ψ if

$$\tilde{f}(z) \sim c \cdot f(z), \quad z \rightarrow 0+, \quad (13.15)$$

where c is a positive constant. If $c = 1$, the multiplicative constant of the blowup rate is also independent of the lens (i.e., $\tilde{\kappa} = \kappa$).

Lemma 13.1 *In the critical NLS, any blowup rate of the form*

$$l(z) \sim \kappa \cdot (Z_c - z)^p (\log |\log(Z_c - z)|)^q, \quad p > 0, \quad q \in \mathbb{R}, \quad (13.16)$$

is unaffected by the addition of a lens, i.e., if we replace ψ_0 with $\tilde{\psi}_0$, see (13.12), then (13.16) still holds with the same p and q . If, in addition, the multiplicative constant κ is also unaffected by the lens, then $p = 1/2$.

Proof Since $\tilde{\psi}$ is given by the lens transformation (8.6) of ψ with $L = 1 - z/F$,

$$|\tilde{\psi}(z, \mathbf{x})| = \frac{1}{L^{\frac{d}{2}}(z)} |\psi(\xi, \mathbf{x})|, \quad \xi = \frac{\mathbf{x}}{L}, \quad \xi = \int_0^z \frac{ds}{L^2(s)}.$$

Therefore,

$$\frac{\frac{2}{d}+1}{\tilde{l}^2(z)} = \int |\tilde{\psi}(z, \mathbf{x})|^{\frac{4}{d}+2} d\mathbf{x} = \frac{1}{L^2(z)} \int |\psi(\xi(z), \mathbf{x})|^{\frac{4}{d}+2} d\mathbf{x} = \frac{1}{L^2(z)} \frac{\frac{2}{d}+1}{l^2(\xi(z))}.$$

Hence, by (13.14),

$$\tilde{f}(\tilde{Z}_c - z) = \tilde{l}(z) = L(z)l(\xi(z)) = L(z)f(Z_c - \xi(z)).$$

To finish the proof, we need to show that

$$\tilde{f}(\tilde{Z}_c - z) \sim c \cdot f(\tilde{Z}_c - z), \quad z \rightarrow \tilde{Z}_c, \quad (13.17a)$$

see (13.15), where \tilde{Z}_c is given by (13.13), and that

$$c = 1 \implies p = \frac{1}{2}. \quad (13.17b)$$

Therefore, we need to show that

$$L(z)f(Z_c - \xi(z)) \sim c \cdot f(\tilde{Z}_c - z), \quad z \rightarrow \tilde{Z}_c. \quad (13.18)$$

We first claim that $L(\tilde{Z}_c) > 0$. If $F < 0$, this is immediate. If $F > 0$, then by (13.13),

$$\frac{1}{\tilde{Z}_c} = \frac{1}{Z_c} + \frac{1}{F} > \frac{1}{F} > 0.$$

Therefore, $\tilde{Z}_c < F$ and $L(\tilde{Z}_c) = 1 - \frac{\tilde{Z}_c}{F} > 0$.

Now, by l'Hospital's rule,

$$\lim_{z \rightarrow \tilde{Z}_c} \frac{Z_c - \xi(z)}{\tilde{Z}_c - z} \tilde{Z}_c - z = \xi'(\tilde{Z}_c) = \frac{1}{L^2(\tilde{Z}_c)} > 0.$$

Hence,

$$Z_c - \xi(z) \sim \frac{\tilde{Z}_c - z}{L^2(\tilde{Z}_c)}, \quad z \rightarrow \tilde{Z}_c.$$

If $l(z)$ is given by (13.16), then

$$f(s) \sim \kappa \cdot s^p (\log |\log s|)^q, \quad s \rightarrow 0+.$$

Therefore, as $z \rightarrow \tilde{Z}_c$,

$$L(z)f(Z_c - \xi(z)) \sim L(\tilde{Z}_c) f\left(\frac{\tilde{Z}_c - z}{L^2(\tilde{Z}_c)}\right) \sim c \cdot f(\tilde{Z}_c - z), \quad c = L^{1-2p}(\tilde{Z}_c),$$

which yields (13.17). \square

Remark Expression (13.16) covers all known blowup rates of the critical NLS: linear, square root, and loglog law.

Remark We already used Lemma 13.1 in the proof of Lemma 10.6 to show that the solution of the critical NLS with $\psi_0 = (1 + \epsilon)\psi_{R^{(0)}}^{\text{explicit}}(z = 0)$ has the same blowup rate as the solution with $\psi_0 = (1 + \epsilon)R^{(0)}$.

Exercise 13.3 Show that in the critical NLS, any blowup rate of the form (13.16) is unaffected by the dilation symmetry $\psi(z, \mathbf{x}) \rightarrow \lambda^{\frac{d}{2}}\psi(\lambda^2 z, \lambda\mathbf{x})$. If, in addition, the multiplicative constant κ in the blowup rate (13.16) is unaffected by dilation, then $p = 1/2$.

Thus, a linear blowup rate, a square-root blowup rate, and the loglog law blowup rate are unaffected by the lens transformation and by dilations.

Corollary 13.3 If the blowup rate is of the form (13.16), and if the multiplicative constant κ is universal (i.e., independent of ψ_0), the blowup rate has to be a square root, with or without a logarithmic correction.

The multiplicative constant κ is universal for loglog collapse, see (14.16), but not for a square-root collapse (Chap. 19) or a linear collapse (Sect. 10.1).

13.2 Convergence to a Self-similar Blowup Profile

In this section we consider the blowup profile of solutions of the critical NLS. We limit the discussion to solutions that collapse at a single point, since collapse at more than one point is unstable (Sect. 13.4). The results in this section are valid for all H^1 singular solutions. Stronger results are available for solutions with power slightly above P_{cr} (Sect. 14.6) and for vortex solutions (Sect. 15.11).

In Theorem 13.3 we will prove that near the singularity, any blowup solution of the critical NLS approaches a quasi self-similar profile. To motivate this result, recall the explicit blowup solution

$$\psi_R^{\text{explicit}}(z, r) = \frac{1}{(Z_c - z)^{\frac{d}{2}}} R \left(\frac{r}{Z_c - z} \right) e^{i\zeta(z) - i\frac{r^2}{4(Z_c - z)}}.$$

The blowup rate of ψ_R^{explicit} is, see (10.12),

$$l(z) = \lambda(Z_c - z), \quad \lambda = \left(\frac{\frac{2}{d} + 1}{\|R\|_{\frac{4}{d}+2}^{\frac{4}{d}+2}} \right)^{\frac{1}{2}}.$$

To “extract” from ψ_R^{explicit} its self-similar profile, let

$$S(\psi)(z, \rho) := l^{\frac{d}{2}}(z)\psi(z, r = l(z)\rho). \tag{13.19}$$

Then

$$S\left(\psi_R^{\text{explicit}}\right)(z, \rho) = \lambda^{\frac{d}{2}} R(\lambda\rho) e^{i\xi(z) - i(Z_c - z)^{\frac{\lambda^2 \rho^2}{4}}}.$$

Therefore, for a fixed ρ ,

$$S\left(\psi_R^{\text{explicit}}\right)(z, \rho) \sim \lambda^{\frac{d}{2}} R(\lambda\rho) e^{i\xi(z)}, \quad z \rightarrow Z_c.$$

Since $\lim_{z \rightarrow Z_c} \xi(z) = \infty$, see (10.5), $S\left(\psi_R^{\text{explicit}}\right)(z, \rho)$ does not have a limit as $z \rightarrow Z_c$. For every sequence $z_k \rightarrow Z_c$, however, we can extract a subsequence z_{k_j} for which $\lim_{j \rightarrow \infty} e^{i\xi(z_{k_j})} = e^{i\theta_0}$ for some $\theta_0 \in \mathbb{R}$. Hence, $S\left(\psi_R^{\text{explicit}}\right)(z_{k_j}, \rho) \rightarrow \lambda^{\frac{d}{2}} R(\lambda\rho) e^{i\theta_0}$.

In Theorem 13.3 we will use transformation (13.19) to “extract” the self-similar profile of singular radial solutions. In the case of nonradial solutions the transformation should be more general, so as to allow for a lateral movement of the collapsing core. Thus, if the center of the collapsing core is located at $\mathbf{x}_0(z)$, $S(\psi)$ should “zoom in” on the neighborhood of $\mathbf{x}_0(z)$.

Theorem 13.3 ([276]) *Let $\psi(z, \mathbf{x})$ be a solution of the critical NLS (13.1) that becomes singular at Z_c at a single point \mathbf{x}_c . Let $l(z) = 1/\|\nabla\psi\|_2$ and*

$$S(\psi)(z, \xi) := l^{\frac{d}{2}}(z) \psi\left(z, l(z)\xi - \mathbf{x}_0(z)\right). \quad (13.20)$$

Then there exists $\mathbf{x}_0(z) \in \mathbb{R}^d$, such that for any sequence $z_k \rightarrow Z_c$, there is a subsequence z_{k_j} such that

$$S(\psi)(z_{k_j}, \xi) \rightarrow \Psi(\xi) \quad \text{strongly in } L^p$$

for all p such that

$$\begin{cases} 2 < p \leq \infty, & \text{if } d \leq 2, \\ 2 < p < \frac{2d}{d-2}, & \text{if } d > 2. \end{cases} \quad (13.21)$$

Furthermore, $\|\Psi\|_{\frac{4}{d}+2}^{\frac{4}{d}+2} = 1 + \frac{2}{d}$ and $\|\Psi\|_2^2 \geq \|R^{(0)}\|_2^2$, where $R^{(0)}$ is the ground state of

$$R''(r) + \frac{d-1}{r} R' - R + |R|^{\frac{4}{d}} R = 0, \quad R'(0) = 0, \quad R(\infty) = 0. \quad (13.22)$$

If, in addition, $\psi = \psi(z, r)$ is radial, then $\mathbf{x}_0(z) \equiv 0$, $S(\psi)(z, \rho)$ is given by (13.19), and $\Psi = \Psi(\rho)$.

Proof We only prove for radial solutions and $d \geq 2$. Let $z_k \rightarrow Z_c$ and

$$\phi_k(\rho) := S(\psi)(z_k, \rho) = l^{\frac{d}{2}}(z_k) \psi(z_k, l(z_k)\rho). \quad (13.23)$$

It is easy to check that

$$\|\phi_k\|_2 = \|\psi_0\|_2, \quad \|\nabla\phi_k\|_2 = 1, \quad H(\phi_k) = l^2(z_k)H(\psi_0).$$

Since the sequence ϕ_k is bounded in H_{radial}^1 , it has a subsequence ϕ_{k_j} that converges weakly in H_{radial}^1 to a function $\Psi \in H_{\text{radial}}^1$. In addition, by Compactness Lemma 5.14, $\phi_{k_j} \rightarrow \Psi$ strongly in L^p for any p in the range (13.21).

We claim that $H(\Psi) \leq 0$ and $\Psi \not\equiv 0$. Therefore, it follows from Corollary 5.10 that $\|\Psi\|_2^2 \geq P_{\text{cr}}$, which concludes the proof.

We first show that $H(\Psi) \leq 0$. Since ϕ_{k_j} converges weakly in H^1 to Ψ , $\nabla\phi_{k_j}$ converge weakly in L^2 to $\nabla\Psi$. Therefore, $\|\nabla\Psi\|_2 \leq \lim_{j \rightarrow \infty} \|\nabla\phi_{k_j}\|_2$, see Lemma B.3. In addition, since $\phi_{k_j} \rightarrow \Psi$ strongly in $L^{\frac{4}{d}+2}$, $\|\Psi\|_{\frac{4}{d}+2} = \lim_{j \rightarrow \infty} \|\phi_{k_j}\|_{\frac{4}{d}+2}$. Therefore,

$$H(\Psi) \leq \lim_{j \rightarrow \infty} H(\phi_{k_j}) = \lim_{j \rightarrow \infty} l^2(z_{k_j})H(\psi_0) = 0.$$

Hence, $H(\Psi) \leq 0$. In addition,

$$\begin{aligned} 0 &= \lim_{j \rightarrow \infty} H(\phi_{k_j}) = \lim_{j \rightarrow \infty} \left(\|\nabla\phi_{k_j}\|_2^2 - \frac{1}{\frac{2}{d} + 1} \|\phi_{k_j}\|_{\frac{4}{d}+2}^{\frac{4}{d}+2} \right) \\ &= 1 - \frac{1}{\frac{2}{d} + 1} \|\Psi\|_{\frac{4}{d}+2}^{\frac{4}{d}+2}. \end{aligned} \tag{13.24}$$

Hence, $\|\Psi\|_{\frac{4}{d}+2}^{\frac{4}{d}+2} = \frac{2}{d} + 1$. In particular, $\Psi \not\equiv 0$. \square

Theorem 13.3, which was proved by Weinstein in 1989, was the first rigorous result that provided information on the local structure of collapsing solutions near the singularity. The ability to extract local information using global quantities (L^p norms) is discussed in Sect. 13.2.2.

Remark In Sect. 14.6 we will see that if the input power is slightly above P_{cr} , the self-similar profile Ψ is universal (i.e., independent of ψ_0) and is given by the ground state $R^{(0)}$. This, however, is not the case with the excited explicit blowup solutions $\psi_{R^{(n)}}^{\text{explicit}}$ with $n \geq 1$, with the ring-type blowup solutions that collapse with the ψ_G profile at a square-root blowup rate (Chap. 19), and with singular vortex solutions (Theorem 15.2).

The extension of Theorem 13.3 to the radial BNLS is

Theorem 13.4 ([14]) *Let $d \geq 2$, and let $\psi(z, r)$ be a radial solution of the critical BNLS (13.10) that becomes singular at Z_c . Let $l_B(z) = \|\Delta\psi\|_2^{-\frac{1}{2}}$ and $S(\psi)(z, \rho) := l_B^{\frac{d}{2}}(z)\psi(z, l_B(z)\rho)$. Then for any sequence $z_k \rightarrow Z_c$, there is a subsequence z_{k_j} , such that*

$$S(\psi)(z_k, \rho) \rightarrow \Psi_B(\rho) \quad \text{strongly in } L^p$$

for all p such that

$$\begin{cases} 2 < p \leq \infty, & \text{if } 2 \leq d \leq 4, \\ 2 < p < \frac{2d}{d-4}, & \text{if } d > 4. \end{cases} \quad (13.25)$$

Furthermore, $\|\Psi_B\|_{\frac{8}{d}+2}^{\frac{8}{d}+2} = 1 + \frac{4}{d}$ and $\|\Psi_B\|_2^2 \geq \|R_B^{(0)}\|_2^2$, where $R_B^{(0)}$ is the ground state of

$$-\Delta^2 R_B - R_B + |R_B|^{\frac{4}{d}} R_B = 0. \quad (13.26)$$

Exercise 13.4 Prove Theorem 13.4. Note that the relevant compactness result is Lemma 5.15.

13.2.1 Radial Solutions

In Lemma 5.5 we saw that if ψ_0 is radial, then ψ remains radial. In the critical case, singular radial solutions always collapse at the origin:

Lemma 13.2 ([188]) Let $\psi(z, r)$ be a singular radial solution of the critical NLS (13.1). Then ψ collapses at the origin.

Proof By Definition 5.7, ψ collapses at the origin if for any $\epsilon > 0$,

$$\lim_{z \rightarrow Z_c} \int_0^\epsilon |\psi(z, r)|^{\frac{4}{d}+2} r^{d-1} dr = \infty.$$

Let $r = l(z)\rho$. Then

$$\begin{aligned} \int_0^\epsilon |\psi(z, r)|^{\frac{4}{d}+2} r^{d-1} dr &= l^d(z) \int_0^{\frac{\epsilon}{l(z)}} |\psi(z, l\rho)|^{\frac{4}{d}+2} \rho^{d-1} d\rho \\ &= l^{-2}(z) \int_0^{\frac{\epsilon}{l(z)}} |S(\psi)(z, \rho)|^{\frac{4}{d}+2} \rho^{d-1} d\rho. \end{aligned}$$

By Theorem 13.3 with $p = \frac{4}{d} + 2$ and Eq. (13.24), as $z \rightarrow Z_c$,

$$\begin{aligned} \int_0^{\frac{\epsilon}{l(z)}} |S(\psi)|^{\frac{4}{d}+2} \rho^{d-1} d\rho &\sim \int_0^\infty |S(\psi)|^{\frac{4}{d}+2} \rho^{d-1} d\rho \\ &\longrightarrow \int_0^\infty |\Psi|^{\frac{4}{d}+2} \rho^{d-1} d\rho = \frac{2}{d} + 1. \end{aligned}$$

Hence,

$$\lim_{z \rightarrow Z_c} \int_0^\epsilon |\psi(z, r)|^{\frac{4}{d}+2} r^{d-1} dr = \left(\frac{2}{d} + 1 \right) \lim_{z \rightarrow Z_c} l^{-2}(z) = \infty. \quad \square$$

Remark The question whether radial solutions collapse only at the origin is still open (Sect. 13.4.1).

Remark Lemma 13.2 does not extend to the supercritical case. Indeed, the supercritical NLS admits radial solutions that collapse on a sphere, and not at the origin (Chap. 22).

Exercise 13.5 Let ψ be a singular radial solution of the critical biharmonic NLS (13.10). Prove that ψ collapses at $r = 0$.

13.2.2 Quasi Self-similar Collapse

“Reversing” transformation (13.19), one obtains

$$\psi(z, r) = \frac{1}{l^{\frac{d}{2}}(z)} S(\psi) \left(z, \frac{r}{l(z)} \right).$$

To interpret Theorem 13.3, assume for a moment that $S(\psi)(z, r) \equiv \Psi(r)$. In that case, $\psi(z, r) = l^{-\frac{d}{2}}(z) \Psi \left(\frac{r}{l(z)} \right)$, i.e., the collapsing solution is self-similar. Therefore, Theorem 13.3 may seem to suggest that as $z_{k_j} \rightarrow Z_c$, ψ approaches a self-similar profile ψ_F , where

$$|\psi_F| := \frac{1}{l^{\frac{d}{2}}(z)} F \left(\frac{r}{l(z)} \right), \quad \|F\|_2^2 \geq P_{\text{cr}}.$$

In fact, Theorem 13.3 “only” shows that the blowup profile is *quasi self-similar*, i.e., that as $z_{k_j} \rightarrow Z_c$,

$$\psi(z, r) \sim \begin{cases} \psi_F, & \text{if } 0 \leq \frac{r}{l(z)} \leq \rho_0, \\ \psi_{\text{outer}}, & \text{if } \frac{r}{l(z)} \gg \rho_0, \end{cases} \quad (13.27)$$

where $\rho_0 \gg 1$. Here, by *quasi self-similar* we mean that, unlike the self-similar solutions ψ_R^{explicit} and ψ_G^{explicit} ,

1. only the inner core of the solution undergoes collapse, while the “outer solution” does not participate in the collapse process (partial-beam collapse),
2. even the inner core is not truly self-similar, since it is not *equal* to ψ_F , but only approaches it as $z_{k_j} \rightarrow Z_c$.

To see that Theorem 13.3 “only” implies that the blowup profile is quasi self-similar, consider the following informal argument. Assume that ψ collapses according to (13.27). Since ψ_{outer} does not participate in the collapse process, it has a finite limit as $z \rightarrow Z_c$, i.e., $\lim_{z \rightarrow Z_c} |\psi_{\text{outer}}(z, r)| = \phi(r)$. Therefore, by (13.19),

$$|S(\psi)(z, \rho)| \sim \begin{cases} F(\rho), & \text{if } 0 \leq \rho \leq \rho_0, \\ l^{\frac{d}{2}}(z)\phi(l(z)\rho), & \text{if } \rho \gg \rho_0. \end{cases}$$

Since

$$\int_{\rho_0}^{\infty} \left(l^{\frac{d}{2}}(z) |\phi(l\rho)| \right)^p \rho^{d-1} d\rho = l^{\frac{(p-2)d}{2}}(z) \int_0^{\infty} |\phi(r)|^p r^{d-1} dr, \quad (13.28)$$

it follows that $S(\psi)(z, \rho) \xrightarrow{L^p} \Psi(\rho)$ for $p > 2$, where

$$|\Psi| = \begin{cases} F(\rho), & \text{if } 0 \leq \rho \leq \rho_0, \\ 0, & \text{if } \rho \gg \rho_0. \end{cases}$$

Hence, the presence of an “outer solution” does not contradict with Theorem 13.3.

Note that Theorem 13.3 does not say that $S(\psi)(z, r) \xrightarrow{L^2} \Psi(r)$. Indeed, if $S(\psi)(z, r) \xrightarrow{L^2} \Psi(r)$ then $\|\psi\|_2^2 = \|\Psi\|_2^2$, and so ψ undergoes a whole-beam collapse. Critical collapse, however, is generically a partial-beam process (Sect. 7.7.1).

Finally, we note that, by (13.27),

$$\begin{aligned} \|\psi\|_p^p &\sim \int_{r < \rho_0 l(z)} |\psi_F|^p d\mathbf{x} + \int_{r > \rho_0 l(z)} |\psi_{\text{outer}}|^p d\mathbf{x} \\ &\sim l^{-\frac{d}{2}(p-2)}(z) \int_{\rho < \rho_0} |F|^p d\xi + \int |\phi|^p d\mathbf{x}. \end{aligned}$$

Therefore, the L^p norm of blowup solutions is only affected by the collapsing core for $p > 2$, but is “equally affected” by the collapsing core and by the outer solution for $p = 2$. In other words, while the L^2 norm cannot “distinguish” between the collapsing core and the non-collapsing background, L^p norms for $p > 2$ can “zoom in” on the collapsing core.

13.2.3 $l(z) \sim c_l L(z)$ in the Critical NLS

Previously, we saw that the collapsing core of a singular solution of the critical NLS approaches a self-similar profile, so that

$$|\psi| \sim |\psi_F| = \frac{1}{L^{\frac{d}{2}}(z)} F\left(\frac{r}{l(z)}\right), \quad r = O(l(z)).$$

Conclusion 13.1 *In the critical NLS, the blowup rate $l(z)$ is linearly proportional to the dimensionless width of the collapsing core.*

Remark This conclusion does not hold in the supercritical case (Sect. 13.6.2).

Since the radial width is only determined up to a multiplicative constant, we sometimes have that

$$|\psi| \sim \frac{1}{L^{\frac{d}{2}}(z)} F\left(\frac{r}{L(z)}\right), \quad r = O(L(z)), \quad (13.29)$$

where $l(z) \sim c_l L(z)$. To find c_l in this case, we note that $\|\psi\|_{\frac{4}{d}+2}^{\frac{4}{d}+2} \sim L^{-2} \|F\|_{\frac{4}{d}+2}^{\frac{4}{d}+2}$. Therefore, by (13.3),

$$l(z) \sim c_l L(z), \quad c_l = \left(\frac{\frac{2}{d} + 1}{\|F\|_{\frac{4}{d}+2}^{\frac{4}{d}+2}} \right)^{\frac{1}{2}}. \quad (13.30)$$

13.2.4 $l_B(z) \sim c_{l_B} L(z)$ in the Critical BNLS

Let ψ be a solution of the critical BNLS (13.10) that becomes singular at Z_c . The blowup rate of ψ is

$$l_B(z) := \frac{1}{\|\Delta\psi\|_2^{\frac{1}{2}}} \sim \left(\frac{\frac{4}{d} + 1}{\|\psi\|_{\frac{8}{d}+2}^{\frac{8}{d}+2}} \right)^{\frac{1}{4}}, \quad (13.31)$$

see Sect. 10.9. By Theorem 13.4, the collapsing core approaches a self-similar profile, so that

$$|\psi| \sim \frac{1}{l_B^{\frac{d}{2}}(z)} F_B\left(\frac{r}{l_B(z)}\right), \quad r = O(l_B(z)).$$

Hence, in the critical BNLS the blowup rate is linearly proportional to the dimensionless width. Since the radial width is only determined up to a multiplicative constant, we sometimes have that

$$|\psi| \sim \frac{1}{L^{\frac{d}{2}}(z)} F_B\left(\frac{r}{L(z)}\right), \quad r = O(L(z)).$$

Therefore, $\|\psi\|_{\frac{8}{d}+2}^{\frac{8}{d}+2} \sim L^{-4}(z) \|F_B\|_{\frac{8}{d}+2}^{\frac{8}{d}+2}$. Hence, by (13.31),

$$l_B(z) \sim c_{l_B} L(z), \quad c_{l_B} = \left(\frac{\frac{4}{d} + 1}{\|F_B\|_{\frac{8}{d}+2}^{\frac{8}{d}+2}} \right)^{\frac{1}{4}}. \quad (13.32)$$

13.2.5 Nawa's Theorem

Additional information on the blowup profile was obtained in 1994 by Nawa:

Theorem 13.5 ([196]) *Let ψ be a solution of the critical NLS (13.1) that blows up at Z_c at a single point \mathbf{x}_c . Let $\{z_n\}$ be a monotonically-increasing sequence such that*

$$\lim_{n \rightarrow \infty} z_n = Z_c \quad \text{and} \quad \sup_{z \in [0, z_n)} \|\psi(z, \mathbf{x})\|_{\frac{4}{d}+2} = \|\psi(z_n, \mathbf{x})\|_{\frac{4}{d}+2}.$$

Let $L_n = \|\psi(z_n, \mathbf{x})\|_{\frac{4}{d}+2}^{-\left(\frac{2}{d}+1\right)}$, and let

$$u_n(z, \mathbf{x}) = L_n^{\frac{d}{2}} \psi^* \left(z_n - L_n^2 z, L_n \mathbf{x} \right), \quad -\frac{Z_c - z_n}{L_n^2} < z \leq \frac{z_n}{L_n^2}.$$

Then there exists a subsequence of $\{u_n\}$, still denoted by $\{u_n\}$, with the following properties: There exist

1. A nontrivial global solution $u(z, \mathbf{x})$ of (13.1) with zero Hamiltonian and momentum, i.e., $H(u) = 0$ and $\operatorname{Im} \int u^* \nabla u \, d\mathbf{x} = 0$.
2. A sequence $\{\mathbf{x}_{0,n}\}$, such that for any $Z > 0$,

$$\lim_{n \rightarrow \infty} \sup_{0 \leq z \leq Z} \|u_n(z, \mathbf{x}) - u(z, \mathbf{x} - \mathbf{x}_{0,n})\|_{\frac{4}{d}+2} = 0,$$

$$\lim_{n \rightarrow \infty} \sup_{0 \leq z \leq Z} \|\nabla u_n(z, \mathbf{x}) - \nabla u(z, \mathbf{x} - \mathbf{x}_{0,n})\|_2 = 0,$$

and

$$\lim_{n \rightarrow \infty} \sup_{0 \leq z \leq Z} \|u_n(z, \mathbf{x}) - u(z, \mathbf{x} - \mathbf{x}_{0,n}) - \phi_n(z, \mathbf{x})\|_2 = 0,$$

where $\phi_n(z, \mathbf{x})$ is the solution of the linear Schrödinger equation

$$i \frac{\partial \phi_n}{\partial z} + \Delta \phi_n = 0, \quad z \geq 0, \quad \mathbf{x} \in \mathbb{R}^d,$$

with the initial condition $\phi_n(0, \mathbf{x}) = u_n(0, \mathbf{x}) - u(0, \mathbf{x} - \mathbf{x}_{0,n})$.

Furthermore, $\|\psi_0\|_2^2 \geq \|u(z, \mathbf{x})\|_2^2 \geq P_{\text{cr}}$.

Remark If the initial condition is radial, then $\mathbf{x}_{0,n} \equiv 0$.

Theorem 13.5 shows that the blowup solution is composed of a localized collapsing core and a dilated solution of the linear Schrödinger equation. The collapsing core has power $\geq P_{\text{cr}}$, and in the rescaled variables it approaches a global zero-Hamiltonian NLS solution. Examples of zero-Hamiltonian global solutions are $u = e^{iz} R^{(n)}(r)$, where $R^{(n)}$ is the n th-state of (13.22). Additional rigorous results by Nawa on the asymptotic profile of blowup solutions are given in [197–199].

13.3 Power Concentration

In Sect. 10.2 we saw that all the power of the explicit blowup solution ψ_R^{explicit} concentrates at the blowup point (*whole-beam collapse*), i.e.,

$$\lim_{z \rightarrow Z_c} |\psi_R^{\text{explicit}}(z, r)|^2 = \|\psi_R^{\text{explicit}}\|^2 \delta(r).$$

The following theorem shows that for any blowup solution of the critical NLS, a finite amount of power, which is at least P_{cr} , concentrates into the blowup point. This result was proved by Merle and Tsutsumi [188] for radial solutions and $d \geq 2$, independently by Weinstein [276] for any dimension and without the assumption of radial symmetry, and was subsequently improved by Nawa [194, 195].

Theorem 13.6 (Power concentration³ [188, 195, 276]) *Let $\psi(z, \mathbf{x})$ be a solution of the critical NLS (13.1) which becomes singular at Z_c . Then there exists a continuous function $\mathbf{x}_0(z)$, such that for all $\epsilon > 0$,*

$$\liminf_{z \rightarrow Z_c} \|\psi(z, \mathbf{x})\|_{L^2(|\mathbf{x}-\mathbf{x}_0(z)|<\epsilon)}^2 \geq P_{\text{cr}},$$

where $P_{\text{cr}} = \|R^{(0)}\|_2^2$ and $R^{(0)}$ is the ground state of (13.22). In particular, if $\psi = \psi(z, r)$ is radial, then $\mathbf{x}_0(z) \equiv 0$, and for all $\epsilon > 0$,

$$\liminf_{z \rightarrow Z_c} \|\psi(z, r)\|_{L^2(r<\epsilon)}^2 \geq P_{\text{cr}}. \quad (13.33)$$

Proof We begin with the case of radial solutions and $d \geq 2$. Assume by negation that there exist $\epsilon_0 > 0$ and a sequence $z_k \rightarrow Z_c$, such that

$$\lim_{k \rightarrow \infty} \|\psi(z_k, r)\|_{L^2(r<\epsilon_0)}^2 < P_{\text{cr}}. \quad (13.34)$$

³ This property is also called *mass concentration* and *L^2 concentration*.

Let ϕ_k be given by (13.23). Then for any $\epsilon > 0$,

$$\|\phi_k(\rho)\|_{L^2\left(\rho < \frac{\epsilon}{l(z_k)}\right)}^2 = \|\psi(z_k, r)\|_{L^2(r < \epsilon)}^2.$$

Hence, since $\lim_{k \rightarrow \infty} l(z_k) = 0$, then for any $\rho_m > 0$, if k is sufficiently large,

$$\|\phi_k(\rho)\|_{L^2(\rho < \rho_m)}^2 \leq \|\psi(z_k, r)\|_{L^2(r < \epsilon)}^2.$$

As in the proof of Theorem 13.3, ϕ_k has a subsequence ϕ_{k_j} that converges weakly to Ψ in L^2 , where $\|\Psi\|_2^2 \geq P_{\text{cr}}$. Therefore, ϕ_{k_j} also converges weakly to Ψ in $L^2(\rho < \rho_m)$. Hence,

$$\|\Psi(\rho)\|_{L^2(\rho < \rho_m)}^2 \leq \liminf_{j \rightarrow \infty} \|\phi_{k_j}(\rho)\|_{L^2(\rho < \rho_m)}^2,$$

and so

$$\|\Psi(\rho)\|_{L^2(\rho < \rho_m)}^2 \leq \liminf_{j \rightarrow \infty} \|\psi(z_{k_j}, r)\|_{L^2(r < \epsilon)}^2.$$

Since this holds for all ρ_m , we have that

$$P_{\text{cr}} \leq \|\Psi\|_2^2 \leq \liminf_{j \rightarrow \infty} \|\psi(z_{k_j}, r)\|_{L^2(r < \epsilon)}^2,$$

which is in contradiction with (13.34).

Weinstein's proof in the nonradial case is based on the concentration compactness method of Lions [159]. A different proof was provided by Nawa [194]. We present here the proof of Hmidi and Keraani, which is based on

Theorem 13.7 (nonradial compactness [127]) *Let $\{v_n(\xi)\}_{n=1}^\infty$ be a bounded sequence of H^1 functions such that*

$$\limsup_{n \rightarrow \infty} \|\nabla v_n\|_2 \leq M \quad \text{and} \quad \limsup_{n \rightarrow \infty} \|v_n\|_{\frac{d}{d+2} + 2} \geq m.$$

Then there exists $\{\xi_{n_j}\}_{j=1}^\infty \subset \mathbb{R}^d$, such that

$$v_{n_j}(\xi + \xi_{n_j}) \rightharpoonup V(\xi) \quad \text{weakly in } H^1.$$

Moreover,

$$\|V\|_2^2 \geq \left(\frac{d}{d+2} \right)^{\frac{d}{2}} \frac{m^{d+2}}{M^d} \|R^{(0)}\|_2^2, \tag{13.35}$$

where $R^{(0)}$ is the ground state of (13.22).

Remark The fact that V satisfies relation (13.35) follows from the Gagliardo-Nirenberg inequality (Exercise 5.10).

To prove Theorem 13.6 in the nonradial case, let $z_n \rightarrow Z_c$, $l_n = \frac{1}{\|\nabla \psi(z_n)\|_2}$, and $v_n(\xi) = l_n^{\frac{d}{2}} \psi(z_n, l_n \xi)$. Then $\|\nabla v_n\|_2 \equiv 1$. In addition,

$$\|v_n\|_{\frac{4}{d}+2}^{\frac{4}{d}+2} = l_n^{d+2} \|\psi(z_n, l_n \xi)\|_{\frac{4}{d}+2}^{\frac{4}{d}+2} = l_n^2 \|\psi(z_n, \mathbf{x})\|_{\frac{4}{d}+2}^{\frac{4}{d}+2}.$$

Therefore, using (10.9),

$$\begin{aligned} 1 &= \lim_{n \rightarrow \infty} \frac{\frac{1}{1+\frac{2}{d}} \|\psi(z_n, \mathbf{x})\|_{\frac{4}{d}+2}^{\frac{4}{d}+2}}{\|\nabla \psi(z_n, \mathbf{x})\|_2^2} = \frac{1}{1 + \frac{2}{d}} \lim_{n \rightarrow \infty} l_n^2 \|\psi(z_n, \mathbf{x})\|_{\frac{4}{d}+2}^{\frac{4}{d}+2} \\ &= \frac{1}{1 + \frac{2}{d}} \lim_{n \rightarrow \infty} \|v_n\|_{\frac{4}{d}+2}^{\frac{4}{d}+2}. \end{aligned}$$

We thus see that v_n satisfies the conditions of Theorem 13.7 with $M = 1$ and $m = (1 + \frac{2}{d})^{\frac{1}{\frac{4}{d}+2}}$. Therefore, there exists $\{\xi_{n_j}\}_{j=1}^{\infty} \subset \mathbb{R}^d$ such that

$$v_{n_j}(\xi + \xi_{n_j}) \rightharpoonup V(\xi) \quad \text{weakly in } H^1$$

and

$$\|V\|_2^2 \geq \left(\frac{d}{d+2} \right)^{\frac{d}{2}} \left(1 + \frac{2}{d} \right)^{\frac{d+2}{\frac{4}{d}+2}} \|R^{(0)}\|_2^2 = \|R^{(0)}\|_2^2.$$

Now, for any $\epsilon > 0$,

$$\|v_n(\xi)\|_{L^2(|\xi - \xi_n| < \frac{\epsilon}{l_n})}^2 = \|\psi(z_n, \mathbf{x})\|_{L^2(|\mathbf{x} - \mathbf{x}_n| < \epsilon)}^2, \quad \mathbf{x}_n = l_n \xi_n.$$

Therefore, for any $\rho_m > 0$, if n is sufficiently large,

$$\|v_n(\xi)\|_{L^2(|\xi - \xi_n| < \rho_m)}^2 \leq \|\psi(z_n, \mathbf{x})\|_{L^2(|\mathbf{x} - \mathbf{x}_n| < \epsilon)}^2.$$

Since $v_{n_j}(\xi + \xi_{n_j})$ converges weakly to $V(\xi)$ in L^2 , it also converges weakly to V in $L^2(|\xi| < \rho_m)$. Hence,

$$\|V(\xi)\|_{L^2(|\xi| < \rho_m)}^2 \leq \liminf_{j \rightarrow \infty} \|v_{n_j}(\xi)\|_{L^2(|\xi - \xi_{n_j}| < \rho_m)}^2.$$

Therefore,

$$\|V(\xi)\|_{L^2(|\xi| < \rho_m)}^2 \leq \liminf_{j \rightarrow \infty} \|\psi(z_{n_j}, \mathbf{x})\|_{L^2(|\mathbf{x} - \mathbf{x}_{n_j}| < \epsilon)}^2.$$

Since this holds for all ρ_m ,

$$\|V\|_2^2 \leq \liminf_{j \rightarrow \infty} \|\psi(z_{n_j}, \mathbf{x})\|_{L^2(|\mathbf{x}-\mathbf{x}_{n_j}|<\epsilon)}^2.$$

Finally, since $P_{\text{cr}} \leq \|V\|_2^2$, we have that

$$P_{\text{cr}} \leq \liminf_{j \rightarrow \infty} \|\psi(z_{n_j}, \mathbf{x})\|_{L^2(|\mathbf{x}-\mathbf{x}_{n_j}|<\epsilon)}^2. \quad \square$$

The Concentration Theorem 13.6 implies a lower bound for the amount of power that collapses into the singularity (see Definition 7.2):

Corollary 13.4 *All singular solutions of the critical NLS undergo a strong collapse with $P_{\text{collapse}} \geq P_{\text{cr}}$.*

Previously, the necessary condition for collapse $\|\psi_0\|_2^2 \geq P_{\text{cr}}$ was derived using a priori estimates (Theorem 5.11). The Concentration Theorem 13.6 provides a more intuitive derivation of this condition: The power that collapses into the singularity satisfies $P_{\text{collapse}} \geq P_{\text{cr}}$, hence the total beam power satisfies $\|\psi\|_2^2 \geq P_{\text{collapse}} \geq P_{\text{cr}}$. Therefore, by power conservation, $\|\psi_0\|_2^2 \geq P_{\text{cr}}$.

Remark By power conservation, the amount of power that does not collapse into the singularity is $\|\psi_0\|_2^2 - P_{\text{collapse}} \leq \|\psi_0\|_2^2 - P_{\text{cr}}$.

Concentration Theorem 13.6 also leads to

Corollary 13.5 *Let ψ be a solution of the critical NLS (13.1) which collapses at Z_c . Then there exists a continuous function $\mathbf{x}_0(z)$, such that for all $\epsilon > 0$,*

$$\liminf_{z \rightarrow Z_c} \|\psi(z, \mathbf{x})\|_{L^\infty(|\mathbf{x}-\mathbf{x}_0(z)|<\epsilon)} = \infty.$$

In particular, if $\psi = \psi(z, r)$ is radial, then $\mathbf{x}_0(z) \equiv 0$, and for all $\epsilon > 0$,

$$\liminf_{z \rightarrow Z_c} \|\psi(z, r)\|_{L^\infty(r<\epsilon)}^2 = \infty.$$

Proof Assume by negation that for any function $\mathbf{x}_0(z)$, there exist $\epsilon_0 > 0$ and $M > 0$ such that

$$\liminf_{z \rightarrow Z_c} \|\psi(z, \mathbf{x})\|_{L^\infty(|\mathbf{x}-\mathbf{x}_0(z)|<\epsilon_0)} < M < \infty.$$

Then for all $0 < \epsilon < \epsilon_0$,

$$\liminf_{z \rightarrow Z_c} \|\psi(z, \mathbf{x})\|_{L^2(|\mathbf{x}-\mathbf{x}_0(z)|<\epsilon)}^2 < M^2 \rho_d \epsilon^d,$$

where ρ_d is the volume of the unit sphere in \mathbb{R}^d . This, however, is in contradiction with Theorem 13.6. \square

Remark In Corollary 5.7 we saw that $\lim_{z \rightarrow Z_c} \|\psi\|_\infty = \infty$ for all singular NLS solutions.

It is tempting to conclude from Corollary 13.5 that the amplitude of the solution at the blowup point $\mathbf{x}_c := \lim_{z \rightarrow Z_c} \mathbf{x}_0(z)$ has to become infinite, i.e., that

$$\lim_{z \rightarrow Z_c} |\psi(z, \mathbf{x}_0(z))| = \infty.$$

This, however, is not always the case. Indeed, in Corollary 15.13 we will see that the critical NLS admits singular vortex solutions that vanish at \mathbf{x}_c .

The extension of Theorem 13.6 to the radial critical BNLS is

Theorem 13.8 ([14]) *Let ψ be a radial solution of the critical BNLS (13.10) which becomes singular at Z_c . Then the origin $r = 0$ is a blowup point, and for all $\epsilon > 0$,*

$$\liminf_{z \rightarrow Z_c} \|\psi(z, r)\|_{L^2(r < \epsilon)}^2 \geq P_{\text{cr}}^B := \|R_B^{(0)}\|_2^2,$$

where $R_B^{(0)}$ is the ground state of (13.26).

Exercise 13.6 Prove Theorem 13.8.

13.3.1 Is $P_{\text{collapse}} = P_{\text{cr}}$?

In the radial case, Theorem 13.6 implies that the solution approaches a δ -function near the singularity point $r = 0$, i.e., as $z \rightarrow Z_c$,

$$|\psi|^2 \rightarrow P_{\text{collapse}} \delta(r) + |\phi(r)|^2, \quad P_{\text{collapse}} \geq P_{\text{cr}},$$

where ϕ is the limit of the “outer” solution, whose power is $\|\psi_0\|_2^2 - P_{\text{collapse}}$. Based on numerical and asymptotic studies carried out since the 1980s (see Sect. 14.1 and Chap. 17), it has been widely believed that regardless of the initial condition, near the singularity the collapsing core “always” approaches the universal blowup profile $\psi_{R^{(0)}}$, so that

$$|\psi(z, r)|^2 \sim |\psi_{R^{(0)}}(z, r)|^2 + |\phi(r)|^2, \tag{13.36a}$$

where

$$|\psi_{R^{(0)}}| = \frac{1}{L^{\frac{q}{2}}(z)} R^{(0)} \left(\frac{r}{L(z)} \right) \tag{13.36b}$$

and $\lim_{z \rightarrow Z_c} L(z) = 0$. In that case

$$P_{\text{collapse}} = P_{\text{cr}}. \tag{13.37}$$

In particular, P_{collapse} is independent of the initial condition.

Obviously, relations (13.36) and (13.37) do not hold for the excited explicit blowup solutions $\psi_{R^{(n)}}^{\text{explicit}}$ with $n \geq 1$. These “counterexamples”, however, are unstable. It

was believed, therefore, that relations (13.36) and (13.37) hold for all stable blowup solutions. In fact, relation (13.36) was rigorously proved in 2005 by Merle and Raphael [181] for all initial conditions with power slightly above P_{cr} (Sect. 14.6). In 2005, however, Fibich, Gavish, and Wang showed that the critical NLS “probably” admits singular solutions that collapse with a ring-type profile ψ_G , such that the amount of power that collapses into the singularity is substantially larger than P_{cr} . These solutions are radially stable but azimuthally unstable. See Chap. 19 for more details.

The two-dimensional critical NLS also admits singular vortex solutions $\psi(z, r, \theta) = e^{im\theta} A(z, r)$. These solutions have the power-concentration property that the amount of power that collapses into the singularity is at least $P_{\text{cr}}(m)$, see Theorem 15.3. In addition, $P_{\text{cr}}(m) > P_{\text{cr}}$, see Corollary 15.7. Hence, $P_{\text{collapse}} > P_{\text{cr}}$ for all singular vortex solutions. In particular, relations (13.36) and (13.37) do not hold for singular vortex solutions.⁴

13.3.2 Rate of Power Concentration

Let $\mathbf{x}_0(z)$ denote the center of the collapsing core. Since the amount of power that collapses into the singularity is at least P_{cr} , we can define $b(z)$ as the radius of a ball around $\mathbf{x}_0(z)$, such that the power within this ball is slightly below P_{cr} , i.e.,

$$\int_{|\mathbf{x}-\mathbf{x}_0(z)| \leq b(z)} |\psi|^2 d\mathbf{x} = (1 - \epsilon_0)P_{\text{cr}},$$

where $0 < \epsilon_0 \ll 1$ is fixed.⁵ We now consider the *rate of power concentration*, i.e., the rate at which $b(z)$ goes to zero as $z \rightarrow Z_c$.

In the case of the explicit blowup solution ψ_R^{explicit} , the rate of power concentration is equal to the blowup rate:

Lemma 13.3 *The rate of power concentration and the blowup rate for ψ_R^{explicit} are both linear.*

Proof In Sect. 10.4.1 we saw that the blowup rate of ψ_R^{explicit} is linear. The rate of power concentration is also linear, because for any $K > 0$,

$$\begin{aligned} \|\psi_R^{\text{explicit}}(z, \mathbf{x})\|_{L^2(|\mathbf{x}| < K(Z_c - z))}^2 &= \frac{1}{(Z_c - z)^d} \int_{|\mathbf{x}| < K(Z_c - z)} \left| R\left(\frac{\mathbf{x}}{Z_c - z}\right) \right|^2 d\mathbf{x} \\ &= \int_{|\xi| < K} |R(\xi)|^2 d\xi = \|R\|_2^2 - \|R\|_{L^2(|\xi| > K)}^2, \end{aligned}$$

and $\lim_{K \rightarrow \infty} \|R\|_{L^2(|\xi| > K)}^2 = 0$. □

⁴ Under azimuthal perturbations, however, singular vortex solutions disintegrate into multiple filaments, each of which collapses with $P_{\text{collapse}} = P_{\text{cr}}$ (see, e.g., Fig. 15.6).

⁵ We do not set $\epsilon_0 = 0$, because in that case $b(z) \equiv \infty$ for $\psi_{R^{(0)}}^{\text{explicit}}$.

More generally, if ψ undergoes a quasi self-similar collapse with the $\psi_{R^{(0)}}$ profile according to (13.36), then the rate of power concentration satisfies $b(z) \sim c_b L(z)$. By (13.30), the blowup rate satisfies $l(z) \sim c_l L(z)$. Therefore, when (13.36) holds, the rate of power concentration is equal to the blowup rate. Relation (13.36), hence the equivalence of the rate of power concentration and of the blowup rate, were rigorously proved for initial conditions with power slightly above P_{cr} (Sect. 14.6). The following theorem, which holds for all radial initial conditions, shows that

$$b(z) \leq K \cdot l(z),$$

i.e., the rate of power concentration is equal to or faster than the blowup rate:

Theorem 13.9 ([256]) *Let ψ be a radial solution of the critical NLS (13.1) with $d \geq 2$ that blows up at Z_c , and let $l(z) = 1/\|\nabla\psi\|_2$.*

1. *If $a(z)$ is a positive, monotonically decreasing function on $[0, Z_c]$ such that*

$$\lim_{z \rightarrow Z_c} a(z) = 0 \quad \text{and} \quad \lim_{z \rightarrow Z_c} \frac{l(z)}{a(z)} = 0,$$

then

$$\liminf_{z \rightarrow Z_c} \|\psi\|_{L^2(r < a(z))}^2 \geq P_{\text{cr}}.$$

2. *For any $\epsilon > 0$, there exists $K > 0$ such that*

$$\liminf_{z \rightarrow Z_c} \|\psi\|_{L^2(r < K \cdot l(z))}^2 \geq (1 - \epsilon)P_{\text{cr}}.$$

Theorem 13.9 was proved in 1990 by Y. Tsutsumi. It is also an immediate consequence of Theorem 13.3, which was proved by Weinstein in 1989:

Exercise 13.7 *Use Theorem 13.3 to prove Theorem 13.9. Hint: The proof is similar to that of Theorem 13.6 in the radial case.*

Remark Assertions 1 and 2 of Theorem 13.9 imply that $b(z) \leq a(z)$ and $b(z) \leq K \cdot l(z)$, respectively.

Remark Theorem 13.9 is optimal, in the sense that the rate of power concentration is equal to the blowup rate for ψ_R^{explicit} (Lemma 13.3).

The upper bound for the concentration rate in Theorem 13.9 is not explicit, because it is given in terms of the blowup rate. An explicit upper bound is given in the following theorem, which shows that *the rate of power concentration is equal to or faster than a square root*:

Theorem 13.10 (rate of power concentration [256]) *Let $\psi(z, r)$ be a radial solution of the critical NLS (13.1) with $d \geq 2$ that blows up at Z_c .*

1. If $a(z)$ is a positive, monotonically decreasing function on $[0, Z_c]$ such that

$$\lim_{z \rightarrow Z_c} a(z) = 0 \quad \text{and} \quad \lim_{z \rightarrow Z_c} \frac{(Z_c - z)^{\frac{1}{2}}}{a(z)} = 0,$$

then

$$\liminf_{z \rightarrow Z_c} \|\psi\|_{L^2(r < a(z))}^2 \geq P_{\text{cr}}.$$

2. For any $\epsilon > 0$, there exists a $K > 0$ such that

$$\liminf_{z \rightarrow Z_c} \|\psi\|_{L^2\left(r < K(Z_c - z)^{\frac{1}{2}}\right)}^2 \geq (1 - \epsilon)P_{\text{cr}}.$$

Proof By Corollary 13.1, $l(z) \leq M(Z_c - z)^{\frac{1}{2}}$. Therefore, Theorem 13.10 follows from Theorem 13.9. \square

Remark Theorem 13.10 implies that $b(z) \leq K(Z_c - z)^{\frac{1}{2}}$.

Exercise 13.8 Let ψ_R^{explicit} be given by (10.3). Show that if $a(z)$ satisfies the conditions of assertion 1 of Theorem 13.10, then

$$\lim_{z \rightarrow Z_c} \|\psi_R^{\text{explicit}}(z)\|_{L^2(r < a(z))}^2 = \|R\|_2^2.$$

Theorem 13.10 implies lower bounds for the blowup rate of the L^p norms:

Corollary 13.6 ([256]) Under the conditions of Theorem 13.10, for any $2 < p \leq \infty$, there exists a positive constant $M_p > 0$, such that

$$\|\psi\|_p \geq M_p (Z_c - z)^{-\frac{d(p-2)}{4p}}, \quad z \rightarrow Z_c.$$

Proof From assertion 2 of Theorem 13.10 and the Hölder inequality

$$\int |fg| \leq \left(\int |f|^q \right)^{\frac{1}{q}} \left(\int |g|^{\frac{p}{2}} \right)^{\frac{2}{p}}, \quad \frac{1}{q} + \frac{1}{\frac{p}{2}} = 1$$

we have that as $z \rightarrow Z_c$,

$$\begin{aligned} (1 - \epsilon)P_{\text{cr}} &\leq \|\psi\|_{L^2\left(r < K(Z_c - z)^{\frac{1}{2}}\right)}^2 = \int_{r < K(Z_c - z)^{\frac{1}{2}}} 1 \cdot |\psi|^2 d\mathbf{x} \\ &\leq \left(\int_{r < K(Z_c - z)^{\frac{1}{2}}} 1 d\mathbf{x} \right)^{\frac{1}{q}} \left(\int_{r < K(Z_c - z)^{\frac{1}{2}}} |\psi|^p d\mathbf{x} \right)^{\frac{2}{p}}. \end{aligned}$$

Hence,

$$\|\psi\|_p^p \geq \int_{r < K(Z_c - z)^{\frac{1}{2}}} |\psi|^p d\mathbf{x} \geq C \left(\int_{r < K(Z_c - z)^{\frac{1}{2}}} 1 d\mathbf{x} \right)^{-\frac{p}{2}}.$$

To finish the proof, note that

$$\frac{1}{q} = \frac{p-2}{p} \quad \text{and} \quad \int_{r < K(Z_c - z)^{\frac{1}{2}}} 1 d\mathbf{x} = c_K (Z_c - z)^{\frac{d}{2}}. \quad \square$$

Remark We already derived this result in Corollary 13.2, but only for $\frac{4}{d} + 2 \leq p \leq \infty$.

Remark It is interesting to contrast Corollary 13.6 with Lemma 8.8, which shows that L^p norms of solutions with power below P_{cr} decay to zero as $z \rightarrow \infty$.

Exercise 13.9 ([14]) Extend Theorems 13.9 and 13.10 to the critical BNLS.

13.4 Collapse at k Points

The possibility that NLS solutions can simultaneously collapse at several points was first discussed by Merle, who suggested the following definition for the set of blowup points:

Definition 13.1 (Collapse at k points [188]) Let ψ be an NLS solution that becomes singular at Z_c . Then $\left\{ \mathbf{x}_c^{(j)} \right\}_{j=1}^k$ is the set of blowup points of ψ , if for all $1 \leq j \leq k$ and for all $\epsilon > 0$, there exists a sequence $z_n \rightarrow Z_c$, such that

$$\lim_{z_n \rightarrow Z_c} \|\psi\|_{H^1(|\mathbf{x} - \mathbf{x}_c^{(j)}| < \epsilon)} = \infty \quad \text{and/or} \quad \lim_{z_n \rightarrow Z_c} \|\psi\|_{L^{2\sigma+2}(|\mathbf{x} - \mathbf{x}_c^{(j)}| < \epsilon)} = \infty.$$

We can use a symmetry argument to show that such solutions exist.

Proposition 13.1 The critical and supercritical NLS admit solutions that collapse at k points for any $k = 2, 3, \dots$

Proof We give an informal proof. Let $f(r) \in H_{\text{radial}}^1$ be such that $H(f) < 0$, and the solution of the critical or supercritical NLS with $\psi_0 = f(r)$ collapses at the origin. By NLS symmetries (Sect. 8.1), the NLS solution with $\psi_0 = \lambda^{\frac{1}{\sigma}} f(\lambda|\mathbf{x} - \mathbf{x}_0^{(j)}|)$ collapses at $\mathbf{x}_c = \mathbf{x}_0^{(j)}$. Consider now the initial condition

$$\psi_0(\mathbf{x}) = \sum_{j=1}^k \lambda^{\frac{1}{\sigma}} f(\lambda|\mathbf{x} - \mathbf{x}_0^{(j)}|), \quad (13.38)$$

which is the sum of k identical input beams. If we fix $\{\mathbf{x}_0^{(j)}\}_{j=1}^k$ and let $\lambda \rightarrow \infty$, then each beam becomes more and more localized, and so the interactions between the k beams become more and more negligible. Since $H(f) < 0$, for λ sufficiently large $H(\psi_0) < 0$, see (13.38), and so the corresponding solution ψ becomes singular. Since there are always some interactions between the beams, generically one beam collapses slightly before the others, and so ψ collapses at a single point. We can, however, force all k beams to collapse at the same distance Z_c , by placing their initial centers $\{\mathbf{x}_0^{(j)}\}_{j=1}^k$ at equal distances along a circle, since in this configuration symmetry dictates that all k beams collapse simultaneously (and that their k collapse points $\{\mathbf{x}_c^{(j)}\}_{j=1}^k$ are equally distanced along a concentric circle).⁶ In principle, the k beams can collapse at the origin, in which case there is a single blowup point. If λ is sufficiently large, however, the interactions between the beams are so weak that each of them collapses “on its own”, i.e., $\mathbf{x}_c^{(j)} \approx \mathbf{x}_0^{(j)}$. \square

Remark See Sect. 27.5 for simulations and experiments of collapse at $k = 2$ points.

In the proof of Proposition 13.1 the k points are equally distanced along a circle. In 1990, Merle proved that one can construct a solution of the critical NLS which blows up simultaneously at *any* k points in \mathbb{R}^d :

Theorem 13.11 ([188]) *Let $\{\mathbf{x}_c^{(j)}\}_{j=1}^k$ be in \mathbb{R}^d , $\{n_j\}_{j=1}^k$ be in $\{0, 1, 2, \dots\}$, $R^{(n)}$ be a nontrivial solution of (13.22), and $\psi_{R^{(n)}, \alpha}$ be given by (10.6). Then there is a constant α_0 , such that for any $\alpha_1, \dots, \alpha_k > \alpha_0$, there exists a solution ψ of the critical NLS (13.1) that blows up at Z_c , such that*

- The set of blowup points in $L^{\frac{4}{d}+2}$ and in H^1 is $\{\mathbf{x}_c^{(j)}\}_{j=1}^k$.
- For all $\rho > 0$ such that the balls $\{B(\mathbf{x}_c^{(j)}, \rho)\}_{j=1}^k$ are disjoint,

$$\lim_{z \rightarrow Z_c} \|\psi\|_{L^2(B(\mathbf{x}_c^{(j)}, \rho))} = \|R^{(n_j)}\|_2^2, \quad j = 1, \dots, k.$$

- For all $\rho > 0$,

$$\lim_{z \rightarrow Z_c} \|\psi\|_{L^2(\mathbb{R}^d \setminus \bigcup_{j=1}^k B(\mathbf{x}_c^{(j)}, \rho))} = 0.$$

In addition, there is a constant $\gamma > 0$, such that

⁶ When k is even, we can also let the initial condition be the sum of k identical out-of-phase input beams, i.e., $\psi_0 = \sum_{j=1}^k (-1)^j \lambda^{\frac{1}{\sigma}} f(\lambda |\mathbf{x} - \mathbf{x}_0^{(j)}|)$, where $\{\mathbf{x}_0^{(j)}\}_{j=1}^k$ are equally distanced along a circle. Such a configuration is called a *necklace beam* (Sect. 15.13).

$$\left\| \psi(z, \mathbf{x}) - \sum_{j=1}^k \psi_{R^{(n_j)}, \alpha_j}^{\text{explicit}} \left(z, \mathbf{x} - \mathbf{x}_c^{(j)} \right) \right\|_{2+\frac{4}{d}} \leq e^{-\frac{\gamma}{Z_c - z}}, \quad 0 \leq z < Z_c.$$

Thus, as $z \rightarrow Z_c$, in the vicinity of each $\mathbf{x}_c^{(j)}$ the solution approaches the explicit blowup solution $\psi_{R^{(n_j)}, \alpha_j}^{\text{explicit}} \left(z, \mathbf{x} - \mathbf{x}_c^{(j)} \right)$. Therefore,

$$\psi \rightharpoonup \sum_{j=1}^k \|R^{(n_j)}\|_2^2 \delta(|\mathbf{x} - \mathbf{x}_c^{(j)}|), \quad z \rightarrow Z_c,$$

where the limit is in the sense of distributions. In particular, all the solution power collapses into the k collapse points.

The solution constructed by Merle is unstable. Intuitively, this is because each of the collapsing component approaches the unstable blowup solution $\psi_{R^{(n_j)}, \alpha_j}^{\text{explicit}}$.⁷

Remarkably, although each component is unstable, and although the k components interact with each other, each component “manages” to collapse with the unstable $\psi_{R^{(n_j)}}^{\text{explicit}}$ profile.

Consider an NLS solution that collapses at $k > 1$ points. If we perturb its initial condition, then generically one of the k filaments will collapse before all the others.

Conclusion 13.2 *Collapse at more than one point in the critical or supercritical NLS is unstable, in the sense that infinitesimal perturbations of the initial condition can cause the solution to collapse at a single point.*

Therefore, NLS solutions that simultaneously collapse at several points are “not physical”. Of course, a physical laser beam can undergo multiple filamentation and collapse at several points (Chap. 25). In that case, however, each filament generically collapses at a different axial distance. The corresponding NLS solution, however, collapses at a single point, which corresponds to the first filament that undergoes collapse.⁸

Remark In [199], Nawa extended Theorem 13.5 to the case of k blowup points.

13.4.1 Is $k \leq P/P_{\text{cr}}$?

In Theorem 13.6 we saw that if ψ collapses at a single point, the amount of power that concentrates at the singularity point is at least P_{cr} . Since collapse in the critical NLS is a local phenomenon, this suggests that when ψ collapses at k points, the amount of power that concentrates at each singularity point is at least P_{cr} . This is indeed the case with Merle’s solutions which collapse at k points (Theorem 13.11),

⁷ Another reason is that collapse at more than one point is always unstable (Conclusion 13.2).

⁸ See also the discussion in Sect. 25.1.1.

and also with the k -symmetric solutions constructed in the proof of Proposition 13.1. So far, however, this result was not rigorously proved, and is therefore formulated as

Conjecture 13.1 Let ψ be an H^1 solution of the critical NLS that collapses at k points. Then the amount of power that concentrates at each singularity point is at least P_{cr} .

Corollary 13.7 Assume that Conjecture 13.1 holds. Then $k \leq P/P_{\text{cr}}$, where $P = \int |\psi_0|^2 dx$ is the initial power. In particular, k is finite.

In Lemma 13.2 we proved that if ψ is a radial singular solution, then it has to collapse at the origin. Intuitively, we expect that ψ collapses only at the origin, since otherwise it collapses on a sphere, in which case it concentrates a power of at least P_{cr} at an infinite number of points. At present, however, this argument is not rigorous.⁹

13.5 Minimal-Power Blowup Solutions

In Theorem 5.11 we saw that a necessary condition for collapse in the critical NLS is that the input power be at least P_{cr} .

Definition 13.2 (minimal-power blowup solution) A minimal-power blowup solution of the critical NLS is a blowup solution whose power is exactly P_{cr} .

The explicit solution $\psi_{R^{(0)}}^{\text{explicit}}$ is a minimal-power blowup solution (Chap. 10). A natural question is whether there exist other minimal-power blowup solutions. The following result shows that this question is only of theoretical interest.

Lemma 13.4 All minimal-power blowup solutions of the critical NLS are strongly unstable.

Proof Any perturbation that reduces the power of the initial condition arrests the collapse. \square

The first characterization of minimal-power blowup solutions was done in 1986 by Weinstein [275], who proved that if $\|\psi_0\|_2^2 = P_{\text{cr}}$ and if ψ blows up at Z_c , then $|\psi| \rightarrow L^{-\frac{d}{2}}(z) R^{(0)} \left(\frac{r}{L(z)} \right)$ strongly in H^1 as $z \rightarrow Z_c$, where $\lim_{z \rightarrow Z_c} L(z) = 0$. Weinstein's result was improved by Merle, who showed in 1992 for radial H^1 solutions with a finite variance, and in 1993 for all H^1 solutions, that $\psi_{R^{(0)}}^{\text{explicit}}$ is the only minimal-power blowup solution (up to NLS symmetries):

Theorem 13.12 ([174, 175]) Let ψ be a solution of the critical NLS (13.1) which blows up at $0 < Z_c < \infty$, such that $\|\psi_0\|_2^2 = P_{\text{cr}}$. Then there exist $\alpha, \theta \in \mathbb{R}$ and $\mathbf{x}_0, \mathbf{c} \in \mathbb{R}^d$, such that for $0 \leq z < Z_c$,

⁹ An informal proof that radial solutions of the critical NLS cannot collapse on a sphere is given in Lemma 22.1.

$$\begin{aligned} \psi(z, \mathbf{x}) &= e^{i\theta} \psi_{R^{(0)}, \alpha, \mathbf{c}}^{\text{explicit}}(z, \mathbf{x} - \mathbf{x}_0) \\ &:= \frac{1}{(\alpha(Z_c - z))^{\frac{d}{2}}} R^{(0)} \left(\left| \frac{\mathbf{x} - \mathbf{x}_0 - z\mathbf{c}}{\alpha(Z_c - z)} \right| \right) e^{i\theta + \frac{i}{\alpha^2(Z_c - z)} - \frac{i|\mathbf{x} - \mathbf{x}_0 - z\mathbf{c}|^2}{4(Z_c - z)} + \frac{i\mathbf{c}(\mathbf{x} - \mathbf{x}_0)}{2} - \frac{i|\mathbf{c}|^2 z}{4}}, \end{aligned} \quad (13.39)$$

where $R^{(0)}$ is the ground state of (13.22).

Remark Here, α is the dilation parameter, \mathbf{x}_0 is the initial position, \mathbf{c} is the tilt parameter, and $\theta = \arg \psi(0, \mathbf{x}_0) - \frac{1}{\alpha^2 Z_c}$ determines the initial on-axis phase.

An immediate, yet important, consequence of Theorem 13.12 is that any blowup solution whose initial profile is not a ground state has power strictly above P_{cr} :

Corollary 13.8 *Let ψ be a singular solution of the critical NLS (13.1). If ψ_0 is not given by*

$$\begin{aligned} e^{i\theta} \psi_{R^{(0)}, \alpha, \mathbf{c}}^{\text{explicit}}(0, \mathbf{x} - \mathbf{x}_0) \\ := \frac{1}{(\alpha Z_c)^{\frac{d}{2}}} R^{(0)} \left(\left| \frac{\mathbf{x} - \mathbf{x}_0}{\alpha Z_c} \right| \right) e^{i\theta + \frac{i}{\alpha^2 Z_c} - \frac{i|\mathbf{x} - \mathbf{x}_0|^2}{4Z_c} + \frac{i\mathbf{c}(\mathbf{x} - \mathbf{x}_0)}{2}}, \end{aligned} \quad (13.40)$$

then $\|\psi_0\|_2^2 > P_{\text{cr}}$.

Intuitively, initial conditions different from (13.40) require more power than P_{cr} in order to collapse, for the following reason. In Sect. 14.6 we shall see that all singular solutions of the critical NLS whose power is close to P_{cr} , collapse with a self-similar $R^{(0)}$ profile. Therefore, when the initial condition is not given by (13.40), the solution needs to evolve into the $R^{(0)}$ profile as it collapses. During this “reorganization stage”, the solution loses some power to the background. Therefore, since the amount of power that eventually collapses into the singularity is P_{cr} , the solution requires some extra power above P_{cr} in order to collapse.

Remark In Sect. 38.2 we will see that Bourgain-Wang solutions can be viewed as “generalized” minimal-power blowup solutions.

13.5.1 Is $P_{\text{th}}[f] > P_{\text{cr}}$ for $f \not\equiv R^{(0)}$?

In Sect. 7.10 we defined the threshold power for collapse $P_{\text{th}} = P_{\text{th}}[f]$ as the minimal power for which any solution of the critical NLS with $\psi_0 = cf(\mathbf{x})$ that satisfies $\|\psi_0\|_2^2 > P_{\text{th}}$, will collapse. By Corollary 7.13, $P_{\text{th}}[R^{(0)}] = P_{\text{cr}}$. Therefore, if $P_{\text{th}}[f] > P_{\text{cr}}$, then f is different from $R^{(0)}$. It is believed that the converse also holds, namely, that if f is different from $R^{(0)}$, then $P_{\text{th}}[f] > P_{\text{cr}}$. This, however, does not

follow from Theorem 13.12, and has not been rigorously proved so far. Of course, if f is different from $R^{(0)}$ and the NLS solution blows up when $\|\psi_0\|_2^2 = P_{\text{th}}$, then it follows from Theorem 13.12 that $P_{\text{th}}[f] > P_{\text{cr}}$. If, however, f is different from $R^{(0)}$ and the NLS solution does not blowup for $\|\psi_0\|_2^2 = P_{\text{th}}$ (but only for $\|\psi_0\|_2^2 > P_{\text{th}}$), then there is no proof that $P_{\text{th}} > P_{\text{cr}}$, although this is suspected to be true.

13.6 Supercritical NLS

The results presented so far in this chapter were for the critical NLS. In this section we briefly present the equivalent theory for the L^2 supercritical NLS. As always, we assume that the NLS is also H^1 subcritical. Therefore, we consider the NLS

$$i\psi_z(z, \mathbf{x}) + \Delta\psi + |\psi|^{2\sigma}\psi = 0, \quad \psi(0, \mathbf{x}) = \psi_0(\mathbf{x}) \in H^1, \quad (13.41a)$$

where

$$\begin{cases} \frac{2}{d} < \sigma < \infty, & \text{if } d \leq 2, \\ \frac{2}{d} < \sigma < \frac{2}{d-2}, & \text{if } d > 2. \end{cases} \quad (13.41b)$$

13.6.1 Blowup Rate

In Sect. 13.1 we saw that in the critical case, the blowup rate $l(z)$ is bounded from below by a square root, and there is no known upper bound. The situation is different in the supercritical case, where $l(z)$ is bounded from below and from above. Indeed, we will shortly see that if the blowup rate is a power law

$$l(z) \sim \kappa(Z_c - z)^p, \quad z \rightarrow Z_c, \quad (13.42)$$

where $\kappa > 0$, then

$$p_{\min} \leq p < 1, \quad p_{\min} := \frac{1}{2} - \frac{\sigma d - 2}{4\sigma}. \quad (13.43)$$

If, in addition, ψ_0 is radial and $\sigma < 2$, one has the stronger result¹⁰ that

$$p_{\min} \leq p \leq p_{\max}, \quad p_{\max} := \frac{1}{1 + \frac{2-\sigma}{\sigma(d-1)}}. \quad (13.44)$$

The bounds p_{\min} and p_{\max} are sharp, in the sense that they are attained by the peak-type solutions ψ_Q and by the shrinking-ring solutions ψ_S , respectively (Sect. 13.6.2). The lower bound p_{\min} is monotonically decreasing in σ from $p_{\min} = \frac{1}{2} -$ at $\sigma = \frac{2}{d} +$

¹⁰ This result is stronger, since $p_{\max} < 1$.

to $p_{\min} = 0+$ at $\sigma = \frac{2}{d-2}-$. Similarly, the upper bound p_{\max} is monotonically increasing in σ from $p_{\max} = \frac{1}{2}+$ at $\sigma = \frac{2}{d}+$ to $p_{\max} = 1-$ at $\sigma = \frac{2}{d-2}-$.

In 1989, Merle proved the following result:

Theorem 13.13 ([187]) *Let $J[\Theta] := \int_0^{Z_c} \|\nabla \psi(z)\|_2^\Theta dz$, where ψ is a solution of the supercritical NLS (13.41) that becomes singular at Z_c . Then $J[\Theta]$ is finite for $\Theta < 1$ and infinite for $\Theta > \frac{1}{p_{\min}}$.*

Therefore, if $l(z) \sim \kappa(Z_c - z)^p$, then $p\Theta < 1$ for $\Theta < 1$ and $p\Theta \geq 1$ for $\Theta > 1/p_{\min}$. Hence,

$$p_{\min} \leq p \leq 1.$$

The lower bound for p also follow from a result of Cazenave and Weissler:

Theorem 13.14 ([41]) *Let $d > 2$, and let ψ be a solution of the supercritical NLS (13.41) that becomes singular at Z_c . Then*

$$l(z) \leq M(Z_c - z)^{p_{\min}}, \quad 0 \leq z < Z_c, \quad (13.45)$$

where $M > 0$ and p_{\min} is given by (13.43).

While Theorem 13.13 “only” shows that $p \leq 1$, the following result, also due to Merle, shows that $p < 1$.

Lemma 13.5 ([187]) *Let ψ be a solution of the supercritical NLS (13.41) that becomes singular at Z_c , such $V(\psi_0) < \infty$. Then*

$$\int_0^{Z_c} (Z_c - z) \|\nabla \psi(z)\|_2^2 dz < \infty.$$

Proof Following Cazenave [39], the variance identity (7.6) can be written as

$$V''(z) = 8H + \frac{d\sigma - 2}{2} \left(H - \|\nabla \psi\|_2^2 \right) \leq a - b \|\nabla \psi\|_2^2$$

for some constants $a, b > 0$. Integrating this inequality between 0 and z gives

$$V'(z) - V'(0) \leq az - b \int_0^z \|\nabla \psi(s)\|_2^2 ds.$$

Integrating this inequality between 0 and z_m , where $0 < z_m < Z_c$, gives

$$V(z_m) - V(0) - z_m V'(0) \leq a \frac{z_m^2}{2} - b \int_{z=0}^{z_m} \int_{s=0}^z \|\nabla \psi(s)\|_2^2 ds dz.$$

By definition, $V(z_m) \geq 0$. Therefore,

$$b \int_{z=0}^{z_m} \int_{s=0}^z \|\nabla \psi(s)\|_2^2 ds dz \leq V(0) + z_m V'(0) + a \frac{z_m^2}{2}.$$

In addition, since $V'(0) = 4 \operatorname{Im} \int \psi_0^* \mathbf{x} \cdot \nabla \psi_0 d\mathbf{x}$, see (7.19c), then

$$|V'(0)| \leq 4 \int |\psi_0^*| |\mathbf{x}| |\nabla \psi_0| d\mathbf{x} \leq 4 \left(V(0) \int |\nabla \psi_0|^2 d\mathbf{x} \right)^{\frac{1}{2}} < \infty.$$

Consequently,

$$\int_{z=0}^{z_m} \int_{s=0}^z \|\nabla \psi(s)\|_2^2 ds dz \leq \frac{V(0) + Z_c |V'(0)| + a \frac{Z_c^2}{2}}{b} < \infty.$$

Therefore, by letting $z_m \rightarrow Z_c$, we get that

$$\int_{z=0}^{Z_c} \int_{s=0}^z \|\nabla \psi(s)\|_2^2 ds dz < \infty.$$

Finally, integration by parts gives

$$\begin{aligned} \int_{z=0}^{Z_c} \int_{s=0}^z \|\nabla \psi(s)\|_2^2 ds dz &= \left[z \int_{s=0}^z \|\nabla \psi(s)\|_2^2 ds \right]_{z=0}^{Z_c} - \int_{z=0}^{Z_c} z \|\nabla \psi(z)\|_2^2 dz \\ &= \int_{z=0}^{Z_c} (Z_c - z) \|\nabla \psi(z)\|_2^2 dz. \end{aligned} \quad \square$$

The proof of Lemma 13.5 makes use of the variance identity. A stronger result was obtained by Merle, Raphael, and Szeftel in the sub-quintic radial case, using a localized version of the variance identity:

Theorem 13.15 ([186]) *Let $d \geq 2$, $\frac{2}{d} < \sigma < \min \left\{ 2, \frac{2}{d-2} \right\}$, and let $\psi(z, r)$ be a radial solution of the supercritical NLS (13.41) that becomes singular at Z_c . Then*

$$\int_z^{Z_c} (Z_c - s) \|\nabla \psi(s)\|_2^2 ds \leq C (Z_c - z)^{\frac{2\alpha}{1+\alpha}}, \quad \alpha = \frac{2-\sigma}{\sigma(d-1)},$$

where $0 < \alpha < 1$ and $0 < C < \infty$.

Therefore, if $l(z) \sim \kappa (Z_c - z)^p$, then $p \leq \frac{1}{1+\alpha} = p_{\max}$.

As in the critical case, Theorem 13.14 allows us to derive bounds for the blowup rates of the L^p norms:

Exercise 13.10 Generalize Corollary 13.2 to the supercritical NLS.

The following exercise extends Exercise 13.3 to the supercritical case.

Exercise 13.11 Show that in the supercritical NLS, any blowup rate of the form (13.16) is unaffected by the dilation symmetry $\psi(z, \mathbf{x}) \rightarrow \lambda^{\frac{1}{\sigma}} \psi(\lambda^2 z, \lambda \mathbf{x})$. If, in addition, the multiplicative constant D in (13.16) is unaffected by dilation, then $p = p_{\min}$.

13.6.2 Types of Singular Solutions

At present, the following singular solutions of the L^2 -supercritical and H^1 -subcritical NLS (13.41) are known:

1. Equation (13.41) admits singular *peak-type solutions* that collapse with the ψ_Q profile, where

$$|\psi_Q(z, r)| = \frac{1}{L^{\frac{1}{\sigma}}(z)} \left| Q\left(\frac{r}{L}\right) \right|,$$

see Chap. 21. The blowup rates of $L(z)$ and ψ are

$$L(z) \sim \kappa(Z_c - z)^{\frac{1}{2}}, \quad l(z) \sim c(Z_c - z)^{p_{\min}}, \quad p_{\min} = \frac{1}{2} - \frac{\sigma d - 2}{4\sigma}.$$

Note that p_{\min} can assume any value in $(0, \frac{1}{2})$.

2. The supercritical sub-quintic NLS ($\frac{2}{d} < \sigma < 2$) with $d > 1$ admits singular *shrinking-ring solutions* that collapse with the ψ_S profile, where

$$|\psi_S| = \frac{1}{L^{\frac{1}{\sigma}}(z)} S\left(\frac{r - r_{\max}(z)}{L}\right), \quad r_{\max}(z) = r_0 L^\alpha(z), \quad \alpha = \frac{2 - \sigma}{\sigma(d - 1)},$$

see Chap. 23. The blowup rates of $L(z)$ and ψ are

$$L(z) \sim \kappa(Z_c - z)^{p_{\max}}, \quad l(z) \sim c(Z_c - z)^{p_{\max}},$$

where

$$p_{\max} = \frac{1}{1 + \alpha} = \frac{1}{2 - \frac{\sigma d - 2}{\sigma(d - 1)}}.$$

Since α can assume any value in $(0, 1)$, p_{\max} can assume any value in $(\frac{1}{2}, 1)$.

3. The supercritical quintic NLS ($\sigma = 2$ and $d > 1$) admits singular *standing-ring solutions* that collapse with the ψ_F profile, where

$$|\psi_F(t, r)| = \frac{1}{L^{\frac{1}{\sigma}}(z)} R_{\text{ID}}\left(\frac{r - r_{\max}(z)}{L(z)}\right), \quad 0 < \lim_{z \rightarrow Z_c} r_{\max}(z) < \infty,$$

see Sect. 22.3. The blowup rates of $L(z)$ and ψ are

$$L(z) \sim \underbrace{\left(\frac{2\pi(Z_c - z)}{\log \log \frac{1}{Z_c - z}} \right)^{\frac{1}{2}}}_{\text{loglog law}}, \quad l(z) \sim c \left(\frac{Z_c - z}{\log \log \frac{1}{Z_c - z}} \right)^{\frac{1}{4} + \frac{1}{2\sigma}}.$$

4. The supercritical super-quintic NLS ($\sigma > 2$) with $d > 1$ admits singular *standing-ring solutions* that collapse with the ψ_F profile, where

$$|\psi_F(t, r)| = \frac{1}{L^{\frac{1}{\sigma}}(z)} Q_{1D} \left(\frac{r - r_{\max}(z)}{L(z)} \right), \quad 0 < \lim_{z \rightarrow Z_c} r_{\max}(z) < \infty,$$

see Sect. 22.4. The blowup rates of $L(z)$ and ψ are

$$L(z) \sim \kappa (Z_c - z)^{\frac{1}{2}}, \quad l(z) \sim c (Z_c - z)^{\frac{1}{4} + \frac{1}{2\sigma}}.$$

5. In the two-dimensional case, each of the above four types has a *vortex analog* of the form $\psi(z, r, \theta) = e^{im\theta} A(z, r)$, see Chap. 15.
6. The supercritical NLS with $d > 2$ admits *combinations of the above types*, e.g., solutions that are a standing-ring in $k > 1$ dimensions and peak-type in the other $d - k$ dimensions (Sect. 22.7).

Remark In Sect. 13.2.3 we saw that $l(z) \sim c_l L(z)$ in the critical NLS. The above examples show that, except for the shrinking-ring ψ_S solutions, this is not the case for the supercritical NLS.

13.6.3 No Minimal-Power and Power-Concentration Properties

In Lemma 5.6 we showed that, unlike the critical NLS, the supercritical NLS admits singular solutions with arbitrarily small power. Therefore, in the supercritical NLS:

1. There is no *critical power for collapse*.
2. There are no *minimal-power blowup solutions*.¹¹
3. The amount of power that collapses into the singularity can be arbitrarily small. In fact, solutions of the supercritical NLS can undergo a weak collapse (Sect. 21.2).
4. There is no *power concentration* property.

In Sect. 13.4 we saw that, as in the critical case, the supercritical NLS admits solutions that collapse at k points, and that these solutions are unstable, in the sense

¹¹ There are, however, “minimal-power” shrinking-ring solutions (Sect. 23.5).

that infinitesimal perturbations can result in collapse at a single point. In the critical case, power concentration suggests that the number of collapse points is bounded by P/P_{cr} , see Corollary 13.7. In the supercritical case there is no such bound, as there is no power-concentration property. Indeed, in Chap. 22 we will see that the supercritical NLS with $\sigma \geq 2$ and $d > 1$ admits *singular standing-ring solutions* that collapse on a sphere, i.e., at an infinite number of points.

In Lemma 13.2 we saw that in the critical case, if the initial condition is radial and the solution becomes singular, the origin has to be a blowup point. For many years, this result was believed to hold for the supercritical NLS as well. The discovery of the singular standing-ring solutions showed that this is not the case, since these radial solutions collapse on a d -dimensional sphere, and not at the origin.

Chapter 14

The Peak-Type Blowup Profile $\psi_{R^{(0)}}$

In Chap. 13 we presented properties shared by *all* singular solutions of the critical NLS

$$i\psi_z(z, \mathbf{x}) + \Delta\psi + |\psi|^{\frac{4}{d}}\psi = 0, \quad \psi(0, \mathbf{x}) = \psi_0(\mathbf{x}) \in H^1, \quad (14.1)$$

such as power concentration, a quasi self-similar collapse, and a square-root bound for the blowup rate. In this chapter we focus on singular solutions which are stable (in the sense of Definition 10.4), and undergo a quasi self-similar collapse with the $\psi_{R^{(0)}}$ profile.

The $\psi_{R^{(0)}}$ profile is given by

$$\psi_{R^{(0)}}(z, r) = \frac{1}{L^{\frac{d}{2}}(z)} R^{(0)}(\rho) e^{i\zeta(z) + i\frac{L_z}{L} \frac{r^2}{4}}, \quad \rho = \frac{r}{L(z)}, \quad \frac{d\zeta}{dz} = \frac{1}{L^2(z)}, \quad (14.2)$$

where $\lim_{z \rightarrow Z_c} L(z) = 0$ and $R^{(0)}$ is the ground state of

$$R''(\rho) + \frac{d-1}{\rho} R' - R + |R|^{\frac{4}{d}} R = 0, \quad R'(0) = 0, \quad R(\infty) = 0. \quad (14.3)$$

Since

$$|\psi_{R^{(0)}}| = \frac{1}{L^{\frac{d}{2}}(z)} R^{(0)} \left(\frac{r}{L(z)} \right), \quad (14.4)$$

and since the maximum of $R^{(0)}$ is attained at $\rho = 0$, the $\psi_{R^{(0)}}$ profile is *peak-type*, i.e., its maximum is attained at $\rho = 0$.¹

¹ The critical NLS also admits *ring-type* singular solutions (Chaps. 11, 19, and 20).

As we shall see, stable collapse with the $\psi_{R^{(0)}}$ profile is “only” quasi self-similar.² Thus, as the solution self-focuses, it splits into

1. an inner core ψ_{coll} that collapses into the singularity point $\mathbf{x}_c := \lim_{z \rightarrow Z_c} \mathbf{x}_0(z)$, where $\mathbf{x}_0(z) := \arg \max_{\mathbf{x}} |\psi(z, \mathbf{x})|$ is the location of the solution’s peak, and
2. an outer, non-collapsing part ψ_{outer} that continues to propagate forward.

Therefore, roughly speaking,

$$\psi(z, \mathbf{x}) = \begin{cases} \psi_{\text{coll}}, & \text{if } |\mathbf{x} - \mathbf{x}_0(z)| = O(L(z)), \\ \psi_{\text{outer}}, & \text{if } |\mathbf{x} - \mathbf{x}_0(z)| \gg L(z), \end{cases}$$

where $L(z)$ is the width of the collapsing core.

When we say that “ ψ collapses with the $\psi_{R^{(0)}}$ profile”, what we mean is that $\psi_{\text{coll}} \rightarrow \psi_{R^{(0)}}$ as $z \rightarrow Z_c$. Thus, $\psi \rightarrow \psi_{R^{(0)}}$ for $\mathbf{x} - \mathbf{x}_0(z) = O(L(z))$, i.e., on a domain that shrinks to the singularity point \mathbf{x}_c . As $z \rightarrow Z_c$, the width of the collapsing core goes to zero and its amplitude becomes infinite, so that

$$|\psi_{\text{coll}}|^2 \sim |\psi_{R^{(0)}}|^2 \rightarrow \|R^{(0)}\|_2^2 \delta(r), \quad z \rightarrow Z_c, \quad (14.5)$$

see (14.4). Hence, the amount of power that collapses into the singularity is $P_{\text{collapse}} = P_{\text{cr}}$. Anywhere but at the singularity point (i.e., for $\mathbf{x} \in \mathbb{R}^d \setminus \mathbf{x}_c$), the limiting solution is given by the non-collapsing outer part ψ_{outer} , which converges to a function $\phi(\mathbf{x})$. The function $\phi(\mathbf{x})$ is rough, i.e., it is in L^2 , but not in H^1 or in L^p for $p > 2$.

Since $\psi_{\text{coll}} \sim \psi_{R^{(0)}}$, the self-focusing dynamics is captured by the function $L(z)$, see (14.4). As we shall see, the rate at which $L(z)$ goes to zero is a square root with a loglog correction, i.e.,

$$L(z) \sim \left(\frac{2\pi(Z_c - z)}{\log \log \frac{1}{Z_c - z}} \right)^{\frac{1}{2}}, \quad z \rightarrow Z_c \quad (\text{loglog law}). \quad (14.6)$$

This blowup rate is slightly faster than the square-root bound (13.6).

Remark The results in this chapter are also relevant for *standing-ring blowup solutions* of the supercritical quintic NLS ($\sigma = 2$ and $d > 1$), which collapse with the one-dimensional quintic $\psi_{R^{(0)}}$ profile at the loglog-law rate (Sect. 22.3).

² The explicit solution $\psi_{R^{(0)}}^{\text{explicit}}$ also collapses with the $\psi_{R^{(0)}}$ profile. This solution, however, is “truly” self-similar, and is unstable.

14.1 Numerical Observations—Convergence to $\psi_{R^{(0)}}$

In this section, we present simulations of singular solutions of the critical NLS that undergo a quasi self-similar collapse with the $\psi_{R^{(0)}}$ profile. We focus on the physical case of the two-dimensional cubic NLS

$$i\psi_z(z, x, y) + \Delta\psi + |\psi|^2\psi = 0, \quad \psi(0, x, y) = \psi_0(x, y). \quad (14.7)$$

Recall that in the two-dimensional case

$$|\psi_{R^{(0)}}| = \frac{1}{L(z)} R^{(0)} \left(\frac{r}{L(z)} \right),$$

where $R^{(0)}$, the *Townes profile* (see Sect. 3.3.3), is the ground state of

$$R''(\rho) + \frac{1}{\rho} R' - R + R^3 = 0, \quad R'(0) = 0, \quad R(\infty) = 0.$$

14.1.1 Radial Initial Conditions

We begin with the case of radial initial conditions. Previously, we proved that if $\psi_0 = \psi_0(r)$, then

1. ψ remains radial (Lemma 5.5).
2. If ψ becomes singular, then it collapses at the origin (Lemma 13.2).
3. The blowup profile is quasi self-similar, so that, roughly speaking, as $z \rightarrow Z_c$,

$$|\psi(z, r)| \sim \begin{cases} \frac{1}{L^{\frac{d}{2}}(z)} F \left(\frac{r}{L(z)} \right) & 0 \leq r \leq \rho_0 L(z), \\ \phi(r) & \rho_0 L(z) \ll r < \infty, \end{cases}$$

where $\rho_0 \gg 1$ and $\|F\|_2^2 \geq P_{\text{cr}}$, see Sect. 13.2.2.

Remark In simulations of the two-dimensional NLS with radial initial conditions, one typically solves the radial NLS

$$i\psi_z(z, r) + \psi_{rr} + \frac{1}{r}\psi_r + |\psi|^2\psi = 0, \quad \psi(0, r) = \psi_0(r). \quad (14.8)$$

Solving (14.8) numerically is easier and faster than solving the “genuinely two-dimensional” NLS (14.7). In addition, when solving (14.8), radial symmetry is

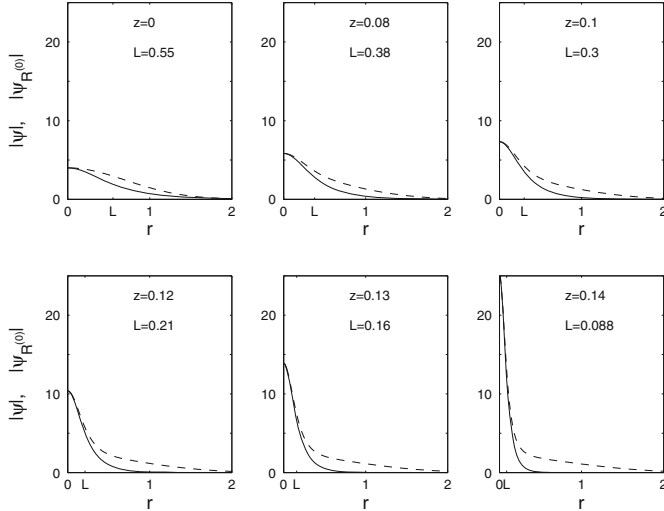


Fig. 14.1 Solution of the two-dimensional cubic NLS with $\psi_0 = 4e^{-r^2}$ ($P \approx 2.1P_{\text{cr}}$, dashes). The collapsing core ($r = O(L)$) approaches the $\psi_{R^{(0)}}$ profile (solid). Outside the collapsing core ($r \gg L$), $|\psi|$ lies above $|\psi_{R^{(0)}}|$

automatically maintained (as it should). If, however, one studies the azimuthal stability of radial solutions (as e.g., in Sect. 14.1.2), then Eq.(14.7) is to be solved.

A typical simulation of the radial critical NLS (14.8) is presented in Fig. 14.1. As ψ self-focuses, its collapsing core near $r = 0$ becomes higher and narrower and it approaches the $\psi_{R^{(0)}}$ profile. Here and elsewhere, when monitoring the agreement between ψ and $\psi_{R^{(0)}}$, the value of $L(z)$ in $\psi_{R^{(0)}}$ is extracted from the numerical solution ψ by using the relation $|\psi(z, r = 0)| \sim |\psi_{R^{(0)}}(z, r = 0)|$,³ which yields

$$L(z) = \left(\frac{R^{(0)}(0)}{|\psi(z, r = 0)|} \right)^{\frac{2}{d}}. \quad (14.9)$$

The convergence of ψ to $\psi_{R^{(0)}}$ occurs only for $r = O(L)$. For $r \gg L$, $|\psi|$ lies above $|\psi_{R^{(0)}}|$, due to the excess power above critical ($P - P_{\text{cr}} \approx 1.1P_{\text{cr}}$) that does not collapse into the singularity.

To better see the convergence of the self-similar profile to $R^{(0)}$, note that by (14.4),

$$L^{\frac{d}{2}} |\psi(z, r)| \sim L^{\frac{d}{2}} |\psi_{R^{(0)}}(z, r)| = R^{(0)}(\rho), \quad \rho = \frac{r}{L(z)}. \quad (14.10)$$

Therefore, in Fig. 14.2 we plot the same data as in Fig. 14.1, but in the rescaled variables (14.10), namely, we plot $L^{\frac{d}{2}} |\psi|$ as a function of ρ , where $L(z)$ is determined

³ I.e., by letting $\psi_{R^{(0)}}$ have the same amplitude at $r = 0$ as ψ .

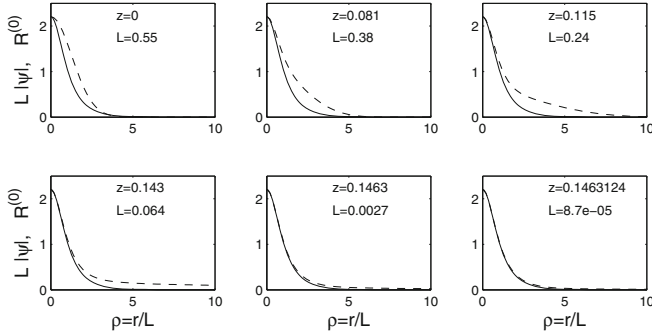


Fig. 14.2 Same simulation as in Fig. 14.1 (dots), but plotted in the rescaled variables (14.10). The self-similar profile of the collapsing core approaches the Townes profile $R^{(0)}$ (solid line). Data is plotted on the fixed domain $0 \leq \rho \leq 10$, which in the physical variable r corresponds to the shrinking domain $[0, 10L(z)]$

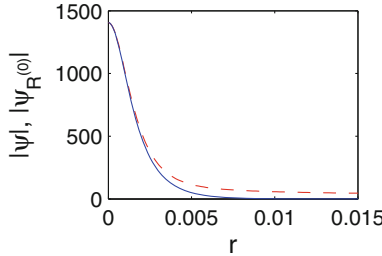


Fig. 14.3 Solution of the two-dimensional cubic NLS with high-power Gaussian initial condition $\psi_0 = 15\sqrt{\frac{\pi}{2}}e^{-r^2}$ ($P \approx 38P_{\text{cr}}$, dashes) at $z = 0.017$. The solid line is $\psi_{R^{(0)}}$. From [73]

from (14.9). This representation clearly shows that the self-similar profile of the collapsing core converges to $R^{(0)}$.

The convergence of the collapsing core of radial solutions to $\psi_{R^{(0)}}$ was also observed:

- At much higher power levels, e.g., for a Gaussian initial condition with $P \approx 38P_{\text{cr}}$ (Fig. 14.3).
- For non-monotone initial conditions, e.g., the perturbed excited state $\psi_0 = (1 \pm 0.01)R^{(1)}(r)$ with $P \approx 6.6P_{\text{cr}}$ (Figs. 14.10 and 14.11).

In general, NLS simulations show that initial profiles that are “closer” to $R^{(0)}$ converge to $\psi_{R^{(0)}}$ after “less” self-focusing. Thus, for example, a Gaussian initial condition with power slightly above P_{cr} converges to $\psi_{R^{(0)}}$ after “less” self-focusing than an equal-power super-Gaussian, or a higher-power Gaussian.

14.1.2 Convergence to a Radial Profile

In what follows, we consider three types of nonradial initial conditions: Elliptic, multiple peaks, and noisy.⁴ Overall, these simulations show that as $z \rightarrow Z_c$:

1. The collapsing core becomes radial about the singularity point \mathbf{x}_c .⁵
2. The profile of the collapsing core approaches the $\psi_{R^{(0)}}$ profile.
3. The non-collapsing “outer tail” does not become radial.

Elliptic Initial Conditions

The standard approach in nonlinear optics for analyzing the effect of input-beam astigmatism has been to consider the NLS (14.7) with the elliptic Gaussian initial conditions

$$\psi_0(x, y) = c e^{-(\frac{x}{a})^2 - (\frac{y}{b})^2}, \quad (14.11)$$

where a , b , and c are constants. Numerical simulations carried out by Landman et al. [152] and by Gross and Manassah [119] showed that ψ becomes radial near the singularity. In [75] Fibich and Ilan pointed out that while the collapsing core (whose power is $\approx P_{\text{cr}}$) becomes radial and approaches $\psi_{R^{(0)}}$, the outer, non-collapsing part of the solution does not become radial (Figs. 14.4 and 14.5).

Remark See [75] for a detailed study of self-focusing of elliptic beams, Sect. 14.5 for experiments with astigmatic beams, Corollary 14.3 for the convergence on the collapsing core to a radial profile, and Sect. 24.6 for the threshold power for collapse of elliptic beams.

Multiple Peaks

The convergence of the collapsing core to a radial profile was observed by Landman et al. [152] in simulations of the critical NLS with initial conditions that have several local maxima. In a simulation with two unequal peaks, the higher peak absorbed the lower peak and then underwent a radial collapse at a single point. When the two peaks were equal, the numerical solution collapsed around two distinct peaks (as it should, see Sect. 13.4).

⁴ Obviously, in these simulations one has to solve the “genuinely two-dimensional” NLS (14.7), and not the radial NLS (14.8).

⁵ In light of Lemma 5.5, the question whether the collapsing core becomes radial is only of interest if ψ_0 is not radial.

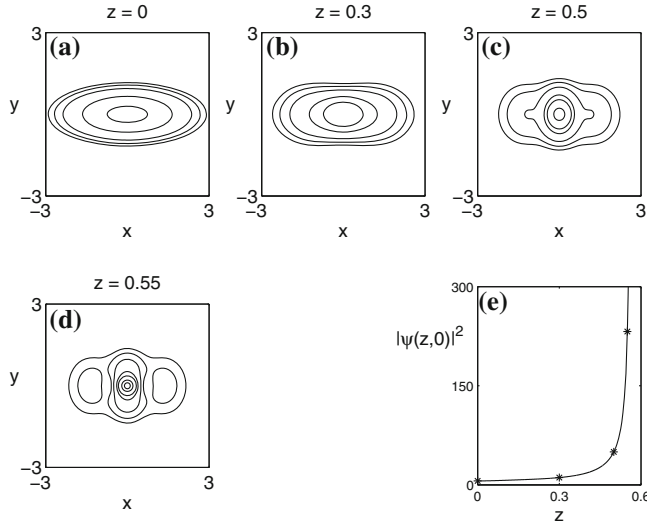


Fig. 14.4 The NLS (14.7) with $\psi_0 = 2\sqrt{0.8P_{\text{cr}}}e^{-(0.4x)^2-y^2}$ ($P = 2P_{\text{cr}}$). **a–d** Contour plots of $|\psi|$ in the (x, y) -plane. Only the collapsing core approaches a radial profile. **e** Evolution of the on-axis intensity. Axial locations of contour plots are denoted by *

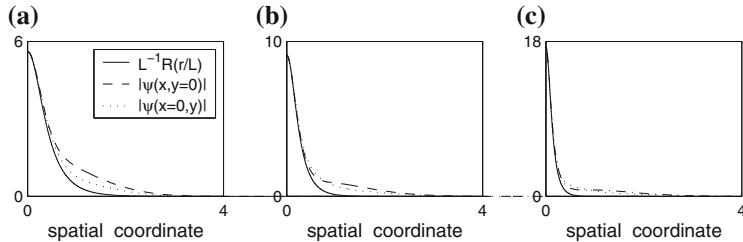


Fig. 14.5 Solution of the two-dimensional cubic NLS with the elliptic initial condition $\psi_0 = 2\sqrt{1.165P_{\text{cr}}}e^{-\left(\frac{3x}{4}\right)^2-y^2}$. The spatial coordinates are x (dashes) and y (dots). The solid line is $\psi_{R^{(0)}}$. **a** $z = 0.22$, $L = 0.52$. **b** $z = 0.28$, $L = 0.32$. **c** $z = 0.31$, $L = 0.165$. From [75]

Noisy Initial Conditions

In [76], Fibich and Ilan solved numerically the NLS (14.7) with noisy high-power Gaussian initial conditions, and observed that the solution collapses at a single point with a radial blowup profile. For example, Fig. 14.6a shows the contour levels of a Gaussian initial condition with $P = 15P_{\text{cr}}$ and 10% complex-valued noise. As the solution collapses, its profile becomes clean and radial (Fig. 14.6b). Since the noise quickly disappears, the evolution of the maximal intensity (hence the collapse distance), with and without noise, are nearly the same (Fig. 14.7).

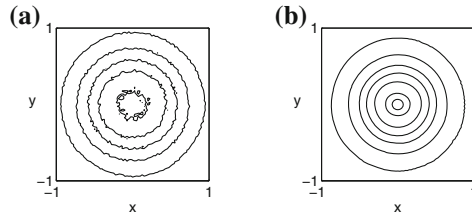


Fig. 14.6 Solution of the NLS (14.7) with a noisy high-power input Gaussian beam with $P = 15P_{\text{cr}}$ and 10% complex-valued noise. Contour plots of $|\psi(x, y, z)|$ at **a** $z = 0$, and **b** $z = 0.026$. From [131]

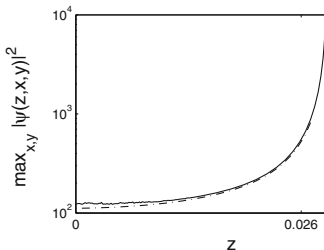


Fig. 14.7 Dynamics of the maximal intensity of the solution of Fig. 14.6 (solid). Dash-dot curve is for same input beam, but without noise. From [131]

In particular, $\psi_{R(0)}$ is an attractor for noisy Gaussian initial conditions with $P = 15P_{\text{cr}}$.

Noise can have a destabilizing effect and lead to multiple filamentation at much higher input powers (Sect. 25.1.1).⁶ Thus, collapse of sufficiently high-power radial solutions is unstable under nonradial perturbations. This Bespalov-Talanov instability, however, is irrelevant to the stability of $\psi_{R(0)}$, because high-power initial conditions are “very far” from $\psi_{R(0)}$. Moreover, when a high-power solution breaks into multiple filaments, each filament ultimately collapses with the $\psi_{R(0)}$ profile.

14.2 Numerical Observations—Blowup Rate

We now consider the blowup rate of solutions that collapse with the $\psi_{R(0)}$ profile. Recall that up to a multiplicative constant, the blowup rate $l(z) := 1/\|\nabla\psi\|_2$ is equal to the solution width $L(z)$, see Sect. 13.2.3, whose value can be conveniently extracted from ψ using (14.9).

⁶ In Sect. 3.6.3 we saw that noise has a destabilizing effect on infinite-power, plane wave solutions.

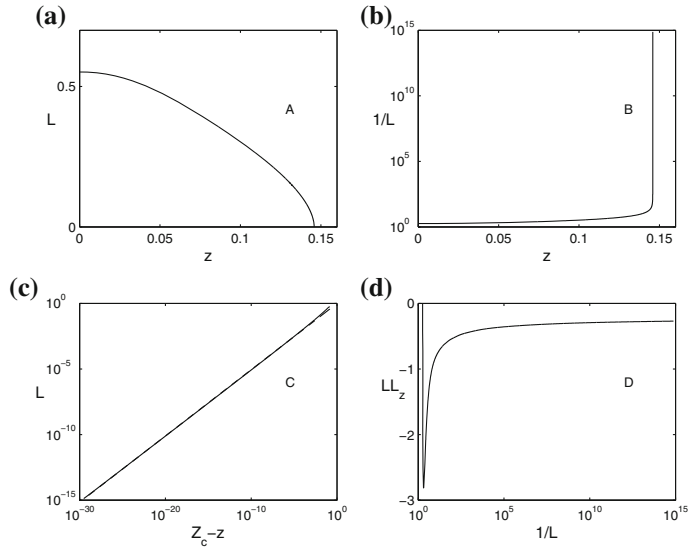


Fig. 14.8 Blowup rate of the solution of Fig. 14.1. **a** $L(z)$. **b** $1/L$ as a function of z , plotted on a semi-logarithmic scale. **c** L as a function of $Z_c - z$, plotted on a loglog scale. *Dashed line* is $L = 0.99(Z_c - z)^{0.505}$. The two curves are nearly indistinguishable. **d** LL_z as a function of $1/L$

Figure 14.8a shows that the width $L(z)$ of the solution of Fig. 14.1 is monotonically decreasing, and that it vanishes at $Z_c \approx 0.146$. Plotting the on-axis amplitude $1/L$, see Fig. 14.8b, shows that relatively little self-focusing takes place during most of the propagation. Then, “all of a sudden”, as the solution approaches the singularity point Z_c , the on-axis amplitude increases faster and faster, becoming infinite at Z_c .⁷

14.2.1 How to Determine Numerically a Power-Law Blowup Rate?

When we try to compute the blowup rate of $L(z)$, we first search for the values of κ and p for which the power-law relation

$$L \sim \kappa(Z_c - z)^p, \quad z \rightarrow Z_c \quad (14.12)$$

provides the best fit to the numerical data. Since

$$\log L \sim \log \kappa + p \log(Z_c - z), \quad (14.13)$$

⁷ As discussed in Sect. 3.2, the self-focusing process accelerates because of a nonlinear feedback mechanism. Thus, as the beam collapses, the intensity at its center increases. Hence so does the index of refraction. This, in turn, increases the attraction towards the beam center, thereby accelerating the self-focusing process.

the values of p and κ can be determined using linear regression. For example, applying this fit to the simulation of Fig. 14.1 yields $p \approx 0.505$, see Fig. 14.8c, showing that the blowup rate is close to a square root.

One problem with this approach is that as $z \rightarrow Z_c$, the computed value of $Z_c - z$ suffers from loss of significant digits. This numerical error can be considerably reduced by searching for the value of Z_c for which the relation between $\log L$ and $\log(Z_c - z)$ is closest to linear.⁸ Alternatively, one can perform the fit between $\log L$ and $\log(Z_c - z)$ for values of z which are sufficiently “far” from Z_c . Note, however, that one cannot use values of z which are “too far” from Z_c , because the power-law relation (14.12) holds only asymptotically as $z \rightarrow Z_c$, and not from $z = 0$.

14.2.2 How to Distinguish Between Loglog and Square-Root Blowup Rates?

In Sect. 14.6 we shall see that the blowup rate of solutions that collapse with the $\psi_{R^{(0)}}$ profile is a square root with a loglog correction (the loglog law), see (14.6). The loglog correction cannot be observed numerically, for reasons explained in Sect. 18.3. We can, however, try to achieve the “less ambitious” goal of determining numerically whether the blowup rate is a “pure” square root or slightly faster (as is the case with the loglog law).

It is tempting to do this by checking whether the fitted value of p is larger than $1/2$. The main problem with this approach is that, regardless of the way in which the value of Z_c is computed, one has to determine manually the range over which the numerical fit is performed, and the choice of the fitting range affects the computed values of p and κ . Although this effect is typically quite small, when trying to determine whether the blowup rate is a square root or slightly faster, we cannot “afford” to have this numerical effect. For example, is the fact that $p \approx 0.505$ in Fig. 14.8c an indication that the blowup rate is faster than a square root, or a numerical artifact?⁹

LL_z Approach

An alternative approach for determining whether the blowup rate is faster than a square root, proposed by Fibich, Gavish, and Wang, is based on computing the limit of LL_z and using the following result:

⁸ i.e., the value of Z_c for which r^2 of the regression curve (14.13) is closest to 1.

⁹ Indeed, even if the blowup rate is a square root, the fitted numerical value of p will never be exactly $1/2$.

Lemma 14.1 ([73]) Let $a := -\lim_{z \rightarrow Z_c} LL_z$.

1. If $0 < a < \infty$, $L(z)$ goes to zero at the square root blowup rate

$$L(z) \sim \alpha \sqrt{Z_c - z}, \quad \alpha = \sqrt{2a} > 0.$$

2. If $a = 0$, the blowup rate of $L(z)$ is faster than a square root.

Proof By l'Hospital's rule,

$$\lim_{z \rightarrow Z_c} \frac{L^2}{Z_c - z} = -2 \lim_{z \rightarrow Z_c} LL_z = 2a.$$

Therefore, the result follows. \square

For example, if $L(z)$ is given by the loglog law (14.6), then

$$-LL_z \sim \frac{\pi}{\log \log \frac{1}{Z_c - z}} \rightarrow 0, \quad z \rightarrow Z_c. \quad (14.14)$$

Exercise 14.1 Let $a = -\lim_{z \rightarrow Z_c} L^\alpha L_z$. Show that:

1. If $0 < a < \infty$, the blowup rate of $L(z)$ is $\frac{1}{1+\alpha}$, i.e.,

$$L(z) \sim \kappa (Z_c - z)^{\frac{1}{1+\alpha}}, \quad \kappa = ((1 + \alpha)a)^{\frac{1}{1+\alpha}} > 0.$$

2. If $a = 0$, the blowup rate of $L(z)$ is faster than $\frac{1}{1+\alpha}$.

Determining whether the blowup rate is equal to or faster than a square root by computing $\lim_{z \rightarrow Z_c} LL_z$ avoids the problems that arise when the blowup rate is computed “directly” by curve fitting $L \sim \kappa(Z_c - z)^\rho$, see Sect. 14.2.1. Indeed, since we do not need the value of Z_c , we avoid the loss of significant digits in the calculation of $Z_c - z$. In addition, since the calculation is local (in z), the results are insensitive to the “fitting range”. One potential problem with the “ LL_z approach” is that it involves numerical differentiation. Indeed, if one computes L_z using values of $L(z_j)$ at adjacent grid nodes $\{z_j\}$, the result is typically quite noisy. This problem can be easily avoided, however, by using values of L at grid nodes that are sufficiently far away from each other.

The main problem with the “ LL_z approach” is that in a loglog collapse, the rate at which LL_z goes to zero is exponentially slower than the rate at which L goes to zero. Indeed, taking the loglog of (14.6) gives $\log \log \frac{1}{Z_c - z} \sim \log \log \frac{1}{L}$. Substituting this relation in (14.14) gives

$$-LL_z \sim \frac{\pi}{\log \log \frac{1}{L}}. \quad (14.15)$$

Therefore, it is not always clear whether LL_z goes to zero, or to a negative constant (see, e.g., Fig. 14.8d).

Remark In the case of shrinking-ring solutions, further support that $a := -\lim_{z \rightarrow z_c} LL_z$ is positive can be obtained from the numerical agreement between the value of $\alpha = \sqrt{2a}$ extracted from the blowup rate, and the value of α extracted from matching the self-similar profile with the best-fitting G profile. See Sect. 19.2.2 for more details.

Blowup-Profile Approach

Another approach for determining whether the blowup rate is faster than a square root is to consider the blowup profile. Indeed, by Proposition 19.2, the blowup rate is faster than a square root if and only if the self-similar profile is a solution of the R equation, see (14.3). Unfortunately, the “blowup profile approach” is not conclusive either, because in principle it is possible that the self-similar profile converges to a solution of the G equation, see (19.8), with $G(0) \approx R^{(0)}(0)$ and $0 < \alpha \ll 1$, which “looks like” $R^{(0)}$ for $\rho = O(1)$,¹⁰ but has a square root blowup rate.

14.2.3 Blowup Rate

We now return to the problem of determining the blowup rate of the solution of Fig. 14.1. From Fig. 14.8d it is not clear whether LL_z ultimately goes to zero or to a negative constant. As noted, this is because when L is given by the loglog law, the rate at which LL_z goes to zero is exponentially slow in $1/L$, see (14.15). In practice, however, when LL_z goes to a negative constant, this is usually very clear from the plot (see, e.g., Fig. 19.5). Therefore, Fig. 14.8d suggests that the blowup rate is slightly faster than a square root. The convergence of the blowup profile to $\psi_{R^{(0)}}$ in Figs. 14.1 and 14.2 provides further support that the blowup rate is slightly faster than a square root.

In Fig. 14.9 we consider the blowup rate of the high-power solution from Fig. 14.3. Since (i) $p \approx 0.503$, (ii) LL_z “appears to” go to zero, and (iii) the blowup profile approaches $\psi_{R^{(0)}}$, the overall numerical evidence suggests that the blowup rate is slightly faster than a square root.

¹⁰ When $G(0) \approx R^{(0)}(0)$, the difference between G and $R^{(0)}$ is evident only for $\rho = O(\alpha^{-2}) \gg 1$. This region, however, is way outside the collapsing-core domain where ψ converges to a self-similar profile.

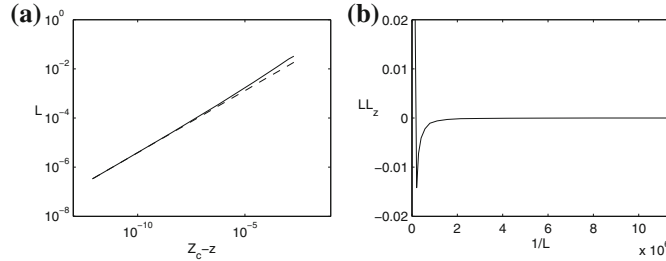


Fig. 14.9 Blowup rate of the solution of Fig. 14.3. **a** L as a function of $Z_c - z$, plotted on a loglog scale (solid). Dashed line is $2.295(Z_c - z)^{0.505}$. **b** LL_z as a function of $1/L$

14.3 Numerical Observations—Perturbed Excited Solitary Waves

In Sect. 6.4.4 we saw that in dimension $d \geq 2$, the critical NLS admits a countable number of radial solitary waves $\psi^{\text{solitary},(n)} = e^{iz} R^{(n)}(r)$, where $n = 0$ is the ground state and $n \geq 1$ are the excited states. In Sect. 7.11.1 we proved that for any $0 < \epsilon \ll 1$, the solution of the critical NLS with $\psi_0 = (1 + \epsilon)R^{(n)}$ blows up at a finite distance. We also saw that if we perturb the ground-state solitary wave in the opposite direction, i.e., $\psi_0 = (1 - \epsilon)R^{(0)}$, the solution exists globally and scatters (diffracts) as $z \rightarrow \infty$.

We now use numerical simulations to address several questions that, at present, are not covered by NLS theory:

1. Do the perturbed excited states $\psi_0 = (1 - \epsilon)R^{(n)}$, where $0 < \epsilon \ll 1$ and $n \geq 1$, become singular? Note that it is not possible to answer this question analytically, because ψ_0 has power above P_{cr} and a positive Hamiltonian (Sect. 7.11.1).
2. When a perturbed excited state $\psi_0 = (1 \pm \epsilon)R^{(n)}$ becomes singular, what is its blowup rate and profile? In particular, does it collapse with the $R^{(n)}$ profile or with the $R^{(0)}$ profile?

In Figs. 14.10 and 14.11 we solve the critical NLS with $\psi_0 = (1 \pm 0.01)R^{(1)}(r)$, where $R^{(1)}$ is the first excited state, see Fig. 6.1, whose power is $P \approx 6.6P_{\text{cr}}$. In both simulations, initially (i.e., for $0 \leq z \leq 1$, top row), the profile of the perturbed solution remains close to $R^{(1)}$. This is to be expected, by continuity from the unperturbed solitary wave $\psi^{\text{solitary},(1)} = e^{iz} R^{(1)}(r)$. Subsequently, there is a transition stage, during which the profile changes from $R^{(1)}$ to $R^{(0)}$ (middle row). This transition is non-monotone. For example, in Fig. 14.10 the profile approaches $R^{(0)}$ between $2 \leq z \leq 2.44$, moves back towards $R^{(1)}$ at $z = 2.7$, and approaches $R^{(0)}$ again at $z = 2.86$. Eventually (bottom row), the collapsing core approaches the $\psi_{R^{(0)}}$ profile.

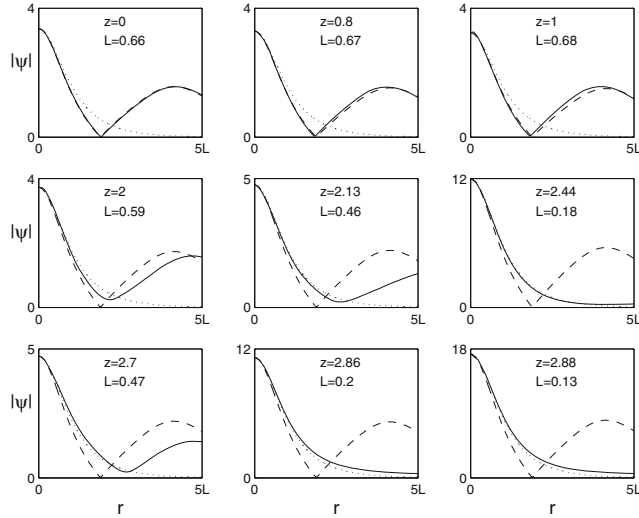


Fig. 14.10 Solution of the critical NLS (14.8) with $\psi_0 = 1.01 R^{(1)}(r)$. Initially, the solution amplitude (solid line) remains close to a modulated excited state $|\psi_{R^{(1)}}| := \frac{1}{L^{(1)}(z)} |R^{(1)}(\frac{r}{L^{(1)}(z)})|$, where $L^{(1)}(z) := \frac{R^{(1)}(0)}{|\psi(z,0)|}$ (dashed line). Ultimately, however, the solution converges to $\psi_{R(0)}$ (dotted line). Because we plot absolute values, $|R^{(1)}|$ and $|\psi|$ are non-smooth at the point where they change sign

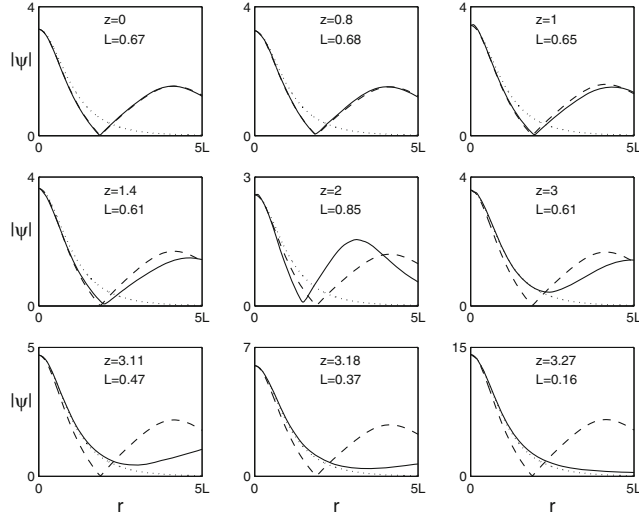


Fig. 14.11 Same as Fig. 14.10 with $\psi_0 = 0.99 R^{(1)}(r)$

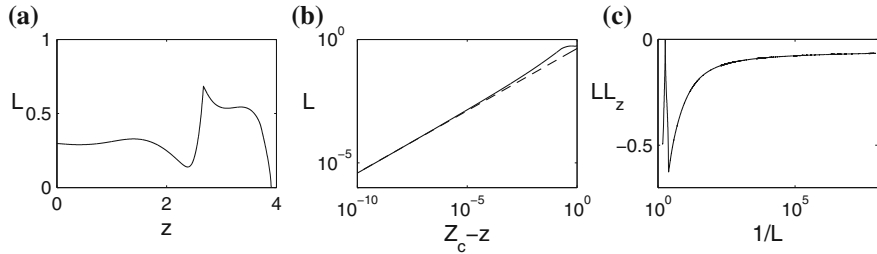


Fig. 14.12 Blowup rate of the solution of Fig. 14.10. **a** $L(z) := \frac{1}{|\psi(z, r=0)|}$ as a function of z . **b** L as a function of $Z_c - z$, plotted on a loglog scale (*solid*). The *dashed line* is $0.43(Z_c - z)^{0.504}$. **c** LL_z as a function of $\frac{1}{L}$

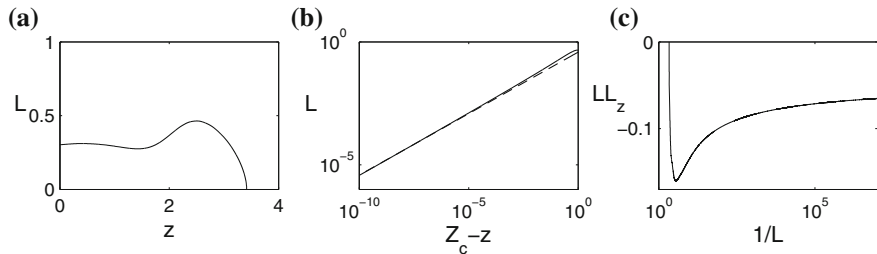


Fig. 14.13 Same as Fig. 14.12, for the solution of Fig. 14.11. The *dashed line* in B is $0.38(Z_c - z)^{0.5002}$

Figures 14.12a and 14.13a show the dynamics of the width $L(z)$ of the perturbed excited state. Initially ($0 \leq z \leq 1$), the solutions remain close to $\psi^{\text{solitary},(1)} = e^{iz} R^{(1)}(r)$, and so $L(z) \approx L(0)$. Subsequently, during the transition from $R^{(1)}$ to $R^{(0)}$, the dynamics of $L(z)$ is non-monotone. Eventually, as the solutions collapse with the $\psi_{R^{(0)}}$ profile, $L(z)$ decreases monotonically to zero.

Plotting L as a function of $Z_c - z$ on a loglog scale shows that the blowup rate of $L(z)$ is close to a square root (Figs. 14.12b and 14.13b). In addition, Figs. 14.12c and 14.13c suggest that $\lim_{L \rightarrow 0} LL_z = 0$. Hence, the blowup rate is slightly faster than a square root.¹¹

Overall, the above simulations suggest

Observation 14.1 *Solutions of the critical NLS with the perturbed excited-state initial conditions $\psi_0 = (1 \pm \epsilon)R^{(n)}(r)$, where $0 < \epsilon \ll 1$ and $n \geq 1$,*

1. *Become singular.*
2. *Have a blowup rate which is slightly faster than a square root.*
3. *Collapse with the $\psi_{R^{(0)}}$ profile.*

¹¹ See Sect. 14.2 on how to determine the blowup rate numerically.

4. Concentrate the power $P_{\text{collapse}} = \|R^{(0)}\|_2^2$ at the singularity.
5. Undergo a partial-beam collapse (since $P_{\text{collapse}} < \|R^{(n)}\|_2^2$).

14.4 Numerical Observations—Perturbed Excited Explicit Blowup Solutions

In Sect. 10.6.3 we saw that there are no analytic results on the stability of the excited explicit blowup solutions $\psi_{R^{(n)}}^{\text{explicit}}$ with $n \geq 1$. Recall, however, that the lens transformation implies that the addition of a focusing lens does not arrest collapse (Lemma 8.5), nor does it affect the blowup rate (Lemma 13.1) or the blowup profile. Therefore, from Observation 14.1 immediately follows

Observation 14.2 *Solutions of the critical NLS with the perturbed excited explicit blowup solutions*

$$\psi_0 = (1 \pm \epsilon)\psi_{R^{(n)}}^{\text{explicit}}(0, r) = (1 \pm \epsilon)R^{(n)}(r)e^{-i\frac{r^2}{4F}},$$

where $0 < \epsilon \ll 1$, $F > 0$, and $n \geq 1$,

1. Become singular.
2. Have a blowup rate which is slightly faster than a square root.
3. Collapse with the $\psi_{R^{(0)}}$ profile.
4. Concentrate the power $P_{\text{collapse}} = \|R^{(0)}\|_2^2$ at the singularity.
5. Undergo a partial-beam collapse.

Therefore, the excited explicit blowup solutions are unstable in the sense of Definition 10.3.

14.5 Experimental Observations

In this section, we present experimental results which show that:

1. Collapsing laser beams undergo a partial-beam collapse, in which the beam core undergoes collapse, but the rest of the beam continues to propagate forward nearly linearly.
2. The collapsing core approaches a radial profile.
3. This radial blowup profile is given by $\psi_{R^{(0)}}$.

The effect of input-beam ellipticity on self-focusing beams was first tested experimentally in 1972 by Giuliano et al. [113]. In these experiments, they used astigmatic lenses, yet observed that “the damaged region was found to possess a circular rather than an elliptic cross section”. In other words, these experiments showed that even when the input beam is astigmatic, the collapsing core becomes radial as it collapses.

In experiments carried out in 2006 by Moll, Fibich, and Gaeta, we studied the blowup profile of intense laser beams that propagated in silica. The input beams had either a randomly-distorted circular profile (Fig. 14.14a) or an astigmatic one (Fig. 14.14c). In both cases, the beam collapsed with a radial blowup profile (Fig. 14.14b, d, respectively).

In that study we also measured the transverse profile of the collapsing core, and observed that it was in excellent agreement with the $\psi_{R^{(0)}}$ profile (Fig. 14.15).¹² Here, the only fitting parameter was the value of $L(z)$, which was determined using (14.9). To the best of our knowledge, this is the first experimental observation of a universal blowup profile in any physical system. In a subsequent study, Grow et al. [122] observed that a noisy Gaussian input beam that propagated in water collapsed with the Townes profile.

Figure 14.15 also shows that outside of the collapsing core, the profile is the same for low- and high-power beams, up to a linear scaling that accounts for the change in power. This shows that optical collapse is a *partial-beam collapse*: While the

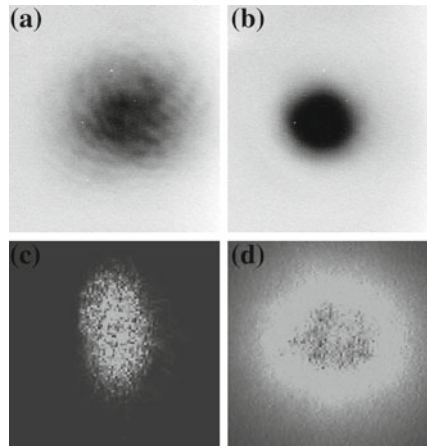


Fig. 14.14 At low powers, **a** a randomly distorted beam and **c** an elliptically-shaped input beam with a 3:1 ratio of major to minor axes are passed through the BK7 sample. As the power is increased, **b** the distorted beam self-focuses, becoming smaller in diameter as well as smooth and symmetric. For the elliptically-shaped beam, **d** circularly symmetric super-continuum generation is formed. An elliptically-shaped Gaussian beam profile fit to the captured image demonstrates that the beam is circular to better than one part in thirty. From [192]

¹² The Townes profile in Fig. 14.15 has a triangular shape, because the y-axis is on a logarithmic scale.

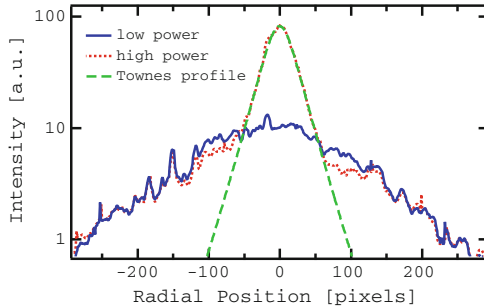


Fig. 14.15 The first experimental observation of the Townes profile $R^{(0)}$. Lineouts along one axis are taken through the center of the beam at two different powers, y -axis is plotted on a logarithmic scale. At sufficiently high powers, a strong on-axis component is observed which matches the $\psi_{R^{(0)}}$ profile. The low-power profile has been scaled by a constant factor, to account for different input powers. Adapted from [192]

collapsing core undergoes a nonlinear dynamics and approaches the $\psi_{R^{(0)}}$ profile, the beam tail propagates nearly linearly.

Remark The remarkable agreement between the experimental results in this section and the predictions of the NLS model, shows that the NLS model remains valid even as the beam undergoes significant self-focusing. See Sect. 1.8 for further discussion.

Remark When the input power is several critical powers or more, input-beam ellipticity can lead to multiple filamentation, i.e., to a complete breakup of radial symmetry. This occurs after the NLS blowup point, and requires the presence of a collapse-arresting mechanism. See Sect. 25.3.2 for more details.

14.6 Collapse with the $\psi_{R^{(0)}}$ Profile at the Loglog Law Blowup Rate

In Sect. 13.2 we rigorously saw that all singular solutions of the critical NLS undergo a quasi self-similar collapse with a self-similar profile whose power is at least P_{cr} . Numerical simulations (similar to those in Sect. 14.1) that were carried out during the 1980s suggested that, regardless of the initial condition, the collapsing core always approaches the peak-type $\psi_{R^{(0)}}$ profile.¹³ This “information” was used in asymptotic studies, also carried out during the 1980s, which showed that the blowup rate is given by a square root with a loglog correction. This blowup rate became known as the *loglog law*.¹⁴

¹³ More recent simulations suggest that there may exist radially-stable solutions that collapse with a ring-type blowup profile which is different from $\psi_{R^{(0)}}$ (Sect. 14.6.8).

¹⁴ The asymptotic analysis that leads to the loglog law is presented in Chaps. 17 and 18.

Following the original informal derivations of the loglog law, a considerable research effort was devoted to observing it in NLS simulations. This research effort failed, for reasons outlined in Sect. 18.3. A rigorous proof of the loglog law and of the convergence to $\psi_{R^{(0)}}$ also turned out to be a formidable challenge. In part, this is because these two properties do not hold for all singular solutions. Thus, the loglog law does not hold for blowup solutions that collapse at a linear rate (Sect. 13.1.1), and the convergences to $\psi_{R^{(0)}}$ does not hold for vortex blowup solutions (Sect. 15.11.2). Although these “counterexamples” are unstable, their existence implies that a rigorous proof of the convergence to $\psi_{R^{(0)}}$ and of the loglog law should somehow be able to distinguish between the stable singular solutions and the unstable “counterexamples”.

The first rigorous proof of the convergence to $\psi_{R^{(0)}}$ and of the loglog law was obtained by Perelman in 2001 for the one-dimensional NLS with a certain class of isotropic initial conditions which are sufficiently close to the ground state. Subsequently, in a series of breakthrough papers published between 2003 and 2006, Merle and Raphaël treated rigorously the general case, using the approach previously developed by Martel and Merle for analysis of collapse in the critical KdV equation [169]. The results of Merle and Raphaël are summarized in the following theorem:¹⁵

Theorem 14.1 ([178–183, 217]) *Let $d = 1, \dots, 5$, and let ψ be a solution of the critical NLS (14.1) that blows up at Z_c . Then there exists a universal constant $\alpha^* > 0$, which depends only on the dimension, such that if $\psi_0 \in B_{\alpha^*}$, where*

$$B_{\alpha^*} := \left\{ \psi_0 \mid \psi_0 \in H^1, \quad P_{\text{cr}} \leq \|\psi_0\|_2^2 \leq P_{\text{cr}} + \alpha^* \right\},$$

the following holds:

1. **Convergence to the universal $\psi_{R^{(0)}}$ profile**

There exist parameters $(\zeta(z), \mathbf{x}_0(z), L(z)) \in \mathbb{R} \times \mathbb{R}^d \times \mathbb{R}^+$, and a function $\phi \in L^2$, such that

$$\psi(z, \mathbf{x}) - \psi_{R^{(0)}}(z, \mathbf{x} - \mathbf{x}_0(z)) \xrightarrow{L^2} \phi(\mathbf{x}), \quad z \rightarrow Z_c,$$

where

$$\psi_{R^{(0)}}(z, \mathbf{x}) = \frac{1}{L^{\frac{d}{2}}(z)} R^{(0)} \left(\frac{|\mathbf{x}|}{L(z)} \right) e^{i\zeta(z)},$$

and $R^{(0)}$ is the ground state of (14.3). Moreover, the blowup point is finite, i.e., $\mathbf{x}_c := \lim_{z \rightarrow Z_c} \mathbf{x}_0(z) \in \mathbb{R}^d$.

¹⁵ We do not present the rigorous proofs of Merle and Raphaël. In Chaps. 17 and 18 we present an informal derivation of the loglog law.

2. Blowup rate

As $z \rightarrow Z_c$, either

$$\|\nabla \psi\|_2 \sim \frac{\|\nabla R^{(0)}\|_2}{\sqrt{2\pi}} \left(\frac{Z_c - z}{\log |\log(Z_c - z)|} \right)^{-\frac{1}{2}} \quad (\text{loglog law}), \quad (14.16)$$

or

$$\|\nabla \psi\|_2 \geq \frac{C^*}{\sqrt{H_G(\psi_0)}} \frac{1}{Z_c - z} \quad (\text{at least linear}), \quad (14.17)$$

where C^* is a universal constant and $H_G(\psi) := H(\psi) - \left(\frac{\operatorname{Im} \int \psi^* \nabla \psi}{\|\psi\|_2} \right)^2$.

3. Sufficient condition for loglog collapse

If $H_G(\psi_0) < 0$ and $P_{\text{cr}} < \|\psi_0\|_2^2 < P_{\text{cr}} + \alpha^*$, then ψ blows up at the loglog rate (14.16).

4. Stability of loglog blowup

The set of initial conditions $\psi_0 \in \mathcal{B}_{\alpha^*}$ for which ψ collapses with the loglog rate (14.16), is open in H^1 .

In what follows, we discuss the results and consequences of Theorem 14.1.

14.6.1 Universal Blowup Profile and Power Quantification

Assertion 1 of Theorem 14.1 states that as $z \rightarrow Z_c$, the solution breaks into a collapsing core that approaches the $\psi_{R^{(0)}}$ profile, and a non-collapsing tail that approaches a function $\phi(\mathbf{x}) \in L^2$. The blowup profile is universal, as it is independent of the initial condition. The limiting tail ϕ , however, depends on ψ_0 .

The function $\mathbf{x}_0(z)$ describes the location of the peak intensity. Thus, for example, if the input beam is radial, then $\mathbf{x}_0(z) \equiv 0$, and if the input beam is radial and titled, then $\mathbf{x}_0(z) = \mathbf{x}_0(0) + z\mathbf{c}$, see Sect. 8.2.

The result that the blowup point \mathbf{x}_c is finite is intuitive, because it corresponds to the blowup point of an intense laser beam. We note, however, that in other nonlinear dispersive equations, such as the critical KdV, the collapse point can escape to infinity [170].

Since the power of $\psi_{R^{(0)}}$ is equal to P_{cr} , it follows from power conservation that the tail limit ϕ contains the rest of the power:

Corollary 14.1 ([180]) Under the conditions of Theorem 14.1,

$$|\psi|^2 \rightharpoonup \|R^{(0)}\|_2^2 \delta(\mathbf{x} - \mathbf{x}_c) + |\phi|^2, \quad z \rightarrow Z_c, \quad (14.18)$$

where $\|\phi\|_2^2 = \|\psi_0\|_2^2 - \|R^{(0)}\|_2^2$. In particular, the amount of power that collapses into the singularity is $P_{\text{collapse}} = \|R^{(0)}\|_2^2$.

Remark The power concentration Theorem 13.6 “only” showed that $P_{\text{collapse}} \geq P_{\text{cr}}$.

In Sect. 7.7 we asked whether singular solutions of the critical NLS undergo a whole-beam or a partial-beam collapse. Corollary 14.1 implies

Corollary 14.2 *Under the conditions of Theorem 14.1, if $P_{\text{cr}} < \|\psi_0\|_2^2 \leq P_{\text{cr}} + \alpha^*$, the NLS solution undergoes a partial-beam collapse.*

Since all minimal-power singular solutions are unstable (Lemma 13.4), this implies that *all stable singular solutions with power below $P_{\text{cr}} + \alpha^*$ undergo a partial-beam collapse*.

Theorem 14.1 also implies

Corollary 14.3 *For all singular solutions whose power is below $P_{\text{cr}} + \alpha^*$, even if the initial condition is not radial, the collapsing core becomes radially-symmetric about the singularity point \mathbf{x}_c .*

In particular, the blowup profile $\psi_{R^{(0)}}$ is azimuthally stable. This result is consistent with NLS simulations (Sect. 14.1.2) and self-focusing experiments (Sect. 14.5).

In Sect. 13.4 we saw that NLS solutions can collapse at more than one point. In Theorem 14.1, however, the NLS solution collapses only at \mathbf{x}_c .

Corollary 14.4 *All singular solutions of the critical NLS whose power is below $P_{\text{cr}} + \alpha^*$ collapse at a single point.*

“Missing” Phase Term

In Chap. 17 we shall see that

$$\psi_{R^{(0)}} = \frac{1}{L^{\frac{d}{2}}(z)} R^{(0)} \left(\frac{r}{L(z)} \right) e^{i\zeta(z) + i \frac{L_z r^2}{L} \frac{r^2}{4}}.$$

The quadratic phase term $\frac{L_z r^2}{L} \frac{r^2}{4}$ does not appear in the expression for $\psi_{R^{(0)}}$ in Theorem 14.1. To confirm that the two expressions for $\psi_{R^{(0)}}$ are asymptotically equivalent, we now show that $e^{i \frac{L_z r^2}{L} \frac{r^2}{4}} \rightarrow 1$ as $z \rightarrow Z_c$. We first note that $\rho = O(1)$ in the collapsing-core region. Hence,

$$\frac{L_z r^2}{L} \frac{r^2}{4} = \frac{LL_z}{4} \rho^2 = O(LL_z).$$

In addition, by (13.30), $l(z) \sim c_l L(z)$. Since $l(z) := 1/\|\nabla \psi\|_2$ goes to zero at the blowup rates (14.16) or (14.17), both of which are faster than a square root, this implies that $LL_z \rightarrow 0$, see Lemma 14.1. Therefore, $\lim_{z \rightarrow Z_c} e^{i \frac{L_z r^2}{L} \frac{r^2}{4}} = 1$.

Remark Since $LL_z \rightarrow 0$, one can ask why we retain the quadratic phase term in the asymptotic analysis in Chap. 17. In short, the answer is that when L goes to zero at the loglog law rate, the rate at which $LL_z \rightarrow 0$ is exponentially slower than the rate

at which $L \rightarrow 0$.¹⁶ Therefore, to leading order,¹⁷ LL_z is a small negative constant, rather than zero.

14.6.2 Blowup Rate

Assertion 2 of Theorem 14.1 shows that when $P_{\text{cr}} \leq \|\psi_0\|_2^2 \leq P_{\text{cr}} + \alpha^*$, there are two possibilities for the blowup rate $l(z)$: Either it is given by the loglog law, or it is at least linear. The loglog law implies that for any $\epsilon > 0$,

$$(Z_c - z)^{\frac{1}{2} + \epsilon} \ll l(z) \ll (Z_c - z)^{\frac{1}{2}}, \quad z \rightarrow Z_c.$$

Therefore, the loglog-law blowup rate is slightly faster than the square-root upper bound, see Sect. 13.1, but is significantly slower than the linear blowup rate of ψ_R^{explicit} and of the Bourgain-Wang solutions (Chap. 10). Note that the multiplicative constant in the loglog law is universal, which is consistent with Corollary 13.3.

The difference between collapse at a linear blowup rate and at the loglog law blowup rate is also captured by the “roughness” of the limiting tail ϕ :

Theorem 14.2 ([180]) *Under the conditions of Theorem 14.1, there exists a universal constant $C^* > 0$, such that $\rho > 0$ small enough we have that:*

1. **Loglog regime:** *If the blowup rate is given by (14.16), then*

$$\frac{1}{C^*} \frac{1}{(\log |\log \rho|)^2} \leq \int_{|\mathbf{x}-\mathbf{x}_c| \leq \rho} |\phi(\mathbf{x})|^2 d\mathbf{x} \leq \frac{C^*}{(\log |\log \rho|)^2}.$$

In particular, $\phi \notin H^1$, and $\phi \notin L^p$ for $p > 2$.

2. **At least linear rate:** *If the blowup rate satisfies (14.17), then*

$$\int_{|\mathbf{x}-\mathbf{x}_c| \leq \rho} |\phi(\mathbf{x})|^2 d\mathbf{x} \leq C^* H_G(\psi_0) \rho^2$$

and $\phi \in H^1$.

Thus, in a loglog collapse, the rate at which $\lim_{\mathbf{x} \rightarrow \mathbf{x}_c} |\phi(\mathbf{x})| = \infty$ is such that ϕ “barely makes it” into L^2 , but does not make it into L^p for $p > 2$. In contrast, in a linear collapse, $\phi(\mathbf{x})$ is in H^1 , and therefore, by the Gagliardo-Nirenberg inequality, is also in L^p . Therefore, although the NLS solution has a strong L^2 limit everywhere but at the singularity point \mathbf{x}_c , the roughness of the non-collapsing tail tells us whether a loglog collapse has taken place.

¹⁶ See (14.14), and also Figs. 14.8c, 14.12c, and 14.13c.

¹⁷ i.e., under the adiabatic approximation (Sect. 18.4).

14.6.3 Sufficient Condition for Loglog Collapse

Assertion 3 of Theorem 14.1 shows that if $H_G(\psi_0) < 0$ and $P_{\text{cr}} < \|\psi_0\|_2^2 < P_{\text{cr}} + \alpha^*$, then ψ blows up at the loglog rate. In Sect. 7.6 we saw that the condition $H_G(\psi_0) < 0$ is equivalent to the condition of a negative Hamiltonian in a tilted coordinate system where the solution has a zero linear momentum.

14.6.4 Stability of Loglog Blowup

Assertion 4 of Theorem 14.1 states that the set of initial conditions $\psi_0 \in \mathcal{B}_{\alpha^*}$ for which ψ collapses at the loglog rate, is open in H^1 . Therefore, solutions that collapse with the $\psi_{R^{(0)}}$ profile at the loglog rate are stable according to Definition 10.4.

14.6.5 Instability of Linear Collapse?

According to Theorem 14.1, the critical NLS can also admit singular solutions that collapse with a blowup rate which is at least linear. Examples of solutions that blowup at a linear rate and are in \mathcal{B}_{α^*} are the explicit blowup solution ψ_R^{explicit} and Bourgain-Wang blowup solutions with $\|\phi\|_2^2 \leq \alpha^*$. These solutions are unstable (Sect. 13.1.1). At present, it is not known whether there exist solutions whose blowup rate is faster than linear, and whether all solutions that collapse at a linear rate are unstable.

14.6.6 Spectral Property

Theorem 14.1 is stated for $1 \leq d \leq 5$. In fact, the only place where the dependence on dimension appears in the proof, is in the assumption that a certain spectral property is satisfied. Hence, Theorem 14.1 is valid in any dimension for which the spectral property holds.

The spectral property was proved by Merle and Raphaël [180] for $d = 1$, by utilizing the explicit expression for $R^{(0)}$, see Sect. 6.4.3. A numerically-aided proof was given by Fibich et al. [90] for $d = 2, 3, 4, 5$. In dimension $d = 6$, the spectral property does not hold. At present, the validity of Theorem 14.1 for $d \geq 6$ is open, and it is not known whether the nature of critical collapse changes at high dimensions.

14.6.7 Value of $\alpha^*(d)$

The exact value of $\alpha^* = \alpha^*(d)$ does not follow from the proof of Theorem 14.1. Therefore, in what follows we derive some basic estimates.

Lemma 14.2

$$\alpha^* \leq P_{\text{cr}}. \quad (14.19)$$

Proof We prove this bound by showing that there exist singular NLS solutions with power slightly above $2P_{\text{cr}}$ that collapse at two different points. Since Theorem 14.1 does not allow for collapse at two different points (Corollary 14.4), the result follows.

Let ψ be the solution of the critical NLS with the two-beam initial condition

$$\psi_0 = (1 + \epsilon)R^{(0)}(\mathbf{x} + \mathbf{x}_0) + (1 + \epsilon)R^{(0)}(\mathbf{x} - \mathbf{x}_0).$$

Let $0 < \epsilon \ll 1$ be fixed. Since $R^{(0)}$ decays exponentially, then for $|\mathbf{x}_0| \gg 1$,

$$\|\psi_0\|_2^2 \approx 2\|(1 + \epsilon)R^{(0)}\|_2^2 = 2(1 + \epsilon)^2 P_{\text{cr}}, \quad H(\psi_0) \approx 2H((1 + \epsilon)R^{(0)}) < 0,$$

see Lemma 7.13. Therefore, ψ becomes singular at a finite distance, and has power slightly above $2P_{\text{cr}}$.

To see that ψ collapses at two points, we provide the following informal argument. The NLS solution with $\psi_0 = (1 + \epsilon)R^{(0)}(\mathbf{x} \mp \mathbf{x}_0)$ collapses at $\mathbf{x} = \pm\mathbf{x}_0$. In addition, when $|\mathbf{x}_0|$ is sufficiently large, the interaction between the two beams is negligible. Therefore, ψ simultaneously blows up at two different points $\pm\mathbf{x}_0(\epsilon) \approx \pm\mathbf{x}_0$.¹⁸ □

The proof of Lemma 14.2 does not apply for radial initial conditions. In that case, we have the following estimate.

Lemma 14.3 *If $\psi_0 = \psi_0(r)$ is radial, then*

$$\alpha_{\text{radial}}^* < \|R^{(1)}\|_2^2 - \|R^{(0)}\|_2^2. \quad (14.20)$$

Proof Theorem 14.1 does not hold for the blowup solution $\psi_{R^{(1)}}^{\text{explicit}}(z, r)$ whose power is $\|R^{(1)}\|_2^2$, see Sect. 8.4.3, because this solution collapses with the $R^{(1)}$ profile and not with the $R^{(0)}$ profile. □

For example, when $d = 2$,

$$\frac{\|R^{(1)}\|_2^2}{\|R^{(0)}\|_2^2} \approx \frac{12.28}{1.86} \approx 6.6,$$

see Sect. 6.4. Therefore, $\alpha_{\text{radial}}^*(d = 2) < 5.6P_{\text{cr}}$.

Remark In Sect. 15.11 we shall see that *all* singular solutions of the two-dimensional critical NLS with vortex initial conditions $\psi_0 = e^{im\theta}A_0(r)$ do not collapse with the $\psi_{R^{(0)}}$ profile. This leads to the bound, see (15.69),

$$\alpha^*(d = 2) < P_{\text{cr}}(m = 1) - P_{\text{cr}} \approx 3.1P_{\text{cr}}.$$

¹⁸ See the symmetry argument in Sects. 13.4 and 27.5 for the dependence of the number of collapse points on the lateral separation distance $2\|\mathbf{x}_0\|_2$.

14.6.8 Universality of $\psi_{R^{(0)}}$ and of Loglog Collapse?

In Sect. 14.6.7 we saw that Theorem 14.1 does not apply for all initial conditions. Nevertheless, in all the numerical simulations carried out since the late 1970s and until 2005, it was always observed that blowup solutions of the critical NLS collapsed with the $\psi_{R^{(0)}}$ profile at a blowup rate slightly faster than a square root. Thus, for example, although Theorem 14.1 does not hold for the excited explicit blowup solutions $\psi_{R^{(n)}}^{\text{explicit}}$ with $n \geq 1$, numerical simulations suggest that when perturbed, these solutions collapse with the $\psi_{R^{(0)}}$ profile at the loglog law rate (Sect. 10.6.3). Collapse with the $\psi_{R^{(0)}}$ profile was also observed for clean Gaussian beams with $P = 38P_{\text{cr}}$, and for noisy Gaussian beams with $P = 15P_{\text{cr}}$ (Figs. 14.3 and 14.6, respectively). Therefore, it was widely believed that the results of Theorem 14.1 are valid for all stable singular solutions.

More recent numerical and asymptotic results by Fibich et al. 2005–2007 suggest that there may exist singular H^1 solutions of the critical NLS that collapse with a self-similar ring profile which is not given by $\psi_{R^{(0)}}$, and at a square root blowup rate without a loglog correction.¹⁹ Moreover, these solutions appear to be stable under radial perturbations. It is not clear, however, whether these solutions maintain the self-similar ring profile all the way up to the singularity. Therefore, *it is currently an open question whether all stable solutions of the critical radial NLS collapse with the $\psi_{R^{(0)}}$ profile at the loglog law rate.*²⁰ See Chap. 19 for more details.

Remark In Sect. 15.11 we shall see that *all* singular radial vortex solutions of the two-dimensional critical NLS *do not* collapse with the $\psi_{R^{(0)}}$ profile. These solutions are, however, azimuthally unstable (Sect. 15.11.1).

14.7 Critical Biharmonic NLS $(\psi_{R_B^{(0)}})$

Peak-type solutions of the critical BNLS

$$i\psi_z(z, \mathbf{x}) - \Delta^2\psi + |\psi|^{\frac{8}{d}}\psi = 0, \quad \psi(0, \mathbf{x}) = \psi_0(\mathbf{x}) \in H^2, \quad (14.21)$$

were studied analytically, asymptotically, and numerically by Fibich et al. [82], and by Baruch et al. [14]. These solutions undergo a quasi self-similar collapse, so that as $z \rightarrow Z_c$,

$$\psi(z, r) \sim \begin{cases} \psi_{R_B^{(0)}}(z, r), & \text{if } 0 \leq \frac{r}{L(z)} \leq \rho_c, \\ \psi_{\text{outer}}(z, r), & \text{if } \frac{r}{L(z)} \geq \rho_c. \end{cases} \quad (14.22)$$

¹⁹ In Chap. 11 we saw that the critical NLS admits the explicit ring-type solutions ψ_G^{explicit} that collapse with a self-similar profile which is different from $\psi_{R^{(0)}}$, at a square root blowup rate. These solutions, however, are not in H^1 .

²⁰ When the dimension d is an integer, these ring-type solutions are unstable under nonradial perturbations.

The asymptotic profile $\psi_{R_B^{(0)}}$ is given by

$$\psi_{R_B^{(0)}}(z, r) = \frac{1}{L^{\frac{d}{2}}(z)} R_B^{(0)} \left(\frac{r}{L(z)} \right) e^{i \int^z \frac{ds}{L^4(s)}}, \quad (14.23)$$

where $R_B^{(0)}(\rho)$ is the ground state of the solitary-wave equation

$$-R_B(\rho) - \Delta_\rho^2 R_B + |R_B|^{\frac{8}{d}} R_B = 0, \quad (14.24a)$$

$$R'_B(0) = R'''_B(0) = R_B(\infty) = R'_B(\infty) = 0. \quad (14.24b)$$

The blowup rate of these peak-type solutions is slightly faster than the quartic-root lower bound (Theorem 13.2), i.e.,

$$\lim_{z \rightarrow Z_c} \frac{L(z)}{(Z_c - z)^p} = \begin{cases} 0, & \text{if } p = \frac{1}{4}, \\ \infty, & \text{if } p > \frac{1}{4}. \end{cases}$$

Therefore, there is a striking analogy between peak-type collapse in the critical NLS and the critical BNLS. See [14, 82] for further details.

Remark The critical BNLS also admits shrinking-ring solutions that collapse with the ψ_{G_B} profile at a quartic-root blowup rate (Sect. 19.7).

Chapter 15

Vortex Solutions

In this chapter, we consider vortex solutions of the two-dimensional NLS

$$i\psi_z(z, x, y) + \Delta\psi + |\psi|^{2\sigma}\psi = 0, \quad \psi(0, x, y) = \psi_0(x, y) \in H^1. \quad (15.1)$$

These solutions are of the form

$$\psi(z, r, \theta) = A(z, r)e^{im\theta}, \quad m = \pm 1, \pm 2, \dots, \quad (15.2)$$

where $x = r \cos \theta$ and $y = r \sin \theta$.

It is relatively easy to produce optical vortices experimentally. As a result, vortices have been intensively studied in nonlinear optics, both theoretically and experimentally. Most of this research effort, however, has been on non-collapsing vortices. Vortex solutions have also been studied theoretically and experimentally in the context of Bose-Einstein condensates.

Singular vortex solutions were studied by Kruglov et al. [146, 147], and more recently by Fibich and Gavish [72]. Obviously, all the results previously derived for all singular solutions, remain valid for the special case of vortex solutions. Singular vortex solutions, however, have some unique characteristics. Thus, because of the phase singularity, the amplitude of vortex solutions has to vanish at $r = 0$. Therefore, *singular vortex solutions have the unique property that their amplitude is identically zero at the singularity point $\mathbf{x}_c = \mathbf{0}$* . As a result, singular vortex solutions of the supercritical NLS cannot collapse with the peak-type ψ_Q profile, and singular vortex solutions of the critical NLS cannot collapse with the peak-type $\psi_{R^{(0)}}$ profile. This, in turn, implies that vortex solutions of the critical NLS concentrate more power at the singularity than non-vortex ones.

Most of the theory of singular vortex solutions is a natural extension of that for non-vortex solutions. There is, however, one surprising difference between the two cases. In the non-vortex case, peak-type singular solutions that collapse with the $R^{(0)}$ profile in the critical case and with the admissible Q profile in the supercritical case, are stable. In the vortex case, however, numerical simulations suggest that the

analogous $R_m^{(0)}$ and Q_m profiles are radially unstable. Rather, it is the G_m and S_m profiles, the vortex analogs of the G and S ring profiles,¹ which are radially stable.²

Remark The asymptotic profiles of collapsing vortex solutions of the critical and supercritical NLS will be discussed in Chap. 20 and in Sect. 23.7.1, respectively.

15.1 Preliminary Results

When analyzing vortex solutions, it is useful to rewrite the two-dimensional NLS (15.1) in cylindrical coordinates

$$i\psi_z(z, r, \theta) + \psi_{rr} + \frac{1}{r}\psi_r + \frac{1}{r^2}\psi_{\theta\theta} + |\psi|^{2\sigma}\psi = 0, \quad \psi(0, r, \theta) = \psi_0(r, \theta). \quad (15.3)$$

Since $d = 2$, this equation is subcritical when $\sigma < 1$ and supercritical when $\sigma > 1$. In the critical case $\sigma = 1$, (15.3) reads

$$i\psi_z(z, r, \theta) + \psi_{rr} + \frac{1}{r}\psi_r + \frac{1}{r^2}\psi_{\theta\theta} + |\psi|^2\psi = 0, \quad \psi(0, r, \theta) = \psi_0(r, \theta). \quad (15.4)$$

In this chapter we mainly consider initial conditions that are a radial vortex with a winding number (topological charge) m , i.e.,

$$\psi_0(r, \theta) = A_0(r)e^{im\theta} \in H^1, \quad m = \pm 1, \pm 2, \dots \quad (15.5)$$

In this case, the solution remains a radial vortex with a winding number m :

Lemma 15.1 *Let ψ be a solution of (15.3) with the initial condition (15.5). Then*

$$\psi(z, r, \theta) = A(z, r)e^{im\theta}, \quad (15.6)$$

where $A(z, r)$ is the solution of

$$iA_z(z, r) + A_{rr} + \frac{1}{r}A_r - \frac{m^2}{r^2}A + |A|^{2\sigma}A = 0, \quad A(0, r) = A_0(r). \quad (15.7)$$

In particular, in the critical case, the equation for $A(z, r)$ reads

$$iA_z(z, r) + A_{rr} + \frac{1}{r}A_r - \frac{m^2}{r^2}A + |A|^2A = 0, \quad A(0, r) = A_0(r). \quad (15.8)$$

¹ The S profile is presented in Chap. 23.

² All singular vortex solutions are azimuthally unstable.

Proof Substituting $\psi = A(z, r)e^{im\theta}$ in (15.3) shows that A is a solution of (15.7). Since θ does not appear in (15.7), A is independent of θ . Since $\psi = A(z, r)e^{im\theta}$ is a solution of the NLS, it follows from uniqueness of NLS solutions that it is the unique solution. \square

Lemma 15.1 will be used extensively in this chapter. Note, however, that radial vortex solutions are unstable under azimuthal perturbations (Sects. 15.4.1, 15.8.3, and 15.9.2).

The following lemma lists some useful relations between the solution $\psi(z, r, \theta) = e^{im\theta}A(z, r)$ of (15.3), and the corresponding solution $A(z, r)$ of (15.7).

Lemma 15.2 *Let $\psi(z, r, \theta)$ be a solution of the NLS (15.3) with the radial vortex initial condition (15.5), and let $A(z, r)$ be the corresponding solution of (15.7). Then*

1. *Power conservation reads* $\|\psi\|_2^2 = \|A\|_2^2 \equiv \|A_0\|_2^2 = \|\psi_0\|_2^2$.

$$2. \quad \|\nabla\psi\|_2^2 = \left\| \frac{dA}{dr} \right\|_2^2 + m^2 \left\| \frac{A}{r} \right\|_2^2.$$

$$3. \quad \|\psi\|_{H^1}^2 = \|A\|_2^2 + \left\| \frac{dA}{dr} \right\|_2^2 + m^2 \left\| \frac{A}{r} \right\|_2^2.$$

4. *Hamiltonian conservation reads*

$$\begin{aligned} H(\psi) &:= \|\nabla\psi\|_2^2 - \frac{1}{\sigma+1} \|\psi\|_{2\sigma+2}^{2\sigma+2} \\ &= \left\| \frac{dA}{dr} \right\|_2^2 - \frac{1}{\sigma+1} \|A\|_{2\sigma+2}^{2\sigma+2} + m^2 \left\| \frac{A}{r} \right\|_2^2 \\ &\equiv \left\| \frac{dA_0}{dr} \right\|_2^2 - \frac{1}{\sigma+1} \|A_0\|_{2\sigma+2}^{2\sigma+2} + m^2 \left\| \frac{A_0}{r} \right\|_2^2 \\ &= \|\nabla\psi_0\|_2^2 - \frac{1}{\sigma+1} \|\psi_0\|_{2\sigma+2}^{2\sigma+2}. \end{aligned}$$

5. *If $0 \not\equiv \psi(z) \in H^1$, then $A(z) \in \mathcal{F}$, where*

$$\mathcal{F} = \left\{ f(r) : \mathbb{R}^+ \rightarrow \mathbb{C} \mid f \not\equiv 0, \quad f, \frac{f}{r}, f_r \in L_2(\mathbb{R}^2) \right\}. \quad (15.9)$$

6. *Conservation of angular momentum reads*

$$M(\psi) := \int \mathbf{x} \times \operatorname{Im}(\psi^* \nabla \psi) d\mathbf{x} = m \|A\|_2^2 \equiv m \|A_0\|_2^2 = m \|\psi_0\|_2^2,$$

where $\mathbf{x} = (x, y)$.

Proof Assertion 1 is immediate. To prove Assertion 2, we use the cylindrical coordinate system $(\hat{e}_r, \hat{e}_\theta)$. Since $\psi = A(z, r)e^{im\theta}$, then

$$\|\nabla\psi\|_2^2 = \|\psi_r \hat{e}_r + \frac{1}{r} \psi_\theta \hat{e}_\theta\|_2^2 = \|\psi_r\|_2^2 + \left\| \frac{1}{r} \psi_\theta \right\|_2^2 = \|A_r\|_2^2 + m^2 \left\| \frac{A}{r} \right\|_2^2.$$

Assertions 3–5 follow directly from Assertion 2. To prove Assertion 6, we note that

$$\begin{aligned} M &= \int r \hat{e}_r \times \operatorname{Im}(\psi^* \nabla \psi) d\mathbf{x} = \int r \hat{e}_r \times \operatorname{Im} \left(\psi^* \left(\psi_r \hat{e}_r + \frac{1}{r} \psi_\theta \hat{e}_\theta \right) \right) d\mathbf{x} \\ &= \int \operatorname{Im}(\psi^* \psi_\theta) d\mathbf{x} = m \|A\|_2^2, \end{aligned}$$

where in the last equality we used (15.6). \square

From the relative signs and magnitudes of the terms in (15.7) we have

Conclusion 15.1 *Vorticity works “with” diffraction and “against” nonlinearity. In addition, the magnitude of vorticity increases with m .*

This conclusion also follows from the relative signs and magnitudes of the terms of the NLS Hamiltonian

$$H(\psi = e^{im\theta} A(z, r)) = \|\nabla_r A\|_2^2 + m^2 \left\| \frac{A}{r} \right\|_2^2 - \frac{1}{\sigma+1} \|A\|_{2\sigma+2}^{2\sigma+2}.$$

We now show that the function $A(z, r)$ is continuous in r :

Lemma 15.3 *Let $A(z, r)$ be in \mathcal{F} . Then A is continuous in r .*

Proof Since $A(z) \in \mathcal{F}$,

$$\left\| \frac{dA}{dr} \right\|_2^2, \left\| \frac{A}{r} \right\|_2^2 < \infty. \quad (15.10)$$

Let $0 \leq r_1 < r_2 < \infty$. Then

$$A^2(r_2) - A^2(r_1) = \int_{r_1}^{r_2} 2A(s)A'(s) ds = \int_{r_1}^{r_2} 2 \frac{A(s)}{\sqrt{s}} (A'(s)\sqrt{s}) ds.$$

Therefore, since $2|ab| \leq a^2 + b^2$,

$$\begin{aligned} 0 \leq |A^2(r_2) - A^2(r_1)| &\leq \int_{r_1}^{r_2} \left[\frac{A^2(s)}{s} + (A'(s))^2 s \right] ds \\ &= \int_{r_1}^{r_2} \left[\frac{A^2(s)}{s^2} + (A'(s))^2 \right] s ds. \end{aligned}$$

Since the integrand in the last integral is in L^1 , see (15.10), this integral tends to zero as $r_2 \rightarrow r_1$. Therefore, $A(r)$ is continuous in r . \square

Since NLS vortex solutions $\psi = A(z, r)e^{im\theta}$ have a phase singularity at $r = 0$, they have to vanish at the origin:

Lemma 15.4 *Let $A(z, r)$ be a solution of (15.7) which is in \mathcal{F} for $0 \leq z < Z_c \leq \infty$. Then*

$$A(z, r = 0) = 0, \quad 0 \leq z < Z_c.$$

Proof Since A is continuous in r , see Lemma 15.3, and $\|\frac{A}{r}\|_2^2 < \infty$, see (15.9), the result follows. \square

Therefore, we also have

Lemma 15.5 *Let $\psi = e^{im\theta}A(z, r)$ be a vortex solution of the NLS (15.3) which is in H^1 for $0 \leq z < Z_c \leq \infty$. Then*

$$\psi(z, r = 0, \theta) = 0, \quad 0 \leq \theta \leq 2\pi, \quad 0 \leq z < Z_c. \quad (15.11)$$

Since ψ and A are in H^1 , they are only defined ‘‘almost everywhere’’. Hence, one can arbitrarily change their value at $r = 0$. Therefore, the correct interpretation of Lemmas 15.4 and 15.5 is that $\lim_{r \rightarrow 0} A(z, r) = \lim_{r \rightarrow 0} \psi(z, r, \theta) = 0$.

15.2 Solitary Vortex Profiles ($R_m^{(n)}$)

The two-dimensional NLS (15.3) admits the solitary vortex solutions

$$\psi_{\text{vortex}}^{\text{solitary}}(z, r, \theta) = R_m(r)e^{iz+im\theta},$$

where R_m is the solution of

$$R_m''(r) + \frac{1}{r}R_m' - \left(1 + \frac{m^2}{r^2}\right)R_m + |R_m|^{2\sigma}R_m = 0, \quad 0 < r < \infty. \quad (15.12)$$

The phase of $\psi_{\text{vortex}}^{\text{solitary}}$ is

$$\arg(\psi_{\text{vortex}}^{\text{solitary}}) = z + m\theta.$$

Therefore, $\psi_{\text{vortex}}^{\text{solitary}}$ rotates around the origin as it propagates. The rotation velocity can be found from the equation

$$\arg(\psi_{\text{vortex}}^{\text{solitary}}) \equiv \text{constant},$$

yielding³

$$\frac{d\theta}{dz} = -\frac{1}{m}. \quad (15.13)$$

Remark The stability of $\psi_{\text{vortex}}^{\text{solitary}}$ will be discussed in Sect. 15.8.

15.2.1 Pohozaev Identities

Let $R(x, y) := R_m(r)e^{im\theta}$. Then $\psi = e^{iz}R(x, y)$ is a solitary wave of the two-dimensional NLS (15.1), and R is a nonradial solution of

$$\Delta R(x, y) - R + |R|^{2\sigma} R = 0. \quad (15.14)$$

Therefore, all the results in Chap. 6 on nonradial solutions of (15.14) are applicable to $R = R_m(r)e^{im\theta}$. For example, from the Pohozaev identities for $R(x)$, see (6.7), we immediately have

Lemma 15.6 (Pohozaev identities for vortex solutions) *Let $R_m(r)$ be a solution of (15.12) in \mathcal{F} . Then*

$$\|R_m\|_2^2 = \frac{2}{2(\sigma+1)} \|R_m\|_{2\sigma+2}^{2\sigma+2}, \quad (15.15a)$$

$$\|\nabla_r R_m\|_2^2 + m^2 \left\| \frac{R_m}{r} \right\|_2^2 = \frac{\sigma}{\sigma+1} \|R_m\|_{2\sigma+2}^{2\sigma+2}. \quad (15.15b)$$

Proof This follows from substituting $R = e^{im\theta} R_m(r)$ and $d = 2$ in (6.7). \square

Lemma 15.7 *Let $R_m(r)$ be a solution of (15.12) in \mathcal{F} . Then*

$$H\left(e^{im\theta} R_m(r)\right) = \frac{2\sigma-2}{2\sigma+2} \|R_m\|_{2\sigma+2}^{2\sigma+2}. \quad (15.16)$$

Proof The proof is the same as in Corollary 7.14. \square

Corollary 15.1 *Let $R_m(r)$ be a nontrivial solution of (15.12) in \mathcal{F} . Then*

$$\begin{cases} H\left(e^{im\theta} R_m(r)\right) < 0, & \text{if } \sigma < 1, \\ H\left(e^{im\theta} R_m(r)\right) = 0, & \text{if } \sigma = 1, \\ H\left(e^{im\theta} R_m(r)\right) > 0, & \text{if } \sigma > 1. \end{cases}$$

Proof This follows directly from (15.16). \square

³ While (15.13) may seem to suggest that vortex solutions can only rotate at a discrete set of velocities, this is not the case. Indeed, by the dilation symmetry, the NLS (15.3) admits the solitary vortex solutions $\psi = R_m^\lambda(r)e^{i\lambda z+im\theta}$, where $R_m^\lambda(r) = \lambda^{\frac{1}{2\sigma}} R_m(\sqrt{\lambda}r)$, whose rotation velocity is $\frac{d\theta}{dz} = -\frac{\lambda}{m}$.

15.2.2 Infinite Number of Solutions

Iaia and Warchall proved that, as in the two-dimensional vortex-free case (Sect. 6.4.4), Eq. (15.12) has a countable number of solutions:

Lemma 15.8 ([130]) *For any integer m , any $\sigma > 0$, and any $n = 0, 1, 2, \dots$, there exists a solution $R_m^{(n)}(r)$ of (15.12) in \mathcal{F} that has exactly n zeros in $(0, \infty)$.*

Figure 15.1 shows solutions of (15.12) with $\sigma = 1$ and $m = 1$ that have $n = 0, 1, 2$, and 3 zeros.

Mizumachi proved that, as in the vortex-free case (Sect. 6.3), the R_m equation has a unique positive solution:

Lemma 15.9 ([189]) *For any integer m and any $\sigma > 0$, there exists a unique solution $R_m^{(0)}(r)$ of (15.12) in \mathcal{F} which is positive in $(0, \infty)$.*

As in the vortex-free case, uniqueness for $n \geq 1$ was observed numerically, but was not proved analytically.

15.2.3 Asymptotic Behavior for $r \ll 1$

We now consider the behavior of $R_m(r)$ near $r = 0$. Since $\psi_{\text{vortex}}^{\text{solitary}}(z, r = 0, \theta) = 0$, see Lemma 15.5, we have that $R_m(0) = 0$. We now show that $R_m(r) \sim cr^m$ for $r \ll 1$:

Lemma 15.10 *Let R_m be a nontrivial solution of (15.12). Then $R_m = r^m r_m(r)$, where $r_m(r)$ is the unique solution of*

$$r_m''(r) + \frac{2m+1}{r} r_m'(r) - r_m(r) + |r|^{2\sigma m} |r_m(r)|^{2\sigma} r_m(r) = 0, \quad (15.17a)$$

subject to

$$r_m(0) = r_{m,0} \neq 0, \quad r_m'(0) = 0. \quad (15.17b)$$

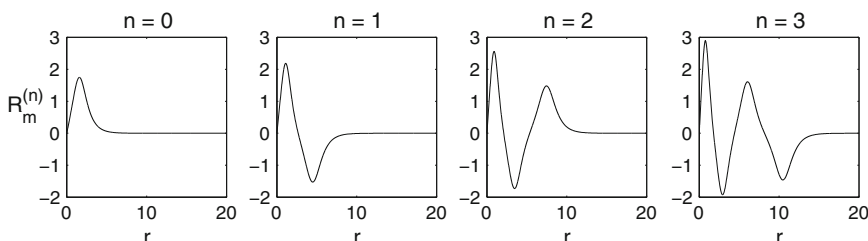


Fig. 15.1 Solutions of (15.12) with $\sigma = 1$ and $m = 1$, for $n = 0, 1, 2, 3$

Therefore,

$$\lim_{r \rightarrow 0} \frac{R_m(r)}{r^m} = r_{m,0} \neq 0.$$

Proof Let us look for a solution of (15.12) of the form $R_m = r^\ell r_m(r)$, where $r_m(0) \neq 0$. Since $R_m(0) = 0$, we have that $\ell > 0$. Substituting $R_m = r^\ell r_m(r)$ in (15.12) gives

$$r''_m(r) + \frac{2\ell + 1}{r} r'_m - r_m + \frac{\ell^2 - m^2}{r^2} r_m + |r|^{2\sigma\ell} |r_m|^{2\sigma} r_m = 0. \quad (15.18)$$

Since $2\sigma\ell > 0$, to leading order, (15.18) reduces to the linear equation

$$r''_m(r) + \frac{2\ell + 1}{r} r'_m - r_m + \frac{\ell^2 - m^2}{r^2} r_m = 0.$$

This equation has a regular-singular point at $r = 0$. Hence, it has two independent solutions of the form $r_m(r) = r^\alpha \sum_{i=0}^{\infty} a_i r^i$, where $a_0 \neq 0$, and α is a root of the indicial equation $\alpha(\alpha - 1) + (2\ell + 1)\alpha + \ell^2 - m^2 = 0$. Since $r_m(0) \neq 0$, $\alpha = 0$ and therefore $\ell_{1,2} = \pm m$. Since $\ell > 0$, then $\ell = m$. Substituting $\ell = m$ in (15.18) gives (15.17). Finally, substituting $r_m(r) = \sum_{i=0}^{\infty} a_i r^i$ in (15.17a) and letting $r \rightarrow 0$ shows that $a_1 = 0$. Therefore, $r'_m(0) = 0$. \square

Corollary 15.2 *For any $r_{m,0} \in \mathbb{C}$, the equation*

$$R''_m(r) + \frac{1}{r} R'_m - \left(1 + \frac{m^2}{r^2}\right) R_m + |R_m|^{2\sigma} R_m = 0, \quad 0 < r < \infty, \quad (15.19a)$$

subject to

$$r_{m,0} = \lim_{r \rightarrow 0} \frac{R_m(r)}{r^m}, \quad (15.19b)$$

has a unique solution.

Thus, unlike the vortex-free case, uniqueness of solutions of (15.19a) does not follow from imposing conditions on $R_m(0)$ and $R'_m(0)$, but rather on $\lim_{r \rightarrow 0} \frac{R_m(r)}{r^m}$.

Corollary 15.3 *Let*

$$r_{m,0}^{(n)} := \lim_{r \rightarrow 0} \frac{R_m^{(n)}(r)}{r^m}, \quad (15.20)$$

where $R_m^{(n)}$ is the n th-state solution of (15.12). Then the solution of (15.19) with $r_{m,0} = r_{m,0}^{(n)}$ is unique, and is given by $R_m^{(n)}$.

Remark It is easy to see that if $r_m(r)$ is a solution of (15.17), then so is $r_m(-r)$. Therefore, $r_m(r)$ is an even function. Since $R_m = r^m r_m(r)$, this implies that $R_m(r)$ is even when m is even, but odd when m is odd. This result may seem surprising, since R_m depends only on r . Note, however, that $R_m(r)$ does not have to be radial, because it is a component of the nonradial vortex profile $R_m(r)e^{im\theta}$.

Remark By l'Hospital's rule,

$$0 \neq r_{m,0} = \lim_{r \rightarrow 0} \frac{R_m(r)}{r^m} = \lim_{r \rightarrow 0} \frac{R'_m(r)}{mr^{m-1}} = \cdots = \frac{1}{m!} \frac{d^m}{dr^m} R_m(r=0).$$

Hence, for example, $R'_{m=1}(0) \neq 0$, showing again that $R_m(r)$ is odd when m is odd.

15.2.4 Ring Profile with an Exponential Tail

As in the vortex-free case, $R_m(r)$ decays exponentially as $r \rightarrow \infty$:

Lemma 15.11 *Let $R_m^{(n)}(r)$ be a solution of (15.12) in \mathcal{F} . Then*

$$R_m^{(n)}(r) \sim A_{m,n} r^{-\frac{1}{2}} e^{-r}, \quad r \gg 1,$$

where $A_{m,n}$ is a constant.

Proof The proof is the same as for Lemma 6.14. □

If R_m is a solution of (15.12), then so is $e^{i\alpha} R_m$. Therefore, without loss of generality, we can assume that $r_{m,0} > 0$. In this case, by Lemma 15.10, $R_m(r) \sim r_{m,0} r^m$ is monotonically increasing for $0 \leq r \ll 1$. In addition, by Lemma 15.11, $R_m(r)$ decays to zero as $r \rightarrow \infty$. Therefore, we have

Lemma 15.12 *For any n , $\{R_m^{(n)}(r)\}$ is a ring-type solution that attains its global maximum at some $r = r_{\max}^{(n)}$, where $0 < r_{\max}^{(n)} < \infty$.*

This is different from the vortex-free case where for any n , $R^{(n)} := R_{m=0}^{(n)}$ attains its global maximum at $r = 0$ (Corollary 6.16).

15.2.5 The Ground State ($R_m^{(0)}$)

Variational Characterization

The ground state $R_m^{(0)}$ is the nontrivial solution of the R_m equation (15.12) with the minimal power (Definition 5.11). In Lemma 5.8 we saw that in the two-dimensional

vortex-free case ($m = 0$), $R^{(0)}$ is the H^1 minimizer of

$$J[u] := \frac{\|\nabla u\|_2^{2\sigma} \|u\|_2^2}{\|u\|_{2\sigma+2}^{2\sigma+2}}.$$

We now look for a similar variational characterization of $R_m^{(0)}$.

Let $u = u(x_1, x_2) = f(r)e^{im\theta}$ be a vortex. Then

$$J[u] = J[f(r)e^{im\theta}] = J_m[f], \quad (15.21)$$

where

$$J_m[f(r)] := \frac{\left(\|\nabla_r f\|_2^2 + m^2 \|\frac{f}{r}\|_2^2\right)^\sigma \|f\|_2^2}{\|f\|_{2\sigma+2}^{2\sigma+2}}. \quad (15.22)$$

Following Fibich and Gavish [72], we now show that the ground state of (15.12) is the minimizer of J_m in \mathcal{F} . We first show that the minimum of J_m in \mathcal{F} is attained:

Lemma 15.13 ([72]) *Let $J_m[f]$ be given by (15.22), and let \mathcal{F} be defined by (15.9). Then $\inf_{f \in \mathcal{F}} J_m[f]$ is attained.*

Proof The proof is similar to the vortex-free case (Sect. 5.12.2). Recall that if $f \in \mathcal{F}$, then $f(r)e^{im\theta} \in H^1$ and $J_m[f] = J[f(r)e^{im\theta}]$. Therefore,

$$\inf_{f \in \mathcal{F}} J_m[f] = \inf_{f \in \mathcal{F}} J[f(r)e^{im\theta}] \geq \inf_{0 \neq u \in H^1} J[u] = \frac{1}{C_{\sigma,d=2}}.$$

From the definition of an infimum, there exists a sequence $f_n \in \mathcal{F}$ such that $J_m[f_n] \rightarrow \inf_{f \in \mathcal{F}} J_m[f]$. Let $f_n^{\lambda,\mu}(r) = \mu f_n(\lambda r)$. Since $J_m[f_n^{\lambda,\mu}] = J_m[f_n]$, we can choose λ_n and μ_n such that $J_m[f_n^{\lambda_n,\mu_n}] = J_m[f_n]$ and $\|f_n^{\lambda_n,\mu_n}\|_2 = \|\nabla f_n^{\lambda_n,\mu_n}\|_2 = 1$. This yields a sequence $f_n = f_n^{\lambda_n,\mu_n}$ such that $f_n \in \mathcal{F}$, $\|f_n\|_2 = \|\nabla f_n\|_2 = 1$, and

$$J_m[f_n] = \frac{\left(1 + m^2 \left\|\frac{f_n}{r}\right\|_2^2\right)^\sigma}{\|f_n\|_{2\sigma+2}^{2\sigma+2}} \rightarrow \inf_{f \in \mathcal{F}} J_m[f]. \quad (15.23a)$$

Since $\{f_n\}$ is bounded in H_{radial}^1 , it has a subsequence, also denoted by $\{f_n\}$, that converges weakly in H^1 to \tilde{f} . Therefore, f_n and ∇f_n converge weakly in L^2 to \tilde{f} and $\nabla \tilde{f}$, respectively. Hence,

$$\|\tilde{f}\|_2 \leq 1, \quad \|\nabla \tilde{f}\|_2 \leq 1. \quad (15.23b)$$

In addition, the Compactness Lemma 5.14 implies that $f_n \rightarrow \tilde{f}$ strongly in $L^{2\sigma+2}$, i.e.,

$$\lim_{n \rightarrow \infty} \frac{1}{\|f_n\|_{2\sigma+2}^{2\sigma+2}} = \frac{1}{\|\tilde{f}\|_{2\sigma+2}^{2\sigma+2}}. \quad (15.23c)$$

Therefore, by (15.23a), $\frac{f_n}{r}$ is bounded in L^2 .

We now show that $\frac{f_n}{r} \rightharpoonup \frac{\tilde{f}}{r}$ weakly in L^2 . Since $\{\frac{f_n}{r}\}$ is bounded in L^2 , it has a subsequence such that $\frac{f_n}{r} \rightharpoonup v$ weakly in L^2 . We claim that $v = \frac{\tilde{f}}{r}$. Indeed, for any test function $\varphi \in \tilde{\mathcal{F}} := \left\{ f \mid f, \frac{f}{r} \in L^2 \right\}$, we have that $\int \frac{f_n}{r} \varphi = \int f_n \frac{\varphi}{r}$. Hence,

$$\int v \varphi = \lim_{n \rightarrow \infty} \int \frac{f_n}{r} \varphi = \lim_{n \rightarrow \infty} \int f_n \frac{\varphi}{r} = \int \tilde{f} \frac{\varphi}{r}.$$

Since $\tilde{\mathcal{F}}$ is dense in L^2 , it follows that for any test function $\varphi \in L^2$,

$$\int v \varphi = \int \frac{\tilde{f}}{r} \varphi.$$

Hence, $v = \frac{\tilde{f}}{r}$ and $\frac{f_n}{r} \rightharpoonup \frac{\tilde{f}}{r}$.

The weak convergence of $\frac{f_n}{r}$ to $\frac{\tilde{f}}{r}$ in L^2 implies that (Lemma B.3)

$$\left\| \frac{\tilde{f}}{r} \right\|_2 \leq \liminf_{n \rightarrow \infty} \left\| \frac{f_n}{r} \right\|_2. \quad (15.23d)$$

By (15.23),

$$J_m[\tilde{f}] \leq \frac{\left(1 + m^2 \left\| \frac{\tilde{f}}{r} \right\|_2^2\right)^\sigma}{\|\tilde{f}\|_{2\sigma+2}^{2\sigma+2}} \leq \liminf_{n \rightarrow \infty} J_m[f_n] = \inf_{f \in \mathcal{F}} J_m[f].$$

Since $\tilde{f} \in \mathcal{F}$, the last inequality implies that $J_m[\tilde{f}] = \inf_{f \in \mathcal{F}} J_m[f]$. \square

Lemma 15.14 ([72]) *The minimum of J_m in \mathcal{F} is attained by $R_m^{(0)}$, the ground state of (15.12). In addition,*

$$\min_{f \in \mathcal{F}} J_m[f] = \frac{\sigma^\sigma}{1 + \sigma} \|R_m^{(0)}\|_2^{2\sigma}. \quad (15.24)$$

Proof As in the vortex-free case (Sect. 5.12), the extremals of J_m are, up to scaling, solutions of (15.12), see [72, Appendix E]. Therefore, the extremals are given

Table 15.1 Comparison of $R^{(0)}$ and $R_m^{(0)}$

	$R^{(0)}$	$R_m^{(0)}$
Minimizer of	J	J_m
Profile	peak-type	ring-type
Monotonicity	monotonically decreasing	non-monotone
Positive in	$[0, \infty)$	$(0, \infty)$
Value at $r = 0$	> 1	0
$r = 0$ is a global	maximum	minimum

by $\{R_m^{(n)}\}_{n=0}^\infty$. In addition, as in the two-dimensional vortex-free case, see (5.38),

$$J_m[R_m^{(n)}] = \frac{\sigma^\sigma}{\sigma + 1} \|R_m^{(n)}\|_2^{2\sigma}. \quad (15.25)$$

Therefore, the ground state of (15.12) is a minimizer of $J_m[f]$. Hence, by Lemma 15.16, the ground state is given by $R_m^{(0)}$. \square

Lemma 15.15 *The minimizer of J_m in \mathcal{F} is positive in $(0, \infty)$.*

Proof Without loss of generality, the minimizer is real (Lemma 5.7). Let $v(r)$ be a minimizer of J_m . Then $|v(r)|$ is also a minimizer, see (5.47). Hence, $|v(r)|$ is a non-negative solution of (15.12). Assume, by negation, that $v(r)$ vanishes at $0 < r_a < \infty$. Then at $r = r_a$ we have that $|v| = |v'| = 0$. Therefore, $|v| \equiv 0$, which is a contradiction. \square

Lemma 15.16 *The ground state of (15.12) is unique, and is given by the positive vortex solution $R_m^{(0)}$.*

Proof By Lemma 15.14, the ground state of (15.12) is a minimizer of J_m . By Lemma 15.15, any minimizer of J_m has to be positive. Since $R_m^{(0)}$ is the unique positive solution of (15.12), see Lemma 15.9, the result follows. \square

The similarities and differences between $R^{(0)}$ and $R_m^{(0)}$ are summarized in Table 15.1.

Analytic Approximation

In order to derive an analytic approximation for $R_m^{(0)}$, we begin with an informal argument. Let $r_{\max} := \arg \max_r |R_m^{(0)}(r)|$ denote the point where $R_m^{(0)}(r)$ attains its global maximum. Assume that $r_{\max} \gg 1$.⁴ Then for $r - r_{\max} = O(1)$,

$$\frac{1}{r} R'_m \ll R''_m(r), \quad \frac{m^2}{r^2} R_m \sim \frac{m^2}{r_{\max}^2} R_m.$$

⁴ This assumption will be justified in Lemma 15.17.

Therefore, Eq.(15.12) can be approximated by

$$R_m''(r) - \lambda^2 R_m + |R_m|^{2\sigma} R_m = 0, \quad \lambda = \sqrt{1 + \frac{m^2}{r_{\max}^2}}.$$

The positive solution of this equation that attains its maximum at r_{\max} is

$$R_\lambda(r - r_{\max}) = \lambda^{\frac{1}{\sigma}} R(\lambda(r - r_{\max})),$$

where $R(x)$ is the positive solution of the one-dimensional solitary-wave equation

$$R''(x) - R + |R|^{2\sigma} R = 0, \quad -\infty < x < \infty,$$

that attains its maximum at $x = 0$. By Lemma 6.15, $R = (1 + \sigma)^{\frac{1}{2\sigma}} \operatorname{sech}^{\frac{1}{\sigma}}(\sigma x)$. Therefore, to leading order, $R_m^{(0)}(r)$ can be approximated by

$$R_\lambda(r - r_{\max}) = \lambda^{\frac{1}{\sigma}} (1 + \sigma)^{\frac{1}{2\sigma}} \operatorname{sech}^{\frac{1}{\sigma}}(\lambda\sigma(r - r_{\max})), \quad \lambda = \sqrt{1 + \frac{m^2}{r_{\max}^2}}. \quad (15.26a)$$

Mizumachi [190] showed that the balance of the next-order terms gives

$$r_{\max} \sim \sqrt{\frac{2}{\sigma}} m. \quad (15.26b)$$

Therefore, $\lambda \sim \sqrt{1 + \frac{\sigma}{2}}$.

Relation (15.26b) shows that the ring radius increases with m and decreases with σ . Indeed, in Conclusion 15.1 we saw that vorticity works “with” diffraction and “against” nonlinearity. Therefore, as m increases and/or σ decreases, nonlinearity becomes weaker compared with the linear terms, and therefore the ring radius increases.

Mizumachi proved rigorously that $R_m^{(0)} \sim R_\lambda(r - r_{\max})$ as $m \rightarrow \infty$:

Lemma 15.17 ([190]) *Let $R_m^{(0)}(r)$ be the positive solution of (15.12), and let R_λ and r_{\max} be given by (15.26). Then for $m \gg 1$,*

$$\|R_m^{(0)}(r) - R_\lambda(r - r_{\max})\|_{H_{\text{radial}}^2} = O(m^{-\frac{1}{2}})$$

and

$$\|R_m^{(0)}(r) - R_\lambda(r - r_{\max})\|_\infty = O(m^{-1}).$$

15.2.6 Critical Case

In the critical case $\sigma = 1$, Eq.(15.12) reads

$$R_m''(r) + \frac{1}{r} R'_m - \left(1 + \frac{m^2}{r^2}\right) R_m + |R_m|^2 R_m = 0, \quad 0 < r < \infty. \quad (15.27)$$

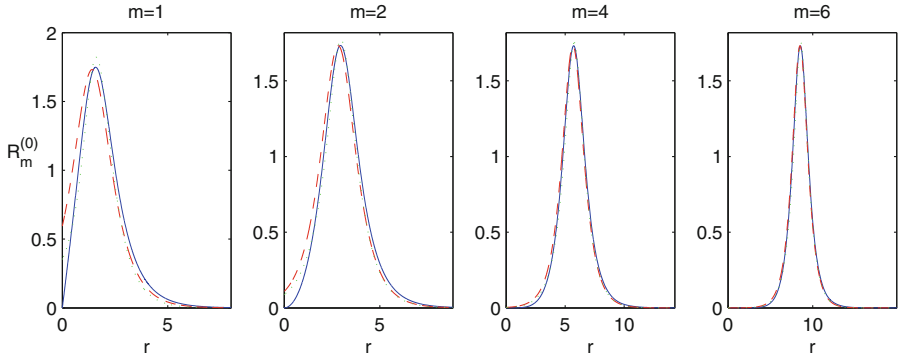


Fig. 15.2 The ground state $R_m^{(0)}(r)$ of (15.27) for $m = 1, 2, 4$, and 6 (solid). The dashed curve is approximation (15.28). From [72]

As noted, this equation has a countable number of solutions $\{R_m^{(n)}\}_{n=0}^{\infty}$ in \mathcal{F} . The solutions for $n = 0, 1, 2$, and 3 are shown in Fig. 15.1.

In Corollary 15.1 we saw that in the critical case, $H(R_m(r)e^{im\theta}) = 0$. More generally, we have

Lemma 15.18 *Let $R_m^{(n)}$ be a nontrivial solution of (15.27) and $c > 0$. Then*

$$\begin{cases} H(cR_m^{(n)}(r)e^{im\theta}) > 0, & \text{if } 0 < c < 1, \\ H(cR_m^{(n)}(r)e^{im\theta}) = 0, & \text{if } c = 1, \\ H(cR_m^{(n)}(r)e^{im\theta}) < 0, & \text{if } c > 1. \end{cases}$$

Proof The proof is the same as in the vortex-free case (Lemma 7.12). □

By Lemma 15.17, the ground state of (15.27) can be approximated by

$$R_m^{(0)}(r) \sim \sqrt{3} \operatorname{sech} \left(\frac{r - r_{\max}}{\sqrt{2/3}} \right), \quad r_{\max} = \sqrt{2}m. \quad (15.28)$$

Although approximation (15.28) was derived for $m \gg 1$, it is reasonably accurate for $m = 1$, and its accuracy quickly improves as m increases, see Fig. 15.2.

15.3 Optimal Constant $C_{\sigma,2}(m)$

In Lemma 5.10 we saw that the optimal constant $C_{\sigma,2} = C_{\sigma,d=2}$ in the Gagliardo-Nirenberg inequality

$$\|f\|_{2\sigma+2}^{2\sigma+2} \leq C_{\sigma,2} \|\nabla f\|_2^{2\sigma} \|f\|_2^2, \quad f(x_1, x_2) \in H^1(\mathbb{R}^2), \quad (15.29)$$

is

$$C_{\sigma,2} = \frac{1+\sigma}{\sigma^\sigma} \frac{1}{\|R^{(0)}\|_2^{2\sigma}},$$

where $R^{(0)}$ is the ground state of

$$R''(r) + \frac{1}{r} R' - R + |R|^{2\sigma} R = 0, \quad (15.30)$$

i.e., of Eq.(15.12) with $m = 0$. In [72], Fibich and Gavish extended this result to the special case where f is a radial vortex:

Lemma 15.19 ([72]) *The optimal constant $C_{\sigma,2}(m)$ in the Gagliardo-Nirenberg inequality*

$$\|f_m\|_{2\sigma+2}^{2\sigma+2} \leq C_{\sigma,2}(m) \|\nabla f_m\|_2^{2\sigma} \|f_m\|_2^2, \quad (15.31a)$$

where

$$f_m(r, \theta) = f(r)e^{im\theta} \in H^1, \quad (15.31b)$$

is

$$C_{\sigma,2}(m) = \frac{1+\sigma}{\sigma^\sigma} \frac{1}{\|R_m^{(0)}\|_2^{2\sigma}}, \quad (15.32)$$

where $R_m^{(0)}$ is the ground state of (15.12).

Proof The optimal constant $C_{\sigma,2}(m)$ is given by

$$\frac{1}{C_{\sigma,2}(m)} = \inf_{0 \neq f_m \in H^1} J[f_m]. \quad (15.33)$$

Since $J[f_m] = J_m[f]$, see (15.21), we have that $C_{\sigma,2}(m) = 1/\inf_{f \in \mathcal{F}} J_m[f]$, where \mathcal{F} is defined in (15.9). In Lemma 15.13 we proved that $\inf_{f \in \mathcal{F}} J_m[f]$ is attained. Therefore, $C_{\sigma,2}(m) = 1/\min_{f \in \mathcal{F}} J_m[f]$. Since $\min_{f \in \mathcal{F}} J_m[f] = \frac{\sigma^\sigma}{1+\sigma} \|R_m^{(0)}\|_2^{2\sigma}$, see Lemma 15.14, the result follows. \square

15.4 Critical Power for Vortex Collapse $P_{\text{cr}}(m)$

In Theorem 5.11 we saw that the critical power for collapse in the two-dimensional critical NLS is $P_{\text{cr}} = \|R^{(0)}\|_2^2$, where $R^{(0)}$ is the ground state of (15.30). This result is valid for any $\psi_0 \in H^1$, vortex or non-vortex. In the case of vortex solutions, Fibich and Gavish proved the stronger result that the critical power for collapse is $P_{\text{cr}}(m) = \|R_m^{(0)}\|_2^2$:

Theorem 15.1 ([71, 72]) Let ψ be a solution of the critical NLS (15.4) with $\psi_0 = e^{im\theta} A_0(r) \in H^1$. Then a necessary condition for ψ to becomes singular is $\|\psi_0\|_2^2 \geq P_{\text{cr}}(m)$, where

$$P_{\text{cr}}(m) = \|R_m^{(0)}\|_2^2 \quad (15.34)$$

is the power of the ground state of (15.27).

Proof As in the proof of Theorem 5.5, from conservation of the Hamiltonian and the power, and from the Gagliardo-Nirenberg inequality (15.31), it follows that for $\psi = A(z, r)e^{im\theta} \in H^1$,

$$\|\nabla \psi\|_2^2 \leq H(0) + \kappa \|\nabla \psi\|_2^2, \quad \kappa = \frac{C_{1,2}(m)}{2} \|\psi_0\|_2^2. \quad (15.35)$$

Therefore, a sufficient condition for global existence (i.e., for $\|\nabla \psi\|_2$ to be bounded) is $\kappa < 1$. Hence

$$P_{\text{cr}}(m) = \frac{2}{C_{1,2}(m)}. \quad (15.36)$$

Finally, by (15.32) with $\sigma = 1$, $P_{\text{cr}}(m) = \|R_m^{(0)}\|_2^2$. \square

Corollary 15.4 A necessary condition for the solution A of (15.8) to become singular is $\|A_0\|_2^2 \geq P_{\text{cr}}(m)$.

The result of Theorem 15.1 is sharp, in the sense that all vortex solutions $\psi = A(z, r)e^{im\theta}$ whose power is strictly below $P_{\text{cr}}(m)$ do not become singular, and there exists a singular vortex solution, the explicit singular vortex solution $\psi_{R_m^{(0)}}^{\text{explicit}}$, see Sect. 15.5.1, whose power is exactly $P_{\text{cr}}(m)$.

Corollary 15.5 Let $\sigma = 1$ and $f_m = e^{im\theta} f(r) \in H^1$. If $H(f_m) \leq 0$ and $f_m \not\equiv 0$, then $\|f_m\|_2^2 = \|f\|_2^2 \geq P_{\text{cr}}(m)$.

Proof From Lemma 15.19 with $\sigma = 1$ and (15.34) we have that $\left(1 - \frac{\|f_m\|_2^2}{P_{\text{cr}}(m)}\right) \|\nabla f_m\|_2^2 \leq H(f_m)$. Hence, the result follows. \square

As in the vortex-free case (Lemma 6.9), the critical power $P_{\text{cr}}(m)$ is also the minimal power of vortex profiles with a non-positive Hamiltonian:

Corollary 15.6 Let $\sigma = 1$. Then

$$P_{\text{cr}}(m) = \min_{0 \neq f_m = f(r)e^{im\theta} \in H^1} \left\{ \|f_m\|_2^2 \mid H(f_m) \leq 0 \right\}. \quad (15.37)$$

Proof By Corollary 15.5, if $f_m \not\equiv 0$ and $H(f_m) \leq 0$, then $\|f_m\|_2^2 \geq P_{\text{cr}}(m)$. Therefore,

$$P_{\text{cr}}(m) \leq \inf_{0 \neq f_m = f(r)e^{im\theta} \in H^1} \left\{ \|f_m\|_2^2 \mid H(f_m) \leq 0 \right\}.$$

Since, in addition, $H(R_m^{(0)} e^{im\theta}) = 0$, see Corollary 15.1, and $\|R_m^{(0)} e^{im\theta}\|_2^2 = P_{\text{cr}}(m)$, see Theorem 15.1, the result follows. \square

We now show that the vortex critical power increases with m :

Corollary 15.7 ([72]) $P_{\text{cr}}(m)$ is monotonically increasing in m , i.e.,

$$\underbrace{P_{\text{cr}}(m=0)}_{=P_{\text{cr}}} < P_{\text{cr}}(m=1) < P_{\text{cr}}(m=2) < \dots$$

Proof By (15.24) and (15.36),

$$P_{\text{cr}}(m) = \|R_m^{(0)}\|_2^2 = 2 \min_{f \in \mathcal{F}} J_m[f].$$

For any given f , the functional $J_m[f]$ is monotonically increasing in m , see (15.22). Hence, so is its minimum $P_{\text{cr}}(m)$. \square

This result can be motivated as follows. In Conclusion 15.1 we saw that vorticity works “with” diffraction and “against” nonlinearity. Therefore, as m increases, more power is required for the nonlinearity to overcome the combined effects of diffraction and vorticity.

Let

$$P_{\text{cr}}(m) = 2\pi P_{\text{cr}}^{\text{radial}}(m), \quad P_{\text{cr}}^{\text{radial}}(m) := \int_0^\infty |R_m^{(0)}|^2 r dr.$$

The numerically-calculated values of $P_{\text{cr}}^{\text{radial}}(m)$ in Table 15.2 confirm that $P_{\text{cr}}(m)$ is monotonically increasing in m . We can also estimate $P_{\text{cr}}^{\text{radial}}(m)$ analytically by using approximation (15.28) for $m \gg 1$:

$$\begin{aligned} P_{\text{cr}}^{\text{radial}}(m) &= \int_0^\infty |R_m^{(0)}|^2 r dr \approx 3 \int_0^\infty \operatorname{sech}^2 \left(\frac{r - \sqrt{2}m}{\sqrt{2/3}} \right) r dr \\ &= 2 \log(e^{2\sqrt{3}m} + 1) \approx 4\sqrt{3}m. \end{aligned}$$

Figure 15.3 shows that $P_{\text{cr}}^{\text{radial}}(m)$ is well approximated by $4\sqrt{3}m$, and that the approximation improves as m increases: For $m = 2$ the approximation error is already less than 3%, and for $m \geq 5$ the error is below 0.4%.

Table 15.2 Numerical values of $P_{\text{cr}}^{\text{radial}}(m) = \int_0^\infty |R_m^{(0)}|^2 r dr$. From [72]

m	0	1	2	3	4	5
$P_{\text{cr}}^{\text{radial}}(m)$	1.86	7.68	14.26	21.05	27.90	34.78
m		6	7	8	9	10
$P_{\text{cr}}^{\text{radial}}(m)$		41.67	48.57	55.48	62.45	69.14

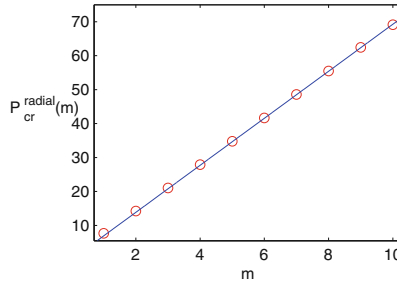


Fig. 15.3 $P_{\text{cr}}^{\text{radial}}(m)$ for $m = 0, 1, \dots, 10$ (\circ). The solid line is $4\sqrt{3}m$. From [72]

Remark See Sect. 24.7 for additional results on the critical power and threshold power for collapse of vortex solutions.

15.4.1 Nonradial Vortex Initial Conditions

In Theorem 15.1 we saw that the critical power for collapse of vortex solutions is $P_{\text{cr}}(m)$. This result was proved, however, only for radial vortex initial conditions $\psi_0 = A_0(r)e^{im\theta}$. A natural question is, therefore, whether this result also holds for nonradial vortex initial conditions. In the non-vortex case, the critical power for collapse⁵ is P_{cr} for both radial and nonradial initial conditions. To show that this is not the case with vortex initial conditions, in Lemma 15.20 we prove that there exist blowup solutions of the critical NLS with nonradial vortex initial conditions and power slightly above P_{cr} , hence significantly below $P_{\text{cr}}(m)$. This shows, in particular, that Theorem 15.1 cannot be extended to nonradial vortex initial conditions.

Lemma 15.20 ([72]) *Let $\epsilon > 0$ and $P_{\text{cr}} = \|R^{(0)}\|_2^2$. Then there exists $\psi_0(x, y) = A_0(x, y)e^{im\theta} \in H^1$, where $A_0(x, y)$ is a real function and $\|\psi_0\|_2^2 \leq P_{\text{cr}} + \epsilon$, such that the solution of the critical NLS (15.4) with the initial condition ψ_0 becomes singular.*

Proof The idea of the proof is as follows. We take a non-vortex radial initial condition with power slightly above P_{cr} that leads to collapse, center it sufficiently far away from the origin, multiply it by $e^{im\theta}$, and then show that it becomes singular.

Let $\mathbf{x} = (x, y)$, and

$$\psi_0(x, y) = v(|\mathbf{x}|)(1 + \epsilon)\lambda R^{(0)}(\lambda(\mathbf{x} - \mathbf{x}_0))e^{im\theta},$$

where $\mathbf{x}_0 = (r_0 \cos \theta_0, r_0 \sin \theta_0)$, $r_0 > 1$, $R^{(0)}$ is the ground state of (15.30), and $v(r)$ is a smooth radial function that behaves like r^m near $r = 0$, is monotonically

⁵ i.e., the optimal lower bound for the threshold power P_{th} for collapse.

increasing in r , and is identically one outside the unit circle.⁶ Since $R^{(0)}(r)$ decays exponentially in r ,

$$\psi_0 \sim (1 + \epsilon)\lambda R^{(0)}(\lambda(\mathbf{x} - \mathbf{x}_0))e^{im\theta_0}, \quad \lambda \gg 1.$$

Therefore, $\lim_{\lambda \rightarrow \infty} \|\psi_0\|_2^2 = (1 + \epsilon)^2 \|R^{(0)}\|_2^2$ and

$$H(\psi_0) \sim \lambda H\left((1 + \epsilon)R^{(0)}\right), \quad \lambda \gg 1.$$

Since $H\left((1 + \epsilon)R^{(0)}\right) < 0$, see Lemma 7.12, then $H(\psi_0) < 0$ for $\lambda \gg 1$. Hence, the solution becomes singular (Theorem 7.2). \square

To illustrate the proof of Lemma 15.20, we solve the critical NLS (15.4) with the off-center vortex initial condition

$$\psi_0 = 2.8e^{-(x-3)^2-(y-3)^2} \tanh^2(4x^2 + 4y^2)e^{im\theta}, \quad m = 2. \quad (15.38)$$

The power of ψ_0 is $\|\psi_0\|_2^2 \approx 1.05P_{\text{cr}}$, i.e., slightly above P_{cr} . This power is sufficient for the vortex-free Gaussian initial condition $\psi_0 = 2.8e^{-(x-3)^2-(y-3)^2}$ to become singular, see Sect. 24.3. In accordance with the proof of Lemma 15.20, the off-center vortex initial condition (15.38) also becomes singular, see Fig. 15.4, even though its power is well below $P_{\text{cr}}(m = 2) \approx 7.7P_{\text{cr}}$. Vorticity has no effect on the collapse characteristics, i.e., the solution collapses with the $\psi_{R^{(0)}}$ profile. In fact, the only noticeable effect of vorticity is that the collapsing solution moves along the tangent line to the circle $x^2 + y^2 = 18$, see Fig. 15.5.

Exercise 15.1 Explain why the solution moves along the tangent line to the circle, rather than rotate along the circle.

The difference between Theorem 15.1 and Lemma 15.20 has to do with the location of the collapse point \mathbf{x}_c . In Theorem 15.1, radial symmetry dictates that the solution collapses at the origin (Lemma 15.33). Since the phase singularity “forces” the solution to behave as r^m near the origin (Lemma 15.10), it cannot collapse with the $R^{(0)}$ profile, but only with the $R_m^{(0)}$ profile. As a result, the critical power for collapse is $P_{\text{cr}}(m)$. When, however, the collapse point is not at $r = 0$, vorticity does not prevent the solution from collapsing with the $R^{(0)}$ profile. This is because in the vicinity of the collapse point $\mathbf{x}_c = r_c e^{im\theta_c}$, vorticity only “adds” a constant phase term $e^{im\theta_c}$. Therefore, the critical power for collapse at any $\mathbf{x}_c \neq 0$ is P_{cr} .

Remark The dependence of the critical power on the location of the collapse point (i.e., whether it coincides with the phase singularity) is a manifestation of the general

⁶ The role of $v(r)$ is to modify the initial condition near the phase singularity at $r = 0$, so that it will be in H^1 , see Lemmas 15.5 and 15.10.

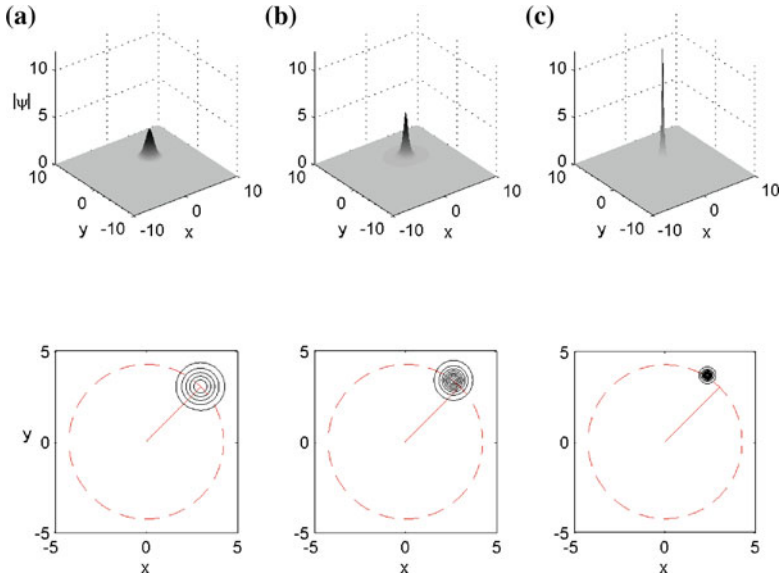


Fig. 15.4 Solution of the NLS (15.4) with the initial condition (15.38) at **a** $z = 0$. **b** $z = 0.54$. **c** $z = 1$. The *dashed curve* is the circle $x^2 + y^2 = 18$. The *solid line* connects the origin with the center of the initial condition at $(3, 3)$. From [72]

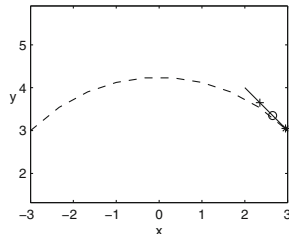


Fig. 15.5 Location of the center-of-mass of the solution from Fig. 15.4 at $z = 0$ (*), $z = 0.54$ (o), and $z = 1$ (+). The *solid line* is the tangent at $(3,3)$ to the *circle* $x^2 + y^2 = 18$ (*dashed line*)

principle that the critical power only depends on local properties near the collapse point \mathbf{x}_c (Sect. 24.10).

The NLS also admits nonradial vortex blowup solutions with power below $P_{\text{cr}}(m)$, whose center of mass is at $r = 0$. To see that, in Fig. 15.6 we solve the critical NLS (15.4) with

$$\psi_0 = 0.98 R_m^{(0)} \left(\sqrt{x^2 + (1.01y)^2} \right) e^{im\theta}, \quad m = 2. \quad (15.39)$$

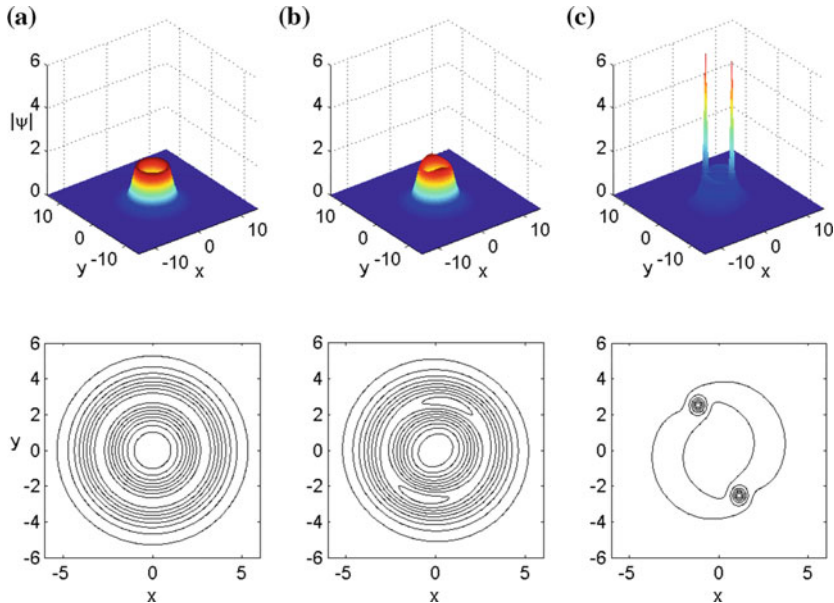


Fig. 15.6 Solution of the critical NLS (15.4) with the slightly elliptic initial condition (15.39) at **a** $z = 0$. **b** $z = 2.19$. **c** $z = 3.45$. From [72]

This initial condition is $\psi_{\text{vortex}}^{\text{solitary}}(z = 0) = e^{im\theta} R_m^{(0)}(r)$, perturbed to be slightly elliptic and to have $\|\psi_0\|_2^2 \approx 0.95P_{\text{cr}}(m = 2) < P_{\text{cr}}(m = 2)$. Because solitary vortex solutions are azimuthally unstable (Sect. 15.8.3), the solution breaks into two filaments, which subsequently undergo collapse. Since the centers of these filaments are not at $r = 0$, each of them only requires the vortex-free critical power P_{cr} in order to collapse.⁷ Therefore, since $\|\psi_0\|_2^2 > 2P_{\text{cr}}$, the solution has sufficient power to collapse at two points.

Remark In the vortex-free critical case, an elliptic initial condition requires more power to collapse than the corresponding radial initial condition (Sect. 24.6). In contrast, elliptic vortex initial conditions require less power to collapse than radial ones. This is because in the vortex-free case, the peak-type $R^{(0)}$ profile remains an attractor under azimuthal perturbations. Since the collapsing core of an elliptic beam loses more power as it evolves into the radial $R^{(0)}$ profile than the corresponding radial beam, it needs more input power in order to collapse. In contrast, in the vortex case, the ring-type $R_m^{(0)}$ profile is unstable under azimuthal perturbations. These perturbations change the asymptotic blowup profile from $R_m^{(0)}$ to $R^{(0)}$, thereby reducing the critical power for collapse.

⁷ When m is even, the symmetry-breaking induced by input-beam ellipticity preserves the symmetries $x \rightarrow -x$ and $y \rightarrow -y$. Therefore, the number of elliptically-induced off-center filaments is even (Lemma 25.1). Hence, elliptic vortex input beams with an even m require at least $2P_{\text{cr}}$ in order to collapse.

15.5 Explicit Blowup Solutions (Critical NLS)

In the vortex-free case the critical NLS admits two explicit blowup solutions:

1. The peak-type solution $\psi_{R^{(n)}}^{\text{explicit}}$, which is in H^1 and has a linear blowup rate (Chap. 10).
2. The ring-type solution ψ_G^{explicit} , which is in $L^{2\sigma+2}$ but not in H^1 , and has a square-root blowup rate (Chap. 11).

These solutions have the following vortex analogs [72]:

1. The explicit solution $\psi_{R_m^{(n)}}^{\text{explicit}}$, which is in H^1 and has a linear blowup rate. This solution is discussed in Sect. 15.5.1.
2. The explicit solution $\psi_{G_m}^{\text{explicit}}$, which is in $L^{2\sigma+2}$ but not in H^1 , and has a square-root blowup rate. This solution is discussed in Sect. 15.6.

Unlike the vortex-free case, both $\psi_{R_m^{(n)}}^{\text{explicit}}$ and $\psi_{G_m}^{\text{explicit}}$ are ring-type, since they vanish at the phase-singularity point $r = 0$.

Remark Stability of $\psi_{R_m^{(n)}}^{\text{explicit}}$ and $\psi_{G_m}^{\text{explicit}}$ will be discussed in Sect. 15.9.

15.5.1 The Explicit Vortex Blowup Solution $\psi_{R_m^{(n)}}^{\text{explicit}}$

In Sect. 8.4.3 we constructed the explicit singular solution $\psi_{R^{(n)}}^{\text{explicit}}$ of the critical NLS, by applying the lens transformation to $\psi^{\text{solitary},(n)} = e^{iz} R^{(n)}(r)$. We now use the same approach to construct the explicit singular vortex solution $\psi_{R_m^{(n)}}^{\text{explicit}}$.

In the case of the two-dimensional critical NLS in cylindrical coordinates, see (15.4), the lens transformation reads as follows. Let $\psi(z, r, \theta)$ be a solution of (15.4), and let

$$\tilde{\psi}(z, r, \theta) = \frac{1}{L(z)} \psi(\zeta, \rho, \theta) e^{i \frac{L_z}{L} \frac{r^2}{4}}, \quad (15.40a)$$

where

$$\rho = \frac{r}{L(z)}, \quad \zeta = \int_0^z \frac{ds}{L^2(s)}, \quad (15.40b)$$

and $L(z)$ is a linear function of z . Then $\tilde{\psi}$ is also a solution of (15.4).⁸ Applying the lens transformation (15.40) with $L(z) = Z_c - z$ to $\psi_{\text{vortex}}^{\text{solitary},(n)} = R_m^{(n)}(r) e^{iz+im\theta}$ leads to

⁸ Thus, the angle θ is unaffected by the lens transformation.

Lemma 15.21 *Let*

$$\psi_{R_m^{(n)}}^{\text{explicit}}(z, r, \theta) = \frac{1}{L(z)} R_m^{(n)}(\rho) e^{i\zeta(z) + im\theta + i\frac{L_z}{L} \frac{r^2}{4}}, \quad (15.41a)$$

where

$$L(z) = Z_c - z, \quad \rho = \frac{r}{L(z)}, \quad \zeta(z) = \int_0^z \frac{ds}{L^2(s)} = \frac{z/Z_c}{Z_c - z}, \quad (15.41b)$$

and $R_m^{(n)}$ is a nontrivial solution of (15.27). Then $\psi_{R_m^{(n)}}^{\text{explicit}}$ is an explicit singular vortex solution of the two-dimensional critical NLS (15.4).

Lemma 15.22 $\psi_{R_m^{(n)}}^{\text{explicit}}$ becomes singular at $\mathbf{x}_c = \mathbf{0}$ (i.e., $r = 0$) as $z \rightarrow Z_c$.

Proof This is a special case of Lemma 10.3. \square

As in the vortex-free case (Sect. 10.2), $\psi_{R_m^{(n)}}^{\text{explicit}}$ undergoes a whole-beam collapse, and its variance vanishes at the singularity. In addition, by Lemma 15.5, $\psi_{R_m^{(n)}}^{\text{explicit}}(z, r = 0, \theta) \equiv 0$.

Corollary 15.8 $\psi_{R_m^{(n)}}^{\text{explicit}}$ vanishes at the singularity point $\mathbf{x}_c = \mathbf{0}$ for $0 \leq z < Z_c$.

In particular, $\lim_{z \rightarrow Z_c} \psi_{R_m^{(n)}}^{\text{explicit}}(z, \mathbf{x}_c) = 0$.

This is exactly the opposite from the non-vortex case, where both $\psi_{R^{(n)}}^{\text{explicit}}$ and ψ_G^{explicit} satisfy $\lim_{z \rightarrow Z_c} |\psi(z, \mathbf{x}_c)| = \infty$.⁹

Remark In Corollary 15.13 we will see that the result of Corollary 15.8 holds for all radial singular vortex solutions of the critical NLS.

The blowup rate of $\psi_{R_m^{(n)}}^{\text{explicit}}$ is linear. Indeed, by (13.2),

$$\frac{1}{\|\nabla \psi_{R_m^{(n)}}^{\text{explicit}}\|_2} \sim \frac{\sqrt{2}}{\|\psi_{R_m^{(n)}}^{\text{explicit}}\|_4^2} = \frac{\sqrt{2}}{\|R_m^{(n)}\|_4^2} (Z_c - z), \quad z \rightarrow Z_c.$$

The phase of $\psi_{R_m^{(n)}}^{\text{explicit}}$ at the rescaled radius $\rho = r/L(z)$ is

$$\arg \left(\psi_{R_m^{(n)}}^{\text{explicit}}(z, \rho, \theta) \right) = \zeta(z) + m\theta - L(z) \frac{\rho^2}{4}.$$

⁹ Since $R^{(n)}(r)$ attains its global maximum at $r = 0$, then obviously $\lim_{z \rightarrow Z_c} |\psi_{R^{(n)}}^{\text{explicit}}(z, 0)| = \infty$. By (11.42), $\lim_{z \rightarrow Z_c} |\psi_G^{\text{explicit}}(z, 0)| = \infty$.

Therefore,

$$\arg \left(\psi_{R_m^{(n)}}^{\text{explicit}}(z, \rho, \theta) \right) \sim \zeta(z) + m\theta, \quad z \rightarrow Z_c. \quad (15.42)$$

Hence, as $z \rightarrow Z_c$, the phase becomes independent of ρ , and it rotates at the angular velocity $\frac{d\zeta}{dz} = L^{-2} \rightarrow \infty$.¹⁰

15.6 The Explicit Vortex Blowup Solution $\psi_{G_m}^{\text{explicit}}$

As in the vortex-free case (Sect. 11.1), we can look for explicit blowup solutions of the two-dimensional critical NLS (15.4) of the form

$$\psi_{G_m}^{\text{explicit}}(z, r, \theta) = \frac{1}{L(z)} G_m(\rho) e^{i\zeta + im\theta + i\frac{L_z}{L} \frac{r^2}{4}}, \quad \zeta = \int_0^z \frac{ds}{L^2(s)}, \quad \rho = \frac{r}{L(z)},$$

where $L(z)$ is not necessarily linear in z . Substituting $\psi_{G_m}^{\text{explicit}}$ in (15.4) gives

$$G_m''(\rho) + \frac{1}{\rho} G_m' - \left(1 + \frac{m^2}{\rho^2} \right) G_m + |G_m|^2 G_m + \frac{1}{4} \beta(z) \rho^2 G_m = 0,$$

where $\beta = L^3 L_{zz}$. Since $G_m(\rho)$ is independent of z , $\beta(z) \equiv \beta$. Hence, the equation for $L(z)$ is

$$L_{zz}(z) = -\frac{\beta}{L^3}. \quad (15.43)$$

As in the vortex-free case, if $\beta < 0$, L cannot go to zero. If $\beta = 0$, the equation for G_m reduces to Eq. (15.27) for R_m , L is linear in z , and we recover the explicit blowup solutions $\psi_{R_m}^{\text{explicit}}$. If $\beta > 0$, $L(z)$ can also go to zero. In this case, the blowup rate is a square root, see Lemma 11.2, and so we have

Lemma 15.23 *Let*

$$\psi_{G_m}^{\text{explicit}}(z, r, \theta) = \frac{1}{L(z)} G_m(\rho) e^{i\zeta(z) + im\theta - i\frac{\alpha^2}{8} \rho^2}, \quad (15.44a)$$

where

$$L(z) = \alpha(Z_c - z)^{\frac{1}{2}}, \quad (15.44b)$$

$$\rho = \frac{r}{L(z)}, \quad \zeta(z) = -\frac{1}{\alpha^2} \ln \left(1 - \frac{z}{Z_c} \right), \quad (15.44c)$$

¹⁰ The acceleration of angular velocity follows from conservation of angular momentum. Thus, as the vortex power (mass) concentrates into a smaller region, the angular velocity has to increase in order that angular momentum be conserved.

G_m is the solution of

$$G_m''(r) + \frac{1}{r} G_m' - \left(1 + \frac{m^2}{r^2}\right) G_m + |G_m|^2 G_m + \gamma r^2 G_m = 0, \quad (15.45a)$$

subject to the initial condition¹¹

$$\lim_{r \rightarrow 0} \frac{G_m(r)}{r^m} = g_{m,0} \neq 0, \quad (15.45b)$$

and $\gamma = \alpha^4/16$. Then $\psi_{G_m}^{\text{explicit}}(z, r, \theta)$ is an explicit solution of the critical NLS (15.4). More generally, let

$$\psi_{G_m}^{\text{explicit}}(z, r, \theta) = \frac{1}{L(z)} G_m(\rho) e^{i\xi(z) + im\theta + i\frac{L_z}{L} \frac{r^2}{4}}, \quad (15.46)$$

where $L(z)$ is the solution of (15.43), and G_m is the solution of (15.45) with $\gamma = \beta/4$. Then $\psi_{G_m}^{\text{explicit}}(z, r, \theta)$ is an explicit solution of (15.4).

Remark In Lemma 15.25 we will see that G_m is in L^4 , but not in H^1 , or even in L^2 . Therefore, $\psi_{G_m}^{\text{explicit}}$ is not in H^1 or in L^2 . It is, however, an L^4 solution that blows up at a square-root rate, see Sect. 15.6.3.

When $\psi_{G_m}^{\text{explicit}}$ is given by (15.44), the phase at $\rho = r/L(z)$ is

$$\arg \left(\psi_{G_m}^{\text{explicit}}(z, \rho, \theta) \right) = \xi(z) + m\theta - \frac{\alpha^2}{8} \rho^2. \quad (15.47)$$

Exercise 15.2 Show that if $\psi_{G_m}^{\text{explicit}}$ is given by (15.46), then

$$\arg \left(\psi_{G_m}^{\text{explicit}}(z, \rho, \theta) \right) \sim \xi(z) + m\theta - \frac{1}{4} \beta^{\frac{1}{2}} \rho^2, \quad z \rightarrow Z_c.$$

Hint: Use Eq. (11.13).

Therefore, unlike $\psi_{R_m}^{\text{explicit}}$, see (15.42), the dependence of $\arg(\psi_{G_m}^{\text{explicit}})$ on ρ does not disappear as $z \rightarrow Z_c$. Rather, the phase of $\psi_{G_m}^{\text{explicit}}$ looks like a spiral that rotates at the angular velocity $\frac{d\xi}{dz} = L^{-2}$, which increases to infinity as $z \rightarrow Z_c$.

¹¹ See Lemma 15.24.

$$15.6.1 \quad \psi_0 = e^{im\theta} G_m(r) e^{-i\frac{r^2}{4F}}$$

The explicit solution (15.44) depends on the two parameters α and Z_c . As in the vortex-free case (Sect. 11.1.1), in the special case where $Z_c = \alpha^{-2}$,

$$\begin{aligned} \psi_{G_m}^{\text{explicit}}(z, r, \theta) &= \frac{1}{L(z)} G_m \left(\frac{r}{L(z)} \right) e^{im\theta} e^{i\zeta(z)} e^{-i\frac{\alpha^2 r^2}{8(1-\alpha^2 z)}} \\ &= \frac{1}{L(z)} G_m \left(\frac{r}{L(z)} \right) e^{im\theta} e^{i\zeta(z)} e^{-i\frac{r^2}{8(Z_c-z)}}, \end{aligned} \quad (15.48a)$$

where

$$L(z) = \sqrt{1 - \alpha^2 z} = \sqrt{1 - \frac{z}{Z_c}}, \quad (15.48b)$$

and

$$\zeta(z) = -\frac{\ln(1 - \alpha^2 z)}{\alpha^2} = -Z_c \ln \left(1 - \frac{z}{Z_c} \right). \quad (15.48c)$$

Substituting $z = 0$ in (15.48) shows that the corresponding initial condition

$$\psi_0 = G_m(r) e^{im\theta} e^{-i\frac{\alpha^2}{8} r^2} = G_m(r) e^{im\theta} e^{-i\frac{r^2}{8Z_c}}$$

is the $e^{im\theta} G_m(r)$ profile, focused by a lens with $F = 2\alpha^{-2} = 2Z_c$.

15.6.2 Analysis of the G_m Equation

Following Fibich and Gavish [72], we present a systematic study of (15.45). When $0 \leq r \ll 1$, the term $\gamma r^2 G_m$ is negligible, and so the G_m equation (15.45) reduces to the R_m equation (15.12). Therefore, the behavior of G_m is similar to that of R_m :

Lemma 15.24 ([72]) *Let $G_m(r)$ be a nontrivial solution of (15.45). Then $G_m(r) = r^m g_m(r)$, where $g_m(r)$ is the unique solution of*

$$g_m''(r) + \frac{2m+1}{r} g_m' - \left(1 - \gamma r^2 \right) g_m + |r|^{2m} |g_m|^2 g_m = 0,$$

subject to

$$g_m(0) = g_{m,0} \neq 0, \quad g_m'(0) = 0.$$

Therefore,

$$\lim_{r \rightarrow 0} \frac{G_m(r)}{r^m} = g_{m,0} \neq 0.$$

Proof The proof is identical to that of Lemma 15.10. \square

Therefore, in particular,

$$G_m(r) \sim cr^m, \quad 0 \leq r \ll 1.$$

When $r \gg 1$, the vorticity term $\frac{m^2}{r^2} G_m$ becomes negligible, and so the G_m equation reduces to the G equation (11.4a). Therefore, the behavior of G_m as $r \rightarrow \infty$ is similar to that of G :

Lemma 15.25 *Let $G_m(r)$ be a solution of (15.45) with $\gamma > 0$. Then*

1. $\lim_{r \rightarrow \infty} G_m(r) = 0$ and $\lim_{r \rightarrow \infty} G'_m(r) = 0$.
2. As $r \rightarrow \infty$,

$$G_m(r) \sim \frac{c_m}{r} \cos(h(r)), \quad G'_m(r) \sim -c_m \sqrt{\gamma} \sin(h(r)),$$

where

$$h(r) \sim \frac{\sqrt{\gamma}}{2} r^2 - \frac{1}{2\sqrt{\gamma}} \ln r + d_m,$$

and c_m and d_m are constants that depend on the value of $g_{m,0}$.

3. G_m and ∇G_m are not in L^2 . In particular, G_m is not in H^1 . G_m is, however, in L^p for any $p > 2$. In particular, G_m is in L^4 .

Proof See Exercise 11.2. \square

We thus see that for any $g_{m,0} \in \mathbb{C}$, the solution G_m of (15.45) decays to zero as $r \rightarrow \infty$. This is exactly the opposite from the initial value problem

$$R''_m(r) + \frac{1}{r} R'_m - \left(1 + \frac{m^2}{r^2}\right) R_m + |R_m|^{2\sigma} R_m = 0, \quad \lim_{r \rightarrow 0} \frac{R_m(r)}{r^m} = r_{m,0},$$

whose solutions decay to zero as $r \rightarrow \infty$ if and only if $R_m = R_m^{(n)}$ for some $n \in \{0, 1, \dots\}$, see Sect. 15.2.2. This, in turn, is the case if and only if $r_{m,0} = r_{m,0}^{(n)}$ for some $n \in \{0, 1, \dots\}$, see Corollary 15.3. Another difference between $R_m^{(n)}$ and G_m is that, as in the vortex-free case, $R_m^{(n)}$ decays exponentially, whereas G_m has an algebraically-decaying, infinite-power oscillatory tail.

So far, we saw that $G_m(r)$ has a local minimum at $r = 0$, and an algebraically-decaying oscillatory tail as $r \rightarrow \infty$. Figure 15.7 shows solutions of the G_m equation (15.45) with $\alpha = 0.35$, for various positive values of $g_{m,0}$. In general, these solutions can be separated into

1. a **ring region** in which G_m is positive with one or several peaks, and
2. a **tail region** in which G_m is oscillatory and has an algebraic decay.

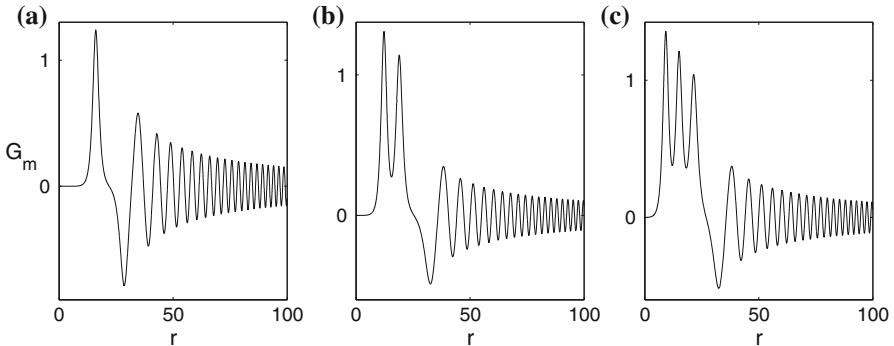


Fig. 15.7 Solutions of (15.45) with $m = 2$ and $\alpha = 0.35$, for various positive values of $g_{m,0} := g_m(0)$: **a** $g_{m,0} = 6.5 \times 10^{-7}$. **b** $g_{m,0} = 2 \times 10^{-5}$. **c** $g_{m,0} = 3.5 \times 10^{-4}$. From [72]

By Lemma 15.25, the tail amplitude is determined by c_m . Therefore, $c_m = O(1)$ for the solutions presented in Fig. 15.7. As in the vortex-free case, for a given value of $g_{m,0}$, we can define the single-ring G_m profile as the single-ring solution of (15.45) with the value of $\alpha = \alpha^{(1)}(g_{m,0})$ that gives rise to the smallest possible value of c_m . Alternatively, for a given α , we can define the single-ring G_m profile as the single-ring solution of (15.45) with the value of $g_{m,0} = g_{m,0}^{(1)}(\alpha)$ that gives rise to the smallest possible value of c_m . More generally, the n -ring profile is the n -ring solution of (15.45) with the minimal value of c_m .

Figure 15.8 shows c_m as a function of $g_{m,0}$ for $m = 2$ and $\alpha = 0.35$. In general, c_m is $O(1)$, but it sharply falls by several orders of magnitude at certain locations. Let us denote the values of $g_{m,0}$ at these minimum points (going from left to right) by $g_{m,0}^{(1)}, g_{m,0}^{(2)}, g_{m,0}^{(3)}, \dots$. Plotting the corresponding G_m profiles shows that $g_{m,0} = g_{m,0}^{(n)}$ corresponds to an n -ring profile (Fig. 15.9). Therefore, Eq. (15.45) admits one-parameter families of n -ring profiles which are determined by $(\alpha, g_{m,0}^{(n)}(\alpha))$. As in the vortex-free case, the n -ring profiles have infinite-power tails, since their value of c_m

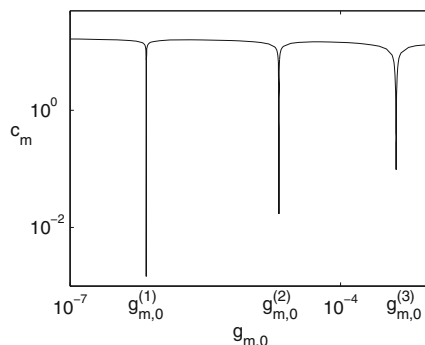


Fig. 15.8 c_m as a function of $g_{m,0}$, for $m = 2$ and $\alpha = 0.35$. From [72]

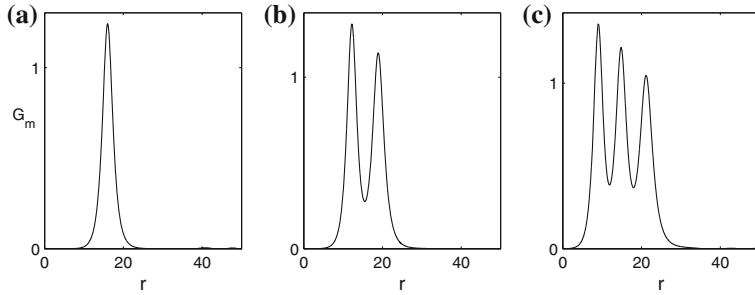


Fig. 15.9 Solutions of (15.45) with $m = 2$ and $\alpha = 0.35$. **a** Single-ring solution with $g_{m,0} = g_{m,0}^{(1)}(\alpha) \approx 7 \times 10^{-7}$. **b** Double-ring solution with $g_{m,0} = g_{m,0}^{(2)}(\alpha) \approx 2 \times 10^{-5}$. **c** Triple-ring solution with $g_{m,0} = g_{m,0}^{(3)}(\alpha) \approx 4 \times 10^{-4}$. From [72]

is small but not zero. In addition, as in the vortex-free case, all the ring peaks of G_m are of the same sign, whereas those of $R_m^{(n)}$ are of alternating signs.

The numerically-calculated curves of $\alpha^{(1)}(g_{m,0})$ and $g_{m,0}^{(1)}(\alpha)$ are plotted in Fig. 15.10 for the case $m = 2$. The thing to note is that the function $\alpha^{(1)}(g_{m,0})$ vanishes at some $g_{m,0} > 0$, see Fig. 15.10a. When α vanishes, however, Eq. (15.45) for G_m reduces to Eq. (15.27) for R_m . Since G_m with $\alpha = \alpha^{(1)}(g_{m,0})$ is a single-ring profile, then so is the limiting R_m profile. Hence, it is given by $R_m^{(0)}$. Therefore, $\alpha^{(1)}(g_{m,0})$ vanishes at $g_{m,0} = r_{m,0}^{(0)} := \lim_{r \rightarrow 0} \frac{R_m^{(0)}(r)}{r^m} > 0$, see (15.20).

Conclusion 15.2 The single-ring $R_m^{(0)}$ profile is the limit of the single-ring G_m profiles as $g_{m,0} \rightarrow r_{m,0}^{(0)} > 0$ and $\alpha^{(1)}(g_{m,0}) \rightarrow \alpha^{(1)}(r_{m,0}^{(0)}) = 0$.

This result is exactly the opposite from the vortex-free case, where $R^{(0)}$ is peak-type, and therefore cannot be the limit of single-ring G profiles.¹²

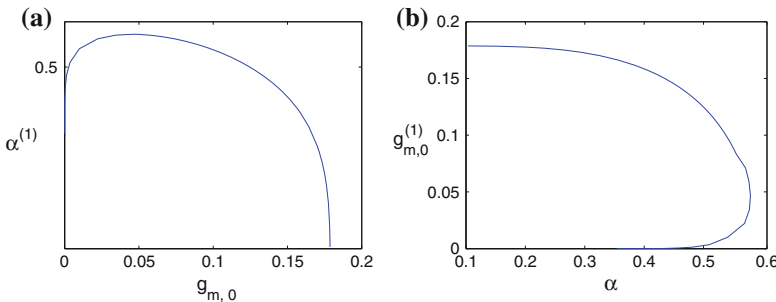


Fig. 15.10 Relation between α and $g_{m,0}$ for single-ring vortex solutions of (15.45) with $m = 2$. **a** $\alpha^{(1)}(g_{m,0})$. **b** $g_{m,0}^{(1)}(\alpha)$

¹² Indeed, since $R^{(0)}(0) > 1$, see Sect. 6.4.5, as $G(0) \rightarrow R^{(0)}(0)$, we have that $G(0) > 1$. Hence, the solutions of the G equation as $G(0) \rightarrow R^{(0)}(0)$ are peak-type and not ring-type (Sect. 11.2.2).

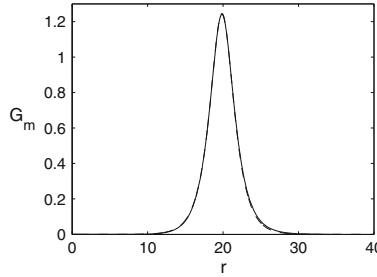


Fig. 15.11 Single-ring G_m profile with $m = 2$, $\alpha = 0.35$, and $g_{m,0} = g_{m,0}^{(1)}(\alpha) \approx 7 \times 10^{-7}$ (solid). The dashed line is approximation (15.49). The two curves are nearly indistinguishable

Remark Conclusion 15.2 provides insight on the instability of solitary vortex solutions (Sect. 15.8.2).

Remark Similar arguments show that $\alpha^{(n)}(g_{m,0})$ vanishes at $g_{m,0} = r_{m,0}^{(n)} := \lim_{r \rightarrow 0} \frac{R_m^{(n)}(r)}{r^m} > 0$, see (15.20). Therefore, the n -ring $R_m^{(n)}$ profile is the limit of the n -ring G_m profiles as $g_{m,0} \rightarrow r_{m,0}^{(n)}$.

As in the vortex-free case (Lemma 11.8), the profile of $G_m(r)$ near the peak of its ring(s) is, up to scaling, that of a one-dimensional solitary wave:

Lemma 15.26 *Let $G_m(r)$ be a solution of (15.45), and let r_{\max} be a local maximum point of G_m such that $1 \ll r_{\max} \leq \gamma^{-\frac{1}{2}}$. Then for $r - r_{\max} = O(1)$,*

$$G_m(r) \sim 2^{\frac{1}{2}} \lambda \operatorname{sech}(\lambda(r - r_{\max})), \quad \lambda = \sqrt{1 + \frac{m^2}{r_{\max}^2} - \gamma r_{\max}^2}. \quad (15.49)$$

Proof The proof is the same as in the vortex-free case (Lemma 11.8). □

Figure 15.11 shows that approximation (15.49) is in excellent agreement with the single-ring G_m solution in the ring region.

15.6.3 Square-Root Blowup Rate (in L^4)

In Lemma 15.24 we saw that G_m is in L^4 , but not in H^1 . Therefore, $\psi_{G_m}^{\text{explicit}}$ is a singular solution in L^4 , but not in H^1 . As in the vortex-free case (Sect. 11.3), since $\|G_m\|_4^4 < \infty$ and $\|\psi_{G_m}^{\text{explicit}}(z)\|_4^2 = \|G_m\|_4^2/L(z)$, we have

Lemma 15.27 $\psi_{G_m}^{\text{explicit}}$ is an explicit solution of the two-dimensional critical NLS that blows up in L^4 as $z \rightarrow Z_c$ at a square-root blowup rate.

15.7 The Explicit Blowup Solution $\psi_{Q_m}^{\text{explicit}}$ (Supercritical NLS)

In Sect. 12.1 we derived the explicit peak-type blowup solution ψ_Q^{explicit} of the supercritical NLS. We now derive its vortex analog for the two-dimensional supercritical NLS

$$i\psi_z(z, r, \theta) + \psi_{rr} + \frac{1}{r}\psi_r + \frac{1}{r^2}\psi_{\theta\theta} + |\psi|^{2\sigma}\psi = 0, \quad \sigma > 2. \quad (15.50)$$

Let

$$\psi(z, r, \theta) = \frac{1}{L^{\frac{1}{\sigma}}(z)} Q_m(\rho) e^{im\theta} e^{i\xi(z)}, \quad \rho = \frac{r}{L(z)}, \quad \xi = \int_0^z \frac{ds}{L^2(s)}.$$

It can be verified by direct substitution that the equation for Q_m is

$$Q''_m(\rho) + \frac{1}{\rho}Q'_m - \left(1 + \frac{m^2}{\rho^2}\right)Q_m - iLL_z \left(\frac{1}{\sigma}Q_m + \rho Q'_m\right) + |Q_m|^{2\sigma}Q_m = 0.$$

Hence, as in Sect. 12.1, there exists a real constant a , such that $L(z) = \sqrt{2a(Z_c - z)}$. Therefore, the equation for Q_m reads

$$Q''_m(\rho) + \frac{1}{\rho}Q'_m - \left(1 + \frac{m^2}{\rho^2}\right)Q_m + ia \left(\frac{1}{\sigma}Q_m + \rho Q'_m\right) + |Q_m|^{2\sigma}Q_m = 0. \quad (15.51)$$

Therefore, we have

Lemma 15.28 *Let $Q_m(\rho)$ be a solution of (15.51), and let*

$$\psi_{Q_m}^{\text{explicit}}(z, r, \theta) = \frac{1}{L^{\frac{1}{\sigma}}(z)} Q_m(\rho) e^{im\theta} e^{i\xi(z)},$$

where

$$L(z) = \sqrt{2a(Z_c - z)}, \quad \rho = \frac{r}{L(z)}, \quad \xi = \int_0^z \frac{ds}{L^2(s)} = \frac{1}{2a} \log \frac{Z_c}{Z_c - z}.$$

Then $\psi_{Q_m}^{\text{explicit}}$ is an explicit solution of the supercritical NLS (15.50).

If we substitute

$$Q_m(\rho) = e^{i\frac{L_z}{L} \frac{r^2}{4}} P_m(\rho) = e^{-i\frac{a\rho^2}{4}} P_m(\rho),$$

the equation for P_m reads

$$P_m''(\rho) + \frac{1}{\rho} P_m' - \left(1 + \frac{m^2}{\rho^2}\right) P_m - ia \frac{\sigma - 1}{\sigma} P_m + \frac{1}{4} a^2 \rho^2 P_m + |P_m|^{2\sigma} P_m = 0.$$

An argument similar to that in the proof of Lemma 15.10 shows that $P_m(\rho) \sim q_{m,0} \rho^m$ for $0 \leq \rho \ll 1$, where $q_{m,0} \in \mathbb{C}$. Hence, $|Q_m(\rho)|$ has a local minimum at $\rho = 0$. Consequently, Q_m is ring-type and not peak-type.

As $\rho \rightarrow \infty$, the vorticity term $\frac{m^2}{\rho^2} Q_m$ becomes negligible, and so the Q_m equation (15.51) reduces to the Q equation (12.6a). Therefore, as with the Q equation (Sect. 12.2), for any $q_{m,0} \in \mathbb{C}$, the solution of (15.51), subject to

$$\lim_{\rho \rightarrow 0} \frac{Q_m(\rho)}{\rho^m} = q_{m,0},$$

decays to zero as $\rho \rightarrow \infty$, and its asymptotic behavior is given by

$$Q_m(\rho) \sim c_1 Q_1(\rho) + c_2 Q_2(\rho), \quad \rho \rightarrow \infty,$$

where c_1 and c_2 are complex numbers, and

$$Q_1 \sim \rho^{-\frac{i}{a} - \frac{1}{\sigma}}, \quad Q_2 \sim e^{-i \frac{a \rho^2}{2}} \rho^{\frac{i}{a} - d + \frac{1}{\sigma}}.$$

Therefore, Q_m is in $L^{2\sigma+2}$ but not in H^1 . Hence, as with ψ_Q^{explicit} , see Sect. 12.3, $\psi_{Q_m}^{\text{explicit}}$ is a singular solution in $L^{2\sigma+2}$ but not in H^1 .

Remark Radial stability of $\psi_{Q_m}^{\text{explicit}}$ is discussed in Sect. 15.10.

15.8 Stability of Solitary Vortex Solutions $\psi_{\text{vortex}}^{\text{solitary},(n)}$

In Sect. 15.2 we saw that the NLS (15.3) admits the solitary vortex solutions

$$\psi_{\text{vortex}}^{\text{solitary},(n)}(z, r, \theta) = e^{iz+im\theta} R_m^{(n)}(r), \quad (15.52)$$

where $R_m^{(n)}$ is a solution of (15.27). We now study the stability of these solutions.

15.8.1 Radial Stability

We first consider the stability of the ground-state solitary vortex solutions $\psi_{\text{vortex}}^{\text{solitary},(n=0)}$ $(z, r, \theta) = e^{iz+im\theta} R_m^{(0)}(r)$ under radial vortex perturbations, i.e., perturbations of the initial condition of the form $e^{im\theta} f(r)$. By the dilation symmetry, the NLS (15.3) admits the solitary vortex solutions $\psi_{\text{vortex},\omega}^{\text{solitary},(n=0)} = R_{m,\omega}^{(0)}(r) e^{i\omega z+im\theta}$, where $R_{m,\omega}^{(0)}(r) = \omega^{\frac{1}{2\sigma}} R_m^{(0)}(\sqrt{\omega}r)$ and $R_m^{(0)}$ is the ground state of (15.27). Hence,

$$\begin{cases} \frac{d}{d\omega} \|R_{m,\omega}^{(0)}\|_2^2 > 0, & \text{if } 0 < \sigma < 1, \\ \frac{d}{d\omega} \|R_{m,\omega}^{(0)}\|_2^2 = 0, & \text{if } \sigma = 1, \\ \frac{d}{d\omega} \|R_{m,\omega}^{(0)}\|_2^2 < 0, & \text{if } \sigma > 1. \end{cases} \quad (15.53)$$

Therefore, by the VK condition (Sect. 9.4.2), the ground-state solitary vortex solutions are radially stable in the subcritical case, and unstable in the supercritical case.

Next, we consider radial stability in the critical case.

Lemma 15.29 *The solitary vortex solutions $\psi_{\text{vortex}}^{\text{solitary},(n)}$ of the critical NLS are strongly unstable.*

Proof This is a special case of Theorem 9.4. \square

We now focus on the *ground-state* solitary vortex solution of the critical NLS $\psi_{\text{vortex}}^{\text{solitary},(n=0)}(z, r, \theta) = e^{iz+im\theta} R_m^{(0)}(r)$. This solution has exactly the critical power, i.e.,

$$\|\psi_{\text{vortex}}^{\text{solitary},(n=0)}\|_2^2 = \|R_m^{(0)}\|_2^2 = P_{\text{cr}}(m).$$

If we perturb its initial condition as

$$\psi_0^{(\epsilon)} = (1 - \epsilon) \psi_{\text{vortex}}^{\text{solitary},(n=0)}(z = 0, r), \quad 0 < \epsilon \ll 1, \quad (15.54)$$

then $\|\psi_0^{(\epsilon)}\|_2^2 < P_{\text{cr}}(m)$. Therefore, the perturbed solution exists globally (Theorem 15.1). Moreover, the perturbed solution scatters as $z \rightarrow \infty$:

Lemma 15.30 (scattering) *Let ψ be a solution of the critical NLS (15.4) with $\psi_0(r, \theta) = A_0(r) e^{im\theta} \in H^1$, and let $\|\psi_0\|_2^2 < P_{\text{cr}}(m)$. Then for all p such that $2 \leq p < \infty$,*

$$\|\psi\|_p^p \leq \frac{C_p}{z^{p-2}}, \quad 0 \leq z < \infty, \quad (15.55)$$

where C_p is a constant that depends on p .

Proof The proof is the same as in the vortex-free case (Lemma 8.8), with P_{cr} replaced by $P_{\text{cr}}(m)$ and the Gagliardo-Nirenberg inequality (15.29) replaced by that for vortex solutions, see (15.31). \square

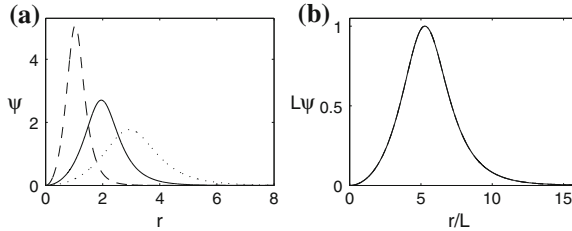


Fig. 15.12 **a** Solution of the critical NLS (15.4) with the initial condition (15.56) at $z = 0$ (dots, $L^{-1} = 1$), $z = 6$ (solid, $L^{-1} = 1.5$) and $z = 7.5$ (dashes, $L^{-1} = 2.8$). **b** The second and third curves from subplot (a) at the focusing levels $L^{-1} = 1.5$ and 2.8 , rescaled according to (15.57). Also plotted is the solution at the focusing level $L^{-1} = 5 \times 10^{14}$ (dash-dots). All three lines are indistinguishable. From [72]

Thus, as in the vortex-free radial case (Sect. 7.12), the ground-state solitary vortex profile $e^{im\theta} R_m^{(0)}(r)$ has the *dual borderline properties*, whereby it has the critical power for collapse (Theorem 15.1) and a zero Hamiltonian (Corollary 15.1). Consequently, it collapses under some perturbations and scatters under others.

15.8.2 A Surprising Result

So far, all the results on stability of solitary vortex solutions were identical to those in the vortex-free case. In what follows, we show a remarkable difference between these two cases. Consider the critical NLS with

$$\psi_0 = (1 + \epsilon)\psi_{\text{vortex}}^{\text{solitary}, (n=0)}(z = 0) = (1 + \epsilon)e^{im\theta} R_m^{(0)}(r), \quad 0 < \epsilon \ll 1. \quad (15.56)$$

Since $H(\psi_0) < 0$, see Lemma 15.18, the solution becomes singular. In the vortex-free case, it follows from Theorem 14.1 that the solution collapses with the self-similar $R^{(0)}$ profile at the loglog law rate. Thus, multiplication by $1 + \epsilon$ changes the blowup rate from linear to the loglog law, but does not change the self-similar profile.

We now use numerical simulations to show that the effect of the same perturbation in the vortex case is more dramatic. Specifically, we solve the critical NLS (15.4) with the initial condition (15.56) for $m = 2$ and $\epsilon = 0.02$.¹³ Figure 15.12 shows that the numerical solution collapses with a ring profile, and that the rescaled solution

$$\psi_{\text{rescaled}} = \frac{1}{L(z)} \psi \left(\frac{r}{L(z)} \right), \quad L(z) := \frac{\max_r |\psi_0|}{\max_r |\psi|} \quad (15.57)$$

¹³ In fact, we compute the solution of (15.8) with $A_0 = (1 + \epsilon)R_m^{(0)}(r)$. This way, radial symmetry is automatically maintained. Moreover, when we solve Eq. (15.4), the numerical solution quickly becomes corrupted, because it is azimuthally unstable (Sect. 15.8.3).

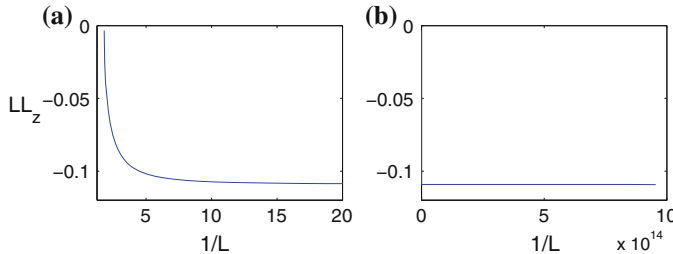


Fig. 15.13 LL_z as a function of $1/L$, for the solution of Fig. 15.12. **a** Initial dynamics ($1 \leq 1/L \leq 20$). **b** Advanced dynamics ($1/L = O(10^{14})$). Subplot (b) is from [72]

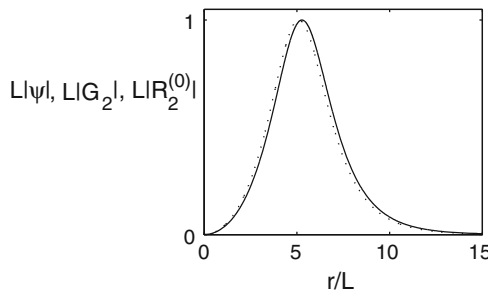


Fig. 15.14 The self-similar profile of the NLS solution from Fig. 15.12b (solid line) is indistinguishable from $G_{m=2}$ with $\alpha = 0.4652$ and $g_{m,0} = g_{m,0}^{(1)}(\alpha) = 0.14$ (dashed line). The dotted line is $R_{m=2}^{(0)}$. All three profiles are rescaled according to (15.57). From [72]

remains unchanged while focusing by 10^{14} . This self-similar collapse is in agreement with Theorem 15.2.¹⁴

We now use Lemma 14.1 to find the blowup rate. Since $\lim_{z \rightarrow z_c} LL_z = -0.109 < 0$, see Fig. 15.13b, the solution collapses at the square-root blowup rate

$$L \sim \alpha \sqrt{Z_c - z}, \quad \alpha \approx \sqrt{2 \cdot 0.109} = 0.467.$$

Therefore, in contrast to the vortex-free case, a solution that started with a perturbed $R_{m=2}^{(0)}$ profile did not collapse at the loglog law rate!

In Sect. 20.1 we shall see that singular vortex solutions of the critical NLS that have a square-root blowup rate, collapse with a single-ring G_m profile. To confirm that this is indeed the case for the solution of Fig. 15.12, we search for the value of α of the single-ring $G_{m=2}$ profile that provides the best fit to the self-similar profile of the collapsing solution, and observe that there is an excellent agreement between the two profiles (Fig. 15.14). In contrast, the agreement of the self-similar profile of the collapsing solution with $R_{m=2}^{(0)}$ is not as good. Moreover, there is an excellent

¹⁴ In Fig. 20.2 we will see that the collapse is “only” quasi self-similar.

agreement, of less than 0.5% difference, between the value $\alpha \approx 0.465$ of the best-fitting single-ring $G_{m=2}$ profile, and the value $\alpha \approx 0.467$ obtained from the blowup rate. Therefore, based on numerical evidence, we formulate

Conjecture 15.1 ([72]) *The solution of the two-dimensional critical NLS with the initial condition (15.56), collapses with a self-similar single-ring G_m profile at a square-root blowup rate, and not with a self-similar $R_m^{(0)}$ profile at the loglog law blowup rate. More generally, singular vortex solutions that collapse with the self-similar $R_m^{(0)}$ profile are radially unstable.*

Remark This is exactly the opposite from the vortex-free case, where the $R^{(0)}$ profile is a strong attractor under radial and nonradial perturbations (Sect. 14.6).

Remark Conjecture 15.1 is in contradiction with a recent result by Simpson and Zwier. See Sect. 20.2 for further details.

The strong-instability dynamics of $\psi_{\text{vortex}}^{\text{solitary},(0)}$ in Figs. 15.12 and 15.13 can be viewed as a movement along the one-parameter family of single-ring solutions

$$\psi_{G_m} := \frac{1}{L(z)} G_m(\rho; \alpha^{(1)}(z)) e^{i\xi + im\theta + i\frac{L_z}{L} \frac{r^2}{4}}, \quad \alpha^{(1)}(z) = \sqrt{-2LL_z}.$$

Indeed, when $\epsilon = 0$, the solution of the two-dimensional critical NLS with the initial condition (15.56) is $\psi = e^{iz+im\theta} R_m^{(0)}$. Therefore, $L(z) \equiv 1$, $\alpha^{(1)}(z) \equiv 0$, and $G_m(\rho; \alpha^{(1)}(z)) = G_m(\rho; \alpha^{(1)} \equiv 0) = R_m^{(0)}$, see Conclusion 15.2. When $0 < \epsilon \ll 1$, as the perturbed solution evolves, LL_z continuously changes from $LL_z \approx 0$ to $LL_z \approx -0.1092$, see Fig. 15.13a. Hence, the value of $\alpha^{(1)}(z)$ continuously changes from $\alpha^{(1)}(z=0) \approx 0$ to $\alpha^{(1)}(z \approx Z_c) \approx \sqrt{2 \cdot 0.1092} = 0.4673$, along the right branch of the $\alpha^{(1)}$ curve in Fig. 15.10a. Therefore, the self-similar profile $G_m(\rho; \alpha^{(1)}(z))$ continuously changes from $G_m(\rho; \alpha^{(1)} \approx 0) \approx R_m^{(0)}(\rho)$ to $G_m(\rho; \alpha^{(1)} \approx 0.4673)$. This characterization of the instability dynamics reveals that the difference between the strong-instability dynamics of $\psi_{\text{vortex}}^{\text{solitary},(0)} = e^{iz} e^{im\theta} R_m^{(0)}(r)$ and that of $\psi^{\text{solitary},(0)} = e^{iz} R^{(0)}(r)$ has to do with the fact that $R_m^{(0)}$ is the limit of single-ring G_m profiles, but $R^{(0)}$ is not the limit of single-ring G profiles.

15.8.3 Azimuthal Instability

In [244, 245], Soto-Crespo and co-workers developed a perturbation method, the Approximate Modulational Instability (AMI) method, for analyzing the azimuthal instability of stationary ring solutions. We now use this method to show that ground-state solitary vortex solutions are azimuthally unstable:¹⁵

¹⁵ In Sect. 11.5 we applied the AMI method to collapsing ring solutions.

Lemma 15.31 Let $\psi_{\text{vortex}}^{\text{solitary},(0)}(z, r, \theta) = e^{iz+im\theta} R_m^{(0)}(r)$ be the ground-state solitary vortex solution of the two-dimensional NLS (15.3). Then $\psi_{\text{vortex}}^{\text{solitary},(0)}$ is azimuthally unstable.

Proof To simplify the notations, we denote $\psi_m := \psi_{\text{vortex}}^{\text{solitary},(0)}$. Let

$$\psi_0(r, \theta) = \left(1 + \mu \cos(k\theta)\right) \psi_m(z=0, r, \theta), \quad |\mu| \ll 1,$$

where $k = 1, 2, \dots$ is the frequency of the perturbation. We look for a solution of the form

$$\psi(z, r, \theta) = \left(1 + \mu \cos(k\theta)e^{\delta_k z} + O(\mu^2)\right) \psi_m(z, r, \theta), \quad (15.58)$$

where δ_k is the growth rate of the k th mode. If $\delta_k > 0$ the k th mode will grow, if $\delta_k < 0$ it will decay, and if δ_k is imaginary it will neither grow nor decrease. Since we want to know whether there are unstable modes, in what follows we will check whether there exist solutions of the form (15.58) for which δ_k is real and positive.

Let us denote $C := \cos(k\theta)e^{\delta_k z}$. Substituting (15.58) in (15.3) and using

$$\begin{aligned} i\psi_z &= i(1 + \mu C)(\psi_m)_z + i\mu C \delta_k \psi_m + O(\mu^2), \\ \Delta\psi &= \Delta_r \psi + \frac{1}{r^2} \psi_{\theta\theta} = (1 + \mu C)\Delta\psi_m - \frac{k^2}{r^2} \mu C \psi_m + O(\mu^2), \end{aligned}$$

and

$$\begin{aligned} |\psi|^{2\sigma} \psi &= |\psi_m|^{2\sigma} \psi_m (1 + \mu C)^{1+\sigma} (1 + \mu^* C)^\sigma + O(\mu^2) \\ &= |\psi_m|^{2\sigma} \psi_m (1 + (1 + \sigma)\mu C) (1 + \sigma \mu^* C) + O(\mu^2) \\ &= |\psi_m|^{2\sigma} \psi_m (1 + (1 + \sigma)\mu C + \mu^* C) + O(\mu^2) \\ &= |\psi_m|^{2\sigma} \psi_m (1 + \mu C + 2\sigma \operatorname{Re}(\mu) C) + O(\mu^2), \end{aligned}$$

we get

$$\begin{aligned} &\underbrace{i \frac{d}{dz} \psi_m(z, r, \theta) + \Delta \psi_m + |\psi_m|^{2\sigma} \psi_m}_{=0} \\ &+ \mu \cos(k\theta) e^{\delta_k z} \left[\underbrace{i \frac{d}{dz} \psi_m + \Delta \psi_m + |\psi_m|^{2\sigma} \psi_m + i\delta_k \psi_m - \frac{k^2}{r^2} \psi_m}_{=0} \right] \\ &+ 2\sigma \mu_r \cos(k\theta) e^{\delta_k z} |\psi_m|^{2\sigma} \psi_m = O(\mu^2). \end{aligned}$$

Balancing the $\mathcal{O}(\mu)$ terms and substituting $\mu = \mu_r + i\mu_i$ and $|\psi_m| = R_m^{(0)}$ gives

$$(\mu_r + i\mu_i) \left(i\delta_k - \frac{k^2}{r^2} \right) + 2\sigma \mu_r |R_m^{(0)}|^{2\sigma} = 0.$$

The equation for the real and imaginary parts reads¹⁶

$$B \begin{pmatrix} \mu_r \\ \mu_i \end{pmatrix} = 0, \quad B = \begin{pmatrix} 2\sigma |R_m^{(0)}(r)|^{2\sigma} - \left(\frac{k}{r}\right)^2 & -\delta_k \\ \delta_k & -\left(\frac{k}{r}\right)^2 \end{pmatrix}.$$

A nontrivial solution exists only if $|B| = 0$, from which it follows that

$$\delta_k = \pm \frac{k}{r} \sqrt{2\sigma |R_m^{(0)}(r)|^{2\sigma} - \left(\frac{k}{r}\right)^2}.$$

The above result is inconsistent with our assumption that δ_k in expression (15.58) is independent of r . Nevertheless, one can argue that since $R_m^{(0)}$ has a ring profile which is localized around its peak at r_{\max} , one can replace r with r_{\max} , yielding

$$\delta_k = \pm \frac{k}{r_{\max}} \sqrt{2\sigma |R_m^{(0)}(r_{\max})|^{2\sigma} - \left(\frac{k}{r_{\max}}\right)^2}. \quad (15.59)$$

Hence, if

$$0 < k < \sqrt{2\sigma} r_{\max} |R_m^{(0)}(r_{\max})|^{\sigma}, \quad (15.60)$$

there exist a solution of the form (15.58) for which the growth rate δ_k is positive.

By Lemma 15.17, $r_{\max} \sim \sqrt{\frac{2}{\sigma}} m$ and $|R_m^{(0)}(r_{\max})|^{\sigma} \sim (1 + \frac{\sigma}{2})^{\frac{1}{2}} (1 + \sigma)^{\frac{1}{2}}$. Therefore, condition (15.60) can be approximated by

$$0 < k < 2m \left(1 + \frac{\sigma}{2}\right)^{\frac{1}{2}} (1 + \sigma)^{\frac{1}{2}}.$$

Since $\sigma > 0$, the modes $k = 1, \dots, 2m$ are unstable, and so the solution is azimuthally unstable. \square

Interestingly, the unstable modes are the low frequencies and not the high frequencies, see (15.60).¹⁷ This explains why the addition of 1% ellipticity, which mainly excites the low frequencies, can lead to the “dramatic” azimuthal instability observed in Fig. 15.6.

¹⁶ Here we use the assumption that δ_k is real.

¹⁷ This is typical for modulational instabilities, see Sect. 3.6.3.

Equation (15.59) shows that δ_k^2 is a parabola in $\left(\frac{k}{r_{\max}}\right)^2$ that vanishes at $\left(\frac{k}{r_{\max}}\right)^2 = 0$ and $\left(\frac{k}{r_{\max}}\right)^2 = 2\sigma|R_m^{(0)}(r_{\max})|^{2\sigma}$. Hence, the maximum of δ_k^2 is attained at $\left(\frac{k}{r_{\max}}\right)^2 = \sigma|R_m^{(0)}(r_{\max})|^{2\sigma}$. Since k has to be an integer, the fastest growing mode is the integer closest to $r_{\max}\sqrt{\sigma}|R_m^{(0)}(r_{\max})|^{\sigma}$. This value provides a quantitative prediction to the number of spikes (filaments) that emerge on the ring, and was found to be in good agreement with NLS simulations of stationary rings [244, 245].¹⁸

Remark We can also explain the azimuthal instability of collapsing rings using the following informal argument. Let us break the radial symmetry by adding a small initial hump somewhere along the ring. Since the intensity is higher at the hump, power will be attracted towards the hump. As a result, the hump will focus faster than the rest of the ring, resulting in the formation of a spike. This instability dynamics can be seen in Fig. 22.9.

15.9 Stability of $\psi_{R_m^{(n)}}^{\text{explicit}}$ and $\psi_{G_m}^{\text{explicit}}$

15.9.1 Radial Stability

We begin with the ground-state solution $\psi_{R_m^{(0)}}^{\text{explicit}}$:

Corollary 15.9 ([72]) *The ground-state explicit singular vortex solution $\psi_{R_m^{(0)}}^{\text{explicit}}$ is strongly unstable (in the sense of Definition 10.2).*

Proof Let ψ be the solution of the critical NLS (15.4) with $\psi_0 = (1 - \epsilon)\psi_{R_m^{(0)}}^{\text{explicit}}$ ($z = 0$), where $0 < \epsilon \ll 1$. Since $\|\psi_0\|_2^2 = (1 - \epsilon)^2\|R_m^{(0)}\|_2^2 < P_{\text{cr}}(m)$, it follows from Theorem 15.1 that ψ exists globally. \square

We now perturb the initial condition in the opposite direction, i.e.,

$$\psi_0 = (1 + \epsilon)\psi_{R_m^{(0)}}^{\text{explicit}}(z = 0), \quad 0 < \epsilon \ll 1. \quad (15.61)$$

This is initial condition (15.56), dilated by $L(0) = Z_c$ and focused by a lens with a focal distance $F = Z_c$. Since dilation and a focusing lens do not prevent the solution from collapsing (Corollary 7.5), nor do they change the blowup rate (Sect. 13.1.6) or the blowup profile, we have

Corollary 15.10 ([72]) *Assume that Conjecture 15.1 holds. Then the solution of the critical NLS (15.4) with the initial condition (15.61) collapses with a self-similar*

¹⁸ In [244, 245], the fastest-growing mode was estimated by the mean value of $r\sqrt{\sigma}|R_m^{(0)}(r)|^{\sigma}$ in the ring region.

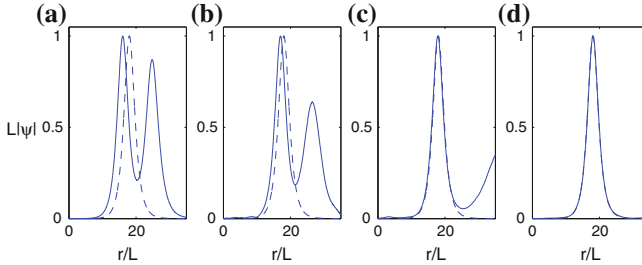


Fig. 15.15 The critical NLS (15.4) with $\psi_0 = \psi_{G_m}^{\text{explicit}}(z = 0)$, where $m = 2$ and G_m is the *double-ring* solution with $\alpha = 0.35$ and $g_{m,0} = g_{m,0}^{(2)}(\alpha) = 2 \times 10^{-5}$. The NLS solution (*solid line*), rescaled according to (15.57), at **a** $z = 0$ ($L^{-1}(z) = 1$). **b** $z = 27$ ($L^{-1}(z) = 3.4$). **c** $z = 27.6$ ($L^{-1}(z) = 7.2$). **d** $z = 27.8$ ($L^{-1}(z) = 36.1$). The *dashed line* is the *single-ring* G_2 profile with $\alpha = \alpha^{(1)} \approx 0.367$ and $g_{m,0} = 2.9 \times 10^{-6}$. From [72]

single-ring G_m profile at a square-root blowup rate, and not with a self-similar $R_m^{(0)}$ profile at the loglog law blowup rate.

The instability dynamics of $\psi_{R_m^{(0)}}^{\text{explicit}}$ under multiplication by $1 + \epsilon$ is different from that of $\psi_{R^{(0)}}^{\text{explicit}}$, which undergoes a loglog collapse with the $\psi_{R^{(0)}}$ profile (Lemma 10.6). As explained in Sect. 15.8.2, this is because $R_m^{(0)}$ is the limit of single-ring G_m profiles, whereas $R^{(0)}$ is not the limit of single-ring G profiles.

To study the radial stability of $\psi_{G_m}^{\text{explicit}}$, in [72] we solved numerically the critical NLS with the initial condition $\psi_{G_m}^{\text{explicit}}(z = 0) = G_m(r)e^{im\theta - i\frac{\alpha^2 r^2}{8}}$, whose analytic solution is given by $\psi_{G_m}^{\text{explicit}}$, see (15.48). When G_m was a single ring profile, the numerical solution remained close to $\psi_{G_m}^{\text{explicit}}$ while focusing over 15 orders of magnitude. When G_m was a double-ring profile, however the numerical solution quickly departed from the analytic one, and ultimately collapsed with a single-ring G_m self-similar profile (Fig. 15.15). Since we used the same numerical parameters (grid resolution, etc.) in both simulations, these (and additional) simulations suggest

Observation 15.1 ([72]) *Single-ring* $\psi_{G_m}^{\text{explicit}}$ *solutions are radially stable, but multi-ring* $\psi_{G_m}^{\text{explicit}}$ *solutions are radially unstable.*

In summary, as in the vortex-free case, $\psi_{R_m^{(n)}}^{\text{explicit}}$ is radially unstable for any n , and $\psi_{G_m}^{\text{explicit}}$ is radially unstable if G_m is a multi-ring solution, but radially stable if G_m is a single-ring solution. However, while in the vortex-free case the perturbed $\psi_{R^{(0)}}^{\text{explicit}}$ solutions collapse with a self-similar $R^{(0)}$ profile, the perturbed $\psi_{R_m^{(0)}}^{\text{explicit}}$ vortex solutions collapse with a self-similar single-ring G_m profile. As noted, this difference is related to the fact that $R^{(0)}$ is not the limit of single-ring G profiles, but $R_m^{(0)}$ is the limit of single-ring G_m profiles.

15.9.2 Azimuthal Instability

By Lemma 11.10, all collapsing self-similar ring solutions of the two dimensional critical NLS are azimuthally unstable. Therefore, we have

Lemma 15.32 ([72]) *The explicit solutions $\psi_{R_m^{(n)}}^{\text{explicit}}$ and $\psi_{G_m}^{\text{explicit}}$ of the two-dimensional critical NLS (15.4) are azimuthally unstable.*

Azimuthal instability of collapsing vortices was studied numerically by Fibich and Gavish [72, Sect. 3.6.6], and experimentally by Vuong et al. [264].

15.10 Radial Instability of $\psi_{Q_m}^{\text{explicit}}$

In Sect. 15.7 we saw that the two-dimensional supercritical NLS admits the explicit blowup vortex solution $\psi_{Q_m}^{\text{explicit}}$. To check numerically whether $\psi_{Q_m}^{\text{explicit}}$ is radially stable, Fibich and Gavish noted that $\psi_{Q_m}^{\text{explicit}}$ has the following two characteristics:¹⁹

1. It undergoes an *equal-rate collapse*, i.e., $r_{\max}(z) \sim cL(z)$ as $z \rightarrow Z_c$, where $r_{\max}(z) := \arg \max_r |\psi|$ is the location of the ring peak, and $L(z) := \frac{\max_r |\psi_0|^{\sigma}}{\max_r |\psi|^{\sigma}}$ is the ring width.
2. The blowup rate of $L(z)$ is a square root.

In Fig. 15.16 we solve numerically the supercritical NLS (15.50) with $\sigma = 1.1$ and $\psi_0 = \psi_{Q_m}^{\text{explicit}}(z = 0)$, where Q_m is the *admissible solution*²⁰ of (15.51) with

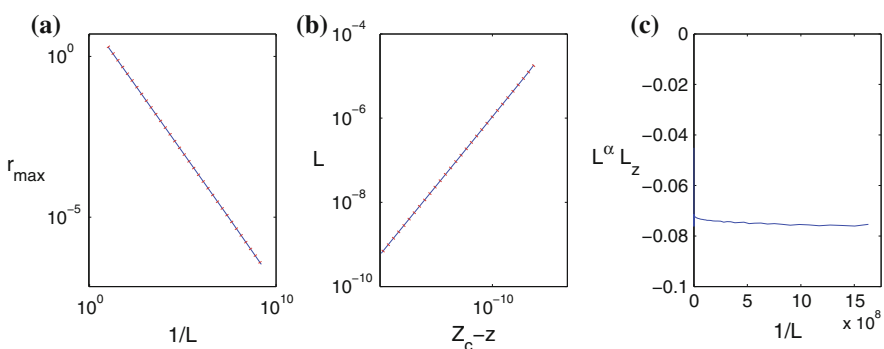


Fig. 15.16 The supercritical NLS (15.50) with $\psi_0 = \psi_{Q_m}^{\text{explicit}}(z = 0)$. **a** r_{\max} as a function of L^{-1} (*solid line*). The *dotted curve* is $13.5L^{-0.823}$. **b** L as a function of $Z_c - z$ on a logarithmic scale (*solid line*). The *dotted curve* is $0.33(Z_c - z)^{0.547}$. **c** $L^\alpha L_z$ as a function of $1/L$. From [72]

¹⁹ The motivation for choosing these two characteristics will become clear in Sect. 23.7.

²⁰ i.e., the zero-Hamiltonian, single-ring solution.

$a = 0.092$ and $q_{m,0} = 4.08 \times 10^{-4}$. Since the analytic solution is given by $\psi_{Q_m}^{\text{explicit}}$, if $\psi_{Q_m}^{\text{explicit}}$ is stable, the numerical solution should undergo an equal-rate collapse and collapse at a square-root blowup rate. Figure 15.16a shows, however, that the best-fitting α for $r_{\max} \approx r_0 L^\alpha$ is $\alpha = 0.823$. In addition, Fig. 15.16b shows that the best-fitting p for $L \sim \kappa(Z_c - z)^p$ is $p \approx 0.547$. Since the numerical solution does not undergo an equal-rate collapse, nor does it collapse at a square-root blowup rate, this suggests

Observation 15.2 ([72]) *The explicit solutions $\psi_{Q_m}^{\text{explicit}}$, where Q_m is an admissible solution of (15.51), are radially unstable.*

The fitted values of α and p are in excellent agreement with those of the ψ_{S_m} profile, which is the vortex analog of the shrinking-ring ψ_S solutions of the supercritical NLS (Sect. 23.7). Indeed, the fitted value $\alpha = 0.823$ differs from the predicted value $\alpha = \frac{2}{\sigma} - 1 = \frac{9}{11} \approx 0.818$ by $\approx 0.6\%$, and the fitted blowup rate $p = 0.547$ differs from the predicted value $p = \frac{\sigma}{2} = 0.550$ by $\approx 0.5\%$. Thus, as in the critical NLS (Sect. 15.9.1), the vortex analog of peak-type solutions are radially unstable. In Sect. 23.7 we shall see that, as in the critical NLS, the vortex analog of ring-type solutions are radially stable.

15.11 Asymptotic Blowup Profile (Critical NLS)

15.11.1 Quasi Self-similar Profile

As in the vortex-free case (Theorem 13.3), all singular radial vortex solutions of the critical NLS collapse with a quasi self-similar vortex profile:

Theorem 15.2 ([72]) *Let ψ be a solution of the critical NLS (15.4) with $\psi_0 = A_0(r)e^{im\theta} \in H^1$ that becomes singular at Z_c , and let*

$$S(\psi)(z, \rho, \theta) := l(z)\psi(z, l(z)\rho, \theta), \quad l(z) := \frac{1}{\|\nabla\psi\|_2}. \quad (15.62)$$

Then for any sequence $z_k \rightarrow Z_c$, there is a subsequence z_{k_j} , such that $S(\psi)(z_{k_j}, \rho, \theta) \rightarrow e^{im\theta}\Psi(\rho)$ strongly in L^p for all $2 < p \leq \infty$. Furthermore,

$$\|\Psi\|_4^4 = 2, \quad \|\Psi\|_2^2 \geq P_{\text{cr}}(m) = \|R_m^{(0)}\|_2^2, \quad \Psi(0) = 0.$$

Proof By Lemma 15.1, $\psi(z, \rho, \theta) = e^{im\theta}A(z, \rho)$. Hence,

$$S(\psi) = e^{im\theta}l(z)A(z, l(z)\rho).$$

To apply Compactness Lemma 5.14, we need to work with radial functions. Therefore, we eliminate the nonradial term $e^{im\theta}$ by defining

$$b_k(\rho) := e^{-im\theta} S(\psi)(z_k, \rho, \theta) = l(z_k) A(z_k, l(z_k)\rho). \quad (15.63)$$

Since $\|b_k\|_2^2 = \|A(z_k, \cdot)\|_2^2 = \|A_0\|_2^2$ and since

$$\|\nabla B_k\|_2^2 = l^2(z_k) \|\nabla A(z_k, \cdot)\|_2^2 = \frac{\|\nabla A(z_k, \cdot)\|_2^2}{\|\nabla \psi(z_k, \cdot)\|_2^2} = \frac{\|A_r\|_2^2}{\|A_r\|_2^2 + m^2 \|\frac{A}{r}\|_2^2} \leq 1,$$

the sequence b_k is bounded in H_{radial}^1 . Hence, it has a subsequence, also denoted by b_k , such that $b_k \rightharpoonup \Psi$ weakly in H_{radial}^1 . Therefore, b_k and ∇B_k converge weakly in L^2 to Ψ and $\nabla \Psi$, respectively. Consequently,

$$\|\Psi\|_2 \leq \liminf_{k \rightarrow \infty} \|b_k\|_2, \quad \|\nabla \Psi\|_2^2 \leq \liminf_{k \rightarrow \infty} \|\nabla b_k\|_2^2. \quad (15.64)$$

In addition, since b_k is bounded in H_{radial}^1 , Compactness Lemma 5.14 ensures strong convergence of b_k to Ψ in L^p for $2 < p < \infty$. In particular,

$$\|\Psi\|_4 = \lim_{k \rightarrow \infty} \|b_k\|_4. \quad (15.65)$$

Let

$$B_k(\rho, \theta) := e^{im\theta} b_k(\rho) = S(\psi)(z_k, \rho, \theta) = l(z_k) \psi(z_k, l(z_k)\rho, \theta). \quad (15.66)$$

Since $B_k - e^{im\theta} \Psi(\rho) = e^{im\theta} (b_k - \Psi(\rho))$, B_k converges to $e^{im\theta} \Psi(\rho)$ strongly in L^p for $2 < p < \infty$. We claim that

$$H(e^{im\theta} \Psi(\rho)) \leq 0 \quad \text{and} \quad \psi \not\equiv 0. \quad (15.67)$$

Therefore, from Corollary 15.5 it follows that $\|\Psi\|_2^2 \geq P_{\text{cr}}(m)$.

To prove inequality (15.67), we first note that, by (15.65),

$$\|\Psi\|_4 = \lim_{k \rightarrow \infty} \|B_k\|_4. \quad (15.68a)$$

In addition, by (15.62) and (15.66),

$$\|\nabla B_k\|_2 = l(z_k) \|\nabla \psi(z_k)\|_2 \equiv 1.$$

Since

$$1 = \|\nabla B_k\|_2^2 = \|\nabla b_k\|_2^2 + m^2 \left\| \frac{b_k}{\rho} \right\|_2^2,$$

we have that $\frac{b_k}{\rho}$ is bounded in L^2 . Hence, as in the proof of Lemma 15.13, $\frac{b_k}{\rho}$ converges weakly in L^2 to $\frac{\Psi}{\rho}$. Therefore,

$$\left\| \frac{\Psi}{\rho} \right\|_2^2 \leq \liminf_{k \rightarrow \infty} \left\| \frac{b_k}{\rho} \right\|_2^2.$$

By this inequality and (15.64),

$$\begin{aligned} \|\nabla(e^{im\theta}\Psi(\rho))\|_2^2 &= \|\nabla\Psi\|_2^2 + m^2 \left\| \frac{\Psi}{\rho} \right\|_2^2 \leq \liminf_{k \rightarrow \infty} \|\nabla b_k\|_2^2 + m^2 \liminf_{k \rightarrow \infty} \left\| \frac{b_k}{\rho} \right\|_2^2 \\ &\leq \liminf_{k \rightarrow \infty} \left(\|\nabla b_k\|_2^2 + m^2 \left\| \frac{b_k}{\rho} \right\|_2^2 \right). \end{aligned}$$

Hence,

$$\|\nabla(e^{im\theta}\Psi)\|_2^2 \leq \liminf_{k \rightarrow \infty} \|\nabla B_k\|_2^2. \quad (15.68b)$$

By (15.66), (15.68), and Hamiltonian conservation,

$$\begin{aligned} H(e^{im\theta}\Psi(\rho)) &\leq \liminf_{k \rightarrow \infty} H(B_k) = \liminf_{k \rightarrow \infty} l^2(z_k)H(\psi(z_k)) \\ &= \liminf_{k \rightarrow \infty} l^2(z_k)H(\psi_0) = 0. \end{aligned}$$

Therefore, $H(e^{im\theta}\Psi(\rho)) \leq 0$. In addition,

$$0 = \lim_{k \rightarrow \infty} H(B_k) = \lim_{k \rightarrow \infty} \|\nabla B_k\|_2^2 - \frac{1}{2} \lim_{k \rightarrow \infty} \|B_k\|_4^4 = 1 - \frac{1}{2} \|\Psi\|_4^4.$$

Therefore, $\psi \not\equiv 0$. Hence, we proved (15.67). Finally, since $\Psi \in \mathcal{F}$, Lemma 15.4 yields $\Psi(0) = 0$. \square

Remark As in the vortex-free case (Sect. 13.2.2), Theorem 15.2 does not show that the solution undergoes a self-similar collapse, but “only” that its collapsing core approaches a self-similar profile.

15.11.2 Blowup Profile is Different from $\psi_{R^{(0)}}$

In Theorem 14.1 we saw that all singular solutions of the two-dimensional critical NLS with power slightly above P_{cr} , collapse with the $\psi_{R^{(0)}}$ profile. In contrast,

Corollary 15.11 *Singular solutions of the critical NLS (15.4) with $\psi_0 = e^{im\theta}A_0(r)$ do not collapse with the $\psi_{R^{(0)}}$ profile.*

Proof This follows from Theorem 15.2, because:

1. $\|\psi_{R^{(0)}}\|_2^2 = P_{\text{cr}} < P_{\text{cr}}(m) \leq \|\Psi\|_2^2$.
2. $\psi_{R^{(0)}}(z, r = 0) \neq 0 = \Psi(0)$.
3. Radial vortex solutions have the $e^{im\theta}$ term, see Lemma 15.1, which $\psi_{R^{(0)}}$ does not have. \square

15.11.3 Upper Bound for $\alpha^*(d = 2)$

In Sect. 14.6.7 we derived some basic estimates for $\alpha^*(d)$, the constant that appears in Theorem 14.1. As Corollary 15.11 shows, Theorem 14.1 is not valid for singular radial vortex solutions, since they do not collapse with the $\psi_{R^{(0)}}$ profile. Since the minimal-power singular vortex solution is $\psi_{R_{m=1}^{(0)}}^{\text{explicit}}$, and its power is $P_{\text{cr}}(m = 1) \approx 4.1P_{\text{cr}}$, see Table 15.2, we have that

$$\alpha^*(d = 2) < P_{\text{cr}}(m = 1) - P_{\text{cr}} \approx 3.1P_{\text{cr}}. \quad (15.69)$$

15.11.4 Azimuthal Instability

Theorem 15.2 shows that any singular radial vortex solution of the critical NLS (15.4) collapses with a quasi self-similar profile Ψ . Since $\Psi(0) = \Psi(\infty) = 0$, this “shows” that Ψ has a ring profile. By Lemma 11.10, however, ring-type singular solutions of (15.4) are azimuthally unstable.

Conclusion 15.3 *All singular radial vortex solutions of the two-dimensional critical NLS (15.4) are azimuthally unstable.*

15.11.5 Power Concentration

As in the vortex-free case (Theorem 13.6), Theorem 15.2 implies that the amount of power that collapses into the singularity is at least $P_{\text{cr}}(m)$:

Theorem 15.3 (Concentration Theorem [72]) *Let ψ be a solution of the critical NLS (15.4) with $\psi_0 = A_0(r)e^{im\theta} \in H^1$ that becomes singular at Z_c . Then for all $\epsilon > 0$,*

$$\liminf_{z \rightarrow Z_c} \|\psi\|_{L^2(r < \epsilon)}^2 \geq P_{\text{cr}}(m).$$

Proof The proof is as in the vortex-free radial case (Theorem 13.6). \square

Corollary 15.12 *Let ψ be as in Theorem 15.3. Then ψ undergoes a strong collapse with $P_{\text{collapse}} \geq P_{\text{cr}}(m)$.*

We stress that these results only apply to *radial* vortex solutions. Indeed, in Sect. 15.4.1 we saw that nonradial vortex initial conditions can become singular, even if their power is below $P_{\text{cr}}(m)$.

15.11.6 Rate of Power Concentration

As in the vortex-free case (Theorem 13.9), one can use Theorem 15.2 to show that the concentration rate is not slower than the blowup rate:

Theorem 15.4 ([72]) *Let ψ be as in Theorem 15.3, and let $l(z) = 1/\|\nabla\psi\|_2$.*

1. *If $a(z)$ is a positive, monotonically-decreasing function on $[0, Z_c]$ such that*

$$\lim_{z \rightarrow Z_c} a(z) = 0 \quad \text{and} \quad \lim_{z \rightarrow Z_c} \frac{l(z)}{a(z)} = 0.$$

Then $\liminf_{z \rightarrow Z_c} \|\psi\|_{L^2(r < a(z))}^2 \geq P_{\text{cr}}(m)$.

2. *For any $\epsilon > 0$, there exists $K > 0$ such that*

$$\liminf_{z \rightarrow Z_c} \|\psi\|_{L^2(r < Kl(z))}^2 \geq (1 - \epsilon)P_{\text{cr}}(m).$$

Since the blowup rate of singular vortex solutions is bounded by a square root (Corollary 13.1), we have

Theorem 15.5 (Rate of power concentration [72]) *Let ψ be as in Theorem 15.3.*

1. *If $a(z)$ is a positive, monotonically-decreasing function on $[0, Z_c]$, such that*

$$\lim_{z \rightarrow Z_c} a(z) = 0 \quad \text{and} \quad \lim_{z \rightarrow Z_c} \frac{\sqrt{Z_c - z}}{a(z)} = 0.$$

Then $\liminf_{z \rightarrow Z_c} \|\psi(z)\|_{L^2(r < a(z))}^2 \geq P_{\text{cr}}(m)$.

2. *For any $\epsilon > 0$, there exists a $K > 0$ such that*

$$\liminf_{z \rightarrow Z_c} \|\psi(z)\|_{L^2(r < K\sqrt{Z_c - z})}^2 \geq (1 - \epsilon)P_{\text{cr}}(m).$$

15.11.7 Collapse at the Origin

In the vortex-free case, all singular radial solutions collapse at the origin (Lemma 13.2). A similar result holds for radial vortex solutions:

Lemma 15.33 *Let ψ be as in Theorem 15.3. Then ψ becomes singular at $r = 0$.*

Proof Let $\epsilon > 0$. By Theorem 15.2 with $p = 4$,

$$\begin{aligned} \int_{r<\epsilon} |\psi(z, r, \theta)|^4 r dr &= L^2(z) \int_{\rho<\frac{\epsilon}{L}} |\psi(z, L\rho, \theta)|^4 \rho d\rho \\ &= L^{-2}(z) \int_{\rho<\frac{\epsilon}{L}} |S(\psi)(z, \rho, \theta)|^4 \rho d\rho. \end{aligned}$$

Therefore, as $z \rightarrow Z_c$,

$$\int_{r<\epsilon} |\psi(z, r, \theta)|^4 r dr \sim L^{-2}(z) \|S\|_4^4 \sim L^{-2}(z) \|\Psi\|_4^4 \rightarrow \infty. \quad (15.70)$$

Hence, by Definition 5.7, ψ becomes singular at $\mathbf{x}_c = 0$. \square

Remark Lemma 15.33 cannot be extended to the supercritical case. Indeed, the two-dimensional NLS with $\sigma \geq 2$ admits radial vortex solutions that collapse on the circle $|\mathbf{x}| = r_c > 0$, see Sect. 22.5.

The most striking property of singular radial vortex solutions is that they vanish at the singularity point:

Corollary 15.13 *Let ψ be as in Theorem 15.3. Then ψ vanishes at the singularity point $\mathbf{x}_c = \mathbf{0}$ for $0 \leq z < Z_c$. In particular,*

$$\lim_{z \rightarrow Z_c} \psi(z, \mathbf{x}_c) = 0.$$

Proof This follows from Lemma 15.5 and Lemma 15.33. \square

Radial vortex solutions, however, become unbounded arbitrarily close to the singularity point:

Corollary 15.14 *Let ψ be as in Theorem 15.3. Then for all $\epsilon > 0$,*

$$\lim_{z \rightarrow Z_c} \|\psi(z, \mathbf{x})\|_{L^\infty(|\mathbf{x}|<\epsilon)} = \infty.$$

Proof By negation, assume that $\lim_{z \rightarrow Z_c} \|\psi(z, \mathbf{x})\|_{L^\infty(|\mathbf{x}|<\epsilon_0)} < \infty$ for some $\epsilon_0 > 0$. Then $\lim_{z \rightarrow Z_c} \int_{r<\epsilon_0} |\psi(z, r, \theta)|^4 r dr < \infty$. This, however, contradicts with (15.70). \square

Thus, the L^∞ norm on any circle around the origin becomes infinite, yet the solution is identically zero at the origin.

15.12 Vortex Solutions in Three Dimensions

So far we studied vortex solutions of the two-dimensional NLS. We now briefly discuss vortex solutions in three dimensions.

In Chap. 36 we will see that the three-dimensional NLS

$$i\psi_z(z, \mathbf{x}) + \Delta\psi + |\psi|^2\psi = 0, \quad \mathbf{x} = (x, y, t), \quad \Delta = \frac{\partial^2}{\partial x^2} + \frac{\partial^2}{\partial y^2} + \frac{\partial^2}{\partial t^2}$$

models the propagation of ultrashort laser pulses in the anomalous regime. This equation admits solutions which are a vortex in the two transverse spatial coordinates, i.e.,

$$\psi(z, x, y, t) = e^{im\theta}A(z, r, t), \quad r = \sqrt{x^2 + y^2}.$$

The equation for the vortex profile is

$$iA_z(z, r, t) + A_{rr} + \frac{1}{r}A_r - \frac{m^2}{r^2}A + A_{tt} + |A|^2A = 0.$$

Hence, these vortex solutions are anisotropic in $|\mathbf{x}| = \sqrt{r^2 + t^2}$.

We can also try to look for isotropic three-dimensional vortex solutions. In the linear case, this is done by replacing $e^{im\theta}$ with the spherical harmonic $Y_{l,m}(\theta, \phi) = P_l^{(m)}(\cos \theta)e^{im\phi}$, where $P_l^{(m)}$ is the associated Legendre function. This yields the vortex solution

$$\psi(z, \mathbf{x}) = Y_{l,m}(\theta, \phi)A(z, \rho), \quad \rho = |\mathbf{x}| = \sqrt{r^2 + t^2},$$

where A is the solution of

$$iA_z(z, \rho) + A_{\rho\rho} + \frac{2}{\rho}A_\rho - \frac{l(l+1)}{\rho^2}A = 0.$$

This approach does not extend to the nonlinear case, because the equation for A becomes

$$iA_z(z, \rho) + A_{\rho\rho} + \frac{2}{\rho}A_\rho - \frac{l(l+1)}{\rho^2}A + |Y_{l,m}(\theta, \phi)|^2|A|^{2\sigma}A = 0.$$

Since $|Y_{l,m}(\theta, \phi)| = |P_l^{(m)}(\cos \theta)|$ depends on θ , A cannot depend only on z and ρ .

15.13 Necklace Solutions

In Sect. 2.15.3 we saw that the two-dimensional linear Schrödinger equation

$$i\psi_z(z, x, y) + \Delta\psi = 0 \quad (15.71)$$

admits the Gaussian beam

$$\psi(z, r) = \frac{1}{L(z)} e^{-\frac{1-4iz}{L^2(z)}|r^2+i\zeta(z)|}, \quad L(z) = \sqrt{1+16z^2}, \quad \zeta = -\frac{1}{2} \arctan(4z).$$

More generally, (15.71) admits the *Laguerre-Gaussian* vortex beams

$$\psi_{\text{LG}}^{\text{vortex}}(z, r, \theta) := \frac{1}{L(z)} \left(\frac{r}{L(z)} \right)^m e^{-\frac{1-4iz}{L^2(z)}|r^2+i\zeta(z)|} e^{im\theta}.$$

It is easy to see that if $\psi = A(z, r)e^{im\theta}$ is a vortex solution of (15.71), then so is $\psi = A(z, r)\cos(m\theta)$. Therefore,

$$\psi_{\text{LG}}^{\text{necklace}} := \frac{1}{L(z)} \left(\frac{r}{L(z)} \right)^m e^{-\frac{1-4iz}{L^2(z)}|r^2+i\zeta(z)|} \cos(m\theta)$$

is a solution of (15.71). Whereas the amplitude of $\psi_{\text{LG}}^{\text{vortex}}$ is radial, that of $\psi_{\text{LG}}^{\text{necklace}}$ has a $|\cos(m\theta)|$ dependence. Therefore, $|\psi_{\text{LG}}^{\text{necklace}}|$ attains its maximum at the $2m$ points

$$(r_j, \theta_j) = \left(r_M(z), \frac{j\pi}{m} \right), \quad r_M(z) := \arg \max_r |\psi_{\text{LG}}^{\text{vortex}}|, \quad j = 1, \dots, 2m.$$

These $2m$ peaks are equally distributed along an expanding circle of radius $r_M(z) = r_M(0)L(z)$, and adjacent peaks have a π phase difference.

In nonlinear propagation, it is no longer true that if $\psi = A(z, r)e^{im\theta}$ is a vortex solution of the NLS, then so is $\psi = A(z, r)\cos(m\theta)$. Nevertheless, the NLS admits solutions that have a structure of a “necklace with $2m$ anti-phase pearls”:

Lemma 15.34 *Let $\psi(z, r, \theta)$ be a solution of the NLS (15.4). If*

$$\psi_0(r, \theta) = f(r) \cos(m\theta), \quad (15.72)$$

then ψ is invariant under rotations by $\frac{2\pi}{m}$, i.e., $\psi(z, r, \theta) = \psi(z, r, \theta + \frac{2\pi}{m})$. In addition, ψ is antisymmetric with respect to the $2m$ rays $\theta \equiv \tilde{\Theta}_j$, i.e.,

$$\psi(z, r, \tilde{\Theta}_j + \theta) = -\psi(z, r, \tilde{\Theta}_j + \theta), \quad \tilde{\Theta}_j := \frac{(\frac{1}{2} + j)\pi}{m}, \quad j = 1, \dots, 2m.$$

In particular, $\psi(z, r, \tilde{\Theta}_j) \equiv 0$ for $j = 1, \dots, 2m$.

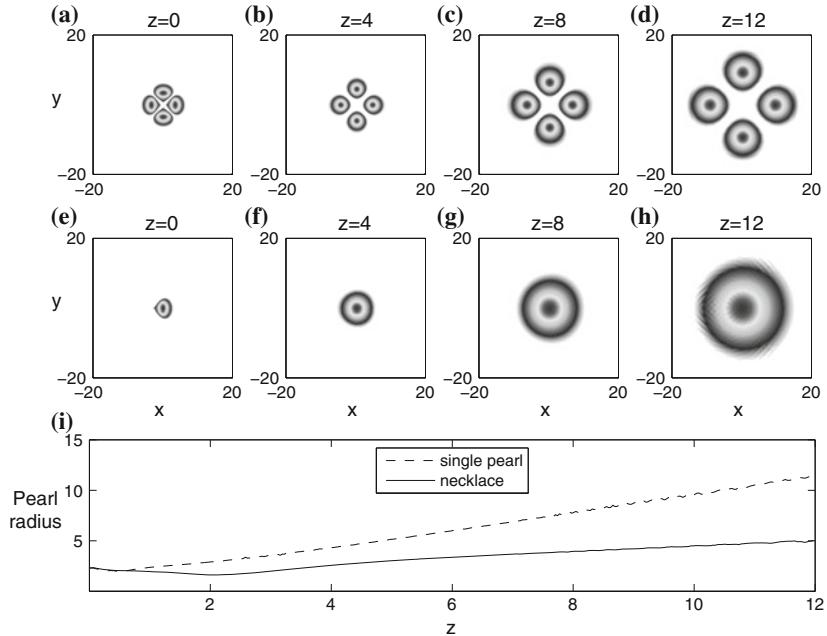


Fig. 15.17 The NLS (15.4) with $\psi_0 = \sqrt{2} \operatorname{sech}(r - 3.4) \cos(2\theta)$. **a–d** Contour plots of $|\psi|$ at different distances. **e–h** The same plots when ψ_0 consists of a single pearl. **i** Radius of a single pearl as a function of z , for the 4-pearl necklace (solid), and for the single pearl (dashes)

Exercise 15.3 Prove Lemma 15.34.

Lemma 15.34 shows that the repulsion between adjacent out-of-phase pearls “induces” a Dirichlet boundary condition on the ray half-way in-between. Because a Dirichlet boundary condition is reflecting (Sect. 16.1), there is no interaction between adjacent pearls (beams). Hence, the dynamics of the j th pearl is governed by the NLS (15.4) in the j th sector $\tilde{\Theta}_j < \theta < \tilde{\Theta}_{j+1}$, subject to Dirichlet boundary conditions on the rays $\theta \equiv \tilde{\Theta}_j$ and $\theta \equiv \tilde{\Theta}_{j+1}$. In particular, the solution preserves its necklace structure.

If the power of each pearl is above P_{cr} , then generically it collapses at a finite distance. In that case, the solution collapses simultaneously at $2m$ points. If, however, the pearl power is below P_{cr} , then it scatters as $z \rightarrow \infty$. This scattering is slower than for a single pearl, since the reflecting boundaries (i.e., the repulsion by adjacent out-of-phase pearls) slows down the pearl expansion. In particular, if one sets the power of each pearl to be slightly below P_{cr} , diffraction is almost balanced by the Kerr nonlinearity and the repulsion by neighboring out-of-phase pearls, and so the expansion is much slower than for a single pearl, see Fig. 15.17. This setup was first proposed by Soljacic et al. [243] as a way to achieve stable propagation in a bulk Kerr medium over long distances. Necklace beams in a Kerr medium were observed experimentally by Grow et al. [121].

Let us briefly discuss the stability of necklace beams. By Lemma 15.34, so long that the initial condition is of the form (15.72), the necklace structure is preserved. Hence, the necklace structure can only be destroyed by perturbations that are not of the form (15.72). Such “azimuthal” perturbations break the antisymmetry with respect to the rays $\theta \equiv \tilde{\Theta}_j$, and thus lead to power transfer between adjacent pearls. Numerical simulations suggest that necklace beams are more stable under azimuthal perturbations than vortex beams [121, 243].

Remark See Sect. 16.4.7 for necklace beams on bounded domains.

Chapter 16

NLS on a Bounded Domain

In this chapter we study the focusing NLS on a bounded domain $\Omega \subset \mathbb{R}^d$

$$i\psi_z(z, \mathbf{x}) + \Delta\psi + |\psi|^{2\sigma}\psi = 0, \quad \mathbf{x} \in \Omega, \quad z \geq 0, \quad (16.1a)$$

subject to the Dirichlet boundary condition

$$\psi(z, \mathbf{x}) = 0, \quad \mathbf{x} \in \partial\Omega, \quad z \geq 0, \quad (16.1b)$$

and the initial condition

$$\psi(0, \mathbf{x}) = \psi_0(\mathbf{x}), \quad \mathbf{x} \in \Omega. \quad (16.1c)$$

We assume that the domain Ω is smooth and convex, and that σ is in the H^1 -subcritical regime (5.2). As always, we pay a special attention to the *critical* NLS on a bounded domain

$$i\psi_z(z, \mathbf{x}) + \Delta\psi + |\psi|^{\frac{4}{d}}\psi = 0, \quad \mathbf{x} \in \Omega, \quad z \geq 0, \quad (16.2a)$$

subject to

$$\psi(z, \mathbf{x}) = 0, \quad \mathbf{x} \in \partial\Omega, \quad z \geq 0, \quad (16.2b)$$

and

$$\psi(0, \mathbf{x}) = \psi_0(\mathbf{x}), \quad \mathbf{x} \in \Omega. \quad (16.2c)$$

In optics, a Dirichlet boundary condition models a boundary (interface) that reflects back all radiation. Since a reflecting boundary works “together” with the focusing nonlinearity and “against” (the defocusing) diffraction, it lowers the threshold power for collapse P_{th} , and it has a stabilizing effect on solitary waves. A reflecting boundary has no effect, however, on the behavior near the singularity, because NLS blowup is a *local* phenomenon. Thus, in the critical case the power concentration property still holds, and the blowup profile and blowup rate are the same as on unbounded domains.

16.1 Physical Motivation

In Chap. 1 we saw that the two-dimensional cubic NLS

$$i\psi_z(z, x, y) + \Delta\psi + |\psi|^2\psi = 0, \quad \Delta = \frac{\partial^2}{\partial x^2} + \frac{\partial^2}{\partial y^2} \quad (16.3)$$

models propagation of intense laser beams in a bulk Kerr medium. It is usually assumed that the Kerr medium extends for $-\infty < x, y < \infty$. This is not the case, however, when the beam propagates in a hollow-core fiber filled with a noble gas.¹ Because of the difference between the index of refraction of the fiber walls and of the gas, when the fiber diameter is much greater than the beam wavelength, the walls reflect back almost all radiation [168].² Therefore, to leading order, one can assume that the electric field $\vec{\mathcal{E}}$ outside the fiber is identically zero. Hence, so is the electric induction field $\vec{\mathcal{D}}$. Consequently, from the continuity of the tangential component of $\vec{\mathcal{E}}$ and of the normal component of $\vec{\mathcal{D}}$ across interfaces [134], it follows that $\vec{\mathcal{E}}$, hence ψ , is identically zero at the fiber walls.

We recall that

$$\frac{d}{dz} \int_{\Omega} |\psi|^2 d\mathbf{x} = \int_{\partial\Omega} \mathbf{J} \cdot \mathbf{n} ds,$$

where $\mathbf{J} = i(\psi^* \nabla \psi - \psi \nabla \psi^*)$ is the power flux density and \mathbf{n} is the outward unit normal to $\partial\Omega$ (Sect. 5.3). Therefore, the boundary condition $\psi \equiv 0$ implies that power does not radiate through the boundary.

Conclusion 16.1 *A Dirichlet boundary condition in the Schrödinger equation reflects back all radiation that reaches the boundary.*

In light of the above, propagation of laser beams in hollow-core fibers can be modeled by the NLS on a bounded domain $\Omega \subset \mathbb{R}^2$

$$i\psi_z(z, x, y) + \Delta\psi + |\psi|^2\psi = 0, \quad (x, y) \in \Omega, \quad z \geq 0, \quad (16.4a)$$

subject to Dirichlet boundary conditions at the fiber walls

$$\psi(z, x, y) = 0, \quad (x, y) \in \partial\Omega, \quad z \geq 0, \quad (16.4b)$$

and

$$\psi(0, x, y) = \psi_0(x, y), \quad (x, y) \in \Omega. \quad (16.4c)$$

¹ A noble gas has a pure $\chi^{(3)}$ Kerr nonlinearity [266], whose magnitude can be controlled by varying the gas pressure.

² This is a consequence of Snell's law, see Sects. 2.2.2 and 2.2.3.

The domain Ω is typically the circle $B_{r_f} := \{0 \leq r \leq r_f\}$, where $r = \sqrt{x^2 + y^2}$ and r_f is the fiber radius. In this case, one can look for radial solutions, which satisfy

$$i\psi_z(z, r) + \psi_{rr} + \frac{1}{r}\psi_r + |\psi|^2\psi = 0, \quad 0 < r < r_f, \quad z \geq 0,$$

subject to

$$\psi_r(z, 0) = 0, \quad \psi(z, r_f) = 0, \quad z \geq 0,$$

and

$$\psi(0, r) = \psi_0(r), \quad 0 \leq r \leq r_f.$$

16.2 Numerical Motivation

When the NLS in free space is solved numerically, the computational domain has to be truncated. Therefore, one needs to impose a boundary condition at the boundary of the computational domain. A common approach is to impose a Dirichlet boundary condition, in which case one ends up computing a solution of (16.1). Therefore, *the NLS on a bounded domain with Dirichlet boundary conditions arises in numerical simulations of the free-space NLS*.

The main advantage of the Dirichlet boundary condition is that it is simple to implement. Unfortunately, it is doing exactly the opposite from what it is supposed to do, namely, it reflects back all radiation that reaches the boundary of the computational domain, rather than let it go through. See Sect. 29.3 for further discussion.

16.3 Invariance and Symmetries

In this chapter, most L^p and H^1 norms are taken over a domain $\Omega \subset \mathbb{R}^d$:

Definition 16.1 (L^p and H^1 norms on a domain) *The L^p and H^1 norms of a function $f(\mathbf{x})$ on a domain $\Omega \subset \mathbb{R}^d$ are*

$$\|f\|_{L^p(\Omega)} := \begin{cases} \left(\int_{\Omega} |f(\mathbf{x})|^p d\mathbf{x} \right)^{\frac{1}{p}}, & \text{if } 1 \leq p < \infty, \\ \sup_{\mathbf{x} \in \Omega} |f(\mathbf{x})|, & \text{if } p = \infty, \end{cases}$$

and $\|f\|_{H^1(\Omega)} := \left(\|f\|_{L^2(\Omega)}^2 + \|\nabla f\|_{L^2(\Omega)}^2 \right)^{\frac{1}{2}}$.

We consider solutions $\psi(z) \in H_0^1(\Omega)$, namely, solutions that vanish on $\partial\Omega$, see (16.1b), and are in $H^1(\Omega)$, i.e., $\|\psi(z)\|_{H^1(\Omega)} < \infty$.

As in free space (Sect. 5.3), the NLS (16.1) conserves the power, i.e.,

$$\|\psi\|_{L^2(\Omega)}^2 \equiv \|\psi_0\|_{L^2(\Omega)}^2 \quad (16.5)$$

and the Hamiltonian, i.e.,

$$H_\Omega(\psi) \equiv H_\Omega(\psi_0), \quad H_\Omega(\psi) := \|\nabla\psi\|_{L^2(\Omega)}^2 - \frac{1}{\sigma+1} \|\psi\|_{L^{2\sigma+2}(\Omega)}^{2\sigma+2}. \quad (16.6)$$

Unlike in free space, linear momentum is not conserved, since any radiation that reaches the boundary is reflected backwards.

As in free space (Sect. 8.1), the following transformations leave the NLS (16.1) on a bounded domain invariant:

1. Axial translations: $\psi(z, \mathbf{x}) \rightarrow \psi(z - z_0, \mathbf{x})$.
2. Phase shifts: $\psi \rightarrow \psi e^{i\theta}$ with θ real.

Because of the Dirichlet boundary condition, however, spatial translation, the Galilean transformation, the dilation transformation, and in the critical case the lens transformation, do not leave (16.1) invariant. The absence of the last two symmetries, which play such an important role in NLS theory, is related to many of the differences between self-focusing in free space and on bounded domains.

16.4 Solitary Waves

The NLS (16.1) on a bounded domain admits the solitary-wave solutions $\psi_\omega^{\text{solitary}} = e^{i\omega z} Q_\omega(\mathbf{x})$, where Q_ω is a real function and ω is a real number. The equation for Q_ω is

$$\Delta Q_\omega(\mathbf{x}) - \omega Q_\omega + |Q_\omega|^{2\sigma} Q_\omega = 0, \quad \mathbf{x} \in \Omega, \quad (16.7a)$$

$$Q_\omega(\mathbf{x}) = 0, \quad \mathbf{x} \in \partial\Omega. \quad (16.7b)$$

In free space, a necessary condition for the existence of solitary waves $\psi_\omega^{\text{solitary}} = e^{i\omega z} R_\omega(\mathbf{x})$ in H^1 is $\omega > 0$, see Lemma 6.1. This condition follows from the requirement that R_ω decays to zero sufficiently fast as $|\mathbf{x}| \rightarrow \infty$. This requirement does not exist on bounded domains. Indeed, on bounded domains the n th state $Q_\omega^{(n)}$ exists for $\omega_n \leq \omega < \infty$ (Sect. 16.4.4). Since $\lim_{n \rightarrow \infty} \omega_n = -\infty$ (Sect. 16.4.3), ω can assume negative values with arbitrarily large absolute values.

The dependence of Q_ω on ω is not as simple as in free space where $R_\omega(\mathbf{x}) = \omega^{\frac{1}{2\sigma}} R_{\omega=1} \left(\omega^{\frac{1}{2}} \mathbf{x} \right)$, see (6.6). Indeed, because of the Dirichlet boundary condition,

$$Q_\omega(\mathbf{x}) \neq \omega^{\frac{1}{2\sigma}} Q_{\omega=1} \left(\omega^{\frac{1}{2}} \mathbf{x} \right).$$

Consequently, we cannot set $\omega = 1$ “without loss of generality”. Nevertheless, as in free space, as have

Lemma 16.1 *Let $Q_\omega(\mathbf{x})$ be a solution of (16.7). Then*

$$\frac{d}{d\omega} H_\Omega(Q_\omega) = -\omega \frac{d}{d\omega} \|Q_\omega\|_{L^2(\Omega)}^2.$$

Proof The proof is the same as in Lemma 6.2. Note that because ψ vanishes at the boundary, there is no contribution from boundary integrals in the integration by parts. \square

16.4.1 Pohozaev Identities

The Pohozaev identities for NLS solitary waves on a bounded domain are as follows.

Lemma 16.2 (Pohozaev identities) *Let $Q_\omega(\mathbf{x})$ be a solution of (16.7) in $H_0^1(\Omega)$. Then*

$$\begin{aligned}\omega \|Q_\omega\|_{L^2(\Omega)}^2 &= \frac{2-\sigma(d-2)}{2(\sigma+1)} \|Q_\omega\|_{L^{2\sigma+2}(\Omega)}^{2\sigma+2} - \frac{1}{2} \int_{\partial\Omega} (\mathbf{x} \cdot \mathbf{n}) (\nabla Q_\omega \cdot \mathbf{n})^2 ds, \\ \|\nabla Q_\omega\|_{L^2(\Omega)}^2 &= \frac{d\sigma}{2(\sigma+1)} \|Q_\omega\|_{L^{2\sigma+2}(\Omega)}^{2\sigma+2} + \frac{1}{2} \int_{\partial\Omega} (\mathbf{x} \cdot \mathbf{n}) (\nabla Q_\omega \cdot \mathbf{n})^2 ds,\end{aligned}$$

where \mathbf{n} is the outward unit normal to $\partial\Omega$.

Proof The proof is the same as that of Lemma 6.3, except that we do not set $\omega = 1$, and we keep nonzero contributions from boundary integrals in the integration by parts. To do that, we first note that because $Q_\omega \equiv 0$ on $\partial\Omega$, ∇Q_ω points in the direction of \mathbf{n} on $\partial\Omega$. Therefore, $|\nabla Q_\omega \cdot \mathbf{n}| = |\nabla Q_\omega|$ and

$$\nabla Q_\omega(\mathbf{x}) = (\nabla Q_\omega \cdot \mathbf{n}) \mathbf{n}, \quad \mathbf{x} \in \partial\Omega. \quad (16.8)$$

Relation (6.8) on bounded domains reads

$$\|\nabla Q_\omega\|_{L^2(\Omega)}^2 + \omega \|Q_\omega\|_{L^2(\Omega)}^2 = \|Q_\omega\|_{L^{2\sigma+2}(\Omega)}^{2\sigma+2}.$$

The first nonzero contribution from the boundary integrals comes from integration by parts in relation (6.9) of the term

$$\int_{\Omega} (\mathbf{x} \cdot \nabla Q_\omega) \Delta Q_\omega d\mathbf{x} = \int_{\partial\Omega} (\mathbf{x} \cdot \nabla Q_\omega) (\nabla Q_\omega \cdot \mathbf{n}) ds - \int_{\Omega} \nabla(\mathbf{x} \cdot \nabla Q_\omega) \cdot \nabla Q_\omega d\mathbf{x}.$$

The second nonzero contribution from boundary integrals comes from integration by parts in relation (6.11) of the term

$$-\int_{\Omega} (\mathbf{x} \cdot \nabla) \left(\frac{(\nabla Q_{\omega})^2}{2} \right) d\mathbf{x} = -\int_{\partial\Omega} (\mathbf{x} \cdot \mathbf{n}) \frac{(\nabla Q_{\omega})^2}{2} d\mathbf{s} + \frac{d}{2} \int_{\Omega} (\nabla Q_{\omega})^2 d\mathbf{x}.$$

By (16.8),

$$\int_{\partial\Omega} (\mathbf{x} \cdot \nabla Q_{\omega})(\nabla Q_{\omega} \cdot \mathbf{n}) d\mathbf{s} = \int_{\partial\Omega} (\mathbf{x} \cdot \mathbf{n}) (\nabla Q_{\omega} \cdot \mathbf{n})^2 d\mathbf{s} = \int_{\partial\Omega} (\mathbf{x} \cdot \mathbf{n})(\nabla Q_{\omega})^2 d\mathbf{s}.$$

Hence, on bounded domains, relation (6.12) reads

$$\begin{aligned} & \frac{d-2}{2} \|\nabla Q_{\omega}\|_{L^2(\Omega)}^2 + \frac{d}{2} \omega \|Q_{\omega}\|_{L^2(\Omega)}^2 + \frac{1}{2} \int_{\partial\Omega} (\mathbf{x} \cdot \mathbf{n}) (\nabla Q_{\omega} \cdot \mathbf{n})^2 d\mathbf{s} \\ &= \frac{d}{2(\sigma+1)} \|Q_{\omega}\|_{L^{2\sigma+2}(\Omega)}^{2\sigma+2}. \end{aligned}$$

The rest of the proof is the same as that of Lemma 6.3. \square

From the second Pohozaev identity in Lemma 16.2 follows

Corollary 16.1 *Let $Q_{\omega}(\mathbf{x})$ be a solution of (16.7) in $H_0^1(\Omega)$. Then*

$$H_{\Omega}(Q_{\omega}) = \frac{d\sigma-2}{2\sigma+2} \|Q_{\omega}\|_{L^{2\sigma+2}(\Omega)}^{2\sigma+2} + \frac{1}{2} \int_{\partial\Omega} (\mathbf{x} \cdot \mathbf{n}) (\nabla Q_{\omega} \cdot \mathbf{n})^2 d\mathbf{s}. \quad (16.9)$$

Remark A different proof of (16.9) is given in Corollary 16.7.

To determine the sign of the boundary integral, we first prove

Lemma 16.3 *Let $Q_{\omega}(\mathbf{x})$ be a solution of (16.7) in $H_0^1(\Omega)$. Then for any $\mathbf{x}_0 \in \mathbb{R}^d$,*

$$\int_{\partial\Omega} ((\mathbf{x} - \mathbf{x}_0) \cdot \mathbf{n}) (\nabla Q_{\omega} \cdot \mathbf{n})^2 d\mathbf{s} = \int_{\partial\Omega} (\mathbf{x} \cdot \mathbf{n}) (\nabla Q_{\omega} \cdot \mathbf{n})^2 d\mathbf{s}$$

or, equivalently, $\int_{\partial\Omega} (\mathbf{x}_0 \cdot \mathbf{n}) (\nabla Q_{\omega} \cdot \mathbf{n})^2 d\mathbf{s} = 0$.

Proof Denote

$$\tilde{Q}_{\omega}(\mathbf{x}) := Q_{\omega}(\mathbf{x} + \mathbf{x}_0), \quad \tilde{\Omega} := \{\mathbf{x} \mid \mathbf{x} + \mathbf{x}_0 \in \Omega\}. \quad (16.10)$$

Clearly, $\tilde{Q}_{\omega}(\mathbf{x})$ is a solution of (16.7) in $H_0^1(\tilde{\Omega})$. Therefore, application of the first Pohozaev identity in Lemma 16.2 to \tilde{Q}_{ω} gives

$$\omega \|\tilde{Q}_{\omega}\|_{L^2(\tilde{\Omega})}^2 = \frac{2-\sigma(d-2)}{2(\sigma+1)} \|\tilde{Q}_{\omega}\|_{L^{2\sigma+2}(\tilde{\Omega})}^{2\sigma+2} - \frac{1}{2} \int_{\partial\tilde{\Omega}} (\mathbf{x} \cdot \mathbf{n}) (\nabla \tilde{Q}_{\omega}(\mathbf{x}) \cdot \mathbf{n})^2 d\mathbf{s}.$$

Using (16.10), we can rewrite this identity as

$$\omega \|Q_\omega\|_{L^2(\Omega)}^2 = \frac{2-\sigma(d-2)}{2(\sigma+1)} \|Q_\omega\|_{L^{2\sigma+2}(\Omega)}^{2\sigma+2} - \frac{1}{2} \int_{\partial\Omega} ((\mathbf{x} - \mathbf{x}_0) \cdot \mathbf{n}) (\nabla Q_\omega(\mathbf{x}) \cdot \mathbf{n})^2 ds.$$

The result follows from comparison of this identity with the first Pohozaev identity in Lemma 16.2. \square

Remark Lemma 16.3 does not hold for arbitrary functions in H_0^1 , but only for solutions of (16.7), see Sect. 16.8.1.

Lemma 16.4 *Let $Q_\omega(\mathbf{x})$ be a nontrivial solution of (16.7) in $H_0^1(\Omega)$. If Ω is convex, then*

$$\int_{\partial\Omega} (\mathbf{x} \cdot \mathbf{n}) (\nabla Q_\omega \cdot \mathbf{n})^2 ds > 0.$$

Proof Let $\mathbf{x}_0 \in \Omega$. Since Ω is convex, $(\mathbf{x} - \mathbf{x}_0) \cdot \mathbf{n} > 0$ for all $\mathbf{x} \in \partial\Omega$. Therefore, $\int_{\partial\Omega} ((\mathbf{x} - \mathbf{x}_0) \cdot \mathbf{n}) (\nabla Q_\omega \cdot \mathbf{n})^2 ds > 0$. Hence, the result follows from Lemma 16.3. \square

Remark The positive sign of the boundary integral reflects the fact that the boundary is reflecting (Sect. 16.8.1).

16.4.2 Critical Case

In the critical case, the Hamiltonian of the free-space solitary waves is zero (Corollary 6.4). On bounded domains, however, the Hamiltonian is positive:

Corollary 16.2 *Let $Q_\omega(\mathbf{x})$ be a solution of (16.7), let $\sigma d = 2$, and let Ω be convex. Then*

$$H_\Omega(Q_\omega) = \frac{1}{2} \int_{\partial\Omega} (\mathbf{x} \cdot \mathbf{n}) (\nabla Q_\omega \cdot \mathbf{n})^2 ds > 0.$$

Proof This follows from Corollary 16.1 and Lemma 16.4. \square

This result has implications to the stability of the critical solitary waves (Sect. 16.5.2).

16.4.3 Linear Solitary Waves

Consider the linear Schrödinger equation on a bounded domain

$$i\psi_z(z, \mathbf{x}) + \Delta\psi = 0, \quad \mathbf{x} \in \Omega, \quad z \geq 0, \tag{16.11a}$$

with the Dirichlet boundary condition

$$\psi(z, \mathbf{x}) = 0, \quad \mathbf{x} \in \partial\Omega, \quad z \geq 0. \quad (16.11b)$$

This equation admits the solitary-wave solutions $\psi = e^{i\omega z} Y_\omega(\mathbf{x})$, where $Y_\omega(\mathbf{x})$ is the solution of

$$\Delta Y_\omega(\mathbf{x}) - \omega Y_\omega = 0, \quad \mathbf{x} \in \Omega, \quad (16.12a)$$

subject to

$$Y_\omega(\mathbf{x}) = 0, \quad \mathbf{x} \in \partial\Omega. \quad (16.12b)$$

Equation (16.12) is a linear eigenvalue problem. It has a countable number of negative eigenvalues $\{\omega_n\}_{n=0}^\infty$ and eigenfunctions $\{Y^{(n)}(\mathbf{x})\}_{n=0}^\infty$, such that³

$$0 > \omega_0 > \omega_1 \geq \omega_2 \geq \dots, \quad \lim_{n \rightarrow \infty} \omega_n = -\infty.$$

In the special case where Ω is the d -dimensional sphere $B_{r_f} := \{|\mathbf{x}| < r_f\}$, we can look for radial eigenfunctions, which are the solutions of

$$Y''(r) + \frac{d-1}{r} Y' = \omega Y, \quad 0 < r < r_f, \quad (16.13a)$$

$$Y'(0) = 0, \quad Y(r_f) = 0. \quad (16.13b)$$

By Sturm-Liouville theory, all eigenvalues are simple, and $Y^{(n)}(r)$ has n zeros in $(0, r_f)$. In particular, in the two-dimensional radial case, $Y^{(n)}(r) = J_0(k_n r / r_f)$, where $J_0(r)$ is the Bessel function of order zero of the first kind, k_n is the n th positive root of $J_0(r)$, and $\omega_n = -k_n^2 / r_f^2$.⁴

Remark Linear solitary waves on a bounded domain represent a perfect balance between diffraction and the reflecting (i.e., focusing) boundary. In free space, there is no boundary to counter diffraction. Consequently, the free-space linear Schrödinger equation does not admit finite-power solitary waves.⁵

16.4.4 Large-Amplitude and Small-Amplitude Regimes

Following Fibich and Merle [89], we consider two asymptotic regimes for the solitary waves of (16.7).

³ To see that all eigenvalues are negative, multiply (16.12a) by Y_ω and integrate by parts.

⁴ Thus, $k_0 \approx 2.405$, $k_1 \approx 5.520$, $k_2 \approx 8.654$, etc.

⁵ The free-space two-dimensional linear Schrödinger equation admits the *Bessel beams* $\psi = e^{i\omega z} J_0(\sqrt{-\omega}r)$ for $-\infty < \omega < 0$. These solitary waves, however, have infinite power, since $J_0(r) \sim (\frac{2}{\pi r})^{\frac{1}{2}} \cos(r - \frac{\pi}{4})$ as $r \rightarrow \infty$.

Large-Amplitude Regime ($\omega \gg 1$)

Let $\mathbf{x}_0(\omega) \in \Omega$ be the point where Q_ω attains its global maximum in Ω . Therefore, $Q_\omega(\mathbf{x} + \mathbf{x}_0(\omega))$ attains its global maximum at $\mathbf{x} = 0$. Let

$$Q_\omega(\mathbf{x} + \mathbf{x}_0) = \omega^{\frac{1}{2\sigma}} F(\sqrt{\omega}\mathbf{x}). \quad (16.14)$$

Then $F(\mathbf{x})$ is a solution of

$$\Delta F(\mathbf{x}) - F + |F|^{2\sigma} F = 0, \quad \mathbf{x} \in \Omega_{\frac{1}{\omega^2}} := \left\{ \sqrt{\omega}\mathbf{x} \mid \mathbf{x} + \mathbf{x}_0(\omega) \in \Omega \right\},$$

subject to

$$F(\mathbf{x}) = 0, \quad \mathbf{x} \in \partial\Omega_{\frac{1}{\omega^2}},$$

which attains its global maximum at $\mathbf{x} = 0$. Since $\lim_{\omega \rightarrow \infty} \Omega_{\frac{1}{\omega^2}} = \mathbb{R}^d$, we have that $\lim_{\omega \rightarrow \infty} F(\mathbf{x}) = R(\mathbf{x})$, where $R(\mathbf{x})$ is a free-space solution of

$$\Delta R(\mathbf{x}) - R + |R|^{2\sigma} R = 0, \quad \mathbf{x} \in \mathbb{R}^d \quad (16.15)$$

which attains its global maximum at $\mathbf{x} = 0$. We thus have

Lemma 16.5 *Equation (16.7) admits the large-amplitude solitary waves*

$$Q_\omega(\mathbf{x}) \sim R_\omega(\mathbf{x} - \mathbf{x}_0(\omega)) := \omega^{\frac{1}{2\sigma}} R(\sqrt{\omega}(\mathbf{x} - \mathbf{x}_0(\omega))), \quad \omega \gg 1, \quad (16.16)$$

where $\mathbf{x}_0(\omega) \in \Omega$, and $R(\mathbf{x})$ is a solution of (16.15) which attains its global maximum at $\mathbf{x} = 0$.

Thus, large-amplitude solitary waves are localized, hence they do not “feel” the boundary, which is why they are similar to the free-space solitary waves.

Corollary 16.3 *Let Q_ω be given by (16.16). Then*

$$\|Q_\omega\|_{L^2(\Omega)}^2 \sim \omega^{\frac{2-\sigma d}{2\sigma}} \|R\|_{L^2(\mathbb{R}^d)}^2, \quad \omega \rightarrow \infty.$$

In particular,

1. In the subcritical case $\sigma d < 2$, $\frac{d}{d\omega} \|Q_\omega\|_{L^2(\Omega)}^2 > 0$ as $\omega \rightarrow \infty$.
2. In the supercritical case $\sigma d > 2$, $\frac{d}{d\omega} \|Q_\omega\|_{L^2(\Omega)}^2 < 0$ as $\omega \rightarrow \infty$.

Remark In Lemma (16.25) we will see that in the critical case $\sigma d = 2$, $\frac{d}{d\omega} \|Q_\omega\|_{L^2(\Omega)}^2 > 0$ as $\omega \rightarrow \infty$.

Corollary 16.4 Let Q_ω be given by (16.16) and $\sigma d = 2$. Then

$$\lim_{\omega \rightarrow \infty} |Q_\omega(\mathbf{x})|^2 = \|R\|_{L^2(\mathbb{R}^d)}^2 \delta(\mathbf{x} - \mathbf{x}_0^\infty), \quad \mathbf{x}_0^\infty := \lim_{\omega \rightarrow \infty} \mathbf{x}_0(\omega).$$

Proof By Lemma 16.5, $Q_\omega(\mathbf{x}) \sim \omega^{\frac{d}{2}} R(\sqrt{\omega}(\mathbf{x} - \mathbf{x}_0(\omega)))$. Therefore, the result follows. \square

Small-Amplitude (Weakly-Nonlinear) Regime

When the nonlinearity is weak, $Q_\omega(\mathbf{x}) \sim a(\omega)Y_\omega(\mathbf{x})$, where $Y_\omega(\mathbf{x})$ is an eigenfunction of (16.12). The following lemma characterizes the weakly-nonlinear solitary waves that bifurcate from $Y^{(n)}$:

Lemma 16.6 Equation (16.7) admits the weakly-nonlinear solitary waves

$$Q_\omega^{(n)}(\mathbf{x}) \sim (\omega - \omega_n)^{\frac{1}{2\sigma}} c_n^{\frac{1}{2\sigma}} Y^{(n)}(\mathbf{x}), \quad 0 < \omega - \omega_n \ll \omega_n,$$

$$\text{where } c_n = \frac{\|Y^{(n)}\|_{L^2(\Omega)}^2}{\|Y^{(n)}\|_{L^{2\sigma+2}(\Omega)}^{2\sigma+2}}.$$

Proof We substitute in (16.7)

$$Q_\omega^{(n)}(\mathbf{x}; \omega) \sim S_0(\mathbf{x}; \omega) + S_1(\mathbf{x}; \omega) + \dots, \quad S_0 \gg S_1 \gg \dots,$$

and

$$\omega = \omega_n + (\omega - \omega_n), \quad \omega - \omega_n \ll \omega_n.$$

The leading-order equation is

$$\Delta S_0 - \omega_n S_0 = 0,$$

whose solution is $S_0 = a(\omega)Y^{(n)}(\mathbf{x})$. The equation for next-order terms is

$$\Delta S_1 - \omega_n S_1 = (\omega - \omega_n)S_0 - |S_0|^{2\sigma} S_0. \quad (16.17)$$

Since S_0 is in the kernel of the left-hand side, the solvability condition for (16.17) is that S_0 is orthogonal to the right-hand side,⁶ i.e.,

$$(\omega - \omega_n)\|S_0\|_{L^2(\Omega)}^2 - \|S_0\|_{L^{2\sigma+2}(\Omega)}^{2\sigma+2} = 0.$$

⁶ To see that, multiply (16.17) by S_0 , integrate over Ω , and use integration by parts to show that the integral over the left-hand side vanishes.

Therefore, $\omega - \omega_n > 0$ and

$$(\omega - \omega_n) a^2(\omega) \|Y^{(n)}\|_{L^2(\Omega)}^2 = a^{2\sigma+2}(\omega) \|Y^{(n)}\|_{L^{2\sigma+2}(\Omega)}^{2\sigma+2}.$$

Hence, $a^{2\sigma}(\omega) = (\omega - \omega_n)c_n$, from which the result follows. \square

Thus, the amplitude of weakly-nonlinear solutions goes to zero as $\omega \rightarrow \omega_n+$. The power of these small-amplitude solitary waves satisfies

$$\|Q_\omega^{(n)}\|_{L^2(\Omega)}^2 \sim (\omega - \omega_n)^{\frac{1}{\sigma}} c_n^{\frac{1}{\sigma}} \|Y^{(n)}\|_{L^2(\Omega)}^2, \quad 0 < \omega - \omega_n \ll \omega_n. \quad (16.18)$$

Hence, the power is monotonically increasing in ω , i.e.,

$$\frac{d}{d\omega} \|Q_\omega^{(n)}\|_{L^2(\Omega)}^2 > 0, \quad 0 < \omega - \omega_n \ll \omega_n, \quad (16.19)$$

and it goes to zero as $\omega \rightarrow \omega_n+$, i.e.,

$$\lim_{\omega \rightarrow \omega_n+} \|Q_\omega^{(n)}\|_{L^2(\Omega)}^2 = 0.$$

16.4.5 Radial Solitary Waves

When Ω is the d -dimensional sphere $B_{r_f} := \{|\mathbf{x}| < r_f\}$, we can look for radial solitary waves, which are the solutions of, see (16.7),

$$Q_\omega''(r) + \frac{d-1}{r} Q_\omega' - \omega Q_\omega + |Q_\omega|^{2\sigma} Q_\omega = 0, \quad 0 < r < r_f, \quad (16.20a)$$

$$Q_\omega'(0) = 0, \quad Q_\omega(r_f) = 0. \quad (16.20b)$$

As in free space (Chap. 6), we have the following results:

- For $d \geq 2$, the ODE (16.20) has a countable number of solutions $\left\{Q_\omega^{(n)}\right\}_{n=0}^\infty$. These solutions can be arranged in increasing order of the action $I_\Omega(Q_\omega) := H_\Omega(Q_\omega) + \omega \|Q_\omega\|_{L^2(\Omega)}^2$, i.e.,

$$I_\Omega(Q_\omega^{(0)}) < I_\Omega(Q_\omega^{(1)}) \leq I_\Omega(Q_\omega^{(2)}) < \dots$$

In addition, $Q_\omega^{(0)}$ is positive in $[0, r_f]$, see [21, 22].

2. For any $\omega > 0$, there exists a unique real positive solution $Q_\omega^{(0)}(r)$ to ODE (16.20), see [149].
3. All positive solutions $Q_\omega(\mathbf{x})$ of the elliptic PDE (16.7) on B_{r_f} are radial and monotonically decreasing in $r = |\mathbf{x}|$, see [110, 111].
4. By the previous three items, for any $\omega > 0$, there is a unique positive solution to PDE (16.7) on $\Omega = B_{r_f}$, which is the positive solution of ODE (16.20), and also the minimizer of I_ω among all nontrivial solutions of ODE (16.20).

By Lemma 16.5, the large-amplitude solitary waves of (16.20) satisfy

$$Q_\omega^{(n)}(r) \sim R_\omega^{(n)}(r) := \omega^{\frac{1}{2\sigma}} R^{(n)}(\sqrt{\omega}r), \quad \omega \gg 1, \quad (16.21)$$

where $R^{(n)}$ is the n th-state free-space solitary wave, which is conjectured to have n zeros (Sect. 6.4.4). Similarly, by Lemma 16.6, small-amplitude solitary waves of (16.20) can be approximated by

$$Q_\omega^{(n)}(r) \sim (\omega - \omega_n)^{\frac{1}{2\sigma}} c_n^{\frac{1}{2\sigma}} Y^{(n)}(r), \quad 0 < \omega - \omega_n \ll \omega_n,$$

where $c_n = \frac{\|Y^{(n)}\|_{L^2(\Omega)}^2}{\|Y^{(n)}\|_{L^{2\sigma+2}(\Omega)}^{2\sigma+2}}$ and $Y^{(n)}$ is the n th eigenfunction of (16.13), which has n zeros in $(0, r_f)$.

The above results suggest the following picture. The n th-state $Q_\omega^{(n)}(r)$ of (16.20) exists for $\omega_n < \omega < \infty$, and has n zeros in $(0, r_f)$. As ω increases, nonlinearity becomes more pronounced and $Q_\omega^{(n)}$ becomes more localized. As a result, the effect of the boundary decreases, hence $Q_\omega^{(n)}$ approaches the free-space solitary wave $R_\omega^{(n)}$. Going in the opposite direction, as ω decreases, the solution becomes less localized. Therefore, nonlinearity becomes weaker, whereas the effect of the reflecting boundary increases. In particular, as $\omega \rightarrow \omega_n+$, nonlinearity becomes negligible, and $Q_\omega^{(n)}$ approaches the n th eigenfunction $Y^{(n)}$ of the linear problem. This description is confirmed numerically in Fig. 16.1 for the two-dimensional cubic case.

16.4.6 Solitary Vortex Solutions

We briefly note that the two-dimensional NLS on the sphere B_{r_f} admits the *solitary vortex solutions*

$$\psi_{\text{vortex},\omega}^{\text{solitary}}(z, r, \theta) = e^{i\omega z} e^{im\theta} Q_{\omega,m}(r),$$

where $Q_{\omega,m}$ is the solution of

$$Q_{\omega,m}''(r) + \frac{1}{r} Q_{\omega,m}' - \left(\omega + \frac{m^2}{r^2} \right) Q_{\omega,m} + |Q_{\omega,m}|^{2\sigma} Q_{\omega,m} = 0, \quad 0 < r < r_f,$$

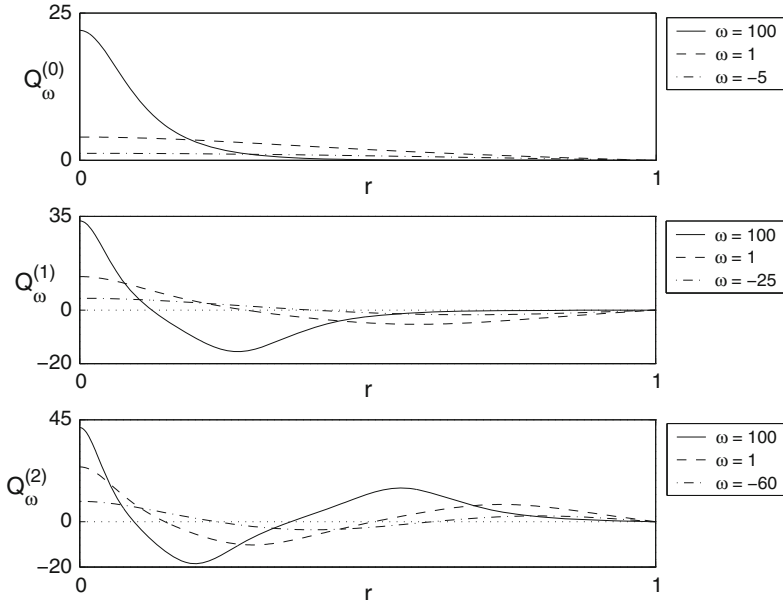


Fig. 16.1 The first three states of (16.20) with $d = 2$ and $\sigma = 1$, for various values of ω . From [89]

subject to

$$Q_{\omega,m}(r_f) = 0.$$

The properties of these solutions follow from those of the free-space solitary vortex waves (Sect. 15.2), and of the non-vortex solitary waves on the two-dimensional sphere (Sect. 16.4.5).

16.4.7 Necklace Solitary Waves

In Sect. 15.13 we considered necklace solutions of the NLS. In free space there are no necklace solitary waves, and so all necklace solutions either scatter or simultaneously collapse at $2m$ points. Necklace solitary waves, however, do exist on bounded domains. For example, let $\psi = e^{iz}Q(r, \theta)$ be a necklace solitary wave on the unit circle $B_1 = \{0 \leq r \leq 1, 0 \leq \theta \leq 2\pi\}$ with $2m$ pearls. Then Q is the solution of

$$\Delta Q(r, \theta) - Q + |Q|^2 Q = 0, \quad (r, \theta) \in B_1, \quad Q(r = 1, \theta) \equiv 0,$$

such that the global maxima and minima of Q are attained at $2m$ points equally distanced along a circle $r = r_{\text{neck}}$. Without loss of generality, assume that these extremum points are $(r_j, \theta_j) = (r_{\text{neck}}, \frac{j\pi}{m})$, where $j = 1, \dots, 2m$. Then, as in Lemma 15.34, Q is invariant under rotations by $2\pi/m$, and is antisymmetric with

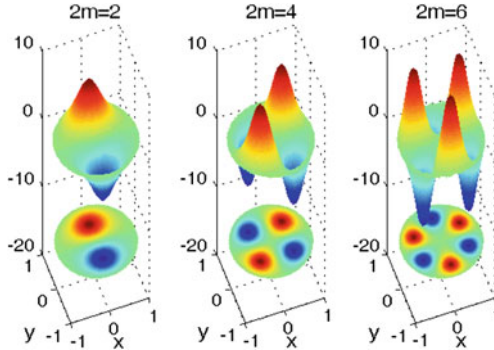


Fig. 16.2 Necklace solitary waves on the unit circle with $2m = 2, 4$, and 6 pearls, computed with the *non-spectral renormalization method* (Sect. 28.3)

respect to the rays $\theta \equiv \tilde{\Theta}_j$, where $\tilde{\Theta}_j := (\frac{1}{2} + j) \pi/m$ and $j = 1, \dots, 2m$. In particular, $Q(r, \tilde{\Theta}_j) \equiv 0$ for $j = 1, \dots, 2m$. Therefore, the j th “pearl” is the positive (or negative) solution of

$$\Delta Q - Q + |Q|^2 Q = 0, \quad (r, \theta) \in \Omega_j := \left\{ 0 \leq r \leq 1, \tilde{\Theta}_{j-1} \leq \theta \leq \tilde{\Theta}_j \right\},$$

subject to $Q \equiv 0$ on $\partial\Omega_j$. Figure 16.2 presents necklace solitary waves with 2, 4, and 6 pearls. Necklace solitary waves can also be constructed on rectangular and annular domains.

16.4.8 Critical Radial Solitary Waves

In the critical case, Eq. (16.20) reads

$$Q_\omega''(r) + \frac{d-1}{r} Q_\omega' - \omega Q_\omega + |Q_\omega|^{\frac{4}{d}} Q_\omega = 0, \quad 0 < r < r_f, \quad (16.22a)$$

$$Q_\omega'(0) = 0, \quad Q_\omega(r_f) = 0. \quad (16.22b)$$

Clearly, all the results of Sect. 16.4.5 are valid in this case. In addition, by Corollary 16.2,

$$H_\Omega(Q_\omega) = \frac{s_d}{2} r_f^d (Q_\omega'(r_f))^2 > 0, \quad (16.23)$$

where s_d is the surface area of the d -dimensional unit-sphere.

In the critical case, the dilation symmetry $R_\omega(r) = \omega^{\frac{4}{d}} R(\omega^{\frac{1}{2}} r)$ implies that the power of the free-space solitary waves is independent of ω , i.e., $\|R_\omega^{(n)}\|_2^2 = \|R^{(n)}\|_2^2$,

where $R^{(n)} := R_{\omega=1}^{(n)}$ is the n th-state solution of

$$\begin{aligned} R''(r) + \frac{d-1}{r}R' - R + |R|^{\frac{4}{d}}R = 0, \quad 0 < r < \infty, \\ R'(0) = 0, \quad \lim_{r \rightarrow \infty} R(r) = 0. \end{aligned} \tag{16.24}$$

This is not the case on bounded domains, however, where there is no such dilation symmetry. Indeed, we already saw that in the weakly-nonlinear regime

$$\frac{d}{d\omega} \|Q_\omega^{(n)}\|_{L^2(\Omega)}^2 > 0, \quad 0 < \omega - \omega_n \ll \omega_n,$$

see (16.19). We can prove a similar result in the large-amplitude regime:

Lemma 16.7 ([89]) *Let $Q_\omega^{(n)}(r)$ be the solution of (16.22) which approaches $R_\omega^{(n)}(r)$ as $\omega \rightarrow \infty$, see (16.21). Then*

$$\frac{d}{d\omega} \|Q_\omega^{(n)}\|_{L^2(B_{r_f})}^2 > 0, \quad \omega \rightarrow \infty, \tag{16.25}$$

and $\lim_{\omega \rightarrow \infty} \|Q_\omega^{(n)}\|_{L^2(B_{r_f})}^2 = \|R^{(n)}\|_2^2$, where $R^{(n)}$ is the n th-state of (16.24).

Proof By relation (16.21) with $\sigma = 2/d$, $\|Q_\omega^{(n)}\|_{L^2(B_{r_f})}^2 \rightarrow \|R_\omega^{(n)}\|_2^2 = \|R^{(n)}\|_2^2$.

In addition, by relation (16.21), $\frac{dQ_\omega^{(n)}}{dr}(r_f) \approx \omega^{\frac{1}{2\sigma} + \frac{1}{2}} \frac{dR_\omega^{(n)}}{dr}(\sqrt{\omega}r_f)$. Since $R_\omega^{(n)}(r)$ decays exponentially as $r \rightarrow \infty$ (Lemma 6.14), then $\lim_{\omega \rightarrow \infty} \frac{dQ_\omega^{(n)}}{dr}(r_f) = 0$. Therefore, by (16.23), $\lim_{\omega \rightarrow \infty} H_\Omega(Q_\omega^{(n)}) = 0$. Since the Hamiltonian is positive for $\omega < \infty$, see (16.23), this shows that there exists a sequence $\omega_k \rightarrow \infty$ such that $\frac{d}{d\omega} H_\Omega(Q_\omega^{(n)})|_{\omega=\omega_k} < 0$. Using additional arguments, Fukuizumi et al. [102] showed that

$$\frac{d}{d\omega} H_\Omega(Q_\omega^{(n)}) < 0, \quad \omega \rightarrow \infty.$$

Relation (16.25) follows from this relation and Lemma 16.1. \square

From (16.19) and Lemma 16.7 follows

Lemma 16.8 *Let $Q_\omega^{(n)}(r)$ be the n th-state of (16.22). Then*

$$\frac{d}{d\omega} \|Q_\omega^{(n)}\|_{L^2(B_{r_f})}^2 > 0 \quad \text{for } 0 < \omega - \omega_n \ll \omega_n \text{ and } 1 \ll \omega < \infty. \tag{16.26}$$

In addition,

$$\lim_{\omega \rightarrow \omega_n+} \|Q_\omega^{(n)}\|_{L^2(B_{r_f})}^2 = 0, \quad \lim_{\omega \rightarrow \infty} \|Q_\omega^{(n)}\|_{L^2(B_{r_f})}^2 = \|R^{(n)}\|_2^2. \tag{16.27}$$

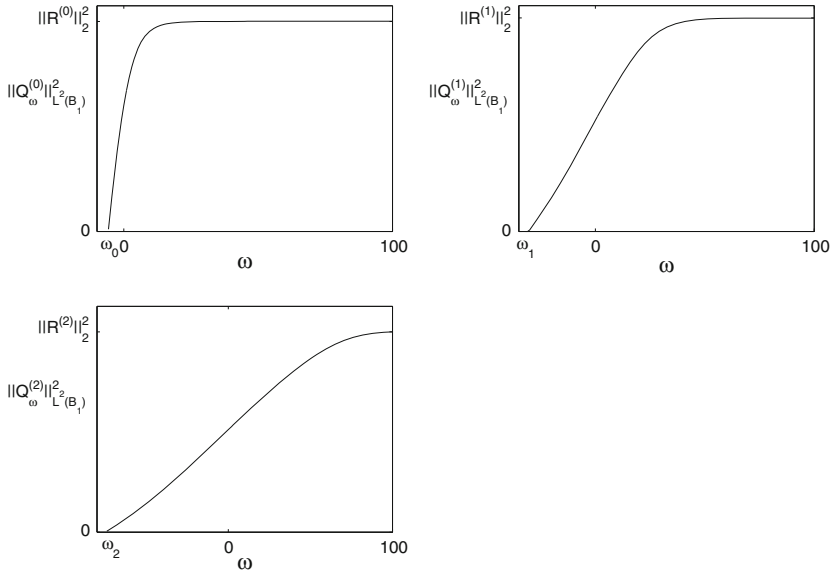


Fig. 16.3 The power of $Q_\omega^{(n)}$ as a function of ω , for the first three states of (16.22) with $d = 2$ and $\Omega = B_1$. Here, $\omega_0 \approx -5.7$, $\omega_1 \approx -32$, $\omega_2 \approx -74$, $\|R^{(0)}\|_2^2 \approx 11.7$, $\|R^{(1)}\|_2^2 \approx 77.3$, and $\|R^{(2)}\|_2^2 \approx 195$. Adapted from [89]

Numerical simulations show that in the two-dimensional critical case, $\|Q_\omega^{(n)}\|_{L^2(B_{r_f})}^2$ is monotonically increasing in ω for $\omega_n < \omega < \infty$, see Fig. 16.3. This result was rigorously proved by Fukuizumi, Hadj Salem, and Kikuchi for the one-dimensional subcritical and critical NLS:

Lemma 16.9 ([102]) *Let $d = 1$ and $0 < \sigma \leq 2$. Then*

$$\frac{d}{d\omega} \|Q_\omega^{(n)}\|_{L^2(B_{r_f})}^2 > 0, \quad \omega_n < \omega < \infty.$$

Therefore, we formulate

Conjecture 16.1 *For any d , and for any σ in the H^1 -subcritical regime,*

$$\frac{d}{d\omega} \|Q_\omega^{(n)}\|_{L^2(B_{r_f})}^2 > 0, \quad \omega_n < \omega < \infty.$$

The motivation for Conjecture 16.1 is as follows. On a bounded domain, a solitary wave represents a perfect balance between diffraction, and the combined focusing effects of the nonlinearity and the reflecting boundary. As ω increases, the solitary wave becomes more localized, hence the focusing effect of the reflecting boundaries decreases, and so the nonlinearity should be stronger in order to balance diffraction. Consequently, the power of the solitary wave increases.

Conjecture 16.1 and (16.27) imply that:

1. $0 < \|Q_\omega^{(n)}\|_{L^2(B_{r_f})}^2 < \|R^{(n)}\|_2^2$ for $\omega \in (\omega_n, \infty)$.
2. For any $P \in (0, \|R^{(n)}\|_2^2)$, there exists a unique $\omega(P) \in (\omega_n, \infty)$ such that $\|Q_{\omega(P)}^{(n)}\|_{L^2(B_{r_f})}^2 = P$.
3. The function $\omega(P)$ is monotonically increasing in P .
4. $\lim_{P \rightarrow 0+} \omega(P) = \omega_n < 0$.
5. $\lim_{P \rightarrow \|R^{(n)}\|_2^2} \omega(P) = +\infty$.

Remark In Sect. 8.4.7 we saw that in the free-space critical case, all solutions with $P < P_{\text{cr}}$ scatter as $z \rightarrow \infty$. In addition, there exist solutions with $P = P_{\text{cr}}$ for which nonlinearity exactly balances diffraction, namely, the ground-state solitary waves $\psi_\omega^{\text{solitary},(0)} = e^{i\omega z} R_\omega^{(0)}(r)$. Therefore, in the free-space critical case, the minimal power needed for nonlinearity to balance diffraction is P_{cr} . In contrast, on a bounded domain, there exist a solitary wave with power P for any $0 < P < P_{\text{cr}}$. Moreover, this is not only true for the ground state, but also for the excited states. Intuitively, this is because in free space, the nonlinearity has to balance diffraction “on its own”, whereas on a bounded domain it is “aided” by the reflecting boundary. Since the boundary can support solitary waves even without the “help” of the nonlinearity (Sect. 16.4.3), it can “easily” support nonlinear solitary waves with arbitrarily low power.

In the free-space critical case, the power and Hamiltonian of $R_\omega^{(0)}$ are independent of ω (Exercise 6.2 and Corollary 6.5). These properties are not true for the critical NLS (16.22) on B_{r_f} . Rather, we have the following variational characterization of bounded-domain ground states $Q_\omega^{(0)}$, due to Fibich and Merle:

Theorem 16.1 ([89]) *Assume that Conjecture 16.1 holds, and let $Q_\omega^{(0)}(r)$ be the unique positive solution of (16.22). Then for any $\omega \in (\omega_0, +\infty)$, $Q_\omega^{(0)}(r)$ is the unique real minimizer of*

$$\inf_{U(\mathbf{x}) \in H_0^1(B_{r_f})} \left\{ H_{B_{r_f}}(U) \mid \|U\|_{L^2(B_{r_f})}^2 = \|Q_\omega^{(0)}\|_{L^2(B_{r_f})}^2 \right\}.$$

In addition, for any $0 < P < P_{\text{cr}}$, there exists a unique $\omega(P) \in (\omega_0, +\infty)$, such that $Q_{\omega(P)}^{(0)}(r)$ is the unique real minimizer of

$$\inf_{U(\mathbf{x}) \in H_0^1(B_{r_f})} \left\{ H_{B_{r_f}}(U) \mid \|U\|_{L^2(B_{r_f})}^2 = P \right\}. \quad (16.28)$$

Thus, the variational characterization of $Q_\omega^{(0)}(r)$ is based on the absence of a dilation invariance on bounded domains.

Remark It is not assumed that $U(\mathbf{x})$ is radial.

Remark In free space, this variational characterization holds in the subcritical case, but not in the critical or supercritical cases (Sect. 6.3.3).

Remark See Lemma 6.10 for the equivalent variational characterization of the free-space critical ground state.

Corollary 16.5 *If the infimum (16.28) is taken over complex functions, the minimizers are given by the one-parameter family $\{e^{i\theta} Q_\omega(r) \mid \theta \in \mathbb{R}\}$.*

Proof Assume that the infimum is attained by $U(\mathbf{x}) = A(\mathbf{x})e^{iS(\mathbf{x})}$, where $A = |U|$ and S are real. Since $A \in H_0^1(B_{r_f})$ and $H_\Omega(U) = H_\Omega(A) + \|A\nabla S\|_2^2 \geq H_\Omega(A)$, one has that $S(\mathbf{x}) \equiv \theta_0$ and A is a minimizer. Hence, by Theorem 16.1, $A = Q_\omega^{(0)}(r)$. \square

16.5 Stability of Solitary Waves

16.5.1 Orbital Stability on a Bounded Domain

In Sect. 9.1 we defined orbital stability as stability up to phase shifts and translations. On a bounded domain the NLS is not invariant under translations, and so orbital stability refers only to stability up to phase shifts:

Definition 16.2 (Orbital stability on a bounded domain) *Let $\psi_\omega^{\text{solitary}} = e^{i\omega z} Q_\omega(\mathbf{x})$ be a solitary wave of the NLS (16.1). We say that ψ is orbitally stable, if for any $\epsilon > 0$, there exists $\delta > 0$, such that if*

$$\|\tilde{\psi}_0(\mathbf{x}) - Q_\omega(\mathbf{x})\|_{H_0^1(\Omega)} < \delta,$$

and if $\tilde{\psi}$ is the solution of (16.1) with the initial condition $\tilde{\psi}_0$, then

$$\inf_{\theta(z) \in \mathbb{R}} \|\tilde{\psi}(z, \mathbf{x}) - e^{i\theta(z)} Q_\omega(\mathbf{x})\|_{H_0^1(\Omega)} < \epsilon, \quad 0 \leq z < \infty.$$

16.5.2 Critical NLS

In Sect. 7.11.1 we saw that the ground-state solitary waves $\psi_\omega^{\text{solitary}, (0)} = e^{i\omega z} R_\omega^{(0)}(r)$ of the free-space critical NLS are unstable. This instability is related to the dual borderline properties of $R_\omega^{(0)}$, namely, that $H(R_\omega^{(0)}) = 0$ and $\|R_\omega^{(0)}\|_2^2 = P_{\text{cr}}$ (Sect. 7.12). Thus, small perturbations can either make the Hamiltonian negative and lead to collapse (Theorem 9.4), or lower the power below P_{cr} and lead to scattering (Sect. 8.4.7).

The situation is different with the ground-state solitary waves of the critical NLS on the bounded domain B_{r_f} , because:

1. Their Hamiltonian is strictly positive, see (16.23).
2. Their power is strictly below P_{cr} , see Lemma 16.8 and Conjecture 16.1.

Indeed, these solitary waves are stable. Intuitively, this is because $Q_\omega^{(0)}$ is the minimizer of the Hamiltonian out of all equal-power profiles (Theorem 16.1). Therefore, if the initial condition is close to $Q_\omega^{(0)}$, the solution has to stay close to $Q_\omega^{(0)}$.⁷

Lemma 16.10 ([89]) *Assume that Conjecture 16.1 holds. Then the ground-state solitary waves $\psi_\omega^{\text{solitary},(0)} = e^{i\omega z} Q_\omega^{(0)}(r)$ of the critical NLS (16.2) on B_{r_f} are orbitally stable.*

Proof By negation. If not, then there exist $\epsilon_0 > 0$ and a sequence $\{\psi_n\}$ of solutions of (16.2) on B_{r_f} such that

$$\|\psi_n(0, \mathbf{x}) - Q_\omega^{(0)}(r)\|_{H_0^1} \rightarrow 0, \quad n \rightarrow \infty, \quad (16.29)$$

and a sequence $\{z_n\}$ such that for all n ,

$$\inf_{\theta \in \mathbb{R}} \|\psi_n(z_n, \mathbf{x}) - e^{i\theta} Q_\omega^{(0)}(r)\|_{H_0^1(B_{r_f})} \geq \epsilon_0 > 0. \quad (16.30)$$

Let $U_n(\mathbf{x}) := \psi_n(z_n, \mathbf{x})$. In what follows, we will show that the variational characterization of $Q_\omega^{(0)}$ in Theorem 16.1 implies that

$$\lim_{n \rightarrow \infty} U_n = e^{i\theta_0} Q_\omega^{(0)} \quad \text{strongly in } H_0^1, \quad (16.31)$$

and hence that

$$\inf_{\theta \in \mathbb{R}} \|\psi_n(z_n, \mathbf{x}) - e^{i\theta} Q_\omega^{(0)}\|_{H_0^1} \leq \|U_n - e^{i\theta_0} Q_\omega^{(0)}\|_{H_0^1} \rightarrow 0, \quad n \rightarrow \infty,$$

which is in contradiction with (16.30).

To prove (16.31), we first note that by (16.29), as $n \rightarrow \infty$,

$$\|\psi_n(0, \mathbf{x})\|_{L^2(B_{r_f})} \rightarrow \|Q_\omega^{(0)}\|_{L^2(B_{r_f})}, \quad H_\Omega(\psi_n(0, \mathbf{x})) \rightarrow H_\Omega(Q_\omega^{(0)}),$$

see Corollary 5.1. Therefore, by power and Hamiltonian conservation

$$\|U_n\|_{L^2(B_{r_f})} = \|\psi_n(0, \mathbf{x})\|_{L^2(B_{r_f})} \rightarrow \|Q_\omega^{(0)}\|_{L^2(B_{r_f})}, \quad n \rightarrow \infty,$$

⁷ This is the same as in the subcritical free-space case, where the variational characterization of the ground state as the minimizer of the Hamiltonian out of all equal-power profiles implies that the ground-state solitary waves are orbitally stable (Sect. 9.4.1).

and

$$H_\Omega(U_n) = H_\Omega(\psi_n(0, \mathbf{x})) \rightarrow H_\Omega(Q_\omega^{(0)}), \quad n \rightarrow \infty.$$

Since the optimal constant in the Gagliardo-Nirenberg inequality on a bounded domain is the same as in free space (Lemma 16.14),

$$\begin{aligned} \|\nabla U_n\|_{L^2(B_{r_f})}^2 &= H_\Omega(U_n) + \frac{1}{\sigma+1} \|U_n\|_{L^{2\sigma+2}(B_{r_f})}^{2\sigma+2} \\ &\leq \max_n H_\Omega(U_n) + \kappa_n \|\nabla U_n\|_{L^2(B_{r_f})}^2, \end{aligned}$$

where $\kappa_n = (\|U_n\|_{L^2(B_{r_f})}^2/P_{\text{cr}})^\sigma$. Since $\lim_{n \rightarrow \infty} \|U_n\|_{L^2(B_{r_f})} = \|Q_\omega^{(0)}\|_{L^2(B_{r_f})}^2 < P_{\text{cr}}$, one has that $\lim_{n \rightarrow \infty} \kappa_n < 1$. Therefore, $\|\nabla U_n\|_2 \leq C$.

We thus showed that U_n is bounded in H_0^1 . Therefore, there is a subsequence U_n which converges weakly in H_0^1 . Hence, U_n converges strongly in L^2 and in $L^{2\sigma+2}$ to \tilde{U} (the proof of Lemma 5.14). Consequently,

$$\|\tilde{U}\|_2 = \|Q_\omega^{(0)}\|_{L^2(B_{r_f})}, \quad H_\Omega(\tilde{U}) \leq \liminf_n H_\Omega(U_n) = H_\Omega(Q_\omega^{(0)}).$$

By Theorem 16.1 and Corollary 16.5, the above relations show that $\tilde{U} = e^{i\theta_0} Q_\omega^{(0)}$ for some θ_0 and $H_\Omega(\tilde{U}) = H_\Omega(Q_\omega^{(0)})$. Therefore, $H_\Omega(U_n) \xrightarrow{n \rightarrow \infty} H_\Omega(\tilde{U})$, hence $\|\nabla U_n\|_2 \xrightarrow{n \rightarrow \infty} \|\nabla \tilde{U}\|_2$, hence $\|U_n\|_{H_0^1} \xrightarrow{n \rightarrow \infty} \|\tilde{U}\|_{H_0^1}$, hence U_n converges strongly in H_0^1 to $\tilde{U} = e^{i\theta_0} Q_\omega^{(0)}$. \square

It is believed that Conjecture 16.1 holds for all ω , in which case all critical ground-state solitary waves on B_{r_f} are orbitally stable. At present, however, Conjecture 16.1 was only proved in some special cases (Lemmas 16.8 and 16.9). Therefore, we have

Theorem 16.2 ([89, 102]) *The ground-state solitary waves $\psi_\omega^{\text{solitary},(0)} = e^{i\omega z} Q_\omega^{(0)}$ of the critical NLS (16.2) on B_{r_f} are orbitally stable for $\omega_0 < \omega < \infty$ if $d = 1$, and for ω sufficiently close to ω_0 or sufficiently large in any dimension.*

Remark The result of Lemma 16.10 is consistent with the VK condition for stability $\frac{d}{d\omega} \|Q_\omega^{(0)}\|_2^2 > 0$, see Sect. 9.3.

Since the critical ground-state solitary waves are orbitally stable, a natural question is whether they are local or global attractors. In fact, they are neither:

Lemma 16.11 ([89]) *Let ψ be the solution of the critical NLS (16.2) on B_{r_f} with the initial condition ψ_0 . Then*

$$\lim_{z \rightarrow \infty} \inf_{\theta \in \mathbb{R}} \|\psi(z, \mathbf{x}) - e^{i\theta} Q_{\bar{\omega}}^{(0)}(r)\|_{H_0^1(B_{r_f})} = 0 \quad \text{for some } \bar{\omega}, \quad (16.32)$$

if and only if $\psi_0 \equiv e^{i\theta_0} Q_{\bar{\omega}}^{(0)}$ for some θ_0 .

Proof If relation (16.32) holds, then $\lim_{z \rightarrow \infty} \|\psi\|_{L^2(B_{r_f})}^2 = \|Q_{\bar{\omega}}^{(0)}\|_{L^2(B_{r_f})}^2$ and $\lim_{z \rightarrow \infty} H_\Omega(\psi) = H_\Omega(Q_{\bar{\omega}}^{(0)})$, see Corollary 5.1. Therefore, by power and Hamiltonian conservation, $\|\psi_0\|_{L^2(B_{r_f})}^2 = \|Q_{\bar{\omega}}^{(0)}\|_{L^2(B_{r_f})}^2$ and $H_\Omega(\psi_0) = H_\Omega(Q_{\bar{\omega}}^{(0)})$. Hence, by Corollary 16.5, $\psi_0 = e^{i\theta_0} Q_{\bar{\omega}}^{(0)}$. \square

Intuitively, a solution can approach a solitary wave in two ways: It can radiate power and approach a lower-power solitary wave, or it can approach an equal-power solitary wave. The first option is not possible on a bounded domain, because all radiated power is reflected backwards by the boundary. The second option is only possible if $\psi_0 \equiv e^{i\theta_0} Q_{\bar{\omega}}^{(0)}$, because otherwise the Hamiltonian of ψ_0 is larger than that of the equal-power ground state.

16.5.3 Linear and Weakly-Nonlinear Modes

We now consider the stability of the linear solitary waves $e^{i\omega_n z} Y_\omega^{(n)}(\mathbf{x})$, presented in Sect. 16.4.3.

Lemma 16.12 *Let ψ be a solution of the linear Schrödinger equation (16.11) with $\psi_0(\mathbf{x}) = Y_\omega^{(n)}(\mathbf{x}) + f(\mathbf{x})$, where $f \in H_0^1(\Omega)$. Then*

$$\|\psi(z, \mathbf{x}) - e^{i\omega_n z} Y_\omega^{(n)}(\mathbf{x})\|_{H^1(\Omega)} \equiv \|f\|_{H^1(\Omega)}, \quad 0 \leq z < \infty.$$

Proof By linearity, $\psi = e^{i\omega_n z} Y_\omega^{(n)}(\mathbf{x}) + u(z, \mathbf{x})$, where $u(z, \mathbf{x})$ is the solution of (16.11) with the initial condition $u_0 = f$. Since in the linear case the H^1 norm is conserved (Corollary 2.6),

$$\|\psi - e^{i\omega_n z} Y_\omega^{(n)}(\mathbf{x})\|_{H^1(\Omega)} = \|u(z)\|_{H^1(\Omega)} \equiv \|u_0\|_{H^1(\Omega)} = \|f\|_{H^1(\Omega)}. \quad \square$$

Thus, linear solitary waves are stable, and not “just” orbitally stable. “By continuity”, weakly-nonlinear solitary waves “should” also be stable, since the reflecting boundaries “enable” them to propagate “nearly linearly”.⁸

Conclusion 16.2 *The weakly-nonlinear solitary waves of the NLS (16.1) on a bounded domain are orbitally stable, because the reflecting boundaries have a stabilizing effect.*

Since we deduced Conclusion 16.2 from a continuity argument, this suggests that it is valid in the subcritical, critical, and supercritical cases, both for ground-state and for excited-states solitary waves.

⁸ Indeed, weakly-nonlinear solitary waves satisfy the VK condition, see (16.19).

16.5.4 Supercritical NLS

In Sect. 9.4 we saw that the solitary waves of the free-space supercritical NLS violate the VK condition, and are thus unstable. We now consider the stability of the ground-state solitary waves of the supercritical NLS on a bounded domain. Intuitively, as $\omega \rightarrow \infty$, the bounded-domain solitary waves become more and more localized, as they approach the free-space solitary waves (Sect. 16.4.4). Hence, large-amplitude solitary waves on a bounded domain also violate the VK condition (Corollary 16.3), and are thus unstable. When ω is slightly above ω_0 , however, the small-amplitude solitary waves are stable, as they inherit the stability of the linear modes (Conclusion 16.2). These results were rigorously proved by Fukuizumi, Hadj Selem, and Kikuchi for $\Omega = B_{r_f}$:

Lemma 16.13 ([102]) *Let $\psi_\omega^{\text{solitary},(0)} = e^{i\omega z} Q_\omega^{(0)}$ be a solitary wave of the NLS (16.1) on B_{r_f} , where $Q_\omega^{(0)}$ is the ground-state of (16.20), let $\sigma d > 2$, and let ω_0 be the eigenvalue of the ground-state linear solitary wave $Y_\omega^{(0)}$ of (16.12) on B_{r_f} . Then there exist λ_1 and λ_2 , where $\omega_0 < \lambda_1 < \lambda_2 < \infty$, such that $\psi_\omega^{\text{solitary},(0)}$ is orbitally-stable for $\omega_0 < \omega < \lambda_1$, and unstable for $\lambda_2 < \omega < \infty$.*

Intuitively, since the free-space supercritical solitary waves are unstable, the bounded-domain ones are stable if and only if the effect of the reflecting boundary is sufficiently large, i.e., if the solitary wave is sufficiently non-localized (which is the case when it is weakly nonlinear).

16.5.5 Excited States

So far, we mostly considered the stability of the ground-state solitary waves. We now briefly discuss the stability of the excited-states solitary waves.

In [89], Fibich and Merle observed numerically that excited-state solitary waves of the two-dimensional critical NLS with power above P_{cr} are strongly unstable, so that when slightly perturbed, they collapse at a finite distance. Excited-state solitary waves with power sufficiently below P_{cr} , however, appeared numerically to be radially stable for quite a long distance. In fact, the excited states appeared to be “as stable” as the ground state. This result was initially surprising, since “in general” excited-state solitary waves are unstable, and decay into a ground-state solitary wave plus radiation. As noted in Conclusion 16.2, however, on bounded domains the small-amplitude excited states are stabilized by the reflecting boundary.

In [102], Fukuizumi, Hadj Selem, and Kikuchi studied the stability of the excited states of the one-dimensional NLS on B_{r_f} . They rigorously proved that the excited states are orbitally stable under perturbations that have the same symmetries as the excited state, in the subcritical and critical case for all ω , and in the supercritical case for ω slightly above ω_n . In addition, they rigorously proved that in the supercritical case, the excited states $Q_\omega^{(n)}$ are orbitally unstable for sufficiently large ω .

Numerically, they observed for the subcritical, critical, and supercritical NLS, that the excited states are stable if ω is close to ω_n , but that there exist “sufficiently large” frequencies ω for which the excited states are orbitally unstable.

Conclusion 16.3 ([89, 102]) *Small-amplitude excited-state solitary waves inherit the stability of the linear ones, whereas large-amplitude excited-state solitary waves inherit the instability of the free-space ones.*

16.6 Optimal Constant $C_{\sigma,d}(\Omega)$

An important tool in the analysis of the free-space NLS is the Gagliardo-Nirenberg inequality for functions $f \in H^1(\mathbb{R}^d)$, see Sect. 5.4. For example, in Theorem 5.5 we used this inequality to find sufficient conditions for global existence in the focusing NLS. The corresponding Gagliardo-Nirenberg inequality for $f \in H_0^1(\Omega)$ reads [104, 105, 202]

$$\|f\|_{L^{2\sigma+2}(\Omega)}^{2\sigma+2} \leq C_{\sigma,d}(\Omega) \|\nabla f\|_{L^2(\Omega)}^{\sigma d} \|f\|_{L^2(\Omega)}^{2\sigma+2-\sigma d}. \quad (16.33)$$

In general, optimal constants in Sobolev inequalities depend on Ω . As noted by Fibich, however, this is not the case for inequality (16.33):

Lemma 16.14 ([66]) *Let $\Omega \subset \mathbb{R}^d$ be a smooth bounded domain in \mathbb{R}^d , and let $C_{\sigma,d}(\Omega)$ be the optimal constant in the Gagliardo-Nirenberg inequality (16.33) for functions $f \in H_0^1(\Omega)$. Then*

- (i) $C_{\sigma,d}(\Omega)$ is independent of Ω .
- (ii) $C_{\sigma,d}(\Omega) = C_{\sigma,d}(\mathbb{R}^d)$, where $C_{\sigma,d}(\mathbb{R}^d)$ is given by (5.40).
- (iii) $\inf_{0 \neq f \in H_0^1(\Omega)} J_\Omega[f] = \inf_{0 \neq f \in H^1(\mathbb{R}^d)} J_{\mathbb{R}^d}[f]$, where

$$J_\Omega[f] = \frac{\|\nabla f\|_{L^2(\Omega)}^{\sigma d} \|f\|_{L^2(\Omega)}^{2+\sigma(2-d)}}{\|f\|_{L^{2\sigma+2}(\Omega)}^{2\sigma+2}}.$$

Proof Since $1/C_{\sigma,d}(\Omega) = \inf_{0 \neq f \in H_0^1(\Omega)} J_\Omega[f]$, see (5.29), it is sufficient to prove assertion (iii). For any $f \in H_0^1(\Omega)$, let

$$\tilde{f} := \begin{cases} f, & \text{if } \mathbf{x} \in \Omega, \\ 0, & \text{if } \mathbf{x} \in \mathbb{R}^d \setminus \Omega. \end{cases} \quad (16.34)$$

Since $\tilde{f} \in H^1(\mathbb{R}^d)$ and $J_\Omega[f] = J_{\mathbb{R}^d}[\tilde{f}]$,

$$\inf_{0 \neq f \in H_0^1(\Omega)} J_\Omega[f] \geq \inf_{0 \neq f \in H^1(\mathbb{R}^d)} J_{\mathbb{R}^d}[f]. \quad (16.35)$$

In what follows, we will construct functions $f_\epsilon \in H_0^1(\Omega)$ such that

$$\lim_{\epsilon \rightarrow 0} J_\Omega[f_\epsilon] = J_{\mathbb{R}^d}[R^{(0)}]. \quad (16.36)$$

This will imply that

$$\inf_{0 \neq f \in H_0^1(\Omega)} J_\Omega[f] \leq \lim_{\epsilon \rightarrow 0} J_\Omega[f_\epsilon] = J_{\mathbb{R}^d}[R^{(0)}] = \inf_{0 \neq f \in H_0^1(\mathbb{R}^d)} J_{\mathbb{R}^d}[f].$$

The proof of (iii) will then follow from this inequality and (16.35).

Since f_ϵ should approach $R^{(0)}$ yet vanish at the boundary of Ω , let us define

$$f_\epsilon(r) = \begin{cases} R^{(0)}\left(\frac{r}{\epsilon}\right), & \text{if } 0 \leq r \leq \frac{r_M}{2}, \\ R^{(0)}\left(\frac{r_M}{2\epsilon}\right)g(r), & \text{if } \frac{r_M}{2} \leq r \leq r_M, \\ 0, & \text{if } r \geq r_M, \end{cases} \quad (16.37)$$

where $r = |\mathbf{x} - \mathbf{x}_0|$, $\mathbf{x}_0 \in \Omega$, r_M is a positive number such that $\{|\mathbf{x} - \mathbf{x}_0| \leq r_M\} \subset \Omega$, $R^{(0)}$ is the minimizer of $J_{\mathbb{R}^d}[f]$, and $g(r)$ is a smooth function that satisfies $g(r_M/2) = 1$ and $g(r_M) = 0$. Now,

$$\begin{aligned} \|f_\epsilon\|_{L^p(\Omega)}^p &= \int_{0 \leq r < \frac{r_M}{2}} \left| R^{(0)}\left(\frac{r}{\epsilon}\right) \right|^p d\mathbf{x} + \left(R^{(0)}\left(\frac{r_M}{2\epsilon}\right) \right)^p C_g \\ &= \epsilon^d \int_{0 \leq r < \frac{r_M}{2\epsilon}} \left| R^{(0)}(r) \right|^p d\mathbf{x} + \left(R^{(0)}\left(\frac{r_M}{2\epsilon}\right) \right)^p C_g, \end{aligned}$$

where $C_g = \int_{\frac{r_M}{2} \leq r < r_M} |g(r)|^p d\mathbf{x}$. Since $R^{(0)}(r)$ decays exponentially,

$$\lim_{\epsilon \rightarrow 0} \epsilon^{-d} \|f_\epsilon\|_{L^p(\Omega)}^p = \|R^{(0)}\|_{L^p(\mathbb{R}^d)}^p.$$

Similarly, it can be shown that

$$\lim_{\epsilon \rightarrow 0} \epsilon^{2-d} \|\nabla f_\epsilon\|_{L^2(\Omega)}^2 = \|\nabla R^{(0)}\|_2^2.$$

Therefore,

$$\lim_{\epsilon \rightarrow 0} J_\Omega[f_\epsilon] = \lim_{\epsilon \rightarrow 0} \frac{\left(\epsilon^{d-2}\right)^{\frac{\sigma d}{2}} \|\nabla R^{(0)}\|_2^{\sigma d} (\epsilon^d)^{\frac{2+\sigma(2-d)}{2}} \|R^{(0)}\|_2^{2+\sigma(2-d)}}{\epsilon^d \|R^{(0)}\|_{2\sigma+2}^{2\sigma+2}} = J_{\mathbb{R}^d}[R^{(0)}],$$

i.e., (16.36) holds. \square

From Lemmas 16.14 and 5.10 follows

Lemma 16.15 *The Gagliardo-Nirenberg inequality (16.33) for functions $f \in H_0^1(\Omega)$ can be written as*

$$\|f\|_{L^{2\sigma+2}(\Omega)}^{2\sigma+2} \leq C_{\sigma,d} \|\nabla f\|_{L^2(\Omega)}^{\sigma d} \|f\|_{L^2(\Omega)}^{2+\sigma(2-d)}, \quad (16.38)$$

where

$$C_{\sigma,d} = \frac{2(\sigma+1)}{(\sigma d)^{\frac{\sigma d}{2}}} [2 + \sigma(2-d)]^{-\left(1-\frac{\sigma d}{2}\right)} \|R^{(0)}\|_2^{-2\sigma}$$

and $R^{(0)}$ is the ground state of (16.15).

An interesting consequence of Lemma 16.14 is

Corollary 16.6 ([66]) *The infimum of $J_\Omega[f]$ over all functions $0 \not\equiv f \in H_0^1(\Omega)$ is not achieved.*

Proof Assume that the infimum of J_Ω is achieved by some $f \in H_0^1(\Omega)$. Let \tilde{f} be given by (16.34). In light of Lemma 16.14, \tilde{f} is a minimizer of $J_{\mathbb{R}^d}[f]$. Hence, by Lemma 6.5, \tilde{f} is positive in \mathbb{R}^d , which is a contradiction. \square

This result is exactly the opposite from the free-space case, where the infimum of $J_{\mathbb{R}^d}[f]$ is achieved (Theorem 5.10).

Exercise 16.1 ([82]) *In the analysis of the biharmonic NLS on a bounded domain, one makes use of the Gagliardo-Nirenberg inequality [104, 105, 202]*

$$\|f\|_{L^{2\sigma+2}(\Omega)}^{2\sigma+2} \leq B_{\sigma,d}(\Omega) \|\Delta f\|_{L^2(\Omega)}^{\frac{\sigma d}{2}} \|f\|_{L^2(\Omega)}^{2+2\sigma-\frac{\sigma d}{2}}, \quad f \in H_0^2(\Omega), \quad (16.39)$$

where

$$\begin{cases} 0 \leq \sigma < \infty, & \text{if } d \leq 4, \\ 0 \leq \sigma < \frac{4}{d-4}, & \text{if } d > 4. \end{cases}$$

Prove that $B_{\sigma,d}(\Omega) = B_{\sigma,d}(\mathbb{R}^d)$.⁹

16.6.1 Critical Case

By Lemma 16.15, the Gagliardo-Nirenberg inequality (16.33) on a bounded domain in the critical case $\sigma d = 2$ reads

$$\|f\|_{L^{\frac{4}{d}+2}(\Omega)}^{\frac{4}{d}+2} \leq C_{\sigma=\frac{2}{d},d} \|f\|_{L^2(\Omega)}^{\frac{4}{d}} \|\nabla f\|_{L^2(\Omega)}^2, \quad C_{\sigma=\frac{2}{d},d} = \frac{\frac{2}{d}+1}{\|R^{(0)}\|_2^{\frac{4}{d}}},$$

⁹ The exponential decay of R_B was proved in Exercise 6.11.

where $R^{(0)}$ is the free-space ground state of (16.24). This inequality can also be written as

$$\|f\|_{L^{\frac{4}{d}+2}(\Omega)}^{\frac{4}{d}+2} \leq \left(\frac{2}{d} + 1\right) \left(\frac{\|f\|_{L^2(\Omega)}^2}{\|R^{(0)}\|_2^2}\right)^{\frac{2}{d}} \|\nabla f\|_{L^2(\Omega)}^2. \quad (16.40)$$

Therefore, it immediately follows that, as in free space (Corollary 5.10), in the critical case

$$\|\psi_0\|_{L^2(\Omega)}^2 < \|R^{(0)}\|_{L^2(\mathbb{R}^d)}^2 \implies H_\Omega(\psi_0) > 0. \quad (16.41)$$

16.7 Global Existence

Local existence in H_0^1 for the NLS on a bounded domain with Dirichlet boundary conditions was proved in [39, Theorem 3.5.1] for $d = 1$, and in [203, 204] for $d = 2$ and $0 < \sigma \leq 1$. As in free space, the local existence theory provides a domain of existence $C([0, Z]; H_0^1(\Omega))$, such that Z is a monotonically decreasing function of $\|\psi_0\|_{H^1(\Omega)}$. Therefore, when $\|\psi\|_{H^1(\Omega)}$ can be formally bounded, this implies global existence in z . Since $\|\psi\|_{L^2(\Omega)}^2$ is bounded, global existence is equivalent to $\|\nabla \psi\|_{L^2(\Omega)}^2$ being bounded.

As in free space, we have

Theorem 16.3 *Let $\psi_0 \in H_0^1(\Omega)$. The following two conditions are sufficient for global existence in the focusing NLS on a bounded domain (16.1):*

1. $\sigma d < 2$.
2. $\sigma d = 2$ and $\|\psi_0\|_{L^2(\Omega)}^2 < P_{\text{cr}}$, where $P_{\text{cr}} = \|R^{(0)}\|_2^2$ and $R^{(0)}$ is the free-space ground state of (16.24).

Proof The proof is identical to the proofs of Theorem 5.5 and Theorem 5.11. Indeed, these proofs are based on power conservation, Hamiltonian conservation and the Gagliardo-Nirenberg inequality, and these three relations are identical in free space and on bounded domains. \square

Therefore, in the critical case, the necessary condition for blowup on bounded domains is the same as on \mathbb{R}^d :

Theorem 16.4 ([66]) *A necessary condition for blowup in the critical NLS (16.2) on a bounded domain Ω is*

$$\|\psi_0\|_{L^2(\Omega)}^2 \geq P_{\text{cr}} = \|R^{(0)}\|_2^2, \quad (16.42)$$

where $R^{(0)}$ is the free-space ground state of (16.24).

The question whether condition (16.42) is sharp is addressed in Sects. 16.8.2 and 24.5.

16.8 Blowup Solutions

16.8.1 Variance Identity

As in free space, the variance identity plays an important role in the theory of singular solutions of the NLS on a bounded domain.

Lemma 16.16 (Variance identity on a bounded domain) *Let ψ be a solution of the NLS (16.1), and let $V_\Omega(z) := \int_\Omega |\mathbf{x}|^2 |\psi|^2 d\mathbf{x}$ be its variance. Then $\frac{d}{dz} V_\Omega(z) = 4 \operatorname{Im} \int_\Omega (\mathbf{x} \cdot \nabla \psi) \psi^* d\mathbf{x}$, and*

$$\frac{d^2}{dz^2} V_\Omega(z) = 8H_\Omega - 8 \frac{d\sigma - 2}{2\sigma + 2} \|\psi\|_{L^{2\sigma+2}(\Omega)}^{2\sigma+2} - 4 \int_{\partial\Omega} (\mathbf{x} \cdot \mathbf{n}) |\nabla \psi \cdot \mathbf{n}|^2 ds, \quad (16.43)$$

where \mathbf{n} is the outward unit normal to $\partial\Omega$.

Proof The proof of Lemma 16.16 is the same as that of Theorem 7.1, except that we keep contributions from boundary integrals in integration by parts. In addition, as in the proof of Lemma 16.2, on $\partial\Omega$ we have that $\psi \equiv 0$, hence $\nabla \psi$ points in the direction of \mathbf{n} . Therefore, $\nabla \psi = (\nabla \psi \cdot \mathbf{n})\mathbf{n}$ and $|\nabla \psi|^2 = |\nabla \psi \cdot \mathbf{n}|^2$.

The only nonzero contribution from boundary integrals comes from integration by parts of, see (7.9),

$$\begin{aligned} & \int_\Omega \mathbf{x} \cdot \nabla \psi^* \Delta \psi d\mathbf{x} + \text{c.c.} \\ &= \int_{\partial\Omega} (\mathbf{x} \cdot \nabla \psi^*) (\nabla \psi \cdot \mathbf{n}) ds - \int_\Omega \nabla (\mathbf{x} \cdot \nabla \psi^*) \cdot \nabla \psi d\mathbf{x} + \text{c.c.} \\ &= \int_{\partial\Omega} (\mathbf{x} \cdot \mathbf{n}) |\nabla \psi \cdot \mathbf{n}|^2 ds - \int_\Omega (\nabla \psi^* + (\mathbf{x} \cdot \nabla) \nabla \psi^*) \cdot \nabla \psi d\mathbf{x} + \text{c.c.} \\ &= 2 \int_{\partial\Omega} (\mathbf{x} \cdot \mathbf{n}) |\nabla \psi \cdot \mathbf{n}|^2 ds - 2 \|\nabla \psi\|_2^2 - \int_\Omega \mathbf{x} \cdot \nabla |\nabla \psi|^2 d\mathbf{x} \\ &= 2 \int_{\partial\Omega} (\mathbf{x} \cdot \mathbf{n}) |\nabla \psi \cdot \mathbf{n}|^2 ds - 2 \|\nabla \psi\|_2^2 - \int_{\partial\Omega} (\mathbf{x} \cdot \mathbf{n}) |\nabla \psi|^2 ds + d \|\nabla \psi\|_2^2 \\ &= \int_{\partial\Omega} (\mathbf{x} \cdot \mathbf{n}) |\nabla \psi \cdot \mathbf{n}|^2 ds + (d-2) \|\nabla \psi\|_2^2. \end{aligned}$$

Therefore, the result follows. \square

When Ω is the ball B_{r_f} , the variance identity (16.43) reads

$$\frac{d^2}{dz^2} V_{B_{r_f}}(z) = 8H_{B_{r_f}} - 8 \frac{d\sigma - 2}{2\sigma + 2} \|\psi\|_{L^{2\sigma+2}(B_{r_f})}^{2\sigma+2} - 4s_d r_f^d |\psi_r(z, r_f)|^2,$$

where s_d is the surface area of the d -dimensional unit ball. In that case, the boundary integral is negative. More generally, the boundary integral in the variance identity (16.43) is negative if Ω is convex and $\mathbf{0} \in \Omega$.

When Ω is convex but $\mathbf{0} \notin \Omega$, it is not clear whether the boundary integral is negative. In order to be able to determine the sign of the boundary integral in the variance identity, let

$$V_\Omega(z; \mathbf{x}_0) := \int_{\Omega} |\mathbf{x} - \mathbf{x}_0|^2 |\psi|^2 d\mathbf{x}.$$

Then $\frac{d}{dz} V_\Omega(z; \mathbf{x}_0) = 4 \operatorname{Im} \int_{\Omega} ((\mathbf{x} - \mathbf{x}_0) \cdot \nabla \psi) \psi^* d\mathbf{x}$, and

$$\frac{d^2}{dz^2} V_\Omega(z; \mathbf{x}_0) = 8H_\Omega - 8 \frac{d\sigma - 2}{2\sigma + 2} \|\psi\|_{L^{2\sigma+2}(\Omega)}^{2\sigma+2} - 4 \int_{\partial\Omega} (\mathbf{x} - \mathbf{x}_0) \cdot \mathbf{n} |\nabla \psi \cdot \mathbf{n}|^2 ds. \quad (16.44)$$

Therefore, we have

Lemma 16.17 *Let ψ be a solution of the NLS (16.1) on a bounded domain Ω . If Ω is convex and $\mathbf{x}_0 \in \Omega$, then*

$$\frac{d^2}{dz^2} V_\Omega(z; \mathbf{x}_0) < 8H_\Omega - 8 \frac{d\sigma - 2}{2\sigma + 2} \|\psi\|_{L^{2\sigma+2}(\Omega)}^{2\sigma+2}.$$

Proof When Ω is convex and $\mathbf{x}_0 \in \Omega$, then $(\mathbf{x} - \mathbf{x}_0) \cdot \mathbf{n} > 0$ on $\partial\Omega$. Therefore, $\int_{\partial\Omega} (\mathbf{x} - \mathbf{x}_0) \cdot \mathbf{n} |\nabla \psi \cdot \mathbf{n}|^2 ds > 0$. Hence, the result follows from (16.44). \square

Remark Intuitively, the contribution of the boundary in the variance identity (16.43) is negative, because reflecting boundaries have a focusing effect, and therefore have the same sign as the nonlinearity.

By Lemma 16.17, if $\sigma d \geq 2$, then $\frac{d^2}{dz^2} V_\Omega(z; \mathbf{x}_0) < 8H_\Omega(0)$. Therefore, as in free space (Theorem 7.2), the condition of a negative Hamiltonian is sufficient for collapse:

Lemma 16.18 *Let ψ be a solution of the focusing NLS (16.1) on a convex bounded domain Ω , and let $\sigma d \geq 2$. If $H_\Omega(0) < 0$, then ψ becomes singular at a finite distance Z_c .*

Remark As in Theorem 7.2, one can also formulate sufficient conditions for collapse when $H_\Omega(0) \geq 0$.

Remark In the second proof of Lemma 7.1 we saw that $\frac{d}{dz} V(z; \mathbf{x}_0) = \frac{d}{dz} V(z) + 2\mathbf{x}_0 \cdot \mathbf{M}$, where \mathbf{M} is linear momentum. Since \mathbf{M} is conserved in free space, this implies that $V_{zz}(z; \mathbf{x}_0) \equiv V_{zz}(z)$ in free space. In contrast, on bounded domains \mathbf{M} is not conserved, hence $\frac{d^2}{dz^2} V_\Omega(z; \mathbf{x}_0) \neq \frac{d^2}{dz^2} V_\Omega(z)$, and so the boundary integral $\int_{\partial\Omega} ((\mathbf{x} - \mathbf{x}_0) \cdot \mathbf{n}) |\nabla \psi \cdot \mathbf{n}|^2 ds$ is not independent of \mathbf{x}_0 .¹⁰

¹⁰ This shows that the result of Lemma 16.3 is not valid for arbitrary functions, but only for solutions of (16.7).

The variance identity provides an alternative proof to Corollary 16.1:

Corollary 16.7 *Let $Q_\omega(\mathbf{x})$ be a solution of (16.7) in $H_0^1(\Omega)$. Then*

$$H_\Omega(Q_\omega) = \frac{d\sigma - 2}{2\sigma + 2} \|Q_\omega\|_{L^{2\sigma+2}(\Omega)}^{2\sigma+2} + \frac{1}{2} \int_{\partial\Omega} (\mathbf{x} \cdot \mathbf{n}) (\nabla Q_\omega \cdot \mathbf{n})^2 ds. \quad (16.45)$$

Proof As in free space (Corollary 7.14), the result is proved by substituting $\psi = e^{i\omega z} Q_\omega(\mathbf{x})$ in the variance identity (16.43). \square

16.8.2 Threshold Power for Collapse (Critical NLS)

So far we saw that, as in free space, a necessary condition for collapse in the critical NLS on bounded domains is $\|\psi_0\|_{L^2(\Omega)}^2 \geq P_{\text{cr}}$, and a sufficient condition is $H_\Omega(\psi_0) < 0$. As in free space (Corollary 7.15), the condition $\|\psi_0\|_{L^2(\Omega)}^2 \geq P_{\text{cr}}$ is sharp in the following sense:

Lemma 16.19 ([89]) *For any $\epsilon > 0$, there exists a singular solution of the critical NLS (16.2) on a bounded domain, such that $\|\psi_0\|_{L^2(\Omega)}^2 \leq (1 + \epsilon)P_{\text{cr}}$.*

Proof Let $\epsilon > 0$, and let

$$\psi_0(\mathbf{x}) = \begin{cases} (1 + \epsilon)^{\frac{1}{2}} \lambda^{\frac{d}{2}} (R^{(0)}(\lambda r) - R^{(0)}(\lambda r_M)), & \text{if } 0 \leq r \leq r_M, \\ 0, & \text{if } r > r_M, \end{cases}$$

where $r = |\mathbf{x} - \mathbf{x}_0|$, $\mathbf{x}_0 \in \Omega$, r_M is a positive number such that $\{|\mathbf{x} - \mathbf{x}_0| \leq r_M\} \subset \Omega$, and $R^{(0)}$ is the free-space ground state of (16.24). Then $\psi_0 \in H_0^1(\Omega)$ and $\|\psi_0\|_{L^2(\Omega)}^2 < (1 + \epsilon)P_{\text{cr}}$. In addition, since $R^{(0)}$ decays exponentially, then $\lim_{\lambda \rightarrow \infty} \lambda^{\frac{d}{2}} R^{(0)}(\lambda r_M) = 0$. Hence, $\lim_{\lambda \rightarrow \infty} H_\Omega(\psi_0) = \lim_{\lambda \rightarrow \infty} \lambda^2 H((1 + \epsilon)^{\frac{1}{2}} R^{(0)}) = -\infty$, where in the last stage we used the result that $H((1 + \epsilon)^{\frac{1}{2}} R^{(0)}) < 0$, see Lemma 7.12. Therefore, if λ is sufficiently large, then $H_\Omega(\psi_0) < 0$. Consequently, the corresponding NLS solution blows up at a finite distance (Lemma 16.18). \square

In Sect. 13.5 we saw that the free-space critical NLS admits singular solutions whose power is exactly P_{cr} . These minimal-power solutions are given by the explicit blowup solution $\psi_{R^{(0)}}^{\text{explicit}}$, up to NLS symmetries. A natural question is, therefore, whether there exist minimal-power singular solutions on a bounded domain.¹¹ This question was answered by Burq et al. [37], who constructed blowup solutions of the critical NLS on a bounded domain that satisfy

¹¹ The free-space minimal-power solution $\psi_{R^{(0)}}^{\text{explicit}}$ can be derived by applying the lens transformation to the ground-state solitary wave $\psi^{\text{solitary},(0)} = e^{iz} R^{(0)}(r)$, see Sect. 8.4.3. On a bounded domain, however, the lens transformation is not an NLS symmetry.

$$\lim_{z \rightarrow Z_c} \left\| \psi(z, \mathbf{x}) - \psi_{R^{(0)}}^{\text{explicit}}(z, |\mathbf{x} - \mathbf{x}_c|) \right\|_{H^1(\Omega)} = 0.$$

Therefore, these solutions have the same power and blowup rate as $\psi_{R^{(0)}}^{\text{explicit}}$. In particular, they are minimal-power solutions that collapse at a linear rate. As in free space, these minimal-power solutions are strongly unstable, since any perturbation that reduces their power arrests the collapse.

Numerical simulations conducted by Fibich and Gaeta [70] and by Fibich and Merle [89] suggest that in the case of the two-dimensional critical NLS on the unit sphere, the condition $\|\psi_0\|_{L^2(\Omega)}^2 > P_{\text{cr}}$ is generically sufficient for collapse (Observation 24.5). This is different from the critical NLS in free space, where generically $P_{\text{th}} > P_{\text{cr}}$ (Theorem 13.12). To motivate this observation, we note that both in free space (Sect. 14.6) and on bounded domains (Sect. 16.8.3), the solution generically collapses with the $\psi_{R^{(0)}}$ profile, so that the amount of power that collapses into the singularity is P_{cr} . In free space, unless the initial profile is $R^{(0)}$, the solution requires some extra power above P_{cr} in order to collapse (Theorem 13.12). As noted in Sect. 13.5, this is because the collapsing core radiates some power as it evolves into the $\psi_{R^{(0)}}$ profile. On a bounded domain, however, all the power which is radiated during this “reorganization stage” is reflected back by the boundary. As a result, no power is lost by the collapsing core as it evolves into the $\psi_{R^{(0)}}$ profile.

As in free space, the condition $\|\psi_0\|_{L^2(\Omega)}^2 > P_{\text{cr}}$ cannot be sufficient for collapse for all initial profiles. Indeed, the initial conditions $\psi_0 = Q_\omega^{(n)}(r)$ with $n \geq 1$ and ω sufficiently large have power above P_{cr} , see Lemma 16.7, yet the corresponding solitary waves $\psi_\omega^{\text{solitary},(n)} = e^{i\omega z} Q_\omega^{(n)}(r)$ exist globally. Numerical simulations suggest that, as in free space, these high-power excited-state solitary waves are unstable [89].

Remark See Sect. 24.5 for further discussion of the threshold power for collapse on a bounded domain.

16.8.3 Local Behavior Near the Singularity (Critical NLS)

In Theorem 13.3 we proved that all solutions of the critical NLS collapse with a quasi self-similar profile. Since critical collapse is a local phenomenon, one can expect that the boundary has no effect near the singularity point, and so that the same result also holds on bounded domains. Indeed we have

Theorem 16.5 *Let $\psi(z, r)$ be a solution of the critical NLS on B_{r_f}*

$$i\psi_z(z, r) + \psi_{rr} + \frac{d-1}{r}\psi_r + |\psi|^{\frac{4}{d}}\psi = 0, \quad 0 < r < r_f, \quad z \geq 0,$$

$$\psi_r(z, 0) = 0, \quad \psi(z, r_f) = 0, \quad z \geq 0,$$

where $\psi(0, r) = \psi_0(r) \in H_0^1(B_{r_f})$. Let $d \geq 2$ and $l(z) = \frac{\|\nabla R^{(0)}\|_2}{\|\nabla \psi\|_{L^2(B_{r_f})}}$, where $R^{(0)}$ is the free-space ground state of (16.24). Let

$$S(\psi)(z, \rho) = \begin{cases} l^{\frac{d}{2}}(z)\psi(z, l(z)\rho), & \text{if } 0 \leq \rho < \frac{r_f}{l(z)}, \\ 0, & \text{if } \rho \geq \frac{r_f}{l(z)}. \end{cases} \quad (16.46)$$

If ψ becomes singular at Z_c , then for any sequence $z_k \rightarrow Z_c$, there is a subsequence z_{k_j} , such that $S(\psi)(z_{k_j}, \rho) \rightarrow \Psi(\rho)$ strongly in $L^p(\mathbb{R}^d)$ for all $2 < p < \frac{2d}{d-2}$. Furthermore, $\|\Psi\|_4^4 = 2$ and $\|\Psi\|_2^2 \geq \|R^{(0)}\|_2^2 = P_{\text{cr}}$.

Proof The proof of Theorem 13.3 in the radial case is based on power conservation, Hamiltonian conservation, the compactness lemma, and the Gagliardo-Nirenberg inequality. Since these four relations remain the same on bounded domains, the result follows. \square

In Sect. 13.3 we used Theorem 13.3 to prove that the amount of power that collapses into the singularity is at least P_{cr} (Theorem 13.6). In exactly the same way, we can use Theorem 16.5 to prove the power concentration property for the critical NLS on a bounded domain:

Theorem 16.6 (Power concentration [89]) *Under the conditions of Theorem 16.5, for all $\epsilon > 0$,*

$$\lim_{z \rightarrow Z_c} \|\psi\|_{L^2(r \leq \epsilon)} \geq P_{\text{cr}}.$$

Theorem 16.5 shows that, as in free space, collapse in the critical NLS on a bounded domain is a local phenomenon. This suggests that the effect of the boundary on the collapse dynamics becomes negligible, in which case the blowup profile and blowup rate on bounded domains are the same as in free space. That this is indeed the case was shown by Planchon and Raphaël [211], who proved the existence and stability of singular solutions of the critical NLS on a bounded domain that collapse with the $\psi_{R^{(0)}}$ profile at the loglog law rate.

16.9 Oscillations for $P < P_{\text{cr}}$

We now consider solutions of the critical NLS with power below P_{cr} . While these solutions exist globally, both in free space and on a bounded domain, their dynamics as $z \rightarrow \infty$ is very different. Thus, in free space these solutions always scatter as $z \rightarrow \infty$ (Sect. 8.4.7). In contrast, the NLS on a bounded domain admits non-diffracting, non-collapsing stable solutions for any $0 < P < P_{\text{cr}}$, namely, the ground-state solitary waves. Moreover, even if the bounded-domain solution is not a solitary wave, the reflecting boundary prevents it from scattering. Since these solutions do not have sufficient power to collapse either, they end up undergoing focusing-defocusing oscillations.

This difference between bounded and unbounded domains is manifested by the variance. Indeed, in free space if $P < P_{\text{cr}}$ then $\lim_{z \rightarrow \infty} V(z) = \infty$, see (8.20). On bounded domains, however, $V_\Omega(z)$ is bounded from above, because

$$V_\Omega(z) \leq \|\psi\|_{L^2(\Omega)}^2 \max_{\mathbf{x} \in \Omega} |\mathbf{x}|^2 < \infty, \quad 0 \leq z < \infty.$$

16.9.1 Informal Analysis

Consider an initial condition with power below P_{cr} , which is not a ground state. Since ground states are typically attractors, the solution “tries” to approach a ground state. It cannot do that, however, because it has a higher Hamiltonian than the equal-power ground state (Lemma 16.11). Therefore, it ends up oscillating around a ground-state profile.

This oscillatory dynamics can be analyzed by assuming that $\psi(z, r) \sim A(z, r)e^{i\zeta(z)+i\frac{\alpha(z)r^2}{2}}$, where $A(z, r)$, $\zeta(z)$, and $\alpha(z)$ are real. Since $F(z) := \frac{1}{2\alpha(z)}$ is the local focal distance (Conclusion 2.12), the function $\alpha(z)$ measures the local focusing angle. Thus, for example, at the peaks and valleys of $|\psi|$ the solution is collimated, and so $\alpha = 0$. Similarly, the focusing angle is maximal roughly half-way between the peaks and valleys, hence $\alpha^2(z)$ is maximal there.¹²

By power and Hamiltonian conservation,

$$\|\psi_0\|_2^2 \equiv \|\psi\|_2^2 \sim \|A\|_2^2, \quad H_\Omega(\psi_0) \equiv H_\Omega(\psi) \sim H_\Omega(A) + \alpha^2(z)V(A),$$

where $V(A)$ is the variance of A .¹³ Therefore, the value of $H_\Omega(A)$ is minimal when $\alpha^2(z)V(A)$ is maximal, which is roughly half-way between the peaks and valleys of $|\psi|$. On the other hand, at the peaks and valleys we have that $\alpha = 0$, hence that $H_\Omega(A)$ is maximal. Since the minimum of $H_\Omega(A)$ subject to the constraint $\|A\|_2^2 = \|Q_\omega^{(0)}\|_2^2$ is attained at $A = Q_\omega^{(0)}$ (Theorem 16.1), we have

Conclusion 16.4 *If $|\psi_0|$ is “sufficiently close” to $Q_\omega^{(0)}$, the solution oscillates around $Q_\omega^{(0)}$, so that the distance between $|\psi|$ and $Q_\omega^{(0)}$ is maximal at the focusing peaks and valleys of $|\psi|$, and is minimal half-way in-between.*

Numerical simulations suggest that Conclusion 16.4 holds for input profiles which are close to a ground state, but not for those not close to a ground state [89].

¹² Since “ $\alpha = \frac{L_z}{2L}$ ”, α is proportional to the “velocity”. Therefore, as in the case of an oscillator, the velocity is zero at the maximal and minimal values, and is maximal half-way through (i.e., at the bottom of the potential well).

¹³ Since α is proportional to the “velocity”, the first and second terms of $H_\Omega(\psi_0)$ are potential and kinetic “energy”, respectively.

16.10 Experiments

Propagation of intense laser pulses in a 6 cm hollow-core photonic crystal fiber (PCF) filled with argon, nitrogen, and atmospheric air, was studied experimentally in 2004 by Konorov et al. [143]. At low powers, where the propagation is linear, the pulse was transmitted through the hollow PCF with no significant changes in its profile at the output of the fiber. When the pulse power was above a certain power threshold P_{th} , the output beam became unstable, suggesting the occurrence of an optical breakdown induced by the collapsing laser beam. In between, at input powers below P_{th} but for which nonlinear effects are important, Konorov et al. observed that regardless of the transverse field distribution of the input beam, the output beam always tended to a radial profile, which is well approximated by a ground state $Q_{\omega}^{(0)}$ of the NLS on a disc (Fig. 16.4).

The results of these experiments are thus in agreement with the predictions of the NLS model on a bounded domain, that (i) solutions undergo collapse if their power exceeds a certain critical power, and (ii) at somewhat lower powers, they oscillate around a stable solitary wave.

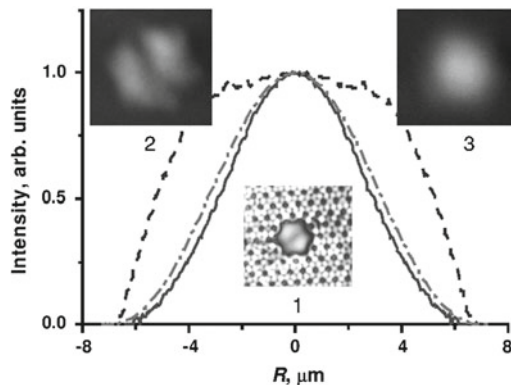


Fig. 16.4 Radial beam profiles measured at the output of a 6 cm PCF filled with atmospheric-pressure air with 30-fs Ti:sapphire input pulses with an energy of (dashed curve) $0.5 \mu\text{J}$ and (solid curve) $4 \mu\text{J}$. The dashed-dotted curve shows the profile of the ground state $Q_{\omega}^{(0)}$. Insets, images of the output beam measured with (1) $0.1 \mu\text{J}$, (2) $0.5 \mu\text{J}$, and (3) $4 \mu\text{J}$ pulses. From [143]

Part III
Asymptotic Analysis
of the Critical NLS

Chapter 17

Derivation of Reduced Equations

In this chapter we derive reduced equations for the dynamics of solutions of the critical NLS

$$i\psi_z(z, \mathbf{x}) + \Delta\psi + |\psi|^{\frac{4}{d}}\psi = 0, \quad \psi(0, \mathbf{x}) = \psi_0(\mathbf{x}) \in H^1$$

that undergo a quasi self-similar collapse with the $\psi_{R^{(0)}}$ profile (Chap. 14). To simplify the presentation, we consider the radial case

$$i\psi_z(z, r) + \psi_{rr} + \frac{d-1}{r}\psi_r + |\psi|^{\frac{4}{d}}\psi = 0, \quad \psi(0, r) = \psi_0(r) \in H_{\text{radial}}^1. \quad (17.1)$$

The reduced equations, however, are also valid in the nonradial case.

We recall that

$$\psi_{R^{(0)}}(z, r) = \frac{1}{L^{\frac{d}{2}}(z)} R^{(0)}(\rho) e^{i\zeta(z) + i\frac{Lz}{L^2} \frac{r^2}{4}}, \quad (17.2a)$$

where

$$\rho = \frac{r}{L(z)}, \quad \frac{d\zeta}{dz} = \frac{1}{L^2(z)}, \quad (17.2b)$$

and $R^{(0)}$ is the ground state of

$$R''(\rho) + \frac{d-1}{\rho}R' - R + |R|^{\frac{4}{d}}R = 0, \quad R'(0) = 0, \quad R(\infty) = 0. \quad (17.3)$$

The information that ψ collapses with the $\psi_{R^{(0)}}$ profile enables us to average the NLS solution over the transverse coordinates. This averaging leads to *reduced equations* for $L(z)$, which are independent of \mathbf{x} :

Proposition 17.1 ([100, 151, 156]) *Let $\psi(z, r)$ be a solution of the critical NLS (17.1) that collapses with the $\psi_{R^{(0)}}$ profile. Then as $z \rightarrow Z_c$, the dynamics of $L(z)$ is governed, to leading order, by the reduced equations*

$$L_{zz}(z) = -\frac{\beta}{L^3}, \quad \beta_z(z) = -\frac{v(\beta)}{L^2}, \quad (17.4a)$$

where $0 < \beta \ll 1$,

$$v(\beta) = c_v e^{-\pi/\sqrt{\beta}}, \quad c_v = \frac{2A_R^2}{M^{\text{radial}}}, \quad (17.4b)$$

$$A_R = \lim_{r \rightarrow \infty} e^r r^{\frac{d-1}{2}} R^{(0)}(r), \quad M^{\text{radial}} = \frac{1}{4} \int_0^\infty r^2 |R^{(0)}|^2 r^{d-1} dr, \quad (17.4c)$$

and $R^{(0)}$ is the ground state of (17.3).

Remark The reduced Eq. (17.4a) are only $O(\beta)$ accurate, see Conclusion 17.2.

Because the reduced equations are ODEs, they are simpler to analyze (and to solve numerically) than the original NLS. Nevertheless, in Chap. 18 we shall see that even this ‘simple’ ODE system offered some challenges of its own.

The derivation of the reduced equations was one of the hardest challenges in NLS research during the 1980s. These equations were first derived in 1985 by Fraiman [100] from a linear-stability analysis of perturbations around $\psi_{R^{(0)}}$. Unaware of Fraiman’s work, these equations were rederived in 1988 by Papanicolaou and coworkers [151, 156] from a solvability condition, by allowing the dimension d to continuously approach the critical value of $2/\sigma$ from above. Malkin [164] derived the reduced equations in 1993 by considering the evolution of the power of the collapsing core.

A rigorous derivation of the reduced equations also turned out to be a formidable challenge. The first rigorous derivation was done in 2001 by Perelman for $d = 1$ and a certain class of initial conditions. A rigorous derivation for all initial conditions whose power is slightly above P_{cr} in dimensions $1 \leq d \leq 5$ was given by Merle and Raphaël in 2003–2006. See Sect. 13.2 for more details.

The derivation of Proposition 17.1 presented in this chapter follows Malkin [164] and Fibich and Papanicolaou [93]. This derivation is not rigorous, and makes use of several assumptions, which were originally based on numerical observations. While its level of rigor is well below that of Merle and Raphaël, this derivation is much shorter, and it provides a physical interpretation to the reduced equations.

17.1 “Failure” of Self-similar Analysis

The first studies that derived a reduced equation for $L(z)$ assumed that the collapsing solution is self-similar (i.e., that the propagation is *aberrationless*). For example, in Sect. 3.5 we saw that Akhmanov, Sukhorukov, and Khokhlov derived a reduced

equation for $L(z)$, under the assumption that the self-focusing solution maintains a self-similar Gaussian profile. Subsequently, other self-similar profiles were considered, such as sech and super-Gaussian profiles. While these studies provided some insight on the initial self-focusing dynamics, the self-similar/aberrationless approach could not resolve the dynamics near the singularity, for reasons that will be discussed in Sects. 17.1.2 and 17.2.

17.1.1 Identifying All Self-similar Solutions

We first identify all the self-similar solutions of the critical radial NLS:

Lemma 17.1 *Let $\psi(z, r)$ be a self-similar solution of the critical radial NLS (17.1), such that $|\psi(z, r)| = L^{-p}(z)V\left(\frac{r}{L(z)}\right)$. Then*

1. *The self-similar solution is given by*

$$\psi(z, r) = \frac{1}{L^{\frac{d}{2}}(z)} V(\rho) e^{iS(z, \rho)}, \quad S = LL_z \frac{\rho^2}{4} + c_1 \zeta(z) + c_2, \quad (17.5a)$$

where ρ and $\zeta(z)$ are given by (17.2b), and c_1 and c_2 are real constants.

2. *The profile V satisfies*

$$\Delta V(\rho) - c_1 V + |V|^{\frac{4}{d}} V + \frac{\beta}{4} \rho^2 V = 0, \quad V'(0) = 0, \quad (17.5b)$$

where β is a real constant.

3. *The width $L(z)$ satisfies*

$$L_{zz}(z) = -\frac{\beta}{L^3}. \quad (17.5c)$$

Proof By power conservation, $p = d/2$. Therefore, $\psi = L^{-\frac{d}{2}}(z)V(\rho)e^{iS(z, \rho)}$, where V and S are real. Substituting this in (17.1) gives

$$\begin{aligned} & i \underbrace{\left(-\frac{d}{2} L^{-\frac{d}{2}-1} L_z V + L^{-\frac{d}{2}} \frac{-rL_z}{L^2} V_\rho + L^{-\frac{d}{2}} Vi \left(S_z + S_\rho \frac{-rL_z}{L^2} \right) \right)}_{i\psi_z} \\ & + L^{-\frac{d}{2}-2} \underbrace{\left(\Delta V + 2iV_\rho S_\rho + V \left(i\Delta S - S_\rho^2 \right) \right)}_{\Delta\psi} + \underbrace{L^{-\frac{d}{2}-2} |V|^{\frac{4}{d}} V}_{|\psi|^{\frac{4}{d}}\psi} = 0. \end{aligned}$$

If we multiply by $L^{\frac{d}{2}+2}$ and rearrange, we get

$$\Delta V - L^2 \left(S_z - S_\rho \frac{\rho L_z}{L} \right) V + |V|^{\frac{4}{d}} V - S_\rho^2 V + iV \left(-\frac{d}{2} LL_z + \Delta S \right) + iV_\rho (-\rho LL_z + 2S_\rho) = 0.$$

Since V and S are real, the equations for the real and imaginary parts are

$$\Delta V - \left(L^2 \left(S_z - S_\rho \frac{\rho L_z}{L} \right) + S_\rho^2 \right) V + |V|^{\frac{4}{d}} V = 0, \quad (17.6a)$$

$$V \left(-\frac{d}{2} LL_z + \Delta S \right) + V_\rho (-\rho LL_z + 2S_\rho) = 0. \quad (17.6b)$$

Let $\xi = \mathbf{x}/L$, so that $|\xi| = \rho$. Then (17.6b) can be rewritten as

$$\nabla \cdot \left(V^2 \left(-\frac{LL_z}{2} \xi + \nabla S \right) \right) = 0.$$

Therefore, for any $0 < \rho_0 < \infty$,

$$\begin{aligned} 0 &= \int_{0 \leq |\xi| \leq \rho_0} \nabla \cdot \left(V^2 \left(-\frac{LL_z}{2} \xi + \nabla S \right) \right) d\xi \\ &= \int_{|\xi| = \rho_0} V^2 \left(-\frac{LL_z}{2} \xi + \nabla S \right) \cdot \mathbf{n} ds \\ &= \rho_0^{d-1} s_d V^2(\rho_0) \left(-\frac{\rho_0}{2} LL_z + S_\rho(\rho_0) \right), \end{aligned}$$

where s_d is the surface area of the d -dimensional unit ball. Hence,

$$-\frac{\rho}{2} LL_z + S_\rho \equiv 0.$$

The solution of this equation is $S = LL_z \frac{\rho^2}{4} + \tilde{\zeta}(z)$. Therefore, since

$$\begin{aligned} &L^2 \left(S_z - S_\rho \frac{\rho L_z}{L} \right) + S_\rho^2 \\ &= L^2 \left((LL_z)_z \frac{\rho^2}{4} + \tilde{\zeta}_z - (L_z)^2 \frac{\rho^2}{2} \right) + (LL_z)^2 \frac{\rho^2}{4} \\ &= -L^3 L_{zz} \frac{\rho^2}{4} - L^2 \tilde{\zeta}_z, \end{aligned}$$

Equation (17.6a) becomes

$$\Delta V - V \left(L^3 L_{zz} \frac{\rho^2}{4} + L^2 \tilde{\zeta}_z \right) + |V|^{\frac{4}{d}} V = 0.$$

Finally, since V should only depend on ρ , this implies that

$$-L^3 L_{zz} \equiv \beta, \quad L^2 \tilde{\zeta}_z \equiv c_1,$$

and so the result follows (with $\tilde{\zeta} = c_1 \zeta$). \square

Thus, all radial self-similar solutions are given by (17.5). These self-similar solutions were already analyzed in Sect. 11.1, where we saw that

$$L^2(z) = (L(0) + z L'(0))^2 - \frac{\beta}{L^2(0)} z^2.$$

Therefore,

1. If $\beta < 0$, $L(z)$ cannot go to zero (i.e., ψ cannot become singular).
2. If $\beta = 0$, then $L(z)$ is linear in z , Eq. (17.5b) for V reduces to Eq. (17.3) for R , and so $\psi = \psi_{R^{(n)}}^{\text{explicit}}$.
3. If $\beta > 0$, $L(z)$ can also go to zero. In that case, V identifies with the G profile, i.e., the solution of

$$G''(\rho) + \frac{d-1}{\rho} G' - c_1 G + |G|^{\frac{4}{d}} G + \gamma \rho^2 G = 0, \quad \gamma > 0 \quad (17.7)$$

with $\gamma = \beta/4$, and so $\psi = \psi_G^{\text{explicit}}$. The self-similar solution ψ_G^{explicit} , however, is not in H^1 (Chap. 11).

Corollary 17.1 *The only H^1 self-similar singular solutions of the critical radial NLS are the explicit blowup solutions $\psi_{R^{(n)}}^{\text{explicit}}$.*

The solutions $\psi_{R^{(n)}}^{\text{explicit}}$, however, are unstable (Sect. 10.6).

Corollary 17.2 *The radial critical NLS does not admit stable H^1 self-similar singular solutions.*

17.1.2 Relation to the Aberrationless Approximation

In Lemma 17.1 we saw that the reduced equation of self-similar solutions of the critical NLS is

$$L_{zz}(z) = -\frac{\beta}{L^3}, \quad \beta \equiv \text{constant}. \quad (17.8)$$

In Sect. 3.5 we derived the same reduced equation by applying the aberrationless approximation, see (3.29). This is not a coincidence, because self-similarity is the same as aberrationless propagation.

The difference between the aberrationless reduced equation (17.8) and the “correct” reduced equations (17.4) is that β is constant in the former but decays in the latter. As we shall see in Sect. 17.3, the decay of β corresponds to power transfer from the collapsing core to the non-collapsing tail. Obviously, this effect cannot be captured by self-similar/aberrationless solutions.

17.2 Dual Borderline Properties of $\psi_{R^{(0)}}$

In Sect. 7.12 we saw that the ground-state solitary wave $\psi^{\text{solitary},(0)} = e^{iz} R^{(0)}(r)$ has the dual borderline properties that any perturbation that lowers its power leads to scattering, whereas any perturbation that makes its Hamiltonian negative leads to collapse. We now show that $\psi_{R^{(0)}}$ inherits these dual borderline properties:

Lemma 17.2 *The profile $\psi_{R^{(0)}}$, see (17.2), is a borderline case for:*

1. *The sufficient condition for global existence $P < P_{\text{cr}}$ (Theorem 5.11).*
2. *The sufficient condition for collapse that follows from the variance identity (third condition of Theorem 7.2).*

Proof Since

$$\|\psi_{R^{(0)}}\|_2^2 = P_{\text{cr}}, \quad (17.9a)$$

$\psi_{R^{(0)}}$ is a borderline case for the condition $P < P_{\text{cr}}$. Indeed, any perturbation that lowers its power arrests collapse and leads to scattering (Sect. 8.4.7). In addition, as Exercise 17.1 shows, $\psi_{R^{(0)}}$ is a borderline case for the third condition of Theorem 7.2. \square

Exercise 17.1 *Show that if $L_z(z) < 0$, then*

$$H(\psi_{R^{(0)}}) > 0, \quad \text{Im} \int \psi_{R^{(0)}}^* \mathbf{x} \cdot \nabla \psi_{R^{(0)}} d\mathbf{x} = -\sqrt{H(\psi_{R^{(0)}}) V(\psi_{R^{(0)}})}. \quad (17.9b)$$

The dual borderline properties of $\psi_{R^{(0)}}$ show that it represents a *delicate balance between nonlinearity and diffraction*. As a result, the self-focusing dynamics is determined by the *small difference* between ψ and $\psi_{R^{(0)}}$, rather than by $\psi_{R^{(0)}}$, see Sect. 18.6.

The delicate balance between nonlinearity and diffraction cannot be captured by an *aberrationless approximation method* with a self-similar profile different from $\psi_{R^{(0)}}$. This is because $\psi_{R^{(0)}}$ is the only profile that satisfies both (17.9a) and (17.9b).¹

¹ This is because $R^{(0)}$ is the only profile that satisfies $H = 0$ and $P = P_{\text{cr}}$ (Corollary 5.11).

Moreover, the dynamics of the small difference between ψ and $\psi_{R^{(0)}}$ is determined by the exponentially-small power transfer from the collapsing core to the non-collapsing tail. The aberrationless approximation, however, “does not allow” for power transfers.

Remark Because of the dual borderline properties of $\psi_{R^{(0)}}$, the addition of small perturbations can have a large effect on the self-focusing dynamics. This sensitivity to small perturbations cannot be captured by aberrationless or variational methods, but only by an asymptotic theory which is based on the dynamics of the small difference between ψ and $\psi_{R^{(0)}}$. Such an asymptotic theory, called *modulation theory*, is developed in Chap. 31.

17.3 Quasi Self-similar Collapse

In what follows, we state several observations on solutions that collapse with the $\psi_{R^{(0)}}$ profile, and then use them to derive the reduced equations (17.4). These observations were originally based on numerical simulations (such as the ones in Sect. 14.1). A rigorous justification of these observations follows from the work of Merle and Raphaël (Sect. 14.6).

Observation 17.1 *A stable collapse with the $\psi_{R^{(0)}}$ profile is a partial-beam collapse and not a whole-beam collapse. Thus,*

$$\psi = \psi_{\text{coll}} + \psi_{\text{outer}},$$

where ψ_{coll} is the high-intensity inner core of the beam that undergoes collapse, and ψ_{outer} is the low-intensity outer “tail” which propagates forward.²

Observation 17.2 *As the inner core collapses, it approaches the $\psi_{R^{(0)}}$ profile. The collapsing core, however, is not equal to $\psi_{R^{(0)}}$, but only approaches it asymptotically, i.e.,*

$$\psi_{\text{coll}} \sim \psi_{R^{(0)}}, \quad z \rightarrow Z_c.$$

Indeed, we will see that the blowup dynamics is determined by the small difference between ψ_{coll} and $\psi_{R^{(0)}}$.

Observations 17.1 and 17.2 are related. Indeed, because the power P of stable singular solutions is above P_{cr} , see Lemma 13.4, and because the power of the collapsing core approaches $\|\psi_{R^{(0)}}\|_2^2 = P_{\text{cr}}$, from power conservation it follows that a positive amount of power ($P - P_{\text{cr}}$) does not collapse into the singularity. Hence, stable collapse with the $\psi_{R^{(0)}}$ profile has to be a partial-beam collapse.

Observation 17.3 *The outer part of the solution does not participate in the collapse process. Rather, it has a limit as $z \rightarrow Z_c$, i.e.,*

² We only consider collapse at a single point, because collapse at several points is unstable (Conclusion 13.2).

$$\lim_{z \rightarrow Z_c} \psi_{\text{outer}}(z, r) = \phi(r) \in L^2. \quad (17.10)$$

The dynamics of the collapsing core and of the outer solution occur on $O(\zeta)$ and $O(z)$ length scales, respectively. Since $dz = L^2 d\zeta$, ψ_{outer} appears to be frozen on the ζ length scale of the collapse. Therefore, relation (17.10) will be referred to as the frozen boundary condition.

Remark Unlike the self-similar solutions discussed in Sect. 17.1:

1. Only the inner part of the solution is “self-similar”.
2. Even this inner part is not equal to the self-similar profile, but only approaches it asymptotically.

Therefore, a stable collapse with the ψ profile is “only” *quasi self-similar*.

Remark Consider a solution that collapses with the $\psi_{R^{(0)}}$ profile. If ψ_0 is not close to $\psi_{R^{(0)}}$, the solution has to undergo a *reorganization stage*, during which it evolves into a collapsing core $\psi_{\text{coll}} \sim \psi_{R^{(0)}}$ and a non-collapsing tail ψ_{outer} . This reorganization stage is typically characterized by a “fast” power transfer from ψ_{coll} to ψ_{outer} (*non-adiabatic* self-focusing). The dynamics during the reorganization stage is not self-similar, since the solution profile changes from ψ_0 to $\psi_{R^{(0)}}$. Therefore, there is no self-similar profile around which one can average the NLS and obtain reduced equations.³

Conclusion 17.1 Generically, the reduced equations are not valid from $z = 0$, but only “sufficiently close” to Z_c , once Observations 17.1–17.3 hold.

Because $R^{(0)}$ decays exponentially as $\rho \rightarrow \infty$, see Lemma 6.14, $L(z)$ is a measure of the width of $\psi_{\text{coll}} \sim \psi_{R^{(0)}}$. Therefore, we can use it to give a more precise definition of ψ_{coll} and ψ_{outer} . A possible definition is

$$\psi = \begin{cases} \psi_{\text{coll}}, & \text{if } 0 \leq r \leq \rho_c L(z), \\ \psi_{\text{outer}}, & \text{if } r \gg \rho_c L(z), \end{cases} \quad (17.11)$$

with $\rho_c = O(1)$. Let us introduce the *quasi self-similar transformation*

$$\psi(z, r) = \frac{1}{L^{\frac{d}{2}}(z)} V(\zeta, \rho) e^{i\zeta + i \frac{L_z}{L} \frac{r^2}{4}}, \quad (17.12)$$

where ρ and $\zeta(z)$ are given by (17.2b). The resulting equation for V is

$$iV_\zeta(\zeta, \rho) + \Delta V - V + |V|^{\frac{4}{d}} V + \frac{1}{4} \beta(z) \rho^2 V = 0, \quad \beta = -L^3 L_{zz}, \quad (17.13)$$

see Lemma 8.2. Transformation (17.12) is only quasi self-similar, because unlike transformation (17.5):

³ Nevertheless, if $\|\psi_0\|_2^2 \gg P_{\text{cr}}$, one can derive reduced equations for the initial dynamics using the *NGO method* (Chap. 26).

1. V can depend on ζ .
2. Transformation (17.12) characterizes the inner core ψ_{coll} , but not the outer part ψ_{outer} . In other words, $V \rightarrow R^{(0)}$ for $0 \leq \rho \leq \rho_c$, but not for $\rho \gg \rho_c$.

Let us expand the solution of (17.13) in an asymptotic series

$$V \sim V_0 + V_1 + V_2 + \dots, \quad V_0 \gg V_1 \gg V_2 \gg \dots . \quad (17.14)$$

We expect that $V(\zeta, \rho) \sim V_0(\zeta, \rho) \sim R^{(0)}(\rho)$ for $0 \leq \rho \leq \rho_c$. Therefore, $V_\zeta \sim V_{0,\zeta} = o(1)$. Hence, the leading-order equation for V_0 in the collapsing-core region is^{4,5}

$$\Delta V_0 - V_0 + |V_0|^{\frac{4}{d}} V_0 + \frac{1}{4} \beta \rho^2 V_0 = 0, \quad 0 \leq \rho \leq \rho_c. \quad (17.15a)$$

In addition, since V_0 is radial,

$$V'_0(0) = 0. \quad (17.15b)$$

When $\beta = 0$, Eq. (17.15) for V_0 reduces to Eq. (17.3) for $R^{(0)}$. Therefore, Observation 17.2 that $V_0 \rightarrow R^{(0)}$ implies that $\beta \rightarrow 0$. In particular, for z sufficiently close to Z_c we should have that $\beta \ll 1$.

Since β is small, we can expand V_0 in an asymptotic series in β , i.e.,

$$V_0(\rho; \beta) \sim R^{(0)}(\rho) + \beta g(\rho) + O(\beta^2), \quad g = \left. \frac{\partial V_0}{\partial \beta} \right|_{\beta=0}. \quad (17.16)$$

Substituting (17.16) in (17.15) and collecting powers of β shows that the equation for g is

$$L_+ g = -\frac{1}{4} \rho^2 R^{(0)}, \quad g'(0) = 0, \quad g(\infty) = 0, \quad (17.17)$$

where $L_+ := \Delta - 1 + \left(\frac{4}{d} + 1\right) |R^{(0)}|^{\frac{4}{d}}$. Both $R^{(0)}$ and g decay exponentially as $\rho \rightarrow \infty$. Indeed, by Lemma 6.14

$$R^{(0)} \sim A_R \rho^{-\frac{d-1}{2}} e^{-\rho}, \quad \rho \gg 1, \quad (17.18)$$

where A_R is a constant.

⁴ In Sect. 17.6.2 we shall see that for the equation for V_0 to hold for $0 \leq \rho < \infty$ (i.e., for V_0 to satisfy the frozen boundary condition as $\rho \rightarrow \infty$), one has to add an exponentially-small imaginary term to Eq. (17.14).

⁵ Equation (17.15) for V_0 is that same as Eq. (11.4) for the G profile. Our convention is that ring-type solutions of this equation are denoted by G , and peak-type solutions (which are close to $R^{(0)}$) by V_0 .

Exercise 17.2 Let $g(\rho)$ be the solution of (17.17). Show that $g(\rho) \sim A_g \rho^3 R^{(0)}(\rho)$ as $\rho \rightarrow \infty$, where A_g is a constant.

Expansion (17.16) is uniform in $0 \leq \rho \leq \rho_c$, i.e., there exists a constant C , such that⁶

$$|V_0 - R^{(0)} - \beta g| \leq C\beta^2, \quad 0 \leq \rho \leq \rho_c.$$

Therefore,

$$\int_0^{\rho_c} |V_0|^2 \rho^{d-1} d\rho = \int_0^{\rho_c} |R^{(0)}|^2 \rho^{d-1} d\rho + 2\beta \int_0^{\rho_c} R^{(0)} g \rho^{d-1} d\rho + O(\beta^2).$$

Since $R^{(0)}$ and g decay exponentially, the error of replacing ρ_c with infinity in the right-hand side integrals is exponentially small.⁷ Therefore,

$$\int_0^{\rho_c} |V_0|^2 \rho^{d-1} d\rho = \int_0^{\infty} |R^{(0)}|^2 \rho^{d-1} d\rho + 2\beta \int_0^{\infty} R^{(0)} g \rho^{d-1} d\rho + O(\beta^2).$$

In Lemma 17.5 we will use regular perturbations to derive the identity

$$\int_0^{\infty} R^{(0)} g \rho^{d-1} d\rho = \frac{1}{8} \int_0^{\infty} \rho^2 |R^{(0)}|^2 \rho^{d-1} d\rho. \quad (17.19)$$

Therefore,

$$\int_0^{\rho_c} |V_0|^2 \rho^{d-1} d\rho = P_{\text{cr}} + \frac{\beta}{4} \int_0^{\infty} \rho^2 |R^{(0)}|^2 \rho^{d-1} d\rho + O(\beta^2).$$

Let $P_{\text{coll}}^{\text{radial}}$ denote the radial power of the collapsing core ψ_{coll} , i.e.,

$$P_{\text{coll}}^{\text{radial}} = P^{\text{radial}}(\psi_{\text{coll}}) = \int_0^{\rho_c L(z)} |\psi|^2 r^{d-1} dr. \quad (17.20)$$

Since

$$P_{\text{coll}}^{\text{radial}} = \int_0^{\rho_c} |V|^2 \rho^{d-1} d\rho \sim \int_0^{\rho_c} |V_0|^2 \rho^{d-1} d\rho,$$

⁶ This expansion is not uniform in $[0, \infty)$, as it is based on the assumption that $\beta\rho^2 \ll 1$. Indeed, while $R^{(0)}$ and g decay exponentially as $\rho \rightarrow \infty$, V_0 only has a polynomial decay (Sect. 11.2.1). This non-uniformity reflects the fact that the quasi self-similar transformation (17.12) is appropriate for the collapsing core ψ_{coll} , but not for the outer solution ψ_{outer} .

⁷ More precisely, we should let $\rho_c \sim \beta^{-q}$ with $q > 0$, so that the error of replacing ρ_c with infinity in the right-hand side integrals is exponentially small in β . We should also impose $q < 1/2$, so that $\beta\rho^2$ would remain a small perturbation in (17.15).

we have the following result, due to Malkin:⁸

Lemma 17.3 ([164]) *Let $P_{\text{coll}}^{\text{radial}}$ be given by (17.20). Then*

$$P_{\text{coll}}^{\text{radial}} = P_{\text{cr}}^{\text{radial}} + \beta M^{\text{radial}} + O(\beta^2), \quad \beta \ll 1, \quad (17.21)$$

where

$$P_{\text{cr}}^{\text{radial}} := \int_0^\infty |R^{(0)}(r)|^2 r^{d-1} dr, \quad M^{\text{radial}} := \frac{1}{4} \int_0^\infty r^2 |R^{(0)}(r)|^2 r^{d-1} dr.$$

Remark If we do not use radial integrals, relation (17.21) reads

$$P_{\text{coll}} = P_{\text{cr}} + \beta M + O(\beta^2),$$

where

$$P_{\text{coll}} = \int_{|\mathbf{x}| \leq \rho_c L(z)} |\psi|^2 d\mathbf{x}, \quad P_{\text{cr}} = \int |R^{(0)}|^2 d\mathbf{x}, \quad M = \frac{1}{4} \int |\mathbf{x}|^2 |R^{(0)}|^2 d\mathbf{x}. \quad (17.22)$$

The variable $\beta(z)$ was defined in (17.13) as

$$\beta = -L^3 L_{zz}. \quad (17.23)$$

As such, it measures the acceleration of the blowup rate. Lemma 17.3 shows, however, that near the blowup point

$$\beta \sim \frac{P_{\text{coll}} - P_{\text{cr}}}{M}. \quad (17.24)$$

Corollary 17.3 β is proportional to the excess power above P_{cr} of the collapsing core.

We can use these *dual interpretations* of β to better understand the collapse process. Thus, by (17.23), as $L(z)$ goes to zero, β has to be positive (Sect. 17.1.1). By (17.24), this implies that the power of the collapsing core is above P_{cr} . In addition, by (17.24), the observation that $\lim_{z \rightarrow z_c} \beta = 0$ implies that the amount of power that collapses into the singularity is exactly P_{cr} .

Malkin calculated the rate of power transfer from ψ_{coll} to ψ_{outer} using the WKB method:

Proposition 17.2 ([164]) *Let P_{coll} be the power of the collapsing core. Then*

$$\frac{d}{d\xi} P_{\text{coll}} \sim -M v(\beta), \quad \beta \rightarrow 0, \quad (17.25)$$

⁸ Here we implicitly assume that the contribution of V_1 to the power of V is at most $O(\beta^2)$. Indeed, from (17.63) it will follow that V_1 is exponentially small in β .

where $v(\beta)$ is given by (17.4b), and P_{coll} and M are given either by (17.20) and (17.4c), respectively, or by (17.22).

Proof See Sect. 17.5, or an alternative proof in Sect. 17.6.3. \square

Thus, the exponentially-small term $v(\beta)$ in the reduced equations (17.4a) accounts for power transfer from ψ_{coll} to ψ_{outer} . In particular, since β is small near the singularity, the self-focusing process becomes *adiabatic*, i.e., the rate at which $L(z)$ goes to zero is exponentially faster than the rate at which the excess power above P_{cr} of the collapsing core goes to zero.

Remark In the rescaled variable ρ , the change in the power of ψ_{coll} can be interpreted as *power transfer* from ψ_{coll} to ψ_{outer} . In the original variable r , however, a more accurate statement is that as ψ_{coll} collapses, it *leaves behind* its excess power above P_{cr} .

If we combine (17.21) with (17.25), we get that

$$\beta_\zeta \sim -v(\beta). \quad (17.26)$$

Rewriting (17.26) in terms of z gives the second reduced equation (17.4a). With this, the goal of reducing the critical NLS to a system of equations that do not depend on the transverse variables has been achieved.

Conclusion 17.2 *The reduced equations have an $O(\beta)$ accuracy.*

Proof The reduced equations are derived using the approximation $\beta \sim (P_{\text{coll}} - P_{\text{cr}})/M$, see Lemma 17.3, which has an $O(\beta)$ accuracy. \square

17.4 Perturbation Analysis for $U = R^{(0)} + \epsilon h$

In this section we use regular perturbations to calculate the leading-order effect of small deviations from the $R^{(0)}$ profile on the power and Hamiltonian. This calculation will be used in Lemma 17.5 to prove the integral identity (17.19). A similar calculation will be needed in Chap. 31, where we analyze the effect of small perturbations. Therefore, we present here a derivation that covers both cases. In particular, since some of the perturbations in Chap. 31 are nonradial, we allow U to depend on \mathbf{x} , rather than only on $|\mathbf{x}|$.

Lemma 17.4 *Let $U(\mathbf{x}; \epsilon)$ be a real function in H^1 that satisfies*

$$\Delta U - U + |U|^{\frac{4}{d}} U + \epsilon w(U) = 0, \quad (17.27)$$

where $w(U)$ is real, and let $H(U) = \int |\nabla U|^2 d\mathbf{x} - \frac{1}{\frac{2}{d}+1} \int |U|^{\frac{4}{d}+2} d\mathbf{x}$. Then

$$H(U) = \epsilon \int w(U) \left[\frac{d}{2} U + \mathbf{x} \cdot \nabla U \right] d\mathbf{x}. \quad (17.28)$$

Let

$$U(\mathbf{x}) = R^{(0)}(r) + \epsilon h(\mathbf{x}) + O(\epsilon^2), \quad |\epsilon| \ll 1, \quad (17.29)$$

where $r = |\mathbf{x}|$, and $R^{(0)}$ is the ground state solution of (17.3). Then h is the solution of

$$L_+ h = -w(R^{(0)}), \quad L_+ := \Delta - 1 + \left(\frac{4}{d} + 1 \right) |R^{(0)}|^{\frac{4}{d}}.$$

In addition, the following integral identities hold:

$$\int R^{(0)} h d\mathbf{x} = -\frac{1}{2} \int w(R^{(0)}) \left[\frac{d}{2} R^{(0)} + r \frac{dR^{(0)}}{dr} \right] d\mathbf{x}, \quad (17.30a)$$

$$\int \nabla R^{(0)} \nabla h d\mathbf{x} = \frac{1}{2} \int w(R^{(0)}) r \frac{dR^{(0)}}{dr} d\mathbf{x}, \quad (17.30b)$$

$$\int |R^{(0)}|^{\frac{4}{d}} R^{(0)} h d\mathbf{x} = -\frac{d}{4} \int w(R^{(0)}) R^{(0)} d\mathbf{x}. \quad (17.30c)$$

Therefore,

$$\|U\|_2^2 = \|R^{(0)}\|_2^2 + 2\epsilon \int R^{(0)} h d\mathbf{x} + O(\epsilon^2) \quad (17.31)$$

$$= \|R^{(0)}\|_2^2 - \epsilon \int w(R^{(0)}) \left[\frac{d}{2} R^{(0)} + r \frac{dR^{(0)}}{dr} \right] d\mathbf{x} + O(\epsilon^2), \quad (17.32)$$

and

$$H(U) = \epsilon \int w(R^{(0)}) \left[\frac{d}{2} R^{(0)} + r \frac{dR^{(0)}}{dr} \right] d\mathbf{x} + O(\epsilon^2) \quad (17.33)$$

$$= -2\epsilon \int R^{(0)} h d\mathbf{x} + O(\epsilon^2). \quad (17.34)$$

Proof We first derive the Pohozaev identities for U . If we multiply (17.27) by U and integrate by parts, we get that

$$-\int (\nabla U)^2 - \int |U|^2 + \int |U|^{\frac{4}{d}+2} + \epsilon \int w(U) U = 0. \quad (17.35)$$

Similarly, if we multiply (17.27) by $\mathbf{x} \cdot \nabla U$ and follow the derivation of (6.12), we get that

$$\frac{d-2}{2} \int (\nabla U)^2 + \frac{d}{2} \int |U|^2 - \frac{d}{\frac{4}{d}+2} \int |U|^{\frac{4}{d}+2} + \epsilon \int w(U) \mathbf{x} \cdot \nabla U = 0. \quad (17.36)$$

Multiplying (17.35) by $d/2$ and adding (17.36) gives (17.28). Equation (17.33) follows from (17.28) and (17.29).

If we multiply (17.3) by U and integrate by parts, we get

$$-\int \nabla R^{(0)} \nabla U - \int U R^{(0)} + \int U |R^{(0)}|^{\frac{4}{d}} R^{(0)} = 0. \quad (17.37)$$

The equation for the $O(\epsilon)$ terms in (17.35) is

$$-2 \int \nabla R^{(0)} \nabla h - 2 \int R^{(0)} h + \left(\frac{4}{d} + 2 \right) \int |R^{(0)}|^{\frac{4}{d}} R^{(0)} h = - \int w(R^{(0)}) R^{(0)}. \quad (17.38a)$$

The equation for the $O(\epsilon)$ terms in (17.36) is

$$(d-2) \int \nabla R^{(0)} \nabla h + d \int R^{(0)} h - d \int |R^{(0)}|^{\frac{4}{d}} R^{(0)} h = - \int w(R^{(0)}) r \frac{dR^{(0)}}{dr}. \quad (17.38b)$$

Finally, the equation for the $O(\epsilon)$ terms in (17.37) is

$$-\int \nabla R^{(0)} \nabla h - \int R^{(0)} h + \int |R^{(0)}|^{\frac{4}{d}} R^{(0)} h = 0. \quad (17.38c)$$

Equations (17.38) can be viewed as three linear equations for the three unknowns $\int R^{(0)} h$, $\int \nabla R^{(0)} \nabla h$, and $\int |R^{(0)}|^{\frac{4}{d}} R^{(0)} h$. Solving this linear system gives (17.30). Equation (17.32) follows from (17.31) and (17.30a). Equation (17.34) follows from (17.33) and (17.30a). \square

Corollary 17.4 *The results of Lemma 17.4 remain unchanged if we replace Eq.(17.27) with the equation*

$$\Delta U - U + |U|^{\frac{4}{d}} U + \epsilon w(U) = O(\epsilon^2).$$

Proof The $O(\epsilon^2)$ right-hand side does not affect the equations for the $O(1)$ and $O(\epsilon)$ terms in the proof of Lemma 17.4. \square

From Eqs. (17.31) and (17.34) it immediately follows that

$$\underbrace{\int |U|^2 - \int |R^{(0)}|^2}_{=O(\epsilon)} = \underbrace{-H(U)}_{=O(\epsilon)} + O(\epsilon^2). \quad (17.39)$$

Corollary 17.5 Let $U(\mathbf{x}) = R^{(0)}(r) + \epsilon h(\mathbf{x}) + O(\epsilon^2)$, where $h \in H^1$, $\epsilon \ll 1$, and $\int R^{(0)} h d\mathbf{x} \neq 0$. Then the two conditions for collapse agree asymptotically, i.e.,

$$H(U) < 0 \iff \int |U|^2 > P_{\text{cr}}. \quad (17.40)$$

This asymptotic agreement only holds for small deviations from the $R^{(0)}$ profile, because $R^{(0)}$ is the unique profile that simultaneously satisfies $\|R^{(0)}\|_2^2 = P_{\text{cr}}$ and $H(R^{(0)}) = 0$, see Sect. 7.12.

Exercise 17.3 Let $U(\mathbf{x}) = R^{(0)}(r) + \epsilon h(\mathbf{x}) + O(\epsilon^2)$, where $h \in H^1$ and $\int R^{(0)} h d\mathbf{x} > 0$. Show that $\|U\|_2^2 < P_{\text{cr}}$ for $-1 \ll \epsilon < 0$, and $H(U) < 0$ for $0 < \epsilon \ll 1$.

17.4.1 Perturbation Analysis for $V_0 \sim R^{(0)} + \beta g$

We now use Lemma 17.4 to prove the integral identity (17.19).

Lemma 17.5 $\int_0^\infty Rg \rho^{d-1} d\rho = \frac{1}{8} \int_0^\infty \rho^2 |R^{(0)}|^2 \rho^{d-1} d\rho$.

Proof We cannot apply Lemma 17.4 with $U = V_0$ directly, because $V_0 \notin L^2$ (Sect. 11.2.1). Therefore, we proceed as follows. Let $\tilde{V}_0 := R^{(0)} + \beta g$. Since $R^{(0)}$ and g decay exponentially (Lemma 6.14 and Exercise 17.2), $\tilde{V}_0 \in H^1$. Hence, we can apply Lemma 17.4 with $U = \tilde{V}_0$.

To find the equation satisfied by \tilde{V}_0 , we add Eqs. (17.3) and (17.17) multiplied by β . This gives

$$\Delta \tilde{V}_0 - \tilde{V}_0 + |R^{(0)}|^{\frac{4}{d}} R^{(0)} + \beta \left(\frac{4}{d} + 1 \right) |R^{(0)}|^{\frac{4}{d}} g + \frac{1}{4} \beta \rho^2 R^{(0)} = 0.$$

Therefore,

$$\begin{aligned} \Delta \tilde{V}_0 - \tilde{V}_0 + |\tilde{V}_0|^{\frac{4}{d}} \tilde{V}_0 + \frac{1}{4} \beta \rho^2 \tilde{V}_0 \\ = |\tilde{V}_0|^{\frac{4}{d}} \tilde{V}_0 - |R^{(0)}|^{\frac{4}{d}} R^{(0)} - \beta \left(\frac{4}{d} + 1 \right) |R^{(0)}|^{\frac{4}{d}} g + \frac{1}{4} \beta \rho^2 (\tilde{V}_0 - R^{(0)}) \\ = O(\beta^2). \end{aligned}$$

Note that the right-hand side is $O(\beta^2)$ for $0 \leq \rho < \infty$, because it consists of the exponentially-decreasing functions $R^{(0)}$ and g . Therefore, by Corollary 17.4, we can apply Lemma 17.4 with $U = \tilde{V}_0$, $\epsilon = \beta$, $w(U) = \frac{1}{4}\rho^2 U$, and $h = g$. Hence, by (17.30a),

$$\begin{aligned} \int_0^\infty R^{(0)} g \rho^{d-1} d\rho &= -\frac{1}{8} \int_0^\infty \rho^2 R^{(0)} \left(\frac{d}{2} R^{(0)} + \rho \frac{dR^{(0)}}{d\rho} \right) \rho^{d-1} d\rho \\ &= -\frac{1}{8} \int_0^\infty \rho^2 \left(R^{(0)} \rho^{\frac{d}{2}} \right)_\rho \left(R^{(0)} \rho^{\frac{d}{2}} \right) d\rho = \frac{1}{8} \int_0^\infty \rho^2 |R^{(0)}|^2 \rho^{d-1} d\rho. \end{aligned}$$

17.5 Calculation of $\frac{dP_{\text{coll}}}{dz}$ (Proof of Proposition 17.2)

We begin with an auxiliary result:

Lemma 17.6 *The rate of change of the power of ψ_{coll} is*

$$\frac{d}{dz} P_{\text{coll}} = \frac{1}{L^2} \left[i\rho^{d-1} V^* V_\rho + \text{c.c.} \right]_{\rho=\rho_c}, \quad (17.41)$$

where V is related to ψ through (17.12), and c.c. stands for complex conjugate.

Proof By definition,

$$\frac{d}{dz} P_{\text{coll}} = \frac{d}{dz} \int_0^{r_c(z)} |\psi|^2 r^{d-1} dr, \quad r_c(z) = L(z)\rho_c.$$

Therefore,

$$\frac{d}{dz} P_{\text{coll}} = r'_c(z) |\psi|^2 r_c^{d-1} + \int_0^{r_c} \frac{d}{dz} |\psi|^2 r^{d-1} dr, \quad r'_c(z) = L_z \rho_c = \frac{L_z}{L} r_c.$$

By (5.5), for any domain $\Omega \subset \mathbb{R}^d$,

$$\int_{\Omega} \frac{d}{dz} |\psi|^2 d\mathbf{x} = \int_{\partial\Omega} [i\psi^* \nabla \psi + \text{c.c.}] \cdot \mathbf{n} ds.$$

In particular, in the radial case,

$$\int_0^{r_c} \frac{d}{dz} |\psi|^2 r^{d-1} dr = \left[i\psi^* \psi_r r^{d-1} + \text{c.c.} \right]_{r=0}^{r=r_c}.$$

Hence,

$$\frac{d}{dz} P_{\text{coll}} = \left[\frac{L_z}{L} r^d |\psi|^2 + \left[i\psi^* \psi_r r^{d-1} + \text{c.c.} \right] \right]_{r=0}^{r=r_c}. \quad (17.42)$$

By (17.12),

$$\psi_r = i \frac{L_z}{L} \frac{r}{2} \psi + \frac{V_\rho}{L^{\frac{d}{2}+1}} e^{i\zeta+i\frac{L_z r^2}{L}}.$$

Therefore,

$$\psi^* \psi_r = i \frac{L_z}{L} \frac{r}{2} |\psi|^2 + \frac{1}{L^{d+1}} V^* V_\rho.$$

Substitution in (17.42) gives (17.41). \square

Our next goal is to compute the right-hand side of (17.41). If we do that by substituting the expansion

$$V \sim V_0 \sim R^{(0)} + \beta g + \dots, \quad 0 \leq \rho \ll \beta^{-\frac{1}{2}}, \quad (17.43)$$

we get zero, because both $R^{(0)}$ and g are real. In fact, even if we continue the expansion to higher orders in β , we would still get zero, because the higher-order terms are also real.⁹ As we shall see, the reason for this is that the rate of power radiation is exponentially small in β . Thus, a power series in β is too crude for this calculation.¹⁰

To carry out this asymptotics-beyond-all-orders calculation, we will calculate the rate of power radiation at $\rho_c \sim 2\beta^{-\frac{1}{2}}$. Because $\beta\rho_c^2 \neq o(1)$, expansion (17.43) is not valid at ρ_c . Therefore, to approximate V_0 at ρ_c , we first rewrite (17.15) as

$$\Delta_\rho V_0(\rho) - UV_0 = 0, \quad U = 1 - |V_0(\rho)|^{\frac{4}{d}} - \frac{1}{4}\beta\rho^2. \quad (17.44)$$

Since

$$V_0 \sim R^{(0)}(\rho), \quad 0 \leq \rho \ll \beta^{-\frac{1}{2}}, \quad (17.45)$$

one has

$$U \sim 1 - |R^{(0)}|^{\frac{4}{d}}, \quad 0 \leq \rho \ll \beta^{-\frac{1}{2}}.$$

Note that $U(0) < 0$, since $R^{(0)}(0) > 1$ (Corollary 6.10). In addition, since $R^{(0)}$ is monotonically decreasing, U changes its sign at the turning point $\rho_a = O(1)$, where $R^{(0)}(\rho_a) \approx 1$, see Fig. 17.1. Since $R^{(0)}$ decays exponentially,

$$U \sim 1 - \frac{1}{4}\beta\rho^2, \quad \rho \gg 1. \quad (17.46)$$

⁹ Indeed, Lemma 17.10 shows that V_0 , the solution of (17.15), is real (up to multiplication by a constant phase).

¹⁰ $\frac{d}{d\zeta} P_{\text{coll}}$ can be calculated from the right-hand side of (17.41), provided we add an exponentially-small imaginary correction to the equation for V_0 (Sect. 17.6.3).

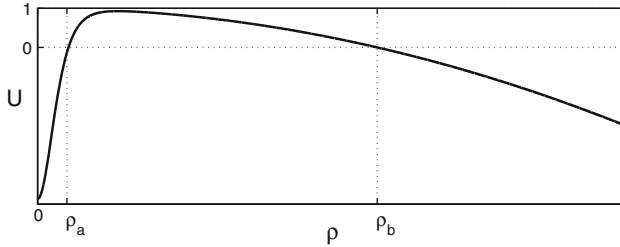


Fig. 17.1 Illustration of the potential U in (17.44)

Therefore, $U \sim 1$ in the overlap region $1 \ll \rho \ll \beta^{-\frac{1}{2}}$, and changes its sign at the second turning point $\rho_b \sim 2\beta^{-\frac{1}{2}}$.

As noted, our goal is to approximate V_0 at $\rho_c \approx \rho_b$.¹¹ To do that, we proceed as follows. When $\rho \gg 1$, the potential U is independent of V_0 , see (17.46), hence Eq.(17.44) is linear. In this linear regime, the potential U changes its sign at ρ_b . The solution is oscillatory in the classically-accessible region $\rho_b < \rho$ where $U < 0$, and exponentially decreasing in the classically-inaccessible region $1 \ll \rho < \rho_b$ where $U > 0$. Since the equation is linear for $\rho \gg 1$, we can approximate the solution using the WKB method (Lemma 17.7). The WKB approximation, however, breaks down at and near the turning point ρ_b . Therefore, we will obtain two WKB approximations: One valid to the right of ρ_b , denoted by $V_0^{\text{WKB,right}}$, and another valid to the left of ρ_b , denoted by $V_0^{\text{WKB,left}}$. Since Eq.(17.44) is of the second order, each of these WKB approximations has two undetermined coefficients; those of $V_0^{\text{WKB,right}}$ will be denoted by c_+ and c_- , see (17.52), and those of $V_0^{\text{WKB,left}}$ by d_1 and d_2 , see (17.57). From the frozen boundary condition (i.e., from matching ψ_{coll} with ψ_{outer}) it will follow that $c_- = 0$ (Lemma 17.8). To find the value of c_+ , we will use the connection formula past the turning point to express d_1 and d_2 in terms of c_+ and c_- , see (17.58). Finally, the value of d_1 , hence of c_+ , will be determined in Lemma 17.9 by matching $V_0^{\text{WKB,left}}$ with the approximation $V_0 \sim R^{(0)}$, which is valid in the nonlinear region $\rho = O(1)$.

To find the asymptotic behavior of V_0 for $\rho > \rho_b$, let

$$s := \delta\rho, \quad \delta := \frac{\beta^{\frac{1}{2}}}{2} \ll 1. \quad (17.47)$$

Then Eq.(17.44) reads

$$\delta^2 \Delta_s V_0 \left(\frac{s}{\delta} \right) - U V_0 = 0, \quad U(s) = 1 - \left| V_0 \left(\frac{s}{\delta} \right) \right|^{\frac{4}{d}} - s^2. \quad (17.48)$$

¹¹ And then substitute this approximation in (17.41).

In terms of the new independent variable s , the turning points are $s_a = \delta\rho_a = O(\delta)$ and $s_b \approx 1$. By (17.18), (17.45), and (17.47),

$$V_0 \sim A_R e^{-\frac{s}{\delta}} \left(\frac{s}{\delta}\right)^{-\frac{d-1}{2}}, \quad \delta \ll s \ll 1. \quad (17.49)$$

This expansion will be matched with $V_0^{\text{WKB, left}}$ in the proof of Lemma 17.9.

When $s \gg s_a = O(\delta)$, the nonlinearity becomes negligible, and so we can solve (17.48) using the WKB method.¹² To do that, let us recall the *quasi-classical limit* in quantum mechanics:

Lemma 17.7 *Let $V(x)$ be a solution of*

$$V''(x) + \frac{d-1}{x} V' + \frac{1}{\epsilon^2} Q(x) V = 0, \quad (17.50)$$

such that $Q(x) \neq 0$. Then $V(x) \sim V^{\text{WKB}}(x)$ as $\epsilon \rightarrow 0$, where

$$V^{\text{WKB}}(x) = \frac{1}{x^{\frac{d-1}{2}} Q^{\frac{1}{4}}(x)} \left[c_- e^{-\frac{i}{\epsilon} \int^x \sqrt{Q}} + c_+ e^{\frac{i}{\epsilon} \int^x \sqrt{Q}} \right]. \quad (17.51)$$

Proof We look for a solution of the form $V \sim e^{\frac{1}{\epsilon} h_0(x) + h_1(x) + \epsilon h_2(x) + \dots}$, where $\frac{1}{\epsilon} h_0(x) \gg h_1(x) \gg \epsilon h_2(x) \gg \dots$ as $\epsilon \rightarrow 0$. Substitution in (17.50) gives

$$\left(\frac{1}{\epsilon} h_0'' + h_1'' + \dots \right) + \left(\frac{1}{\epsilon} h_0' + h_1' + \dots \right)^2 + \frac{d-1}{x} \left(\frac{1}{\epsilon} h_0' + h_1' + \dots \right) + \frac{Q}{\epsilon^2} \sim 0.$$

Balancing the leading $O(\epsilon^{-2})$ terms gives

$$(h_0')^2 + Q = 0.$$

Therefore,

$$h_0' = \pm i \sqrt{Q}, \quad h_0 = \pm i \int^x \sqrt{Q}.$$

Balancing the $O(\epsilon^{-1})$ terms gives

$$h_0'' + 2h_0'h_1' + \frac{d-1}{x} h_0' = 0.$$

Thus,

$$h_1' = -\frac{d-1}{2x} - \frac{h_0''}{2h_0'}, \quad h_1 = -\frac{d-1}{2} \log x - \frac{1}{2} \log h_0'.$$

¹² For an introduction to the WKB method, see e.g., [20, 193].

It can be verified that $\epsilon h_2(x) = o(1)$. Therefore, the result follows. \square

The WKB expansion (17.51) is valid provided that $\frac{h_0(x)}{\epsilon} \gg h_1(x) \gg \epsilon h_2(x)$ and $\epsilon h_2(x) = o(1)$. These conditions are indeed satisfied when $Q(x) \neq 0$ and $\epsilon \rightarrow 0$. It can be shown that when $Q(x_0) = 0$ and $Q'(x_0) \neq 0$, the above conditions for the validity of the WKB expansion (17.51) are satisfied if $|x - x_0| \gg \epsilon^{\frac{2}{3}}$, see e.g., [20, Sect. 10.4].

We now use the WBK expansion (17.51) with

$$Q = -U = s^2 - 1 + \left| V_0 \left(\frac{s}{\delta} \right) \right|^{\frac{4}{d}}$$

to solve (17.48) for $s \gg \delta$. In this domain $Q \sim s^2 - 1$ has a turning point at $s_b \sim 1$. Since $Q'(s_b) \neq 0$, expansion (17.51) is valid when $|s - 1| \gg \delta^{\frac{2}{3}}$. Hence,

$$V_0 \sim V_0^{\text{WKB,right}}, \quad s - 1 \gg \delta^{\frac{2}{3}}, \quad \delta \rightarrow 0,$$

where

$$V_0^{\text{WKB,right}} = \frac{1}{s^{\frac{d-1}{2}} Q^{\frac{1}{4}}} \left[c_- e^{-i \frac{\delta}{\delta} \int_{s_b}^s \sqrt{Q}} + c_+ e^{+i \frac{\delta}{\delta} \int_{s_b}^s \sqrt{Q}} \right]. \quad (17.52)$$

Since we intend to calculate the rate of power radiation by substituting (17.52) in (17.41), we need to find the values of c_- and c_+ .

Lemma 17.8 *If ψ satisfies the frozen boundary condition (17.10), then $c_- = 0$.*¹³

Proof Since $Q \sim s^2$ for $s \gg 1$, it follows from (17.52) that

$$V_0^{\text{WKB,right}} \sim \frac{1}{s^{\frac{d}{2}}} \left[c_- e^{-i \frac{s^2}{2\delta}} + c_+ e^{+i \frac{s^2}{2\delta}} \right], \quad s \gg 1.$$

Since

$$\psi \sim \frac{V_0}{L^{\frac{d}{2}}} e^{i\zeta + i \frac{L_z}{L} \frac{r^2}{4}}, \quad \frac{s^2}{2\delta} = \frac{\delta}{2} \rho^2 = \frac{\beta^{\frac{1}{2}}}{4} \rho^2 = \frac{\beta^{\frac{1}{2}}}{4L^2} r^2,$$

we have that when $r \gg L/\beta^{\frac{1}{2}}$ (so that $s \gg 1$),

$$\psi \sim \frac{e^{i\zeta}}{(\delta r)^{\frac{d}{2}}} \left[c_- e^{i \frac{LL_z - \beta^{\frac{1}{2}}}{L^2} \frac{r^2}{4}} + c_+ e^{i \frac{LL_z + \beta^{\frac{1}{2}}}{L^2} \frac{r^2}{4}} \right].$$

¹³ i.e., there are no left-going waves as $\rho \rightarrow \infty$.

We claim that

$$\lim_{z \rightarrow Z_c} \frac{LL_z - \beta^{\frac{1}{2}}}{L^2} = -\infty, \quad \lim_{z \rightarrow Z_c} \frac{LL_z + \beta^{\frac{1}{2}}}{L^2} < \infty. \quad (17.53)$$

Therefore, ψ_{outer} satisfies the frozen boundary condition (17.10), and thus avoids having infinitely-fast spatial oscillations, only if $c_- = 0$.

To prove relations (17.53), we first assume that β is constant. In this case, if we multiply the equation

$$L_{zz} = -\frac{\beta}{L^3}$$

by $2L_z$, integrate, and multiply by L^2 , we get

$$L^2 L_z^2 = \beta + c_0 L^2. \quad (17.54)$$

Therefore, $\lim_{z \rightarrow Z_c} LL_z = \pm\sqrt{\beta}$. Since $L > 0$ and $L_z < 0$ as $z \rightarrow Z_c$, then

$$\lim_{z \rightarrow Z_c} LL_z = -\sqrt{\beta}.$$

Therefore, by (17.54), as $z \rightarrow Z_c$,

$$\frac{LL_z + \sqrt{\beta}}{L^2} = \frac{L^2 L_z^2 - \beta}{L^2 (LL_z - \sqrt{\beta})} \rightarrow -\frac{c_0}{2\sqrt{\beta}} < \infty$$

and

$$\lim_{z \rightarrow Z_c} \frac{LL_z - \sqrt{\beta}}{L^2} = \lim_{z \rightarrow Z_c} \frac{-2\sqrt{\beta}}{L^2} = -\infty.$$

If β is not a constant but varies significantly slower than L , these relations remain valid. In Sect. 18.5 we shall see that this is indeed the case. This will provide an a posteriori justification for the validity of (17.53). \square

Substituting $c_- = 0$ in (17.52) gives

$$V_0^{\text{WKB,right}} = \frac{c_+}{s^{\frac{d-1}{2}} Q^{\frac{1}{4}}} e^{+\frac{i}{\delta} \int_{s_b}^s \sqrt{Q}}. \quad (17.55)$$

Lemma 17.9

$$c_+ = A_R \delta^{\frac{d-1}{2}} e^{-\frac{\pi}{4\delta} + \frac{i\pi}{4}}. \quad (17.56)$$

Proof Application of the WKB expansion (17.51) to Eq.(17.48), to the left of the turning point $s_b \sim 1$, gives

$$V_0 \sim V_0^{\text{WKB,left}}, \quad \{s \gg \delta\} \cap \{1 - s \gg \delta^{\frac{2}{3}}\}, \quad \delta \rightarrow 0,$$

where

$$V_0^{\text{WKB, left}} = \frac{1}{s^{\frac{d-1}{2}} |Q|^{\frac{1}{4}}} \left[d_1 e^{-\frac{1}{\delta} \int_{s_b}^s \sqrt{|Q|}} + d_2 e^{+\frac{1}{\delta} \int_{s_b}^s \sqrt{|Q|}} \right], \quad (17.57)$$

and $|Q| = -Q = U \sim 1 - s^2$. To determine the values of d_1 and d_2 , one needs to connect expansion (17.55) for $V_0^{\text{WKB, right}}$ with expansion (17.57) for $V_0^{\text{WKB, left}}$. The connection formula is¹⁴

$$d_1 = c_+ e^{-i\frac{\pi}{4}}, \quad d_2 = 0. \quad (17.58)$$

Hence,

$$V_0^{\text{WKB, left}} = \frac{c_+ e^{-i\frac{\pi}{4}}}{s^{\frac{d-1}{2}} |Q|^{\frac{1}{4}}} e^{-\frac{1}{\delta} \int_{s_b}^s \sqrt{|Q|}}. \quad (17.59)$$

In particular, when $\delta \ll s \ll 1$, then $|Q| \sim 1$ and

$$V_0^{\text{WKB, left}} \sim \frac{c_+ e^{-i\frac{\pi}{4}}}{s^{\frac{d-1}{2}}} e^{-\frac{1}{\delta} \left(\int_1^0 \sqrt{1-s^2} ds + \int_0^s \sqrt{1-s^2} ds \right)} \sim \frac{c_+}{s^{\frac{d-1}{2}}} e^{-\frac{i\pi}{4} + \frac{\pi}{4\delta} - \frac{s}{\delta}},$$

where we used $s_b \sim 1$, $\int_0^1 \sqrt{1-s^2} ds = \pi/4$ and $\int_0^s \sqrt{1-s^2} ds \sim s$. Matching this expansion for $V_0^{\text{WKB, left}}$ with expansion (17.49) gives (17.56). \square

Rewriting (17.55) in terms of $\rho = s/\delta$ gives

$$V_0^{\text{WKB, right}} = \frac{c_+}{(\delta\rho)^{\frac{d-1}{2}} Q^{\frac{1}{4}}} e^{+i \int_{\rho_b}^{\rho} \sqrt{Q}}.$$

This approximation is valid for $\rho - \rho_b \gg \beta^{-\frac{1}{6}}$. If we substitute it into the right-hand side of (17.41) and use (17.47) and (17.56), we get that

$$\frac{1}{L^2} \left(i\rho^{d-1} V^* V_\rho + \text{c.c.} \right) \sim -\frac{1}{L^2} \frac{2|c_+|^2}{\delta^{d-1}} = -\frac{2A_R^2}{L^2} e^{-\frac{\pi}{\sqrt{\beta}}}, \quad \rho - \rho_b \gg \beta^{-\frac{1}{6}}.$$

Combining this with (17.41) proves (17.25). \square

17.5.1 A Remark on the Derivation

The WKB calculation in Sect. 17.5 shows that if ψ_{coll} satisfies the frozen boundary condition (17.10), then V_0 is complex to the right of s_b , see (17.55), but real (up to multiplication by a constant phase) to the left of s_b , see (17.59). On the other hand, we have

¹⁴ See e.g., [20, Chap. 10, Eq. (10.6.18)] and [150, Chap. 7, Eq. (50.2)].

Lemma 17.10 *Let V_0 be a solution of*

$$V_0''(\rho) + \frac{d-1}{\rho} V_0' - V_0 + |V_0|^{\frac{4}{d}} V_0 + \frac{1}{4} \beta \rho^2 V_0 = 0. \quad (17.60)$$

If $V_0'(0) = 0$, then $V_0(\rho)$ is real for all ρ (up to multiplication by $e^{i\alpha}$).

Proof Same as the proof of Lemma 6.12. \square

Corollary 17.6 *Let V_0 be a solution of (17.60). Then V_0 cannot simultaneously satisfy the symmetry condition $V_0'(0) = 0$ and the frozen boundary condition¹⁵ as $\rho \rightarrow \infty$.*

However, V_0 should satisfy both boundary conditions, since it is radial and since ψ_{outer} should satisfy the frozen boundary condition. To resolve this “contradiction”, we recall that the connection formula beyond the turning point at s_b is directional. Therefore, one cannot use it to go from the left of s_b (where V_0 is real) to the right of s_b (where V_0 is complex), but only in the opposite direction (see, e.g., [20, 150]). Moreover, the connection formula is only $O(\delta)$ accurate, and so $d_2 = O(\delta)$ and not zero. This implies that the second term in expression (17.57) is not identically zero, hence that V_0 is not “100% real” to the left of s_b . This second term is, however, quite small, since $d_2 = O(\delta)$ and since it decays exponentially as s decreases.

We thus see that if V_0 satisfies the frozen boundary condition as $\rho \rightarrow \infty$, it should have an exponentially-small imaginary component for $\rho = O(1)$. Therefore, in particular, the equation for V_0 cannot be (17.60). Indeed, in Sect. 17.6.2 we shall see that for V_0 to satisfy both the condition $V_0'(0) = 0$ and the frozen boundary condition, one has to add to Eq. (17.60) an exponentially-small imaginary term, see (17.61).

17.6 Derivation of Reduced Equations from a Solvability Condition

We now sketch a completely different derivation of the reduced equations, in which we consider singular solutions of the supercritical NLS, and take their limit $\sigma d \rightarrow 2+$. This approach was used by Landman et al. in their original derivation of the reduced system [151, 156]. A clear presentation of this derivation is given in [249].

17.6.1 “Correct” Equation for V_0

In Corollary 17.6 we saw that the solution of (17.60) cannot simultaneously satisfy the symmetry condition at the origin and the frozen boundary condition as $\rho \rightarrow \infty$.

¹⁵ i.e., be of the form (17.55).

To resolve this problem, Landman et al. considered the equation for V_0 in the *slightly-supercritical* regime

$$\sigma d = 2 + \epsilon, \quad 0 < \epsilon \ll 1.$$

The equation for the self-similar profile in the supercritical case¹⁶ is

$$\frac{d^2 V_0(\rho)}{d\rho^2} + \frac{d-1}{\rho} \frac{dV_0}{d\rho} - V_0 + |V_0|^{2\sigma} V_0 + \frac{\beta}{4} \rho^2 V_0 - i\sqrt{\beta} \frac{\sigma d - 2}{2\sigma} V_0 = 0, \quad 0 < \rho < \infty,$$

see (12.21),¹⁷ subject to

$$\frac{dV_0}{d\rho}(0) = 0, \quad V_0(\infty) = 0.$$

Adding the constraint that V_0 should be an *admissible solution*,¹⁸ so that it approaches $R^{(0)}$ as $\sigma d \rightarrow 2+$ (Sect. 12.6.1), determines a unique $\beta = \beta(\sigma, d)$. In particular, as $\sigma d \rightarrow 2+$, the equation for the admissible V_0 becomes, see (12.26),

$$\frac{d^2 V_0(\rho)}{d\rho^2} + \frac{d-1}{\rho} \frac{dV_0}{d\rho} - V_0 + |V_0|^{\frac{4}{d}} V_0 + \frac{\beta}{4} \rho^2 V_0 - i \frac{M}{2P_{\text{cr}}} v(\beta) V_0 = 0, \quad 0 < \rho < \infty. \quad (17.61)$$

Conclusion 17.3 *In the critical case, for the equation for V_0 to be valid for $0 < \rho < \infty$, it must contain an imaginary term, which is exponentially small in β .*

17.6.2 Solvability Condition

The remainder of the derivation in [151,156] is as follows.¹⁹ As before, the equation for V is

$$iV_\zeta(\zeta, \rho) + \Delta V - V + |V|^{\frac{4}{d}} V + \frac{1}{4} \beta(z) \rho^2 V = 0,$$

see (17.13). Since $V \sim V_0 + V_1 + \dots$, where $V_0(\rho; \beta(\zeta))$ is the solution of (17.61), the equation for V_1 reads

$$\begin{aligned} \Delta V_1 - V_1 + \left(1 + \frac{2}{d}\right) |V_0|^{\frac{4}{d}} V_1 + \frac{2}{d} |V_0|^{\frac{4}{d}} V_1^* + \frac{1}{4} \beta \rho^2 V_1 \\ = -i \frac{\partial V_0}{\partial \zeta} - i \frac{M}{2P_{\text{cr}}} v(\beta) V_0. \end{aligned} \quad (17.62)$$

¹⁶ i.e., the supercritical analog of (17.60).

¹⁷ In Chap. 12, V_0 is denoted by P .

¹⁸ i.e., that $|V_0(\rho)|$ is monotonically decreasing and $H(e^{-i\frac{\sqrt{\beta}\rho^2}{4}} V_0) = 0$, see Sect. 12.6.1.

¹⁹ Alternatively, at this stage we could also proceed by using (17.61) to prove Proposition 17.2, see Sect. 17.6.3.

As before, for $0 \leq \rho \ll \beta^{-\frac{1}{2}}$ we can expand

$$V_0(\zeta, \rho) \sim R^{(0)}(\rho) + \beta(\zeta)g(\rho) + O(\beta^2),$$

where $R^{(0)}$ and g are the solutions of (17.3) and (17.17), respectively. Therefore,

$$V_0 \sim R^{(0)}, \quad \beta\rho^2 = o(1), \quad \frac{dV_0}{d\zeta} \sim g \frac{d\beta}{d\zeta}.$$

Hence, to leading order, Eq. (17.62) reads

$$\Delta V_1 - V_1 + \left(1 + \frac{2}{d}\right) |R^{(0)}|^{\frac{4}{d}} V_1 + \frac{2}{d} |R^{(0)}|^{\frac{4}{d}} V_1^* = -i \frac{d\beta}{d\zeta} g - i \frac{M}{2P_{\text{cr}}} v(\beta) R^{(0)}. \quad (17.63)$$

Lemma 17.11 *Let V_1 be the solution of*

$$\Delta V_1(\mathbf{x}) - V_1 + \left(1 + \frac{2}{d}\right) |R^{(0)}|^{\frac{4}{d}} V_1 + \frac{2}{d} |R^{(0)}|^{\frac{4}{d}} V_1^* = iq(\mathbf{x}), \quad (17.64)$$

where $q(\mathbf{x})$ is real and $R^{(0)}$ is the ground state of (17.3). Then the solvability condition for V_1 is $\int R^{(0)} q d\mathbf{x} = 0$.

Proof Let $V_1 = S + iT$, where S and T are real. Then (17.64) reads

$$L_+ S = 0, \quad L_- T = q,$$

where

$$L_+ = \Delta - 1 + \left(1 + \frac{4}{d}\right) |R^{(0)}|^{\frac{4}{d}}, \quad L_- = \Delta - 1 + |R^{(0)}|^{\frac{4}{d}}.$$

The operators L_+ and L_- are self-adjoint, and their null spaces are $N(L_+) = \text{span}\{\nabla R^{(0)}\}$ and $N(L_-) = \text{span}\{R^{(0)}\}$, see Lemma 17.12 below. Therefore, by the Fredholm Alternative Theorem, the equation for S is solvable. The equation for T is solvable, however, only if its right-hand side is orthogonal to $R^{(0)}$. \square

Lemma 17.12 ([273]) *L_- and L_+ are self-adjoint operators in L^2 with null spaces $N(L_-) = \text{span}\{R^{(0)}\}$ and $N(L_+) = \text{span}\left\{\frac{\partial R^{(0)}}{\partial x_j}\right\}_{j=1}^d$, respectively.*

Proof

1. Since $L_- R^{(0)} = 0$ and $R^{(0)} \in L^2$, $R^{(0)}$ is in the null space of L_- . Since $R^{(0)}$ is positive, it is the ground state of the eigenvalue problem $L_- u = \lambda u$. Because the ground state of an eigenvalue problem is unique, there are no other functions in the null space.

2. Differentiating (17.3) with respect to x_j gives $L_+ \frac{\partial R^{(0)}}{\partial x_j} = 0$. Therefore, since $\frac{\partial R^{(0)}}{\partial x_j} \in L^2$, it is in the null space of L_+ . That the null space only consists of $\nabla R^{(0)}$, was proved in [273] for the case $d = 1$ and $\sigma > 0$ and for the case $d = 3$ and $0 < \sigma \leq 1$, and in [93] for the radial case in any dimension. \square

By Lemma 17.11, the solvability condition for (17.63) is

$$\int R^{(0)} \left[g\beta_\zeta + \frac{M}{2P_{\text{cr}}} v(\beta) R^{(0)} \right] d\mathbf{x} = 0.$$

Since $\int |R^{(0)}|^2 d\mathbf{x} = P_{\text{cr}}$ and $\int R^{(0)} g d\mathbf{x} = M/2$, see Lemma 17.5, the solvability condition leads to (17.26).

17.6.3 Alternative Proof of Proposition 17.2

In Lemma 17.6 we proved that

$$\frac{d}{d\zeta} P_{\text{coll}}^{\text{radial}} = \left[i\rho^{d-1} V^* \frac{dV}{d\rho} + \text{c.c.} \right]_{\rho=\rho_c}.$$

In Sect. 17.5 we could not use this relation with $V \sim V_0$ to calculate the right-hand side at $1 \ll \rho_c \ll \beta^{-\frac{1}{2}}$, since the solution V_0 of (17.15) is real at ρ_c . Once we know that the correct equation for V_0 is (17.61), however, we can proceed as follows. If we multiply (17.61) by $\rho^{d-1} V_0^*$, subtract the complex-conjugate equation, and integrate between $\rho = 0$ and $\rho = \rho_c$, we get

$$\left[\rho^{d-1} V_0^* \frac{dV_0}{d\rho} + \text{c.c.} \right]_{\rho=\rho_c} = i \frac{M}{P_{\text{cr}}} v(\beta) \int_0^{\rho_c} |V_0|^2 \rho^{d-1} d\rho.$$

Therefore,

$$\frac{d}{d\zeta} P_{\text{coll}}^{\text{radial}} \sim - \frac{M}{P_{\text{cr}}} v(\beta) \int_0^{\rho_c} |R^{(0)}|^2 \rho^{d-1} d\rho \sim -M^{\text{radial}} v(\beta).$$

17.7 Numerical Values of P_{cr} , M , A_R , and c_v

In this section we provide the numerical values of

$$P_{\text{cr}} = \int |R^{(0)}|^2 d\mathbf{x}, \quad M = \frac{1}{4} \int |\mathbf{x}|^2 |R^{(0)}|^2 d\mathbf{x},$$

$$\begin{aligned} P_{\text{cr}}^{\text{radial}} &= \int_0^\infty |R^{(0)}|^2 r^{d-1} dr, & M^{\text{radial}} &= \frac{1}{4} \int_0^\infty r^2 |R^{(0)}|^2 r^{d-1} dr, \\ A_R &= \lim_{r \rightarrow \infty} e^r r^{\frac{d-1}{2}} R^{(0)}(r), & c_v &= \frac{2A_R^2}{M^{\text{radial}}}. \end{aligned}$$

Clearly, $P_{\text{cr}} = s_d \cdot P_{\text{cr}}^{\text{radial}}$ and $M = s_d \cdot M^{\text{radial}}$, where s_d is the surface area of the unit sphere in d dimensions, i.e.,

$$s_2 = 2\pi, \quad s_3 = 4\pi, \quad s_4 = 2\pi^2, \quad s_5 = \frac{8}{3}\pi^2, \dots \quad (17.65)$$

17.7.1 $d = 1$

When $d = 1$, $R^{(0)}(x) = 3^{\frac{1}{4}} \cosh^{-\frac{1}{2}}(2x)$, see Lemma 6.15. Therefore,

$$\begin{aligned} P_{\text{cr}} &= \int_{-\infty}^\infty |R^{(0)}(x)|^2 dx = \int_{-\infty}^\infty 3^{\frac{1}{2}} \cosh^{-1}(2x) dx \approx 2.7207, \\ P_{\text{cr}}^{\text{radial}} &= \int_0^\infty |R^{(0)}(x)|^2 dx = \int_0^\infty 3^{\frac{1}{2}} \cosh^{-1}(2x) dx \approx 1.3603. \end{aligned}$$

In addition,

$$R^{(0)} = 3^{\frac{1}{4}} \left(\frac{e^{2x} + e^{-2x}}{2} \right)^{-\frac{1}{2}} \sim 3^{\frac{1}{4}} 2^{\frac{1}{2}} e^{-x}, \quad x \rightarrow \infty.$$

Therefore, $A_R = \lim_{r \rightarrow \infty} e^r R^{(0)}(r) = 3^{\frac{1}{4}} 2^{\frac{1}{2}} \approx 1.8612$. Finally,

$$M^{\text{radial}} = \frac{1}{4} \int_0^\infty r^2 3^{\frac{1}{2}} \cosh^{-1}(2r) dr \approx 0.2098, \quad c_v = \frac{2A_R^2}{M^{\text{radial}}} \approx 33.02.$$

17.7.2 $d = 2$

When $d = 2$, Eq. (17.3) has a countable number of solutions. The ground state can be calculated numerically, see Chap. 28, yielding

$$P_{\text{cr}} = \int_{\mathbb{R}^2} |R^{(0)}|^2 dxdy \approx 11.701, \quad P_{\text{cr}}^{\text{radial}} = \int_0^\infty |R^{(0)}|^2(r) r dr \approx 1.8623,$$

$$A_R = \lim_{r \rightarrow \infty} e^r r^{\frac{1}{2}} R^{(0)}(r) \approx 3.52, \quad M^{\text{radial}} = \frac{1}{4} \int_0^\infty r^2 |R^{(0)}|^2 r dr \approx 0.5529,$$

and $c_v = \frac{2A_R^2}{M^{\text{radial}}} \approx 44.8$.

Remark If one computes A_R directly from $A_R = \lim_{r \rightarrow \infty} e^r r^{\frac{1}{2}} R^{(0)}(r)$, the obtained value depends on the numerical values of $R^{(0)}$ at large r . Since $R^{(0)}$ is exponentially decaying, these numerical values are considerably less accurate than those for $r = O(1)$.²⁰ One can, however, obtain a more accurate value by calculating A_R from the identity

$$A_R = \left(\frac{\pi}{2}\right)^{\frac{1}{2}} \int_0^\infty (R^{(0)})^3(r) I_0(r) r dr, \quad (17.66)$$

where $I_0(r)$ is the solution of the modified Bessel equation

$$I_0''(r) + \frac{1}{r} I_0'(r) - I_0(r) = 0$$

which is bounded as $r \rightarrow 0$ and satisfies

$$I_0'(0) = 0, \quad I_0(r) \sim \frac{e^r}{\sqrt{2\pi r}} \quad \text{as } r \rightarrow \infty. \quad (17.67)$$

Exercise 17.4 Prove (17.66) using integration by parts and (17.67).

²⁰ This is especially the case if one computes $R^{(0)}$ using the *shooting* method (Sect. 28.1).

Chapter 18

Loglog Law and Adiabatic Collapse

In Chap. 17 we considered solutions of the critical NLS

$$i\psi_z(z, \mathbf{x}) + \Delta\psi + |\psi|^{\frac{4}{d}}\psi = 0, \quad \psi(0, \mathbf{x}) = \psi_0(\mathbf{x}) \in H^1 \quad (18.1)$$

that undergo a stable, quasi self-similar collapse with the $\psi_{R^{(0)}}$ profile. We saw that to leading order, the dynamics of the collapsing core ψ_{coll} evolves according to the *reduced equations*

$$L_{zz}(z) = -\frac{\beta}{L^3}, \quad \beta_z(z) = -\frac{\nu(\beta)}{L^2}, \quad (18.2)$$

where $\nu(\beta) = c_v e^{-\pi/\sqrt{\beta}}$, c_v is a positive constant, L is the width of ψ_{coll} , and β is proportional to its excess power above P_{cr} .

Equations (18.2) were derived by Fraiman, and independently by Landman, LeMesurier, Papanicolaou, Sulem, and Sulem. By solving (18.2) asymptotically, they showed that $L(z)$ goes to zero as a square root with a loglog correction:

Proposition 18.1 ([100, 151, 156]) *Let $L(z)$ be a solution of (18.2), such that $\beta(0) > 0$, $L(0) > 0$, and $\lim_{z \rightarrow Z_c} L(z) = 0$. Then*

$$L(z) \sim \left(\frac{2\pi(Z_c - z)}{\log \log \frac{1}{Z_c - z}} \right)^{\frac{1}{2}}, \quad z \rightarrow Z_c \quad (\text{loglog law}). \quad (18.3)$$

Proof See Sect. 18.2. □

By Lemma 18.1 below, the blowup rate of solutions that collapse with the $\psi_{R^{(0)}}$ profile satisfies

$$l(z) := \frac{1}{\|\nabla\psi\|_2} \sim \frac{L(z)}{\|\nabla R^{(0)}\|_2}, \quad z \rightarrow Z_c.$$

Therefore, Proposition 18.1 implies

Proposition 18.2 ([100, 151, 156]) *Let ψ be a solution of the critical NLS (18.1) that undergoes a stable quasi self-similar collapse with the $\psi_{R^{(0)}}$ profile. Then*

$$l(z) \sim \frac{\sqrt{2\pi}}{\|\nabla R^{(0)}\|_2} \left(\frac{Z_c - z}{\log \log \frac{1}{Z_c - z}} \right)^{\frac{1}{2}}, \quad z \rightarrow Z_c. \quad (18.4)$$

Remark A rigorous proof of (18.4) took almost twenty years, see Sect. 14.6.

After the discovery of the loglog law, researchers tried to observe it numerically, but did not succeed. It later turned out that the reason for this is that the loglog law does not become valid even after the NLS solution focuses by 10^{15} . The validity of the NLS as a physical model for laser propagation, however, breaks down much earlier, at focusing levels of 10^2 – 10^3 (Sect. 1.8). This “failure” of the loglog law in the domain of physical interest has nothing to do with the validity of the reduced equations. Indeed, once solved by means of the *adiabatic approach*, the reduced equations lead to the *adiabatic laws for critical collapse*, which become valid after moderate self-focusing. The adiabatic laws and the loglog law are in asymptotic agreement as $z \rightarrow Z_c$. Their domains of validity, however, differ considerably.

18.1 Preliminary Observations

The reduced equations (18.2) were derived for NLS solutions that collapse with the $\psi_{R^{(0)}}$ profile, where

$$\psi_{R^{(0)}}(z, r) = \frac{1}{L^{\frac{d}{2}}(z)} R^{(0)}(\rho) e^{i\zeta + i \frac{L_z}{L} \frac{r^2}{4}}, \quad \rho = \frac{r}{L(z)}, \quad \zeta(z) = \int_0^z \frac{ds}{L^2(s)}, \quad (18.5)$$

and $R^{(0)}$ is the ground state of

$$R''(\rho) + \frac{d-1}{\rho} R' - R + |R|^{\frac{4}{d}} R = 0, \quad R'(0) = 0, \quad R(\infty) = 0. \quad (18.6)$$

Here $L(z)$, ρ , and ζ are the dimensionless width, the rescaled transverse coordinate, and the rescaled axial coordinate, respectively, of the collapsing core $\psi_{\text{coll}} \sim \psi_{R^{(0)}}$. The relation between the blowup rates of $L(z)$ and $l(z)$ is as follows:

Lemma 18.1 *Under the conditions of Proposition 18.2,*

$$l(z) \sim \frac{L(z)}{\|\nabla R^{(0)}\|_2}, \quad z \rightarrow Z_c. \quad (18.7)$$

Proof By (13.30), $l(z) \sim c_l L(z)$, where $c_l = \left(\left(\frac{2}{d} + 1 \right) / \|R^{(0)}\|_2^{\frac{4}{d}+2} \right)^{\frac{1}{2}}$. In addition, by (6.7b), $\|R^{(0)}\|_2^{\frac{4}{d}+2} / \left(\frac{2}{d} + 1 \right) = \|\nabla R^{(0)}\|_2^2$. \square

Let

$$A(z) := \frac{1}{L(z)}. \quad (18.8)$$

By (18.5), A is proportional to the on-axis amplitude, i.e.,

$$A(z) = c_A |\psi_{R^{(0)}}(z, 0)|^{\frac{2}{d}} \sim c_A |\psi(z, 0)|^{\frac{2}{d}}, \quad c_A = (R^{(0)}(0))^{-\frac{2}{d}}.$$

Therefore, collapse corresponds to $\lim_{z \rightarrow Z_c} A(z) = \infty$. By (18.2) and (18.8),

$$\beta = \frac{A_{\xi\xi}}{A}, \quad \xi(z) = \int_0^z \frac{ds}{L^2(s)}. \quad (18.9)$$

Therefore, the reduced equations (18.2) can be written in terms of ξ as

$$A_{\xi\xi}(\xi) = \beta A, \quad (18.10a)$$

$$\beta_{\xi}(\xi) = -v(\beta), \quad (18.10b)$$

$$z_{\xi}(\xi) = \frac{1}{A^2}. \quad (18.10c)$$

This formulation has two advantages (which will be utilized in Sect. 18.2): The equation for β is decoupled from the equations for A and z , and the equation for A is linear.

Exercise 18.1 Prove relation (18.9).

Let us make some additional observations.

Proposition 18.3 Let ψ be as in Proposition 18.2, and let β and ξ be the corresponding variables of the reduced equations. Then

$$\lim_{z \rightarrow Z_c} \xi(z) = \infty, \quad (18.11)$$

$$\lim_{\xi \rightarrow \infty} \beta(\xi) = 0, \quad \lim_{z \rightarrow Z_c} \beta(z) = 0. \quad (18.12)$$

Proof By (18.7),

$$\xi(z) = \int_0^z \frac{ds}{L^2(s)} \sim \frac{1}{\|\nabla R^{(0)}\|_2^2} \int_0^z \|\nabla \psi(s)\|_2^2 ds.$$

In Theorem 13.1 we saw that $\|\nabla\psi(z)\|_2^2 \geq K^2(Z_c - z)^{-1}$. Therefore,

$$\lim_{z \rightarrow Z_c} \zeta(z) \geq \frac{K^2}{\|\nabla R^{(0)}\|_2^2} \lim_{z \rightarrow Z_c} \int_0^z \frac{ds}{Z_c - s} = \infty,$$

which proves (18.11).

By (18.11), $\lim_{z \rightarrow Z_c} \beta(z) = \lim_{\zeta \rightarrow \infty} \beta(\zeta)$. In addition, by (18.10b), β is monotonically decreasing and $\beta \rightarrow 0$ as $\zeta \rightarrow \infty$. Hence, (18.12) follows. \square

Relation (18.12) has two interpretations:

1. If we think of $\beta \sim (P_{\text{coll}} - P_{\text{cr}})/M$ as the excess power above P_{cr} of the collapsing core ψ_{coll} , see Lemma 17.3, relation (18.12) implies

Corollary 18.1 *Let ψ be as in Proposition 18.2. Then the amount of power that collapses into the singularity is exactly P_{cr} .*

2. If we think of $\beta = -L^3 L_{zz}$ as a measure of the acceleration of the blowup rate, and recall that by Lemma 11.2, $\beta(z) \equiv \text{constant}$ implies the square-root blowup rate $L(z) \sim (4\beta)^{\frac{1}{4}}(Z_c - z)^{\frac{1}{2}}$, then (18.12) implies

Corollary 18.2 *Let ψ be as in Proposition 18.2. Then its blowup rate is faster than a square root.*

Finally, we list some useful relations among the reduced-equations variables:

Lemma 18.2 *Let $\beta = -L^3 L_{zz}$ and $\zeta = \int_0^z L^{-2}$. Then*

$$\beta = \frac{1}{4}(y_z)^2 - \frac{1}{2}yy_{zz} = \frac{A_\zeta \zeta}{A} = a^2 + a_\zeta \quad (18.13a)$$

and

$$\beta_z = -\frac{1}{2}yy_{zzz}, \quad (18.13b)$$

where

$$y = L^2, \quad A = \frac{1}{L}, \quad a = -LL_z = -\frac{L_\zeta}{L} = \frac{A_\zeta}{A}.$$

18.2 Derivation of the Loglog Law (Proof of Proposition 18.1)

In the reduced equations (18.10), Eq. (18.10b) for β is decoupled from the other two equations, and Eq. (18.10b) for A is decoupled from Eq. (18.10c) for z . This suggests the following approach for solving (18.10):

1. Solve Eq. (18.10b) for $\beta(\zeta)$.
2. Use the solution for $\beta(\zeta)$ and Eq. (18.10a) to solve for $A(\zeta)$.
3. Use the solution for $A(\zeta)$ and Eq. (18.10c) to express A as a function of z .

We now use this approach to derive the *loglog law* (18.3).

18.2.1 Solve Eq. (18.10b) for $\beta(\zeta)$

Equation (18.10b) for β cannot be solved exactly. To solve it asymptotically, we first rewrite it as

$$\lambda_\zeta(\zeta) = \frac{c_v}{2\pi^2} \lambda^3 e^{-\lambda}, \quad \lambda = \frac{\pi}{\sqrt{\beta}}. \quad (18.14)$$

From (18.12) we have that $\lim_{\zeta \rightarrow \infty} \lambda = \infty$. Therefore, we can use the fact that $\lambda \gg 1$ to solve (18.14) to leading order:

Lemma 18.3 *Let $\lambda(\zeta)$ be the solution of (18.14) with $\lambda(0) = \lambda_0 \gg 1$. Then*

$$\zeta \sim \frac{2\pi^2}{c_v} \frac{e^\lambda}{\lambda^3}, \quad \lambda - \lambda_0 \gg 1. \quad (18.15)$$

Proof From (18.14) we have that

$$\zeta = \int_{\lambda_0}^{\lambda} \frac{d\xi}{d\lambda} d\lambda = \int_{\lambda_0}^{\lambda} \left(\frac{d\lambda}{d\xi} \right)^{-1} d\lambda = \frac{2\pi^2}{c_v} \int_{\lambda_0}^{\lambda} \lambda^{-3} e^\lambda d\lambda.$$

We can use integration by parts to expand the integral in an asymptotic series in λ^{-1} :

$$\begin{aligned} \int_{\lambda_0}^{\lambda} \lambda^{-3} e^\lambda d\lambda &= \lambda^{-3} e^\lambda \Big|_{\lambda_0}^{\lambda} + 3 \int_{\lambda_0}^{\lambda} \lambda^{-4} e^\lambda d\lambda \\ &= \lambda^{-3} e^\lambda \Big|_{\lambda_0}^{\lambda} + 3 \lambda^{-4} e^\lambda \Big|_{\lambda_0}^{\lambda} + 12 \int_{\lambda_0}^{\lambda} \lambda^{-5} e^\lambda d\lambda = \dots . \end{aligned}$$

Therefore,

$$\int_{\lambda_0}^{\lambda} \lambda^{-3} e^\lambda d\lambda \sim e^\lambda \left(\lambda^{-3} + 3\lambda^{-4} + \dots \right) \Big|_{\lambda_0}^{\lambda}.$$

Since $\lambda - \lambda_0 \gg 1$, we have that $e^\lambda \gg e^{\lambda_0}$. Since, in addition, $\lambda \gg 1$, we get that $\int_{\lambda_0}^{\lambda} \lambda^{-3} e^\lambda d\lambda \sim e^\lambda \lambda^{-3}$, from which the result follows. \square

Taking the log of both sides of relation (18.15) gives

$$\log \zeta \sim \log \frac{2\pi^2}{c_v} + \lambda - 3 \log \lambda \sim \lambda, \quad \zeta \rightarrow \infty.$$

Therefore, by (18.14),

$$\beta \sim \frac{\pi^2}{\log^2 \zeta}, \quad \zeta \rightarrow \infty. \quad (18.16)$$

As expected, see (18.12), β vanishes at the singularity. Note that the constant c_v has no effect on the leading-order behavior of $\beta(\zeta)$, hence also on that of $L(\zeta)$.

18.2.2 Use the Solution for $\beta(\zeta)$ and Eq. (18.10a) to Solve for $A(\zeta)$

We are now in a position to solve for $A(\zeta)$:

Lemma 18.4 *Let $A(\zeta)$ be a solution of (18.10a), where β satisfies (18.16). Then as $\zeta \rightarrow \infty$,*

$$A \sim c_A e^{f_0(\zeta) + f_1(\zeta)}, \quad (18.17a)$$

where

$$f_0 \sim \zeta \sqrt{\beta} \sim \frac{\pi \zeta}{\log \zeta}, \quad f_1 \sim \log \beta^{-\frac{1}{4}} \sim \log \left(\frac{\pi}{\log \zeta} \right)^{-\frac{1}{2}}. \quad (18.17b)$$

Proof We look for a solution of the form

$$A \sim e^{f_0(\zeta) + f_1(\zeta) + \dots}, \quad f_0(\zeta) \gg f_1(\zeta) \gg \dots, \quad \zeta \rightarrow \infty. \quad (18.18)$$

Substitution in (18.10a) gives

$$(f_0'' + f_1'' + \dots) + (f_0' + f_1' + \dots)^2 - \beta = 0.$$

Collecting the leading-order terms, one obtains

$$f_0'' + (f_0')^2 - \beta \sim 0. \quad (18.19)$$

Using the method of dominant balance, it can be shown that $f_0'' \ll (f_0')^2$ (Exercise 18.2). Therefore,

$$f_0' = \pm \sqrt{\beta}.$$

To compute f_0 , we first use integration by parts to get

$$\int^{\zeta} \sqrt{\beta} = \zeta \sqrt{\beta} - \int^{\zeta} \zeta \frac{d}{d\zeta} \sqrt{\beta}.$$

By (18.16),

$$\frac{d}{d\zeta} \sqrt{\beta} \sim \frac{d}{d\zeta} \frac{\pi}{\log \zeta} = -\frac{\pi}{\zeta \log^2 \zeta} \sim -\sqrt{\beta} \frac{1}{\zeta \log \zeta}.$$

Hence

$$-\int^{\zeta} \zeta \frac{d}{d\zeta} \sqrt{\beta} \sim \int^{\zeta} \frac{\sqrt{\beta}}{\log \zeta} \ll \int^{\zeta} \sqrt{\beta}.$$

Therefore, $\int^{\zeta} \sqrt{\beta} \sim \zeta \sqrt{\beta}$. Since the solution with the minus sign corresponds to a decaying exponential, we have that

$$f'_0 = \sqrt{\beta} \sim \frac{\pi}{\log \zeta}. \quad (18.20)$$

Hence $f_0 \sim \zeta \sqrt{\beta} \sim \frac{\pi \zeta}{\log \zeta}$. Balancing the next-order terms gives

$$f''_0 + 2f'_0 f'_1 = 0.$$

Therefore, $f'_1 = -\frac{f''_0}{2f'_0}$ and so

$$f_1 = -\frac{1}{2} \log |f'_0| \sim -\frac{1}{2} \log \sqrt{\beta} \sim -\frac{1}{2} \log \left(\frac{\pi}{\log \zeta} \right).$$

Balancing the next-order terms gives $f_2 = o(1)$, see Exercise 18.3. Hence, $A \sim c_A e^{f_0 + f_1}$. \square

Exercise 18.2 Assume that the leading-order balance in (18.19) is given either by $f''_0 + (f'_0)^2 = 0$ or by $f''_0 - \beta = 0$. Show that this leads to an inconsistency, i.e., that in both cases the neglected term is larger than the two terms that are being retained.

Exercise 18.3 Show that $f_2 = o(1)$.

18.2.3 Use the Solution for $A(\zeta)$ and Eq. (18.10c) to Express A as a Function of z

Lemma 18.4 gives the blowup rate in terms of ζ . To express it in terms of z , we first take the log of both sides of relation (18.18) to get

$$\log A \sim f_0.$$

Taking the log of this relation and using (18.17) gives

$$\log \log A \sim \log \zeta. \quad (18.21)$$

Using (18.10c), (18.17), (18.20), and integration by parts gives

$$\begin{aligned} Z_c - z &= \int_{\zeta}^{\infty} \frac{dz}{d\zeta} d\zeta = \int_{\zeta}^{\infty} \frac{1}{A^2(\zeta)} d\zeta \sim c_A^{-2} \int_{\zeta}^{\infty} e^{-2(f_0+f_1)} d\zeta \\ &= c_A^{-2} \int_{\zeta}^{\infty} \left(e^{-2(f_0+f_1)} \right)' \frac{-1}{2(f'_0 + f'_1)} d\zeta \\ &= \frac{c_A^{-2}}{2(f'_0 + f'_1)} e^{-2(f_0+f_1)} - \frac{c_A^{-2}}{2} \int_{\zeta}^{\infty} e^{-2(f_0+f_1)} \left(\frac{-1}{f'_0 + f'_1} \right)' d\zeta \\ &\sim \frac{1}{2(f'_0 + f'_1)} \frac{1}{A^2} + \frac{1}{2} \int_{\zeta}^{\infty} \frac{1}{A^2} \left(\frac{1}{f'_0 + f'_1} \right)' d\zeta. \end{aligned} \quad (18.22)$$

From Lemma 18.4 it follows that $f'_0 \sim \pi/\log \zeta$ and $f'_1 \ll f'_0$. Hence,

$$\left(\frac{1}{f'_0 + f'_1} \right)' \sim \left(\frac{1}{f'_0} \right)' \sim \left(\frac{\log \zeta}{\pi} \right)' = \frac{1}{\pi \zeta},$$

and so the second term in (18.22) is $O(1/\zeta)$ smaller than the first term. Consequently,

$$Z_c - z \sim \frac{1}{2(f'_0 + f'_1)} \frac{1}{A^2} \sim \frac{1}{2f'_0} \frac{1}{A^2} \sim \frac{\log \zeta}{2\pi} \frac{1}{A^2}. \quad (18.23)$$

Therefore, by (18.21),

$$Z_c - z \sim \frac{\log \log A}{2\pi A^2}, \quad (18.24)$$

or equivalently

$$\frac{1}{Z_c - z} \sim \frac{2\pi A^2}{\log \log A}.$$

Taking the loglog of this relation gives

$$\log \log \frac{1}{Z_c - z} \sim \log \log A.$$

Combining this relation with (18.24) gives the loglog law (18.3).

18.3 “Failure” of the Loglog Law

The asymptotic analysis that led to the loglog law consisted of

1. derivation of the reduced equations (Chap. 17), and
2. asymptotic solution of the reduced equations (Sect. 18.2).

In parallel to this asymptotic research, a considerable research effort during the 1980s consisted of numerical investigations of singular NLS solutions. These simulations required specialized numerical methods, because standard PDE solvers cannot handle the ever-increasing gradients near the singularity, and therefore break down after the solution focuses by 10^2 – 10^3 .¹

To compute NLS solutions “sufficiently close” to the singularity, McLaughlin et al. [171] developed the method of *dynamic rescaling* (Sect. 29.4.1), which can “easily” reach focusing levels of 10^{15} . NLS simulations with the dynamic-rescaling method showed that the blowup rate is indeed very close to a square root. These simulations, however, failed to detect the loglog correction. In fact, they could not even show conclusively that the blowup rate is faster than a square root (Sect. 14.2.2).

Initially, it was believed that the loglog correction was not detected numerically because it was too small to be observed, even after focusing by 10^{15} . Another possible explanation for the failure to detect the loglog correction was that the reduced equations become valid only at focusing levels above 10^{15} . In [93], Fibich and Papanicolaou resolved this issue by checking at which focusing levels the solution $L(z)$ of the reduced equations reaches the loglog law asymptotics (18.3). Indeed, the loglog law (18.4) for the NLS blowup rate $l(z)$ is derived from the reduced equations, and not directly from the NLS. Therefore, if the solution $L(z)$ of the reduced equations has not yet reached the loglog law asymptotics (18.3), then by Lemma 18.1, the blowup rate $l(z)$ of the corresponding NLS solution ψ has not reached the loglog law asymptotics (18.4) either. This approach has the advantage that it is much easier to analyze or solve numerically the reduced equations instead of the NLS. Indeed, we have

Conclusion 18.1 ([93]) *The loglog law (18.3) for $L(z)$ becomes the leading-order solution of the reduced equations (18.2) only at extremely large amplifications, well above 10^{15} .*

In fact, we can identify the exact stage in the derivation of the loglog law which leads to this ‘failure’:

Conclusion 18.2 ([93]) *The approximation $\beta \sim \pi^2/\log^2 \zeta$, see (18.16), becomes the leading-order solution of (18.14) only at extremely large amplifications, well above 10^{15} .*

¹ See Chap. 30 for what can happen when one tries to compute a singular NLS solution with a standard numerical solver.

To see this, we prove

Lemma 18.5 ([93]) *A necessary condition for $\beta \sim \pi^2/\log^2 \zeta$ to be the leading-order solution of (18.14) is*

$$A(z) \gg e^{\frac{2}{\nu(\beta_0)} \frac{\beta_0^2}{v(\beta_0)}}, \quad \beta_0 = \beta(0). \quad (18.25)$$

Proof In the proof of Lemma 18.3 which led to (18.16), we made the approximation

$$\lambda^{-3} e^\lambda \Big|_{\lambda_0}^\lambda \sim \lambda^{-3} e^\lambda.$$

A necessary condition for this to hold is $\lambda - \lambda_0 \gg 1$. Since $\lambda(\zeta) \geq \lambda_0 \gg 1$, from Eq.(18.14) we see that $\lambda_\zeta = \lambda^3 e^{-\lambda}$ is monotonically decreasing for $\zeta \geq 0$. Hence $\lambda - \lambda_0 = \int_0^\zeta \lambda_\zeta d\zeta < \zeta \lambda_\zeta(0)$. We thus see that a necessary condition for (18.16) to be the leading-order solution of (18.14) is

$$\zeta \gg \frac{1}{\lambda_\zeta(0)} = \frac{2\pi^2}{c_v} e^{\lambda_0} \lambda_0^{-3} = \frac{2}{\pi} \frac{\beta_0^{\frac{3}{2}}}{\nu(\beta_0)}, \quad (18.26a)$$

where in the last two equalities we used (18.14). In addition, by (18.17),

$$A(\zeta) \gg e^{\zeta \sqrt{\beta}}. \quad (18.26b)$$

The result follows from relations (18.26). \square

Exercise 18.4 Show that a sufficient condition for $\beta(\zeta)$ to get below $\beta(0)/4$ is $\zeta \geq \frac{3}{4} \frac{\beta(0)}{\nu(\beta(0)/4)}$.

Condition (18.25) shows that *the focusing level at which the loglog law becomes valid is double exponentially large*. For example, when $d = 2$, then $c_v \approx 45$ (Sect. 17.7.2). If, in addition, $\beta_0 = 0.05$, then by (18.25), a necessary condition for the loglog to hold is

$$A \gg 10^{48}.$$

Even with specialized methods such as *dynamic rescaling*, the accuracy of the numerical solution of the NLS becomes questionable after focusing by 10^{15} . In contrast, we can use standard numerical methods to solve the reduced equations over hundreds of orders of magnitudes, without a significant deterioration in the numerical accuracy. To do that, we recall that

$$\beta = a^2 + a_\zeta, \quad a = -\frac{L_\zeta}{L},$$

see (18.13a). Therefore, we can solve numerically the equivalent form of the reduced equations

$$\beta_\zeta(\zeta) = -\nu(\beta), \quad a_\zeta(\zeta) = \beta - a^2, \quad (18.27a)$$

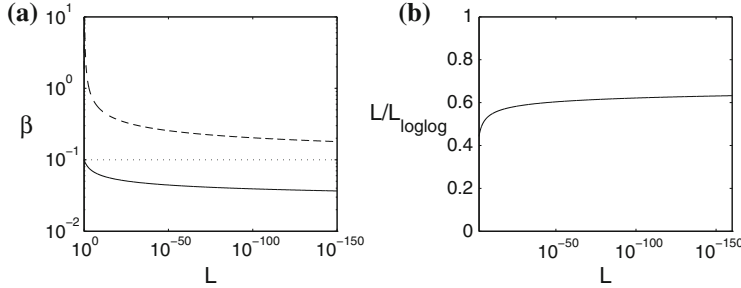


Fig. 18.1 The reduced equations (18.27) with $d = 2$, $\beta(0) = 0.1$, $L(0) = 1$, and $L_z(0) = 0$. **a** $\beta(z)$ as a function of $L(z)$. Even after focusing by 10^{150} , strict adiabaticity [$\beta \equiv \beta(0)$, dots] is a better approximation to the numerical solution of (18.27) [solid] than the asymptotic approximation $\beta \sim \frac{\pi^2}{\log^2 \zeta}$ [dashes] that leads to the loglog law. **b** The ratio (18.28)

and then recover $L(\zeta)$ and $Z_c - z$ from numerical quadratures of

$$L(\zeta) = L(0) e^{-\int_0^\zeta a(s) ds}, \quad Z_c - z = \int_\zeta^\infty \frac{dz}{d\zeta} d\zeta = \int_\zeta^\infty L^2(\zeta) d\zeta. \quad (18.27b)$$

A typical simulation of the reduced equations (18.27) is presented in Fig. 18.1. Even after focusing by 10^{150} , the approximation $\beta \sim \pi^2/\log^2 \zeta$, which leads to the loglog law, is not valid (Fig. 18.1a). Note that for these parameters, condition (18.25) “only” gives $A \gg 1340$. Therefore, even when condition (18.25) is satisfied, the loglog law is not necessarily valid.

To check whether the numerical solution of the reduced system in Fig. 18.1 has reached the loglog regime, we plot the ratio

$$\frac{L(z)}{L_{\text{loglog}}(z)}, \quad L_{\text{loglog}}(z) := \left(\frac{2\pi(Z_c - z)}{\log \log \frac{1}{Z_c - z}} \right)^{\frac{1}{2}}. \quad (18.28)$$

While we know that this ratio goes to 1 as $z \rightarrow Z_c$, Fig. 18.1b shows that it does not approach this value even after focusing by 10^{150} . Therefore, we conclude that the solution of the reduced equations did not reach the loglog regime even after focusing by 10^{150} .²

As noted, if the solution of the reduced equations does not reach the loglog regime, then neither does the NLS solution. Indeed, in Fig. 18.4 we shall see that in NLS simulations, the blowup rate does not reach the loglog regime even after focusing by 10^{10} . Since the physical validity of the NLS model breaks down after focusing

² Since the ratio (18.28) may appear to approach a constant ≈ 0.6 in Fig. 18.1b, one might argue that $L(z)$ did reach the loglog regime. This is wrong, however, because there is no free multiplicative constant in the loglog law. Thus, the ratio (18.28) has to approach 1 in the loglog regime. The ratio (18.28) appears to approach a constant simply because both $L(z)$ and $L_{\text{loglog}}(z)$ are ‘almost’ a square root.

by 10^2 – 10^3 (Sect. 1.8), the NLS model becomes invalid long before its solution has reached the loglog regime.

Conclusion 18.3 *The loglog law (18.4) is not “physical”, i.e., it is not valid in the regime where optical collapse is modeled by the NLS.*

This ‘failure’ of the loglog law has nothing to do with the validity of the reduced equations. Indeed, in Sect. 18.8 we will see that once analyzed with the *adiabatic approach*, predictions of the reduced equations become valid at mild focusing levels, which are still in the domain of physical interest.

Conclusion 18.4

1. *The reduced equations become valid at moderate focusing levels.*
2. *The blowup rate of the solution ψ of the critical NLS approaches the loglog law (18.4) only at extremely large amplifications, because the blowup rate of the solution $L(z)$ of the reduced equations (18.2) approaches the loglog law (18.3) only at such large amplifications.*

18.4 Adiabatic Approach

In order to derive an asymptotic law for $L(z)$ which is valid in the domain of physical interest (i.e., when $L(z)$ is moderately small), and not only in the “mathematical limit” as $L \rightarrow 0$, we note that the two reduced equations (18.2) evolve on very different length scales:

$$L_{zz}(z) = -\frac{\beta}{L^3} \quad (\text{fast scale}), \quad (18.29a)$$

$$\beta_z(z) = -\frac{\nu(\beta)}{L^2} \quad (\text{slow scale}). \quad (18.29b)$$

Indeed, the characteristic length scales for changes in L and in β are

$$[z^{(L)}] = \left(\frac{[L]}{[L_{zz}]} \right)^{\frac{1}{2}} = \left(\frac{[L]}{[\beta L^{-3}]} \right)^{\frac{1}{2}} = \frac{L^2}{\beta^{\frac{1}{2}}}, \quad [z^{(\beta)}] = \frac{[\beta]}{[\beta_z]} = \frac{\beta L^2}{\nu(\beta)}.$$

Therefore, the ratio

$$\frac{[z^{(L)}]}{[z^{(\beta)}]} = \frac{\nu(\beta)}{\beta^{\frac{3}{2}}} \quad (18.30)$$

becomes exponentially small as $z \rightarrow Z_c$.

Conclusion 18.5 *While both L and β go to zero as $z \rightarrow Z_c$, changes in β are exponentially slower than in L .*

For example, as L decreases by 10^{150} in Fig. 18.1, β decreases by less than 10.

Exercise 18.5 Use the reduced equations (18.10) to show that the length scales in ζ for changes in A and in β are $[\zeta^{(A)}] = \beta^{-\frac{1}{2}}$ and $[\zeta^{(\beta)}] = \frac{\beta}{v(\beta)}$. Conclude that $\frac{[\zeta^{(A)}]}{[\zeta^{(\beta)}]} = \frac{v(\beta)}{\beta^{\frac{1}{2}}}$, which is the same as (18.30).

To derive the loglog law, we first solved the slow-scale equation (18.29b) to leading order, and then used its approximate solution to solve the fast-scale equation (18.29a). In problems with multiple scales, however, the correct approach is to solve the fast-scale equation while ignoring the changes in the slow scales, and only then use the solution of the fast scale to solve the slow-scale equation.^{3,4} Of course, if we could solve the slow-scale equation (18.29b) exactly, then the leading-order solution of the fast-scale equation would be valid at a much earlier stage.

Conclusion 18.6 The “failure” of the loglog law at physical focusing levels is due to the combination of

1. solving the reduced equations in the “wrong order”, and
2. the fact that the leading-order approximation of the slow-scale equation becomes valid only at extremely large amplifications.

Therefore, in [64] we suggested to reverse the order in which the reduced equations are solved, namely:

1. First solve Eq. (18.29a) for $L(z)$ while ignoring the slow changes in β , i.e., under the approximation $\beta(z) \approx \beta(0)$.
2. Only then take into account the slow changes in β according to (18.29b).

When we solved the reduced equations in Fig. 18.1, as L decreased by 10^{150} , β decreased by less than 10. This simulation thus provides a strong support for analyzing the reduced equations with a multiple-scales approach. In fact, in this simulation, even after focusing by 10^{150} , the approximation $\beta \equiv \beta(0)$ [i.e., completely neglecting the slow-scale dynamics] is considerably more accurate than the asymptotic approximation $\beta \sim \pi^2/\log^2 \zeta$ that leads to the loglog law.

From the “NLS perspective”, since β is proportional to the excess power above P_{cr} of the collapsing core ψ_{coll} (Lemma 17.3), the physical interpretation of the above multiple-scales approach is that the rate at which the collapsing-core leaves behind

³ For example, when we solved the linear Helmholtz equation in Sect. 2.1 using geometrical optics, we first solved the fast-scale Eikonal equation for the phase S , and only then used its solution to solve the slow-scale transport equation for the amplitude A . Similarly, when we solved the weakly-nonlinear Helmholtz equation (1.34) in Sect. 1.7, we first assumed that the fast-scale dynamics is given by the carrier oscillations $e^{ik_0 z}$, and only then used this assumption to derive the slow-scale equation for the amplitude ψ .

⁴ In general, in problems with multiple scales it is not possible to solve the slow-scale equation before the fast-scale equation. This ‘order reversal’ was possible here because the slow-scale equation (18.10b) is decoupled from the fast-scale equation (18.10a).

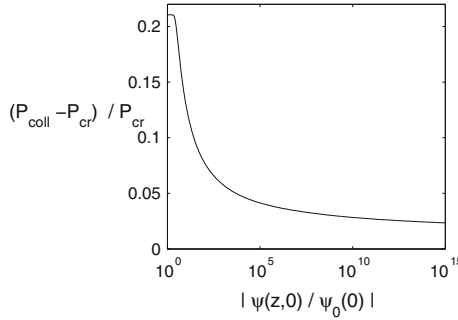


Fig. 18.2 The two-dimensional critical NLS with $\psi_0 = 1.1R^{(0)}$. The rate at which the excess power of ψ_{coll} above P_{cr} goes to zero is exponentially smaller than the rate at which its on-axis amplitude goes to infinity

its excess power above P_{cr} is exponentially slower than the rate at which its width shrinks to zero. To illustrate this, in Fig. 18.2 we solve the critical NLS and observe that as the on-axis amplitude increases by 10^{15} , the excess power of the collapsing core decreases by less than 10.

Conclusion 18.7 *Near the singularity, self-focusing becomes adiabatic, in the sense that the collapsing core shrinks with almost no power losses.*

The above multiple-scales approach thus amounts to first solving for the dynamics of the width L under the assumption of *strict adiabaticity* and only then taking into account the slow nonadiabatic changes.

18.5 Strict Adiabatic Law

We begin by considering the self-focusing dynamics under strict adiabaticity, i.e., when nonadiabatic changes are completely neglected:

Lemma 18.6 ([64]) *Let z_0 be in the adiabatic regime where the reduced equations hold. Then under the approximation of strict adiabaticity, the self-focusing dynamics is given by*

$$L^2(z) = L_0^2 + 2L_0L'_0(z - z_0) + C_0(z - z_0)^2 = (L_0 + (z - z_0)L'_0)^2 - \frac{\beta_0}{L_0^2}(z - z_0)^2 \quad (18.31a)$$

for $z_0 \leq z < Z_c$, where $L_0 = L(z_0) > 0$, $L'_0 = L_z(z_0)$, $C_0 = C(z_0)$, and

$$C(z) := L_z^2 - \frac{\beta}{L^2} = (L^2)_{zz}. \quad (18.31b)$$

Proof Since z_0 is in the adiabatic regime, the reduced equations are valid for $z_0 \leq z < Z_c$. Under the approximation of strict adiabaticity, (18.29b) reduces to $\beta(z) \equiv \beta_0$, and so (18.29a) reads

$$L_{zz}(z) = -\frac{\beta_0}{L^3}, \quad \beta_0 = \beta(z_0).$$

The solution of this equation follows from Lemma 2.8. \square

Exercise 18.6 Derive the strict adiabatic law (18.31a) from the reduced equations (18.10). Hint: Under strict adiabaticity, Eqs. (18.10a) and (18.10b) reduce to $A_{\zeta\zeta} = \beta_0 A$.

18.5.1 $Z_c - z_0 \approx Z_c^{\text{adiabatic}}$

Setting $L(Z_c) = 0$ in (18.31a) gives

$$C_0(Z_c - z_0)^2 + 2L_0 L'_0 (Z_c - z_0) + L_0^2 = 0.$$

The roots of this quadratic equation are

$$\begin{aligned} Z_c^{(1),(2)} - z_0 &= \frac{-L_0 L'_0 \mp \sqrt{L_0^2 L_z^2(0) - L_0^2 C_0}}{C_0} = \frac{-L_0 L'_0 \mp \sqrt{\beta_0}}{(L'_0)^2 - \frac{\beta_0}{L_0^2}} \\ &= L_0^2 \frac{L_0 L'_0 \pm \sqrt{\beta_0}}{(\sqrt{\beta_0} + L_0 L'_0)(\sqrt{\beta_0} - L_0 L'_0)}. \end{aligned} \quad (18.32)$$

Therefore,

$$Z_c^{(1)} - z_0 = \frac{L_0^2}{\sqrt{\beta_0} - L_0 L'_0}, \quad Z_c^{(2)} - z_0 = \frac{L_0^2}{-\sqrt{\beta_0} - L_0 L'_0}. \quad (18.33)$$

Since collapse occurs if at least one of these two roots is real and positive, a necessary condition for collapse is $\beta_0 > 0$. In light of Lemma 17.3, this means that the power of the collapsing core $P_{\text{coll}} = P(\psi_{\text{coll}})$ is above P_{cr} ,⁵ or equivalently that the focusing nonlinearity is stronger than diffraction. When $L'_0 > 0$, $Z_c^{(2)} - z_0$ is always negative, and $Z_c^{(1)} - z_0$ is positive if and only if $L_0 L'_0 \leq \sqrt{\beta_0}$. When $L'_0 < 0$, then regardless of the sign of $Z_c^{(2)} - z_0$, $Z_c^{(1)} - z_0$ is the smaller positive solution. Therefore, we have

Lemma 18.7 ([64, 93]) Under the approximation of strict adiabaticity, the remaining distance to the blowup point is approximated by $Z_c - z_0 \approx Z_c^{\text{adiabatic}}$, where

⁵ Therefore, $\beta_0 > 0$ is the asymptotic analog of the necessary condition $P(0) > P_{\text{cr}}$.

$$Z_c^{\text{adiabatic}} = \begin{cases} \frac{L_0^2}{\sqrt{\beta_0} - L_0 L'_0}, & \text{if } \beta_0 > 0 \text{ and } L_0 L'_0 \leq \sqrt{\beta_0}, \\ \text{no collapse,} & \text{otherwise.} \end{cases} \quad (18.34)$$

According to (18.34), when the “input” beam $\psi_0 := \psi(z_0)$ is collimated or converging ($L'_0 \leq 0$), the condition $\beta_0 > 0$ (i.e., $P_{\text{coll}} > P_{\text{cr}}$) is also sufficient for blowup.⁶ If, however, the input beam is diverging ($L'_0 > 0$), the necessary and sufficient condition for blowup is $\beta_0 \geq (L_0 L'_0)^2$, i.e., the input power should be sufficiently high so that the focusing nonlinearity be stronger than the combined effects of diffraction and input-beam divergence.⁷

Lemma 18.8 ([93]) *The approximation $Z_c^{\text{adiabatic}}$, see (18.34), preserves the lens-transformation symmetry of the critical NLS.*

Proof Let $\psi_0 := \psi(z_0)$. If ψ_0 is real, then $L'_0 = 0$, and so

$$Z_c^{\text{adiabatic}} = \frac{L_0^2}{\sqrt{\beta_0}}.$$

Now, let $\tilde{\psi}_0 = \psi_0 e^{-i \frac{r^2}{4F}}$, where ψ_0 is real. Since the addition of $e^{-i \frac{r^2}{4F}}$ does not affect the initial width and power, $\tilde{L}_0 = L_0$ and $\tilde{P}_{\text{coll}} = P_{\text{coll}}$, where the tildes denote the corresponding quantities for $\tilde{\psi}$. Therefore, by Lemma 17.3,

$$\tilde{\beta}_0 \sim \frac{\tilde{P}_{\text{coll}} - P_{\text{cr}}}{M} = \frac{P_{\text{coll}} - P_{\text{cr}}}{M} \sim \beta_0.$$

In addition, comparison of the phases of $\tilde{\psi}_0$ and $\psi_{R^{(0)}}$, see (18.5), shows that

$$\frac{\tilde{L}'_0}{\tilde{L}_0} = -\frac{1}{F}. \quad (18.35)$$

Therefore, by (18.34),

$$\tilde{Z}_c^{\text{adiabatic}} = \frac{L_0^2}{\sqrt{\beta_0} + \frac{L_0^2}{F}}.$$

Since

$$\frac{1}{\tilde{Z}_c^{\text{adiabatic}}} = \frac{1}{Z_c^{\text{adiabatic}}} + \frac{1}{F},$$

⁶ For NLS solutions, the condition $P > P_{\text{cr}}$ is not sufficient for collapse (Corollary 13.8 and Chap. 24). The reduced equations, however, are derived under the assumption that the self-similar profile of the collapsing core is close to $R^{(0)}$. In that case, the condition $P > P_{\text{cr}}$ is asymptotically equivalent to the condition $H < 0$, see Corollary 17.5, and is therefore sufficient for collapse.

⁷ These results are similar to those obtained with the aberrationless approximation method in Sect. 3.5. This is because aberrationless propagation is, by definition, strictly adiabatic. The important difference from Sect. 3.5 is that here we used the correct asymptotic profile.

approximation (18.34) preserves the lens-transformation property of the collapse distance (Lemma 8.5). \square

Remark The adiabatic approximation $Z_c^{\text{adiabatic}}$ is further discussed in Sect. 27.2.1.

Exercise 18.7 Show that $Z_c^{\text{adiabatic}}$, see (18.34), preserves the dilation symmetry $\psi \rightarrow \lambda^{\frac{d}{2}}\psi(\lambda^2z, \lambda x)$ of the critical NLS.

18.5.2 Blowup Rate

To find the blowup rate under strict adiabaticity, we rewrite the strict adiabatic law (18.31a) in terms of $Z_c - z$, the remaining distance to the singularity:

Lemma 18.9 The strict adiabatic law (18.31a) reads

$$L(z) = \sqrt{2\sqrt{\beta_0}(Z_c^{\text{adiabatic}} - z) + C_0(Z_c^{\text{adiabatic}} - z)^2}, \quad (18.36)$$

where $Z_c^{\text{adiabatic}}$ is given by (18.34).

Proof We can use relations (18.33) to rewrite (18.31a) as

$$L^2 = C_0(Z_c^{(1)} - z)(Z_c^{(2)} - z) = C_0(Z_c^{(1)} - z)^2 + C_0(Z_c^{(1)} - z)(Z_c^{(2)} - Z_c^{(1)}).$$

In addition, by (18.32), $C_0(Z_c^{(2)} - Z_c^{(1)}) = 2\sqrt{\beta_0}$. \square

Near the singularity, the strict adiabatic law (18.36) reduces to

$$L(z) = \sqrt{2\sqrt{\beta_0}(Z_c^{\text{adiabatic}} - z)}. \quad (18.37)$$

Corollary 18.3 Strict adiabaticity corresponds to a square-root blowup rate.

We already derived the square-root blowup rate (18.37) in Sect. 3.5.2 and in Lemma 11.2 for aberrationless/self-similar propagation. As noted, aberrationless/self-similar propagation implies strict adiabaticity.

18.6 Delicate Balance Between Two Giants

Consider the focused input beam $\tilde{\psi}_0 = \psi_0 e^{-i\frac{r^2}{4F}}$, where ψ_0 is real, $L_0 = 1$, and $z_0 = 0$. Since $\frac{L'_0}{L_0} = -\frac{1}{F}$, see (18.35), the strict adiabatic law (18.31) reads

$$L^2(z) = \left(1 - \frac{z}{F}\right)^2 - \beta_0 z^2.$$

In Sect. 3.5 we used the aberrationless approximation method to obtain

$$L^2(z) = \left(1 - \frac{z}{F}\right)^2 + \left(\frac{1}{L_{\text{diff}}^2} - \frac{4n_2}{n_0} \frac{E_c^2}{r_0^2}\right) z^2.$$

Comparison of these two relations shows that the coefficient β_0 represents the balance of nonlinearity and diffraction.⁸

Conclusion 18.8 *In critical selffocusing, once the reduced equations become valid, the balance of the focusing nonlinearity and diffraction is $O(\beta)$ smaller than each of these terms separately, i.e.,*

$$\frac{\Delta\psi + |\psi|^{\frac{4}{d}}\psi}{\Delta\psi} = O(\beta), \quad \frac{\Delta\psi + |\psi|^{\frac{4}{d}}\psi}{|\psi|^{\frac{4}{d}}\psi} = O(\beta).$$

We can also derive Conclusion 18.8 as follows. In Sect. 17.3 we saw that

$$\psi_{\text{coll}} \sim \frac{1}{L^{\frac{d}{2}}(z)} V_0(\rho) e^{i\zeta + i \frac{L_z}{L} \frac{r^2}{4}}, \quad V_0 \sim R^{(0)} + \beta g.$$

When $\beta = 0$, then $V_0 = R^{(0)}$. Consequently, nonlinearity and diffraction are exactly balanced.⁹ For $0 < \beta \ll 1$, the $O(\beta)$ deviation of V_0 from $R^{(0)}$ leads to $O(\beta)$ changes in the nonlinearity and diffraction. As a result, their balance changes from zero to $O(\beta)$. Hence, it is $O(\beta)$ smaller than their individual magnitudes.

Conclusion 18.8 shows that we can visualize adiabatic self focusing as a competition between two giants, nonlinearity and diffraction, with nearly equal strength. Therefore, a dwarf whose strength is comparable to the *difference* in strength between these two giants can shift the balance in either direction:¹⁰

Conclusion 18.9 (Balance of the giants principle) *Once a collapsing solution of the critical NLS enters the adiabatic regime, any perturbation which is $O(\beta)$ smaller than nonlinearity and diffraction, becomes comparable to their balance. Therefore, it has an $O(1)$ effect on the self-focusing dynamics.*

Applications of this principle are given in Sects. 31.5, 32.4.2, 34.1, and 36.6, where we analyze the effect of various perturbations on critical collapse. This sensitivity to small perturbations is a unique characteristic of the critical NLS. In a way, it reflects the fact that the critical NLS is the borderline between the subcritical NLS, where all solutions exist globally, and the supercritical NLS, where solutions can become singular.

⁸ This observation is consistent with the results that nonlinearity and diffraction are balanced when $P = P_{\text{cr}}$, and that β is proportional to the excess power above P_{cr} .

⁹ Indeed, since $\beta = -L^{-3}L_{zz}$, then $\beta = 0 \implies L_{zz} = 0$, i.e., there is no acceleration or deceleration.

¹⁰ This is a consequence of the dual borderline properties of the $\psi_{R^{(0)}}$ profile (Sect. 17.2).

18.7 Nonadiabatic Effects

Self-focusing, as given by (18.31a) or by (18.36), is strictly adiabatic. In order to maintain the $O(\beta)$ accuracy of the reduced equations all the way up to the singularity, the slow changes in $\beta(z)$ and $C(z)$ should be included. To do that, we replace (18.36) by

$$L(z) \sim \sqrt{2\sqrt{\beta(z)}(Z_c - z) + C(z)(Z_c - z)^2}, \quad (18.38)$$

which is *Fibich's adiabatic law* [64]. The evolution of β is determined from (18.29b). In addition, by (18.13a) and (18.31b),

$$C(z) = L_z^2 - \frac{\beta}{L^2} = \frac{a^2 - \beta}{L^2} = -\frac{a_\zeta}{L^2}. \quad (18.39)$$

Lemma 18.10

$$a_\zeta \sim -\frac{v(\beta)}{2\sqrt{\beta}}, \quad z \rightarrow Z_c. \quad (18.40)$$

Proof We first prove the result under the strict-adiabaticity approximation. In this case $\beta \equiv \beta_0$, and so $L_{zz} = -L^{-3}\beta_0$. Multiplying by $2L_z$, integrating, and using $a = -LL_z$, gives $a^2 = \beta_0 + C_0L^2$. Therefore,

$$\lim_{\zeta \rightarrow \infty} a^2 = \beta_0. \quad (18.41a)$$

Since $a_\zeta = \beta - a^2$, this implies that

$$\lim_{\zeta \rightarrow \infty} a_\zeta = 0. \quad (18.41b)$$

Hence, by (18.41),

$$\lim_{\zeta \rightarrow \infty} \frac{a_\zeta}{a^2} = 0.$$

Relations (18.41) were derived under the strict-adiabaticity approximation. Nevertheless, because changes in β are exponentially slower than compared in L ,¹¹ the solution of the reduced equations satisfies $a_\zeta \ll a^2$ as $\zeta \rightarrow \infty$. Hence

$$a^2 \sim \beta, \quad z \rightarrow Z_c,$$

and so $\beta_\zeta \sim 2aa_\zeta \sim 2\sqrt{\beta}a_\zeta$. Since $\beta_\zeta \sim -v(\beta)$, the result follows. \square

¹¹ See Conclusion 18.5.

18.8 Comparison of the Adiabatic and Loglog Laws

As noted, under strict adiabaticity the blowup rate is given by (18.37). Adding the slow changes in β leads to *Malkin's adiabatic law*:

Lemma 18.11 ([164]) *Let $L(z)$ be a solution of the reduced Eqs (18.2) such that $\beta(0) > 0$, $L(0) > 0$, and $\lim_{z \rightarrow Z_c} L(z) = 0$. Then*

$$L(z) \sim \sqrt{2\sqrt{\beta}(Z_c - z)}, \quad z \rightarrow Z_c. \quad (18.42)$$

Proof In the derivation of the loglog law we saw that $f'_0 \sim \sqrt{\beta}$, see (18.20), and $Z_c - z \sim \frac{L^2}{2f'_0}$, see (18.23). Combining these relations gives (18.42). \square

The proof of Lemma 18.11 shows that *Malkin's adiabatic law* (18.42) and the *loglog law* agree asymptotically as $z \rightarrow Z_c$. Note that here we used the systematic derivation of the loglog law to prove Malkin's adiabatic law. Similarly, we can use the systematic derivation of the loglog law (and of Malkin's law) to prove Fibich's adiabatic law, by establishing the asymptotic agreement between Fibich's adiabatic law (18.38) and Malkin's adiabatic law (18.42):

Lemma 18.12

$$\lim_{z \rightarrow Z_c} \frac{C(z)(Z_c - z)^2}{2\sqrt{\beta}(Z_c - z)} = 0.$$

Proof By (18.39) and (18.40), $C(z) \sim \frac{v(\beta)}{2\sqrt{\beta}L^2}$ as $z \rightarrow Z_c$. Therefore,

$$\frac{C(z)(Z_c - z)^2}{2\sqrt{\beta}(Z_c - z)} \sim \frac{v(\beta)(Z_c - z)}{4\beta L^2}.$$

By (18.42), $Z_c - z \sim \frac{L^2}{2\sqrt{\beta}}$. Therefore, since $\beta \rightarrow 0$, see Proposition 18.3,

$$\frac{C(z)(Z_c - z)^2}{2\sqrt{\beta}(Z_c - z)} \sim \frac{v(\beta)}{8\beta^{\frac{3}{2}}} \rightarrow 0, \quad z \rightarrow Z_c. \quad (18.43)$$

\square

Thus, we have

Proposition 18.4 *The loglog law (18.3), Malkin's adiabatic law (18.42), and Fibich's adiabatic law (18.38) are asymptotically equivalent as $z \rightarrow Z_c$.*

The domain of validity of the three laws, however, differ considerably. Indeed, for the adiabatic laws to be applicable, β should be moderately small so that $\beta^{-\frac{3}{2}}v(\beta) \ll 1$, see (18.30). In contrast, a necessary condition for the loglog law

to be valid is $\lambda - \lambda_0 \gg 1$, i.e., that β be considerably smaller than β_0 . Since self-focusing is adiabatic, satisfying this condition requires extremely large focusing levels (Lemma 18.5).

Fibich's adiabatic law (18.38) becomes valid before Malkin's adiabatic law (18.42), because in addition to the collapsing-core power (β), it also incorporates the focusing angle (L_z). After some focusing, however, the difference between the two laws becomes exponentially small.

18.8.1 Simulations

In Fig. 18.3 we solve the reduced equations with $L(0) = 1$, $L_z(0) = 0$, and $\beta(0) = 0.02$, and plot the relative errors of the three laws. As expected, even after focusing by 10^{10} , the loglog law is not valid. Fibich's adiabatic law is accurate from $z = 0$, and Malkin's adiabatic law becomes accurate after some focusing takes place. From this point on, the two adiabatic laws are essentially identical. The relative error of the adiabatic laws remains fairly constant. This is because the accuracy of the reduced equations, hence of the adiabatic laws, is $O(\beta)$, see Conclusion 17.2, and because β hardly changes as L decreases by 10^{10} .

In Fig. 18.4 we solve the critical NLS with $\psi_0 = 1.02R^{(0)}(r)$ and with $\psi_0 = 4e^{-r^2}$. For both initial conditions, Malkin's adiabatic law (18.42) and Fibich's adiabatic law (18.38) become $O(\beta)$ accurate early on and maintain this accuracy, while the loglog law (18.3) is not valid even after focusing by 10^{10} . In Fig. 18.4a, ψ_0 is close to $\psi_{R^{(0)}}$. Hence, the reduced equations are valid from $z = 0$. Consequently, the relative errors of the three laws are qualitatively the same as in the simulation of the reduced equations in Fig. 18.3. In particular, Fibich's law is valid from $z = 0$, whereas Malkin's requires some focusing to be valid. In Fig. 18.4b, ψ_0 is not close to $\psi_{R^{(0)}}$. Therefore, the initial dynamics is not governed by the reduced equations. Hence, the two adiabatic laws require more focusing before they become valid. At that stage,

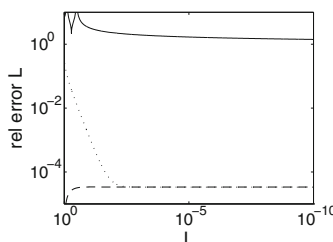


Fig. 18.3 The relative error in L of Fibich's adiabatic law (18.38) [dashed line], Malkin's adiabatic law (18.42) [dotted line], and the loglog law (18.3) [solid line]. Here, L is the solution of the reduced equations (18.27) with $d = 2$, $L(0) = 1$, $L_z(0) = 0$, and $\beta(0) = 0.02$

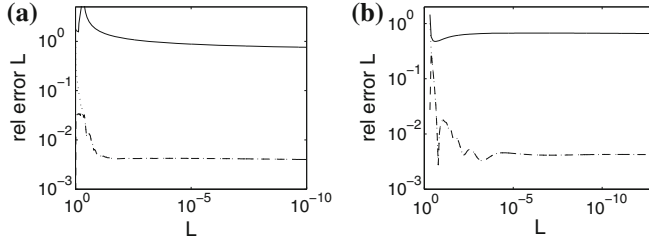


Fig. 18.4 The two-dimensional critical NLS with **a** $\psi_0 = 1.02 R^{(0)}(r)$, and **b** $\psi_0 = 4e^{-r^2}$. The plots show the relative error in $L(z) := \frac{R^{(0)}(0)}{|\Psi(z,0)|}$ of Fibich's adiabatic law (18.38) [dashed line], Malkin's adiabatic law (18.42) [dotted line], and the loglog law (18.3) [solid line]. From [93]

they are already in the domain where they agree. See [93] for additional numerical comparisons of the three laws.

18.9 In Retrospect

The search for the blowup rate of the critical NLS took a long time. This problem was already addressed by Kelley [140] in his celebrated 1965 Physical Review Letter (Sect. 3.4). Based on numerical simulations, Kelley suggested the relation $|\psi(z,0)|^2 \sim |\psi(0,0)|^2 (Z_c^2 - z^2)^{-\frac{1}{2}}$, which implies that $L \sim |\psi(z,0)|^{-1} \sim (Z_c - z)^{\frac{1}{4}}$, i.e., a one-fourth blowup rate. Between 1976 and 1991, several formulae were suggested and tested numerically: $L \sim (Z_c - z)^{\frac{2}{3}}$ [142, 250, 284], $L \sim (Z_c - z)^{\frac{1}{2}}$ [226], $L \sim \left(\frac{Z_c - z}{\log \frac{1}{Z_c - z}} \right)^{\frac{1}{2}}$ [225, 263, 278], and $L \sim \frac{(Z_c - z)^{\frac{1}{2}}}{(\log \frac{1}{Z_c - z})^\gamma}$ where $0.35 \leq \gamma \leq 0.65$ depends on ψ_0 [145, 236, 283]. The loglog law was first discovered in 1985 by Fraiman [100]. Because of a misprint, however, the double log in [100] appeared as a single log. The loglog law was rediscovered three years later (in a completely different way) by Papanicolaou and coworkers [151, 156].

During the 1990s, Malkin and Fibich and Papanicolaou [64, 93, 164] showed that the loglog law asymptotics is only reached at extremely large focusing levels, well above 10^{50} . The validity of the NLS model, however, breaks down after focusing by $10^2 - 10^3$. Therefore, *in retrospect, the discovery that the blowup rate of the critical NLS is given by the loglog law had no physical relevance*. Nevertheless, the effort invested in the derivation of the loglog law was not in vain. Indeed, in retrospect, the main achievement of these studies was the derivation of the reduced equations. As was later shown by Malkin and Fibich and Papanicolaou [64, 93, 164], the reduced equations can be solved in the domain of physical interest by employing the adiabatic approach. Moreover, the asymptotic methods used to derive the reduced equations can be generalized to perturbed critical NLS equations (Chap. 31), which provide more realistic models for physical self focusing.

The exponentially small $\nu(\beta)$ term is the main reason why finding the blowup rate of the critical NLS was so hard. Ironically, once perturbations are added to the NLS, $\nu(\beta)$ becomes negligible. Therefore, in retrospect, asymptotic analysis of the perturbed critical NLS is much easier than of the unperturbed critical NLS.

Chapter 19

Singular H^1 Ring-Type Solutions (ψ_G)

In this chapter we study solutions of the critical radial NLS

$$i\psi_z(z, r) + \psi_{rr} + \frac{d-1}{r}\psi_r + |\psi|^{\frac{4}{d}}\psi = 0, \quad d > 1 \quad (19.1a)$$

that collapse with the *ring-type* profile ψ_G . Unlike the ring-type solution ψ_G^{explicit} from Chap. 11, these solutions are in H^1 , i.e.,

$$\psi(0, r) = \psi_0(r) \in H^1. \quad (19.1b)$$

These solutions were discovered in 2005 by Fibich et al. [73] for the two-dimensional critical radial NLS

$$i\psi_z(z, r) + \psi_{rr} + \frac{1}{r}\psi_r + |\psi|^2\psi = 0, \quad \psi(0, r) = \psi_0(r) \in H^1. \quad (19.2)$$

That study provided the first example of (i) a singular solution of the critical NLS that does not collapse with an $R^{(n)}$ profile, (ii) a stable singular solution of the critical radial NLS that does not collapse with the “universal” $\psi_{R^{(0)}}$ profile, and (iii) a stable singular solution of the radial NLS (critical or supercritical) that does not collapse with a peak-type profile. Subsequently, Fibich et al. extended the results to the critical NLS in any dimension $d > 1$ [74].

19.1 Preliminary Simulations

Consider the NLS (19.2) with $\psi_0 = 15e^{-r^4}$. This super-Gaussian initial condition is flat-top (Fig. 19.1a), is in H^1 , and its power is highly above critical ($P \approx 38P_{\text{cr}}$). The NLS solution initially evolves into a ring-type profile (Fig. 19.1b).¹ As the solution

¹ In Chap. 26 we will use the *NGO method* to explain why high-power super-Gaussian initial conditions evolve into a ring profile.

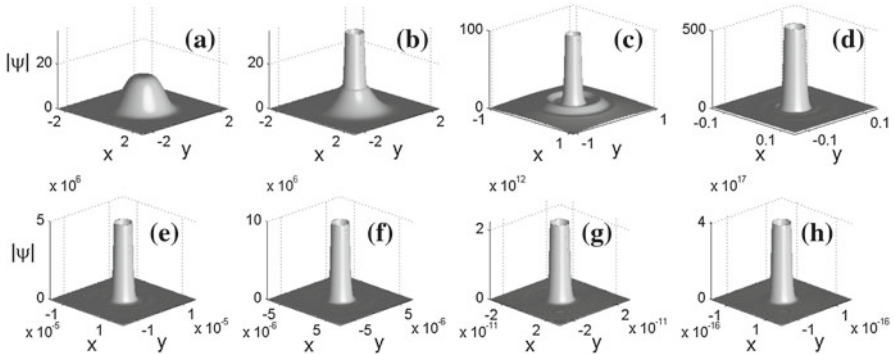


Fig. 19.1 Solution of the NLS (19.2) with $\psi_0 = 15e^{-r^4}$ at: **a** $z = 0, A(z) = 1$; **b** $z = 0.020, A(z) = 2.3$; **c** $z = 0.027, A(z) = 6.4$; **d** $z = 0.0286, A(z) = 35$; **e** $z = 0.0288, A(z) = 3.3 \times 10^5$; **f** $A(z) = 6.6 \times 10^5$; **g** $A(z) = 4.6 \times 10^{10}$; **h** $A(z) = 6.5 \times 10^{15}$. Values of z in subplots **e–h** differ in the 14th digit. From [73]

continues to collapse, it maintains a ring profile that becomes taller in amplitude, smaller in radius and narrower in its annular width (Fig. 19.1c–h), up to focusing levels of $A(z) = O(10^{15})$, where

$$A(z) = \frac{\max_r |\psi(z, r)|}{\max_r |\psi(0, r)|}. \quad (19.3)$$

The key thing to note in Fig. 19.1 is that the collapsing core does not evolve into the peak-type $\psi_{R^{(0)}}$ profile, but rather maintains a ring profile. This numerical observation was very surprising, because at that time it was widely believed that all stable solutions of the critical NLS collapse with the $\psi_{R^{(0)}}$ profile. In fact, just two years earlier, Merle and Raphaël proved this result rigorously (Sect. 14.6). Although the proof of Merle and Raphaël is “limited” to solutions with power below $\|R^{(1)}\|_2^2$, see Lemma 14.3, and $\|R^{(1)}\|_2^2 \approx 6.6P_{\text{cr}}$ for $d = 2$, see Sect. 6.4, it was believed that this restriction is technical, and that all stable solutions of the critical NLS collapse with the $\psi_{R^{(0)}}$ profile. Indeed, a Gaussian initial condition with the same power as $\psi_0 = 15e^{-r^4}$ does collapse with the $\psi_{R^{(0)}}$ profile (Fig. 14.3).

Remark The question whether the solution of Fig. 19.1 will maintain a ring profile all the way up to the singularity is still open, see Sect. 19.6.

19.1.1 Quasi Self-similar Ring Profile

Figure 19.1 suggests that the collapsing solution is self similar. This is to be expected, since the collapsing core of any H^1 solution of the radial critical NLS approaches

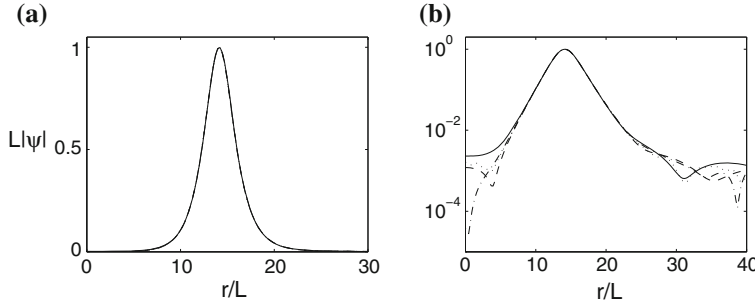


Fig. 19.2 **a** Data of Fig. 19.1e–h, rescaled according to (19.5): $A(z) = 3.3 \times 10^5$ (solid), $A(z) = 6.6 \times 10^5$ (dashes), $A(z) = 4.6 \times 10^{10}$ (dots) and $A(z) = 6.5 \times 10^{15}$ (dash-dots); all four lines are indistinguishable. **b** Same data on a semi-logarithmic scale. From [73]

the self-similar form

$$|\psi(z, r)| \sim \frac{1}{L^{\frac{d}{2}}(z)} F(\rho), \quad \rho = \frac{r}{L(z)}, \quad (19.4)$$

see Sect. 13.2. To observe the convergence to self similarity, we plot the data of Fig. 19.1e–h, rescaled according to²

$$\psi_{\text{rescaled}}(z, r) = L^{\frac{d}{2}}(z) \psi(z, \rho), \quad \rho = \frac{r}{L(z)}, \quad L(z) = \|\psi(z)\|_{\infty}^{-\frac{2}{d}}. \quad (19.5)$$

The four rescaled plots are indistinguishable (Fig. 19.2a), showing that the collapsing ring maintains the self-similar form (19.4) while focusing by 10^{10} .

Plotting the same data on a semi-logarithmic scale (Fig. 19.2b) shows that the collapsing solution is “only” *quasi self-similar*: It is self-similar in the ring region $\rho - \rho_{\max} = O(1)$, but not near the center ($0 \leq \rho \ll \rho_{\max}$), or far outside ($\rho - \rho_{\max} \gg 1$), where $\rho_{\max} \approx 14$ is the radius of the rescaled ring.³

Next, we increase the input power and solve (19.2) with $\psi_0 = 20e^{-r^4}$ ($P \approx 67P_{\text{cr}}$). This solution also collapses with a self-similar ring profile (Fig. 19.3a), whose radius $\rho_{\max} \approx 20$ is larger than that in Fig. 19.2. More generally, numerical simulations show that the radius of the rescaled ring profile increases with input power.⁴

High-power initial conditions different from $\psi_0 = ce^{-r^4}$ can also lead to a ring-type collapse. This is the case, e.g., with $\psi_0 = 15e^{-r^8}$ ($P \approx 43P_{\text{cr}}$), see Fig. 19.3b, and also with the non-monotone multi-ring initial conditions that collapse with the

² Under rescaling (19.5), $\|\psi_{\text{rescaled}}(z)\|_{\infty} = 1$.

³ The fact that the blowup profile is “only” quasi self-similar is consistent with Theorem 13.3, see Sect. 13.2.2.

⁴ Since different initial conditions collapse with ring profiles that have different rescaled radii, the self-similar ring profile is not universal.

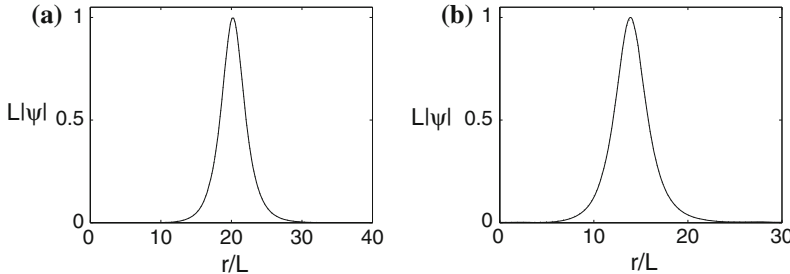


Fig. 19.3 Solution of the NLS (19.2), rescaled according to (19.5). **a** $\psi_0 = 20e^{-r^4}$. Solution plotted at the focusing levels $A(z) = 1.1 \times 10^3$ (solid) and $A(z) = 1.8 \times 10^5$ (dots). **b** $\psi_0 = 15e^{-r^8}$, $A(z) = 6.6 \times 10^3$ (solid) and $A(z) = 2.7 \times 10^4$ (dots). In both cases, the solid and dotted curves are indistinguishable. From [73]

single-ring ψ_G profile (Sect. 11.4.1). Not all high-power initial conditions, however, collapse with a ring profile. For example, a Gaussian initial condition with the same power as the super-Gaussian initial condition from Fig. 19.1 collapses with the $\psi_{R(0)}$ profile (Fig. 14.3).⁵

19.2 Blowup Profile and Blow Rate

In Sect. 13.2 we saw that for any H^1 singular solution of the radial critical NLS, the collapsing core approaches the self-similar form (19.4). Therefore, the solution is peak-type if $\rho_{\max} = 0$ and ring-type if $0 < \rho_{\max} < \infty$, where $\rho_{\max} := \arg \max_\rho F(\rho)$ is the location of the global maximum of F .

Following Fibich, Gavish, and Wang, we now use informal analysis to show that ring-type blowup solutions have a square-root blowup rate, and that their self-similar ring profile is a solution of the G equation:

Proposition 19.1 ([73, 74]) *Let ψ be a solution of the critical NLS (19.1). Assume that ψ collapses with a ring-type self-similar profile, i.e., $\psi(z, r) \sim \psi_G(z, r)$, where*

$$\psi_G(z, r) = \frac{1}{L^{\frac{d}{2}}(z)} G(\rho) e^{i\xi + i \frac{L_z}{4L} r^2}, \quad \xi = \int_0^z \frac{ds}{L^2(s)}, \quad \rho = \frac{r}{L(z)}, \quad (19.6)$$

and $G(\rho)$ has a ring profile, i.e., its global maximum is attained at $0 < \rho_{\max} < \infty$. Then

1. The blowup rate of $L(z)$ is a square root, i.e.,

$$L(z) \sim \alpha \sqrt{Z_c - z}, \quad z \rightarrow Z_c, \quad \alpha > 0. \quad (19.7)$$

⁵ In Chap. 26 we will use the *NGO method* to explain why high-power super-Gaussian initial conditions evolve into a ring profile, but equal-power Gaussian initial conditions evolve into a peak profile.

2. The self-similar ring profile $G(\rho)$ is a solution of

$$G''(\rho) + \frac{d-1}{\rho} G' - G + |G|^{\frac{4}{d}} G + \frac{\alpha^4}{16} \rho^2 G = 0, \quad \alpha > 0, \quad (19.8a)$$

subject to

$$0 \neq G(0) \in \mathbb{C}, \quad G'(0) = 0. \quad (19.8b)$$

Proof Substituting $\psi(z, r) \sim \psi_G(z, r)$ in (19.1) shows that the equation for G is, see Lemma 8.2,

$$G''(\rho) + \frac{d-1}{\rho} G' - G + |G|^{\frac{4}{d}} G + \frac{1}{4} \beta(z) \rho^2 G = 0, \quad (19.9)$$

where $\beta(z) = -L^3 L_{zz}$. Since $G(\rho)$ is independent of z , $\beta(z) \equiv \beta$. Hence, the equation for $L(z)$ reads

$$L_{zz}(z) = -\frac{\beta}{L^3},$$

where β is a constant. For $L(z)$ to vanish, β must be non-negative (Sect. 11.1). If $\beta \equiv 0$, Eq.(19.9) reduces to the R equation

$$R''(\rho) + \frac{d-1}{\rho} R' - R + |R|^{\frac{4}{d}} R = 0. \quad (19.10)$$

By Lemma 6.16, all solutions of (19.10) attain their global maximum at $\rho = 0$. Since, however, G attains its global maximum at $\rho_{\max} > 0$, it follows that $\beta > 0$. As in Sect. 11.1, this implies that $L(z) \sim \alpha \sqrt{Z_c - z}$, where $\alpha = (4\beta)^{\frac{1}{4}}$. Therefore, $\beta = \alpha^4/4$. \square

The proof of Proposition 19.1 suggests that there are only two types of singular solutions of the radial critical NLS:⁶

Proposition 19.2 ([74]) *Let ψ be a solution of the critical NLS (19.1) that collapses with the quasi self-similar profile*

$$\psi_F(z, r) = \frac{1}{L^{\frac{d}{2}}(z)} F(\rho) e^{i\xi + i \frac{L_z}{4L} r^2}, \quad \rho = \frac{r}{L(z)}, \quad \xi = \int_0^z \frac{ds}{L^2(s)}.$$

Then the blowup rate of $L(z)$ is either equal to or faster than a square root.

- (1) *If the blowup rate is equal to a square root, then $F(\rho)$ is a ring-type or a peak-type solution of the G equation (19.8) with $\alpha > 0$.*

⁶ The critical NLS also admits vortex-type singular solutions (Sects. 15.5, 15.6, and Chap. 20). These solutions, however, are not radial.

- (2) If the blowup rate is faster than a square root, then $F(\rho)$ is a peak-type solution of the R equation (19.10).

Proof From the proof of Proposition 19.1 it follows that $\beta \geq 0$. Therefore, the blowup rate of $L(z)$ is either equal to or faster than a square root.⁷

- (1) If the blowup rate is equal to a square root, then $\beta > 0$. Hence, F is a solution of the G equation, and is thus ring-type if $0 < G(0) < 1$ and peak-type if $G(0) > 1$ (Sect. 11.2.2).
- (2) If the blowup rate is faster than a square root, then $\beta = 0$. Hence, F is a solution of the R equation, whose H^1 solutions are always peak-type (Lemma 6.16). \square

Remark Case (1) of Proposition 19.2 applies to ψ_G^{explicit} (Chap. 11) and to the H^1 solutions that collapse with the ψ_G profile which are discussed in this chapter. Case (2) of Proposition 19.2 applies to H^1 solutions that collapse with the $\psi_{R^{(0)}}$ profile at the loglog law blowup rate (Chap. 14), and to ψ_R^{explicit} and Bourgain-Wang solutions that have a linear blowup rate (Chap. 10).

By Proposition 19.2, the self-similar profile of singular ring-type solutions is a solution of the G equation (19.8). When $0 < G(0) \ll 1$, solutions of (19.8) consist of a ring region in which G is positive with one or several peaks, and an algebraically-decaying oscillatory tail (Sect. 11.2). In particular, Eq. (19.8) admits a one-parameter family of single-ring solutions with a minimal tail (Sect. 11.2.5). The numerical simulations in Sect. 19.2.1 suggest

Observation 19.1 ([73]) *The self-similar profile of stable singular ring-type H^1 solutions of the critical NLS (19.1) is a single-ring solution of the G equation (19.8).*

At present, the only analytic support to Observation 19.1 is Proposition 19.1. Note, however, that while Proposition 19.1 says that the self-similar profile is a solution of the G equation, it does not say that $\alpha = \alpha^{(1)}(G_0)$, i.e., that this solution has a single-ring profile with a minimal tail.

19.2.1 Quasi Self-similar Blowup Profile

In Figs. 19.2 and 19.3 we presented three NLS solutions that collapse with a self-similar ring profile. We now show (numerically) that the self-similar profile of these solutions is a single-ring solution of the G equation. Since the single-ring G profiles constitute a one-parameter family (Sect. 11.2.5), we need to find the single-ring G profile that provides the best fit to the self-similar profile of ψ . To do that, we apply rescaling (19.5) to ψ and to the single-ring G profiles, and then fit ψ_{rescaled} with the G_{rescaled} that has the same radius.⁸

⁷ This also follows from the results that in the critical case the blowup rates of ψ and of $L(z)$ are the same (Sect. 13.2.3), and the blowup rate of ψ is at least a square root (Theorem 13.1).

⁸ The rescaled profiles G_{rescaled} can be parameterized by their radius (Fig. 11.9).

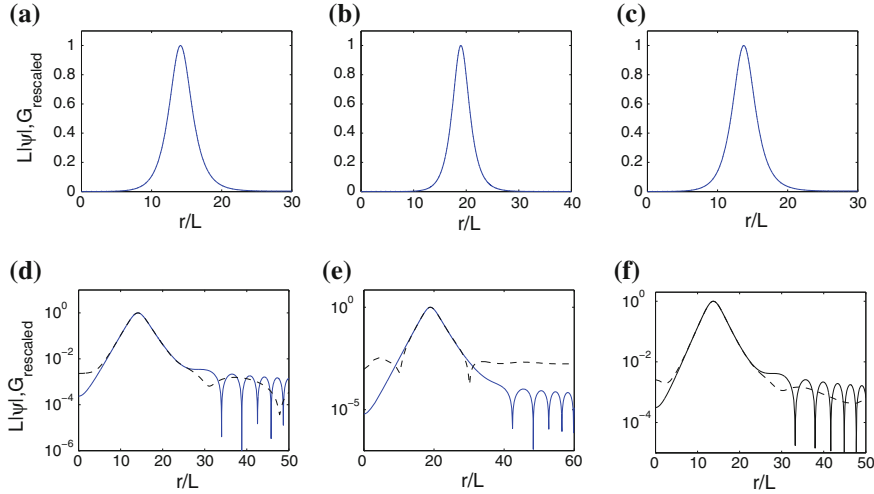


Fig. 19.4 Solution of the NLS (19.2) (dashes) and the best-fitting single-ring G profile (solid), both rescaled according to (19.5). **a** $\psi_0 = 15e^{-r^4}$, rescaled profile of ψ at $A(z) = 6.5 \cdot 10^{15}$, G profile with $G_0 = 2.9 \times 10^{-4}$ and $\alpha = \alpha^{(1)}(G_0) \cong 0.413$; the two lines are indistinguishable. **b** Same as (a) with $\psi_0 = 20e^{-r^4}$, $A(z) = 1.6 \times 10^5$, $G_0 = 7.6 \times 10^{-6}$ and $\alpha = \alpha^{(1)}(G_0) \cong 0.36$. **c** Same as (a) with $\psi_0 = 15e^{-r^8}$, $A(z) = 2.7 \times 10^4$, $G_0 = 3.8 \times 10^{-4}$ and $\alpha = \alpha^{(1)}(G_0) \cong 0.42$. **d–f** Same data as on top, but on a semi-logarithmic scale. From [73]

Figure 19.4a–c shows that each of the three self-similar profiles from Figs. 19.2 and 19.3 is in excellent match with the rescaled single-ring G profile that has the same radius. Plotting the same data on a semi-logarithmic scale (Fig. 19.4d–f) shows that the G profile provides an excellent match to the self-similar profile in the ring region $\rho - \rho_{\max} = O(1)$, but not for $\rho = O(1)$ or for $\rho \gg \rho_{\max}$. This “mismatch” is to be expected, since (i) the NLS solution does not maintain a self-similar profile outside the ring region (Fig. 19.2b), and (ii) G has an infinite-power tail, whereas the power of ψ is finite.

The NLS solution in the outer region $\rho \gg \rho_{\max}$, denoted by ψ_{outer} , does not participate in the collapse process, since the nonlinearity is negligible there. The NLS solution in the inner region $0 \leq \rho \ll \rho_{\max}$, denoted by ψ_{inner} , contains the power which is radiated inwards by the collapsing ring. Since this power is “trapped”, it bounces back and forth between the origin and the ring region.

Observation 19.2 ([73]) *Let ψ be a ring-type blowup solution of the critical NLS (19.1). Then ψ undergoes a quasi self-similar collapse, so that*

$$\psi(z, r) \sim \begin{cases} \psi_{\text{inner}}, & \text{if } 0 \leq r \ll L\rho_{\max}, \\ \psi_G, & \text{if } r - L\rho_{\max} = O(L), \\ \psi_{\text{outer}}, & \text{if } r \gg L\rho_{\max}, \end{cases} \quad (19.11)$$

where ψ_G is given by (19.6), and G is a single-ring solution of (19.8).

19.2.2 Blowup Rate of ψ_G

According to Proposition 19.1, collapsing ring-type solutions have a square-root blowup rate, without a loglog correction. Since the proof of Proposition 19.1 is not rigorous, we would like to confirm this prediction numerically. A priori, this may seem an impossible goal, since in Sect. 18.3 we argued that one cannot detect the loglog correction numerically. However, as noted by Fibich et al. [73], in order to show that the blowup rate is a “pure” square root, one does not need to detect the loglog correction, but only to tell whether the blowup rate is equal to or faster than a square root. This “less ambitious” goal can be achieved by computing numerically the limit of LL_z (Sect. 14.2.1).

We now apply the “ LL_z approach” to the ring-type blowup solution from Fig. 19.1 with $\psi_0 = 15e^{-r^4}$. Since $a := -\lim_{z \rightarrow Z_c} LL_z \approx 0.085$ (Fig. 19.5), the blowup rate is

$$L(z) \sim \alpha \sqrt{Z_c - z}, \quad \alpha \approx \sqrt{2 \times 0.085} = 0.412, \quad (19.12)$$

see Lemma 14.1. In particular, the blowup rate is a “pure” square root, without a loglog correction. In order to confirm the robustness of the “ LL_z approach”, we applied it to the NLS solution with an equal-power Gaussian initial condition. In this case $\lim_{z \rightarrow Z_c} LL_z = 0$, see Fig. 19.5b, which implies a faster-than-a-square-root blowup rate. Indeed, this solution collapses with the $\psi_{R(0)}$ profile (Fig. 14.3).

In Proposition 19.1 we saw that the blowup rate is faster than a square root when the blowup profile is $\psi_{R(0)}$, and equal to a square root when the blowup profile is ψ_G . Therefore, Fig. 19.4a provide additional support that the blowup rate of $\psi_0 = 15e^{-r^4}$ is a square root. Moreover, when we find the best-fitting G profile, the value of α in the G equation is determined from the condition that the rescaled G profile has the same radius as the rescaled self-similar profile. For example, for $\psi_0 = 15e^{-r^4}$ this fitting yields $\alpha \approx 0.413$. The value of α can be independently extracted from the numerical blowup rate, see (19.12), yielding $\alpha \approx 0.412$. *The excellent agreement between the values of α extracted from the blowup rate and from the self-similar*

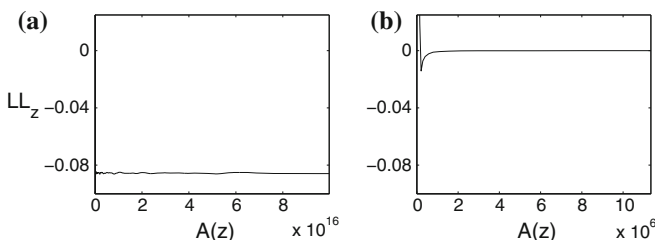


Fig. 19.5 LL_z as a function of $A(z) = \frac{\max_r |\psi(z,r)|}{\max_r |\psi(0,r)|}$ for solutions of the NLS (19.2) with **a** $\psi_0 = 15e^{-r^4}$, and **b** $\psi_0 = 15\sqrt{\frac{\pi}{2}}e^{-r^2}$. Adapted from [73]

profile provides a strong numerical support that the blowup rate is a square root, and that the self-similar profile is a single-ring solution of the G equation.

19.2.3 $d = 7/4$

So far, the numerical results in this chapter were for the two-dimensional critical NLS. The results of Proposition 19.1 and Observation 19.2, however, are formulated for any $d > 1$. In particular, d does not have to be an integer. Indeed, a systematic numerical study confirmed the validity of Proposition 19.1 and Observation 19.1 for ring-type singular solutions of the critical NLS (19.1) with $d = 7/4$. See [74, Sect. 2] for further details.

19.3 Azimuthal Instability

In Sect. 11.4 we saw numerically that when G has a single-ring profile, the explicit blowup solution ψ_G^{explicit} is stable as a solution of the radial critical NLS. When $d = 2$, however, ψ_G^{explicit} is azimuthally unstable as a solution of

$$i\psi_z(z, x, y) + \psi_{xx} + \psi_{yy} + |\psi|^2\psi = 0. \quad (19.13)$$

Indeed, under azimuthal perturbations, ψ_G^{explicit} breaks into filaments, each of which collapses with the peak-type $\psi_{R^{(0)}}$ profile.

The situation is similar with singular solutions that collapse with the quasi self-similar ψ_G profile. Indeed, the numerical simulations of Sect. 19.1 suggest that these solutions are radially stable, and the informal analysis in Sect. 11.5 suggests that they are azimuthally unstable.

Observation 19.3 *Singular ring-type solutions of the two-dimensional critical NLS are stable as solutions of the radial NLS (19.2), but unstable as solutions of the NLS (19.13).*

The issue of azimuthal stability arises only when d is an integer. Thus, for example, singular ring-type solutions of the critical NLS (19.1) with $d = 7/4$ are stable “without any restrictions” [74].

19.4 Experiments with Super-Gaussian Beams

In Sect. 19.1 we saw numerically (and in Chap. 26 we shall show asymptotically) that high-power super-Gaussian initial conditions initially evolve into a ring profile. Since a ring structure is azimuthally unstable (Observation 19.3), it breaks into a *ring of filaments*, i.e., into multiple filaments located on a circle.

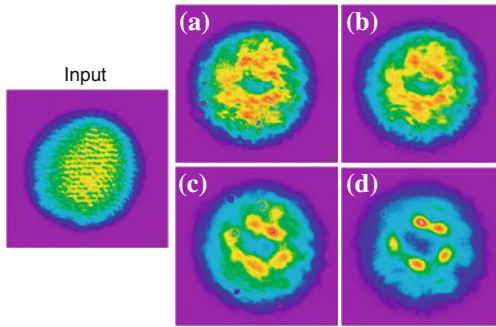


Fig. 19.6 (Experimental) propagation dynamics of a super-Gaussian input beam in water. The image area is 0.3×0.3 mm. *Left* Input profile. *Right* Output profile, when the length of the water cell is: **a** 1.3 cm, **b** 2.0 cm, **c** 3.0 cm, **d** 4.3 cm. From [122]

In [122], Grow et al. studied *experimentally* the propagation of high-power super-Gaussian input beams in water, see Fig. 19.6⁹, and observed that:

1. The beams initially evolved into a ring profile.
2. Subsequently, the rings became azimuthally unstable and broke into several filaments located on a circle.

These experimental results are, therefore, in agreement with the predictions of the NLS model. As such, they provide further support to the physical validity of the NLS model (Sect. 1.8).

19.5 Ring Power Collapsing into the Singularity

As noted, peak-type blowup solutions of the critical NLS collapse with the $\psi_{R^{(0)}}$ profile. These solutions undergo a strong collapse with $P_{\text{collapse}} = P_{\text{cr}}$ (Corollary 14.1). In particular, P_{collapse} is independent of ψ_0 .

The situation is different with ring-type blowup solutions. The power that collapses into the singularity is $P_{\text{collapse}} \approx P_{\text{ring}}$, the power of the G profile in the ring region, which is highly above P_{cr} (Sect. 11.2.5). In addition, P_{ring} increases with input power.¹⁰ Thus, *ring-type collapse is more efficient than peak-type collapse in concentrating power into the singularity*. For example, since a Gaussian initial condition with $P = 40P_{\text{cr}}$ collapses with the $\psi_{R^{(0)}}$ profile, only 2.5% of its power collapses into the singularity. In contrast, an equal-power super-Gaussian collapses with a ring profile that concentrates 70% of its power into the singularity [73].

⁹ These experiments are also discussed in Sect. 26.7.2.

¹⁰ Intuitively, a higher-power initial condition collapses with a G profile that has a larger radius (Sect. 19.1.1), and so has a higher ring power (Fig. 11.8d).

In theory, ring-type collapse offers the possibility to concentrate much more power into a small region than peak-type collapse. In practice, however, because the collapsing ring is azimuthally unstable, it breaks into filaments, each of which collapses with $P_{\text{collapse}} = P_{\text{cr}}$. Therefore, azimuthal instability limits the extent to which one can use ring-type collapse to increase the amount of power which is deposited in a small region.

19.6 Open Question

In Chap. 11 we saw that the critical NLS admits the solution ψ_G^{explicit} , which maintains a ring profile all the way up to the singularity. In addition, numerical simulations suggest that when G is a single-ring profile, ψ_G^{explicit} is radially stable. This solution, however, is not in H^1 .

In this chapter we presented simulations of H^1 solutions of the critical radial NLS that collapse with the quasi self-similar ring profile ψ_G at a square-root blowup rate, up to focusing levels of $A(z) = O(10^{16})$. We now ask

Open Question 19.1 *Can H^1 solutions of the critical radial NLS maintain the ring-type ψ_G profile all the way up to the singularity, or do they ultimately collapse with the peak-type $\psi_{R^{(0)}}$ profile?*

To motivate this question, consider the NLS (19.2) with $\psi_0 = 9.4e^{-r^4}$ ($P = 15P_{\text{cr}}$). The solution collapses with a ring profile up to $A(z) = O(10^7)$, see Fig. 19.7b–d. Based on these data, one might conclude that the solution collapses with the ψ_G profile all the way up to the singularity. As we continue the simulation to $A(z) = O(10^{10})$, however, the solution’s peak moves to the origin (Fig. 19.7e), and eventually the solution collapses with the $\psi_{R^{(0)}}$ profile (Fig. 19.7f).

This simulation shows that just because the solution of Fig. 19.1 maintained a ring profile up to $A(z) = 10^{15}$, this does not imply that it will maintain a ring profile all the way up to the singularity. Since any numerical solver becomes unreliable at sufficiently high focusing levels, Question 19.1 cannot be answered numerically, but only analytically. Nevertheless, numerical simulations of singular H^1 vortex solutions of the critical NLS provide a strong indirect support to the possibility that the quasi self-similar ψ_G ring profile can be maintained up to the singularity (Sect. 20.3).

It is worth noting that the existence of singular H^1 ring-type solutions does not contradict the rigorous theory of the critical NLS. Indeed,

- In Sect. 14.6 we saw that Merle and Raphaël proved that singular solutions of the critical NLS (19.2) collapse with the $\psi_{R^{(0)}}$ profile at the loglog law rate. This result may seem to suggest that H^1 solutions cannot collapse with the ψ_G profile at a square-root rate. The result of Merle and Raphaël, however, was “only” proved for initial conditions with power below $\|R^{(1)}\|_2^2$. In addition, $\|R^{(1)}\|_2^2 \approx 6.6P_{\text{cr}}$ for $d = 2$, see Sect. 6.4. The power of the ring-type solutions presented in this chapter, however, is considerably higher ($P \geq 38P_{\text{cr}}$).

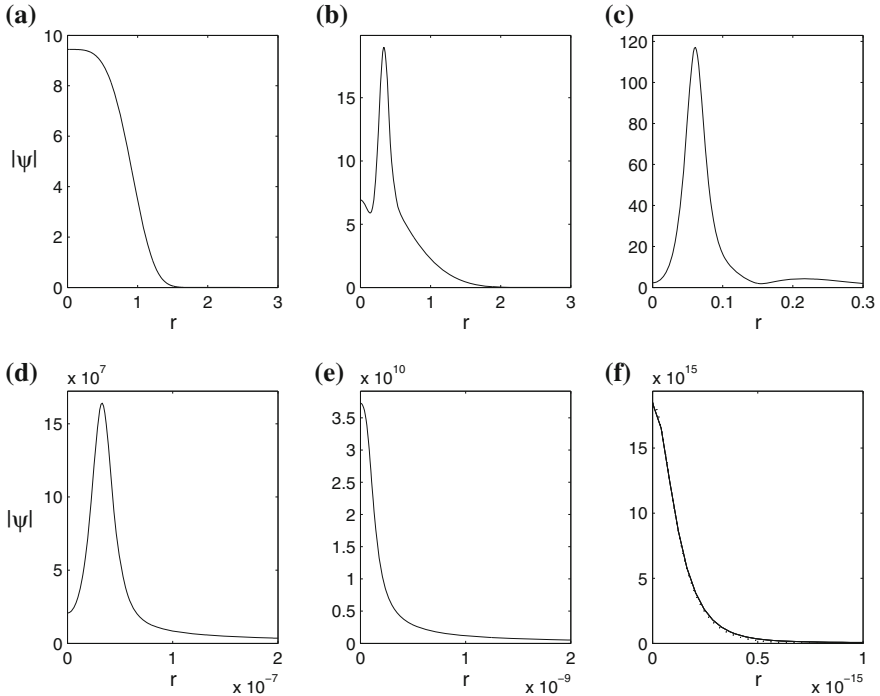


Fig. 19.7 Solution of (19.2) with $\psi_0 = \sqrt{\frac{60}{\pi} P_{\text{cr}}} e^{-r^4}$ ($P = 15P_{\text{cr}}$) at the following focusing levels: **a** $A = 1$, **b** $A = 2$, **c** $A = 12$, **d** $A = 1.7 \times 10^7$, **e** $A = 4 \times 10^9$, **f** $A = 2 \times 10^{15}$. The dotted line in (f) is $\psi_{R^{(0)}}$. From [73]

- The power of the G profile is infinite (Corollary 11.2). This may seem to suggest that finite-power solutions cannot collapse with the infinite-power ψ_G profile. Observation 19.2 shows, however, that $\psi \sim \psi_G$ only in the ring region. Therefore, the infinite-power tail of the G profile is “irrelevant” to NLS ring-type solutions.¹¹

Whether the self-similar ring profile is maintained “only” up to $A(z) = 10^{16}$, or up to the singularity, is a purely mathematical issue, because:

1. For any conceivable physical application, the validity of the NLS model breaks down long before reaching such focusing levels (Sect. 1.8).
2. Collapsing ring-type solutions are stable only if we impose the non-physical assumption of radial symmetry.¹²

¹¹ The situation where an infinite-power tail is “irrelevant” because the collapse is only quasi self-similar, occurs also for peak-type blowup solutions of the critical and supercritical NLS (Sects. 17.3 and 21.1, respectively).

¹² When d is not an integer, all solutions are radial, and therefore collapsing ring solutions are stable “without any restrictions”. A non-integer d , however, is not physical.

Conclusion 19.1 *Collapsing ring solutions can be observed experimentally at the early stages of the collapse (Sect. 19.4). The singular limit of these solutions, however, is only of mathematical interest.*

19.7 Critical Biharmonic NLS (ψ_{G_B})

In [13], Baruch et al. conducted a numerical study of ring-type blowup solutions of the critical radial BNLS

$$i\psi_z(z, r) - \Delta^2 \psi + |\psi|^{\frac{8}{d}} \psi = 0, \quad \psi(0, r) = \psi_0(r) \in H^2,$$

where $\Delta^2 = \left(\frac{\partial^2}{\partial r^2} + \frac{d-1}{r} \frac{\partial}{\partial r} \right)^2$. These solutions undergo a quasi self-similar collapse with the ψ_{G_B} profile

$$\psi_{G_B}(z, r) = \frac{1}{L^{\frac{d}{2}}(z)} G_B \left(\frac{r}{L(z)} \right) e^{i \int_0^z \frac{1}{L^4} + i S_B(z, r)},$$

where G_B and S_B are real.¹³ Their blowup rate is a quartic root, i.e.,

$$L(z) \sim \kappa \sqrt[4]{Z_c - z}, \quad z \rightarrow Z_c, \quad \kappa > 0.$$

Therefore, up to the change $2 \rightarrow 4$, these solutions are completely analogous to solutions of the critical NLS that collapse with the ψ_G profile. We stress that these results are purely numerical, as the existence of singular solutions of the biharmonic NLS is still open. See [13, Sect. 4] for further details.

¹³ In the critical BNLS, the explicit expression for the radial phase term (i.e., the biharmonic analog of $e^{i \frac{L_z}{L} \frac{r^2}{4}}$) is not known. Therefore, $S_B(z, r)$ is the BNLS analog of $e^{i \frac{L_z}{L} \frac{r^2}{4}}$.

Chapter 20

Singular H^1 Vortex Solutions (ψ_{R_m} and ψ_{G_m})

In Sects. 15.5.1 and 15.6 we saw that the two-dimensional critical NLS

$$i\psi_z(z, r, \theta) + \psi_{rr} + \frac{1}{r}\psi_r + \frac{1}{r^2}\psi_{\theta\theta} + |\psi|^2\psi = 0, \quad \psi(0, r, \theta) = e^{im\theta}A_0(r), \quad (20.1)$$

admits the explicit blowup vortex solutions $\psi_{R_m}^{\text{explicit}}$ and $\psi_{G_m}^{\text{explicit}}$. In this chapter we follow Fibich and Gavish [72] and study blowup vortex solutions of (20.1) that are radially stable (unlike $\psi_{R_m}^{\text{explicit}}$), and in H^1 (unlike $\psi_{G_m}^{\text{explicit}}$). Blowup vortex solutions of the supercritical NLS are discussed in Sects. 22.5 and 23.7.

20.1 Two Potential Blowup Profiles

In Chap. 15 we saw that solutions of (20.1) maintain a radial vortex profile $\psi(z, r, \theta) = e^{im\theta}A(z, r)$, where A is the solution of

$$iA_z(z, r) + A_{rr} + \frac{1}{r}A_r - \frac{m^2}{r^2}A + |A|^2A = 0, \quad A(0, r) = A_0(r). \quad (20.2)$$

We also saw that their blowup profile cannot be given by $\psi_{R^{(0)}}$, because vortex solutions vanish at $r = 0$.

By analogy with vortex-free ring solutions (Proposition 19.1), we assume that vortex solutions undergo a quasi self-similar collapse with the blowup profile

$$\psi_{B_m}(z, r, \theta) = \frac{1}{L(z)}B_m(\rho)e^{i\xi+im\theta+i\frac{L_z}{L}\frac{r^2}{4}}, \quad \xi = \int_0^z \frac{ds}{L^2(s)}, \quad \rho = \frac{r}{L(z)}.$$

As in Sect. 15.6, it can be shown that B_m is the solution of

$$B_m''(\rho) + \frac{1}{\rho} B_m' - \left(1 + \frac{m^2}{\rho^2}\right) B_m + B_m^3 + \frac{\beta_c}{4} \rho^2 B_m = 0, \quad \beta_c = \lim_{z \rightarrow Z_c} L^3 L_{zz},$$

and that the following two possibilities exist:

1. If $\beta_c = 0$, then $\lim_{z \rightarrow Z_c} \frac{L(z)}{\sqrt{Z_c - z}} = 0$, i.e., the blowup rate is faster than a square root. The profile B_m is a solution of the R_m equation

$$R_m''(r) + \frac{1}{r} R_m' - \left(1 + \frac{m^2}{r^2}\right) R_m + R_m^3 = 0,$$

and the blowup profile is

$$\psi_{R_m}(z, r, \theta) = \frac{1}{L(z)} R_m(\rho) e^{i\xi + im\theta + i \frac{L_z}{L} \frac{r^2}{4}}.$$

2. If $\beta_c > 0$, then $L(z) \sim \sqrt{\frac{\beta_c}{2}(Z_c - z)}$, i.e., the blowup rate is a square root. The profile B_m is a solution of the G_m equation

$$G_m''(\rho) + \frac{1}{\rho} G_m' - \left(1 + \frac{m^2}{\rho^2}\right) G_m + G_m^3 + \frac{\beta_c}{4} \rho^2 G_m = 0, \quad (20.3)$$

and the blowup profile is

$$\psi_{G_m}(z, r, \theta) = \frac{1}{L(z)} G_m(\rho) e^{i\xi + im\theta + i \frac{L_z}{L} \frac{r^2}{4}}. \quad (20.4)$$

Thus, there are two potential blowup profiles for H^1 vortex solutions of the critical NLS (20.1): ψ_{R_m} and ψ_{G_m} .

In the H^1 non-vortex case there are also two blowup profiles: $\psi_{R^{(0)}}$ and ψ_G . It is easy to distinguish between them numerically, because $\psi_{R^{(0)}}$ is peak-type and ψ_G is ring-type. “Unfortunately”, one cannot use this approach to distinguish numerically between ψ_{R_m} and ψ_{G_m} , because both are ring-type. Moreover, because the single-ring G_m profiles bifurcate from $R_m^{(0)}$ (Conclusion 15.2), G_m can be arbitrarily close to $R_m^{(0)}$. Therefore, Fibich and Gavish [72] suggested to distinguish numerically between ψ_{R_m} and ψ_{G_m} according to the blowup rate. Thus, if $a := -\lim_{z \rightarrow Z_c} LL_z = 0$, the blowup rate is faster than a square root (Lemma 14.1), and so the vortex solution collapses with the ψ_{R_m} profile. If $a > 0$, however, the blowup rate is a square root, and so the vortex solution collapses with the ψ_{G_m} profile.

As in the vortex-free case (Sect. 19.2.1), when $a > 0$ we can gain additional confidence that the solution collapses with the ψ_{G_m} profile, as follows. We find the G_m profile that provides the best match to the self-similar profile of the collapsing

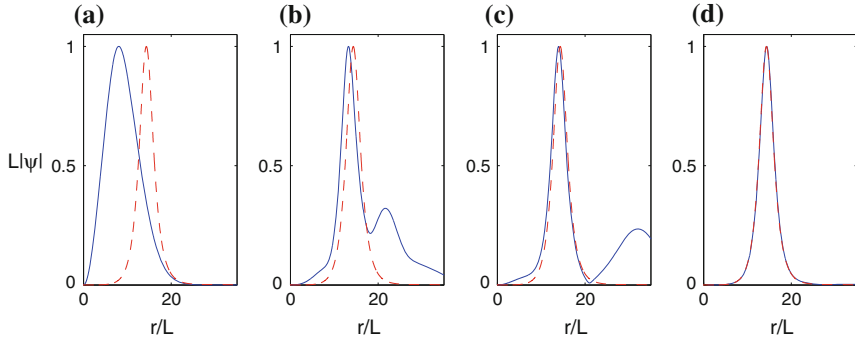


Fig. 20.1 Solution of (20.1) with $\psi_0 = \frac{1}{3}r^2 e^{-(\frac{r}{4})^2+i2\theta}$ (solid). The dashed curve is the single-ring G_2 vortex profile with $\alpha^{(1)} \approx 0.410$. Both curves are rescaled according to (20.7). **a** $z = 0$, $L^{-1}(z) = 1$, **b** $z = 1.1$, $L^{-1}(z) = 3.8$, **c** $z = 1.4$, $L^{-1}(z) = 5.3$, **d** $z = 1.8$, $L^{-1}(z) = 26$. From [72]

solution.¹ Then we confirm that the value of $\alpha = \alpha^{(1)}(g_{m,0})$ of the best-matching single-ring G_m profile agrees with the value of

$$\alpha = (2a)^{\frac{1}{2}}, \quad a = -\lim_{z \rightarrow Z_c} LL_z \quad (20.5)$$

which is extracted from the blowup rate (see e.g., Fig. 20.1).

20.2 Simulations

In the simulations presented in this section we enforce radial symmetry by solving Eq. (20.2) for $A(z, r)$, rather than Eq. (20.1) for $\psi(z, r, \theta)$. In fact, we have to do that, because radial vortex solutions of (20.1) are azimuthally unstable (Sect. 20.4).

In Sect. 15.8.2 we saw that the solution of the critical NLS (20.1) with

$$\psi_0 = 1.02 R_m^{(0)}(r) e^{im\theta}, \quad m = 2 \quad (20.6)$$

collapses with a self-similar single-ring G_m profile at a square-root blowup rate, and not with a self-similar $R_m^{(0)}$ profile at a loglog law blowup rate. Then, in Fig. 15.15 we saw that the numerical solution of (20.1) with

$$\psi_0 = \psi_{G_m}(z = 0) = G_m(r) e^{im\theta - i \frac{\alpha^2 r^2}{8}},$$

¹ i.e., the G_m profile that has the same rescaled radius as the self-similar profile.

where G_m is a double-ring profile, collapses with a self-similar single-ring G_m profile, and not with a double-ring G_m profile. These two simulations suggest that $\psi_{R_m^{(0)}}$ and the multi-ring ψ_{G_m} are radially-unstable, and that the single-ring ψ_{G_m} profile is a strong attractor for collapsing radial vortex solutions.

To further support this observation, we solve (20.1) with a Laguerre-Gaussian initial condition whose power is $P = 4.1P_{\text{cr}}(m=2) \approx 32P_{\text{cr}}$. After focusing by 26, the rescaled solution

$$\psi_{\text{rescaled}} = \frac{1}{L(z)} \psi \left(\frac{r}{L} \right), \quad L(z) = \frac{\max_r |\psi_0|}{\max_r |\psi|} \quad (20.7)$$

is indistinguishable from the single-ring G_2 profile with $\alpha^{(1)} \approx 0.410$, see Fig. 20.1. This value of α is in an excellent agreement with the value $\alpha \approx 0.409$ which is extracted from the blowup rate using (20.5).

Observation 20.1 ([72]) *The single-ring ψ_{G_m} profile is a strong attractor for singular radial vortex solutions of the critical NLS. The $\psi_{R_m^{(0)}}$ and multi-ring ψ_{G_m} profiles, however, are radially unstable.*

This is different from the non-vortex radial case, where both $\psi_{R^{(0)}}$ and the single-ring ψ_G are attractors.

Recently, Simpson and Zwier proved that when $m = 1$, there exists an open set of radial vortex initial conditions, for which the corresponding NLS solutions collapse with the $\psi_{R_m^{(0)}}$ profile at the loglog law rate [238]. This rigorous result is in disagreement with Observation 20.1, which is based on numerical simulations (such as in Sect. 15.8.2). At present, we do not know how to reconcile these two results. One possibility is that there is a mistake, either in the numerical simulations or in the rigorous proof. Another possibility is that solutions that “appear” to collapse with the ψ_{G_m} profile, ultimately collapse with the $\psi_{R_m^{(0)}}$ profile.² This explanation, however, is inconsistent with the simulations in Sect. 15.8.2 where a perturbed $\psi_{R_m^{(0)}}$ profile moves away from $\psi_{R_m^{(0)}}$ and towards ψ_{G_m} . Yet another possibility is that $\psi_{R_m^{(0)}}$ is an attractor for $m = 1$, but unstable for $m = 2$. We checked numerically that this is not the case, however, by repeating the simulations of Sect. 15.8.2 with $m = 1$. It is also possible that $\psi_{R_m^{(0)}}$ solutions are stable, but their basin of stability is so small that they become unstable under a 2% perturbation.

Further support to Observation 20.1 comes from the existence of an analogous numerical result in the supercritical case (Observation 23.3), namely, that ψ_{S_m} (the vortex-analog of the ring-type solution) is radially stable, but ψ_{Q_m} (the vortex-analog of the peak-type solution) is radially unstable. Note that Observation 23.3 is more solid than Observation 20.1, because it is easy to distinguish numerically between ψ_{S_m} and ψ_{Q_m} .

² This explanation is motivated by the simulation of Fig. 19.7, in which the solution collapses with the ψ_G profile “for a long time”, but ultimately collapse with the ψ_R profile.

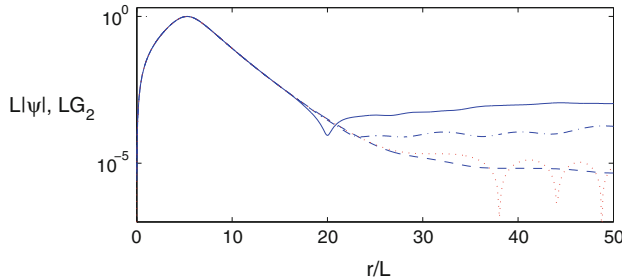


Fig. 20.2 Figure 15.12b, re-plotted on a semi-logarithmic scale. The *dotted curve* is the single-ring G_m vortex profile from Fig. 15.14. From [72]

20.2.1 Quasi Self-similar Collapse

As noted, Theorem 15.2 implies that the blowup profile is quasi self-similar. To show that stable vortex solutions undergo a quasi self-similar collapse and not a self-similar collapse, in Fig. 20.2 we re-plot Fig. 15.12b,³ on a semi-logarithmic scale. For $0 \leq \frac{r}{L} \leq 15$, the rescaled NLS solution remains unchanged while focusing by 10^{15} , and is in excellent agreement with the best-matching single-ring G_m profile. For $\frac{r}{L} > 20$, however, the rescaled solution does change. In particular, it is completely “unrelated” to the infinite-power oscillatory tail of G_m .

In Sect. 19.2.1 we saw that singular non-vortex ring-type H^1 solutions approach the ψ_G profile in the ring region $\frac{r}{L} - \rho_{\max} = O(1)$, but not in the inner region $\frac{r}{L} = O(1)$ or in the outer region $\frac{r}{L} - \rho_{\max} \gg 1$. In contrast, collapsing vortex solutions approach the ψ_{G_m} profile both in the ring region and in the inner region. Intuitively, this is because both ψ and ψ_{G_m} have to vanish at $r = 0$ (Lemma 15.5).

Observation 20.2 ([72]) Let $\psi = e^{im\theta} A(z, r)$ be a radially-stable blowup H^1 vortex solution of the critical NLS (20.1). Then ψ undergoes a quasi self-similar collapse with a single-ring ψ_{G_m} profile, so that

$$\psi(z, r) \sim \begin{cases} \psi_{G_m}(z, r), & \text{if } 0 \leq \frac{r}{L(z)} \leq \rho_{\max} + O(1), \\ \psi_{\text{outer}}(z, r), & \text{if } \frac{r}{L(z)} - \rho_{\max} \gg 1, \end{cases}$$

where ψ_{G_m} is given by (20.4), G_m is a single-ring solution of (20.3), and $\rho_{\max} = \arg \max G_m(\rho)$.

³ i.e., the solution of (20.1) with the initial condition (20.6).

20.3 Open Question

At present, the following question is open:

Open Question 20.1 *Can H^1 vortex solutions of the critical NLS (20.1) maintain a single-ring ψ_{G_m} profile all the way up to the singularity, or do they ultimately collapse with the $\psi_{R_m^{(0)}}$ profile?*

The simulations in Sect. 20.2 suggest that radially-stable singular vortex solutions of the critical NLS undergo a quasi self-similar collapse with a single-ring ψ_{G_m} profile. By Lemma 15.25, however, ψ_{G_m} has infinite power. This may seem to suggest that ψ_{G_m} cannot be the asymptotic profile of H^1 vortex solutions of the critical NLS. In Sect. 20.2.1 we saw, however, that ψ_{G_m} does not characterize the outer region. Hence, the infinite-power tail of ψ_{G_m} is “irrelevant” to collapsing vortex solutions (see e.g., Fig. 20.2).

A similar situation occurs in the vortex-free case, where numerical simulations suggest that ring-type singular solutions collapse with the ψ_G profile, which also has an infinite-power tail. In that case, ψ_G also does not characterize the “outer solution” (Sect. 19.6). Thus, the infinite-power tail of ψ_G is also “irrelevant”.

As noted in Sect. 19.6, it is impossible to determine numerically whether singular solutions maintain the ring-type ψ_G profile all the way up to the singularity, or whether they ultimately collapse with the peak-type $\psi_{R_m^{(0)}}$ profile. It is therefore an open question whether there exist H^1 non-vortex solutions of the critical NLS that collapse with the ψ_G profile at a square-root rate. Similarly, it is impossible to determine numerically whether singular vortex solutions can maintain the ψ_{G_m} profile all the way up to the singularity. The surprising numerical observation that $\psi_{R_m^{(0)}}$ is not an attractor (Observation 20.1), however, suggests that there may be “no other alternative”, i.e., that singular vortex solutions “have to” collapse with the ψ_{G_m} profile. In that case, however, “there is no reason” why non-vortex solutions cannot collapse with the ψ_G profile. Whether this is the case is an open question.

20.4 Azimuthal Instability

Lemma 11.10 showed that collapsing self-similar ring solutions of the two-dimensional critical NLS are azimuthally unstable. Therefore, we have

Lemma 20.1 ([72]) *All singular radial vortex solutions of the critical NLS (20.1) are azimuthally unstable.*

Once a vortex solution becomes azimuthally unstable, it disintegrates into filaments. These filaments are typically not centered at the phase singularity. Therefore, they collapse with the non-vortex $\psi_{R_m^{(0)}}$ profile (as e.g., in Fig. 15.6). See [72, 260, 264] for further analysis and simulations of the azimuthal instability of collapsing vortex solutions.

Part IV
Asymptotic Analysis
of the Supercritical NLS

Chapter 21

Singular H^1 Peak-Type Solutions (ψ_Q)

In this chapter we consider peak-type blowup solutions of the supercritical NLS

$$i\psi_z(z, \mathbf{x}) + \Delta\psi + |\psi|^{2\sigma}\psi = 0, \quad \psi(0, \mathbf{x}) = \psi_0(\mathbf{x}) \in H^1, \quad \sigma d > 2. \quad (21.1)$$

We assume that (21.1) is also H^1 -subcritical, see (5.2). Therefore, σ is in the range

$$\begin{cases} \frac{2}{d} < \sigma < \infty, & \text{if } d \leq 2, \\ \frac{2}{d} < \sigma < \frac{2}{d-2}, & \text{if } d > 2. \end{cases} \quad (21.2)$$

In Chap. 12 we saw that the supercritical NLS admits the explicit peak-type blowup solution

$$\psi_Q^{\text{explicit}}(z, r) = \frac{1}{L^{\frac{1}{\sigma}}(z)} Q(\rho) e^{i\zeta(z)},$$

where

$$L(z) = \kappa \sqrt{Z_c - z}, \quad \kappa = \sqrt{2a}, \quad \rho = \frac{r}{L(z)}, \quad \zeta = \int_0^z \frac{ds}{L^2(s)},$$

and Q is a solution of

$$Q''(\rho) + \frac{d-1}{\rho} Q' - Q + ia \left(\frac{1}{\sigma} Q + \rho Q' \right) + |Q|^{2\sigma} Q = 0, \quad Q'(0) = 0. \quad (21.3)$$

This explicit solution, however, is not in H^1 . In this chapter we study peak-type blowup solutions of the supercritical NLS that are in H^1 . As we shall see, these solutions undergo a quasi self-similar collapse with the peak-type profile ψ_Q .

To simplify the presentation, we assume that ψ_0 is radial. In that case ψ remains radial (Lemma 5.5), and so the dynamics is governed by the radial supercritical NLS

$$i\psi_z(z, r) + \psi_{rr} + \frac{d-1}{r} \psi_r + |\psi|^{2\sigma} \psi = 0, \quad \psi(0, r) = \psi_0(r) \in H^1, \quad \sigma d > 2. \quad (21.4)$$

The assumption of radial symmetry is reasonable for collapsing peak-type solutions. Indeed, Landman et al. [152] observed numerically that, as in the critical case (Sect. 14.1.2 and Corollary 14.3), even if ψ_0 is not radial, the collapsing core of peak-type supercritical solutions approaches a radial profile near the singularity.

Remark The results of this chapter are also relevant to standing-ring blowup solutions of the supercritical NLS with $\sigma > 2$ and $d > 1$ (Sect. 22.4).

21.1 Quasi Self-similar Collapse

In Sect. 12.2 we saw that all nontrivial solutions of the Q equation (21.3) are not in H^1 . Therefore, ψ_Q^{explicit} cannot be an attractor for blowup solutions of (21.4) on $0 \leq r < \infty$. LeMesurier et al. [155] and Shvetz et al. [235] observed numerically that peak-type blowup solutions of (21.4) undergo a quasi self-similar collapse, so that as $z \rightarrow Z_c$,

$$\psi(z, r) \sim \begin{cases} \psi_Q(z, r), & \text{if } 0 \leq r \leq r_c, \\ \psi_{\text{outer}}(z, r), & \text{if } r \geq r_c, \end{cases} \quad (21.5)$$

where

$$\psi_Q(z, r) = \frac{1}{L^{\frac{1}{\sigma}}(z)} Q(\rho) e^{i\xi(z)}, \quad \rho = \frac{r}{L(z)}, \quad (21.6a)$$

and r_c depends on ψ_0 . As in the derivation of ψ_Q^{explicit} (Sect. 12.1), substituting $\psi \sim \psi_Q$ in (21.4) shows that Q is a solution of (21.3), and that

$$L(z) = \sqrt{2a(Z_c - z)}, \quad \xi = \int_0^z \frac{ds}{L^2(s)}. \quad (21.6b)$$

While the inner-core solution ($0 \leq r \leq r_c$) approaches ψ_Q , this is not the case with the non-collapsing outer part ψ_{outer} . Rather, as in the critical case (Sect. 17.3), its dynamics appears to be frozen as $z \rightarrow Z_c$, compared with the ever faster dynamics of the collapsing core.

In Sect. 17.3 we saw that stable peak-type solutions of the critical NLS undergo a quasi self-similar collapse with the $\psi_{R^{(0)}}$ profile, so that as $z \rightarrow Z_c$,

$$\psi(z, r) \sim \begin{cases} \psi_{R^{(0)}}(z, r), & \text{if } 0 \leq r \leq \rho_c L(z), \\ \psi_{\text{outer}}(z, r), & \text{if } r \geq \rho_c L(z). \end{cases}$$

There is, however, an important difference between the two cases. In the critical case the collapsing core approaches $\psi_{R^{(0)}}$ on a fixed domain $0 \leq \rho \leq \rho_c$ in the rescaled

transverse variable. In physical variables, this domain corresponds to the domain $0 \leq r \leq \rho_c L(z)$, which shrinks to a point as $z \rightarrow Z_c$. In the supercritical case, however, the collapsing core approaches ψ_Q on a fixed domain $0 \leq r \leq r_c$ in the physical transverse variable. In the rescaled variables, this domain corresponds to the domain $0 \leq \rho \leq r_c/L(z)$, which becomes infinite as $z \rightarrow Z_c$ [235].

In the critical case, the Hamiltonian of the self-similar peak-type profile is zero (Corollary 7.14). A similar result exists in the supercritical case:

Lemma 21.1 *Let ψ be a solution of the supercritical NLS (21.4) that undergoes a quasi self-similar collapse according to (21.5) and (21.6). Then*

$$H(Q) := \int_0^\infty \left(|\nabla Q(\rho)|^2 - \frac{1}{\sigma+1} |Q|^{2\sigma+2} \right) \rho^{d-1} d\rho = 0.$$

Proof We provide an informal proof. By (21.5), $H(\psi) \sim H(\psi_Q) + H(\psi_{\text{outer}})$, where

$$\begin{aligned} H(\psi_Q) &= \int_0^{r_c} \left(|\nabla \psi_Q|^2 - \frac{1}{\sigma+1} |\psi_Q|^{2\sigma+2} \right) r^{d-1} dr, \\ H(\psi_{\text{outer}}) &= \int_{r_c}^\infty \left(|\nabla \psi_{\text{outer}}|^2 - \frac{1}{\sigma+1} |\psi_{\text{outer}}|^{2\sigma+2} \right) r^{d-1} dr. \end{aligned}$$

Since ψ_{outer} does not participate in the collapse process, $H(\psi_{\text{outer}})$ remains bounded as $z \rightarrow Z_c$. Since $H(\psi) \equiv H(\psi_0)$, this implies that $H(\psi_Q)$ remains bounded as $z \rightarrow Z_c$. Now, by (21.6),

$$H(\psi_Q) = L^{d-\frac{2}{\sigma}-2}(z) \int_0^{\frac{r_c}{L(z)}} \left(|\nabla Q(\rho)|^2 - \frac{1}{\sigma+1} |Q|^{2\sigma+2} \right) \rho^{d-1} d\rho.$$

Because σ is in the range (21.2), we have that $d - \frac{2}{\sigma} - 2 < 0$. Consequently, $L^{d-\frac{2}{\sigma}-2} \rightarrow \infty$ as $L \rightarrow 0$. Since $H(\psi_Q)$ should remain bounded, this implies that $\lim_{L \rightarrow 0} \int_0^{\frac{r_c}{L}} \left(|\nabla Q(\rho)|^2 - \frac{1}{\sigma+1} |Q|^{2\sigma+2} \right) \rho^{d-1} d\rho = 0$. \square

In Sect. 12.2 we saw that as $\rho \rightarrow \infty$,

$$Q(\rho) \sim c_1 Q_1(\rho) + c_2 Q_2(\rho), \quad Q_1 \sim \rho^{-\frac{i}{a} - \frac{1}{\sigma}}, \quad Q_2 \sim e^{-i \frac{a\rho^2}{2}} \rho^{\frac{i}{a} - d + \frac{1}{\sigma}}.$$

We also saw that if $H(Q) = 0$, then $c_2 = 0$ and $Q \sim c_1 Q_1$ has infinite power. Since $\psi \rightarrow \psi_Q$ on $\rho \in [0, \frac{r_c}{L(z)}] \rightarrow [0, \infty)$, it may seem that we approximate a finite-power solution (ψ) with an infinite-power blowup profile (ψ_Q). This issue was clarified by Bergé and Pesme, who showed that the limiting power of ψ_Q in $[0, r_c]$ is finite:

Lemma 21.2 ([23, 24]) Let Q be a zero-Hamiltonian solution of (21.3), and let ψ_Q be given by (21.6). Then

$$\lim_{z \rightarrow Z_c} \int_0^{r_c} |\psi_Q(z, r)|^2 r^{d-1} dr = |c_1|^2 \frac{r_c^{d-\frac{2}{\sigma}}}{d - \frac{2}{\sigma}}, \quad (21.7)$$

where $c_1 = \lim_{\rho \rightarrow \infty} \frac{Q(\rho)}{Q_1(\rho)}$.

Proof This relation was already proved in Lemma 12.5, see (12.12). \square

Lemmas 21.1 and 21.2 show that

1. The Q profile of ψ_Q has an infinite power and a zero Hamiltonian.
2. There is no contradiction between ψ_Q having an infinite power and ψ having a finite power.

In Sect. 12.7 we saw that the Q equation (21.3) admits a countable number of zero-Hamiltonian solutions. We also saw that there is a unique zero-Hamiltonian solution which is monotonically decreasing (the *admissible solution*). Numerical simulations show that the self-similar profile of collapsing peak-type supercritical solutions is monotonically decreasing, and that the blowup solutions ψ_Q^{explicit} with non-monotone, zero-Hamiltonian Q profiles are unstable [35]:¹

Observation 21.1 ([155, 235]) Let $\psi(z, r)$ be a stable singular peak-type solution of the supercritical NLS (21.4). Then ψ undergoes a quasi self-similar collapse with the ψ_Q profile according to (21.5) and (21.6). The Q profile is the unique admissible solution of (21.3), which is obtained for²

$$a = a_Q(\sigma, d), \quad Q(0) = Q_0(\sigma, d). \quad (21.8)$$

In particular, the blowup profile of peak-type solutions of the supercritical NLS is universal (i.e., independent of ψ_0).

21.2 Weak Collapse

In the critical case all singular solutions undergo a strong collapse (Corollary 13.4). This is not true in the supercritical case:

¹ This is similar to the critical case, where the monotone $R^{(0)}$ profile is an attractor for the self-similar profile (Chap. 14), but the non-monotone, excited-state $R^{(n)}$ profiles are unstable (Sect. 10.6.3). It is also “similar” to the explicit singular ring-type solutions ψ_G^{explicit} of the critical NLS, where the single-ring solution is stable but the multi-rings solutions are unstable (Sect. 11.4.1). In that case, the single-ring solution is the “least non-monotone” (single- or multi-) ring profiles.

² See Sect. 12.6.

Corollary 21.1 *Let ψ be as in Lemma 21.1. Then ψ undergoes a weak collapse.*

Proof The proof is the same as that of Lemma 12.5. \square

Therefore, by Corollary 7.6, the variance of these solutions is strictly positive at the singularity.

Not all H^1 singular solutions of the supercritical NLS undergo a weak collapse. Indeed, in Sect. 23.4 we will see that singular shrinking-ring solutions of the supercritical NLS undergo a strong collapse.

21.3 Blowup of L^p Norms

In the critical case, the solution blows up in L^p for $p > 2$ (Corollary 13.6 and Theorem 14.2). The extension of this result to the supercritical case is

Lemma 21.3 *Let ψ be as in Lemma 21.1. Then*

$$\begin{cases} \lim_{z \rightarrow Z_c} \|\psi\|_p^p < \infty, & \text{if } 2 \leq p < \sigma d, \\ \lim_{z \rightarrow Z_c} \|\psi\|_p^p = \infty, & \text{if } p \geq \sigma d. \end{cases}$$

Proof As in Lemma 21.1, an informal proof follows from Eqs. (21.5) and (21.6a) and from Exercise 12.5. \square

21.4 Blowup Rate

Let ψ be a solution of the supercritical NLS that undergoes a quasi self-similar collapse with the ψ_Q profile, where Q is the unique admissible profile. By (21.6b) and (21.8), the blowup rate of $L(z)$ is a square root, i.e.,

$$L(z) \sim \kappa_Q \sqrt{Z_c - z}, \quad z \rightarrow Z_c, \tag{21.9a}$$

where

$$\kappa_Q = \sqrt{2a_Q(\sigma, d)}. \tag{21.9b}$$

Therefore, *the multiplicative constant κ_Q of the blowup rate is universal*. This is different from the ring-type blowup solutions of the critical NLS (which also have a square-root blowup rate), for which the multiplicative constant depends on the initial condition (Sect. 11.3).

We now consider the blowup rate of ψ :

Lemma 21.4 *Let ψ be as in Lemma 21.1, and let Q be the admissible solution of (21.3). Then the blowup rate of ψ is given by*

$$l(z) := \|\nabla\psi\|_2^{-1} \sim \kappa_\psi(\sigma, d) (Z_c - z)^{p_{\min}}, \quad p_{\min} := \frac{1}{2} - \frac{\sigma d - 2}{4\sigma},$$

where $\kappa_\psi = \|\nabla Q\|_2^{-1} \kappa_Q^{p_{\min}}$ and κ_Q is given by (21.9b).

Proof As $z \rightarrow Z_c$,

$$\begin{aligned} \|\nabla\psi\|_2^2 &\sim \frac{1}{\sigma+1} \|\psi\|_{2\sigma+2}^{2\sigma+2} \sim \frac{1}{\sigma+1} \|\psi_Q\|_{2\sigma+2}^{2\sigma+2} \sim \frac{1}{\sigma+1} L^{d-2-\frac{2}{\sigma}} \|Q\|_{2\sigma+2}^{2\sigma+2} \\ &\sim L^{d-2-\frac{2}{\sigma}} \|\nabla Q\|_2^2, \end{aligned}$$

where in the last step we used $H(Q) = 0$. Since $L \sim \kappa_Q \sqrt{Z_c - z}$, the result follows. \square

Thus, the blowup rate of ψ is equal to the rigorous lower bound (13.45) of Cazenave and Weissler.

21.5 Rigorous Results

The rigorous theory for solutions of the supercritical NLS that undergo a peak-type collapse is considerably less developed than for the critical NLS. Recently, Merle, Raphaël, and Szeftel used the “loglog analysis” of Merle and Raphaël for the critical case (Sect. 14.6), to prove existence and stability for solutions that undergo a quasi self-similar collapse with the ψ_Q profile in the slightly-supercritical regime $0 < \sigma d - 2 \ll 1$:

Theorem 21.1 ([184]) *Let $1 \leq d \leq 5$. There exists $\sigma^* > \frac{2}{d}$, such that for any $\sigma \in (\frac{2}{d}, \sigma^*)$, there exists $\delta(\sigma) > 0$ with $\delta(\sigma) \rightarrow 0$ as $\sigma \rightarrow \frac{2}{d}+$, there exists $a_Q(\sigma, d) > 0$ with*

$$\sigma d - 2 = \frac{2\sigma A_R^2}{P_{\text{cr}}^{\text{radial}}} \exp\left(-\frac{\pi}{a_Q(\sigma, d)}(1 + \delta(\sigma))\right),$$

where $A_R = \lim_{r \rightarrow \infty} r^{\frac{d-1}{2}} e^r R^{(0)}(r)$, $P_{\text{cr}}^{\text{radial}} = \int_0^\infty |R^{(0)}|^2 r^{d-1} dr$, and $R^{(0)}$ is the ground state of

$$R''(r) + \frac{d-1}{r} R' - R + |R|^{\frac{4}{d}} R = 0, \quad R'(0) = 0, \quad R(\infty) = 0, \quad (21.10)$$

and an open set $\mathcal{O} \subset H^1$ of initial conditions, such that for any $\psi_0 \in \mathcal{O}$, the corresponding solution of the NLS (21.1) blows up at some Z_c , $0 < Z_c < \infty$, according to the following dynamics:

1. There exist $(L(z), \mathbf{x}_0(z), \zeta(z)) \in \mathbb{R}^+ \times \mathbb{R}^d \times \mathbb{R}$ and $\tilde{Q}, \epsilon(z) \in H^1$, such that for $0 \leq z < Z_c$,

$$\psi(z, \mathbf{x}) = \frac{1}{L^{\frac{1}{\sigma}}(z)} e^{i\zeta(z)} \left[\tilde{Q}(\xi) + \epsilon(z, \xi) \right], \quad \xi = \frac{\mathbf{x} - \mathbf{x}_0(z)}{L(z)},$$

and $\|\nabla \epsilon(z)\|_2 \leq \delta(\sigma)$.

2. The blowup point is finite, i.e., $\lim_{z \rightarrow Z_c} \mathbf{x}_0(z) \in \mathbb{R}^d$.

3. The blowup rate is a square root, i.e.,

$$1 - \delta(\sigma) \leq \frac{L(z)}{\sqrt{2a_Q(\sigma, d)(Z_c - z)}} \leq 1 + \delta(\sigma).$$

Note that the function \tilde{Q} in Theorem 21.1 is not the admissible Q profile, but only a sufficiently good approximation of it. Indeed, Theorem 21.1 says that $\epsilon(z)$ is small, but does not say that it goes to zero at the singularity.

21.6 Simulations

In this section we present numerical simulations, due to Baruch et al. [12], of peak-type blowup solutions of the one-dimensional supercritical NLS

$$i\psi_z(z, x) + \psi_{xx} + |\psi|^{2\sigma}\psi = 0, \quad \sigma > 2. \quad (21.11)$$

The one-dimensional ψ_Q profile is given by

$$\psi_Q(z, x) = \frac{1}{L^{\frac{1}{\sigma}}(z)} Q(\xi) e^{i\zeta(z)}, \quad \xi = \frac{x}{L(z)}, \quad \zeta = \int_0^z \frac{ds}{L^2(s)}, \quad (21.12a)$$

where

$$L(z) = \kappa_Q \sqrt{Z_c - z}, \quad \kappa_Q = \sqrt{2a_Q(\sigma, d = 1)}. \quad (21.12b)$$

The admissible self-similar profile $Q = Q(\xi; \sigma, d = 1)$ is the monotonically decreasing solution of

$$Q''(\xi) - Q + ia \left(\frac{1}{\sigma} Q + \xi Q' \right) + |Q|^{2\sigma} Q = 0, \quad (21.13a)$$

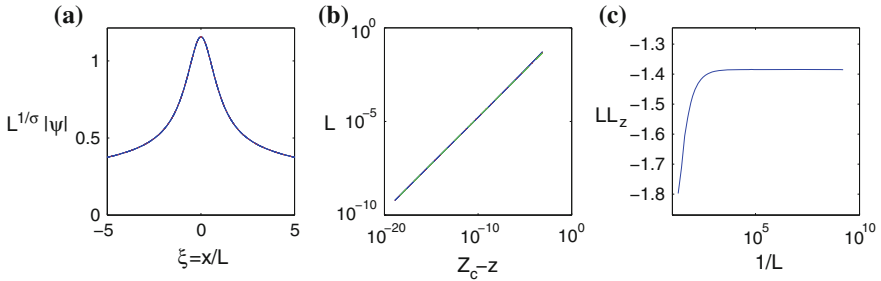


Fig. 21.1 Solution of the supercritical NLS (21.11) with $\sigma = 3$ and $\psi_0 = 2e^{-2x^2}$. **a** The rescaled solution (21.14) at the focusing levels $L^{-1} = 10^4$ (solid) and $L^{-1} = 10^8$ (dashed). The dotted curve is the admissible $Q(\xi; \sigma = 3, d = 1)$. All three curves are indistinguishable. **b** L as a function of $Z_c - z$, on a logarithmic scale. The dotted curve is $L = 1.7(Z_c - z)^{0.5007}$. The two curves are indistinguishable. **c** LL_z as a function of L^{-1} . From [12]

subject to

$$Q'(0) = 0, \quad \lim_{\xi \rightarrow \infty} \xi \left(Q' + \left(\frac{i}{a} + \frac{1}{\sigma} \right) \frac{Q}{\xi} \right) = 0. \quad (21.13b)$$

This solution is obtained for, see Sect. 12.6,

$$a = a_Q(\sigma, d = 1), \quad Q(0) = Q_0(\sigma, d = 1).$$

In Fig. 21.1 we solve (21.11) with $\sigma = 3$ and $\psi_0(x) = 2e^{-2x^2}$. To show that the NLS solution collapses with the ψ_Q profile (21.12), we plot the rescaled solution

$$\psi_{\text{rescaled}}(z, x) = L^{\frac{1}{\sigma}}(z) \left| \psi \left(\frac{x}{L(z)} \right) \right|, \quad L = \left(\frac{\|Q\|_\infty}{\|\psi\|_\infty} \right)^\sigma = \left(\frac{Q_0(\sigma, d = 1)}{\|\psi\|_\infty} \right)^\sigma. \quad (21.14)$$

The rescaled profiles at focusing levels of $1/L = 10^4$ and $1/L = 10^8$ are indistinguishable (Fig. 21.1a), indicating that the solution is indeed self-similar while focusing by 10^4 . Moreover, the rescaled profiles are in perfect fit with the admissible profile $Q(\xi; \sigma = 3, d = 1)$.

Next, we consider the blowup rate of $L(z)$. The power-law fit $L(z) \sim \kappa(Z_c - z)^\rho$ yields $\rho \approx 0.5007$, see Fig. 21.1b, indicating that the blowup rate of L is a square root or slightly faster. To confirm that the blowup rate is a square root, we compute the limit of LL_z , see Lemma 14.1. Since $\lim_{z \rightarrow Z_c} LL_z = -1.384 < 0$, see Fig. 21.1c, the blowup rate is indeed a square root, i.e.,

$$L(z) \sim \kappa \sqrt{Z_c - z}, \quad \kappa \approx \sqrt{2 \cdot 1.384} \approx 1.664. \quad (21.15)$$

Additional support that the blowup rate is a square root is provided by Fig. 21.1a. Indeed, if the blowup rate is faster than a square root, then $a := -\lim_{z \rightarrow z_c} LL_z = 0$. In this case, the Q equation (21.3) reduces to the R equation (21.10), whose solutions decay exponentially. The rescaled profile in Fig. 21.1a, however, has a slow algebraic decay (e.g., it decreases by less than 3 between $\xi = 0$ and $\xi = 5$), which is consistent with Q but inconsistent with R .

The value of κ can be extracted numerically in two independent ways:

1. From the blowup rate of the NLS solution, see (21.15).³
2. From the admissible Q profile. Indeed, by (12.28), $a_Q(\sigma = 3, d = 1) \approx 1.384$ for the admissible profile $Q(\xi; \sigma = 3, d = 1)$. Therefore, by (21.12b),

$$\kappa_Q = \sqrt{2a_Q(\sigma = 3, d = 1)} \approx 1.664. \quad (21.16)$$

The 4-digit agreement between the values of κ in (21.15) and (21.16) provides a strong support to Observation 21.1. This agreement confirms, in particular, that the multiplicative constant κ of the blowup rate is universal.

Finally, we verify that the solution approaches ψ_Q for $r \in [0, r_c]$, i.e., on a fixed domain in the unrescaled transverse variable, as follows. In Fig. 21.2 we plot the solution, rescaled according to (21.14), at the focusing levels $1/L = 10, 10^3$ and 10^5 . The rescaled profiles bifurcate from the Q profile at increasing values of $\xi = x/L$. The “bifurcation positions” (which are marked by circles in Fig. 21.2) are located at $\xi \approx 0.09/L$. Therefore, the region where $\psi \sim \psi_Q$ is roughly $\xi \in \left[0, \frac{0.09}{L(z)}\right]$, which corresponds to $r \in [0, r_c]$ with $r_c \approx 0.09$.

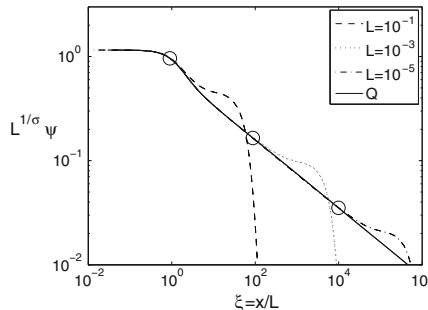


Fig. 21.2 The solution of Fig. 21.1, rescaled according to (21.14), at the focusing levels $L = 10^{-1}$ (dashes), $L = 10^{-3}$ (dots), and $L = 10^{-5}$ (dash-dots). The circles mark the approximate position where each curve bifurcates from the admissible Q profile (solid)

³ The function $L(z)$ can be extracted from the NLS solution ψ using relation (21.14).

21.7 Supercritical Biharmonic NLS (ψ_{Q_B})

Peak-type blowup solutions of the supercritical radial BNLS

$$i\psi_z(z, r) - \Delta^2\psi + |\psi|^{2\sigma}\psi = 0, \quad \psi(0, r) = \psi_0(r) \in H^2, \quad \sigma d > 4,$$

where $\Delta^2 = \left(\frac{\partial^2}{\partial r^2} + \frac{d-1}{r}\frac{\partial}{\partial r}\right)^2$, were studied asymptotically and numerically by Baruch and Fibich [11]. These solutions undergo a quasi self-similar collapse, so that as $z \rightarrow Z_c$,

$$\psi(z, r) \sim \begin{cases} \psi_{Q_B}(z, r), & \text{if } 0 \leq r \leq r_c, \\ \psi_{\text{outer}}(z, r), & \text{if } r \geq r_c, \end{cases} \quad (21.17)$$

where r_c is a number, whose value depends on the initial condition. The asymptotic profile ψ_{Q_B} is given by

$$\psi_{Q_B}(z, r) = \frac{1}{L^{\frac{2}{\sigma}}(z)} Q_B \left(\frac{r}{L(z)} \right) e^{i \int^z \frac{1}{L^4}},$$

where $Q_B(\rho)$ is a zero-Hamiltonian solution of a nonlinear eigenvalue problem

$$-Q_B(\rho) + i\frac{\kappa^4}{4} \left(\frac{2}{\sigma} Q_B + \rho Q'_B \right) - \Delta^2 Q_B + |Q_B|^{2\sigma} Q_B = 0, \quad (21.18a)$$

$$Q'_B(0) = Q''_B(0) = 0. \quad (21.18b)$$

The blowup rate of $L(z)$ is a quartic root, i.e.,

$$L(z) \sim \kappa (Z_c - z)^{\frac{1}{4}}, \quad z \rightarrow Z_c, \quad (21.19)$$

where $\kappa > 0$ is the nonlinear eigenvalue of (21.18). Thus, there is a striking analogy between peak-type blowup solutions of the supercritical NLS and of the supercritical BNLS. See [11] for further details.

Chapter 22

Singular Standing-Ring Solutions (ψ_F)

Previously, we saw that solutions of the critical NLS can collapse with the explicit peak-type profile ψ_R^{explicit} (Chap. 10), the Bourgain-Wang profile ψ_{BW} (Sect. 10.8), the asymptotic peak-type profile $\psi_{R^{(0)}}$ (Chap. 14), the explicit ring-type profile ψ_G^{explicit} (Chap. 11), or the asymptotic ring-type profile ψ_G (Chap. 19). Similarly, solutions of the supercritical NLS can collapse with the explicit peak-type profile ψ_Q^{explicit} (Chap. 12) or the asymptotic peak-type profile ψ_Q (Chap. 21). In two dimensions, these blowup solutions also have vortex analogs (Chaps. 15, 20, and Sect. 23.7.1).

All these singular solutions share the common feature that they collapse at a single point. In Sect. 13.4 we saw that NLS solutions can also collapse at several points. In the critical case, power concentration suggests that the number of collapse points is bounded by P/P_{cr} , see Sect. 13.4.1. Although there is no similar bound in the supercritical case (Sect. 13.6.3), until 2006 it was believed that all singular H^1 solutions of the supercritical NLS collapse at a finite number of points.

In 2006, Raphaël rigorously proved that the two-dimensional quintic NLS ($d = 2$, $\sigma = 2$) admits solutions that collapse on a circle [218]. This breakthrough paper showed, in particular, that the supercritical NLS admits solutions that collapse at an infinite number of points. In 2007, Fibich et al. showed that the quintic NLS admits solutions that collapse on a d -dimensional sphere for any $d > 1$ [74]. In 2010, Baruch et al. [12] showed that the NLS admits solutions that collapse on a d -dimensional sphere for any $d > 1$ and $\sigma \geq 2$. This chapter is devoted to the study of these standing-ring blowup solutions.

22.1 Standing-Ring and Shrinking-Ring Solutions

In this chapter we consider blowup solutions of the radial NLS

$$i\psi_z(z, r) + \psi_{rr} + \frac{d-1}{r}\psi_r + |\psi|^{2\sigma}\psi = 0, \quad d > 1. \quad (22.1)$$

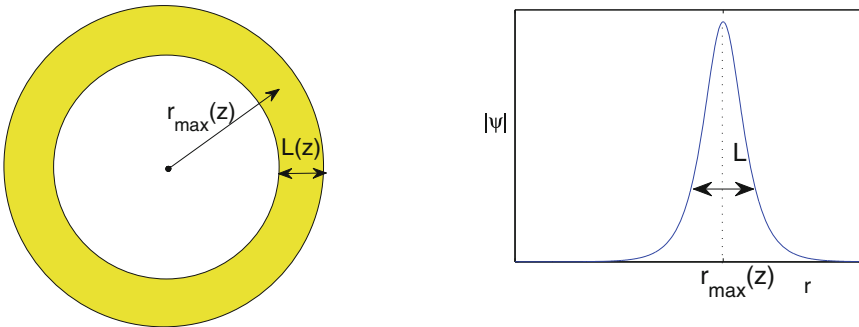


Fig. 22.1 Illustration of ring radius $r_{\max}(z)$ and ring width $L(z)$

Let us denote the location of the maximal amplitude by

$$r_{\max}(z) := \arg \max_r |\psi|. \quad (22.2)$$

Definition 22.1 (ring-type and peak-type blowup solutions) *Let $\psi(z, r)$ be an NLS solution that blows up at Z_c .*

- We say that ψ is a ring-type blowup solution, if $r_{\max}(z) > 0$ for $0 \leq z < Z_c$, and if $|\psi|$ is monotonically increasing in r for $0 \leq r < r_{\max}(z)$ and monotonically decreasing for $r_{\max}(z) < r < \infty$.
- We say that ψ is a peak-type blowup solution, if $r_{\max}(z) \equiv 0$ for $0 \leq z < Z_c$, and if $|\psi|$ is monotonically decreasing in r for $0 \leq r < \infty$.

We distinguish between three types of ring-type blowup solutions:

1. If $\lim_{z \rightarrow Z_c} r_{\max}(z) = 0$, ψ collapses at $r = 0$. Such a solution is called a *shrinking-ring blowup solution*.
2. If $0 < \lim_{z \rightarrow Z_c} r_{\max}(z) < \infty$, ψ collapses on a d -dimensional sphere. Such a solution is called a *standing-ring blowup solution*.
3. If $\lim_{z \rightarrow Z_c} r_{\max}(z) = \infty$, ψ is called a *expanding-ring blowup solution*. Non-existence of such NLS solutions will be discussed in Sect. 23.8.

As we shall see, for all known ring-type blowup solutions of the NLS, the blowup profile is of the self-similar form

$$|\psi_F(t, r)| = \frac{1}{L^{\frac{1}{\sigma}}(z)} |F(\rho)|, \quad \rho = \frac{r - r_{\max}(z)}{L(z)},$$

where $F(\rho)$ is a function that attains its global maximum at $\rho = 0$, and decreases monotonically as $|\rho|$ increases.¹ Therefore, $r_{\max}(z)$ is the ring radius and $L(z)$ is the ring width (Fig. 22.1). Regardless of whether the ring-type blowup solution is shrinking or standing, we always have that $\lim_{z \rightarrow Z_c} L(z) = 0$, i.e., the ring width goes to zero and the ring amplitude goes to infinity at the singularity.

22.2 Preliminary Observations

The following result, due to Baruch, Fibich, and Gavish, shows that a standing-ring collapse can only occur for $\sigma \geq 2$:

Lemma 22.1 ([12]) *Let $\psi(z, r)$ be a standing-ring blowup solution of the NLS (22.1), such that $\psi \sim \psi_F$ for $|r - r_{\max}(z)| \leq \rho_c L(z)$, where $\rho_c = O(1)$ is a constant,*

$$|\psi_F(z, r)| = \frac{1}{L^{\frac{1}{\sigma}}(z)} |F(\rho)|, \quad \rho = \frac{r - r_{\max}(z)}{L(z)}, \quad (22.3a)$$

$$r_{\max}(z) = \arg \max_r |\psi|, \quad (22.3b)$$

$F(\rho)$ attains its global maximum at $\rho = 0$,

$$\lim_{z \rightarrow Z_c} L(z) = 0, \quad (22.3c)$$

and

$$0 < \lim_{z \rightarrow Z_c} r_{\max}(z) < \infty. \quad (22.3d)$$

Then $\sigma \geq 2$.

Proof The power of the collapsing core ψ_F is

$$\begin{aligned} \|\psi_F\|_{L^2(|r - r_{\max}| \leq \rho_c L(z))}^2 &= L^{-\frac{2}{\sigma}}(z) \int_{r_{\max} - \rho_c L(z)}^{r_{\max} + \rho_c L(z)} \left| F\left(\frac{r - r_{\max}}{L}\right) \right|^2 r^{d-1} dr \\ &= L^{-\frac{2}{\sigma}}(z) \int_{-\rho_c}^{\rho_c} |F(\rho)|^2 (L\rho + r_{\max})^{d-1} L d\rho \\ &\sim L^{1-\frac{2}{\sigma}}(z) r_{\max}^{d-1}(Z_c) \int_{-\rho_c}^{\rho_c} |F(\rho)|^2 d\rho. \end{aligned}$$

¹ The variable ρ measures the distance from the ring peak in units of $L(z)$. Therefore, ρ is negative for $0 \leq r < r_{\max}$ and positive for $r_{\max} < r < \infty$.

Since $\|\psi_F\|_{L^2(|r-r_{\max}| \leq \rho_c L(z))}^2 \leq \|\psi\|_2^2 = \|\psi_0\|_2^2 < \infty$, $L^{1-\frac{2}{\sigma}}$ has to remain bounded as $L \rightarrow 0$. Hence, $\sigma \geq 2$. \square

By (22.3), in the ring region, i.e., for $|r - r_{\max}| \leq \rho_c L(z)$,

$$[\psi_{rr}] \sim \frac{[\psi]}{L^2(z)}, \quad \left[\frac{\psi_r}{r} \right] \sim \frac{1}{r_{\max}(Z_c)} \frac{[\psi]}{L(z)}.$$

Therefore,

$$\frac{d-1}{r} \psi_r \ll \psi_{rr}, \quad z \rightarrow Z_c.$$

Hence, to leading order, (22.1) reduces to the one-dimensional NLS²

$$i\phi_z(z, x) + \phi_{xx} + |\phi|^{2\sigma} \phi = 0. \quad (22.4)$$

This shows that

$$\psi(z, r) \sim \phi(z, x = r - r_{\max}(z)), \quad (22.5)$$

where $\phi(z, x)$ is a peak-type solution of the one-dimensional NLS (22.4) that collapses at $x = 0$. In particular,

$$\psi_F(z, r) = \phi_{1D}^{\text{peak}}(z, x = r - r_{\max}(z)), \quad (22.6)$$

where $\phi_{1D}^{\text{peak}}(z, x)$ is the blowup profile of peak-type solutions of the one-dimensional NLS (22.4) that collapse at $x = 0$. These informal arguments lead to

Proposition 22.1 ([12]) *Under the conditions of Lemma 22.1, the blowup profile ψ_F and blowup rate $L(z)$ of standing-ring blowup solutions of the d-dimensional NLS (22.1) are the same as those of peak-type solutions of the one-dimensional NLS (22.4).*

Remark Since the one-dimensional NLS (22.4) admits blowup solutions only if $\sigma \geq 2$, we recover the result of Lemma 22.1.

The one-dimensional NLS (22.4) is critical when $\sigma = 2$ and supercritical when $\sigma > 2$. In what follows, we consider “critical standing rings” ($\sigma = 2$) in Sect. 22.3, and “supercritical standing-rings” ($\sigma > 2$) in Sect. 22.4.

Exercise 22.1 Let $|\psi_F|$ be given by (22.3). Show that

$$\|\psi_F\|_{2\sigma+2}^{2\sigma+2} \sim L^{-1-\frac{2}{\sigma}}(z) r_{\max}^{d-1}(Z_c) \int_{-\infty}^{\infty} |F(\rho)|^{2\sigma+2} d\rho.$$

² For clarity, in this chapter we denote the solutions of the one-dimensional NLS by ϕ .

Conclude that the relation between the blowup rates of ψ and $L(z)$ is

$$l(z) \sim c_l L^{\frac{1}{2} + \frac{1}{\sigma}}(z), \quad z \rightarrow Z_c. \quad (22.7)$$

22.2.1 Standing-Ring Solutions of the BNLS and Other Nonlinear PDEs

In [12], Baruch et al. noted that the informal analysis of Sect. 22.2 can be applied to other nonlinear PDEs, such as the *biharmonic NLS*, the *nonlinear heat equation*, and the *nonlinear biharmonic heat equation*. For example, we have

Lemma 22.2 ([12]) *Let ψ be a standing-ring blowup solution of the radial biharmonic NLS*

$$i\psi_z(z, r) - \Delta^2\psi + |\psi|^{2\sigma}\psi = 0, \quad (22.8)$$

such that $\psi \sim \psi_{F_B}(z, r)$ for $|r - r_{\max}(z)| \leq \rho_c L(z)$, where

$$|\psi_{F_B}(z, r)| = \frac{1}{L^{\frac{1}{2\sigma}}(z)} |F_B(\rho)|, \quad \rho = \frac{r - r_{\max}(z)}{L(z)},$$

$\rho_c = O(1)$ is a constant, $F_B(\rho)$ attains its global maximum at $\rho = 0$, $\lim_{z \rightarrow Z_c} L(z) = 0$, and $0 < \lim_{z \rightarrow Z_c} r_{\max}(z) < \infty$. Then

1. $\sigma \geq 4$.
2. $\psi_{F_B}(z, r) = \phi_{B,1D}^{\text{peak}}(z, x = r - r_{\max}(z))$, where $\phi_{B,1D}^{\text{peak}}(z, x)$ is the blowup profile of peak-type solutions of the one-dimensional BNLS

$$i\phi_z(z, x) - \phi_{xxxx} + |\phi|^{2\sigma}\phi = 0 \quad (22.9)$$

that collapse at $x = 0$.

3. *The blowup profile ψ_{F_B} and the blowup rate of $L(z)$ of collapsing standing-ring solutions of the BNLS (22.8) are the same as those of collapsing peak-type solutions of the one-dimensional BNLS (22.9).*

Exercise 22.2 Prove Lemma 22.2.

Remark Peak-type blowup solutions of the critical and supercritical BNLS are considered in Sects. 14.7 and 21.7, respectively.

22.3 “Critical” Standing Rings ($\sigma = 2$)

In this section we study standing-ring blowup solutions of the supercritical radial quintic NLS

$$i\psi_z(z, r) + \psi_{rr} + \frac{d-1}{r}\psi_r + |\psi|^4\psi = 0, \quad d > 1. \quad (22.10)$$

22.3.1 Informal Analysis

By Proposition 22.1, standing-ring blowup solutions of (22.10) have the same blowup profile and blowup rate as peak-type blowup solutions of the one-dimensional critical NLS

$$i\phi_z(z, x) + \phi_{xx} + |\phi|^4\phi = 0. \quad (22.11)$$

In Chap. 14 we saw that peak-type solutions of (22.11) collapse at the loglog law blowup rate with the one-dimensional $\psi_{R^{(0)}}$ profile, which we shall denote here by $\phi_{R_{1D}}$,³ where

$$\phi_{R_{1D}}(z, x) = \frac{1}{L^{\frac{1}{2}}(z)} R_{1D}(\xi) e^{i\xi(z) + i\frac{L_z}{4L}x^2}, \quad \xi = \frac{x}{L},$$

and

$$R_{1D}(\xi) = 3^{\frac{1}{4}} \operatorname{sech}^{\frac{1}{2}}(2\xi) \quad (22.12)$$

is the unique one-dimensional critical solitary wave (Lemma 6.15). In addition, the relation between the blowup rates of ψ and $L(z)$ is given by (22.7). Therefore, we have the following result, due to Fibich, Gavish, and Wang:

Lemma 22.3 ([74]) *Let ψ be a standing-ring blowup solution of the quintic NLS (22.10). Then*

1. *ψ approaches the standing-ring ψ_F profile in the ring region, i.e., $\psi \sim \psi_F$ for $r - r_{\max} = O(L(z))$, where*

$$\psi_F(z, r) = \phi_{R_{1D}}(z, r - r_{\max}(z)) \quad (22.13a)$$

$$= \frac{1}{L^{\frac{1}{2}}(z)} R_{1D}(\rho) e^{i\xi(z) + i\frac{L_z}{4L}(r - r_{\max}(z))^2},$$

R_{1D} is given by (22.12),

$$\rho = \frac{r - r_{\max}(z)}{L(z)}, \quad \xi(z) = \int_0^z \frac{ds}{L^2(s)}, \quad (22.13b)$$

$$\lim_{z \rightarrow Z_c} L(z) = 0, \text{ and } 0 < \lim_{z \rightarrow Z_c} r_{\max}(z) < \infty.$$

³ We drop the $^{(0)}$ superscript, because in one dimension there is a unique solitary wave.

2. The blowup rates of $L(z)$ and ψ are given by the loglog law, i.e.,

$$L(z) \sim \left(\frac{2\pi(Z_c - z)}{\log \log \frac{1}{Z_c - z}} \right)^{\frac{1}{2}}, \quad l(z) \sim c_l L(z), \quad z \rightarrow Z_c. \quad (22.14)$$

Remark The quadratic phase term $e^{i \frac{L_z}{4L} (r - r_{\max}(z))^2}$ accounts for focusing towards the ring peak at $r = r_{\max}(z)$, i.e., for the narrowing of the ring width $L(z)$.

22.3.2 Rigorous Results

In 2006, Raphaël proved existence and stability of standing-ring blowup solutions for the quintic two-dimensional radial NLS

$$i\psi_z(z, r) + \psi_{rr} + \frac{1}{r}\psi_r + |\psi|^4\psi = 0, \quad \psi(0, r) = \psi_0(r). \quad (22.15)$$

This result was extended to $d \geq 3$ by Raphaël and Szeftel in 2009.

Theorem 22.1 ([218, 219]) *There exists an open set of initial conditions $\mathcal{O} \subset H_{\text{radial}}^1(\mathbb{R}^2)$ if $d = 2$, and $\mathcal{O} \subset H_{\text{rad}}^d(\mathbb{R}^d)$ if $d \geq 3$, such that the following holds. Let $\psi_0 \in \mathcal{O}$. Then the corresponding solution of the quintic NLS (22.10) blows up at Z_c , where $0 < Z_c < \infty$, according to the following dynamics:*

1. *There exist $L(z) > 0$, $r_{\max}(z) > 0$, and $\zeta(z) \in \mathbb{R}$, such that*

$$\psi(z, r) - \frac{1}{L^{\frac{1}{2}}(z)} R_{1D}(\rho) e^{i\zeta(z)} \xrightarrow{L^2} u(r), \quad z \rightarrow Z_c, \quad (22.16)$$

where R_{1D} and ρ are given by (22.12) and (22.13b), respectively.

2. *The radius of the singular circle converges to a positive constant, i.e., $0 < \lim_{z \rightarrow Z_c} r_{\max}(z) < \infty$.*
3. *The blowup rate of $L(z)$ is given by the loglog law (22.14).*

Theorem 22.1 is the rigorous version of Lemma 22.3. Note, however, that according to Theorem 22.1, the asymptotic profile of the collapsing core is $\frac{1}{L^{\frac{1}{2}}(z)} R_{1D}(\rho) e^{i\zeta(z)}$. By Lemma 22.3, however, the asymptotic profile also has the quadratic phase term $e^{i \frac{L_z}{4L} (r - r_{\max}(z))^2}$. To confirm the agreement of these two asymptotic profiles, we first note that $\rho = O(1)$ in the ring region. In addition, since $L(z)$ is given by the loglog law, $\lim_{z \rightarrow Z_c} LL_z = 0$, see (14.14). Therefore, as $z \rightarrow Z_c$,

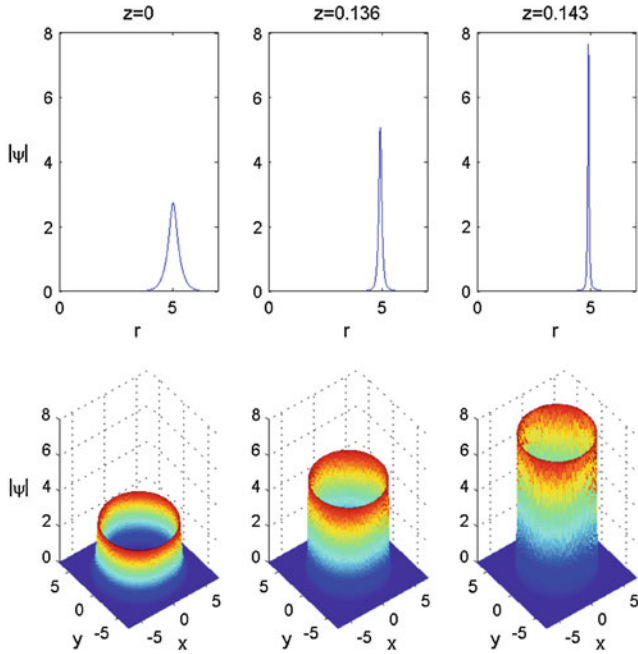


Fig. 22.2 Solution of (22.15) with $\psi_0 = R_{1D}(r - 5)$. From [74]

$$\frac{L_z}{4L} (r - r_{\max}(z))^2 = \frac{LL_z}{4} \rho^2 \rightarrow 0.$$

Remark The quadratic phase term $e^{i \frac{L_z}{4L} (r - r_{\max}(z))^2}$ will play a key role in the analysis of shrinking-ring solutions in Chap. 23.

22.3.3 Simulations

Standing-ring Collapse

In [74] Fibich et al. solved the two-dimensional quintic radial NLS (22.15) with the ring-type initial condition⁴

$$\psi_0 = R_{1D}(r - 5) = \sqrt[4]{3} \sqrt{\operatorname{sech}(2(r - 5))}. \quad (22.17)$$

Figure 22.2 shows the early stage of the dynamics. As ψ self-focuses by ≈ 3 , the ring amplitude increases, the ring width decreases, and the ring radius converges

⁴ The dimension d does not have to be an integer. See [74, Sect. 6.2] for a numerical study of standing-ring blowup solutions of the quintic NLS with $d = 3/2$.

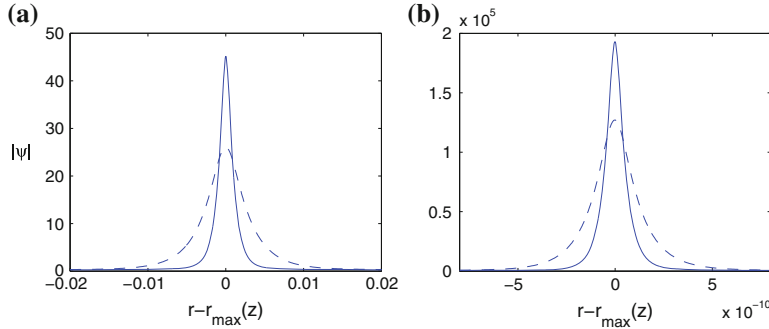


Fig. 22.3 The solution of Fig. 22.2 at several focusing levels. **a** $L^{-1} = 390$ (dashes) and $L^{-1} = 1,174$ (solid). **b** $L^{-1} = 9.3 \cdot 10^9$ (dashes) and $L^{-1} = 2.1 \cdot 10^{10}$ (solid). From [74]

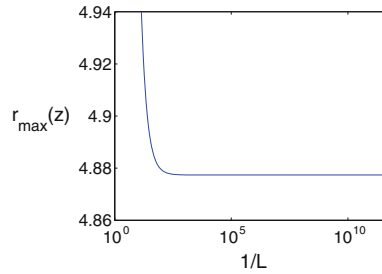


Fig. 22.4 Ring radius as a function of the focusing level, for the solution of Fig. 22.2. From [74]

to a positive constant ($r_{\max}(z) \approx 5$). These characteristics persist as ψ collapses over 10 orders of magnitude, see Fig. 22.3. Figure 22.4 shows the ring radius $r_{\max}(z)$ as a function of the focusing level $L^{-1} = \frac{\max_r |\psi|^2}{\max_r |\psi_0|^2}$, see (22.19b). Since $\lim_{L \rightarrow 0} r_{\max}(z) \approx 4.88 > 0$, the ring is indeed standing and not shrinking.

Quasi Self-similar Collapse

To confirm that the singular part of the solution is of the self-similar form

$$|\psi| \sim \frac{1}{L^{\frac{1}{2}}(z)} R_{1D} \left(\frac{r - r_{\max}(z)}{L(z)} \right), \quad (22.18)$$

see (22.13), we rescale the solution as

$$\psi_{\text{rescaled}}(z, r) := L^{\frac{1}{2}}(z) \psi(z, \rho), \quad (22.19a)$$

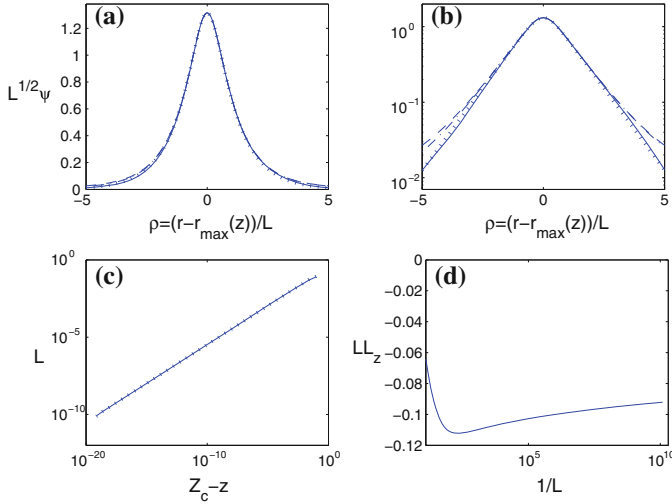


Fig. 22.5 The solution of Fig. 22.2. **a** Solution rescaled according to (22.19), at the focusing levels $L^{-1} = 5$ (solid), $L^{-1} = 3.6 \cdot 10^5$ (dashes), and $L^{-1} = 1.35 \cdot 10^{10}$ (dash-dot). The dotted curve is $R_{1D} = \sqrt[4]{3} \sqrt{\operatorname{sech}(2\rho)}$. The four curves are nearly indistinguishable. **b** Same data on a semi-logarithmic scale. **c** L as a function of $Z_c - z$ (solid). The dotted curve is $0.34 \cdot (Z_c - z)^{0.5001}$. **d** LL_z as a function of the focusing level L^{-1} . From [74]

where

$$\rho = \frac{r - r_{\max}(z)}{L}, \quad L = \frac{\max_r |\psi_0|^2}{\max_r |\psi|^2}, \quad r_{\max}(z) = \arg \max_r |\psi|. \quad (22.19b)$$

Figure 22.5a shows the rescaled profile at the focusing levels $L^{-1} = 5$, $L^{-1} = 3.6 \cdot 10^5$, and $L^{-1} = 1.35 \cdot 10^{10}$. The three profiles are indistinguishable from each other and from R_{1D} , showing that the solution maintains the self-similar profile (22.13) while focusing over 10 orders of magnitude. Plotting the same data on a semi-logarithmic scale (Fig. 22.5b) shows that the rescaled profiles are self-similar in the ring region $\rho = O(1)$ [i.e., $r - r_{\max}(z) = O(L)$], but not near the beam center ($\rho \ll 1$ or $r_{\max} - r \gg L$) or far outside ($\rho \gg 1$ or $r - r_{\max} \gg L$). Hence, as with the critical peak-type solutions (Sects. 13.2.2 and 17.3), “critical” standing-ring solutions are “only” quasi self-similar.

Blowup Rate

To determine numerically the blowup rate of standing-ring solutions, we first perform the power-law fit $L(z) \sim \kappa(Z_c - z)^p$.⁵ This yields $p \approx 0.5001$, see Fig. 22.5c,

⁵ See Sect. 14.2.1.

indicating that the blowup rate is close to a square root. To check whether L is slightly faster than a square root, we compute the limit of LL_z , see Lemma 14.1. It is not clear from Fig. 22.5d, however, whether LL_z goes to zero or to a negative constant. In this case, however, we *know* from Theorem 22.1 that LL_z goes to zero. The slow decrease to zero of LL_z is a consequence of the loglog law, see (14.15).

Radial Stability

To test for radial stability of standing-ring solutions, we randomly perturb the initial ring profile (22.17) from Fig. 22.2 as

$$\psi_0^{\text{noise}}(r) = (1 + \epsilon_1(r))R_{1D}(r - 5) + \epsilon_2(r), \quad (22.20)$$

where $\epsilon_1(r)$ and $\epsilon_2(r)$ are uniformly distributed in $[-0.3, 0.3]$ and $[-0.1, 0.1]$, respectively (Fig. 22.6a). After focusing by ≈ 1.2 , the noise in the ring region (i.e., the area of high nonlinearity) disappears (Fig. 22.6b). Subsequently, the noise at the inner and outer regions also decreases, so that after focusing by ≈ 6 , the solution approaches a clean standing-ring profile (Fig. 22.6c). Therefore, we conclude that the standing-ring profile $\psi_F(z, r) = \phi_{R_{1D}}(z, r - r_{\max}(z))$, see (22.13), is a strong attractor under radial perturbations.

Of course, we know from Theorem 22.1 that standing-ring blowup solutions are stable under sufficiently small radial perturbations. Theorem 22.1, however, does not indicate the size of the basin of attraction. Figure 22.6 suggests that the basin of attraction of standing-ring solutions is of a significant size.

Remark Standing-ring solutions are unstable under azimuthal perturbations (Sect. 22.6).

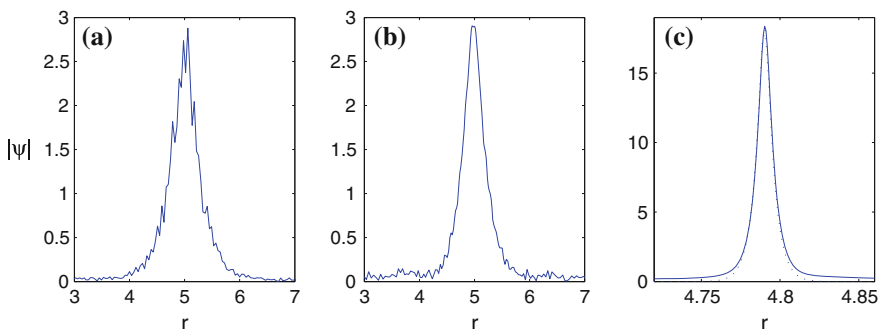


Fig. 22.6 Solution of the quintic 2D NLS (22.15) with the noisy initial condition (22.20). **a** $z = 0$, $L^{-1} = 1.5$, **b** $z = 0.066$, $L^{-1} = 1.7$, **c** $z = 0.195$, $L^{-1} = 10.6$ (solid). The dotted curve is a fitted $\phi_{R_{1D}}$ profile. From [74]

22.4 “Supercritical” Standing Rings ($\sigma > 2$)

In this section we study standing-ring blowup solutions of the radial *super-quintic* NLS (22.1) with $d > 1$ and $\sigma > 2$.

22.4.1 Informal Analysis

By Proposition 22.1, standing-ring blowup solutions of the radial NLS (22.1) with $d > 1$ and $\sigma > 2$ have the same blowup profile and blowup rate as peak-type blowup solutions of the supercritical one-dimensional NLS

$$i\phi_z(z, x) + \phi_{xx} + |\phi|^{2\sigma}\phi = 0, \quad \sigma > 2. \quad (22.21)$$

In Chap. 21 we saw that peak-type solutions of (22.21) collapse at a square-root blowup rate with the one-dimensional ψ_Q profile, which we shall denote here by $\phi_{Q_{1D}}$, where

$$\phi_{Q_{1D}}(z, x) = \frac{1}{L^{\frac{1}{\sigma}}(z)} Q_{1D}(\xi) e^{i\xi(z)}, \quad \xi = \frac{x}{L(z)},$$

and $Q_{1D}(\xi) := Q(\xi; d = 1)$ is the admissible solution of the one-dimensional Q equation.⁶ Finally, the relation between the blowup rate of ψ and $L(z)$ is given by (22.7). Therefore, we have the following result, due to Baruch, Fibich, and Gavish:

Lemma 22.4 ([12]) *Let ψ be a standing-ring blowup solution of the supercritical NLS (22.1) with $d > 1$ and $\sigma > 2$. Then*

1. *The solution approaches the standing-ring ψ_F profile in the ring region, i.e., $\psi \sim \psi_F$ for $r - r_{\max} = O(L)$, where*

$$\psi_F(z, r) = \phi_{Q_{1D}}(z, x = r - r_{\max}(z)) = \frac{1}{L^{\frac{1}{\sigma}}(z)} Q_{1D}(\rho) e^{i\xi(z)}, \quad (22.22a)$$

$$\rho = \frac{r - r_{\max}(z)}{L(z)}, \quad \xi = \int_0^z \frac{ds}{L^2(s)}, \quad (22.22b)$$

$\lim_{z \rightarrow Z_c} L(z) = 0$, $0 < \lim_{z \rightarrow Z_c} r_{\max}(z) < \infty$, and Q_{1D} is the admissible solution of

⁶ See Sect. 12.6 for definition of admissible solutions, and Sect. 12.6.2 for one-dimensional admissible solutions.

$$Q''(x) - Q + ia \left(\frac{1}{\sigma} Q + x Q_x \right) + |Q|^{2\sigma} Q = 0, \quad Q'(0) = 0,$$

with

$$a = a_Q(\sigma, d = 1), \quad Q(0) = Q_0(\sigma, d = 1). \quad (22.23)$$

2. The blowup rate of $L(z)$ is a square root, i.e.,

$$L(z) \sim \kappa_{\text{standing}}(\sigma) \sqrt{Z_c - z}, \quad z \rightarrow Z_c, \quad (22.24a)$$

where

$$\kappa_{\text{standing}}(\sigma) = \sqrt{2a_Q(\sigma, d = 1)}. \quad (22.24b)$$

3. The blowup rate of ψ is

$$l(z) \sim c_l(Z_c - z)^{\frac{1}{4} + \frac{1}{2\sigma}}, \quad z \rightarrow Z_c.$$

The constant κ_{standing} in the blowup rate of standing-ring solutions, see (22.24), is equal to the constant $\kappa(\sigma, d = 1)$ in the blowup rate of one-dimensional peak-type solutions, see (21.9), since both are given by $\sqrt{2a_Q(\sigma, d = 1)}$, where $a_Q(\sigma, d = 1)$ is the nonlinear eigenvalue that corresponds to the admissible one-dimensional profile $Q(\xi; \sigma, d = 1)$.

Corollary 22.1 *The constant κ_{standing} is universal, (i.e., independent of ψ_0). Furthermore, κ_{standing} is also independent of the dimension d .*

Obviously, κ_{standing} depends on the nonlinearity exponent σ .

22.4.2 Simulations

In [12], Baruch et al. solved the NLS (22.1) with $d = 2$, $\sigma = 3$, and the ring-type initial condition $\psi_0 = 2e^{-2(r-5)^2}$. Figure 22.7 shows the ring radius as the solution self-focuses by 10^{10} . Since $\lim_{z \rightarrow Z_c} r_{\max}(z) \approx 5.001 > 0$, the ring is indeed standing. To show that initial conditions which are not ring-shaped can also undergo a standing-ring collapse, we solve (22.1) with $\psi_0(r) = 2e^{-r^4}$, and observe that the solution evolves into a ring (Fig. 22.8a-d).⁷ Since $\lim_{z \rightarrow Z_c} r_{\max}(z) \approx 0.33$ (Fig. 22.8e), the solution undergoes a standing-ring collapse. Since $\lim_{z \rightarrow Z_c} LL_z = -1.384 < 0$ (Fig. 22.8f), $L(z)$ has the predicted square-root blowup rate

$$L(z) \sim \kappa_{\text{standing}} \sqrt{Z_c - z}, \quad \kappa_{\text{standing}} \approx \sqrt{2 \cdot 1.384} = 1.664.$$

⁷ In Chap. 26 we use the *NGO method* to explain why strongly nonlinear super-Gaussian initial conditions evolve into a ring profile.

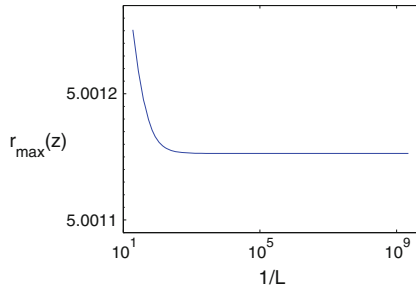


Fig. 22.7 Ring radius as a function of the focusing level, for the solution of the NLS (22.1) with $d = 2$, $\sigma = 3$, and $\psi_0 = 2e^{-2(r-5)^2}$. From [12]

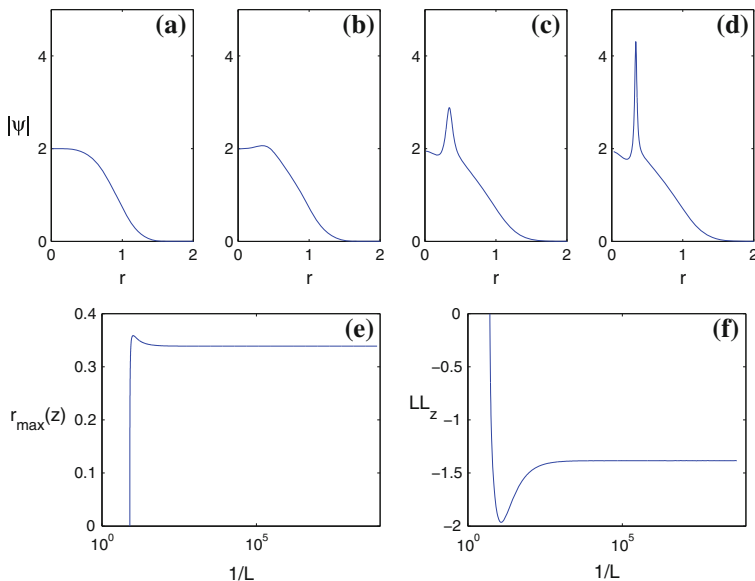


Fig. 22.8 Solution of the NLS (22.1) with $d = 2$, $\sigma = 3$, and $\psi_0 = 2e^{-r^4}$. **a** $z = 0$. **b** $z = 0.01$. **c** $z = 0.019$. **d** $z = 0.02$. **e** Ring radius as a function of $1/L$. **f** LL_z as a function of $1/L$. From [12]

22.5 Singular Standing Vortex Solutions

In Chap. 15 we saw that the two-dimensional NLS

$$i\psi_z(z, x, y) + \Delta\psi + |\psi|^{2\sigma}\psi = 0, \quad \psi(0, x, y) = \psi_0(x, y) \quad (22.25)$$

admits vortex blowup solutions of the form $\psi(z, r, \theta) = A(z, r)e^{im\theta}$. As in the vortex-free case, Eq. (22.25) admits standing vortex blowup solutions for $\sigma \geq 2$. For further details, see [72, Sect. 5.3.1.2] for the case $\sigma = 2$, and [12, Sect. 5] for the case $\sigma > 2$.

22.6 Azimuthal Instability

We now show that standing-ring blowup solutions of the NLS are radially-stable but azimuthally-unstable. In the quintic case, Theorem 22.1 shows that these solutions are stable under sufficiently small radial perturbations. In addition, the simulations in Sects. 22.3.3 and 22.4.2 show that standing-ring collapse occurs for large classes of radial initial conditions. To show that standing-ring collapse is unstable under non-radial perturbations, we consider the two-dimensional NLS

$$i\psi_z(z, r, \theta) + \psi_{rr} + \frac{1}{r}\psi_r + \frac{1}{r^2}\psi_{\theta\theta} + |\psi|^{2\sigma}\psi = 0 \quad (22.26)$$

with

$$\psi_0^{(\epsilon)}(r, \theta) = \psi_0(r)(1 + \epsilon h(\theta)),$$

where ψ_0 is such that when $\epsilon = 0$, the (radial) solution blows up with the standing-ring profile ψ_F . By continuity, when $0 < \epsilon \ll 1$, the solution initially evolves into a slightly-nonradial standing ring. Since NLS solutions are attracted towards higher-intensity regions, the local-maxima bumps along the ring will attract power from their surroundings, thereby further enhancing the breakup of radial symmetry.

To observe this instability process numerically, we solve (22.26) with $\sigma = 3$ and

$$\psi_0(r, \theta) = 2e^{-2(r-5)^2} \left[1 + 0.01e^{-100\theta^2} \right], \quad (22.27)$$

which is the standing-ring initial condition from Fig. 22.7 with a 1% bump at $\theta = 0$, see Fig. 22.9a. As predicted, as the solution evolves, the bump attracts power from its surroundings (Fig. 22.9b, c), thereby enhancing the breakup of radial symmetry.

We can also break radial symmetry by adding a small astigmatism to the input beam. For example, in Fig. 22.10 we solve the NLS

$$i\psi_z(z, x, y) + \Delta\psi + |\psi|^4\psi = 0 \quad (22.28a)$$

with

$$\psi_0^{\text{elliptic}}(x, y) = R_{1D} \left(\sqrt{1.02x^2 + y^2} - 5 \right), \quad (22.28b)$$

which is the slightly-elliptic version of (22.17). After mild focusing (≈ 1.5), the ring breaks into two filaments that are located at the intersection of the ring with the x -axis.⁸ Therefore, standing-ring blowup solutions are unstable under elliptic perturbations.

⁸ This filamentation pattern is typical for elliptic input beams, see Lemma 25.1.

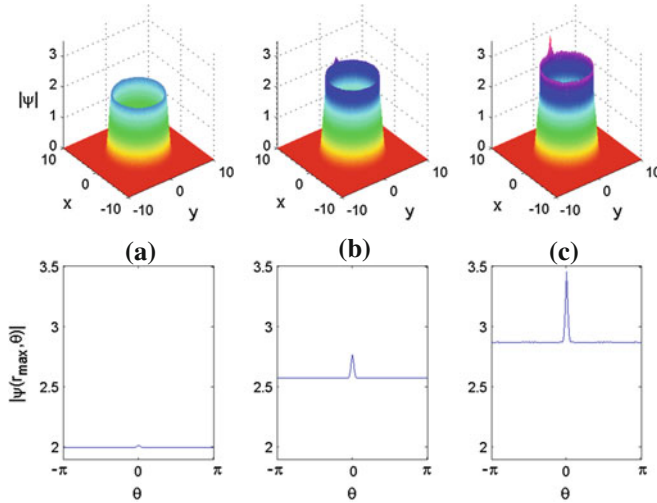


Fig. 22.9 Solution of (22.26) with $\sigma = 3$ and the initial condition (22.27). **a** $z = 0$. **b** $z = 0.0140$, **c** $z = 0.0147$. Top Surface plot. Bottom Amplitude along the ring peak $|\psi(z, r_{\max}(z), \theta)|$ as function of θ . From [12]

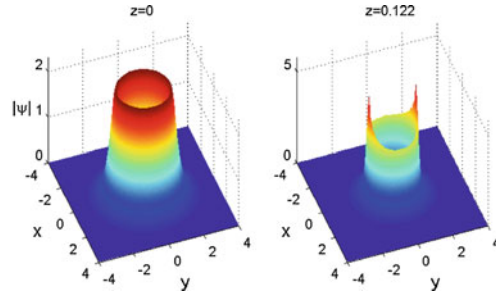


Fig. 22.10 Solution of the NLS (22.28a) with the slightly-elliptic initial condition (22.28b). From [74]

22.7 Mixed Standing-Ring/Peak-Type Solutions

We briefly note that the d -dimensional NLS

$$i\psi_z(z, \mathbf{x}) + \Delta\psi + |\psi|^{2\sigma}\psi = 0, \quad \mathbf{x} \in \mathbb{R}^d \quad (22.29)$$

admits blowup solutions that are a standing ring in k dimensions and peak-type in the other $d - k$ dimensions, where $1 < k < d$. Without loss of generality, these solutions blowup on the k -dimensional sphere

$$S_{r_{\max}}^k = \left\{ x_1^2 + \cdots + x_k^2 \equiv r_{\max}^2 > 0, \quad x_{k+1} = \cdots = x_d = 0 \right\}.$$

To apply the informal analysis of Sect. 22.2, we rewrite (22.29) as

$$i\psi_z(z, r, x_{k+1}, \dots, x_d) + \psi_{rr} + \frac{k-1}{r}\psi_r + \sum_{j=k+1}^d \psi_{x_j x_j} + |\psi|^{2\sigma}\psi = 0,$$

where $r = \sqrt{x_1^2 + \cdots + x_k^2}$. If ψ undergoes a mixed standing-ring/peak-type collapse on $S_{r_{\max}}^k$, the equation for ψ can be approximated by

$$i\psi_z(z, \mathbf{y}) + \Delta_{\mathbf{y}}\psi + |\psi|^{2\sigma} = 0,$$

where $\mathbf{y} = (r, x_{k+1}, \dots, x_d) \in \mathbb{R}^{d-k+1}$ and $\Delta_{\mathbf{y}}\psi = \psi_{rr} + \sum_{j=k+1}^d \psi_{x_j x_j}$. Therefore, a mixed standing-ring/peak-type collapse:

1. Is possible if $\sigma(d - k + 1) \geq 2$.
2. Is equivalent to a one-dimensional critical collapse if $\sigma(d - k + 1) = 2$, and to a one-dimensional supercritical collapse if $\sigma(d - k + 1) > 2$.

For example, consider the three-dimensional NLS

$$i\psi_z(z, r, t) + \Delta\psi + |\psi|^2\psi = 0, \quad \Delta = \frac{\partial^2}{\partial r^2} + \frac{1}{r}\frac{\partial}{\partial r} + \frac{\partial^2}{\partial t^2},$$

which models the propagation of laser pulses in the anomalous regime (Conclusion 36.1). This equation admits blowup solutions which are a standing ring in the radial coordinate and peak-type in the temporal coordinate. The collapse dynamics of these solutions is given, to leading order, by the critical two-dimensional NLS

$$i\psi_z(z, r, t) + \left(\frac{\partial^2}{\partial r^2} + \frac{\partial^2}{\partial t^2} \right) \psi + |\psi|^2\psi = 0.$$

Therefore, near the singularity,

$$\begin{aligned} \psi(z, r, t) &\sim \psi_{R^{(0)}} \left(z, \sqrt{(r - r_{\max})^2 + t^2} \right) \\ &= \frac{1}{L(z)} R^{(0)} \left(\frac{\sqrt{(r - r_{\max}(z))^2 + t^2}}{L(z)} \right) e^{i\xi(z) + i\frac{L_z}{L} \frac{(r - r_{\max}(z))^2 + t^2}{4}}, \end{aligned}$$

where $R^{(0)}$ is the two-dimensional Townes profile, and $L(z)$ goes to zero at the loglog blowup rate. A rigorous proof of existence and stability of these solutions was given by Zwiers [287] and by Holmer and Roudenko [129]. Moreover, in Sect. 37.4 we will use the *NGO method* to show that this mixed-type blowup solution is an attractor for strongly-nonlinear initial conditions which are super-Gaussian in r and Gaussian in t , i.e.,

$$\psi_0 = c e^{-r^{2m}} e^{-t^2}, \quad m > 1, \quad c \gg 1.$$

Chapter 23

Singular Shrinking-Ring Solutions (ψ_S)

In Chap. 19 we saw that the critical NLS ($\sigma = 2/d$) with $d > 1$ admits shrinking-ring solutions that collapse with the ψ_G profile at a point. Then in Chap. 22 we saw that the supercritical NLS with a quintic nonlinearity ($\sigma = 2$) and $d > 1$ admits standing-ring solutions that collapse with the ψ_F profile on a sphere. In this chapter we follow Fibich et al. [74], and show that these two seemingly-unrelated ring-type solutions belong to the boundary of a two-parameter family of shrinking-ring solutions of the supercritical sub-quintic radial NLS

$$i\psi_z(z, r) + \psi_{rr} + \frac{d-1}{r}\psi_r + |\psi|^{2\sigma}\psi = 0, \quad \frac{2}{d} < \sigma < 2, \quad d > 1. \quad (23.1)$$

As always with ring solutions, we exclude the case $d = 1$, since there are no ring solutions in one dimension.¹

23.1 Review of Ring-Type Blowup Solutions

In Sect. 22.1 we saw that collapsing ring solutions are characterized by their radius $r_{\max}(z) := \arg \max_r |\psi(z, r)|$ and width $L(z)$, see Fig. 22.1. We distinguished between shrinking-ring solutions for which $\lim_{z \rightarrow Z_c} r_{\max} = 0$, and standing-ring solutions for which $0 < \lim_{z \rightarrow Z_c} r_{\max} < \infty$.

In Sect. 11.2.5 we saw that single-ring $G(r)$ profiles attain their global maximum at some $r_{\max}^G \gg 1$. Let $\tilde{G}(r) := G\left(r + r_{\max}^G\right)$. Then we can rewrite ψ_G as, see (19.6),

$$\psi_G(z, r) = \frac{1}{L^{\frac{1}{\sigma}}(z)} \tilde{G}(\rho) e^{i\zeta + i\frac{L_z}{4L}r^2}, \quad (23.2a)$$

¹ As in one dimension $x = 0$ is not different from $x > 0$.

where

$$\rho = \frac{r - r_{\max}(z)}{L(z)}, \quad \zeta = \int_0^z \frac{ds}{L^2(s)}, \quad r_{\max}(z) = r_{\max}^G L(z), \quad (23.2b)$$

and the global maximum of \tilde{G} is attained at $\rho = 0$. Since the ring radius and width go to zero at the same rate, we say that ψ_G undergoes an *equal-rate collapse*.²

The blowup profile of the standing-ring solutions of the supercritical quintic NLS ($\sigma = 2$ and $d > 1$) is

$$\psi_F(z, r) = \frac{1}{L^{\frac{1}{\sigma}}(z)} F(\rho) e^{i\zeta + i \frac{L_z}{4L}(r - r_{\max}(z))^2}, \quad (23.3a)$$

see (22.13), where

$$\rho = \frac{r - r_{\max}(z)}{L(z)}, \quad \zeta = \int_0^z \frac{ds}{L^2(s)}, \quad 0 < \lim_{z \rightarrow Z_c} r_{\max}(z) < \infty, \quad (23.3b)$$

and the global maximum of $F = R_{1D}$ is attained at $\rho = 0$. Hence, ψ_G and ψ_F are similar, except for two important differences:

1. The quadratic phase term is centered at $r = 0$ for ψ_G , see (23.2a), corresponding to focusing towards the origin, but at $r = r_{\max}(z)$ for ψ_F , see (23.3a), corresponding to focusing towards the ring peak at $r_{\max}(z)$.
2. ψ_G is a shrinking ring, see (23.2b), whereas ψ_F is a standing ring, see (23.3b).

23.2 A New Type of Ring-Type Blowup Solutions

In 1975, Degtiarev et al. [54] discovered that the three-dimensional cubic NLS admits radial solutions that collapse with a ring-type profile at the origin. These solutions were rediscovered in 2005 by Fibich et al. [73], see Fig. 23.1. The radius of these ring solutions shrinks to zero as

$$r_{\max}(z) \sim c L^{\frac{1}{2}}(z), \quad z \rightarrow Z_c.$$

² The collapsing core of a blowup solution of the radial critical NLS approaches the self-similar form $|\psi(z, r)| \sim L^{-\frac{d}{2}}(z) Q(\frac{r}{L(z)})$ for some function Q (Sect. 13.2). If the singular solution is ring-type, the global maximum of $Q(\rho)$ is attained at some $0 < \rho_{\max} < \infty$. Hence, $r_{\max}(z) = \rho_{\max} L(z)$. Therefore, ring-type blowup solutions of the critical NLS “have to” undergo an equal-rate collapse.

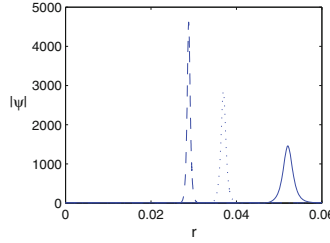


Fig. 23.1 Solution of the NLS (23.1) with $d = 3$, $\sigma = 1$, and $\psi_0 = 10e^{-r^4}$, at $z_1 = 0.038711$ (solid), $z_2 = z_1 + 9 \times 10^{-6}$ (dots) and $z_3 = z_1 + 12 \times 10^{-6}$ (dashes). From [73]

Since these solutions do not undergo an equal-rate or a standing-ring collapse, they are different from the ring solutions that we saw so far.

In 2007, Fibich, Gavish, and Wang showed that these solutions belong to a two-parameter family of shrinking-ring solutions that exist in the supercritical sub-quintic regime $\frac{2}{d} < \sigma < 2$ and $d > 1$:

Proposition 23.1 ([74]) *The supercritical sub-quintic NLS (23.1) admits shrinking-ring blowup solutions that undergo a quasi self-similar collapse with the ψ_S profile, i.e., $\psi(z, r) \sim \psi_S(z, r)$ for $r - r_{\max}(z) = O(L(z))$, where*

$$\psi_S(z, r) \sim \frac{1}{L^{\frac{1}{\sigma}}(z)} R_{1D}(\rho) e^{ic_s \xi(z) + i \frac{L_z}{4L} [\alpha r^2 + (1-\alpha)(r - r_{\max}(z))^2]}, \quad (23.4a)$$

$$\rho = \frac{r - r_{\max}(z)}{L(z)}, \quad \xi = \int_0^z \frac{ds}{L^2(s)}, \quad r_{\max}(z) = r_{\max}^0 L^\alpha(z), \quad (23.4b)$$

$c_s = 1 + \frac{2-\sigma}{\alpha(\sigma+2)}$, and

$$R_{1D}(\rho) = (1 + \sigma)^{\frac{1}{2\sigma}} \operatorname{sech}^{\frac{1}{\sigma}}(\sigma\rho). \quad (23.5)$$

In addition,

1. The shrinkage parameter α is given by

$$\alpha = \alpha_{\text{ring}} := \frac{2 - \sigma}{\sigma(d - 1)}. \quad (23.6)$$

In particular, $0 < \alpha < 1$.

2. The blowup rates of $L(z)$ and ψ are

$$L(z) \sim \kappa(Z_c - z)^p, \quad l(z) \sim c_l(Z_c - z)^p, \quad z \rightarrow Z_c,$$

where $\kappa, c_l > 0$, and

$$p = \frac{1}{1 + \alpha_{\text{ring}}} = \frac{1}{1 + \frac{2-\sigma}{\sigma(d-1)}} = \frac{1}{2 - \frac{\sigma d - 2}{\sigma(d-1)}}.$$

In particular, $\frac{1}{2} < p < 1$.

Proof See Sect. 23.3. □

The self-similar profile of ψ_S is the one-dimensional solitary wave R_{1D} , which is the solution of

$$R'' - R + |R|^{2\sigma} R = 0, \quad R'(0) = 0, \quad R(\infty) = 0.$$

Hence, it is independent of d . In addition, since

$$\zeta(z) \sim \int_0^z (Z_c - s)^{-\frac{2}{1+\alpha_{\text{ring}}}} ds \sim (Z_c - z)^{-\frac{1-\alpha_{\text{ring}}}{1+\alpha_{\text{ring}}}}, \quad z \rightarrow Z_c,$$

the phase of ψ_S becomes infinite at the singularity.³

The radial phase $i \frac{L_z}{4L} [\alpha r^2 + (1-\alpha)(r - r_{\max})^2]$ is a weighted sum of two lens-type terms. Thus, $e^{i \frac{L_z}{4L} \alpha r^2}$ corresponds to a “global” shrinkage towards the origin (i.e., $r_{\max}(z) \rightarrow 0$), whereas $e^{i \frac{L_z}{4L} (1-\alpha)(r - r_{\max})^2}$ corresponds to a “local” narrowing of the ring width (i.e., $L(z) \rightarrow 0$). This double-lens phase is a unique feature of the ψ_S profile.

The ψ_S profile can also be written as, see Sect. 23.3.4,

$$\psi_S(z, r) \sim \frac{1}{L^{\frac{1}{\sigma}}(z)} R_{1D}(\rho) e^{i \frac{4}{2+\sigma} \zeta(z) - i \sqrt{\frac{2-\sigma}{\sigma+2}} \rho}. \quad (23.7)$$

Since $\arg(\psi_S)$ is linear in ρ , the ring is tilted in the “moving-frame” variable ρ (Conclusion 8.1). The rescaled profile satisfies the zero-Hamiltonian condition

$$H_{1d} \left(R_{1D}(\rho) e^{-i \sqrt{\frac{2-\sigma}{\sigma+2}} \rho} \right) = 0,$$

where H_{1d} is the one-dimensional Hamiltonian (Lemma 23.9).

23.2.1 $\frac{d-1}{r} \psi_r$ Is Not Negligible

The ψ_S profile satisfies

$$r_{\max}(z) \sim L^\alpha, \quad \psi_S \sim L^{-\frac{1}{\sigma}}, \quad \frac{\partial}{\partial r} \psi_S \sim L^{-(1+\frac{1}{\sigma})}. \quad (23.8)$$

³ This is the case with all known singular NLS solutions.

Since $0 < \alpha < 1$,

$$\frac{d-1}{r}\psi_r \sim \frac{d-1}{r_{\max}(z)}\psi_r \sim L^{-(\alpha+1+\frac{1}{\sigma})} \ll \psi_{rr} \sim L^{-\left(2+\frac{1}{\sigma}\right)}, \quad z \rightarrow Z_c.$$

Therefore, $\frac{d-1}{r}\psi_r = o(\psi_{rr})$ as $z \rightarrow Z_c$. This may seem to suggest that the d -dimensional NLS (23.1) can be approximated by the one-dimensional NLS

$$i\psi_z(z, r) + \psi_{rr} + |\psi|^{2\sigma}\psi = 0. \quad (23.9)$$

Indeed, a similar argument was extremely useful in the analysis of standing-ring blowup solutions (Sect. 22.2). Since $\sigma < 2$, however, the NLS (23.9) is subcritical, and therefore does not admit singular solutions. We thus conclude that *although $\frac{d-1}{r}\psi_r$ becomes smaller and smaller than ψ_{rr} , it cannot be neglected in the analysis.*⁴

23.3 Finding the Blowup Profile and Blowup Rate

In this section we follow the informal derivation of Fibich et al. [74] and find the blowup profile and blowup rate of ring-type blowup solutions of the NLS (23.1), such as the one in Fig. 23.1.

23.3.1 “Interpolation” of ψ_G and ψ_F

Since $r_{\max}(z) \sim cL^\alpha(z)$, where $\alpha = 1$ for ψ_G , $\alpha = 1/2$ for the solution of Fig. 23.1, and $\alpha = 0$ for ψ_F , this suggests that ψ_S is “between” ψ_G and ψ_F . Therefore, we find ψ_S from “interpolation” of ψ_G and ψ_F .

We begin with the “common components” of ψ_G and ψ_F . The amplitudes of ψ_G and ψ_F are self-similar around the ring peak at $r_{\max}(z)$, i.e.,

$$|\psi_G|, |\psi_F| = \frac{1}{L^{\frac{1}{\sigma}}(z)}S(\rho), \quad \rho = \frac{r - r_{\max}(z)}{L}.$$

Therefore, we retain this form in $|\psi_S|$. Similarly, both profiles have the non-radial phase term $e^{i\xi(z)}$, where $\xi = \int_0^z L^{-2}$. Hence, this term is also retained.

Next, we “interpolate” the “different components” of ψ_G and ψ_F :

1. We assume that the radial phase of ψ_S is a weighted sum of the radial phases of ψ_G , see (23.2a), and of ψ_F , see (23.3a). Hence,

$$\arg \psi_S = \xi(z) + \gamma(z)r^2 + \eta(z)(r - r_{\max}(z))^2.$$

⁴ Indeed, ψ_S depends on d (through α_{ring} and p), whereas ψ_F does not.

This sum corresponds to a simultaneous “global” shrinkage of the ring radius $r_{\max}(z)$ and “local” shrinkage of the ring width $L(z)$, respectively.

2. We let $r_{\max}(z) = r_{\max}^0 L^\alpha(z)$, so that ψ_G and ψ_F correspond to $\alpha = 1$ and $\alpha = 0$, respectively, and ψ_S corresponds to $0 < \alpha < 1$.

Therefore, our starting point is

$$\psi_S(z, r) = \frac{1}{L^{\frac{1}{\alpha}}(z)} S(\rho) e^{i\zeta(z) + i\gamma(z)r^2 + i\eta(z)(r - r_{\max}(z))^2}, \quad (23.10a)$$

where

$$\rho = \frac{r - r_{\max}(z)}{L(z)}, \quad \zeta = \int_0^z \frac{ds}{L^2(s)}, \quad r_{\max}(z) = r_{\max}^0 L^\alpha(z), \quad (23.10b)$$

and

$$0 < \alpha < 1. \quad (23.10c)$$

Substitution of this profile in the NLS (23.1) gives

$$S_{\rho\rho}(\rho) + \frac{(d-1)L}{L\rho + r_{\max}^0 L^\alpha} S_\rho - S + |S|^{2\sigma} S + AS + i(B + \rho C)S_\rho + iDS = 0,$$

where

$$\begin{aligned} A(z) &= -(L\rho + r_{\max}^0 L^\alpha)^2 L^2 \gamma' - L^4 \rho^2 \eta' + 2\alpha \rho r_{\max}^0 L^{2+\alpha} L_z \eta \\ &\quad - 4L^2 \left(\gamma \left(L\rho + r_{\max}^0 L^\alpha \right) + \eta L\rho \right)^2, \\ B(z) &= -r_{\max}^0 \alpha L^\alpha L_z + 4\gamma r_{\max}^0 L^{\alpha+1}, \\ C(z) &= -LL_z + 4(\gamma + \eta)L^2, \\ D(z) &= -\frac{1}{\sigma} LL_z + 2[\gamma d + \eta] L^2 + 2(d-1)\eta \frac{L^3 \rho}{L\rho + r_{\max}^0 L^\alpha}. \end{aligned}$$

Since the G and F profiles are real, we “require” that the “interpolated” profile S be real as well.⁵ Therefore, $B(z)$, $C(z)$, and $D(z)$ should vanish as $z \rightarrow Z_c$. Since, in addition, S only depends on ρ , $A(z)$ should have a finite limit as $z \rightarrow Z_c$.

Setting $B(z) \equiv 0$ gives

$$\gamma(z) = \alpha \frac{L_z}{4L}. \quad (23.11a)$$

⁵ The requirement that S be real, i.e., that $\arg(\psi)$ is of the form $\zeta + \gamma r^2 + \eta(r - r_{\max})^2$, is not obvious. Indeed, the self-similar profile of peak-type solutions of the supercritical NLS is a *complex-valued* function multiplied by a quadratic radial phase term (Sect. 12.5). This requirement will be justified a posteriori by the agreement of the asymptotic analysis with numerical simulations (Sect. 23.6).

Setting $C(z) \equiv 0$ and using (23.11a) gives

$$\eta(z) = (1 - \alpha) \frac{L_z}{4L}. \quad (23.11b)$$

Substituting (23.11) in (23.10a) gives rise to the ring-type profile

$$\psi_S(z, r) = \frac{1}{L^{\frac{1}{\sigma}}(z)} S(\rho) e^{i\zeta + i\alpha \frac{L_z}{4L} r^2 + i(1-\alpha) \frac{L_z}{4L} (r - r_{\max}(z))^2}, \quad (23.12)$$

where S is the solution of

$$S_{\rho\rho}(\rho) + \frac{(d-1)L}{L\rho + r_{\max}^0 L^\alpha} S_\rho - S + |S|^{2\sigma} S + AS + iDS = 0, \quad (23.13a)$$

and

$$A = -\frac{1}{4} \left(L^3 \rho^2 + 2\alpha r_{\max}^0 L^{2+\alpha} \rho + \alpha \left(r_{\max}^0 \right)^2 L^{1+2\alpha} \right) L_{zz} \\ + \frac{1}{4} \alpha(1-\alpha) r_{\max}^0 \left(r_{\max}^0 L^{2\alpha} + 2L^{\alpha+1} \rho \right) L_z^2, \quad (23.13b)$$

$$D = \frac{d-1}{2} \left[\alpha - \frac{2-\sigma}{\sigma(d-1)} + (1-\alpha) \frac{L\rho}{L\rho + r_{\max}^0 L^\alpha} \right] LL_z. \quad (23.13c)$$

Note that, by (23.12),

$$\arg(\psi_S) = \zeta(z) + \alpha \frac{L_z}{4L} r^2 + (1-\alpha) \frac{L_z}{4L} (r - r_{\max}(z))^2. \quad (23.14)$$

Conclusion 23.1 *The radial phase of ψ_S is a linear interpolation of the radial phases of ψ_G and ψ_F .*

As noted, this interpolation corresponds to a simultaneous “global” shrinkage of the ring radius $r_{\max}(z)$ and “local” shrinkage of the ring width $L(z)$.

23.3.2 The Shrinkage Parameter α

The parameter α relates the shrinkage of the ring radius $r_{\max}(z)$ and of the ring width $L(z)$. We begin by discussing the possible values of α :

- **$\alpha = 1$:** Since $r_{\max}(z) = r_{\max}^0 L(z)$, the solution undergoes an *equal-rate collapse*. In addition, the phase term $(1-\alpha) \frac{L_z}{4L} (r - r_{\max}(z))^2$ in $\arg(\psi_S)$ vanishes. Therefore, ψ_S reduces to ψ_G .

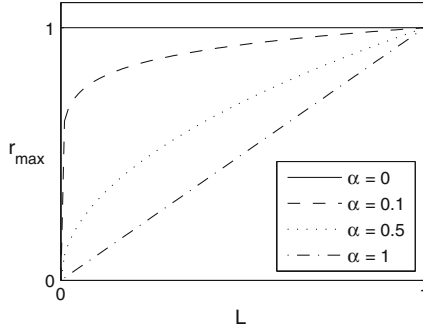


Fig. 23.2 Plot of $r_{\max} = L^\alpha$ for $\alpha = 0, 0.1, 0.5$, and 1

- $\alpha = 0$: Since $r_{\max}(z) \equiv r_{\max}^0$, the solution undergoes a standing-ring collapse. In addition, the phase term $\alpha \frac{L_z}{4L} r^2$ disappears. Therefore, ψ_S reduces to ψ_F .
- $0 < \alpha < 1$: Both radial phase terms are present. Therefore, ψ_S does not reduce to ψ_G or to ψ_F . Since $r_{\max}(z) = r_{\max}^0 L^\alpha(z)$, the shrinkage of $r_{\max}(z)$ is initially slower than in an equal-rate collapse, but near the singularity it becomes faster than in an equal-rate collapse (Fig. 23.2).
- $\alpha > 1$: This case does not correspond to a ring solution, because the ring radius becomes smaller than the ring width as L goes to zero.
- $\alpha < 0$: The ring radius increases to infinity as L goes to zero. Hence, the solution is an expanding ring.

The above arguments further motivate the initial assumption that $0 < \alpha < 1$, see (23.10c). We now obtain a sharper lower bound for α :

Lemma 23.1 *Let ψ be a ring-type blowup solution of the NLS (23.1) that collapses with the ψ_S profile (23.12). Then*

$$\alpha \geq \alpha_{\text{ring}}, \quad \alpha_{\text{ring}} := \frac{2 - \sigma}{\sigma(d - 1)} > 0.$$

Proof Since $\alpha < 1$, the (radial) power of ψ_S can be approximated by

$$\begin{aligned} \int_0^\infty |\psi_S|^2 r^{d-1} dr &= L^{-\frac{2}{\sigma}} \int_0^\infty |S(\rho)|^2 r^{d-1} dr \\ &= L^{-\frac{2}{\sigma}} \int_{-\frac{r_{\max}^0}{L^{1-\alpha}}}^\infty |S(\rho)|^2 \left(L\rho + r_{\max}^0 L^\alpha \right)^{d-1} L d\rho \\ &\approx L^{-\frac{2}{\sigma} + \alpha(d-1)+1} \left(r_{\max}^0 \right)^{d-1} \int_{-\infty}^\infty |S(\rho)|^2 d\rho. \end{aligned}$$

Assume by negation that $\alpha < \alpha_{\text{ring}}$. Then

$$-\frac{2}{\sigma} + \alpha(d-1) + 1 < -\frac{2}{\sigma} + \alpha_{\text{ring}}(d-1) + 1 = 0.$$

Therefore, $\int |\psi_S|^2 \rightarrow \infty$ as $L \rightarrow 0$. This, however, is in contradiction with power conservation, since $\int |\psi_S|^2 \leq \int |\psi|^2 \equiv \int |\psi_0|^2$. \square

As noted, $\alpha < 1$. An additional upper bound for α is as follows:

Lemma 23.2 *Under the conditions of Lemma 23.1, $\alpha < \frac{2+\sigma}{\sigma(d-1)}$.*

Proof By (23.12),

$$\|\psi_S\|_{2\sigma+2}^{2\sigma+2} = \frac{1}{L^{\frac{2\sigma+2}{\sigma}}} \int_{-\frac{r_{\max}^0}{L^{1-\alpha}}}^{\infty} |S(\rho)|^{2\sigma+2} \left(L\rho + r_{\max}^0 L^\alpha \right)^{d-1} L d\rho.$$

Since $\alpha < 1$,

$$\|\psi_S\|_{2\sigma+2}^{2\sigma+2} \sim L^{\alpha(d-1)-1-\frac{2}{\sigma}} (r_{\max}^0)^{d-1} \int_{-\infty}^{\infty} |S(\rho)|^{2\sigma+2} d\rho, \quad L \rightarrow 0. \quad (23.15)$$

Therefore, since $\|\psi_S\|_{2\sigma+2}^{2\sigma+2} \rightarrow \infty$, we conclude that

$$\alpha(d-1) - 1 - \frac{2}{\sigma} < 0, \quad (23.16)$$

and so the result follows. \square

Depending on the values of σ and d , this upper bound can be above or below the upper bound $\alpha < 1$.

23.3.3 Bounds for the Blowup Rate

We now derive upper and lower bounds for the blowup rate.

Lemma 23.3 *Let the conditions of Lemma 23.1 hold. If, in addition,*

$$L(z) \sim \kappa(Z_c - z)^p, \quad z \rightarrow Z_c,$$

where $\kappa > 0$, then

$$p \geq \frac{1}{1+\alpha}. \quad (23.17)$$

Proof Consider Eq. (23.13) for S . Since $0 < \alpha < 1$, we have that as $z \rightarrow Z_c$,

$$\begin{aligned} A &\sim -\frac{\alpha (r_{\max}^0)^2}{4} \left[L^{2\alpha+1} L_{zz} - (1-\alpha)L^{2\alpha} L_z^2 \right] \\ &\sim -\frac{\alpha (r_{\max}^0)^2}{4} p(\alpha p - 1) \kappa^{2(1+\alpha)} (Z_c - z)^{2((\alpha+1)p-1)}. \end{aligned} \quad (23.18)$$

Since $\lim_{z \rightarrow Z_c} A(z)$ should be finite, the result follows. \square

Next, we derive an upper bound for p :

Lemma 23.4 *Under the conditions of Lemma 23.3,*

$$p \leq \frac{2}{1 + \frac{2}{\sigma} - \alpha(d-1)} \frac{1}{1 + \alpha_{\text{ring}}} = \frac{1}{1 - \frac{d-1}{2} (\alpha - \alpha_{\text{ring}})} \frac{1}{1 + \alpha_{\text{ring}}},$$

where $\alpha_{\text{ring}} := \frac{2-\sigma}{\sigma(d-1)}$.

Proof By Hamiltonian conservation, see (10.9),

$$\|\nabla \psi\|_2^2 \sim \frac{1}{\sigma+1} \|\psi\|_{2\sigma+2}^{2\sigma+2} \sim \frac{1}{\sigma+1} \|\psi_S\|_{2\sigma+2}^{2\sigma+2}, \quad z \rightarrow Z_c.$$

In addition, by (23.15), $\|\psi_S\|_{2\sigma+2}^{2\sigma+2} \sim c L^{\alpha(d-1)-1-\frac{2}{\sigma}}$, where c is a generic positive constant. Therefore,

$$\|\nabla \psi\|_2^2 \sim c L^{\alpha(d-1)-1-\frac{2}{\sigma}} \sim c (Z_c - z)^{p(\alpha(d-1)-1-\frac{2}{\sigma})}, \quad z \rightarrow Z_c. \quad (23.19)$$

By Theorem 13.15,

$$\int_z^{Z_c} (Z_c - s) \|\nabla \psi(s)\|_2^2 ds \leq C (Z_c - z)^{\frac{2\alpha_{\text{ring}}}{1+\alpha_{\text{ring}}}}. \quad (23.20)$$

Relations (23.19) and (23.20) imply that

$$p \left(\alpha(d-1) - 1 - \frac{2}{\sigma} \right) + 2 \geq \frac{2\alpha_{\text{ring}}}{1 + \alpha_{\text{ring}}}.$$

The result follows from this inequality and (23.16). \square

Combining Lemmas 23.3 and 23.4, we have that

$$\frac{1}{1 + \alpha} \leq p \leq \frac{1}{1 - \frac{d-1}{2} (\alpha - \alpha_{\text{ring}})} \frac{1}{1 + \alpha_{\text{ring}}}. \quad (23.21)$$

Exercise 23.1 ([12]) Use Lemma 13.5 to show that if $\alpha = \alpha_{\text{ring}}$, then $p < 1$.⁶

Exercise 23.2 Show that Theorem 13.14 implies that under the conditions of Lemma 23.3, $p \geq \frac{1}{2} - \frac{\sigma d - 2}{4\sigma}$. Verify that this lower bound is less sharp than the one in Lemma 23.3.

23.3.4 Self-similar Profile

The self-similar profile approaches a rescaled one dimensional solitary wave:

Lemma 23.5 $S(\rho) = \omega^{\frac{1}{2\sigma}} R_{1D} \left(\omega^{\frac{1}{2}} \rho \right)$, where $R_{1D}(\rho) = (1 + \sigma)^{\frac{1}{2\sigma}} \operatorname{sech}^{\frac{1}{\sigma}}(\sigma \rho)$ and

$$\omega = \begin{cases} 1 - \frac{\alpha (r_{\max}^0)^2}{4(1+\alpha)^2} \kappa^{2(1+\alpha)}, & \text{if } p = \frac{1}{1+\alpha}, \\ 1, & \text{if } p > \frac{1}{1+\alpha}. \end{cases}$$

Proof By (23.18),

$$\lim_{z \rightarrow Z_c} A(z) = \begin{cases} \frac{\alpha (r_{\max}^0)^2}{4(1+\alpha)^2} \kappa^{2(1+\alpha)}, & \text{if } p = \frac{1}{1+\alpha}, \\ 0 & \text{if } p > \frac{1}{1+\alpha}. \end{cases}$$

In addition, since $0 < \alpha < 1$, $\frac{(d-1)L}{L\rho + r_{\max}^0 L^\alpha} \rightarrow 0$. By Lemma 23.3, $p \geq \frac{1}{1+\alpha}$, hence $2p - 1 \geq \frac{1-\alpha}{1+\alpha} > 0$, and so

$$LL_z \sim -p\kappa^2(Z_c - z)^{2p-1} \rightarrow 0. \quad (23.22)$$

Therefore, by (23.13c),

$$\lim_{z \rightarrow Z_c} D(z) = \lim_{z \rightarrow Z_c} \frac{d-1}{2} \left[\alpha - \frac{2-\sigma}{\sigma(d-1)} + (1-\alpha) \frac{L\rho}{L\rho + r_{\max}^0 L^\alpha} \right] LL_z = 0.$$

In light of all the above, as $z \rightarrow Z_c$, Eq. (23.13) reduces to the one-dimensional solitary wave equation

$$S_{\rho\rho}(\rho) - \omega S + |S|^{2\sigma} S = 0.$$

⁶ When $\alpha = \alpha_{\text{ring}}$, the upper bound in Lemma 23.4 yields $p \leq \frac{1}{1+\alpha_{\text{ring}}}$. This upper bound is sharper than the one in Exercise 23.1. Note, however, that Lemma 23.4 is only valid for $\sigma < 2$, whereas Exercise 23.1 is valid for any σ in the H^1 -subcritical regime. This is because the proof of Lemma 23.4 makes use of Lemma 13.15, which is only valid for $\sigma < 2$, whereas the proof of Exercise 23.1 makes use of Lemma 13.5, which is valid for any σ in the H^1 -subcritical regime. This distinction will become important in the proof of Lemma 23.11.

Since S attains its global maximum at $\rho = 0$, the result follows from Lemma 6.15. \square

The dual-lens term, see (23.14), approaches a linear phase term in the “moving-frame” variable ρ :

Lemma 23.6 *As $z \rightarrow Z_c$,*

$$\frac{L_z}{4L} \left[\alpha r^2 + (1 - \alpha)(r - r_{\max}(z))^2 \right] \sim \frac{\alpha}{2} L_z r_{\max}(z) \rho + \alpha \frac{L_z}{4L} r_{\max}^2(z).$$

Proof Since $LL_z \rightarrow 0$, see (23.22), and

$$\begin{aligned} \frac{L_z}{4L} \left[\alpha r^2 + (1 - \alpha)(r - r_{\max}(z))^2 \right] &= \frac{L_z}{4L} \left[\alpha(\rho L + r_{\max})^2 + (1 - \alpha)(\rho L)^2 \right] \\ &= \frac{LL_z}{4} \rho^2 + \frac{\alpha}{2} L_z r_{\max} \rho + \alpha \frac{L_z}{4L} r_{\max}^2, \end{aligned}$$

the result follows. \square

Therefore, the rescaled radial profile approaches $S(\rho) e^{i \frac{\alpha}{2} L_z r_{\max} \rho}$, and

$$\psi_S \sim \frac{1}{L^{\frac{1}{\sigma}}(z)} S(\rho) e^{i \frac{\alpha}{2} L_z r_{\max}(z) \rho + i \xi_2(z)}, \quad \xi_2(z) := \xi(z) + \alpha \frac{L_z}{4L} r_{\max}^2(z). \quad (23.23)$$

As noted by Merle, Raphaël, and Szeftel, the limiting rescaled profile satisfies a zero-Hamiltonian condition:

Lemma 23.7 ([186]) *Let $H_{1d}(f(\rho)) := \int_{-\infty}^{\infty} |f'|^2 d\rho - \frac{1}{\sigma+1} \int_{-\infty}^{\infty} |f|^{2\sigma+2} d\rho$ be the one-dimensional Hamiltonian. Then*

$$\lim_{z \rightarrow Z_c} H_{1d} \left(S(\rho) e^{i \frac{\alpha}{2} L_z r_{\max} \rho} \right) = 0.$$

Proof Since ψ_S is given by (23.23), a calculation similar to that of (23.15) yields

$$\int_0^{\infty} |\psi_S|^{2\sigma+2} r^{d-1} dr \sim L^{\alpha(d-1)-1-\frac{2}{\sigma}} \left(r_{\max}^0 \right)^{d-1} \int_{-\infty}^{\infty} |S(\rho)|^{2\sigma+2} d\rho$$

and

$$\int_0^{\infty} |\nabla_r \psi_S|^2 r^{d-1} dr \sim L^{\alpha(d-1)-1-\frac{2}{\sigma}} \left(r_{\max}^0 \right)^{d-1} \int_{-\infty}^{\infty} |\nabla_{\rho} (S(\rho) e^{i \frac{\alpha}{2} L_z r_{\max} \rho})|^2 d\rho.$$

Therefore,

$$H(\psi_S) \sim L^{\alpha(d-1)-1-\frac{2}{\sigma}} \left(r_{\max}^0\right)^{d-1} H_{1d} \left(S(\rho) e^{i\frac{\alpha}{2} L_z r_{\max} \rho}\right).$$

Since $\alpha(d-1)-1-\frac{2}{\sigma} < 0$, see (23.16), the condition that $H(\psi_S)$ remains bounded as $L \rightarrow 0$ implies that $H_{1d} \left(S(\rho) e^{i\frac{\alpha}{2} L_z r_{\max} \rho}\right) \rightarrow 0$.⁷ \square

Lemma 23.8 ([186])

$$\lim_{z \rightarrow Z_c} \frac{\alpha}{2} L_z r_{\max} = -\sqrt{\omega} \sqrt{\frac{2-\sigma}{\sigma+2}}. \quad (23.24)$$

Proof Since $S = \omega^{\frac{1}{2\sigma}} R_{1D} \left(\omega^{\frac{1}{2}} \rho\right)$ is real,

$$H_{1d} \left(S(\rho) e^{i\frac{\alpha}{2} L_z r_{\max} \rho}\right) = H_{1d}(S) + \frac{\alpha^2}{4} L_z^2 r_{\max}^2 \|S\|_2^2.$$

By Exercise 6.2 with $d = 1$,

$$\|S\|_2^2 = \omega^{\frac{2-\sigma}{2\sigma}} \|R_{1D}\|_2^2, \quad H_{1d}(S) = \omega^{1+\frac{2-\sigma}{2\sigma}} H_{1d}(R_{1D}).$$

By the Pohozaev identities (6.7) and Eq.(6.15) with $d = 1$,

$$H_{1d}(R_{1D}) = \frac{\sigma-2}{2\sigma+2} \|R_{1D}\|_{2\sigma+2}^{2\sigma+2} = \frac{\sigma-2}{\sigma+2} \|R_{1D}\|_2^2.$$

Combining the above with Lemma 23.7 gives

$$\omega^{1+\frac{2-\sigma}{2\sigma}} \frac{\sigma-2}{\sigma+2} \|R_{1D}\|_2^2 + \frac{\alpha^2}{4} L_z^2 r_{\max}^2 \omega^{\frac{2-\sigma}{2\sigma}} \|R_{1D}\|_2^2 \rightarrow 0.$$

Therefore,

$$\frac{\alpha^2}{4} L_z^2 r_{\max}^2 \rightarrow \omega \frac{2-\sigma}{\sigma+2}.$$

Since $L_z < 0$ as $z \rightarrow Z_c$, the result follows. \square

By Lemmas 23.5 and 23.8, the limiting rescaled radial profile satisfies

$$S(\rho) e^{i\frac{\alpha}{2} L_z r_{\max} \rho} \rightarrow \omega^{\frac{1}{2\sigma}} R_{1D} \left(\omega^{\frac{1}{2}} \rho\right) e^{-i\sqrt{\omega} \sqrt{\frac{2-\sigma}{\sigma+2}} \rho}.$$

⁷ $H(\psi_S)$ remains bounded because $H(\psi)$ is conserved and the Hamiltonian of the “outer solution” is bounded.

From this limit and Lemma 23.7 follows

Lemma 23.9 ([186]) $H_{1d} \left(R_{1D}(\rho) e^{-i\sqrt{\frac{2-\sigma}{\sigma+2}}\rho} \right) = 0$.

We are now in a position to find the relation between p and α :

Corollary 23.1 *Under the conditions of Lemma 23.3, $p = \frac{1}{1+\alpha}$.*

Proof From (23.24) we have that $-\infty < \lim_{z \rightarrow Z_c} L_z r_{\max}(z) < 0$. Since

$$L_z r_{\max}(z) = L_z r_{\max}^0 L^\alpha \sim -r_{\max}^0 p \kappa^{1+\alpha} (Z_c - z)^{(1+\alpha)p-1}, \quad (23.25)$$

the result follows. \square

Corollary 23.2 *Under the conditions of Lemma 23.3,*

$$\omega = \frac{\alpha}{\alpha + \frac{2-\sigma}{\sigma+2}}. \quad (23.26)$$

Proof Substituting $p = \frac{1}{1+\alpha}$ in (23.25) and using (23.24) gives

$$-\frac{\alpha}{2} r_{\max}^0 \frac{1}{1+\alpha} \kappa^{1+\alpha} \sim \frac{\alpha}{2} L_z r_{\max}(z) \rightarrow -\sqrt{\omega} \sqrt{\frac{2-\sigma}{\sigma+2}}.$$

Taking the square, one obtains

$$\frac{\alpha^2}{4} (r_{\max}^0)^2 \frac{1}{(1+\alpha)^2} \kappa^{2(1+\alpha)} = \omega \frac{2-\sigma}{\sigma+2}.$$

Since $\frac{\alpha^2}{4} (r_{\max}^0)^2 \frac{1}{(1+\alpha)^2} \kappa^{2(1+\alpha)} = \alpha(1-\omega)$, see Lemma 23.5, we get

$$\alpha(1-\omega) = \omega \frac{2-\sigma}{\sigma+2}.$$

Therefore, ω is given by (23.26). \square

Corollary 23.3 *As $z \rightarrow Z_c$,*

$$\xi_2(z) := \xi(z) + \alpha \frac{L_z}{4L} r_{\max}^2(z) \sim c_2 \xi(z), \quad c_2 = 1 - \omega \frac{1-\alpha}{\alpha} \frac{2-\sigma}{2+\sigma}.$$

Proof By (23.24) and Corollary 23.2,

$$\alpha \frac{L_z}{4L} r_{\max}^2(z) = \frac{1}{\alpha} \frac{1}{LL_z} \frac{\alpha^2}{4} L_z^2 r_{\max}^2(z) \sim \frac{1}{\alpha} \frac{1}{LL_z} \omega \frac{2-\sigma}{2+\sigma}.$$

In addition, since $L \sim \kappa(Z_c - z)^{\frac{1}{1+\alpha}}$,

$$\zeta = \int_0^z \frac{ds}{L^2(s)} \sim \int_0^z \frac{ds}{\kappa^2 (Z_c - s)^{\frac{2}{1+\alpha}}} \sim \frac{1}{\kappa^2} \frac{1+\alpha}{1-\alpha} (Z_c - z)^{-\frac{1-\alpha}{1+\alpha}}$$

and $LL_z \sim -\kappa^2 \frac{1}{1+\alpha} (Z_c - z)^{\frac{1-\alpha}{1+\alpha}}$. By the above, $1/LL_z \sim -(1-\alpha)\zeta$. Hence, $\xi_2(z) \sim \zeta(z) \left(1 - \omega \frac{1-\alpha}{\alpha} \frac{2-\sigma}{2+\sigma}\right)$, as claimed. \square

The analysis so far showed that

$$\psi_S \sim \frac{\omega^{\frac{1}{2\sigma}}}{L^{\frac{1}{\sigma}}(z)} R_{1D}(\omega^{\frac{1}{2}}\rho) e^{i\xi_2(z) - i\sqrt{\omega} \sqrt{\frac{2-\sigma}{\sigma+2}} \rho},$$

where

$$\rho = \frac{r - r_{\max}(z)}{L(z)}, \quad r_{\max}(z) = r_{\max}^0 L^\alpha(z), \quad \xi_2 \sim c_2 \int_0^z \frac{1}{L^2}.$$

To bring ψ_S to a canonical form, let

$$\tilde{L}(z) := \frac{L(z)}{\sqrt{\omega}}. \quad (23.27)$$

Then

$$\psi_S \sim \frac{1}{\tilde{L}^{\frac{1}{\sigma}}(z)} R_{1D}(\tilde{\rho}) e^{i\xi_2(z) - i\sqrt{\frac{2-\sigma}{\sigma+2}} \tilde{\rho}},$$

where

$$\tilde{\rho} = \frac{r - r_{\max}(z)}{\tilde{L}(z)} = \omega^{\frac{1}{2}} \rho, \quad r_{\max}(z) = \widetilde{r_{\max}^0} \tilde{L}^\alpha, \quad \widetilde{r_{\max}^0} := r_{\max}^0 \omega^{\frac{\alpha}{2}},$$

and

$$\xi_2 \sim \frac{c_2}{\omega} \int_0^z \frac{1}{\tilde{L}^2}, \quad \frac{c_2}{\omega} = \frac{1}{\omega} - \frac{1-\alpha}{\alpha} \frac{2-\sigma}{2+\sigma} = \frac{4}{2+\sigma},$$

where in the last equality we used (23.26). Dropping the tildes, we obtain (23.7). Alternatively, if we apply rescaling (23.27) to the original double-lens phase, we get

$$i\alpha \frac{L_z}{4L} r^2 + i(1-\alpha) \frac{L_z}{4L} (r - r_{\max}(z))^2 = i\alpha \frac{\tilde{L}_z}{4\tilde{L}} r^2 + i(1-\alpha) \frac{\tilde{L}_z}{4\tilde{L}} (r - r_{\max}(z))^2$$

and

$$\zeta = \int_0^z \frac{1}{L^2} = \frac{1}{\omega} \int_0^z \frac{1}{\tilde{L}^2} = \frac{\alpha + \frac{2-\sigma}{\sigma+2}}{\alpha} \int_0^z \frac{1}{\tilde{L}^2}.$$

Therefore, dropping the tildes, we get (23.4a).

23.3.5 $\alpha = \alpha_{\text{ring}}$ and $p = \frac{1}{1+\alpha_{\text{ring}}}$

In Sect. 23.3.2 we saw that

$$\frac{2-\sigma}{\sigma(d-1)} = \alpha_{\text{ring}} \leq \alpha < \min \left\{ 1, \frac{2+\sigma}{\sigma(d-1)} \right\}.$$

The simulations in Sect. 23.6.2 strongly suggest that α is equal to its lower bound.⁸

Observation 23.1 ([74]) $\alpha = \alpha_{\text{ring}}$.

Substituting $\alpha = \alpha_{\text{ring}}$ in inequalities (23.21) gives

$$p = \frac{1}{1 + \alpha_{\text{ring}}}.$$

Therefore, by (23.19), the blowup rate of ψ is

$$l(z) \sim c(Z_c - z)^{\frac{1}{1+\alpha_{\text{ring}}}}.$$

The simulations in Sect. 23.6.2 show that this is indeed the blowup rate, providing further support to Observation 23.1. This concludes the informal derivation of Proposition 23.1.

23.4 Strong Collapse

In Sect. 21.2 we saw that peak-type blowup solutions of the supercritical NLS undergo a weak collapse.⁹ We now show that shrinking-ring blowup solutions of the supercritical NLS undergo a strong collapse:

⁸ I.e., that ψ_S undergoes a strong collapse (Exercise 23.3).

⁹ See Sect. 7.7 for definitions of weak and strong collapse.

Lemma 23.10 *Under the conditions of Proposition 23.1, the amount of power that collapses into the singularity is*

$$P_{\text{collapse}} = \left(r_{\max}^0\right)^{d-1} \int_{-\infty}^{\infty} |R_{1D}|^2 d\rho > 0. \quad (23.28)$$

Hence, ψ_S undergoes a strong collapse.

Proof Calculations similar to those in the proof of Lemma 23.1 give

$$P_\epsilon := \lim_{z \rightarrow Z_c} \int_{0 \leq r < \epsilon} |\psi_S|^2 r^{d-1} dr \sim \left(r_{\max}^0\right)^{d-1} \int_{-\infty}^{\infty} |S|^2 d\rho.$$

Since $P_{\text{collapse}} := \lim_{\epsilon \rightarrow 0+} P_\epsilon$ and $S = R_{1D}$, the result follows. \square

Exercise 23.3 Let ψ_S be given by (23.12). Show that ψ_S undergoes a strong collapse if $\alpha = \alpha_{\text{ring}}$ and a weak collapse if $\alpha > \alpha_{\text{ring}}$.

23.5 “Minimal-Power” Shrinking-Ring Solutions

The derivation of Proposition 23.1 is based on informal analysis and numerical evidence. Recently, Merle, Raphaël, and Szeftel rigorously proved the existence of a “minimal-power” shrinking-ring solution:

Theorem 23.1 ([186]) *Let $d \geq 2$, $\frac{2}{d} < \sigma < \min\{2, \frac{2}{d-2}\}$, $Z_c \in \mathbb{R}$, $\alpha_{\text{ring}} = \frac{2-\sigma}{\sigma(d-1)}$, and $R_{1D}(\rho) = (1+\sigma)^{\frac{1}{2\sigma}} \operatorname{sech}^{\frac{1}{\sigma}}(\sigma\rho)$. Then there exist $\Delta Z > 0$ and a radial solution $\psi(z, r) \in C([Z_c - \Delta Z, Z_c], H^1)$ of the NLS (23.1) that becomes singular at Z_c , with the following dynamics. There exist parameters $(r_{\max}(z), L(z), \zeta(z)) \in \mathbb{R}_+ \times \mathbb{R}_+ \times \mathbb{R}$, such that as $z \rightarrow Z_c$,*

$$\psi(z, r) - \frac{1}{L^{\frac{1}{\sigma}}(z)} R_{1D}(\rho) e^{-i\sqrt{\frac{2-\sigma}{\sigma+2}}\rho} e^{i\zeta(z)} \rightarrow 0 \quad \text{in } L^2(\mathbb{R}^d), \quad (23.29)$$

where $\rho = \frac{r-r_{\max}(z)}{L(z)}$. In addition, as $z \rightarrow Z_c$, $L(z) \sim \kappa (Z_c - z)^{\frac{1}{1+\alpha_{\text{ring}}}}$, $r_{\max}(z) \sim r_{\max}^0 L^{\alpha_{\text{ring}}}$, $\zeta(z) \sim c_1 L^{-(1-\alpha_{\text{ring}})}$, and $\|\nabla \psi\|_2 \sim c_2 (Z_c - z)^{-\frac{1}{1+\alpha_{\text{ring}}}}$.

By (23.29),

$$|\psi|^2 \rightarrow \|\psi_0\|_2^2 \delta(r), \quad z \rightarrow Z_c.$$

Hence, the solution in Theorem 23.1 undergoes a whole-beam collapse (Sect. 7.7). Since the solution does not have a non-collapsing tail, it can be viewed as a “minimal-power” shrinking-ring blowup solution.

In the critical case, all minimal-power blowup solutions are strongly unstable, since any perturbation that reduces the power arrests collapse (Sect. 13.5).

The situation in the supercritical case is different, because there is no notion of a critical power (Sect. 5.11.3). At present, the stability of the “minimal-power” solutions of Theorem 23.1 is open. In Sect. 23.6.3 we will see numerically that solutions that collapse with the ψ_S profile are radially stable. These solutions, however, have nontrivial tails, and are thus different from those of Theorem 23.1.

23.6 Simulations

23.6.1 Self-similar Ring-Type Profile

We solve the radial NLS (23.1) with $\sigma = 1.1$ and $d = 2.1$. By (23.6),

$$\alpha_{\text{ring}} = \frac{2 - 1.1}{1.1(2.1 - 1)} \approx 0.7438. \quad (23.30)$$

We use the initial condition

$$\psi_S^0(r) = 2R_{1D}(2^\sigma(r - 5))e^{-i[\alpha_{\text{ring}}r^2 + (1 - \alpha_{\text{ring}})(r - 5)^2]}. \quad (23.31)$$

Since this initial condition is equal to the asymptotic profile, the solution collapses with the ψ_S profile from $z = 0$, and not only after an initial transient. Figure 23.3a, b shows that the numerical solution indeed undergoes a shrinking-ring collapse. To check for self similarity, in Fig. 23.3c we plot the rescaled solution

$$\psi_{\text{rescaled}} = L^{\frac{1}{\sigma}}(z)\psi\left(\frac{r - r_{\max}(z)}{L(z)}\right), \quad (23.32a)$$

$$L(z) := \frac{\max_r |\psi_0|^\sigma}{\max_r |\psi|^\sigma}, \quad r_{\max}(z) := \arg \max_r |\psi| \quad (23.32b)$$

at various focusing levels between $L^{-1} = 4.4$ and $L^{-1} = 6.2 \times 10^7$. The rescaled profiles are nearly indistinguishable from each other and from R_{1D} , indicating that the solution indeed collapses with the ψ_S profile. Plotting the same data on a semi-logarithmic scale (Fig. 23.3d) shows that the collapse is “only” quasi self-similar, i.e., ψ_S characterizes the collapsing ring region ($-5 \leq \rho \leq 5$), but not the inner and outer regions ($|\rho| \geq 5$). The existence of a nontrivial tail implies, in particular, that this is not a “minimal-power” shrinking-ring solution (Sect. 23.5).

23.6.2 $\alpha = \alpha_{\text{ring}}$ and $p = \frac{1}{1+\alpha_{\text{ring}}}$

To confirm that $r_{\max}(z) \sim r_{\max}^0 L^{\alpha_{\text{ring}}}(z)$, we solve the NLS (23.1) with the initial condition (23.31) for $d = 2, 2.1$, and 3 , and for $\sigma = 1, 1.1, \dots, 2$, extract $r_{\max}(z)$ and $L(z)$ from ψ using (23.32b), and then search for the value of α that provides the

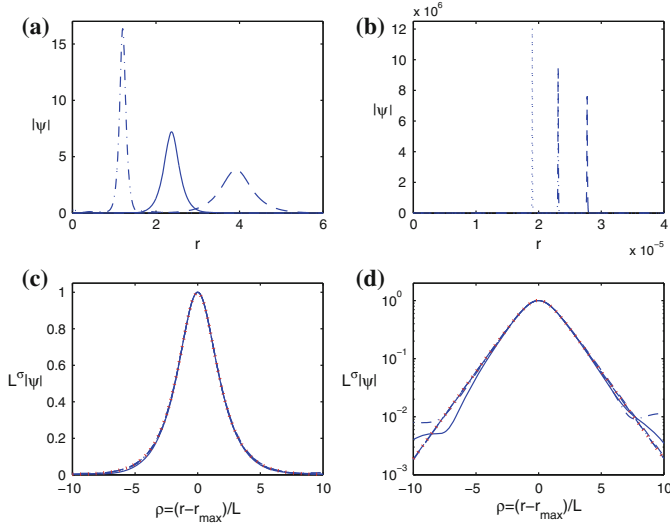


Fig. 23.3 Solution of the NLS (23.1) with $\sigma = 1.1$, $d = 2.1$, and the initial condition (23.31) at: **a** $z = 0.072$, ($L^{-1} = 4.4$, dashes), $z = 0.17$, ($L^{-1} = 8.8$, solid) and $z = 0.24$, ($L^{-1} = 21.6$, dash-dots), **b** $L^{-1} = 3.7 \times 10^7$ (dashes), $L^{-1} = 4.7 \times 10^7$ (dash-dots) and $L^{-1} = 6.2 \times 10^7$ (dots). **c** The six curves from (a) and (b), rescaled according to (23.32) and superimposed. The bold dotted curve is the R_{1D} profile (23.5). All seven curves are nearly indistinguishable. **d** Same data as in (c), on a semi-logarithmic scale. From [74]

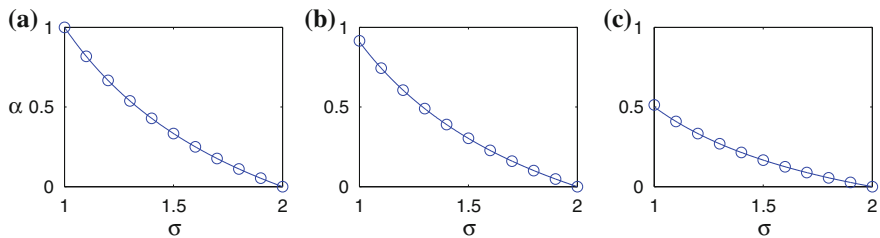


Fig. 23.4 Fitted values of α (circles) for $\sigma = 1, 1.1, \dots, 2$. The solid curve is $\alpha_{\text{ring}} = \frac{2-\sigma}{\sigma(d-1)}$. **a** $d = 2$. **b** $d = 2.1$. **c** $d = 3$. From [74]

best fit in $r_{\max}(z) \sim c L^\alpha(z)$. In all 3×11 cases, the difference between the fitted value of α and α_{ring} is less than 0.1%, see Fig. 23.4.

Similarly, to confirm that $p = \frac{1}{1+\alpha_{\text{ring}}}$, we ran a series of simulations with $d = 2$ and $\sigma = 1, 1.1, \dots, 1.9$, and found p from the power-law fit $L(z) \sim \kappa(Z_c - z)^p$.

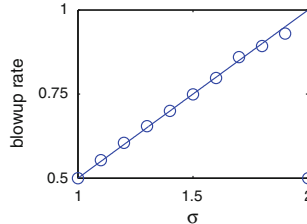


Fig. 23.5 Fitted values of p (circles) for $d = 2$ and $\sigma = 1, 1.1, \dots, 2$. The solid curve is $p = \frac{1}{1+\alpha_{\text{ring}}}$. From [74]

In all 10 cases, the difference between the fitted value of p and $\frac{1}{1+\alpha_{\text{ring}}}$ is less than 2%, see Fig. 23.5.¹⁰

Remark When $\sigma = 2$ the blowup rate is slightly faster than a square root (Theorem 22.1). Therefore, there is a *jump discontinuity* in the blowup rate at $\sigma = 2$. This issue is further discussed in Sect. 23.9.1.

23.6.3 Stability of ψ_S

In Fig. 23.6 we solve the supercritical NLS (23.1) with $d = 2.1$, $\sigma = 1.1$, and $\psi_0(r) = 15e^{-r^4}$. Initially, the solution evolves into a ring profile (Fig. 23.6b).¹¹ As the solution continues to collapse, it converges to ψ_S (Fig. 23.6d). This and additional simulations [74] suggest that ψ_S is a strong attractor for solutions of the radial NLS (23.1).

To test stability under non-radial perturbations,¹² in Fig. 23.7 we solve the two-dimensional NLS

$$i\psi_z(z, x, y) + \psi_{xx} + \psi_{yy} + |\psi|^{2\sigma}\psi = 0, \quad \sigma = 1.5, \quad (23.33a)$$

with the slightly-elliptic initial condition

$$\psi_S^{0,\text{elliptic}} = \psi_S^0 \left(\sqrt{1.02x^2 + y^2} \right), \quad (23.33b)$$

where ψ_S^0 is given by (23.31). After little focusing, two filaments emerge at the intersection of the ring with the y -axis.¹³ Therefore, we conclude that ψ_S is unstable under azimuthal perturbations.

¹⁰ In Sect. 23.9.1 we explain why the worst fit occurs for $\sigma = 1.9$.

¹¹ In Chap. 26 we use the *NGO method* to explain why strongly-nonlinear super-Gaussian initial conditions evolve into a ring profile.

¹² Obviously, this test can only be conducted for integer values of d .

¹³ This filamentation pattern is typical for elliptic initial conditions (Lemma 25.1).

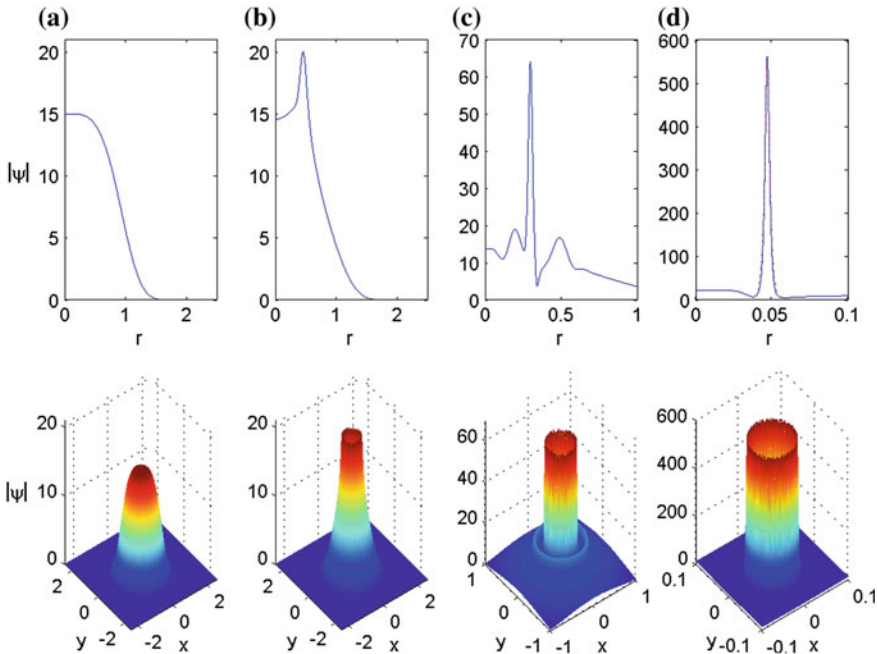
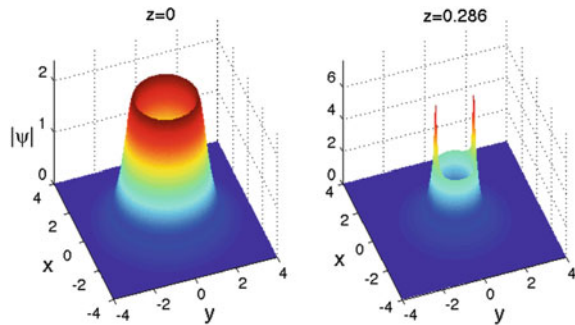


Fig. 23.6 *Top* Solution of the NLS (23.1) with $d = 2.1$, $\sigma = 1.1$, and $\psi_0 = 15e^{-r^4}$. **a** $z = 0$ ($L^{-1} = 1$), **b** $z = 0.011$ ($L^{-1} = 1.3$), **c** $z = 0.017$, ($L^{-1} = 4.3$), **d** $z = 0.019$ ($L^{-1} = 37.4$). The dotted curve in d is $|\psi_S|$; the two curves are nearly indistinguishable. *Bottom* Same data as in *top* graphs. From [74]

Fig. 23.7 Solution of (23.33). From [74]



Observation 23.2 ([74]) *The shrinking-ring profile ψ_S is stable under radial perturbations, but unstable under azimuthal perturbations.*

23.7 Singular Shrinking-Vortex Solutions (ψ_{S_m})

In two dimensions, shrinking-ring blowup solutions have a vortex analog:

Proposition 23.2 ([72]) *The two-dimensional supercritical subquintic NLS*

$$i\psi_z(z, r, \theta) + \psi_{rr} + \frac{1}{r}\psi_r + \frac{1}{r^2}\psi_{\theta\theta} + |\psi|^{2\sigma}\psi = 0, \quad 1 < \sigma < 2, \quad (23.34a)$$

with radial vortex initial conditions

$$\psi(0, r, \theta) = e^{im\theta} A_0(r), \quad (23.34b)$$

admits vortex solutions that undergo a quasi self-similar collapse with the ψ_{S_m} blowup profile, where $\psi_{S_m}(z, r, \theta) = e^{im\theta} \psi_S(z, r)$, and ψ_S is as in Proposition 23.1. In particular,

$$r_{\max}(z) \sim r_{\max}^0 L^{\alpha_{\text{ring}}}(z), \quad \alpha_{\text{ring}} = \frac{2 - \sigma}{\sigma},$$

and

$$L(z) \sim \kappa(Z_c - z)^p, \quad p = \frac{1}{1 + \alpha_{\text{ring}}} = \frac{\sigma}{2}.$$

Thus, the shrinking-ring profile ψ_S , multiplied by $e^{im\theta}$, is an asymptotic blowup profile of vortex solutions of (23.34).

23.7.1 Stability of Collapsing Supercritical Vortex Solutions

Recall that in the vortex-free case, solutions of the two-dimensional supercritical sub-quintic NLS (23.34a) can collapse with:

1. The peak-type profile ψ_Q , for which the blowup rate of $L(z)$ is $p = \frac{1}{2}$ (Chap. 21).
2. The shrinking-ring profile ψ_S , for which $r_{\max}(z) \sim r_{\max}^0 L^{\alpha_{\text{ring}}}$ where $\alpha_{\text{ring}} = \frac{2}{\sigma} - 1$, and $p = \frac{1}{1 + \alpha_{\text{ring}}} = \frac{\sigma}{2}$ (Proposition 23.1).

Similarly, when $m > 0$, there are two *potential* asymptotic blowup profiles [72]:

1. The ring-type profile $\psi_{Q_m} = L^{-\frac{1}{\sigma}}(z)Q_m\left(\frac{r}{L}\right)e^{im\theta}e^{i\xi(z)}$, which undergoes an equal-rate collapse ($\alpha = 1$) with $p = \frac{1}{2}$.
2. The ring-type profile $\psi_{S_m} = e^{im\theta}\psi_S$, for which $r_{\max}(z) \sim r_{\max}^0 L^{\alpha_{\text{ring}}}$ where $\alpha_{\text{ring}} = \frac{2}{\sigma} - 1$, and $p = \frac{1}{1+\alpha_{\text{ring}}} = \frac{\sigma}{2}$.

In contrast to the vortex-free case, both ψ_{Q_m} and ψ_{S_m} are ring type. Note that S_m is given by R_{1D} , and is thus independent of m . This is different from Q_m , which depends on m , see (15.51).

In the vortex-free case, numerical simulations show that ψ_Q is stable and ψ_S is radially stable. In contrast, in the vortex case, we already saw in Fig. 15.16 that a radial solution that started with the ψ_{Q_m} profile underwent a ψ_{S_m} collapse. This and additional simulations suggest

Observation 23.3 ([72]) ψ_{S_m} is a strong attractor for radial vortex solutions of the supercritical NLS (23.34), whereas ψ_{Q_m} is radially unstable.

Observation 23.3 is the supercritical analog of Observation 20.1, which says that in the critical case, ψ_{G_m} (the vortex analog of the ring-type solution ψ_G) is radially stable, but $\psi_{R_m^{(0)}}$ (the vortex analog of the peak-type solution $\psi_{R^{(0)}}$) is unstable. In the critical case, it is hard to tell ψ_{G_m} and $\psi_{R_m^{(0)}}$ apart numerically, because both profiles undergo an equal-rate collapse, and because there is a loglog difference between their blowup rates. In contrast, in the supercritical case it is easy to distinguish numerically between ψ_{Q_m} and ψ_{S_m} , because there are $O(1)$ differences between their values of α and p .¹⁴ Hence, the numerical support for Observation 23.3 is much stronger.

23.8 Non-existence of Expanding Rings

In [12], Baruch, Fibich, and Gavish asked whether the two-parameter family of ring-type ψ_S solutions can be extended to the super-quintic regime $\sigma > 2$. When $\sigma > 2$, then $\alpha_{\text{ring}} < 0$, and so $\lim_{z \rightarrow Z_c} r_{\max}(z) = \infty$, i.e., the solution is an expanding ring. These expanding rings do not violate power conservation. Indeed, calculations similar to those in the proof of Lemma 23.1 show that

$$\|\psi_S\|_2^2 = \int_{r_{\max}-\rho_c L(z)}^{r_{\max}+\rho_c L(z)} |\psi_S|^2 r^{d-1} dr \sim (r_{\max}^0)^{d-1} \int_{-\rho_c}^{\rho_c} |S|^2 d\rho, \quad z \rightarrow Z_c,$$

i.e., the power of an expanding ψ_S remains bounded. Nevertheless, we can prove that there are no expanding solutions with the ψ_S profile:

¹⁴ Thus, $\alpha = 1$ and $p = \frac{1}{2}$ for ψ_{Q_m} , whereas $\alpha = \alpha_{\text{ring}}$ and $p = \frac{\sigma}{2}$ for ψ_{S_m} .

Lemma 23.11 ([12]) *There are no NLS solutions that collapse with the ψ_S profile (23.4), such that $\alpha = \alpha_{\text{ring}} < 0$ and $L(z) \sim \kappa(Z_c - z)^p$.*

Proof By Lemma 23.3 and Exercise 23.1,¹⁵ $\frac{1}{1+\alpha} \leq p < 1$. Hence, α cannot be negative. \square

Indeed, numerical simulations suggest that when $\sigma > 2$, all ring-type blowup solutions are standing and not expanding. See [12, Sect. 4] for more details.

Remark The collapse point can escape to infinity in other nonlinear dispersive equations, such as the critical KdV [170].

23.9 Classification of Ring-Type Blowup Solutions

Figure 23.8 summarizes the classification of ring-type blowup solutions of the radial NLS

$$i\psi_z(z, r) + \psi_{rr} + \frac{d-1}{r}\psi_r + |\psi|^{2\sigma}\psi = 0, \quad d > 1.$$

- (A) In the subcritical regime $\sigma < \frac{2}{d}$, there are no blowup solutions.
- (B) In the critical case $\sigma = \frac{2}{d}$, the NLS admits shrinking-ring solutions that undergo an equal-rate collapse with the ψ_G profile at a square-root blowup rate (Chap. 19).

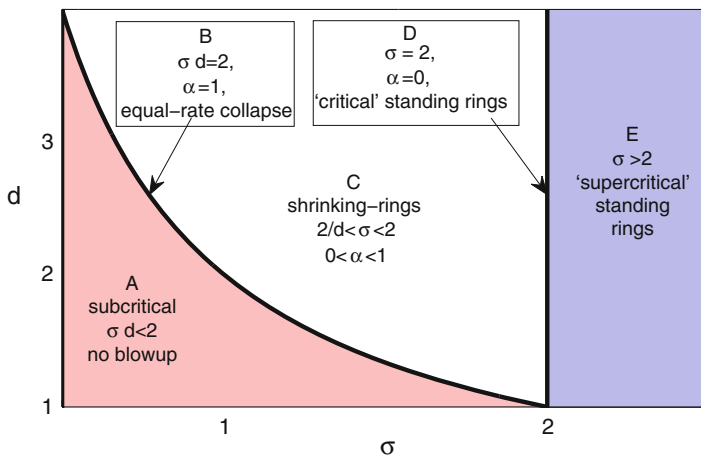


Fig. 23.8 Classification of ring-type blowup solutions of the NLS

¹⁵ We cannot use the upper bound for p from Lemma 23.4, because its proof is based on Lemma 13.15, which is only valid for $\sigma < 2$. We can use the upper bound from Exercise 23.1, however, because its proof is based on Lemma 13.5, which is valid for any σ in the H^1 -subcritical regime.

- (C) In the supercritical sub-quintic regime $\frac{2}{d} < \sigma < 2$, the NLS admits shrinking-ring solutions that collapse with the ψ_S profile, where $S = R_{1D}$, the ring radius $r_{\max}(z)$ shrinks to zero as $L^{\alpha_{\text{ring}}}(z)$ with $\alpha_{\text{ring}} = \frac{2-\sigma}{\sigma(d-1)}$, and the blowup rate is $p = \frac{1}{1+\alpha_{\text{ring}}}$. These solutions are analyzed in this chapter.
- (D) The quintic NLS ($\sigma = 2$) admits “critical” standing-ring solutions that collapse with the ψ_F profile where $F = R_{1D}$, at the loglog law blowup rate (Sect. 22.3).
- (E) The super-quintic NLS ($\sigma > 2$) admits “supercritical” standing-ring solutions that collapse with the ψ_F profile where $F = Q_{1D}$, at a square-root blowup rate (Sect. 22.4).

23.9.1 Critical Exponent and Phase Transition

In Fig. 23.9a we plot the blowup-rate exponent p of the width $L(z)$ of ring-type blowup NLS solutions. As σ increases from $\frac{2}{d}$ to $2-$, p increases monotonically from $\frac{1}{2}$ to $1-$. When $\sigma = 2$, the blowup rate is $p = \frac{1}{2}$ with a loglog correction (loglog law). Finally, $p = \frac{1}{2}$ for $\sigma > 2$.

Since

$$\lim_{\sigma \rightarrow 2-} p = 1, \quad \lim_{\sigma \rightarrow 2+} p = \frac{1}{2},$$

the blowup rate has a jump discontinuity at $\sigma = 2$.¹⁶ In addition, the blowup dynamics changes at $\sigma = 2$ from a shrinking ring ($\sigma < 2$) to a standing ring ($\sigma \geq 2$), see Fig. 23.9c.

Conclusion 23.2 *The critical exponent for ring-type blowup in the NLS is $\sigma = 2$.*

To understand why $\sigma = 2$ is a critical exponent, recall that standing-ring solutions are ‘equivalent’ to peak-type solutions of the one-dimensional NLS with the same nonlinearity exponent σ (Sect. 22.2). Since $\sigma = 2$ is the critical exponent for collapse in the one-dimensional NLS, it is also the critical exponent for a standing-ring collapse.

At $\sigma = 2$ ring-type solutions undergo a *phase transition* from collapse at a point (for $\sigma < 2$) to collapse on a sphere (for $\sigma \geq 2$). Consequently, when σ is slightly below 2, the solution initially behaves as a standing ring (i.e., $r_{\max}(z) \approx \text{constant}$). Eventually, however, the solution “remembers” that it “should” collapse at a point, and therefore it shrinks extremely fast, see Fig. 23.2. It is because of this “sudden” change that simulations of shrinking rings are considerably more demanding when σ is slightly below 2. This explains, for example, why in Fig. 23.5 the worst numerical agreement with the theoretical prediction occurs for $\sigma = 1.9$.

¹⁶ In Sect. 10.5 we saw another example where the blowup rate has a discontinuity.

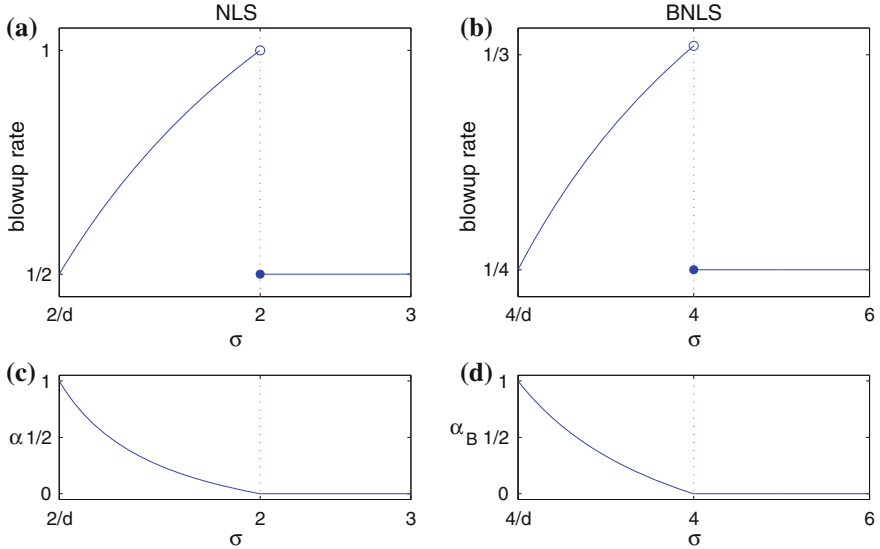


Fig. 23.9 **a** The blowup rate of ring-type blowup NLS solutions increases monotonically from $p = \frac{1}{2}$ at $\sigma = \frac{2}{d}$ to $p = 1-$ at $\sigma = 2-$. For $\sigma = 2$ (full circle) $p = \frac{1}{2}$ (with a loglog correction) and for $\sigma > 2$, $p = \frac{1}{2}$. **b** The blowup rate of ring-type blowup BNLS solutions increases monotonically from $p = \frac{1}{4}$ at $\sigma = \frac{4}{d}$ to $p = \frac{1}{3}-$ at $\sigma = 4-$. For $\sigma = 4$ (full circle) $p = \frac{1}{4}$ (with a loglog correction?) and for $\sigma > 4$, $p = \frac{1}{4}$. **c** The shrinkage parameter α_{ring} of ring-type NLS solutions. For $\frac{2}{d} \leq \sigma < 2$, α_{ring} decreases monotonically from 1 to 0+ (shrinking rings). For $\sigma \geq 2$, $\alpha_{\text{ring}} = 0$ (standing rings). **d** The shrinkage parameter α_B^{ring} of ring-type BNLS solutions. For $\frac{4}{d} \leq \sigma < 4$, α_B^{ring} decreases monotonically from 1 to 0+ (shrinking rings). For $\sigma \geq 4$, $\alpha_B^{\text{ring}} = 0$ (standing rings). From [12]

23.10 Biharmonic NLS

23.10.1 Shrinking-Ring Blowup Solutions (ψ_{S_B})

We briefly discuss shrinking-ring blowup solutions of the supercritical BNLS. See [13] for further details. The BNLS analog of Lemma 23.1 is

Lemma 23.12 ([13]) *Let ψ be a ring-type blowup solution of the radial BNLS*

$$i\psi_z(z, r) - \Delta^2\psi + |\psi|^{2\sigma}\psi = 0, \quad d > 1, \quad \frac{4}{d} < \sigma < 4 \quad (23.35)$$

that undergoes a quasi self-similar collapse with the ψ_{S_B} profile, where¹⁷

¹⁷ Since we do not know the BNLS analog of the quadratic radial phase term $e^{i\frac{L_z}{L} \frac{r^2}{4}}$, we cannot write explicitly the double-phase representation of the ψ_{S_B} profile. Therefore, $S_B(\rho)$ is the BNLS analog of $S(\rho)e^{i\frac{L_z}{4L}(\alpha r^2 + (1-\alpha)(r-r_{\max})^2)}$.

$$\psi_{S_B}(z, r) = \frac{1}{L^{\frac{2}{\sigma}}(z)} S_B(\rho) e^{i\zeta(z)}, \quad (23.36a)$$

$$\rho = \frac{r - r_{\max}(z)}{L(z)}, \quad r_{\max}(z) \sim r_{\max}^0 L^\alpha(z), \quad \zeta(z) = \int_0^z \frac{ds}{L^4(s)}, \quad (23.36b)$$

$\lim_{z \rightarrow Z_c} L(z) = 0$, and $S_B(\rho)$ attains its global maximum at $\rho = 0$. Then

$$\alpha_{\text{ring}}^B \leq \alpha \leq 1, \quad \alpha_{\text{ring}}^B := \frac{4 - \sigma}{\sigma(d - 1)} > 0.$$

Exercise 23.4 Prove Lemma 23.12.

Similarly to the NLS, see Exercise 23.3, ψ_{S_B} undergoes a *strong collapse* if $\alpha = \alpha_{\text{ring}}^B$ and a *weak collapse* if $\alpha > \alpha_{\text{ring}}^B$. Numerical simulations suggest that $\alpha = \alpha_{\text{ring}}^B$, and that the blowup rate of L is

$$L(z) \sim \kappa(Z_c - z)^p, \quad p = \frac{1}{4 - \frac{\sigma d - 4}{\sigma(d - 1)}} = \frac{1}{3 + \alpha_{\text{ring}}^B}. \quad (23.37)$$

Therefore, $0 < \alpha_{\text{ring}}^B < 1$ and $\frac{1}{4} < p < \frac{1}{3}$. Finally, substituting (23.36) and (23.37) in (23.35) shows that the equation for S_B is

$$-S_B(\rho) - i \frac{\left(1 - \alpha_{\text{ring}}^B\right) r_{\max}^0}{3 + \alpha_{\text{ring}}^B} \kappa^{3 + \alpha_{\text{ring}}^B} (S_B)_\rho - (S_B)_{\rho\rho\rho\rho} + |S_B|^{2\sigma} S_B = 0.$$

23.10.2 Classification of Ring-Type Blowup Solutions

Figure 23.10 summarizes the classification of ring-type blowup solutions of the radial BNLS

$$i\psi_z(z, r) - \Delta^2 \psi + |\psi|^{2\sigma} \psi = 0, \quad d > 1.$$

- (A) In the subcritical regime $\sigma < \frac{4}{d}$ there are no blowup solutions.
- (B) In the critical case $\sigma = \frac{4}{d}$, the BNLS admits shrinking-ring solutions that undergo an equal-rate collapse with the ψ_{G_B} profile at a quartic-root blowup rate (Sect. 19.7).
- (C) When $\frac{4}{d} < \sigma < 4$, the BNLS admits shrinking-ring solutions that collapse with the ψ_{S_B} profile, $r_{\max}(z)$ shrinks to zero as $L^{\alpha_{\text{ring}}^B}(z)$ with $\alpha_{\text{ring}}^B = \frac{4 - \sigma}{\sigma(d - 1)}$, and the blowup rate of $L(z)$ is $p = \frac{1}{3 + \alpha_{\text{ring}}^B}$ (Sect. 23.10.1).

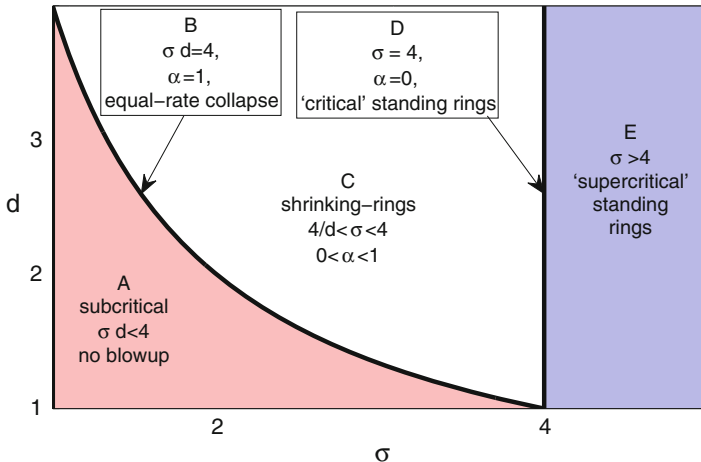


Fig. 23.10 Classification of ring-type blowup solutions of the BNLS

- (D) The BNLS with $\sigma = 4$ admits “critical” standing-ring solutions that collapse with the ψ_{F_B} profile where $F_B = R_{B,1D}$, at a slightly-faster-than-a-quartic-root blowup rate (Lemma 22.2 and [12]).
- (E) The BNLS with $\sigma > 4$ admits “supercritical” standing-ring solutions that collapse with the ψ_{F_B} profile where $F_B = Q_{B,1D}$, at a quartic-root blowup rate (Lemma 22.2 and [12]).

Conclusion 23.3 ([13]) *Up to the change $2 \rightarrow 4$, the classification of ring-type blowup solutions of the BNLS is completely analogous to that of the NLS, cf. Figs. 23.8 and 23.10.*

In particular, BNLS ring-type blowup solutions undergo a phase transition from a shrinking-ring to a standing-ring collapse at the *critical exponent* $\sigma = 4$ (Fig. 23.9d). As a result, the blowup rate has a jump discontinuity at $\sigma = 4$ (Fig. 23.9b).

Part V
NLS in Nonlinear Optics II

Chapter 24

Critical and Threshold Powers for Collapse (P_{cr} and P_{th})

Previously, we saw that a necessary condition for collapse in the critical NLS

$$i\psi_z(z, \mathbf{x}) + \Delta\psi + |\psi|^{\frac{4}{d}}\psi = 0, \quad \psi(0, \mathbf{x}) = \psi_0(\mathbf{x}) \in H^1 \quad (24.1)$$

is that the input power $P = \int |\psi_0|^2 d\mathbf{x}$ is at least the critical power P_{cr} . This condition, however, is not sufficient. Rather, for any profile $f(\mathbf{x}) \in H^1$, there exists a threshold power $P_{\text{th}} = P_{\text{th}}[f]$, generically above P_{cr} , such that all solutions of (24.1) with $\psi_0 = cf(\mathbf{x})$ and power above P_{th} undergo collapse.

The critical power sets a (universal) lower bound on the amount of power that is needed for optical collapse. In contrast, the threshold power sets a (profile-dependent) upper bound on the amount of power that can be propagated in a Kerr medium. This is because above the threshold power, once the beam collapses, its intensity becomes sufficiently high so as to ionize the Kerr medium. Since an ionized medium is not transparent, the beam experiences significant power losses beyond the collapse point.

In this chapter we consider the critical and threshold powers for collapse. We mainly focus on the physical case of the two-dimensional critical NLS

$$i\psi_z(z, x, y) + \Delta\psi + |\psi|^2\psi = 0, \quad \psi(0, x, y) = \psi_0(x, y). \quad (24.2)$$

We do not consider the supercritical NLS, because in that case there is no critical power for collapse (Sect. 5.11.3).¹

¹ There is, however, a critical H^1 -norm for collapse (Theorem 5.9), as well as a profile-dependent threshold power for collapse (Corollary 7.12), in the supercritical NLS.

24.1 Review: P_{cr} , P_{th} , and $P_{\text{sufficient}}$

In Theorem 5.11 we saw that a necessary condition for collapse in the critical NLS (24.1) is

$$P \geq P_{\text{cr}} := \int |R^{(0)}|^2 d\mathbf{x},$$

where $R^{(0)} = R^{(0)}(r)$ is the ground state of

$$R''(r) + \frac{d-1}{r} R' - R + |R|^{\frac{4}{d}} R = 0, \quad R'(0) = 0, \quad R(\infty) = 0,$$

and $r = |\mathbf{x}|$. The critical power P_{cr} is thus equal to the power of $R^{(0)}$. Its value can be calculated analytically when $d = 1$, and numerically in higher dimensions (Sect. 17.7 and Chap. 28).

In the two-dimensional case, $R^{(0)}$ is sometimes called the *Townes profile* (Sect. 3.3.3). It is the positive solution of

$$R''(r) + \frac{1}{r} R' - R + R^3 = 0, \quad R'(0) = 0, \quad R(\infty) = 0,$$

and its power is

$$P_{\text{cr}} = \int |R^{(0)}|^2 dx dy = 2\pi P_{\text{cr}}^{\text{radial}}, \quad P_{\text{cr}}^{\text{radial}} = \int_{r=0}^{\infty} |R^{(0)}|^2 r dr \approx 1.8623.$$

For the critical NLS (24.1) with the one-parameter family of initial conditions $\psi_0 = cf(\mathbf{x})$, the sufficient condition for collapse $H(\psi_0) < 0$ can be written as (Sect. 7.10.1)

$$P > P_{\text{sufficient}}[f] := \left(\left(\frac{2}{d} + 1 \right) \frac{\|f\|_2^{\frac{4}{d}} \|\nabla f\|_2^2}{\|f\|_{\frac{4}{d}+2}^{\frac{4}{d}+2}} \right)^{\frac{d}{2}},$$

where $P = |c|^2 \int |f|^2 d\mathbf{x}$. For example, in the two-dimensional case, this condition reads

$$P > P_{\text{sufficient}}[f] := 2 \frac{\|f\|_2^2 \|\nabla f\|_2^2}{\|f\|_4^4}.$$

Since ψ collapses for $P > P_{\text{sufficient}}[f]$ and exists globally for $P < P_{\text{cr}}$, we have

Lemma 24.1 *For any profile $f \in H^1$, there exists a threshold power $P_{\text{th}} = P_{\text{th}}[f]$, such that the solution of the critical NLS with $\psi_0 = cf(\mathbf{x})$ collapses for any $P > P_{\text{th}}$. Furthermore,*

$$0 < P_{\text{cr}} \leq P_{\text{th}}[f] \leq P_{\text{sufficient}}[f] < \infty.$$

It is tempting to conclude that for any $f \in H^1$, there exists $P_{\text{th}} = P_{\text{th}}[f]$, such that the solution of the critical NLS with $\psi_0 = cf(\mathbf{x})$ exists globally for $0 \leq P < P_{\text{th}}$ and collapses for $P_{\text{th}} < P < \infty$. This, however, is not true. For example, in Sect. 14.3 we saw (numerically) that if $\psi_0 = cR^{(1)}(r)$, ψ collapses for $c = 1 \pm 0.01$ but exists globally for $c = 1$.

In Sect. 7.10.1 we saw that

$$P_{\text{sufficient}}[f] = P_{\text{cr}} \iff f = \mu e^{i\alpha} R^{(0)}(\lambda(\mathbf{x} - \mathbf{x}_0)).$$

Therefore,

$$P_{\text{th}}[R^{(0)}] = P_{\text{cr}}, \quad (24.3)$$

and $P_{\text{sufficient}}[f] > P_{\text{cr}}$ if $f \neq \mu e^{i\alpha} R^{(0)}(\lambda(\mathbf{x} - \mathbf{x}_0))$. We also saw that

$$\lim_{\substack{H^1 \\ f_n \rightarrow R^{(0)}}} P_{\text{th}}[f_n] = P_{\text{cr}}, \quad (24.4)$$

see Exercise 7.6. This limit suggests

Observation 24.1 *Initial profiles which are “closer” to $R^{(0)}$ have lower threshold powers for collapse.*

The limit (24.4) suggests that Observation 24.1 holds for profiles near $R^{(0)}$. In addition, in Sect. 24.3 we will present numerical evidence that Observation 24.1 also holds for profiles which are not close to $R^{(0)}$. Intuitively, the threshold power is higher than P_{cr} , because the collapsing core always leaves behind some power as it approaches the $\psi_{R^{(0)}}$ profile during the initial “reorganization” stage (Sect. 17.3). Therefore, when the initial profile is closer to $R^{(0)}$, the minimal amount of power which has to be left behind is smaller. Hence, the threshold power for collapse is lower.

24.1.1 A Historical Note

In 1964, Chiao, Gamire, and Townes calculated the critical power for self trapping from the condition that the diffraction angle of a uniform beam is equal to the critical angle for total internal reflection (Sect. 3.3.2). This led to the estimate $P_{\text{cr}}^{\text{Chiao, radial}} = \frac{1.22^2 \pi^2}{8} = 1.84$, which (by a pure coincidence) is close to the power of the Townes profile.² A year later, Kelley estimated the critical power for collapse from the condition that the diffraction length is equal to the self-focusing distance, and obtained the estimate $P_{\text{cr}}^{\text{radial}} = \frac{1.22^2 \pi^2}{32} = 0.46$ (Sect. 3.4.2). In his 1975 review paper on self focusing (Sect. 3.7), Marburger gives the value $P_{\text{cr}}^{\text{radial (2)}} = 1.86$, based on numerical simulations.

² See Sect. 24.11 for the relation between the critical powers for collapse and for self-trapping.

For some reason, there has been a persisting confusion in the nonlinear-optics literature regarding the critical power. For example, the 1996 handbook of nonlinear optics lists all the above three values: One for self-trapping, one for “weak self-focusing”, and one for self-focusing. This is wrong; there is a unique critical power P_{cr} , which is the universal lower bound for the threshold power for collapse.

24.2 Dimensional Dependence

In Sect. 1.6 we saw that propagation of linearly-polarized, paraxial, cw laser beams in a Kerr medium is governed by the dimensional NLS

$$2ik_0\psi_z(z, x, y) + \Delta_{x,y}\psi + k_0^2 \frac{4n_2}{n_0} |\psi|^2 \psi = 0, \quad \psi_0(x, y) = A \left(\frac{x}{r_0}, \frac{y}{r_0} \right) e^{ik_0 S(x, y)},$$

where A and S are real, and r_0 is the input-beam width. The dimensional input beam power (in MKS units) is

$$P^{\text{dim}} = 2\epsilon_0 n_0 c \int |\psi_0|^2 dx dy. \quad (24.5)$$

If we change to the dimensionless variables

$$\tilde{x} = \frac{x}{r_0}, \quad \tilde{y} = \frac{y}{r_0}, \quad \tilde{z} = \frac{z}{2L_{\text{diff}}}, \quad \tilde{\psi} = 2k_0 r_0 \sqrt{\frac{n_2}{n_0}} \psi,$$

where $L_{\text{diff}} = k_0 r_0^2$, the resulting dimensionless NLS is

$$i\tilde{\psi}_{\tilde{z}}(\tilde{x}, \tilde{y}, \tilde{z}) + \Delta_{\tilde{x}, \tilde{y}}\tilde{\psi} + |\tilde{\psi}|^2 \tilde{\psi} = 0, \quad \tilde{\psi}_0(\tilde{x}, \tilde{y}) = 2k_0 r_0 \sqrt{\frac{n_2}{n_0}} A(\tilde{x}, \tilde{y}) e^{ik_0 S(r_0 \tilde{x}, r_0 \tilde{y})},$$

and the relation between the dimensional input power P^{dim} and the dimensionless input power $P = \int |\tilde{\psi}_0(\tilde{x}, \tilde{y})|^2 d\tilde{x} d\tilde{y}$ is

$$P^{\text{dim}} = \frac{2\epsilon_0 c n_0^2}{4k_0^2 n_2} P = \frac{\lambda^2 \epsilon_0 c n_0^2}{8\pi^2 n_2} P,$$

where $\lambda = 2\pi/k_0$ is the free-space wavelength. Therefore, we have

Conclusion 24.1 *The relations between the dimensional and dimensionless critical powers and threshold powers are*

$$P_{\text{cr}}^{\text{dim}} = \frac{\lambda^2 \epsilon_0 c n_0^2}{8\pi^2 n_2} P_{\text{cr}}, \quad P_{\text{th}}^{\text{dim}}[f] = \frac{\lambda^2 \epsilon_0 c n_0^2}{8\pi^2 n_2} P_{\text{th}}[f].$$

Thus, the dimensional critical and threshold powers are proportional to the square of the wavelength, and inversely proportional to the Kerr coefficient n_2 . They do not, however, depend on the input-beam width r_0 . As noted in Sect. 3.4.2, this is because if we vary r_0 while keeping the input power unchanged, both diffraction and the Kerr nonlinearity scale as r_0^3 .

Remark The first experimental demonstration that the threshold power is independent of input-beam width was done in 1966 by Wang [267].

24.3 Threshold Power

The threshold power of the Townes profile is $P_{\text{th}}[R^{(0)}] = P_{\text{cr}}$, see (24.3). Unfortunately, there is no analytic method for calculating the threshold power of other profiles. Numerical computations show that P_{th} is 1.8% above P_{cr} for Gaussian profiles and 8.8% above P_{cr} for super-Gaussian profiles (Table 24.1). Such values may lead to the impression that the threshold power of all radial profiles is slightly above P_{cr} . This, however, is not the case. For example, the bottom raw in Table 24.1 shows that $P_{\text{th}} \approx 2.2P_{\text{cr}}$ for $\psi_0 = c \operatorname{sech}(r - 5)$. Intuitively, this threshold power is much higher than P_{cr} , because the collapsing core has to lose a lot of power as it evolves from the initial ring-type profile into the peak-type $R^{(0)}$ profile. Finally, we note that Table 24.1 provides numerical support to Observation 24.1 that initial profiles which are closer to $R^{(0)}$ have lower threshold powers.

24.3.1 Inaccuracy of the Zero-Hamiltonian Condition

Table 24.1 also lists the theoretical lower and upper bounds for P_{th} . Inspection of this data suggests

Table 24.1 The radial threshold power for collapse $P_{\text{th}}^{\text{radial}}[f] := \frac{1}{2\pi} P_{\text{th}}[f]$ in the two-dimensional NLS (24.2) with $\psi_0 = cf(r)$

Initial profile $f(r)$	$P_{\text{th}}^{\text{radial}}[f]$		
	Lower bound	Numerical value	Upper bound $P_{\text{sufficient}}^{\text{radial}}[f]$
$R^{(0)}(r)$	$P_{\text{cr}}^{\text{radial}}$	$P_{\text{cr}}^{\text{radial}}$	$P_{\text{cr}}^{\text{radial}}$
$e^{-\frac{r^2}{2}}$	$P_{\text{cr}}^{\text{radial}}$	1.896	2
$e^{-\frac{r^4}{2}}$	$P_{\text{cr}}^{\text{radial}}$	2.03	$2\sqrt{2}$
$\operatorname{sech}(r - 5)$	$P_{\text{cr}}^{\text{radial}}$	4.04	10.1

Also shown are the theoretical lower bound $P_{\text{cr}}^{\text{radial}} \approx 1.8623$ (left column) and upper bound $P_{\text{sufficient}}^{\text{radial}}[f] := \frac{1}{2\pi} P_{\text{sufficient}}[f]$ (right column). Data in first three rows are from [70]

Observation 24.2 *The upper bound $P_{\text{sufficient}}$ provides a less accurate estimate for P_{th} than the lower bound P_{cr} , i.e.,*

$$P_{\text{th}} - P_{\text{cr}} \ll P_{\text{sufficient}} - P_{\text{th}}.$$

Indeed, even for the ring-type profile $\psi_0 = c \operatorname{sech}(r - 5)$, whose threshold power is more than twice the critical power, $P_{\text{th}}^{\text{radial}} \approx 4.04$ is closer to $P_{\text{cr}}^{\text{radial}} \approx 1.86$ than to $P_{\text{sufficient}}^{\text{radial}} \approx 10.1$.

The upper bound $P_{\text{sufficient}}$ is nothing but the zero-Hamiltonian condition. Therefore, we have

Observation 24.3 *The zero-Hamiltonian condition typically leads to a significant overestimate of the threshold power for collapse.*

Additional numerical support for Observations 24.2 and 24.3 is given in Sects. 24.5, 24.6.2, and 24.7.

24.3.2 Failure of the Aberrationless Approximation

In some studies P_{cr} and P_{th} were estimated theoretically by employing the aberrationless approximation that

$$|\psi| = \frac{1}{L^{\frac{d}{2}}(z)} f \left(\frac{\mathbf{x}}{L(z)} \right), \quad (24.6)$$

i.e., that the solution maintains a self-similar profile.³ Originally, the aberrationless approximation was implemented with a truncated Taylor series expansion (Sect. 3.5). Subsequent studies adopted a *variational method* [55].⁴ Regardless of the specific details, in all these aberrationless approximation methods, one replaces the NLS with a reduced system of ODEs for the solution width $L(z)$. The aberrationless approximation for the critical power is then found from the condition that $L(z)$ goes to zero at a finite propagation distance.⁵

To analyze the error introduced by calculating the critical power with the aberrationless approximation, we note that substituting the aberrationless ansatz (24.6) in

³ For example, in Sect. 3.5 the aberrationless approximation led to estimate $P_{\text{cr}} \approx P_{\text{cr}}^{\text{Akhmanov}}$, see (3.32).

⁴ In the variational method one assumes that the NLS solution maintains a self-similar profile, substitutes this profile into the NLS Lagrangian density, average the Lagrangian over the transverse coordinates, and then computes its variational derivative.

⁵ See, e.g., [49, Eq.(2.9)].

the critical variance identity $V_{zz} = 8H$ gives

$$(L^2)_{zz} = 8 \frac{H(\psi_0)}{V(f)}, \quad (24.7)$$

see (7.4). Equation (24.7) is thus the reduced equation for $L(z)$ under the aberration-less approximation. If the input beam is collimated (i.e., ψ_0 is real) then $L_z(0) = 0$,⁶ and so $L(z)$ goes to zero if and only if $H(\psi_0) < 0$. If the input beam is focused (i.e., $\tilde{\psi}_0 = \psi_0 e^{-i\frac{|\mathbf{x}|^2}{4F}}$), then $L(z)$ goes to zero if and only if $H(|\tilde{\psi}_0|) = H(\psi_0) < 0$, see Sect. 7.5. Therefore, we have

Conclusion 24.2 *Under the aberrationless approximation (24.6), the critical and threshold powers for collapse are approximated by the power of the initial condition $\psi_0 = cf(\mathbf{x})$ that satisfies $H(\psi_0) = 0$,⁷ i.e.,*

$$P_{\text{cr}}^{\text{aberrationless}} = P_{\text{th}}^{\text{aberrationless}} = P_{\text{sufficient}}[f].$$

Since

$$\begin{aligned} P_{\text{cr}}^{\text{aberrationless}} - P_{\text{cr}} &= P_{\text{sufficient}}[f] - P_{\text{cr}} \\ &= \underbrace{P_{\text{sufficient}}[f] - P_{\text{th}}[f]}_{\text{error 1}} + \underbrace{P_{\text{th}}[f] - P_{\text{cr}}}_{\text{error 2}}, \end{aligned}$$

the error of approximating P_{cr} by $P_{\text{cr}}^{\text{aberrationless}}$ is the sum of the following two positive errors:

1. The error $P_{\text{sufficient}}[f] - P_{\text{th}}[f]$ of over-estimating the threshold power with the zero-Hamiltonian condition.
2. The error $P_{\text{th}}[f] - P_{\text{cr}}$ of over-estimating the critical power with the threshold power. The magnitude of this error depends on how far f is from $R^{(0)}$, see Observation 24.1.

Note that by Observation 24.2, the first error is typically much larger than the second.

In conclusion, from Observation 24.3 and Conclusion 24.2 follows

Observation 24.4 *The aberrationless approximation typically leads to a significant overestimate of the critical power.*

⁶ See Conclusion 2.9

⁷ Note that $f(\mathbf{x})$ is real, see (24.6).

24.4 Biharmonic NLS

The critical power for collapse in the critical BNLS

$$i\psi_z(z, \mathbf{x}) - \Delta^2\psi + |\psi|^{\frac{8}{d}}\psi = 0, \quad \psi(0, \mathbf{x}) = \psi_0(\mathbf{x}) \in H^2 \quad (24.8)$$

is $P_{\text{cr}}^B = \int |R_B^{(0)}|^2 d\mathbf{x}$, where $R_B^{(0)}$ is the ground state of

$$-\Delta^2 R_B - R_B + |R_B|^{\frac{8}{d}} R_B = 0.$$

Numerical calculation of $R_B^{(0)}$, see Sect. 28.4, yields

$$P_{\text{cr}}^B(d=1) = \int_{-\infty}^{\infty} |R_B^{(0)}(x)|^2 dx \approx 2.9868,$$

$$P_{\text{cr}}^B(d=2) = \int_{-\infty}^{\infty} \int_{-\infty}^{\infty} |R_B^{(0)}(x, y)|^2 dx dy \approx 13.143,$$

$$P_{\text{cr}}^B(d=3) = \int_{-\infty}^{\infty} \int_{-\infty}^{\infty} \int_{-\infty}^{\infty} |R_B^{(0)}(x_1, x_2, x_3)|^2 dx_1 dx_2 dx_3 \approx 44.88,$$

see [14, 82]. Simulations of (24.8) suggest that, as in the critical NLS, the threshold power for collapse P_{th}^B is slightly above P_{cr}^B for peak-type solutions. For example, in one dimension $1.003P_{\text{cr}}^B \leq P_{\text{th}}^B[e^{-x^2}] \leq 1.004P_{\text{cr}}^B$, $1.01P_{\text{cr}}^B \leq P_{\text{th}}^B[\text{sech}(x)] \leq 1.02P_{\text{cr}}^B$, and $1.005P_{\text{cr}}^B \leq P_{\text{th}}^B[\frac{1}{1+x^4}] \leq 1.01P_{\text{cr}}^B$ [82].

24.5 Bounded Domains (Hollow-Core Fibers)

In Sect. 16.1 we saw that propagation of intense laser beams in hollow-core fibers can be modeled by the two-dimensional cubic NLS on a bounded domain Ω . In Theorem 16.4 we saw that the critical power for collapse on a bounded domain is equal to the free-space critical power P_{cr} . The negative Hamiltonian condition for blowup (which leads to the upper bound $P_{\text{sufficient}}$) is also the same as in free space (Lemma 16.18). Therefore, we have

Lemma 24.2 *Let ψ be the solution of the d -dimensional critical NLS (16.2) on a bounded domain Ω with $\psi_0 = cf(\mathbf{x}) \in H_0^1(\Omega)$. Then the threshold power for collapse $P_{\text{th}}[f]$ is bounded from below and from above as follows:*

$$P_{\text{cr}} \leq P_{\text{th}}[f] \leq P_{\text{sufficient}}[f] := \left(\left(\frac{2}{d} + 1 \right) \frac{\|f\|_{L^2(\Omega)}^{\frac{4}{d}} \|\nabla f\|_{L^2(\Omega)}^2}{\|f\|_{L^{\frac{4}{d}+2}(\Omega)}^{\frac{4}{d}+2}} \right)^{\frac{d}{2}}.$$

Table 24.2 Same as Table 24.1 on the bounded domain $B_1 := \{0 \leq r \leq 1\}$

Initial profile $f(r)$	$P_{\text{th}}^{\text{radial}}[f]$		
	Lower bound	Numerical value	Upper bound $P_{\text{sufficient}}^{\text{radial}}[f]$
$J_0(k_1 r)$	$P_{\text{cr}}^{\text{radial}}$	$P_{\text{cr}}^{\text{radial}}$	2.76
$\cos(\pi r/2)$	$P_{\text{cr}}^{\text{radial}}$	$P_{\text{cr}}^{\text{radial}}$	2.99
$1 - r^2$	$P_{\text{cr}}^{\text{radial}}$	$P_{\text{cr}}^{\text{radial}}$	3.33
$\sin(\pi r)$	$P_{\text{cr}}^{\text{radial}}$	$P_{\text{cr}}^{\text{radial}}$	6.58

Here $k_1 \approx 2.405$. From [70]

In [70], Fibich and Gaeta computed $P_{\text{th}}[f]$ numerically for the two-dimensional critical NLS on the unit disc B_1 with various profiles $f \in H_0^1(B_1)$, see Table 24.2. Unlike in free space (Sect. 24.3), the value of P_{th} was found to be *equal* to P_{cr} for “all” profiles. Similar numerical results were obtained in [89].

Observation 24.5 ([70, 89]) *The threshold power for collapse P_{th} on a bounded domain is generically equal to the lower bound P_{cr} . In other words, the condition $P > P_{\text{cr}}$ is generically sufficient for collapse.*

The “disclaimer” *generically* is needed because Observation 24.5 does not hold for all solutions. For example, the power of the bounded-domain solitary waves $\psi_\omega^{\text{solitary}} = e^{i\omega z} Q_\omega^{(n)}(\mathbf{x})$ is strictly above P_{cr} when $n \geq 1$ and ω is sufficiently large (Sect. 16.4.8). Since solitary waves exist globally, Observation 24.5 does not hold for high-power excited solitary waves. Note, however, that these “counterexamples” are unstable (Sect. 16.5.5).

Remark The result of Observation 24.5 is different from the free-space case, where generically $P_{\text{th}} > P_{\text{cr}}$. As noted in Sect. 16.8.2, the reason for this difference is that the reflecting boundaries prevent the collapsing core from losing power to the background.

Remark Since on bounded domains generically $P_{\text{th}} = P_{\text{cr}}$, the upper bound $P_{\text{sufficient}}$ leads to an even larger overestimate of the threshold power on bounded domains than in free space.

24.6 Elliptic Input Beams

The effect of input-beam ellipticity on the self-focusing dynamics was first considered in 1972 by Giuliano et al. [113]. They analyzed the two-dimensional NLS (24.2) with the elliptic Gaussian initial conditions

$$\psi_0(x, y) = \frac{c}{\sqrt{a_0 b_0}} e^{-\left(\frac{x}{a_0}\right)^2 - \left(\frac{y}{b_0}\right)^2},$$

where a_0 and b_0 are the initial widths in the x - and y -directions, respectively. By making the aberrationless approximation that the beam maintains an elliptic Gaussian profile during its propagation. i.e.,

$$|\psi|^2 = \frac{c^2}{a(z)b(z)} e^{-\left(\frac{x}{a(z)}\right)^2 - \left(\frac{y}{b(z)}\right)^2}, \quad (24.9)$$

where $a(0) = a_0$ and $b(0) = b_0$, they reduced the NLS to a system of two coupled ODEs for $a(z)$ and $b(z)$. Based on this reduced system, they predicted that the threshold power for collapse increases with input-beam ellipticity as

$$P_{\text{th}}(e) = h(e) P_{\text{th}}[e^{-r^2}], \quad h(e) = \frac{e + e^{-1}}{2}, \quad e = \frac{b_0}{a_0}, \quad (24.10)$$

where $P_{\text{th}}[e^{-r^2}] = P_{\text{th}}(e = 1)$ is the threshold power of a circular Gaussian.

In what follows we show that relation (24.10) is qualitatively correct, in the sense that P_{th} indeed increases with e . Relation (24.10) is quantitatively inaccurate, however, because it is based on the aberrationless approximation (Observation 24.4).

24.6.1 Lower and Upper Bounds

The lower and upper bounds for the threshold power for collapse of elliptic initial conditions were determined by Fibich and Ilan:

Lemma 24.3 ([75]) *The threshold power for collapse in the two-dimensional NLS (24.2) of the elliptic initial conditions*

$$\psi_0(x, y) = cf\left(\sqrt{\frac{x^2}{a_0^2} + \frac{y^2}{b_0^2}}\right) \in H^1 \quad (24.11)$$

is bounded from below and from above by

$$P_{\text{cr}} \leq P_{\text{th}}\left[f\left(\sqrt{\frac{x^2}{a_0^2} + \frac{y^2}{b_0^2}}\right)\right] \leq h(e) P_{\text{sufficient}}[f(r)].$$

Proof By Theorem 5.11, the lower bound is equal to P_{cr} . The upper bound is derived in Exercise 24.1. \square

Exercise 24.1 Show that

1. The elliptic initial condition (24.11) satisfies the sufficient condition for blowup $H < 0$ if $|c|^2 > \left(\frac{1}{a_0^2} + \frac{1}{b_0^2}\right) \frac{\int |\nabla f|^2 dx dy}{\int |f|^4 dx dy}$.

2. This inequality can be written as $P > P_{\text{sufficient}} \left[f \left(\sqrt{\frac{x^2}{a_0^2} + \frac{y^2}{b_0^2}} \right) \right]$, where

$$P_{\text{sufficient}} \left[f \left(\sqrt{\frac{x^2}{a_0^2} + \frac{y^2}{b_0^2}} \right) \right] = h(e) P_{\text{sufficient}}[f(r)]. \quad (24.12)$$

Comparison of (24.12) with (24.10) shows that, as noted in Conclusion 24.2, under the aberrationless approximation, P_{th} is approximated by $P_{\text{sufficient}}$.

24.6.2 Threshold Power

The threshold power for collapse of elliptic Gaussian, super-Gaussian, and Townesian initial conditions was computed by Fibich and Ilan [75]. This calculation suggested that the relative increase in the threshold power due to input-beam ellipticity can be approximated by, see Fig. 24.1,

$$\frac{P_{\text{th}}(e) - P_{\text{th}}[f(r)]}{P_{\text{th}}[f(r)]} \approx 0.4(h(e) - 1). \quad (24.13)$$

Here, the values of $P_{\text{th}}[f(r)] = P_{\text{th}}(e = 1)$ are $1.018P_{\text{cr}}$, $1.088P_{\text{cr}}$, and P_{cr} , respectively (Sect. 24.3). Intuitively, P_{th} increases with e because the more elliptic the input beam, the more power the collapsing core has to lose as it evolves into the radial $\psi_{R^{(0)}}$ profile.

By (24.13), the relative increase in P_{th} is $0.4(h(e) - 1)$, rather than the aberrationless-approximation prediction of $h(e) - 1$, see (24.10).

Observation 24.6 ([75]) *The increase of the threshold power for collapse due to input-beam ellipticity is only 40% of the aberrationless-approximation prediction (24.10).*

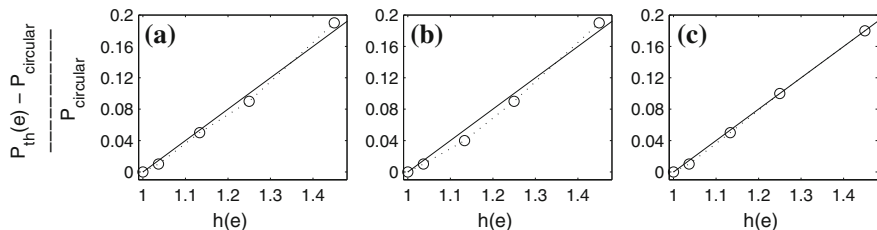


Fig. 24.1 Relative increase of the threshold power for collapse in the two-dimensional NLS (24.2) due to input-beam ellipticity [circles and dotted curve] is well approximated with $0.4(h(e) - 1)$ [solid line]. Initial profiles are: **a** $\psi_0 = ce^{-s^2}$, **b** $\psi_0 = ce^{-s^4}$, and **c** $\psi_0 = cR^{(0)}(s)$, where $s = \sqrt{\frac{x^2}{a_0^2} + \frac{y^2}{b_0^2}}$ and $e = \frac{b_0}{a_0}$. From [75]

This shows again that the zero-Hamiltonian condition leads to inaccurate predictions for the threshold power.

In [58], Diubietis et al. observed experimentally that the threshold power for filamentation increases with input-beam ellipticity (Sect. 25.3.2). Since the threshold power for filamentation is roughly the same as for collapse (Sect. 24.11), that study provided an *experimental confirmation that P_{th} increases with e* .

24.7 Vortex Beams

In Chap. 15 we studied collapsing vortex solutions of the two-dimensional critical NLS (24.2). We now consider the critical and threshold powers for collapse of radial vortex initial conditions $\psi_0 = e^{im\theta} A_0(r)$. In Theorem 15.1 we saw that a necessary condition for collapse is

$$P \geq P_{\text{cr}}(m) = 2\pi P_{\text{cr}}^{\text{radial}}(m), \quad P_{\text{cr}}^{\text{radial}}(m) := \int_0^\infty |R_m^{(0)}|^2 r dr,$$

where $R_m^{(0)}$ is the ground state of

$$R_m''(r) + \frac{1}{r} R_m' - \left(1 + \frac{m^2}{r^2}\right) R_m + |R_m|^2 R_m = 0.$$

We also saw that $P_{\text{cr}}^{\text{radial}}(m)$ increases with m , and that $P_{\text{cr}}^{\text{radial}}(m) \approx 4\sqrt{3}m$.

In [71], Fibich and Gavish analyzed the threshold power for collapse of vortex ring-type profiles, as follows. Let

$$\psi_0 = cf(r)e^{im\theta}, \quad f(r) = Q(\rho), \quad \rho = \frac{r - r_{\max}}{L},$$

where $Q(\rho)$ attains its global maximum at $\rho = 0$ and decreases monotonically with $|\rho|$. Motivated by the vortex-free case (Observation 24.1), we can expect that the closer f is to a dilated ground state $R_m^{(0)}(cr)$, the closer $P_{\text{th}}[f]$ is to its lower bound $P_{\text{cr}}(m)$, and so the lower $P_{\text{th}}[f]$ is.⁸ Now, a ring profile f is characterized by its width L and radius r_{\max} (Fig. 22.1). By (15.28), the radius and width of $R_m^{(0)}(cr)$ satisfy $r_{\max} \approx \frac{\sqrt{2}m}{c}$ and $L \approx \frac{1}{c}\sqrt{\frac{2}{3}}$. We can always choose c so that $R_m^{(0)}(cr)$ has either the same radius or the same width as $f(r)$. We cannot, however, choose c so

⁸ As in the vortex-free case, the only minimal-power vortex blowup solutions [i.e., vortex blowup solutions with $P = P_{\text{cr}}(m)$] are the explicit solutions $\psi_{R_m^{(0)}}^{\text{explicit}}$ (Sect. 15.5.1).

Table 24.3 Numerically-calculated values of $\frac{P_{\text{th}}[\psi_0] - P_{\text{cr}}(m)}{P_{\text{cr}}(m)}$

m	Input beams		
	$\psi_0^{\text{LG}}(\%)$	$\psi_0^{\text{sech}}(\%)$	$\psi_0^{\text{modified sech}}(\%)$
1	0.65	20	0.13
2	0.80	4.5	0.91
3	7	1.9	0.71
4	11	2.9	0.32
5	14	9	0.17
6	19	14	0.34

From [71]

that $R_m^{(0)}(cr)$ has the same radius and the same width as $f(r)$. Therefore, since the one-parameter family $\{R_m^{(0)}(cr)\}_{0 < c < \infty}$ is characterized by

$$\frac{\text{radius}}{\text{width}} \approx \sqrt{3}m, \quad (24.14)$$

we can use this relation to estimate the “distance” between a ring profile $f(r)$ and $\{R_m^{(0)}(cr)\}_{0 < c < \infty}$.

To illustrate this, Table 24.3 lists the excess power of P_{th} above $P_{\text{cr}}(m)$ for several vortex ring-type profiles. Consider first the Laguerre-Gaussian profiles $\psi_0^{\text{LG}} = cr^m e^{-r^2} e^{im\theta}$, which are the vortex modes of the linear Schrödinger equation. The maximum of ψ_0^{LG} is attained at $r_{\max} = \sqrt{\frac{m}{2}}$. Therefore, these modes are characterized by $\frac{\text{radius}}{\text{width}} \approx \sqrt{\frac{m}{2}}$. This ratio is closest to relation (24.14) for $m = \frac{1}{6}$, explaining why $\frac{P_{\text{th}}(m)}{P_{\text{cr}}(m)}$ is minimal at $m = 1$. The sech-ring input profile $\psi_0^{\text{sech}} = cr^2 \text{sech}(r - 5)e^{im\theta}$ is characterized by $\frac{\text{radius}}{\text{width}} = 5$. This ratio is closest to relation (24.14) for $m = \frac{5}{\sqrt{3}} \approx 2.9$, explaining why $\frac{P_{\text{th}}(m)}{P_{\text{cr}}(m)}$ is minimal for $m = 3$. Finally, for the “modified sech” profiles $\psi_0^{\text{modified sech}} = cr^2 \text{sech}(r - \sqrt{3}m)e^{im\theta}$, which were constructed so that they satisfy relation (24.14), the threshold powers are less than 1% above $P_{\text{cr}}(m)$ for $1 \leq m \leq 6$.

In [146], Kruglov et al. estimated the (radial) critical power for vortex collapse as

$$P_{\text{cr}}^{\text{Kruglov, radial}}(m) = \frac{2^{2m+1} m!(m+1)!}{(2m)!}. \quad (24.15)$$

This estimate was derived by assuming that the solution maintains a self-similar Laguerre-Gaussian profile. By Conclusion 24.2, under this aberrationless approximation P_{cr} is approximated by $P_{\text{sufficient}}[\psi_0^{\text{LG}}]$, as is confirmed directly in the following exercise:

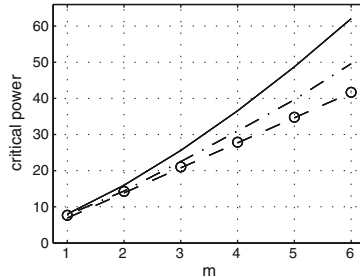


Fig. 24.2 Critical power $P_{\text{cr}}^{\text{radial}}(m) = \int_0^\infty |R_m^{(0)}|^2 r dr$ (o), the approximation $4\sqrt{3}m$ (dashed line), the threshold power of the Laguerre-Gaussian modes ($P_{\text{th}}^{\text{radial}}[\psi_0^{\text{LG}}]$, dash-dotted line), and the aberrationless estimate $P_{\text{cr}}^{\text{Kruglov, radial}}(m)$ (solid line). From [71]

Exercise 24.2 Verify that $P_{\text{sufficient}}^{\text{radial}}[\psi_0^{\text{LG}}] = \frac{2^{2m+1}m!(m+1)!}{(2m)!}$.

While the aberrationless estimate (24.15) captures the increase of the critical power with m , it is quantitatively inaccurate (Fig. 24.2). In fact, even the threshold power of the Laguerre-Gaussian modes is closer to $P_{\text{cr}}(m)$ than to $P_{\text{cr}}^{\text{aberrationless}}(m)$, in agreement with Observation 24.2. We thus see once more that the aberrationless approximation leads to a significant overestimate of the critical power (Observation 24.4).

24.7.1 Effect of Symmetry Breaking

In Sect. 24.6 we saw that deviations from radial symmetry increase the threshold power for collapse of non-vortex initial conditions. For vortex initial conditions, however, deviations from radial symmetry *decrease* the threshold power for collapse. This is because radial vortex solutions have to collapse with the $R_m^{(0)}$ profile, whereas non-radial vortex solutions can collapse with the lower-power $R^{(0)}$ profile. See Sect. 15.4.1 for more details.

24.8 Circular, Radial, and Azimuthal Polarizations

In this section we consider the critical power of input beams that are not linearly polarized. Let ψ_\pm denote the amplitudes of the circular components $\hat{e}_\pm = \frac{\hat{e}_x \pm i\hat{e}_y}{\sqrt{2}}$. The equation for each circular component is⁹

$$i \frac{\partial \psi_\pm}{\partial z}(z, x, y) + \Delta \psi_\pm + \frac{2}{3} \left[|\psi_\pm|^2 + 2|\psi_\mp|^2 \right] \psi_\pm = 0.$$

⁹ See [80] and the references therein for self-focusing of circularly-polarized beams.

If $\psi_- \equiv 0$ (a circular polarization state), this equation reduces to

$$i \frac{\partial \psi_+}{\partial z} + \Delta \psi_+ + \frac{2}{3} |\psi_+|^2 \psi_+ = 0. \quad (24.16)$$

Because the Kerr effect is weaker by a factor of $\frac{2}{3}$ compared with the linear polarization state, see (24.2), the critical power for collapse of circularly-polarized beams is larger by $\frac{3}{2}$, i.e.,¹⁰

$$P_{\text{cr}}^{\text{circular pol.}} = \frac{3}{2} P_{\text{cr}}.$$

Similarly, the critical power of circularly-polarized vortex beams [i.e., $\psi_- \equiv 0$ and $\psi_+ = e^{im\theta} A(z, r)$] is

$$P_{\text{cr}}^{\text{circular pol.}}(m) = \frac{3}{2} P_{\text{cr}}(m).$$

Next, we consider the cases of radial and azimuthal polarizations,

$$\psi^{\text{radial pol.}} = A(z, r)[e^{i\theta} \hat{e}_- + e^{-i\theta} \hat{e}_+], \quad \psi^{\text{azim. pol.}} = A(z, r)[e^{i\theta} \hat{e}_- - e^{-i\theta} \hat{e}_+].$$

Because \hat{e}_{\pm} are orthogonal to each other, $|\psi|^2 = |\psi_+|^2 + |\psi_-|^2$. Since, in addition, $|\psi_+| = |\psi_-| = |A|$, the equation for each component is

$$i \frac{\partial \psi_{\pm}}{\partial z} + \Delta \psi_{\pm} + 2|\psi_{\pm}|^2 \psi_{\pm} = 0, \quad \psi_{\pm}(0, r, \theta) = A(0, r)e^{\pm i\theta}.$$

Therefore, the Kerr effect is twice as strong as in the linear polarization state. Hence, $P_{\text{cr}}(\psi_+) = P_{\text{cr}}(\psi_-) = \frac{1}{2} P_{\text{cr}}(m = 1)$. Finally, since the power of $\psi^{\text{azim. pol.}}$ and of $\psi^{\text{radial pol.}}$ is the sum of the powers of ψ_+ and ψ_- , we have that [71]

$$P_{\text{cr}}^{\text{radial pol.}} = P_{\text{cr}}^{\text{azim. pol.}} = P_{\text{cr}}(\psi_+) + P_{\text{cr}}(\psi_-) = P_{\text{cr}}(m = 1) \approx 4.12 P_{\text{cr}},$$

where the value of $P_{\text{cr}}(m = 1)$ is taken from Table 15.4.

24.9 Interpretation of the Ratio P/P_{cr}

The critical power P_{cr} is the minimal power required for the focusing nonlinearity to balance diffraction. Indeed, all solutions with power below P_{cr} scatter as $z \rightarrow \infty$ (Sect. 8.4.7), and there exists a solution whose power is exactly P_{cr} , the ground-state solitary wave $\psi^{\text{solitary},(0)} = e^{iz} R^{(0)}(r)$, for which nonlinearity balances diffraction.

¹⁰ This follows from the observation that if ψ is a solution of the NLS (24.2), then $\psi_+(z, x, y) = \sqrt{\frac{3}{2}} \psi(z, x, y)$ is a solution of the NLS (24.16).

Conclusion 24.3 In the critical NLS, the ratio P/P_{cr} is a measure of the “nonlinearity level” of the propagation.¹¹

Specifically,

- When $P \approx P_{\text{cr}}$, the magnitudes of nonlinearity and diffraction are comparable. Hence, the propagation is nonlinear.
- When $P \ll P_{\text{cr}}$, diffraction dominates over nonlinearity. Hence, the propagation is linear or weakly nonlinear.
- When $P \gg P_{\text{cr}}$, nonlinearity dominates over diffraction. Hence, the propagation is strongly nonlinear.¹²

The above characterization holds for collimated peak-type input beams, such as Gaussians or super-Gaussians. There are cases, however, for which this characterization fails. For example, if the initial condition consists of numerous well-separated low-power input beams, the propagation is weakly nonlinear even if the total power P is $\gg P_{\text{cr}}$. Another example is provided by ring-type initial conditions. Because their threshold power is well above P_{cr} (Sect. 24.3), propagation of ring-type initial conditions with $P \approx P_{\text{cr}}$ is weakly nonlinear. Finally, the initial dynamics of beams with $P \gg P_{\text{cr}}$ is weakly nonlinear if they are focused by a sufficiently strong lens or phase mask (Sect. 25.3.4). Therefore, a more reliable measure for the “nonlinearity level” is provided by the ratio $\frac{[|\psi|^{\frac{4}{d}}\psi]}{[\Delta\psi]}$.

24.10 Local Nature of the Critical Power

The NLS (24.1) is invariant under spatial translations $\mathbf{x} \rightarrow \mathbf{x} - \mathbf{x}_0$. Therefore, the critical power for collapse is independent of the transverse location \mathbf{x}_c at which the solution collapses. When translation invariance is lost, however, the critical power can depend on \mathbf{x}_c . For example, consider the inhomogeneous critical NLS

$$i\psi_z(z, \mathbf{x}) + \Delta\psi + \eta(\mathbf{x})|\psi|^{\frac{4}{d}}\psi = 0, \quad (24.17)$$

which models the propagation of laser beams in an inhomogeneous medium in which the linear index of refraction is constant, but the nonlinear index of refraction depends on the transverse coordinate.¹³ Assume that a solution of (24.17) collapses at \mathbf{x}_c . Intuitively, as the collapsing core concentrates at \mathbf{x}_c , its dynamics is effectively governed by the homogeneous critical NLS

$$i\psi_z(z, \mathbf{x}) + \Delta\psi + \eta(\mathbf{x}_c)|\psi|^{\frac{4}{d}}\psi = 0.$$

¹¹ This characterization is analogous to the one in Sect. 3.1.2.

¹² This high-power regime is analyzed in Chap. 26.

¹³ Self-focusing in the inhomogeneous critical NLS (24.17) was studied in [96, 99, 177].

By Theorem 5.6, the critical power for collapse in this equation is $\eta^{-\frac{d}{2}}(\mathbf{x}_c)P_{\text{cr}}$. Hence, the critical power for collapse at \mathbf{x}_c in the inhomogeneous critical NLS (24.17) depends on $\eta(\mathbf{x}_c)$.

More generally, the concentration of the collapsing core suggests

Conclusion 24.4 *The critical power for collapse at \mathbf{x}_c depends on the “local conditions” near \mathbf{x}_c .*

Conclusion 24.4 explains why the critical power for collapse on a bounded domain is the same as in free space (Sect. 16.7), and also why the critical power of vortex solutions is $P_{\text{cr}}(m)$ for solutions that collapse at the phase singularity (Theorem 15.1), but P_{cr} for those collapsing elsewhere (Sect. 15.4.1).

24.11 Critical and Threshold Powers for Self Trapping

Self-trapping (*filamentation*) refers to the situation where after a laser beam collapses, it continues to propagate in a tightly-focused state over a long distance. In Sect. 9.4.2 we saw that the solitary waves of the critical NLS are unstable, so that once perturbed, they either collapse or scatter. Hence, there is no self-trapping in the critical NLS model.

Self-trapping becomes possible if one adds a dispersive collapse-arresting mechanism, such as a saturating nonlinearity (Sect. 32.5) or nonparaxiality (Sect. 34.3). To be self-trapped, a laser beam should first undergo collapse. Therefore, the threshold power for filamentation of $\psi_0 = cf(\mathbf{x})$, denoted by $P_{\text{th}}^{\text{filamentation}}[f]$, is at least the threshold power for collapse $P_{\text{th}}[f]$. In fact, $P_{\text{th}}^{\text{filamentation}}[f]$ is somewhat higher than $P_{\text{th}}[f]$, since after the arrest of collapse, the high-intensity core of a self-trapped beam undergoes focusing-defocusing oscillations (Sect. 31.5.2), during which it loses some power to the background [164, 259]. Moreover, as the high-intensity core defocuses, it needs some “extra power” above P_{cr} in order to refocus, because the Kerr nonlinearity has to overcome the combined effects of diffraction and linear defocusing.¹⁴

Motivated by the definition of the critical power for collapse, we can define the *critical power for filamentation* $P_{\text{cr}}^{\text{filamentation}}$ as the minimal power required for self trapping, i.e., $P_{\text{cr}}^{\text{filamentation}} := \inf_{f \in H^1} P_{\text{th}}^{\text{filamentation}}[f]$.

Conclusion 24.5 *Consider a perturbed critical NLS model that admits self-trapping. Then the critical power for filamentation is equal to the critical power for collapse, i.e., $P_{\text{cr}}^{\text{filamentation}} = P_{\text{cr}}$.*

Proof We give a very informal proof. Denote by $P(\omega)$ the power of the ground-state solitary wave $\psi_\omega^{\text{solitary},(0)} = e^{i\omega z} R_\omega^{(\epsilon)}(\mathbf{x})$ of the perturbed NLS. Because solitary waves are self-trapped, $P_{\text{cr}}^{\text{filamentation}} \leq P(\omega)$ for any ω . We will show

¹⁴ We encountered a similar situation in Conclusion 3.4 and the subsequent remark.

below that $\inf_{\omega} P(\omega) = P_{\text{cr}}$. Therefore, $P_{\text{cr}}^{\text{filamentation}} \leq P_{\text{cr}}$. In addition, since $P_{\text{th}}^{\text{filamentation}}[f] \geq P_{\text{th}}[f] \geq P_{\text{cr}}$, it follows that $P_{\text{cr}}^{\text{filamentation}} := \inf_f P_{\text{th}}^{\text{filamentation}}[f] \geq P_{\text{cr}}$. Therefore, $P_{\text{cr}}^{\text{filamentation}} = P_{\text{cr}}$.

To prove that $\inf_{\omega} P(\omega) = P_{\text{cr}}$, we first note that $P(\omega) > P_{\text{cr}}$, because in addition to diffraction, the nonlinearity should also balance the collapse-arresting mechanism. To proceed, we consider the saturated NLS

$$i\psi_z(z, x, y) + \Delta_{x,y}\psi + |\psi|^2\psi - \epsilon|\psi|^4\psi = 0,$$

which provides a phenomenological model for self-trapping (Sect. 32.5). In this case, $R_{\omega}^{(\epsilon)}$ is the ground state of

$$\Delta R_{\omega} - \omega R_{\omega} + |R_{\omega}|^2 R_{\omega} - \epsilon|R_{\omega}|^4 R_{\omega} = 0.$$

Now, $R_{\omega}^{(\epsilon)}(r) = \omega^{\frac{1}{2}} R^{(\epsilon\omega)}(\omega^{\frac{1}{2}}r)$, where $R^{(\epsilon\omega)} := R_1^{(\epsilon\omega)}$ is the ground state of

$$\Delta R - R + |R|^2 R - \epsilon\omega|R|^4 R = 0.$$

By continuity, $R^{(\epsilon\omega)}$ approaches the Townes profile $R^{(0)}$ as $\epsilon\omega \rightarrow 0$. Therefore, for any fixed ϵ ,

$$\int |R_{\omega}^{(\epsilon)}|^2 dx dy = \int |R^{(\epsilon\omega)}|^2 dx dy \rightarrow \int |R^{(0)}|^2 dx dy, \quad \omega \rightarrow 0.$$

Hence, $\inf_{\omega} P(\omega) = P_{\text{cr}}$. □

Intuitively, the critical powers for collapse and for self-trapping are the same, because both correspond to the borderline case where nonlinearity and diffraction are exactly balanced.

Chapter 25

Multiple Filamentation

In Sect. 3.6 we presented the first studies on multiple filamentation. Briefly, in 1965 Pilipetskii and Rustamov [209] observed experimentally that when the power of a collapsing laser beam was several critical powers, it sometimes broke up into several long and narrow filaments, a phenomenon which has been called *multiple filamentation, beam breakup, or small-scale self-focusing*. Because multiple filamentation represents a complete breakup of radial symmetry, it has to be initiated by a symmetry-breaking mechanism. In 1966, Bespalov and Talanov [27] suggested that the symmetry-breaking mechanism that leads to multiple filamentation is input-beam noise. For many years, this has been the only theoretical explanation for multiple filamentation.

25.1 Validity of Bespalov-Talanov Analysis

Let $\psi^{\text{PW}} := \alpha e^{i\alpha^2 z}$ be a plane-wave solution of the NLS

$$i\psi_z(z, x, y) + \Delta\psi + |\psi|^2\psi = 0, \quad \psi(0, x, y) = \psi_0(x, y). \quad (25.1)$$

Bespalov and Talanov showed that (Sect. 3.6.3):

1. ψ^{PW} is linearly unstable.
2. The characteristic distance of this *modulational instability* (L_{MI}) scales as α^{-2} .

Then, with a “leap of faith”, they concluded from this that:

1. Input-beam noise leads to multiple filamentation of laser beams.
2. The characteristic distance for multiple filamentation of laser beams (L_{MF}) scales as $1/P$, where P is the input power.

The validity of these two conclusions was not clear, since unlike plane waves, physical laser beams have a finite power. Moreover, because plane waves have no transverse dynamics, the instabilities can grow while the leading-order solution ψ^{PW} remains unchanged. In contrast, collapsing laser beams undergo transverse changes, which are unaccounted for in the Bespalov-Talanov analysis. One could argue that because $\psi_0^{\text{PW}} \equiv \alpha$ is the zeroth-order Taylor approximation of $\psi_0 = \alpha e^{-r^2}$ near $r = 0$, $\psi^{\text{PW}} = \alpha e^{i\alpha^2 z}$ is the leading-order approximation of the NLS solution with $\psi_0 = \alpha e^{-r^2}$. The validity of this argument, however, is not clear.

When the validity of an informal analysis is not clear, the natural thing to do is to test it numerically. Specifically, in the case of the Bespalov-Talanov analysis, this means solving the NLS (25.1) with a noisy high-power initial condition, and checking whether the solution indeed breaks up into multiple filaments. This numerical test could not be done in the 1960s, because it requires solving the NLS numerically without imposing radial symmetry. At that time, even solving the radial NLS was quite demanding. Numerical simulations of nonradial NLS solutions became possible in the late 1970s. For example, in 1979 Konno and Suzuki [142] solved numerically the *saturated NLS*¹

$$i\psi_z(z, x, y) + \Delta\psi + \frac{|\psi|^2\psi}{1 + \epsilon_{\text{sat}}|\psi|^2} = 0, \quad 0 < \epsilon_{\text{sat}} \ll 1 \quad (25.2)$$

without imposing radial symmetry, and observed that in some simulations, solutions with radial initial conditions underwent multiple filamentation (Sect. 25.2). For some reason, however, in the twenty years that followed, the Bespalov-Talanov prediction that high-power noisy solutions of the *unperturbed* NLS (25.1) undergo multiple filamentation was not tested numerically. One can only speculate as to why this numerical test was not done. One possibility is that by the time such simulations became possible, the Bespalov-Talanov explanation for multiple filamentation was widely believed to be true. Another possibility is that the addition of nonlinear saturation was seen as a technical issue, and therefore simulations such as those of Konno and Suzuki were viewed as numerical confirmations of the Bespalov-Talanov analysis.²

25.1.1 Threshold Power for a Bespalov-Talanov Multiple Filamentation ($P_{\text{th}}^{\text{MF}}$)

The first numerical test of the Bespalov-Talanov explanation for multiple filamentation of laser beams was done in 2001 by Fibich and Ilan [76]. In that study, we solved the NLS (25.1) with the noisy high-power initial conditions

¹ This equation is analyzed in Sects. 32.4 and 32.5.

² Which they are not, see Sects. 25.2 and 25.5.

$$\psi_0(x, y) = c_1 e^{-x^2-y^2} [1 + c_2 \cdot \text{rand}(x, y)], \quad (25.3)$$

where $\text{rand}(x, y)$ is a random complex function, and c_1 and c_2 determine the power and noise levels, respectively. In these simulations the solution always collapsed at a single point with a radial blowup profile (see, e.g., Fig. 14.6b). Moreover, the collapse dynamics, with and without noise, was nearly the same (Fig. 14.7). Since these simulations were conducted with high-power initial conditions (e.g., $P = 15P_{\text{cr}}$), they suggested that input-beam noise does not lead to multiple filamentation in the NLS (25.1), and therefore that the Bespalov-Talanov explanation for multiple filamentation is incorrect.

In 2005, Fibich et al. [68] observed numerically that noise can lead to multiple filamentation of collapsing solutions of (25.1), but only at much higher powers, typically above $100P_{\text{cr}}$. For example, Fig. 25.2 shows three solutions of (25.1) that have the same initial noise realization but different powers.³ The spatial profile of the beams, just as they begin to collapse, shows a single filament for $P = 20P_{\text{cr}}$, the emergence of additional small filaments for $P = 40P_{\text{cr}}$, and numerous filaments for $P = 150P_{\text{cr}}$. Thus, the same noise realization does not have a destabilizing effect at $P = 20P_{\text{cr}}$, but leads to multiple filamentation at $P = 150P_{\text{cr}}$. This result was surprising, since both solutions are in the high-power regime $P \gg P_{\text{cr}}$.⁴

The explanation of this result is that *the dynamics of noisy high-power solutions depends on the competition between the clean selffocusing dynamics and modulation instability* [68]. Thus, when the self-focusing distance L_{SF} is much smaller than the modulational-instability distance L_{MI} , the instabilities do not have enough distance to grow. Therefore, noise remains small, and the solution collapses as a single filament. When $L_{\text{SF}} \gg L_{\text{MI}}$, however, the instabilities grow before the solution begins to self-focus.⁵ Therefore, the solution develops minor spikes. Since spikes have a higher index of refraction, they attract power from their neighborhoods. As a result, they further increase and evolve into filaments.⁶

Let $P_{\text{th}}^{\text{MF}}$ denote the power at which $L_{\text{MI}} = L_{\text{SF}}$. By (3.38),

$$L_{\text{MI}} \sim P^{-1}, \quad P \gg P_{\text{cr}}.$$

In addition, by (3.21),⁷

$$L_{\text{SF}} \sim P^{-\frac{1}{2}}, \quad P \gg P_{\text{cr}}.$$

³ i.e., the three initial conditions only differ in the value of c_1 in (25.3).

⁴ Moreover, in the high-power regime the self-focusing dynamics is, up to dilations, independent of P (Corollary 26.1).

⁵ In this case the solution initially “behaves like a plane wave”, in the sense that it only undergoes self-phase modulations (Sect. 26.1).

⁶ The growth of a spike can be seen in Fig. 22.9.

⁷ This also follows from Conclusion 26.2 with $\sigma = 1$.

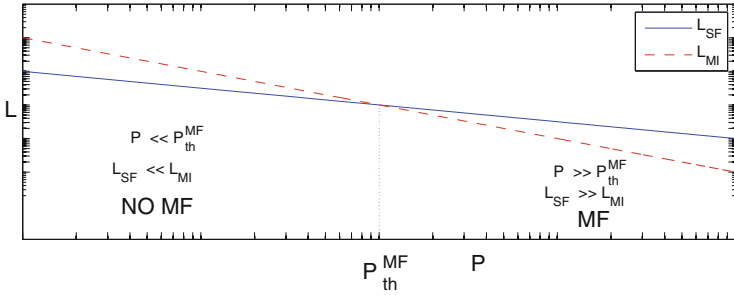


Fig. 25.1 A Bespalov-Talanov type multiple filamentation (MF) occurs in the very high-power regime $P \gg P_{\text{th}}^{\text{MF}}$, but not in the high-power regime $P_{\text{cr}} \ll P \ll P_{\text{th}}^{\text{MF}}$. Plot is on a loglog scale

Hence,

$$\begin{cases} L_{\text{SF}} \ll L_{\text{MI}}, & \text{if } P \ll P_{\text{th}}^{\text{MF}}, \\ L_{\text{SF}} \gg L_{\text{MI}}, & \text{if } P \gg P_{\text{th}}^{\text{MF}}, \end{cases}$$

see Fig. 25.1. At present, there is no analytic estimate for $P_{\text{th}}^{\text{MF}}$.⁸ Informal arguments and numerical simulations suggests that it is on the order of $100P_{\text{cr}}$ [68].

Conclusion 25.1 Let ψ be a solution of the NLS (25.1) with a noisy initial condition, such that in the absence of noise the solution collapses at a single point with the $\psi_{R^{(0)}}$ profile. Then there exists a threshold power $P_{\text{th}}^{\text{MF}}$, which is on the order of $100P_{\text{cr}}$, such that

1. If $P \ll P_{\text{th}}^{\text{MF}}$, the effect of noise remains small. Therefore, the solution collapses at a single point with the $\psi_{R^{(0)}}$ profile.
2. If $P \gg P_{\text{th}}^{\text{MF}}$, the solution breaks up into multiple filaments as it collapses.

Remark In Sect. 27.2.3 we will use the same arguments to show that the collapse distance scales as

$$Z_c \sim \begin{cases} P^{-\frac{1}{2}}, & \text{if } P_{\text{cr}} \ll P \ll P_{\text{th}}^{\text{MF}}, \\ P^{-1}, & \text{if } P \gg P_{\text{th}}^{\text{MF}}. \end{cases} \quad (25.4)$$

Remark Noisy beams with $P \ll P_{\text{th}}^{\text{MF}}$ can also undergo multiple filamentation because of input-beam noise. In that case, however, the multiple filamentation process is very different. In particular, it requires the presence of an additional collapse-arresting mechanism, and it only occurs *after* collapse has been arrested. See Sects. 25.2 and 25.5 for more details.

Remark In the simulation of the NLS (25.1) with $P = 150P_{\text{cr}}$ in Fig. 25.2, one of the spikes ultimately collapses before all others. Therefore, the NLS solution

⁸ This threshold power is not universal (i.e., $P_{\text{th}}^{\text{MF}}$ depends on the initial profile).

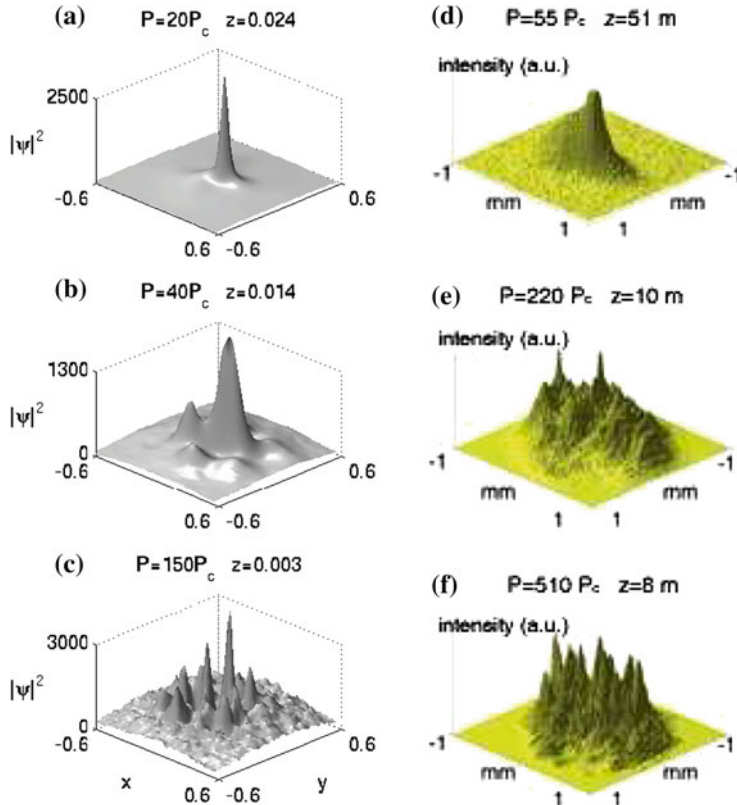


Fig. 25.2 Left (numerical) simulations of the NLS (25.1) with the Gaussian initial condition (25.3) with 10% frozen noise, for **a** $P = 20P_{\text{cr}}$, **b** $40P_{\text{cr}}$, **c** $150P_{\text{cr}}$. Plots show the spatial intensity profile just as the solution begins to collapse (at $z = 0.024, 0.014$, and 0.003 , respectively). Right (experimental) spatial profile of pulses that propagate in air, just as they begin to collapse. Pulse power and collapse distance are: **d** $P = 55P_{\text{cr}}$, $z = 51 \text{ m}$. **e** $P = 220P_{\text{cr}}$, $z = 10 \text{ m}$. **f** $P = 510P_{\text{cr}}$, $z = 8 \text{ m}$. Note the qualitative similarity between the two columns. From [68]

collapses at a single point. Physically, however, the collapse of this spike will be arrested by some mechanism which is neglected in (25.1). Subsequently, some of the other spikes will collapse at longer propagation distances. Therefore, the physical solution that corresponds to this simulation undergoes multiple filamentation, in the sense that it collapses at $k > 1$ transverse locations $\left\{ \mathbf{x}_c^{(j)} \right\}_{j=1}^k$ and axial distances $\left\{ Z_c^{(j)} \right\}_{j=1}^k$. See also Sect. 13.4 on the difference between the number of collapse points from a mathematical and a physical perspective, and Chap. 38 on continuations of NLS solutions beyond the singularity.

25.1.2 Experiments

In Fig. 27.3 we will present experimental results on the collapse distance of high-power pulses in air [68]. Roughly speaking, in these experiments the collapse distance scaled as $P^{-\frac{1}{2}}$ in the high-power regime $P_{\text{cr}} \ll P \ll P_{\text{th}}^{\text{MF}}$ and as P^{-1} in the very high-power regime $P \gg P_{\text{th}}^{\text{MF}}$, in agreement with (25.4). In these experiments, the pulse spatial profile, just as it began to collapse, always consisted of a single filament in the $P^{-\frac{1}{2}}$ regime, and of multiple filaments in the P^{-1} regime (Fig. 25.2d–f). Therefore, these experimental results confirm that a pre-collapse multiple filamentation goes hand-in-hand with a P^{-1} collapse.

25.2 Noise and Saturated Nonlinearities

In 1968, Marburger and Dawes solved numerically the saturated NLS (25.2) with clean high-power Gaussian input beams [166]. They observed that the numerical solution did not collapse, but rather oscillated between a focused peak profile and a defocused ring profile. Marburger and Dawes noted that because a ring profile is azimuthally unstable, it breaks up into multiple filaments. Such a beam breakup could not be observed in their simulations, however, because they used a radial code.

In 1979, Konno and Suzuki [142] solved the saturated NLS (25.2) on a Cartesian grid in the (x, y) -plane. In some of their simulations, solutions with radial initial conditions underwent multiple filamentation. Because radial symmetry is preserved by NLS solutions (Lemma 5.5), however, the multiple filamentation observed in their simulations was a numerical artifact, probably due to the preferred directions that are induced by the Cartesian discretization (Sect. 30.2).

In 1991–2, Soto-Crespo et al. pointed out that the transition from radial symmetry to multiple filamentation in the saturated NLS (25.2) is associated with the appearance of a ring profile as the solution defocuses [244, 245]. They developed an asymptotic method, the Approximate Modulational Instability (AMI) method, for analyzing the modulational instability of stationary rings.⁹ This method also provided a theoretical estimate for the fastest-growing unstable azimuthal mode $e^{ik\theta}$, hence for the expected number of spikes (filaments).

In Fig. 25.3 we solve the saturated NLS (25.2) with the high-power noisy input beam (25.3) with $P \approx 15P_{\text{cr}}$. After the arrest of collapse, the high-intensity core oscillates between a focused peak profile and a defocused ring profile. Because of input-beam noise, the rings have some imperfections. As a result, after several focusing-defocusing cycles, the solution breaks up into three filaments.¹⁰ Note that in

⁹ This method is used in the proof of Lemma 15.31. An extension of this method to collapsing rings is used in the proof of Lemma 11.10.

¹⁰ The symmetry-breaking mechanism that leads to multiple filamentation can also be deterministic (e.g., input-beam ellipticity [58, Fig. 4]).

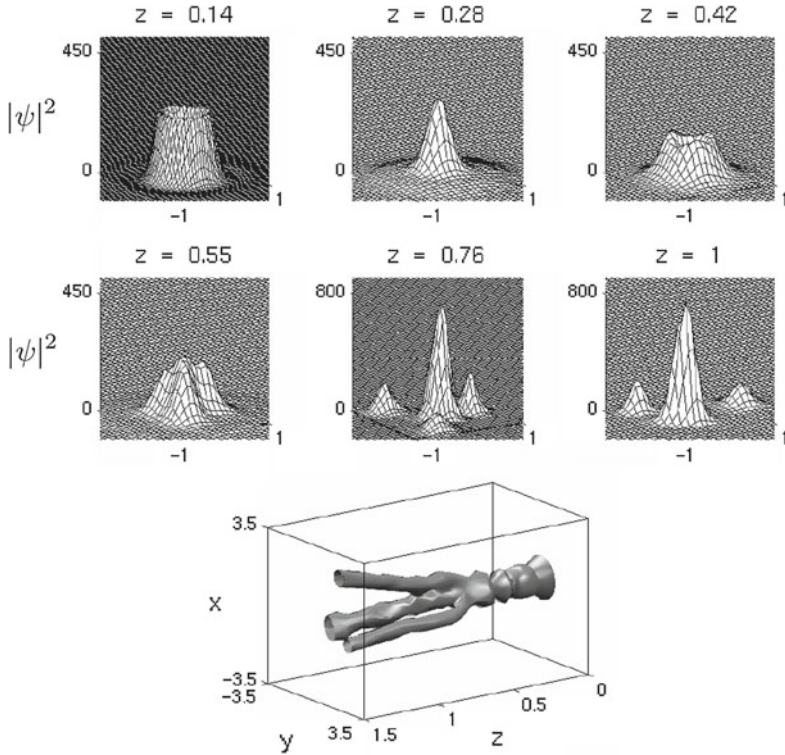


Fig. 25.3 *Top* Solution of the saturated NLS (25.2) with $\epsilon_{\text{sat}} \approx 0.0144$, for the noisy input beam (25.3) with $P \approx 15P_{\text{cr}}$ and noise level $c_2 = 2\%$. *Bottom* Iso-intensity surface plot of the solution. The beam propagates from right to left. From [76]

In this simulation the solution does not undergo multiple filamentation during the initial collapse, but only after collapse was arrested. Therefore, this noise-induced multiple filamentation is not of a Bespalov-Talanov type,¹¹ but is rather of a post-collapse, ring-breakup type. See Sect. 25.5 for further discussion.

25.3 Deterministic Multiple Filamentation

As noted, for many years the only explanation for multiple filamentation was that it is initiated by input beam noise. Since noise is, by definition, random, the resulting multiple filamentation patterns are different from shot to shot. In particular, the number and location of the filaments are unpredictable. This constituted a serious drawback

¹¹ This is to be expected, since $P = 15P_{\text{cr}} \ll P_{\text{th}}^{\text{MF}}$, see Conclusion 25.1.

in applications that required a precise localization. Therefore, it was desirable to find a way to control the multiple filamentation process.

25.3.1 Vectorial Effects

In 2001 Fibich and Ilan suggested that multiple filamentation can also be induced by the polarization state of linearly-polarized input beams. Because linear polarization breaks up radial symmetry in a deterministic way, the resulting multiple filamentation pattern is deterministic.

To see that, recall that the NLS (25.1) is “only” the leading-order model for propagation of linearly-polarized beams in a Kerr medium. A more comprehensive model is the *vectorial nonlinear Helmholtz equation* (NLH)

$$\left\{ \begin{array}{l} \Delta_{x,y,z}\vec{\mathcal{E}} - \vec{\nabla}(\nabla \cdot \vec{\mathcal{E}}) + k_0^2 \vec{\mathcal{E}} = -\frac{k_0^2}{\epsilon_0 n_0^2} \vec{\mathcal{P}}_{\text{NL}}, \\ \nabla \cdot \vec{\mathcal{E}} = -\frac{1}{\epsilon_0 n_0^2} \nabla \cdot \vec{\mathcal{P}}_{\text{NL}}, \end{array} \right. \quad (25.5a)$$

where $\vec{\mathcal{E}} = (\mathcal{E}_1, \mathcal{E}_2, \mathcal{E}_3)$ is the electric field, $\Delta_{x,y,z} = \frac{\partial^2}{\partial x^2} + \frac{\partial^2}{\partial y^2} + \frac{\partial^2}{\partial z^2}$, and

$$\vec{\mathcal{P}}_{\text{NL}} = \frac{4\epsilon_0 n_0 n_2}{1+\gamma} \left[(\vec{\mathcal{E}} \cdot \vec{\mathcal{E}}^*) \vec{\mathcal{E}} + \gamma (\vec{\mathcal{E}} \cdot \vec{\mathcal{E}}) \vec{\mathcal{E}}^* \right], \quad (25.5b)$$

is the nonlinear-polarization field (Sect. 1.4.4). Let us consider a linearly-polarized input beam

$$\vec{\mathcal{E}}^{\text{input}} = \left(\mathcal{E}_1^{\text{input}}, 0, 0 \right) \quad (25.6)$$

that impinges on the Kerr-medium interface at $z = 0$. In the vectorial NLH (25.5), such an input beam breaks up radial symmetry by inducing a preferred direction in the transverse (x, y) -plane; the direction of linear polarization. In [76, 77] Fibich and Ilan asked whether this symmetry breakup can lead to a deterministic multiple filamentation. Testing this question numerically requires solving the vectorial NLH (25.5) without imposing radial symmetry and for input powers well above P_{cr} . Even solving the scalar NLH with radial symmetry and for input powers slightly above P_{cr} , however, is still a challenge (Sect. 34.8). Therefore, in [76, 77] we first used a systematic asymptotic analysis to approximate (25.5) by the following perturbed scalar NLS for A_1 , the rescaled amplitude of \mathcal{E}_1 :

$$\begin{aligned} & iA_{1,z}(z, x, y) + \Delta_{x,y}A_1 + |A_1|^2 A_1 \\ &= -f^2 \left[\frac{1}{4}A_{1,zz} + \frac{4+6\gamma}{1+\gamma} |A_{1,x}|^2 A_1 + (A_{1,x})^2 A_1^* \right. \\ & \quad \left. + \frac{1+2\gamma}{1+\gamma} \left(|A_1|^2 A_{1,xx} + A_1^2 A_{1,xx}^* \right) \right]. \end{aligned} \quad (25.7)$$

Here, $f = \frac{1}{r_0 k_0}$ is the small nonparaxiality parameter (Sect. 2.12), $A_{1,zz}$ accounts for nonparaxial effects, and the remaining $O(f^2)$ terms represent the leading-order effect of the vectorial coupling between \mathcal{E}_1 and \mathcal{E}_3 .¹² As expected, these terms are anisotropic, and they preserve the preferred direction induced by the linear-polarization state of the input beam (25.6).

Figure 25.4 shows the numerical solution of (25.7) with a clean Gaussian input beam with $P = 5P_{\text{cr}}$.¹³ As the beam propagates, it goes through the following stages: (i) self-focusing to a peak profile, (ii) defocusing to a ring profile with two minor bumps, (iii) second self-focusing to a peak, (iv) defocusing of central peak and emergence of two side-filaments, (v) decay of the central filament and self-focusing of the two side filaments. The two side filaments propagate forward in the z -direction while moving away from each other at a constant velocity along the direction of the initial linear polarization.

The multiple filamentation in Fig. 25.4 is deterministic. Intuitively, it occurs because after the arrest of collapse, the solution defocuses into a ring profile, which is unstable under the anisotropic vectorial effects. This multiple filamentation process is thus qualitatively similar to the noise-induced multiple filamentation in the saturated NLS (Sect. 25.2). In particular, it occurs after collapse was arrested. In other simulations of (25.7) the solution broke into two filaments along the direction perpendicular to that of the initial linear polarization, into four side filaments, or into a central filament and four side filaments [77]. These simulations thus showed that, in theory, vectorial effects can lead to deterministic multiple filamentation.

To determine whether in a specific experiment multiple filamentation is initiated by vectorial effects, Fibich and Ilan noted that from all the mechanisms that are neglected in the derivation of the NLS from Maxwell's equations, vectorial effects is the only one that breaks up radial symmetry by inducing a preferred direction in the transverse plane, which is that of the initial linear-polarization state. Therefore, if multiple filamentation is initiated by vectorial effects,

1. The filamentation pattern should be deterministic (i.e., reproducible shot to shot).
2. If the direction of linear polarization of the input beam is rotated in the transverse plane, the multiple filamentation pattern should follow the same rotation.
3. When a beam splits into two filaments, the splitting should occur either in the direction of initial polarization or in the perpendicular direction.¹⁴

¹² The effect of the coupling between \mathcal{E}_1 and \mathcal{E}_2 is only $O(f^4)$ [76].

¹³ To solve (25.7) as an initial value problem, $A_{1,zz}$ was replaced with an $O(f^2)$ “equivalent” term, see (34.9).

¹⁴ In two dimensions, whenever there is a preferred direction, the perpendicular direction is also a preferred direction.

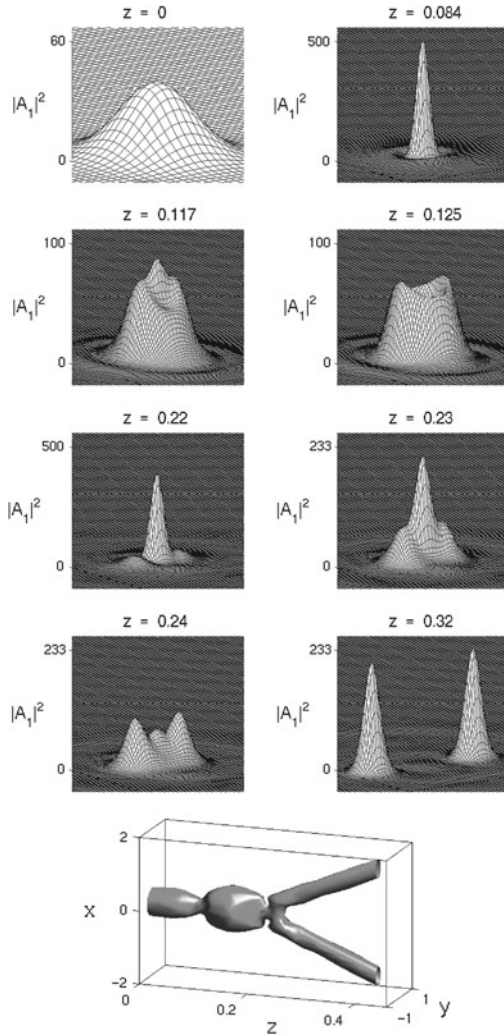


Fig. 25.4 *Top* Solution of (25.7) with $f = 0.025$, $\gamma = 0.5$, and the clean input beam $A_1(z = 0, x, y) = 2\sqrt{5P_{\text{cr}}}e^{-(x^2+y^2)}$. *Bottom* Isosurface plot. From [77]

In [58] Dubietis et al. carried out self-focusing experiments in water in which the multiple filamentation patterns were deterministic (Sect. 25.3.2). When, however, we rotated the direction of linear polarization of the input beam, this had no effect on the orientation of the multiple filamentation pattern. Similar results were later obtained by Grow and Gaeta in multiple filamentation experiments in glass [120]. Therefore, in those two studies multiple filamentation was deterministic, yet it was not induced by vectorial effects.

So far, there has been no experimental evidence of multiple filamentation induced by vectorial effects. This is probably because for vectorial effects to be sufficiently strong so as to lead to multiple filamentation, the beam radius should narrow down to a wavelength scale. For example, in the simulation of Fig. 25.4, before the beam breaks into two filaments, it narrows down to a two-wavelengths radius. In experiments, however, self-focusing is typically arrested at a much earlier stage by plasma effects. For example, in the experiments of Dubietis et al. the wavelength was $\approx 0.5 \mu\text{m}$, and the diameters of the filaments were $\approx 20 \mu\text{m}$. Therefore, vectorial effects were too weak to lead to multiple filamentation.

In retrospect, the main contribution of the 2001 studies of Fibich and Ilan was the suggestion that deterministic multiple filamentation is possible. Whether there exists a physical setup in which vectorial effects lead to multiple filamentation is still an open question.

25.3.2 *Elliptic (Astigmatic) Input Beams*

In 1991 Grantham et al. [115] predicted theoretically and observed experimentally (for laser pulses that propagated in sodium vapor) that input-beam astigmatism can lead to a deterministic multiple filamentation pattern.¹⁵ Unfortunately, this study was for the most part unnoticed by the “multiple filamentation community”, probably because it presented the results in the context of “bifurcations of optical transverse solitary waves”, and did not mention its implications to multiple filamentation.¹⁶

In 2002–3, Fibich and Ilan [78, 80] showed numerically that deterministic multiple filamentation can be induced by input-beam ellipticity, by solving the vectorial NLH (25.5) for clean circularly-polarized¹⁷ elliptic Gaussian input beams

$A_+(z = 0, x, y) = ce^{-\frac{x^2}{a_0^2} - \frac{y^2}{b_0^2}}$. In these simulations, collapse was arrested by vectorial effects and nonparaxiality. Subsequently, the solutions oscillated between a focused peak profile and a defocused ring profile. The radial symmetry of the ring was broken by input-beam ellipticity,¹⁸ which induced two preferred directions: the directions of the ellipse major and minor axes. As a result, when the input beam was sufficiently powerful and sufficiently elliptic, the solution underwent a deterministic post-collapse ring-breakup multiple filamentation.

In 2004, Dubietis et al. [58] showed experimentally that deterministic multiple filamentation can be induced by input-beam ellipticity. Figure 25.5 shows the filamentation pattern of a laser pulse after propagation through a 31 mm water cell,

¹⁵ In Sect. 14.5 we presented experimental results of astigmatic input beams that collapsed with a single filament that had a circular profile. The experiments of Grantham et al., however, were carried out at much higher powers.

¹⁶ This is illustrated by the fact that this study did not even reference the Bespalov-Talanov paper!

¹⁷ See Sect. 24.8 and [80] for self-focusing of circularly-polarized beams.

¹⁸ A circular polarization state does not break the radial symmetry of the input beam. Therefore, it cannot induce a deterministic multiple filamentation [78, 80].

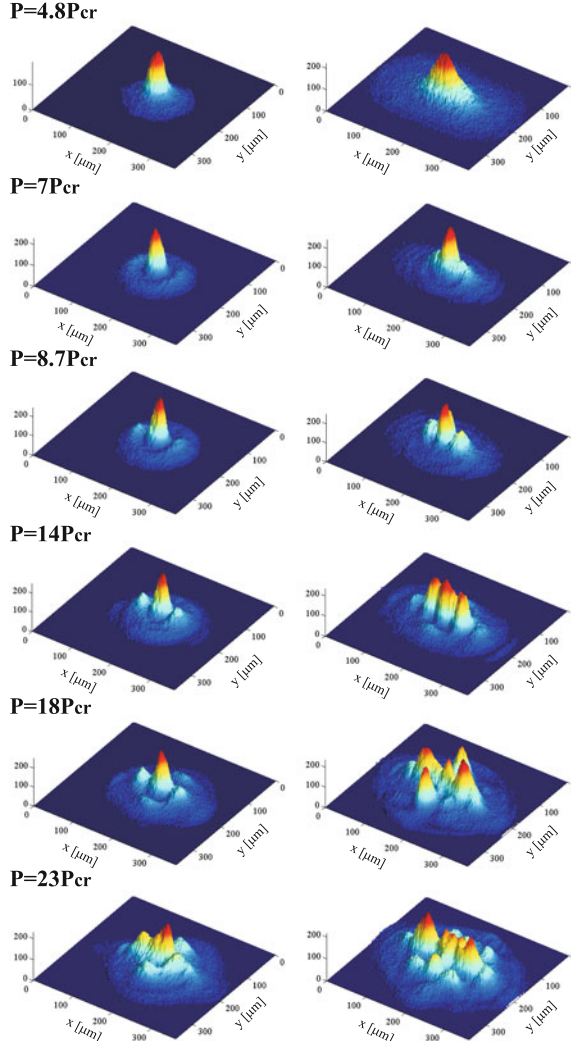


Fig. 25.5 (Experimental) filamentation patterns after propagation through a 31 mm water cell, for a nearly-circular ($e = 1.09$, left panel) and elliptic ($e = 2.2$, right panel) input beams, at various input powers. The major axis of the ellipse lies along the x -axis of the plots. Adapted from [58]

for a nearly-circular input beam ($e = 1.09$) and for an elliptic one ($e = 2.2$), where $e := b_0/a_0$. The experimental results show that:

1. At powers moderately above the threshold for multiple filamentation, in addition to the central filament, there are two filaments along the major axis of the ellipse. At higher powers, additional filaments in the perpendicular direction

emerge. At even higher powers ($P = 23P_{\text{cr}}$), one can observe a quadruple of filaments along the bisectors of the major and minor axes.

2. The multiple filamentation patterns in Fig. 25.5 were reproducible shot to shot. Therefore, they were not induced by random noise.
3. The threshold power for multiple filamentation is much smaller for the elliptic beam.
4. Whereas ellipticity decreases the threshold power for multiple filamentation, it increases the threshold power for filamentation (i.e., for the formation of a single filament). Indeed, the threshold powers for observing a single filament at $z = 31$ mm were $4.9P_{\text{cr}}$ and $6P_{\text{cr}}$ for the nearly-circular and elliptic beams, respectively. This 20% increase is in reasonable agreement with the theoretical prediction of a 13% increase in the threshold power for collapse due to input-beam ellipticity.¹⁹
5. The number of filaments increases with input power.
6. The filaments in Fig. 25.5 consist of a central filament, pairs located symmetrically along the major and/or minor axis, and/or quadruples located symmetrically along the bisectors of the major and minor axes.

The last observation is a consequence of a symmetry argument:

Lemma 25.1 ([58]) *In an isotropic propagation model, any multiple filamentation pattern which is induced by input-beam ellipticity can only consist of a combination of*

1. *A single on-axis filament.*
2. *Pairs of identical filaments located along the ellipse major axis at $(\pm x_{\text{fil}}, 0)$.*
3. *Pairs of identical filaments located along the minor axis at $(0, \pm y_{\text{fil}})$.*
4. *Quadruples of filaments located at $(\pm x_{\text{fil}}, \pm y_{\text{fil}})$.*

These four possibilities are shown in Fig. 25.6 in blue, red, yellow, and green, respectively.

Proof When the propagation model is isotropic, the symmetry breaking induced by input-beam ellipticity preserves the symmetries $x \rightarrow -x$ and $y \rightarrow -y$ (Corollary 5.9). Therefore, the filamentation pattern has to preserve these two symmetries. \square

¹⁹ Indeed, by (24.13),

$$\frac{P_{\text{th}}(e) - P_{\text{th}}[f(r)]}{P_{\text{th}}[f(r)]} \approx 0.4 \left(\frac{e + e^{-1}}{2} - 1 \right) \approx \begin{cases} 0.15\%, & \text{if } e = 1.09, \\ 13\%, & \text{if } e = 2.2. \end{cases}$$

Therefore,

$$\frac{P_{\text{th}}(e = 2.2) - P_{\text{th}}(e = 1.09)}{P_{\text{th}}(e = 1.09)} \approx 13\%.$$

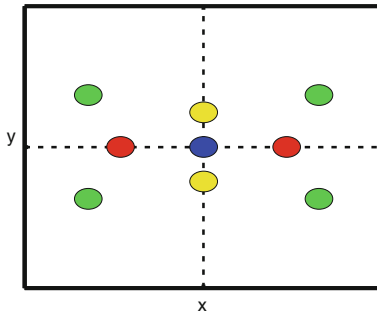


Fig. 25.6 The four possible types of multiple filaments induced by input-beam ellipticity

In another experiment, Dubietis et al. [58] rotated the ellipse in the transverse plane. The multiple filamentation pattern did not change, but simply rotated with the ellipse orientation. This further confirmed that in these experiments multiple filamentation was induced by input-beam ellipticity.

In Sect. 25.3.1 we saw that vectorial effects can also lead to deterministic multiple filamentation. In that case, however, the orientation of the filamentation pattern is determined by the direction of linear polarization. To confirm that this is not the case, we rotated the direction of linear polarization of the input beam, and observed that this rotation had no effect on the orientation of the multiple filamentation pattern [58].

To theoretically show that the multiple filamentation patterns in Fig. 25.5 could be induced by ellipticity, we solved the saturated NLS (25.2) with clean elliptic Gaussian initial conditions. The addition of nonlinear saturation was phenomenological, and was done in order to arrest collapse and lead to filamentation (Chap. 32). In these simulations, all four types of multiple filaments listed in Lemma 25.1 were observed.

The above experimental, analytic, and numerical results lead to

Conclusion 25.2 *Multiple filamentation which is induced by input-beam ellipticity (astigmatism) is a generic process that does not depend on the specific optical properties of the medium (air, water, silica, etc.), on the collapse-arresting mechanism, or on pulse duration.*

Remark Similar results were later obtained by Grow and Gaeta for laser pulses that propagated in glass [120]. They also observed experimentally and numerically that highly-elliptic ($e \gg 1$) input pulses can breakup into a line (or several lines) of filaments that are parallel to the ellipse major axis.

Remark Input-beam ellipticity can also lead to multiple filamentation of ring-type solutions (Figs. 22.10 and 23.7).

25.3.3 Tilted Lens Setup

Once it became clear that a deterministic breakup of input-beam symmetry can lead to a deterministic multiple filamentation, other approaches for controlling the multiple filamentation process were proposed. For example, Fibich et al. [69], and independently Méchain et al. [172], showed that multiple filamentation can be controlled with a tilted lens. In this approach a lens is placed on a rotating holder, so that the angle ϕ between the normal to the lens surface and the beam's direction of propagation can be continuously varied, thereby providing a smooth control of the “astigmatism level”.

In [69], we launched 200 fs input pulses with power $65.5 \text{ GW} \approx 20P_{\text{cr}}$ that propagated in air. The input-pulse spatial profile was noisy and elliptic ($e \approx 2.3$), and it varied considerably between shots (Fig. 25.7). Initially, the lens was set in the “traditional way”, i.e., perpendicular to the pulse direction of propagation ($\phi = 0^\circ$). The typical filamentation pattern consisted of a strong central filament with two additional weaker filaments along the ellipse minor axis (Fig. 25.8, top-left). Averaging over 1,000 shots (Fig. 25.8, top-right) showed that the central and lower filaments were stable, but that the upper filament sometimes disappeared or merged with the central one. It is remarkable that despite the high noise level, the filamentation pattern was quite stable. This shows that the filamentation pattern was predominantly determined by input-beam astigmatism. Indeed, the filamentation pattern is very close to the theoretical prediction for elliptic initial conditions (Lemma 25.1).

When we rotated the lens by $\phi = 5^\circ$, the two side filaments moved further away from the central one along the minor axis (Fig. 25.8, second line). Upon further rotation to $\phi = 10^\circ$ (third line), the two filaments along the minor axis disappeared. Instead, two strong filaments appeared along the major axis, and the central filament became weaker than the side ones. The left filament was stronger than the right one, but both were quite stable. Finally, at $\phi = 20^\circ$ (fourth line) we observed a single filament, which was highly stable in space.

A well-known difficulty in experiments with high-power lasers is that the transverse location of the filaments can change from shot to shot, due to the random nature of the noise that leads to multiple filamentation. Our results show that large astigmatism can remedy this problem. Indeed, even in the traditional setup ($\phi = 0^\circ$), astigmatism leads to a stable pattern in which the standard deviation of the location

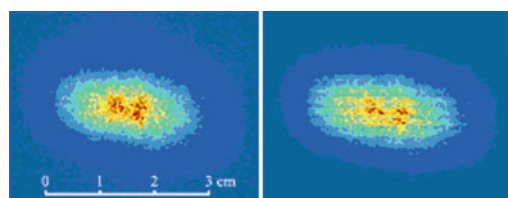


Fig. 25.7 (Experimental) input-beam spatial profile. *Left* typical single shot. *Right* average over 100 shots. From [69]

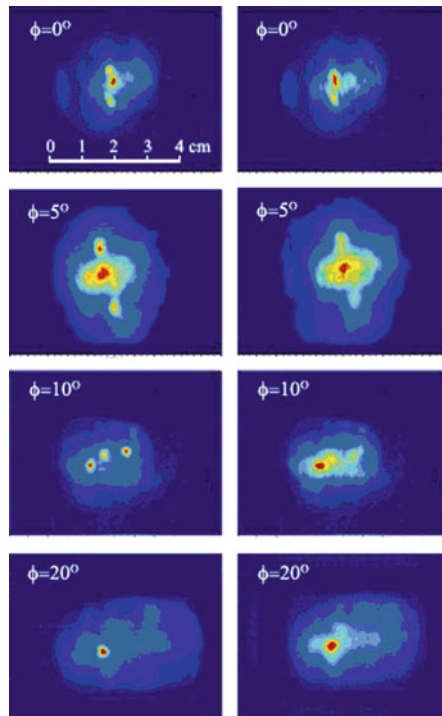


Fig. 25.8 (Experimental) filamentation patterns in air. *Left* Typical single shot. *Right* Average over 1,000 shots. From [69]

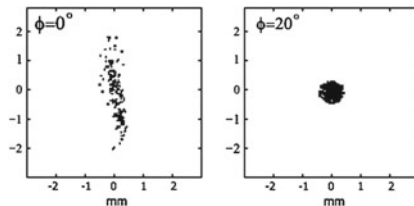


Fig. 25.9 Location of central filament in 320 shots. From [69]

of the strong central filament was 0.15 ± 0.08 mm and 0.75 ± 0.04 mm along the directions of the minor and major axis, respectively (Fig. 25.9). At $\phi = 20^\circ$, the (single) filament was extremely localized, with standard deviation of 0.14 ± 0.04 mm in both directions. This shows that the multiple filamentation pattern can be controlled with input-beam ellipticity and a tilted lens setup.

Conclusion 25.3 *Rather than trying to control the filamentation pattern by lowering the initial noise level, one can control it by adding a sufficiently large deterministic astigmatism.*

25.3.4 Amplitude and Phase Masks

In [172] Méchain et al. showed experimentally and numerically that the multiple filamentation pattern can also be controlled with an amplitude mask. Specifically, non-circular diaphragms with a trefoil or a five-foil shape led to a deterministic beam break-up.

Rohwetter et al. [223] showed experimentally that multiple filamentation can be controlled with a smooth phase mask. Although in that experiment the input power was highly above P_{cr} , the initial multiple filamentation process was linear, because the phase-mask effects dominated the nonlinear Kerr effect as the input beam evolved into multiple filaments.²⁰

25.3.5 Chaotic Post-collapse Interactions

In Sects. 25.3.1–25.3.4 we presented several methods for controlling the *initial* multiple filamentation pattern deterministically. We note, however, that because of the *loss of phase* phenomenon, subsequent interactions between filaments are chaotic. Therefore, these interactions cannot be controlled deterministically. See Sect. 39.2 for more details.

25.4 Predicting the Initial Filamentation Pattern

Most studies on multiple filamentation are numerical. Ideally, however, we would like to predict the multiple filamentation pattern analytically. In Lemma 25.1 we characterized the multiple filamentation patterns which are induced by input-beam ellipticity. Another analytic approach is the *nonlinear geometrical optics (NGO) method*. This method predicts the initial dynamics of high-power beams for which the Kerr nonlinearity dominates over diffraction. Thus, for example, the NGO method shows that high-power super-Gaussian input beams initially evolve into a ring profile. Since the ring is azimuthally unstable, it subsequently breaks into a ring of filaments. The NGO method also shows that high-power square beams initially evolve into four filaments located on a square. The NGO method, however, cannot predict the dynamics beyond the initial multiple filamentation stage. See Chaps. 26 and 37 for more details.

²⁰ Therefore, this multiple filamentation experiment can be modeled by the linear Schrödinger equation.

25.5 Summary—Four Types of Multiple Filamentation

In this chapter we saw that various processes can lead to multiple filamentation:

1. **A Bespalov-Talanov pre-collapse multiple filamentation** occurs at very high input powers, typically above $100P_{\text{cr}}$. Beam breakup is initiated by input-beam noise. As the beam propagates, the noise increases exponentially via a modulation-instability process, leading to the formation of multiple spikes. The spikes further grow by attracting power from their surroundings, and those with power above P_{cr} undergo collapse. Multiple filamentation occurs as the beam collapses, at a distance $L_{\text{MF}} \sim 1/P$.
2. In a **post-collapse ring-breakup multiple filamentation**, after the arrest of collapse, the beam oscillates between a focused peak profile and a defocused ring profile. Because a ring is unstable under azimuthal perturbations, it breaks into a “ring of filaments”.

There are two necessary ingredients for this type of multiple filamentation:

- (a) A *collapse-arresting mechanism* that leads to focusing-defocusing oscillations, so that the beam profile at the defocusing stage is a ring. Examples for such mechanisms are nonlinear saturation, nonparaxiality, and vectorial effects.
- (b) A *symmetry-breaking mechanism*. This mechanism can be random (e.g., input beam noise) or deterministic (e.g., input beam ellipticity, a tilted lens, or a linear polarization state).

This type of multiple filamentation can occur at power levels of several P_{cr} . Since it occurs after the arrest of collapse, the multiple filamentation distance L_{MF} scales as $P^{-\frac{1}{2}}$.

3. **An NGO pre-collapse multiple filamentation** results from self-phase modulations of clean high-power input beams with flat-top profiles. Examples are square input beams that initially break into a “square of four filaments”, and radial super-Gaussian input beams that evolve into rings, which subsequently break into a “ring of filaments”. In this type of multiple filamentation, the power has to be sufficiently above P_{cr} so that nonlinearity initially dominates over diffraction, but it can be well below $100P_{\text{cr}}$. The multiple filamentation distance L_{MF} scales as $P^{-\frac{1}{2}}$.
4. **A linear pre-collapse multiple filamentation** occurs when input-beam phase dominates the initial dynamics and leads to multiple filamentation (e.g., in the case of a phase mask). Multiple filamentation occurs before the beam collapses, and is a linear phenomenon.

Chapter 26

Nonlinear Geometrical Optics (NGO) Method

In this chapter we present an asymptotic method, the Nonlinear Geometrical Optics (NGO) method, for analyzing the initial self-focusing dynamics of strongly-nonlinear solutions of the NLS¹

$$i\psi_z(z, \mathbf{x}) + \Delta\psi + |\psi|^{2\sigma}\psi = 0, \quad \psi(0, \mathbf{x}) = \psi_0(\mathbf{x}). \quad (26.1)$$

Here, by *strongly nonlinear* we mean that nonlinearity initially dominates over diffraction, i.e.,

$$\Delta\psi_0 \ll |\psi_0|^{2\sigma}\psi_0. \quad (26.2)$$

In the critical NLS, relation (26.2) implies that the input power is highly above P_{cr} (Sect. 24.9).

A priori, the analysis in the strongly-nonlinear regime should be harder than when nonlinearity and diffraction are of comparable magnitudes. Thus, for example, in the critical NLS, all blowup solutions for which nonlinearity and diffraction are of comparable magnitudes collapse with the $\psi_{R^{(0)}}$ profile. In contrast, strongly-nonlinear solutions can collapse with the $\psi_{R^{(0)}}$ profile, with the ψ_G profile, or breakup into multiple filaments. Therefore, the dynamics in the strongly-nonlinear regime is richer, and there is no universal attractor. Nevertheless, we shall see that the analysis in the strongly-nonlinear regime is, in a sense, much simpler. This is because there is a natural large parameter in the problem, the ratio of the magnitudes of nonlinearity and diffraction. The availability of this large parameter enables us to derive *linear ODEs* that approximate the *initial* self-focusing dynamics of strongly-nonlinear solutions.²

¹ The NGO method can be extended to NLS equations with other nonlinearities (Sect. 26.2) and with anomalous dispersion (Chap. 37).

² In contrast, the reduced equations for collapse with the $\psi_{R^{(0)}}$ profile (Chap. 17) approximate the *final* self-focusing dynamics (i.e., as $z \rightarrow Z_c$).

26.1 Derivation of NGO Equations

The NGO rays equation was derived in 2006 by Grow et al. [122]. Subsequently, Gavish et al. derived the NGO amplitude equation [106]. Both derivations started from the nonlinear Helmholtz equation. In this section we present a simpler derivation, directly from the NLS.

Let ψ be a solution of the NLS (26.1) with a strongly-nonlinear initial condition, see (26.2). By continuity, during the initial propagation stage

$$\Delta\psi \ll |\psi|^{2\sigma}\psi. \quad (26.3)$$

Hence, (26.1) can be approximated by

$$i\psi_z(z, \mathbf{x}) + |\psi|^{2\sigma}\psi = 0, \quad \psi(0, \mathbf{x}) = \psi_0(\mathbf{x}). \quad (26.4)$$

By Lemma 3.1, the solution of (26.4) is $\psi = \psi_{\text{SPM}}$, where

$$\psi_{\text{SPM}}(z, \mathbf{x}) := \psi_0(\mathbf{x})e^{i|\psi_0(\mathbf{x})|^{2\sigma}z}. \quad (26.5)$$

Conclusion 26.1 *NLS solutions with strongly-nonlinear initial conditions initially undergo self phase modulations (SPM), while their amplitude remains nearly unchanged.*

To demonstrate this conclusion, in Fig. 26.1 we solve the critical NLS with high-power Gaussian initial conditions. As predicted, during the initial propagation stage (roughly for $0 \leq z \leq 0.5Z_c$) the phase increases as $|\psi_0|^{2\sigma}z$, whereas the amplitude remains nearly unchanged.

As self-phase modulations accumulate, the magnitude of $\Delta\psi \approx \Delta\psi_{\text{SPM}}$ increases, while that of $|\psi|^{2\sigma}\psi \approx |\psi_{\text{SPM}}|^{2\sigma}\psi_{\text{SPM}}$ remains unchanged. Therefore, the relative

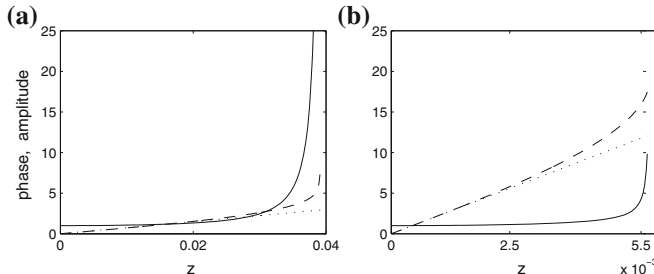


Fig. 26.1 On-axis phase $\arg \psi(z, 0)$ (dashes) and normalized on-axis amplitude $\frac{|\psi(z, 0)|}{|\psi_0(0)|}$ (solid) for the solution of the two-dimensional cubic NLS with $\psi_0 = 2\sqrt{P}e^{-r^2}$. The dotted line is $|\psi_0(0)|^2 z$. **a** $P = 10P_{\text{cr}}$. **b** $P = 300P_{\text{cr}}$. From [68]

magnitude of diffraction increases until it can no longer be neglected. To find the initial effect of diffraction,³ we decompose the NLS solution as

$$\psi = A(z, \mathbf{x}) e^{iS(z, \mathbf{x})},$$

where A and S are real. Substitution in (26.1) gives

$$-AS_z + iA_z + \Delta A + 2i\nabla A \cdot \nabla S + A \left[-(\nabla S)^2 + i\Delta S \right] + |A|^{2\sigma} A = 0.$$

Separating the real and imaginary parts gives the *paraxial eikonal equation*

$$S_z + (\nabla S)^2 = \frac{\Delta A}{A} + |A|^{2\sigma} \quad (26.6a)$$

and the *paraxial transport equation*

$$A_z + 2\nabla S \cdot \nabla A = -A\Delta S. \quad (26.6b)$$

The initial conditions for Eqs. (26.6) are

$$S(0, \mathbf{x}) = \arg(\psi_0(\mathbf{x})), \quad A(0, \mathbf{x}) = |\psi_0(\mathbf{x})|.$$

During the initial propagation stage where (26.4) holds, all the derivatives with respect to \mathbf{x} are negligible, and so (26.6) reduces to

$$S_z = |A|^{2\sigma}, \quad A_z = 0. \quad (26.7)$$

The solution of (26.7) is

$$S(z, \mathbf{x}) = \arg(\psi_0(\mathbf{x})) + |\psi_0(\mathbf{x})|^{2\sigma} z, \quad A(z, \mathbf{x}) \equiv |\psi_0(\mathbf{x})|,$$

i.e., the solution already calculated in (26.5). To find the initial dynamics of A , we substitute $S = |\psi_0|^{2\sigma} z$ in the paraxial transport Eq. (26.6b) and solve it with the *method of characteristics*. The characteristic equations are

$$\frac{dz}{d\sigma} = 1, \quad \frac{d\mathbf{x}}{d\sigma} = 2\nabla S, \quad \frac{dA}{d\sigma} = -A\Delta S.$$

Since $z = \sigma$, these equations read

$$\frac{d\mathbf{x}(z)}{dz} = 2\nabla S(z, \mathbf{x}(z)), \quad \frac{dA(z, \mathbf{x}(z))}{dz} = -A(z, \mathbf{x}(z))\Delta S(z, \mathbf{x}(z)).$$

³ I.e., the effect of diffraction when it is still smaller than nonlinearity, but no longer negligible.

Therefore, we obtain

Proposition 26.1 ([106, 122]) *Let ψ be a solution of the NLS (26.1). If $\Delta\psi_0 \ll |\psi_0|^{2\sigma}\psi_0$, then during the initial propagation stage⁴*

$$\psi \approx \psi_{\text{NGO}} := Ae^{iS_{\text{NGO}}},$$

where

$$S_{\text{NGO}}(z, \mathbf{x}) = \arg(\psi_0(\mathbf{x})) + |\psi_0(\mathbf{x})|^{2\sigma}z \quad (\text{NGO phase equation}), \quad (26.8a)$$

the trajectories of the rays satisfy

$$\frac{d\mathbf{x}(z)}{dz} = 2\nabla S_{\text{NGO}} \quad (\text{NGO rays equation}), \quad (26.8b)$$

and the amplitude evolution along each ray is

$$\frac{dA(z, \mathbf{x}(z))}{dz} = -A\Delta S_{\text{NGO}} \quad (\text{NGO amplitude equation}). \quad (26.8c)$$

26.2 NGO Method

To illustrate the NGO method, consider the one-dimensional cubic NLS

$$i\psi_z(z, x) + \psi_{xx} + |\psi|^2\psi = 0 \quad (26.9)$$

with $\psi_0 = ce^{-x^4}$ and $c \gg 1$. Since $\frac{d^2\psi_0}{dx^2} \sim c$ and $|\psi_0|^2\psi_0 \sim c^3$, the condition $\frac{d^2\psi_0}{dx^2} \ll |\psi_0|^2\psi_0$ holds, and so we can apply the NGO method. Since $S_{\text{NGO}} = c^2e^{-2x^4}z$, see (26.8a), the NGO rays equation reads, see (26.8b),

$$\frac{dx}{dz} = 2\frac{\partial}{\partial x}S_{\text{NGO}} = -16c^2x^3ze^{-2x^4}. \quad (26.10a)$$

The numerical solution of (26.10a) for $0 \leq z \leq 0.07$ shows that rays that originate in $0.25 \approx a < |x| < b \approx 1.4$ bend toward the center and concentrate near $x = \pm a$, see Fig. 26.2a. In contrast, rays that originate in $|x| < a$ and in $|x| > b$ remain essentially parallel. Hence, we conclude that the input beam splits into two beams (filaments), centered at $x \approx \pm a$.

⁴ The term “initial propagation stage” will be made precise in Lemma 26.3.

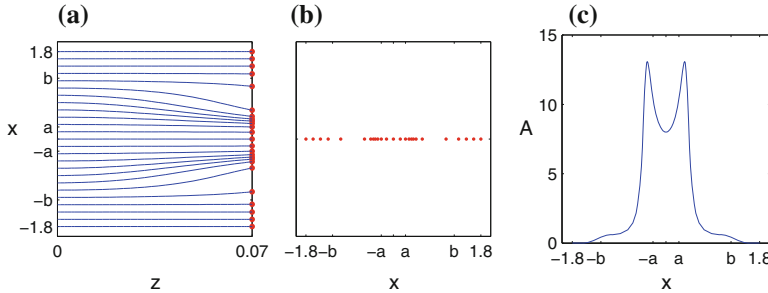


Fig. 26.2 NGO approximation of the one-dimensional NLS (26.9) with $\psi_0 = 8e^{-x^4}$. **a** Trajectories of NGO rays. **b** Location of NGO rays at $z = 0.07$. **c** NGO amplitude distribution at $z = 0.07$. From [106]

The above conclusion is based on the implicit assumption that when the initial distribution of rays is uniform, a higher concentration of rays correspond to a region with a higher intensity.⁵ The problem with this assumption is that it does not distinguish between rays that originate in high-intensity regions and those that originate in low-intensity regions. To illustrate this, consider the location of the rays at $z = 0.07$ (Fig. 26.2b). If we assume that a higher concentration of rays implies a higher intensity, Fig. 26.2b suggests that in addition to the two spikes at $\pm a$, there are two minor spikes at the solution wings.

To overcome this problem and improve the quality of the graphical representation, Gavish et al. [106] derived the NGO amplitude equation (26.8c). In our example, this equation reads

$$\frac{d}{dz}A(z, x(z)) = -A \frac{\partial^2}{\partial x^2} \left(c^2 e^{-2x^4} z \right), \quad (26.10b)$$

where $x = x(z)$ is the solution of (26.10a) which was calculated earlier. In Fig. 26.2c we plot the solution of (26.10b) at $z = 0.07$ (i.e., at the same z as in Fig. 26.2b). This plot clearly shows that the beam splits into two filaments at $x = \pm a$, and that there are no additional humps at the wings. This NGO prediction will be later confirmed in Fig. 26.8c by a direct simulation of the NLS (26.9). Therefore, the amplitude representation in Fig. 26.2c is both cleaner and more informative than the ray representation in Fig. 26.2b.

The generalization of the NGO method to higher dimensions is straightforward. For example, consider the two-dimensional cubic NLS

$$i\psi_z(z, x, y) + \psi_{xx} + \psi_{yy} + |\psi|^2\psi = 0 \quad (26.11)$$

with $\psi_0 = 6.55e^{-x^4-y^4}$. The NGO rays equation is, see (26.8a) and (26.8b),

$$\frac{d}{dz}(x(z), y(z)) = 2 \left(\frac{\partial}{\partial x}, \frac{\partial}{\partial y} \right) \left(6.55^2 e^{-2x^4-2y^4} z \right).$$

⁵ This assumption is motivated by the conservation of power along ray bundles (Sect. 2.1.2).

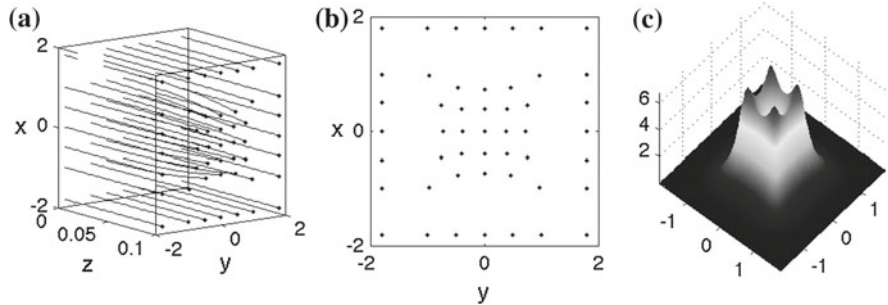


Fig. 26.3 NGO approximation of the two-dimensional NLS (26.11) with $\psi_0 = 6.55e^{-x^4-y^4}$. **a** Trajectories of NGO rays. **b** Location of NGO rays at $z = 0.1$. **c** NGO amplitude distribution at $z = 0.1$. From [106]

The NGO rays are plotted in Fig. 26.3a. At any distance z , we can plot the location of the rays in the (x, y) -plane (Fig. 26.3b). As in the one-dimensional case, however, the locations of the rays do not provide a clear description of the beam profile. For example, in Fig. 26.3b it looks as though at $z = 0.1$ the beam is flat-top at the center. In order to find the amplitude distribution, we solve the NGO amplitude equation

$$\frac{d}{dz} A(z, x(z), y(z)) = -A \Delta_{x,y} \left(6.55^2 e^{-2x^4-2y^4} z \right),$$

see (26.8c). The solution of this equation shows that the beam evolves into four filaments located at the corners of a square (Fig. 26.3c). This NGO prediction will be confirmed in Fig. 26.16b by a direct simulation of (26.11).

In summary, the NGO method for the NLS (26.1) with strongly-nonlinear initial conditions is:

1. Choose starting points \mathbf{x}_i for the rays at $z = 0$.
2. For each ray, find its trajectory and amplitude by solving

$$\frac{d}{dz} \mathbf{x}(z) = 2 \nabla S, \quad \frac{d}{dz} A(z, \mathbf{x}(z)) = -A \Delta S, \quad (26.12a)$$

with the initial conditions

$$\mathbf{x}(0) = \mathbf{x}_i, \quad A(0) = |\psi_0(\mathbf{x}_i)|,$$

where

$$S = S_{\text{NGO}}(z, \mathbf{x}(z)) = \arg(\psi_0(\mathbf{x})) + |\psi_0(\mathbf{x}(z))|^{2\sigma} z. \quad (26.12b)$$

```

function[] = NGO()
% Solve the NGO equations in one dimension
amplitude = [];rays = [];
rayStartingPoints = linspace(-1.4,1.4,35);
z_array = [0:0.001:0.05];
for x=rayStartingPoints
    psi_0 = 8*exp(-x^8);
    % Find ray trajectory and amplitude
    [z,X] = ode45(@NGO_ODEs, z_array, [x psi_0]); %X = [x(z), A(z)]
    rays = [X(:,1)';rays];
    amplitude = [X(:,2)';amplitude];
end
subplot(2,2,1); plot(z,rays);
subplot(2,2,2);surf(amplitude,'EdgeColor','none');shading interp,
shg
end

function dXdz = NGO_ODEs(z,X)
x=X(1); A=X(2);
psi_0 = 8*exp(-x^8);
grad_S = -16*x^7*psi_0^2*z;
delta_S = 16*psi_0^2*x^6*(16*x^8-7)*z;
dXdz = [2*grad_S; -A*delta_S];
end

```

Fig. 26.4 A sample Matlab code for computing the NGO rays and amplitude in Fig. 26.9a, b

The beauty of the NGO method is that it replaces a nonlinear PDE (the NLS) with linear ODEs for each ray. Therefore, numerical implementation of the NGO method is much simpler, and requires a few lines of code (Fig. 26.4). Moreover, the NGO method can also simplify the *analysis* of the initial self-focusing dynamics.

Remark The NGO method can be easily extended to NLS equations of the form⁶

$$i\psi_z(z, \mathbf{x}) + \Delta\psi + F(|\psi|^2)\psi = 0, \quad \psi(0, \mathbf{x}) = \psi_0(\mathbf{x}). \quad (26.13)$$

Indeed, the only change is that (26.12b) is replaced by

$$S = S_{\text{NGO}}(z, \mathbf{x}(z)) = \arg(\psi_0(\mathbf{x})) + F(|\psi_0(\mathbf{x}(z))|^2)z. \quad (26.14)$$

⁶ Examples of such nonlinearities are cubic-quintic and saturated nonlinearities (Chap. 32).

26.2.1 Direction of NGO Rays

Previously we saw that under the geometrical optics approximation, the rays are perpendicular to the wavefronts of $S^{(E)}$ (Lemma 2.1). In the strongly nonlinear regime, we have the following result:

Lemma 26.1 *The NGO rays of the dimensionless NLS (26.13) are perpendicular, to leading order, to the wavefronts $S_{\text{NGO}}^{(E)}(z, \mathbf{x}) \equiv \text{constant}$, where*

$$S_{\text{NGO}}^{(E)} := \frac{z}{2} + S_{\text{NGO}}^{(\psi)} \quad (26.15)$$

is the NGO approximation of the dimensionless NLH phase, and $S_{\text{NGO}}^{(\psi)}$ is given by (26.8a).

Proof The phases of the dimensionless Helmholtz and Schrödinger solutions are related by⁷

$$S^{(E)} = \frac{z}{2} + S^{(\psi)}. \quad (26.16)$$

Since in the NGO regime $S^{(\psi)} \sim S_{\text{NGO}}^{(\psi)}$, then $S^{(E)} \sim S_{\text{NGO}}^{(E)}$. By (26.8b), the direction of the NGO rays is

$$\left(\frac{dz}{dz}, \frac{d\mathbf{x}}{dz} \right) = (1, 2\nabla_{\mathbf{x}} S_{\text{NGO}}^{(\psi)}). \quad (26.17)$$

By the slowly-varying envelope approximation, $\frac{\partial}{\partial z} S^{(E)} \sim \frac{\partial}{\partial z} \frac{z}{2} = \frac{1}{2}$. Hence, we can rewrite (26.17) as $\left(\frac{dz}{dz}, \frac{d\mathbf{x}}{dz} \right) \sim 2\nabla_{z, \mathbf{x}} S_{\text{NGO}}^{(E)}$. \square

26.3 (In)dependence on Beam Power

Consider the power-law NLS (26.1) with $\psi_0 = cg(\mathbf{x})$, where c and $g(\mathbf{x})$ are real, and c is sufficiently large so that $|\psi_0|^{2\sigma} \psi_0 \gg \Delta\psi_0$. We can use the NGO method to analyze how the NLS solution changes with c , i.e., as we fix the input profile and vary the power $P = c^2 \int |g|^2 d\mathbf{x}$.

Lemma 26.2 *Consider the NGO equations (26.12) with initial conditions that corresponds to $\psi_0 = cg(\mathbf{x})$, where ψ_0 is real. Then the evolution of the NGO amplitude along the ray $\mathbf{x}(z; c)$ is given by the dilation*

$$A(z, \mathbf{x}(z; c); c) = c\tilde{A}(\tilde{z}, \tilde{\mathbf{x}}(\tilde{z})), \quad \tilde{z} = c^\sigma z,$$

⁷ The relation between $S^{(E)}$ and $S^{(\psi)}$ for the dimensional Helmholtz and Schrödinger solutions is $k_0 S^{(E)} = k_0 z + k_0 S^{(\psi)}$, see (2.31). When changing to dimensionless variables, then $k_0 S^{(E)} \rightarrow S^{(E)}$, $k_0 S^{(\psi)} \rightarrow S^{(\psi)}$, and $k_0 \rightarrow 1/2$. Therefore, we get (26.16).

where $\tilde{\mathbf{x}}(z) = \mathbf{x}(z; c = 1)$ and $\tilde{A}(z, \mathbf{x}) = A(z, \mathbf{x}; c = 1)$ are independent of c . In particular,

1. The NGO self-focusing dynamics is independent of c .
2. The NGO self-focusing distance scales as $c^{-\sigma} \sim P^{-\frac{\sigma}{2}}$.

Proof Since $S_{\text{NGO}}(z = 0) = 0$ and $A(z = 0) = cg$, then

$$S_{\text{NGO}} = c^{2\sigma} g^{2\sigma}(\mathbf{x})z, \quad (26.18)$$

and so the NGO equations (26.12) read

$$\frac{d\mathbf{x}}{dz} = 2c^{2\sigma} z \nabla g^{2\sigma}(\mathbf{x}), \quad \frac{dA}{dz} = -c^{2\sigma} z A \Delta g^{2\sigma}(\mathbf{x}).$$

Therefore, if we define $\tilde{z} = c^\sigma z$, then

$$\frac{d\mathbf{x}}{d\tilde{z}} = 2\tilde{z} \nabla g^{2\sigma}(\mathbf{x}), \quad \frac{dA}{d\tilde{z}} = -\tilde{z} A \Delta g^{2\sigma}(\mathbf{x}).$$

Since these equations are independent of c , and the initial conditions are $\mathbf{x}(0) = \mathbf{x}_0$ and $A(0) = c g(\mathbf{x}_0)$, the result follows. \square

Lemma 26.2 implies

Corollary 26.1 *The NLS self focusing dynamics in the strongly-nonlinear regime is, up to dilation, independent of P .*

This is very different from the “low-power” regime, where changes in P can lead to qualitative changes in the self-focusing dynamics (Figs. 27.7 and 27.9), and even to a change from blow up to scattering (Lemmas 7.13 and 9.7).

26.3.1 L_{SPM} and L_{SF}

Equation (26.18) and Lemma 26.2 lead to

Conclusion 26.2 *Consider the power-law NLS (26.1) with $\psi_0 = cg(\mathbf{x})$ in the strongly-nonlinear regime $c \gg 1$. Then the characteristic distances for self-phase modulations and for self-focusing scale as*

$$L_{\text{SPM}} \sim c^{-2\sigma} \sim P^{-\sigma}, \quad L_{\text{SF}} \sim c^{-\sigma} \sim P^{-\frac{\sigma}{2}}.$$

Proof In the strongly-nonlinear regime, the dynamics can be approximated by the NGO equations. Since $S_{\text{NGO}} = \arg(\psi_0) + c^{2\sigma} g^{2\sigma}(\mathbf{x})z \sim c^{2\sigma} g^{2\sigma}(\mathbf{x})z$, one can use Lemma 26.2 even if ψ_0 is not real. \square

Remark By Corollary 26.2, $L_{\text{SPM}} \ll L_{\text{SF}}$ as $P \rightarrow \infty$. This observation is the key for understanding the destabilizing effect of input-beam noise on peak-type collapse. See Sects. 25.1.1 and 27.2.3 for further details.

The value of L_{SF} provides a good estimate for the collapse distance Z_c . This is because once self-focusing begins, it accelerates very fast (see e.g., Fig. 26.1). Since $L_{\text{SF}} \sim P^{-\frac{\sigma}{2}}$, this suggests that $Z_c \sim P^{-\frac{\sigma}{2}}$ in the strongly-nonlinear regime. See Sect. 27.2.2 for further discussion.

26.3.2 “Counter-Intuitive” Effect of Small Diffraction

Let us point out two “counter-intuitive” results.

1. In Sect. 26.1 we saw that in the absence of diffraction the solution only undergoes self-phase modulations. Once diffraction is added, however, the solution also undergoes self-focusing. Thus, diffraction is defocusing, yet adding it has a “focusing effect”.
2. Consider the NLS

$$i\psi_z(z, \mathbf{x}) + \alpha \Delta \psi + |\psi|^{2\sigma} \psi = 0, \quad \psi(0, \mathbf{x}) = \psi_0(\mathbf{x}), \quad \alpha > 0 \quad (26.19)$$

with real, strongly-nonlinear initial conditions (i.e., $\alpha \Delta \psi_0 \ll |\psi_0|^{2\sigma} \psi_0$). The corresponding NGO equations are

$$\frac{d\mathbf{x}(z)}{dz} = 2\alpha \nabla S, \quad \frac{dA(z, \mathbf{x}(z))}{dz} = -\alpha A \Delta S, \quad S = |\psi_0|^{2\sigma} z. \quad (26.20)$$

Exercise 26.1 Derive Eq. (26.20).

If we make the change of variable $\tilde{z} := \sqrt{\alpha}z$, Eq. (26.20) becomes independent of α . Therefore,

$$\mathbf{x} = \mathbf{x}(\sqrt{\alpha}z), \quad A = A(\sqrt{\alpha}z, \mathbf{x}(\sqrt{\alpha}z)).$$

Conclusion 26.3 The initial self-focusing dynamics in the α -NLS (26.19) with strongly-nonlinear initial conditions is faster/slower by a factor of $\sqrt{\alpha}$, compared with the NLS (26.1).

Thus, as α increases, the magnitude of diffraction increases, yet the self-focusing dynamics becomes faster and not slower.

These results appear to be “counter-intuitive”, because we implicitly assume that diffraction is always defocusing. Such a linear superposition approach, however, is inappropriate in the strongly-nonlinear regime. Indeed, according to this linear approach, self-focusing should be fastest when there is no diffraction, which is not the case.⁸

⁸ See Sects. 3.4.1, 30.4, and 36.8.1 for other failures of the linear superposition approach.

26.4 Limitations of the NGO Method

In the derivation of the NGO equations we first calculated the effect of the initial amplitude $|\psi_0|$ on the phase, yielding $S \approx S_{\text{NGO}}$. Then we used S_{NGO} to calculate the evolution of the amplitude $A = |\psi|$. In the NLS, once $|\psi|$ increases, self-phase modulations become faster than $|\psi_0|^{2\sigma}z$, hence the self-focusing process accelerates (see, e.g., Fig. 26.1). In the NGO method, however, this feedback effect of A on S is neglected.

Conclusion 26.4 *Self focusing in the NGO equations is slower than in the NLS. In particular, the self-focusing distance of the NGO solution is larger than that of the NLS solution.*

The feedback effect of changes in A on S , which is neglected in the NGO method, becomes significant once A undergoes $O(1)$ changes.

Conclusion 26.5 *The NGO equations capture the initial self-focusing dynamics of strongly-nonlinear beams, but their validity breaks down once the amplitude undergoes $O(1)$ changes.*

By Conclusion 26.2, the solution undergoes self-phase modulations for $z = O(L_{\text{SPM}})$ and self-focusing for $z = O(L_{\text{SF}})$, where $L_{\text{SPM}} \sim P^{-\sigma}$ and $L_{\text{SF}} \sim P^{-\frac{\sigma}{2}}$. Since the NGO equations only capture the initial self-focusing dynamics, we have

Lemma 26.3 *Let ψ be a solution of the NLS (26.1), and let $\Delta\psi_0 \ll |\psi_0|^{2\sigma}\psi_0$. Then*

1. $\psi \approx \psi_{\text{SPM}}$ for $z = O(P^{-\sigma})$,
2. $\psi \approx \psi_{\text{NGO}}$ for $0 \leq z \ll P^{-\frac{\sigma}{2}}$,

where ψ_{SPM} is given by (26.5) and ψ_{NGO} is as in Proposition 26.1.

Finally, we note that the NGO phase equation (26.8a) was derived by neglecting the $(\nabla S)^2$ term in the paraxial eikonal equation (26.6a), i.e., by assuming that the initial evolution of the phase is predominantly due to self-phase modulations. The assumption that $S \approx S_{\text{NGO}}$ is valid when condition (26.2) holds. It becomes invalid, however, when the input beam is focused by a sufficiently-strong lens or phase mask.⁹

⁹ For example, consider the focused input beam $\psi_0 = Ae^{-\frac{|\mathbf{x}|^2}{4F}}$. If we keep the $(\nabla S)^2$ term in (26.6a) and neglect the nonlinearity, the equation for S becomes

$$S_z(z, \mathbf{x}) + (\nabla S)^2 = 0, \quad S(0, \mathbf{x}) = -\frac{|\mathbf{x}|^2}{4F}.$$

The solution of this equation is $S = \frac{|\mathbf{x}|^2}{4(z-F)}$, see Sect. 2.9. Therefore, unless the lens effect on the phase is negligible compared with self phase modulations, S cannot be approximated with $S_{\text{NGO}} = -\frac{|\mathbf{x}|^2}{4F} + |\psi_0|^{2\sigma}z$.

Conclusion 26.6 *The NGO equations (26.12) are not valid when the initial phase distribution has a non-negligible effect on the self-focusing dynamics.*

Remark In Sect. 26.8 we will discuss how to incorporate the effect of a lens into the NGO method.

26.5 One Spatial Dimension

In this section we analyze the one-dimensional cubic NLS

$$i\psi_z(z, x) + \psi_{xx} + |\psi|^2\psi = 0 \quad (26.21a)$$

with the collimated input beam

$$\psi_0(x) = ce^{-x^{2m}}, \quad (26.21b)$$

where c is sufficiently large so that $|\psi_0|^2\psi_0 \gg \frac{d^2\psi_0}{dx^2}$.

26.5.1 Analysis

By (26.12),

$$S_{\text{NGO}} = c^2 e^{-2x^{2m}} z, \quad (26.22)$$

and so the NGO equations read

$$\frac{dx(z)}{dz} = 2c^2 z \frac{\partial}{\partial x} e^{-2x^{2m}}, \quad (26.23a)$$

$$\frac{dA(z, x(z))}{dz} = -c^2 z A \frac{\partial^2}{\partial x^2} e^{-2x^{2m}}. \quad (26.23b)$$

Proposition 26.2 ([106]) *Consider the NLS (26.21) with a strongly nonlinear initial condition $(|\psi_0|^2\psi_0 \gg \frac{d^2\psi_0}{dx^2})$. Then initially the solution localizes to a single peak if $m = 1$, but splits into two peaks for $m > 1$.*

Proof We prove the result for $m > 1$ by showing that rays that originate near $x = 0$ and far away from the beam center remain parallel, while those that originate between these two regions bend toward $x = 0$. Indeed, by (26.23a),

$$\frac{dx}{dz} = -8mc^2 x^{2m-1} e^{-2x^{2m}} z. \quad (26.24)$$

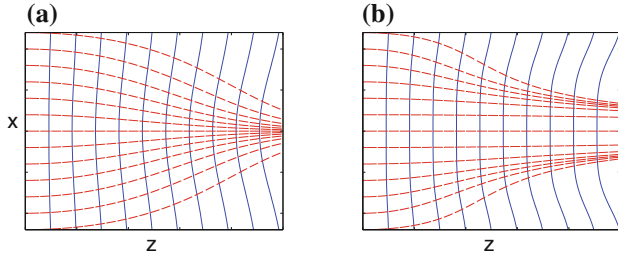


Fig. 26.5 NGO rays (dashes) are nearly perpendicular to the level sets of the approximate NLH phase $S_{\text{NGO}}^{(E)}$ (solid). Initial profile is: **a** Gaussian ($m = 1$). **b** Super-Gaussian ($m > 1$). From [122]

Therefore, all rays bend toward $x = 0$. For a ray that starts at $x(0) = x$ to “get close” to the beam center at a finite distance Z , its bending should be sufficiently large so that $Z \frac{dx}{dz} = O(x)$, or equivalently $\frac{1}{x} \frac{dx}{dz} = O(\frac{1}{Z})$. By (26.24), $\frac{1}{x} \frac{dx}{dz} \ll 1$ for $|x| \gg 1$. Hence, rays that are far from the beam center are essentially parallel. In addition, since for $m > 1$ we have that $\frac{1}{x} \frac{dx}{dz} \ll 1$ for $|x| \ll 1$, rays near the beam center are also parallel. Finally, since $\frac{1}{x} \frac{dx}{dz} = O(1)$ for $x = O(1)$, these rays bend toward $x = 0$.

For $m = 1$,

$$\frac{1}{x} \frac{dx}{dz} = -8c^2 e^{-2x^2} z.$$

Hence, the rays near $x = 0$ are not parallel, but rather bend toward the center. Therefore, the solution localizes into a single filament at $x = 0$. \square

The proof of Proposition 26.2 leads to

Conclusion 26.7 *The difference between self focusing of strongly-nonlinear Gaussian and super-Gaussian input beams has to do with their curvatures near $x = 0$ (and not, e.g., with their behaviors as $|x| \rightarrow \infty$).*

To further motivate Conclusion 26.7, in Fig. 26.5 we plot the NGO approximation of the wavefronts of the corresponding NLH solutions

$$S_{\text{NGO}}^{(E)} := \frac{z}{2} + S_{\text{NGO}} = \left(\frac{1}{2} + c^2 e^{-2x^{2m}} \right) z \equiv \text{constant}, \quad (26.25)$$

see (26.15). The wavefronts near the beam center are flat for the super-Gaussian beam, but depressed for the Gaussian beam. Since NGO rays are perpendicular to NLH wavefronts (Lemma 26.1), the flat-top profile of the wavefronts of the super-Gaussian beam focuses the rays into two off-center filaments. In contrast, the depressed profile of the wavefronts of the Gaussian beam focuses all rays towards the center. Therefore, we see again that the difference between Gaussian and super-Gaussian input beams has to do with the flatness of the initial profile at $x = 0$.

Remark When m is only slightly larger than 1, the splitting occurs only at very high input powers, and after very long propagation distances.

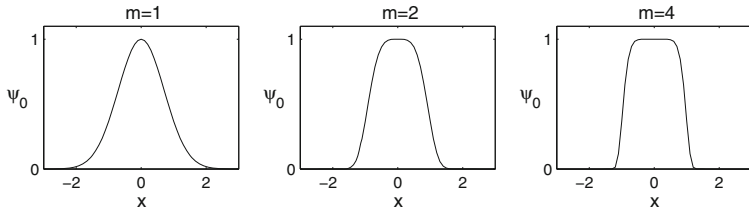


Fig. 26.6 The initial condition (26.21b) for $m = 1, 2$, and 4

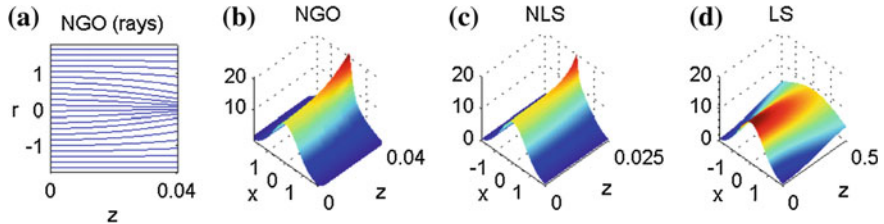


Fig. 26.7 The one-dimensional cubic NLS (26.21a) with $\psi_0 = 8.9e^{-x^2}$. **a** NGO rays. **b** NGO amplitude. **c** NLS solution. **d** Solution of the linear Schrödinger (LS) equation with the same initial condition. From [106]

26.5.2 Simulations

Consider the NLS (26.21). The initial condition is peak-type if $m = 1$, and flat-top if $m > 1$ (Fig. 26.6). In the latter case, m characterizes the steepness of the transition from the flap-top region to zero. Hence, $m = 2$ and $m = 4$ represent a uniform beam that passes through a soft and a hard aperture, respectively.

When $m = 1$, the solution of the NGO ray equation (26.23a) shows that all NGO rays bend towards $x = 0$ (Fig. 26.7a), suggesting that the beam localizes to a single peak at $x = 0$. This behavior is also observed in Fig. 26.7b, where we solve the NGO amplitude equation (26.23b). This NGO prediction is confirmed in direct simulations of the NLS (26.21a) in Fig. 26.7c.

In Fig. 26.8 we consider a flat-top soft-aperture initial condition ($m = 2$). In this case, rays that originate in $0.35 \approx a < |x| < b \approx 1.4$ bend toward the center and concentrate near $x = \pm a$. In contrast, rays that originate in $|x| < a$ and in $|x| > b$ remain essentially parallel. Therefore, the input beam splits into two beams localized around $x = \pm a$ (Fig. 26.8a). A similar dynamics is evident in Fig. 26.8b, where we plot the NGO amplitude. Figure 26.8c shows that the corresponding NLS solution indeed splits into two filaments.

In Fig. 26.9 we consider a hard-aperture flap-top initial condition ($m = 4$). As in the soft-aperture case, rays that originate in $0.67 \approx a < |x| < b \approx 1.2$ bend toward the center and concentrate near $x = \pm a$. In contrast, rays that originate in $|x| < a$ and in $|x| > b$ remain essentially parallel. Therefore, the input beam splits into two

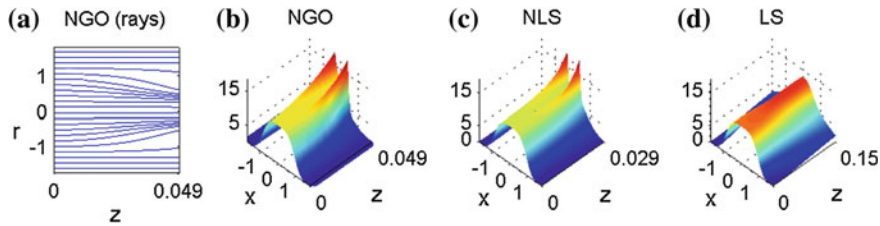


Fig. 26.8 Same as Fig. 26.7 with $\psi_0 = 8e^{-x^4}$. From [106]

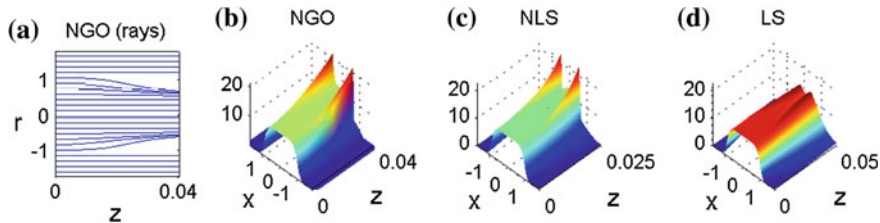


Fig. 26.9 Same as Fig. 26.7 with $\psi_0 = 8.09e^{-x^8}$. From [106]

beams localized around $x = \pm a$ (Fig. 26.9a, b). This NGO prediction is confirmed by direct NLS simulations in Fig. 26.9c.

Remark As predicted in Conclusion 26.4, the self-focusing distance of the NLS solutions in Figs. 26.7, 26.8 and 26.9 is shorter than that of the corresponding NGO solutions.

26.6 “Failure” of the Linear Schrödinger Model

The NGO method is valid in the strongly-nonlinear regime where nonlinearity dominates over diffraction. One-dimensional flat-top input beams, however, can also split in linear propagation. This raises the question whether diffraction could also produce the filamentation patterns in Figs. 26.7, 26.8 and 26.9. In other words, are these filamentation patterns a linear or a nonlinear phenomenon? To answer this question, we solve the linear Schrödinger equation with the same input beams. In the case of a Gaussian input beam, the linear solution broadens with propagation (Fig. 26.7d), whereas the NLS solution localizes into a single filament. For a soft-aperture super-Gaussian input beam ($m = 2$), after a minor initial localization toward one peak, the linear solution also broadens with propagation rather than split into two filaments (Fig. 26.8). Only in the case of a hard aperture super-Gaussian input beam ($m = 4$), both the linear and the nonlinear solutions split into two (Fig. 26.9). Even in that case, however, the linear solution splits as its intensity decreases, whereas the NLS and NGO solutions split as their intensities increase.

Conclusion 26.8 ([106]) *The initial self-focusing dynamics of strongly-nonlinear collimated input beams is captured by the NGO equations, but not by the linear Schrödinger equation.*

Remark Conclusion 26.8 also holds in higher dimensions, see [106] for further details.

Neither the NGO method nor the linear model can accurately predict the self-focusing distance of the NLS solution. As noted in Conclusion 26.4, the NGO self-focusing distance is always larger than the NLS self-focusing distance. The NGO method does capture, however, the property that the NLS self-focusing distance decreases as the input power increases (Lemma 26.2 and Chap. 27). This property is not captured by the linear model, in which the dynamics is independent of input power.

26.7 Two Spatial Dimensions

We now consider the initial self-focusing dynamics of strongly-nonlinear solutions of the two-dimensional cubic NLS

$$i\psi_z(z, x, y) + \Delta\psi + |\psi|^2\psi = 0, \quad \psi(0, x, y) = \psi_0(x, y). \quad (26.26)$$

26.7.1 Radial Beams

Consider the radial initial conditions

$$\psi_0 = ce^{-r^{2m}}, \quad r = \sqrt{x^2 + y^2}, \quad (26.27)$$

where c is sufficiently large so that $|\psi_0|^2\psi_0 \gg \Delta\psi_0$. Since the solution remains radial (Lemma 5.5), the NLS (26.26) reads

$$i\psi_z(z, r) + \psi_{rr} + \frac{1}{r}\psi_r + |\psi|^2\psi = 0. \quad (26.28)$$

By (26.8), the NGO rays equation is

$$\frac{dr(z)}{dz} = 2\frac{\partial}{\partial r}S_{\text{NGO}} = 2c^2z\frac{\partial}{\partial r}e^{-2r^{2m}}. \quad (26.29)$$

Up to the change $r \longleftrightarrow x$, this is the one-dimensional NGO rays equation (26.23a). Since a split in the radial coordinate corresponds to a ring in the (x, y) -plane, Proposition 26.2 implies

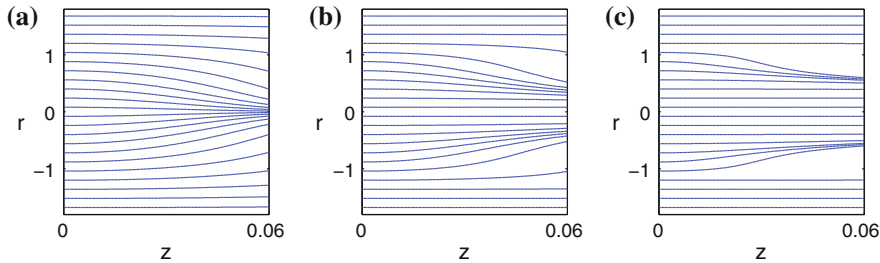


Fig. 26.10 NGO rays of the solution of the two-dimensional NLS (26.28). **a** $\psi_0 = 8e^{-r^2}$. **b** $\psi_0 = 7.1e^{-r^4}$. **c** $\psi_0 = 6.5e^{-r^8}$. From [106]

Proposition 26.3 ([106, 122]) Assume that the input beam (26.27) is strongly non-linear ($|\psi_0|^2\psi_0 \gg \Delta\psi_0$). Then the solution of (26.28) initially evolves into a single peak if $m = 1$, and into a ring if $m > 1$.

Indeed, plotting the NGO rays in Fig. 26.10 shows that for $m = 1$ the beam localizes to a single peak centered at $r = 0$, while for $m = 2$ and $m = 4$ the beam evolves into a ring.

By (26.8), the NGO amplitude equation is

$$\frac{dA(z, r(z))}{dz} = -c^2 z A \left[\frac{\partial^2}{\partial r^2} + \frac{1}{r} \frac{\partial}{\partial r} \right] e^{-2r^{2m}}. \quad (26.30)$$

This equation is similar (but not identical) to the one-dimensional NGO amplitude equation (26.23b). In Fig. 26.11a we plot the NGO amplitude for $m = 1$. As predicted by the NGO rays, the beam localized to a single peak at $r = 0$. This NGO prediction is confirmed by direct NLS simulations in Fig. 26.11b. In Figs. 26.12a and 26.13a we plot the NGO amplitude for $m = 2$ and $m = 4$, respectively. In both cases, in accordance with Proposition 26.3, the NGO solution evolves into a ring, as is confirmed by direct simulations of the NLS (Figs. 26.12b and 26.13b).

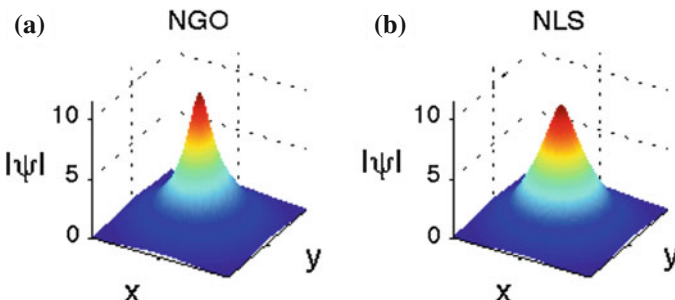


Fig. 26.11 The two-dimensional NLS (26.28) with $\psi_0 = 8e^{-r^2}$. **a** NGO amplitude at $z \approx 0.04$. **b** NLS solution at $z \approx 0.026$. From [106]

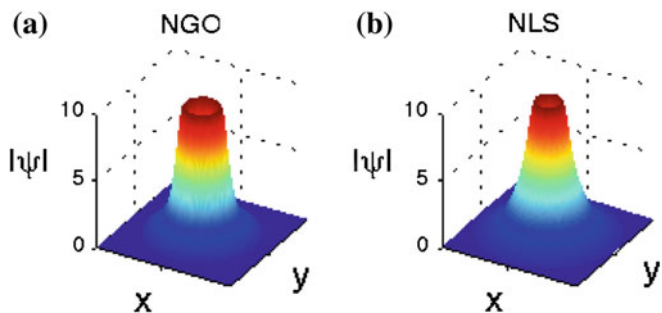


Fig. 26.12 Same as Fig. 26.11 with $\psi_0 = 7.1e^{-r^4}$. **a** NGO amplitude at $z \approx 0.05$. **b** NLS solution at $z \approx 0.04$. From [106]

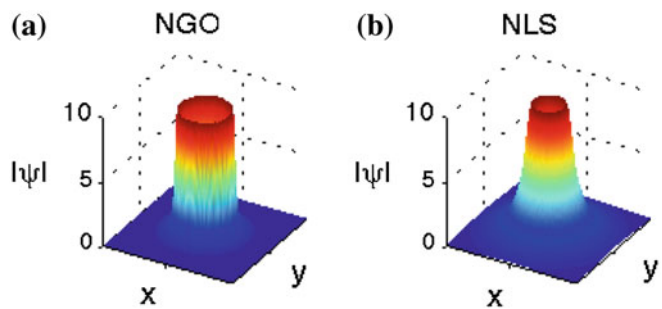


Fig. 26.13 Same as Fig. 26.11 with $\psi_0 = 6.5e^{-r^8}$. **a** NGO amplitude at $z \approx 0.045$. **b** NLS solution at $z \approx 0.04$. From [106]

Remark NLS solutions with a ring profile are unstable under azimuthal perturbations (Sects. 11.4.2, 11.5, and 15.8.3). Therefore, upon further propagation, they disintegrate into a “ring of filaments”. This ring-instability dynamics, however, is not captured by the NGO method.

26.7.2 Experiments

In [122], Grow et al. demonstrated experimentally the difference between the collapse dynamics of strongly-nonlinear Gaussian and super-Gaussian beams, see Fig. 26.14.¹⁰ Initially, an input pulse with a Gaussian spatial profile propagated through a 7 cm water cell and emerged with a peak-type profile. When the input profile was altered to be more flat-top (which approximates a super-Gaussian profile), the pulse emerged from the water cell with a (broken) ring profile.

¹⁰ These experiments were already discussed in Sect. 19.4.

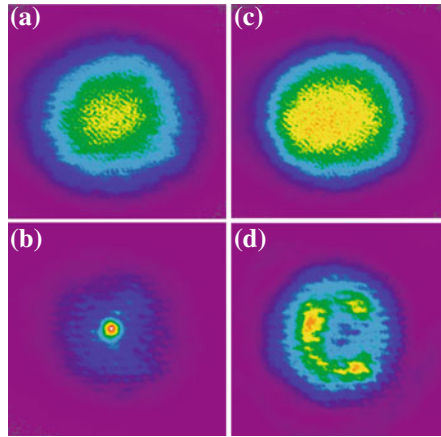


Fig. 26.14 Input and output spatial intensity profiles for a 7 cm propagation distance in water (0.9 mm \times 0.9 mm). **a** Gaussian input profile with input energy $E = 5.6 \mu\text{J}$. **b** The corresponding output beam has a peak profile. **c** Super-Gaussian input profile with $E = 5.0 \mu\text{J}$. **d** The corresponding output beam has a *ring* profile. From [122]

The agreement of the experimental results with NGO predictions provides further support to the physical validity of the NLS model before and during the early stages of the collapse (Sect. 1.8). It also illustrates the robustness of the NGO method, since the input beams in these experiments (Fig. 26.14a, c) were quite noisy.¹¹ Additional experimental confirmation of the NGO method is presented in Sect. 37.5.

26.7.3 Square Input Beams

We now consider the two-dimensional NLS (26.26) with

$$\psi_0 = ce^{-x^{2m}} e^{-y^{2m}}, \quad (26.31)$$

where c is sufficiently large so that nonlinearity initially dominates over diffraction. This input beam has a square profile in the (x, y) -plane for $m > 1$, see Fig. 26.15a. This is different from a Gaussian input beam ($m = 1$) which has a circular profile (Fig. 26.15b).

By (26.12), the NGO equations are

$$\frac{dx(z)}{dz} = 2c^2 z e^{-2y^{2m}} \frac{\partial}{\partial x} e^{-2x^{2m}}, \quad (26.32a)$$

¹¹ See Sect. 26.9 for further discussion of the robustness of the NGO method.

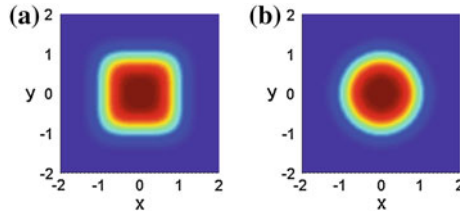


Fig. 26.15 **a** Square profile $\psi_0 = ce^{-x^4-y^4}$. **b** Circular profile $\psi_0 = ce^{-x^2-y^2}$. From [106]

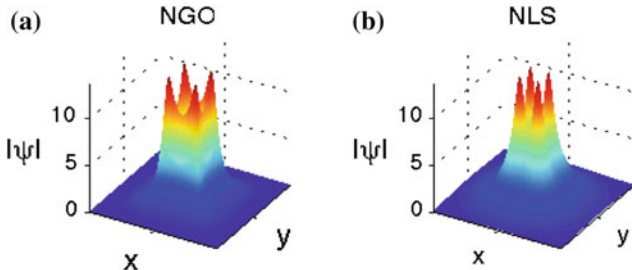


Fig. 26.16 The NLS (26.26) with $\psi_0 = 6.55e^{-x^4}e^{-y^4}$. **a** NGO amplitude at $z \approx 0.075$. **b** NLS solution at $z \approx 0.05$. From [106]

$$\frac{dy(z)}{dz} = 2c^2ze^{-2x^{2m}} \frac{\partial}{\partial y} e^{-2y^{2m}}, \quad (26.32b)$$

$$\frac{dA(z, x(z), y(z))}{dz} = -c^2zA \left[\frac{\partial^2}{\partial x^2} + \frac{\partial^2}{\partial y^2} \right] e^{-2x^{2m}} e^{-2y^{2m}}. \quad (26.32c)$$

When $m = 2$, the NGO solution breaks into four filaments located at the corners of a square, as is confirmed in direct simulations of the NLS (Fig. 26.16).

26.7.4 One-Dimensional Building Blocks

The evolution of the square input beam $\psi_0 = ce^{-x^4}e^{-y^4}$ into a square of four filaments can be explained by considering separately the dynamics in the x - and y -directions, as follows. The solution of the one-dimensional NGO rays equation (26.23a) with $\psi_0 = ce^{-x^4}$ splits into two beams located at $x = \pm a$, see Fig. 26.8 and Proposition 26.2. Hence, the solution of the one-dimensional NGO rays equation (26.32a) with $\psi_0 = c(y)e^{-x^4}$ splits into two vertical stripes centered at $x = \pm a$. Likewise, $\psi_0 = c(x)e^{-y^4}$ splits into two horizontal stripes centered at $y = \pm a$. The “product” of the vertical stripes at $x = \pm a$ and the horizontal stripes at $y = \pm a$ gives four filaments centered at $(\pm a, \pm a)$, see Fig. 26.17a. Therefore, we have

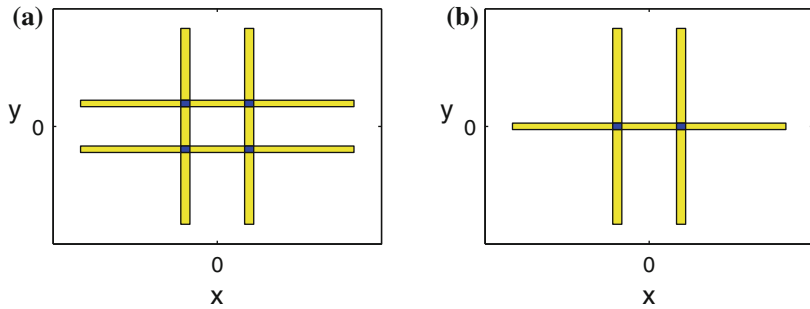


Fig. 26.17 Illustration of the one-dimensional building blocks approach. **a** $\psi_0 = ce^{-x^4} e^{-y^4}$. **b** $\psi_0 = ce^{-x^4} e^{-y^2}$

Proposition 26.4 Consider the input beam (26.31). If $m > 1$ and the input beam is strongly nonlinear, the solution of the NLS (26.26) initially evolves into four filaments located at the corners of a square.

Remark When the input power is sufficiently high, additional filaments can develop along the sides of the square. This, however, occurs after the initial collapse into four filaments, and is therefore not captured by the NGO method (Conclusion 26.5).

To further illustrate the *one-dimensional building blocks* approach, let

$$\psi_0 = ce^{-x^4} e^{-y^2}, \quad c \gg 1.$$

The x -component e^{-x^4} splits into two vertical strips centered at $x = \pm a$, while the y -component e^{-y^2} localizes into a single horizontal strip centered at $y = 0$. The “product” of the two vertical strips and the horizontal stripe gives two filaments centered at $(\pm a, 0)$, see Fig. 26.17b. Therefore, the beam splits into two beams along the x -direction. This splitting is indeed observed in simulations of the NGO equations, and confirmed in NLS simulations (Fig. 26.18).

Remark See Sects. 26.7.5, 37.4, and 37.6 for additional applications of the one-dimensional building blocks approach.

26.7.5 Rectangular Beams

We can also use the one-dimensional building blocks approach to analyze the initial dynamics of *rectangular beams*. Let

$$\psi_0 = ce^{-x^4} e^{-4y^4}.$$

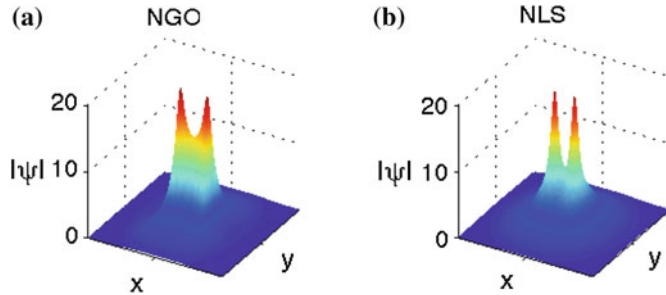


Fig. 26.18 Same as Fig. 26.16, with $\psi_0 = 7.23e^{-x^4}e^{-y^2}$. **a** NGO amplitude at $z = 0.08$. **b** NLS solution at $z \approx 0.05$. From [106]

Under the rescaling $\tilde{y} = \sqrt{2}y$, (26.26) changes into the anisotropic NLS

$$i\psi_z(z, x, \tilde{y}) + \psi_{xx} + 2\psi_{\tilde{y}\tilde{y}} + |\psi|^2\psi = 0, \quad (26.33)$$

with the square input beam $\psi_0 = ce^{-x^4}e^{-\tilde{y}^4}$. Hence, the x -component e^{-x^4} splits into two vertical strips, the \tilde{y} -component $e^{-\tilde{y}^4}$ splits into two horizontal strips, and their “product” gives four filaments located at $(\pm a, \pm a)$ in the rescaled variables, or at $(\pm a, \pm \frac{a}{\sqrt{2}})$ in the original variables. Because of the anisotropy of the NLS (26.33), the dynamics in \tilde{y} is faster than in x (Conclusion 26.3). Hence, the solution first splits in the y -direction into two horizontal strips which are nearly uniform in x , and later undergoes a second splitting in the x -direction into four filaments. These predictions are confirmed in simulations of the NGO and NLS equations (Fig. 26.19).

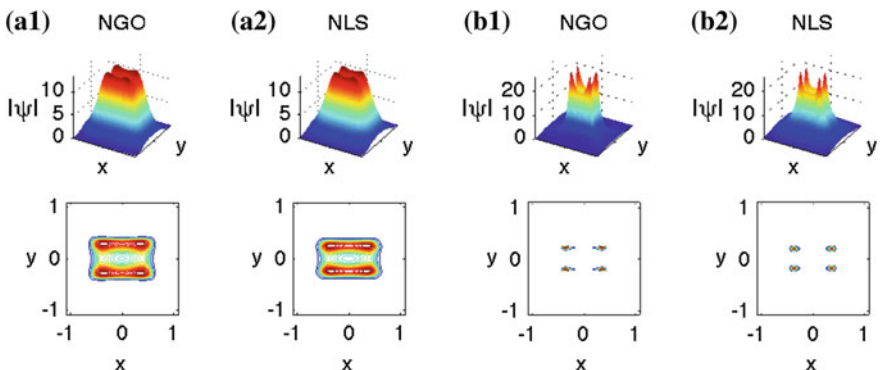


Fig. 26.19 The NLS (26.26) with $\psi_0 = 6.55e^{-x^4}e^{-4y^4}$. Top surface plot. Bottom level sets of $|\psi|$. **a1** NGO amplitude at $z = 0.02$. **a2** NLS solution at $z = 0.016$. **b1** NGO amplitude at $z = 0.07$. **b2** NLS solution at $z = 0.024$. From [106]

26.8 Effect of a Lens

The NGO equations were derived under the assumption that the effect of the initial phase is negligible compared with that of the nonlinearity (Sect. 26.4). We now briefly discuss the effect of a lens on self-focusing of strongly-nonlinear beams.

Lemma 26.4 *The filamentation pattern in the critical NLS is unaffected by a lens.*

Proof This is a consequence of the lens transformation (Sect. 8.4.1). \square

When the NLS is subcritical or supercritical, the lens changes the balance between nonlinearity and diffraction, see Sect. 8.4.2. Hence, a lens can change the filamentation pattern. See [106, Sect. IV] for further details.

26.9 Robustness of NGO Method

So far, we only presented NLS simulations with clean input beams. Numerical simulations of the NLS with high-power noisy input beams suggest that the filamentation pattern is relatively insensitive to input-beam noise. Hence, it can be predicted by the NGO method. Thus, for example, a noisy square input beam splits into four filaments, located more or less at the corners of a square. See [106] for further details.

The robustness of the NGO method is further supported by the agreement between its predictions and experimental results (Sects. 26.7.2 and 37.5). Note, however, that at sufficiently high power levels, the instabilities induced by input beam noise dominate the “clean” self-focusing dynamics which is captured by the NGO equations (Sect. 25.1.1). Consequently, in this “very strongly-nonlinear” regime, the NGO method does not predict the filamentation pattern.

Chapter 27

Location of Singularity (Z_c)

In this chapter we consider the *location of the singularity*, denoted by Z_c ,¹ for solutions of the NLS

$$i\psi_z(z, \mathbf{x}) + \Delta\psi + |\psi|^{2\sigma}\psi = 0, \quad \psi(0, \mathbf{x}) = \psi_0(\mathbf{x}). \quad (27.1)$$

As always, we mainly focus on the critical NLS

$$i\psi_z(z, \mathbf{x}) + \Delta\psi + |\psi|^{\frac{4}{d}}\psi = 0, \quad \psi(0, \mathbf{x}) = \psi_0(\mathbf{x}), \quad (27.2)$$

and in particular on the two-dimensional cubic NLS

$$i\psi_z(z, x, y) + \Delta\psi + |\psi|^2\psi = 0, \quad \psi(0, x, y) = \psi_0(x, y). \quad (27.3)$$

There is no explicit formula for Z_c as a function of ψ_0 . Therefore, in what follows we present a collection of rigorous, asymptotic, numerical, and experimental results.

27.1 Rigorous Results

27.1.1 Consequences of NLS Symmetries

We can use NLS symmetries (Chap. 8) to derive some elementary relations:

Lemma 27.1 *Let $\psi(z, \mathbf{x})$ be a solution of the NLS (27.1) that becomes singular at $z = Z_c$ and $\mathbf{x} = \mathbf{x}_c$. Then*

1. *The solution $\psi^\lambda(z, \mathbf{x})$ of (27.1) with the initial condition $\psi_0^\lambda(\mathbf{x}) = \lambda^{\frac{1}{\sigma}}\psi_0(\lambda\mathbf{x})$ becomes singular at $Z_c^\lambda = \frac{Z_c}{\lambda^2}$ and $\mathbf{x}_c^\lambda = \frac{\mathbf{x}_c}{\lambda}$.*

¹ Z_c is also called the *collapse distance*, the *blowup point*, and the *filamentation distance*.

2. The solution $\psi^{\text{GL}}(z, \mathbf{x})$ of (27.1) with the initial condition $\psi_0^{\text{GL}}(\mathbf{x}) = \psi_0(\mathbf{x})e^{i\frac{\mathbf{c}\mathbf{x}}{2}}$ becomes singular at $Z_c^{\text{GL}} = Z_c$ and $\mathbf{x}_c^{\text{GL}} = \mathbf{x}_c + Z_c\mathbf{c}$.
3. The solution $\psi^{(F)}(z, \mathbf{x})$ of the critical NLS (27.2) with the initial condition $\psi_0^{(F)}(\mathbf{x}) = \psi_0(\mathbf{x})e^{-i\frac{|\mathbf{x}|^2}{4F}}$, where $\frac{1}{F} > -\frac{1}{Z_c}$, becomes singular at $Z_c^{(F)} = \frac{Z_c F}{Z_c + F}$ and $\mathbf{x}_c^{(F)} = \left(1 - \frac{Z_c}{F}\right)\mathbf{x}_c$.

Proof Recall that ψ collapses at Z_c if $\lim_{z \rightarrow Z_c} \|\psi\|_{2\sigma+2} = \infty$, and at \mathbf{x}_c if $\lim_{z \rightarrow Z_c} \|\psi\|_{L^{2\sigma+2}(|\mathbf{x}-\mathbf{x}_c|<\epsilon)} = \infty$ for any $\epsilon > 0$.

1. By the dilation symmetry, $\psi^\lambda(z, \mathbf{x}) = \lambda^{\frac{1}{\sigma}}\psi(\lambda^2 z, \lambda\mathbf{x})$. Since ψ collapses at Z_c and \mathbf{x}_c , the result follows.
2. By Galilean invariance, $\psi^{\text{GL}}(z, \mathbf{x}) = \psi(z, \mathbf{x} - \mathbf{c}z)e^{i\frac{\mathbf{c}\mathbf{x}}{2} - i\frac{|\mathbf{c}|^2 z}{4}}$. Hence, the result follows.
3. This follows from Eqs. (8.9b) and (8.19), which are a consequence of the lens transformation.

□

27.1.2 Upper Bound for Z_c

In Sect. 7.3 we used the variance identity to show that $V(z) \leq P_2(z)$ for solutions of the critical and supercritical NLS, where $V = \int |\mathbf{x}|^2 |\psi|^2 d\mathbf{x}$ and

$$P_2(z) = V(0) + zV'(0) + 4z^2 H(0), \quad V'(0) = 4 \operatorname{Im} \int \psi_0^* \mathbf{x} \cdot \nabla \psi_0 d\mathbf{x}. \quad (27.4)$$

Therefore, if there exists $Z_* > 0$ such that $P_2(Z_*) = 0$, the NLS solution becomes singular at $Z_c \leq Z_*$. If $P_2(z)$ has two positive roots, the upper bound Z_* is the smaller of the two.

If ψ_0 is real, then $V'(0) = 0$ and so $P_2(z) = V(0) + 4z^2 H(0)$. Therefore, if ψ_0 is real and $H(0) < 0$, we have that

$$Z_c \leq Z_* = \sqrt{\frac{V(0)}{-4H(0)}}.$$

For example, consider the two-dimensional cubic NLS (27.3) with $\psi_0 = ce^{-r^2}$. Then

$$\begin{aligned} V(0) &= c^2 \int_0^\infty r^2 e^{-2r^2} r dr = \frac{c^2}{8}, \\ H(0) &= c^2 \int_0^\infty (-2r)^2 e^{-2r^2} r dr - \frac{c^4}{2} \int_0^\infty e^{-4r^2} r dr = \frac{c^2}{2} - \frac{c^4}{16}. \end{aligned}$$

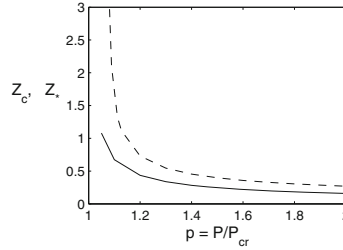


Fig. 27.1 (numerical) The collapse distance Z_c as a function of fractional input power (*solid*), for the NLS (27.3) with $\psi_0 = ce^{-r^2}$. The *dashed line* is the variance-identity upper bound Z_* , see (27.5)

Therefore,

$$Z_* = \sqrt{\frac{c^2/8}{c^4/4 - 2c^2}} = \sqrt{\frac{1}{2(c^2 - 8)}}. \quad (27.5)$$

Numerical simulations show that Z_c is well below Z_* , the variance-identity upper bound (Fig. 27.1). The reason why Z_* does not provide a good estimate for Z_c was discussed in Sect. 7.4.

Lemma 27.2 Consider the NLS (27.1) with $\psi_0 = cf(\mathbf{x})$, let $\sigma d \geq 2$, let $P_2(z; c)$ be given by (27.4), and let $Z_*(c)$ be the smaller positive root of $P_2(z; c)$, if it exists (otherwise, we set $Z_*(c) = \infty$). Then

- (1) There exists $0 < c_* < \infty$, such that

$$\begin{cases} Z_*(c) = \infty, & \text{if } 0 \leq c < c_*, \\ 0 < Z_*(c) < \infty, & \text{if } c_* < c < \infty. \end{cases}$$

- (2) $Z_*(c)$ is monotonically decreasing for $c_* < c < \infty$.

- (3) There exists a positive constant A_f , which depends on f , such that

$$Z_*(c) \sim A_f c^{-\sigma}, \quad c \rightarrow \infty.$$

In particular, $\lim_{c \rightarrow \infty} Z_*(c) = 0$.

Proof

- (1) Let $c_* = \inf_{c \geq 0} \{c \mid Z_*(c) < \infty\}$. We first claim that $0 < c_* < \infty$. Indeed, since $H(\psi_0) = c^2 \|\nabla f\|_2^2 - \frac{c^{2\sigma+2}}{\sigma+1} \|f\|_{2\sigma+2}^{2\sigma+2}$,

$$H < 0 \quad \text{for } c > c_{\text{th}} := \left((\sigma + 1) \frac{\|\nabla f\|_2^2}{\|f\|_{2\sigma+2}^{2\sigma+2}} \right)^{\frac{1}{2\sigma}}.$$

Hence, $P_2(z; c)$ has a positive root for any $c > c_{\text{th}}$ (Theorem 7.2). Therefore, $c_* \leq c_{\text{th}} < \infty$.

In assertion (2) we will prove that if $Z_*(c_1) < \infty$ and $c_2 > c_1$, then $Z_*(c_2) < Z_*(c_1)$. Therefore, $Z_*(c) < \infty$ for any $c > c_*$.

(2) Let $\tilde{P}_2(z; c) = P_2(z; c)/c^2$. Then

$$\tilde{P}_2(z; c) = V[f] + zV'[f] + 4z^2 \left(\|\nabla f\|_2^2 - \frac{c^{2\sigma}}{\sigma+1} \|f\|_{2\sigma+2}^{2\sigma+2} \right),$$

where $V[f] = \int |\mathbf{x}|^2 |f|^2 d\mathbf{x}$ and $V'[f] = 4 \operatorname{Im} \int f^* (\mathbf{x} \cdot \nabla f) d\mathbf{x}$. Therefore, if $Z_*(c_1) < \infty$,

$$\begin{aligned} 0 &= \tilde{P}_2(Z_*(c_1); c_1) \\ &= V[f] + Z_*(c_1)V'[f] + 4Z_*^2(c_1) \left(\|\nabla f\|_2^2 - \frac{c_1^{2\sigma}}{\sigma+1} \|f\|_{2\sigma+2}^{2\sigma+2} \right). \end{aligned}$$

Hence, $\tilde{P}_2(Z_*(c_1); c_2) < 0$ for any $c_2 > c_1$. Since, in addition, $\tilde{P}_2(z = 0; c_2) > 0$, it follows that $Z_*(c_2) < Z_*(c_1)$.

(3) As $c \rightarrow \infty$, the roots of $\tilde{P}_2(z; c) = 0$ satisfy $z_{1,2} \sim \pm \left(\frac{(\sigma+1)V[f]}{4\|f\|_{2\sigma+2}^{2\sigma+2}} \right)^{\frac{1}{2}} c^{-\sigma}$, see Exercise 27.1. Therefore, $Z_* \sim \left(\frac{(\sigma+1)V[f]}{4\|f\|_{2\sigma+2}^{2\sigma+2}} \right)^{\frac{1}{2}} c^{-\sigma}$. \square

Exercise 27.1 Let $x^{1,2}$ be the roots of $(A_1 - \lambda^2 A_2)x^2 + Bx + C = 0$. Show that $x^{1,2} \sim \pm \frac{1}{\lambda} \sqrt{\frac{C}{A_2}}$ as $\lambda \rightarrow \infty$.

Since $Z_c \leq Z_*$, Lemma 27.2 immediately leads to

Lemma 27.3 Let $\sigma d \geq 2$, let ψ be the solution of the NLS (27.1) with $\psi_0 = cf(\mathbf{x})$, and let $Z_c(c)$ be its blowup point.² Then

$$Z_c(c) \leq A_f c^{-\sigma}, \quad c \rightarrow \infty, \tag{27.6}$$

where A_f is a positive constant that depends on f . In particular,

$$\lim_{c \rightarrow \infty} Z_c(c) = 0. \tag{27.7}$$

We can rewrite Lemma 27.3 in terms of the solution power:

Lemma 27.4 Under the conditions of Lemma 27.3,

$$Z_c(P) \leq B_f P^{-\frac{\sigma}{2}}, \quad P \rightarrow \infty, \tag{27.8}$$

where $P = \|\psi_0\|_2^2$ and B_f is a positive constant that depends on f .

² $Z_c = \infty$ if ψ exists globally.

In Fig. 27.1 the upper bound Z_* provided a significant overestimate for Z_c . In fact, Z_* can even be *qualitatively different* from Z_c . For example,

1. By Lemma 27.2, $Z_*(c)$ is monotonically decreasing in c . While generically $Z_c(c)$ is monotonically decreasing in c (see e.g., Sect. 27.3), it can also be non-monotone (Sect. 27.6).
2. By Lemma 27.2, $Z_*(P) \sim P^{-\frac{\sigma}{2}}$ as $P \rightarrow \infty$. While $Z_c(P) \sim P^{-\frac{\sigma}{2}}$ for clean initial conditions (Conclusion 27.1), $Z_c(P) \sim P^{-\sigma}$ for noisy initial conditions (Sect. 27.2.3).

Therefore, while it is ‘tempting’ to make qualitative and quantitative predictions for Z_c based on the explicit expression for Z_* , this approach is ‘dangerous’.

27.2 Asymptotic Results

27.2.1 Adiabatic Approximation (Critical NLS)

In Lemma 18.7 we saw that in the critical NLS (27.2), if ψ_0 is real and close to a rescaled ground state $R_{L_0}^{(0)} := L_0^{-\frac{d}{2}} R^{(0)}(\frac{r}{L_0})$, the location of the singularity can be approximated using the strict adiabatic law, yielding

$$Z_c \sim Z_c^{\text{adiabatic}} := \frac{L_0^2}{\sqrt{\beta_0}}. \quad (27.9)$$

Here, L_0 is the width of ψ_0 , and $\beta_0 \sim \frac{P - P_{\text{cr}}}{M}$ is proportional to its excess power above P_{cr} , see (17.24). Numerical simulations [64] show that approximation (27.9) is fairly accurate for Townesian, Gaussian, and super-Gaussian initial conditions in the power range $P_{\text{cr}} < P < 2P_{\text{cr}}$.

Approximation (27.9) shows that Z_c scales as the square of the initial width,³ that Z_c is monotonically decreasing in P , and that

$$Z_c \sim \alpha(P - P_{\text{cr}})^{-\frac{1}{2}}, \quad 0 < P - P_{\text{cr}} \ll P_{\text{cr}}. \quad (27.10)$$

It is tempting to conclude that $Z_c \sim P^{-\frac{1}{2}}$ as $P \rightarrow \infty$. Note, however, that approximation (27.9) was derived under the assumption that $\psi_0 \sim R_{L_0}^{(0)}$, which implies that $0 < P - P_{\text{cr}} \ll P_{\text{cr}}$. Therefore, the scaling of Z_c for $P \gg P_{\text{cr}}$ can be different from $P^{-\frac{1}{2}}$. Indeed, in the one-dimensional critical NLS ($d = 1$ and $\sigma = 2$), it follows from Lemma 27.4 that $Z_c \leq B_f P^{-1}$ as $P \rightarrow \infty$. Hence, Z_c cannot

³ We already derived this result from the dilation symmetry (Lemma 27.1).

scale as $P^{-\frac{1}{2}}$. Rather, in Conclusion 27.1 we will see that for clean initial conditions $Z_c \sim P^{-\frac{\sigma}{2}}$. Therefore, $Z_c \sim P^{-\frac{1}{2}}$ as $P \rightarrow \infty$ only if $\sigma = 1$.

Remark The adiabatic approximation (27.9) for the collapse distance was derived for ψ_0 real, which corresponds to a collimated input beam. In the case of the focused input beam $\tilde{\psi}_0 = \psi_0 e^{-i\frac{x^2}{4F}}$, this approximation reads

$$\tilde{Z}_c^{\text{adiabatic}} = \frac{L_0^2}{\sqrt{\beta_0} + \frac{L_0^2}{F}},$$

see Lemma 18.8. In particular, $\tilde{Z}_c^{\text{adiabatic}}$ and $Z_c^{\text{adiabatic}}$ are related by the lens relation

$$\frac{1}{\tilde{Z}_c^{\text{adiabatic}}} = \frac{1}{Z_c^{\text{adiabatic}}} + \frac{1}{F}.$$

27.2.2 Clean High-Power Initial Conditions

Consider the NLS (27.1) with $\psi_0 = cf(\mathbf{x})$. In Sect. 26.3 we used the *NGO method* to show that the self-focusing distance scales as

$$L_{\text{SF}} \sim c^{-\sigma} \sim P^{-\frac{\sigma}{2}}, \quad c, P \rightarrow \infty. \quad (27.11)$$

The self-focusing distance L_{SF} provides a good estimate for the collapse distance Z_c . This is because once the solution's amplitude and width undergo $O(1)$ changes, the solution blows up “immediately afterwards”.⁴ Therefore, we have

Conclusion 27.1 *Let $\sigma d \geq 2$, let ψ be a solution of the NLS (27.1) with $\psi_0 = cf(\mathbf{x})$, let $P = \int |\psi_0|^2 d\mathbf{x}$, and let Z_c be the blowup point of ψ . If ψ_0 is a clean initial condition, then*

$$Z_c \sim \alpha P^{-\frac{\sigma}{2}}, \quad P \rightarrow \infty. \quad (27.12)$$

Remark The scaling exponent in relation (27.12) depends on the nonlinearity exponent σ , but not on the dimension.

Remark Conclusion 27.1 is consistent with the upper bound (27.8).

27.2.3 Noisy High-Power Initial Conditions

In the derivation of relation (27.11) which led to Conclusion 27.1, we implicitly assumed that the self-focusing dynamics is determined by the competition between

⁴ See, e.g., Figs. 3.4, 14.8a and 26.1.

nonlinearity and diffraction.⁵ In the case of noisy initial conditions, however, one should also consider the role of modulational instability (MI).

Following the discussion in Sect. 25.1.1, the characteristic distances for modulational instability and for self-focusing scale as

$$L_{\text{MI}} \sim P^{-\sigma}, \quad L_{\text{SF}} \sim P^{-\frac{\sigma}{2}}.$$

Let $P_{\text{th}}^{\text{MF}}$ denote the power at which $L_{\text{MI}} = L_{\text{SF}}$. If $P \ll P_{\text{th}}^{\text{MF}}$, then $L_{\text{MI}} \gg L_{\text{SF}}$, and so input-beam noise has a minor effect on the collapse dynamics, hence also on Z_c . When $P \gg P_{\text{th}}^{\text{MF}}$, however, then $L_{\text{MI}} \ll L_{\text{SF}}$, and so the solution becomes unstable before it had the chance to collapse. Once the solution becomes unstable, it develops spikes whose width is much smaller than the initial width L_0 (see, e.g., Fig. 25.2). Since the collapse distance scales as the square of the characteristic width (Sect. 27.1.1), the additional distance required for the spikes to collapse is much smaller than L_{MI} . Therefore,

$$Z_c^{\text{noisy}} \approx L_{\text{MI}} \sim \alpha P^{-\sigma}.$$

This scaling law was discovered in 1966 by Bespalov and Talanov (Sect. 3.6.1), rediscovered in 1974 by Campillo, Shapiro, and Suydam, and re-rediscovered in 2005 by Fibich et al.:

Conclusion 27.2 ([27, 38, 68]) *Let ψ be the solution of the NLS (27.1) with $\psi_0 = cf(\mathbf{x})$, let $\sigma d \geq 2$, $P = \int |\psi_0|^2 d\mathbf{x}$, and Z_c be the corresponding collapse point. If ψ_0 is noisy, then*

$$Z_c \sim \begin{cases} \alpha_1 P^{-\frac{\sigma}{2}}, & \text{if } 1 \ll P \ll P_{\text{th}}^{\text{MF}}, \\ \alpha_2 P^{-\sigma}, & \text{if } P \gg P_{\text{th}}^{\text{MF}}. \end{cases}$$

In particular,

$$Z_c \sim \alpha_2 P^{-\sigma}, \quad P \rightarrow \infty. \quad (27.13)$$

Thus, the collapse distance of high-power noisy beams decays much faster than for equal-power clean beams, see (27.12):

Conclusion 27.3 *In the case of sufficiently high-power beams, input-beam noise leads to a considerable reduction in the collapse distance, i.e.,*

$$Z_c^{\text{noisy}} \ll Z_c^{\text{clean}}.$$

Numerical and experimental confirmations of Conclusions 27.2 and 27.3 are given in Fig. 27.3.

⁵ The *NGO method*, which was used to derive (27.11), relies on this assumption.

Remark The change in the scaling of Z_c from $P^{-\frac{\sigma}{2}}$ to $P^{-\sigma}$ is accompanied by a transition from a single-filament collapse to multiple-filaments collapse (Sects. 25.1.1 and 25.1.2).

27.3 Gaussian Initial Conditions (Critical NLS)

In 1969, Dawes and Marburger [53] computed numerically the location of the singularity for the two-dimensional cubic NLS (27.3) with $\psi_0 = ce^{-r^2}$. From these values they obtained the curve-fitted formula⁶

$$Z_c \sim 0.184 \left[\left(\left(\frac{P}{P_2} \right)^{\frac{1}{2}} - 0.852 \right)^2 - 0.0219 \right]^{-\frac{1}{2}}, \quad P_2 = 1.013P_{\text{cr}}. \quad (27.14)$$

Over the years, the Dawes-Marburger formula was frequently used in the nonlinear optics literature. This formula, however, has a 10% error in the range $1.05P_{\text{cr}} \leq P \leq 2P_{\text{cr}}$, see Fig. 27.2a. Therefore, Fibich and Papanicolaou [93] suggested an improved curve-fitted formula

$$Z_c \sim 0.1585 \left(\frac{P}{P_{\text{cr}}} - 1 \right)^{-0.6346} \quad (27.15)$$

which has a 1% error in this range (Fig. 27.2a).

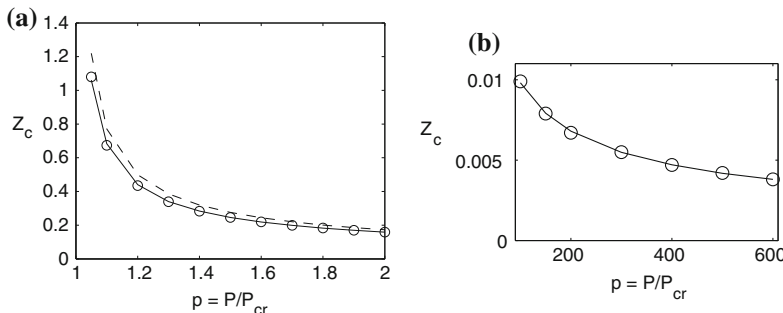


Fig. 27.2 Location of singularity (o) as a function of fractional power in the two-dimensional cubic NLS (27.3) with $\psi_0 = ce^{-r^2}$. **a** The power regime $1.05P_{\text{cr}} \leq P \leq 2P_{\text{cr}}$. Also shown are the curve-fitted formula (27.15) of Fibich and Papanicolaou (solid line) and the curve-fitted formula (27.14) of Dawes and Marburger (dashed line). **b** The power regime $100P_{\text{cr}} \leq P \leq 600P_{\text{cr}}$. Solid line is the curve-fitted formula (27.16)

⁶ The value of Z_c in (27.14) is half of that in [53], because the initial condition in [53] was $\psi_0 = ce^{-\frac{r^2}{2}}$.

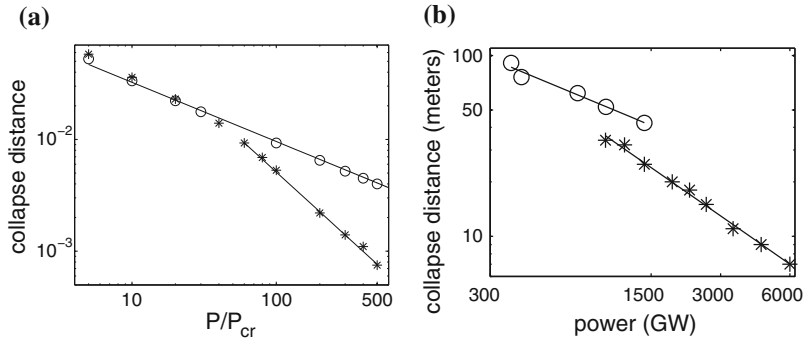


Fig. 27.3 **a** (numerical): Collapse distance of clean (o) and noisy (*) Gaussian initial conditions for the two-dimensional NLS (27.3), as a function of fractional input power. Solid lines are $Z_c = \alpha P^b$ with $b = -0.53$ (top) and $b = -1.18$ (bottom). **b** (experimental): Collapse distance in atmospheric propagation as a function of input power. Circles and stars represent data where a single amplifier and two amplifiers were used, respectively. Solid lines are $Z_c = \alpha P^b$ with $b = -0.53$ (top) and $b = -0.89$ (bottom). From [68]

The curve-fitted formulae (27.14) and (27.15) are not valid for $P \gg P_{\text{cr}}$. Simulations of (27.3) with $\psi_0 = ce^{-r^2}$ showed that [68]

$$Z_c \sim 0.11 \left(\frac{P}{P_{\text{cr}}} \right)^{-0.53}, \quad 100P_{\text{cr}} \leq P \leq 600P_{\text{cr}}, \quad (27.16)$$

see Fig. 27.2b. This approximation has a relative accuracy of 1.5%, and is in good agreement with the $P^{-\frac{1}{2}}$ theoretical prediction (Conclusion 27.1).

To observe the effect of noise on the collapse distance, in Fig. 27.3a we added 10% frozen noise by setting $\psi_0 = c(e^{-r^2} + 0.1 \text{ ran } d(x, y))$ and using the same noise realization as we varied c . As predicted in Conclusions 27.2 and 27.3, at “low” powers ($P_{\text{cr}} \ll P \leq 40P_{\text{cr}}$) noise has a little effect on the collapse distance, which continued to scale roughly as $P^{-\frac{1}{2}}$. At sufficiently high powers, however, noise leads to a considerable reduction in Z_c , which scales roughly as P^{-1} . In particular, these simulations confirm the transition from $Z_c \sim P^{-\frac{\sigma}{2}}$ to $Z_c \sim P^{-\sigma}$ for noisy input beams.

27.4 Experiments

In 1966, Wang [267] measured the collapse distance of laser beams in liquids (benzene, toluene, and nitrobenzene) as a function of input power. Wang observed that for $P_{\text{cr}} < P \leq 6P_{\text{cr}}$ the experimental data lie on the curves

$$\sqrt{P} = \sqrt{P_{\text{cr}}} + \frac{C}{Z_c},$$

where C depends on the Kerr medium. These results are in agreement with the $P^{-\frac{1}{2}}$ scaling law for values of P which are moderately above P_{cr} (Conclusion 27.1).

In 1974, Campillo et al. [38] measured the collapse distance of laser beams that propagated in CS_2 . At sufficiently high input powers the collapse distance scaled as $1/P$, in agreement with Conclusion 27.2.

The dependence of the scaling of the collapse distance on the power level was observed by Fibich et al. [68] for 45fs laser pulses propagating in air. In this experiment the collapse distance was defined as the shortest propagation distance at which the laser pulse created a visible damage to a Polyvinyl Chloride (PVC) target.⁷ Initially we used a single amplifier, hence the input profile had a relatively low noise level. A power-law fit $Z_c \sim \alpha P^b$ of the experimental data yielded $b = -0.53$, see Fig. 27.3b, in agreement with the theoretical prediction $b = -1/2$. When we added a second amplifier, we increased both the power range and the noise level. In these experiments the power-law fit yielded $b = -0.89$, in agreement with the theoretical prediction $b = -1$. See Sect. 25.1.2 for further discussion of this experiment.

27.5 Coupled Optical Beams

In 2007, Ishaaya et al. [133] studied the collapse dynamics of two parallel Gaussian beams. To do that, they solved the NLS

$$4i\psi_z(z, x, y) + \Delta\psi + |\psi|^2\psi = 0 \quad (27.17a)$$

with the two-beam initial condition

$$\psi_0(x, y) = ce^{-\left(x-\frac{\Delta_0}{2}\right)^2-y^2} + e^{i\phi_0}ce^{-\left(x+\frac{\Delta_0}{2}\right)^2-y^2}, \quad (27.17b)$$

where Δ_0 and ϕ_0 are the lateral separation and phase difference between the two input beams, respectively. As noted in Sect. 3.2.2, the two beams attract each other if $\phi_0 = 0$ (in-phase), and repel each other if $\phi_0 = \pi$ (out-of-phase).

When $\phi_0 = 0$, the initial condition (27.17b) is symmetric with respect to $x = 0$. In addition, if $\psi(z, x, y)$ is a solution of (27.17a), then so is $\psi(z, -x, y)$. Therefore, by uniqueness of NLS solutions, ψ maintains the symmetry with respect to $x = 0$ for all $z > 0$. Consequently, if ψ collapses, there are two possibilities for the collapse dynamics:

1. If the two beams remain separated, they collapse at the same distance Z_c , and the transverse locations of their collapse points are symmetric with respect to

⁷ PVC damage patterns from this experiment are presented in Fig. 25.2d–f.

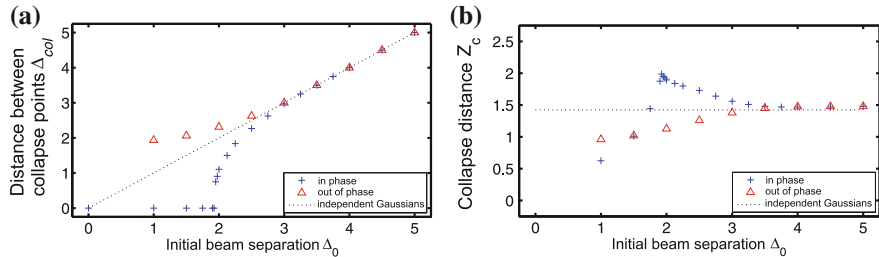


Fig. 27.4 Collapse dynamics of two coupled Gaussian beams with $P = 2.5P_{\text{cr}}$ in Kerr media (numerical). **a** Lateral separation between the collapse points, and **b** collapse distance, as functions of the initial separation between the beams, for 0 and π relative phases. From [133]

$x = 0$, i.e., $(x_c, y_c) = \left(\pm \frac{\Delta_{\text{col}}}{2}, 0 \right)$, where Δ_{col} is the lateral distance between the two collapse points.

2. If the two beams merge and collapse as a single beam, there is a unique collapse point, which by symmetry has to be at $(x_c, y_c) = (0, 0)$.

When $\phi_0 = \pi$, similar arguments show that the solution is antisymmetric with respect to $x = 0$, i.e., $\psi(z, x, y) = -\psi(z, -x, y)$ for $z \geq 0$. In particular, $\psi(z, x = 0, y) \equiv 0$ for all $z > 0$ and $-\infty < y < \infty$. Thus, the repulsion that each beam experiences is equivalent to the presence of a reflecting boundary at $x = 0$ (Sect. 16.1). Consequently, the two beams cannot merge and collapse as a single beam. By antisymmetry, the only possible collapse dynamics is that the two beams collapse at the same axial distance Z_c at two symmetric points $(x_c, y_c) = \left(\pm \frac{\Delta_{\text{col}}}{2}, 0 \right)$.

Figure 27.4 shows Z_c and Δ_{col} as functions of the initial separation Δ_0 . In these simulations the combined power of the two beams was $P = 2.5P_{\text{cr}}$. When the initial separation was sufficiently large, in both the in-phase and out-of-phase cases, the two beams were essentially independent of each other. Therefore, the lateral distance between the collapse points was equal to the initial separation, and the collapse distance was independent of initial separation.

In the in-phase case, as the initial separation decreased, the collapsing beams were attracted towards each other, hence Δ_{col} also decreased. At some critical value ($\Delta_0^{\text{critical}} \approx 1.9$), a sharp transition to a single collapsing beam was observed. This transition was accompanied by a 40% increase of the collapse distance (relative to independent-beam collapse). Intuitively, when $\Delta_0 \approx \Delta_0^{\text{critical}}$ the opposite forces that pull the solution towards a single-beam collapse and towards a two-beam collapse are nearly equal. As a result, the solution “cannot decide” which way to go, resulting in lengthening of the collapse distance.

Conclusion 27.4 *The lengthening of the collapse distance represents a critical slowing down, associated with a phase transition between independent two-beam collapse and fusion into a single beam.*

The effect of the initial separation on the collapse dynamics is different in the out-of-phase case. As Δ_0 decreases, the collapsing beams repel each other, rather than

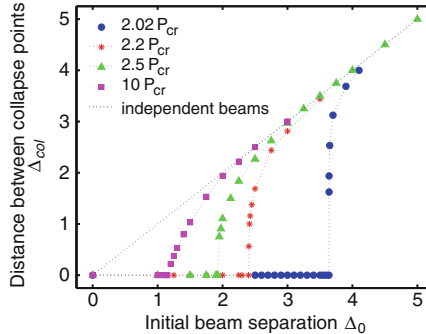


Fig. 27.5 (Numerical) spatial separation between collapse points as a function of initial spatial separation between two in-phase Gaussian beams, for various input powers. From [133]

fuse into a single beam. Since this repulsion is effectively a one-sided focusing effect that accelerates the collapse, the collapse distance is *shorter* than in the independent-beams case.

The dependence of the critical separation (where phase transition occurs) on the combined input power P is shown in Fig. 27.5. As P decreases towards $2P_{cr}$ (i.e., one critical power per beam), the critical separation at which the transition occurs increases, and the transition becomes steeper. For example, the critical separation with $P = 2.02P_{cr}$ is nearly 3 times larger than with $P = 10P_{cr}$. Intuitively, this is because as $P \rightarrow 2P_{cr}$, the collapse distance of each beam becomes considerably longer, see (27.10). This allows the beams to attract each other over a longer distance. Therefore, they can be set further apart, and yet eventually fuse into a single beam.

Ishaaya et al. also carried out experiments with coupled beams that confirmed the above theoretical predictions, see Fig. 27.6. Thus, in the in-phase case, two collapse points were observed when initial separation was large, but only one when initial separation was small. In the out-of-phase case, two collapse points were always observed.

Remark The above interactions between optical beams are deterministic. In Sect. 39.2 we shall see that because of the *loss of phase* property, interactions between beams or filaments that already underwent collapse are stochastic.

27.6 Monotonicity and Non-monotonicity of $Z_c(P)$

Let ψ be a solution of the critical or supercritical NLS (27.1) with $\psi_0 = cf(x)$. In all the analytic, asymptotic, and numerical results in Sects. 27.1, 27.2 and 27.3, the collapse distance was always monotonically decreasing in c . This is intuitive: As $P = c^2 \int |f|^2 dx$ increases, the focusing nonlinearity becomes stronger than diffraction. Hence, self focusing occurs faster, and so Z_c decreases. In Sect. 27.5 we saw, however, that the dependence of Z_c on the initial separation between two in-phase beams is non-monotone. This non-monotonicity results from the sharp

increase in the collapse distance in the transition between a single-beam collapse and a two-beam collapse.

The same type of non-monotonicity occurs if instead of fixing the power and varying the initial separation, we fix the initial separation and vary the power. Indeed, if the power of each beam is sufficiently high, it undergoes an independent collapse. In this two-beam collapse regime, the collapse distance is monotonically decreasing in P . As we lower the power, the distance over which the two beams attract each other increases. Therefore, at “sufficiently low” powers the two beams merge and collapse as a single beam. In this single-beam collapse regime, the collapse distance is also monotonically decreasing in P . In the transition between these two regimes, however, the collapse distance increases dramatically, because the solution “cannot determine which way to go”. As a result, there is loss of monotonicity in the phase-transition regime.

Non-monotonicity of $Z_c(P)$ was studied numerically in 2008 by Besse et al. [28]. Their results can be summarized as follows:

- If ψ_0 corresponds to a single beam or to the sum of two beams that move away from each other, Z_c is monotonically decreasing in P .
- If ψ_0 corresponds to the sum of two beams that travel towards each other, there are two main regimes: Either each beam collapses separately before they meet, or they merge and blowup at a single point. In each of these regimes, Z_c is monotonically decreasing in P . In the transition between these two regimes, however, Z_c increases dramatically, and thus ceases to be monotone.

In what follows, we present examples of the loss of monotonicity.

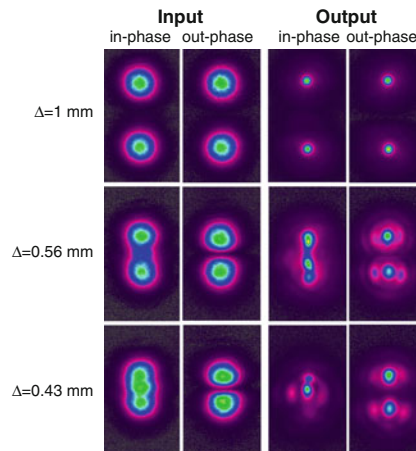


Fig. 27.6 (Experimental) input and output intensity-distributions of two collapsing beams with different initial separations for the in- and out-of-phase cases. The Gaussian beam waist is 0.29 mm, the total energy of the two beams is $7.2 \mu\text{J}$, and the propagation distance in the BK7 glass sample is 28 cm. From [133]

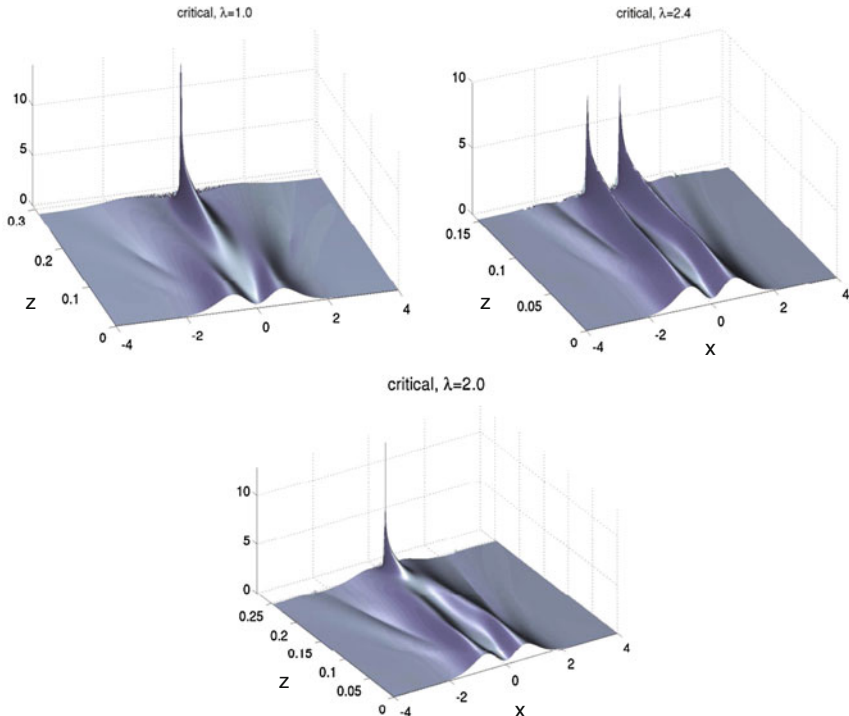


Fig. 27.7 Solution of (27.18) with $\lambda = 1$, $\lambda = 2$, and $\lambda = 2.4$. From [28]

27.6.1 Loss of Monotonicity

In [28], Besse et al. solved numerically the one-dimensional critical NLS

$$i\psi_z(z, x) + \psi_{xx} + \lambda|\psi|^4\psi = 0 \quad \psi(0, x) = \psi_0(x) \quad (27.18a)$$

with the two-beam initial condition

$$\psi_0(x) = 4(e^{-x^2} - 0.9e^{-3x^2})e^{-i\log(e^x+e^{-x})}. \quad (27.18b)$$

The amplitude of ψ_0 has two peaks at $x = \pm 0.7$, see Fig. 27.7, and its phase behaves as e^{-ix} for $x \gg 1$ and as e^{ix} for $x \ll -1$. Therefore, the two peaks move towards each other as they propagate forward (Exercise 2.6).

The dependence of Z_c on λ is shown in Fig. 27.8.⁸ For sufficiently low and high nonlinearities ($\lambda < 1.6$ and $\lambda > 2.2$, respectively), Z_c is monotonically decreasing in λ . In-between, however, there is loss of monotonicity. Figure 27.7 shows the dynamics in the three regimes. In the low-nonlinearity regime ($\lambda = 1$), the two beams

⁸ Varying λ and fixing P is equivalent to varying P and fixing λ .

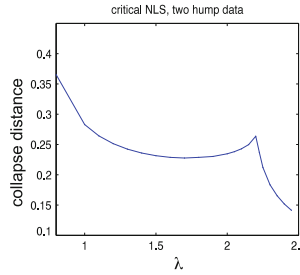


Fig. 27.8 Z_c as a function of λ for the solution of (27.18). From [28]

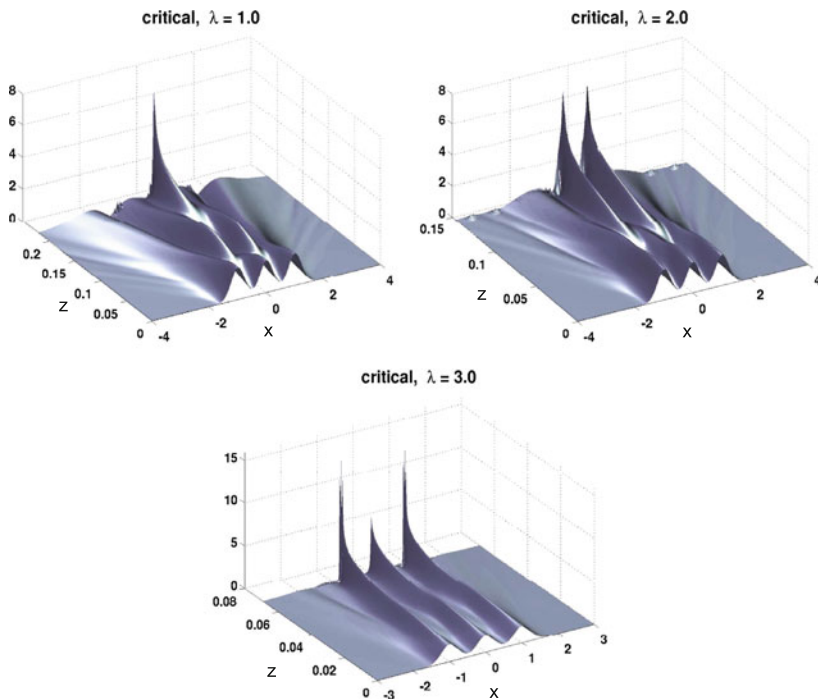


Fig. 27.9 Solution of (27.18a) with the initial condition (27.19) for $\lambda = 1$, $\lambda = 2$, and $\lambda = 3$. From [28]

merge and collapse at a single point. In the high-nonlinearity regime ($\lambda = 2.4$), the two beams remain separated and collapse simultaneously at two points. In the phase transition regime ($\lambda = 2$), the two beams remain separated over a considerable distance, but eventually merge and collapse at a single point.

To show that it is possible to have more than one non-monotonicity region, Besse et al. solved (27.18a) with the three-beam initial condition

$$\psi_0(x) = 2 \left(e^{-(3(x-1))^2} + e^{-(3x)^2} + e^{-(3(x+1))^2} \right) e^{-i \log(e^x + e^{-x})}. \quad (27.19)$$

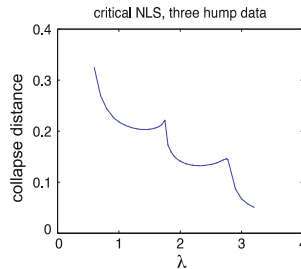


Fig. 27.10 Z_c as a function of λ for the solution of (27.18a) with the initial condition (27.19). From [28]

If λ is sufficiently large, each of the three beams self-focuses and collapses individually. At smaller values of λ , the three beams merge into two beams that collapse individually. At even smaller values of λ , the two beams merge into a single beam before collapsing. These three possible scenarios are shown in Fig. 27.9, and correspond to the three regimes in Fig. 27.10 where $Z_c(\lambda)$ is monotonically decreasing. In between these three regimes, there are two phase transitions where $Z_c(\lambda)$ is non-monotone.

Remark See Sects. 27.7.2 and 33.1.6 for other examples of non-monotonicity of Z_c .

27.7 Effect of a Lens

Let ψ be a solution of the NLS (27.1) with the initial condition $\psi_0^{(F)} = \psi_0 e^{-i \frac{|x|^2}{4F}}$. The quadratic phase term models a lens with focal distance F which is located at $z = 0$ (Conclusion 2.12). Intuitively, one can expect that a focusing lens accelerates collapse and so leads to a shorter collapse distance, i.e., that $Z_c^{(F)}$ is monotonically decreasing in $1/F$. In what follows we will see that this is usually the case, but not always.

27.7.1 Monotonicity (Critical Case)

In Sect. 8.4.5 we used the lens transformation to show that in the critical NLS (27.2), the addition of a lens with focal length F changes the collapse distance from Z_c to

$$Z_c^{(F)} = \frac{Z_c F}{Z_c + F}, \quad (27.20)$$

so that

$$\frac{1}{Z_c^{(F)}} = \frac{1}{Z_c} + \frac{1}{F}. \quad (27.21)$$

Therefore, for any initial profile, the collapse distance is monotonically increasing in F .

Corollary 27.1 *Let ψ be a solution of the critical NLS (27.2) with the initial condition $\psi_0^{(F)} = \psi_0 e^{-i \frac{|x|^2}{4F}}$, and let $Z_c^{(F)}$ be the corresponding collapse point ($Z_c^{(F)} = \infty$ if ψ does not collapse). Then*

1. $Z_c^{(F)}$ is monotonically increasing in F .
2. In the case of defocusing lenses ($-\infty < F < 0$), $Z_c^{(F)}$ becomes infinite as $-F$ approaches Z_c from above, i.e.,

$$\lim_{-F \rightarrow Z_c^+} Z_c^{(F)} = +\infty. \quad (27.22)$$

Proof This follows directly from (27.20). □

The results of Corollary 27.1 are illustrated in Fig. 27.11.

It is instructive to distinguish between three cases:

1. When $-Z_c < F < 0$, the lens is defocusing and its focal length is smaller than the collapse distance of the collimated beam. Since $Z_c^{(F)} < 0$, see (27.20), the defocusing lens arrests the collapse (Fig. 27.12d).
2. When $F < -Z_c < 0$, the lens is defocusing and its focal length is larger than the collapse distance of the collimated beam. Since $Z_c < Z_c^{(F)} < \infty$, see (27.20), collapse is delayed but not arrested (Fig. 27.12b). In particular, if $-F$ is slightly larger than Z_c , the collapse distance increases dramatically (see (27.22) and Fig. 27.12c).
3. When $0 < F$, the lens is focusing. Since $0 < Z_c^{(F)} < Z_c$, see (27.20), collapse is accelerated.

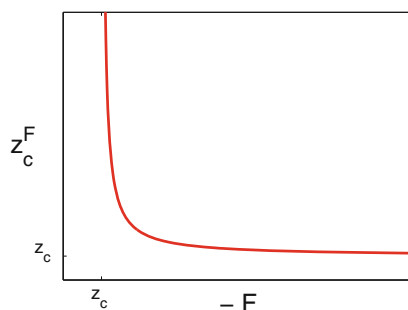


Fig. 27.11 Collapse distance in the critical NLS (27.2) as a function of the focal length of a defocusing lens. From [95]

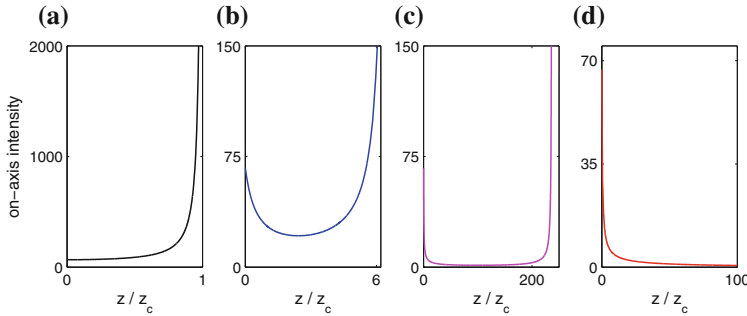


Fig. 27.12 $|\psi(z, 0, 0)|^2$ as a function of propagation distance, for the solution of the two-dimensional critical NLS (27.3) with a Gaussian input beam with $P = 9P_{\text{cr}}$, which is defocused at $z = 0$ by a lens with focal length F . **a** No lens ($F = \infty$). Collapse distance is $Z_c \approx 0.0423$. **b** $-F = 1.18Z_c$. **c** $-F = 1.0034Z_c$. **d** $-F = 0.9975Z_c$. From [95]

27.7.2 Loss of Monotonicity (Supercritical Case)

By Corollary 27.1, in the critical NLS the collapse distance is monotonically decreasing in F for any initial profile. Intuitively, this is because the lens does not change the relative magnitudes of nonlinearity and diffraction. Therefore, the lens does not change the dynamics, except for the longitudinal and transverse length scales over which it occurs. The situation is different in the supercritical case, where the lens changes the relative magnitudes of nonlinearity and diffraction (Sect. 8.4.2). As a result, the lens can lead to a qualitative change in the dynamics, from collapse at two points to collapse at a single point. This, in turn, can result in the loss of monotonicity of the collapse distance. To illustrate this, Besse et al. [28] solved numerically the one-dimensional supercritical NLS

$$i\psi_z(z, x) + \psi_{xx} + |\psi|^6\psi = 0 \quad (27.23a)$$

with the two-beam initial condition

$$\psi_0 = 1.8 \left(e^{-(3x)^2} + e^{-(3(x-1.5))^2} \right) e^{-i \frac{|x|^2}{4F}}, \quad (27.23b)$$

and observed that the collapse distance is non-monotone in F (Fig. 27.13). As in Sect. 27.6.1, non-monotonicity occurs in the phase transition regime between two-beam collapse and a single-beam collapse.

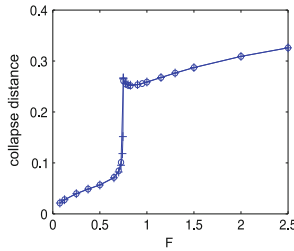


Fig. 27.13 $Z_c^{(F)}$ (crosses and circles) as a function of F for the solution of (27.23). Adapted from [28]

27.8 Controlling the Collapse Distance

One of the challenges in atmospheric propagation of intense laser pulses has been to delay and control the collapse (filamentation) distance. For many years, the standard approach has been to delay the onset of collapse by adding a negative *chirp*⁹ to the input pulse (see, e.g., [50]).

27.8.1 Deformable Mirror

In 2005, Jin et al. [135] introduced a cw (continuous-wave) approach to this problem. Specifically, they demonstrated experimentally that for a given input pulse, the collapse distance in air can be controlled by changing the initial divergence angle θ with a deformable mirror.¹⁰

The experimental results of Jin et al. were theoretically explained by Fibich et al. [95] using the lens transformation, as follows. The relation between the divergence angle and the focal length is $\tan \theta = -r_0/F$. Therefore, rewriting the (exact) relation (27.21) in terms of θ gives

$$\frac{1}{Z_c(\theta)} = \frac{1}{Z_c} - \frac{\tan \theta}{r_0}. \quad (27.24)$$

Figure 27.14 shows the experimental results of Jin et al. at three different power levels. Motivated by (27.24), we plotted $1/Z_c(\theta)$ as a function of $\tan \theta$. As expected, for each power level the data lie on a straight line. Moreover, all three lines have the same slope. This is also in agreement with (27.24), because varying the input power only affects the collapse distance Z_c .

⁹ See Sect. 36.2.4.

¹⁰ A deformable mirror acts as a lens, except that the focused (or defocused) beam is reflected rather than transmitted.

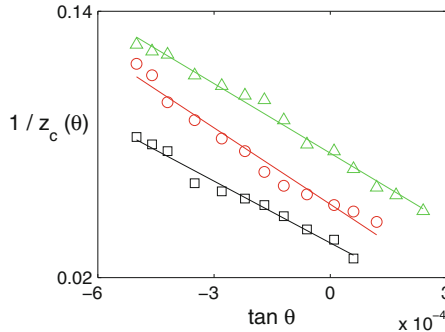


Fig. 27.14 Experimental data extracted from [135, Fig. 8]. Collapse distance in air as a function of divergence angle of deformable mirror. Input power is 300 GW (squares), 350 GW (circles), and 400 GW (triangles). From [95]

27.8.2 Double Lens Setup

An alternative cw approach for controlling the collapse distance was proposed in 2006 by Fibich et al. [95], and independently by Liu et al. [160]. In this approach one uses a double-lens setup that consists of a defocusing lens with focal length $F_1 < 0$ at $z = 0$, and a focusing lens with focal length $F_2 > 0$ at $z = d$ (Fig. 27.15). The collapse distance is controlled by varying the distance d between the two lenses (i.e., a *variable telescope*). Since the goal in atmospheric applications is to extend the collapse distance, the defocusing lens is chosen to be stronger than the focusing one (i.e., $-F_1 < F_2$), so that the overall lensing is defocusing.

Lemma 27.5 ([95]) *The double-lens setup changes the collapse distance from Z_c to $Z_c^{(F_1, F_2)}$, where*

$$Z_c^{(F_1, F_2)} = d + F_2 \frac{Z_c(F_1 - d) - dF_1}{(F_1 + F_2 - d)Z_c + F_1F_2 - dF_1}.$$

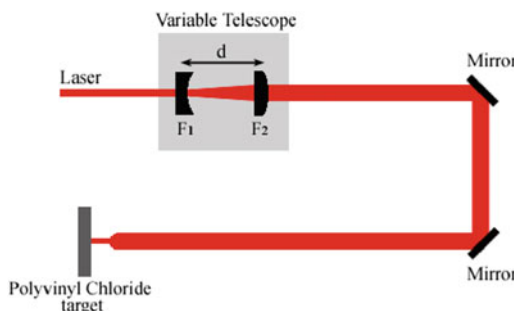


Fig. 27.15 Experimental setup of the double-lens system. From [95]

Proof The effect of the double-lens setup on the collapse distance is calculated by two successive applications of the lens transformation. By (27.21), the first lens at $z = 0$ maps the collapse distance from Z_c to $Z_c^{(F_1)}$, where

$$\frac{1}{Z_c^{(F_1)}} = \frac{1}{Z_c} + \frac{1}{F_1}.$$

Similarly, the second lens at $z = d$ maps the collapse distance from $Z_c^{(F_1)}$ to $Z_c^{(F_1, F_2)}$, where

$$\frac{1}{Z_c^{(F_1, F_2)} - d} = \frac{1}{Z_c^{(F_1)} - d} + \frac{1}{F_2}.$$

Eliminating $Z_c^{(F_1)}$ gives the result. \square

Remark In the proof of Lemma 27.5 we implicitly assumed that in the absence of the double-lens system the beam undergoes collapse (i.e., $Z_c > 0$), and that its collapse point Z_c is mapped by the first lens beyond the second lens (i.e., $Z_c^{(F_1)} > d$).

Obviously, if $Z_c^{(F_1)} < d$, the second lens has no effect on the collapse point. In that case, if $-F_1 < Z_c$, the defocusing beam arrests the collapse, whereas if $-F_1 > Z_c$ the beam collapses between the two lenses.

The expression for $Z_c^{(F_1, F_2)}$ can be rewritten as

$$Z_c^{(F_1, F_2)} = Z_c \frac{-F_1 F_2 - d F_1 + d^2}{(Z_c + F_1)(d - d_c)}, \quad d_c = \frac{(F_1 + F_2)Z_c + F_1 F_2}{Z_c + F_1}. \quad (27.25)$$

The denominator in (27.25) vanishes at $d = d_c$. When d is slightly below d_c , $Z_c^{(F_1, F_2)}$ is negative (i.e., there is no collapse). In other words, the defocusing effect of the double lens is stronger than the Kerr nonlinearity. This case is thus equivalent to a single defocusing lens with $-F < Z_c$ (Sect. 27.7). When d is slightly above d_c , the collapse point is mapped to “near infinity”. As d increases from d_c , $Z_c^{(F_1, F_2)}$ decreases from $+\infty$. Because of the $d_c - d$ term in the denominator, $Z_c^{(F_1, F_2)}$ is sensitive to changes in d near $d = d_c$ (Fig. 27.16).

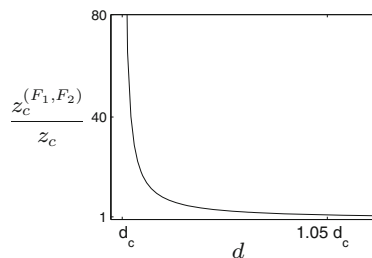


Fig. 27.16 (Theoretical) the collapse distance in the double-lens setup as a function of the distance between the two lenses. Here $F_1 = -0.5F_2 < 0$. Note the similarity to Fig. 27.11. From [95]

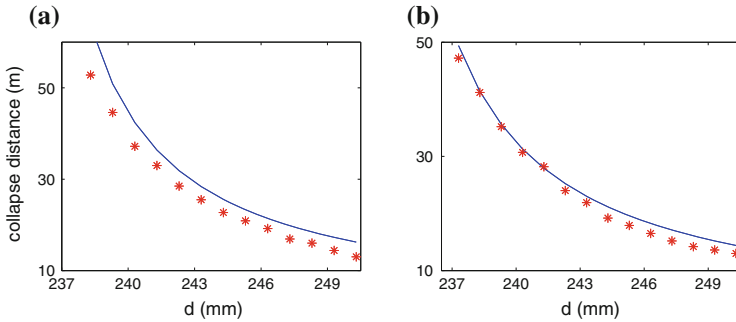


Fig. 27.17 (Experimental) collapse distance in atmospheric propagation as a function of distance between the two lenses (stars). Solid line is the theoretical prediction (27.25). **a** $P \approx 660P_{\text{cr}}$ and $Z_c = 11$ m; **b** $P \approx 780P_{\text{cr}}$ and $Z_c = 8.2$ m. From [95]

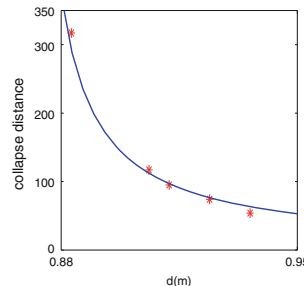


Fig. 27.18 Same as Fig. 27.17 with $P \approx 60P_{\text{cr}}$ and $Z_c = 16$ m. From [60]

Remark If we let $d \rightarrow 0$ in (27.25), we get that

$$\frac{1}{Z_c^{(F_1, F_2)}} = \frac{1}{Z_c} + \left(\frac{1}{F_1} + \frac{1}{F_2} \right).$$

Indeed, in this case the two lenses can be replaced with a single lens with focal length F , such that $\frac{1}{F} = \frac{1}{F_1} + \frac{1}{F_2}$ (Exercise 8.2).

In [95], Fibich et al. demonstrated in an indoor experiment that the double-lens setup can delay the collapse distance in air by a factor of 4, from $Z_c \approx 11$ meters to $Z_c^{(F_1, F_2)} \approx 50$ meters. Subsequently, Eisenmann et al. [60] repeated this experiment in an outdoor setting, and used the double-lens setup to delay the collapse distance by a factor of 20, from $Z_c \approx 16$ meters to $Z_c^{(F_1, F_2)} \approx 330$ meters. In both experiments the collapse distance with the double-lens setup was found to be in good agreement with the theoretical prediction (27.25), see Figs. 27.17 and 27.18.

Part VI

Numerical Methods

Chapter 28

Computation of Solitary Waves

Let $\psi^{\text{solitary}} = e^{iz} R(\mathbf{x})$ be a solitary wave of the NLS. Then the equation for R reads

$$\Delta R(\mathbf{x}) - R + |R|^{2\sigma} R = 0. \quad (28.1)$$

Since explicit solutions are only available in the one-dimensional case (Sect. 6.4.3), in higher dimensions $R(\mathbf{x})$ can only be computed numerically. In this chapter we present two popular methods for computing $R(\mathbf{x})$: *Shooting* and *renormalization*. For additional methods, see [137, Sect. 7.2].

28.1 Shooting Method

The shooting method can be used in the radial case, where R is a solution of the boundary value problem

$$R''(r) + \frac{d-1}{r} R' - R + |R|^{2\sigma} R = 0, \quad R'(0) = 0, \quad R(\infty) = 0.$$

In this method, one searches for the value(s) $R_0 \in \mathbb{R}$, such that the solution of the initial value problem

$$R''(r) + \frac{d-1}{r} R' - R + |R|^{2\sigma} R = 0, \quad R(0) = R_0, \quad R'(0) = 0 \quad (28.2)$$

satisfies $R(\infty) = 0$. By Corollary 6.10, one can limit the search to $R_0 > (1 + \sigma)^{\frac{1}{2\sigma}}$.

The shooting method is easy to implement,¹ and it can compute both the ground state $R^{(0)}$ and the excited states $\{R^{(n)}\}_{n \geq 1}$. The main disadvantage of shooting is that it becomes unstable at large values of r . To see this, note that as $r \rightarrow \infty$, (28.2) can be approximated by

$$R''(r) + \frac{d-1}{r} R' - R = 0.$$

The solution of this equation behaves as (see the proof of Lemma 6.14)

$$R(r) \sim r^{-\frac{d-1}{2}} (ae^{-r} + be^r), \quad r \rightarrow \infty.$$

The values of a and b depend on R_0 . If $R_0 = R^{(n)}(0)$, then $b = 0$, and so the analytic solution of (28.2) has the correct exponential decay as $r \rightarrow \infty$. Because of roundoff errors, however, the value of b in the numerical solution of (28.2) can be small, but it cannot be identically zero. Therefore, the increasing exponential corrupts the numerical solution at large r .

Remark When solving (28.2) numerically, the $\frac{1}{r} R'$ term can lead to significant roundoff errors for $0 < r \ll 1$. To avoid this, we can replace this term near $r = 0$ with its Taylor series approximation

$$\frac{R'}{r} \sim R''(0) + \frac{r^2}{6} R'''(0), \quad 0 \leq r \ll 1,$$

where $R''(0)$ and $R'''(0)$ are given by (6.43) and (6.44), respectively.

28.2 Spectral Renormalization Method

The spectral renormalization method was introduced in 1975 by Petviashvili [208], and re-introduced in the early 2000s by Ablowitz and co-workers (see [1] and the references therein). This method is not limited to radial solutions, it does not suffer from the instabilities of shooting at large r , and it converges to $R^{(0)}$ “quickly” and for “any” initial guess. Therefore, this method is very useful for computing ground states, but it cannot compute the excited states. A rigorous proof that the spectral renormalization method converges to the ground state was given by Pelinovsky and Stepantsvili [206].

Taking the d -dimensional Fourier transform of (28.1) and rearranging gives

$$\mathcal{F}(R) = \frac{\mathcal{F}(|R|^{2\sigma} R)}{|\mathbf{k}|^2 + 1}. \quad (28.3)$$

¹ See sample Matlab code in Fig. 28.1.

```

function []=shooting()
% Calculate R(r) in d dimensions using shooting
% Output is r_sol=[r0:dr:rf], R_sol=R(r_sol) and dR=R'(r_sol).
global R0 Dim r_inf dr_Taylor tol sigma options
Dim =2; sigma = 1; r_inf = 15; dr=0.01; tol = 1e-10;
dr_Taylor = 1e-6; %when to switch from Taylor to direct formula
R0_guess = 2.2; %initial guess for R(0)
options = odeset('RelTol',tol,'AbsTol',tol);
R0 = fzero(@shoot_for_R0,R0_guess); %Find R(0) using shooting
% X is [R, R', I_R2 I_dR2 I_2sigma_2], where I_R2=int R^2 r^(d-1),
% I_dR2=int R'^2 r^(d-1), I_2sigma_2=int R^(2 sigma+2) r^(d-1)
X0 = [R0 0 0 0]; %X0=X(0)
[r_sol,X] = ode45(@R_profile, [0:dr:r_inf], X0, options);
R_sol = X(:,1); dR_sol=X(:,2);
plot(r_sol,R_sol,r_sol,dR_sol); legend('R','dR'); xlabel('r'); shg
% Verifications - check Pohozaev identities
I_R2 = X(end,3); I_dR2 = X(end,4); I_2sigma_2 = X(end,5);
Pohozaev1 = I_R2-(2-sigma*(Dim-2))/2/(sigma+1)*I_2sigma_2
Pohozaev2 = I_dR2-sigma*Dim/2/(sigma+1)*I_2sigma_2
end
%
function R_inf = shoot_for_R0(R0) %R(r_inf) as function of R0
global r_inf options
X0 = [R0 0 0 0];
[r_sol,X] = ode45(@R_profile, [0 r_inf], X0, options);
R_inf = X(end,1);
end
%
function dX = R_profile(r,X) %Evaluate R and associated integrals
global dr_Taylor R0 Dim sigma
R = X(1); dR = X(2); dX = zeros(5,1); dX(1) = dR;
R_2sigma = abs(R)^(2*sigma);
if (r >= dr_Taylor)
    dX(2) = R-R_2sigma*R-(Dim-1)*dR/r; % R''(r)
else % Near the origin, approximate R'/r with R''(0)
    if isempty(R0)== 1
        R0=0; %set arbitrary value to R0 before it is being used
    end
    ddR0 = R0*(1-abs(R0)^(2*sigma))/Dim; %R''(0)
    dX(2) = R-R_2sigma*R-(Dim-1)*ddR0; %R''(r)
end
dX(3) = r^(Dim-1)*R^2; %for I_R2
dX(4) = r^(Dim-1)*dR^2; %for I_dR2
dX(5) = r^(Dim-1)*R_2sigma*R^2; %for I_2sigma_2
end

```

Fig. 28.1 A sample Matlab code for calculating $R^{(n)}(r)$ using shooting

Equation (28.3) can be solved with the fixed-point iterations²

$$\mathcal{F}(R_{(j+1)}) = \frac{\mathcal{F}(|R|^{2\sigma} R_{(j)})}{|\mathbf{k}|^2 + 1}, \quad j = 0, 1, \dots, \quad (28.4)$$

or equivalently $R_{(j+1)}(\mathbf{x}) = \mathcal{F}^{-1}\left(\frac{\mathcal{F}(|R_{(j)}|^{2\sigma} R_{(j)})}{|\mathbf{k}|^2 + 1}\right)$. Note that $R_{(0)}$, the initial guess,

is a function and not a scalar (e.g., $R_{(0)} = e^{-|\mathbf{x}|^2}$).

Numerical simulations show that the iterations (28.4) generically converge to the fixed points $R_{(\infty)} \equiv 0$ or $R_{(\infty)} \equiv \infty$, rather than to the ground state $R^{(0)}$. This observation can be motivated by the result that for any $0 < \epsilon \ll 1$, the iterations (28.4) with $R_{(0)} = (1-\epsilon)R^{(0)}$ converge to zero, and those with $R_{(0)} = (1+\epsilon)R^{(0)}$ converge to infinity:

Lemma 28.1 ([96]) *Consider the fixed-point iterations (28.4) with the initial guess $R_{(0)} = cR(\mathbf{x})$, where R is a nontrivial solution of (28.1). Then*

$$\lim_{j \rightarrow \infty} R_{(j)}(\mathbf{x}) \equiv \begin{cases} 0, & \text{if } 0 < c < 1, \\ \infty, & \text{if } 1 < c < \infty. \end{cases}$$

Proof By (28.4),

$$\mathcal{F}(R_{(1)}) = \frac{\mathcal{F}(|cR|^{2\sigma} cR)}{|\mathbf{k}|^2 + 1} = c^{2\sigma+1} \frac{\mathcal{F}(|R|^{2\sigma} R)}{|\mathbf{k}|^2 + 1} = c^{2\sigma+1} \mathcal{F}(R).$$

Therefore, if $R_{(0)} = cR$ then $R_{(1)} = c^{2\sigma+1}R$. Hence, the next iteration gives

$$R_{(2)} = \left(c^{2\sigma+1}\right)^{2\sigma+1} R = c^{(2\sigma+1)^2} R.$$

By induction, $R_{(j)} = c^{(2\sigma+1)^j} R$ for $j = 0, 1, \dots$, and so the result follows. \square

Lemma 28.1 shows that any small neighborhood of $R^{(0)}$ contains initial guesses for which the iterations (28.4) diverge away from $R^{(0)}$ towards zero or towards infinity. Therefore, for $R_{(j)}$ to converge to $R^{(0)}$, we need to prevent this divergence. To do that, we multiply (28.3) by $[\mathcal{F}(R)]^*$ and integrate over \mathbf{k} . This gives the integral identity

$$\text{SL}[R] = \text{SR}[R], \quad (28.5a)$$

where

$$\text{SL}[R] := \int |\mathcal{F}(R)|^2 d\mathbf{k}, \quad \text{SR}[R] := \int \frac{\mathcal{F}(|R|^{2\sigma} R) [\mathcal{F}(R)]^*}{|\mathbf{k}|^2 + 1} d\mathbf{k}. \quad (28.5b)$$

² In this section $R_{(j)} = R_{(j)}(\mathbf{x})$ denotes the j th iteration. Thus, $R_{(0)}$ is the initial guess, $R_{(1)}$ is the first iteration, etc.

In general, $R_{(j)}$ does not satisfy the integral identity (28.5). Therefore, we let $R_{(j+\frac{1}{2})} := c_j R_{(j)}$, where c_j is a positive constant which is chosen so that $R_{(j+\frac{1}{2})}$ satisfies (28.5). Specifically, let

$$\text{SL}_j := \text{SL}[R_{(j)}], \quad \text{SR}_j := \text{SR}[R_{(j)}]. \quad (28.6)$$

Then c_j is chosen so that

$$\text{SL}[c_j R_{(j)}] = \text{SR}[c_j R_{(j)}].$$

Therefore,

$$|c_j|^2 \text{SL}_j = |c_j|^{2\sigma+2} \text{SR}_j.$$

This equation has three solutions: $c_j = 0$ (corresponding to $R_{(\infty)} \equiv 0$), $c_j = \infty$ (corresponding to $R_{(\infty)} \equiv \infty$), and

$$c_j = \left| \frac{\text{SL}_j}{\text{SR}_j} \right|^{\frac{1}{2\sigma}},$$

corresponding to $R_{(\infty)} = R$. Therefore, to avoid the convergence to $R_{(\infty)} \equiv \infty$ or $R_{(\infty)} \equiv 0$, we apply the iterations (28.4) to $R_{(j+\frac{1}{2})}$, instead of to $R_{(j)}$. Since

$$\mathcal{F}\left(|R_{(j+\frac{1}{2})}|^{2\sigma} R_{(j+\frac{1}{2})}\right) = c_j^{2\sigma+1} \mathcal{F}\left(|R_{(j)}|^{2\sigma} R_{(j)}\right),$$

we arrive at the following.³

Spectral Renormalization Method:

$$\mathcal{F}(R_{(j+1)}) = \left| \frac{\text{SL}_j}{\text{SR}_j} \right|^{\frac{2\sigma+1}{2\sigma}} \frac{\mathcal{F}(|R_{(j)}|^{2\sigma} R_{(j)})}{|\mathbf{k}|^2 + 1}, \quad j = 0, 1, \dots, \quad (28.7)$$

where SL_j and SR_j are given by (28.6).

Remark Numerical simulations suggest that the iterations (28.7) converge to $R^{(0)}$ for essentially “any” initial guess $R_{(0)}$.

Remark A sample Matlab code of the spectral renormalization method is given in Fig. 28.2.

³ The above informal argument explains why renormalization prevents the divergence to zero or infinity. It does not explain, however, why these iterations generically converge to the ground state and not to an excited state.

```

function [ ] = Spectral_renormal()
%Calculate the R profile in 1 dimension using spectral renormalization
Nx=100; Xmax=10;sigma=2; thresh=1e-4; max_iter=50;
dx = 2*Xmax/Nx;
x = [-Xmax:dx:Xmax-dx];
dk = pi/Xmax;
k = fftshift([-Nx/2:Nx/2-1]*dk);
beta = (2*sigma+1)/(2*sigma); % exponent of SL/SR
R0 = exp(-x.^2); %initial guess
Rn = R0; m=1; error = 1;
while(error > thresh && m < max_iter)
    Rn_hat = fft(Rn);
    NL_hat = fft((abs(Rn)).^(2*sigma).*Rn);
    SL = dk*sum(conj(Rn_hat).*Rn_hat);
    SR = dk*sum(conj(Rn_hat).*NL_hat./(1+k.^2));
    Rn_hat = (SL/SR)^beta.*NL_hat./(1+k.^2);
    Rn = ifft(Rn_hat);
    error = abs(SL/SR-1); % check whether SL/SR is close to 1
    m = m+1;
end
%compare numerical solution with explicit expression
R_analytic = (1+sigma)^(1/(2*sigma))*(sech(sigma*x)).^(1/sigma);
plot(x,Rn,'-',x,R_analytic,'--');
xlabel('x'), ylabel('R^{(0)}','Rotation',0)
legend('numerical','analytic')
shg
end

```

Fig. 28.2 A sample Matlab code for calculating the one-dimensional ground state using the spectral renormalization method

Remark Intuitively, the renormalization by c_j prevents the divergence to zero or to infinity by restricting the iterations to functions that satisfy the integral identity (28.5), i.e., to functions that are bounded away from $R_{(\infty)} \equiv 0$ and from $R_{(\infty)} \equiv \infty$. This explanation suggests that one can also prevent the divergence by imposing other integral identities, and that the iterations do not have to be spectral. See Sect. 28.3 for more details.

Remark The iterations (28.7) can be rewritten as

$$\mathcal{F}(R_{(j+1)}) = \left(\frac{\text{SL}_j}{\text{SR}_j} \right)^\beta \frac{\mathcal{F}(|R_{(j)}|^{2\sigma} R_{(j)})}{|\mathbf{k}|^2 + 1}, \quad (28.8a)$$

where

$$\beta = \beta^* := \frac{2\sigma + 1}{2\sigma}. \quad (28.8b)$$

Numerical simulations show that the iterations (28.8a) converge to $R^{(0)}$ for $1 < \beta < 1 + \frac{1}{\sigma}$, and not only for $\beta = \beta^*$. To see why this is the case, assume as before that $R_{(0)} = cR$. Since $SL[R_{(0)}] = c^2 SL[R]$, $SR[R_{(0)}] = c^{2\sigma+2} SR[R]$, and $SL[R] = SR[R]$, the next iteration reads

$$\mathcal{F}(R_{(1)}) = \left(\frac{c^2}{c^{2\sigma+2}} \right)^\beta \frac{\mathcal{F}(c^{2\sigma+1}|R|^{2\sigma}R)}{|\mathbf{k}|^2 + 1} = c^\gamma \mathcal{F}(R), \quad (28.9)$$

where $\gamma = 2\sigma + 1 - 2\sigma\beta$. Therefore, $R_{(1)} = c^\gamma R$ and by induction $R_{(j)} = c^{\gamma^j} R$ for $j = 0, 1, \dots$. These iterations converge to R if and only if $c^{\gamma^j} \rightarrow 1$, i.e., if $|\gamma| < 1$. Therefore, the iterations (28.8a) converge to $R^{(0)}$ for $1 < \beta < 1 + \frac{1}{\sigma}$, as was indeed rigorously proved by Pelinovsky and Stepanyants [206]. The fastest convergence occurs for $\beta = \beta^*$, because in this case $\gamma = 0$ and so $R_{(1)} = R$.

In dimensions $d \geq 2$, one can utilize the radial symmetry of the ground state and work with one-dimensional integrals. In that case, however, one cannot use the Fourier transform. Therefore, in practice, when $d = 2$ or 3, it is sometimes simpler not to exploit radial symmetry and implement (28.7) using d -dimensional FFT. Alternatively, one can exploit radial symmetry and apply a non-spectral version of the renormalization method (Sect. 28.3).

28.3 Non-spectral Renormalization Method

In [11], Baruch and Fibich noted that the renormalization method does not have to be “spectral”, i.e., it can be implemented without changing to the transformed variables. Indeed, the heart of this method is the renormalization by c_j that prevents the divergence to zero or to infinity, whereas the change to Fourier space is a “technical issue”.

The spatial analog of (28.3) is

$$L(R) = -|R|^{2\sigma} R, \quad L(R) := \Delta R - R, \quad (28.10)$$

or equivalently,

$$R = -L^{-1} [|R|^{2\sigma} R]. \quad (28.11)$$

Therefore, before renormalization, the fixed-point iterations read

$$R_{(j+1)} = -L^{-1} [|R_{(j)}|^{2\sigma} R_{(j)}], \quad j = 0, 1, \dots, \quad (28.12)$$

Lemma 28.2 Consider the fixed-point iterations (28.12) with $R_{(0)} = cR(\mathbf{x})$, where R is a nontrivial solution of (28.1). Then

$$\lim_{j \rightarrow \infty} R_{(j)}(\mathbf{x}) \equiv \begin{cases} 0, & \text{if } 0 < c < 1, \\ \infty, & \text{if } 1 < c < \infty. \end{cases}$$

Exercise 28.1 Prove Lemma 28.2.

Hence, we need to add an integral constraint that will prevent the divergence. One possibility is to multiply (28.11) by R and integrate. This yields $\text{SL}^{\text{ns}}[R] = \text{SR}^{\text{ns}}[R]$,⁴ where

$$\text{SL}^{\text{ns}}[R] := \int |R|^2 d\mathbf{x} \quad \text{SR}^{\text{ns}}[R] := - \int RL^{-1} [|R|^{2\sigma} R] d\mathbf{x}. \quad (28.13)$$

As before, let $R_{(j+\frac{1}{2})} := c_j R_{(j)}$ satisfy $\text{SL}^{\text{ns}}[c_j R_{(j)}] = \text{SR}^{\text{ns}}[c_j R_{(j)}]$. Then

$$c_j = \left| \frac{\text{SL}^{\text{ns}}[R_{(j)}]}{\text{SR}^{\text{ns}}[R_{(j)}]} \right|^{\frac{1}{2\sigma}}.$$

Hence, the resulting non-spectral renormalization iterations read as follows.

Non-spectral renormalization method:

$$R_{(j+1)} = - \left| \frac{\text{SL}^{\text{ns}}[R_{(j)}]}{\text{SR}^{\text{ns}}[R_{(j)}]} \right|^{\frac{2\sigma+1}{2\sigma}} L^{-1} [|R_{(j)}|^{2\sigma} R_{(j)}], \quad j = 0, 1, \dots,$$

where L is given by (28.10), and $\text{SL}^{\text{ns}}[R_{(j)}]$ and $\text{SR}^{\text{ns}}[R_{(j)}]$ are given by (28.13).

Examples where spectral renormalization cannot be used but non-spectral renormalization can, are:

1. When the equation has variable coefficients [11].
2. When the ground state is defined on a bounded domain (see Chap. 16 and in particular Sect. 16.4.7).
3. In dimensions $d \geq 2$, when one wants to exploit radial symmetry to work with one-dimensional integrals.

28.4 Biharmonic Solitary Waves

The equation for the profile of the solitary waves of the biharmonic NLS is

$$-\Delta^2 R_B(\mathbf{x}) - R_B + |R_B|^{2\sigma} R_B = 0. \quad (28.14)$$

⁴ The superscript *ns* (*non-spectral*) emphasizes that the integral quantities are different from those in the spectral case.

If we look for radial solutions, this equation reads

$$-\Delta_r^2 R_B(r) - R_B + |R_B|^{2\sigma} R_B = 0, \quad (28.15)$$

where $\Delta_r^2 = \frac{\partial^4}{\partial r^4} + \frac{2(d-1)}{r} \frac{\partial^3}{\partial r^3} + \frac{(d-1)(d-3)}{r^2} \frac{\partial^2}{\partial r^2} - \frac{(d-1)(d-3)}{r^3} \frac{\partial}{\partial r}$ is the radial biharmonic operator.

When we compute radial solutions using shooting, (28.15) is solved for $0 < r < \infty$, with the initial conditions⁵

$$R_B(0) = R_{B,0}, \quad R'_B(0) = 0, \quad R''_B(0) = R''_{B,0}, \quad R'''_B(0) = 0.$$

Therefore, one needs to conduct a *two-parameter search* for $R_{B,0}$ and $R''_{B,0}$, for which $R_B(\infty) = 0$.

When $d = 1$, Eq. (28.15) reads

$$-R_B^{(4)}(x) - R_B + |R_B|^{2\sigma} R_B = 0. \quad (28.16)$$

In this case the search can be simplified as follows. If we multiply (28.16) by R'_B , substitute $R_B^{(4)} R'_B = \left[R_B^{(3)} R'_B - \frac{R''_B''}{2} \right]'$, integrate, and impose the condition of decay at infinity, we get

$$-R_B^{(3)} R'_B + \frac{1}{2} R''_B - \frac{1}{2} R_B^2 + \frac{1}{2\sigma+2} R_B^{2\sigma+2} = 0.$$

Substituting $x = 0$ gives $R''_B(0) = \pm \sqrt{R_B^2(0) - \frac{1}{\sigma+1} R_B^{2\sigma+2}(0)}$. Therefore, in the one-dimensional case, one only needs to conduct a one-parameter search for $R_{B,0}$ [82].

Following [14], the ground state $R_B^{(0)}$ of (28.14) can be computed with the spectral renormalization iterations

$$\mathcal{F}(R_{(j+1)}) = \left(\frac{\text{SL}_j}{\text{SR}_j} \right)^\beta \frac{\mathcal{F}(|R_{(j)}|^{2\sigma} R_{(j)})}{|\mathbf{k}|^4 + 1}, \quad j = 0, 1, \dots, \quad (28.17)$$

where

$$\text{SL}_j := \int |\mathcal{F}(R_{(j)})|^2 d\mathbf{k}, \quad \text{SR}_j := \int \frac{\mathcal{F}(|R_{(j)}|^{2\sigma} R_{(j)}) [\mathcal{F}(R_{(j)})]^*}{|\mathbf{k}|^4 + 1} d\mathbf{k},$$

and $\beta = \beta^* := \frac{2\sigma+1}{2\sigma}$. Therefore, to apply this method, one only needs to replace $|\mathbf{k}|^2 + 1$ with $|\mathbf{k}|^4 + 1$ in Fig. 28.2. This method is superior to shooting for $d \geq 1$.

⁵ Since $R_B(r)$ is even, all odd derivatives of R_B must vanish at $r = 0$.

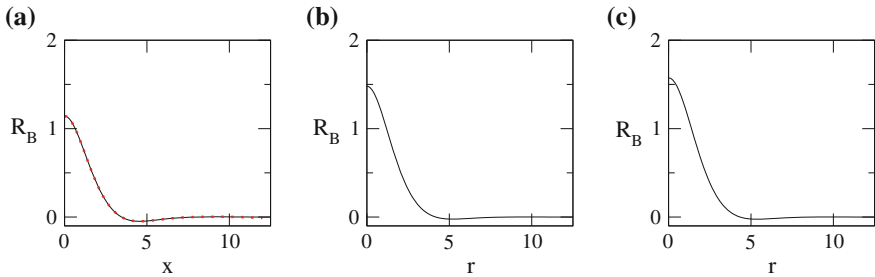


Fig. 28.3 The ground state $R_B^{(0)}$ of Eq.(28.14) with $\sigma = 4/d$, computed with the spectral renormalization method. **a** $d = 1$. The dotted line was computed with the shooting method. **b** $d = 2$. **c** $d = 3$. From [14]

Figure 28.3 shows the critical biharmonic ground states $R_B^{(0)}$ in one, two, and three dimensions, which were calculated with the spectral renormalization method. In one dimension the solution coincides with the one computed using shooting.

Exercise 28.2 Let $R_B^{(0)}$ be the ground state of (28.14).

1. Show that, generically, the spectral iterations without renormalization

$$\mathcal{F}(R_{(j+1)}) = \frac{\mathcal{F}(|R_{(j)}|^{2\sigma} R_{(j)})}{|\mathbf{k}|^4 + 1}, \quad j = 0, 1, \dots$$

diverge to zero or to infinity.

2. Show that a necessary condition for the iterations (28.17) to converge to $R_B^{(0)}$ is $1 < \beta < \frac{2\sigma+2}{2\sigma}$, and argue why the fastest convergence is obtained for $\beta = \beta^*$.

28.5 Consistency Checks

The following consistency checks can (and should) be applied to any numerical solver of (28.1). Here $R^{\text{num}}(\mathbf{x})$ denotes the numerical solution of (28.1).

1. In the one-dimensional case, compare R^{num} with the explicit solution (6.37).
2. Verify that R^{num} satisfies the Pohozaev identities (6.3).
3. Verify that the numerical solution of the NLS with the initial condition $\psi_0 = R^{\text{num}}(\mathbf{x})$ remains “close” to $\psi = e^{iz} R^{\text{num}}(\mathbf{x})$.⁶

⁶ If the solitary wave is unstable, this agreement will only persist for a “short” distance.

Chapter 29

Numerical Methods for the NLS

In this chapter we provide a very brief introduction to finite-difference methods for the NLS

$$i\psi_z(z, \mathbf{x}) + \Delta\psi + |\psi|^{2\sigma}\psi = 0, \quad \psi(0, \mathbf{x}) = \psi_0(\mathbf{x}). \quad (29.1)$$

Other approaches for computing NLS solutions include pseudo-spectral and split-step methods.¹ These methods, however, have been mainly used for non-collapsing solutions.

29.1 Spatial Discretization

Let $\Delta^h\psi$ denote a finite-difference approximation of $\Delta\psi$ on the uniform grid $\{\mathbf{x}_m = h\mathbf{m} \mid \mathbf{m} \in \mathbb{Z}^d\}$, and let $\psi_m(z) := \psi(z, \mathbf{x}_m)$. Thus, in one dimension, ψ_{xx}^h denotes a finite-difference approximation of ψ_{xx} on the grid $\{x_m = hm \mid m \in \mathbb{Z}\}$, and $\psi_m(z) := \psi(z, x_m)$. In two dimensions, $\Delta_{x,y}^h\psi$ denotes a finite-difference approximation of $\Delta_{x,y}\psi$ on the grid $\{(x_{m_1}, y_{m_2}) = (m_1h, m_2h) \mid (m_1, m_2) \in \mathbb{Z}^2\}$, and $\psi_{m_1, m_2}(z) := \psi(z, x_{m_1}, y_{m_2})$.

In one dimension, the standard three-point center-difference scheme for ψ_{xx} is

$$\psi_{xx}^h(z, x_m) := \frac{\psi_{m-1} - 2\psi_m + \psi_{m+1}}{h^2}. \quad (29.2)$$

This scheme is $O(h^2)$ accurate, i.e., $\psi_{xx} = \psi_{xx}^h + O(h^2)$. Similarly, the standard five-point $O(h^4)$ center-difference scheme for ψ_{xx} is

$$\psi_{xx}^h(z, x_m) := \frac{-\psi_{m-2} + 16\psi_{m-1} - 30\psi_m + 16\psi_{m+1} - \psi_{m+2}}{12h^2}. \quad (29.3)$$

¹ See e.g. [251, 270, 280] and the references therein.

In two dimensions, the $O(h^2)$ center-difference scheme for $\Delta_{x,y}\psi$ is

$$\begin{aligned} \Delta_{x,y}^h \psi(z, x_{m_1}, y_{m_2}) \\ := \frac{\psi_{m_1-1,m_2} + \psi_{m_1,m_2-1} - 4\psi_{m_1,m_2} + \psi_{m_1,m_2+1} + \psi_{m_1+1,m_2}}{h^2}, \end{aligned} \quad (29.4)$$

and the $O(h^4)$ center-difference scheme is

$$\begin{aligned} \Delta_{x,y}^h \psi(z, x_{m_1}, y_{m_2}) \\ := \frac{-\psi_{m_1,m_2-2} + 16\psi_{m_1,m_2-1} - 30\psi_{m_1,m_2} + 16\psi_{m_1,m_2+1} - \psi_{m_1,m_2+2}}{12h^2} \\ + \frac{-\psi_{m_1-2,m_2} + 16\psi_{m_1-1,m_2} - 30\psi_{m_1,m_2} + 16\psi_{m_1+1,m_2} - \psi_{m_1+2,m_2}}{12h^2}. \end{aligned} \quad (29.5)$$

Substituting any of the above discretizations in (29.1) gives the *semi-discrete NLS*

$$i \frac{d}{dz} \psi_{\mathbf{m}}(z) + \Delta^h \psi_{\mathbf{m}} + |\psi_{\mathbf{m}}|^{2\sigma} \psi_{\mathbf{m}} = 0, \quad \psi_{\mathbf{m}}(0) = \psi_0(\mathbf{x}_{\mathbf{m}}), \quad (29.6)$$

where $\mathbf{m} \in \mathbb{Z}^d$.²

29.1.1 Radial NLS

Consider the radial NLS

$$i \psi_z(z, r) + \psi_{rr} + \frac{d-1}{r} \psi_r + |\psi|^2 \psi = 0 \quad (29.7)$$

on the uniform grid $\{r_m = hm \mid m = 0, 1, \dots\}$, and let $\psi_m(z) := \psi(z, r_m)$. The $O(h^2)$ center-difference schemes for ψ_r and ψ_{rr} are

$$\psi_r^h(z, r_m) := \frac{-\psi_{m-1} + \psi_{m+1}}{2h}, \quad \psi_{rr}^h(z, r_m) := \frac{\psi_{m-1} - 2\psi_m + \psi_{m+1}}{h^2}.$$

The $O(h^4)$ center-difference schemes for ψ_r and ψ_{rr} are

$$\psi_r^h(z, r_m) := \frac{-\psi_{m-2} + 8\psi_{m-1} - 8\psi_{m+1} + 8\psi_{m+2}}{12h},$$

$$\psi_{rr}^h(z, r_m) := \frac{-\psi_{m-2} + 16\psi_{m-1} - 30\psi_m + 16\psi_{m+1} - \psi_{m+2}}{12h^2}.$$

² In Chap. 30 we study the effect of spatial discretization by analyzing (29.6).

Note that $r_0 = 0$ is an interior point at which the NLS is satisfied. In addition, by l'Hospital's rule, $\lim_{r \rightarrow 0} \frac{\psi_r}{r} \psi_{rr}(r = 0)$. Therefore, $\Delta_r \psi = d \cdot \psi_{rr}$ at $r_0 = 0$. To compute the difference schemes at $r_0 = 0$ and $r_1 = h$, we can use radial symmetry to add the two fictitious points $\psi_{-1} = \psi_1$ and $\psi_{-2} = \psi_2$.

29.2 “Temporal” Discretization

In this section we consider the discretization in the time-like variable z .

29.2.1 Explicit Methods

The semi-discrete NLS (29.6) is an infinite system of ODEs, indexed by $\mathbf{m} \in \mathbb{Z}^d$, which are coupled through the discretized Laplacian. In practice, this system is truncated and solved for $M_i^1 \leq m_i \leq M_i^r$, i.e., on the bounded domain $M_i^1 h \leq x_i \leq M_i^r h$, where $i = 1, \dots, d$. The truncated system can be solved with any explicit solver of ODEs. A popular choice is Runge-Kutta methods, such as Matlab's ODE45.

29.2.2 Implicit Methods

The semi-discrete NLS (29.6) can also be solved with an implicit Crank-Nicolson approach. To do that, let

$$z^n := n dz, \quad \psi_{\mathbf{m}}^n := \psi(z^n, \mathbf{x}_{\mathbf{m}}), \quad z^{n+\frac{1}{2}} := z^n + \frac{dz}{2}, \quad \psi_{\mathbf{m}}^{n+\frac{1}{2}} := \psi\left(z^{n+\frac{1}{2}}, \mathbf{x}_{\mathbf{m}}\right).$$

We first note that

$$\frac{\partial}{\partial z} \psi_{\mathbf{m}}^{n+\frac{1}{2}} = \frac{\psi_{\mathbf{m}}^{n+1} - \psi_{\mathbf{m}}^n}{dz} + O(dz^2), \quad \Delta^h \psi_{\mathbf{m}}^{n+\frac{1}{2}} = \frac{\Delta^h \psi_{\mathbf{m}}^{n+1} + \Delta^h \psi_{\mathbf{m}}^n}{2} + O(dz^2).$$

Therefore, with $O(dz^2)$ accuracy, (29.6) can be approximated at $z^{n+\frac{1}{2}}$ by

$$i \frac{\psi_{\mathbf{m}}^{n+1} - \psi_{\mathbf{m}}^n}{dz} + \frac{\Delta^h \psi_{\mathbf{m}}^{n+1} + \Delta^h \psi_{\mathbf{m}}^n}{2} + N\left(\psi_{\mathbf{m}}^{n+\frac{1}{2}}\right) = 0, \quad N(\psi) := |\psi|^{2\sigma} \psi.$$

This equation can be rewritten as

$$\left[\mathbf{I} - i \frac{dz}{2} \Delta^h \right] \psi_{\mathbf{m}}^{n+1} = \left[\mathbf{I} + i \frac{dz}{2} \Delta^h \right] \psi_{\mathbf{m}}^n + i dz N\left(\psi_{\mathbf{m}}^{n+\frac{1}{2}}\right), \quad \mathbf{m} \in \mathbb{Z}^d,$$

where \mathbf{I} is the identity operator. The above system of equations is iteratively solved for $n = 0, 1, \dots$, subject to the initial condition $\psi_{\mathbf{m}}^0 = \psi_0(\mathbf{x}_{\mathbf{m}})$.

At each iteration, we need to solve an implicit system of nonlinear equations. To do that, we can approximate the nonlinear term at $z^{n+\frac{1}{2}}$ using linear extrapolation or interpolation, i.e.,

$$\begin{aligned} N\left(\psi_{\mathbf{m}}^{n+\frac{1}{2}}\right) &= \frac{3}{2}N\left(\psi_{\mathbf{m}}^n\right) - \frac{1}{2}N\left(\psi_{\mathbf{m}}^{n-1}\right) + O\left(dz^2\right) \\ &= \frac{N\left(\psi_{\mathbf{m}}^{n+1}\right) + N\left(\psi_{\mathbf{m}}^n\right)}{2} + O\left(dz^2\right). \end{aligned}$$

Therefore, the predictor stage is

$$\left[\mathbf{I} - i \frac{dz}{2} \Delta^h\right] \psi_{\mathbf{m}, \text{pred}}^{n+1} = \left[\mathbf{I} + i \frac{dz}{2} \Delta^h\right] \psi_{\mathbf{m}}^n + i dz \frac{3N\left(\psi_{\mathbf{m}}^n\right) - N\left(\psi_{\mathbf{m}}^{n-1}\right)}{2},$$

and the corrector stage is

$$\left[\mathbf{I} - i \frac{dz}{2} \Delta^h\right] \psi_{\mathbf{m}}^{n+1} = \left[\mathbf{I} + i \frac{dz}{2} \Delta^h\right] \psi_{\mathbf{m}}^n + i dz \frac{N\left(\psi_{\mathbf{m}, \text{pred}}^{n+1}\right) + N\left(\psi_{\mathbf{m}}^n\right)}{2}.$$

Both the predictor and the corrector stages require solving a linear system of equations with the coefficient matrix $A := \mathbf{I} - i \frac{dz}{2} \Delta^h$. The matrix A is sparse, and does not depend on z . Hence, the (sparse) LU decomposition of A needs to be calculated only once, at the beginning of the simulation.

29.2.3 Explicit of Implicit?

Explicit methods are easier to implement than implicit ones. Unfortunately, they are usually less efficient. In short, this is because the CFL condition for stability is $dz = O(h^2)$ in the explicit case and $dz = O(h)$ in the implicit case. As noted, the implicit Crank-Nicolson method requires the LU factorization of A . In the one-dimensional case and in the multidimensional radial case, A is a tridiagonal or a pentadiagonal matrix. Therefore, its LU factorization is inexpensive. In higher dimensions, however, the LU factorization of A become more demanding. In such cases, one may resort to using explicit methods.

29.3 Boundary Conditions

When solving the NLS in \mathbb{R}^d numerically, we have to truncate the computational domain. Therefore, we need to impose boundary conditions at the boundary of the computational domain. Ideally, these boundary conditions should not reflect back any radiation, i.e., they should transmit (absorb) all outgoing radiation. This is not

easy to achieve, however, because the NLS is a *dispersive equation* in which different frequencies travel at different phase velocities.^{3,4} In one dimension, there are some ad hoc absorbing boundary conditions that perform reasonably well [123]. At present, however, there are no satisfactory absorbing boundary conditions for the NLS in higher dimensions.

The boundary conditions which are simplest to implement are Dirichlet and periodic. Both, however, have adverse effects on the computed solution: Dirichlet boundary conditions reflect back all radiation that reaches the computational domain boundary (Sect. 16.2), whereas periodic boundary conditions let it enter the domain from the “other side”. Therefore, when using Dirichlet or periodic boundary conditions, one has to make sure that they do not corrupt the solution. This can be done with a *domain-convergence test*, whereby the size of the computational domain is increased until a further increase has a “negligible” effect on the computed solution in the domain of interest.

Reflections from the computational domain boundary are of most concern when the solution is defocusing, because more radiation reaches the boundary. Therefore, reflections are less of an issue in simulations of collapsing solutions than for solitary waves or solutions that undergo focusing-defocusing oscillations, less for solitary waves than for defocusing solutions, and less for the focusing NLS than for the linear Schrödinger equation.

29.4 Moving-Mesh Methods

As an NLS solution collapses, it develops larger and larger gradients in z and in \mathbf{x} . Once these gradients cannot be resolved on the numerical grid, the validity of the simulation breaks down. Therefore, for a numerical solution to get closer and closer to the singularity, the numerical algorithm should use smaller and smaller mesh sizes in z and in \mathbf{x} while handling ever increasing function values. This requires specialized methods that can dynamically change the computational grid.

29.4.1 Dynamic Rescaling

The first specialized method for computing NLS blowup solutions was that of *dynamic rescaling*, which was developed in 1986 by McLaughlin et al. [171]. In this method, the width $L(z)$ of a radial solution $\psi(z, r)$ is used to dynamically rescale the dependent and independent variables, so that the rescaled solution remains smooth and bounded as $z \rightarrow Z_c$. Therefore, the rescaled equation can be solved with standard methods.

³ See Sect. 2.15.4.

⁴ See, e.g., [126] for absorbing boundary conditions for dispersive equations.

The method of dynamic rescaling is based on pre-knowledge of the scaling of the singular part of the solution. Specifically, the known scalings of $\psi_{R^{(0)}}$ and ψ_Q , the collapsing cores of peak-type singular NLS solutions (see Chaps. 14 and 21, respectively), motivate the transformation

$$\psi(z, r) = \frac{1}{L^{\frac{1}{\sigma}}(z)} u(\xi, \rho), \quad \rho = \frac{r}{L(z)}, \quad \xi = \int_0^z \frac{ds}{L^2(s)}. \quad (29.8)$$

Substitution in the NLS (29.1) shows that the equation for $u(\xi, \rho)$ is

$$iu_\xi(\xi, \rho) + \Delta_\rho u + ia(\xi) \left(\frac{u}{\sigma} + \rho u_\rho \right) + |u|^{2\sigma} u = 0, \quad (29.9)$$

where $a(\xi) := -L \frac{dL}{dz} = -\frac{1}{L} \frac{dL}{d\xi}$ and $\Delta_\rho := \partial_{\rho\rho} + \frac{d-1}{\rho} \partial_\rho$. The function $L(\xi)$ is chosen so that u remains bounded as $\xi \rightarrow \infty$. For example, the choice $L = \|\psi\|_\infty^{-\sigma}$ ensures that $|u|_\infty \equiv 1$. Similarly, the choice $L = \left(\frac{\|\nabla u_0\|_2^2}{\|\nabla \psi\|_2^2} \right)^{\frac{1}{2+\frac{2}{\sigma}-d}}$ ensures that $\|\nabla u\|_2^2 \equiv \|\nabla u_0\|_2^2$. Because u remains smooth and bounded, the rescaled equation (29.9) can be solved with standard methods. The original variables are recovered from $u(\xi, \rho)$ and $L(\xi)$ using $\psi = L^{-\frac{1}{\sigma}} u$, $z = \int_0^\xi L^2$, and $r = \rho L$. A significant improvement to the original dynamic rescaling method comes from the use of approximate boundary conditions [145].

Dynamic rescaling was extremely successful in computing radial peak-type blowup solutions of the NLS (29.1), “easily” reaching focusing levels of 10^{15} . While this method can be extended to nonradial solutions [152], its capabilities in the non-radial case are far less spectacular. For additional information on dynamic rescaling, see [249, Sect. 6.1.2] and the references therein.

29.4.2 Remeshing Without Prior Knowledge

In the method of dynamic rescaling, the solution is discretized on a fixed grid $[\rho_0, \dots, \rho_N]$ in the rescaled ρ variable. Therefore, in the original variables the solution is discretized on the uniformly-shrinking mesh $[r_0, \dots, r_N]$, where $r_n = \rho_n L(z)$. For peak-type solutions the mesh points move into the singular region at just the correct rate, so that the collapsing core is well resolved. Unfortunately, dynamic rescaling is “at a loss” when there is no prior knowledge of the scaling of the collapsing core,⁵ or when the scaling of the collapsing core is more complex than a uniform contraction towards a fixed point.⁶

⁵ This is the case in simulations of pulse splitting in the NLS with normal dispersion (Chap. 36).

⁶ This is the case with standing-ring and shrinking-ring blowup solutions (Chaps. 22 and 23, respectively).

In 1996, Budd et al. [36] developed a moving-mesh method for the NLS, in which mesh points are redistributed without any prior knowledge of the solution profile near the singularity. In order to ensure that grid points move into regions with higher gradients (so that the solution will be well resolved in these regions), they coupled the NLS to a PDE that governs the dynamic location of the grid points.

In 2000, Ren and Wang [222] replaced the dynamic PDE for the mesh points with a semi-static variational approach. Specifically, they defined a global smoothness criterion for the solution, and applied a grid-remeshing procedure only when this criterion is violated. The remeshing procedure was based on an iterative solution of a variational problem with a weight function, hence the name the Iterative Grid Redistribution (IGR) method. The IGR method was highly successful in computing singular solutions. In particular, it managed to handle problems that could not be solved with dynamic rescaling, such as solving the NLS with small normal dispersion beyond the pulse splitting (Sect. 36.8.8 and [94]), and computing standing-ring and shrinking-ring blowup solutions (Chaps. 22 and 23 and [74]).

In [57], Ditkowsky and Gavish improved the IGR method by replacing the iterative remeshing with a single-step procedure, by deriving a robust methodology for designing the weight function, and by controlling the fraction of grid points that move into the singular region. These capabilities enabled the solution of even more challenging cases, such as vortex blowup solutions [72]. See also [13, 94, 268] for additional improvements and modifications to IGR, and [42] for the moving-mesh algorithm of Ceniceros and Hou.

29.5 Consistency Checks

Regardless of the numerical method used to solve the NLS, there are several consistency checks that should be performed:

1. The order of accuracy of the numerical solver can be tested with the following problems that possess an explicit stable solution:
 - (a) The solution of the d -dimensional linear Schrödinger equation

$$i\psi_z(z, \mathbf{x}) + \Delta\psi = 0, \quad \psi_0 = e^{-|\mathbf{x}|^2}$$

is $\psi = (1 + 4iz)^{-\frac{d}{2}} e^{-\frac{1-4iz}{1+16z^2} |\mathbf{x}|^2}$. This solution can be used to test the linear part of the code.

- (b) The solution of the NLS (29.1) with $\psi_0 = R^{(0)}(|\mathbf{x}|)$ is the solitary wave $\psi^{\text{solitary},(0)} = e^{iz} R^{(0)}(|\mathbf{x}|)$. The ground state $R^{(0)}$ is given explicitly in the one-dimensional case (Lemma 6.15), and can be computed numerically in higher dimensions (Chap. 28). In the subcritical case, $\psi^{\text{solitary},(0)}$ is stable. In the critical and supercritical cases where $\psi^{\text{solitary},(0)}$ is unstable, the

numerical solution should agree with $\psi^{\text{solitary},(0)}$ over a “short” distance, whose length increases as the grid is refined.

- (c) The solution of the one-dimensional cubic NLS

$$i\psi_z(z, x) + \psi_{xx} + |\psi|^2\psi = 0, \quad \psi_0 = \sqrt{2} \operatorname{sech}(x)e^{\frac{ix}{2}}$$

is the moving soliton $\psi(z, x) = \sqrt{2} \operatorname{sech}(x - z)e^{\frac{ix}{2} + \frac{3}{4}iz}$.

2. A qualitative test of the code is that the solution of the critical NLS

$$i\psi_z + \Delta\psi + |\psi|^{\frac{4}{d}}\psi = 0, \quad \psi_0 = (1 + \epsilon)R^{(0)},$$

should collapse for $0 < \epsilon \ll 1$ and scatter for $0 < -\epsilon \ll 1$.

3. When solving the NLS with a general initial condition, one should:

- (a) Monitor the conservation of the power and the Hamiltonian. Note that as the solution collapses, the two terms of the Hamiltonian go to infinity. As a result, the numerical evaluation of the Hamiltonian suffers from cancellation of significant digits. Therefore, the numerical Hamiltonian may appear to be “less conserved” than the numerical power.
- (b) Verify that the solution at the lateral boundaries of the computational domain is “sufficiently” small.
- (c) Verify that further refining the grid size in z and in x and further enlarging the computational domain has a “negligible” effect on the solution in the domain of interest.

Chapter 30

Effects of Spatial Discretization

In this chapter we consider what can happen when we try to compute a singular solution of the critical or supercritical NLS

$$i\psi_z(z, \mathbf{x}) + \Delta\psi + |\psi|^{2\sigma}\psi = 0, \quad \sigma d \geq 2 \quad (30.1)$$

with a *naive* finite-difference scheme. We do not give a comprehensive answer. Rather, following Fibich and Ilan [79], we focus on the effect of discretizing the Laplacian with the standard second-order or fourth-order center-difference schemes. As we shall see, this discretization initially accelerates self-focusing, but later arrests collapse, leading instead to focusing-defocusing oscillations.

30.1 Spatial Discretization

We assume that the mesh size in z is sufficiently fine, so that the effects of discretization in z are negligible, compared with those of discretization in \mathbf{x} . Therefore, in what follows we treat z as a continuous variable.

Consider the one-dimensional NLS

$$i\psi_z(z, x) + \psi_{xx} + |\psi|^{2\sigma}\psi = 0, \quad (30.2)$$

discretized on the uniform grid $\{x_m = mh \mid m \in \mathbb{Z}\}$. Substituting the standard $O(h^2)$ center-difference scheme for ψ_{xx} , see (29.2), yields

$$i\frac{d}{dz}\psi_m(z) + \frac{\psi_{m-1} - 2\psi_m + \psi_{m+1}}{h^2} + |\psi_m|^{2\sigma}\psi_m = 0, \quad m \in \mathbb{Z}, \quad (30.3)$$

where $\psi_m(z) := \psi(z, x_m)$.¹ Similarly, substituting the standard $O(h^4)$ center-difference scheme for ψ_{xx} , see (29.3), yields

$$\begin{aligned} i \frac{d}{dz} \psi_m(z) + \frac{-\psi_{m-2} + 16\psi_{m-1} - 30\psi_m + 16\psi_{m+1} - \psi_{m+2}}{h^2} \\ + |\psi_m|^{2\sigma} \psi_m = 0, \quad m \in \mathbb{Z}. \end{aligned} \quad (30.4)$$

For the two-dimensional NLS

$$i\psi_z(z, x, y) + \Delta_{x,y}\psi + |\psi|^{2\sigma}\psi = 0 \quad (30.5)$$

on the uniform grid $\{(x_{m_1}, y_{m_2}) = (m_1 h, m_2 h) \mid (m_1, m_2) \in \mathbb{Z}^2\}$, substituting the $O(h^2)$ center-difference scheme for $\Delta_{x,y}\psi$, see (29.4), yields

$$\begin{aligned} i \frac{d}{dz} \psi_{m_1, m_2}(z) + \frac{\psi_{m_1-1, m_2} + \psi_{m_1, m_2-1} - 4\psi_{m_1, m_2} + \psi_{m_1, m_2+1} + \psi_{m_1+1, m_2}}{h^2} \\ + |\psi_{m_1, m_2}|^{2\sigma} \psi_{m_1, m_2} = 0, \quad (m_1, m_2) \in \mathbb{Z}^2, \end{aligned} \quad (30.6)$$

while substituting the $O(h^4)$ center-difference scheme for $\Delta_{x,y}\psi$, see (29.5), yields

$$\begin{aligned} i \frac{d}{dz} \psi_{m_1, m_2}(z) \\ + \frac{-\psi_{m_1, m_2-2} + 16\psi_{m_1, m_2-1} - 30\psi_{m_1, m_2} + 16\psi_{m_1, m_2+1} - \psi_{m_1, m_2+2}}{12h^2} \\ + \frac{-\psi_{m_1-2, m_2} + 16\psi_{m_1-1, m_2} - 30\psi_{m_1, m_2} + 16\psi_{m_1+1, m_2} - \psi_{m_1+2, m_2}}{12h^2} \\ + |\psi_{m_1, m_2}|^{2\sigma} \psi_{m_1, m_2} = 0, \quad (m_1, m_2) \in \mathbb{Z}^2, \end{aligned} \quad (30.7)$$

where $\psi_{m_1, m_2}(z) := \psi(z, x_{m_1}, y_{m_2})$.

30.2 Modified Equations

By Taylor expansion,

$$\frac{\psi_{m-1} - 2\psi_m + \psi_{m+1}}{h^2} = \psi_{xx}(z, x_m) + \frac{h^2}{12} \psi_{xxxx} + O(h^4).$$

¹ To avoid too many notations, ψ_m denotes both the solution of the NLS (30.2) at x_m , and the solutions of the semi-discrete NLS (30.3) and (30.4).

Hence, the semi-discrete NLS (30.3) is more accurately approximated by the *modified equation*

$$i\psi_z(z, x) + \psi_{xx} + |\psi|^{2\sigma}\psi + \frac{h^2}{12}\psi_{xxxx} = 0, \quad (30.8)$$

than by the original NLS (30.2). Similarly, since

$$\begin{aligned} & \frac{\psi_{m_1-1,m_2} + \psi_{m_1,m_2-1} - 4\psi_{m_1,m_2} + \psi_{m_1,m_2+1} + \psi_{m_1+1,m_2}}{h^2} \\ &= \Delta_{x,y}\psi(z, x_{m_1}, y_{m_2}) + \frac{h^2}{12}(\psi_{xxxx} + \psi_{yyyy}) + O(h^4), \end{aligned}$$

the semi-discrete NLS (30.6) is more accurately approximated by the modified equation

$$i\psi_z(z, x, y) + \Delta_{x,y}\psi + |\psi|^{2\sigma}\psi + \frac{h^2}{12}(\psi_{xxxx} + \psi_{yyyy}) = 0, \quad (30.9)$$

than by the original NLS (30.5).

Fourth-order diffraction $\Delta_{x,y}^2\psi = \psi_{xxxx} + 2\psi_{xxyy} + \psi_{yyyy}$ is isotropic, i.e., it is invariant under rotations in \mathbb{R}^2 . In contrast, $\psi_{xxxx} + \psi_{yyyy}$ is only invariant under rotations by 90° . This anisotropy in (30.9) is induced by the preferred directions of the Cartesian discretization. In Lemma 30.1 we shall see that the anisotropy of $\psi_{xxxx} + \psi_{yyyy}$ is “mild”, in the sense that its L^2 norm is equivalent to that of $\Delta_{x,y}^2\psi$.²

More generally, we have

Conclusion 30.1 *The leading-order effect of second-order center-difference discretization of $\sum_{i=1}^d \frac{\partial^2 \psi}{\partial x_i^2}$ is equivalent to that of mildly-anisotropic fourth-order diffraction $\frac{h^2}{12} \sum_{i=1}^d \frac{\partial^4 \psi}{\partial x_i^4}$.*

Similar arguments show that the semi-discrete NLS (30.4) is more accurately approximated by the modified equation

$$i\psi_z(z, x) + \psi_{xx} + |\psi|^{2\sigma}\psi - \frac{2h^4}{15}\frac{\partial^6 \psi}{\partial x^6} = 0, \quad (30.10)$$

than by the ‘original’ NLS (30.2), and the semi-discrete NLS (30.7) is more accurately approximated by the modified equation

$$i\psi_z(z, x, y) + \Delta\psi + |\psi|^{2\sigma}\psi - \frac{2h^4}{15}\left(\frac{\partial^6 \psi}{\partial x^6} + \frac{\partial^6 \psi}{\partial y^6}\right) = 0, \quad (30.11)$$

than by the ‘original’ NLS (30.5).

² Nevertheless, this “mild” anisotropy can lead to multiple filamentation in NLS simulations (Sect. 25.2).

Conclusion 30.2 The leading-order effect of fourth-order center-difference discretization of $\sum_{i=1}^d \frac{\partial^2 \psi}{\partial x_i^2}$ is equivalent to that of negative mildly-anisotropic sixth-order diffraction $-\frac{2h^4}{15} \sum_{i=1}^d \frac{\partial^6 \psi}{\partial x_i^6}$.

30.2.1 Rigorous Analysis

The modified equations (30.8)–(30.11) are special cases of the NLS with small high-order mildly-anisotropic diffraction

$$i\psi_z(z, \mathbf{x}) + \Delta\psi + |\psi|^{2\sigma}\psi + (-1)^k\epsilon \sum_{i=1}^d \frac{\partial^{2k}\psi}{\partial x_i^{2k}} = 0, \quad 0 < \epsilon \ll 1, \quad (30.12)$$

where $\epsilon = c_k h^{2k-2}$ and $2k - 2$ is the order of the center-difference scheme. We now prove that all solutions of (30.12) exist globally. We first establish this result for the NLS with *isotropic* high-order diffraction.

Theorem 30.1 ([82]) Let ψ be a solution of

$$i\psi_z(z, \mathbf{x}) + \Delta\psi + |\psi|^{2\sigma}\psi + (-1)^k\epsilon\Delta^k\psi = 0, \quad \psi(0, \mathbf{x}) = \psi_0(\mathbf{x}) \in H^k,$$

where $k \geq 2$ is an integer. Then $\epsilon > 0$ is a sufficient condition for global existence.

Proof The case $k = 2$ was proved in Theorem 5.8. The extension to $k > 2$ is straightforward. \square

Remark Note that $\epsilon > 0$ is the defocusing case.

We now show that the anisotropy of $\sum_{i=1}^d \frac{\partial^{2k}\psi}{\partial x_i^{2k}}$ is “mild”, in the sense that its L^2 norm is equivalent to that of the corresponding isotropic term.

Lemma 30.1 Let $f(\mathbf{x}) \in H^k(\mathbb{R}^d)$, and let $k = 2, 3, \dots$

1. If k is even, then

$$\sum_{i=1}^d \left\| \frac{\partial^k f}{\partial x_i^k} \right\|_2^2 \leq \|\Delta^{\frac{k}{2}} f\|_2^2 \leq d^k \sum_{i=1}^d \left\| \frac{\partial^k f}{\partial x_i^k} \right\|_2^2.$$

2. If k is odd, then

$$\sum_{i=1}^d \left\| \frac{\partial^k f}{\partial x_i^k} \right\|_2^2 \leq \|\Delta^{\frac{k-1}{2}} \nabla f\|_2^2 \leq d^k \sum_{i=1}^d \left\| \frac{\partial^k f}{\partial x_i^k} \right\|_2^2,$$

where $\|\Delta^{\frac{k-1}{2}} \nabla f\|_2^2 := \sum_{i=1}^d \|\Delta^{\frac{k-1}{2}} \frac{\partial f}{\partial x_i}\|_2^2$.

Proof Let $\hat{f}(\mathbf{w})$ be the Fourier transform of $f(\mathbf{x})$, and let k be even. By Parseval's relation,

$$\sum_{i=1}^d \left\| \frac{\partial^k f}{\partial x_i^k} \right\|_2^2 = \sum_{i=1}^d \| w_i^k \hat{f} \|^2_2 = \sum_{i=1}^d \int |w_i|^{2k} |\hat{f}|^2 d\mathbf{w},$$

and

$$\|\Delta^{\frac{k}{2}} f\|_2^2 = \| |\mathbf{w}|^k \hat{f} \|_2^2 = \int |\mathbf{w}|^{2k} |\hat{f}|^2 d\mathbf{w}.$$

Therefore, it is sufficient to prove that

$$\sum_{i=1}^d w_i^{2k} \leq \left(\sum_{i=1}^d w_i^2 \right)^k \leq d^k \sum_{i=1}^d w_i^{2k}.$$

The left inequality is immediate. The right inequality follows from

$$\left(\sum_{i=1}^d w_i^2 \right)^k \leq \left(d \cdot \max_i w_i^2 \right)^k = d^k \max_i w_i^{2k} \leq d^k \sum_{i=1}^d w_i^{2k}. \quad \square$$

Exercise 30.1 Prove Lemma 30.1 for k odd.

Using Lemma 30.1, we can generalize Theorem 30.1 to the NLS with mildly-anisotropic high-order diffraction:

Theorem 30.2 ([79]) Let ψ be a solution of (30.12) such that $\psi(0, \mathbf{x}) \in H^k$, and let $k \geq 2$ be an integer. Then ψ exists globally.

Proof We first note that power and Hamiltonian conservation for (30.12) read $\|\psi\|_2^2 \equiv \|\psi_0\|_2^2$ and $H(z) \equiv H(0)$, where

$$H = \underbrace{\|\nabla \psi\|_2^2}_{\text{diffraction}} - \underbrace{\frac{1}{\sigma+1} \|\psi\|_{2\sigma+2}^{2\sigma+2}}_{\text{nonlinearity}} - \epsilon \underbrace{\sum_{i=1}^d \left\| \frac{\partial^k \psi}{\partial x_i^k} \right\|_2^2}_{\text{discretization}}. \quad (30.13)$$

We begin with the case where k is even. By power conservation, Hamiltonian conservation, and inequality (5.16),

$$\begin{aligned} \epsilon \sum_{i=1}^d \left\| \frac{\partial^k \psi}{\partial x_i^k} \right\|_2^2 &= -H(0) + \|\nabla \psi\|_2^2 - \frac{1}{\sigma+1} \|\psi\|_{2\sigma+2}^{2\sigma+2} \\ &\leq -H(0) + \|\psi\|_2 \|\Delta \psi\|_2 = -H(0) + \|\psi_0\|_2 \|\Delta \psi\|_2. \end{aligned}$$

From Parseval's relation and the inequality $|\mathbf{w}|^4 \leq 1 + |\mathbf{w}|^{2k}$,³ we have that

$$\|\Delta\psi\|_2^2 = \int |\mathbf{w}|^4 |\hat{\psi}|^2 d\mathbf{w} \leq \int (1 + |\mathbf{w}|^{2k}) |\hat{\psi}|^2 d\mathbf{w} = \|\psi\|_2^2 + \|\Delta^{\frac{k}{2}}\psi\|_2^2.$$

In addition, by Lemma 30.1, $\|\Delta^{\frac{k}{2}}\psi\|_2^2 \leq \sum_{i=1}^d \left\| \frac{\partial^k \psi}{\partial x_i^k} \right\|_2^2$. Combining the above gives $\epsilon d^{-k} \|\Delta^{\frac{k}{2}}\psi\|_2^2 \leq -H(0) + \|\psi_0\|_2 \sqrt{\|\psi_0\|_2^2 + \|\Delta^{\frac{k}{2}}\psi\|_2^2}$, from which we conclude that $\|\Delta^{\frac{k}{2}}\psi\|_2^2$ is bounded. Since in addition $\|\psi\|_2^2 \equiv \|\psi_0\|_2^2$, we have that $\|\psi\|_{H^k}$ is bounded (Exercise 30.2). Hence, ψ exists globally. When k is odd, global existence follows from similar estimates for $\|\Delta^{\frac{k-1}{2}}\nabla\psi\|_2^2$. \square

Exercise 30.2 Let k be even. Show that if $\|\Delta^{\frac{k}{2}}\psi\|_2$ and $\|\psi\|_2$ are bounded, then $\psi \in H^k$.

30.3 Analysis of the Semi-discrete NLS

Theorem 30.2 shows that all solutions of the modified equations (30.8)–(30.11) exist globally. While this suggests that solutions of the corresponding semi-discrete NLS equations do not blowup, it does not prove it. This is because if a solution of the semi-discrete NLS does blowup, the validity of the Taylor expansion of the discretized Laplacian, hence of the modified equation as an approximation of the semi-discrete NLS, breaks down near the singularity.

To rigorously prove that solutions of the above semi-discrete NLS do not blowup, we analyze these equations directly in a discrete framework. We begin with the following definitions:⁴

$$\begin{aligned} \{\psi_m\} \in l^2(\mathbb{Z}) &\iff \|\psi_m\|_{l^2} := \left(h \sum_{m=-\infty}^{\infty} |\psi_m|^2 \right)^{\frac{1}{2}} < \infty, \\ \{\psi_{m_1, m_2}\} \in l^2(\mathbb{Z}^2) &\iff \|\psi_{m_1, m_2}\|_{l^2} := \left(h^2 \sum_{m_1, m_2=-\infty}^{\infty} |\psi_{m_1, m_2}|^2 \right)^{\frac{1}{2}} < \infty. \end{aligned}$$

Lemma 30.2 (discrete power conservation) Let $\{\psi_m(z)\}$ be a solution of the semi-discrete NLS (30.3) or (30.4), such that $\{\psi_m(z)\} \in l^2$. Then

$$\|\psi_m(z)\|_{l^2} \equiv \|\psi_m(0)\|_{l^2}.$$

³ To prove this inequality, simply consider separately the cases $|\mathbf{w}| \leq 1$ and $|\mathbf{w}| > 1$.

⁴ These discrete norms are the composite trapezoidal rules for $\|\psi\|_2$.

Similarly, let $\{\psi_{m_1, m_2}(z)\}$ be a solution of the semi-discrete NLS (30.6) or (30.7), such that $\{\psi_{m_1, m_2}(z)\} \in l^2$. Then

$$\|\psi_{m_1, m_2}(z)\|_{l^2} \equiv \|\psi_{m_1, m_2}(0)\|_{l^2}.$$

Proof The proof is the discrete analog of that of Lemma 5.1. Let $\{\psi_m(z)\}$ be a solution of (30.3). Multiplying this equation by ψ_m^* gives

$$i\psi_m^* \frac{d}{dz} \psi_m + \psi_m^* \frac{\psi_{m-1} - 2\psi_m + \psi_{m+1}}{h^2} + |\psi_m|^{2\sigma+2} = 0.$$

Subtracting the complex-conjugate equation gives

$$i \frac{d}{dz} |\psi_m|^2 + \psi_m^* \frac{\psi_{m-1} + \psi_{m+1}}{h^2} - \psi_m \frac{\psi_{m-1}^* + \psi_{m+1}^*}{h^2} = 0.$$

Taking the sum over all m gives

$$i \frac{d}{dz} \sum_{m=-\infty}^{\infty} |\psi_m|^2 = i \sum_{m=-\infty}^{\infty} \frac{d}{dz} |\psi_m|^2 = 0.$$

The proof for the other cases is similar. \square

When the discrete power (l^2 norm) is conserved, the semi-discrete solution cannot become infinite, and therefore the semi-discrete solution exists globally:

Lemma 30.3 *Let $\{\psi_m\}$ be a solution of a semi-discrete one-dimensional NLS, for which $\|\psi_m(z)\|_{l^2}$ is conserved. If $\{\psi_m(0)\} \in l^2$, then $\{\psi_m\}$ exist globally in l^2 . Furthermore,*

$$\|\psi_m(z)\|_{l^\infty} \leq h^{-\frac{1}{2}} \|\psi_m(0)\|_{l^2}, \quad 0 \leq z < \infty,$$

where $\|\psi_m\|_{l^\infty} := \sup_m |\psi_m|$.

Similarly, let $\{\psi_{m_1, m_2}\}$ be a solution of a semi-discrete two-dimensional NLS, for which $\|\psi_{m_1, m_2}(z)\|_{l^2}$ is conserved. If $\{\psi_{m_1, m_2}(0)\} \in l^2$, then $\{\psi_{m_1, m_2}\}$ exist globally in l^2 . Furthermore,

$$\|\psi_{m_1, m_2}(z)\|_{l^\infty} \leq h^{-1} \|\psi_{m_1, m_2}(0)\|_{l^2}, \quad 0 \leq z < \infty,$$

where $\|\psi_{m_1, m_2}\|_{l^\infty} := \sup_{m_1, m_2} |\psi_{m_1, m_2}|$.

Proof We prove the lemma for $\{\psi_m\}$; the proof for $\{\psi_{m_1, m_2}\}$ is identical. By the local existence theory for ODEs, there exists $0 < Z < \infty$ such that $\{\psi_m(z)\}$ exists and is continuous in $[0, Z]$. Assume by negation that $\{\psi_m\}$ does not exist in l^2 for $0 \leq z < \infty$. Then there exists $0 < Z_c < \infty$ such that either $\{\psi_m\}$ is defined at $z = Z_c$ but $\lim_{z \rightarrow Z_c} \|\psi_m(z)\|_{l^2} = \infty$, or $\{\psi_m\}$ is not defined at $z = Z_c$, in

which case $\lim_{z \rightarrow Z_c} \sup_m |\psi_m(z)| = \infty$. For both possibilities, because power conservation holds for $0 \leq z < Z_c$,

$$\sup_m |\psi_m(z)|^2 \leq \sum_{m=-\infty}^{\infty} |\psi_m(z)|^2 \equiv h^{-1} \|\psi_m(0)\|_{l^2}^2 < \infty,$$

where the left inequality holds because a single term cannot exceed the sum of non-negative terms. Since $\{\psi_m\}$ is continuous in z , this implies

$$\lim_{z \rightarrow Z_c} \sup_m |\psi_m(z)|^2 \leq h^{-1} \lim_{z \rightarrow Z_c} \|\psi_m(z)\|_{l^2}^2 \leq h^{-1} \|\psi_m(0)\|_{l^2}^2.$$

This, however, is in contradiction with both possibilities. \square

Corollary 30.1 *Let $\{\psi_m(0)\} \in l^2$. Then the solutions of the semi-discrete equations (30.3) and (30.4) exist globally in l^2 . Furthermore,*

$$\|\psi_m(z)\|_{l^\infty} \leq h^{-\frac{1}{2}} \|\psi_m(0)\|_{l^2}, \quad 0 \leq z < \infty.$$

Similarly, let $\{\psi_{m_1, m_2}(0)\} \in l^2$. Then the solutions of the semi-discrete equations (30.6) and (30.7) exist globally in l^2 . Furthermore,

$$\|\psi_{m_1, m_2}(z)\|_{l^\infty} \leq h^{-1} \|\psi_{m_1, m_2}(0)\|_{l^2}, \quad 0 \leq z < \infty.$$

Proof This follows from Lemma 30.3. \square

Remark The result of Lemma 30.3 does not hold in the continuous case. For example, consider a solution ψ of the critical NLS with $\psi_0 \in H^1$. If ψ becomes singular in H^1 , it also becomes singular in L^2 (Sect. 5.7.2). Therefore, $\psi_0 \in L^2$, yet ψ does not exist globally in L^2 . In this case ψ becomes singular in L^2 not because its L^2 norm goes to infinity, but rather because it approaches a delta function (Sect. 13.3), which is not in L^2 . The discrete delta function, however, is in l^2 . Thus, the difference between the discrete and continuous cases has to do with the fact that the set $\{\|f^n\|_{l^2} \equiv C\}$ is compact, whereas the set $\{\|f(\mathbf{x})\|_{L^2} \equiv C\}$ is not.

30.4 Informal Analysis

The analysis in Sects. 30.2.1 and 30.3 shows that solutions of the above semi-discrete NLS equations do not become singular. It does not, however, provide information on the dynamics of these solutions. To gain insight on the effect of discretization, we recall the two ‘rules’ from Sect. 5.9:

1. Diffraction is defocusing.
2. Nonlinearity is defocusing when it has the same sign as diffraction, and focusing when it has the opposite sign.

To apply these ‘rules’ to the modified equation (30.12), we inspect the three terms of its Hamiltonian (30.13). Since $0 < \epsilon \ll 1$, the dominant terms are initially diffraction and nonlinearity (first and second terms), whereas discretization (third term) is small. Since discretization has the same sign as nonlinearity, it works with nonlinearity and against diffraction, i.e., it is focusing. As the solution self-focuses, the discretization term increases faster than diffraction, because it consists of higher-order derivatives. Therefore, the dominant terms become discretization and nonlinearity. Since both have the same sign, nonlinearity becomes defocusing. Hence, collapse is arrested.

Conclusion 30.3 *Center-difference discretization of $\Delta\psi$ initially accelerates self-focusing, but later arrests it.*

Remark Conclusion 30.3 shows that discretization is initially focusing, but is later defocusing. This shows again⁵ that one cannot analyze the NLS with a linear superposition approach.

Since collapse is arrested once $\Delta\psi \ll \epsilon \sum_{i=1}^d \frac{\partial^{2k}\psi}{\partial x_i^{2k}}$, we can estimate the maximal amplitude of semi-discrete solutions from the condition that $\Delta\psi$ and $\epsilon \sum_{i=1}^d \frac{\partial^{2k}\psi}{\partial x_i^{2k}}$ have equal magnitudes. Recall that $|\psi| \sim L^{-\frac{1}{\sigma}}(z)F(\frac{r}{L})$ for NLS peak-type solutions.⁶ Hence,

$$\Delta\psi \sim \frac{[\psi]}{L^2}, \quad \epsilon \sum_{i=1}^d \frac{\partial^{2k}\psi}{\partial x_i^{2k}} \sim \frac{\epsilon[\psi]}{L^{2k}}.$$

Therefore, the equal-magnitude condition implies that the minimal width of semi-discrete solutions scales as $L_{\min} \sim \epsilon^{\frac{1}{2k-2}}$. Hence, by (30.12),

$$L_{\min} \sim h.$$

This result is intuitive, because the width of a discrete solution cannot be smaller than the mesh size. Since $\max |\psi| \sim L_{\min}^{-\frac{1}{\sigma}}$, we have

Conclusion 30.4 *The maximal amplitude of semi-discrete solutions scales as*

$$\max_{z,x} |\psi| \sim h^{-\frac{1}{\sigma}}. \tag{30.14}$$

⁵ See Sects. 3.4.1, 26.3.2, and 36.8.1.

⁶ See Sect. 13.2 for the critical case and Chap. 21 for the supercritical case.

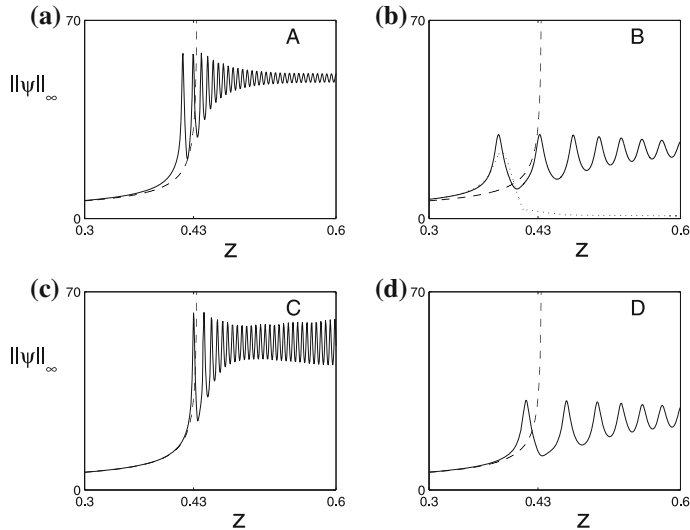


Fig. 30.1 A singular NLS solution (dashes), computed (solid) using: **a** Second-order discretization (Eq. (30.6) with $h = 0.05$). **b** Same as (a) with $h = 0.1$. Dotted line is solution of the modified equation (30.9). **c** Fourth-order discretization (Eq. (30.7) with $h = 0.05$). **d** Same as (c) with $h = 0.1$. From [79]

In particular, *the scaling of the maximal amplitude is independent of the order of the finite-difference scheme*. This result is surprising, because higher-order schemes should be able to handle steeper gradients. Note, however, that by the ‘time’ the maximal amplitude has been reached, the numerical solution has long bifurcated from the analytic one (see, e.g., Fig. 30.1), because the arrest of collapse is an indication that the dynamics of the semi-discrete solution is dominated by numerical effects. Therefore we have

Conclusion 30.5 *The maximal amplitude of the numerical solution is not a reliable measure for its accuracy.*

30.5 Simulations

Consider the two-dimensional NLS (30.5) with $\sigma = 1$ and $\psi_0 = 3e^{-x^2-y^2}$. This solution is singular, because its Hamiltonian is negative. In Fig. 30.1 we compute it using second-order and fourth-order center-difference discretization of $\Delta\psi$. We let dz be sufficiently small, so that discretization in z has a negligible effect. The computed solutions (i.e., the solutions of the second-order and fourth-order semi-discrete NLS) do not blowup. Rather, they undergo focusing-defocusing oscillations.

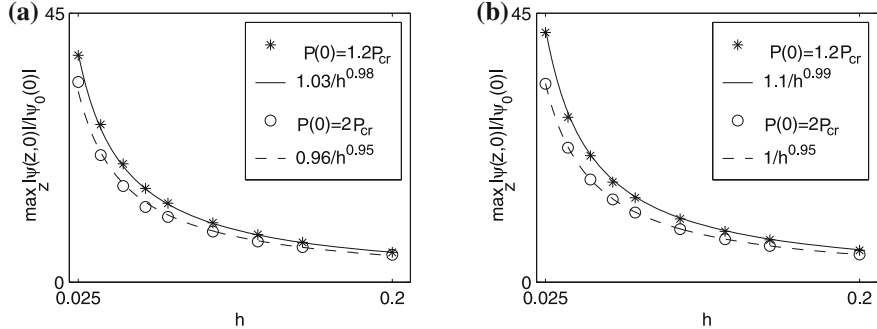


Fig. 30.2 Maximal focusing as a function of grid size for solutions of the semi-discrete two-dimensional NLS. Initial conditions are Gaussians with $P = 1.2P_{\text{cr}}$ (*) or $P = 2P_{\text{cr}}$ (o). Solid and dashed lines are power-law fits of data points. **a** Second-order discretization Eq. (30.6). **b** Fourth-order discretization Eq. (30.7). From [79]

Comparison with the “exact” NLS solution⁷ shows that, as predicted in Conclusion 30.3, discretization initially accelerates self-focusing, but later arrests the collapse and leads to focusing-defocusing oscillations. The solution of the modified equation (30.9) is in good agreement with the semi-discrete solution during the first focusing-defocusing event, but does not capture the subsequent focusing-defocusing oscillations (Fig. 30.1b). Rather, after the first focusing event, the solution of the modified equation simply scatters (diffracts).

In Fig. 30.2 we plot the maximal amplitude reached by the numerical solutions, as a function of the spatial mesh size h . As predicted in Conclusion 30.4, for both second-order and fourth-order discretization, the maximal amplitude scales as $h^{-\frac{1}{\sigma}} = h^{-1}$. In fact, fourth-order discretization yields only slightly higher maximal amplitude than second-order discretization. Note, however, that fourth-order discretization does yield more accurate results than second-order discretization during the initial stage of the simulation (Fig. 30.1).

⁷ i.e., the numerical solution, computed with sufficiently refined grids in \mathbf{x} and z .

Part VII
The Perturbed Critical NLS

Chapter 31

Modulation Theory

In Chap. 1 we saw that propagation of intense laser beams in a Kerr medium can be modeled by the two-dimensional cubic NLS

$$i\psi_z(z, x, y) + \Delta\psi + |\psi|^2\psi = 0. \quad (31.1)$$

According to (31.1), high-power laser beams undergo an optical collapse, in which the electric field becomes infinite at a finite propagation distance Z_c . Since physical quantities do not become infinite, this indicates that the NLS model breaks down at or before Z_c . In other words, some of the terms that were neglected in the derivation of (31.1) from Maxwell's equations become important near Z_c .

Equation (31.1) is a special case of the d -dimensional critical NLS

$$i\psi_z(z, \mathbf{x}) + \Delta\psi + |\psi|^{\frac{4}{d}}\psi = 0. \quad (31.2)$$

In Sect. 17.3 we saw that stable collapse in (31.2) consists of¹

1. a **nonadiabatic stage** that starts at $z = 0$ and ends shortly before Z_c , during which the solution “splits” into a collapsing core ψ_{coll} that approaches the $\psi_{R^{(0)}}$ profile and a non-collapsing outer tail ψ_{outer} , and
2. an **adiabatic stage** that starts shortly before Z_c and ends at Z_c , during which “most of the collapse” takes place.

During the initial nonadiabatic stage the effects of small perturbations are minor, and so the propagation can be modeled by the NLS. Indeed, Eq. (31.1) has been very successful in predicting the pre-collapse dynamics of laser beams (Sect. 1.8). The situation is very different during the adiabatic stage. This is because once ψ_{coll} is close to $\psi_{R^{(0)}}$, nonlinearity and diffraction nearly balance each other (Sect. 18.6), and so the net effect of nonlinearity and diffraction is much smaller than that of each of them

¹ Here we only consider peak-type blowup solutions, since ring-type blowup solutions are azimuthally unstable (Sect. 19.3).

separately (*i.e.*, $\Delta\psi + |\psi|^{\frac{4}{d}}\psi \ll \Delta\psi, |\psi|^{\frac{4}{d}}\psi$). As a result, small perturbations have $O(1)$ effects on the dynamics as soon as they become comparable to $\Delta\psi + |\psi|^{\frac{4}{d}}\psi$, even though at this stage they are still considerably smaller than $\Delta\psi$ and $|\psi|^{\frac{4}{d}}\psi$. This shows (again) that to model beam propagation near and beyond the NLS singularity point Z_c , some of the terms that are neglected in the NLS model should be retained.

In general, direct analysis of perturbed NLS equations can be hard. In this chapter we present an asymptotic theory called *modulation theory*, which was developed by Fibich and Papanicolaou [92, 93], that approximates any perturbed critical NLS equation by *reduced equations* that are independent of the transverse variable \mathbf{x} . Since the reduced equations are much simpler to analyze than the original perturbed NLS, they enable us to better understand the effect of a small perturbation. Is it focusing or defocusing? In the latter case, does it lead to focusing-defocusing oscillations or to a complete defocusing? What is the continuation of a singular solution beyond Z_c if we let the perturbation go to zero?²

31.1 Derivation of Reduced Equations

In Chap. 17 we utilized the fact that $\psi_{\text{coll}} \sim \psi_{R^{(0)}}$ as $z \rightarrow Z_c$ to average the critical NLS (31.2) over the transverse coordinates and obtain the reduced equations

$$L_{zz}(z) = -\frac{\beta}{L^3}, \quad \beta_z(z) = -\frac{\nu(\beta)}{L^2}. \quad (31.3)$$

In Chap. 18 we solved (31.3) asymptotically and saw that the blowup rate is given by the loglog law. The loglog law asymptotics, however, is only reached at extremely large focusing levels, at which the NLS model is physically irrelevant. Once analyzed with the adiabatic approach, however, predictions of the reduced equations (31.3) become valid at moderate focusing levels at which the NLS model is still physically valid.

In this chapter we generalize this approach to the perturbed critical NLS³

$$i\psi_z(z, \mathbf{x}) + \Delta\psi + |\psi|^{\frac{4}{d}}\psi + \epsilon F(\psi) = 0, \quad \epsilon \ll 1. \quad (31.4)$$

Specifically,

1. We utilize the fact that $\psi_{\text{coll}} \sim \psi_{R^{(0)}}$ to average (31.4) over the transverse coordinates and thus obtain reduced equations that are independent of \mathbf{x} .
2. We analyze the reduced equations with the adiabatic approach, *i.e.*, by neglecting the weak coupling between ψ_{coll} and ψ_{outer} .

² Continuations of singular solutions are discussed in Chap. 38.

³ Examples of physical perturbations are $F = -|\psi|^{\frac{4}{d}+2}\psi$ (high-order nonlinearity, Chap. 32), $F = \psi_{zz}$ (nonparaxiality, Sect. 34.3), $F = i|\psi|^q\psi$ (linear and nonlinear damping, Chap. 33), and $F = \psi_{tt}$ (dispersion, Chap. 36).

31.1.1 Three Conditions for Validity of Modulation Theory

Modulation theory is valid when the following three conditions hold:

Condition 1. The perturbation is considerably smaller than diffraction and nonlinearity, i.e., $\epsilon F \ll \Delta\psi, |\psi|^{\frac{4}{d}}\psi$.

Condition 2. The high-intensity core ψ_{coll} is close to the $\psi_{R^{(0)}}$ profile, where

$$\psi_{R^{(0)}}(z, r) = \frac{1}{L^{\frac{d}{2}}(z)} R^{(0)}(\rho) e^{iS}, \quad (31.5a)$$

$$\rho = \frac{r}{L}, \quad S = \xi(z) + \frac{L_z}{L} \frac{r^2}{4}, \quad \frac{\partial \xi}{\partial z} = \frac{1}{L^2}, \quad (31.5b)$$

and $R^{(0)}$ is the ground state of

$$R''(\rho) + \frac{d-1}{\rho} R' - R + |R|^{\frac{4}{d}} R = 0, \quad R'(0) = 0, \quad R(\infty) = 0. \quad (31.6)$$

Condition 3. Let $\beta(z) := -L^3 L_{zz}$. Then $|\beta| \ll 1$.

Remark For the collapsing core ψ_{coll} to approach the $\psi_{R^{(0)}}$ profile (and remain close to it), the dynamics should be dominated by nonlinearity and diffraction. Therefore, Conditions 1 and 2 are closely related.

Remark Condition 2 implies that $P_{\text{coll}} := P(\psi_{\text{coll}}) \sim P(\psi_{R^{(0)}}) = P_{\text{cr}}$, i.e., that the power of the collapsing core is close to P_{cr} .

Remark In the unperturbed critical NLS, during the adiabatic stage, β is proportional to $P_{\text{coll}} - P_{\text{cr}}$ (Corollary 17.3). Therefore, Condition 2 implies Condition 3. In the perturbed critical NLS (31.4), however, β is generically proportional to $P_{\text{coll}} - P_{\text{cr}}$ for nonconservative perturbations, but not for conservative ones (Sect. 31.4.1). Hence, Condition 2 does not necessarily imply Condition 3.

Remark Because β is not necessarily proportional to $P_{\text{coll}} - P_{\text{cr}}$, it can be negative even when $P_{\text{coll}} > P_{\text{cr}}$. Hence, in what follows β is allowed to assume both positive and negative values.

31.1.2 Three (or Five) Stages of Propagation

Consider the perturbed critical NLS (31.4) with an initial condition ψ_0 which in the unperturbed critical NLS (31.2) leads to a peak-type collapse with the $\psi_{R^{(0)}}$ profile at Z_c . If ϵ is sufficiently small so that

$$\epsilon F(\psi_0) \ll \Delta\psi_0 + |\psi_0|^{\frac{4}{d}}\psi_0,$$

the dynamics of the perturbed solution can be initially modeled by (31.2). Unless ψ_0 is already close to $\psi_{R^{(0)}}$, however, Condition 2 does not hold at $z = 0$. Since the perturbed solution initially evolves as the unperturbed one, its core approaches $\psi_{R^{(0)}}$ as $z \rightarrow Z_c$, and so Conditions 2 and 3 become satisfied. It is at this stage that diffraction and nonlinearity nearly balance each other, so that small perturbations can affect the leading-order dynamics. Therefore, generically, one can identify three stages in the dynamics of the perturbed solution:

- (1) **Unperturbed nonadiabatic stage.** The dynamics is the same as in the *non-adiabatic stage* of the unperturbed solution. Only Condition 1 holds. This stage lasts from $z = 0$ and until shortly before Z_c .
- (2) **Unperturbed adiabatic stage.** The dynamics is the same as in the *adiabatic stage* of the unperturbed solution. In particular, Conditions 1–3 hold. Here we assume that ϵ is sufficiently small so that at the beginning of the adiabatic stage the perturbation is still smaller than the combined effect of diffraction and nonlinearity,⁴ i.e.,

$$\epsilon F(\psi) \ll \Delta\psi + |\psi|^{\frac{4}{d}}\psi \ll \Delta\psi, |\psi|^{\frac{4}{d}}\psi. \quad (31.7)$$

This stage lasts over a short distance in z and ends before Z_c .

- (3) **Weakly-perturbed stage.** Most perturbations increase in magnitude as ψ collapses. If this increase is slower than that of nonlinearity and diffraction,⁵ the effect of the perturbation decreases as ψ collapses. If, however, the perturbation increases faster than nonlinearity and diffraction, the collapsing solution reaches a stage where the perturbation is still smaller than diffraction and nonlinearity, but is comparable to their balance, i.e.,

$$[\epsilon F] = \left[\Delta\psi + |\psi|^{\frac{4}{d}}\psi \right] \ll \Delta\psi, |\psi|^{\frac{4}{d}}\psi.$$

Therefore, the perturbation affects the leading-order dynamics. During this stage, which begins roughly at Z_c , Conditions 1–3 hold.

If the perturbation arrests collapse, it remains comparable to the balance of nonlinearity and diffraction. Therefore, Conditions 1–3 remain valid for all future z , and so the solution remains in the *weakly-perturbed stage* as it evolves (see, e.g., Sect. 31.5.5). If, however, collapse is not arrested and the growth of the perturbation is faster than that of diffraction and nonlinearity, self-focusing enters a fourth stage during which the perturbation becomes dominant:

⁴ Otherwise, the leading-order dynamics is affected by all three terms in (31.4), i.e., the solution “jumps” from stage 1 to stage 5.

⁵ This is the case, e.g., with linear damping (see Sect. 33.1.5).

- (4) **Strongly-perturbed stage.** The perturbation dominates the balance of nonlinearity and diffraction, i.e., $\epsilon F \gg \Delta\psi + |\psi|^{\frac{4}{d}}\psi$. Therefore, to leading order, the dynamics is governed by

$$i\psi_z + \epsilon F(\psi) = 0.$$

Because the dynamics is no longer dominated by nonlinearity and diffraction, the collapsing core ψ_{coll} moves away from the $\psi_{R^{(0)}}$ profile. Consequently, Conditions 1 and 2 are not satisfied.

- (5) **Perturbed stage.** As ψ_{coll} moves away from $\psi_{R^{(0)}}$, diffraction and nonlinearity do not balance each other anymore. Consequently, $\Delta\psi + |\psi|^{\frac{4}{d}}\psi$ increases and becomes comparable to the perturbation, as well as to diffraction and to the nonlinearity, i.e.,

$$[\epsilon F] = \left[\Delta\psi + |\psi|^{\frac{4}{d}}\psi \right] = \left[\Delta\psi \right] = \left[|\psi|^{\frac{4}{d}}\psi \right].$$

As a result, the leading-order dynamics is determined by all three terms in (31.4).⁶ In particular, Conditions 1 and 2 are not valid.

Conditions 1–3 hold during the second and third stages. These two stages are thus covered by modulation theory, and will be henceforth called the *modulation-theory stage*.

31.1.3 Main Result

The main result of modulation theory is

Proposition 31.1 ([92, 93]) *Let Conditions 1–3 hold. Then self-focusing in the perturbed critical NLS (31.4) is governed, to leading order, by the reduced equations*

$$\beta_z(z) + \frac{v(\beta)}{L^2} = \frac{\epsilon}{2M} f'_1(z) - \frac{2\epsilon}{M} f_2(z), \quad (31.8a)$$

$$L_{zz}(z) = -\frac{\beta}{L^3}, \quad (31.8b)$$

⁶ This is the case, e.g., with the NLS with small normal dispersion after the pulse splitting (see Sect. 36.8.8 and in particular Fig. 36.4). In some cases, however, the leading order-dynamics during the fifth stage is only determined by two terms, one of which is the perturbation. For example, when $F = |\psi|^{\frac{4}{d}+2}\psi$ and $0 < \epsilon \ll 1$, as ψ_{coll} collapses, the supercritical nonlinearity eventually dominates over the critical nonlinearity, and so the leading-order dynamics is determined by the supercritical nonlinearity and diffraction (Sect. 32.3.2). Similarly, when $F = -\Delta^2\psi$ and $0 < \epsilon \ll 1$, as ψ_{coll} collapses, fourth-order diffraction eventually dominates over diffraction, and so the leading-order dynamics is determined by fourth-order diffraction and nonlinearity.

where

$$\nu(\beta) = \begin{cases} c_v e^{-\pi/\sqrt{\beta}}, & \text{if } \beta > 0, \\ 0, & \text{if } \beta \leq 0, \end{cases} \quad (31.9)$$

$$c_v = \frac{2\omega_d A_R^2}{M}, \quad A_R = \lim_{r \rightarrow \infty} e^r r^{\frac{d-1}{2}} R^{(0)}(r), \quad M = \frac{1}{4} \int |\mathbf{x}|^2 |R^{(0)}|^2 d\mathbf{x},$$

$R^{(0)}$ is the ground state of (31.6), and ω_d is the surface area of the d -dimensional unit sphere.⁷ The auxiliary functions f_1 and f_2 are given by

$$f_1(z) = L^{2-\frac{d}{2}}(z) \operatorname{Re} \int F(\psi_{R^{(0)}}) e^{-iS} \left[d \cdot R^{(0)}(\rho) + 2\rho \frac{dR^{(0)}}{d\rho} \right] d\mathbf{x}, \quad (31.10a)$$

$$f_2(z) = \operatorname{Im} \int F(\psi_{R^{(0)}}) \psi_{R^{(0)}}^* d\mathbf{x}, \quad (31.10b)$$

where $\psi_{R^{(0)}}$, ρ , and S are given by (31.5).

Proof See Sect. 31.2. □

Remark When $\epsilon = 0$, Eqs. (31.8) are the reduced equations for the unperturbed critical NLS, see (31.3).

Remark Assuming we can carry out the integration in (31.10), f_1 and f_2 are explicit functions of L , β , ζ , and their derivatives.

If we change the integration variable from \mathbf{x} to

$$\xi = \frac{\mathbf{x}}{L}, \quad (31.11)$$

the auxiliary functions f_1 and f_2 read

$$f_1(z) = L^{2+\frac{d}{2}}(z) \operatorname{Re} \int F(\psi_{R^{(0)}}) e^{-iS} \left[d \cdot R^{(0)}(\rho) + 2\rho \frac{dR^{(0)}}{d\rho} \right] d\xi, \quad (31.12a)$$

$$f_2(z) = L^{\frac{d}{2}}(z) \operatorname{Im} \int F(\psi_{R^{(0)}}) e^{-iS} R^{(0)}(\rho) d\xi. \quad (31.12b)$$

If ψ_0 is radial and F is isotropic, then ψ remains radial for all z , and Proposition 31.1 reads as follows.

Proposition 31.2 *Let Conditions 1–3 hold and let F be isotropic. Then self-focusing in the perturbed critical radial NLS*

$$i\psi_z(z, r) + \psi_{rr} + \frac{d-1}{r}\psi_r + |\psi|^{\frac{4}{d}}\psi + \epsilon F(\psi) = 0, \quad \epsilon \ll 1,$$

⁷ See (17.65).

is governed, to leading order, by

$$\beta_z(z) + \frac{v(\beta)}{L^2} = \frac{\epsilon}{2M^{\text{radial}}} \left(f_1^{\text{radial}} \right)'(z) - \frac{2\epsilon}{M^{\text{radial}}} f_2^{\text{radial}}(z), \quad (31.13a)$$

$$L_{zz}(z) = -\frac{\beta}{L^3}, \quad (31.13b)$$

where $v(\beta)$ is given by (31.9), $c_v = \frac{2A_R^2}{M^{\text{radial}}}$, $M^{\text{radial}} = \frac{1}{4} \int_0^\infty r^2 |R^{(0)}|^2 r^{d-1} dr$, and

$$\begin{aligned} f_1^{\text{radial}}(z) &= L^{2-\frac{d}{2}}(z) \operatorname{Re} \int_0^\infty F(\psi_{R^{(0)}}) e^{-iS} \left[d \cdot R^{(0)}(\rho) + 2\rho \frac{dR^{(0)}}{d\rho} \right] r^{d-1} dr \\ &= L^{2+\frac{d}{2}}(z) \operatorname{Re} \int_0^\infty F(\psi_{R^{(0)}}) e^{-iS} \left[d \cdot R^{(0)}(\rho) + 2\rho \frac{dR^{(0)}}{d\rho} \right] \rho^{d-1} d\rho, \end{aligned} \quad (31.14a)$$

$$\begin{aligned} f_2^{\text{radial}}(z) &= \operatorname{Im} \int_0^\infty F(\psi_{R^{(0)}}) \psi_{R^{(0)}}^* r^{d-1} dr \\ &= L^{\frac{d}{2}}(z) \operatorname{Im} \int_0^\infty F(\psi_{R^{(0)}}) e^{-iS} R^{(0)}(\rho) \rho^{d-1} d\rho. \end{aligned} \quad (31.14b)$$

31.1.4 The Physical Case $d = 2$

The critical case of physical interest is the two-dimensional cubic NLS. In this case, the perturbed critical NLS reads

$$i\psi_z(z, x, y) + \Delta\psi + |\psi|^2\psi + \epsilon F(\psi) = 0, \quad \epsilon \ll 1, \quad (31.15)$$

Eqs. (31.10) read

$$f_1(z) = 2L(z) \operatorname{Re} \int F(\psi_{R^{(0)}}) e^{-iS} \left[R^{(0)}(\rho) + \rho \frac{dR^{(0)}}{d\rho} \right] dx dy, \quad (31.16a)$$

$$f_2(z) = \operatorname{Im} \int F(\psi_{R^{(0)}}) \psi_{R^{(0)}}^* dx dy, \quad (31.16b)$$

Eqs. (31.12) read

$$f_1(z) = 2L^3(z) \operatorname{Re} \int F(\psi_{R^{(0)}}) e^{-iS} \left[R^{(0)}(\rho) + \rho \frac{dR^{(0)}}{d\rho} \right] d\xi d\eta, \quad (31.17a)$$

$$f_2(z) = L(z) \operatorname{Im} \int F(\psi_{R^{(0)}}) e^{-iS} R^{(0)}(\rho) d\xi d\eta, \quad (31.17b)$$

where $\xi = \frac{x}{L}$, $\eta = \frac{y}{L}$, and $\rho = \sqrt{\xi^2 + \eta^2}$, and Eqs. (31.14) read

$$\begin{aligned} f_1^{\text{radial}}(z) &= 2L(z) \operatorname{Re} \int_0^\infty F(\psi_{R^{(0)}}) e^{-iS} \frac{d}{d\rho} \left[\rho R^{(0)}(\rho) \right] r dr \\ &= 2L^3(z) \operatorname{Re} \int_0^\infty F(\psi_{R^{(0)}}) e^{-iS} \frac{d}{d\rho} \left[\rho R^{(0)}(\rho) \right] \rho d\rho, \end{aligned} \quad (31.18a)$$

$$\begin{aligned} f_2^{\text{radial}}(z) &= \operatorname{Im} \int_0^\infty F(\psi_{R^{(0)}}) \psi_{R^{(0)}}^* r dr \\ &= L(z) \operatorname{Im} \int_0^\infty F(\psi_{R^{(0)}}) e^{-iS} R^{(0)}(\rho) \rho d\rho. \end{aligned} \quad (31.18b)$$

31.1.5 Multiple Perturbations

As noted, numerous small terms are neglected in the derivation of the NLS from Maxwell's equations. Therefore, in some cases one is interested in the combined effect of several small perturbations. Since the reduced equations are linear in F , one simply adds the contribution of each perturbation:

Proposition 31.3 *Consider the perturbed critical NLS*

$$i\psi_z(z, \mathbf{x}) + \Delta\psi + |\psi|^{\frac{4}{d}}\psi + \sum_{k=1}^K \epsilon_k F_k(\psi) = 0,$$

and assume that Conditions 1–3 hold.⁸ Then self-focusing is governed, to leading order, by

$$\beta_z(z) + \frac{v(\beta)}{L^2} = \sum_{k=1}^K \frac{\epsilon_k}{2M} f'_{k,1}(z) - \sum_{k=1}^K \frac{2\epsilon_k}{M} f_{k,2}(z), \quad L_{zz}(z) = -\frac{\beta}{L^3},$$

⁸ In the case of multiple perturbations, Condition 1 reads $\epsilon_k F_k \ll \Delta\psi, |\psi|^{\frac{4}{d}}\psi$ for $k = 1, \dots, K$.

where

$$\begin{aligned} f_{k,1}(z) &= L^{2-\frac{d}{2}}(z) \operatorname{Re} \int F_k(\psi_{R^{(0)}}) e^{-iS} \left[d \cdot R^{(0)}(\rho) + 2\rho \frac{dR^{(0)}}{d\rho} \right] d\mathbf{x}, \\ f_{k,2}(z) &= \operatorname{Im} \int F_k(\psi_{R^{(0)}}) \psi_{R^{(0)}}^* d\mathbf{x}. \end{aligned}$$

31.1.6 Perturbations that “Add a Dimension”

Some perturbations “add a dimension” to the critical NLS. For example, the canonical model for propagation of ultrashort pulses in a bulk medium is the two-dimensional cubic NLS with small temporal dispersion

$$i\psi_z(z, x, y, t) + \psi_{xx} + \psi_{yy} + |\psi|^2\psi - \epsilon\psi_{tt} = 0, \quad (31.19)$$

see Sect. 35.3. Since t “behaves” as a third spatial variable (Sect. 35.1.4), dispersion “adds a dimension” to the critical NLS. Consequently, the reduced equations of (31.19) are PDEs in z and t , i.e., $L = L(z, t)$, and similarly for β , ζ , f_1 , and f_2 . See Sect. 36.8.3 for more details.

As another example, consider the evolution of Bose-Einstein condensates with attractive interactions, which is modeled by the three-dimensional cubic NLS/GP equation (Sect. 4.2)

$$i\psi_t(t, x, y, z) + \psi_{xx} + \psi_{yy} + \psi_{zz} + |\psi|^2\psi = 0.$$

In some setups an external potential confines the initial condensate to a two-dimensional trap. As a result, it has a cigar shape, i.e.,

$$\psi_0(x, y, z) = ce^{-x^2-y^2-\delta^2z^2}, \quad \delta \ll 1.$$

Under the rescaling $\tilde{z} = z/\delta$, the NLS/GP reads

$$i\psi_t(t, x, y, \tilde{z}) + \psi_{xx} + \psi_{yy} + |\psi|^2\psi + \delta^2\psi_{\tilde{z}\tilde{z}} = 0.$$

This equation can be viewed as the two-dimensional critical NLS with a perturbation that “adds a dimension”. In fact, this equation is nothing but (31.19) with $\epsilon = -\delta^2$.

31.2 Derivation of Main Result (Proposition 31.1)

In this section we present two informal derivations of the reduced equations (31.18): A “mathematical” derivation from a solvability condition, and a “physical” one from balance of power.

31.2.1 Derivation from a Solvability Condition

This derivation generalizes that for the unperturbed critical NLS in Sect. 17.6. Let

$$\psi(z, \mathbf{x}) = \frac{1}{L^{\frac{d}{2}}(z)} V^\epsilon(\zeta, \xi) e^{iS}, \quad (31.20)$$

where ζ , S , and ξ are defined in (31.5b) and (31.11).⁹ If we substitute (31.20) in the perturbed NLS (31.4), the equation for V^ϵ is

$$i \frac{\partial V^\epsilon}{\partial \zeta}(\zeta, \xi) + \Delta V^\epsilon - V^\epsilon + |V^\epsilon|^{\frac{4}{d}} V^\epsilon + \frac{\beta}{4} \rho^2 V^\epsilon + \epsilon L^{2+\frac{d}{2}} F(\psi) e^{-iS} = 0, \quad (31.21)$$

where $\Delta = \Delta_\xi$ and $\rho = |\xi|$. By Condition 2, $\psi_{\text{coll}} \sim \psi_{R^{(0)}}$. Hence, $V^\epsilon(\zeta, \xi) \sim R^{(0)}(\rho)$ for $\xi = O(1)$. As in the unperturbed case, we expand

$$V^\epsilon \sim V_0^\epsilon + V_1^\epsilon + \dots, \quad (31.22)$$

we assume that $V_0^\epsilon(\zeta, \xi) = V_0^\epsilon(\xi; \beta(\zeta))$,¹⁰ and that V_0^ϵ satisfies

$$\Delta V_0^\epsilon - V_0^\epsilon + |V_0^\epsilon|^{\frac{4}{d}} V_0^\epsilon + \frac{\beta}{4} \rho^2 V_0^\epsilon - i \frac{M}{2P_{\text{cr}}} v^\epsilon(\beta) V_0^\epsilon + \epsilon w(V_0^\epsilon) = 0, \quad (31.23a)$$

where

$$w(V_0^\epsilon) := L^{2+\frac{d}{2}} \operatorname{Re} \left[F(\psi_{V_0^\epsilon}) e^{-iS} \right], \quad \psi_{V_0^\epsilon} := \frac{1}{L^{\frac{d}{2}}} V_0^\epsilon e^{iS}. \quad (31.23b)$$

When $\epsilon = 0$, this is Eq.(17.61) for $V_0 := V_0^{\epsilon=0}$. We thus added to the equation for V_0^ϵ the real part of the perturbation. We did not add the imaginary part of the perturbation, because we assume that, as in the unperturbed case, V_0^ϵ is “essentially” real for $\xi = O(1)$. The exponentially-small imaginary term v^ϵ is “only” added to have the correct behavior as $\xi \rightarrow \infty$. We assume that the perturbation has a small effect on the radiation term v^ϵ , i.e., that there is a perturbed pair $V_0^\epsilon \sim V_0$ and $v^\epsilon \sim v$ that satisfies (31.23).

Equation (31.8a) is obtained from the solvability condition for the next-order term V_1^ϵ , as follows. By (31.21)–(31.23), the equation for V_1^ϵ reads

⁹ Unlike the derivation in the unperturbed case, we allow V^ϵ to depend on ξ (rather than only on ρ). This will enable us to consider anisotropic perturbations such as vectorial effects [76], propagation in fiber arrays [93], and propagation of ultrashort pulses in planar waveguides with fourth-order dispersion [81].

¹⁰ i.e. that V_0^ϵ is quasi steady.

$$\begin{aligned} \Delta V_1^\epsilon - V_1^\epsilon + \left(1 + \frac{2}{d}\right) |V_0^\epsilon|^{\frac{4}{d}} V_1^\epsilon + \frac{2}{d} (V_0^\epsilon)^{\frac{2}{d}+1} (V_0^{\epsilon*})^{\frac{2}{d}-1} V_1^{\epsilon*} + \frac{1}{4} \beta \rho^2 V_1^\epsilon \\ = -i \left[\frac{\partial V_0^\epsilon}{\partial \zeta} + \frac{M}{2P_{\text{cr}}} v^\epsilon(\beta) V_0^\epsilon \right] - i\epsilon L^{\frac{d}{2}+2} \operatorname{Im} \left[F(\psi_{V_0^\epsilon}) e^{-iS} \right]. \end{aligned}$$

By (31.23), in the domain $\xi = O(1)$ we can expand V_0^ϵ in ϵ and β as

$$V_0^\epsilon(\xi; \beta(\zeta)) = R^{(0)}(\rho) + \beta(\zeta)g(\rho) + \epsilon h(\zeta, \xi) + O(\beta^2, \beta\epsilon, \epsilon^2). \quad (31.24)$$

Therefore, since β and ϵ are small, the following approximations hold in the domain $\xi = O(1)$:

$$V_0^\epsilon \sim R^{(0)}, \quad -V_1^\epsilon + \frac{\beta}{4} \rho^2 V_1^\epsilon \sim -V_1^\epsilon, \quad \frac{\partial V_0^\epsilon}{\partial \zeta} \sim \beta_\zeta g + \epsilon h_\zeta, \quad v^\epsilon \sim v, \quad \psi_{V_0^\epsilon} \sim \psi_{R^{(0)}}.$$

Hence, to leading order, the equation for V_1^ϵ reads

$$\begin{aligned} \Delta V_1^\epsilon - V_1^\epsilon + \left(1 + \frac{2}{d}\right) |R^{(0)}|^{\frac{4}{d}} V_1^\epsilon + \frac{2}{d} |R^{(0)}|^{\frac{4}{d}} V_1^{\epsilon*} \\ = -i \left[g\beta_\zeta + \epsilon h_\zeta + \frac{M}{2P_{\text{cr}}} v(\beta) R^{(0)} \right] - i\epsilon L^{2+\frac{d}{2}} \operatorname{Im} \left[F(\psi_{R^{(0)}}) e^{-iS} \right]. \quad (31.25) \end{aligned}$$

By Lemma 17.11, the solvability condition for (31.25) is that $R^{(0)}$ is orthogonal to its right-hand side, i.e.,

$$\int R^{(0)} \left[g\beta_\zeta + \epsilon h_\zeta + \frac{Mv(\beta)}{2P_{\text{cr}}} R^{(0)} + \epsilon L^{2+\frac{d}{2}} \operatorname{Im} \left[F(\psi_{R^{(0)}}) e^{-iS} \right] \right] d\xi = 0. \quad (31.26)$$

Lemma 31.1

$$\int R^{(0)} h d\xi = -\frac{1}{4} f_1. \quad (31.27)$$

Proof Applying Lemma 17.4 to Eq. (31.23a) with $\beta = 0$ yields

$$\int R^{(0)} h d\xi = -\frac{1}{4} \int \left[d \cdot R^{(0)}(\rho) + 2\rho \frac{dR^{(0)}(\rho)}{d\rho} \right] w(R^{(0)}) d\xi,$$

where $w(R^{(0)}) := L^{2+\frac{d}{2}} \operatorname{Re} \left[F(\psi_{R^{(0)}}) e^{-iS} \right]$, see (17.30a). Therefore, the result follows from (31.12a). \square

Let us substitute in the solvability condition (31.26) the following relations: $\int |R^{(0)}|^2 d\xi = P_{\text{cr}}$, (31.12b), (31.27), $d\xi = L^{-d} dx$, and

$$\int R^{(0)} g d\xi = \frac{M}{2}, \quad (31.28)$$

see Lemma 17.5. This gives

$$\frac{M}{2}\beta_\zeta - \frac{\epsilon}{4}(f_1)_\zeta + \frac{M}{2}\nu(\beta) + \epsilon L^2 f_2 = 0.$$

Multiplying by L^{-2} and changing from ζ to z , see (31.5b), gives (31.8a).

31.2.2 Derivation from Balance of Power

As in the unperturbed critical NLS (Sect. 17.3), we can also derive the reduced equations from balance of power, as follows. If we multiply (31.4) by ψ^* , subtract the conjugate equation, and integrate over \mathbf{x} , we get that the rate of power change in the perturbed critical NLS (31.4) is

$$\frac{d}{dz} \int |\psi|^2 d\mathbf{x} = -2\epsilon \operatorname{Im} \int \psi^* F(\psi) d\mathbf{x}. \quad (31.29)$$

The dynamics during the *unperturbed adiabatic stage* of (31.4) is the same as during the *adiabatic stage* of the unperturbed critical NLS (Sect. 31.1.2). Hence, the solution of (31.4) can be written as, see (17.11),

$$\psi = \begin{cases} \psi_{\text{coll}}, & \text{if } 0 \leq r \leq \rho_c L(z), \\ \psi_{\text{outer}}, & \text{if } r \geq \rho_c L(z), \end{cases}$$

and its power can be decomposed as

$$\int |\psi|^2 d\mathbf{x} = P_{\text{coll}} + P_{\text{outer}}, \quad (31.30)$$

where

$$P_{\text{coll}} := P(\psi_{\text{coll}}) = \int_{|\mathbf{x}| < \rho_c L(z)} |\psi|^2 d\mathbf{x}, \quad P_{\text{outer}} := P(\psi_{\text{outer}}) = \int_{|\mathbf{x}| > \rho_c L(z)} |\psi|^2 d\mathbf{x}.$$

Lemma 31.2 *Let Conditions 1–3 hold. Then*

$$P_{\text{coll}}(z) \sim P_{\text{cr}} + M\beta(z) - \frac{\epsilon}{2} f_1(z). \quad (31.31)$$

Proof Since

$$\psi_{\text{coll}} \sim \frac{1}{L^{\frac{d}{2}}} V_0^\epsilon e^{iS}, \quad (31.32)$$

where V_0^ϵ is a solution of (31.23), P_{coll} can be approximated by, see (31.24),

$$P_{\text{coll}} = \int_{0 \leq |\xi| \leq \rho_c} |V_0^\epsilon|^2 d\xi \approx \int_{0 \leq |\xi| \leq \rho_c} (R + \beta g + \epsilon h)^2 d\xi.$$

Therefore, since R , g , and h decay exponentially,

$$P_{\text{coll}} \approx \int |R^{(0)}|^2 d\xi + 2\beta \int R^{(0)} g d\xi + 2\epsilon \int R^{(0)} h d\xi + O(\beta^2, \beta\epsilon, \epsilon^2).$$

Substituting the integral identities (31.27) and (31.28) proves the result. \square

Differentiating (31.31) with respect to z gives

$$\frac{d}{dz} P_{\text{coll}} \sim M\beta_z - \frac{\epsilon}{2} f'_1(z). \quad (31.33)$$

In addition, since the perturbation is small, power radiation from the high-intensity core to the background is still given, to leading order, by (17.25). Hence,

$$\frac{d}{dz} P_{\text{outer}} \sim + \frac{M\nu(\beta)}{L^2}.$$

By the above, the left-hand side of (31.29) can be approximated by

$$\frac{d}{dz} \int |\psi|^2 d\mathbf{x} \sim M\beta_z - \frac{\epsilon}{2} f'_1 + \frac{M\nu(\beta)}{L^2}.$$

Since $\psi_{\text{coll}} \sim \psi_{R^{(0)}}$, the right-hand side of (31.29) can be approximated by

$$-2\epsilon \operatorname{Im} \int \psi^* F(\psi) d\mathbf{x} \sim -2\epsilon \operatorname{Im} \int \psi_{R^{(0)}}^* F(\psi_{R^{(0)}}) d\mathbf{x} = -2\epsilon f_2,$$

see (31.10b). Substituting the last two approximations in (31.29) yields (31.8a).

31.2.3 Variational Derivation

When the perturbed critical NLS has a Lagrangian density $\mathcal{L}(\psi, \psi^*)$, one can compute the averaged Lagrangian density $\bar{\mathcal{L}} = \int \mathcal{L}(\psi_{R^{(0)}}, \psi_{R^{(0)}}^*) d\mathbf{x}$ and then obtain the reduced equations from the variational derivative of $\bar{\mathcal{L}}$.¹¹ There are, however, several disadvantages to this variational approach. For one thing, it can only be applied to perturbed NLS equations that have a variational formulation. In addition, with this approach one can only analyze adiabatic effects, because power radiation from ψ_{coll}

¹¹ This approach was applied in [88] to the time-dispersive NLS (31.19).

to ψ_{outer} is not captured by the averaged Lagrangian. Finally, we note that in some studies the variational approach was applied with the wrong ansatz (e.g., a Gaussian or a sech). Because only $\psi_{R^{(0)}}$ captures the delicate balance between nonlinearity and diffraction in critical self-focusing, using any other ansatz might lead to erroneous predictions. Unlike the systematic derivations from a solvability condition or from balance of power, however, the variational approach does not indicate whether the assumed ansatz is inconsistent with the NLS.

31.3 The β Principle

When we apply modulation theory to a specific perturbation, the expressions for f_1 and f_2 can contain numerous terms. The following results provide a quick, informal approach for determining their relative magnitudes.

Conclusion 31.1 (The β principle) *Let Condition 3 hold, let $[L]$ be the characteristic magnitude of L , and let $[Z]$ be the characteristic length scale for changes in $L(z)$. Then*

$$\frac{[L]^4}{[Z]^2} = O(\beta) \ll 1.$$

Proof Since $\beta = -L^3 L_{zz}$, from dimensional arguments we have that $[\beta] = [L]^4 [Z]^{-2}$. In addition, by Condition 3, $\beta \ll 1$. \square

For example, we can use Conclusion 31.1 to “prove” the following results:

Conclusion 31.2 *Let Conditions 1–3 hold. Then*

$$LL_z \ll 1, \quad \left(\frac{L_z}{L} \right)_z \frac{r^2}{4} \ll \frac{1}{L^2}.$$

Proof The first inequality follows from

$$[LL_z] = \frac{[L]^2}{[Z]} = [\beta]^{\frac{1}{2}} \ll 1.$$

To prove the second inequality, we first note that $[r] = [L]$, since $r = L\rho$ and $\rho = O(1)$ in the collapsing core region. Therefore, we need to show that

$$\frac{[L]^2}{[Z]^2} \ll \frac{1}{[L]^2},$$

and this follows from Conclusion 31.1. \square

Exercise 31.1 Let $S = \zeta(z) + \frac{L_z}{L} \frac{r^2}{4}$. Show that

$$S_z \sim \frac{1}{L^2}. \quad (31.34)$$

Conclusion 31.3 Let Conditions 1–3 hold. Then

$$|\psi_{R^{(0)}}|^{\frac{4}{d}} \psi_{R^{(0)}} = \frac{e^{iS}}{L^{2+\frac{d}{2}}} |R^{(0)}|^{\frac{4}{d}} R^{(0)} = O\left(\frac{1}{L^{2+\frac{d}{2}}}\right), \quad (31.35a)$$

$$\Delta_r \psi_{R^{(0)}} \sim \frac{e^{iS}}{L^{2+\frac{d}{2}}} \Delta_\rho R^{(0)}(\rho) = O\left(\frac{1}{L^{2+\frac{d}{2}}}\right). \quad (31.35b)$$

Proof Relation (31.35a) is immediate. To prove relation (31.35b), note that

$$\frac{\partial}{\partial r} \psi_{R^{(0)}}(z, r) = \frac{e^{iS}}{L^{\frac{d}{2}}} \left(\frac{1}{L} \frac{dR^{(0)}(\rho)}{d\rho} + i \frac{L_z}{L} \frac{r}{2} R^{(0)} \right).$$

Now,

$$\left[\frac{1}{L} \frac{dR^{(0)}}{d\rho} \right] = \frac{1}{[L]}, \quad \left[i \frac{L_z}{L} \frac{r}{2} R^{(0)} \right] = \frac{[L_z]}{[L]} [L] = [L_z].$$

In addition, by Conclusion 31.2, $[L]^{-1} \gg [L_z]$. Hence,

$$\frac{\partial}{\partial r} \psi_{R^{(0)}} \sim \frac{e^{iS}}{L^{\frac{d}{2}}} \frac{1}{L} \frac{dR^{(0)}(\rho)}{d\rho}.$$

Differentiating again with respect to r and using similar arguments proves relation (31.35b). \square

Conclusion 31.4 Let Conditions 1–3 hold. Then

$$\epsilon f_1 = o(1), \quad \epsilon f_2 = o\left(\frac{1}{L^2}\right). \quad (31.36)$$

Proof From Condition 2 we have that $\epsilon F(\psi_{R^{(0)}}) \ll \Delta \psi_{R^{(0)}}$. Therefore, by (31.10a),

$$\epsilon f_1 \ll L^{2-\frac{d}{2}}(z) \int \Delta \psi_{R^{(0)}} e^{-iS} \left[d \cdot R^{(0)}(\rho) + 2\rho \frac{dR^{(0)}}{d\rho} \right] d\mathbf{x}.$$

Since $d\mathbf{x} = O(L^d)$ and $\Delta \psi_{R^{(0)}} = O(L^{-2-\frac{d}{2}})$, see (31.35), the right-hand side of this inequality is $O(1)$. Hence, $\epsilon f_1 = o(1)$. The proof for f_2 is similar. \square

Conclusion 31.5 Let $f_2 \not\equiv 0$. Then generically $\frac{[f'_1]}{[f_2]} = O\left(\beta^{\frac{1}{2}}\right) \ll 1$.

Proof By (31.12),

$$\frac{[f'_1]}{[f_2]} = \frac{[L^2]}{[Z]} \frac{\left[\operatorname{Re} \int F(\psi_{R^{(0)}}) e^{-iS} \left[d \cdot R^{(0)} + 2\rho \frac{dR^{(0)}}{d\rho} \right] d\xi \right]}{\left[\operatorname{Im} \int F(\psi_{R^{(0)}}) e^{-iS} R^{(0)} d\xi \right]}.$$

Now, generically, we can “expect” that¹²

$$\left[\operatorname{Re} \left\{ F(\psi_{R^{(0)}}) e^{-iS} \right\} \right] = \left[\operatorname{Im} \left\{ F(\psi_{R^{(0)}}) e^{-iS} \right\} \right],$$

hence also that

$$\left[\operatorname{Re} \int F(\psi_{R^{(0)}}) e^{-iS} \left[d \cdot R^{(0)} + 2\rho \frac{dR^{(0)}}{d\rho} \right] d\xi \right] = \left[\operatorname{Im} \int F(\psi_{R^{(0)}}) e^{-iS} R^{(0)} d\xi \right].$$

Therefore,

$$\frac{[f'_1]}{[f_2]} = \frac{[L^2]}{[Z]} \sim \beta^{\frac{1}{2}},$$

where at the last stage we used Conclusion 31.1. \square

By the last two conclusions, the two terms in the reduced equation (31.8a) which are induced by the perturbation, generically satisfy

$$\epsilon f'_1 \ll \epsilon f_2 \ll \frac{1}{L^2}.$$

In fact, so long that Condition 3 holds, $\epsilon f'_1$ and ϵf_2 can be at most $O(\beta L^{-2})$. Indeed, if either of these terms is $\gg \beta L^{-2}$, then $\beta_z \gg \beta L^{-2}$, and so $\beta_\zeta \gg \beta$. Consequently, β does not remain small, in violation of Condition 3.

31.4 Conservative and Non-conservative Perturbations

The analysis of the reduced equations (31.8) can be significantly simplified by distinguishing between conservative and non-conservative perturbations.

Definition 31.1 (*conservative and non-conservative perturbations*) Let ψ be a solution of the perturbed NLS (31.4). The perturbation F is called *conservative* if the power of ψ is conserved, i.e., if $\frac{d}{dz} \int |\psi(z, \mathbf{x})|^2 d\mathbf{x} \equiv 0$. Otherwise, F is called a *non-conservative perturbation*.

¹² This is not always the case, see, e.g., relation (34.17).

Lemma 31.3 *If F is conservative, then $f_2 \equiv 0$.*

Proof This follows directly from (31.10b) and (31.29). \square

We can also prove Lemma 31.3 as follows. By (31.33) and (31.8a),

$$\frac{d}{dz} P_{\text{coll}} = -\frac{Mv(\beta)}{L^2} - 2\epsilon f_2.$$

Therefore, under the adiabatic approximation

$$\frac{d}{dz} P_{\text{coll}} \sim -2\epsilon f_2. \quad (31.37)$$

Hence,

$$\frac{d}{dz} P_{\text{coll}} = 0 \iff f_2 \equiv 0. \quad (31.38)$$

31.4.1 Dual Interpretations for β

The variable $\beta := -L^3 L_{zz}$ measures the acceleration of the blowup rate. In Corollary 17.3 we saw that in the unperturbed critical NLS, once self-focusing becomes adiabatic, then

$$\beta(z) \sim \frac{P_{\text{coll}}(z) - P_{\text{cr}}}{M}. \quad (31.39)$$

Hence, β has the dual interpretation of being proportional to the excess power above critical of the collapsing core. This interpretation remains valid when the perturbation in (31.4) is “purely non-conservative”:

Corollary 31.1 *Let Conditions 1–3 hold, and let $f_1 \equiv 0$. Then relation (31.39) holds.*

Proof This follows directly from (31.31). \square

More generally, this dual interpretation remains valid for “generic” non-conservative perturbations:¹³

Lemma 31.4 *Let Conditions 1–3 hold, and let $f'_1 \ll f_2$. Then relation (31.39) holds.*

Proof Let z_0^{ad} be in the *unperturbed adiabatic stage* where the effect of the perturbation is negligible (Sect. 31.1.2). Then

$$\beta(z_0^{\text{ad}}) \sim \frac{P_{\text{coll}}(z_0^{\text{ad}}) - P_{\text{cr}}}{M}. \quad (31.40a)$$

¹³ i.e., those satisfying $f'_1 \ll f_2$, see Conclusion 31.5.

In addition, by (31.31) and (31.37),

$$M\beta_z - \frac{\epsilon}{2} f'_1 \sim \frac{d}{dz} P_{\text{coll}} \sim -2\epsilon f_2.$$

Therefore, the condition $f'_1 \ll f_2$ implies that $M\beta_z \sim -2\epsilon f_2$, and so

$$\frac{d}{dz} P_{\text{coll}} \sim -2\epsilon f_2 \sim M\beta_z, \quad z \geq z_0^{\text{ad}}. \quad (31.40b)$$

Finally, by Eq. (31.40),

$$\begin{aligned} \frac{P_{\text{coll}}(z) - P_{\text{cr}}}{M\beta(z)} &= \frac{P_{\text{coll}}(z_0^{\text{ad}}) - P_{\text{cr}} + \int_{z_0^{\text{ad}}}^z \frac{d}{dz} P_{\text{coll}} dz}{M\beta(z_0) + M \int_{z_0^{\text{ad}}}^z \beta_z dz} \\ &= \frac{M\beta(z_0^{\text{ad}})(1+o(1)) + \int_{z_0^{\text{ad}}}^z M\beta_z(1+o(1)) dz}{M\beta(z_0^{\text{ad}}) + M \int_{z_0^{\text{ad}}}^z \beta_z dz} = 1 + o(1). \quad \square \end{aligned}$$

In the conservative case, β is not proportional to $P_{\text{coll}} - P_{\text{cr}}$, see (31.31). Indeed, while P_{coll} is conserved, see (31.38), changes in β are “allowed”, as they can be “compensated” by changes in f_1 .

31.4.2 Non-conservative Perturbations

In Conclusion 31.5 we saw that, generically, non-conservative perturbations satisfy

$$\frac{[f'_1]}{[f_2]} = O\left(\beta^{\frac{1}{2}}\right) \ll 1. \quad (31.41)$$

In that case, the reduced equations can be further simplified, as follows:

Proposition 31.4 *Let Conditions 1–3 hold, and let F be a non-conservative perturbation, such that (31.41) holds. Then the reduced equations (31.8) can be further approximated by*

$$\beta_z = -\frac{2\epsilon}{M} f_2, \quad L_{zz} = -\frac{\beta}{L^3}. \quad (31.42)$$

Proof By (31.41), the leading-order behavior of (31.8) is given by

$$\beta_z + \frac{v(\beta)}{L^2} = -\frac{2\epsilon}{M} f_2, \quad L_{zz} = -\frac{\beta}{L^3}.$$

Since the accuracy of neglecting f'_1 is $O\left(\beta^{\frac{1}{2}}\right)$, there is no point in keeping the exponentially-small term $\nu(\beta)$. \square

By Lemma 31.4, Eq. (31.42) for β_z can be rewritten as

$$\frac{d}{dz}P_{\text{coll}} = -2\epsilon f_2, \quad (31.43)$$

which is Eq. (31.37). Hence, *in the non-conservative case, the reduced equation for β coincides with the equation for the dynamics of the power of the collapsing core.* This is to be expected, since in the nonconservative case β is proportional to $P_{\text{coll}} - P_{\text{cr}}$ (Sect. 31.4.1).

Non-conservative perturbations that are analyzed in this book using modulation theory include linear and nonlinear damping (Sects. 33.3 and 38.6), nonparaxiality (Sect. 34.3), dispersion (Sects. 36.8.3–36.8.5), dispersion and nonparaxiality (Sect. 36.9.1), and the Complex Ginzburg-Landau equation (Sect. 38.7).

31.4.3 Conservative Perturbations

The reduced equations can also be simplified when the perturbation is conservative:

Proposition 31.5 *Let Conditions 1–3 hold. If $f_2 \equiv 0$, then to leading order, Eq. (31.8) reduce to*

$$-L^3 L_{zz}(z) = \beta_0 + \frac{\epsilon}{2M} f_1(z), \quad z \geq z_0^{\text{ad}}, \quad (31.44a)$$

where

$$\beta_0 := \beta\left(z_0^{\text{ad}}\right) - \frac{\epsilon}{2M} f_1\left(z_0^{\text{ad}}\right), \quad (31.44b)$$

and z_0^{ad} is in the unperturbed adiabatic stage.¹⁴ Furthermore, β_0 is proportional to the excess power of the collapsing core above P_{cr} , i.e.,

$$\beta_0 \sim \frac{P_{\text{coll}}(z_0^{\text{ad}}) - P_{\text{cr}}}{M} \sim \frac{P_{\text{coll}}(z) - P_{\text{cr}}}{M}. \quad (31.45)$$

Proof Since $f_2 \equiv 0$, Eq. (31.8a) reads

$$\beta_z + \frac{\nu(\beta)}{L^2} = \frac{\epsilon}{2M} f'_1, \quad L_{zz} = -\frac{\beta}{L^3}. \quad (31.46)$$

¹⁴ See Sect. 31.1.2.

Neglecting the exponentially small $v(\beta)$ term in the left equation¹⁵ and integrating gives

$$\beta(z) = \beta_0 + \frac{\epsilon}{2M} f_1(z), \quad \beta_0 = \beta\left(z_0^{\text{ad}}\right) - \frac{\epsilon}{2M} f_1\left(z_0^{\text{ad}}\right).$$

Therefore, we obtain (31.44a). The relation between β_0 and $P_{\text{coll}}(z_0^{\text{ad}}) - P_{\text{cr}}$ follows from (31.31). Conservation of $P_{\text{coll}}(z)$ follows from (31.37). \square

Lemma 31.5 *Let Conditions 1–3 hold, let $0 < \beta^2 \ll |\epsilon| \ll 1$, and let $H_{\text{coll}} := H(\psi_{\text{coll}}) = \int |\nabla \psi_{\text{coll}}|^2 d\mathbf{x} - \frac{1}{1+\frac{2}{d}} \int |\psi_{\text{coll}}|^{2+\frac{4}{d}} d\mathbf{x}$. Then*

$$H_{\text{coll}} \sim M \left(L_z^2 - \frac{\beta}{L^2} \right) + \frac{\epsilon f_1}{2L^2} = \frac{M}{2} (L^2)_{zz} + \frac{\epsilon f_1}{2L^2}. \quad (31.47)$$

Proof By (31.32), since V_0^ϵ is “essentially” real for $\rho = O(1)$,

$$H(\psi_{\text{coll}}) \sim H \left(\frac{V_0^\epsilon e^{iS}}{L^{\frac{d}{2}}} \right) \sim \frac{L_z^2}{4} \int |\rho|^2 |V_0^\epsilon|^2 d\xi + \frac{H(V_0^\epsilon)}{L^2}. \quad (31.48a)$$

Since $V_0^\epsilon \sim R^{(0)}$, we have that $\frac{1}{4} \int |\rho|^2 |V_0^\epsilon|^2 d\xi \sim M$. In addition, by (17.39) and (31.31),

$$H(V_0^\epsilon) \sim -(P_{\text{coll}} - P_{\text{cr}}) = -\beta M + \frac{\epsilon}{2} f_1. \quad (31.48b)$$

Approximation (31.47) follows from the above relations and $\beta = -L^3 L_{zz}$.

Approximation (31.47) is not valid in the unperturbed case ($\epsilon = 0$). Indeed, substituting $\epsilon = 0$ in (31.47) yields

$$H_{\text{coll}} \sim M \left(L_z^2 - \frac{\beta}{L^2} \right). \quad (31.49)$$

By (18.39) and (18.40), however, when $\epsilon = 0$,

$$L_z^2 - \frac{\beta}{L^2} = \frac{a^2 - \beta}{L^2} = \frac{-a_\xi}{L^2} \sim \frac{v(\beta)}{2\sqrt{\beta} L^2}.$$

Hence, the right-hand side of (31.49) is exponentially small in β . This implies that the leading-order behavior of H_{coll} is determined by the $O(\beta^2)$ terms that were neglected in the expansion of H_{coll} , see (31.48). Consequently, for (31.47) to be valid, ϵ should be larger than the neglected $O(\beta^2)$ terms. \square

¹⁵ i.e., neglecting the coupling between ψ_{coll} and ψ_{outer} .

31.5 Generic Effect of Conservative Perturbations

As we shall see, for various conservative perturbations

$$f_1 \sim -\frac{C_{\text{gen}}}{L^2}, \quad L \rightarrow 0,$$

where C_{gen} is a constant. This is the case, e.g., for a small quintic nonlinearity (Sect. 32.3), saturating nonlinearities (Sect. 32.4), arrays of coupled waveguides [93], fourth-order dispersion [81, 82], discretization effects [79], and “in a way”, also for non-conservative perturbations such as nonparaxiality (Sect. 34.3) and vectorial effects [76].

The following series of lemmas cover this generic case. Lemmas 31.6–31.10 deal with adiabatic effects, Lemma 31.11 concerns nonadiabatic effects, Lemma 31.12 shows that the reduced equations remain valid for all z when the perturbation is defocusing, and Lemma 31.13 shows that the validity of the reduced equations breaks down when the perturbation is focusing.

Lemma 31.6 *Let $L(z)$ be the solution of (31.44) and*

$$f_1 \sim -\frac{C_{\text{gen}}}{L^2}, \quad L \rightarrow 0, \quad (31.50)$$

Then $y(z) := L^2(z)$ is the solution of

$$y_z^2 = 4\beta_0 - \frac{\epsilon C_{\text{gen}}}{M} \frac{1}{y} + \frac{4H_0}{M} y, \quad (31.51)$$

or, equivalently,

$$y_z^2 = \frac{-4H_0}{M} \frac{1}{y} (y_M - y)(y - y_m), \quad (31.52)$$

where

$$y_M = \frac{\sqrt{\beta_0^2 + \frac{\epsilon C_{\text{gen}} H_0}{M^2}} + \beta_0}{-2H_0/M} = \frac{M\beta_0}{-H_0} \left[1 + O\left(\frac{\epsilon H_0}{\beta_0^2}\right) \right], \quad (31.53a)$$

$$y_m = \frac{\epsilon C_{\text{gen}}}{2M} \frac{1}{\sqrt{\beta_0^2 + \frac{\epsilon C_{\text{gen}} H_0}{M^2}} + \beta_0} = \frac{\epsilon C_{\text{gen}}}{4M\beta_0} \left[1 + O\left(\frac{\epsilon H_0}{\beta_0^2}\right) \right], \quad (31.53b)$$

$$\beta_0 = \beta\left(z_0^{\text{ad}}\right) + \frac{\epsilon C_{\text{gen}}}{2ML_0^2} \sim \frac{P_{\text{coll}}(z_0^{\text{ad}}) - P_{\text{cr}}}{M}, \quad L_0 = L\left(z_0^{\text{ad}}\right), \quad (31.53c)$$

and

$$H_0 = ML_z^2(z_0^{\text{ad}}) - \frac{M\beta_0}{L_0^2} + \frac{\epsilon C_{\text{gen}}}{4L_0^4} \sim H_{\text{coll}}(z_0^{\text{ad}}) + \frac{3\epsilon C_{\text{gen}}}{4} \frac{1}{L_0^4}. \quad (31.53d)$$

Proof When f_1 is given by (31.50), Eq. (31.44) reads

$$-L^3 L_{zz} = \beta_0 - \frac{\epsilon C_{\text{gen}}}{2M} \frac{1}{L^2}, \quad \beta_0 := \beta(z_0^{\text{ad}}) + \frac{\epsilon C_{\text{gen}}}{2ML_0^2}. \quad (31.54)$$

If we multiply this equation by $2L^{-3}L_z$ and integrate, we get

$$L_z^2 = \frac{\beta_0}{L^2} - \frac{\epsilon C_{\text{gen}}}{4M} \frac{1}{L^4} + \frac{H_0}{M}, \quad H_0 := ML_z^2(z_0^{\text{ad}}) - \frac{M\beta_0}{L_0^2} + \frac{\epsilon C_{\text{gen}}}{4L_0^4}. \quad (31.55)$$

To relate H_0 and $H(\psi_{\text{coll}})$, we use (31.47) and (31.50) to get

$$H_{\text{coll}} \sim M \left(L_z^2 - \frac{\beta}{L^2} \right) + \frac{\epsilon f_1}{2L^2} \sim M \left(L_z^2 - \frac{\beta}{L^2} \right) - \frac{\epsilon C_{\text{gen}}}{2L^4}.$$

Therefore,

$$H_0 = H_{\text{coll}}(z_0^{\text{ad}}) + \frac{3}{4} \frac{\epsilon C_{\text{gen}}}{2L_0^4}. \quad (31.56)$$

Multiplying (31.55) by $4L^2 = 4y$ gives

$$y_z^2 = 4\beta_0 - \frac{\epsilon C_{\text{gen}}}{M} \frac{1}{y} + \frac{4H_0}{M} y. \quad (31.57)$$

Therefore, we proved (31.51).

Equation (31.57) can be rewritten as

$$y_z^2 = \frac{-4H_0}{M} \frac{1}{y} \left(-y^2 - \frac{\beta_0 M}{H_0} y + \frac{\epsilon C_{\text{gen}}}{4H_0} \right) = \frac{-4H_0}{M} \frac{1}{y} (y_M - y)(y - y_m),$$

where y_m and y_M are the two roots of the quadratic equation

$$\frac{H_0}{M} y^2 + \beta_0 y - \frac{\epsilon C_{\text{gen}}}{4M} = 0. \quad (31.58)$$

Therefore,

$$y_m = \frac{\beta_0 - \sqrt{\beta_0^2 + \frac{\epsilon C_{\text{gen}} H_0}{M^2}}}{-2H_0/M}, \quad y_M = \frac{\beta_0 + \sqrt{\beta_0^2 + \frac{\epsilon C_{\text{gen}} H_0}{M^2}}}{-2H_0/M}. \quad (31.59)$$

□

By (31.54), when $\epsilon C_{\text{gen}} > 0$ the perturbation increases L_{zz} , i.e., it is defocusing. In fact, when $\epsilon C_{\text{gen}} > 0$ collapse is always arrested:

Lemma 31.7 *Assume the conditions of Lemma 31.6. If*

$$\epsilon C_{\text{gen}} > 0, \quad (31.60)$$

the perturbation always arrests collapse in (31.44) and in (31.51), i.e., $L(z)$ and $y(z)$ remain strictly positive for all z .

Proof Let $\epsilon C_{\text{gen}} > 0$. As $y \rightarrow 0+$, the right-hand side of (31.51) becomes negative. This is not possible, however, because the left-hand side is non-negative. \square

Remark A priori, when the perturbation arrests collapse at $y = y_m$, its magnitude should be comparable to that of the focusing nonlinearity, i.e., $[\epsilon F] = \left[|\psi|^{\frac{4}{d}} \psi \right]$.

Since¹⁶

$$\frac{[\epsilon F]}{\left[|\psi|^{\frac{4}{d}} \psi \right]} \sim \frac{\epsilon}{L^2}, \quad (31.61)$$

this suggests that $y_m = O(\epsilon)$. By (31.51), however,

$$y_z^2 \sim 4\beta_0 - \frac{\epsilon C_{\text{gen}}}{M} \frac{1}{y}, \quad y \rightarrow 0.$$

Therefore, since $y_z = 0$ at $y = y_m$,

$$y_m \sim \frac{\epsilon C_{\text{gen}}}{4M\beta_0} = O\left(\frac{\epsilon}{\beta_0}\right) \gg \epsilon,$$

i.e., collapse is arrested at a much earlier stage. This result is consistent with the *balance of the giants principle* (Conclusion 18.9) that collapse is arrested as soon as the perturbation becomes comparable to the balance between nonlinearity and diffraction, which is $O(\beta)$ smaller than each of them separately.

31.5.1 Periodic Focusing-Defocusing Oscillations

The case of most interest is that of a weakly defocusing perturbation ($0 < \epsilon C_{\text{gen}} \ll 1$) that acts on a solution that collapses in the unperturbed NLS. During the *unperturbed*

¹⁶ By (31.12a) and (31.50), $[f_1] = L^{2+\frac{d}{2}} [F]$ and $[f_1] = L^{-2}$, respectively. Therefore, $[F] = L^{-4-\frac{d}{2}}$. In addition, $\left[|\psi|^{\frac{4}{d}} \psi \right] \sim \left[|\psi_{R^{(0)}}|^{\frac{4}{d}} \psi_{R^{(0)}} \right] = L^{-2-\frac{d}{2}}$, see (31.35a). Therefore, (31.61) follows.

adiabatic stage the solution self-focusses and so $P_{\text{coll}} > P_{\text{cr}}$. Therefore, $\beta_0 > 0$, see (31.53c). In addition, since in the unperturbed NLS, $P_{\text{coll}} > P_{\text{cr}}$ if and only if $H_{\text{coll}} < 0$, see (17.40), and since $H_0 = H_{\text{coll}} + O(\epsilon)$, see (31.56), then generically $H_0 < 0$. In this case, the solution undergoes periodic focusing-defocusing oscillations (Fig. 31.2a):

Lemma 31.8 *Let $L(z)$ be the solution of (31.44) with f_1 given by (31.50), and let $\beta_0 > 0$, $H_0 < 0$, and $0 < \epsilon C_{\text{gen}} < \frac{(M\beta_0)^2}{-H_0}$. Then*

$$0 < L_m \leq L(z) \leq L_M < \infty, \quad (31.62)$$

where $L_m := \sqrt{y_m}$ and $L_M := \sqrt{y_M}$, see (31.53). In addition, $L(z)$ oscillates periodically between L_m and L_M . The period of the oscillations is

$$\Delta Z = 2 \sqrt{\frac{My_M}{-H_0}} E \left(1 - \frac{y_m}{y_M} \right), \quad (31.63)$$

where $E(\kappa) := \int_0^{\frac{\pi}{2}} (1 - \kappa \sin^2 \theta)^{\frac{1}{2}} d\theta$ is the complete elliptic integral of the second kind.

Proof By Lemma 31.6, the equation for $y = L^2$ is given by (31.52). The left-hand side of (31.52) is non-negative. Since $0 < y_m < y_M$, see (31.59), the right-hand side of (31.52) is non-negative if and only if $y_m \leq y \leq Y_M$. Therefore, we proved (31.62). Since (31.52) is an autonomous nonlinear oscillator, its solution is periodic.

To evaluate ΔZ , note that by (31.52),

$$\Delta Z = 2 \int_{y_m}^{y_M} z_y dy = \sqrt{\frac{M}{-H_0}} \int_{y_m}^{y_M} \sqrt{\frac{y}{(y_M - y)(y - y_m)}} dy.$$

To bring this integral into a more familiar form, let $\frac{y - y_m}{y_M - y_m} = \cos^2 u$. Then

$$\begin{aligned} \frac{dy}{y_M - y_m} &= -2 \cos u \sin u du = -2 \sqrt{\frac{y - y_m}{y_M - y_m}} \sqrt{1 - \frac{y - y_m}{y_M - y_m}} du \\ &= -2 \sqrt{\frac{y - y_m}{y_M - y_m}} \sqrt{\frac{y_M - y}{y_M - y_m}} du, \end{aligned}$$

and so

$$\sqrt{\frac{y}{(y_M - y)(y - y_m)}} dy = -2 \sqrt{y} du.$$

In addition,

$$\begin{aligned} y &= y_m + (y_M - y_m) \cos^2 u = y_m + (y_M - y_m) \left(1 - \sin^2 u\right) \\ &= y_M \left(1 - \frac{y_M - y_m}{y_M} \sin^2 u\right). \end{aligned}$$

Combining the above gives

$$\Delta Z = 2 \sqrt{\frac{My_M}{-H_0}} \int_0^{\pi/2} \left(1 - \frac{y_M - y_m}{y_M} \sin^2 u\right)^{\frac{1}{2}} du. \quad \square$$

31.5.2 Self Trapping (Filamentation)

One of the earliest observations of nonlinear effects in optics was that of *self-trapping* (filamentation), i.e., of laser beams that collapse and then continue to propagate in a tightly focused state over long distances (Sect. 3.3.1). Initially, self-trapping was explained as propagation of solitary waves of the two-dimensional cubic NLS (Sect. 3.3). It later turned out, however, that these solitary waves are unstable (Sect. 7.11.1). In 1974, Bjorkholm and Ashkin [29] showed experimentally that the width of laser filaments is not constant, but rather varies periodically in z , see Fig. 31.1. “As a result”, over the years, “whenever” it was found that a perturbation leads to periodic focusing-defocusing oscillations, it was suggested as an explanation

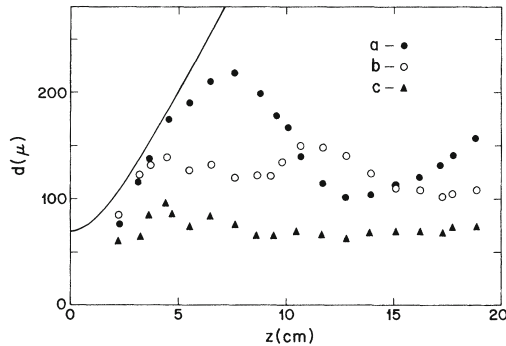


Fig. 31.1 (Experimental) half-power diameter of a laser beam that propagates in a cell filled with sodium vapor, as a function of propagation distance. The input power and side-arm temperature were **a** 15 mW and 180°, **b** 23 mW and 180°, **c** 23 mW and 200°. The *solid curve* shows the free-space propagation. From [29]

for filamentation. Lemma 31.8 clarifies the situation by showing that, generically, “any” conservative mechanism can lead to filamentation.

Remark See also Sect. 32.5 on filamentation due to high-order nonlinear effects.

31.5.3 Other Cases

As noted, the case of most interest is $\epsilon C_{\text{gen}} > 0$, $\beta_0 > 0$, and $H_0 < 0$. For completeness, we now discuss the other cases. When $H_0 > 0$ the solution scatters, rather than remain self-trapped:

Lemma 31.9 *Let $L(z)$ be the solution of (31.44) with f_1 given by (31.50), and let $\epsilon C_{\text{gen}} > 0$, $\beta_0 > 0$, and $H_0 > 0$. Then*

1. *If $L_z(0) < 0$, collapse is arrested once $L = L_m > 0$. Subsequently, $L(z)$ increases monotonically to infinity (see Fig. 31.2b).*
2. *If $L_z(0) > 0$, $L(z)$ increases monotonically to infinity for $0 \leq z < \infty$.*

Proof By (31.53), $y_M < 0 < y_m$. Therefore, (31.52) can be rewritten as

$$y_z^2 = \frac{4|H_0|}{M} \frac{1}{y} (y + |y_M|)(y - y_m).$$

Since the left-hand side is non-negative, $y(z) \geq y_m$ for all z . In addition, $y_z = 0$ if and only if $y = y_m$. Therefore, if $y_z(0) < 0$, y decreases to y_m and then increases monotonically to infinity. If $y_z(0) > 0$, y increases monotonically to infinity. \square

When the perturbation is focusing, solutions of the reduced equation can become singular (Fig. 31.2c):

Lemma 31.10 *Let $L(z)$ be the solution of (31.44) with f_1 given by (31.50), and let $\epsilon C_{\text{gen}} < 0$ and $\beta_0 > 0$. If either of the following two conditions holds:*

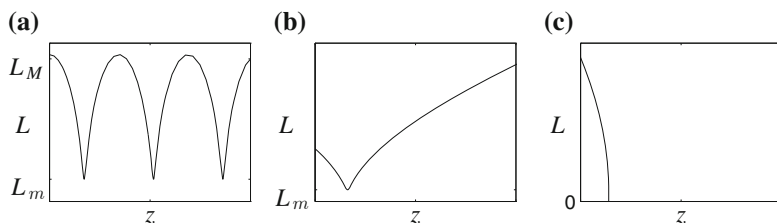


Fig. 31.2 Leading-order effect of the generic conservative perturbation (31.50). **a** Defocusing perturbation and $H_0 < 0$ (Lemma 31.8). **b** Defocusing perturbation, $H_0 > 0$, and $L_z(0) < 0$ (Lemma 31.9). **c** Focusing perturbation and $L_z(0) < 0$ (Lemma 31.10). In all cases $\beta_0 > 0$. From [93]

1. $0 < H_0 < \frac{M^2 \beta_0^2}{-\epsilon C_{\text{gen}}}$ and $L_z(0) < 0$, or
2. $H_0 < 0$,

then $L(z)$ vanishes at a finite distance, i.e., there exists $Z_c^{(\epsilon)}$ such that $0 < Z_c^{(\epsilon)} < \infty$ and $L(Z_c^{(\epsilon)}) = 0$.

Proof By (31.53), if $\epsilon C_{\text{gen}} < 0$, $\beta_0 > 0$, and $0 < H_0 < \frac{M^2 \beta_0^2}{-\epsilon C_{\text{gen}}}$, then $y_m, y_M < 0$. Therefore, (31.52) can be rewritten as

$$y_z^2 = \frac{4|H_0|}{M} \frac{1}{y} (y + |y_M|)(y + |y_m|).$$

Since y_z does not vanish for any $y > 0$, collapse is not arrested if $y_z(0) < 0$.

Similarly, if $\epsilon C_{\text{gen}} < 0$, $\beta_0 > 0$, and $H_0 < 0$, then $y_m < 0 < y_M$. Therefore, (31.52) can be rewritten as

$$y_z^2 = \frac{4|H_0|}{M} \frac{1}{y} (y_M - y)(y + |y_m|).$$

Since the left-hand side is non-negative, $y(z) \leq y_M$ for all z . Hence, even if the beam is initially defocusing, defocusing will be arrested at $y = y_M$, after which y would go to zero. \square

In Lemma 31.13 we will see that under the conditions of Lemma 31.10, the validity of reduced equations break down *before* $Z_c^{(\epsilon)}$. Therefore, Lemma 31.10 suggests, but does not prove, that the corresponding solutions of the perturbed NLS become singular.

31.5.4 Nonadiabatic Effects

Propositions 31.4 and 31.5 show that, regardless of whether the perturbation is conservative or nonconservative, as long as f_1 and f_2 are not both identically zero, the $v(\beta)$ term does not affect the leading-order behavior in the reduced equations (31.8). This is different from the unperturbed critical NLS, where retaining $v(\beta)$ was essential for finding the loglog correction to the blowup rate (Chap. 18).¹⁷

There is, however, one case in which retaining $v(\beta)$ in the reduced equations of a perturbed NLS is essential. Indeed, consider the generic conservative perturbation (31.50) with $\epsilon C_{\text{gen}} > 0$, $\beta_0 > 0$, and $H_0 < 0$. If nonadiabatic effects are neglected, then the solution undergoes periodic focusing-defocusing oscillations (Lemma 31.8). Therefore, in this case $v(\beta)$ provides the only mechanism for the

¹⁷ Under the adiabatic approximation, however, $v(\beta)$ is neglected also in the unperturbed critical NLS (Sects. 18.4–18.5).

decay of the oscillations in the reduced equations. To analyze this nonadiabatic effect, we “go back” from Eq. (31.44a) to the equation¹⁸

$$\beta_z(z) + \frac{v(\beta)}{L^2} = \frac{\epsilon}{2M} f'_1, \quad L_{zz} = -\frac{\beta}{L^3}. \quad (31.64)$$

This equation can be rewritten as, see (31.33),

$$\frac{d}{dz} P_{\text{coll}}(z) = -M \frac{v(\beta)}{L^2}. \quad (31.65)$$

Therefore, the power of ψ_{coll} decreases with propagation. Let

$$\Delta P_{\text{coll}} := P_{\text{coll}}(z + \Delta Z) - P_{\text{coll}}(z)$$

denote the power-loss per oscillation, where ΔZ is the oscillation period, see (31.63). If $\Delta P_{\text{coll}} \ll P_{\text{coll}}$ the solution is nearly periodic, and so we can approximate ΔP_{coll} by

$$\Delta P_{\text{coll}} \sim -M \int_z^{z+\Delta Z} \frac{v(\beta)}{L^2} dz, \quad (31.66)$$

where $L(z)$ is the periodic solution of (31.44).

Lemma 31.11 ([65, 93]) *Assume the conditions of Lemma 31.8, and let $\beta = -L^3 L_{zz}$, $v(\beta)$ be given by (31.9), and ΔP_{coll} be given by (31.66). Then*

$$\Delta P_{\text{coll}} \sim -M v(\beta_M) \beta_M^{-\frac{1}{4}} \left(\frac{y_M - y_m}{y_m} \right)^{\frac{1}{2}}, \quad \beta_M \rightarrow 0, \quad (31.67)$$

where $\beta_M := \beta(y = y_M) = -\frac{H_0}{M}(y_M - y_m)$.

Proof Since $L(z)$ is periodic with period ΔZ , so is $\beta(z)$. In addition, since $v(\beta) = c_v e^{-\pi/\sqrt{\beta}}$ decreases exponentially as $\beta \rightarrow 0$, essentially all the contribution to the integral in (31.66) comes from the neighborhood of the point z_M where $\beta(z)$ attains its global maximum in $[z, z + \Delta Z]$. This observation suggests that we can approximate the integral in (31.66) using the Laplace method for integrals (see e.g., [20, 193]). Briefly, let $h(z)$ be a smooth function that attains its global maximum in the interval $[a, b]$ at an interior point $z_M \in (a, b)$. If $h_{zz}(z_M) < 0$, then by the Laplace method,

$$\int_a^b e^{\lambda h(z)} g(z) dz \sim e^{\lambda h(z_M)} g(z_M) \sqrt{\frac{2\pi}{-h_{zz}(z_M)\lambda}}, \quad \lambda \rightarrow \infty. \quad (31.68)$$

¹⁸ Here we make the approximation $v^\epsilon(\beta) \sim v(\beta)$, i.e., we assume that nonadiabatic effects are, to leading order, unaffected by the perturbation. See [164] for a detailed analysis of nonadiabatic effects.

To make use of (31.68), we first express β in terms of y . Specifically, we show that

$$\beta = \frac{-y_M H_0}{M} \left(1 + \frac{y_m}{y_M} - \frac{2y_m}{y} \right). \quad (31.69)$$

To see this, recall that

$$\beta = \frac{1}{4} y_z^2 - \frac{1}{2} y y_{zz}, \quad (31.70a)$$

see (18.13a). In addition, by (31.52),

$$\frac{1}{4} y_z^2 = \frac{-H_0}{M} (y_M - y) \left(1 - \frac{y_m}{y} \right). \quad (31.70b)$$

Differentiating this equation and dividing by y_z gives

$$\frac{1}{2} y_{zz} = \frac{-H_0}{M} \left(-1 + \frac{y_m y_M}{y^2} \right). \quad (31.70c)$$

Relation (31.69) follows from relations (31.70).

By (31.69), β is monotonically increasing in y . Therefore, the maximum of $\beta(y)$ is attained at y_M , see (31.53a), and is given by

$$\beta_M := \beta(y_M) = -\frac{H_0}{M} (y_M - y_m). \quad (31.71)$$

We can rewrite ΔP_{coll} as, see (31.66),

$$\begin{aligned} \Delta P_{\text{coll}} &\sim -M v(\beta_M) \int_z^{z+\Delta Z} \frac{1}{y} \frac{e^{-\pi/\sqrt{\beta}}}{e^{-\pi/\sqrt{\beta_M}}} dz \\ &= -M v(\beta_M) \int_z^{z+\Delta Z} g(z) e^{\lambda h(z)} dz, \end{aligned} \quad (31.72a)$$

where

$$\lambda := \frac{\pi}{\sqrt{\beta_M}}, \quad h = 1 - \sqrt{\frac{\beta_M}{\beta(z)}}, \quad g = \frac{1}{y}. \quad (31.72b)$$

Since $\beta_M \ll 1$, see Condition 3, then $\lambda \gg 1$. Therefore, we can approximate the integral using Laplace method for integrals. This yields, see (31.68),

$$\int_z^{z+\Delta Z} g(z) e^{\lambda h(z)} dz \sim \frac{\beta_M^{1/4}}{y_M} \sqrt{\frac{2}{-h_{zz}(z_M)}}, \quad (31.73)$$

where $z_M = \arg \max y(z)$.

In standard applications of Laplace method, the function $h(z)$ is given explicitly. This is not the case here, however, since $h(z)$ depends on $\beta(z)$, which in turn depends on $y(z)$, which is not given explicitly. Nevertheless, we can compute $h_{zz}(z_M)$ explicitly, as follows. By (31.72b),

$$h_z(z) = \frac{1}{2} \sqrt{\beta_M} \beta^{-\frac{3}{2}} \beta_z.$$

Since $\beta(z)$ attains its maximum at z_M , then $\beta_z(z_M) = 0$. Therefore,

$$h_{zz}(z_M) = \frac{1}{2} \sqrt{\beta_M} \beta_M^{-\frac{3}{2}} \beta_{zz}(z_M) = \frac{1}{2\beta_M} \beta_{zz}(z_M). \quad (31.74a)$$

Similarly, by (31.69),

$$\beta_z = \frac{-H_0 y_M}{M} \frac{2y_m}{y^2} y_z.$$

Since $y(z)$ attains its maximum at z_M , $y_z(z_M) = 0$. Therefore,

$$\beta_{zz}(z_M) = \frac{-2H_0 y_m}{My_M} y_{zz}(z_M). \quad (31.74b)$$

Substituting $y = y_M$ in (31.70c) and using (31.71) gives

$$y_{zz}(z_M) = \frac{-2H_0}{M} \left(-1 + \frac{y_m}{y_M} \right) = -\frac{2\beta_M}{y_M}. \quad (31.74c)$$

Therefore, by (31.74)

$$h_{zz}(z_M) = \frac{2H_0 y_m}{My_M^2}.$$

Substituting this expression in (31.73) and using (31.71) gives

$$\int_z^{z+\Delta Z} \frac{1}{y(z)} e^{\lambda h(z)} dz \sim \beta_M^{\frac{1}{4}} \sqrt{\frac{M}{-H_0 y_m}} = \beta_M^{-\frac{1}{4}} \sqrt{\frac{y_M - y_m}{y_m}}.$$

Therefore, by (31.72a), the result follows. \square

Remark The proof of Lemma 31.11 shows that most of the radiation occurs when $y \approx y_M$, i.e., when the solution is the most defocused.

The calculation of ΔP_{coll} in Lemma 31.11 was done under the assumption that $y(z)$ and $\beta(z)$ are periodic. This assumption is reasonable if $\Delta P_{\text{coll}} \ll P_{\text{coll}}$. By Lemma 31.11, this is indeed the case as $\beta_M \rightarrow 0$, since then $v(\beta_M) \beta_M^{-\frac{1}{4}}$ decays exponentially to zero. Note, however, that by (31.53a) and (31.53b),

$$\Delta P_{\text{coll}} \sim \left(\frac{y_M}{y_m} \right)^{\frac{1}{2}} \sim \epsilon^{-\frac{1}{2}}, \quad \epsilon \rightarrow 0.$$

Therefore, the dynamics is nearly periodic when ϵ is moderately small, but not if ϵ is “too small”.

31.5.5 Global Validity of Modulation Theory

When the generic conservative perturbation (31.50) is defocusing, we can use the reduced equations to prove that ϵF remains a small perturbation. Hence, modulation theory remains valid throughout the propagation:

Lemma 31.12 *Let F be a conservative perturbation, such that f_1 is given by (31.50) with $\epsilon C_{\text{gen}} > 0$. If Conditions 1–3 hold at z_0^{ad} , they remain valid for all $z \geq z_0^{\text{ad}}$.*

Proof We give an informal proof. We first use the reduced equations to show that ϵF remains $O(\beta)$ smaller than nonlinearity and diffraction (i.e., that Condition 1 holds) for all $z \geq z_0^{\text{ad}}$. Indeed, since Conditions 1–3 hold at z_0^{ad} , modulation theory is valid for $0 \leq z - z_0^{\text{ad}} \ll 1$. To estimate the relative magnitude of the perturbation, recall that $[\epsilon F]/[|\psi|^{\frac{4}{d}} \psi] \sim \frac{\epsilon}{L^2}$, see (31.61). In addition, under the adiabatic approximation $L^2 \geq y_m = O\left(\frac{\epsilon}{\beta_0}\right)$, see Lemma 31.8. Clearly, this bound also holds if we add nonadiabatic effects, as they reduce the strength of the focusing nonlinearity. Therefore,

$$\frac{[\epsilon F]}{[\Delta \psi]} \sim \frac{\epsilon}{L^2} \leq \frac{\epsilon}{y_m} = O(\beta_0) \ll 1.$$

Thus, even at the most focused state, ϵF remains $O(\beta)$ smaller than nonlinearity and diffraction. Hence, Condition 1 holds.

Since Condition 1 holds, the leading-order balance in the perturbed NLS remains between nonlinearity and diffraction. Hence, ψ_{coll} remains close to $\psi_{R(0)}$. Therefore, Condition 2 also holds for $z \geq z_0^{\text{ad}}$.

Finally, since $\beta = \beta_0 + \frac{\epsilon}{2M} f_1$, $\beta_0 \ll 1$, and

$$\frac{\epsilon}{2M} |f_1| = \frac{\epsilon}{2M} \frac{|C_{\text{gen}}|}{L^2} \ll \frac{\epsilon}{2M} \frac{|C_{\text{gen}}|}{y_m} = O(\beta_0) \ll 1,$$

Condition 3 also remains valid for $z \geq z_0^{\text{ad}}$. □

An intuitive explanation of Lemma 31.12 is as follows. By the *balance of the giants principle* (Conclusion 18.9), a defocusing perturbation arrests collapse when it is still $O(\beta)$ smaller than nonlinearity and diffraction. Since the relative magnitude of the perturbation decreases as the solution defocuses, the perturbation remains $O(\beta)$ small.

Finally, we consider the case where the generic conservative perturbation is focusing and leads to collapse (Lemma 31.10).

Lemma 31.13 *Let $L(z)$ be a solution of (31.44) with f_1 given by (31.50), and let $\epsilon C_{\text{gen}} < 0$. If $L(z)$ collapses at $Z_c^{(\epsilon)}$, then $\lim_{z \rightarrow Z_c^{(\epsilon)}} \beta(z) = \infty$.*

Proof By (31.59) and (31.69), as $z \rightarrow Z_c^{(\epsilon)}$,

$$\beta \sim \frac{y_M H_0}{M} \frac{2y_m}{y} = \frac{-\epsilon C_{\text{gen}}}{4M} \frac{1}{L^2} \rightarrow \infty. \quad \square$$

Lemma 31.13 shows that Condition 3 is not satisfied as $z \rightarrow Z_c^{(\epsilon)}$. Therefore, *the validity of modulation theory breaks down before the singularity*. For example, in the case of a small focusing supercritical nonlinearity, this breakdown is associated with the transition from critical to supercritical collapse (Sect. 32.3.2).

An alternative proof to Lemma 31.13 is given by the following exercise.

Exercise 31.2 *Let $L(z)$ be as in Lemma 31.13. Show that $L \sim c_L (Z_c^{(\epsilon)} - z)^{\frac{1}{3}}$ as $z \rightarrow Z_c^{(\epsilon)}$. Conclude that $\beta := -L^3 L_{zz} \sim c_\beta (Z_c^{(\epsilon)} - z)^{-\frac{2}{3}} \rightarrow \infty$.*

Chapter 32

Cubic-Quintic and Saturated Nonlinearities

In this chapter we consider the two-dimensional cubic-quintic NLS

$$i\psi_z(z, x, y) + \Delta\psi + |\psi|^2\psi - \epsilon|\psi|^4\psi = 0, \quad \psi(0, x, y) = \psi_0(x, y) \in H^1. \quad (32.1)$$

We show that when $\epsilon < 0$, the quintic nonlinearity accelerates self-focusing. As a result, blowup solutions undergo a supercritical collapse. When $\epsilon > 0$, however, the quintic nonlinearity always arrests collapse. In addition, when $0 < \epsilon \ll 1$, the self-focusing dynamics in (32.1) is “the same” as in the NLS with a rational saturated nonlinearity,

$$i\psi_z(z, x, y) + \Delta\psi + \frac{|\psi|^2}{1 + \epsilon|\psi|^2}\psi = 0, \quad \psi(0, x, y) = \psi_0(x, y) \in H^1, \quad (32.2)$$

as well as in the NLS with an exponential saturated nonlinearity,

$$i\psi_z(z, x, y) + \Delta\psi + \frac{1 - e^{-2\epsilon|\psi|^2}}{2\epsilon}\psi = 0, \quad \psi(0, x, y) = \psi_0(x, y) \in H^1. \quad (32.3)$$

In particular, solutions of (32.1)–(32.3) can undergo *filamentation (self trapping)* and *multiple filamentation*.

32.1 Physical Motivation

In Sect. 1.4.2 we saw that, typically, the polarization field of laser beams in isotropic media is weakly nonlinear ($\mathcal{P}_{\text{nl}} \ll \mathcal{P}_{\text{lin}}$). The nonlinear component of the polarization field can be expanded in the Taylor series

$$\mathcal{P}_{\text{nl}}(\mathcal{E}) = \chi^{(3)}\mathcal{E}^3 + \chi^{(5)}\mathcal{E}^5 + \chi^{(7)}\mathcal{E}^7 + \dots, \quad (32.4)$$

where \mathcal{E} is electric field and $\chi^{(i)}$ is the i th-order optical susceptibility. When \mathcal{E} is “sufficiently small”, each term in (32.4) is considerably smaller than its predecessor, i.e.,

$$\chi^{(3)}\mathcal{E}^3 \gg \chi^{(5)}\mathcal{E}^5 \gg \chi^{(7)}\mathcal{E}^7 \gg \dots . \quad (32.5)$$

Therefore, to leading order, nonlinear polarization has a cubic dependence on the electric field, i.e.,

$$\mathcal{P}_{\text{nl}} \approx \chi^{(3)}\mathcal{E}^3.$$

Substituting this relation in the scalar nonlinear Helmholtz equation and applying the paraxial approximation (see Chap. 1) leads to the two-dimensional cubic NLS

$$i\psi_z(z, x, y) + \Delta\psi + |\psi|^2\psi = 0. \quad (32.6)$$

According to (32.6), high-power laser beams collapse at a finite propagation distance. As the electric-field intensity increases to infinity, however, the quintic nonlinearity increases faster than the cubic one. As a result, collapsing beams may reach a regime where $\chi^{(5)}\mathcal{E}^5$ is still smaller than $\chi^{(3)}\mathcal{E}^3$, but is not longer negligible.¹ By (32.5), at that stage septic and higher-order nonlinearities can still be neglected.² Hence, nonlinear polarization has the cubic-quintic dependence

$$\mathcal{P}_{\text{nl}} \approx \chi^{(3)}\mathcal{E}^3 + \chi^{(5)}\mathcal{E}^5.$$

Substituting this relation in the scalar nonlinear Helmholtz equation and applying the paraxial approximation yields (32.1). In addition, since $\chi^{(5)}\mathcal{E}^5 \ll \chi^{(3)}\mathcal{E}^3$, we have that $|\epsilon| \ll 1$.

32.2 Global Existence and Singular Solutions

The NLS (32.1) conserves the power $\|\psi\|_2^2$ and the Hamiltonian

$$H := \|\nabla\psi\|_2^2 - \frac{1}{2}\|\psi\|_4^4 + \frac{\epsilon}{3}\|\psi\|_6^6.$$

Exercise 32.1 *Prove conservation of power and Hamiltonian for (32.1).*

In Sects. 32.2.1 and 32.2.2 we will see that (32.1) admits singular solutions when $\epsilon < 0$, but not when $\epsilon > 0$. Intuitively, this is because global existence is determined

¹ Recent experimental measurements suggest, however, that the nonlinear optical response of various materials remains cubic up to laser intensities near the ionization threshold [265, 266].

² Roughly speaking, if the ratio between consecutive terms in expansion (32.4) is $O(\epsilon)$, we retain the $O(\epsilon)$ effect of the quintic nonlinearity, but neglect the $O(\epsilon^2)$ effect of septic and higher-order nonlinearities.

by diffraction and the highest-order nonlinearity. Hence, as far as global existence is concerned, (32.1) is equivalent to the supercritical NLS

$$i\psi_z(z, x, y) + \Delta\psi - \epsilon|\psi|^4\psi = 0. \quad (32.7)$$

When $\epsilon > 0$, the NLS (32.7) is defocusing. Therefore, all its solutions exist globally. When $\epsilon < 0$, however, the NLS (32.7) is focusing and supercritical. Therefore, it admits singular solutions.

32.2.1 Focusing Quintic Nonlinearity

The following exercise rigorously shows that when $\epsilon < 0$, the cubic-quintic NLS (32.1) admits singular solutions:

Exercise 32.2

1. Use (7.16) to write the variance identity for (32.1).
2. Show that when $\epsilon < 0$, (32.1) admits solutions that become singular at a finite distance.

Note that if a solution of (32.1) collapses, it undergoes a supercritical collapse, because the quintic nonlinearity dominates the cubic one near the singularity.

32.2.2 Defocusing Quintic Nonlinearity

When $\epsilon > 0$ the quintic nonlinearity is defocusing. As a result, regardless of how small ϵ is, the solution does not collapse:

Lemma 32.1 *Let ψ be a solution of (32.1). If $\epsilon > 0$, then $\|\psi\|_{H^1}$ remains bounded for all $z \geq 0$.*

Proof By Hamiltonian conservation

$$\|\nabla\psi\|_2^2 + \frac{\epsilon}{3}\|\psi\|_6^6 = H(0) + \frac{1}{2}\|\psi\|_4^4. \quad (32.8a)$$

To bound $\|\psi\|_4^4$, recall the interpolation inequality for L^p norms (Appendix A)

$$\|f\|_q \leq \|f\|_r^\alpha \|f\|_p^{1-\alpha}, \quad 1 \leq r \leq q \leq p \leq \infty,$$

where α is given by

$$\frac{1}{q} = \frac{\alpha}{r} + \frac{1-\alpha}{p}.$$

Substituting $r = 2$, $q = 4$, and $p = 6$ gives $\alpha = 1/4$ and

$$\|\psi\|_4^4 \leq \|\psi\|_2 \|\psi\|_6^3. \quad (32.8b)$$

Making use of the Cauchy's inequality with $\epsilon/3$

$$ab \leq \frac{\epsilon}{3}a^2 + \frac{3}{4\epsilon}b^2,$$

see Appendix A, gives

$$\|\psi\|_6^3 \|\psi\|_2 \leq \frac{\epsilon}{3} \|\psi\|_6^6 + \frac{3}{4\epsilon} \|\psi\|_2^2. \quad (32.8c)$$

By (32.8) and power conservation,

$$\|\nabla\psi\|_2^2 + \frac{\epsilon}{3} \|\psi\|_6^6 \leq H(0) + \frac{1}{2} \|\psi\|_6^3 \|\psi\|_2 \leq H(0) + \frac{1}{2} \left(\frac{3}{4\epsilon} \|\psi_0\|_2^2 + \frac{\epsilon}{3} \|\psi\|_6^6 \right).$$

Therefore, $\|\nabla\psi\|_2^2$ is bounded. \square

32.3 Dynamics

We now use *modulation theory* (Chap. 31) to find the leading-order effect of a small quintic nonlinearity. We begin with a technical result.

Lemma 32.2 *Let $d = 2$ and $F = -|\psi|^4\psi$. Then the auxiliary functions of modulation theory are*

$$f_1(z) = -\frac{\frac{4}{3} \int |R^{(0)}|^6 d\mathbf{x}}{L^2(z)} \approx -\frac{8P_{\text{cr}}}{L^2(z)}, \quad f_2(z) = 0.$$

Proof By (31.18b),

$$f_2^{\text{radial}} = \text{Im} \int F(\psi_{R^{(0)}}) \psi_{R^{(0)}}^* r dr = \text{Im} \int \left[-|\psi_{R^{(0)}}|^4 \psi_{R^{(0)}} \right] \psi_{R^{(0)}}^* r dr = 0.$$

Indeed, since a quintic nonlinearity is a conservative perturbation (Exercise 32.1), from Lemma 31.3 it follows that $f_2 = 0$.

Next, by (31.18a),

$$\begin{aligned} f_1^{\text{radial}} &= 2L^3 \text{Re} \int_0^\infty F(\psi_{R^{(0)}}) e^{-iS} \left[\rho R^{(0)}(\rho) \right]_\rho \rho d\rho \\ &= -2L^3 \int \frac{|R^{(0)}|^5}{L^5} \left[R^{(0)} + \rho \frac{dR^{(0)}}{d\rho} \right] \rho d\rho \end{aligned}$$

$$\begin{aligned}
&= -\frac{2}{L^2} \left(\int |R^{(0)}|^6 \rho d\rho + \int \left(R^{(0)} \right)^5 \frac{dR^{(0)}}{d\rho} \rho^2 d\rho \right) \\
&= -\frac{2}{L^2} \left(\int |R^{(0)}|^6 \rho d\rho - \frac{2}{6} \int |R^{(0)}|^6 \rho d\rho \right) = -\frac{\frac{4}{3} \int |R^{(0)}|^6 \rho d\rho}{L^2}.
\end{aligned}$$

Finally, a numerical computation [93] yields

$$\int |R^{(0)}|^6 d\mathbf{x} \approx 6.07 \int |R^{(0)}|^2 d\mathbf{x} \approx 6P_{\text{cr}}. \quad \square$$

Lemma 32.2 shows that a small quintic nonlinearity is a special case of the generic conservative perturbation (31.50) with

$$C_{\text{gen}} = \frac{4}{3} \int |R^{(0)}|^6 d\mathbf{x} \approx 8P_{\text{cr}}.$$

Therefore, all the results in Sect. 31.5 can be applied with $C_{\text{gen}} \approx 8P_{\text{cr}}$. For example, by Lemma 31.6, once the solution of (32.1) reaches the adiabatic stage where $\psi_{\text{coll}} \sim \psi_{R^{(0)}}$, self-focusing is governed to leading order by³

$$(y_z)^2 = \frac{-4H_0}{M} \frac{1}{y} (y_M - y)(y - y_m), \quad y(z) := L^2(z), \quad (32.9a)$$

where

$$y_M \sim \frac{M\beta_0}{-H_0}, \quad y_m \sim \frac{\epsilon \int |R^{(0)}|^6 d\mathbf{x}}{3M\beta_0} \approx \frac{2\epsilon P_{\text{cr}}}{M\beta_0}. \quad (32.9b)$$

32.3.1 Small Defocusing Quintic Nonlinearity

When the quintic nonlinearity is small and defocusing ($0 < \epsilon \ll 1$), it follows from Lemma 31.7 that collapse is always arrested in the reduced equation (32.9), in agreement with Lemma 32.1. If, in addition, $\beta_0 > 0$ and $H_0 < 0$, the solution of (32.9) undergoes periodic focusing-defocusing oscillations (Lemma 31.8). In the derivation of (32.9), however, non-adiabatic radiation from the high-intensity core is neglected. Once added, it leads to the decay of the oscillations (Sect. 31.5.4). Thus, modulation theory predicts that if ψ_0 is an initial condition with power moderately above P_{cr} and a negative Hamiltonian, the addition of a small defocusing quintic nonlinearity arrests collapse and leads to slowly-decaying oscillations. This prediction is confirmed in direct simulations of the cubic-quintic NLS, see e.g., Fig. 32.1.

³ Equation (32.9) was first derived by Malkin [164] using an approach that later evolved into *modulation theory*.

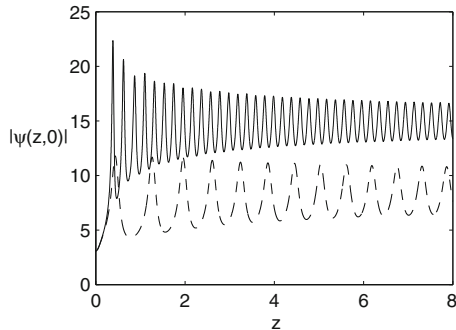


Fig. 32.1 Solution of the cubic-quintic NLS (32.1) with $\psi_0(r) = 3.08e^{-r^2}$ for $\epsilon = 0.5 \times 10^{-3}$ (solid) and $\epsilon = 2 \times 10^{-3}$ (dashes). From [85]

Remark A detailed analysis of non-adiabatic effects in the cubic-quintic NLS was done by Malkin [164].

Remark After the arrest of collapse, the high-intensity core oscillates between a focused peak profile and a defocused ring profile.

Remark Continuation of singular NLS solutions with a vanishing defocusing quintic nonlinearity is discussed in Sect. 38.4.

32.3.2 Small Focusing Quintic Nonlinearity

When the quintic nonlinearity is small and focusing ($0 < -\epsilon \ll 1$), solutions of the reduced equation (32.9) may undergo collapse (Lemma 31.10). This asymptotic result is in agreement with the rigorous result that solutions of the cubic-quintic NLS (32.1) with a focusing quintic nonlinearity can collapse (Exercise 32.2). Note, however, that when a solution of (32.1) collapses, the validity of the reduced equations breaks down *before* the singularity (Lemma 31.13). This breakdown is associated with the transition from critical to supercritical dynamics. Indeed, as a solution of (32.1) collapses, the quintic nonlinearity dominates over the cubic one, and so to leading order, the dynamics is governed by the supercritical NLS (32.7). Hence, if ϵ is sufficiently small, ψ initially approaches the critical $\psi_{R(0)}(r; d = 2, \sigma = 1)$ profile, but ultimately collapses with the supercritical $\psi_Q(r; d = 2, \sigma = 2)$ profile. Consequently, Condition 2 of modulation theory is not satisfied, and so the validity of the reduced equations breaks down.

Remark A similar transition from critical to supercritical collapses occurs in the critical NLS with a small anomalous dispersion (Sect. 36.7).

32.4 Saturated Nonlinearities

32.4.1 Physical Motivation

The physical validity of (32.1) was sometimes criticized because the sign of the nonlinearity $|\psi|^2 - \epsilon|\psi|^4$ changes from positive to negative as $|\psi|$ increases, i.e., the effect of the nonlinear polarization field \mathcal{P}_{nl} changes from focusing to defocusing as $|\mathcal{E}|$ increases. In addition, since relation (32.4) is the Taylor series expansion of $\mathcal{P}_{\text{nl}}(\mathcal{E})$ for small \mathcal{E} , “there is no reason” why it should hold for non-small \mathcal{E} . Therefore, some studies replaced the cubic-quintic nonlinearity with a saturated one. Since

$$\frac{|\psi|^2}{1 + \epsilon|\psi|^2} \sim \begin{cases} |\psi|^2 - \epsilon|\psi|^4, & \text{if } \epsilon|\psi|^2 \ll 1, \\ \frac{1}{\epsilon}, & \text{if } \epsilon|\psi|^2 \gg 1, \end{cases}$$

and

$$\frac{1 - e^{-2\epsilon|\psi|^2}}{2\epsilon} \sim \begin{cases} |\psi|^2 - \epsilon|\psi|^4, & \text{if } \epsilon|\psi|^2 \ll 1, \\ \frac{2}{\epsilon}, & \text{if } \epsilon|\psi|^2 \gg 1, \end{cases}$$

both (32.2) and (32.3) can be viewed as *regularizations* of (32.1): The nonlinearity is asymptotically the same as in (32.1) when $\epsilon|\psi|^2 \ll 1$, but it has a finite positive limit as $|\psi|$ goes to infinity.

32.4.2 Equivalence of Cubic-Quintic and Saturated Nonlinearities

Consider the cubic-quintic NLS (32.1) with $0 < \epsilon \ll 1$ and an initial condition that leads to a peak-type collapse in the cubic NLS (32.6). Initially, it was believed that collapse is arrested when the nonlinearity changes its sign from focusing to defocusing, i.e., once the quintic nonlinearity becomes comparable to the cubic one. At such focusing levels there are $O(1)$ differences between (32.1), (32.2), and (32.3). Therefore, it was believed that there are significant differences between these three models. By the *balance of the giants principle* (Sect. 18.6), however, the quintic nonlinearity arrests collapse when it is still considerably smaller than the cubic one. At such focusing levels the cubic-quintic nonlinearity is asymptotically equivalent to the saturated nonlinearities. Therefore, all three models have the same leading-order dynamics:

Conclusion 32.1 ([93]) *Let ψ_0 be an initial condition for which the solution of the cubic NLS (32.6) collapses with the $\psi_{R^{(0)}}$ profile, and let $0 < \epsilon \ll 1$. Then the solutions of (32.1), (32.2), and (32.3) are “close” to each other.*

Proof We give a very informal proof. If ϵ is sufficiently small, the initial dynamics in (32.1), (32.3), and (32.2) are the same as in (32.6). In particular, all three solutions

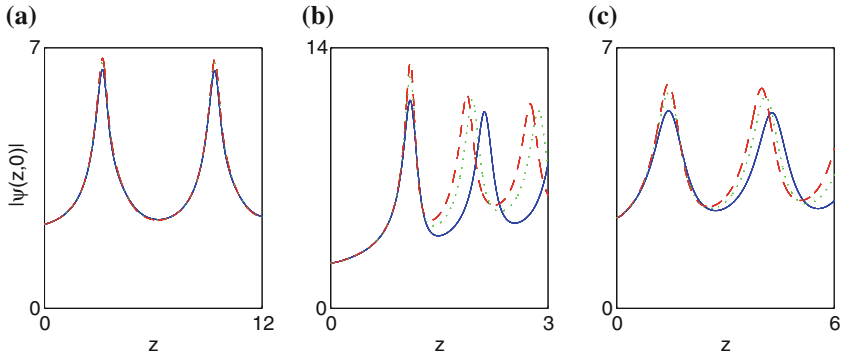


Fig. 32.2 Solutions of Eqs. (32.1) (solid), (32.2) (dashes), and (32.3) (dots) with $\psi_0 = (1 + \delta) R^{(0)}(r)$. **a** $\delta = 0.02$ and $\epsilon = 0.0025$. **b** $\delta = 0.1$ and $\epsilon = 0.0025$. **c** $\delta = 0.1$ and $\epsilon = 0.01$

go through “the same” initial non-adiabatic stage during which the collapsing core approaches the $\psi_{R^{(0)}}$ profile.

We now show that the solutions of (32.1), (32.3), and (32.2) remain close in the modulation-theory stage.⁴ The perturbations that correspond to (32.2) and (32.3) are

$$F = \frac{1}{\epsilon} \left(\frac{|\psi|^2}{1 + \epsilon |\psi|^2} - |\psi|^2 \right) \psi \quad \text{and} \quad F = \frac{1}{\epsilon} \left(\frac{1 - e^{-2\epsilon |\psi|^2}}{2\epsilon} - |\psi|^2 \right) \psi,$$

respectively. These perturbations are conservative, and satisfy

$$F = -|\psi|^4 \psi \left(1 + O(\epsilon |\psi|^2) \right), \quad \epsilon |\psi|^2 \ll 1.$$

Therefore, as long as $\epsilon |\psi|^2 \ll 1$, the leading-order dynamics in (32.2) and in (32.3) are the same as in (32.1). Hence, it is enough to prove that $\epsilon |\psi|^2 \ll 1$ for $0 \leq z < \infty$ in (32.1). If ϵ is sufficiently small, this holds during the initial non-adiabatic stage. In the modulation-theory stage, the leading-order behavior of the solution of (32.1) is governed by the reduced equation (32.9), whose solution y is bounded from below by $y_m = O(\epsilon/\beta_0)$, where $\beta_0 \ll 1$. Hence,

$$\epsilon |\psi|^2 \sim \epsilon |\psi_{R^{(0)}}|^2 \sim \frac{\epsilon}{L^2} \leq \frac{\epsilon}{y_m} = O(\beta_0) \ll 1.$$

Finally, we note that by Lemma 31.12, the solution remains in the modulation-theory stage throughout its propagation. \square

The agreement between solutions of (32.1), (32.2), and (32.3) is illustrated numerically in Fig. 32.2. As expected, the best agreement occurs when ψ_0 is the closest to $\psi_{R^{(0)}}$.

⁴ i.e., during the unperturbed adiabatic stage and the weakly-perturbed stage (Sect. 31.1.2).

32.5 Filamentation and Multiple Filamentation

Consider a collapsing solution of the cubic NLS (32.6) with power moderately above P_{cr} . In Sects. 32.1 and 32.4.2 we saw that the addition of a small defocusing quintic nonlinearity or nonlinear saturation leads to the arrest of collapse, followed by focusing-defocusing oscillations. Physically, this dynamics corresponds to a laser beam that self-focuses to a small radius and then continues to propagate in a tightly focused state, i.e., to a laser beam that undergoes *filamentation (self-trapping)*.⁵ Therefore, the NLS with a cubic-quintic or a saturated nonlinearity can serve as a model for beam filamentation. These high-order nonlinear effects, however, are only one possible explanation for filamentation, since “any” conservative mechanism can lead to filamentation (Sect. 31.5.2). Whether filamentation is caused by high-order nonlinear effects depends probably on the specific physical setup of the filamentation experiment.

As noted, after the arrest of collapse, the beam oscillates between a focused peak profile and a defocused ring profile. Because rings are azimuthally unstable, *solutions of the NLS with a cubic-quintic or a saturated nonlinearity can break up into multiple filaments*. Nonradial perturbations that lead to multiple filamentation can be random or deterministic, see Sects. 25.2 and 25.3.2, respectively.

⁵ Indeed, the width of laser filaments is not constant, but rather undergoes focusing-defocusing oscillations (Sect. 31.5.2).

Chapter 33

Linear and Nonlinear Damping

In the mathematical models considered so far, the laser beam propagated in the Kerr medium without experiencing any power losses. Even in the visible spectrum, however, there is always some absorption by the medium. In this chapter we consider the effects of linear and nonlinear absorption (damping) on collapsing solutions.

33.1 Linear Damping

33.1.1 Physical Origin

In Sect. 1.6 we saw that propagation of linearly-polarized laser beams in a Kerr medium is governed by the scalar nonlinear Helmholtz equation (NLH)

$$\left[\frac{\partial^2}{\partial z^2} + \Delta \right] E(x, y, z) + k^2 E = 0, \quad k^2 = k_0^2 \left(1 + \frac{4n_2}{n_0} |E|^2 \right),$$

where $\Delta = \frac{\partial^2}{\partial x^2} + \frac{\partial^2}{\partial y^2}$, $k_0 = \omega_0 n_0 / c$, ω_0 is frequency, c is speed of light, n_0 is the linear index of refraction, and n_2 is the Kerr coefficient. Substituting $E = e^{ik_0 z} \psi(z, x, y)$, changing to the nondimensional variables

$$\tilde{x} = \frac{x}{r_0}, \quad \tilde{y} = \frac{y}{r_0}, \quad \tilde{z} = \frac{z}{2L_{\text{diff}}}, \quad \tilde{\psi} = r_0 k_0 \sqrt{\frac{4n_2}{n_0}} \psi, \quad (33.1)$$

where r_0 is the radius of the input beam and $L_{\text{diff}} := r_0^2 k_0$ is the diffraction length, applying the paraxial approximation, and dropping the tilde signs, yields the (undamped) NLS

$$i\psi_z(z, x, y) + \Delta\psi + |\psi|^2\psi = 0. \quad (33.2)$$

In the above derivation we assumed that $|E| = |\psi|$. This is indeed the case when n_0 is real, since then so is k_0 . Except in vacuum, however, n_0^2 always has a positive imaginary component, i.e.,

$$n_0^2 = \operatorname{Re}(n_0^2) + i \operatorname{Im}(n_0^2), \quad \operatorname{Im}(n_0^2) > 0.$$

Therefore, while ideal transparency corresponds to $\operatorname{Im}(n_0^2) = 0$, physical transparency means that $0 < \operatorname{Im}(n_0^2) \ll \operatorname{Re}(n_0^2)$. For example, for water in the visible regime we have that $\operatorname{Im}(n_0^2)/\operatorname{Re}(n_0^2) \approx 10^{-7}$ [134].

To model beam propagation in the presence of linear damping, we replace k_0 in the above derivation by

$$\bar{k}_0 := \sqrt{\operatorname{Re}(k_0^2)} = \frac{\omega_0}{c} \sqrt{\operatorname{Re}(n_0^2)}.$$

Substituting $E = e^{i\bar{k}_0 z} \psi(z, x, y)$ in the scalar NLH, changing to the nondimensional variables (33.1), and applying the paraxial approximation, yields the linearly-damped NLS

$$i\psi_z(z, x, y) + \Delta\psi + |\psi|^2\psi + i\delta\psi = 0, \quad (33.3)$$

where

$$\delta = r_0^2 \frac{\omega_0^2}{c^2} \operatorname{Im}(n_0^2) = r_0^2 \bar{k}_0^2 \frac{\operatorname{Im}(n_0^2)}{\operatorname{Re}(n_0^2)} > 0.$$

Since $r_0^2 \bar{k}_0^2 = f^{-2} \gg 1$ (Observation 1.2), δ is not necessarily small in the visible regime.

33.1.2 Linear Damping Parameter (δ)

The damping parameter δ is dimensionless. To understand its meaning, we begin with the following result:

Conclusion 33.1 *Let $0 < \operatorname{Im}(n_0^2) \ll \operatorname{Re}(n_0^2)$, and let L_{damp} denote the characteristic distance for linear damping. Then $L_{\text{damp}} = \left(\bar{k}_0 \frac{\operatorname{Im}(n_0^2)}{\operatorname{Re}(n_0^2)}\right)^{-1}$.*

Proof Since damping is a linear effect, we can calculate L_{damp} using the linear Helmholtz equation

$$\left[\frac{\partial^2}{\partial z^2} + \Delta \right] E(x, y, z) + k_0^2 E = 0.$$

This equation admits the plane-wave solutions $E(z) = E_0 e^{ik_0 z}$. Since $|E| = |E_0| e^{-\operatorname{Im}(k_0)z}$, the characteristic distance for linear damping is

$$L_{\text{damp}} = \frac{1}{\operatorname{Im}(k_0)}.$$

In addition, since $\text{Im}(n_0^2) \ll \text{Re}(n_0^2)$,

$$\begin{aligned}\text{Im}(n_0) &= \text{Im} \left(\sqrt{\text{Re}(n_0^2) + i \text{Im}(n_0^2)} \right) = \sqrt{\text{Re}(n_0^2)} \text{Im} \left(\sqrt{1 + i \frac{\text{Im}(n_0^2)}{\text{Re}(n_0^2)}} \right) \\ &\approx \sqrt{\text{Re}(n_0^2)} \text{Im} \left(1 + \frac{i}{2} \frac{\text{Im}(n_0^2)}{\text{Re}(n_0^2)} \right) = \frac{\sqrt{\text{Re}(n_0^2)}}{2} \frac{\text{Im}(n_0^2)}{\text{Re}(n_0^2)}.\end{aligned}$$

Therefore,

$$\text{Im}(k_0) = \frac{\omega_0}{c} \text{Im}(n_0) \approx \frac{\bar{k}_0}{2} \frac{\text{Im}(n_0^2)}{\text{Re}(n_0^2)}.$$

□

Corollary 33.1 $\delta = \frac{L_{\text{diff}}}{L_{\text{damp}}}$, where $L_{\text{diff}} = \bar{k}_0 r_0^2$.

Thus, the parameter δ is the ratio of the magnitudes of linear damping and diffraction. In particular, $\delta \ll 1$ means that the effect of linear damping over propagation distances of several diffraction lengths is small.

33.1.3 Conditions for Collapse

Equation (33.3) is a special case of the linearly-damped critical NLS

$$i\psi_z(z, \mathbf{x}) + \Delta\psi + |\psi|^{\frac{4}{d}}\psi + i\delta\psi = 0, \quad \psi(0, \mathbf{x}) = \psi_0(\mathbf{x}) \in H^1. \quad (33.4)$$

Multiplying (33.4) by ψ^* and subtracting the conjugate equation gives

$$\|\psi\|_2^2 = e^{-2\delta z} \|\psi_0\|_2^2. \quad (33.5)$$

Therefore, the power decreases exponentially with the propagation distance.

In Corollary 5.12 we saw that in the undamped critical NLS, a necessary condition for collapse is $\|\psi_0\|_2^2 \geq P_{\text{cr}}$. This condition was generalized by Fibich to the linearly-damped critical NLS:

Lemma 33.1 ([66]) Let ψ be a solution of the linearly-damped critical NLS (33.4) that blows up at Z_c^δ , where $0 < Z_c^\delta < \infty$. Then

$$\|\psi_0\|_2^2 \geq e^{2\delta Z_c^\delta} P_{\text{cr}}. \quad (33.6)$$

This result is intuitive. Indeed, by (33.5), inequality (33.6) can be rewritten as

$$\lim_{z \rightarrow Z_c^\delta} \|\psi\|_2^2 \geq P_{\text{cr}}.$$

Hence, Lemma 33.1 says that the power at the blowup point has to be at least P_{cr} .

The following is an immediate consequence of Lemma 33.1:

Corollary 33.2 *Let $\|\psi_0\|_2^2 \leq P_{\text{cr}}$ and $\delta > 0$. Then the solution of (33.3) exists for all $0 \leq z < \infty$.*

At present, there is no rigorous proof that solutions of the linearly-damped critical NLS (33.4) can collapse. In [255], Tsutsumi proved for the linearly-damped supercritical NLS

$$i\psi_z(z, \mathbf{x}) + \Delta\psi + |\psi|^{2\sigma}\psi + i\delta\psi = 0, \quad \sigma d > 2$$

that the two conditions

$$H(0) \leq 0 \quad \text{and} \quad \delta \frac{2\sigma}{\sigma d - 2} V(0) + V'(0) \leq 0,$$

where V is the variance, are sufficient for collapse. This result, however, does not extend to the critical case.

33.1.4 $u = e^{\delta z}\psi$

The damping term $i\delta\psi$ can be “eliminated” from (33.4) by substituting $u(z, \mathbf{x}) = e^{\delta z}\psi(z, \mathbf{x})$. This yields

$$iu_z(z, \mathbf{x}) + \Delta u + e^{-\frac{4}{d}\delta z}|u|^{\frac{4}{d}}u = 0, \quad u(0, \mathbf{x}) = \psi_0(\mathbf{x}) \in H^1. \quad (33.7)$$

Note that the power of u is conserved, i.e.,

$$\|u\|_2^2 \equiv \|\psi_0\|_2^2.$$

Intuitively, (33.7) shows that linear damping reduces the magnitude of the focusing nonlinearity, and that this effect builds up gradually as the solution propagates. This is different from nonlinear damping, whose effect is mainly localized near the blowup point (Sects. 33.2.2 and 33.3.2).

As $z \rightarrow Z_c^\delta$, Eq. (33.7) approaches the undamped NLS

$$iu_z(z, \mathbf{x}) + \Delta u + \kappa|u|^{\frac{4}{d}}u = 0, \quad \kappa = e^{-\frac{4}{d}\delta Z_c^\delta}. \quad (33.8)$$

Since the critical power for collapse in (33.8) is $P_{\text{cr}}\kappa^{-\frac{d}{2}}$ (Theorem 5.6), and since $\|u\|_2^2 \equiv \|\psi_0\|_2^2$, we recover the result of Lemma 33.1.

33.1.5 Blowup Profile and Rate

Equation (33.8) suggests that the effect of linear damping becomes negligible near the singularity,¹ and consequently that solutions of the linearly-damped NLS collapse with the blowup profile and blowup rate of the undamped NLS. This conclusion is supported by asymptotic analysis [66, Sect. 3.5]. Note, however, that while linear damping does not affect the blowup rate, it increases the blowup distance (Sect. 33.1.6).

33.1.6 Monotonicity and Non-monotonicity of Z_c^δ

Since damping slows down the collapse, it seems reasonable to expect that for a given initial condition ψ_0 , the collapse distance Z_c^δ is monotonically increasing in δ . Numerical simulations suggest that this is indeed the generic case (see, e.g., [66, Fig. 1]). Monotonicity of Z_c^δ was also shown asymptotically for initial conditions that are close to $\psi_{R^{(0)}}$ [66, Sect. 3.3].

In [28], Besse et al. showed numerically that Z_c^δ can be non-monotone in δ . As in Sects. 27.5 and 27.6, this loss of monotonicity was observed for initial conditions that correspond to two input beams that travel towards each other, in the phase-transition regime between collapse at a single point and at two points.

33.1.7 Threshold Damping Parameter (δ_{th})

As noted, collapse in the critical NLS is highly sensitive to small perturbations. In particular, small perturbations can arrest collapse regardless of how small they initially are. Therefore, the question arises as to whether small linear damping can arrest collapse, and whether it always does so.

At present, there is no rigorous answer to this question. Numerical and asymptotic studies suggest the following, at least generically:

Observation 33.1 ([5, 53, 66, 114, 207, 221]) *Let ψ_0 be an initial condition that leads to collapse in the undamped critical or supercritical NLS. Then there exists a threshold value δ_{th} , which depends on ψ_0 , such that the solution of the linearly-damped NLS with this initial condition collapses when $0 < \delta < \delta_{\text{th}}$, but exists globally when $\delta > \delta_{\text{th}}$.*

¹ Intuitively, this is because near the singularity collapse occurs “all at once” (see e.g., Fig. 14.8b), whereas the effect of linear damping is proportional to the propagation distance, see (33.6).

Thus, for a given initial condition that leads to collapse in the undamped NLS, “sufficiently large” linear damping arrests collapse, but “sufficiently small” linear damping does not.²

33.2 Nonlinear Damping

We now consider the nonlinearly-damped NLS

$$i\psi_z(z, \mathbf{x}) + \Delta\psi + |\psi|^p\psi + i\delta|\psi|^q\psi = 0, \quad q > 0. \quad (33.9)$$

33.2.1 Physical Motivation

In nonlinear optics the origin of nonlinear damping is multiphoton absorption. In the case of solids, the damping exponent q corresponds to the number of photons needed to make a transition from the valence band to the conduction band. Similarly, in the case of free atoms, q corresponds to the number of photons needed to make a transition from the ground state to an excited state or to the continuum. Therefore, in nonlinear optics q can take integer values between 2 and 8. In Bose-Einstein condensates a quintic nonlinear damping corresponds to losses from three-body inelastic recombinations. Nonlinear damping appears also in the complex Ginzburg-Landau equation (Sect. 38.7).

33.2.2 Power Losses

If we multiply (33.9) by ψ^* , add the complex-conjugate equation, and integrate by parts, we get that

$$\frac{d}{dz} \int |\psi|^2 d\mathbf{x} = -2\delta \int |\psi|^{q+2} d\mathbf{x}. \quad (33.10)$$

By Corollary 5.8, singular solutions of (33.9) with $\delta = 0$ blow up in L^r for all $r \geq 2\sigma + 2 = p + 2$. In other words, for any $q \geq p$, the integral $\int |\psi|^{q+2} d\mathbf{x}$ becomes infinite as ψ collapses. Therefore, intuitively, when $0 < \delta \ll 1$, power losses become important only as ψ approaches the collapse point. This is different from linear damping ($q = 0$), where the power loss between z_1 and z_2 is independent of the dynamics of ψ between z_1 and z_2 , see (33.6).

² An informal proof of the second part of this conclusion in the critical case is as follows. Generically, the collapse distance Z_c^δ is monotonically increasing in δ . In particular, $Z_c^\delta > Z_c$, where $Z_c = Z_c^{\delta=0}$ is the collapse point in the absence of damping. Therefore, by Lemma 33.1, if ψ collapses at Z_c^δ , then $\|\psi_0\|_2^2 \geq e^{2\delta Z_c^\delta} P_{\text{cr}} \geq e^{2\delta Z_c} P_{\text{cr}}$. Consequently, collapse cannot occur when this inequality does not hold, i.e., for $\delta > \delta_c := \frac{1}{2Z_c} \log \frac{\|\psi_0\|_2^2}{P_{\text{cr}}}$. Hence, $\delta_{\text{th}} \leq \delta_c$.

Conclusion 33.2 Power losses due to linear damping are “independent of the dynamics”, whereas those due to nonlinear damping increase as the solution collapses. In particular, if q is sufficiently large, the effect of nonlinear damping is localized near the collapse point.

See also Sect. 33.3.2 for an asymptotic derivation of Conclusion 33.2.

The above discussion also implies

Conclusion 33.3 Nonlinear losses place a limit on the length of laser filaments, but have a minor effect on the collapse (filamentation) distance.

33.2.3 Arrest of Collapse—Rigorous Results

The following theorem was proved by Passot, Sulem, and Sulem for $d = 2$, and by Antonelli and Sparber for $d = 1$ and $d = 3$:

Theorem 33.1 ([7, 205]) *The cubic NLS with sup-cubic nonlinear damping*

$$i\psi_z(z, \mathbf{x}) + \Delta\psi + |\psi|^2\psi + i\delta|\psi|^q\psi = 0, \quad \delta > 0, \quad \psi(0, \mathbf{x}) = \psi_0(\mathbf{x}) \in H^1,$$

where $2 < q < \infty$ if $d = 1, 2$, and $2 < q < 4$ if $d = 3$, has a unique global solution.

Thus, when the nonlinear-damping exponent q is higher than that of the focusing nonlinearity, collapse is arrested for any $\delta > 0$. This is different from the linear damping case, where collapse is only arrested for $\delta > \delta_{\text{th}}$ (Observation 33.1).

Antonelli and Sparber also proved global existence when the nonlinear-damping exponent is equal to that of the focusing nonlinearity and δ is sufficiently large:

Theorem 33.2 ([7]) *The cubic NLS with a cubic nonlinear damping*

$$i\psi_z(z, \mathbf{x}) + \Delta\psi + (1 + i\delta)|\psi|^2\psi = 0, \quad \psi(0, \mathbf{x}) = \psi_0(\mathbf{x}) \in H^1,$$

where $\mathbf{x}\psi_0 \in L^2$, $d \leq 3$, and $\delta \geq 1$, has a unique global solution.

In the supercritical NLS, numerical simulations indeed suggest that when the nonlinear-damping exponent is higher than that of the focusing nonlinearity ($q > p$), collapse is arrested for any positive δ , but that when the nonlinear-damping exponent is equal to that of the focusing nonlinearity, δ has to be “sufficiently large” in order to arrest collapse. See [86, Sect. 4] for further details. In contrast, for the critical NLS with a critical nonlinear damping ($p = q = 4/d$), the restriction on δ in Theorem 33.2 is not really needed, as collapse is arrested for any $\delta > 0$:

Theorem 33.3 *The critical NLS with critical nonlinear damping*

$$i\psi_z(z, \mathbf{x}) + \Delta\psi + (1 + i\delta)|\psi|^{\frac{4}{d}}\psi = 0, \quad \delta > 0, \quad \psi(0, \mathbf{x}) = \psi_0(\mathbf{x}) \in H^1 \tag{33.11}$$

has a unique global solution.

Proof This proof was shown to me by Pierre Raphael. By (33.10) with $q = 4/d$,

$$\frac{d}{dz} \int_{\mathbb{R}^d} |\psi|^2 d\mathbf{x} + 2\delta \int_{\mathbb{R}^d} |\psi|^{\frac{4}{d}+2} d\mathbf{x} = 0.$$

Hence,

$$\int_{\mathbb{R}^d} |\psi|^2 d\mathbf{x} + 2\delta \int_0^z \left(\int_{\mathbb{R}^d} |\psi|^{\frac{4}{d}+2} d\mathbf{x} \right) dz = \int |\psi_0|^2 d\mathbf{x}.$$

Therefore, the Strichartz norm

$$\|\psi\|_{L^{\frac{4}{d}+2}((0,z), L^{\frac{4}{d}+2}(\mathbb{R}^d))}^{\frac{4}{d}+2} := \int_0^z \left(\int_{\mathbb{R}^d} |\psi|^{\frac{4}{d}+2} d\mathbf{x} \right) dz$$

is globally bounded for $0 \leq z < \infty$.

By [39, Theorem 4.7.1], the solution of the critical NLS blows up if and only if this Strichartz norm blows up. This result also holds for (33.11), because solving in Strichartz “does not care” for the damping term. Therefore, the solution of (33.11) exists globally. \square

Finally, we note that the asymptotic analysis in Sect. 33.3.2 suggests that in the critical NLS with subcritical nonlinear damping ($q < 4/d$), δ has to be sufficiently large in order to arrest collapse. Therefore, critical and supercritical nonlinear damping can play the role of a regularizing mechanism (“viscosity”) that allows the continuation of solutions of the critical NLS beyond the blowup point, whereas subcritical nonlinear damping cannot play that role. In the supercritical case, nonlinear damping can allow the continuation of singular solutions only if its exponent is higher than that of the focusing nonlinearity. See Sect. 38.6 and [66, 86] for more details.

33.3 Asymptotic Analysis

33.3.1 Derivation of Reduced Equations

Following Fibich and Levy [66, 87], we can use *modulation theory* to analyze the effect of small damping in the critical NLS

$$i\psi_z(z, \mathbf{x}) + \Delta\psi + |\psi|^{\frac{4}{d}}\psi + i\delta|\psi|^q\psi = 0, \quad 0 < \delta \ll 1. \quad (33.12)$$

Since $F = i|\psi|^q\psi$, the auxiliary functions are, see (31.10),

$$f_1 \equiv 0, \quad f_2 = \frac{c_q}{L^{\frac{qd}{2}}}, \quad c_q = \|R^{(0)}\|_{q+2}^{q+2} > 0.$$

Therefore, by Proposition 31.1, once $\psi \sim \psi_{R^{(0)}}$, self-focusing in (33.12) is governed, to leading order, by the reduced equations

$$L_{zz}(z) = -\frac{\beta}{L^3}, \quad \beta_z(z) = -\frac{\nu(\beta)}{L^2} - \frac{\tilde{\delta}}{L^{\frac{qd}{2}}}, \quad \tilde{\delta} = \frac{2c_q\delta}{M} > 0, \quad (33.13)$$

where $L(z)$ is the solution width and $\beta(z)$ is proportional to the excess power above P_{cr} of the collapsing core (Corollary 31.1).

33.3.2 Dynamics

In the reduced equation for β , see (33.13), the first and second terms correspond to power radiation from the collapsing core to the background and to power losses due to damping, respectively. If we neglect the exponentially small radiation term $\nu(\beta)$, this equation becomes

$$\beta_z(z) = -\tilde{\delta}L^{-\frac{qd}{2}}. \quad (33.14)$$

Therefore, we recover the result of Conclusion 33.2 that power losses due to nonlinear damping ($q > 0$) increase as the solution focuses (i.e., as $L \rightarrow 0$), whereas power losses due to linear damping ($q = 0$) are independent of the dynamics.³

It is useful to change from the physical variable z to the rescaled variable $\zeta = \int_0^z L^{-2}$. Since $\frac{dz}{d\zeta} = L^2$, Eq. (33.14) reads

$$\beta_\zeta(\zeta) = -\tilde{\delta}L^{-\frac{d}{2}\left(q-\frac{4}{d}\right)}. \quad (33.15)$$

Equation (33.15) shows that the effect of nonlinear damping on solutions of the critical NLS that collapse with the peak-type $\psi_{R^{(0)}}$ profile depends on the sign of $q - \frac{4}{d}$:

- When $q < 4/d$ (*subcritical nonlinear damping*), the effect of damping becomes negligible as $L \rightarrow 0$.⁴ Hence, the effect of subcritical nonlinear damping is qualitatively the same as that of linear damping (Observation 33.1), namely, there exists a threshold value δ_{th} , which depends on ψ_0 and on q , such that:

³ i.e., β_z is independent of L when $q = 0$.

⁴ By (33.14), for any $q > 0$ the effect of nonlinear damping increases as $L \rightarrow 0$. By (33.15), however, the effect of nonlinear damping decreases as $L \rightarrow 0$ for $0 < q < \frac{4}{d}$. To resolve this “inconsistency”, we recall that when $\psi \sim \psi_{R^{(0)}}$, $\Delta\psi, |\psi|^{\frac{4}{d}}\psi \sim L^{-2+\frac{d}{2}}$, see (31.35), and $i|\psi|^q\psi \sim L^{-\frac{d}{2}(q+1)}$. Therefore, for any $q > 0$, nonlinear damping increases as $L \rightarrow 0$. When $0 < q < \frac{4}{d}$, however, this increase is slower than that of nonlinearity and diffraction. As a result, the relative effect of damping becomes negligible as $L \rightarrow 0$.

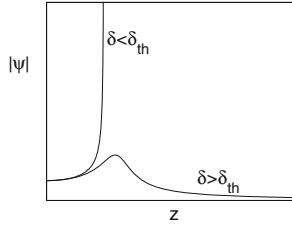


Fig. 33.1 Generic effect of subcritical nonlinear damping on critical collapse. When $\delta < \delta_{\text{th}}$, collapse is not arrested. When $\delta > \delta_{\text{th}}$, collapse is arrested, there is a single focusing-defocusing event, and the solution exists globally

- When $\delta > \delta_{\text{th}}(\psi_0; q)$, the solution power gets below P_{cr} before the solution has a chance to collapse. Therefore, collapse is arrested. After the arrest of collapse the power continues to decrease. Consequently, there is a single focusing-defocusing cycle. In particular, the solution exists globally.
- When $\delta < \delta_{\text{th}}(\psi_0; q)$, the solution collapses before its power gets below P_{cr} . Therefore, damping slows down the collapse, but does not arrest it. Near the singularity, subcritical nonlinear damping becomes negligible compared with nonlinearity and diffraction. Hence, the blowup rate and profile are the same as in the undamped critical NLS.

These two possibilities are illustrated in Fig. 33.1.

- When $q = 4/d$ (*critical nonlinear damping*), Eq. (33.15) reads $\beta_\zeta = -\tilde{\delta}$. Therefore,

$$\beta = \beta_0 - \tilde{\delta}\zeta. \quad (33.16)$$

Following Fibich and Levy [87], if we make the change of variables

$$A = \frac{1}{L}, \quad s = \tilde{\delta}^{-\frac{2}{3}} (\beta_0 - \tilde{\delta}\zeta)$$

and use the relation $\beta = A_\zeta \zeta / A$, see (18.9), Eq. (33.16) transforms into Airy's equation

$$A_{ss}(s) = sA.$$

The initial conditions are given at $s_0 := s(\zeta = 0) = \tilde{\delta}^{-\frac{2}{3}} \beta_0 > 0$. Since $s(z)$ is monotonically decreasing, the Airy equation is solved for decreasing values of s . Recall that the solution of Airy's equation is a linear combination of the Airy and Bairy functions, i.e., $A(s) = k_1 \text{Ai}(s) + k_2 \text{Bi}(s)$, where k_1 and k_2 are constants that depend on the initial conditions at s_0 . Since $0 < \tilde{\delta} \ll 1$, we have that $s_0 \gg 1$. When $s \gg 1$, $\text{Ai}(s)$ decays exponentially while $\text{Bi}(s)$ increases exponentially (Fig. 33.2). Therefore, as s decreases from s_0 , $k_2 \text{Bi}(s)$ decays

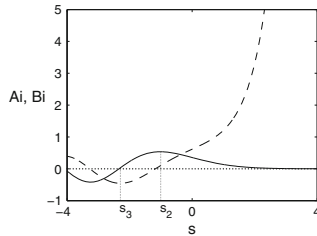


Fig. 33.2 The Airy functions Ai (solid) and Bi (dashes)

exponentially, while $k_1 \text{Ai}(s)$ increases exponentially. Consequently, once $s = O(1), A \sim k_1 \text{Ai}(s)$. This implies that collapse is arrested near $s_2 \approx -1.0$ where $\text{Ai}(s)$ attains its global maximum, see Fig. 33.2. Since A cannot be negative, the reduced equations cannot be valid for $s < s_3^\delta \approx s_3$, where $A(s = s_3^\delta) = 0$ and $s_3 \approx -2.3$ is the point where $\text{Ai}(s)$ vanishes for the first time. Indeed, in Lemma 38.8 we will show that $s \rightarrow s_3^\delta +$ corresponds to $z \rightarrow \infty$. Therefore, $A(s = s_3^\delta) = 0$ corresponds to $L(z = \infty) = \infty$, i.e., to scattering.

In summary, the reduced equations show that for an initial condition which leads to a peak-type collapse with the $\psi_{R^{(0)}}$ profile in the undamped critical NLS, the addition of small critical nonlinear damping always arrests collapse and leads to scattering, *regardless of how small δ is*. This conclusion is confirmed numerically in Fig. 38.8 (left).

3. When $q > 4/d$ (*supercritical nonlinear damping*), damping effects are even stronger. As a result, damping arrests collapse *regardless of how small δ is*, in agreement with Theorem 33.1. If, in addition, $\psi_0 \sim \psi_{R^{(0)}}$, after the arrest of collapse the solution scatters.⁵

The above informal analysis suggests

Conclusion 33.4 let ψ be a solution of the undamped critical NLS with power moderately above P_{cr} that undergoes a peak-type collapse with the $\psi_{R^{(0)}}$ profile. If collapse is arrested by the addition of a small linear or nonlinear damping, after the arrest of collapse the solution scatters.

This is different from the generic effect of dispersive perturbations, which is to arrest collapse and lead to slowly-decaying focusing-defocusing cycles (Sect. 31.5.1). The difference between these two cases has to do with the power of the collapsing core when collapse is arrested, which is below P_{cr} in the dissipative case, but above it in the dispersive one.

Remark See Sect. 38.6 and [86] for additional results on nonlinear damping.

⁵ When the initial power is highly above P_{cr} , numerical simulations reveal a pattern of several focusing-defocusing cycles, with abrupt power losses due to nonlinear damping at the locations of maximal focusing [154].

Chapter 34

Nonparaxiality and Backscattering (Nonlinear Helmholtz Equation)

In Chap. 1 we saw that the two-dimensional cubic NLS

$$i\psi_z(z, x, y) + \Delta\psi + |\psi|^2\psi = 0, \quad \Delta = \frac{\partial^2}{\partial x^2} + \frac{\partial^2}{\partial y^2} \quad (34.1)$$

is the leading-order model for propagation of intense laser beams in a bulk Kerr medium. Briefly, Maxwell equations for intense continuous-wave (cw) beams can be approximated by the vectorial nonlinear Helmholtz equations. Under the approximation that the electric field is linearly-polarized, these equations reduce to the scalar nonlinear Helmholtz equation (NLH)

$$\left(\frac{\partial^2}{\partial z^2} + \Delta \right) E + k_0^2 \left(1 + \frac{4n_2}{n_0} |E|^2 \right) E = 0. \quad (34.2)$$

Substituting $E = \psi e^{ik_0 z}$ and applying the paraxial approximation yields (34.1).

The NLS (34.1) admits solutions that become singular. Physical quantities, however, do not become singular. Therefore, if we employ a sufficiently more comprehensive model, its solutions will exist globally. Since the last stage in the derivation of the NLS is the paraxial approximation, it is natural to ask

Open Question 34.1 Consider the singular solutions of the critical NLS (34.1). Do the corresponding solutions of the scalar NLH (34.2) exist globally?

After many years of research, this question is still open. In this chapter we present rigorous, asymptotic, and numerical results that suggest that the answer is affirmative.

34.1 Breakdown of the Paraxial Approximation

Let $E = \psi e^{ik_0 z}$. We can rewrite the scalar NLH (34.2) in terms of ψ as

$$\psi_{zz}(z, x, y) + 2ik_0\psi_z + \Delta\psi + k_0^2 \frac{4n_2}{n_0} |\psi|^2\psi = 0.$$

Changing to the dimensionless variables

$$\tilde{x} = \frac{x}{r_0}, \quad \tilde{y} = \frac{y}{r_0}, \quad \tilde{z} = \frac{z}{2r_0 k_0^2}, \quad \tilde{\psi} = \left(r_0^2 k_0^2 \frac{4n_2}{n_0} \right)^{\frac{1}{2}} \psi$$

and dropping the tildes gives the dimensionless NLH

$$\epsilon \psi_{zz}(z, x, y) + i \psi_z + \Delta \psi + |\psi|^2 \psi = 0, \quad (34.3)$$

where

$$\epsilon = \frac{f^2}{4}, \quad f = \frac{1}{k_0 r_0} = \frac{1}{2\pi} \frac{\lambda}{r_0}.$$

The wavelength λ is typically much smaller than the initial radius r_0 . Hence,¹

$$0 < \epsilon \ll 1,$$

which suggests that $\epsilon \psi_{zz}$ can be neglected. Under this *paraxial approximation*, the NLH (34.3) reduces to the NLS (34.1). Mathematically, however, this is a very problematic approximation, since by neglecting the highest-order derivative in z , we change the nature of the equation from a boundary value problem (NLH) to an initial value one (NLS). Indeed, in the case of collapsing NLS solutions, the paraxial approximation breaks down *before* the singularity:

Lemma 34.1 *Let ψ be a solution of the two-dimensional critical NLS (34.1) that collapses at Z_c with the $\psi_{R^{(0)}}$ profile. Then the paraxial approximation breaks down before Z_c .*

Proof As $z \rightarrow Z_c$, the collapsing core of ψ approaches the two-dimensional $\psi_{R^{(0)}}$ profile, see Chap. 14, where

$$\psi_{R^{(0)}} = \frac{R^{(0)}(\rho)}{L(z)} e^{iS}, \quad \rho = \frac{r}{L}, \quad S = \zeta + \frac{L_z}{L} \frac{r^2}{4}, \quad \zeta = \int_0^z \frac{ds}{L^2(s)}. \quad (34.4)$$

By (31.35),

$$\Delta \psi_{R^{(0)}} = O(L^{-3}), \quad |\psi_{R^{(0)}}|^2 \psi_{R^{(0)}} = O(L^{-3}). \quad (34.5a)$$

In addition, the leading-order behavior of the nonparaxial term is

$$\epsilon \psi_{zz} \sim \epsilon (\psi_{R^{(0)}})_{zz} \sim -\epsilon \frac{R^{(0)}}{L^5} e^{iS} = O(\epsilon L^{-5}), \quad (34.5b)$$

see Exercise 34.1. Therefore, the paraxial approximation $\epsilon \psi_{zz} \ll \Delta \psi$ breaks down when $\epsilon L^{-5} \sim L^{-3}$, i.e., when $L = O(\sqrt{\epsilon})$. \square

¹ In fact, $\epsilon \ll 1$ even if $r_0 = \lambda$, since then $\epsilon = \frac{1}{16\pi^2} \sim \frac{1}{160}$.

Remark Intuitively, the paraxial approximation breaks down because collapsing beams propagate perpendicularly (rather than parallel) to the z -axis as $z \rightarrow Z_c$.

Exercise 34.1 Use the β principle (Conclusion 31.1) to show that

$$(\psi_{R^{(0)}})_z \sim \frac{i\psi_{R^{(0)}}}{L^2} = O\left(\frac{1}{L^3}\right), \quad (\psi_{R^{(0)}})_{zz} \sim -\frac{\psi_{R^{(0)}}}{L^4} = O\left(\frac{1}{L^5}\right). \quad (34.6)$$

The proof of Lemma 34.1 suggests that the paraxial approximation breaks down when $L = O(\sqrt{\epsilon})$. In fact, it breaks down much earlier:

Conclusion 34.1 Let ψ be as in Lemma 34.1. Then the paraxial approximation breaks down when $L = O(\sqrt{\epsilon/\beta}) \gg \sqrt{\epsilon} = \frac{1}{4\pi} \frac{\lambda}{r_0}$.

Proof We give an informal proof. By the *balance of the giants principle* (Conclusion 18.9), nonparaxiality becomes important as soon as it becomes comparable to the “sum” of nonlinearity and diffraction, and this sum is $O(\beta)$ smaller than their individual magnitudes, i.e., as soon as

$$\epsilon[\psi_{zz}] \sim [\Delta\psi + |\psi|^2\psi] \sim \beta[\Delta\psi]. \quad (34.7)$$

Hence, by (34.5), the paraxial approximation breaks down when $\epsilon L^{-5} \sim \beta L^{-3}$. \square

Remark Conclusion 34.1 also follows from Corollary 34.2, which will be proved using *modulation theory*.

34.2 Early Simulations

In 1987, Vlasov [261] used informal calculations to derive a perturbed NLS that includes the leading-order effect of nonparaxiality, as follows. By (34.3),

$$\psi_z = iW + O(\epsilon), \quad W := \Delta\psi + |\psi|^2\psi. \quad (34.8)$$

Differentiating (34.8) with respect to z yields

$$\begin{aligned} \psi_{zz} &= iW_z + O(\epsilon) = i\Delta\psi_z + i\left(\psi^2\psi^*\right)_z + O(\epsilon) \\ &= i\Delta\psi_z + 2i|\psi|^2\psi_z + i\psi^2\psi_z^* + O(\epsilon). \end{aligned} \quad (34.9)$$

Substituting ψ_z and W from (34.8) gives

$$\begin{aligned} \psi_{zz} &= -\Delta W - 2|\psi|^2W + \psi^2W^* + O(\epsilon) \\ &= -\Delta^2\psi - \Delta(|\psi|^2\psi) - 2|\psi|^2\Delta\psi + \psi^2\Delta\psi^* - |\psi|^4\psi + O(\epsilon), \end{aligned}$$

where $\Delta^2 = \Delta\Delta$ is the biharmonic operator. Therefore, the NLH (34.3) is formally $O(\epsilon^2)$ equivalent to the “nonparaxial NLS”

$$i\psi_z + \Delta\psi + |\psi|^2\psi + \epsilon[-\Delta^2\psi - \Delta(|\psi|^2\psi) - 2|\psi|^2\Delta\psi + \psi^2\Delta\psi^* - |\psi|^4\psi] = 0. \quad (34.10)$$

Vlasov solved (34.10) numerically, and observed that collapse is arrested for initial conditions that lead to collapse in the paraxial NLS (34.1).

In 1988, Feit and Fleck [62] derived a different nonparaxial NLS. They solved it numerically, and also observed that collapse is arrested for initial conditions that lead to collapse in the paraxial NLS (34.1). After the arrest of collapse, the solutions underwent several focusing-defocusing oscillations, whose magnitude decreased with propagation.

The numerical studies of Vlasov and of Feit and Fleck suggested that nonparaxiality arrests collapse. Both studies, however, did not solve the NLH, but only an approximation of this equation. In particular, in both studies the NLH was approximated by an initial value problem, thereby neglecting the effect of the backscattered wave.² Since collapse in the critical NLS is highly sensitive to small perturbations (Sect. 18.6), it was unclear whether replacing the NLH with these approximate equations is legitimate.

34.3 Asymptotic Analysis of Nonparaxial Effects

In 1996, Fibich analyzed the effect of small nonparaxiality by using an asymptotic approach that later evolved into *modulation theory*.

Lemma 34.2 ([65]) *Consider the NLH (34.3) as the perturbed two dimensional critical NLS (31.15) with $F = \psi_{zz}$.³ Then the auxiliary functions of modulation theory satisfy*

$$(f_1)_z \ll f_2 \sim P_{\text{cr}} \left(\frac{1}{L^2} \right)_z. \quad (34.11)$$

Proof In Exercise 34.1 we saw that

$$(\psi_{R^{(0)}})_{zz} \sim -\frac{1}{L^4} \psi_{R^{(0)}} = -\frac{1}{L^5} R^{(0)} e^{iS}. \quad (34.12)$$

² Simulations of the NLH as a genuine boundary value problem were performed many years later (Sect. 34.8).

³ An informal a posteriori justification for treating nonparaxiality as a small perturbation is given in Conclusion 34.4.

Therefore, by (31.18b),

$$f_2 = L \cdot \operatorname{Im} \int_0^\infty (\psi_{R^{(0)}})_{zz} e^{-iS} R^{(0)} \rho d\rho \sim -\frac{1}{L^4} \operatorname{Im} \int_0^\infty R^{(0)} R^{(0)} \rho d\rho = 0.$$

In addition, by (31.18a),

$$\begin{aligned} f_1 &= 2L^3 \operatorname{Re} \int_0^\infty (\psi_{R^{(0)}})_{zz} e^{-iS} \frac{d}{d\rho} (\rho R^{(0)}) \rho d\rho \\ &\sim -\frac{2}{L^2} \int_0^\infty R^{(0)} \frac{d}{d\rho} (\rho R^{(0)}) \rho d\rho = 0, \end{aligned} \quad (34.13)$$

where the last stage follows from

$$\begin{aligned} \int_0^\infty R^{(0)} \frac{d}{d\rho} (\rho R^{(0)}) \rho d\rho &= \int_0^\infty (\rho R^{(0)}) \frac{d}{d\rho} (\rho R^{(0)}) d\rho \\ &= \frac{1}{2} \int_0^\infty \frac{d}{d\rho} (\rho R^{(0)})^2 d\rho = 0. \end{aligned} \quad (34.14)$$

Since both f_1 and f_2 vanish, we need to go beyond the leading-order contribution of $(\psi_{R^{(0)}})_{zz}$. By (34.4),

$$(\psi_{R^{(0)}})_{zz} = \left(\left(\frac{R^{(0)}(\rho)}{L} \right)_{zz} + 2i \left(\frac{R^{(0)}(\rho)}{L} \right)_z S_z + \frac{R^{(0)}}{L} (iS_{zz} - S_z^2) \right) e^{iS}.$$

Hence,

$$\begin{aligned} \operatorname{Im} \left\{ e^{-iS} (\psi_{R^{(0)}})_{zz} \right\} &= 2 \left(\left(\frac{R^{(0)}(\rho)}{L} \right)_z S_z + \frac{R^{(0)}}{L} S_{zz} \right), \\ \operatorname{Re} \left\{ e^{-iS} (\psi_{R^{(0)}})_{zz} \right\} &= \left(\left(\frac{R^{(0)}(\rho)}{L} \right)_{zz} - \frac{R^{(0)}}{L} S_z^2 \right). \end{aligned} \quad (34.15)$$

Since $S_z \sim L^{-2}$, see (31.34), and

$$\begin{aligned} \left(\left(\frac{R^{(0)}(\rho)}{L} \right)_z \right) &= \left(\frac{1}{L} \right)_z R^{(0)} + \frac{1}{L} (R^{(0)})_\rho \rho_z = \left(\frac{1}{L} \right)_z \left(R^{(0)} + \rho \frac{dR^{(0)}}{d\rho} \right) \\ &= \left(\frac{1}{L} \right)_z \frac{d}{d\rho} (\rho R^{(0)}), \end{aligned}$$

we have that

$$\text{Im}\left\{e^{-iS}(\psi_{R^{(0)}})_{zz}\right\} \sim 2\left(\frac{1}{L}\right)_z \frac{d}{d\rho} \left(\rho R^{(0)}\right) \frac{1}{L^2} + \frac{R^{(0)}}{L} \left(\frac{1}{L^2}\right)_z. \quad (34.16)$$

Substituting in (31.18b) and using (34.14) gives

$$\begin{aligned} f_2 &= L \cdot \text{Im} \int_0^\infty (\psi_{R^{(0)}})_{zz} e^{-iS} R^{(0)} \rho d\rho \sim \left(\frac{1}{L^2}\right)_z \int_0^\infty (R^{(0)})^2 \rho d\rho \\ &= \left(\frac{1}{L^2}\right)_z P_{\text{cr}}. \end{aligned}$$

We now turn to f_1 . By (31.18a) and (34.15),

$$\begin{aligned} f_1 &= 2L^3 \cdot \text{Re} \int_0^\infty (\psi_{R^{(0)}})_{zz} e^{-iS} \frac{d}{d\rho} \left(\rho R^{(0)}\right) \rho d\rho \\ &= 2L^3 \int_0^\infty \left[\left(\frac{R^{(0)}}{L}\right)_{zz} - \frac{R^{(0)}}{L} S_z^2 \right] \frac{d}{d\rho} \left(\rho R^{(0)}\right) \rho d\rho. \end{aligned}$$

In addition, as in Exercise 31.34,

$$S_z^2 = \left(\frac{1}{L^2} + \left(\frac{L_z}{L}\right)_z \frac{r^2}{4}\right)^2 \sim \frac{1}{L^4} + 2\frac{1}{L^2} \left(\frac{L_z}{L}\right)_z \frac{r^2}{4} = \frac{1}{L^4} + \left(\frac{L_z}{L}\right)_z \frac{\rho^2}{2}.$$

Since the contribution of the leading-order L^{-4} term vanishes, see (34.13),

$$f_1 \sim 2L^3 \int_0^\infty \left[\left(\frac{R^{(0)}}{L}\right)_{zz} - \frac{R^{(0)}}{L} \left(\frac{L_z}{L}\right)_z \frac{\rho^2}{2} \right] \frac{d}{d\rho} \left(\rho R^{(0)}\right) \rho d\rho.$$

Finally, by the β principle (Conclusion 31.1),⁴

$$[(f_1)_z] = \frac{[L]^2}{[Z]^3} \ll \frac{1}{[L]^2[Z]} = [f_2]. \quad \square$$

⁴ In Conclusion 31.5 we saw that generically $(f_1)_z \ll f_2$. We could not Conclusion 31.5 here, however, because its proof is based on the assumption that $[\text{Re}\{F(\psi_{R^{(0)}})e^{-iS}\}] = [\text{Im}\{F(\psi_{R^{(0)}})e^{-iS}\}]$, and hence that $[\text{Re} \int F(\psi_{R^{(0)}})e^{-iS}(\rho R^{(0)})_\rho \rho d\rho] = [\text{Im} \int F(\psi_{R^{(0)}})e^{-iS} R^{(0)} \rho d\rho]$. By (34.12), (34.16), and the β principle, however, we have that

$$\text{Re}\left\{F(\psi_{R^{(0)}})e^{-iS}\right\} \sim \frac{1}{L^5} \gg \frac{1}{L^3[Z]} \sim \text{Im}\left\{F(\psi_{R^{(0)}})e^{-iS}\right\}. \quad (34.17)$$

Nevertheless, we do have that $(f_1)_z \ll f_2$, because the contribution of the L^{-5} term vanishes in the integration, see (34.13).

By Proposition 31.1 and (34.11), the reduced equations for nonparaxial effects are

$$\beta_z(z) + \frac{\nu(\beta)}{L^2} = -\frac{2\epsilon}{M} f_2 = -\frac{2\epsilon P_{\text{cr}}}{M} \left(\frac{1}{L^2} \right)_z, \quad \beta = -L^3 L_{zz}. \quad (34.18)$$

Neglecting the exponentially-small non-adiabatic term, we get

Proposition 34.1 ([65]) *Under the adiabatic approximation, the reduced equations for the scalar NLH (34.3) read*

$$\beta_z(z) = -\frac{2\epsilon P_{\text{cr}}}{M} \left(\frac{1}{L^2} \right)_z, \quad \beta = -L^3 L_{zz}. \quad (34.19)$$

Since these equations are nothing but the reduced equations for a generic conservative perturbation with $C_{\text{gen}} = 4P_{\text{cr}}$, see (31.54), we have

Conclusion 34.2 *Although nonparaxiality is a nonconservative perturbation,⁵ its leading-order effect is the same as that of the generic conservative perturbations.*

Therefore, we can apply all the results of Sect. 31.5. Thus, for example, by Proposition 31.6, the dynamics of $y := L^2$ is governed by

$$(y_z)^2 = \frac{-4H_0}{M} \frac{1}{y} (y_M - y)(y - y_m), \quad y_M \sim \frac{M\beta_0}{-H_0}, \quad y_m \sim \frac{\epsilon P_{\text{cr}}}{M\beta_0}. \quad (34.20)$$

Hence, by Lemma 31.7,

Corollary 34.1 *The solution of (34.20) satisfies $y(z) \geq y_m > 0$. In particular, it does not vanish.*

This leads to

Conclusion 34.3 ([65]) *Nonparaxiality arrests collapse of peak-type solutions of the critical NLS.*

In addition, we have

Corollary 34.2 ([65]) *Nonparaxiality arrests collapse when $L = O(\sqrt{\epsilon/\beta})$.*

Proof By (34.20), $\min_z L(z) = \min_z \sqrt{y(z)} = \sqrt{y_m} \sim \sqrt{\epsilon/\beta_0}$. \square

Remark Previously, we used the *balance of the giants principle* to conclude that nonparaxiality becomes important once it is $O(\beta)$ smaller than nonlinearity and diffraction, see (34.7). The result of Corollary 34.2 is stronger, because it also shows that the effect of nonparaxiality is to arrest collapse.

⁵ More precisely, nonparaxiality is a nonconservative perturbation in the NLS model. The NLH power P_{NLH} , however, is conserved (Sect. 34.8).

By Lemma 31.8, if $\beta_0 > 0$ and $H_0 < 0$, the solution of (34.20) undergoes focusing-defocusing oscillations. These oscillations decay with propagation because of non-adiabatic effects, see (34.18).

In summary, the asymptotic analysis of (34.3) predicts that:

1. Nonparaxiality arrests collapse.
2. Subsequently, it leads to decaying focusing-defocusing oscillations.

These two predictions are in agreement with the numerical studies of Vlasov and of Feit and Fleck, see Sect. 34.2. Note, however, that backscattering effects are also neglected in the asymptotic analysis.

34.3.1 Global Validity of Reduced Equations

In Lemma 34.1 we saw that as $L \rightarrow 0$, nonparaxiality dominates nonlinearity and diffraction. This may seem to undermine the validity of the reduced equations, which were derived under the assumption that nonparaxiality is a small perturbation (see Condition 1 in Sect. 31.1.1). By Corollary 34.1, however, the relative magnitude of nonparaxiality satisfies

$$\frac{[\epsilon \psi_{zz}]}{[|\psi|^2 \psi]} = \frac{\epsilon L^{-5}}{L^{-3}} = \frac{\epsilon}{L^2} \leq \frac{\epsilon}{y_m} = O(\beta).$$

Conclusion 34.4 ([65]) *Throughout the propagation, nonparaxiality remains $O(\beta)$ smaller than nonlinearity and diffraction.*

In particular, Conclusion 34.4 provides an a posteriori informal justification for treating nonparaxiality as a small perturbation in the asymptotic analysis.

34.4 Backscattering and Vectorial Effects

We now discuss very briefly and informally the overall error which is introduced by replacing the vectorial NLH with the scalar NLS. When we approximate the vectorial NLH with the scalar NLH, we neglect the vectorial nature of the electric field. This approximation amounts to neglecting $O(f^2)$ terms, see (25.7). In addition, in the derivation of the NLS from the scalar NLH we substitute $E = e^{ik_0 z} \psi$ and neglect the ψ_{zz} term. The error introduced by this paraxial approximation is generically also $O(f^2)$, see (34.3).

In fact, when we approximate the scalar NLH with the NLS, we also make the implicit assumption that we can neglect backscattering. To see that, we note that a more accurate ansatz for the electric field is⁶

$$E(z, x, y) = e^{ik_0 z} \psi(z, x, y) + e^{-ik_0 z} B(z, x, y), \quad (34.21)$$

where B is the slowly-varying amplitude of the backscattered wave. Therefore, by using the ansatz $E = e^{ik_0 z} \psi$ and assuming that ψ is slowly-varying in z , we implicitly assume that we can set $B \equiv 0$.

At present, there is little understanding of backscattering in the scalar NLH, beyond the general belief that it is “small”. We now use informal arguments to show that the error introduced by neglecting backscattering is also $O(f^2)$.

Substituting the ansatz (34.21) in the scalar NLH (34.2), we obtain

$$\begin{aligned} 0 &= e^{ik_0 z} \left[\psi_{zz} + 2ik_0 \psi_z + \Delta \psi + |\psi + e^{-2ik_0 z} B|^2 \psi \right] \\ &\quad + e^{-ik_0 z} \left[B_{zz} - 2ik_0 B_z + \Delta B + |\psi + e^{-2ik_0 z} B|^2 B \right]. \end{aligned} \quad (34.22)$$

We first prove an auxiliary result.

Lemma 34.3 *Consider the equation*

$$e^{ik_0 z} F(\psi(z)) + e^{-ik_0 z} G(B(z)) = 0, \quad (34.23)$$

where F and G are dimensionless smooth functions. Let the characteristic length for changes in $\psi(z)$ and $B(z)$ be $L_{\text{diff}} := k_0 r_0^2$, i.e.,

$$\frac{\left[\frac{d^m \psi(z)}{dz^m} \right]}{[\psi]} = O\left(\frac{1}{L_{\text{diff}}^m}\right), \quad m = 1, 2,$$

and similarly for $B(z)$. Then the coupling between the equations for ψ and B is $O(f^2)$, where $f = \frac{1}{r_0 k_0}$, i.e.,

$$F(\psi(z)) = O(f^2), \quad G(B(z)) = O(f^2).$$

Proof If we multiply (34.23) by $e^{-ik_0 z}$ and average the result between $z_0 - \frac{\delta z}{2}$ and $z_0 + \frac{\delta z}{2}$, where $\delta z = \frac{\pi}{k_0}$, we get

$$\frac{1}{\delta z} \int_{z_0 - \frac{\delta z}{2}}^{z_0 + \frac{\delta z}{2}} F(\psi(z)) dz = \frac{-1}{\delta z} \int_{z_0 - \frac{\delta z}{2}}^{z_0 + \frac{\delta z}{2}} e^{-2ik_0 z} G(B(z)) dz. \quad (34.24)$$

⁶ The motivation for this ansatz will become more apparent in Sect. 34.6.

Substituting the Taylor expansion

$$F(\psi(z)) = F(\psi(z_0)) + (z - z_0) \frac{dF(\psi(z))}{dz} \Big|_{z_0} + \frac{(z - z_0)^2}{2} \frac{d^2F(\psi(z))}{dz^2} \Big|_{z_0} + \dots$$

in the left-hand side of (34.24), we obtain

$$\frac{1}{\delta z} \int_{z_0 - \frac{\delta z}{2}}^{z_0 + \frac{\delta z}{2}} F(\psi(z)) dz = F(\psi(z_0)) + \frac{d^2F(\psi(z))}{dz^2} \Big|_{z_0} \cdot O((\delta z)^2).$$

Since the characteristic length for changes in $\psi(z)$ is L_{diff} , we have that $\frac{d^2F(\psi(z))}{dz^2} \Big|_{z_0} = O\left(\frac{1}{L_{\text{diff}}^2}\right)$. Therefore,

$$\frac{d^2F(\psi(z))}{dz^2} \Big|_{z_0} (\delta z)^2 \sim \frac{1}{r_0^4 k_0^4} = f^4.$$

Similarly,

$$\begin{aligned} & \frac{1}{\delta z} \int_{z_0 - \frac{\delta z}{2}}^{z_0 + \frac{\delta z}{2}} e^{-2ik_0 z} G(B(z)) dz \\ & \approx \frac{1}{\delta z} \int_{z_0 - \frac{\delta z}{2}}^{z_0 + \frac{\delta z}{2}} e^{-2ik_0 z} \left[G(B(z_0)) + (z - z_0) \frac{dG(B(z))}{dz} \Big|_{z_0} \right] dz. \end{aligned}$$

Now, $\int_{z_0 - \frac{\delta z}{2}}^{z_0 + \frac{\delta z}{2}} e^{-2ik_0 z} dz = 0$ and

$$\begin{aligned} \int_{z_0 - \frac{\delta z}{2}}^{z_0 + \frac{\delta z}{2}} e^{-2ik_0 z} (z - z_0) dz &= \left[\frac{e^{-2ik_0 z}}{-2ik_0} (z - z_0) \right]_{z_0 - \frac{\delta z}{2}}^{z_0 + \frac{\delta z}{2}} - \underbrace{\int_{z_0 - \frac{\delta z}{2}}^{z_0 + \frac{\delta z}{2}} \frac{e^{-2ik_0 z}}{-2ik_0} dz}_{=0} \\ &= \frac{e^{-2ik_0 z_0}}{-2ik_0} \left[\frac{\delta z}{2} \underbrace{e^{-ik_0 \delta z}}_{=e^{-i\pi}=-1} + \frac{\delta z}{2} \underbrace{e^{ik_0 \delta z}}_{=e^{i\pi}=-1} \right] = \delta z \frac{e^{-2ik_0 z_0}}{2ik_0}. \end{aligned}$$

In addition, since the characteristic length for changes of $B(z)$ is L_{diff} , we have that $\frac{dG(B(z))}{dz} \Big|_{z_0} = O\left(\frac{1}{L_{\text{diff}}}\right)$. Combining the above gives

$$\begin{aligned} \frac{1}{\delta z} \int_{z_0 - \frac{\delta z}{2}}^{z_0 + \frac{\delta z}{2}} e^{-2ik_0 z} G(B(z)) dz &\approx \frac{1}{\delta z} \frac{dG(B(z))}{dz} \Big|_{z_0} \int_{z_0 - \frac{\delta z}{2}}^{z_0 + \frac{\delta z}{2}} e^{-2ik_0 z} (z - z_0) dz \\ &= O\left(\frac{1}{L_{\text{diff}} k_0}\right) = O(f^2). \end{aligned}$$

Summarizing the above, Eq. (34.24) reduces to

$$F(\psi(z)) + O(f^4) = O(f^2).$$

Therefore, the result follows. \square

Since backscattering is typically “small”, let us assume that it is $O(f)$ smaller than the forward-propagating wave. In that case, it immediately follows from (34.22) that neglecting backscattering introduces an $O(f)$ error to the forward-propagating component ψ . In fact, this error is $O(f^2)$:

Corollary 34.3 *Let $\frac{B}{\psi} = O(f)$. Then setting $B \equiv 0$ in (34.22) leads to an $O(f^2)$ error in ψ .*

Proof This result “almost” follows from Lemma 34.3. Indeed, (34.22) is not exactly of the form (34.23), because B appears in the equation for ψ in the term $|\psi + e^{-2ik_0z}B|^2\psi$. Note, however, that

$$\begin{aligned} |\psi + e^{-2ik_0z}B|^2 &= |\psi|^2 + |B|^2 + (\psi^*e^{-2ik_0z}B + \text{c.c.}) \\ &= |\psi|^2(1 + O(f^2)) + (\psi^*e^{-2ik_0z}B + \text{c.c.}). \end{aligned}$$

As in the proof of Lemma 34.3, the fast oscillations decrease the effect of the last term by $O(f^2)$. Since, in addition, $\frac{B}{\psi} = O(f)$, the effect of the last term is $O(f^3)$. Therefore, the result follows. \square

Conclusion 34.5 *Let $\frac{B}{\psi} = O(f)$. Then neglecting backscattering in the derivation of the NLS from the scalar NLH amounts to neglecting $O(f^2)$ terms.*

Therefore, we have

Conclusion 34.6 *Let $\frac{B}{\psi} = O(f)$. Then the overall error of replacing the vectorial NLH with the scalar NLS is $O(f^2)$.*

Obviously, these conclusions are far from optimal, since we had to assume that $\frac{B}{\psi} = O(f)$.

34.5 Continuity of E and E_z Across Interfaces

At the Kerr medium interface at $z = 0$ there is a discontinuity in the coefficients of the Helmholtz equation. Let us recall the following result.

Lemma 34.4 *Let $\vec{E}(x, y, z) = [E_1(x, y, z), 0, 0]$ be a linearly-polarized electric field. Then E_1 and $\frac{\partial E_1}{\partial z}$ are continuous across the interface $z \equiv \text{constant}$.*

Proof Since the tangential components of the electric and magnetic fields are continuous across interfaces [134], this implies the continuity of E_1 and H_2 across

$z \equiv \text{constant}$. From Maxwell's equations for time-harmonic fields in a dielectric medium with a constant permittivity ($\mu \equiv \mu_0$) we have that $\nabla \times \vec{E} = i\omega_0 \mu_0 \vec{H}$, see (1.1). Therefore, taking into account that $E_3 \equiv 0$,

$$i\omega_0 \mu_0 H_2 = \frac{\partial E_1}{\partial z} - \frac{\partial E_3}{\partial x} = \frac{\partial E_1}{\partial z}.$$

Hence, the continuity of H_2 implies the continuity of $\frac{\partial E_1}{\partial z}$. \square

34.6 The (0 + 1)D NLH

Consider the $(2 + 1)$ D scalar Helmholtz equation

$$\left(\frac{\partial^2}{\partial z^2} + \Delta \right) E(x, y, z) + k^2 E = 0, \quad \Delta = \frac{\partial^2}{\partial x^2} + \frac{\partial^2}{\partial y^2}.$$

If we look for plane-wave solutions $E = E(z)$, this equation reduces to

$$E_{zz}(z) + k^2 E = 0. \quad (34.25)$$

In the linear homogeneous case $k^2 \equiv k_0^2$, (34.25) can be rewritten as

$$\left(\frac{d}{dz} + ik_0 \right) \left(\frac{d}{dz} - ik_0 \right) E = 0.$$

Since the solution of $\left(\frac{d}{dz} \mp ik_0 \right) E = 0$ is $E = c_{\pm} e^{\pm ik_0 z}$, the general solution of (34.25) with $k^2 \equiv k_0^2$ is $E = c_+ e^{ik_0 z} + c_- e^{-ik_0 z}$, i.e., a linear combination of right- and left-propagating waves.

Consider now the case where $z = 0$ is the interface between two linear media, i.e.,

$$k^2(z) = \begin{cases} k_{0,l}^2, & \text{if } z < 0, \\ k_{0,r}^2, & \text{if } z > 0. \end{cases}$$

The general solution of (34.25) is

$$E(z) = \begin{cases} c_+ e^{ik_{0,l} z} + c_- e^{-ik_{0,l} z}, & \text{if } z < 0, \\ d_+ e^{ik_{0,r} z} + d_- e^{-ik_{0,r} z}, & \text{if } z > 0. \end{cases}$$

Assume that the problem is driven by a right-propagating wave $E_0^{\text{inc}} e^{ik_{0,l} z}$, which travels from $z = -\infty$ and impinges on the interface $z = 0$ from the left. Part of this wave is transmitted by the interface, and the rest is reflected backwards. For $z > 0$,

however, the solution only consists of a right-traveling wave. Therefore,

$$E(z) = \begin{cases} E_0^{\text{inc}} e^{ik_{0,1}z} + R e^{-ik_{0,1}z}, & \text{if } z < 0, \\ T e^{ik_{0,r}z}, & \text{if } z > 0, \end{cases}$$

where R and T are the coefficients of the reflected and transmitted waves, respectively. Since both E and E_z are continuous at $z = 0$ (Lemma 34.4), we have that

$$E_0^{\text{inc}} + R = T, \quad k_{0,1}(E_0^{\text{inc}} - R) = k_{0,r}T.$$

A simple calculation gives

$$R = \frac{k_{0,1} - k_{0,r}}{k_{0,1} + k_{0,r}} E_0^{\text{inc}}, \quad T = \frac{2k_{0,1}}{k_{0,1} + k_{0,r}} E_0^{\text{inc}}.$$

Hence, the reflected component increases with the difference $k_{0,1} - k_{0,r}$. In addition, since,

$$(E_0^{\text{inc}})^2 k_{0,1} = R^2 k_{0,1} + T^2 k_{0,r},$$

the power of the incident beam is equal to that of the reflected and transmitted beams.

Consider now a homogeneous nonlinear Kerr slab of a finite length z_{\max} , immersed in a linear homogeneous background. In this case

$$n^2(z, |E|) = \begin{cases} n_{0,b}^2, & \text{if } z < 0, \\ n_{0,sl}^2 + \epsilon |E|^2, & \text{if } 0 < z < z_{\max}, \\ n_{0,b}^2, & \text{if } z > z_{\max}, \end{cases}$$

where $\epsilon = 4n_{0,sl}n_{2,sl}$. As before, we assume that the system is driven by the right-propagating wave $E_0^{\text{inc}} e^{ik_0 z}$ which impinges on the interface $z = 0$.

Lemma 34.5 *The electric field inside the Kerr slab is the solution of*

$$E''(z) + \frac{\omega^2}{c^2} (n_{0,sl}^2 + \epsilon |E|^2) E = 0, \quad 0 < z < z_{\max}, \quad (34.26a)$$

subject to the boundary conditions

$$\left(\frac{d}{dz} + ik_0 \right) E = 2ik_0 E_0^{\text{inc}}, \quad z = 0+, \quad (34.26b)$$

$$\left(\frac{d}{dz} - ik_0 \right) E = 0, \quad z = z_{\max}-, \quad (34.26c)$$

where $k_0 = \omega_0 n_{0,b} / c$.

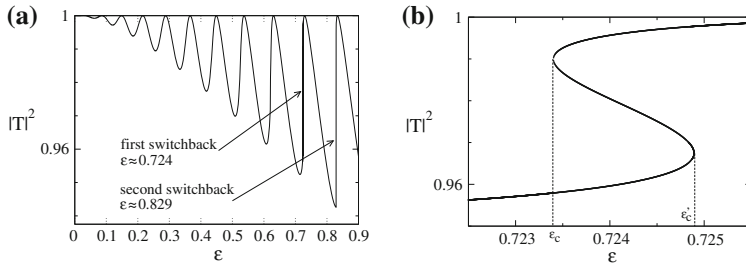


Fig. 34.1 Solution of the (0 + 1)D NLH (34.26) with $n_{0,b} = n_{0,sl} = 1$, $k_0 = 8$, $E_0^{\text{inc}} = 1$, and $Z_{\max} = 10$. **a** The transmittance $|T|^2$ as a function of ϵ . **b** Zoom-in on the first region of nonuniqueness $0.7234 \approx \epsilon_c \leq \epsilon \leq \epsilon'_c \approx 0.7249$. From [15]

Proof Since there are no waves coming from $+\infty$, $E = Te^{ik_0 z}$ for $z > z_{\max}$. Therefore, $\frac{dE}{dz} = ik_0 E$ for $z > z_{\max}$. In particular, $\left(\frac{d}{dz} - ik_0\right) E|_{z_{\max}+} = 0$. Since both E and E_z are continuous across interfaces (Lemma 34.4), we get (34.26c). For $z < 0$ the electric field consists of the known forward-propagating wave and an unknown backscattered wave, i.e., $E = E_0^{\text{inc}} e^{ik_0 z} + Re^{-ik_0 z}$. Therefore, $E_z + ik_0 E = 2ik_0 E_0^{\text{inc}} e^{ik_0 z}$ for $z < 0$. In particular, $\left(\frac{d}{dz} + ik_0\right) E|_{0-} = 2ik_0 E_0^{\text{inc}}$. Since both E and E_z are continuous across interfaces, we get (34.26b). \square

Closed-form solutions of (34.26a) were obtained by Wilhelm [277] for real fields, and by Marburger and Felber [167] for complex ones. Chen and Mills [43] used these solutions to solve the boundary value problem (34.26), as follows. The second-order ODE (34.26a), together with the boundary condition (34.26c) and a specific choice of the transmitted-field amplitude T , constitute an initial value problem at $z = Z_{\max}$ that has a unique solution $E = E(z; T, \epsilon)$.^{7,8} In general, for an arbitrary value of T , the solution $E(z; T, \epsilon)$ does not satisfy the boundary condition (34.26b) at $z = 0$. Chen and Mills derived an algebraic equation (which involves a Jacobi elliptic function) which is satisfied if and only if (34.26b) is satisfied. One can therefore use a *shooting approach*⁹ to find the value(s) of $T = T(\epsilon)$ for which the algebraic equation is satisfied. For these values, the solution $E(z; T, \epsilon)$ of the initial value problem will satisfy (34.26b), and will thus be a solution of the boundary value problem (34.26).

A typical plot of $T(\epsilon)$ is shown in Fig. 34.1. When ϵ is sufficiently small, $T(\epsilon)$ is single-valued. When ϵ exceeds a certain threshold, however, $T(\epsilon)$ becomes multi-valued, which corresponds to nonuniqueness of the solution of the boundary value problem (34.26). This nonuniqueness occurs at certain intervals of ϵ and is of a switchback type, see Fig. 34.1b.

⁷ The boundary value problem (34.26) can be rescaled as $\tilde{E} = E/E_0^{\text{inc}}$ and $\tilde{\epsilon} = \epsilon|E_0^{\text{inc}}|^2$. Under this rescaling $\tilde{E}_0^{\text{inc}} = 1$, and variations of $\tilde{\epsilon}$ correspond to variations of the input power.

⁸ Note that as $|E(Z_{\max})| = |T|$, a choice of T is equivalent to a choice of E at $z = Z_{\max}$.

⁹ See Sect. 28.1.

34.6.1 Radiation Boundary Conditions

The boundary condition (34.26c) at z_{\max} ensures that there are only right-going waves for $z > z_{\max}$. Therefore, we shall refer to it as a *radiation-to-the-right boundary condition*. The boundary condition (34.26b) at $z = 0$ is different; it ensures that for $z < 0$ the incoming wave $E_{\text{inc}}(z) = E_0^{\text{inc}} e^{ik_0 z}$ travels to the right, and simultaneously allows for a backscattered wave with an a priori unknown amplitude to travel to the left. Therefore, this boundary condition will be referred to as a *two-way radiation boundary condition*.

Because of the radiation boundary conditions, the boundary value problem (34.26) is not self-adjoint. Indeed, radiation boundary conditions cannot be of the self-adjoint form $aE + bE_z|_{z_0} = 0$, where a and b are real. This is because in that case there is no power radiation through z_0 , as the power flux at z_0 is

$$S_z(z_0) = k_0 \text{Im} \left(E^* \frac{\partial E}{\partial z} \right) \Big|_{z_0} = -k_0 \text{Im} \left(E^* \frac{a}{b} E \right) \Big|_{z_0} = 0,$$

see (34.31). Thus, *although the coefficients of the Helmholtz equation are real, it is “because” of the radiation boundary conditions that traveling solutions of Helmholtz equation are complex*.

34.7 Boundary Conditions for the $(2+1)$ D NLH

We now go back to the original problem of propagation of intense laser beams in a bulk Kerr medium. Let us first assume that the Kerr medium is located at $0 < z < z_{\max}$, and the propagation is linear for $-\infty < z < 0$ and for $z_{\max} < z < \infty$. The problem is driven by an incoming beam $E^{\text{inc}}(z, x, y)$ that travels from $z = -\infty$ in the positive z -direction and impinges on the Kerr medium at $z = 0$. In this setup the electric field E has no left-propagating components for $z > z_{\max}$. At $z < 0$, E has a known right-propagating incoming component and an unknown left-propagating backscattered component. Therefore, the NLH (34.2) is solved for $0 < z < z_{\max}$, subject to a two-way boundary condition at $z = 0$, and a radiation-to-the-right boundary condition at $z = z_{\max}$.

The radiation boundary conditions in the multi-dimensional case are more complex than in one dimension, see (34.26b, 34.26c), because they have to account for waves that impinge on the interfaces $z = 0$ and z_{\max} at oblique angles. Briefly, in the linear regimes $z < 0$ and $z > z_{\max}$ we can expand the electric field as

$$E(x, y, z) = \frac{1}{2\pi} \int \hat{E}(z; k_x, k_y) e^{i(k_x x + k_y y)} dk_x dk_y.$$

Therefore, the (k_x, k_y) mode satisfies the one-dimensional Helmholtz equation

$$\frac{d^2}{dz^2} \hat{E}(z; k_x, k_y) + k_m^2 \hat{E} = 0, \quad k_m^2 = k_0^2 - k_x^2 - k_y^2.$$

The radiation boundary conditions for this one-dimensional equation are of the form (34.26b, 34.26c). Therefore, when transforming back, the resulting radiation boundary conditions for (34.2) become nonlocal. See [18, 97] for further details.

Consider now a Kerr medium which is located at $0 < z < \infty$. Since the electric field E has no left-propagating components as $z \rightarrow \infty$, it satisfies a radiation-to-the-right boundary condition as $z \rightarrow \infty$. When one solves this problem numerically, the computational domain is truncated at some $0 < z_{\max} < \infty$. Since the propagation for $z > z_{\max}$ is nonlinear, E should satisfy a nonlinear radiation-to-the-right boundary condition at z_{\max} . At present, the formulation of this nonlinear boundary condition is not known. If, however, the electric field decays to zero as $z \rightarrow \infty$, then for z_{\max} sufficiently large the propagation is essentially linear for $z > z_{\max}$, and so one can impose a linear radiation-to-the-right boundary condition at z_{\max} . This is the case e.g., with collapsing beams that scatter after the arrest of collapse (Sect. 34.8.1), but not for soliton-type solutions whose propagation remains nonlinear as $z \rightarrow \infty$ (Sect. 34.8.2).

The formulation of the boundary condition in the lateral coordinate $r = \sqrt{x^2 + y^2}$ is similar. The electric field should satisfy a nonlinear radiation condition as $r \rightarrow \infty$ that will ensure that there are no waves coming from $r = \infty$. If the computational lateral boundary is sufficiently far away, this condition can be approximated by a linear radiation condition. See [98] for further details.

34.8 Genuine Boundary Value Simulations

Numerical simulations of the NLH are considerably harder than of the NLS. This is because the NLH is a boundary value problem, whereas the NLS is an initial value problem. An additional computational obstacle is that, unlike the NLS which governs the slowly-varying envelope, the NLH has to be discretized with a sub-wavelength resolution.¹⁰

The first simulations of the NLH (34.2) with no simplifying assumptions, and in particular with the backscattering included, were performed by Fibich and Tsynkov [97] in 2001. To do that, we developed a numerical method for solving, as a genuine boundary value problem, the (1 + 1)D NLH

$$\left(\frac{\partial^2}{\partial z^2} + \frac{\partial^2}{\partial x^2} \right) E(z, x) + k_0^2 \left(1 + \epsilon |E|^4 \right) E = 0 \quad (34.27)$$

in the domain $0 < z < z_{\max}$ and $-x_{\max} < x < x_{\max}$, subject to a two-way radiation condition at $z = 0$, a radiation-to-the-right condition at $z = z_{\max}$, and a Dirichlet boundary condition at $x = \pm x_{\max}$. This method is based on fixed-point iterations, in which the nonlinearity is frozen at each iteration. One of the key issues was to

¹⁰ A typical rule of thumb is to have at least 10 points per wavelength. In some cases, finer resolutions are required.

construct a two-way boundary condition at $z = 0$ that would let the incoming beam propagate forward, and simultaneously allow the (unknown) backscattered wave to propagate backwards. Numerical simulations of the “critical” NLH (34.27) with the fixed-point iterative method converged for input powers of up to $0.9P_{\text{cr}}$, but diverged for higher powers. Therefore, the simulations in [97] did not provide any insight to Question 34.1.

In [84], Fibich and Tsynkov applied the fixed-point iteration method to the linearly-damped $(1 + 1)\text{D}$ NLH

$$\left(\frac{\partial^2}{\partial z^2} + \frac{\partial^2}{\partial x^2} \right) E(z, x) + k_0^2(1 + i\delta + \epsilon|E|^4)E = 0, \quad \delta > 0. \quad (34.28)$$

These simulations showed that there exist initial conditions for which the solution of the linearly-damped critical NLS¹¹

$$i\psi_z(z, x) + \psi_{xx} + |\psi|^4\psi + i\frac{\delta}{f^2}\psi = 0$$

becomes singular, but the corresponding solution of (34.28) exists globally. Therefore, in these simulations collapse was arrested by nonparaxiality and backscattering. Unfortunately, the damping parameter δ was much larger than in actual physical settings, and could not be reduced to zero (i.e., the fixed-point iterations diverged when δ was “too small”).

The Dirichlet boundary condition at the numerical lateral boundary $x = \pm x_{\text{max}}$ is not physical, as it reflects back all radiation. Therefore, in [98], Fibich and Tsynkov replaced it with the local radiation boundary condition $E_x \mp ik_0 E|_{x=\pm x_{\text{max}}} = 0$. This led to an expansion in bi-orthogonal eigenfunctions in the transverse direction. The improved algorithm converged for input powers of up to $0.99P_{\text{cr}}$, but still diverged for $P > P_{\text{cr}}$. In [16], Baruch, Fibich, and Tsynkov extended the algorithm to the $(2 + 1)\text{D}$ radial cubic NLH

$$\left(\frac{\partial^2}{\partial z^2} + \frac{\partial^2}{\partial r^2} + \frac{1}{r} \frac{\partial}{\partial r} \right) E(z, r) + k_0^2 \left(1 + \epsilon|E|^2 \right) E = 0. \quad (34.29)$$

In that study, the algorithm also diverged for $P > P_{\text{cr}}$.

At that stage of the research, it was unclear whether the numerical divergence above P_{cr} was an indication that collapse is not arrested in the scalar NLH, or a numerical artifact of the fixed-point iterations method. To answer this question, Baruch, Fibich, and Tsynkov considered the $(0 + 1)\text{D}$ NLH (34.26), because it had been known that its solutions always exist, and become non-unique above a certain power threshold (Sect. 34.6). Numerical simulations of (34.26) with the fixed-point iterations method converged at sufficiently low powers, but diverged well below the non-uniqueness threshold. This showed that *the divergence of the fixed-point*

¹¹ This equation is analyzed in Sect. 33.1.

iterations method is a numerical artifact. Therefore, in [15] we developed an alternative method for the $(0+1)$ D NLH, which is based on Newton's iterations. The new method converged both below and above the non-uniqueness threshold. In a subsequent study [18], the Newton's iterations methodology was extended to the $(1+1)$ D NLH (34.27) and to the $(2+1)$ D NLH (34.29), and was again observed to converge much better than the original fixed-point iterations method.

34.8.1 Arrest of Collapse in the NLH

Figure 34.2a shows the numerical solution of the $(2+1)$ D cubic NLH (34.29) with the incoming collimated Gaussian beam $E_0^{\text{inc}} = (\sqrt{\epsilon}r_0k_0)^{-1}e^{-(r/r_0)^2}$, computed using Newton's iterations. The initial width was $r_0 = 1.27\lambda_0$, corresponding to $f^2 = (k_0r_0)^{-2} = 1/64$ and $P = 1.29P_{\text{cr}}$. The NLH solution self-focuses until $z_{\text{arrest}} \approx 0.8L_{\text{DF}}$ where its collapse is arrested, and defocuses from then on. The corresponding NLS solution collapses at $Z_c \approx 0.68L_{\text{DF}}$, see Fig. 34.2c. *Comparison of these NLH and NLS solutions provided the first direct numerical evidence that collapse is arrested in the scalar NLH model.*

The fast oscillations of $|E|^2$ in the z -direction in Fig. 34.2a, c are not a numerical artifact, but rather account for the actual physics. Indeed, since E is a combination of forward and backward traveling fields, i.e.,

$$E \approx \psi e^{ik_0 z} + B e^{-ik_0 z}, \quad (34.30)$$

then $|E|^2 \approx |\psi|^2 + |B|^2 + 2 \operatorname{Re}(\psi B^* e^{i2k_0 z})$. Hence, $|E|^2$ should have oscillations with wavenumber $\approx 2k_0$, as is indeed the case in Fig. 34.2a.

To find a smoother representation of the solution, we recall that while the conserved power of the NLS is $P = \int |\psi|^2 dx dy$, the conserved power of the NLH (34.2)

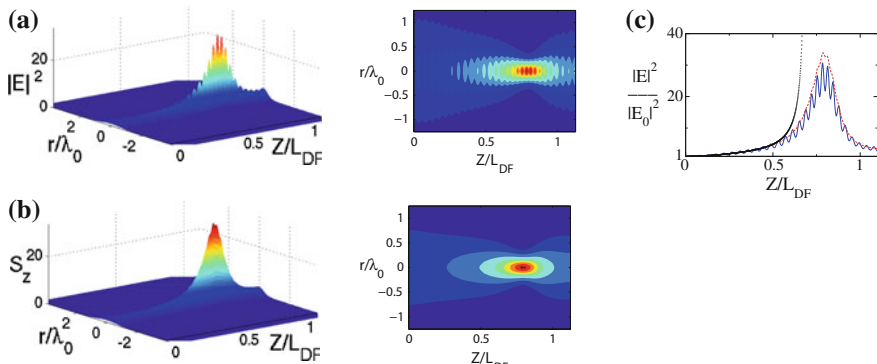


Fig. 34.2 Arrest of collapse in the $(2+1)$ D cubic NLH. **a** $|E|^2$. **b** S_z . **c** Normalized on-axis $|E|^2$ (solid), S_z (dashes), and NLS solution (dots). From [17]

is $P_{\text{NLH}} = \int S_z dx dy$, where $\mathbf{S} = k_0 \text{Im}(E^* \nabla E)$ is the power flux (Poynting vector), and

$$S_z = k_0 \text{Im} \left(E^* \frac{\partial E}{\partial z} \right) \quad (34.31)$$

is its z -component. Specifically, for the field (34.30), S_z is the flux difference between ψ and B , i.e., $S_z \approx k_0^2 (|\psi|^2 - |B|^2)$. It is therefore much smoother than $|E|^2$, and provides a more natural description of the NLH solution (as is confirmed by comparing S_z of Fig. 34.2b with $|E|^2$ of Fig. 34.2a). The energy flux S_z also provides a smoother picture of the on-axis arrest of collapse and of the focusing-defocusing dynamics (Fig. 34.2c).

34.8.2 Nonparaxial Solitons

The Newton's iterations methodology can also be used to compute nonparaxial propagation in the subcritical case. Recall that the one-dimensional cubic NLS admits stable solitary waves called solitons (Sect. 9.4.1). It has been generally believed that the paraxial approximation breaks down when the beam width r_0 becomes comparable to λ_0 , and consequently that there are no solitons with sub-wavelength width.

To show that this is not the case, we solved the (1 + 1)D cubic NLH

$$\left(\frac{\partial^2}{\partial z^2} + \frac{\partial^2}{\partial x^2} \right) E(z, x) + k_0^2 \left(1 + \epsilon |E|^2 \right) E = 0$$

for $0 < z < z_{\max}$ and $-\infty < x < \infty$, subject to the incoming beam

$$E_0^{\text{inc}}(x) = \frac{1}{\sqrt{\epsilon} r_0 k_0} \text{sech} \left(\frac{x}{r_0} \right), \quad r_0 = \frac{\lambda_0}{2},$$

which is the NLS soliton with a half-wavelength width. The NLH solution “behaves as a soliton”, in the sense that it propagates nearly unchanged over 40 diffraction lengths (Fig. 34.3a). Even for such a narrow beam, the nonparaxiality parameter is

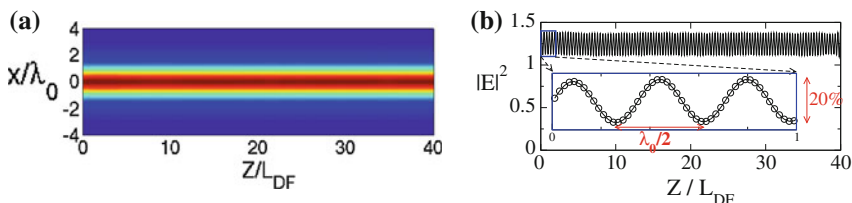


Fig. 34.3 Propagation of a soliton with a half-wavelength width in a Kerr medium slab of length $z_{\max} = 40L_{\text{diff}}$. **a** S_z . **b** On-axis $|E|^2$. From [17]

still small, since $f^2 = \frac{1}{\pi^2} \approx 0.1$, which explains why the dynamics is similar to that of the NLS soliton. As in the $(2+1)$ D case (Fig. 34.2), because part of the forward-propagating beam is backscattered, $|E|^2$ exhibits fast $2k_0$ oscillations (Fig. 34.3b), while S_z is smooth.

34.9 Rigorous Analysis

In 2006, Sever [231] employed a Palais-Smale type argument to prove the existence (hence the arrest of collapse) of solutions of the NLH with self-adjoint boundary conditions. Propagating fields, however, satisfy radiation boundary conditions which are not self-adjoint (Sect. 34.6.1). Unfortunately, Sever's proof heavily relies on self-adjointness, and therefore does not provide an answer to Question 34.1.

Chapter 35

Ultrashort Pulses

So far in this book we considered the propagation of continuous-wave (cw) laser beams, which correspond to time-harmonic solutions of Maxwell's equations. This led to stationary models, such as the NLS or the NLH, in which there is no temporal dynamics. When the laser emits a pulse with a finite-time duration, however, the electric field is no longer time-harmonic, and so the propagation is no longer stationary. Typically, temporal effects are negligible for nanosecond or longer pulses. For picosecond or shorter pulses, however, temporal effects can become important.

35.1 Derivation from Maxwell's Equations

In Chap. 1 we saw that Maxwell's equation for the electric field is

$$\Delta_{x,y,z} \vec{\mathcal{E}}(t, x, y, z) - \nabla(\nabla \cdot \vec{\mathcal{E}}) = \mu_0 \frac{\partial^2 \vec{\mathcal{D}}}{\partial t^2},$$

see (1.3). Under the approximation that the electric field is linearly polarized, this equation becomes

$$\Delta_{x,y,z} \mathcal{E}(t, x, y, z) = \mu_0 \frac{\partial^2 \mathcal{D}}{\partial t^2}.$$

Since $\mathcal{D} = \epsilon_0 \mathcal{E} + \mathcal{P}_{\text{lin}} + \mathcal{P}_{\text{nl}}$, see (1.27), and

$$\epsilon_0 \mu_0 = \frac{1}{c^2}, \quad (35.1)$$

we have that

$$\Delta_{x,y,z} \mathcal{E}(t, x, y, z) = \frac{1}{c^2} \frac{\partial^2 (\mathcal{E} + \epsilon_0^{-1} \mathcal{P}_{\text{lin}})}{\partial t^2} + \mu_0 \frac{\partial^2 \mathcal{P}_{\text{nl}}}{\partial t^2}. \quad (35.2)$$

Let $\hat{\mathcal{E}} = \mathcal{F}(\mathcal{E})$ be the Fourier transform in time of \mathcal{E} , i.e.,

$$\hat{\mathcal{E}}(\omega, x, y, z) = \mathcal{F}(\mathcal{E}) = \frac{1}{\sqrt{2\pi}} \int_{-\infty}^{\infty} \mathcal{E}(t, x, y, z) e^{i\omega t} dt,$$

and let $\mathcal{E} = \mathcal{F}^{-1}(\hat{\mathcal{E}})$ be the inverse Fourier transform, i.e.,

$$\mathcal{E}(t, x, y, z) = \mathcal{F}^{-1}(\hat{\mathcal{E}}) = \frac{1}{\sqrt{2\pi}} \int_{-\infty}^{\infty} \hat{\mathcal{E}}(\omega, x, y, z) e^{-i\omega t} d\omega.$$

Similarly, let $\hat{\mathcal{P}}_{\text{lin}}$ and $\hat{\mathcal{P}}_{\text{nl}}$ be the Fourier transforms of \mathcal{P}_{lin} and \mathcal{P}_{nl} , respectively. Since

$$\hat{\mathcal{E}} + \epsilon_0^{-1} \hat{\mathcal{P}}_{\text{lin}} = n_0^2(\omega) \hat{\mathcal{E}}, \quad (35.3)$$

see Sect. 1.4, the Fourier transform of Eq.(35.2) reads¹

$$\Delta_{x,y,z} \hat{\mathcal{E}}(\omega, x, y, z) + k^2 \hat{\mathcal{E}} + \mu_0 \omega^2 \hat{\mathcal{P}}_{\text{nl}} = 0, \quad k^2(\omega) = \frac{\omega^2 n_0^2(\omega)}{c^2}. \quad (35.4)$$

35.1.1 Dispersion

Consider for a moment the case where $\mathcal{P}_{\text{nl}} \equiv 0$ and n_0 is independent of ω . Then Eq.(35.4) reads

$$\Delta_{x,y,z} \hat{\mathcal{E}} + \frac{\omega^2 n_0^2}{c^2} \hat{\mathcal{E}} = 0.$$

Taking the inverse Fourier transform, one obtains the wave equation

$$\mathcal{E}_{tt}(t, x, y, z) = \frac{c^2}{n_0^2} \Delta_{x,y,z} \mathcal{E}. \quad (35.5)$$

This equation admits the plane-wave solution²

$$\mathcal{E} = E_c e^{-i\omega_0 t + ik_0 z} + \text{c.c.}, \quad k_0 = \frac{\omega_0 n_0}{c} \quad (35.6)$$

which propagates in the positive z -direction. More generally, (35.5) admits solutions of the form

$$\mathcal{E}(t, z) = G(t^*), \quad t^* = t - \frac{z}{c/n_0}. \quad (35.7)$$

¹ The index of refraction is defined in frequency space. Therefore, we substitute relation (35.3) after we take the Fourier transform of Eq.(35.2).

² Since solutions of Maxwell's equation are real, we add the complex-conjugate term.

These solutions travel in the positive z -direction at the velocity $v = c/n_0$ without changing their shape.

When n_0 varies with ω , different frequencies travel at different phase velocities

$$v_{\text{phase}}(\omega) := \frac{\omega}{k(\omega)} = \frac{c}{n_0(\omega)}.$$

As a result, the solution shape is not preserved during propagation, a phenomenon known as *dispersion*.

35.1.2 Slowly-Varying Envelope Approximation

Motivated by the plane-wave solution (35.6), we look for solutions of (35.2) of the form

$$\mathcal{E}(t, x, y, z) = A(t, x, y, z)e^{-i\omega_0 t + ik_0 z} + \text{c.c.}, \quad (35.8)$$

where the amplitude is slowly varying in z and t , compared with the carrier oscillations, i.e.,

$$A_z \ll k_0 A, \quad A_t \ll \omega_0 A. \quad (35.9)$$

We thus look for solutions of (35.4) which are the Fourier transform of expression (35.8), i.e.,

$$\begin{aligned} \hat{\mathcal{E}} &= \mathcal{F}(A(t, x, y, z)e^{-i\omega_0 t + ik_0 z} + \text{c.c.}) \\ &= \hat{A}(\omega - \omega_0, x, y, z)e^{ik_0 z} + \hat{A}^*(\omega + \omega_0, x, y, z)e^{-ik_0 z}. \end{aligned} \quad (35.10)$$

Let us denote by T_0 and $\Delta\omega$ the temporal and spectral widths of A , respectively. For example, a possible definition is

$$T_0 := \sqrt{\frac{\int |t|^2 |A(t, 0)|^2 dt}{\int |A(t, 0)|^2 dt}}, \quad \Delta\omega := \sqrt{\frac{\int |\omega|^2 |\hat{A}(\omega, 0)|^2 d\omega}{\int |\hat{A}(\omega, 0)|^2 d\omega}}.$$

By the uncertainty principle, see (7.21),

$$T_0 \Delta\omega \geq \frac{1}{4}. \quad (35.11a)$$

In addition, since A is slowly varying in t , see (35.9), then

$$\Delta\omega \ll \omega_0. \quad (35.11b)$$

In other words, $\hat{A}(\omega - \omega_0, \cdot)$ is localized at $\omega - \omega_0 = O(\Delta\omega) \ll \omega_0$.

Let us define the dimensionless parameter

$$\delta := \frac{1}{T_0 \omega_0}.$$

By (35.11),

$$\frac{1}{T_0 \omega_0} \ll \frac{1}{T_0 \Delta\omega} \leq 4.$$

We thus see that if A is slowly varying in t , then

$$0 < \delta \ll 1.$$

Let us also decompose the nonlinear polarization field as

$$\mathcal{P}_{\text{nl}}(t, x, y, z) = p_{\text{nl}}(t, x, y, z)e^{-i\omega_0 t + ik_0 z} + \text{c.c..} \quad (35.12)$$

Then

$$\hat{\mathcal{P}}_{\text{nl}} = \hat{p}_{\text{nl}}(\omega - \omega_0, x, y, z)e^{ik_0 z} + \widehat{p}_{\text{nl}}^*(\omega + \omega_0, x, y, z)e^{-ik_0 z}. \quad (35.13)$$

If we substitute (35.10) and (35.13) in (35.4), we get that

$$\begin{aligned} & e^{ik_0 z} \left\{ \hat{A}_{zz}(\omega - \omega_0) + 2ik_0 \hat{A}_z + \Delta_{x,y} \hat{A} + (k^2 - k_0^2) \hat{A} + \mu_0 \omega^2 \hat{p}_{\text{nl}}(\omega - \omega_0) \right\} \\ & + e^{-ik_0 z} \left\{ \widehat{A}_{zz}^*(\omega + \omega_0) - 2ik_0 \widehat{A}_z^* + \Delta_{x,y} \widehat{A}^* + (k^2 - k_0^2) \widehat{A}^* + \mu_0 \omega^2 \widehat{p}_{\text{nl}}^*(\omega + \omega_0) \right\} \\ & = 0. \end{aligned}$$

By Lemma 34.3, the equations for $\hat{A}(\omega - \omega_0)$ and $\widehat{A}^*(\omega + \omega_0)$ can be decoupled with $O(f^2)$ accuracy. Therefore, with $O(f^2)$ accuracy, the equation for \hat{A} is

$$\begin{aligned} & \hat{A}_{zz}(\omega - \omega_0, x, y, z) + 2ik_0 \hat{A}_z + \Delta_{x,y} \hat{A} + (k^2 - k_0^2) \hat{A} \\ & + \mu_0 \omega^2 \hat{p}_{\text{nl}}(\omega - \omega_0, x, y, z) = 0. \end{aligned} \quad (35.14)$$

Since \hat{A} and \hat{p}_{nl} are localized around the carrier frequency ω_0 , we expand k^2 in a Taylor series around ω_0 , i.e.,

$$k^2(\omega) = \sum_{m=0}^{\infty} \alpha_m (\omega - \omega_0)^m, \quad \alpha_m = \frac{1}{m!} \frac{d^m(k^2)}{d\omega^m} \Big|_{\omega_0}.$$

Since $k = \omega n_0(\omega)/c$, see (35.4),

$$k^2(\omega) - k_0^2 = \frac{2k_0}{c_g} (\omega - \omega_0) + \left(\frac{1}{c_g^2} + k_0 k_0'' \right) (\omega - \omega_0)^2 + \sum_{m=3}^{\infty} \alpha_m (\omega - \omega_0)^m, \quad (35.15a)$$

where $c_g := 1/k'(\omega_0)$ and $k_0'' := k''(\omega_0)$ are *group velocity* and *group-velocity dispersion* (GVD), respectively.³ Similarly, we expand ω^2 around ω_0 as

$$\omega^2 = (\omega_0 + (\omega - \omega_0))^2 = \omega_0^2 \left(1 + \frac{1}{\omega_0}(\omega - \omega_0)\right)^2. \quad (35.15b)$$

Substituting (35.15) in (35.14) and transforming back gives⁴

$$\begin{aligned} A_{zz}(z, x, y, t) + 2ik_0 A_z + \Delta_{x,y} A + i \frac{2k_0}{c_g} A_t - \left(\frac{1}{c_g^2} + k_0 k_0''\right) A_{tt} \\ + \sum_{m=3}^{\infty} \alpha_m \left(i \frac{\partial}{\partial t}\right)^m A + \mu_0 \omega_0^2 \left(1 + \frac{i}{\omega_0} \frac{\partial}{\partial t}\right)^2 p_{nl} = 0. \end{aligned} \quad (35.16)$$

35.1.3 Moving-Frame Coordinate System

In the dispersionless case $n_0(\omega) \equiv n_0$ we have that $dk/d\omega = n_0/c$. Hence,

$$c_g = \frac{c}{n_0}. \quad (35.17)$$

Therefore, the linear dispersionless solution (35.7) can be written as

$$\mathcal{E}(t, z) = G(t^*), \quad t^* = t - \frac{z}{c_g}.$$

The dispersionless solution depends on z and t only through the *retarded time* t^* . Once dispersion is added, however, this no longer holds. Nevertheless, when the solution is localized around a carrier frequency ω_0 which is in the transparency spectrum, the phase velocities of “most frequencies” are “nearly” the same, see Sect. 35.2, and so the solution dependence on z and t is “predominantly” through t^* . This suggests that we change to the *moving-frame coordinate system*

$$z^* = z, \quad t^* = t - \frac{z}{c_g}. \quad (35.18)$$

³ The reason we write separately the terms for $m = 1$ and $m = 2$ in (35.15a) will become clear once we change to the moving-frame coordinate system (35.18).

⁴ Since $A(t, \cdot) = (2\pi)^{-\frac{1}{2}} \int \hat{A}(\omega - \omega_0, \cdot) e^{-i(\omega - \omega_0)t} d\omega$, we have that

$$\mathcal{F}^{-1} \left((\omega - \omega_0)^n \hat{A}(\omega - \omega_0, \cdot) \right) = \left(i \frac{\partial}{\partial t} \right)^n A,$$

and similarly for p_{nl} .

Since

$$\frac{\partial}{\partial t} = \frac{\partial}{\partial t^*}, \quad \frac{\partial}{\partial z} = \frac{\partial}{\partial z^*} - \frac{1}{c_g} \frac{\partial}{\partial t^*},$$

we have that

$$\frac{\partial^2}{\partial t^2} = \frac{\partial^2}{\partial t^{*2}}, \quad \frac{\partial^2}{\partial z^2} = \frac{\partial^2}{\partial z^{*2}} - \frac{2}{c_g} \frac{\partial^2}{\partial z^* \partial t^*} + \frac{1}{c_g^2} \frac{\partial^2}{\partial t^{*2}}.$$

Therefore, (35.16) reads⁵

$$\begin{aligned} & A_{z^*z^*}(z^*, x, y, t^*) - \frac{2}{c_g} A_{z^*t^*} + 2ik_0 A_{z^*} + \Delta_{x,y} A - k_0 k_0'' A_{t^*t^*} \\ & + \sum_{m=3}^{\infty} \alpha_m \left(i \frac{\partial}{\partial t^*} \right)^m A + \mu_0 \omega_0^2 \left(1 + \frac{i}{\omega_0} \frac{\partial}{\partial t^*} \right)^2 p_{\text{nl}} = 0. \end{aligned} \quad (35.19)$$

As in the stationary case (Sect. 3.1), we change to the dimensionless spatial variables

$$\tilde{x} = \frac{x}{r_0}, \quad \tilde{y} = \frac{y}{r_0}, \quad \tilde{z} = \frac{z^*}{2L_{\text{diff}}}, \quad (35.20a)$$

where r_0 is the input pulse radius and $L_{\text{diff}} = k_0 r_0^2$ is the diffraction length. We also normalize time by the input pulse duration T_0 , i.e.,

$$\tilde{t} = \frac{t^*}{T_0}. \quad (35.20b)$$

Rewriting (35.19) in the dimensionless variables (35.20) and multiplying by r_0^2 leads to

Proposition 35.1 Consider a linearly-polarized laser pulse that propagates in the positive z -direction. Then the evolution of the pulse amplitude is governed by

$$\begin{aligned} & \frac{1}{4} f^2 A_{\tilde{z}\tilde{z}}(\tilde{t}, \tilde{x}, \tilde{y}, \tilde{z}) - \delta \frac{c/n_0}{c_g} A_{\tilde{z}\tilde{t}} + iA_{\tilde{z}} + \Delta_{\tilde{x}, \tilde{y}} A - \gamma_2 A_{\tilde{t}\tilde{t}} \\ & + \sum_{m=3}^{\infty} \gamma_m \left(i \frac{\partial}{\partial \tilde{t}} \right)^m A + \mu_0 \omega_0^2 r_0^2 \left(1 + i\delta \frac{\partial}{\partial \tilde{t}} \right)^2 p_{\text{nl}} = 0, \end{aligned} \quad (35.21)$$

⁵ In the absence of dispersion we have that $k_0'' = 0$. Hence, the coefficient of the dispersion term in (35.19) vanishes, as it should. This is not the case, however, with Eq. (35.16), thus providing further “support” to the change to the moving-frame coordinate system.

where the moving-frame dimensionless variables are

$$\tilde{t} = \frac{t - z/c_g}{T_0}, \quad \tilde{x} = \frac{x}{r_0}, \quad \tilde{y} = \frac{y}{r_0}, \quad \tilde{z} = \frac{z}{2L_{\text{diff}}},$$

and the dimensionless parameters are

$$f = \frac{1}{r_0 k_0}, \quad \delta = \frac{1}{\omega_0 T_0},$$

and

$$\gamma_2 = \frac{r_0^2 k_0 k''_0}{T_0^2}, \quad \gamma_m = \frac{1}{m!} \left. \frac{r_0^2}{T_0^m} \frac{d^m(k^2)}{d\omega^m} \right|_{\omega_0}, \quad m = 3, 4, \dots \quad (35.22)$$

Remark In the derivation of (35.21) from Maxwell's equations we neglected the vectorial nature of the electric field. This approximation amounts to neglecting $O(f^2)$ terms, see (25.7). We also neglected the coupling between the equations for A^* and for \tilde{A}^* . This approximation also amounts to neglecting $O(f^2)$ terms (Lemma 34.3). Therefore, although we retain the $O(f^2)$ nonparaxial term, the accuracy of (35.21) is $O(f^2)$.

35.1.4 Boundary Conditions

Equation (35.16) is solved in the half-space $0 < z < \infty$ and $-\infty < x, y, t < \infty$, subject to a two-way boundary condition at $z = 0$ and a radiation-to-the-right boundary condition at $z = +\infty$ (Sect. 34.7). In particular, the input pulse amplitude $A^{\text{inc}}(z = 0, x, y, t)$ is prescribed for $-\infty < x, y, t < \infty$. Therefore, mathematically, t plays the role of a third spatial variable.

After we change to the moving-frame coordinates, (35.21) is solved in the half-space $0 < \tilde{z} < \infty$ and $-\infty < \tilde{x}, \tilde{y}, \tilde{t} < \infty$. At $\tilde{z} = 0$, the input pulse amplitude $A^{\text{inc}}(\tilde{z} = 0, \tilde{x}, \tilde{y}, \tilde{t}) = A^{\text{inc}}(z = 0, \frac{\tilde{x}}{r_0}, \frac{\tilde{y}}{r_0}, \frac{\tilde{t}}{T_0})$ is prescribed for $-\infty < \tilde{x}, \tilde{y}, \tilde{t} < \infty$. Therefore, \tilde{t} also plays the role of a third spatial variable.

35.1.5 The Slowly-Varying Envelope Parameter $\delta = \frac{1}{T_0 \omega_0}$

In Sect. 1.7 we saw that the nonparaxiality parameter can be written as

$$f = \frac{1}{2\pi} \frac{\lambda}{r_0}.$$

Therefore, f is proportional to the ratio of the spatial period λ and the input pulse radius r_0 . Since the visible spectrum is $0.4 \mu\text{m} \leq \lambda \leq 0.7 \mu\text{m}$, and since the input pulse radius is typically $\gg 1 \mu\text{m}$, the parameter f is small.

The parameter δ is the temporal analogue of f . Indeed, let $T_{\text{carrier}} = 2\pi/\omega_0$ denote the temporal period of the carrier. Then

$$\delta = \frac{1}{2\pi} \frac{T_{\text{carrier}}}{T_0}.$$

Therefore, δ is proportional to the ratio of the temporal period T_{carrier} and the input-pulse duration T_0 . In particular, when $\delta \ll 1$, the envelope is slowly varying in time, compared with the carrier oscillations.⁶

Since

$$\frac{2\pi}{\lambda} = k_0 = \frac{\omega_0 n_0}{c} = \frac{2\pi n_0}{c T_{\text{carrier}}},$$

then $T_{\text{carrier}} = \lambda n_0 / c$. Hence, in the visible spectrum

$$1 \text{ fs} \approx \frac{0.4 \times 10^{-6} \text{ m}}{3 \times 10^8 \text{ m/s}} \leq \frac{T_{\text{carrier}}}{n_0} \leq \frac{0.7 \times 10^{-6} \text{ m}}{3 \times 10^8 \text{ m/s}} \approx 2 \text{ fs}.$$

Therefore, if $T_0 \gg 1 \text{ fs}$, the parameter δ is small, and so the assumption that the pulse amplitude A is slowly varying in time is justified.

35.1.6 Instantaneous Kerr Response

In Sect. 1.4 we saw that the nonlinear Kerr effect can result from various mechanisms, such as molecular orientation, electrostriction, and nonresonant electrons. Each of these mechanisms has a characteristic time-scale. For example, the distortion of the positions of nonresonant electrons occurs on a time scale of 10^{-16} s . Therefore, when $T_0 \gg 10^{-16} \text{ s}$, the nonlinear Kerr response due to nonresonant electrons is effectively instantaneous, and is given by, see (1.26),

$$\mathcal{P}_{\text{nl}} \approx 4\epsilon_0 n_0 n_2 |A|^2 (A e^{-i\omega_0 t + ik_0 z} + \text{c.c.}).$$

Therefore, by (35.12),

$$p_{\text{nl}} \approx 4\epsilon_0 n_0 n_2 |A|^2 A.$$

Substituting this relation in (35.21) and using (35.1) and (35.6) gives

$$\begin{aligned} & \frac{1}{4} f^2 A_{\tilde{z}\tilde{z}} - \delta \frac{c/n_0}{c_g} A_{\tilde{z}\tilde{t}} + i A_{\tilde{z}} + \Delta_{\tilde{x},\tilde{y}} A - \gamma_2 A_{\tilde{t}\tilde{t}} + \sum_{m=3}^{\infty} \gamma_m \left(i \frac{\partial}{\partial \tilde{t}} \right)^m A \\ & + \frac{4n_2}{n_0} r_0^2 k_0^2 \left(1 + i \delta \frac{\partial}{\partial \tilde{t}} \right)^2 |A|^2 A = 0. \end{aligned} \quad (35.23)$$

⁶ We already reached this conclusion in Sect. 35.1.2.

Let us rescale the amplitude as $A = \left(\frac{4n_2}{n_0} r_0^2 k_0^2\right)^{-\frac{1}{2}} \psi$. Then the equation for ψ reads

$$\begin{aligned} & \frac{1}{4} f^2 \psi_{\tilde{z}\tilde{z}} (\tilde{t}, \tilde{x}, \tilde{y}, \tilde{z}) - \delta \frac{c/n_0}{c_g} \psi_{\tilde{z}\tilde{t}} + i \psi_{\tilde{z}} + \Delta_{\tilde{x}, \tilde{y}} \psi - \gamma_2 \psi_{\tilde{t}\tilde{t}} \\ & + \sum_{m=3}^{\infty} \gamma_m \left(i \frac{\partial}{\partial \tilde{t}} \right)^m \psi + \left(1 + i \delta \frac{\partial}{\partial \tilde{t}} \right)^2 |\psi|^2 \psi = 0. \end{aligned} \quad (35.24)$$

35.2 Dispersion and Transparency

Experimental measurements of the linear index of refraction of transparent materials, such as water [214] and silica [163], show that when ω is in the transparency spectrum,⁷ $n_0(\omega)$ is nearly independent on ω , i.e.,

$$\omega \frac{dn_0}{d\omega} \ll n_0. \quad (35.25)$$

For example, for water in the visible spectrum we have that [63]

$$\omega \frac{dn_0}{d\omega} \approx 0.03. \quad (35.26)$$

The fact that *small dispersion goes hand in hand with small absorption* (and that no dispersion goes hand in hand with no absorption) can also be established theoretically. Indeed, the exact Kramers-Kronig relations and the approximate Sellmeier formula imply that changes in $n_0(\omega)$ mainly occur near resonant frequencies. Since, by definition, there are no resonant frequencies in the transparency spectrum, changes in $n_0(\omega)$ in the transparency spectrum are small. For more details, see, e.g., [30, 134].

By (35.25),

$$\frac{1}{c_g} = \frac{dk}{d\omega} = \frac{d}{d\omega} \frac{\omega n_0}{c} = \frac{1}{c} \left(n_0 + \omega \frac{dn_0}{d\omega} \right) \approx \frac{n_0}{c}.$$

Hence, in the transparency spectrum we can make the approximation

$$\frac{c/n_0}{c_g} \approx 1. \quad (35.27)$$

⁷ i.e., when $\text{Im}(n_0^2(\omega)) \ll \text{Re}(n_0^2(\omega))$, see Sect. 33.1.1.

Indeed, this relation follows by continuity from the dispersionless relation $\frac{c/n_0}{c_g} = 1$, see (35.17). Similarly, by (35.22), in the dispersionless case we have that $\gamma_m \equiv 0$ for $m \geq 2$. Therefore, “by continuity”, if the carrier frequency ω_0 is in the transparency spectrum, then $\{\gamma_m\}_{m \geq 2}$ are “small”.

Typically, when γ_2 is small, the effects of third- and higher-order dispersion can be neglected. If we also use approximation (35.27) and neglect $O(\delta^2)$ terms, (35.24) reduces to

$$\begin{aligned} i\psi_{\tilde{z}}(\tilde{z}, \tilde{x}, \tilde{y}, \tilde{t}) + \Delta_{\tilde{x}, \tilde{y}}\psi + |\psi|^2\psi \\ + \frac{f^2}{4}\psi_{\tilde{z}\tilde{z}} - \delta\psi_{\tilde{z}\tilde{t}} + 2i\delta\frac{\partial}{\partial\tilde{t}}(|\psi|^2\psi) - \gamma_2\psi_{\tilde{t}\tilde{t}} = 0. \end{aligned} \quad (35.28)$$

35.3 Models for Propagation of Ultrashort Pulses

Equation (35.28) can be viewed as the NLS with four perturbation terms: Nonparaxiality ($\psi_{\tilde{z}\tilde{z}}$), the mixed term $\psi_{\tilde{z}\tilde{t}}$, the *shock term* $i\frac{\partial}{\partial\tilde{t}}(|\psi|^2\psi)$, and dispersion ($\psi_{\tilde{t}\tilde{t}}$). The magnitudes of these terms are

$$\frac{f^2}{4} = \frac{1}{4r_0^2k_0^2}, \quad \delta = \frac{1}{\omega_0 T_0}, \quad \delta = \frac{1}{\omega_0 T_0}, \quad \gamma_2 = \frac{r_0^2 k_0 k_0''}{T_0^2},$$

respectively. Since $\gamma_2 \sim T_0^{-2}$, $\delta \sim T_0^{-1}$, and f^2 is independent of T_0 , for sufficiently short pulses we have that $f^2 \ll \delta \ll |\gamma_2|$. In that case (35.28) reduces to⁸

$$i\psi_{\tilde{z}}(\tilde{t}, \tilde{x}, \tilde{y}, \tilde{z}) + \Delta_{\tilde{x}, \tilde{y}}\psi + |\psi|^2\psi - \gamma_2\psi_{\tilde{t}\tilde{t}} = 0, \quad (35.29)$$

which is the *canonical equation for propagation of ultrashort pulses*. This equation is analyzed in Chaps. 36 and 37.

When the $O(\delta)$ terms are also retained, the propagation is governed by

$$i\psi_{\tilde{z}}(\tilde{t}, \tilde{x}, \tilde{y}, \tilde{z}) + \Delta_{\tilde{x}, \tilde{y}}\psi + |\psi|^2\psi - \delta\psi_{\tilde{z}\tilde{t}} + 2i\delta\frac{\partial}{\partial\tilde{t}}(|\psi|^2\psi) - \gamma_2\psi_{\tilde{t}\tilde{t}} = 0. \quad (35.30)$$

We can rewrite this equation as

$$i\left(1 + i\delta\frac{\partial}{\partial\tilde{t}}\right)\psi_{\tilde{z}}(\tilde{t}, \tilde{x}, \tilde{y}, \tilde{z}) + \Delta_{\tilde{x}, \tilde{y}}\psi + |\psi|^2\psi + 2i\delta\frac{\partial}{\partial\tilde{t}}(|\psi|^2\psi) - \gamma_2\psi_{\tilde{t}\tilde{t}} = 0.$$

⁸ Note that T_0 should also be “sufficiently long” (i.e., $T_0 \gg 1/\omega_0$) so that $\delta \ll 1$.

Applying the operator $\left(1 + i\delta \frac{\partial}{\partial \tilde{t}}\right)^{-1} = 1 - i\delta \frac{\partial}{\partial \tilde{t}} + O(\delta^2)$ to this equation and neglecting $O(\delta^2)$ and $O(\delta\gamma_2)$ terms, we get

$$i\psi_{\tilde{z}}(\tilde{t}, \tilde{x}, \tilde{y}, \tilde{z}) + \Delta_{\tilde{x}, \tilde{y}}\psi + |\psi|^2\psi - i\delta\Delta_{\tilde{x}, \tilde{y}}\psi_{\tilde{t}} + i\delta \frac{\partial}{\partial \tilde{t}}(|\psi|^2\psi) - \gamma_2\psi_{\tilde{t}\tilde{t}} = 0. \quad (35.31)$$

The combined effects of dispersion and the $O(\delta)$ terms are considered in Sect. 36.9.

The parameter δ is proportional to the geometric mean of $\frac{f^2}{4}$ and γ_2 , i.e.,

$$\delta^2 = \frac{f^2}{4} |\gamma_2| H, \quad H := \frac{4k_0}{\omega_0^2 |k_0''|}.$$

Lemma 35.1 ([91]) *In the visible spectrum, $H \gg 1$.*

Proof Since $k = \omega n_0(\omega)/c$, then $k''(\omega) = (2n'_0 + \omega n''_0)/c$. Similarly to relation (35.25), since n_0 is hardly changing in the transparency spectrum, $\omega n''_0 \ll n'_0$. Therefore, $k''_0 \sim 2n'_0/c$, and so

$$H \sim \frac{2n_0}{|\omega n'_0(\omega)|} \gg 1. \quad (35.32) \quad \square$$

For example, by (35.26) and (35.32), in the case of water,

$$H \approx \frac{2 \cdot 1.33}{0.03} \approx 90.$$

Following Fibich and Papanicolaou [91], let $T_b := 2L_{\text{diff}}\sqrt{k_0|k_0''|}$ denote the pulse duration for which dispersion and nonparaxiality are of equal magnitudes, i.e., for which $\frac{f^2}{4} = |\gamma_2|$. We have the following cases:

- When $T_0 \gg T_b\sqrt{H} = \frac{4}{f^2\omega_0}$, then $|\gamma_2| \ll \delta \ll f^2$. Therefore, (35.28) reduces to

$$i\psi_{\tilde{z}}(\tilde{t}, \tilde{x}, \tilde{y}, \tilde{z}) + \Delta_{\tilde{x}, \tilde{y}}\psi + |\psi|^2\psi + \frac{1}{4}f^2\psi_{\tilde{z}\tilde{z}} = 0.$$

Thus, when the pulse is sufficiently long, temporal effects are negligible compared with nonparaxiality.

- When $T_0 \approx T_b\sqrt{H} = \frac{4}{f^2\omega_0}$, then $f^2 \approx \delta \gg |\gamma_2|$. Therefore, (35.28) reduces to

$$i\psi_{\tilde{z}}(\tilde{t}, \tilde{x}, \tilde{y}, \tilde{z}) + \Delta_{\tilde{x}, \tilde{y}}\psi + |\psi|^2\psi + \frac{1}{4}f^2\psi_{\tilde{z}\tilde{z}} - \delta\psi_{\tilde{z}\tilde{t}} + 2i\delta\frac{\partial}{\partial\tilde{t}}(|\psi|^2\psi) = 0.$$

3. When $T_0 \approx T_b = 2L_{\text{diff}}\sqrt{k_0|k_0''|}$, then $f^2 \approx |\gamma_2| \ll \delta$. Therefore, (35.28) reduces to

$$i\psi_{\tilde{z}}(\tilde{t}, \tilde{x}, \tilde{y}, \tilde{z}) + \Delta_{\tilde{x}, \tilde{y}}\psi + |\psi|^2\psi - \delta\psi_{\tilde{z}\tilde{t}} + 2i\delta\frac{\partial}{\partial\tilde{t}}(|\psi|^2\psi) = 0.$$

4. When $T_0 \approx \frac{T_b}{\sqrt{H}} = L_{\text{diff}}\omega_0|k_0''|$, then $|\gamma_2| \approx \delta \gg f^2$. Therefore, (35.28) reduces to (35.30) or (35.31).
5. When $T_0 \ll \frac{T_b}{\sqrt{H}} = L_{\text{diff}}\omega_0|k_0''|$, then $f^2 \ll \delta \ll |\gamma_2|$. Therefore, when the pulse is sufficiently short, (35.28) reduces to (35.29).

In most studies, the $O(\delta)$ mixed term and shock term are assumed to be negligible. In the visible spectrum, however, they can dominate both nonparaxiality and dispersion, see Case 3 above. In particular, *it is inconsistent to include nonparaxiality and dispersion without retaining also the mixed term and shock term* [91].

Chapter 36

Normal and Anomalous Dispersion

In Chap. 35 we saw that the canonical model for propagation of ultrashort laser pulses in a Kerr medium is the NLS with temporal dispersion

$$i\psi_z(z, x, y, t) + \Delta\psi - \gamma_2\psi_{tt} + |\psi|^2\psi = 0, \quad \Delta = \frac{\partial^2}{\partial x^2} + \frac{\partial^2}{\partial y^2}, \quad (36.1)$$

where

$$\gamma_2 = \frac{r_0^2 k_0 k_0''}{T_0^2}, \quad (36.2)$$

see (35.29) and (35.22), respectively. In this chapter we analyze the effect of dispersion on self-focusing pulses.

36.1 Initial Conditions

The NLS (36.1) is an initial value problem in z , in which the moving-frame (*retarded time*) variable t plays the role of a third spatial coordinate (Sect. 35.1.4). Therefore, Eq. (36.1) is solved for $0 < z < \infty$ and $-\infty < x, y, t < \infty$, subject to the initial condition

$$\psi(z = 0, x, y, t) = \psi_0(x, y, t), \quad -\infty < x, y, t < \infty,$$

where $\psi_0(x, y, t)$ is the slowly-varying envelope of the input pulse at $z = 0$.

36.2 Linear Dispersive Propagation

If we neglect diffraction and nonlinearity, Eq. (36.1) reduces to the linear Schrödinger equation

$$i\psi_z(z, t) - \gamma_2\psi_{tt} = 0. \quad (36.3)$$

We now briefly discuss this equation.

36.2.1 Dispersion Length (L_{disp})

If we go back to the dimensional variables $z \rightarrow 2L_{\text{diff}}z$ and $t \rightarrow T_0t$, see Sect. 35.1.3, (36.3) becomes

$$2ik_0\psi_z - k_0k_0''\psi_{tt} = 0.$$

The characteristic distance $[Z]$ at which dispersion becomes important can be found from the condition that the above two terms are of comparable magnitudes,¹ i.e.,

$$\frac{k_0[\psi]}{[Z]} = \frac{k_0k_0''[\psi]}{T_0^2}.$$

Therefore, the *dispersion length* is given by

$$L_{\text{disp}} = \frac{T_0^2}{|k_0''|}.$$

For example, the group-velocity dispersion (GVD) of air is [279]

$$k_0''(\text{air}) \approx 0.2 \text{ f s}^2/\text{cm} = 2 \times 10^{-29} \text{ s}^2/\text{m}.$$

Therefore, the dispersion length of a 100 fs pulse that propagates in air is

$$L_{\text{disp}} = \frac{(100 \text{ f s})^2}{0.2 \text{ f s}^2/\text{cm}} = 5 \times 10^4 \text{ cm} = 0.5 \text{ km}.$$

The GVD of water is three orders of magnitude larger [229]:

$$k_0''(\text{water}) \approx 250 \text{ f s}^2/\text{cm} = 2.5 \times 10^{-26} \text{ s}^2/\text{m}.$$

Therefore, the dispersion length of a 100 fs pulse that propagates in water is three orders of magnitude smaller:

$$L_{\text{disp}} = \frac{(100 \text{ f s})^2}{250 \text{ f s}^2/\text{cm}} = 40 \text{ cm} = 0.4 \text{ m}.$$

¹ In Sect. 2.11 we used a similar argument to calculate the diffraction length L_{diff} .

36.2.2 Dispersion Parameter (γ_2)

In general, the linear refractive index n_0 is an increasing function of the frequency ω_0 , except near resonant frequencies (see, e.g., [134, Sect. 7.5]). This motivates the following definitions:

Definition 36.1 (normal and anomalous dispersion) *Dispersion is called normal when $k''(\omega_0) > 0$ and anomalous when $k''(\omega_0) < 0$.*

The dispersion of air and water in the visible spectrum is always normal. For silica the transparency spectrum is $0.5 \mu\text{m} \leq \lambda \leq 2 \mu\text{m}$, and dispersion is normal for $0.5 \mu\text{m} \leq \lambda < \lambda_D$ and anomalous for $\lambda_D < \lambda \leq 2 \mu\text{m}$, where $\lambda_D \approx 1.3 \mu\text{m}$.

Conclusion 36.1 *The NLS (36.1) with $\gamma_2 > 0$ ($\gamma_2 < 0$) models the propagation of ultrashort pulses in a Kerr medium with normal (anomalous) dispersion.*

Proof By (36.2), γ_2 is positive when dispersion is normal and negative when dispersion is anomalous. \square

The parameter γ_2 is dimensionless, and can be written as

$$\gamma_2 = \operatorname{sgn}(k_0'') \frac{L_{\text{diff}}}{L_{\text{disp}}}.$$

Therefore, $|\gamma_2| \ll 1$ if and only if $L_{\text{diff}} \ll L_{\text{disp}}$, i.e., diffraction dominates over dispersion. Similarly, $|\gamma_2| \gg 1$ if and only if $L_{\text{diff}} \gg L_{\text{disp}}$, i.e., dispersion dominates over diffraction.

For example, consider a 100 fs input pulse with $r_0 = 1 \text{ mm}$ and $\lambda = 0.5 \mu\text{m}$. Then the diffraction length is

$$L_{\text{diff}} = r_0^2 k_0 = r_0^2 \frac{2\pi}{\lambda} = (1 \text{ mm})^2 \frac{2\pi}{0.5 \mu\text{m}} = 4\pi \text{ m} \approx 13 \text{ m}.$$

This value is considerably smaller than the dispersion length in air, but considerably larger than the dispersion length in water (Sect. 36.2.1). Therefore, γ_2 is small in the first case and large in the second case.

36.2.3 Temporal Broadening

Consider Eq.(36.3) with $\psi(z = 0, t) = e^{-t^2}$. By Lemma 2.13, the solution is given by

$$\psi(z, t) = \frac{1}{(1 - 4i\gamma_2 z)^{\frac{1}{2}}} e^{-\frac{t^2}{1 - 4i\gamma_2 z}}. \quad (36.4)$$

Since

$$|\psi| = \frac{1}{L^{\frac{1}{2}}(z)} e^{-\frac{t^2}{L^2(z)}}, \quad L(z) = \sqrt{1 + 16\gamma_2^2 z^2},$$

we see that dispersion leads to temporal broadening. The broadening rate depends on the absolute value of γ_2 , but not on its sign.

36.2.4 Chirping

We now add a quadratic temporal phase to the initial condition. Thus, we consider

$$i\psi_z(z, t) - \gamma_2\psi_{tt} = 0, \quad \psi(z=0, t) = e^{-t^2} e^{-iCt^2}. \quad (36.5)$$

In optics, an input pulse is called *negatively chirped* when $C < 0$, and *positively chirped* when $C > 0$. The solution of (36.5) is, see Lemma 2.13,

$$\psi(z, t) = \frac{1}{(1 - 4i\gamma_2 z(1 + iC))^{\frac{1}{2}}} e^{-\frac{t^2}{1 - 4i\gamma_2 z(1 + iC)}}.$$

Since

$$|\psi| = \frac{1}{L^{\frac{1}{2}}(z)} e^{-\frac{t^2}{L^2(z)}}, \quad L(z) = \sqrt{(1 + 4C\gamma_2 z)^2 + 16\gamma_2^2 z^2},$$

we see that chirping leads to temporal focusing when $C\gamma_2 < 0$, and to temporal defocusing when $C\gamma_2 > 0$.

The focusing/defocusing effect of chirping is not unique to Gaussian pulses. Indeed, the chirp term e^{-iCt^2} is the temporal analog of the spatial phase term $e^{-\frac{i x^2}{4F}}$ with $C = \frac{1}{4F}$. Therefore, the analogy between the spatial Schrödinger equation $i\psi_z(z, x) + \psi_{xx} = 0$ and the temporal Schrödinger equation (36.5) with anomalous dispersion shows that in the anomalous regime, positive chirping is focusing and negative chirping is defocusing. If we take the complex conjugate of (36.5), the signs of γ_2 and C are reversed. Since ψ focuses (defocuses) if and only ψ^* focuses (defocuses), we conclude that in the normal regime, positive chirping leads to temporal defocusing and negative chirping to temporal focusing.

36.3 Temporal Solitons

We now consider the combined effects of dispersion and nonlinearity (but still neglect diffraction). In that case, (36.1) reduces to

$$i\psi_z(z, t) - \gamma_2\psi_{tt} + |\psi|^2\psi = 0. \quad (36.6)$$

Since $\sigma = d = 1$, this NLS is subcritical. Therefore, regardless of the sign of γ_2 , all its solutions exist globally. Equation (36.6) received a lot of attention, because it is the canonical equation for propagation of laser pulses in nonlinear optical fibers, and because it is *integrable*.

The qualitative effects of dispersion and nonlinearity can be found using the informal arguments of Sect. 5.9. Thus,

- Dispersion is always defocusing.²
- When dispersion is normal, it has “the same sign” as nonlinearity, and so nonlinearity is also defocusing. Therefore, (36.6) with $\gamma_2 > 0$ is the *defocusing* one-dimensional cubic NLS.
- When dispersion is anomalous, it has “the opposite sign” to nonlinearity, and so nonlinearity is focusing. Therefore, (36.6) with $\gamma_2 < 0$ is the *focusing* one-dimensional cubic NLS. This equation admits the solitary-wave solution

$$\psi^{\text{solitary}} = e^{iz} R_{\text{1D}} \left(\frac{t}{\sqrt{-\gamma_2}} \right), \quad R_{\text{1D}}(\tau) := \sqrt{2} \operatorname{sech}(\tau),$$

where R_{1D} is the solution of $R'' - R + R^3 = 0$, see (6.38). This solitary wave is called a *temporal soliton*, and it plays a key role in nonlinear fiber optics [2].

36.4 Invariance

We now return to the NLS (36.1). This equation preserves the L^2 norm, i.e.,

$$E(z) := \int |\psi(z, x, y, t)|^2 dx dy dt \equiv \int |\psi_0(x, y, t)|^2 dx dy dt = E(0). \quad (36.7)$$

Here we denote the L^2 norm by E and not by P , because in optics it corresponds to the *pulse energy* $E(z) = \int P(z, t) dt$, where $P(z, t) = \int |\psi|^2 dx dy$ is the power at the propagation distance z of the t cross-section.³ Since

$$\frac{\partial P(z, t)}{\partial z} = 2\gamma_2 \operatorname{Im} \int \psi^* \psi_{tt} dx dy, \quad (36.8)$$

the power of each t cross-section is generically not conserved in z . In addition, the conserved Hamiltonian of (36.1) is

² We already reached this conclusion in Sect. 36.2.3.

³ i.e., of the two-dimensional plane $(x, y, t \equiv \text{constant})$.

$$\begin{aligned} H(z) &= \int |\nabla_{x,y}\psi(z, x, y, t)|^2 dx dy dt - \gamma_2 \int |\psi_t(z, x, y, t)|^2 dx dy dt \\ &\quad - \frac{1}{2} \int |\psi(z, x, y, t)|^4 dx dy dt \equiv H(0). \end{aligned} \quad (36.9)$$

Exercise 36.1 Prove relations (36.7)–(36.9).

36.5 Solitary Waves

In Exercise 6.4 we proved that the defocusing NLS

$$i\psi_z + \Delta\psi - |\psi|^{2\sigma}\psi = 0$$

does not admit localized solitary waves. Intuitively, this is because in the case of a localized solitary wave, nonlinearity cancels the defocusing effect of diffraction, whereas in the defocusing NLS nonlinearity is also defocusing. Similarly, there are no localized solitary waves when dispersion is normal, because both normal dispersion and nonlinearity are defocusing in the temporal coordinate:

Lemma 36.1 ([25]) *The NLS (36.1) with $\gamma_2 > 0$ does not admit nontrivial localized solitary wave solutions of the form $\psi_\omega^{\text{solitary}} = e^{i\omega z} R_\omega(x, y, t)$.*

Proof Assume, by negation, that there is such a solution. Then R_ω satisfies

$$-\omega R_\omega + \Delta_{x,y} R_\omega - \gamma_2 \frac{\partial^2}{\partial t^2} R_\omega + |R_\omega|^2 R_\omega = 0. \quad (36.10)$$

If we multiply (36.10) by $x \frac{\partial R_\omega^*}{\partial x} + y \frac{\partial R_\omega^*}{\partial y}$, add the complex-conjugate equation, and integrate by parts, we get that

$$\omega \|R_\omega\|_2^2 - \gamma_2 \|\frac{\partial}{\partial t} R_\omega\|_2^2 = \frac{1}{2} \|R_\omega\|_4^4.$$

Similarly, if we multiply (36.10) by $t \frac{\partial R_\omega^*}{\partial t}$, add the complex-conjugate equation, and integrate by parts, we get that

$$\omega \|R_\omega\|_2^2 + \|\nabla_{x,y} R_\omega\|_2^2 + \gamma_2 \|\frac{\partial}{\partial t} R_\omega\|_2^2 = \frac{1}{2} \|R_\omega\|_4^4.$$

Taking the difference of the last two equations gives

$$\|\nabla_{x,y} R_\omega\|_2^2 = -2\gamma_2 \|\frac{\partial}{\partial t} R_\omega\|_2^2.$$

Since $\gamma_2 > 0$, the two sides are of opposite signs, which is a contradiction. \square

36.5.1 Optical Bullets

When dispersion is anomalous, (36.1) admits the localized solitary waves

$$\psi_\omega^{\text{solitary}} = e^{i\omega z} R_\omega(x, y, \tilde{t} = t/\sqrt{-\gamma_2}), \quad (36.11a)$$

where R_ω is the solution of

$$-\omega R_\omega(x, y, \tilde{t}) + \Delta_{x,y,\tilde{t}} R_\omega + |R_\omega|^2 R_\omega = 0. \quad (36.11b)$$

These solitary waves are localized in time and in space. In the nonlinear optics literature, they are sometimes called *optical bullets* [237]. Optical bullets can be extremely useful for applications, since they propagate localized spatiotemporal energy packets over long distances. Unfortunately, because the NLS (36.1) with anomalous dispersion is supercritical, the optical bullets (36.11) are unstable (Theorem 9.3). Stabilization of “optical bullets” is still one of the holy grails of nonlinear optics.

36.6 Initial Propagation Stage ($|\gamma_2| \ll 1$)

When $|\gamma_2| \ll 1$,⁴ the initial propagation stage can be analyzed by setting $\gamma_2 = 0$ in (36.1). Under this approximation, the propagation is governed by the stationary two-dimensional NLS

$$i\psi_z(z, x, y; t) + \Delta_{x,y}\psi + |\psi|^2\psi = 0, \quad \psi(z=0, x, y; t) = \psi_0(x, y; t), \quad (36.12)$$

and so each t cross-section evolves independently of the other t cross-sections. Since each t cross-section has a different initial condition, it collapses at a different propagation distance, which we shall denote by $Z_c(t)$.⁵ Therefore, solutions of (36.12) blowup at the singularity curve $Z_c(t)$ in the (z, t) -plane.

Consider, for example, Eq.(36.12) with $\psi_0 = ce^{-(t-t_m)^2}e^{-x^2-y^2}$. Since the collapse distance of Gaussian initial conditions decreases monotonically with input power (Sect. 27.3), $Z_c(t)$ attains its minimum at t_m . Hence,

$$Z'_c(t_m) = 0, \quad Z''_c(t_m) > 0.$$

We now show that dispersion cannot be neglected in (36.1) all the way up to the singularity curve $Z_c(t)$, by estimating the magnitudes of diffraction, nonlinearity, and the neglected dispersion, for collapsing solutions of the stationary NLS (36.12):

⁴ i.e., when $L_{\text{diff}} \ll L_{\text{disp}}$, see Sect. 36.2.2.

⁵ $Z_c(t) = \infty$ if the t cross-section does not collapse.

Lemma 36.2 Let ψ be a solution of (36.12) that collapses with the $\psi_{R^{(0)}}$ profile at the singularity curve $Z_c(t)$. Then as $z \rightarrow Z_c(t)$,

$$|\psi|^2\psi = O(L^{-3}), \quad \Delta\psi = O(L^{-3}), \quad \psi_{tt} = O(L^{-5}), \quad L \rightarrow 0.$$

Proof The $\psi_{R^{(0)}}$ profile only depends on the distance from the singularity (Chap. 14). Therefore, near the singularity curve $Z_c(t)$, the solution of (36.12) can be approximated by

$$\psi(z, x, y, t) \sim \psi_{R^{(0)}}(z - Z_c(t), x, y) = \frac{1}{L} R^{(0)} \left(\frac{r}{L} \right) e^{i\zeta + i \frac{L_z}{L} \frac{r^2}{4}}, \quad (36.13a)$$

where

$$L = L(z - Z_c(t)) \rightarrow 0, \quad z \rightarrow Z_c(t), \quad (36.13b)$$

and

$$\zeta = \zeta(z - Z_c(t)) \rightarrow \infty, \quad z \rightarrow Z_c(t). \quad (36.13c)$$

Previously we saw that $|\psi_{R^{(0)}}|^2\psi_{R^{(0)}} = O(L^{-3})$ and $\Delta\psi_{R^{(0)}} = O(L^{-3})$, see (31.35). To estimate the magnitude of $\psi_{tt} \sim (\psi_{R^{(0)}})_{tt}$, we note that since $\psi_{R^{(0)}}$ depends on z and t only through $z - Z_c(t)$, we have that $(\psi_{R^{(0)}})_t = -Z'_c(t)(\psi_{R^{(0)}})_z$ and

$$(\psi_{R^{(0)}})_{tt} = -Z''_c(t)(\psi_{R^{(0)}})_z + (Z'_c(t))^2(\psi_{R^{(0)}})_{zz}. \quad (36.14)$$

Since $(\psi_{R^{(0)}})_z = O(L^{-3})$ and $(\psi_{R^{(0)}})_{zz} = O(L^{-5})$, see (34.6), the result follows. \square

Lemma 36.2 shows that the dispersionless solution satisfies

$$\frac{\gamma_2 \psi_{tt}}{|\psi|^2 \psi} \sim \frac{\gamma_2 \psi_{tt}}{\Delta \psi} \sim \frac{\gamma_2}{L^2}. \quad (36.15)$$

Therefore, as $L \rightarrow 0$, the neglected dispersion dominates over nonlinearity and diffraction.

Corollary 36.1 Even when dispersion is initially negligible in (36.1), it cannot be neglected as $z \rightarrow Z_c(t)$.

Relation (36.15) suggests that dispersion becomes important when $L \sim \sqrt{|\gamma_2|}$. In fact, it becomes important at an earlier stage:

Conclusion 36.2 Under the conditions of Lemma 36.2, dispersion becomes important when $L \gg \sqrt{|\gamma_2|}$.

Proof By the *balance of the giants principle* (Conclusion 18.9), dispersion becomes important when

$$\gamma_2 \psi_{tt} \sim \Delta_{x,y} \psi + |\psi|^2 \psi \sim \frac{\beta}{L^3},$$

where $\beta \ll 1$. By Lemma 36.2, $\gamma_2 \psi_{tt} \sim L^{-5}$. Hence, $L \sim \sqrt{\frac{|\gamma_2|}{\beta}} \gg \sqrt{|\gamma_2|}$.⁶ \square

Remark The results in this section are valid for both normal and anomalous dispersion.

36.7 Small Anomalous Dispersion

When dispersion is anomalous, the Kerr nonlinearity is self-focusing both spatially and temporally. Indeed, in the absence of dispersion, (36.1) reduces to the focusing NLS

$$i\psi_z(z, x, y) + \Delta_{x,y}\psi + |\psi|^2\psi = 0.$$

Hence, the Kerr nonlinearity is self-focusing in the spatial (x, y) coordinates. Similarly, in the absence of diffraction, (36.1) reduces to the focusing NLS

$$i\psi_z(z, t) - \gamma_2 \psi_{tt} + |\psi|^2\psi = 0.$$

Hence, the Kerr nonlinearity is self-focusing in the temporal coordinate.

If anomalous dispersion is small ($0 < -\gamma_2 \ll 1$), the solution initially undergoes a two-dimensional spatial collapse in each t cross-section according to the stationary NLS (36.12). Since by Lemma 36.2 dispersion increases faster than diffraction, the temporal compression increases faster than the spatial one.⁷ Therefore, collapse begins as a spatial process, but then evolves into a *spatiotemporal one*.⁸

To find the blowup profile near the singularity, we note that under the rescaling $\tilde{t} = t/\sqrt{-\gamma_2}$, Eq. (36.1) becomes the isotropic three dimensional cubic NLS

$$i\psi_z(z, x, y, \tilde{t}) + \Delta_{x,y,\tilde{t}}\psi + |\psi|^2\psi = 0. \quad (36.16)$$

In Chap. 21 we saw that singular peak-type solutions of (36.16) collapse with the spherical supercritical profile $\psi_Q(z, r)$, where $Q(r; \sigma = 1, d = 3)$ is the admissible solution of the Q equation with $\sigma = 1$ and $d = 3$ (Sect. 12.6). Therefore, singular peak-type solutions of (36.1) with $\gamma_2 < 0$ undergo a spatiotemporal collapse with the profile $\psi_Q(z, \rho)$, where $\rho = \sqrt{x^2 + y^2 + \frac{t^2}{|\gamma_2|}}$.

Since the three-dimensional cubic NLS (36.16) is supercritical, solutions of (36.1) with $0 < -\gamma_2 \ll 1$ initially undergo a critical collapse, but eventually undergo

⁶ In Sect. 36.8.5 we will derive this relation from the reduced equations.

⁷ See Sect. 26.3.2 for why an increase of small dispersion leads to an increase (and not a decrease) of temporal self-focusing.

⁸ The transition from spatial to spatiotemporal collapse is analyzed in Sects. 36.8.4 and 36.8.5 using the reduced equations (36.21).

a supercritical collapse. A similar transition from critical to supercritical collapse occurs for solutions of the critical NLS with a small focusing supercritical nonlinearity (Sect. 32.3.2).⁹

36.7.1 Cigar-Shaped Bose-Einstein Condensates

The dynamics of Bose-Einstein condensates with attractive interactions can be modeled by the NLS/GP

$$i\psi_t(t, x, y, z) + \Delta_{x,y,z}\psi + |\psi|^2\psi = 0,$$

see Sect. 4.2. Let us consider the case where the initial condensate is a cigar-shaped Gaussian, i.e.,

$$\psi(t=0, x, y, z) = ce^{-x^2-y^2-\epsilon^2z^2}, \quad 0 < \epsilon \ll 1.$$

Under the rescaling $\tilde{z} = \epsilon z$, the condensate evolution is governed by

$$i\psi_t(t, x, y, \tilde{z}) + \Delta_{x,y}\psi + \epsilon^2\psi_{\tilde{z}\tilde{z}} + |\psi|^2\psi = 0, \quad \psi(t=0, x, y, \tilde{z}) = ce^{-x^2-y^2-\tilde{z}^2}.$$

This equation is completely analogous to (36.1) with $0 < -\gamma_2 = \epsilon^2 \ll 1$. Therefore, the above analysis shows that the condensate initially undergoes a two-dimensional collapse in each z cross-section according to

$$i\psi_t(t, x, y; \tilde{z}) + \Delta_{x,y}\psi + |\psi|^2\psi = 0, \quad \psi(t=0, x, y, \tilde{z}) = ce^{-x^2-y^2-\tilde{z}^2}.$$

Since the compression increases faster in z than in (x, y) , the condensate approaches a spherical shape and collapses with the ψ_Q profile, where $\psi_Q = \psi_Q(z, \rho)$, $\rho = \sqrt{x^2 + y^2 + z^2}$, and $Q(\rho; \sigma = 1, d = 3)$ is the admissible solution of the Q equation with $\sigma = 1$ and $d = 3$.

36.8 Small Normal Dispersion

Analysis of (36.1) with normal dispersion is considerably more complex than with anomalous dispersion, because of the opposite signs of diffraction and dispersion.

⁹ In the case of (36.16), the transition is from a 2D critical collapse to a 3D supercritical collapse. In the case of the critical NLS with a small focusing supercritical nonlinearity, however, the transition is from a 2D critical collapse to a 2D supercritical collapse.

36.8.1 Failure of Linear Superposition Analysis

When dispersion is normal, the Kerr nonlinearity is self-focusing in the spatial (x, y) coordinates, but self-defocusing in the temporal coordinate. Since the total pulse energy is conserved, see (36.7), temporal self defocusing reduces the peak cross-sectional power. This suggests, therefore, that normal dispersion slows down the spatial collapse. The problem with this informal argument is that we apply a linear superposition approach to a genuinely-nonlinear process. Thus, this approach may hold in some cases but fail in others. In particular, because this linear approach does not capture the delicate balance between nonlinearity and diffraction as the solution collapses with the $\psi_{R^{(0)}}$ profile, it fails to predict the pulse-splitting phenomenon (Sects. 36.8.4).¹⁰

36.8.2 Early Simulations

The first study on the effect of small normal dispersion on collapsing ultrashort pulses was done in 1986 by Zharova et al. [285]. In that study, they used informal arguments to conclude that as the pulse collapses, power flows away from the pulse peak, leading to the arrest of collapse at the peak. As a result, the pulse splits into two peaks, which continue to self-focus. Zharova et al. argued that the new peaks will split again and again, until the power of all peaks will get below the critical power for collapse P_{cr} . Therefore, they concluded that small normal dispersion arrests collapse through multiple splittings. This informal analysis appeared to be supported by their numerical simulations, in which they solved (36.1) with $\gamma_2 = 1$ and $\psi_0 = 4e^{-\frac{x^2+y^2}{2}-\frac{t^2}{32}}$, and observed temporal splitting into two peaks, followed by a second temporal splitting into four peaks.¹¹

The pulse splitting phenomenon was rediscovered in 1992 by Rothenberg [224] and by Chernev and Petrov [44]. In these studies, however, a second splitting was not observed numerically.

36.8.3 Reduced Equations

The studies of Zharova et al. [285], Rothenberg [224], and Chernev and Petrov [44], led to the following questions:

¹⁰ See Sects. 3.4.1, 26.3.2, and 30.4 for other failures of a linear superposition approach for the NLS.

¹¹ The second splitting turned out to be a numerical artifact (Sect. 36.8.8).

1. What is the mechanism that leads to pulse splitting?
2. Will the two peaks split again? And again?
3. For initial conditions $\psi_0(x, y, t)$ that lead to collapse in the stationary NLS (36.12), will collapse be arrested by small normal dispersion?

These questions could not be studied numerically in the early 1990s, because the available numerical solvers broke down shortly after the pulse splitting. To address these questions analytically, Fibich, Malkin, and Papanicolaou derived in 1995 reduced equations for the critical NLS with small dispersion, using an asymptotic approach that later evolved into *modulation theory* (Chap. 31). In what follows, we derive and analyze these reduced equations.

Following the discussion in Sects. 31.1.2 and 36.6, when $|\gamma_2|$ is sufficiently small, the pulse initially undergoes a two-dimensional collapse at each t cross-section. As it approaches the singularity curve $Z_c(t)$ of the stationary NLS (36.12), dispersion grows faster than diffraction and nonlinearity (Lemma 36.2). If γ_2 is sufficiently small, the solution reaches the adiabatic stage of the unperturbed NLS before dispersion starts to affect the self-focusing dynamics. In that case, the solution approaches the $\psi_{R^{(0)}}$ profile, see (36.13), and so the three conditions of modulation theory¹² are satisfied. These conditions remain satisfied as long as dispersion remains smaller than diffraction and nonlinearity, (i.e., $\gamma_2 \psi_{tt} \ll \Delta\psi, |\psi|^2\psi$).

Lemma 36.3 ([88]) Consider (36.1) as a perturbed two-dimensional critical NLS with $F = \psi_{tt}$. Then the auxiliary functions of modulation theory satisfy $(f_1)_z \ll f_2 \sim P_{\text{cr}} \zeta_{tt}$.

Proof Since

$$\psi_{R^{(0)}}(z, r, t) = \frac{R^{(0)}(\rho)}{L(z, t)} e^{iS}, \quad (36.17a)$$

where

$$\rho = \frac{r}{L(z, t)}, \quad S = \zeta + \frac{L_z}{L} \frac{r^2}{4}, \quad \frac{\partial \zeta}{\partial z} = \frac{1}{L^2(z, t)}, \quad (36.17b)$$

we have that

$$\begin{aligned} \text{Im} \left\{ e^{-iS} (\psi_{R^{(0)}})_{tt} \right\} &= 2 \left(\frac{R^{(0)}}{L} \right)_t S_t + \frac{R^{(0)}}{L} S_{tt}, \\ \text{Re} \left\{ e^{-iS} (\psi_{R^{(0)}})_{tt} \right\} &= \left(\frac{R^{(0)}}{L} \right)_{tt} - \frac{R^{(0)}}{L} S_t^2. \end{aligned}$$

¹² See Sect. 31.1.1.

Therefore, by (31.17b),

$$\begin{aligned} f_2(z, t) &= L(z, t) \operatorname{Im} \int (\psi_{R^{(0)}})_{tt} e^{-iS} R^{(0)}(\rho) d\xi d\eta \\ &= L \int \left[2 \left(\frac{R^{(0)}}{L} \right)_t S_t + \frac{R^{(0)}}{L} S_{tt} \right] R^{(0)}(\rho) d\xi d\eta, \end{aligned}$$

where $\xi = x/L$ and $\eta = y/L$. It can be verified that

$$S_t \sim \zeta_t, \quad S_{tt} \sim \zeta_{tt}, \quad (36.18)$$

see Exercise 36.2, and that

$$\left(\frac{R^{(0)}}{L} \right)_t = \left(\frac{1}{L} \right)_t \frac{d}{d\rho} (\rho R^{(0)}). \quad (36.19)$$

Hence,

$$f_2 \sim L \int \left[2\zeta_t \left(\frac{1}{L} \right)_t \frac{d}{d\rho} (\rho R^{(0)}) + \frac{R^{(0)}}{L} \zeta_{tt} \right] R^{(0)}(\rho) d\xi d\eta = P_{\text{cr}} \zeta_{tt},$$

where in the last stage we used the identity

$$\int \frac{d}{d\rho} (\rho R^{(0)}) R^{(0)} d\xi d\eta = 2\pi \int \frac{d}{d\rho} (\rho R^{(0)}) R^{(0)} \rho d\rho = 0, \quad (36.20)$$

see (34.14). Similarly, by (31.17a),

$$\begin{aligned} f_1(z, t) &= L^3 \operatorname{Re} \int (\psi_{R^{(0)}})_{tt} e^{-iS} \frac{d}{d\rho} (\rho R^{(0)}) d\xi d\eta \\ &= L^3 \int \left[\left(\frac{R^{(0)}}{L} \right)_{tt} - S_t^2 \frac{R^{(0)}}{L} \right] \frac{d}{d\rho} (\rho R^{(0)}) d\xi d\eta. \end{aligned}$$

By Eqs. (36.18) and (36.20),

$$\int S_t^2 \frac{R^{(0)}}{L} \frac{d}{d\rho} (\rho R^{(0)}) d\xi d\eta \sim \frac{\zeta_t^2}{L} \int R^{(0)} \frac{d}{d\rho} (\rho R^{(0)}) d\xi d\eta = 0.$$

Since the contribution of the leading-order term vanishes, we compute the contribution of the next-order term. We have

$$\begin{aligned}
\int S_t^2 \frac{R^{(0)}}{L} \frac{d}{d\rho} (\rho R^{(0)}) d\xi d\eta &= \int \left(\zeta_t + \left(\frac{L_z}{L} \right)_t \frac{r^2}{4} \right)^2 \frac{R^{(0)}}{L} \frac{d}{d\rho} (\rho R^{(0)}) d\xi d\eta \\
&\sim \int 2\zeta_t \left(\frac{L_z}{L} \right)_t \frac{r^2}{4} \frac{R^{(0)}}{L} \frac{d}{d\rho} (\rho R^{(0)}) d\xi d\eta \\
&= \frac{1}{2} \zeta_t L \left(\frac{L_z}{L} \right)_t \int \rho^2 R^{(0)} \frac{d}{d\rho} (\rho R^{(0)}) d\xi d\eta.
\end{aligned}$$

Therefore,

$$[f_1] = \frac{L^2}{[T]^2} + \frac{[\zeta]L^4}{[T]^2[Z]}.$$

To finish the proof, we need to show that

$$[f_2] = [\zeta_{tt}] = \frac{[\zeta]}{[T]^2} \gg \frac{L^2}{[T]^2[Z]} + \frac{[\zeta]L^4}{[T]^2[Z]^2} = [(f_1)_z],$$

i.e., that

$$1 \gg \frac{L^2}{[Z][\zeta]} + \frac{L^4}{[Z]} = \frac{L^2}{[Z]} \left(\frac{1}{[\zeta]} + \frac{L^2}{[Z]} \right).$$

By the β principle (Conclusion 31.1)

$$\frac{L^2}{[Z]} = O(\beta) \ll 1, \quad [\zeta] \gg 1.$$

Hence, the result follows. \square

Exercise 36.2 Use the β principle to show that $S_t \sim \zeta_t$ and $S_{tt} \sim \zeta_{tt}$.

Proposition 36.1 ([88]) The reduced equations for the NLS (36.1) with $|\gamma_2| \ll 1$ are

$$\beta_z(z, t) = \tilde{\gamma}_2 \zeta_{tt}, \quad \tilde{\gamma}_2 := \frac{2P_{\text{cr}}}{M} \gamma_2, \quad (36.21a)$$

$$L_{zz}(z, t) = -\frac{\beta}{L^3}, \quad (36.21b)$$

$$\zeta_z(z, t) = \frac{1}{L^2}. \quad (36.21c)$$

Proof This follows from Proposition 31.5 and Lemma 36.3. \square

Remark The reduced equations (36.21) are different from the ones we saw so far, because they include the modulation variable ζ (and not just L and β), and because the modulation variables L , β , and ζ depend on z and t , and not only on z .¹³

¹³ Therefore, these reduced equations are PDEs and not ODEs. Nevertheless, analysis and simulations of (36.21) are considerably simpler than for the NLS (36.1).

The modulation variables have the following interpretation:

- $L(z, t)$ is the radial width of the t cross-section, and is inversely proportional to its on-axis amplitude.
- $\beta(z, t) = -L^3 L_{zz}$ measures the acceleration of the collapse of the t cross-section. It is also proportional to the excess power above P_{cr} of the collapsing core of the t cross-section, i.e.,

$$\beta(z, t) \sim \frac{P_{\text{coll}}(z, t) - P_{\text{cr}}}{M}, \quad P_{\text{coll}}(z, t) = \int_{|(x,y)| < \rho_c L(z, t)} |\psi|^2 dx dy, \quad (36.22)$$

where $\rho_c = O(1)$ and $M = \frac{1}{4} \int (x^2 + y^2) |R^{(0)}|^2 dx dy$, see Lemma 31.4.

- $\zeta(z, t)$ measures the on-axis phase of the t cross-section, see (36.17). It can also be viewed as its local axial distance.

Note that the reduced equations (36.21) are valid for both normal and anomalous dispersion.

36.8.4 Analysis of Pulse Splitting

The reduced equation (36.21a) can be rewritten as¹⁴

$$\frac{\partial}{\partial z} P_{\text{coll}}(z, t) = 2\gamma_2 P_{\text{cr}} \zeta_{tt}(z, t), \quad (36.23)$$

see (31.43). This equation shows that dispersion leads to power transfer between the collapsing cores of different t cross-sections. Let t_m denote the t cross-section with the maximal input power. Since β is proportional to the excess power above P_{cr} , see (36.22), as long as temporal power transfer is negligible, the maximal value of $\beta(\cdot, t)$ remains at t_m , and so the fastest collapse occurs at t_m , see (36.21b). As a result, $\zeta(\cdot, t)$ attains its maximum at t_m , see (36.21c). Therefore,

$$\zeta_{tt}(z, t_m) < 0. \quad (36.24)$$

Normal Dispersion

When dispersion is normal, then by (36.23) and (36.24),

$$\frac{\partial}{\partial z} P_{\text{coll}}(z, t_m) < 0,$$

¹⁴ Equation (36.23) is the modulation-theory analog of Eq. (36.8).

i.e., the power decreases at t_m . Once the power at t_m gets below P_{cr} , collapse is arrested there. By continuity, collapse is also arrested at nearby t cross-sections. Since the pulse energy is conserved, see (36.7), the power decrease at and near t_m is accompanied by a power increase at the further-away t cross-sections for which $\zeta_{tt} > 0$,¹⁵ see (36.23), resulting in a temporal peak-splitting of the cross-sectional power curve $P(\cdot, t)$. Since the higher the power the faster spatial collapse is, see (36.21b), the temporal splitting of the cross-sectional power leads to a temporal splitting of the width L .

Conclusion 36.3 *Small normal dispersion leads to power radiation from the peak, resulting in peak splitting of the cross-sectional power curve. This, in turn, leads to a temporal splitting of the pulse into two pulses.*

Anomalous Dispersion

When dispersion is anomalous, then by (36.23) and (36.24),

$$\frac{\partial}{\partial z} P_{coll}(z, t_m) > 0.$$

Therefore, the power increases at and near t_m , and decreases at further-away t cross-sections for which $\zeta_{tt} > 0$. As a result, collapse is accelerated at and near t_m and decelerated further away from t_m , resulting in a three-dimensional supercritical spatiotemporal collapse (Sect. 36.7).

36.8.5 Self-similar Analysis

Following Fibich et al. [88], we can further analyze the initial effect of dispersion as follows. As noted, when dispersion is initially negligible, the solution of (36.1) can be approximated by the solution of the stationary NLS (36.12). Near the singularity curve $Z_c(t)$, the on-axis phase of the solution of (36.12) only depends on the distance from the singularity curve, i.e.,

$$\zeta = \zeta(z - Z_c(t)), \quad (36.25)$$

see (36.13c). If γ_2 is sufficiently small, this relation also holds, to leading order, for the solution of (36.1). Hence, $\zeta_t = -Z'_c(t)\zeta_z$,¹⁶

$$\zeta_{tt} = -Z''_c(t)\zeta_z + (Z'_c(t))^2\zeta_{zz}, \quad (36.26)$$

¹⁵ Since $\zeta(\cdot, t)$ assumes its maximum at t_m and since $\lim_{t \rightarrow \pm\infty} \zeta = 0$, there must be t cross-sections for which $\zeta_{tt} > 0$.

¹⁶ Relation (36.26) is the modulation-theory analog of relation (36.14).

and so (36.21a) reads

$$\beta_z = \tilde{\gamma}_2 \left[-Z_c''(t)\zeta_z + (Z_c'(t))^2 \zeta_{zz} \right].$$

Integrating this equation gives

$$\beta(z, t) = \beta_0(t) + \tilde{\gamma}_2 \left[-Z_c''(t)\zeta(z, t) + (Z_c'(t))^2 \frac{1}{L^2(z, t)} \right], \quad (36.27)$$

where

$$\beta_0(t) = \beta(0, t) - \tilde{\gamma}_2 \left[-Z_c''(t)\zeta(0, t) + (Z_c'(t))^2 \frac{1}{L^2(0, t)} \right].$$

As noted, $Z_c(t)$ attains its minimum at t_m , the t cross-section with the maximal input power. Therefore,

$$Z_c'(t_m) = 0, \quad Z_c''(t_m) > 0.$$

By (36.27), the evolution of $\beta(z, t_m)$ is governed by

$$\beta(z, t_m) = \beta_0(t_m) - \tilde{\gamma}_2 Z_c''(t_m) \zeta. \quad (36.28)$$

Since β is proportional to the excess power above P_{cr} , see (36.22), Eq. (36.28) shows that normal dispersion decreases the power of the t_m cross-section, so that it goes below critical at $\zeta = \frac{\beta_0(t_m)}{\tilde{\gamma}_2 Z_c''(t_m)}$. In contrast, since $L^{-2} = \zeta_z \gg \zeta$, Eq. (36.27) shows that for t cross-sections which are not in the near vicinity of t_m , the evolution of the excess power is given by

$$\beta(z, t) \sim \beta_0(t) + \tilde{\gamma}_2 (Z_c'(t))^2 \frac{1}{L^2(z, t)}. \quad (36.29)$$

Hence, normal dispersion increases the power of t cross-sections that are not in the near vicinity of t_m .

Conclusion 36.4 *Small normal dispersion decreases the power at and near t_m , but increases the power of further-away t cross-sections.*

Similar arguments lead to

Conclusion 36.5 *Small anomalous dispersion increases the power at and near t_m , but decreases the power of further-away t cross-sections.*

Both conclusions are in agreement with the analysis in Sect. 36.8.4.

To analyze the effect of these power changes on the dynamics of L , it is convenient to make a change of variable from the pulse width L to the pulse amplitude $A = 1/L$, so that collapse corresponds to $A \rightarrow +\infty$. Since $\beta = A\zeta/A$, see (18.13a), Eq. (36.27) can be rewritten as

$$A_{\zeta\zeta}(\zeta; t) = (\beta_0(t) - \tilde{\gamma}_2 Z_c''(t)\zeta)A + \tilde{\gamma}_2 (Z_c'(t))^2 A^3. \quad (36.30)$$

When $\gamma_2 > 0$, then up to scaling, (36.30) is the second Painlevé transcendent

$$B''(s) = sB + 2B^3.$$

Using a connection result for $B(s)$ of Hastings and McLeod [124], Fibich et al. [88] proved that collapse in (36.30) is only arrested in an exponentially-small neighborhood of t_m .

Equation (36.30) was derived under the assumption that the solution of the reduced equations (36.21) is self-similar, see (36.25). This assumption breaks down, however, as dispersion begins to affect the dynamics.¹⁷ Therefore, the self-similar analysis in this subsection describes the onset of pulse splitting, but its validity for solutions of the reduced equations (36.21), hence for solutions of the NLS (36.1), breaks down “soon afterwards”.¹⁸

Remark Equation (36.29) shows that dispersion becomes important when $\tilde{\gamma}_2(Z'_c(t))^2 \frac{1}{L^2} \sim \beta_0(t)$, i.e., for $L \sim \sqrt{\frac{\beta}{\gamma_2}}$, as was noted in Conclusion 36.2.

36.8.6 Simulations

Figure 36.1 shows the numerical solution of (36.1) with $\gamma_2 = 0.01$ and

$$\psi_0(r, t) = b(t) R^{(0)}(r) e^{-i\sqrt{(b^2(t)-1)\frac{P_{\text{cr}}}{M}}\frac{r^2}{4}}, \quad (36.31)$$

where $b(t) = 1.03 + 0.01 \sin(2\pi t)$ and $R^{(0)}$ is the Townes profile. For technical reasons, in the t coordinate we imposed a periodic boundary condition $\psi(z, r, t = 0) = \psi(z, r, t = 1)$. Initially, the fastest collapse occurs at $t_m = 1/4$, the t cross-section with the maximal input power. At $z_0 = 0.89$ (top row), the peak amplitude is still at t_m , but the power of this cross-section is already below P_{cr} (since $\beta(t_m) < 0$). As a result (second row), collapse is arrested at t_m , and the amplitude also undergoes a temporal splitting. This behavior agrees with Conclusion 36.3 that the temporal splitting of the amplitude is preceded by a temporal splitting of the cross-sectional power.

We also compared numerically the NLS (36.1) with the reduced equations (36.21), as follows. For a given z_0 , we extracted $L(z_0, t)$, $\beta(z_0, t)$, and $\zeta(z_0, t)$ from the NLS solution $\psi(z_0, x, y, t)$. Then, we solved the reduced equations for $z > z_0$, using as initial conditions the extracted values of L , β , and ζ at z_0 . The quantitative agreement

¹⁷ i.e., as the solution of (36.1) bifurcates from that of the stationary NLS (36.12).

¹⁸ For example, as $L \rightarrow 0$, Eqs. (36.21b) and (36.29) reduce to

$$-L^3 L_{zz} = \beta \sim \tilde{\gamma}_2 (Z'_c(t))^2 \frac{1}{L^2}.$$

It can be verified that this equation admits blowup solutions of the form $L \sim c (Z_c - z)^{\frac{1}{3}}$ [88]. For these blowup solutions, however, we have that $\beta \rightarrow \infty$, which implies that the validity of the reduced equations breaks down.

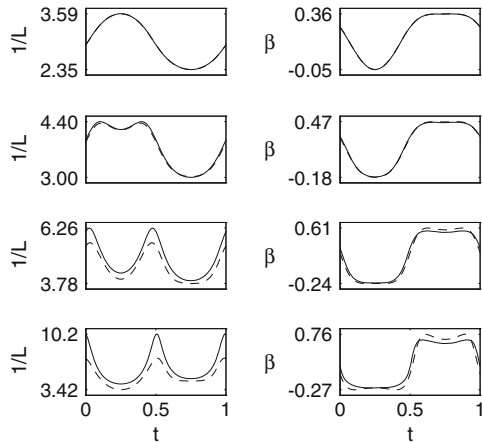


Fig. 36.1 Solution of the NLS (36.1) with $\gamma_2 = 0.01$ and the initial condition (36.31) (dashed curve), at $z_0 = 0.89$ (top row), $z_1 = 0.95$ (second row), $z_2 = 1.00$ (third row), and $z_3 = 1.02$ (bottom row). The solid curve is the corresponding solution of the reduced equations (36.21). Left column: amplitude. Right column: power. From [88]

between the solution of the reduced equation and the NLS solution in Fig. 36.1 provided a strong support to the validity of the reduced equations before and during the pulse splitting.¹⁹

36.8.7 Why only One Splitting?

The analysis of the reduced equations (36.21) in Sects. 36.8.4 and 36.8.5 leads to

Conclusion 36.6 ([88]) *Temporal peak splitting in the NLS (36.1) with small normal dispersion is associated with the transition from a two dimensional self-similar spatial collapse according to the stationary NLS (36.12), to a three-dimensional spatio-temporal dynamics.*

After the splitting, the dynamics becomes fully three dimensional. Therefore, Fibich, Malkin, and Papanicolaou argued that “there is no reason” why the two

¹⁹ Obtaining a quantitative agreement between the NLS (36.1) and the reduced equations turned out to be a nontrivial task. For one thing, the two equations are in agreement only when modulation theory is valid, i.e., after the NLS solution approaches the $\psi_{R^{(0)}}$ profile, but before dispersion becomes comparable to nonlinearity or diffraction. In addition, because modulation theory is only $O(\beta)$ accurate, there is an $O(\beta)$ error in extracting the reduced-equations variables from the NLS solution. To obtain a quantitative agreement, however, this error should be smaller than the temporal variation of the reduced-equations variables. Moreover, the temporal variation of the reduced-equations variables by itself has to be small, since dispersion should be smaller than nonlinearity and diffraction for modulation theory to be valid.

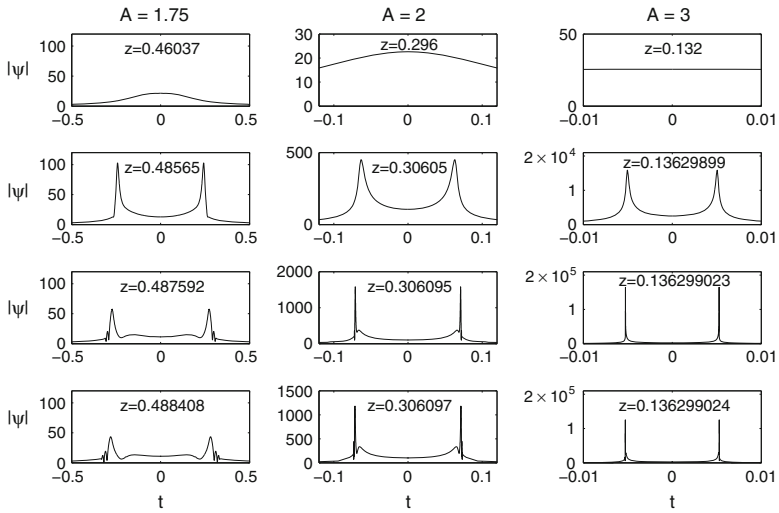


Fig. 36.2 On-axis amplitude $|\psi(z, r = 0, t)|$ of the solution of (36.1) with $\gamma_2 = \frac{1}{32}$ and $\psi_0 = A\sqrt{2}e^{-\frac{x^2+y^2}{2}-t^2}$. Left column: $A = 1.75$. Center column: $A = 2$. Right column: $A = 3$. From [94]

peaks should split again, and conjectured that there is a single peak splitting. This conjecture could not be tested using the reduced equations, because their validity breaks down as the two peaks continue to collapse (Sect. 36.8.9). Testing this conjecture by direct numerical simulations of the NLS (36.1) was not possible at the time, because after the pulse splitting, the two peaks develop very steep temporal gradients (see, e.g., Fig. 36.2). Indeed, continuing the simulation beyond the pulse splitting requires specialized numerical solvers, which were only developed in the early 2000s (Sect. 36.8.8).²⁰

Conclusion 36.6 also implies that solutions of the NLS (36.1) with normal dispersion can self focus without undergoing a peak splitting. This occurs when dispersion is sufficiently large and/or the initial profile is sufficiently far from $\psi_{R^{(0)}}$, so that temporal effects become important before the solution approaches the $\psi_{R^{(0)}}$ profile, thereby “skipping” the two-dimensional self-similar stage.

36.8.8 Post-splitting Simulations

The first solid simulations of the NLS (36.1) beyond the pulse splitting were performed in 2001 by Germaschewski et al. [108] using an adaptive mesh refinement method. These simulations showed that the two peaks do not split again, but rather decay in a “dispersive manner”. Similar results were obtained by Coleman and

²⁰ In fact, the original motivation of Ren and Wang for developing their moving-mesh IGR method (Sect. 29.4.2) was to solve (36.1) beyond the pulse splitting. This goal was achieved in [94].

Sulem [48] using a dynamic mesh refinement method, and by Fibich et al. [94] using the semi-static moving-mesh IGR method of Ren and Wang (Sect. 29.4.2).

Recall that when Zharova et al. [285] computed the solution of (36.1) with $\gamma_2 = 1$ and $\psi_0 = 4e^{-\frac{x^2+y^2}{2}-\frac{t^2}{32}}$, they observed that after the peak splitting, each of the two peaks underwent a second splitting. Although it has been suspected that the second splitting was a numerical artifact due to under-resolution, this specific problem turned out to be computationally challenging. In fact, even the robust solver of Germaschewski et al. [108] could not handle this problem. Eventually, “the Zharova problem” was solved numerically in 2003 by Fibich et al. [94]. This simulation confirmed that there is a single splitting, followed by a dispersive arrest of collapse.

In Fig. 36.2 we present simulations of (36.1) with $\gamma_2 = 1/32$ for three Gaussian initial conditions, whose peak power at $t_m = 0$ is $1.65P_{\text{cr}}$, $2.15P_{\text{cr}}$, and $4.8P_{\text{cr}}$. In all three cases, after the peak splitting, the two peaks continue to focus for some “time”, during which they develop very steep temporal gradients. Eventually, the collapse of the two peaks is arrested, as they decay into small-scale temporal oscillations. The overall arrest of collapse by small normal dispersion can be clearly seen in Fig. 36.3.

Figure 36.4 shows the evolution of the magnitudes of dispersion, nonlinearity, and diffraction. Initially, dispersion is negligible, i.e.,

$$\gamma_2 \psi_{tt} \ll \Delta_{x,y} \psi, |\psi|^2 \psi.$$

Hence, each t cross-section self-focuses independently of the other t cross-sections according to the stationary NLS (36.12). As the solution enters the adiabatic

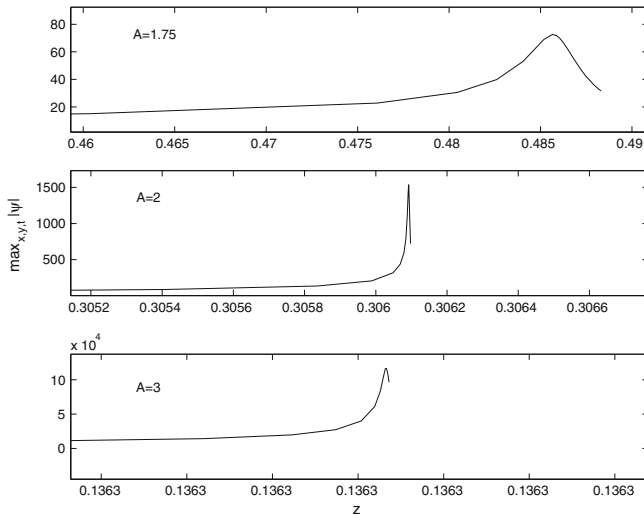


Fig. 36.3 $\max_{x,y,t} |\psi|$ as a function of z , for the simulations of Fig. 36.2. From [94]

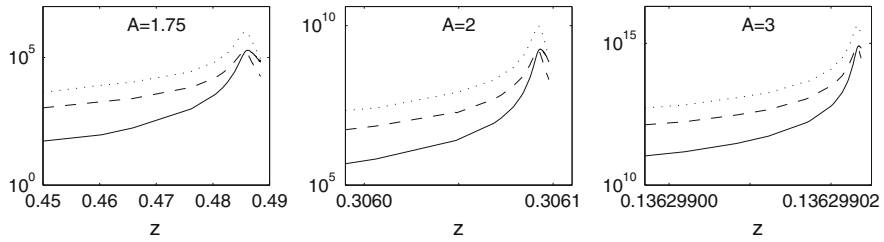


Fig. 36.4 $\max_{x,y,t} |\gamma_2 \psi_{tt}|$ (solid), $\max_{x,y,t} |\Delta_{x,y} \psi|$ (dotted), and $\max_{x,y,t} |\Delta_{x,y} \psi + |\psi|^2 \psi|$ (dashed) as function of z , for the simulations of Fig. 36.2. From [94]

stage, diffraction and nonlinearity become larger while nearly balancing each other. Therefore,

$$\Delta_{x,y} \psi + |\psi|^2 \psi \ll \Delta_{x,y} \psi, |\psi|^2 \psi.$$

Since the growth of dispersion is faster than that of diffraction and nonlinearity (Lemma 36.2), as the solution continues to collapse, it reaches a stage where dispersion becomes comparable to the “sum” of diffraction and nonlinearity, but is still smaller than each of them separately, i.e.,

$$\gamma_2 \psi_{tt} \approx \Delta_{x,y} \psi + |\psi|^2 \psi \ll \Delta_{x,y} \psi, |\psi|^2 \psi.$$

It is at this stage that dispersion leads to the arrest of collapse at t_m , followed by temporal splitting. As the two new peaks self-focus, they develop sharp temporal edges (shocks). As a result, dispersion becomes *larger* than the “sum” of diffraction and nonlinearity, i.e.,

$$\gamma_2 \psi_{tt} \gg \Delta_{x,y} \psi + |\psi|^2 \psi.$$

At this post-splitting stage the dynamics is governed, to leading order, by the one-dimensional linear Schrödinger equation

$$i\psi_z - \gamma_2 \psi_{tt} = 0.$$

Hence, the pulse undergoes linear dispersion, which leads to the disintegration of the two peaks into small-scale temporal oscillations. Note that at this stage the cross-sectional power is above P_{cr} (Fig. 36.5). This does not imply, however, that the pulse self-focuses spatially, since this conclusion holds when the dominant mechanisms are nonlinearity and diffraction, whereas at this stage the dominant mechanism is dispersion. Ultimately, the power of all t cross-sections goes below P_{cr} , and the pulse amplitude decays to zero as diffraction, dispersion, and nonlinearity are all of comparable magnitudes.

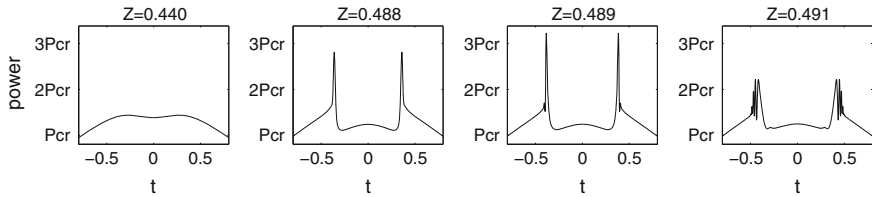


Fig. 36.5 Cross-sectional power $P(z, t) = \int |\psi(z, x, y, t)|^2 dx dy$ for the simulation of Fig. 36.2 with $A = 1.75$. From [94]

36.8.9 Summary: Self-focusing with Small Normal Dispersion

Let $\psi_0(x, y, t)$ be such that in the absence of dispersion, the solution collapses on a singularity curve $Z_c(t)$. The results of Sect. 36.8 suggest that in the presence of small normal dispersion, the propagation consists of five stages:

Initial non-adiabatic 2D spatial dynamics Since dispersion is initially negligible, each t cross-section undergoes a non-adiabatic two dimensional spatial collapse according to the stationary NLS (36.12).

Adiabatic 2D spatial dynamics As the solution approaches the singularity curve $Z_c(t)$ of the stationary NLS (36.12), the collapsing core of each t cross-section approaches the $\psi_{R^{(0)}}$ profile, and so the spatial collapse becomes adiabatic. The fastest collapse occurs at the t_m cross-section with the maximal input power. Since $\psi_{R^{(0)}}$ only depends on the distance from the singularity, collapse is self-similar in $z - Z_c(t)$.

Small-dispersion 3D spatio-temporal dynamics As the solution further approaches the singularity curve $Z_c(t)$, dispersion increases faster than nonlinearity and diffraction. Therefore, the solution reaches the stage where dispersion is still smaller than nonlinearity and diffraction, but is comparable to their balance. At this stage, dispersion leads to a power transfer away from t_m . As a result, the power at t_m goes below critical, and there is a temporal splitting of the power curve. This, in turn, leads to the arrest of collapse at t_m , and thus to a splitting of the pulse amplitude into two peaks.

Linear dispersion 1D temporal dynamics As the two peaks continue to collapse, they develop steeper and steeper temporal gradients. As a result, dispersion becomes larger than the balance of nonlinearity and diffraction. Hence, the propagation is governed, to leading order, by linear dispersion, which leads to a dispersive arrest of collapse of the two peaks.

Final defocusing stage The amplitudes of the two peaks decay to zero, as the solution undergoes a spatiotemporal scattering.

In the above description we implicitly assumed that γ_2 is sufficiently small, so that the solution reaches the *adiabatic 2D spatial dynamics* stage before dispersion becomes important. In this case, modulation theory covers the *adiabatic 2D spatial dynamics* stage and the *small-dispersion 3D spatio-temporal dynamics* stage. The validity of modulation theory breaks down once the solution enters the *linear dispersion 1D temporal dynamics* stage. This breakdown is evident in Fig. 36.4, which shows that dispersion becomes comparable to diffraction, thereby violating Condition 1 of modulation theory (Sect. 31.1.1). This is also evident from Fig. 36.5, which shows that the power of the two collapsing peaks is $\approx 3P_{\text{cr}}$, since this implies that the spatial profile is different from $\psi_{R^{(0)}}$, in violation of Condition 2 of modulation theory.

36.8.10 Open Question

As noted, the asymptotic and numerical studies of the NLS with small normal dispersion suggest that after the pulse splitting:

1. There are no additional splittings.
2. The collapse of the two peaks is arrested by “linear dispersion”.

At present, however, the following question is still open:

Open Question 36.1 *Do all solutions of (36.1) with $\gamma_2 > 0$ and $\psi_0(x, y, t) \in H^1$ exist globally?*

36.9 Asymmetric Pulse Splitting

In the peak-splitting simulations in Sect. 36.8.8, the two peaks are identical. This property follows from a symmetry argument:

Lemma 36.4 *Let ψ be a solution of (36.1) with an initial condition that is symmetric in time, i.e., $\psi_0(t, x, y) = \psi_0(-t, x, y)$. Then ψ remains symmetric in time, i.e., $\psi(z, t, x, y) = \psi(z, -t, x, y)$ for $z > 0$. In particular, if ψ undergoes a temporal splitting, the two pulses are symmetric with respect to $t = 0$.*

Proof The proof is similar to that of Lemma 5.5. □

Lemma 36.4 holds for solutions of (36.1). This equation, however, is only an approximate model for propagation of ultrashort pulses. Indeed, in Sect. 35.3 we saw that a more comprehensive model is given by, see (35.28),

$$i\psi_z(z, x, y, t) + \Delta_{x,y}\psi + |\psi|^2\psi + \frac{f^2}{4}\psi_{zz} - \delta\psi_{zt} - \gamma_2\psi_{tt} = 0. \quad (36.32)$$

The $O(\delta)$ term breaks the invariance under the transformation $t \rightarrow -t$, hence also the symmetry with respect to $t = 0$. We now show that once this term is added, pulse splitting becomes asymmetric.

36.9.1 Reduced Equations

In 1997, Fibich and Papanicolaou [91] used modulation theory to show that the reduced equations of (36.32) are

$$\beta_z(z, t) = -\frac{f^2 P_{\text{cr}}}{2M} \left(\frac{1}{L^2} \right)_z - \frac{48P_{\text{cr}}}{M} \left(\frac{1}{L^2} \right)_t + \frac{2\gamma_2 P_{\text{cr}}}{M} \xi_{tt}, \quad (36.33a)$$

$$L_{zz}(z, t) = -\frac{\beta}{L^3}, \quad (36.33b)$$

$$\zeta_z(z, t) = \frac{1}{L^2}. \quad (36.33c)$$

Figure 36.6 shows the numerical solution of (36.33) with $f^2 = 5.2 \times 10^{-6}$, $\delta = 5 \times 10^{-3}$, and $\gamma_2 = 1.5 \times 10^{-1}$ ²¹ and the initial conditions

$$\beta(0, t) = \frac{P_{\text{cr}}(1.05e^{-t^2} - 1)}{M}, \quad L(0, t) \equiv 1, \quad \zeta(0, t) \equiv 0.$$

As expected, the $O(\delta)$ term leads to an asymmetric split. This simulation also revealed that the front peak is lower than the rear one.

Exercise 36.3 Derive the reduced equations (36.33).

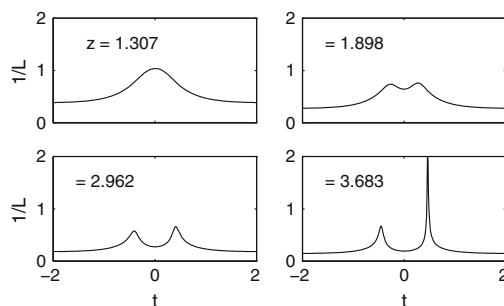


Fig. 36.6 On-axis intensity as a function of time, for the solution of the reduced equations (36.33) at the propagation distances indicated. From [91]

²¹ These values correspond to the pulse-splitting experiment of Ranka, Schirmer, and Gaeta (Sect. 36.10).

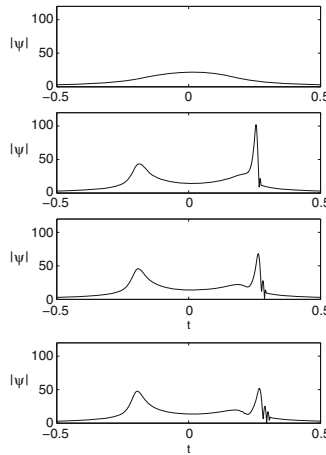


Fig. 36.7 Solution of (36.34) with $\gamma_2 = \frac{1}{32}$, $\delta = \frac{0.001}{\sqrt{32}}$, and $\psi_0 = 1.75\sqrt{2}e^{-\frac{x^2+y^2}{2}-t^2}$. From [94]

36.9.2 Simulations

When the pulse is sufficiently ultrashort, (36.32) reduces to, see (35.31),

$$i\psi_z(z, x, y, t) + \Delta_{x,y}\psi + |\psi|^2\psi + i\delta \left[(|\psi|^2\psi)_t - \Delta_{x,y}\psi_t \right] - \gamma_2\psi_{tt} = 0. \quad (36.34)$$

In Fig. 36.7 we solved (36.34) numerically, for the same parameters and initial condition as in the left column of Fig. 36.2, but with $\delta = \frac{0.001}{\sqrt{32}}$ instead of $\delta = 0$. This simulation confirmed the prediction of modulation theory that the pulse splits asymmetrically, with the front peak being lower than the rear peak (Sect. 36.9.1). The arrest of collapse of the rear peak takes place in a dispersive manner, reminiscent of the case $\delta = 0$ in Fig. 36.2.

36.10 Experimental Observation of Pulse Splitting (Normal Regime)

The first experimental observation of temporal splitting was done in 1996 by Ranka et al. for ultrashort pulses that propagated in glass [216]. Subsequently, pulse splitting was observed by Diddams et al. in fused silica [56]. Interestingly, both studies observed a second splitting at higher input powers. This does not imply, however, that solutions of (36.1) undergo multiple splittings, because the second splitting was observed at such high powers where the validity of (36.1) probably breaks down. An example of experimental pulse splitting is presented in Fig. 36.8.

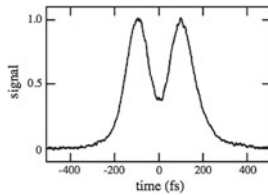


Fig. 36.8 (Experimental) cross-correlation measurement of temporal pulse splitting of an initially 80 fs pulse at 800 nm in a fused-silica glass sample. From [103]

In 1998, Ranka and Gaeta [215] observed experimentally and numerically that the pulse splits in an asymmetric fashion, with the front peak being lower than the rear peak, thus conforming the theoretical predictions of Fibich and Papanicolaou (Sect. 36.9.1). In addition, they observed that the higher rear peak becomes lower than the front peak with further propagation.

Remark See Sect. 37.5 for experimental observation of temporal splitting in the anomalous regime.

Chapter 37

NGO Method for Ultrashort Pulses with Anomalous Dispersion

In Chap. 26 we presented the nonlinear geometrical optics (NGO) method, for analyzing the initial self-focusing dynamics of strongly nonlinear solutions of the NLS

$$i\psi_z(z, \mathbf{x}) + \Delta\psi + |\psi|^{2\sigma}\psi = 0.$$

In this chapter we apply this method to strongly nonlinear solutions of the cubic NLS with anomalous dispersion

$$\begin{aligned} i\psi_z(z, x, y, t) + \psi_{xx} + \psi_{yy} - \gamma_2\psi_{tt} + |\psi|^2\psi &= 0, & \gamma_2 < 0, \\ \psi(0, x, y, t) &= \psi_0(x, y, t), \end{aligned} \tag{37.1}$$

which models the propagation of ultrashort pulses in a Kerr medium with anomalous dispersion (Conclusion 36.1). Here, by *strongly nonlinear* we mean that the Kerr nonlinearity initially dominates over diffraction and dispersion, i.e.,

$$\left(\frac{\partial^2}{\partial x^2} + \frac{\partial^2}{\partial y^2} - \gamma_2 \frac{\partial^2}{\partial t^2} \right) \psi_0 \ll |\psi_0|^2 \psi_0. \tag{37.2}$$

37.1 NGO Method

Under the rescaling

$$\tilde{t} = \frac{t}{(-\gamma_2)^{\frac{1}{2}}}, \tag{37.3}$$

Equation (37.1) becomes the isotropic three-dimensional NLS

$$i\psi_z(z, x, y, \tilde{t}) + \Delta\psi + |\psi|^2\psi = 0, \quad \Delta = \psi_{xx} + \psi_{yy} + \psi_{\tilde{t}\tilde{t}}. \tag{37.4}$$

By Proposition 26.1, if ψ is a solution of (37.4) with an initial condition ψ_0 that satisfies $\Delta\psi_0 \ll |\psi_0|^2\psi_0$, then during the initial propagation stage $\psi \approx \psi_{\text{NGO}} := Ae^{iS_{\text{NGO}}}$ where $S_{\text{NGO}} = |\psi_0|^2z$, the trajectories of the rays satisfy

$$\frac{d\mathbf{x}(z)}{dz} = 2\nabla S_{\text{NGO}}, \quad (37.5a)$$

where $\mathbf{x} = (x, y, \tilde{t})$ and $\nabla = \left(\frac{\partial}{\partial x}, \frac{\partial}{\partial y}, \frac{\partial}{\partial \tilde{t}}\right)$, and the amplitude evolution along each ray is

$$\frac{dA(z, \mathbf{x}(z))}{dz} = -A\Delta S_{\text{NGO}}, \quad (37.5b)$$

where $\Delta = \frac{\partial^2}{\partial x^2} + \frac{\partial^2}{\partial y^2} + \frac{\partial^2}{\partial \tilde{t}^2}$. Changing back from \tilde{t} to t gives

Proposition 37.1 *Let ψ be a solution of the NLS (37.1). If ψ_0 is strongly nonlinear, see (37.2), then during the initial propagation stage $\psi \approx \psi_{\text{NGO}} := Ae^{iS_{\text{NGO}}}$, where*

$$S_{\text{NGO}} = |\psi_0(x, y, t)|^2z, \quad (37.6a)$$

the trajectories of the rays satisfy

$$\frac{dx}{dz} = 2\frac{\partial S_{\text{NGO}}}{\partial x}, \quad \frac{dy}{dz} = 2\frac{\partial S_{\text{NGO}}}{\partial y}, \quad \frac{dt}{dz} = -2\gamma_2 \frac{\partial S_{\text{NGO}}}{\partial t}, \quad (37.6b)$$

and the amplitude evolution along each ray is

$$\frac{d}{dz}A(z, x(z), y(z), t(z)) = -A\left(\frac{\partial^2}{\partial x^2} + \frac{\partial^2}{\partial y^2} - \gamma_2 \frac{\partial^2}{\partial t^2}\right)S_{\text{NGO}}. \quad (37.6c)$$

37.2 One Temporal Dimension

Consider the one-dimensional temporal NLS with anomalous dispersion

$$i\psi_z(z, t) - \gamma_2\psi_{tt} + |\psi|^2\psi = 0, \quad \gamma_2 < 0, \quad \psi(0, t) = \psi_0(t) = c e^{-t^{2m}}. \quad (37.7)$$

Under rescaling (37.3), this equation reads

$$i\psi_z(z, \tilde{t}) + \psi_{\tilde{t}\tilde{t}} + |\psi|^2\psi = 0.$$

This equation is identical to the one-dimensional spatial NLS

$$i\psi_z(z, x) + \psi_{xx} + |\psi|^2\psi = 0. \quad (37.8)$$

Therefore, *all* the results obtained in Sect. 26.5 for Eq. (37.8) are valid for Eq. (37.7). In particular, we have

Conclusion 37.1 ([106]) *Let $\psi(z, t)$ be a solution of (37.7) with a strongly nonlinear initial condition (i.e., $|\psi_0|^2\psi_0 \gg \gamma_2 \frac{\partial^2 \psi_0}{\partial t^2}$). Then ψ initially localizes to a single temporal pulse if $m = 1$, but splits into two pulses if $m > 1$.*

37.3 Spherical Spatio-Temporal Input Pulses

Consider a solution of (37.1) with the spherical initial condition

$$\psi_0(x, y, t) = c e^{-\rho^{2m}}, \quad \rho = \sqrt{r^2 + \frac{t^2}{|\gamma_2|}}, \quad r = \sqrt{x^2 + y^2}. \quad (37.9)$$

In this case dispersion and diffraction have exactly the same magnitude. Indeed, under rescaling (37.3), ψ is a solution of the isotropic NLS (37.4) with the spherical initial condition $\psi_0(x, y, \tilde{t}) = c e^{-\rho^{2m}}$, where $\rho = \sqrt{r^2 + \tilde{t}^2}$. Therefore, the solution remains spherical as it propagates, i.e., $\psi = \psi(z, \rho)$.

Let c be sufficiently large so that $|\psi_0|^2\psi_0 \gg \Delta_{x,y,\tilde{t}}\psi_0$. By (37.5), the NGO rays equation is

$$\frac{d}{dz}\rho(z) = 2c^2 z \frac{\partial}{\partial \rho} e^{-2\rho^{2m}}. \quad (37.10a)$$

Up to the change $\rho \longleftrightarrow x$, this is the one-dimensional NGO rays equation (26.23a). Therefore, by Proposition 26.2, the solution localizes towards $\rho = 0$ when $m = 1$, but splits in ρ for $m > 1$. Since a split in ρ corresponds to a spherical shell in the (x, y, \tilde{t}) -space, we have

Conclusion 37.2 ([106]) *Let ψ be a solution of the NLS (37.1) with a strongly nonlinear spherical initial condition, see (37.2) and (37.9). Then ψ initially evolves into a spatio-temporal peak profile if $m = 1$, but into a spatio-temporal spherical shell if $m > 1$.*

By (37.5), the NGO amplitude equation is

$$\frac{dA(z)}{dz} = -c^2 z A(z) \left[\frac{\partial}{\partial \rho^2} + \frac{2}{\rho} \frac{\partial}{\partial \rho} \right] e^{-2\rho^{2m}}. \quad (37.10b)$$

This equation is similar (but not identical) to the one-dimensional NGO amplitude equation, see (26.23b).

In Fig. 37.1 we consider the three-dimensional NLS (37.1) with $\gamma_2 = -1$ and the spherical super-Gaussian input pulse (37.9) with $m = 2$. As expected, the corresponding solution of the NGO equations (37.10) initially evolves into a spherical shell (Fig. 37.1a). This prediction is confirmed by direct NLS simulations (Fig. 37.1b).

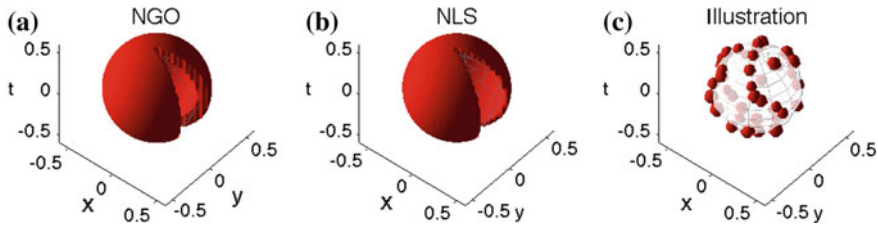


Fig. 37.1 The NLS (37.1) with $\gamma_2 = -1$, $\psi_0 = 17.8e^{-\rho^4}$, and $\rho = \sqrt{x^2 + y^2 + t^2}$. **a** NGO solution at $z = 0.025$. **b** NLS solution at $z = 0.02$. **c** Illustration of the subsequent multiple-filamentation dynamics. In (a) and (b), a portion of the shell was removed for the graphical presentation. From [106]

Remark A shell profile is unstable under azimuthal perturbations, which break it into spatio-temporal wave packets located on the shell.¹ Since observing a shell breakup numerically requires solving the NLS in $(3+1)$ dimensions, in Fig. 37.1c we only present a schematic illustration of a shell breakup into a “shell of spatio-temporal wave packets”.

A spatio-temporal Gaussian input pulse is the product of a spatial Gaussian with a temporal one, i.e., $e^{-\rho^2} = e^{-r^2}e^{-\tilde{t}^2}$. This is not the case, however, with spatio-temporal super-Gaussian input pulses. For example,

$$e^{-\rho^4} = e^{-(r^2+\tilde{t}^2)^2} = e^{-r^4-2r^2\tilde{t}^2-\tilde{t}^4} \neq e^{-r^4}e^{-\tilde{t}^4}.$$

Hence, while it is easy to produce a spatio-temporal Gaussian input pulse, it is not clear whether one can actually produce a spatio-temporal super-Gaussian input pulse of the form (37.9). Consequently, the results of this section may be more relevant in Bose-Einstein condensates, where the dynamics is described by the three-dimensional focusing NLS/GP, and the initial condensate can have a three-dimensional spherical super-Gaussian (flat-top) spatial profile.

37.4 Cylindrical Spatio-Temporal Input Pulses

Consider the solution of the NLS (37.1) with

$$\psi_0(x, y, t) = ce^{-r^{2m}-t^{2n}}, \quad r = \sqrt{x^2 + y^2}. \quad (37.11)$$

¹ This is similar to breakup of spatial rings into rings of filaments (Sect. 11.5 and Fig. 19.6).

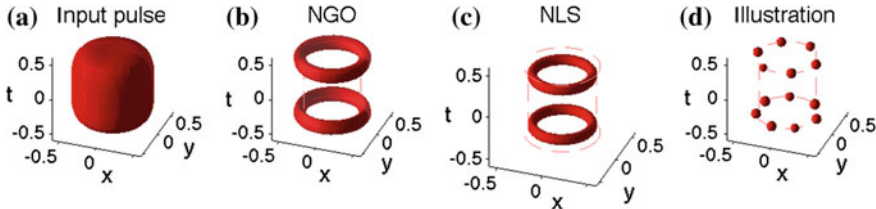


Fig. 37.2 The NLS (37.1) with $\gamma_2 = -1$ and $\psi_0 = 7.1e^{-r^4-t^4}$, where $r = \sqrt{x^2 + y^2}$. **a** Initial condition. **b** NGO solution at $z = 0.05$. **c** NLS solution at $z \approx 0.039$. **d** Illustration of the subsequent ring instability dynamics. From [106]

When $m, n > 1$, ψ_0 has a spatio-temporal cylindrical profile (Fig. 37.2a), which is a square in the (r, t) -plane. By (37.6), when c is sufficiently large, the NGO rays equation is

$$\frac{d}{dz}(r(z), t(z)) = 2c^2 z \left(\frac{\partial}{\partial r}, -\gamma_2 \frac{\partial}{\partial t} \right) e^{-2r^{2m}-2t^{2n}}, \quad (37.12a)$$

and the NGO amplitude equation is

$$\frac{dA(z)}{dz} = -c^2 z A(z) \left[\frac{\partial}{\partial r^2} + \frac{1}{r} \frac{\partial}{\partial r} - \gamma_2 \frac{\partial}{\partial t^2} \right] e^{-2r^{2m}-2t^{2n}}. \quad (37.12b)$$

Equation (37.12a) is the same, up to scaling, as Eq. (26.32a–b) for two-dimensional square input beams. Therefore, we can analyze the initial dynamics using the *one-dimensional building blocks approach* (Sect. 26.7.4). Thus, for example, when $m, n > 1$, the pulse simultaneously splits in the radial and temporal coordinates, resulting in four “filaments” in the (r, t) -plane. Since a split in r corresponds to a tube in the (x, y, t) -space, a simultaneous split in the radial and temporal coordinates corresponds to two pulses in the (x, y, t) -space, each of which is a spatial ring (Fig. 37.2b). This NGO prediction is confirmed by direct NLS simulations in Fig. 37.2c.

Conclusion 37.3 Let ψ be the solution of the NLS (37.1) with a spatio-temporal initial condition (37.11) with $m, n > 1$ which is strongly nonlinear; see (37.2). Then ψ initially evolves into two pulses, each of which is a spatial ring.

Remark Since NLS rings are unstable (Sect. 11.5 and Fig. 19.6), each of the rings in Fig. 37.2b will later disintegrate into spatio-temporal wavepackets. Observing this ring breakup numerically, however, requires solving the NLS in $(3+1)$ dimensions. Therefore, in Fig. 37.2d we only present a schematic illustration of two rings of spatio-temporal wavepackets.

We can also use the one-dimensional building blocks to analyze the initial dynamics of

$$\psi_0 = ce^{-r^2} e^{-t^4}, \quad c \gg 1, \quad (37.13)$$

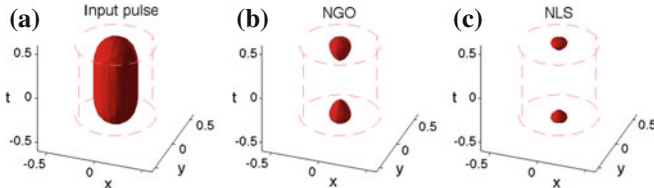


Fig. 37.3 The NLS (37.1) with $\gamma_2 = -1$ and $\psi_0 = 20e^{-r^2-t^4}$. **a** Initial condition. **b** NGO solution at $z = 0.04$. **c** NLS solution at $z = 0.01$. From [106]

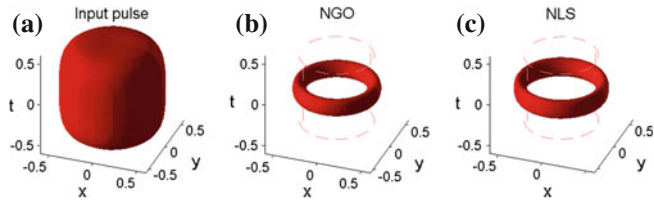


Fig. 37.4 The NLS (37.1) with $\gamma_2 = -1$ and $\psi_0 = 20e^{-r^4-t^2}$. **a** Initial condition. **b** NGO solution at $z = 0.02$. **c** NLS solution at $z = 0.01$

see Fig. 37.3a. Since the radial component is a Gaussian, it localizes to a single peak. The temporal component is a super-Gaussian, which splits into two pulses. The “product” of these two profiles gives two temporal pulses (Fig. 37.3b). Therefore, we have

Conclusion 37.4 ([106]) *Let ψ be the solution of the NLS (37.1) with the initial condition (37.13). Then ψ splits into two peak-type pulses. In other words, in the anomalous regime high-power input pulses which are peak-type spatially and flat-top temporally undergo a temporal splitting into two pulses as they propagate.*

This NGO prediction of is confirmed by direct NLS simulations in Fig. 37.3c, and experimentally in Sect. 37.5.

Finally, for

$$\psi_0 = ce^{-r^{2m}}e^{-t^2}, \quad m > 1, \quad c \gg 1,$$

the radial component evolves into a ring, and the temporal one into a single peak at $t = 0$. Therefore, the solution initially evolves into a two-dimensional spatial ring at $t = 0$ (Fig. 37.4b). This NGO prediction is confirmed by direct NLS simulations in Fig. 37.4c.²

37.4.1 Non-isotropic Case

We now consider Eq.(37.1) in the non-isotropic case. This case is similar to the two-dimensional anisotropic NLS (26.33), see Sect. 26.7.5.

² Ultimately, these solutions undergo a mixed standing-ring/peak-type collapse (Sect. 22.7).

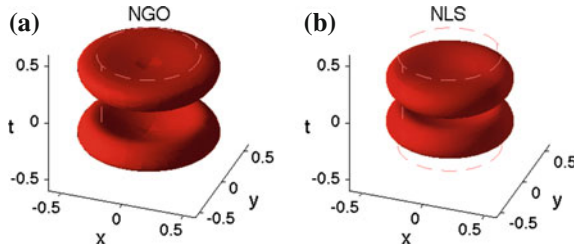


Fig. 37.5 The NLS (37.1) with $\gamma_2 = -1$ and $\psi_0 = 7.1e^{-r^4-4t^4}$. **a** NGO solution at $z = 0.035$. **b** NLS solution at $z \approx 0.02$. From [106]

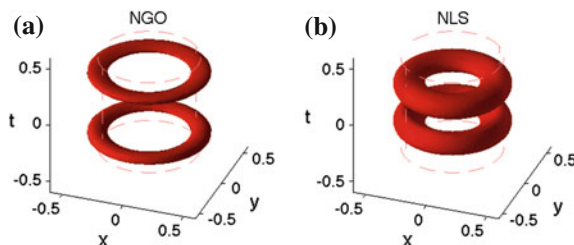


Fig. 37.6 Same as Fig. 37.5. **a** NGO solution at $z = 0.05$. **b** NLS solution at $z = 0.033$. From [106]

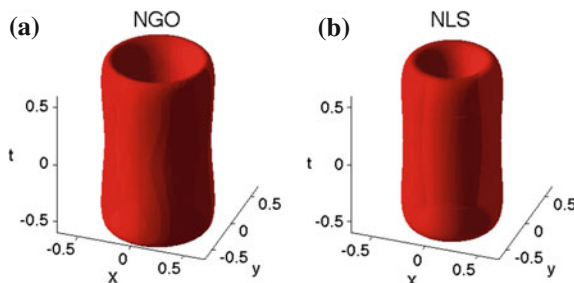


Fig. 37.7 The NLS (37.1) with $\gamma_2 = -1$ and $\psi_0 = 7.1e^{-r^4-\frac{t^4}{4}}$. **a** NGO solution at $z = 0.05$. **b** NLS solution at $z = 0.033$. From [106]

When anomalous dispersion is stronger than diffraction ($-\gamma > 1$), temporal self-focusing is faster than the spatial one (Conclusion 26.3). Hence, if $m, n > 1$, the solution first splits in time into two pulses, each of which has a flat-top (disc) spatial profile (Fig. 37.5a). Subsequently, each spatial disc evolves into a spatial ring (Fig. 37.6a). This NGO prediction is confirmed in direct NLS simulations in Figs. 37.5b and 37.6b.

Similarly, when $m, n > 1$ and diffraction is stronger than anomalous dispersion ($0 < -\gamma < 1$), the solution first evolves into a tube which is nearly constant in time (Fig. 37.7a). Subsequently, the tube splits in time into two shorter pulses, each of which has a ring profile (Fig. 37.8a). This NGO prediction is confirmed in direct NLS simulations in Figs. 37.7b and 37.8b.

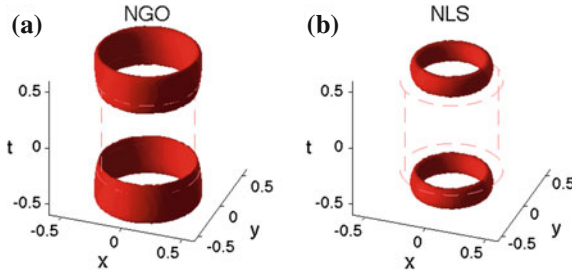


Fig. 37.8 Same as Fig. 37.7. **a** NGO solution at $z = 0.075$. **b** NLS solution at $z = 0.047$. From [106]

37.5 Experimental Observation of Pulse Splitting (Anomalous Regime)

As noted, in 2008 Gavish et al. used the NGO method to predict that pulses which are flat-top temporally undergo a temporal splitting in the anomalous regime (Conclusion 37.4). This theoretical prediction was confirmed experimentally in 2011 by Schrauth et al. [230]. The pulse wavelength of $\lambda = 1.510 \mu\text{m}$ was chosen to be in the anomalous-GVD regime for fused silica (Sect. 36.2.2). Autocorrelations of the pulse after it propagated through a 30 mm fused-silica sample are shown in Fig. 37.9 for various input powers. When the input pulse had a Gaussian temporal profile, the traces did not show any indication of pulse splitting (Fig. 37.9a). In contrast, the traces for temporal super-Gaussian input profiles in Fig. 37.9b exhibited pulse splitting even at the lowest peak power (as evidenced by the appearance of shoulders on the autocorrelation trace). As the power is increased, pulse splitting becomes more pronounced.

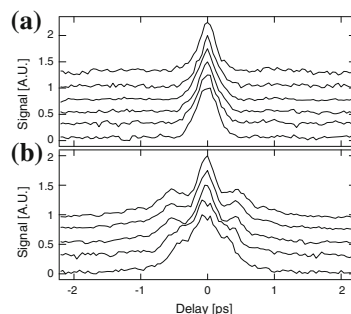


Fig. 37.9 (Experimental) autocorrelation traces after propagation through 30 mm of fused silica in the anomalous regime. **a** Temporal Gaussian input profiles with peak power increasing from 15.7 MW (bottom) to 62.8 MW (top). **b** Temporal super-Gaussian input profiles with peak power increasing from 11.2 MW (bottom) to 26.9 MW (top). From [230]

Remark See Sect. 36.10 for experimental observation of pulse splitting in the normal regime.

37.6 Spatio-Temporal Cubic Input Pulses

Finally, we consider solutions of (37.1) with

$$\psi_0 = ce^{-x^{2m}-y^{2m}-t^{2n}}, \quad c \gg 1. \quad (37.14)$$

By (37.6), the NGO rays equations are

$$\frac{d}{dz} (x(z), y(z), t(z)) = 2c^2 z \left(\frac{\partial}{\partial x}, \frac{\partial}{\partial y}, -\gamma_2 \frac{\partial}{\partial t} \right) e^{-2x^{2m}-2y^{2m}-2t^{2n}}, \quad (37.15a)$$

and the NGO amplitude equation is

$$\frac{dA(z)}{dz} = -c^2 z A(z) \left[\frac{\partial^2}{\partial x^2} + \frac{\partial^2}{\partial y^2} - \gamma_2 \frac{\partial^2}{\partial t^2} \right] e^{-2x^{2m}-2y^{2m}-2t^{2n}}. \quad (37.15b)$$

We can use the *one-dimensional building blocks approach* to predict the initial dynamics. For example, consider the spatio-temporal cube profile $\psi_0 = ce^{-x^4-y^4-t^4}$ (Fig. 37.10a). Each one-dimensional component e^{-x^4} , e^{-y^4} , and e^{-t^4} splits into two components centered at $x = \pm a$, $y = \pm a$ and $t = \pm a$, respectively. The “product” of these building blocks attains its maximum at eight vertices of the cube ($x = \pm a$, $y = \pm a$, $t = \pm a$). Indeed, solving the NGO equations numerically shows that the pulse evolves into a cube of eight pulses (Fig. 37.10).

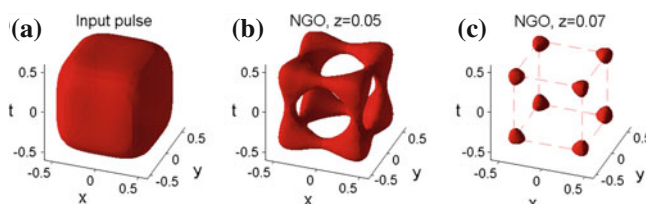


Fig. 37.10 Solution of the NGO equations (37.15) with $\psi_0 = 6.5e^{-x^4-y^4-t^4}$. **a** $z = 0$. **b** $z = 0.05$. **c** $z = 0.07$. From [106]

Chapter 38

Continuations Beyond the Singularity

The two-dimensional cubic NLS models the propagation of intense laser beams in a Kerr medium. Therefore, when an NLS solution collapses at a finite distance, the question arises as to how to continue it beyond the singularity. The laser beam, however, “does not care” about such “mathematical issues”, and so it continues to propagate forward.

Of course, physical quantities do not become singular. Rather, when an NLS solution blows up, this indicates that some of the terms neglected in the derivation of the NLS from Maxwell’s equations (see Chap. 1) become important near the singularity. Hence, the standard approach for continuing NLS solutions beyond the singularity has been to use more comprehensive models, in which collapse is arrested. Indeed, collapse is arrested if the propagation model includes nonlinear saturation (Chap. 32), nonlinear damping (Chap. 33), nonparaxiality (Chap. 34), or normal dispersion (Chap. 36).

In this chapter we adopt a different approach, and ask

Question 38.1 *Can singular NLS solutions be continued beyond the singularity within the framework of the NLS model?*

By this we mean that the solution satisfies the (unperturbed) NLS both before and after the singularity, and some matching (“jump”) condition at the singularity. The motivation for this approach comes from hyperbolic equations, where in the absence of viscosity, solutions can become singular (develop *shocks*).¹ In that case, there is a huge body of literature on how to continue inviscid solutions beyond the singularity, which consists of Riemann problems, vanishing-viscosity solutions, entropy conditions, Rankine-Hugoniot jump conditions, specialized numerical methods, etc. (see, e.g. [157]). Although it has been known that the NLS model breaks down when the input power is sufficiently high since 1965 (Sect. 3.4), an “equivalent” theory for the NLS has yet to be developed.

¹ In a shock wave the function remains bounded, but its derivative becomes infinite.

We adopt the following definition of a continuation:

Definition 38.1 (Continuation beyond the singularity) *Let $\psi(z, \mathbf{x})$ be an NLS solution that collapses at Z_c . Let $\psi^{(\epsilon)}(z, \mathbf{x})$ be a one-parameter family, which is smooth in ϵ , such that*

1. *For any $0 < \epsilon \ll 1$, $\psi^{(\epsilon)}$ exists for $0 \leq z < \infty$.*
2. $\lim_{\epsilon \rightarrow 0+} \psi^{(\epsilon)} = \psi$ *for $0 \leq z < Z_c$.*

Then the continuation of ψ beyond the singularity is defined as

$$\psi^{\text{continuation}} := \lim_{\epsilon \rightarrow 0+} \psi^{(\epsilon)}, \quad Z_c < z < \infty.$$

As we shall see, there are various ways to continue NLS solutions beyond the singularity. Ideally, we would like the continuation to remain close to the physical solution beyond the singularity. The physical continuation of NLS/GP solutions in Bose-Einstein condensates, however, may be different from that in nonlinear optics. Even in nonlinear optics, different physical setups may call for different continuations, since the continuation depends on the dominant collapse-arresting mechanism. Therefore, there is probably no universal physical continuation of NLS solutions.

We distinguish between two types of continuations:

1. Continuations that lead to a **point singularity**, in which the limiting solution is singular at Z_c , but regular (i.e., in L^2) for $z > Z_c$.
2. Continuations that lead to a **filament singularity**, in which the limiting solution has a δ -function singularity for $Z_c \leq z \leq z_0$, where $Z_c < z_0 \leq \infty$.

In nonlinear optics, experiments show that collapsing beams evolve into long and narrow filaments (Sect. 3.3.1), which can be viewed as “extended δ -functions”. This suggests that physical continuations of the NLS in nonlinear optics should lead to a filament singularity.

38.1 Rigorous Continuations

38.1.1 Merle's Explicit Continuation of $\psi_{R^{(0)}, \alpha}^{\text{explicit}}$

The first continuation of singular NLS solutions was proposed by Merle in 1992 for the explicit blowup solution $\psi_{R^{(0)}, \alpha}^{\text{explicit}}$. Recall that the critical NLS

$$i\psi_z(z, \mathbf{x}) + \Delta\psi + |\psi|^{\frac{4}{d}}\psi = 0, \quad \psi_0(0, \mathbf{x}) = \psi_0(\mathbf{x}) \quad (38.1)$$

admits the explicit solution

$$\psi_{R^{(0)}}^{\text{explicit}}(z, r) = \frac{1}{L^{\frac{d}{2}}(z)} R^{(0)} \left(\frac{r}{L(z)} \right) e^{i\zeta + i \frac{L_z}{L} \frac{r^2}{4}}, \quad (38.2a)$$

where

$$L = Z_c - z, \quad \zeta = \int_0^z \frac{ds}{L^2(s)} = \frac{1}{Z_c - z} - \frac{1}{Z_c}, \quad (38.2b)$$

and $R^{(0)}$ is the ground state solution of

$$R''(r) + \frac{d-1}{r} R' - R + |R|^{\frac{4}{d}} R = 0, \quad R'(0) = 0, \quad R(\infty) = 0.$$

More generally, (38.1) admits the explicit solutions

$$\psi_{R^{(0)}, \alpha}^{\text{explicit}}(z, r) = \frac{1}{L_{\alpha}^{\frac{d}{2}}(z)} R^{(0)} \left(\frac{r}{L_{\alpha}(z)} \right) e^{i\zeta_{\alpha} + i \frac{(L_{\alpha})_z}{L_{\alpha}} \frac{r^2}{4}}, \quad (38.3a)$$

where

$$L_{\alpha} = \alpha(Z_c - z), \quad \zeta_{\alpha} = \int_0^z \frac{ds}{L_{\alpha}^2(s)} = \frac{1}{\alpha^2} \left(\frac{1}{Z_c - z} - \frac{1}{Z_c} \right), \quad (38.3b)$$

and $\alpha > 0$. The explicit solutions (38.2) and (38.3) blowup at Z_c . These *minimal-power blowup solutions* are strongly unstable, because any perturbation that decreases their power arrests the collapse. See Chap. 10 and Sect. 13.5 for more details.

To continue $\psi_{R^{(0)}, \alpha}^{\text{explicit}}$ beyond the singularity, Merle considered the solution $\psi^{(\epsilon)}$ of (38.1) with the initial condition

$$\psi_0^{(\epsilon)}(r) = (1 - \epsilon) \psi_{R^{(0)}, \alpha}^{\text{explicit}}(0, r), \quad 0 < \epsilon \ll 1. \quad (38.4)$$

Since the power of $\psi^{(\epsilon)}$ is below P_{cr} , it exists globally. Therefore, it is possible to continue $\psi_{R^{(0)}, \alpha}^{\text{explicit}}$ beyond the singularity by taking the limit of $\psi^{(\epsilon)}$ as $\epsilon \rightarrow 0+$. By continuity, $\psi^{(\epsilon)}$ converges to $\psi_{R^{(0)}, \alpha}^{\text{explicit}}$ before the singularity. The interesting limit is, therefore, after the singularity.

Theorem 38.1 ([174]) *Let $\psi^{(\epsilon)}$ be the solution of the critical NLS (38.1) with the initial condition (38.4). Then for any $\theta \in \mathbb{R}$ there exists a sequence $\epsilon_n \rightarrow 0+$ (depending on θ), such that*

$$\psi^{(\epsilon_n)}(z, r) \xrightarrow{H^1} \begin{cases} \psi_{R^{(0)}, \alpha}^{\text{explicit}}(z, r), & \text{if } 0 \leq z < Z_c, \\ e^{i\theta} \psi_{R^{(0)}, \alpha}^{\text{explicit}*}(2Z_c - z, r), & \text{if } Z_c < z < \infty. \end{cases} \quad (38.5)$$

Theorem 38.1 shows that the amplitude of the limiting solution is symmetric with respect to Z_c , i.e.,

$$\lim_{\epsilon \rightarrow 0+} |\psi^{(\epsilon)}(Z_c + z, r)| = \lim_{\epsilon \rightarrow 0+} |\psi^{(\epsilon)}(Z_c - z, r)|, \quad z > 0. \quad (38.6)$$

Therefore, if we define the width of $\psi^{(\epsilon)}$ as

$$L_\epsilon(z) := \left| \frac{R^{(0)}(0)}{\psi^{(\epsilon)}(z, 0)} \right|^{\frac{2}{d}}, \quad (38.7)$$

see (38.3b), then the limiting width is symmetric with respect to Z_c , i.e.,

$$\lim_{\epsilon \rightarrow 0+} L_\epsilon(z) = \alpha |Z_c - z|, \quad 0 \leq z < \infty. \quad (38.8)$$

The “full” limiting solution (amplitude+phase) is completely determined after the singularity, but only up to multiplication by $e^{i\theta}$, i.e.,

$$\lim_{\epsilon_n \rightarrow 0+} \psi^{(\epsilon_n)}(Z_c + z, r) = e^{i\theta} \lim_{\epsilon_n \rightarrow 0+} \psi^{*(\epsilon_n)}(Z_c - z, r), \quad z > 0.$$

Thus, Merle’s continuation has two key properties:

1. **Symmetry property:** The continuation is symmetric with respect to the singularity point Z_c .
2. **Phase-loss property:** After the singularity, the solution is only determined up to multiplication by $e^{i\theta}$.

Note that the symmetry property is a “matching condition”.

Motivation

The result of Theorem 38.1 can be motivated as follows. Since

$$\lim_{z \rightarrow Z_c^-} \lim_{\epsilon \rightarrow 0+} |\psi^{(\epsilon)}|^2 = \lim_{z \rightarrow Z_c^-} |\psi_{R^{(0)}, \alpha}^{\text{explicit}}|^2 = P_{\text{cr}} \delta(r), \quad (38.9)$$

and since the continuation is power preserving, we have that

$$\lim_{z \rightarrow Z_c^+} \lim_{\epsilon \rightarrow 0+} |\psi^{(\epsilon)}|^2 = P_{\text{cr}} \delta(r).$$

Therefore, for $z > Z_c$, $\lim_{\epsilon \rightarrow 0+} \psi^{(\epsilon)}$ is a *minimal-power blowup solution* that becomes singular as $z \rightarrow Z_c+$. In addition, since $\psi^{(\epsilon)}$ is radial, the so is $\lim_{\epsilon \rightarrow 0+} \psi^{(\epsilon)}$. Therefore, by Theorem 13.12, for $z > Z_c$, $\lim_{\epsilon \rightarrow 0+} \psi^{(\epsilon)}$ has to be given by $e^{i\theta} \psi_{R^{(0)}, \tilde{\alpha}}^{\text{explicit}*}$ for some $\tilde{\alpha} > 0$.²

² The conjugation comes from the fact that z is decreasing as $z \rightarrow Z_c+$.

For any $\epsilon > 0$, the Hamiltonian of $\psi^{(\epsilon)}$ is conserved. Therefore, the continuation in Theorem 38.1 is also Hamiltonian preserving, i.e.,

$$H\left(\psi_{R^{(0)}, \alpha}^{\text{explicit}}\right) = H\left(\psi_{R^{(0)}, \tilde{\alpha}}^{\text{explicit*}}\right).$$

In addition, since $H(R^{(0)}) = 0$, then

$$H\left(\psi_{R^{(0)}, \alpha}^{\text{explicit}}\right) = ML_z^2 = M\alpha^2, \quad H\left(\psi_{R^{(0)}, \tilde{\alpha}}^{\text{explicit*}}\right) = M\tilde{\alpha}^2, \quad (38.10)$$

where $M = \frac{1}{4} \int |\mathbf{x}|^2 |R^{(0)}|^2 d\mathbf{x}$, see (7.25). Therefore, $\alpha = \tilde{\alpha}$. Hence, the symmetry property follows.³

To motivate the phase-loss property, we note that since

$$\arg\left(\psi_{R^{(0)}, \alpha}^{\text{explicit}}(z, 0)\right) = \xi(z) = \frac{1}{\alpha^2} \frac{1}{Z_c - z} \rightarrow \infty, \quad z \rightarrow Z_c -,$$

then $\lim_{\epsilon \rightarrow 0+} \arg \psi^{(\epsilon)}(Z_c, 0) = \infty$. Consequently, the post-collapse phase of the continuation is “beyond infinity”. Thus, for $z \geq Z_c$, $\arg(\psi^{(\epsilon)})$ is continuous in ϵ and it goes to infinity as $\epsilon \rightarrow 0$. Hence, for any θ and $z \geq Z_c$, one can choose a sequence $\epsilon_n \rightarrow 0$ such that $e^{i \arg(\psi^{(\epsilon_n)}(z, 0))} = e^{i\theta}$.

Simulations

Let $\psi^{(\epsilon)}(z, x)$ be the solution of the one-dimensional critical NLS

$$i\psi_z(z, x) + \psi_{xx} + |\psi|^4\psi = 0, \quad \psi_0^{(\epsilon)}(x) = (1 - \epsilon)\psi_{R^{(0)}}^{\text{explicit}}(0, x). \quad (38.11)$$

The solution width, see (38.7), satisfies $\lim_{\epsilon \rightarrow 0+} L_\epsilon(z) = |Z_c - z|$, both for $0 \leq z < Z_c$ and for $z > Z_c$, see Fig. 38.1a, in accordance with the symmetry property (38.8).

To observe the post-collapse phase-loss property, we note that if the phase of the limiting solution is lost, the phase of $\psi^{(\epsilon)}$ with $0 < \epsilon \ll 1$ is “almost lost”, i.e., it becomes highly sensitive to small changes in ϵ . Indeed, Fig. 38.1b shows that $O(10^{-4})$ changes in ϵ have a negligible effect on the pre-collapse phase, but an $O(1)$ effect on the post-collapse phase.

38.1.2 Continuation of Bourgain-Wang Solutions

In Sect. 10.8 we presented the Bourgain-Wang singular solutions ψ_{BW} . These solutions have a collapsing core that approaches $\psi_{R^{(0)}, \alpha}^{\text{explicit}}$ and blows up at a linear rate.

³ See Sect. 38.3 for another explanation of the symmetry property.

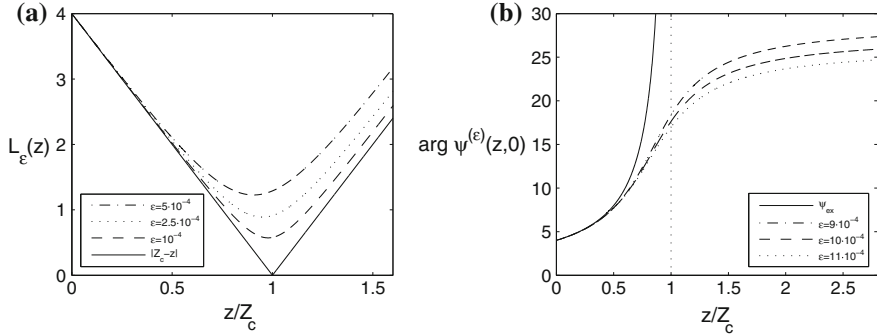


Fig. 38.1 Solution of (38.11). **a** $L_\epsilon(z)$ for $\epsilon = 5 \cdot 10^{-4}, 2.5 \cdot 10^{-4}$ and 10^{-4} . The solid line is $L = |Z_c - z|$. **b** Accumulated on-axis phase for $\epsilon = 1.1 \cdot 10^{-3}, 10^{-3}$, and $0.9 \cdot 10^{-3}$. The solid line is $\arg \left(\psi_{R^{(0)}}^{\text{explicit}}(z, 0) \right)$. From [85]

Unlike $\psi_{R^{(0)}, \alpha}^{\text{explicit}}$, however, these solutions also have a nontrivial tail, denoted by u , which does not participate in the collapse process. The L^2 limit of the tail is denoted by ϕ .

Let ψ_{BW} denote the unique Bourgain-Wang solution that collapses at Z_c with the limiting blowup profile $\psi_{R^{(0)}, \alpha}^{\text{explicit}}$ and tail ϕ . By Theorem 10.2, ψ_{BW} inherits the dual instabilities of $\psi_{R^{(0)}, \alpha}^{\text{explicit}}$, see Sect. 10.6.2, in the sense that it can be embedded into a one-parameter family of NLS solutions, denoted by $\psi^{(\eta)}$, such that $\psi^{(\eta=0)} = \psi_{\text{BW}}$, $\psi^{(\eta)}$ scatters when perturbed in one direction ($\eta > 0$), but collapses when perturbed in the other direction ($\eta < 0$).

Since $\psi^{(\eta)}$ exists globally for $0 < \eta \ll 1$, one can define the continuation of ψ_{BW} as the limit of $\psi^{(\eta)}$ as $\eta \rightarrow 0+$. By continuity,

$$\lim_{\eta \rightarrow 0+} \psi^{(\eta)} = \psi_{\text{BW}} \quad z < Z_c.$$

The post-collapse limit was calculated by Merle, Raphaël, and Szeftel:

Theorem 38.2 ([185]) Let $0 < \eta \leq 1$ and let $\psi^{(\eta)} \in C(\mathbb{R}, \Sigma)$ be the global solution built in Theorem 10.2, where $\Sigma := \{u(\mathbf{x}) \mid \mathbf{x}u \in L^2\} \cap H^1$. Then for any $\theta \in \mathbb{R}$ there exists a sequence $\eta_n \rightarrow 0+$, such that

$$\forall z > Z_c, \quad \lim_{\eta_n \rightarrow 0+} \psi^{(\eta_n)}(z, \mathbf{x}) = e^{i\theta} \psi_{\text{BW}}^*(2Z_c - z, \mathbf{x}) \quad \text{in } \Sigma.$$

In particular, the Merle-Raphaël-Szeftel continuation of Bourgain-Wang solutions satisfies the symmetry and phase-loss properties.

Remark See Sect. 38.2 for additional results on continuation of Bourgain-Wang solutions.

38.1.3 Tao's Continuation

In 2009, Tao [254] presented a rigorous continuation of singular solutions of the critical NLS in the semi-Strichartz class. Intuitively, these solutions are formed by solving the NLS in the Strichartz class whenever possible, and deleting any power that escapes to spatial or frequency infinity when the solution leaves the Strichartz class. These solutions, however, do not depend continuously on the initial conditions. Hence, the problem is not well-posed in this class of solutions. Consequently, this continuation does not seem to be relevant to physical models.

38.1.4 Vanishing Nonlinear-Saturation Continuation

In 1992, Merle presented a rigorous continuation which is based on arresting collapse with nonlinear saturation. This continuation is presented in Sect. 38.4.1.

38.2 Sub-threshold Power Continuation

The main weakness of Theorem 38.1 is that it only applies to the unstable minimal-power blowup solution $\psi_{R^{(0)}, \alpha}^{\text{explicit}}$. In 2011, Fibich and Klein generalized this result as follows. Let $\psi(z, \mathbf{x}; K)$ be the solution of the critical NLS with

$$\psi_0(\mathbf{x}; K) = K f(\mathbf{x}), \quad f(\mathbf{x}) \in H^1, \quad K > 0,$$

and let

$$K_{\text{th}} := \inf\{K \mid \psi(z, \mathbf{x}; K) \text{ collapses at } Z_c(K), 0 < Z_c(K) < \infty\}. \quad (38.12)$$

Assume that the infimum is attained, i.e., that $\psi(z, \mathbf{x}; K_{\text{th}})$ blows up at a finite distance Z_c .⁴ In this case, $\psi(z, \mathbf{x}; K_{\text{th}})$ is the “minimal-power” blowup solution of the one-parameter family $\psi(z, \mathbf{x}; K)$. By construction, the solution $\psi^{(\epsilon)}$ of the critical NLS with the initial condition

$$\psi_0^{(\epsilon)}(\mathbf{x}) = (1 - \epsilon) K_{\text{th}} f(\mathbf{x}), \quad (38.13)$$

exists globally for $0 < \epsilon \ll 1$ and blows up for $\epsilon = 0$. Therefore, as in Theorem 38.1, we can define the continuation of $\psi(z, \mathbf{x}; K_{\text{th}})$ as $\psi^{(\epsilon=0)} := \lim_{\epsilon \rightarrow 0+} \psi^{(\epsilon)}$. By continuity, $\psi^{(\epsilon=0)} = \psi(z, \mathbf{x}; K_{\text{th}})$ before the singularity.

⁴ For example, the infimum is attained when $f = R^{(0)}(r)e^{-ir^2}$, but not when $f = R^{(0)}(r)$.

Proposition 38.1 ([85]) Let $\psi^{(\epsilon)}$ be the solution of the critical NLS (38.1) with the initial condition (38.13), where $f(r)$ is radial. Assume that $\psi^{(\epsilon=0)}$ blows up at Z_c , where $0 < Z_c < \infty$. Assume further that $\psi^{(\epsilon=0)}$ blows up with the $\psi_{R^{(0)}}$ profile.⁵ Then there exist $\alpha \in \mathbb{R}^+$ and $\phi \in L^2$ such that the following hold:

1. **(before the singularity)** There exist $\theta_0 \in \mathbb{R}$ such that

$$\lim_{z \rightarrow Z_c^-} \left[\psi^{(\epsilon=0)}(z, r) - e^{i\theta_0} \psi_{R^{(0)}, \alpha}^{\text{explicit}}(z, r) \right] = \phi(r),$$

where $\psi_{R^{(0)}, \alpha}^{\text{explicit}}$ is given by (38.3).

2. **(after the singularity)** For any $\theta \in \mathbb{R}$, there exist a sequence $\epsilon_n \rightarrow 0+$, depending on θ , such that

$$\lim_{z \rightarrow Z_c^+} \left[\lim_{\epsilon_n \rightarrow 0+} \psi^{(\epsilon_n)}(z, r) - e^{i\theta} \psi_{R^{(0)}, \alpha}^{\text{explicit}*}(2Z_c - z, r) \right] = \phi(r).$$

3. The limiting width of the collapsing core satisfies

$$\lim_{\epsilon \rightarrow 0+} L_\epsilon(z) \sim \alpha |Z_c - z|, \quad z \rightarrow Z_c \pm. \quad (38.14)$$

Proof An informal asymptotic proof is given in Sect. 38.2.1. \square

Corollary 38.1 Let $\psi(z, r; K_{\text{th}})$ be a “minimal-power” blowup solution that collapses with the $\psi_{R^{(0)}}$ profile.

1. If $\|\psi(z; \mathbf{x}; K_{\text{th}})\|_2^2 = P_{\text{cr}}$, then $\phi \equiv 0$ and so $\psi(z, r; K_{\text{th}}) \equiv e^{i\theta_0} \psi_{R^{(0)}, \alpha}^{\text{explicit}}$.
2. If $\|\psi(z; \mathbf{x}; K_{\text{th}})\|_2^2 > P_{\text{cr}}$, then $\phi \not\equiv 0$ and so $\psi(z, r; K_{\text{th}})$ is the unique Bourgain-Wang solution with singular core $e^{i\theta_0} \psi_{R^{(0)}, \alpha}^{\text{explicit}}$ and limiting tail ϕ .

Proof Proposition 38.1 shows that the singular core of $\psi(z, r; K_{\text{th}})$ is given by $\psi_{R^{(0)}, \alpha}^{\text{explicit}}$, and that $\|\psi(z, r; K_{\text{th}})\|_2^2 = P_{\text{cr}} + \|\phi\|_2^2$. By Theorem 13.12, $\|\psi(z, r; K_{\text{th}})\|_2^2 = P_{\text{cr}}$ if and only if $\psi(z, r; K_{\text{th}})$ is equal to $e^{i\theta_0} \psi_{R^{(0)}, \alpha}^{\text{explicit}}$. \square

Corollary 38.2 ([85]) If $\|\psi(z; \mathbf{x}; K_{\text{th}})\|_2^2 > P_{\text{cr}}$, the limiting solution in Proposition 38.1 is a Bourgain-Wang solution, both before and after the singularity.

Since Bourgain-Wang blowup solutions are unstable, they were viewed as “non-generic”. Corollary 38.1 shows, however, that they are “generic” in the following sense:

⁵ This is the case, e.g., if $0 \leq \|\psi(0; \mathbf{x}; K_{\text{th}})\|_2^2 - P_{\text{cr}} \ll 1$, see Theorem 14.1.

Conclusion 38.1 ([85]) Any “minimal-power” blowup solution $\psi(z, r; K_{\text{th}})$ that has power above P_{cr} and collapses with the $\psi_{R^{(0)}}$ profile, is a Bourgain-Wang solution.

38.2.1 Proof of Proposition 38.1

Theory Review

In Sect. 17.3 we saw that collapse of peak-type radial solutions can be divided into

1. An initial non-adiabatic stage, during which the solution splits into a collapsing core ψ_{coll} and a non-collapsing tail ψ_{outer} , i.e.,

$$\psi(z, r) \sim \begin{cases} \psi_{\text{coll}}, & \text{if } 0 \leq \frac{r}{L(z)} \leq \rho_0, \\ \psi_{\text{outer}}, & \text{if } \frac{r}{L(z)} \gg \rho_0, \end{cases} \quad (38.15a)$$

where $L(z)$ is the collapsing-core width and $\rho_0 = O(1)$.

2. A final adiabatic stage as $z \rightarrow Z_c$, during which ψ_{coll} approaches the blowup profile

$$\psi_{R^{(0)}} = \frac{1}{L^{\frac{d}{2}}(z)} R^{(0)}(\rho) e^{i\zeta + i \frac{L_z}{L} \frac{r^2}{4}}, \quad \rho = \frac{r}{L}, \quad \frac{d\zeta}{dz} = \frac{1}{L^2}, \quad (38.15b)$$

and ψ_{outer} approaches a “regular” profile $\phi(\mathbf{x}) \in L^2$, see Theorem 14.1.

Once $\psi_{\text{coll}} \sim \psi_{R^{(0)}}$, the dynamics of the collapsing core is governed by

$$\beta_z(z) = -\frac{\nu(\beta)}{L^2}, \quad L_{zz} = -\frac{\beta}{L^3}, \quad (38.16a)$$

see Proposition 17.1, where

$$\nu(\beta) = \begin{cases} c_v e^{-\pi/\sqrt{\beta}}, & \text{if } \beta > 0, \\ 0, & \text{if } \beta \leq 0, \end{cases} \quad (38.16b)$$

and

$$c_v = \frac{2A_R^2}{M^{\text{radial}}}, \quad A_R = \lim_{r \rightarrow \infty} e^r r^{\frac{d-1}{2}} R^{(0)}(r), \quad M^{\text{radial}} = \frac{1}{4} \int_0^\infty r^2 (R^{(0)})^2 r^{d-1} dr. \quad (38.16c)$$

In addition, β is proportional to the excess power above P_{cr} of the collapsing core, i.e.,

$$\beta \sim \frac{P_{\text{coll}} - P_{\text{cr}}}{M}, \quad P_{\text{coll}} = \|\psi_{\text{coll}}\|_2^2, \quad M = \frac{1}{4} \int |\mathbf{x}|^2 |R^{(0)}|^2 d\mathbf{x}, \quad (38.17)$$

see (17.24).

Asymptotic Analysis

Let $0 \leq z_0 < Z_c$ denote a distance at which $\psi_{\text{coll}}^{(\epsilon=0)}(z_0) \sim \psi_{R^{(0)}}$, so that the reduced equations (38.16) hold for $z \geq z_0$. By continuity, $\psi_{\text{coll}}^{(\epsilon)}(z_0) \sim \psi_{R^{(0)}}$ for $0 < \epsilon \ll 1$. Let $\beta(z; \epsilon)$ and $L(z; \epsilon)$ denote the solution of (38.16) that corresponds to $\psi^{(\epsilon)}$. Under the adiabatic approximation, $\psi^{(\epsilon)}$ collapses if and only if the power of its collapsing core $\psi_{\text{coll}}^{(\epsilon)}$ is at least P_{cr} (Corollary 17.5). Therefore, by construction,

$$\begin{cases} P_{\text{coll}}^{(\epsilon)}(z_0) \geq P_{\text{cr}}, & \text{if } \epsilon < 0, \\ P_{\text{coll}}^{(\epsilon)}(z_0) < P_{\text{cr}}, & \text{if } \epsilon > 0. \end{cases}$$

Hence, by (38.17),

$$\begin{cases} \beta_0^{(\epsilon)} \geq 0, & \text{if } \epsilon < 0, \\ \beta_0^{(\epsilon)} < 0, & \text{if } \epsilon > 0, \end{cases} \quad (38.18)$$

where $\beta_0^{(\epsilon)} := \beta(z_0; \epsilon)$.

Lemma 38.1 *Let $\epsilon > 0$. Then Eq. (38.16a) reduce to*

$$L_{zz}(z; \epsilon) = -\frac{\beta_0^{(\epsilon)}}{L^3}, \quad z > z_0, \quad (38.19)$$

where $\beta_0^{(\epsilon)}$ is independent of z .

Proof By (38.18), if $\epsilon > 0$, then $\beta_0^{(\epsilon)} < 0$. Hence, by (38.16b), $v(\beta) = 0$. Therefore, by (38.16a), $\beta_z = 0$ and so $\beta \equiv \beta_0^{(\epsilon)}$. \square

Equation (38.19) is solved subject to initial conditions of the form

$$L(z_0; \epsilon) = L_0^{(\epsilon)}, \quad L_z(z_0; \epsilon) = L_{z,0}^{(\epsilon)}. \quad (38.20)$$

Lemma 38.2 *Let $L(z; \epsilon)$ be the solution of (38.19)–(38.20). Then*

$$\lim_{\epsilon \rightarrow 0+} L(z; \epsilon) = \alpha |Z_c - z|, \quad z_{\text{ad}} \leq z < \infty, \quad (38.21)$$

where

$$\alpha := \lim_{\epsilon \rightarrow 0+} L_{z,0}^{(\epsilon)}, \quad Z_c := \lim_{\epsilon \rightarrow 0+} \frac{L_0^{(\epsilon)}}{-L_{z,0}^{(\epsilon)}}.$$

Proof As in the proof of Lemma 2.8, the solution of (38.19)–(38.20) is

$$L^2 = c_1^{(\epsilon)} \left(z + \frac{L_0^{(\epsilon)} L_{z,0}^{(\epsilon)}}{c_1^{(\epsilon)}} \right)^2 - \frac{\beta_0^{(\epsilon)}}{c_1^{(\epsilon)}}, \quad c_1^{(\epsilon)} = \left(L_{z,0}^{(\epsilon)} \right)^2 - \frac{\beta_0^{(\epsilon)}}{L_0^{(\epsilon)}}. \quad (38.22)$$

By (38.18), $\lim_{\epsilon \rightarrow 0+} \beta_0^{(\epsilon)} = 0$. Therefore, $\lim_{\epsilon \rightarrow 0+} c_1^{(\epsilon)} = \alpha^2$. Consequently, $\lim_{\epsilon \rightarrow 0+} L^2(z; \epsilon) = \alpha^2(z - Z_c)^2$. \square

Corollary 38.3 $\lim_{\epsilon \rightarrow 0+} \zeta(z = Z_c; \epsilon) = \infty$.

Proof By (38.15b) and (38.21),

$$\lim_{\epsilon \rightarrow 0+} \zeta(z = Z_c; \epsilon) = \lim_{\epsilon \rightarrow 0+} \int_0^{Z_c} \frac{dz}{L^2(z; \epsilon)} = \int_0^{Z_c} \frac{dz}{\alpha^2(Z_c - z)^2} = \infty. \quad \square$$

To go back from $L(z)$ to ψ , we make use of

Lemma 38.3 Let $\psi_{R^{(0)}}$ be given by (38.15b). If $L(z) = \alpha|Z_c - z|$, then

$$\psi_{R^{(0)}}(z, r) = \begin{cases} e^{i\theta_0} \psi_{R^{(0)}, \alpha}^{\text{explicit}}(z, r), & \text{if } 0 \leq z < Z_c, \\ e^{i\theta_1} \psi_{R^{(0)}, \alpha}^{\text{explicit}*}(2Z_c - z, r), & \text{if } z > Z_c, \end{cases} \quad (38.23)$$

where $\psi_{R^{(0)}, \alpha}^{\text{explicit}}$ is given by (38.3) and $\theta_0, \theta_1 \in \mathbb{R}$.

Proof of Proposition 38.1

In Lemma 38.2 we saw that the solution of the reduced system is given by (38.21) for $z_{\text{ad}} \leq z < \infty$. Therefore, by Lemma 38.3, when $z_{\text{ad}} \leq z < Z_c$, then $\psi_{R^{(0)}}(z, r) = \psi_{R^{(0)}, \alpha}^{\text{explicit}}(z, r) e^{i\theta_0}$, and when $z > Z_c$, then $\psi_{R^{(0)}}(z, r) = \psi_{R^{(0)}, \alpha}^{\text{explicit}*}(2Z_c - z, r) \lim_{\epsilon_n \rightarrow 0} e^{i\theta_1(\epsilon_n)}$.

Since $\arg \psi(z, 0) \sim \arg \psi_{R^{(0)}}(z, 0) = \zeta(z)$, Corollary 38.3 shows that the limiting phase becomes infinite at Z_c , hence also for $z > Z_c$. Therefore, for a given $z > Z_c$ and $\theta \in \mathbb{R}$, there exists a sequence $\epsilon_n \rightarrow 0+$ such that $e^{i \arg \psi^{(\epsilon_n)}(z, 0)} = e^{i\theta}$. Since $\psi_{\text{coll}} \rightarrow \psi_{R^{(0)}}$ and $\psi_{\text{outer}} \rightarrow \phi(\mathbf{x}) \in L^2$ as $z \rightarrow Z_c$, the proposition follows.

38.2.2 Comparison of Proposition 38.1 and Theorem 10.2

In Theorem 10.2, Merle, Raphaël, and Szeftel showed that any Bourgain-Wang blowup solution lies on the boundary of an H^1 open set of global solutions that scatter forward and backward in z , and also on the boundary of an H^1 open set of

solutions that undergo a loglog blowup at a finite z . These results follow immediately from the reduced equation (38.16) and relation (38.18), since

- The Bourgain-Wang blowup solution ψ_{BW} corresponds to $\epsilon = 0$. Indeed, $\beta(\epsilon = 0) = 0$ implies that $L_{zz} = 0$, i.e., the blowup rate is linear.
- For any $\epsilon > 0$, $\beta_0^{(\epsilon)} < 0$. Hence, by (38.22), $L(z)$ remains strictly positive and satisfies $\lim_{z \rightarrow \pm\infty} L(z) = \infty$.
- For any $\epsilon < 0$, $\beta_0^{(\epsilon)} > 0$. Hence, $L(z)$ goes to zero at some finite $Z_c^{(\epsilon)}$ at the loglog rate (Proposition 18.1). In addition, $\lim_{\epsilon \rightarrow 0+} Z_c^{(\epsilon)} = Z_c$.

A notable difference between these two results is that in Theorem 10.2, Merle, Raphaël, and Szeftel started from the Bourgain-Wang solution at the singularity point Z_c , and then found a smooth deformation such that the deformed solutions belong to the above two open sets on either side of the Bourgain-Wang solution. In Proposition 38.1, Fibich and Klein started from the initial condition $\psi_0 = Kf(\mathbf{x})$, and obtained the Bourgain-Wang solution as $K \rightarrow K_{\text{th}}-$.⁶

38.3 Reversible Continuations

The continuation in Proposition 38.1 preserves the symmetry property of Theorem 38.1. More generally, the symmetry property holds for any continuation that preserves the NLS invariance under the *reversibility transformation*

$$z \rightarrow -z \quad \text{and} \quad \psi \rightarrow \psi^*, \quad (38.24)$$

and also satisfies the constant-phase condition (38.26):

Lemma 38.4 ([85]) *Let ψ be a solution of the critical or supercritical NLS*

$$i\psi_z(z, \mathbf{x}) + \Delta\psi + |\psi|^{2\sigma}\psi = 0, \quad \psi_0(0, \mathbf{x}) = \psi_0(\mathbf{x}), \quad \sigma d \geq 2 \quad (38.25)$$

that blows up at Z_c , and let $\psi^{(\epsilon)}(z, \mathbf{x})$ be a one-parameter family which is smooth in ϵ and satisfies the following four conditions:

1. $\psi^{(\epsilon)}$ exists globally for $0 < \epsilon \ll 1$.
2. $\lim_{\epsilon \rightarrow 0+} \psi^{(\epsilon)} = \psi$ for $0 \leq z < Z_c$.
3. $\psi^{(\epsilon)}$ is invariant under (38.24).

⁶ Another difference is that, unlike Proposition 38.1, the proof of Theorem 10.2 is rigorous.

4. Let Z_{\max}^ϵ denote the point at which the collapse of $\psi^{(\epsilon)}$ is arrested.⁷ Then there exists $\alpha^{(\epsilon)} \in \mathbb{R}$ such that for all $\mathbf{x} \in \mathbb{R}^d$,

$$\arg \psi^{(\epsilon)}(Z_{\max}^\epsilon, \mathbf{x}) \equiv \alpha^{(\epsilon)} \quad (\text{constant-phase condition}). \quad (38.26)$$

Then the continuation satisfies the symmetry property

$$\lim_{\epsilon \rightarrow 0+} \left| \psi^{(\epsilon)}(Z_c + z, \mathbf{x}) \right| = |\psi(Z_c - z, \mathbf{x})|, \quad z > 0.$$

If, in addition, ψ satisfies the fifth condition

$$5. \lim_{z \rightarrow Z_c} \arg \psi(z, 0) = \infty,$$

then the continuation also satisfies the phase-loss property, i.e., for any $\theta \in \mathbb{R}$, there exists a sequence $\epsilon_n \rightarrow 0+$ (depending on θ), such that

$$\lim_{\epsilon_n \rightarrow 0+} \psi^{(\epsilon_n)}(Z_c + z, \mathbf{x}) = e^{i\theta} \psi^*(Z_c - z, \mathbf{x}), \quad z > 0.$$

Proof A proof similar to that of Lemma 2.16 gives

$$\psi^{(\epsilon)}(Z_{\max}^\epsilon + z, \mathbf{x}) = e^{2i\alpha^{(\epsilon)}} \psi^{(\epsilon)*}(Z_{\max}^\epsilon - z, \mathbf{x}), \quad z > 0. \quad (38.27)$$

Since $\lim_{z \rightarrow Z_c} \|\psi(z)\|_{2\sigma+2} = \infty$ and $\lim_{\epsilon \rightarrow 0} \|\psi^\epsilon(z)\|_{2\sigma+2} = \|\psi(z)\|_{2\sigma+2} < \infty$ for $0 \leq z < Z_c$, it follows that $\lim_{\epsilon \rightarrow 0+} Z_{\max}^\epsilon = Z_c$. The symmetry property follows by taking the limit of (38.27) as $\epsilon \rightarrow 0+$.

Finally, by conditions 4 and 5,

$$\lim_{\epsilon \rightarrow 0+} \alpha^{(\epsilon)} = \lim_{\epsilon \rightarrow 0+} \arg \psi^{(\epsilon)}(Z_{\max}^\epsilon, 0) = \lim_{z \rightarrow Z_c} \arg \psi(z, 0) = \infty.$$

Hence, for any θ , there exists $\epsilon_n \rightarrow 0+$ such that $e^{2i\alpha^{(\epsilon)}} = e^{i\theta}$. Therefore, the phase-loss property follows. \square

The interpretation of Lemma 38.4 is as follows. Conditions 1 and 2 say that $\lim_{\epsilon \rightarrow 0+} \psi^{(\epsilon)}$ is a continuation of ψ . Condition 3 says that the continuation is reversible in z . The constant-phase condition (Condition 4) says that the solution is collimated at $z = Z_{\max}^\epsilon$. Intuitively, this is because the solution is focusing for $z < Z_{\max}^\epsilon$ and defocusing for $z > Z_{\max}^\epsilon$. By Conditions 3 and 4, the propagation dynamics to the left and to the right of Z_{\max}^ϵ are identical, see (38.27).⁸ Therefore, letting $\epsilon \rightarrow 0$, we obtain the symmetry property. Condition 5 says that the phase of the singular solution ψ becomes infinite at the singularity. This condition holds

⁷ For example, we can set $Z_{\max}^\epsilon := \arg \max_z \|\psi^{(\epsilon)}(z)\|_{2\sigma+2}$.

⁸ See Sect. 2.16 for a similar situation in the linear case.

for all known singular solutions of the critical and supercritical NLS. Therefore, the post-collapse phase is lost.

The conditions of Lemma 38.4 are not sharp. For example, in Sect. 38.6.6 we shall see that the vanishing linear-damping continuation of $\psi_{R^{(0)}, \alpha}^{\text{explicit}}$ satisfies the symmetry and phase-loss properties, even though $\psi^{(\epsilon)}$ is not reversible in z .

An immediate consequence of Lemma 38.4 is

Corollary 38.4 *Under conditions 1–4 of Lemma 38.4, $\lim_{\epsilon_n \rightarrow 0+} \psi^{(\epsilon_n)}$ is in H^1 for $z > Z_c$. Hence, continuations that satisfy these four conditions lead to a point singularity and not to a filament singularity.*

In Sect. 38.4 we will see that reversible continuations can also lead to a filament singularity. In such cases, however, the constant-phase condition does not hold.

38.4 Vanishing Nonlinear-Saturation Continuation

In this section we consider a continuation which is based on the addition of small nonlinear saturation. The motivation for this approach comes from the *vanishing-viscosity solutions* of hyperbolic conservation laws. Of course, the key question is which physical mechanism plays the role of “viscosity” in the NLS. In the nonlinear optics context, there are numerous candidates, namely all the mechanisms neglected in the derivation of the NLS from Maxwell’s equations: Nonparaxiality, high-order nonlinearities, dispersion, damping, etc. Of course, for a physical mechanism to play the role of “viscosity”, it should arrest collapse regardless of how small it is, so that one can let this term go to zero and still have global solutions. This requirement rules out some candidates such as linear damping (Sect. 33.2.3), but still leaves plenty of potential candidates, such as nonlinear saturation, nonparaxiality and nonlinear damping.

The addition of small nonlinear saturation is “physical”. Indeed, In Sect. 32.1 we saw that the cubic Kerr nonlinearity is only the leading-order approximation to the nonlinear polarization field, and that a more accurate description includes higher-order nonlinearities.

38.4.1 Merle’s Rigorous Analysis

In 1992, Merle rigorously analyzed the continuation which is based on arresting collapse with a small nonlinear saturation:⁹

⁹ Strictly speaking, this continuation is based on the addition of a defocusing supercritical nonlinearity. The effect of this perturbation is, however, equivalent to that of nonlinear saturation (Sect. 32.4.2).

Theorem 38.3 ([173]) Let $d \geq 2$ and $\psi_0 \in \Sigma_{\text{radial}} := H_{\text{radial}}^1 \cap \{r\psi_0 \in L^2\}$, such that the solution of the critical NLS (38.1) blows up in finite distance Z_c . For $\epsilon > 0$ and $\frac{4}{d} < q < \frac{4}{d-2}$, let $\psi^{(\epsilon)}$ be the solution of the saturated critical NLS

$$i\psi_z(z, \mathbf{x}) + \Delta\psi + |\psi|^{\frac{4}{d}}\psi - \epsilon|\psi|^q\psi = 0, \quad \psi(0, \mathbf{x}) = \psi_0(r). \quad (38.28)$$

Assume that there exist $z_0 > Z_c$ and a constant $C > 0$ such that

$$\int |\mathbf{x}|^2 |\psi^{(\epsilon)}(z_0, \mathbf{x})|^2 d\mathbf{x} \leq C. \quad (38.29)$$

Then

1. There exists a function $\tilde{\psi}(z, \mathbf{x})$ defined for $z < z_0$, such that for all $r_0 > 0$, $\tilde{\psi} \in \mathcal{C}([0, z_0), L^2(|\mathbf{x}| \geq r_0))$, and $\psi^{(\epsilon)}(z, \mathbf{x}) \rightarrow \tilde{\psi}(z, \mathbf{x})$ in $\mathcal{C}([0, z_0), L^2(|\mathbf{x}| \geq r_0))$ as $\epsilon \rightarrow 0$.
2. For $z < z_0$, there exists a function $P_{\text{filament}}(z) \geq 0$, such that

$$|\psi^{(\epsilon)}(z, \mathbf{x})|^2 \rightarrow P_{\text{filament}}(z) \delta(\mathbf{x}) + |\tilde{\psi}(z, \mathbf{x})|^2, \quad \epsilon \rightarrow 0,$$

in the sense of distributions. Furthermore,

- (a) If $P_{\text{filament}}(z) \neq 0$, then $\lim_{\epsilon \rightarrow 0} \|\psi^{(\epsilon)}(z)\|_{H^1} = \infty$ and $P_{\text{filament}}(z) \geq P_{\text{cr}}$.
- (b) If $P_{\text{filament}}(z) = 0$, then there is a constant $c > 0$ such that for all ϵ , $\|\psi^{(\epsilon)}(z)\|_{H^1} < c$, and $\psi^{(\epsilon)}(z) \rightarrow \tilde{\psi}(z)$ in L^2 .

3. For all $z < z_0$, $P_{\text{filament}}(z) + \int |\tilde{\psi}(z, \mathbf{x})|^2 d\mathbf{x} = \int |\psi_0(\mathbf{x})|^2 d\mathbf{x}$.

Condition (38.29) is believed to hold generically. Therefore, case 2(a) of Theorem 38.3 shows that if the vanishing nonlinear-saturation continuation has a singular component, this continuation consists of an on-axis filament with power $\geq P_{\text{cr}}$, and a regular component elsewhere.

38.4.2 Malkin's Asymptotic Analysis

In 1993, Malkin [164] analyzed asymptotically the dynamics of solutions of the saturated critical NLS (38.28) with $d = 2$ and $q = 4$, for initial conditions that collapse with the $\psi_{R^{(0)}}$ profile in the unsaturated critical NLS (Sect. 32.3). Malkin showed that initially, the solution collapses as in the non-saturated case. Then collapse is arrested by nonlinear saturation, followed by focusing-defocusing oscillations. During each oscillation the collapsing core loses some power to the background. As

a result, the magnitude of the oscillations decreases, so that ultimately the solution approaches a solitary wave of the saturated NLS.

If we fix the initial condition ψ_0 , then as ϵ decreases towards zero, collapse is arrested after more focusing takes place, and so the oscillations occur at higher amplitudes (Fig. 32.1). Hence, it is reasonable to conclude that the amplitude of the limiting solitary wave goes to infinity as $\epsilon \rightarrow 0+$. In addition, as $\epsilon \rightarrow 0+$, the solitary waves of (38.28) approach the solitary waves of the unsaturated critical NLS, and so their power approaches P_{cr} . Hence, Malkin's analysis suggests that

$$P_{\text{filament}}(z) \equiv P_{\text{cr}}, \quad Z_c \leq z < \infty,$$

i.e., after the singularity, the limiting solution consists of a semi-infinite filament with power P_{cr} , and a regular part with power $\|\psi_0\|_2^2 - P_{\text{cr}}$.

38.4.3 Importance of Power Radiation

The analysis of Merle and of Malkin suggest

Conclusion 38.2 *The vanishing nonlinear-saturation continuation of singular solutions of the critical NLS leads to a filament singularity. In addition, the filament power is P_{cr} .*

Since the saturated NLS is reversible in z , Conclusion 38.2 appears to be in violation of Lemma 38.4, see Corollary 38.4. Note, however, that in Lemma 38.4 we assumed that the phase is constant at the point Z_{\max}^ϵ where collapse is arrested. If this constant-phase condition were to hold for the solution of the saturated NLS, then by Lemma 38.4 the solution at $z = 2Z_{\max}^\epsilon$ would have gone back to its initial value and be given by ψ_0^* . Figure 32.1 shows, however, that this is not the case. To understand why this is so, recall that in Sect. 32.3.1 we saw that in the absence of radiation, the collapsing core of the solution of saturated NLS undergoes periodic oscillations, rather than approaches a solitary wave. Therefore, *the nonadiabatic radiation of the collapsing core plays a key role in changing the vanishing nonlinear-saturation continuation from a point singularity to a filament singularity.*

Remark The asymptotic profile of the collapsing core is given by

$$\psi_{\text{coll}}^{(\epsilon)} \sim \psi_{R^{(0)}} = \frac{1}{L^{\frac{d}{2}}(z)} R^{(0)} \left(\frac{r}{L} \right) e^{i\zeta + i \frac{L_z}{L} \frac{r^2}{4}}.$$

Since $L(z)$ attains its minimum at Z_{\max}^ϵ , we have that $L_z(Z_{\max}^\epsilon) = 0$. Hence, the constant-phase condition does hold asymptotically for the collapsing core. As the above results show, this is not enough for Lemma 38.4 to hold.

38.5 Shrinking-Hole Continuation

In this section we present a continuation of ring-type blowup solutions which is based on placing a reflecting hole at the origin and then letting it shrink to a point.

38.5.1 Theory Review

In Chap. 11 we saw that the two-dimensional radial critical NLS

$$i\psi_z(z, r) + \psi_{rr} + \frac{1}{r}\psi_r + |\psi|^2\psi = 0, \quad \psi(0, r) = \psi_0(r) \quad (38.30)$$

admits the explicit ring-type solutions

$$\psi_G^{\text{explicit}}(z, r) = \frac{1}{L(z)}G\left(\frac{r}{L(z)}\right)e^{i\xi(z)+i\frac{L_z}{L}\frac{r^2}{4}}, \quad (38.31a)$$

where

$$L(z) = \sqrt{1 - \alpha^2 z}, \quad \xi = \int_0^z \frac{ds}{L^2(s)} = -\frac{1}{\alpha^2} \ln(1 - \alpha^2 z), \quad (38.31b)$$

and $G(\rho)$ is a solution of

$$G''(\rho) + \frac{G'}{\rho} + \left[\frac{\alpha^4}{16}\rho^2 - 1\right]G + G^3 = 0, \quad 0 \neq G(0) \in \mathbb{R}, \quad G'(0) = 0.$$

This solution blows up in L^4 at $Z_c = \alpha^{-2}$. Setting $z = 0$ in (38.31) gives the corresponding initial condition

$$\psi_{G,0}^{\text{explicit}}(r) = G(r)e^{-\frac{i\alpha^2}{8}r^2}. \quad (38.32)$$

The explicit solution ψ_G^{explicit} is not in H^1 , since it has an infinite power. In Chap. 19 we saw, however, that the critical NLS admits H^1 solutions that (probably) collapse with the ring-type ψ_G profile.

38.5.2 Explicit Continuation of ψ_G^{explicit}

The sub-threshold power continuation of Sect. 38.2 cannot be applied to ψ_G^{explicit} , because these solutions have infinite power.¹⁰ Therefore, to continue ψ_G^{explicit} beyond

¹⁰ This continuation cannot be applied also to H^1 solutions that collapse with the ring-type ψ_G profile, since these solutions only exist for $P \gg P_{\text{cr}}$ (Sect. 19.6).

the singularity, we cut a hole around the origin with radius r_0 , and impose a Dirichlet boundary condition at $r = r_0$. Physically, this is equivalent to placing a reflecting wall at $r = r_0$ (Sect. 16.1). Since $\psi_0 = \psi_{G,0}^{\text{explicit}}$ does not satisfy the Dirichlet boundary condition, we modify it as $\psi_0(r; r_0) := \psi_{G,0}^{\text{explicit}}(r) H_s\left(\frac{r}{r_0}\right)$, where $H_s(\rho) \equiv 0$ for $0 \leq \rho \leq 1$, $H_s(\rho) \equiv 1$ for $\rho \geq 2$, and $H_s(\rho)$ increases smoothly and monotonically for $1 < \rho < 2$. We thus solve the radial NLS

$$i\psi_z(z, r) + \psi_{rr} + \frac{1}{r}\psi_r + |\psi|^2\psi = 0, \quad r_0 < r < \infty, \quad z > 0, \quad (38.33a)$$

subject to the initial condition

$$\psi(0, r) = \psi_{G,0}^{\text{explicit}}(r) H_s\left(\frac{r}{r_0}\right), \quad r_0 < r < \infty, \quad (38.33b)$$

and the Dirichlet boundary condition

$$\psi(z, r_0) = 0, \quad z \geq 0. \quad (38.33c)$$

A typical simulation is shown in Fig. 38.2. Initially the ring becomes higher and narrower as it shrinks towards the hole. After the ring is reflected by the hole, it becomes lower and wider as it expands.

Let $Z_{\text{ref}}^{(r_0)}$ denote the reflection distance, so that the ring shrinks for $0 \leq z < Z_{\text{ref}}^{(r_0)}$ and expands for $Z_{\text{ref}}^{(r_0)} < z < \infty$. Since the ring is collimated at $Z_{\text{ref}}^{(r_0)}$, it is reasonable to assume that there exists $\alpha^{(r_0)} \in \mathbb{R}$ such that

$$\arg \psi(Z_{\text{ref}}^{(r_0)}, r; r_0) \equiv \alpha^{(r_0)}, \quad r_0 \leq r < \infty. \quad (38.34)$$

Under this assumption, we can use Lemma 38.4 to calculate the shrinking-hole continuation of ψ_G^{explicit} :

Proposition 38.2 ([85]) *Let $\psi(z, r; r_0)$ be the solution of (38.33), and assume that condition (38.34) holds. Then for any $\theta \in \mathbb{R}$, there exists a sequence $r_{0,n} \rightarrow 0+$ (depending on θ), such that*

$$\lim_{r_{0,n} \rightarrow 0+} \psi(z, r; r_{0,n}) = \begin{cases} \psi_G^{\text{explicit}}(z, r), & \text{if } 0 \leq z < Z_c, \\ \psi_G^{\text{explicit}*}(2Z_c - z, r)e^{i\theta}, & \text{if } z > Z_c, \end{cases}$$

where $\psi_G^{\text{explicit}}(z, r)$ is given by (38.31) and $Z_c = \alpha^{-2}$. Hence, this continuation satisfies the symmetry and phase-loss properties. In particular, the limiting width is

$$\lim_{r_0 \rightarrow 0+} L(z; r_0) = \sqrt{\left|1 - \frac{z}{Z_c}\right|}. \quad (38.35)$$

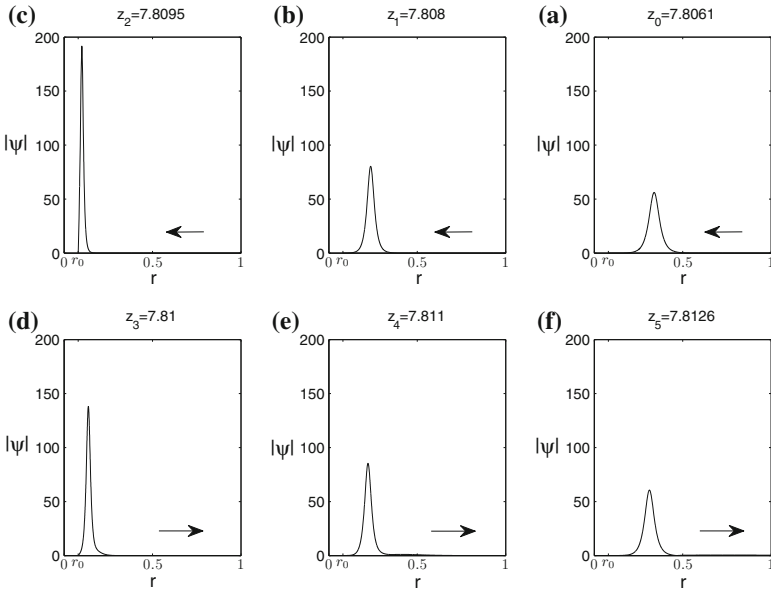


Fig. 38.2 Solution of (38.33) with $r_0 = 0.08$ at **a** $z_0 \approx 7.806$, **b** $z_1 \approx 7.808$, **c** $z_2 \approx 7.8095$, **d** $z_3 \approx 7.810$, **e** $z_4 \approx 7.811$, **f** $z_5 \approx 7.8126$. The arrows denote the direction in which the ring moves. From [85]

Proof We give an informal proof that the conditions of Lemma 38.4 hold.

1. The solution of (38.33) exists globally, since otherwise it collapses at some $0 < r_c < \infty$ (a standing ring), or at $r_c = \infty$ (an expanding ring). The first option is only possible, however, if the nonlinearity is quintic or higher (Lemma 22.1). The second option is not possible for any nonlinearity (Sect. 23.8).
2. By continuity, $\lim_{r_0 \rightarrow 0+} \psi = \psi_G^{\text{explicit}}$ for $0 \leq z < Z_c$.
3. The NLS (38.33a) is reversible in z .
4. The constant-phase condition is (38.34).
5. $\lim_{z \rightarrow Z_c} \arg \psi_G^{\text{explicit}} = \infty$, see (38.31b). □

The main weakness of Proposition 38.2 is that it relies on the assumption that (38.34) holds. Indeed, in Sect. 38.4.3 we saw that the constant-phase condition is not always satisfied when collapse is arrested, and that this can lead to violation of Lemma 38.4 even when the continuation is reversible. Nevertheless, the numerical simulations in [85] provided a strong support to Proposition 38.2. For example, in Fig. 38.3a we plot $L(z; r_0)$ for $r_0 = 0.15, 0.125, 0.1$, and 0.08 . The curve obtained from extrapolation of these curves to $r_0 = 0$, see Fig. 38.3b, is nearly identical to the limiting curve (38.35) predicted by Proposition 38.2.

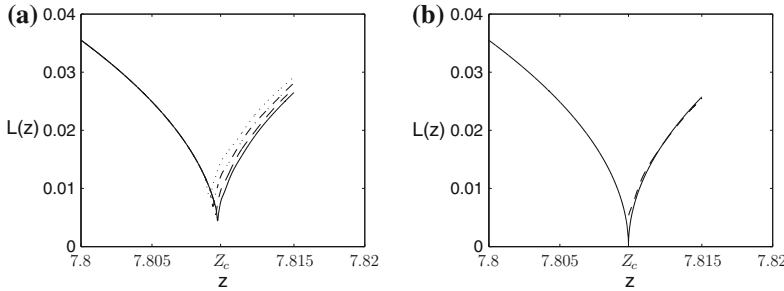


Fig. 38.3 Solution of (38.33). **a** The width of $\psi(z, r; r_0)$ for $r_0 = 0.15$ (dots), $r_0 = 0.125$ (dashed-dots), $r_0 = 0.1$ (dashes), and $r_0 = 0.08$ (solid). Here, $L(z; r_0) := G(0)/|\psi(z, 0; r_0)|$. **b** Extrapolation of the four curves in subplot (a) to $r_0 = 0$ (dashed). The solid line is $L(z) = \sqrt{|1 - z/Z_c|}$. From [85]

38.6 Vanishing Nonlinear-Damping Continuation

38.6.1 Physical Motivation

In this section we present a continuation based on the addition of nonlinear damping. The addition of nonlinear damping is “physical”, see Sect. 33.2.1. As with the vanishing nonlinear-saturation continuation, the motivation for this approach comes from vanishing-viscosity solutions of hyperbolic equations (Sect. 38.4). Here, however, “viscosity = nonlinear damping”.

38.6.2 Arrest of Collapse by Nonlinear Damping—Review

Let $\psi^{(\delta)}$ be the solution of the damped NLS

$$i\psi_z(z, \mathbf{x}) + \Delta\psi + |\psi|^p\psi + i\delta|\psi|^q\psi = 0, \quad \psi(0, \mathbf{x}) = \psi_0(\mathbf{x}). \quad (38.36)$$

Assume that ψ_0 is such that the undamped solution $\psi^{(\delta=0)}$ becomes singular. If the solution of (38.36) exists globally for any $0 < \delta \ll 1$, we can define the vanishing-damping continuation of $\psi^{(\delta=0)}$ as

$$\psi^{\text{continuation}} := \lim_{\delta \rightarrow 0+} \psi^{(\delta)}. \quad (38.37)$$

In Sects. 33.2.3 and 33.2.2 we saw that generically, in the critical case $p = 4/d$, subcritical nonlinear damping ($q < 4/d$) arrests collapse only if δ is “sufficiently large”. When nonlinear damping is critical or supercritical ($q \geq 4/d$), however, it arrests collapse for any $0 < \delta \ll 1$.

Conclusion 38.3 *Critical and supercritical nonlinear damping can play the role of a regularizing mechanism (“viscosity”) that allows the continuation of the critical NLS beyond the blowup point, but subcritical nonlinear damping cannot play that role.*¹¹

In Sect. 33.2.3 we saw that in the supercritical case $p > 4/d$, nonlinear damping arrests collapse for any $0 < \delta \ll 1$ if $q > p$, but (probably) not when $q \leq p$.

Conclusion 38.4 *Nonlinear damping can play the role of a regularizing mechanism that allows the continuation of the supercritical NLS beyond the blowup point only if $q > p$.*

38.6.3 Explicit Continuation of $\psi_{R^{(0)},\alpha}^{\text{explicit}}$ with Critical Nonlinear Damping

In 2011, Fibich and Klein calculated explicitly the vanishing critical nonlinear damping continuation of $\psi_{R^{(0)},\alpha}^{\text{explicit}}$:

Proposition 38.3 ([85]) *Let $\psi^{(\delta)}(z, r)$ be the solution of the critical NLS with critical nonlinear damping*

$$i\psi_z(z, \mathbf{x}) + \Delta\psi + (1 + i\delta)|\psi|^{\frac{4}{d}}\psi = 0, \quad \delta > 0, \quad (38.38)$$

subject to

$$\psi_0(\mathbf{x}) = \psi_{R^{(0)},\alpha}^{\text{explicit}}(0, r), \quad (38.39)$$

see (38.3a). Then for any $\theta \in \mathbb{R}$, there exists a sequence $\delta_n \rightarrow 0+$, depending on θ , such that

$$\lim_{\delta_n \rightarrow 0+} \psi^{(\delta_n)}(z, r) = \begin{cases} \psi_{R^{(0)},\alpha}^{\text{explicit}}(z, r), & \text{if } 0 \leq z < Z_c, \\ \psi_{R^{(0)},\tilde{\alpha}}^{\text{explicit}*}(2Z_c - z, r)e^{i\theta}, & \text{if } Z_c < z < \infty, \end{cases} \quad (38.40)$$

where

$$\tilde{\alpha} = \kappa\alpha$$

and $\psi_{R^{(0)},\alpha}^{\text{explicit}}$ is given by (38.3). In particular, the limiting width is

$$\lim_{\delta \rightarrow 0+} L(z; \delta) = \begin{cases} \alpha(Z_c - z), & \text{if } 0 \leq z < Z_c, \\ \kappa\alpha(z - Z_c), & \text{if } Z_c < z < \infty. \end{cases} \quad (38.41)$$

¹¹ The minimal-power blowup solutions $\psi_{R^{(0)},\alpha}^{\text{explicit}}$, however, can be continued with a subcritical nonlinear damping (Sect. 38.6.6).

The constant κ is given by

$$\kappa = \pi [\text{Bi}(0)\text{Ai}'(s^*) - \text{Ai}(0)\text{Bi}'(s^*)] = \frac{\text{Ai}(0)}{-\text{Ai}(s^*)} \approx 1.614, \quad (38.42)$$

where Ai and Bi are the Airy and Bairy functions, respectively, and $s^* \approx -2.6663$ is the first negative root of $G(s) = \sqrt{3}\text{Ai}(s) - \text{Bi}(s)$, see Fig. 38.6a.

Proof See Sect. 38.6.4 and (38.71). \square

In Theorem 38.1 we presented Merle's sub-threshold power continuation of $\psi_{R^{(0)},\alpha}^{\text{explicit}}$. Proposition 38.3 provides a different continuation of $\psi_{R^{(0)},\alpha}^{\text{explicit}}$. In both continuations the post-collapse limit is only determined up to multiplication by $e^{i\theta}$. This phase-loss property follows from the fact that the phase of $\psi_{R^{(0)},\alpha}^{\text{explicit}}$ becomes infinite at Z_c . Therefore, it holds for any continuation of $\psi_{R^{(0)},\alpha}^{\text{explicit}}$.

As in the motivation for Merle's continuation (Sect. 38.1.1), since

$$\lim_{z \rightarrow Z_c^-} \lim_{\delta \rightarrow 0+} |\psi^{(\delta)}|^2 = \lim_{z \rightarrow Z_c^-} |\psi_{R^{(0)},\alpha}^{\text{explicit}}|^2 = P_{\text{cr}} \delta(r),$$

$\lim_{\delta \rightarrow 0+} \psi^{(\delta)}$ for $z > Z_c$ is a *minimal-power blowup solution* that collapses as $z \rightarrow Z_c+$. In addition, since $\psi^{(\delta)}$ is radial, then so is $\lim_{\delta \rightarrow 0+} \psi^{(\delta)}$. Therefore, by Theorem 13.12, $\lim_{\delta \rightarrow 0+} \psi^{(\delta)}$ for $z > Z_c$ has to be given by $\psi_{R^{(0)},\tilde{\alpha}}^{\text{explicit}*}$ for some $\tilde{\alpha} > 0$. Since

$$H(\psi_{R^{(0)},\alpha}^{\text{explicit}}) = M\alpha^2, \quad H(\psi_{R^{(0)},\tilde{\alpha}}^{\text{explicit}*}) = M\tilde{\alpha}^2,$$

see (38.10), the value of $\tilde{\alpha}$ depends on the limiting Hamiltonian. In Merle's continuation the Hamiltonian is conserved for any $\epsilon > 0$, hence also as $\epsilon \rightarrow 0+$. Therefore, in Merle's continuation $\tilde{\alpha} = \alpha$. Nonlinear damping, however, increases the Hamiltonian for any $\delta > 0$, and even as $\delta \rightarrow 0+$, see Sect. 38.6.5. Indeed, by (38.40),

$$\lim_{\delta \rightarrow 0+} H(\psi^{(\delta)}) = \begin{cases} M\alpha^2, & \text{if } 0 \leq z < Z_c, \\ M\alpha^2\kappa^2, & \text{if } Z_c < z < \infty. \end{cases}$$

Conclusion 38.5 The vanishing critical nonlinear damping continuation of $\psi_{R^{(0)},\alpha}^{\text{explicit}}$ leads to a finite increase of the Hamiltonian at Z_c .

As a result, the defocusing velocity (angle) $\tilde{\alpha} = \kappa\alpha$ is higher than the focusing velocity (angle) α , as illustrated in Fig. 38.4.

Corollary 38.5 The vanishing critical nonlinear-damping continuation of $\psi_{R^{(0)},\alpha}^{\text{explicit}}$ is asymmetric with respect to Z_c . In particular, it does not satisfy the symmetry property.

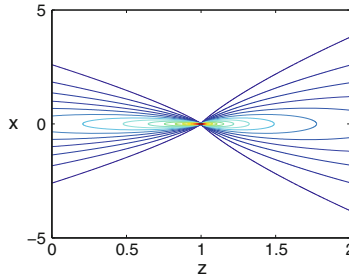


Fig. 38.4 Contour plot of the vanishing critical nonlinear damping continuation of $\psi_{R^{(0)},\alpha}^{\text{explicit}}$, see (38.40). Here, $d = 1$ and $Z_c = 1$. Note the asymmetry with respect to Z_c . From [85]

The “loss of symmetry” is to be expected, since the damped NLS (38.38) is not invariant under the reversibility transformation (38.24). Intuitively, this is because the nonlinear damping term $i\delta|\psi|^{\frac{4}{d}}\psi$ reduces the power as z increases, but increases it as z decreases.

Simulations

To illustrate Proposition 38.3 numerically, we solved the damped NLS (38.38) with the initial condition (38.39). Figure 38.5a shows that as $\delta \rightarrow 0+$, the maximal amplitude is attained at $Z_{\max}^{(\delta)} \rightarrow Z_c$. Figure 38.5b, c confirm that $\lim_{\delta \rightarrow 0+} L(z; \delta)$ is given by (38.41), and that

$$\lim_{\delta \rightarrow 0} L_z(z; \delta) = \begin{cases} -\alpha, & \text{if } 0 \leq z < Z_c, \\ \kappa\alpha, & \text{if } Z_c < z < \infty, \end{cases} \quad (38.43)$$

where κ is defined in (38.42). In Fig. 38.5d we plot the accumulated phase at $x = 0$, and observe that small changes in δ have a negligible effect before the collapse but an $O(1)$ effect after the collapse, which is an indication of the phase-loss property.

38.6.4 Proof of Proposition 38.3

To prove Proposition 38.3, we first approximate the NLS (38.38) by a reduced system of ODEs. Then we solve the reduced system explicitly as $\delta \rightarrow 0+$. Without loss of generality we can set $\alpha = 1$.

Derivation of Reduced Equations

We first show that the three conditions of modulation theory (Sect. 31.1.1) are valid at $z = 0$. Indeed, since $\psi_0 = \psi_{R^{(0)}}^{\text{explicit}}(z = 0)$ and $0 < \delta \ll 1$, Conditions 1 and 2

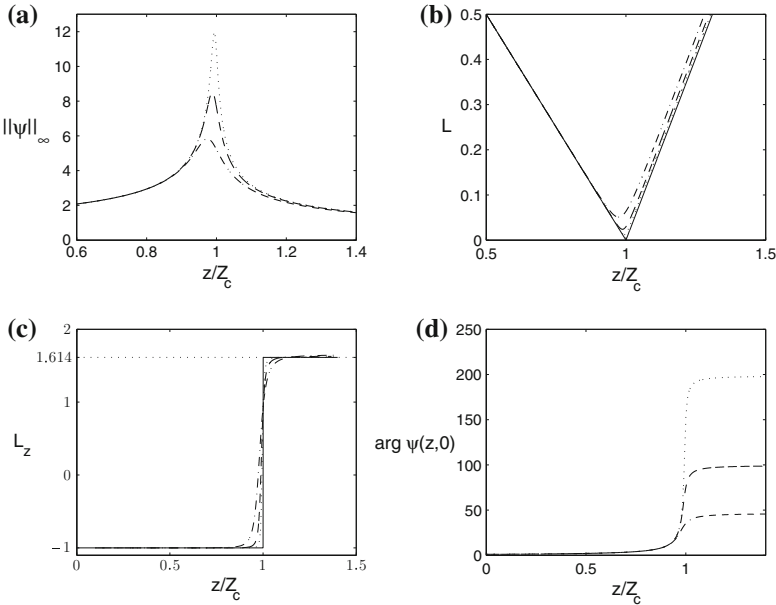


Fig. 38.5 Solution of the damped NLS (38.38) with $d = 1$ and the initial condition (38.39) with $\alpha = 1$ and $Z_c = 1$, for $\delta = 10^{-5}$ (dashes-dots), $\delta = 10^{-6}$ (dashes) and $\delta = 1.25 \cdot 10^{-7}$ (dots). **a** $\|\psi\|_\infty$. **b** $L(z; \delta)$, recovered from ψ using (38.7). The solid line is (38.41). **c** $L_z(z; \delta)$. The solid line is (38.43). **d** Accumulated phase at $x = 0$. From [85]

are satisfied. In addition, in Lemma 38.5 we will prove that $\beta(0) = 0$.¹² Hence, Condition 3 also holds.

Since modulation theory is valid, $\psi^{(\delta)} \sim \psi_{R^{(0)}} = \frac{1}{L^{\frac{d}{2}}(z)} R^{(0)}(\rho) e^{i\xi + i \frac{L_z z^2}{L} \frac{r^2}{4}}$,¹³ and the dynamics of $L(z)$ is governed, to leading order, by the reduced equations of modulation theory.

Lemma 38.5 *Let $\psi^{(\delta)}$ be the solution of the damped NLS (38.38) with the initial condition (38.39) with $\alpha = 1$. Then the reduced equations for $L(z)$ are*

$$\beta_z(z) = -\frac{\tilde{\delta}}{L^2}, \quad \tilde{\delta} := \frac{2c_d \delta}{M}, \quad (38.44a)$$

$$L_{zz}(z) = -\frac{\beta}{L^3}, \quad (38.44b)$$

¹² This also follows from relation (31.39) and the fact that $\|\psi_0\|_2^2 = P_{\text{cr}}$.

¹³ Typically, only the collapsing core approaches the $\psi_{R^{(0)}}$ profile, i.e., $\psi_{\text{coll}}^{(\delta)} \sim \psi_{R^{(0)}}$. Since the initial condition has exactly the critical power, however, ψ has “no tail”. Therefore, $\psi^{(\delta)} \sim \psi_{R^{(0)}}$.

with the initial conditions

$$\beta(0) = 0, \quad L(0) = Z_c, \quad L_z(0) = -1, \quad (38.45)$$

where $c_d = \|R^{(0)}\|_{\frac{4}{d}+2}^{\frac{4}{d}+2}$ and $M = \frac{1}{4} \int |\mathbf{x}|^2 |R^{(0)}|^2 d\mathbf{x}$.

Proof The reduced equations for the damped NLS (38.38) are, see (33.1.3),

$$\beta_z(z) = -\frac{\nu(\beta)}{L^2} - \frac{\tilde{\delta}}{L^2}, \quad \beta(z) = -L^3 L_{zz}, \quad (38.46)$$

where $\nu(\beta)$ is given by (38.16b). We recall that when $\delta = 0$, the initial condition (38.39) leads to the explicit solution (38.2), for which $L(z) = Z_c - z$. Therefore, when $\delta = 0$,

$$L(0) = Z_c, \quad L_z(0) = -1, \quad L_{zz}(0) = 0. \quad (38.47)$$

Since the initial conditions are independent of the subsequent dynamics, they are independent of δ . Consequently, when $\delta > 0$ the initial conditions are also given by (38.47). Therefore, since $\beta(z) = -L^3 L_{zz}$, then $\beta(0) = 0$. Now, since $\nu(\beta = 0) = 0$, see (38.16b), by (38.46) we have that $\beta_z < 0$. Therefore, $\beta \leq 0$, and consequently $\nu(\beta) \equiv 0$, see (38.16b). \square

Explicit Solution of the Reduced Equations

Our ultimate goal is to solve the reduced equations (38.44) with the initial conditions (38.45) explicitly as $\delta \rightarrow 0+$. We first obtain an explicit solution for any $\delta > 0$:

Lemma 38.6 *The solution of (38.44)–(38.45) can be written as $L(z) = 1/A(s(z))$, where*

$$A(s) = \pi \left[\tilde{\delta}^{-\frac{1}{3}} \text{Ai}(0) - \frac{1}{Z_c} \text{Ai}'(0) \right] \left[\sqrt{3} \text{Ai}(s) - \text{Bi}(s) \right] + \frac{1}{Z_c} \frac{\text{Bi}(s)}{\text{Bi}(0)}, \quad (38.48)$$

$\text{Ai}(s)$ and $\text{Bi}(s)$ are the Airy and Bairy functions, respectively, and

$$s(z; \tilde{\delta}) = -\tilde{\delta}^{\frac{1}{3}} \int_0^z A^2(w) dw. \quad (38.49)$$

Proof Equation (38.44a) can be rewritten as $\beta_\xi = -\tilde{\delta}$, where $\xi = \int_0^z L^{-2}$. Since $\beta(z = 0) = \beta(\xi = 0) = 0$, one has that $\beta(\xi) = -\tilde{\delta}\xi$. We recall that, see (18.13a),

$$\beta = \frac{A_\xi \xi}{A}, \quad A = \frac{1}{L}. \quad (38.50)$$

Combining the last two relations gives $A_{\zeta\zeta} = -\tilde{\delta}\zeta A$. The change of variable $s = -\tilde{\delta}^{\frac{1}{3}}\zeta$ transforms this equation into Airy's equation

$$A_{ss} = sA. \quad (38.51)$$

By (38.45), (38.49), and (38.50), the initial conditions for (38.51) are

$$A(s=0) = \frac{1}{L(z=0)} = \frac{1}{Z_c}, \quad (38.52a)$$

$$A_s(s=0) = (L^{-1})_z \frac{dz}{d\zeta} \frac{d\zeta}{ds} = -\frac{L_z(0)}{L^2} L^2 (-\tilde{\delta}^{-\frac{1}{3}}) = -\tilde{\delta}^{-\frac{1}{3}}. \quad (38.52b)$$

The general solution of Airy's equation reads

$$A(s) = k_1 \text{Ai}(s) + k_2 \text{Bi}(s). \quad (38.53)$$

Substituting (38.53) in (38.52) gives

$$k_1 = \frac{\tilde{\delta}^{-\frac{1}{3}} \text{Bi}(0) + \frac{1}{Z_c} \text{Bi}'(0)}{\text{Ai}(0)\text{Bi}'(0) - \text{Ai}'(0)\text{Bi}(0)}, \quad k_2 = -\frac{\tilde{\delta}^{-\frac{1}{3}} \text{Ai}(0) + \frac{1}{Z_c} \text{Ai}'(0)}{\text{Ai}(0)\text{Bi}'(0) - \text{Ai}'(0)\text{Bi}(0)}.$$

We recall that the Wronskian of the Airy and Bairy functions is

$$\text{Ai}(s)\text{Bi}'(s) - \text{Ai}'(s)\text{Bi}(s) = \frac{1}{\pi}. \quad (38.54)$$

Therefore,

$$k_1 = \pi \left(\tilde{\delta}^{-\frac{1}{3}} \text{Bi}(0) + \frac{\text{Bi}'(0)}{Z_c} \right), \quad k_2 = -\pi \left(\tilde{\delta}^{-\frac{1}{3}} \text{Ai}(0) + \frac{\text{Ai}'(0)}{Z_c} \right). \quad (38.55)$$

We also recall that the Airy and Bairy functions satisfy

$$\text{Ai}(0) = \frac{\text{Bi}(0)}{\sqrt{3}}, \quad \text{Ai}'(0) = -\frac{\text{Bi}'(0)}{\sqrt{3}}. \quad (38.56)$$

By (38.54) and (38.56),

$$2\pi \text{Ai}'(0)\text{Bi}(0) = -1, \quad 2\pi \text{Ai}(0)\text{Bi}'(0) = 1. \quad (38.57)$$

Substituting (38.55) in (38.53) and using (38.56) and (38.57) leads to (38.48). \square

Calculation of $\lim_{\tilde{\delta} \rightarrow 0+} s(z; \tilde{\delta})$

Relation (38.49) for $s(z; \tilde{\delta})$ is explicit, but not very informative. Numerical integration suggests that $s(z; \tilde{\delta})$ tends to a step function as $\tilde{\delta} \rightarrow 0+$, see Fig. 38.6b. Indeed, we have

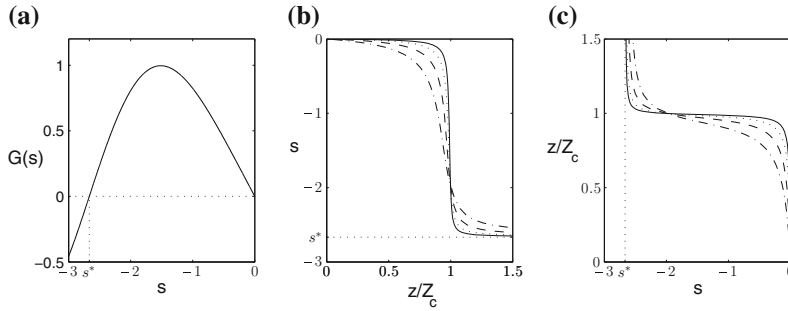


Fig. 38.6 **a** The function $G(s)$, see (38.59). Here, s^* is the first negative root of $G(s) = 0$. **b** $s(z; \tilde{\delta})$, as calculated from numerical integration of (38.49) with $\tilde{\delta} = 10^{-4}$ (dash-dots), $\tilde{\delta} = 10^{-5}$ (dashes), $\tilde{\delta} = 10^{-6}$ (dots), and $\tilde{\delta} = 1.25 \cdot 10^{-7}$ (solid). **c** Same as (b) for the inverse function $z(s; \tilde{\delta})$. From [85]

Lemma 38.7

$$\lim_{\tilde{\delta} \rightarrow 0+} s(z; \tilde{\delta}) = \begin{cases} 0, & \text{if } 0 \leq z < Z_c, \\ s^*, & \text{if } Z_c < z < \infty, \end{cases} \quad (38.58)$$

where $s^* \approx -2.6663$ is the first negative root of $G(s) = 0$, and

$$G(s) = \sqrt{3} \operatorname{Ai}(s) - \operatorname{Bi}(s). \quad (38.59)$$

Proof This result will follow from Corollary 38.7 and Lemma 38.13. The value of s^* was computed numerically, see Fig. 38.6a. \square

Inverting relation (38.49) gives

$$z(s; \tilde{\delta}) = \tilde{\delta}^{-\frac{1}{3}} \int_s^0 \frac{1}{A^2(s)} ds. \quad (38.60)$$

The limit of $z(s; \tilde{\delta})$ is also a step function, see Fig. 38.6c. We begin by computing this limit analytically.

Lemma 38.8 Let $s_{\tilde{\delta}}^*$ be the first negative root of $A(s; \tilde{\delta})$, see (38.48). Then $\lim_{s \rightarrow s_{\tilde{\delta}}^*+} z(s; \tilde{\delta}) = \infty$.

Proof For any $0 < \epsilon \ll 1$,

$$z\left(s_{\tilde{\delta}}^*\right) > \tilde{\delta}^{-\frac{1}{3}} \int_{s_{\tilde{\delta}}^*}^{s_{\tilde{\delta}}^* + \epsilon} \frac{1}{A^2(s)} ds.$$

By definition, $A(s_{\tilde{\delta}}^*; \tilde{\delta}) = 0$. Furthermore, since $A(s; \tilde{\delta})$ is a nontrivial solution of Airy's equation, one has that $A_s(s_{\tilde{\delta}}^*; \tilde{\delta}) \neq 0$, since otherwise by uniqueness one gets $A(s; \tilde{\delta}) \equiv 0$. Therefore, there exists $\epsilon > 0$ such that

$$A(s; \tilde{\delta}) \sim \left(s - s_{\tilde{\delta}}^* \right) A_s \left(s_{\tilde{\delta}}^*; \tilde{\delta} \right), \quad s_{\tilde{\delta}}^* \leq s \leq s_{\tilde{\delta}}^* + \epsilon. \quad (38.61)$$

Hence,

$$\int_{s_{\tilde{\delta}}^*}^{s_{\tilde{\delta}}^* + \epsilon} \frac{1}{A^2(s)} ds \sim \frac{1}{A_s^2 \left(s_{\tilde{\delta}}^*; \tilde{\delta} \right)} \int_{s_{\tilde{\delta}}^*}^{s_{\tilde{\delta}}^* + \epsilon} \frac{1}{\left(s - s_{\tilde{\delta}}^* \right)^2} ds = \infty,$$

and so $z(s_{\tilde{\delta}}^*) = \infty$. \square

By (38.49) and Lemma 38.8, $s(z; \tilde{\delta})$ is monotonically decreasing from $s(z=0) = 0$ to $s(z = \infty) = s_{\tilde{\delta}}^*$. Hence, the interval $0 \leq z < \infty$ is mapped to $0 \geq s > s_{\tilde{\delta}}^*$. Since $\text{Ai}(s)$ and $\text{Bi}(s)$ are bounded for $s \leq 0$, see Fig. 33.2, $A(s; \tilde{\delta})$ is finite for $s \leq 0$, see (38.48). This shows that the solution of the damped NLS (38.38) does not collapse. Note that $A(s = s_{\tilde{\delta}}^*) = 0$ corresponds to $L(z = \infty) = \infty$, i.e., to scattering.

Lemma 38.9 $\lim_{\tilde{\delta} \rightarrow 0+} s_{\tilde{\delta}}^* = s^*$.

Proof By (38.48), as $\tilde{\delta} \rightarrow 0+$,

$$A(s) \sim \pi \text{Ai}(0) \tilde{\delta}^{-\frac{1}{3}} \left[\sqrt{3} \text{Ai}(s) - \text{Bi}(s) \right] = \pi \text{Ai}(0) \tilde{\delta}^{-\frac{1}{3}} G(s). \quad (38.62)$$

Therefore, $\lim_{\tilde{\delta} \rightarrow 0+} s_{\tilde{\delta}}^*$ satisfies (38.59). \square

Lemma 38.10 Let $0 < -s \ll 1$. Then $\lim_{\tilde{\delta} \rightarrow 0+} z(s; \tilde{\delta}) = Z_c$.

Proof Expression (38.48) can be rewritten as $A(s; \tilde{\delta}) = E(s) \tilde{\delta}^{-\frac{1}{3}} + \frac{1}{Z_c} F(s)$, where

$$E(s) := \pi \text{Ai}(0) G(s), \quad F(s) := \frac{\text{Bi}(s)}{\text{Bi}(0)} - \pi \text{Ai}'(0) G(s). \quad (38.63)$$

Therefore,

$$z(s; \tilde{\delta}) = \tilde{\delta}^{-\frac{1}{3}} \int_s^0 \frac{1}{A^2(w)} dw = \int_s^0 \frac{\tilde{\delta}^{\frac{1}{3}}}{\left(E(w) + \frac{\tilde{\delta}^{\frac{1}{3}}}{Z_c} F(w) \right)^2} dw. \quad (38.64)$$

From (38.56), (38.57), (38.59), and (38.63) it follows that $E(0) = 0$, $F(0) = 1$, and

$$E'(0) = \pi \text{Ai}'(0) \left(\sqrt{3} \text{Ai}'(0) - \text{Bi}'(0) \right) = -2\pi \text{Ai}(0) \text{Bi}'(0) = -1. \quad (38.65)$$

Hence,

$$E(s) \sim -s, \quad F(s) \sim 1, \quad -1 \ll s \leq 0.$$

Substituting this in (38.64) gives

$$z(s; \tilde{\delta}) \sim \int_s^0 \frac{\tilde{\delta}^{\frac{1}{3}}}{\left(-w + \frac{\tilde{\delta}^{\frac{1}{3}}}{Z_c}\right)^2} dw = Z_c - \frac{\tilde{\delta}^{\frac{1}{3}}}{-s + \frac{\tilde{\delta}^{\frac{1}{3}}}{Z_c}}, \quad (38.66)$$

and so the result follows. \square

Lemma 38.11 *Let $s^* < s_2 < s_1 < 0$. Then $\lim_{\tilde{\delta} \rightarrow 0} (z(s_2; \tilde{\delta}) - z(s_1; \tilde{\delta})) = 0$.*

Proof By (38.64),

$$z(s_2) - z(s_1) = \int_{s_2}^{s_1} \frac{\tilde{\delta}^{\frac{1}{3}}}{\left(E(s) + \frac{\tilde{\delta}^{\frac{1}{3}}}{Z_c} F(s)\right)^2} ds.$$

Since $E(s) = \pi \text{Ai}(0)G(s)$ and $G(s) > 0$ for $s^* < s < 0$, then $E(s) \geq c > 0$ for $s^* < s_2 \leq s \leq s_1 < 0$, where c is independent of $\tilde{\delta}$. Therefore,

$$\lim_{\tilde{\delta} \rightarrow 0} (z(s_2) - z(s_1)) \sim \lim_{\tilde{\delta} \rightarrow 0} \tilde{\delta}^{\frac{1}{3}} \int_{s_2}^{s_1} \frac{1}{E^2(s)} ds = 0. \quad \square$$

Corollary 38.6 *Let $s^* < s < 0$. Then $\lim_{\tilde{\delta} \rightarrow 0} z(s; \tilde{\delta}) = Z_c$.*

Proof This follows from Lemmas 38.10 and 38.11. \square

Lemma 38.12 *The function $z(s; \tilde{\delta})$ tends to the step function*

$$\lim_{\tilde{\delta} \rightarrow 0+} z(s; \tilde{\delta}) = \begin{cases} \infty, & \text{if } s = s^*, \\ Z_c, & \text{if } s^* < s < 0, \\ 0, & \text{if } s = 0. \end{cases}$$

Proof The top limit follows from Lemmas 38.8 and 38.9, the middle limit from Corollary 38.6, and the bottom one from (38.60). \square

We now go back to $s(z; \tilde{\delta})$.

Corollary 38.7 *Let $0 \leq z < Z_c$. Then $\lim_{\tilde{\delta} \rightarrow 0+} s(z; \tilde{\delta}) = 0$.*

Proof From (38.66) it follows that

$$\lim_{\tilde{\delta} \rightarrow 0+} z(s_1 = -c\tilde{\delta}^{\frac{1}{3}}; \tilde{\delta}) = Z_c - \frac{1}{c + \frac{1}{Z_c}} = \frac{Z_c}{1 + \frac{1}{c} \frac{1}{Z_c}}.$$

Therefore, $z(s; \tilde{\delta})$ has a boundary layer of thickness $\tilde{\delta}^{\frac{1}{3}}$ near $s = 0$, in which it increases monotonically from 0 to Z_c . \square

Lemma 38.13 Let $Z_c < z < \infty$. Then $\lim_{\tilde{\delta} \rightarrow 0+} s(z; \tilde{\delta}) = s^*$.

Proof Since $s(z; \tilde{\delta})$ is monotonically decreasing, see (38.49), $z(s; \tilde{\delta}) \approx Z_c$ for $s_{\tilde{\delta}}^* < s < 0$ (Corollary 38.6), and $\lim_{s \rightarrow s_{\tilde{\delta}}^*} z(s; \tilde{\delta}) = \infty$ (Lemma 38.8), it follows that $s(z; \tilde{\delta})$ has a boundary layer near $s_{\tilde{\delta}}^*$ in which it changes from Z_c to ∞ . Therefore, the values $Z_c < z < \infty$ are attained in the boundary layer around $s_{\tilde{\delta}}^*$. Since $\lim_{\tilde{\delta} \rightarrow 0+} s_{\tilde{\delta}}^* = s^*$, the result follows. \square

This concludes the proof of Lemma 38.7.

Calculation of $\lim_{\tilde{\delta} \rightarrow 0+} L(z; \tilde{\delta})$

Lemma 38.14

$$\lim_{\tilde{\delta} \rightarrow 0+} L(z; \tilde{\delta}) = \begin{cases} Z_c - z, & \text{if } 0 \leq z < Z_c, \\ \kappa(z - Z_c), & \text{if } Z_c < z < \infty, \end{cases} \quad (38.67)$$

where κ is given by (38.42).

Proof Using the relations $L = A^{-1}$ and (38.53), one obtains

$$L_z = -A^{-2} A_s \frac{ds}{dz} = -A^{-2} A_s \left(-\tilde{\delta}^{\frac{1}{3}} A^2 \right) = \tilde{\delta}^{\frac{1}{3}} A_s = \tilde{\delta}^{\frac{1}{3}} [k_1 \text{Ai}'(s) + k_2 \text{Bi}'(s)]. \quad (38.68)$$

By (38.55),

$$\lim_{\tilde{\delta} \rightarrow 0+} \tilde{\delta}^{\frac{1}{3}} k_1 = \pi \text{Bi}(0), \quad \lim_{\tilde{\delta} \rightarrow 0+} \tilde{\delta}^{\frac{1}{3}} k_2 = -\pi \text{Ai}(0).$$

Therefore,

$$\lim_{\tilde{\delta} \rightarrow 0} L_z(z; \tilde{\delta}) = \pi \left[\text{Bi}(0) \text{Ai}'(s^{(\tilde{\delta}=0)}(z)) - \text{Ai}(0) \text{Bi}'(s^{(\tilde{\delta}=0)}(z)) \right],$$

where $s^{(\tilde{\delta}=0)}(z) = \lim_{\tilde{\delta} \rightarrow 0} s(z; \tilde{\delta})$. Hence, by (38.58),

$$\lim_{\tilde{\delta} \rightarrow 0} L_z(z) = \begin{cases} \pi [\text{Bi}(0) \text{Ai}'(0) - \text{Ai}(0) \text{Bi}'(0)], & \text{if } 0 \leq z < Z_c, \\ \pi [\text{Bi}(0) \text{Ai}'(s^*) - \text{Ai}(0) \text{Bi}'(s^*)], & \text{if } Z_c < z < \infty. \end{cases}$$

Since $\pi [\text{Bi}(0) \text{Ai}'(0) - \text{Ai}(0) \text{Bi}'(0)] = -1$, see (38.54),

$$\lim_{\tilde{\delta} \rightarrow 0} L_z(z) = \begin{cases} -1, & \text{if } 0 \leq z < Z_c, \\ \kappa, & \text{if } Z_c < z < \infty, \end{cases}$$

where κ is given by (38.42). Since $L(0) = Z_c$, (38.67) follows. \square

Our last observation concerns the phase. Using $\zeta = \int_0^z L^{-2}$ and (38.67),

$$\lim_{\tilde{\delta} \rightarrow 0+} \zeta(Z_c) = \int_0^{Z_c} \frac{ds}{(Z_c - s)^2} = \infty. \quad (38.69)$$

Therefore, the phase information is lost at the singularity.

Proof of Proposition 38.3

We saw that $\psi^\delta \sim \psi_{R^{(0)}}$, where $L(z)$ is given by (38.67). Therefore, by Lemma 38.3, $\psi_{R^{(0)}}(z, r) = \psi_{R^{(0)}}^{\text{explicit}}(z, r)$ for $0 \leq z < Z_c$ and $\psi_{R^{(0)}}(z, r) = \psi_{R^{(0)}, \kappa}^{\text{explicit}*}(2Z_c - z, r)$ for $z > Z_c$. Since $\arg(\psi(z, 0)) \sim \arg(\psi_{R^{(0)}}(z, 0)) = \zeta(z)$, relation (38.69) shows that the limiting phase becomes infinite at and after the singularity. Hence, for a given $z > Z_c$ and $\theta \in \mathbb{R}$, there exists a sequence $\delta_n \rightarrow 0+$, such that $\lim_{\delta_n \rightarrow 0+} \arg \psi^{(\delta_n)}(z, 0) = \theta$. Thus, Proposition 38.3 follows.

38.6.5 Nonlinear Damping and the Hamiltonian

In the case of a purely non-conservative perturbation¹⁴ such as nonlinear damping, the Hamiltonian of ψ can be approximated by, see (31.47),

$$H(\psi) \sim \frac{M}{2} (L^2)_{zz}. \quad (38.70)$$

Since $-\frac{1}{2} L^2 (L^2)_{zzz} = \beta_z = -\tilde{\delta} L^{-2}$, see (18.13b) and (38.44a),

$$H_z \sim \frac{M}{2} (L^2)_{zzz} = -M \frac{\beta_z}{L^2} = M \frac{\tilde{\delta}}{L^4}.$$

Therefore, *nonlinear damping increases the Hamiltonian*. In fact, even a *vanishing* critical nonlinear damping increases the Hamiltonian:

Lemma 38.15 *Let $\psi^{(\delta)}$ be the solution of the NLS (38.38) with the initial condition (38.39) with $\alpha = 1$. Let $\Delta H := H^{(\delta=0)}(z = \infty) - H^{(\delta=0)}(z = 0)$, where $H^{(\delta=0)}(z) := \lim_{\delta \rightarrow 0} H(\psi^{(\delta)})$ is the limiting Hamiltonian. Then*

$$\Delta H = M \left(\left(\frac{\text{Ai}(0)}{\text{Ai}(s^*)} \right)^2 - 1 \right).$$

¹⁴ i.e., when $f_1(z) \equiv 0$, see Sect. 31.4.1.

Proof By (38.49) and (38.62),

$$H_s = H_z \frac{dz}{ds} = M \frac{\tilde{\delta}}{L^4} \frac{1}{-\tilde{\delta}^{\frac{1}{3}} A^2} = -M \tilde{\delta}^{2/3} A^2 \sim -M \pi^2 A_i^2(0) G^2(s).$$

Therefore,

$$\Delta H := H^{(\delta=0)}(\infty) - H^{(\delta=0)}(0) = \int_0^{s^*} H_s^{(\delta=0)} ds = M \pi^2 A_i^2(0) \int_{s^*}^0 G^2(s) ds.$$

Now,

$$\int_{s^*}^0 G^2 ds = G^2 s \Big|_{s^*}^0 - \int_{s^*}^0 2s G G_s ds = -2 \int_{s^*}^0 s G G_s ds.$$

Since G is a linear combination of $\text{Ai}(s)$ and $\text{Bi}(s)$, $G_{ss} = sG$. Hence,

$$\int_{s^*}^0 G^2 ds = -2 \int_{s^*}^0 G_{ss} G_s ds = -G_s^2 \Big|_{s^*}^0.$$

Therefore, $\Delta H = -M \pi^2 A_i^2(0) G_s^2 \Big|_{s^*}^0$.

Since the Wronskian of the Airy equation is a constant,

$$W(G, A) = G(s) A'_i(s) - A_i(s) G'(s) \equiv G(0) A'_i(0) - A_i(0) G'(0).$$

Therefore, since G vanishes at $s = 0$ and $s = s^*$, $G'(s^*) = \frac{A_i(0)G'(0)}{A_i(s^*)}$. Hence,

$$\Delta H = -M \pi^2 A_i^2(0) G_s^2(0) \left(1 - \left(\frac{\text{Ai}(0)}{\text{Ai}(s^*)} \right)^2 \right).$$

Since $-1 = E'(0) = \pi A_i(0) G'(0)$, see (38.65), the result follows. \square

We can use Lemma 38.15 to obtain a different expression for κ . Indeed, by (38.40) with $\alpha = 1$ and (38.10),

$$\Delta H = H \left(\psi_{R^{(0)}, \kappa}^{\text{explicit}*} \right) - H \left(\psi_{R^{(0)}}^{\text{explicit}} \right) = M (\kappa^2 - 1).$$

Comparison of this expression with Lemma 38.15 gives

$$\kappa = \frac{\text{Ai}(0)}{|\text{Ai}(s^*)|}. \quad (38.71)$$

Exercise 38.1 Show that critical nonlinear damping reduces the power of $\psi_{R^{(0)}, \alpha}^{\text{explicit}}$, but a vanishing critical nonlinear damping does not.

38.6.6 Continuations of $\psi_{R^{(0)},\alpha}^{\text{explicit}}$ with Subcritical and Supercritical Nonlinear Damping

In Proposition 38.3 we considered the continuation of $\psi_{R^{(0)},\alpha}^{\text{explicit}}$ with a critical nonlinear damping. The extension of this result to subcritical and supercritical nonlinear damping, also due to Fibich and Klein, is as follows:

Proposition 38.4 ([86]) *Let $\psi^{(\delta)}(z, r)$ be the solution of the nonlinearly-damped critical NLS*

$$i\psi_z(z, \mathbf{x}) + \Delta\psi + |\psi|^{\frac{4}{d}}\psi + i\delta|\psi|^q\psi = 0, \quad \psi(0, r) = \psi_{R^{(0)},\alpha}^{\text{explicit}}(0, r). \quad (38.72)$$

Then for any $q \geq 0$, there exists $\kappa(q) \geq 1$, such that the following holds. For any $\theta \in \mathbb{R}$, there exists a sequence $\delta_n \rightarrow 0+$, depending on θ , such that

$$\lim_{\delta_n \rightarrow 0+} \psi^{(\delta_n)}(z, r) = \begin{cases} \psi_{R^{(0)},\alpha}^{\text{explicit}}(z, r), & \text{if } 0 \leq z < Z_c, \\ \psi_{R^{(0)},\tilde{\alpha}}^{\text{explicit}*}(2Z_c - z, r)e^{i\theta}, & \text{if } Z_c < z < \infty, \end{cases}$$

where $\tilde{\alpha} = \kappa(q)\alpha$. In particular, the limiting width of the solution is

$$\lim_{\delta \rightarrow 0+} L(z; \delta) = \begin{cases} \alpha(Z_c - z), & \text{if } 0 \leq z < Z_c, \\ \kappa(q)\alpha(z - Z_c), & \text{if } Z_c < z < \infty. \end{cases} \quad (38.73)$$

Proof We sketch an informal proof. Since $\lim_{z \rightarrow Z_c-} |\psi_{R^{(0)},\alpha}^{\text{explicit}}|^2 = P_{\text{cr}} \delta(r)$, then for $z > Z_c$, $\lim_{\epsilon \rightarrow 0+} \psi^{(\epsilon)}$ is a *minimal-power blowup solution* that collapses as $z \rightarrow Z_c+$. In addition, since $\psi^{(\epsilon)}$ is radial, so is $\lim_{\epsilon \rightarrow 0+} \psi^{(\epsilon)}$. Therefore, by Theorem 13.12, $\lim_{\epsilon \rightarrow 0+} \psi^{(\epsilon)}$ for $z > Z_c$ has to be given by $\psi_{R^{(0)},\tilde{\alpha}}^{\text{explicit}*}$ for some $\tilde{\alpha} > 0$. Since nonlinear damping increases the Hamiltonian, $\tilde{\alpha} = \kappa(q) \cdot \alpha \geq \alpha$. Therefore, $\kappa(q) \geq 1$. The phase-loss property holds, because the phase of $\psi_{R^{(0)},\alpha}^{\text{explicit}}$ becomes infinite at Z_c . \square

In Proposition 38.3 the value of $\kappa(q = \frac{4}{d})$ was calculated analytically by solving the reduced equations explicitly as $\delta \rightarrow 0$. The values of $\kappa(q)$ for $q \neq 4/d$ were calculated numerically in Fig. 38.7 by solving the reduced equations of the damped NLS (38.72) as $\delta \rightarrow 0$. These calculations showed that $\kappa(0) = 1$, i.e., that

$$\lim_{\delta \rightarrow 0+} L(z; \delta, q = 0) = \alpha|Z_c - z|, \quad 0 \leq z < \infty.$$

Thus, the vanishing linear-damping continuation of $\psi_{R^{(0)},\alpha}^{\text{explicit}}$ is symmetric with respect to Z_c , even though the equation for $\psi^{(\delta)}$ is not reversible in z . As the nonlinear damping exponent q increases, it leads to a larger increase in the Hamiltonian at the singularity. As a result, the post-collapse defocusing angle $\tilde{\alpha} = \kappa(q)\alpha$ increases with q .

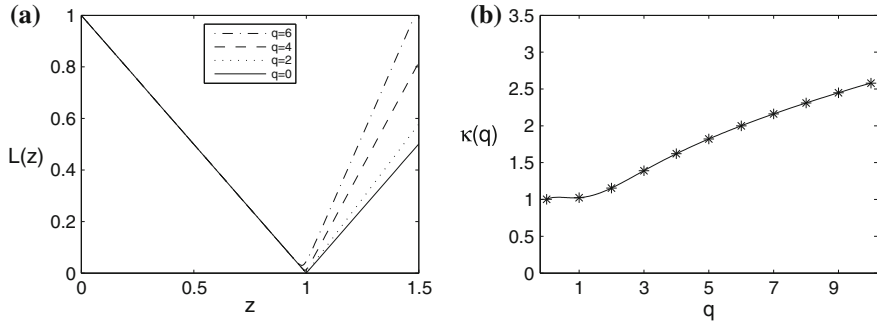


Fig. 38.7 Continuation of $\psi_{R^{(0)},\alpha}^{\text{explicit}}$ with the vanishing nonlinear damping $i\delta|\psi|^q\psi$. **a** The limiting width, see (38.73), for $q = 0$ (solid), $q = 2$ (dots), $q = 4$ (dashes), and $q = 6$ (dash-dot). Here, $\alpha = Z_c = 1$. **b** $\kappa(q)$ for $q = 0, 1, \dots, 10$. From [86]

Remark In Sect. 38.6.2 we noted that subcritical nonlinear damping cannot be used in the continuation of the critical NLS. In the special case of $\psi_{R^{(0)},\alpha}^{\text{explicit}}$, however, we can define the continuation with for $q \geq 0$ (and in particular for $q < \frac{4}{d}$), because even an infinitesimal amount of damping reduces the solution power below P_{cr} and thus arrests collapse.

38.6.7 Continuation of Loglog Collapse

In Sect. 33.3.2 we analyzed the effect of small nonlinear damping on solutions of the critical NLS that undergo a loglog collapse with the peak-type $\psi_{R^{(0)}}$ profile. We saw that in the case of a small critical or supercritical nonlinear damping, collapse is arrested, followed by scattering. We now consider the vanishing nonlinear damping limit of these solutions. The following result is based on informal arguments and numerical simulations:

Proposition 38.5 ([85, 86]) *Let ψ be a solution of the undamped critical NLS (38.1) with an initial condition ψ_0 that collapses with the $\psi_{R^{(0)}}$ profile at the loglog law blowup rate at Z_c . Let $\psi^{(\delta)}$ be the solution of the critical NLS with a critical or supercritical nonlinear damping*

$$i\psi_z(z, \mathbf{x}) + \Delta\psi + |\psi|^{\frac{4}{d}}\psi + i\delta|\psi|^q\psi = 0, \quad q \geq \frac{4}{d},$$

subject to the same initial condition ψ_0 . Then $\lim_{\delta \rightarrow 0+} \psi^{(\delta)} = \psi$ for $0 \leq z < Z_c$. In addition, for any $0 < \delta \ll 1$, there exist $\theta(\delta) \in \mathbb{R}$ and $\phi \in L^2$ such that

$$\lim_{\delta \rightarrow 0+} \left[\psi^{(\delta)}(z, r) - \psi_{R^{(0)}}^*(2Z_c - z, r; \delta) e^{i\theta(\delta)} \right] \xrightarrow{L^2} \phi(r), \quad z \rightarrow Z_c+,$$

where $\psi_{R^{(0)}}$ is given by (38.15b) with some function $L(z; \delta)$, such that

$$\lim_{z \rightarrow Z_c+} \lim_{\delta \rightarrow 0+} L(z; \delta) = 0, \quad \lim_{z \rightarrow Z_c+} \lim_{\delta \rightarrow 0+} L_z(z; \delta) = \infty, \quad \lim_{\delta \rightarrow 0+} \theta(\delta) = \infty.$$

Proof We give a very informal proof. By continuity, as $\delta \rightarrow 0+$, the limiting solution undergoes a loglog collapse. Therefore, by Theorem 14.1, as $z \rightarrow Z_c-$, the collapsing core approaches the $\psi_{R^{(0)}}$ profile, and the non-collapsing tail has an L^2 limit, denoted by ϕ .

After the arrest of collapse by nonlinear damping, the solution defocuses and does not refocus (Sect. 33.3.2). Since as $\delta \rightarrow 0+$ the amount of power that collapses into the singularity is exactly P_{cr} , the expanding core is given by $\psi_{\text{coll}}^{(\delta)} \sim \psi_{R^{(0)}, \alpha}^{\text{explicit}*}(2Z_c - z, r)$, where $\alpha = \alpha(\delta) = \lim_{z \rightarrow Z_c+} L_z(z; \delta)$. We claim that $\lim_{\delta \rightarrow 0+} \alpha(\delta) = +\infty$. Indeed, since $L(z; \delta = 0)$ blows up at the loglog law rate, $\lim_{z \rightarrow Z_c-} L_z(z; \delta = 0) = -\infty$. In addition, since nonlinear damping increases the Hamiltonian (Sect. 38.6.5), the post-collapse defocusing velocity is higher than the pre-collapse focusing velocity. Therefore,

$$\infty = \lim_{z \rightarrow Z_c-} L_z^2(z; \delta = 0) \leq \lim_{\delta \rightarrow 0+} \lim_{z \rightarrow Z_c+} L_z^2(z; \delta) = \lim_{\delta \rightarrow 0+} \alpha^2(\delta).$$

Finally, $\theta(\delta) \rightarrow \infty$, since the phase of loglog solutions becomes infinite as $z \rightarrow Z_c$. \square

Thus, similarly to the continuation of $\psi_{R^{(0)}, \alpha}^{\text{explicit}}$, see Propositions 38.3 and 38.4, this continuation has the phase-loss property. Unlike the continuation of $\psi_{R^{(0)}, \alpha}^{\text{explicit}}$, however, the post-collapse velocity of the expanding core becomes infinite. This is a consequence of the infinite pre-collapse velocity of collapsing loglog solutions, and of the increase of the Hamiltonian at the singularity due to nonlinear damping. Note that because of the infinite velocity of the expanding core, it “immediately” interacts with the non-collapsing tail.

Simulations

To illustrate Proposition 38.5 numerically, in Fig. 38.8a we solve the critical NLS with a critical nonlinear damping with $\psi_0 = \sqrt{1.05} \psi_{R^{(0)}}^{\text{explicit}}(z = 0)$ for several values of δ . All the solutions are highly asymmetric with respect to the point $Z_{\max}^{(\delta)}$ where collapse is arrested. In addition, as $\delta \rightarrow 0+$, the post-collapse expansion of the singular core becomes faster and faster. Similar results were obtained in numerical simulations of loglog solutions of the critical NLS with supercritical nonlinear damping [86].

38.6.8 Continuation of the Supercritical NLS

In [86], Fibich and Klein also studied numerically the vanishing nonlinear damping continuation of solutions of the supercritical NLS that collapse with the peak-type

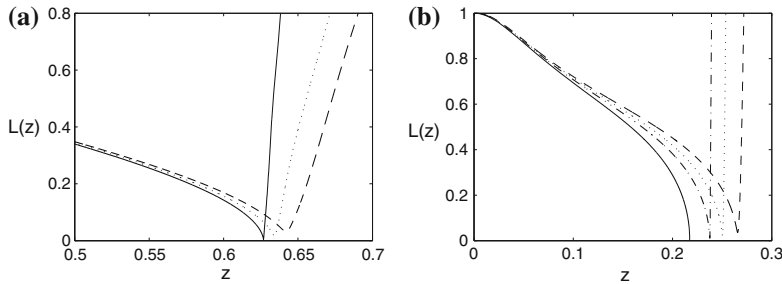


Fig. 38.8 The width $L(z; \delta) := (|\psi(0, 0)|/|\psi(z, 0)|)^{\frac{p-1}{2}}$ of the solution of: **a** the damped critical NLS (38.38) with $d = 1$, $\psi_0(r) = \sqrt{1.05} \psi_{R^{(0)}}^{\text{explicit}}(z = 0, r)$, and $Z_c = 1$, for $\delta = 2.5 \times 10^{-3}$ (dashes), $\delta = 2 \times 10^{-3}$ (dots), and $\delta = 10^{-3}$ (solid). From [85]. **b** the damped supercritical NLS $i\psi_z(z, x) + \psi_{xx} + |\psi|^6\psi + i\delta|\psi|^8\psi = 0$ with $\psi_0(x) = 1.3e^{-x^2}$, for $\delta = 0$ (solid), $\delta = 5 \times 10^{-3}$ (dashed-dots), $\delta = 7.5 \times 10^{-3}$ (dots), and $\delta = 10^{-2}$ (dashes). From [86]

ψ_Q profile. Figure 38.8b shows a typical simulation. As with peak-type singular solutions of the critical NLS (Sect. 38.6.7), nonlinear damping arrests the collapse in a highly asymmetric way, the post-collapse defocusing velocity of the singular core “appears” to increase to infinity as $\delta \rightarrow 0+$, and the post-collapse phase is lost.

38.7 Complex Ginzburg-Landau Continuation

The two-dimensional Complex Ginzburg-Landau equation (CGL)

$$i\psi_t(t, x, y) + \Delta\psi + |\psi|^2\psi - i\epsilon_1\psi - i\epsilon_2\Delta\psi + i\epsilon_3|\psi|^2\psi = 0,$$

arises in models of chemical turbulence, analysis of Poiseuille flow, Rayleigh-Bénard convection and Taylor-Couette flow. Its name comes from the field of superconductivity, where it models phase transitions of materials between superconducting and non-superconducting phases. In [87], Fibich and Levy used modulation theory to show that as $\epsilon_1, \epsilon_2, \epsilon_3 \rightarrow 0$, the collapse dynamics is governed, to leading order, by the reduced equations (38.44) with

$$\tilde{\delta} = \frac{2P_{\text{cr}}}{M}(\epsilon_2 + 2\epsilon_3).$$

Therefore, Propositions 38.3 and 38.5 hold also for the CGL continuation of the critical NLS.

38.8 Vanishing-Diffraction Continuation of the Linear Schrödinger Equation

In the linear Schrödinger equation, under the geometrical optics approximation, a focused input beam collapses at the focal point (Lemma 2.7). Once diffraction is not neglected, however, the focused beam does not collapse to a point, but rather narrows down to a positive diffraction-limited width, and then spreads out with further propagation (Sect. 2.10). Therefore, *diffraction can play the role of “viscosity” in the continuation of singular geometrical optics linear solutions.*

Consider the d -dimensional linear Schrödinger equation

$$2ik_0\psi_z(z, \mathbf{x}) + \Delta\psi = 0, \quad (38.74a)$$

see (1.18), with a focused Gaussian initial condition

$$\psi_0(\mathbf{x}) = e^{-\frac{r^2}{2}} e^{-\frac{ik_0 r^2}{2F}}, \quad r = |\mathbf{x}|, \quad (38.74b)$$

where k_0 is the wavenumber and $F > 0$ is the focal point.

Lemma 38.16 *Under the geometrical optics approximation ($k_0 \rightarrow \infty$), the solution of (38.74) for $0 \leq z < F$ is*

$$\psi_{\text{go}}(z, \mathbf{x}) = \frac{1}{L_{\text{go}}^{\frac{d}{2}}(z)} e^{-\frac{1}{2} \frac{r^2}{L_{\text{go}}^2(z)}} e^{ik_0 \frac{r^2}{2} \frac{L'_{\text{go}}(z)}{L_{\text{go}}(z)}}, \quad L_{\text{go}}(z) = 1 - \frac{z}{F}. \quad (38.75)$$

Proof As in Sect. 2.10, Let $\psi = Ae^{ik_0 S}$, where A and S are real. Substitution in (38.74) gives

$$(\nabla S)^2 + 2S_z - \frac{1}{k_0^2} \frac{\Delta A}{A} = 0, \quad \left(A^2\right)_z + \nabla S \cdot \nabla \left(A^2\right) + A^2 \Delta S = 0, \quad (38.76)$$

with the initial conditions, see (38.74b),

$$S(\mathbf{x}, 0) = -\frac{r^2}{2F}, \quad A^2(\mathbf{x}, 0) = e^{-r^2}. \quad (38.77)$$

Since $k_0 \gg 1$, we can apply the geometrical optics approximation, and neglect the diffraction term ΔA . In this case, (38.76) becomes

$$(\nabla S)^2 + 2S_z = 0, \quad \left(A^2\right)_z + \nabla S \cdot \nabla \left(A^2\right) + A^2 \Delta S = 0. \quad (38.78)$$

The solution of (38.78), subject to the initial conditions (38.77), is

$$S = \frac{r^2}{2} \frac{L_z}{L}, \quad A^2(z, \mathbf{x}) = \frac{1}{L^d(z)} e^{-\frac{r^2}{L^2(z)}}, \quad L(z) = 1 - \frac{z}{F}.$$

Therefore, the result follows. \square

Since $\lim_{z \rightarrow F} |\psi_{\text{go}}|^2 = \|\psi_0\|_2^2 \delta(\mathbf{x})$, the geometrical optics solution blows up at the focal point $z = F$. Equation (38.74) can be solved exactly (i.e., without making the geometrical optics approximation, see Sect. 2.15.3), yielding

$$\psi^{\text{lin}}(z, \mathbf{x}) = \frac{1}{L^{\frac{d}{2}}(z)} e^{-\frac{1}{2} \frac{r^2}{L^2(z)}} e^{ik_0 \frac{r^2}{2} \frac{L_z}{L} + i\zeta(z; k_0)}, \quad (38.79a)$$

where

$$L(z; k_0) = \sqrt{\frac{1}{F} \frac{(z - z_{\min})^2}{z_{\min}} + L_{\min}^2}, \quad (38.79b)$$

$$\zeta(z; k_0) = -\frac{d}{2} \left[\arctan \left(\frac{z - z_{\min}}{L_{\min} \sqrt{F \cdot z_{\min}}} \right) + \arctan \left(\frac{k_0}{F} \right) \right], \quad (38.79c)$$

and

$$z_{\min} = \frac{F}{1 + F^2/k_0^2}, \quad L_{\min} = \frac{F}{\sqrt{F^2 + k_0^2}}. \quad (38.79d)$$

Since $L_{\min} > 0$, $L(z; k_0)$ does not shrink to zero at any $z > 0$. Therefore, ψ^{lin} exists for all $0 \leq z < \infty$, and in particular for $z > F$.

The vanishing-diffraction continuation of ψ_{go} is as follows:

Lemma 38.17 ([85]) *Let ψ^{lin} be the solution of (38.74). Then*

$$\lim_{k_0 \rightarrow \infty} \psi^{\text{lin}}(z, \mathbf{x}) = \begin{cases} \psi_{\text{go}}(z, \mathbf{x}), & \text{if } 0 \leq z < F, \\ (\psi_{\text{go}})^*(2F - z, \mathbf{x}) e^{-i\frac{d}{2}\pi}, & \text{if } F < z < \infty, \end{cases} \quad (38.80)$$

where ψ_{go} is given by (38.75).

Proof It is easy to verify that the limiting width of ψ^{lin} is

$$\lim_{k_0 \rightarrow \infty} L(z; k_0) = \left| 1 - \frac{z}{F} \right| = |L_{\text{go}}(z)|. \quad (38.81)$$

In addition, since $\lim_{k_0 \rightarrow \infty} z_{\min} = F$ and $\lim_{k_0 \rightarrow \infty} L_{\min} = 0$,

$$\lim_{k_0 \rightarrow \infty} \zeta(z; k_0) = \begin{cases} 0, & \text{if } 0 \leq z < F, \\ -\frac{d}{2}\pi, & \text{if } F < z < \infty. \end{cases} \quad (38.82)$$

Therefore, the result follows. \square

Thus, $\lim_{k_0 \rightarrow \infty} \psi^{\text{lin}}$ identifies with ψ_{go} before the focal point, as could be expected by continuity. Beyond the focal point, there is a finite jump in the limiting phase. Other than that, the continuation is symmetric with respect to $Z_c = F$. Indeed, symmetry follows from Lemma 38.4, since the linear Schrödinger equation (38.74) is invariant under the reversibility transformation (38.24), and the phase of ψ^{lin} is constant at the location z_{\min} where its collapse is arrested.¹⁵

By Lemma 38.17, the limiting phase is unique after the singularity. This is the opposite from the nonlinear case, where the post-collapse limiting phase is non-unique.

Conclusion 38.6 ([85]) *The post-collapse loss of phase is a nonlinear phenomenon.*

Indeed, it is because of the nonlinear self-phase modulations that the solution phase blows up at the singularity, which leads to the loss of phase.

38.9 Summary

In this chapter, we presented the available theory on continuations of singular NLS solutions. At present, this theory is quite limited. In particular, it is not clear whether any of the continuations which are presented is “physical”. As noted, there is probably no “universal continuation”, i.e., different physical setups calls for different continuations.

Let us consider the continuation of a collapsing laser beam, which is modeled by a solution of the critical NLS that collapses with the $\psi_{R^{(0)}}$ profile. Since the collapsing core approaches a δ -function with power P_{cr} , it can either be continued with a δ -function filament with power P_{cr} (i.e., a *filament singularity*), or with an expanding $\psi_{R^{(0)}}^*$ profile (i.e., a *point singularity*). Specifically,

- When the collapse-arresting mechanism is conservative (e.g., nonlinear saturation), it generically leads to focusing-defocusing oscillations (Sect. 31.5). Therefore, *continuations based on conservative perturbations generically lead to a filament singularity*.
- When the collapse-arresting mechanism is non-conservative (e.g., nonlinear damping), the solution scatters after its collapse has been arrested, since its power gets below P_{cr} . Therefore, *continuations based on non-conservative perturbations generically lead to a point singularity*. In that case, the continuation will be asymmetric with respect to Z_c , since symmetry generically requires that the continuation be reversible.

The above arguments suggest that any “vanishing-viscosity” continuation of the NLS that leads to a point singularity is asymmetric with respect to Z_c . Therefore, *the*

¹⁵ This is because $L_z(z_{\min}) = 0$, see (38.79).

symmetry property is non-generic. In contrast, the post-collapse phase-loss property appears to be a universal feature of all NLS continuations. Indeed, since the phase of singular NLS solutions become infinite at the singularity, the post-collapse phase is lost, regardless of the continuation mechanism. The consequences of this property are discussed in Chap. 39. Finally, we note that collapsing laser beams typically evolve into filaments. This suggest that physical continuations should lead to a filament singularity, and so that the dominant collapse-arresting mechanism (“viscosity”) should be conservative.

Chapter 39

Loss of Phase and Chaotic Interactions

In Chap. 38 we presented several continuations of the NLS beyond the singularity. All the continuations shared the phase-loss property that after the singularity, the limiting solution is only determined up to multiplication by $e^{i\theta}$. As noted, this is because the phase of all singular NLS solutions becomes infinite at the singularity. Therefore, regardless of the specific collapse-arresting mechanism used in the continuation, the post-collapse phase is “beyond infinity”. Consequently, the initial phase information is lost at the singularity.¹

A priori, the loss of phase has no importance, since NLS solutions are invariant under multiplication by $e^{i\theta}$. As we shall see, however, because of the phase-loss property, interactions between beams that already underwent collapse become chaotic.

39.1 Phase-Loss Property

39.1.1 Physical Perspective

NLS continuations are obtained by letting the collapse-arresting mechanism go to zero. Since the accumulated phase due to self phase modulations becomes infinite at the singularity, the information of the initial phase is completely lost. Hence, the post-collapse phase of the continuation is uniformly distributed in $[0, 2\pi]$.

Physically, the collapse-arresting mechanism is small but not zero. Therefore, the corresponding mathematical solution exists globally and is unique. In particular, the post-collapse accumulated phase is finite and unique. Nevertheless, since the phase accumulated due to self phase modulations (SPM) is “almost infinity”, the initial phase information is “almost lost”. By this, we mean that because small perturbations

¹ Loss of information at singularities occurs also in e.g., shock waves and black holes.

can have an $O(1)$ effect on the phase accumulated during the collapse event,² the initial phase is blurred by the large shot-to-shot fluctuations of the accumulated phase.

Conclusion 39.1 *The post-collapse phase of laser beams is highly sensitive to small perturbations.*

In what follows, we present numerical and experimental evidence for the high sensitivity of the post-collapse phase.³

39.1.2 Simulations

In [234], Shim et al. solved the NLS with a small high-order defocusing nonlinearity

$$i\psi_z(z, x, y) + \Delta\psi + |\psi|^2\psi - \epsilon|\psi|^q\psi = 0, \quad q \geq 4, \quad 0 < \epsilon \ll 1 \quad (39.1)$$

and Gaussian initial conditions. The addition of a high-order nonlinearity was phenomenological, and was done so that it would arrest collapse and lead to filamentation (Chap. 32 and Sect. 38.4). Figure 39.1a shows that as the fractional input power $p = P/P_{\text{cr}}$ increases by 8% (from 1.275 to 1.377), the on-axis accumulated phase at $z = 0.85$, which is beyond the location of the initial collapse z_{arrest} , increases by 2π . In Fig. 39.1b we plot the non-cumulative phase in 56 realizations in which p is uniformly distributed between 1.275 and 1.377, and observe that the phase is more or less uniformly distributed in $[0, 2\pi]$. In Fig. 39.1c, d we repeat these simulations with different values of q and ϵ and obtain similar results. We also solved numerically a perturbed NLS that includes dispersion, space-time focusing, self-steepening, multi-photon absorption, and plasma, which models the experiment described in Sect. 39.1.3. In these simulations we also observe that the on-axis phase for 21 randomly-chosen input powers between 240 MW and 260 MW shows the loss of phase, see Fig. 39.1e. Overall, the simulations in Fig. 39.1 confirm that loss of phase is a universal phenomenon, which is independent of the specific collapse-arresting mechanism. In other simulations we saw that the phase sensitivity increases with propagation distance.

39.1.3 Experiments

The first experimental observation of the phase-loss property was made in 2012 by Shim et al. [234]. Figure 39.2 shows the on-axis phase of a laser beam as it exits from

² A small perturbation leads to a small relative change in the accumulated phase. Since, however, the amount of accumulated phase is “almost infinity”, a small relative change can correspond to an $O(1)$ absolute change. Indeed, assume that a perturbation of size ϵ arrests collapse at $z_{\text{arrest}} = z_{\text{arrest}}(\epsilon)$. The on-axis accumulated phase at z_{arrest} is $\zeta(z_{\text{arrest}}) = \int_0^{z_{\text{arrest}}} L^{-2}$. Since $\lim_{\epsilon \rightarrow 0} \zeta(z_{\text{arrest}}) = \int_0^{z_c} L^{-2} = \infty$, small changes in ϵ can lead to $O(1)$ changes in $\zeta(z_{\text{arrest}})$.

³ We already saw the high sensitivity of the post-collapse phase in Fig. 38.1b.

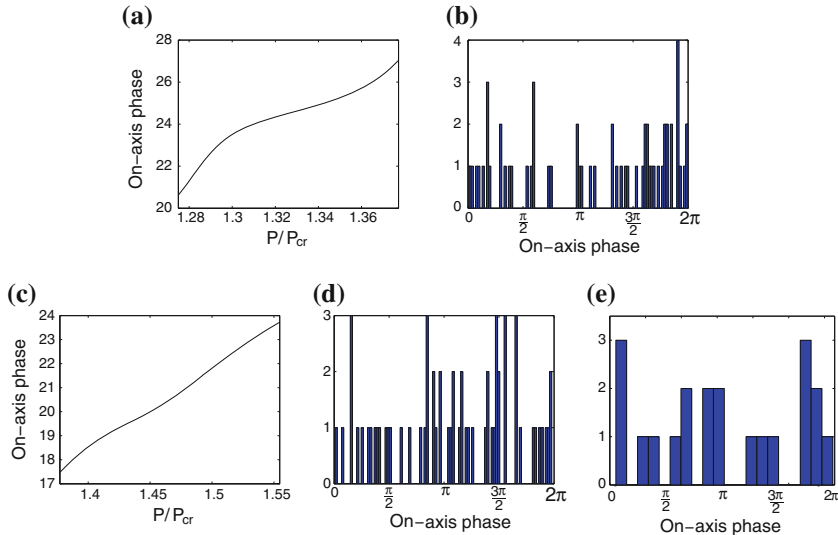


Fig. 39.1 (Numerical) **a** On-axis accumulated phase as a function of fractional input power for the solution of (39.1) with $q = 4$ and $\epsilon = 5 \cdot 10^{-4}$ at $z = 0.85$. **b** Histogram of the on-axis phase at $z = 0.85$ for 56 simulations, when p is uniformly distributed between 1.275 and 1.377. **c** and **d** Same as (a) and (b), respectively, with $q = 10$, $\epsilon = 0.3 \cdot 10^{-8}$, $z = 1.4$, and $1.38 \leq p \leq 1.55$. **e** Histogram of the on-axis phase of collapsing beams after propagation of 24 cm in water, in 21 simulations in which the input power is uniformly distributed between 240 and 260 MW. From [234]

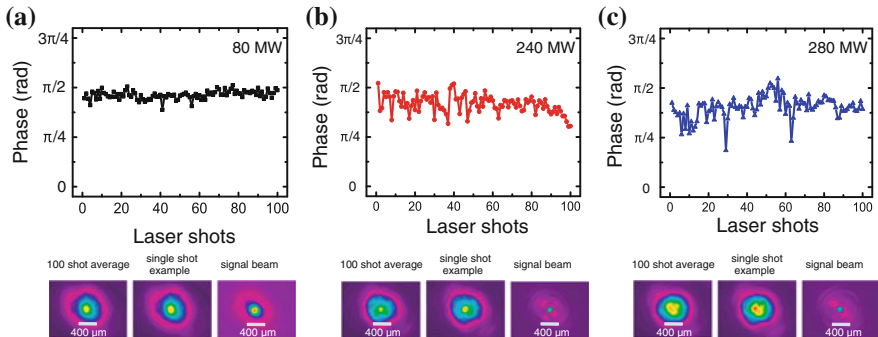


Fig. 39.2 (Experimental) **Top** On-axis phase of a laser beam that propagates through a 24 cm water cell, for 100 consecutive laser shots. **Bottom left** Average over 100 shots of the interferometry image with a reference beam that propagates in air. **Bottom center** A typical single-shot interferometry image. **Bottom right** The signal output image. Peak input powers are **a** $P = 80$ MW, **b** $P = 240$ MW, and **c** $P = 280$ MW. From [234]

a 24 cm water cell. At “low” input powers ($P = 80$ MW), the phase fluctuations are minor. Significant phase fluctuations appear at $P = 240$ MW, and larger fluctuations at $P = 280$ MW. Imaging the beam as it exits from the water cell (bottom-right figure at each power level) shows that it did not collapse inside the water cell for $P = 80$ MW, but that it did collapse for $P = 240$ and 280 MW. Therefore, this experiment confirms that the shot to shot fluctuations of the input beam have a small effect on the pre-collapse phase, but a large one on the post-collapse phase. This experiment also shows that the phase fluctuations increase with input power.

39.2 Chaotic Interactions

A priori, the loss of phase should have no effect on the dynamics, since NLS solutions are invariant under multiplication by $e^{i\theta}$. When, however, two beams (or filaments) interact, their phases determine whether they interact constructively or destructively.⁴ Hence, as was first noted in 1992 by Merle,

Conclusion 39.2 ([174]) *The phase-loss property implies that interactions between post-collapse beams or filaments are chaotic.*

Here again we should distinguish between the mathematical continuation and the physical solution. As the collapse-arresting mechanism goes to zero, the post-collapse phase of each of the two beams is uniformly distributed in $[0, 2\pi]$. Hence, the phase difference between intersecting post-collapse beams is uniformly distributed in $[0, 2\pi]$. In the case of a physical solution, however, the collapse-arresting mechanism is small but not zero. Therefore, for any given initial data, the phase difference between intersecting post-collapse beams is deterministic. This deterministic value, however, is blurred by the large shot-to-shot fluctuations in the phases of the two beams that are accumulated when they collapse.

39.2.1 Simulations

To illustrate the chaotic nature of post-collapse interactions, we consider the one-dimensional critical NLS

$$i\psi_z(z, x) + \psi_{xx} + |\psi|^4\psi = 0, \quad \psi(0, x) = \psi_0(x) \quad (39.2a)$$

with

$$\psi_0(x) = \psi_{R^{(0)}}^{\text{explicit}}(0, x \mp x_0)e^{\pm\frac{ix}{2}}, \quad (39.2b)$$

⁴ See Sects. 3.2.2 and 27.5.

where $\psi_{R^{(0)}}^{\text{explicit}}$ is the explicit blowup solution (38.2) with $d = 1$. The solution of (39.2) is, see Sect. 10.3,

$$\psi(z, x) = \psi_{R^{(0)}}^{\text{explicit}}(z, x \mp x_0 \pm cz)e^{\pm \frac{icx}{2} - i\frac{|c|^2 z}{4}}.$$

This solution is initially centered at $x = \pm x_0$, is tilted, and it blows up at Z_c . In addition, if we multiply the initial condition (39.2b) by $1 - \epsilon$, where $0 < \epsilon \ll 1$, the solution self-focuses until shortly before Z_c , and then defocuses.⁵

Consider now the NLS (39.2a) with

$$\psi_0(x) = \psi_0^{(1)}(x) + \psi_0^{(2)}(x), \quad (39.3a)$$

where

$$\psi_0^{(1)} = (1 - \epsilon)\psi_{R^{(0)}}^{\text{explicit}}(0, x - x_0)e^{i\frac{cx}{2}}, \quad (39.3b)$$

$$\psi_0^{(2)} = e^{i\Delta\theta}(1 - \epsilon - \Delta\epsilon)\psi_{R^{(0)}}^{\text{explicit}}(0, x + x_0)e^{-i\frac{cx}{2}}, \quad (39.3c)$$

and $\epsilon = 10^{-3}$. This initial condition corresponds to two input beams centered at $\pm x_0$, tilted toward each other, each with power slightly below P_{cr} , and with different powers when $\Delta\epsilon \neq 0$. The two input beams are in phase when $\Delta\theta = 0$, and out of phase when $\Delta\theta = \pi$. Figure 39.3a shows the NLS solution when the two input beams are of equal power and in-phase. Since each beam has power slightly below P_{cr} , it focuses up to a certain distance ($z \approx 0.3$), and then defocuses. As the two beams defocus, they intersect at $z \approx 0.6$. Since the two input beams are identical and in phase, the NLS solution satisfies $\psi(z, x) = \psi(z, -x)$. In particular, the two beams are in-phase for all $z > 0$. Therefore, when they cross at $z \approx 0.6$, they interact constructively. Since the combined power of the two beams is almost $2P_{\text{cr}}$, the NLS solution collapses.

In Fig. 39.3b we repeat this simulation with out-of-phase, equal-power input beams. Before the two beams intersect, their dynamics are the same as in Fig. 39.3a. Since the two input beams are identical and out-of-phase, they remain so for all $z > 0$. Therefore, as the two beams approach each other at $z \approx 0.6$, they repel each other.⁶ Since the power of each beam is below P_{cr} , there is no collapse.

In Fig. 39.3c the two input beams are again in-phase, but the power of the second beam is slightly reduced ($\Delta\epsilon = 2.7 \cdot 10^{-4}$). Although initially the two beams are in-phase, as they get closer at $z \approx 0.6$ they repel each other, and so there is no collapse. This dynamics is thus qualitatively the same as in Fig. 39.3b, suggesting that when the two beams in Fig. 39.3c intersect, their phase difference is $\approx \pi$. To verify that this is indeed the case, let $\psi_1(z, x)$ and $\psi_2(z, x)$ denote the solutions of the NLS (39.2a) with the initial conditions $\psi_0^{(1)}$ and $\psi_0^{(2)}$, respectively. Figure 39.4 shows the difference

⁵ This dynamics is shown in Fig. 38.1a for the un-tilted case ($c = 0$).

⁶ Since $\psi(z, x) = -\psi(z, -x)$, it follows that $\psi(z, x = 0) \equiv 0$. Therefore, the line $x = 0$ reflects the beams away from each other. See Sects. 16.1 and 27.5 for more details.

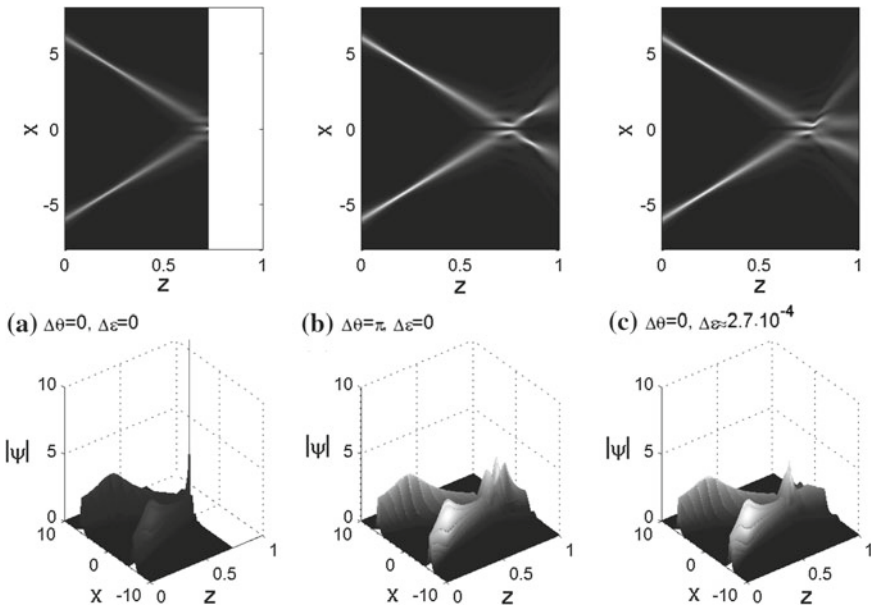


Fig. 39.3 Solution of the NLS (39.2a) with the initial condition (39.3), where $\psi_{R(0)}^{\text{explicit}}$ is given by (38.2) with $d = 1, Z_c = 0.25, x_0 = 6, c = 8$, and $\epsilon = 10^{-3}$. **a** In-phase identical beams ($\Delta\theta = 0$ and $\Delta\epsilon = 0$). **b** Out-of-phase identical beams ($\Delta\theta = \pi$ and $\Delta\epsilon = 0$). **c** In-phase input beams with slightly different powers ($\Delta\theta = 0$ and $\Delta\epsilon \approx 2.7 \cdot 10^{-4}$). From [85]

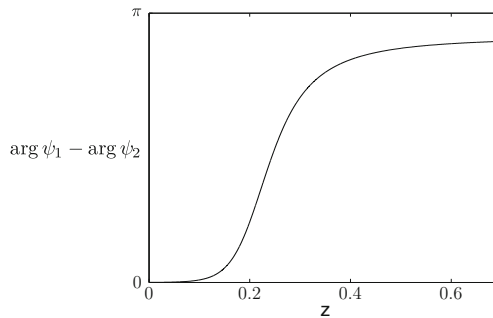


Fig. 39.4 $\arg \psi_1(z, x = x_0 - cz) - \arg \psi_2(z, x = -x_0 + cz)$. From [85]

between the on-axis phases of ψ_1 and ψ_2 . Initially this difference is negligible. As the two beams collapse at $z \approx 0.3$, there is a dramatic increase in their phase difference. Thus, the $O(10^{-4})$ difference in their input powers leads to an $O(1)$ difference in their accumulated phases once they collapse. In particular, at the intersection point ($z \approx 0.6$) the phase difference is $\approx \pi$. We thus conclude that the $O(10^{-4})$ change in the

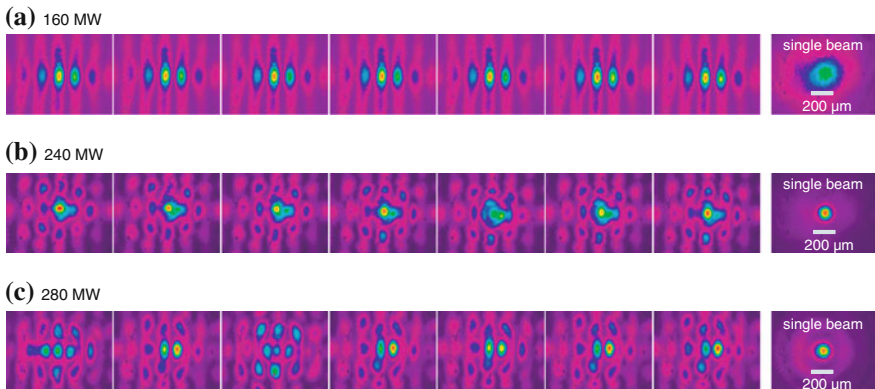


Fig. 39.5 Seven consecutive single-shot images of two crossing beams with initial zero phase at the output face of a 24 cm long water cell for **a** 160 MW, **b** 240 MW, and **c** 280 MW peak input powers. The *right* figure in each row shows a single-beam image at the output face. From [234]

power of the second input beam led to a completely different post-collapse interaction pattern, and that this chaotic behavior is a consequence of the phase-loss property.

39.2.2 Experiments

Because the phase-loss property is universal, we can conclude that interactions between post-collapse beams or filaments are chaotic, even without knowing the correct physical continuation. The first experimental demonstration of this theoretical prediction was performed in 2012 by Shim et al. [234]. Two input beams with nominally the same power and initial phase were sent into a 24 cm water cell at a 0.2° crossing angle, so that they spatially combine near the output face of the water cell. Figure 39.5 shows seven consecutive, single-shot images taken at the output face. The intensity profiles show little fluctuations for $P = 160$ MW. For $P = 240$ MW, however, there are significant shot-to-shot fluctuations in the intensity shapes and peak intensities. For $P = 280$ MW, the shot-to-shot fluctuations are even larger. In order to determine whether the beams collapsed inside the water cell (i.e., before they combined at the output face), we blocked one of the beams and imaged the second beam as it exits the water cell (rightmost figure in each row). These single-beam images show that the two beams do not collapse inside the water cell for $P = 160$ MW, but that they collapse inside the water cell at $P = 240$ MW and 280 MW. Therefore, this experiment confirms that pre-collapse interactions are stable,⁷ post-collapse interactions are unstable, and the effect of loss of phase increases with input power.

⁷ As we already saw in Sect. 27.5.

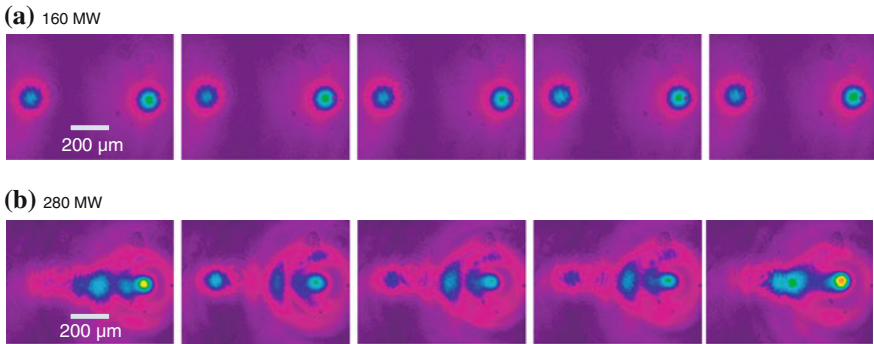


Fig. 39.6 Five consecutive single-shot images of two parallel beams with an initial π phase at the output face of a 24 cm long water cell for **a** 160 MW and **b** 280 MW peak input powers. From [234]

In another experiment, we launched two parallel input beams with a π phase difference.⁸ Figure 39.6a shows that for $P = 160$ MW the two beams do not interact as they propagate, which indicates that the π phase difference is maintained during the propagation. As we increase the power to $P = 280$ MW, however, the output intensity profiles show significant fluctuations, see Fig. 39.6b. This indicates that the two beams sometimes interact, i.e., that the π phase difference is not maintained during the propagation, which we attribute to the post-collapse loss of phase.

39.3 Summary

Most of the theoretical and experimental research on collapsing beams has focused on the amplitude of the blowup profile and the blowup rate (which are given by a rescaled Townes profile and by the loglog and adiabatic laws, respectively). While it has been noted that the on-axis phase becomes infinite at the singularity, the implications of this observation remained, for the most part, unnoticed.

In this chapter we saw that the “blowup of the phase” leads to a loss of phase at the singularity. This property, in turn, implies that interactions between post-collapse filaments are chaotic. Thus, for example, the loss of phase provides the first theoretical explanation for the turbulent behavior observed numerically and experimentally for pulses that contain multiple filaments [26, 191].

For many years it was believed that because multiple filamentation is initiated by input-beam noise, it cannot be controlled. It later turned out that it is possible to control the *initial* multiple filamentation pattern deterministically (Sect. 25.3). The phase-loss property implies, however, that post-collapse multiple-filamentation patterns are highly sensitive to small changes in the input beam. The “bad news” is, thus, that it is not possible to have a deterministic theory (or control) for interactions

⁸ Recall that out of phase beams repel each other (Sect. 3.2.2).

between multiple filaments after they collapsed. The “good news”, however, is that because the initial phases are completely lost, we do know that the limiting relative phase between post-collapse filaments is uniformly distributed in $[0, 2\pi]$. Therefore, it may be possible to develop a stochastic theory for post-collapse interactions.

Appendix A

Elementary Inequalities

The following inequalities are elementary. For proofs, see e.g. [61, Appendix B.2]

Cauchy's inequality: Let $a, b \in \mathbb{R}$. Then

$$ab \leq \frac{a^2}{2} + \frac{b^2}{2}.$$

Cauchy's inequality with ϵ : Let $a, b \in \mathbb{R}$ and let $\epsilon > 0$. Then

$$ab \leq \epsilon a^2 + \frac{1}{4\epsilon} b^2.$$

Young's inequality: Let $1 < p, q < \infty$ such that $\frac{1}{p} + \frac{1}{q} = 1$, and let $a, b > 0$. Then

$$ab \leq \frac{a^p}{p} + \frac{b^q}{q}.$$

Young's inequality with ϵ : Let $a, b, \epsilon > 0$. Then

$$ab \leq \epsilon a^p + C(\epsilon) b^q, \quad C(\epsilon) = \frac{1}{(\epsilon p)^{\frac{q}{p}}} \frac{1}{q}.$$

Hölder's inequality: Let $1 < p, q < \infty$ such that $\frac{1}{p} + \frac{1}{q} = 1$, and let $f \in L^p(\Omega)$ and $g \in L^q(\Omega)$. Then

$$\int_{\Omega} |fg| \leq \|f\|_{L^p(\Omega)} \|g\|_{L^q(\Omega)}. \tag{A.1}$$

Interpolation inequality for L^p norms: Let $1 \leq r \leq q \leq p \leq \infty$, and let

$$\frac{1}{q} = \frac{\alpha}{r} + \frac{1-\alpha}{p}.$$

If $f \in L^r(\Omega) \cap L^p(\Omega)$, then $f \in L^q(\Omega)$, and

$$\|f\|_{L^q(\Omega)} \leq \|f\|_{L^r(\Omega)}^\alpha \|f\|_{L^p(\Omega)}^{1-\alpha}.$$

Appendix B

Strong and Weak Convergence

In this appendix we assume that $1 < p, q < \infty$, and that $\frac{1}{p} + \frac{1}{q} = 1$.

Definition B.1 (*Strong convergence in L^p*) Let $f_n, f \in L^p$. We say that f_n converges to f strongly in L^p , if $\lim_{n \rightarrow \infty} \|f_n - f\|_p = 0$.

Lemma B.1 *If f_n converges to f strongly in L^p , then $\lim_{n \rightarrow \infty} \|f_n\|_p = \|f\|_p$.*

Proof By the triangle inequality, $0 \leq |\|f_n\|_p - \|f\|_p| \leq \|f_n - f\|_p$. □

Definition B.2 (*Weak convergence in L^p*) Let $f_n, f \in L^p$. We say that f_n converges to f weakly in L^p , if for any $g \in L^q$, $\lim_{n \rightarrow \infty} \int f_n g = \int f g$.

Lemma B.2 *If f_n converges to f strongly in L^p , then f_n converges to f weakly in L^p .*

Proof Let $g \in L^q$. Then, by Hölder's inequality (A.1),

$$\left| \int f_n g - \int f g \right| \leq \int |f_n - f| |g| \leq \|f_n - f\|_p \|g\|_q \rightarrow 0, \quad n \rightarrow \infty.$$

□

Lemma B.3 *If f_n converges to f weakly in L^p , $\|f\|_p \leq \liminf_{n \rightarrow \infty} \|f_n\|_p$.*

Proof Since $\frac{1}{p} + \frac{1}{q} = 1$, we have that $(p-1)q = p$. Therefore, if $f \in L^p$, then $g := f^{p-1} \in L^q$. Hence, from the weak convergence it follows that

$$\lim_{n \rightarrow \infty} \int f_n f^{p-1} = \int f^p = \|f\|_p^p.$$

By Hölder's inequality (A.1),

$$\int f_n f^{p-1} \leq \int |f_n| |f^{p-1}| \leq \|f_n\|_p \|f^{p-1}\|_q.$$

Hence

$$\|f\|_p^p = \lim_{n \rightarrow \infty} \int f_n f^{p-1} = \liminf_{n \rightarrow \infty} \int f_n f^{p-1} \leq \|f^{p-1}\|_q \liminf_{n \rightarrow \infty} \|f_n\|_p.$$

Since

$$\|f^{p-1}\|_q = \left(\int f^{(p-1)q} \right)^{\frac{1}{q}} = \left(\int f^p \right)^{1-\frac{1}{p}} = \frac{\|f\|_p^p}{\|f\|_p},$$

the result follows. \square

In some cases, weak convergence implies strong convergence:

Lemma B.4 *Let $0 < p < \infty$. If f_n converges to f weakly in L^p , and if $\|f\|_p = \lim_{n \rightarrow \infty} \|f_n\|_p$, then f_n also converges to f strongly in L^p .*

Proof When $p = 2$ the result is immediate, since

$$\|f_n - f\|_2^2 = \int (f_n - f)^2 = \int f_n^2 + \int f^2 - 2 \int f_n f \rightarrow \int f^2 + \int f^2 - 2 \int f f = 0.$$

More generally, if f_n converges to f weakly in L^p , then f_n has a subsequence f_{n_j} that converges pointwise to f almost everywhere. In addition, since $\|f\|_p = \lim_{n \rightarrow \infty} \|f_n\|_p$, then $\|f_{n_j}\|_p$ are uniformly bounded. Therefore, by the Brézis-Lieb Theorem (see e.g. [156, Theorem 1.9]) we have that

$$\lim_{j \rightarrow \infty} \int | |f_{n_j}|^p - |f_{n_j} - f|^p - |f|^p | d\mathbf{x} = 0.$$

Since

$$\left| \int |f_{n_j}|^p - |f_{n_j} - f|^p - |f|^p d\mathbf{x} \right| \leq \int | |f_{n_j}|^p - |f_{n_j} - f|^p - |f|^p | d\mathbf{x}$$

and $\int |f_{n_j}|^p \rightarrow |f|^p$, we have that $\int |f_{n_j} - f|^p \rightarrow 0$. Since this holds for any subsequence, the result follows. \square

In this book we often make use of the following weak compactness result:

Lemma B.5 *Any bounded sequence in a Hilbert space (L^2 , H^1 , H^2) has a subsequence which converges weakly.*

References

1. M.J. Ablowitz, Z.H. Musslimani, Spectral renormalization method for computing self-localized solutions to nonlinear systems. *Opt. Lett.* **30**, 2140–2142 (2005)
2. G.P. Agrawal, *Nonlinear Fiber Optics*, 3rd edn. (Academic Press, San Diego, 2001)
3. T. Akahori, H. Nawa, Blowup and scattering problems for the nonlinear Schrödinger equations. *Kyoto J. Math.* **53**, 629–672 (2013)
4. S.A. Akhmanov, A.P. Sukhorukov, R.V. Khokhlov, Self-focusing and self-trapping of intense light beams in a nonlinear medium. *JETP* **23**, 1025–1033 (1966)
5. G.D. Akrivis, V.A. Dougalis, O.A. Karakashian, W.R. McKinney. Numerical approximation of singular solutions of the damped nonlinear Schrödinger equation. In ENUMATH 97 (Heidelberg), (World Scientific Publishing, River Edge, 1998), pp. 117–124
6. D. Anderson, M. Bonnedal, M. Lisak, Self-trapped cylindrical laser beams. *Phys. Fluids* **22**, 1838–1840 (1979)
7. P. Antonelli, C. Sparber, Global well-posedness for cubic NLS with nonlinear damping. *Comm. Partial. Diff. Equat.* **35**, 2310–2328 (2010)
8. G.A. Askar'yan, Effects of the gradient of a strong electromagnetic beam on electrons and atoms. *JETP* **15**, 1088–1090 (1962)
9. W. Bao, Y. Cai, Mathematical theory and numerical methods for Bose-Einstein condensation. *Kinet. Relat. Models* **6**, 1–135 (2013)
10. W. Bao, Y. Ge, D. Jaksch, P.A. Markowich, R.M. Weishaeupl, Convergence rate of dimension reduction in Bose-Einstein condensate. *Comput. Phys. Comm.* **177**, 832–850 (2007)
11. G. Baruch, G. Fibich, Singular solutions of the L^2 supercritical biharmonic nonlinear Schrödinger equation. *Nonlinearity* **24**, 1843–1859 (2011)
12. G. Baruch, G. Fibich, N. Gavish, Singular standing-ring solutions of nonlinear partial differential equations. *Physica D* **239**, 1968–1983 (2010)
13. G. Baruch, G. Fibich, E. Mandelbaum, Ring-type singular solutions of the biharmonic nonlinear Schrödinger equation. *Nonlinearity* **23**, 2867–2887 (2010)
14. G. Baruch, G. Fibich, E. Mandelbaum, Singular solutions of the biharmonic nonlinear Schrödinger equation. *SIAM J. Appl. Math.* **70**, 3319–3341 (2010)
15. G. Baruch, G. Fibich, S.V. Tsynkov, High-order numerical method for the nonlinear Helmholtz equation with material discontinuities in one space dimension. *J. Comput. Phys.* **227**, 820–850 (2007)
16. G. Baruch, G. Fibich, S.V. Tsynkov, High-order numerical solution of the nonlinear Helmholtz equation with axial symmetry. *J. Comput. Appl. Math.* **204**, 477–492 (2007)
17. G. Baruch, G. Fibich, S.V. Tsynkov, Simulations of the nonlinear Helmholtz equation: arrest of beam collapse, nonparaxial solitons and counter-propagating beams. *Opt. Express* **16**, 13323–13329 (2008)

18. G. Baruch, G. Fibich, S.V. Tsynkov, A high-order numerical method for the nonlinear Helmholtz equation in multidimensional layered media. *J. Comput. Phys.* **228**, 3789–3815 (2009)
19. M. Ben-Artzi, H. Koch, J.-C. Saut, Dispersion estimates for fourth order Schrödinger equations. *C. R. Acad. Sci. Paris Sér. I Math.* **330**, 87–92 (2000)
20. C.M. Bender, S. Orszag, *Advanced Mathematical Methods for Scientists and Engineers* (McGraw-Hill, New York, 1978)
21. H. Berestycki, T. Gallouët, O. Kavian, Equations de champs scalaires euclidiens non linéaires dans le plan. (French) [Nonlinear Euclidean scalar field equations in the plane]. *C. R. Acad. Sci. Paris. Série I* **297**, 307–310 (1983)
22. H. Berestycki, P.L. Lions, Nonlinear scalar field equations II. Existence of infinitely many solutions. *Arch. Ration. Mech. Anal.* **82**, 347–375 (1983)
23. L. Bergé, D. Pesme, Time dependent solutions of wave collapse. *Phys. Lett. A* **166**, 116–122 (1992)
24. L. Bergé, D. Pesme, Bounded spatial extension of the self-similar collapsing solutions of the nonlinear Schrödinger equation. *Phys. Scr.* **43**, 323–327 (1993)
25. L. Bergé, J.J. Rasmussen, E.A. Kuznetsov, E.G. Shapiro, S.K. Turitsyn, Self-focusing of chirped optical pulses in media with normal dispersion. *J. Opt. Soc. Am. B* **13**, 1879–1891 (1996)
26. L. Bergé, S. Skupin, F. Lederer, G. Méjean, J. Yu, J. Kasparian, E. Salmon, J.P. Wolf, M. Rodriguez, L. Wöste, R. Bourayou, R. Sauerbrey, Multiple filamentation of terawatt laser pulses in air. *Phys. Rev. Lett.* **92**, 225002 (2004)
27. V.I. Bespalov, V.I. Talanov, Filamentary structure of light beams in nonlinear media. *Trans. JETP Lett.* **3**, 307–310 (1966)
28. C. Besse, R. Carles, N.J. Mauser, H.P. Stimming, Monotonicity properties of the blow-up time for nonlinear Schrödinger equations: numerical evidence. *Disc. Cont. Dyn. Sys. B* **9**, 11–36 (2008)
29. J.E. Bjorkholm, A. Ashkin, CW self-focusing and self-trapping of light in sodium vapor. *Phys. Rev. Lett.* **32**, 129–132 (1974)
30. Z. Bor, B. Rácz, Dispersion of optical materials used for picosecond spectroscopy. *Appl. Opt.* **24**, 3440–3441 (1985)
31. J. Bourgain, W. Wang., Construction of blowup solutions for the nonlinear Schrödinger equation with critical nonlinearity. *Ann. Scuola Norm. Sup. Pisa Cl. Sci.* **25**, 197–215 (1997)
32. R.W. Boyd, *Nonlinear Optics*, 2nd edn. (Academic Press, Boston, 2003)
33. R.W. Boyd, S.G. Lukishova, Y.R. Shen (eds.), *Self-focusing: Past and Present* (Springer, Berlin, 2009)
34. C.J. Budd, Asymptotics of multibump blow-up self-similar solutions of the nonlinear Schrödinger equation. *SIAM J. Appl. Math.* **62**, 801–830 (2001)
35. C.J. Budd, S. Chen, R.D. Russel, New self-similar solutions of the nonlinear Schrödinger equation with moving mesh computations. *J. Comput. Phys.* **152**, 756–789 (1999)
36. C.J. Budd, W. Huang, R.D. Russel, Moving mesh methods for problems with blow-up. *SIAM J. Sci. Comput.* **17**, 305–327 (1996)
37. N. Burq, P. Gérard, N. Tzvetkov, Two singular dynamics of the nonlinear Schrödinger equation on a plane domain. *Geom. Funct. Anal.* **13**, 1–19 (2003)
38. A.J. Campillo, S.L. Shapiro, B.R. Suydam, Relationship of self-focusing to spatial instability modes. *Appl. Phys. Lett.* **24**, 178–180 (1974)
39. T. Cazenave, *Semilinear Schrödinger Equations*, volume 10 of Courant Lecture Notes in Mathematics (New York University, Courant Institute of Mathematical Sciences, New York, 2003)
40. T. Cazenave, P.-L. Lions, Orbital stability of standing waves for some nonlinear Schrödinger equations. *Comm. Math. Phys.* **85**, 549–561 (1982)
41. T. Cazenave, F.B. Weissler, The Cauchy problem for the critical nonlinear Schrödinger equation in H^s . *Nonlin. Anal.* **14**, 807–836 (1990)

42. H.D. Ceniceros, T.Y. Hou, An efficient dynamically adaptive mesh for potentially singular solutions. *J. Comput. Phys.* **172**, 609–639 (2001)
43. W. Chen, D.L. Mills, Optical response of a nonlinear dielectric film. *Phys. Rev. B* **35**, 524–532 (1987)
44. P. Chernev, V. Petrov, Self-focusing of light pulses in the presence of normal group-velocity dispersion. *Opt. Lett.* **17**, 172–174 (1992)
45. S. Chi, Q. Guo, Vector theory of self-focusing of an optical beam in Kerr media. *Opt. Lett.* **20**, 1598–1560 (1995)
46. R.Y. Chiao, E. Garmire, C.H. Townes, Self-trapping of optical beams. *Phys. Rev. Lett.* **13**, 479–482 (1964)
47. R.Y. Chiao, M.A. Johnson, S. Krinsky, C.H. Townes, E. Garmire, 6A1—a new class of trapped light filaments. *IEEE J. Quant. Elec.* **2**, 467–469 (1966)
48. J. Coleman, C. Sulem, Numerical simulations of blow-up solutions of the vector nonlinear Schrödinger equation. *Phys. Rev. E* **66**, 036701 (2002)
49. F. Cooper, C. Lucheroni, H. Shepard, Variational method for studying self-focusing in a class of nonlinear Schrödinger equations. *Phys. Lett. A* **70**, 184–188 (1992)
50. A. Couairon, A. Mysyrowicz, Femtosecond filamentation in transparent media. *Phys. Rep.* **441**, 47189 (2007)
51. R. Courant, D. Hilbert, *Methods of Mathematical Physics*, vol. II (Wiley, New York, 1989)
52. S. Le Coz, R. Fukizumi, G. Fibich, B. Kshetrimayum, Y. Sivan, Instability of bound states of a nonlinear Schrödinger equation with a Dirac potential. *Physica D* **237**, 1103–1128 (2008)
53. E.L. Dawes, J.H. Marburger, Computer studies in self-focusing. *Phys. Rev.* **179**, 862–868 (1969)
54. L. Degtiarev, V.E. Zakharov, L.I. Rudakov, Two examples of Langmuir wave collapse. *JETP* **41**, 5761 (1975)
55. M. Desaix, D. Anderson, M. Lisak, Variational approach to collapse of optical pulses. *J. Opt. Soc. Am. B* **8**, 2082–2086 (1991)
56. S.A. Diddams, H.K. Eaton, A.A. Zozulya, T.S. Clement, Amplitude and phase measurements of femtosecond pulse splitting in nonlinear dispersive media. *Opt. Lett.* **23**, 379–381 (1998)
57. A. Ditkowski, N. Gavish, A grid redistribution method for singular problems. *J. Comput. Phys.* **228**, 2354–2365 (2009)
58. A. Dubietis, G. Tamaišauskas, G. Fibich, B. Ilan, Multiple filamentation induced by input-beam ellipticity. *Opt. Lett.* **29**, 1126–1128 (2004)
59. H.S. Eisenberg, Y. Silberberg, R. Morandotti, J.S. Aitchison, Diffraction management. *Phys. Rev. Lett.* **85**, 1863–1866 (2000)
60. S. Eisenmann, E. Louzon, Y. Katzir, T. Palchan, A. Zigler, Y. Sivan, G. Fibich, Control of the filamentation distance and pattern in long-range atmospheric propagation. *Opt. Express* **15**, 2779–2784 (2007)
61. L.C. Evans, *Partial Differential Equations* (American Mathematical Society, Providence, Rhode Island, 1998)
62. M.D. Feit, J.A. Fleck, Beam nonparaxiality, filament formation, and beam breakup in the self-focusing of optical beams. *J. Opt. Soc. Am. B* **5**, 633–640 (1988)
63. G. Fibich. *Self-Focusing in the Nonlinear Schrödinger Equation for Ultrashort Laser-Tissue Interactions*. Ph.D. thesis, Courant Institute, New York University, 1994
64. G. Fibich, An adiabatic law for self-focusing of optical beams. *Opt. Lett.* **21**, 1735–1737 (1996)
65. G. Fibich, Small beam nonparaxiality arrests self-focusing of optical beams. *Phys. Rev. Lett.* **76**, 4356–4359 (1996)
66. G. Fibich, Self-focusing in the damped nonlinear Schrödinger equation. *SIAM. J. Appl. Math.* **61**, 1680–1705 (2001)
67. G. Fibich, Singular solutions of the subcritical nonlinear Schrödinger equation. *Physica D* **240**, 1119–1122 (2011)
68. G. Fibich, S. Eisenmann, B. Ilan, Y. Erlich, M. Fraenkel, Z. Henis, A.L. Gaeta, A. Zigler, Self-focusing distance of very high power laser pulses. *Opt. Express* **13**, 5897–5903 (2005)

69. G. Fibich, S. Eisenmann, B. Ilan, A. Zigler, Control of multiple filamentation in air. *Opt. Lett.* **29**, 1772–1774 (2004)
70. G. Fibich, A. Gaeta, Critical power for self-focusing in bulk media and in hollow waveguides. *Opt. Lett.* **25**, 335–337 (2000)
71. G. Fibich, N. Gavish, Critical power of collapsing vortices. *Phys. Rev. A* **77**, 045803 (2008)
72. G. Fibich, N. Gavish, Theory of singular vortex solutions of the nonlinear Schrödinger equation. *Physica D* **237**, 2696–2730 (2008)
73. G. Fibich, N. Gavish, X.P. Wang, New singular solutions of the nonlinear Schrödinger equation. *Physica D* **211**, 193–220 (2005)
74. G. Fibich, N. Gavish, X.P. Wang, Singular ring solutions of critical and supercritical nonlinear Schrödinger equations. *Physica D* **231**, 55–86 (2007)
75. G. Fibich, B. Ilan, Self focusing of elliptic beams: an example of the failure of the aberrationless approximation. *J. Opt. Soc. Am. B* **17**, 1749–1758 (2000)
76. G. Fibich, B. Ilan, Vectorial and random effects in self-focusing and in multiple filamentation. *Physica D* **157**, 112–146 (2001)
77. G. Fibich, B. Ilan, Vectorial effects in self-focusing and multiple filamentation. *Opt. Lett.* **26**, 840–842 (2001)
78. G. Fibich, B. Ilan, Multiple filamentation of circularly polarized beams. *Phys. Rev. Lett.* **89**, 013901 (2002)
79. G. Fibich, B. Ilan, Discretization effects in the nonlinear Schrödinger equation. *Appl. Numer. Math.* **44**, 63–75 (2003)
80. G. Fibich, B. Ilan, Self-focusing of circularly polarized beams. *Phys. Rev. E* **67**, 036622 (2003)
81. G. Fibich, B. Ilan, Optical light bullets in a pure Kerr medium. *Opt. Lett.* **29**, 887–889 (2004)
82. G. Fibich, B. Ilan, G. Papanicolaou, Self focusing with fourth-order dispersion. *SIAM. J. Appl. Math.* **62**, 1437–1462 (2002)
83. G. Fibich, B. Ilan, S. Schochet, Critical exponents and collapse of nonlinear Schrödinger equations with anisotropic fourth-order dispersion. *Nonlinearity* **16**, 1809–1821 (2003)
84. G. Fibich, B. Ilan, S.V. Tsynkov, Backscattering and nonparaxiality arrest collapse of nonlinear waves. *SIAM. J. Appl. Math.* **63**, 1718–1736 (2003)
85. G. Fibich, M. Klein, Continuations of the nonlinear Schrödinger equation beyond the singularity. *Nonlinearity* **24**, 2003–2045 (2011)
86. G. Fibich, M. Klein, Nonlinear-damping continuation of the nonlinear Schrödinger equation—a numerical study. *Physica D* **241**, 519–527 (2012)
87. G. Fibich, D. Levy, Self-focusing in the complex Ginzburg-Landau limit of the critical nonlinear Schrödinger equation. *Phys. Lett. A* **249**, 286–294 (1998)
88. G. Fibich, V.M. Malkin, G.C. Papanicolaou, Beam self-focusing in the presence of small normal time dispersion. *Phys. Rev. A* **52**, 4218–4228 (1995)
89. G. Fibich, F. Merle, Self-focusing on bounded domains. *Physica D* **155**, 132–158 (2001)
90. G. Fibich, F. Merle, P. Raphaël, Proof of a spectral property related to the singularity formation for the L^2 critical nonlinear Schrödinger equation. *Physica D* **220**, 1–13 (2006)
91. G. Fibich, G.C. Papanicolaou, Self-focusing in the presence of small time dispersion and nonparaxiality. *Opt. Lett.* **22**, 1379–1381 (1997)
92. G. Fibich, G.C. Papanicolaou, A modulation method for self-focusing in the perturbed critical nonlinear Schrödinger equation. *Phys. Lett. A* **239**, 167–173 (1998)
93. G. Fibich, G.C. Papanicolaou, Self-focusing in the perturbed and unperturbed nonlinear Schrödinger equation in critical dimension. *SIAM J. Applied Math.* **60**, 183–240 (1999)
94. G. Fibich, W. Ren, X.P. Wang, Numerical simulations of self focusing of ultrafast laser pulses. *Phys. Rev. E* **67**, 056603 (2003)
95. G. Fibich, Y. Sivan, Y. Ehrlich, E. Louzon, M. Fraenkel, S. Eisenmann, Y. Katzir, A. Zigler, Control of the collapse distance in atmospheric propagation. *Opt. Express* **14**, 4946–4957 (2006)
96. G. Fibich, Y. Sivan, M.I. Weinstein, Bound states of nonlinear Schrödinger equations with a periodic nonlinear microstructure. *Physica D* **217**, 3157 (2006)

97. G. Fibich, S.V. Tsynkov, High-order two-way artificial boundary conditions for nonlinear wave propagation with backscattering. *J. Comput. Phys.* **171**, 1–46 (2001)
98. G. Fibich, S.V. Tsynkov, Numerical solution of the nonlinear Helmholtz equation using nonorthogonal expansions. *J. Comput. Phys.* **210**, 183–224 (2005)
99. G. Fibich, X.P. Wang, Stability of solitary waves for nonlinear Schrödinger equations with inhomogeneous nonlinearities. *Physica D* **175**, 96–108 (2003)
100. G.M. Fraiman, Asymptotic stability of manifold of self-similar solutions in self-focusing. *Sov. Phys. JETP* **61**, 228–233 (1985)
101. B. Franchi, E. Lanconelli, J. Serrin, Existence and uniqueness of nonnegative solutions of quasilinear equations in \mathbb{R}^n . *Adv. Math.* **118**, 177–243 (1996)
102. R. Fukizumi, F.H. Selem, H. Kikuchi, Stationary problem related to the nonlinear Schrödinger equation on the unit ball. *Nonlinearity* **25**, 2271–2301 (2012)
103. A.L. Gaeta, Spatial and temporal dynamics of collapsing ultrashort laser pulses, in *Self-focusing: Past and Present*, ed. by R.W. Boyd, S.G. Lukishova, Y.R. Shen (Springer, Berlin, 2009), pp. 399–411 (chapter 16)
104. E. Gagliardo, Proprieta di alcune classi di funzioni in piu varibili. *Ricerche di Math.* **7**, 102–137 (1958)
105. E. Gagliardo, Ulteriora proprieta di alcune classi di funzioni in piu varibili. *Ricerche di Math.* **8**, 24–51 (1959)
106. N. Gavish, G. Fibich, L.T. Vuong, A.L. Gaeta, Predicting the filamentation of high-power beams and pulses without numerical integration: a nonlinear geometrical optics method. *Phys. Rev. A* **78**, 043807 (2008)
107. I.M. Gelfand, S.V. Fomin, *Calculus of Variations* (Prentice-Hall, New Jersey, 1963)
108. K. Germaschewski, R. Grauer, L. Berge, V.K. Mezentsev, J.J. Rasmussen, Splittings, coalescence, bunch and snake patterns in the 3D nonlinear Schrödinger equation with anisotropic dispersion. *Physica D* **151**, 175–198 (2001)
109. J.M. Gerton, D. Strekalov, I. Prodan, R.G. Hulet, Direct observation of growth and collapse of a Bose-Einstein condensate with attractive interactions. *Nature* **408**, 692–695 (2000)
110. B. Gidas, W.M. Ni, L. Nirenberg, Symmetry of positive solutions of nonlinear elliptic equations in \mathbb{R}^n , in *Mathematical Analysis and Applications, Part A* (Academic Press, New York, 1981), pp. 369–402
111. B. Gidas, W.M. Ni, L. Nirenberg, Symmetry and related properties via the maximum principle. *Comm. Math. Phys.* **68**, 209–243 (1979)
112. J. Ginibre, G. Velo, On a class of nonlinear Schrödinger equations. I: the Cauchy problem, general case. *J. Funct. Anal.* **32**, 1–32 (1979)
113. C.R. Giuliano, J.H. Marburger, A. Yariv, Enhancement of self-focusing threshold in sapphire with elliptical beams. *Appl. Phys. Lett.* **32**, 58–60 (1972)
114. M.V. Goldman, K. Rydpal, B. Hafizi, Dimensionality and dissipation in Langmuir collapse. *Phys. Fluids* **23**, 945–955 (1980)
115. J.W. Grantham, H.M. Gibbs, G. Khitrova, J.F. Valley, J.J. Xu, Kaleidoscopic spatial instability: bifurcations of optical transverse solitary waves. *Phys. Rev. Lett.* **66**, 1422–1425 (1991)
116. M. Grillakis, Linearized instability for nonlinear Schrödinger and Klein-Gordon equations. *Comm. Pure Appl. Math.* **41**, 747–774 (1988)
117. M. Grillakis, Existence of nodal solutions of semilinear equations in \mathbb{R}^N . *J. Diff. Equat.* **85**, 367–400 (1990)
118. M. Grillakis, J. Shatah, W. Strauss, Stability theory of solitary waves in the presence of symmetry. I. *J. Funct. Anal.* **74**, 160–197 (1987)
119. B. Gross, J.T. Manassah, Numerical solution for the propagation of an elliptic Gaussian beam in a Kerr medium. *Phys. Lett. A* **169**, 371–378 (1992)
120. T.D. Grow, A.L. Gaeta, Dependence of multiple filamentation on beam ellipticity. *Opt. Express* **13**, 4594–4599 (2005)
121. T.D. Grow, A.A. Ishaaya, L.T. Vuong, A.L. Gaeta, Collapse and stability of necklace beams in Kerr media. *Phys. Rev. Lett.* **99**, 133902 (2007)

122. T.D. Grow, A.A. Ishaaya, L.T. Vuong, A.L. Gaeta, N. Gavish, G. Fibich, Collapse dynamics of super-gaussian beams. *Opt. Express* **14**, 5468–5475 (2006)
123. G.R. Hadley, Transparent boundary condition for beam propagation. *Opt. Lett.* **16**, 624–626 (1991)
124. S.P. Hastings, J.B. McLeod, A boundary value problem associated with the second Painlevé transcendent and the Korteweg-de Vries equation. *Arch. Rat. Mech. Anal.* **73**, 31–51 (1980)
125. M. Hercher, Laser-induced damage in transparent media. *J. Opt. Soc. Am.* **54**, 563 (1964)
126. R.L. Higdon, Radiation boundary conditions for dispersive waves. *SIAM J. Numer. Anal.* **31**, 64–100 (1994)
127. T. Hmidi, S. Keraani, Remarks on the blowup for the L^2 -critical nonlinear Schrödinger equations. *SIAM J. Math. Anal.* **38**, 1035–1047 (2006)
128. J. Holmer, R. Platte, S. Roudenko, Blow-up criteria for the 3D cubic nonlinear Schrödinger equation. *Nonlinearity* **23**, 977–1030 (2010)
129. J. Holmer, S. Roudenko, A class of solutions to the 3D cubic nonlinear Schrödinger equation that blows up on a circle. *Appl. Math. Res. Express. AMRX* **2011**, 23–94 (2011)
130. J. Iaia, H. Warchall, Nonradial solutions of semilinear elliptic equation in two dimensions. *J. Diff. Equat.* **119**, 533–558 (1995)
131. B. Ilan, *Vectorial Effects and Multiple Filamentation in Self-Focusing of Laser Beams*. Ph.D. thesis, Tel Aviv University, 2002
132. B. Ilan, Y. Sivan, G. Fibich, A quantitative approach to soliton instability. *Opt. Lett.* **36**, 397–399 (2011)
133. A.A. Ishaaya, T.D. Grow, S. Gosh, L.T. Vuong, A.L. Gaeta, Self-focusing dynamics of coupled optical beams. *Phys. Rev. A* **75**, 023813 (2007)
134. J.D. Jackson, *Classical Electrodynamics* (Wiley, New York, 1975)
135. Z. Jin, J. Zhang, M.H. Xu, X. Lu, Y.T. Li, Z.H. Wang, Z.Y. Wei, X.H. Yuan, W. Yu, Control of filaments induced by femtosecond laser pulses propagating in air. *Opt. Express* **13**, 10424–10430 (2005)
136. R. Johnson, X. Pan, On an elliptic equation related to the blow-up phenomenon in the nonlinear Schrödinger equation. *Proc. Roy. Soc. Edinb. Sect. A* **123**, 763–782 (1993)
137. J. Yang, *Nonlinear Waves in Integrable and Nonintegrable Systems* (SIAM, Philadelphia, 2010)
138. M. Karlsson, Optical beams in saturable self-focusing media. *Phys. Rev. A* **46**, 2726–2734 (1992)
139. T. Kato, On nonlinear Schrödinger equations. *Ann. Inst. H. Poincaré. Phys. Théor.* **46**, 113–129 (1987)
140. P.L. Kelley, Self-focusing of optical beams. *Phys. Rev. Lett.* **15**, 1005–1008 (1965)
141. Y.S. Kivshar, G.P. Agrawal, *Optical Solitons* (Academic Press, San Diego, California, 2003)
142. K. Konno, H. Suzuki, Self-focusing of a laser beam in nonlinear media. *Physica Scripta* **20**, 382–386 (1979)
143. S.O. Koronov, A.M. Zheltikov, P. Zhou, A.P. Tarasevitch, D. von der Linde, Self-channeling of subgigawatt femtosecond laser pulses in a ground-state waveguide induced in the hollow core of a photonic crystal fiber. *Opt. Lett.* **29**, 1521–1523 (2004)
144. N. Koppel, M. Landman, Spatial structure of the focusing singularity of the nonlinear Schrödinger equation: a geometrical analysis. *SIAM J. Appl. Math.* **55**, 1297–1323 (1995)
145. N.E. Kosmatov, V.F. Shvets, V.E. Zakharov, Computer simulation of wave collapses in the nonlinear Schrödinger equation. *Physica D* **52**, 16–35 (1991)
146. V.I. Kruglov, Y.A. Logvin, V.M. Volkov, The theory of spiral laser beams in nonlinear media. *J. Mod. Opt.* **39**, 2277–2291 (1992)
147. V.I. Kruglov, V.M. Volkov, R.A. Vlasov, V.V. Drits, Auto-waveguide propagation and the collapse of spiral light beams in non-linear media. *J. Phys. A: Math. Gen.* **21**, 4381–4395 (1988)
148. E.A. Kuznetsov, J.J. Rasmussen, K. Rypdal, S.K. Turitsyn, Sharper criteria for the wave collapse. *Physica D* **87**, 273–284 (1995)

149. M.K. Kwong, Uniqueness of positive solutions of $\Delta u - u + u^p p = 0$ in \mathbb{R}^n . *Arch. Ration. Mech. Anal.* **105**, 243–266 (1989)
150. L.D. Landau, E.M. Lifshitz, *Quantum Mechanics* (Pergamon Press, Oxford, 1977)
151. M.J. Landman, G.C. Papanicolaou, C. Sulem, P.L. Sulem, Rate of blowup for solutions of the nonlinear Schrödinger equation at critical dimension. *Phys. Rev. A* **38**, 3837–3843 (1988)
152. M.J. Landman, G.C. Papanicolaou, C. Sulem, P.L. Sulem, X.P. Wang, Stability of isotropic singularities for the nonlinear Schrödinger equation. *Physica D* **47**, 393–415 (1991)
153. M. Lax, W.H. Louisell, W.B. McKnight, From Maxwell to paraxial wave optics. *Phys. Rev. A* **11**, 1365–1370 (1975)
154. B.J. LeMesurier, Dissipation at singularities of the nonlinear Schrödinger equation through limits of regularisations. *Physica D* **138**, 334–343 (2000)
155. B.J. LeMesurier, G. Papanicolaou, C. Sulem, P.L. Sulem, Focusing and multi-focusing solutions of the nonlinear Schrödinger equation. *Physica D* **31**, 78–102 (1988)
156. B.J. LeMesurier, G.C. Papanicolaou, C. Sulem, P.L. Sulem, Local structure of the self-focusing singularity of the nonlinear Schrödinger equation. *Physica D* **32**, 210–226 (1988)
157. R.J. Leveque, *Numerical Methods for Conservation Laws* (Birkhauser, Basel, 1992)
158. E.H. Lieb, M. Loss, *Analysis*, 2nd edn. (American Mathematical Society, Providence, 2001)
159. P.L. Lions, The concentration-compactness principle in the calculus of variations. The compact case. Part 1. *Ann. Inst. H. Poincaré Anal. Nonlinéaire* **1**, 109–145 (1984)
160. W. Liu, F. Théberge, J.F. Daigle, P.T. Simrad, Y. Kamali, H.L. Xu, S.L. Chin, An efficient control of ultrashort laser filament location in air for the purpose of remote sensing. *Appl. Phys. B* **85**, 55–58 (2006)
161. P.D. Maker, R.W. Terhune, Study of optical effects due to an induced third order polarization in the electric field strength. *Phys. Rev.* **137**, A801–A819 (1965)
162. P.D. Maker, R.W. Terhune, C.M. Savage, Intensity-dependent changes in the refractive index of liquids. *Phys. Rev. Lett.* **12**, 507–509 (1964)
163. I.H. Malitson, Interspecimen comparison of the refractive index of fused silica. *J. Opt. Soc. Am.* **55**, 1205–1209 (1965)
164. V.M. Malkin, On the analytical theory for stationary self-focusing of radiation. *Physica D* **64**, 251–266 (1993)
165. J.H. Marburger, Self-focusing: theory. *Prog. Quant. Electr.* **4**, 35–110 (1975)
166. J.H. Marburger, E.L. Dawes, Dynamical formation of small-scale filaments. *Phys. Rev. Lett.* **21**, 556–558 (1968)
167. J.H. Marburger, F.S. Felber, Theory of a lossless nonlinear Fabry-Perot interferometer. *Phys. Rev. A* **17**, 335–342 (1978)
168. E.A.J. Marcatili, R.A. Schmeltzer, Hollow metallic and dielectric waveguides for long distance optical transmission and lasers. *Bell Syst. Tech. J.* **43**, 1783–1809 (1964)
169. Y. Martel, F. Merle, Stability of blow-up profile and lower bounds for blow-up rate for the critical generalized KdV equation. *Ann. Math.* **155**, 235–280 (2002)
170. Y. Martel, F. Merle, P. Raphael, Blow up for the critical gKdV equation I: dynamics near the soliton. [arXiv:1204.4625](https://arxiv.org/abs/1204.4625), (2012)
171. D.W. McLaughlin, G.C. Papanicolaou, C. Sulem, P.L. Sulem, Focusing singularity of the cubic Schrödinger equation. *Phys. Rev. A* **34**, 1200–1210 (1986)
172. G. Méchain, A. Couairon, M. Franco, B. Prade, A. Mysyrowicz, Organizing multiple femtosecond filaments in air. *Phys. Rev. Lett.* **93**, 035003 (2004)
173. F. Merle, Limit behavior of saturated approximations of nonlinear Schrödinger equation. *Comm. Math. Phys.* **149**, 377–414 (1992)
174. F. Merle, On uniqueness and continuation properties after blow-up time of self-similar solutions of nonlinear Schrödinger equation with critical exponent and critical mass. *Comm. Pure Appl. Math.* **45**, 203–254 (1992)
175. F. Merle, Determination of blow-up solutions with minimal mass for nonlinear Schrödinger equation with critical power. *Duke Math. J.* **69**, 427–454 (1993)
176. F. Merle, Lower bounds for the blow-up rate of solutions of the Zakharov equation in dimension two. *Comm. Pure Appl. Math.* **49**, 765–794 (1996)

177. F. Merle, Nonexistence of minimal blow-up solutions of equations $iu_t = -\delta u - k(x)|u|^{4/N}u$ in r^n . Ann. Inst. Henri Poincaré **64**, 33–85 (1996)
178. F. Merle, P. Raphael, Sharp upper bound on the blow-up rate for the critical nonlinear Schrödinger equation. Geom. Funct. Anal. **13**, 591–642 (2003)
179. F. Merle, P. Raphael, On universality of blow-up profile for L^2 critical nonlinear Schrödinger equation. Invent. Math. **156**, 565–672 (2004)
180. F. Merle, P. Raphael, Blow-up dynamics and upper bound on the blow-up rate for the critical nonlinear Schrödinger equation. Ann. Math. **161**, 157–222 (2005)
181. F. Merle, P. Raphael, Profiles and quantization of the blow-up mass for critical nonlinear Schrödinger equation. Commun. Math. Phys. **253**, 675–704 (2005)
182. F. Merle, P. Raphael, On a sharp lower bound on the blow-up rate for the L^2 critical nonlinear Schrödinger equation. J. Amer. Math. Soc. **19**, 37–90 (2006)
183. F. Merle, P. Raphael, On one blow up point solutions to the critical nonlinear Schrödinger equation. J. Hyperbolic Diff. Equat. **2**, 919–962 (2006)
184. F. Merle, P. Raphael, J. Szeftel, Stable self similar blow up dynamics for slightly L^2 supercritical NLS equations. Geom. Funct. Anal. **20**, 1028–1071 (2010)
185. F. Merle, P. Raphael, J. Szeftel, The instability of Bourgain-Wang solutions for the L^2 critical NLS. Amer. J. Math. **135**, 967–1017 (2013)
186. F. Merle, P. Raphael, J. Szeftel, On collapsing ring blow-up solutions to the mass supercritical nonlinear Schrödinger equation. Duke Math. J. **163**, 369–431 (2014)
187. F. Merle, Y. Tsutsumi, Limit of the solution of a nonlinear Schrödinger equation at blow-up time. J. Funct. Anal. **84**, 201–214 (1989)
188. F. Merle, Y. Tsutsumi, L^2 concentration of blow-up solutions for the nonlinear Schrödinger equation with critical power nonlinearity. J. Diff. Equat. **84**, 205–214 (1990)
189. T. Mizumachi, Vortex solitons for 2d focusing nonlinear Schrödinger equation. Diff. Int. Equat. **18**, 431–450 (2004)
190. T. Mizumachi, Instability of vortex solitons for 2d focusing NLS. Adv. Diff. Equat. **12**, 241–264 (2007)
191. M. Mlejnek, M. Kolesik, J.V. Moloney, E.M. Wright, Optically turbulent femtosecond light guide in air. Phys. Rev. Lett. **83**, 2938–2941 (1999)
192. K.D. Moll, A.L. Gaeta, G. Fibich, Self-similar optical wave collapse: observation of the Townes profile. Phys. Rev. Lett. **90**, 203902 (2003)
193. J.D. Murray, *Asymptotic Analysis* (Springer, New York, 1984)
194. H. Nawa, Mass-concentration phenomenon for the nonlinear Schrödinger equation with the critical power nonlinearity II. Kodai Math. J. **13**, 333–348 (1990)
195. H. Nawa, “Mass concentration” phenomenon for the nonlinear Schrödinger equation with the critical power nonlinearity. Funkcial. Ekvac. **35**, 1–18 (1992)
196. H. Nawa, Asymptotic profiles of blow-up solutions of the nonlinear Schrödinger equation with critical power nonlinearity. J. Math. Soc. Jpn. **46**, 557–586 (1994)
197. H. Nawa, Asymptotic profiles of blow-up solutions of the nonlinear Schrödinger equation with critical power nonlinearity II. unpublished, 1997
198. H. Nawa, Asymptotic profiles of blow-up solutions of the nonlinear Schrödinger equation with critical power nonlinearity III. unpublished, 1997
199. H. Nawa, Asymptotic and limiting profiles of blow-up solutions of the nonlinear Schrödinger equation with critical power. Comm. Pure Appl. Math. **52**, 193–270 (1999)
200. H. Nawa, M. Tsutsumi, On blow-up for the pseudo-conformally invariant nonlinear Schrödinger equation. Funkcial. Ekvac. **32**, 417–428 (1989)
201. H. Nawa, M. Tsutsumi, On blow-up for the pseudo-conformally invariant nonlinear Schrödinger equation II. Comm. Pure Appl. Math. **51**, 373–383 (1998)
202. L. Nirenberg, On elliptic partial differential equations. Ann. Scuola Norm. Sup. Pisa **13**, 115–162 (1959)
203. T. Ogawa, A proof of Trudinger’s inequality and its application to nonlinear Schrödinger equations. Nonlinear Anal. **14**, 765–769 (1990)

204. T. Ogawa, T. Ozawa, Trudinger type inequalities and uniqueness of weak solutions for the nonlinear Schrödinger mixed problem. *J. Math. Anal. Appl.* **155**, 531–540 (1991)
205. T. Passot, C. Sulem, P.L. Sulem, Linear versus nonlinear dissipation for critical NLS equation. *Physica D* **203**, 167–184 (2005)
206. D.E. Pelinovsky, YuA Stepanyants, Convergence of Petviashvili's iteration method for numerical approximation of stationary solutions of nonlinear wave equations. *SIAM J. Numer. Anal.* **42**, 1110–1127 (2004)
207. V. Peréz-García, M. Porras, L. Vázquez, The nonlinear Schrödinger equation with dissipation and the moment method. *Phys. Lett. A* **202**, 176–182 (1995)
208. V.I. Petviashvili, Equation of an extraordinary soliton. *Sov. J. Plasma Phys.* **2**, 257–258 (1976)
209. N.F. Pilipetskii, A.R. Rustamov, Observation of self-focusing of light in liquids. *JETP Lett.* **2**, 55–56 (1965)
210. Y. Pinchover, J. Rubinstein, *An Introduction to Partial Differential Equations* (Cambridge University Press, Cambridge, 2005)
211. F. Planchon, P. Raphaël, Existence and stability of the log-log blow-up dynamics for the L^2 -critical nonlinear Schrödinger equation in a domain. *Ann. Henri Poincaré* **8**, 1177–1219 (2007)
212. S. Pohozaev, Eigenfunctions of the equation $\Delta u + \lambda f(u) = 0$. *Soviet Math. Dokl.* **6**, 1408–1411 (1965)
213. G. Polya, G. Szegő, *Isoperimetric Inequalities in Mathematical Physics* (Princeton University Press, Princeton, 1951)
214. M.R. Querry, D.M. Wieliczka, D.J. Segelstein, Water (H_2O), in *Handbook of Optical Constants of Solids II*, ed. by E.D. Palik (Academic Press, San-Diego, 1991), pp. 1059–1077
215. J.K. Ranka, A.L. Gaeta, Breakdown of the slowly varying envelope approximation in the self-focusing of ultrashort pulses. *Opt. Lett.* **23**, 534–536 (1998)
216. J.K. Ranka, R.W. Schirmer, A.L. Gaeta, Observation of pulse splitting in nonlinear dispersive media. *Phys. Rev. Lett.* **77**, 3783–3786 (1996)
217. P. Raphael, Stability of the log-log bound for blow up solutions to the critical non linear Schrödinger equation. *Math. Ann.* **331**, 577–609 (2005)
218. P. Raphael, Existence and stability of a solution blowing up on a sphere for a L^2 supercritical non linear Schrödinger equation. *Duke Math. J.* **134**, 199–258 (2006)
219. P. Raphael, J. Szeftel, Standing ring blow up solutions to the N -dimensional quintic nonlinear Schrödinger equation. *Comm. Math. Phys.* **290**, 973–996 (2009)
220. J.J. Rasmussen, K. Rypdal, Blow-up in nonlinear Schrödinger equations. I. A general review. *Phys. Scr.* **33**, 481–497 (1986)
221. K.O. Rasmussen, O. Bang, P.I. Christiansen, Driving and collapse in a nonlinear Schrödinger equation. *Phys. Lett. A* **184**, 241–244 (1994)
222. W. Ren, X.P. Wang, An iterative grid redistribution method for singular problems in multiple dimensions. *J. Comput. Phys.* **159**, 246–273 (2000)
223. P. Rohwetter, M. Queißer, K. Stelmaszczyk, M. Fechner, L. Wöste, Laser multiple filamentation control in air using a smooth phase mask. *Phys. Rev. A* **77**, 013812 (2008)
224. J.E. Rothenberg, Pulse splitting during self-focusing in normally dispersive media. *Opt. Lett.* **17**, 583–585 (1992)
225. K. Rypdal, J.J. Rasmussen, Blowup in nonlinear schrodinger equations. II. Similarity structure of the blow-up singularity. *Phys. Scr.* **33**, 498–504 (1986)
226. K. Rypdal, J.J. Rasmussen, K. Thomsen, Similarity structure of wave-collapse. *Physica D* **16**, 339–357 (1985)
227. C.A. Sackett, J.M. Gerton, M. Welling, R.G. Hulet, Measurements of collective collapse in a Bose-Einstein condensate with attractive interactions. *Phys. Rev. Lett.* **82**, 876–879 (1999)
228. B.A. Saleh, M.C. Teich, *Fundamentals of Photonics* (Wiley, New York, 1991)
229. T.D. Scarborough, C. Petersen, C.J.G.J. Uiterwaal, Measurements of the GVD of water and methanol and laser pulse characterization using direct imaging methods. *N. J. Phys.* **10**, 103011 (2008)

230. S.E. Schrauth, B. Shim, A.D. Slepkov, L.T. Vuong, A.L. Gaeta, N. Gavish, G. Fibich, Pulse splitting in the anomalous group-velocity-dispersion regime. *Opt. Express* **19**, 9309–9314 (2011)
231. M. Sever, An existence theorem for some semilinear elliptic systems. *J. Diff. Equat.* **226**, 572–593 (2006)
232. J. Shatah, W.A. Strauss, Instability of nonlinear bound states. *Commun. Math. Phys.* **100**, 173–190 (1985)
233. Y.R. Shen, Self-focusing: experimental. *Prog. Quant. Electr.* **4**, 1–34 (1975)
234. B. Shim, S.E. Schrauth, A.L. Gaeta, M. Klein, G. Fibich, Loss of phase of collapsing beams. *Phys. Rev. Lett.* **108**, 043902 (2012)
235. V.F. Shvets, N.E. Kosmatov, B.J. LeMesurier, On collapsing solutions of the nonlinear Schrödinger equation in supercritical case, in *Singularities in Fluids, Plasmas and Optics*, ed. by R.E. Caflisch, G.C. Papanicolaou (Kluwer, Dordrecht, 1993), pp. 317–321
236. V.F. Shvets, V.E. Zakharov, Computer simulations of wave collapses and wave turbulence, in *Nonlinear World*, IVth International Workshop on Nonlinear and Turbulent Processes in Physics (Kiev, 1989), ed. by V.G. Baryakhtsr, V.M. Chernousenko, N.S. Erokin, A.G. Silenko, Z.E. Zakharov (World Scientific, Singapore, 1990), pp. 671–692
237. Y. Silberberg, Collapse of optical pulses. *Opt. Lett.* **15**, 1282–1284 (1990)
238. G. Simpson, I. Zwiers, Vortex collapse for the L^2 -critical nonlinear Schrödinger equation. *J. Math. Phys.* **52**, 083503 (2011)
239. Y. Sivan, G. Fibich, N.K. Efremidis, S. Bar-Ad, Analytic theory of narrow lattice solitons. *Nonlinearity* **21**, 509–536 (2008)
240. Y. Sivan, G. Fibich, B. Ilan, Drift instability and tunneling of lattice solitons. *Phys. Rev. E* **77**, 045601(R) (2008)
241. Y. Sivan, G. Fibich, B. Ilan, M.I. Weinstein, Qualitative and quantitative analysis of stability and instability dynamics of positive lattice solitons. *Phys. Rev. E* **78**, 046602 (2008)
242. Y. Sivan, G. Fibich, M.I. Weinstein, Waves in nonlinear lattices: ultrashort optical pulses and Bose-Einstein condensates. *Phys. Rev. Lett.* **97**, 193902 (2006)
243. M. Soljacić, S. Sears, M. Segev, Self-trapping of “necklace” beams in self-focusing Kerr media. *Phys. Rev. Lett.* **81**, 4851–4854 (1998)
244. J. Soto-Crespo, D. Heatley, E. Wright, N. Akhmediev, Stability of the higher-bound states in a saturable self-focusing medium. *Phys. Rev. A* **44**, 636–644 (1991)
245. J.M. Soto-Crespo, E.M. Wright, N.N. Akhmediev, Recurrence and azimuthal-symmetry breaking of a cylindrical Gaussian beam in a saturable self-focusing medium. *Phys. Rev. A* **45**, 3168–3174 (1992)
246. W.A. Strauss, Existence of solitary waves in higher dimensions. *Comm. Math. Phys.* **55**, 149–162 (1977)
247. W.A. Strauss, *Nonlinear Wave Equations* (American Mathematical Society, Providence, 1989)
248. J. Stubbe, Global solutions and stable ground states of nonlinear Schrödinger equations. *Physica D* **48**, 259–272 (1991)
249. C. Sulem, P.L. Sulem, *The Nonlinear Schrödinger Equation* (Springer, New York, 1999)
250. P.L. Sulem, C. Sulem, A. Patera, Numerical simulations of singular solutions of the two-dimensional cubic Schrödinger equation. *Comm. Pure Appl. Math.* **37**, 755–778 (1984)
251. T.R. Taha, M.I. Ablowitz, Analytical and numerical aspects of certain nonlinear evolution equations. II. Numerical, nonlinear Schrödinger equation. *J. Comput. Phys.* **55**, 203–230 (1984)
252. V.I. Talanov, Focusing of light in cubic media. *JETP Lett.* **11**, 199–201 (1970)
253. T. Tao, *Nonlinear Dispersive Equations*, vol. 106, CBMS Regional Conference Series in Mathematics (Published for the Conference Board of the Mathematical Sciences, Washington, DC, 2006)
254. T. Tao, Global existence and uniqueness results for weak solutions of the focusing mass-critical nonlinear Schrödinger equation. *Anal. PDE* **2**, 61–81 (2009)
255. M. Tsutsumi, Nonexistence of global solutions to the Cauchy problem for the damped nonlinear Schrödinger equations. *Siam J. Math. Anal.* **15**, 357–366 (1984)

256. Y. Tsutsumi, Rate of L^2 concentration of blow-up solutions for the nonlinear Schrödinger equation with critical power. *Nonlin. Anal.* **15**, 719–724 (1990)
257. S.K. Turitsyn, Nonstable solitons and sharp criteria for wave collapse. *Phys. Rev. E* **47**, R13–R16 (1993)
258. N.G. Vakhitov, A.A. Kolokolov, Stationary solutions of the wave equation in a medium with nonlinearity saturation. *Radiophys. Quant. Elec.* **16**, 783–789 (1973)
259. F. Vidal, T.W. Johnston, Electromagnetic beam breakup—multiple filaments, single beam equilibria and radiation. *Phys. Rev. Lett.* **77**, 1282–1285 (1996)
260. A. Vincotte, L. Berge, Atmospheric propagation of gradient-shaped and spinning femtosecond light pulses. *Physica D* **223**, 163–173 (2006)
261. S.N. Vlasov, Structure of the field of wave beams with circular polarization near a nonlinear focus in a cubic medium. *Sov. J. Quant. Electron.* **17**, 1191–1193 (1987)
262. S.N. Vlasov, V.A. Petrishchev, V.I. Talanov, Averaged description of wave beams in linear and nonlinear media. *Radiophys. Quant. Electron.* **14**, 1062–1070 (1971)
263. S.N. Vlasov, L.V. Piskunova, V.I. Talanov, Structure of the field near a singularity arising from self-focusing in a cubically nonlinear medium. *Sov. Phys. JETP* **48**, 808–812 (1978)
264. L.T. Vuong, T.D. Grow, A. Ishaaya, A.L. Gaeta, G.W. Hooft, E.R. Eliel, G. Fibich, Collapse of optical vortices. *Phys. Rev. Lett.* **96**, 133901 (2005)
265. J.K. Wahlstrand, Y.-H. Cheng, Y.-H. Chen, H.M. Milchberg, Optical nonlinearity in Ar and N_2 near the ionization threshold. *Phys. Rev. Lett.* **107**, 103901 (2011)
266. J.K. Wahlstrand, Y.-H. Cheng, H.M. Milchberg, High field optical nonlinearity and the Kramers-Kronig relations. *Phys. Rev. Lett.* **109**, 113904 (2012)
267. C.C. Wang, Length-dependent threshold for stimulated Raman effect and self-focusing of laser beams in liquids. *Phys. Rev. Lett.* **16**, 344–346 (1966)
268. D. Wang, X.P. Wang, A three-dimensional adaptive method based on the iterative grid redistribution. *J. Comput. Phys.* **199**, 423–436 (2004)
269. X.P. Wang, *On singular solutions of the nonlinear Schrödinger and Zakharov equations*. Ph.D. thesis, Courant Institute, New York University, 1990
270. J. Weideman, B. Herbst, Split-step methods for the solution of the nonlinear Schrödinger equation. *SIAM J. Numer. Anal.* **23**, 485–507 (1986)
271. H.F. Weinberger, *Variational Methods for Eigenvalue Approximation* (SIAM, Philadelphia, 1974)
272. M.I. Weinstein, Nonlinear Schrödinger equations and sharp interpolation estimates. *Comm. Math. Phys.* **87**, 567–576 (1983)
273. M.I. Weinstein, Modulational stability of ground states of nonlinear Schrödinger equations. *SIAM J. Math. Anal.* **16**, 472–490 (1985)
274. M.I. Weinstein, Lyapunov stability of ground states of nonlinear dispersive evolution equations. *Commun. Pure Appl. Math.* **39**, 51–68 (1986)
275. M.I. Weinstein, On the structure and formation of singularities in solutions to nonlinear dispersive evolution equations. *Comm. Part. Diff. Equat.* **11**, 545–565 (1986)
276. M.I. Weinstein, The nonlinear Schrödinger equations—singularity formation, stability and dispersion. *Contemp. Math.* **99**, 213–232 (1989)
277. H. Wilhelm, Analytical solution of the boundary-value problem for the nonlinear Helmholtz equation. *J. Math. Phys.* **11**, 824–826 (1970)
278. D. Wood, The self-focusing singularity in the nonlinear Schrödinger equation. *Stud. Appl. Math.* **71**, 103–115 (1984)
279. Y. Yamaoka, K. Minoshima, H. Matsumoto, Direct measurement of the group refractive index of air with interferometry between adjacent femtosecond pulses. *Appl. Opt.* **42**, 4318–4324 (2002)
280. J. Yang, *Nonlinear Waves in Integrable and Nonintegrable Systems*, Mathematical Modeling and Computations (SIAM, Philadelphia, 2010)
281. V.E. Zakharov, *Handbook of Plasma Physics*, vol. 2 (Elsevier, New York, 1984)
282. V.E. Zakharov, A.B. Shabat, Exact theory of two-dimensional self focusing and one-dimensional self modulation of waves in nonlinear media. *Sov. Phys. JETP* **34**, 62–69 (1972)

283. V.E. Zakharov, V.F. Shvets, Nature of wave collapse in the critical case. *JETP Lett.* **47**, 275–278 (1988)
284. V.E. Zakharov, V.S. Synakh, The nature of the self-focusing singularity. *Sov. Phys. JETP* **41**, 465–468 (1976)
285. N.A. Zharova, A.G. Litvak, T.A. Petrova, A.M. Sergeev, A.D. Yunakovskiy, Multiple fractionation of wave structures in a nonlinear medium. *JETP Lett.* **44**, 13–17 (1986)
286. S. Zhu, J. Zhang, H. Yang, Limiting profile of the blow-up solutions of the fourth-order nonlinear Schrödinger equation. *Dyn. PDE* **7**, 187–205 (2010)
287. I. Zwiers, Standing ring blowup solutions for cubic nonlinear Schrödinger equations. *Anal. PDE* **4**, 677–727 (2011)

Index

A

A priori estimate, 101, 156
Aberrationless approximation, 76–83, 168–169, 422, 425, 427, 464, 558–559, 562, 565
method, 76, 466
Aberrationless propagation, 42, 147
Adiabatic approach, 460–465
Adiabatic law, 462–465
of Fibich, 467–469
of Malkin, 468–470
Admissible solutions, 265–269, 373, 444, 498, 516
Amount of power that collapses into the singularity, 163
Approximate modulational instability (AMI) method, 245–247, 368–371
Azimuthal instability, 244–247, 368–371, 373, 481–482, 492, 519, 576, 577
Azimuthal stability, 107, 312–314, 322–323, 327

B

Backscattering, 63–64, 730–734
Balance of the giants principle, 466, 691, 699, 707, 725, 729, 762
Beam breakup, 83, *see also* multiple filamentation
Beam power, 24, 68, 556
Bespalov-Talanov model, 8, 571, 575, 588, 619
 β principle, 682–684, 725, 728, 768
Biharmonic NLS, 96, 99, 100, 104, 108, 110, 112, 115, 120, 124, 127, 130–131, 152, 173, 176, 180, 216–217, 251,

286–287, 409, 509, 548–550, 644–646
critical, 106, 111, 113, 121, 122, 276–277, 282–284, 292, 296, 331–332, 485, 560
supercritical, 256, 258, 504
blowup alternative, 101
Blowup point, *see* location of singularity
Blowup profile
critical NLS, 280–288
Blowup rate, 208–217, 273–280, 314–318
and the lens transformation, 277–280
biharmonic NLS, 216–217, 286–287
critical NLS, 285–286
linear, 208, 274
square root, 82, 239–240, 465, 499, 501
square-root bound, 275–276
supercritical NLS, 301–303
under adiabatic approximation, 465
BNLS, *see* Biharmonic NLS
Bose-Einstein condensates, 65, 92, 189, 333, 677, 716, 764, 786
Boundary condition
Dirichlet, 386, 387
frozen, 428, 429, 438, 440–443
radiation, 34, 737–739
Bounded domain, 385, 417, 560–561
Bourgain-Wang solutions, 214–216, 300, 328, 797–798, 800, 801, 803, 804

C

Center of mass, 97
Chirp, 631, 758
Collapse
and instability, 200
at k points, 296–299

equal-rate, 524
partial beam, 148, 166–168, 214, 274, 284, 322, 323, 327, 427
quasi self-similar, 284–285, 414, 415, 427–432
strong, 163, 164, 167, 378, 538–539, 549
weak, 164, 167, 498–499
whole beam, 24, 162–167, 203, 206, 274, 355, 427, 539

Collapse distance, *see* location of singularity
Collective coordinate method, 83
Continuations beyond the singularity, 793–832
Continuous dependence on initial conditions, 102
Continuous wave (cw), 6
Coupled optical beams, 65–66, 839–840
Critical exponent
 for blowup, 111, 112, 200
 for ring-type collapse, 547, 550
 for stability, 200
Critical NLS, 111–113
Critical power
 for collapse, 74–75, 110, 111, 121, 122, 553–569
 for self trapping, 68, 569–570
 for vortex collapse, 347–350
Cubic-quintic nonlinearity, 701–709, 807–808

D

Damping
 linear, 711–716, 739, 825
 nonlinear, 716–721, 812–828
Defocusing NLS, 107–109, 130, 154
Diffraction length, 43–47, 757
Diffraction-limited width, 41, 45
Dilation symmetry, 175, 176
Dispersion, 57, 744–745
 anomalous, 757
 length, 756–757
 normal, 757
 relation, 5, 57
Dispersive equations, 57
Dual borderline properties, 135, 366, 427
Dynamic rescaling, 457

E

Eikonal equation, 20–23, 591
 paraxial, 39
Elliptic initial conditions, 89, 107, 244, 245, 312, 561, 564, 581–585

Excited states

definition, 119
instability of, 203
Explicit blowup solutions
 critical peak-type, 205–214
 critical ring-type, 219–247
 subcritical, 270–272
 supercritical peak-type, 249–269

F

Filament singularity, 794, 806, 808, 831, 832
Filamentation, *see* self trapping
Filamentation distance, *see* location of singularity
Focusing NLS, 107, 109–111
Fourier transform, 51

G

Gagliardo-Nirenberg inequality, 99, 100, 115, 116, 120, 121, 134, 346, 347, 407–410
Galilean invariance, 175–177
Geometrical optics, 19–25, 64–65, 79
 nonlinear, *see* NGO method
Gross-Pitaevski equation, 92
Ground state, 119, 131–138
Group velocity, 747
 dispersion (GVD), 747, 756

H

H^1 -subcritical, 95, 114
 H^1 norm, 51, 52, 387
 H^2 -subcritical, 100
 H^2 norm, 52
Hamiltonian, 96
 of the BNLS, 99

I

Index of refraction, 10, 13, 26
Instability
 of singular solutions, 209–211
 strong, 209

K

Kerr
 coefficient, 12
 effect, 750
 nonlinearity, 12–17

L

L^2 concentration, 288, *see also* power concentration
 L^2 -critical, 114
 L^2 -subcritical, 114
 L^2 -supercritical, 114
Lens
 effect of, 159–160, 181–183
 representation, 31, 35–36
Lens transformation, 177–191, 354, 388, 631, 633
Linear momentum, 96
Linear polarization, 5
linear Schrödinger equation, 35–60
 continuation of, 829–831
Linear waveguides
 cylindrical, 28–29
 planar, 26–28, 90, 91
 LL_z approach, 316–318, 480
Location of singularity, 78–83, 87, 463–465, 613–634, 717
 non-monotonicity of, 623, 625–628, 630, 715
Loglog law, 324–331, 449, 450, 452–460, 468–470
Loss of phase, 587, 625, 796–798, 805, 806, 810, 814, 815, 825, 827, 832–841
 L^p norm, 51, 387
 interpolation inequality for, 103, 844

M

Mass concentration, 288, *see also* power concentration
Maxwell's equations, 3
Method of characteristics, 21, 591
Minimal-power blowup solutions, 174, 299–301, 305, 796, 814, 825
Modulational instability, 86, 247, 571, 619
Multiple filamentation, 83–88, 481, 571–588, 701, 709, 840

N

Necklace beam, 297, 381–383, 397, 398
NGO method, 428, 473, 476, 517, 522, 542, 587–611, 618, 619, 783–791
Noisy initial conditions, 84–88, 313–314, 571–577, 618–620
Non-directionality, *see also* reversibility, 57–59
Nonlinear Helmholtz equation
 scalar, 15, 60–62, 723–742
 vectorial, 14, 63–64, 578–581, 730, 733

Nonlinear saturation, 701–709, 799–808
Nonparaxiality parameter, 16, 47, 62

O

Optical fiber, 28, 92
Optimal constant, 115–121, 346–347, 407–410

P

Parabolic approximation, 35, *see also* paraxial approximation
Paraxial approximation, 9, 35, 47–48, 62, 723–725, 730, 741
Parseval's relation, 51
 P_{collapse} , 163, 291–293, 322, 326, 378, 539
Phase loss, *see* loss of phase
Plane wave, 5
 paraxial, 7
Pohozaev identities, 127–131, 338, 389, 390, 433, 646
Polarization field, 9–12, 701, 707
Power, 96
 concentration, 288–296, 305, 377–378, 415
 conservation of, 54, 97, 99
Pseudo-conformal transformation, 179, *see also* lens transformation
Pulse splitting
 in anomalous regime, 785, 787–788, 790
 in normal regime, 765, 766, 769–770, 772–781

R

Rayleigh length, 45, *see also* diffraction length
Renormalization method
 non-spectral, 398, 643–644
 spectral, 638–643
Reversibility, 23, 57–59, 804
Ring-type solutions
 continuation of, 809–811
 critical, 473–485
 explicit, 219–247
 shrinking, 523–550
 standing, 505–522

S

Self defocusing, *see also* defocusing NLS, 65
Self focusing, *see also* focusing NLS, 64–65, 71–74

Self focusing distance, 71–74, 87
 Self phase modulations, 72, 590
 Self trapping, 67–69, 71, 74, 569–570, 693–694, 701, 709
 Shooting method, 143, 637–638
 Small-scale self focusing, 83, *see also* multiple filamentation
 Snell’s law, 25–26
 Solitary waves, 125–145
 computation of, 637–646
 instability rate and dynamics of, 203–204
 linear stability of, 195–198
 necklace, 397, 398
 orbital stability of, 193–195, 402, 407
 stability analysis of, 193–204
 strong instability of, 201, 209
 variational characterization, 136–138, 401, 402
 Solitons, 88, 112, 142, 199, 654, 759
 nonparaxial, 741–742
 Steiner symmetrization, 122
 Subcritical NLS, 111–112
 Sufficient power for collapse, 168–172
 Supercritical NLS, 111, 113–114, 156–158, 167, 301–306
 Symmetries, 175–180

T

Third-harmonic generation, 12
 Threshold power for collapse, 168–172, 413–414, 453–566
 Threshold power for filamentation, 564
 Tilted beams, 36–37, 49–50, 161, 176–177
 Townes profile, 70, 323
 Transport equation, 23–25, 591
 paraxial, 39
 Trapping efficiency, 27, 65

U

Ultrashort pulses, 743–791

V

Variance identity, 99, 147–168, 411–413
 Variational method, 83, 168, 558
 Virial theorem, 148, *see also* variance identity
 VK condition, 198–199, 204, 404, 406
 Vortex solutions, 38, 105, 333–379, 487–492, 544–545, 564–566

W

Wavefront, 22